Source and timing of alkali metasomatism and associated critical element mineralization in the Pool Creek map area, southeastern Yukon

by

Tiera Venesse Naber

B.Sc. (Hons), University of Calgary, 2018

THIS THESIS SUBMITTED IN PARTIAL FUFILLMENT OF THE REQUIREMENTS FOR THE DEGREE OF

MASTER OF SCIENCE

in

The Faculty of Graduate and Postdoctoral Studies

(Geological Sciences)

THE UNIVERSITY OF BRITISH COLUMBIA

(Vancouver)

April 2023

The following individuals certify that they have read, and recommend to the Faculty of Graduate and Postdoctoral Studies for acceptance, the thesis entitled:

Source and timing of alkali metasomatism and associated critical element mineralization in the Pool Creek map area, southeastern Yukon

submitted by	Tiera Naber	in partial fulfilment of the requirements for
the degree of	Master of Science	
in	Geological Sciences	

Examining Committee:

Lee A. Groat, Earth, Ocean & Atmospheric Sciences, UBC
Supervisor

Maya Kopylova, Earth, Ocean & Atmospheric Sciences, UBC
Supervisory Committee Member

James K. Russell, Earth, Ocean & Atmospheric Sciences, UBC
Supervisory Committee Member

James S. Scoates, Earth, Ocean & Atmospheric Sciences, UBC
Additional Examiner

Additional Supervisory Committee Members:

Matthijs A. Smit, Earth, Ocean & Atmospheric Sciences, UBC
Supervisory Committee Member

Abstract

Rare-earth element (REE) and high field strength element (HFSE) bearing Eocene and Neoproterozoic intrusions occur throughout southeastern Yukon, Canada. Poorly exposed outcrops of a REE-HFSE bearing fenite of unknown origin are found adjacent to the Neoproterozoic Pool Creek nepheline syenite, which is superimposed by Eocene volcanism. Fenites hold critical information about the original composition of their source intrusions and have implications as a vector towards associated REE-HFSE mineralization; however, fenites associated with syenitic intrusions are understudied in the literature. Rock and mineral textures and compositions of the Pool Creek nepheline syenite, altered syenite suites, fenites, and host units (quartzite and argillite) were compared to determine the source and timing of the fenitization event and to contribute to the collective knowledge of fenites associated with syenitic intrusions. The altered syenite and fenite suites show geochemical and mineralogical compositions that are transitional between their respective host units and the Pool Creek nepheline syenite. Interestingly, the fenitized units hosted in argillite have REE-HFSE contents up to 15x greater than those hosted in quartzite. The style of mineralization observed in this study is consistent with that of a silicate roof zone type deposit, indicating the orientation of the intrusive system. Relationships between unaltered and altered zircon textures and dates show that the ages of crystallization of multiple intrusive units and associated fenitization occurred between 620 to 660 Ma. Overlapping ages of different syenitic units suggest that the Pool Creek nepheline syenite forms a composite alkaline-silicate complex, rather than a single intrusive event. These lines of evidence suggest that the source of the fenitization that produced the alteration observed in the altered syenite and fenite suites is the Neoproterozoic Pool Creek nepheline syenite, and therefore that fenitization was driven by contact metasomatism between the nepheline syenite and host units. These findings show that the characteristics of the host rocks strongly influence the composition and distribution of fenite aureoles and REE-HFSE mineralization associated with syenitic systems. These conclusions demonstrate that understanding the compositional relationship between the source intrusion, associated fenite, and host yields a plethora of information about the magmatic system and controls on associated mineralization.

Lay Summary

The goals of this research were to investigate the source of an alteration zone in southeast Yukon, Canada. This type of alteration is known to form around the top of cooling magma chambers that are rich in alkali elements, such as potassium (K) and sodium (Na). Such alteration is of public and scientific interest because the altered rocks are commonly enriched in elements such as lanthanum (La), cerium (Ce), and niobium (Nb), that are used in high technology applications.

Using textural and chemical evidence from altered and unaltered rock and mineral samples, the author determined that the alteration zones formed by the cooling of an ancient intrusion known as the Pool Creek nepheline syenite. This research contributes to our knowledge of the geologic characteristics of this type of alteration. This knowledge contributes to our understanding of what methods may be used to explore for similar alteration zones around the globe.

Preface

This dissertation is original, unpublished, independent work by the author, T.V. Naber.

Chapter 4. Figure 4.7 displays X-ray map images collected by Dr. Anette von der Handt and used with permission.

Table of Contents

List of Tables

List of Figures

List of Abbreviations

Analytical

2σ – two standard deviations

λ – radioactive decay constant

avg. – average

BSE – backscattered electron

CA-TIMS – chemical abrasion thermal ionization mass spectrometry

CL – cathodoluminescence

CNMNC – Commission on New Minerals, Nomenclature, and Classification

EMP – electron microprobe

eTh – equivalent thorium

eU – equivalent uranium

HFSE – high field strength element

HREE – heavy rare earth elements

ID-TIMS – isotope dilution thermal ionization mass spectrometry

LA-ICP-MS – laser ablation inductively coupled plasma mass spectrometry

LILE – large ion lithophile element

LREE – light rare earth elements

MREE – middle rare earth elements

MSWD – mean squared weighted deviation

n – number

REE – rare earth element

SEM – scanning electron microscope

SI – international system of units

SIMS – secondary ion mass spectrometry

Units

apfu – atoms per formula unit

cm – centimetre

Ma – millions of years

m – metre

mol % – mole percent

mm – millimetre

nT – nanotesla

ppm – parts per million

μm – micrometre or micron

wt. % - weight percent

Minerals

Ab – albite

Act – actinolite

Ae – aegirine

Aln – allanite

Amph – amphibole

An – anorthite

Ann – annite

Ap – apatite

Arf – arfvedsonite

Cal – calcite

Chl – chlorite

Col – columbite

Di – diopside

Eas – eastonite

En – enstatite

Ep – epidote

Fl – fluorite

Fs – ferrosilite

Hd – hedenbergite

Hem – hematite

Ksp – potassium feldspar

Mnz – monazite

Ms – muscovite

Ne – nepheline

Or – orthoclase

Pcl – pyrochlore

Pg – phengite

Phl – phlogopite

Qtz – quartz

Rt – rutile

Ser – sericite

Sid – siderophyllite

Th – thorite

Ttn – titanite

Wo – wollastonite

Zrn – zircon

Acknowledgements

I gratefully and respectfully acknowledge that the field research for this project was conducted in the traditional, ancestral, and unceded territory of the Kaska Dena Nation, and the laboratory research and writing of this thesis was conducted in the ancestral, traditional, and unceded territory of the xʷməθkʷəy̓əm people.

I have much gratitude for all my colleagues, friends, and family who supported me during this M.Sc. degree. I would first like to thank my supervisor, Professor Lee Groat, for supporting me and my research, and for always encouraging my professional development interests with respect to teaching. Thank you for helping me navigate and overcome personal and academic challenges during the COVID-19 pandemic. I am truly grateful for the research and employment opportunities that you have provided me with while I have been part of your research group.

I am grateful for my committee members, Professors Kelly Russell, Maya Kopylova, and Matthijs Smit for their kindness, insight, guidance, and support while serving on my committee. Kelly, thank you for your encouragement from the start of my degree back in 2018, and your feedback on my project plans as they have changed throughout the years. Maya, thank you for taking the time to look at my funky rock samples with me, for the insightful conversations about my petrographic interpretations, and for providing me with constructive feedback on my thesis. Matthijs, thank you for helping me to better understand my samples with respect to mineral textural and geochemical contexts, and considering creative ways to report and discuss my zircon data and interpretations.

Thank you to Professor James Scoates for being a fantastic external examiner and for helping me to consider the broader applications of my research.

My sincerest thanks to Dr. Anouk Borst for taking the time to connect with me and taking an interest in my research project. I am grateful for the many productive conversations about alkaline-silicate intrusions and fenites; I am truly inspired by your passion for this field of research. I am thankful to you for providing me with insightful questions and feedback on my project, particularly in Chapter 3 and Chapter 5. I have learnt for much from our conversations and appreciate you taking the time to teach and share your knowledge and ideas with me.

I am grateful to the kind and caring technicians in our department that I was privileged to learn from during this research. Thank you to Dr. Jacob Kabel, Jenny Lai, and Lan Kato for the opportunity to work as a Laboratory Assistant on your team in 2019, and for letting me use the scanning electron microscope for my research. Dr. Anette von der Handt, thank you for training me on the electron microprobe and its associated software, and taking the time to teach me about the science behind the electron microprobe. Thank you, Dr. Marghaleray Amini, for training me how to use the LA-ICP-MS instrument and helping me to learn the processing software. Dr. Corey Wall, thank you for providing me with suggestions and feedback on the processing of my zircon ablation chemistry and U-Pb dates.

I would like to express my sincerest gratitude to my colleagues at the Centre for Teaching, Learning and Technology at UBC. Thank you to Drs. Joseph Topornycky and Shaya Golparian for your ongoing support, compassion, encouragement, and mentorship during my degree and time on the Graduate Student Development Team. I am thankful for the vast learning, teaching, and leadership opportunities you both provided me with. I am grateful to have learned so much from the both of you and our wonderful team of graduate facilitators. A shout out to my colleague Natalie Westwood for always making time for chai and chats.

I am truly grateful for the assistance, encouragement, and friendship of Mackenzie Parker during my research. I am thankful for your in-depth edits on many of my academic and non-academic documents. Thank you for helping me stay accountable to my thesis goals, for lending me a shoulder to cry on, and for always believing in me.

To my lab mates, thank you for your friendship and support over the years, and for making our lab space a fun place to be. A special thanks to Lindsey Abdale and Mary Macquistan for your assistance during my 2020 field work. Thank you to Catriona Breasley for our coffee chats and for teaching me how to use handy programs such as Inkscape and ArcGIS Pro. Furthermore, thank you to all my friends who I have grown up with that have continued to check in on me during my degree and who have kept my company while researching and writing.

Lastly, to my parents, Troy and Dora, sisters, Priscilla, and Salina, and partner, Justin, I love you all. Thank you all for always believing in me and for providing me with unconditional love and support throughout my life. I dedicate this thesis to you all.

1 Introduction

This thesis focuses on the origin of alkali metasomatism (i.e., fenitization) within and around a nepheline syenite in the southeastern Yukon Territory of Canada. This area of fenitization occurs on Pyrochlore Dome and Corundum, located within the Bandito property claims owned by Endurance Gold Corp. The objectives of this research are to determine:

(1) the source(s) of alkali metasomatic (i.e., fenitizing) fluids and the timing of the associated metasomatic alteration of the sampled fenitized units on Pyrochlore Dome and Corundum Dome within the Bandito property,
(2) the distribution of rare earth element and high field strength element mineralization across the sampled area on the Bandito property, and
(3) the mechanisms responsible for rare earth element and high field strength element mineralization across the sampled area on the Bandito property.

These questions will be addressed through petrogenetic investigation of the intrusive, country rock, and fenitized rock samples by thin section petrography, mineral compositions, zircon trace element composition and dating, whole rock compositions, and radiometric (gamma ray) spectrometry and magnetic susceptibility measurements. Details of each method are described at the start of each respective chapter. A review of relevant literature related to alkaline-silicate intrusions and their associated metasomatic processes and mineralization is presented in this chapter.

The outcomes of this research will contribute to the understanding of the petrogenetic history of southeast Yukon and alkaline-silicate magmatism in the Canadian Cordillera. Furthermore, the outcomes of this research will contribute to the general understanding of using rock and mineral textures, mineral and bulk rock compositions, mineral dating, and radiometric surveys to

(1) recognize characteristics of metasomatic alteration associated with alkaline-silicate intrusions,
(2) trace the source and interpret the factors that cause metasomatic alteration associated with alkaline-silicate intrusions,

(3) interpret the metasomatic processes that control the distribution of critical element mineralization associated with alkaline-silicate intrusions, and
(4) develop guidelines for the exploration of critical element mineralization associated with metasomatically altered alkaline-silicate intrusions.

Review of alkaline-silicate magmatism

An alkaline rock is defined by the presence of alkaline minerals (real or normative) which formed due to high concentrations of alkaline elements (e.g., Na_2O, K_2O, and CaO) with respect to silica (SiO_2) and alumina (Al_2O_3). Alkaline minerals include modal alkali amphiboles, pyroxenes, and feldspathoids (Sørensen 1997; Le Maitre 2002). Alkaline igneous rocks include a diverse spectrum of silicate rocks (i.e., alkaline-silicate rocks), such as granites/rhyolites, syenites/trachytes, foidites, gabbros/basalts, lamprophyres, lamproites, kimberlites, orangeites, and rare alkaline carbonatites called natrocarbonatites (e.g., Le Maitre 2002).

Alkaline igneous rocks have compositions ranging from silica-oversaturated to silica-undersaturated (e.g., Le Maitre 2002; Frost & Frost 2008, 2011). Rocks defined on the basis of alkalis versus silica are divided into either an alkaline or subalkaline series (Iddings 1892; MacDonald 1968; Irvine & Baragar 1971; Le Maitre 2002), where the subalkaline series can be subdivided into a tholeiitic and calc-alkaline series (Peacock 1931; Tilley 1950; Yoder & Tilley 1962; Irvine & Baragar 1971). The alkalis versus silica method of determining alkalinity is most useful for unaltered volcanic silicate rocks (Le Maitre 2002). Rocks defined on the basis of alkalis versus alumina are divided into the peralkalinity series, which is comprised of three categories (Shand 1927): (1) peraluminous [$Al_2O_3 > (CaO + Na_2O + K_2O$], (2) metaluminous [$Al_2O_3 < (CaO + Na_2O + K_2O)$ but $Al_2O_3 > (Na_2O + K_2O)$], and (3) peralkaline [$Al_2O_3 < (Na_2O + K_2O)$]. The peralkaline index, $(Na_2O + K_2O) / Al_2O_3$, can also be used to define a rock as peralkaline if the ratio is > 1 (Ussing 1912; Le Maitre 2002).

Although the terms “peralkaline index” and “agpaitic index” have been used interchangeably throughout the literature (Ussing 1912), they are not synonymous (Sørensen 1997; Le Maitre 2002). According to Sørensen (1997) and Le Maitre (2002), the term agpaitic specifically

describes a variety of silica-undersaturated peralkaline syenitic rocks (i.e., nepheline syenites and phonolites) that contain high concentrations of rare earth elements (REEs), Li, Be, Nb, Ta, volatiles such as Cl and F, and complex Zr and Ti minerals such as eudialyte, apatite, and rinkite. This definition was challenged by Marks et al. (2011) to include silica-oversaturated peralkaline rocks (i.e., peralkaline granitic compositions) with comparable mineralogical parameters.

A classification system for the agpaitic nature of nepheline syenite rocks was suggested by Khomyakov (1995) based on a rocks typomorphic mineralogical assemblage which is known as the alkalinity modulus (K_{alk}), where $K_{alk} = [x / (x + y + p)] * 100$, and x, y, and p are coefficients in the general mineral formula $A_xM_ySi_pO_q$. The alkalinity modulus categorizes syenites into hyperagpaitic (Kalk = > 40 %), highly agpaitic (K_{alk} = 35–40 %), medium agpaitic (K_{alk} = 25–35 %), low agpaitic (K_{alk} = 15–25 %), and miaskitic (K_{alk} = << 15 %). Although the classification scheme of Khomyakov (1995) is commonly used in the literature, a recent review on agpaitic rocks by Marks & Markl (2017) suggested that its use should be discontinued because, in practice, frequent misuse of the terms causes confusion. Instead, they called for redefinition of the terms agpaitic and miaskitic, suggesting descriptive textural and mineralogical criteria to characterize these rocks, rather than their whole-rock compositions. Marks & Markl (2017) emphasized that, with this new classification, only primary magmatic mineral assemblages should be considered when determining the agpaitic or miaskitic affinity of a rock. A comparison of the new classification of Marks & Markl (2017) to that of Khomyakov (1995) is shown in Table 1.1.

Table 1.1. Examples of minerals in the new classification system for alkaline rocks proposed by Marks & Markl (2017) compared to the nomenclature scheme for nepheline syenites from Khomyakov (1995) after Marks & Markl (2017).

Marks & Markl (2017)		**Khomyakov (1995)**	
Modifier	Diagnostic minerals, excluding post-magmatic and secondary minerals	Group	Diagnostic minerals
Miaskitic	zircon/baddeleyite, perovskite/titanite	Miaskitic	allanite, zircon, ilmenite, hastingsite
		Medium agpaitic	apatite, titanite, nosean, arfvedsonite
Transitional agpaitic	ilmenite, perovskite/titanite, aenigmatite, astrophyllite, baddeleyite/zircon, eudialyte, dalyite, wadeite, elpidite, catapleite	Low agpaitic	eudialyte, låvenite, titanite, zircon, apatite, katophorite
Agpaitic	minerals of the eudialyte, rinkite, and wöhlerite groups and aenigmatite, astrophyllite, dalyite, elpidite, hilairite, lamprophyllite, lorenzite, lovozerite, parakeldyshite, vlasovite, wadeite	Highly agpaitic	eudialyte, lamprophyllite, aenigmatite, astrophyllite, Li-arfvedsonite, nepheline, analcime, sodalite, villiaumite
Hyperagpaitic	steenstrupine-(Ce)/voronkovite, naujakasite, lovozerite/zirsinalite, lomonosovite, natrophosphate, vitusite, natrosilite, ussingite	Hyperagpaitic	zirsinalite, vuonnemite, vitusite, steenstrupine, chkalovite, Li-arfvedsonite, ussingite, natrosilite, villiaumite

Alkaline rocks, especially those with a peralkaline affinity, are commonly rich in halogens, large ion lithophile elements (LILEs), rare earth elements (REEs), and high field strength elements (HFSEs) (e.g., Marks et al. 2011; Marks & Markl 2017). Chemical diversity in alkaline rocks leads to a large variety of complex minerals (Sørensen 1997; Marks & Markl 2017). The extreme compositions and mineralogical diversity of alkaline rocks make their associated mineralization economically important, as they are known to host critical elements (i.e., those essential for producing high technology required for the generation of renewable energy) such as REE, Nb, Ta, P, Zr, and Ti (e.g., Chakhmouradian & Zaitsev 2012; Marks & Markl 2017; Beard et al. 2023). A recent review by Beard et al. (2023) presented a geologic model of critical element resources hosted in alkaline-silicate magmatic systems and made recommendations for geophysical and geochemical approaches and environmental precautions to consider when exploring for resources in these systems.

Global timing, tectonic setting, and source

Alkaline magmatism has occurred from the Late Archean, Proterozoic, Phanerozoic to the present day and has become more common through geologic time (Balashov & Glaznev 2006; Marks & Markl 2017; Beard et al. 2023) and has been observed to increase during the formation of supercontinents (Balashov & Glaznev 2006; Woolley & Bailey 2012; Marks & Markl 2017; Beard et al. 2023). With respect to agpaitic rocks, no Archean occurrences are known, and very few Proterozoic occurrences have been observed in comparison to Phanerozoic showings (Marks & Markl 2017). Interestingly, only one agpaitic occurrence is known to occur between the Neoproterozoic and Late Cambrian, where the majority are Phanerozoic in age and younger than the Early Devonian (Marks & Markl 2017). Mineralization in agpaitic rocks follows this trend, where most deposits are Paleozoic in age (Beard et al. 2023).

In general, the geodynamic settings that alkaline rocks occur in include subduction, oceanic and continental intraplate, and continental rift zones (Marks & Markl 2017). Examples of alkaline complexes from around the world are shown in Table 1.2 with their respective Eons and tectonic settings.

Table 1.2. Examples of alkaline complexes with timing and tectonic affinity.

Alkaline complex	Geologic Eon	Tectonic affinity	Reference
Boa Vista Island, Cape Verde	Phanerozoic	Intraplate	Dyhr & Holm (2010)
Trans-Pecos, United States of America		Subduction	Parker et al. (2012)
Khibina and Lovozero, Kola Peninsula, Russia		Continental rift	Kramm & Kogarko (1994)
Ambohimirahavavy Complex, Madagascar		Intraplate	Estrade et al. (2014)
Oldoinyo Lengai, Tanzania		Continental rift	Bell & Simonetti (1996)
Ilímaussaq, Gardar Province, Greenland	Proterozoic	Continental rift	Marks & Markl (2015)
Nechalacho layered suite, Blatchford Lake Igneous Complex, Canada		Intraplate	Möller & Williams-Jones (2016)
Pilanesberg Complex, South Africa		Intraplate	Elburg & Cawthorn (2017)
Skjoldungen alkaline province, Greenland	Archean	Intraplate	Nielsen & Rosing (1990)

Winter (2010) and Woolley & Kjarsgaard (2008) reviewed theories of sources and genesis of alkaline-silicate rocks and carbonatites from around the world. Examples of genesis and transition from miaskitic to agpaitic rocks in alkaline complexes are reviewed in sources such as Marks & Markl (2015) and Andersen et al. (2018). Sørensen (1997) and Marks & Markl (2017) focused on the sources and genesis of agpaitic rocks. Reviews of sources and genesis of A-type granitoids were discussed by Eby (1990) and Frost & Frost (2011). Lee & Wyllie (1998), Mitchell (2005), and Winter (2010) reviewed the three theories of carbonatite genesis, which are (1) partial melt of metasomatized mantle and differentiation of carbonatite magma from parent silicate magma by (2) liquid immiscibility or by (3) fractional crystallization.

As reviewed by Sørensen (1997), Mark et al. (2010), and Marks & Markl (2017), parental alkaline magmas are thought to be produced from low-degree initial melts of metasomatized mantle, because incompatible elements become more enriched in a melt with a lower degree of melting. Parental melts for peralkaline rocks are thought to have alkali basaltic, basanitic, and nephelinitic compositions based on their common association with peralkaline rocks (e.g., Marks & Markl 2017). Magmatic differentiation of parental magmas by crystal fractionation is an important process in the formation of more evolved silica-undersaturated peralkaline compositions (e.g., Marks & Markl 2017). In contrast, the formation of peralkaline silica-saturated to silica-oversaturated compositions in composite complexes is attributed to crustal contamination by assimilation of crustal melts or country rock into the parental magma (e.g., Marks & Markl 2017).

Morphology

Alkaline-silicate rocks can occur as plutonic and volcanic types and can form large intrusive complexes that commonly include both miaskitic and agpaitic units (e.g., Andersen et al. 2017; Marks & Markl 2017). In such complexes, agpaitic units are typically younger than miaskitic units, and there is great variability in the field relations between these units (Marks & Markl 2017). Alkaline-silicate complexes are commonly composed of distinct ring-shaped intrusions (Marks & Markl 2017), such as the Ting Creek intrusion, Yukon, Canada, (Harrison 1982); the Khibina Complex, Russia (Kramm & Kogarko 1994); and the Pilanesberg Complex, South

Africa (Andersen et al. 2017). Within alkaline-silicate complexes, agpaitic rocks can form a variety of magmatic structures at shallow depths, such as sills, laccoliths, domes, and dikes, and a common feature in agpaitic rocks is magmatic layering (Figure 1.1; Marks & Markl 2017).

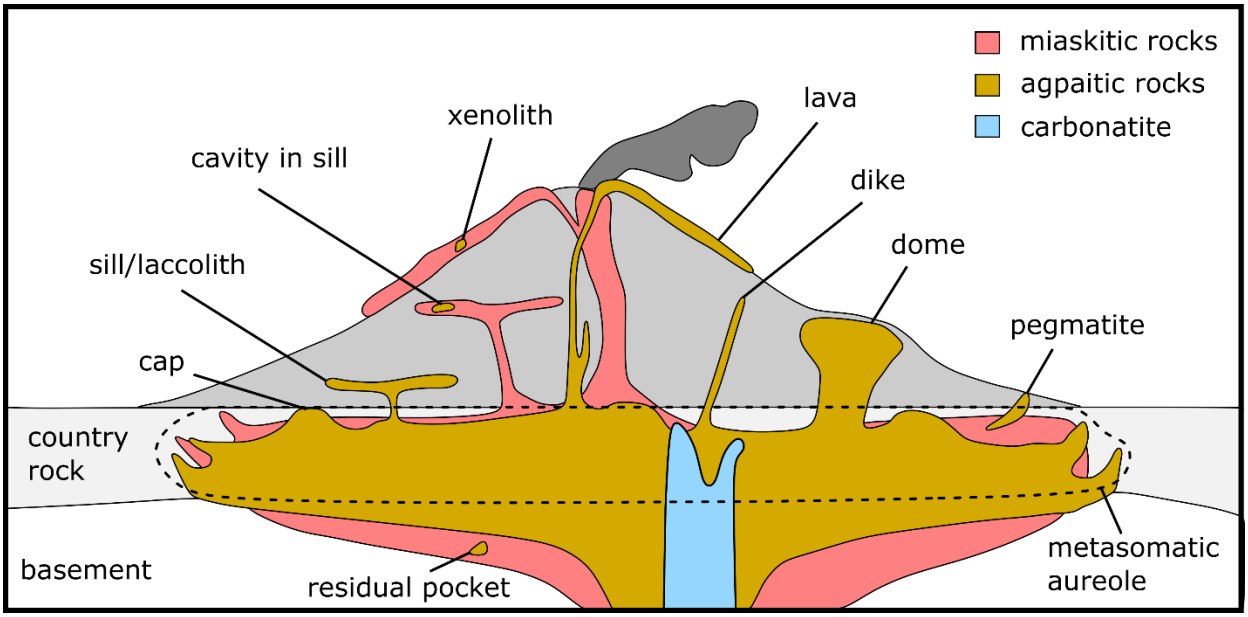

Figure 1.1. Schematic cross-section of the field characteristics of alkaline-silicate rocks adapted from Marks & Markl (2017).

Alkaline-silicate rocks are commonly spatially and genetically associated with carbonatites, which are igneous rocks composed of over 50 modal % carbonate minerals (e.g., Woolley & Kempe 1989; Woolley & Kjarsgaard 2008). Of the 527 carbonatite occurrences known, 76% are associated with alkaline-silicate rocks, such lamprophyres, kimberlites; and ijolites, urtites, melilitolites, foid syenites, alkali gabbro, and ultramafic rocks, and their extrusive equivalents (Woolley & Kjarsgaard 2008). In general, carbonatites tend to form relatively minor portions of alkaline-silicate complexes and postdate the intrusions (Woolley & Kjarsgaard 2008; Marks & Markl 2017), such as those throughout the Gardar province in Greenland (Upton et al. 2003) and throughout India (Krishnamurthy 2019).

Metasomatism

Alteration aureoles in the surrounding host rock are characteristic of alkaline-silicate and carbonatite complexes. The alteration process impacting the host rock is termed fenitization, and the altered host is termed fenite (Brögger 1921; von Eckermann 1948; Heinrich 1966). Fenitizing fluids are alkali-rich and originate from crystallizing alkaline-silicate or carbonatite magmas and can be on the scale of centimeters to several kilometers from the intrusion (e.g., Morogan 1994; Le Bas 2008; Elliott et al. 2018). A conceptual model of fenitization associated with an alkaline-silicate complex in cross-section is presented in Elliott et al. (2018).

Fenitization: An overview

Metasomatism is a metamorphic process in which hot aqueous fluids infiltrate and alter the chemical composition of a rock (which remains in a solid state) via the addition and/or subtraction of ions and molecules from the rock (Zharikov et al. 2007). Metasomatic rocks generally have granoblastic or granofelsic structures (e.g., crystals are equigranular and randomly oriented), however they can exhibit variable grain sizes (e.g., fine to course), and they may show banding (Zharikov et al. 2007). As reviewed by Zharikov et al. (2007), metasomatism:

(1) involves chemical reactions more complex than those involved in isochemical metamorphism (i.e., hydration/dehydration or carbonation/decarbonation reactions);
(2) involves the pseudomorphic replacement of one mineral by another (or by a mixture of minerals) and thus the maintenance of constant volume;
(3) displays mineral zonation around the conduit through which metasomatic fluids flow, where the number of mineral phases decreases towards the conduit; and
(4) forms a regular set of zones of alteration characterizing metasomatic facies (i.e., a metasomatic column).

Metasomatic processes that can alter a rock are diffusional or infiltrational, where varieties of these two types of metasomatism are recognized to occur in and around different zones of a magmatic source (Zharikov et al. 2007). Types of metasomatic processes summarized by Zharikov et al. (2007) are listed in Table 1.3. As reviewed by Zharikov et al. (2007), there are

two metasomatic stages associated with magmatism: the magmatic stage, where fluids radiating from a magma alter the host rock, and the post-magmatic stage, a retrogressive process where fluids radiating from the crystallizing magma (or other heated exogenic sources) alter the magmatic body and/or host rock. As metasomatic fluids travel and exchange chemical components in a rock, the fluids become buffered with respect to the rock (Zharikov et al. 2007). The degree of metasomatic alteration that a rock undergoes depends on the fluid:rock ratio (Zharikov et al. 2007); the greater the ratio of fluid-rock interaction, the more metasomatically altered the rock will be.

Table 1.3. Metasomatic processes described by Zharikov et al. (2007).

Type of metasomatism	Description
Diffusional	Takes place by the diffusion of a solute (rock) through a stagnant solution (fluid). Diffusion is driven by chemical activity gradients in the rock and solution. Typically forms thinly zoned bodies (rims) along cracks, veins, and contact surfaces. Compositions of minerals may vary gradually across each metasomatic zone effected by diffusion.
Infiltrational	Takes place by the transfer of material in solution, infiltrating through the host rock. Infiltration is driven by pressure and concentration gradients between infiltrating and stagnant solutions. Generally, occupy much greater volumes than diffusional metasomatism. The composition of minerals is constant across each of the metasomatic zones effected by infiltration.
Autometasomatism	Forms at the top of cooling magmatic bodies during the early post-magmatic stage. For example, albitization of granitic pluton.
Boundary	Occurs at the contact between two rock types.
Contact (endocontact and exocontact)	Occurs at or near the contact between a magmatic body and another rock. This may occur at various stages in the magmatic evolution. Endocontact zones develop by replacement of the magmatic rocks and exocontact zones are formed by the replacement of the host rocks.
Bimetasomatism	A variety of boundary metasomatism. Alteration of two rock types in contact due to two-way diffusion of the components across the contact.
Near-vein	A variety of diffusional metasomatism. Symmetrical metasomatic zonation forms on either side of an infiltrational metasomatic vein (or a vein in-filling).

Understanding metasomatic processes and mineralogy has important implications for the exploration of critical element resources (e.g., Cu, REE, Zr, and Nb). For instance, metasomatic aureoles that form around magmatic ore deposits (i.e., orthomagmatic deposits) can be used as a vector towards critical element mineralization (e.g., Highland Valley Cu porphyry deposits, British Columbia, Canada; Byrne et al. 2020). Metasomatic fluids can also alter primary critical

element mineralogy and remobilize critical elements in magmatic ore deposits (e.g., Aley hosted Nb deposit, British Columbia, Canada; Chakhmouradian et al. 2015; Nechalacho Layered Suite REE-Zr-Nb deposit, Northwest Territories, Canada; Möller & Williams-Jones 2016; rinkite-(Ce) bearing nepheline syenite pegmatite, Saima alkaline complex, northeastern China; Wu et al. 2019). Sokół et al. (2022) evaluated a fenite associated with a syenitic magma at Illerfissalik, Greenland, and showed that metasomatic fluids can transport high quantities of REE-HFSE away from the source intrusion and deposit them into the adjacent country rock.

Zharikov et al. (2007) outlined 11 metasomatic families, each of which is characterized by specific temperature and pH conditions. This thesis focuses on the fenite family, a high-temperature and corrosive variety of metasomatic alteration that is associated with syenitic and carbonatite intrusions. This thesis will assess the source and age of a poorly exposed fenite aureole that is adjacent to a Neoproterozoic nepheline syenite intrusion in SE Yukon, Canada (Pigage & Mortensen 2004; Swanton 2011; 2012).

Definition of a fenite

The term fenite was first used by Brögger (1921) to describe alkali metasomatism in the country rock intruded by the igneous rocks of the Fen Complex in Norway. Subsequently, alkali metasomatism related to igneous intrusions like those at the Fen Complex, such as carbonatites and peralkaline alkaline-silicate intrusions, has been referred to as fenitization and the fenitized country rock as fenite (von Eckermann 1948). In general, fenite is characterized by a chemical and mineralogical change in the host rock that occurs at high temperatures with fenitizing fluids producing alkali-rich mineralogy such as alkali feldspars, alkali amphiboles, and alkali pyroxenes (e.g., Heinrich 1966, 1985; Zharikov et al. 2007; Le Bas 2008). In the current literature, only a few papers assess fenites associated with carbonatite complexes (e.g., Heinrich 1966; Le Bas 2008; Elliott et al. 2018), and even less assess fenites associated with alkaline-silicate complexes (Sokół et al. 2022; Beard et al. 2023). Sokół et al. (2022) showed that fenites hold essential information about the magmatic evolution of the source intrusion. Beard et al. (2023) summarized the current knowledge of fenites associated with select alkaline-silicate complexes. Le Bas (2008) suggested that this gap in the literature results from (1) difficulty

distinguishing between fenites caused by carbonatites and those caused by alkaline-silicate intrusions and (2) fenites being mistaken for magmatic syenite due to similar looking textures and whole-rock geochemistry.

Classification

Verwoerd (1966) classified three main types of fenite based on the whole-rock ratio of Na to K: sodic, intermediate, and potassic. Fenite compositions change with depth and distance from the source intrusion (e.g., Heinrich 1966; Sindern & Kramm 2000; Le Bas 2008; Elliott et al. 2018). Compositionally, fenites are typically sodic at deeper levels and become more potassic at shallower levels; they transition from higher grade (more intensely fenitized) immediately adjacent to the intrusion to low grade (less intensely fenitized) distally, although this change is not uniform because changes in the host rock composition, fluid composition, and structure control the distribution of fenitization (e.g., Le Bas 2008; Elliott et al. 2018; Anenburg et al. 2020).

As reviewed by Heinrich (1985) and more recently by Le Bas (2008), there are a variety of fenite compositions, and a fenite may have the composition of rocks formed by other geologic processes (e.g., albitite, orthoclasite, and syenite). The naming of such rock types is associated with the environment of formation (i.e., syenite implies a magmatic origin), thus naming a fenite based on its composition is likely to cause confusion in the literature regarding the origin of the rock type. Instead of naming fenites based on their compositions, the IUGS nomenclature classification scheme recommends that fenites be named using structural and mineralogical modifiers, e.g., fluorite-veined aegirine-albite fenite (Zharikov et al. 2007).

Structures that formed in a rock preceding fenitization may be preserved as relict structures (i.e., bedding, metamorphic foliation, fracturing, and brecciation) in the fenitized host rock (e.g., Heinrich 1966; Zharikov et al. 2007). Relict structures in a fenite may become obscured by or confused with similar structures associated with fenitization (i.e., fracturing, brecciation, compositional banding; Heinrich 1966; Zharikov et al. 2007; Elliott et al. 2018). Brecciation is common around potassic fenites at shallower levels and uncommon with sodic fenites (Le Bas 2008; Elliott et al. 2018).

Some workers have suggested that a fenite can be formed by rheomorphism although this has been disputed (summarized by Elliott et al. 2018). Rheomorphism is the process of diffusion of materials with partial or complete melting of a rock by volatiles exsolved from a magma (e.g., Le Bas 2008; Elliott et al. 2018). Brögger (1921) did not ascribe rheomorphism to the fenitizing process. However, Le Bas (2008) suggested the use of the term rheomorphism and extending the definition of fenitization to include rheomorphic rocks. As reviewed by Elliott et al. (2018), fenites formed by rheomorphism are suggested to be mobilized as a crystal mush which may occur as dikes, sills, or plugs.

Mineralogy

Mineral assemblages in fenites are highly variable and depend on the following factors: temperature, pressure, protolith mineralogy, structure and permeability, and fluid composition (e.g., Heinrich 1966, Le Bas 2008, Elliott et al. 2018; Anenburg et al. 2020). As summarized by Elliott et al. (2018), potassic fenites are most commonly dominated by K-rich feldspars, however, potassic fenites may be dominated by phlogopite (i.e., glimmerite) if the country rock is rich in Mg. Sodic fenites are dominated by alkali amphibole, sodic pyroxene, and Na- and K-feldspars. Sodic-potassic fenites have compositions intermediate between the two endmembers. Pyroxene and amphibole chemistries are sensitive to changing grades of fenitization (Elliott et al. 2018), where proximal to the intrusion they are alkali-rich (e.g., Na-rich aegirine, richterite, and magnesio-arfvedsonite), and distally they are lower in alkalis (e.g., diopside to hedenbergite, and arfvedsonite and riebeckite). A common feature of fenite-formed pyroxene and amphibole is non-stoichiometric Si content, where Si is in excess (Elliott et al. 2018). This apparent excess Si could be due to incorporation of light elements in the crystal structure that are undetectable by electron microprobe analyses (Pfaff et al. 2008).

Fluid transport

As reviewed by Elliott et al. (2018), fenitizing fluids flow through permeable planes of weakness (i.e., joints and fractures), grain boundaries, mineral cleavage planes (porous flow), and fractures in a rock. Veining in fenites can be pervasive or localized, where pervasive veins cut the host rock and localized veins follow pre-existing weaknesses. Chemical zoning in the veins results

from changes in the fenitizing fluid. Multiple pulses of fluids utilize the same fractures, which is evidenced by multiple zones of differing minerals that are mirrored on both sides of the fracture. The sources of the Na and K cations in the fenitizing fluids are carbonatite and alkaline-silicate melts (Le Bas 2008). These fluids are rich in halides, primarily F, and have variable H_2O, where variations in the water content may be dependent on the composition of H_2O-bearing minerals in the country rocks (Le Bas 2008).

Fluid reactions and mineralization

As summarized by Elliott et al. (2018), fenite aureoles around alkaline-silicate intrusions (meter-scale) are typically smaller in scale than aureoles around carbonatite intrusions (meter- to kilometer-scale) because water is more soluble in alkaline-silicate melts than in carbonatite melts. Fenitization alters igneous, sedimentary, and metamorphic rock types, however, the extent and intensity of fenitization is largely dependent on the characteristics of the host rock (e.g., Le Bas 2008; Elliott et al. 2018; Anenburg et al. 2020). Host rocks with a large chemical gradient (more reactive) with respect to the fenitizing fluids, such as granite, granitic gneisses, or meta-sediments, will lead to intense fenitization. In contrast, host rocks with a lower chemical gradient (less reactive), such as sandstone and quartzite will typically exhibit much less intense fenitization. When fenitizing fluids react with the host rocks, these rocks trend towards a state of equilibrium with the fluids, where alkali elements in the fluid are typically exchanged for silica in the host rock. The evolution of the fenitizing fluid is marked by mineral compositions and zoning or rimming of minerals, for example, K-feldspar rimmed by albite (e.g., Elliott et al. 2018). If the host rocks are chemically simple (i.e., quartzite) then the compositional change resulting from fenitization can be easily assessed (Heinrich 1985).

Fenitizing fluids in alkaline-silicate and carbonatitic magmatic systems are associated with mineralization, where the extent and type of mineralization can be influenced by fluid composition and temperature, host rock lithology, and depth of intrusion (e.g., Elliott et al. 2018; Anenburg et al. 2020; Sokół et al. 2022; Beard et al. 2023). Metasomatic reactions between fenitizing fluids and primary magmatic minerals in alkaline-silicate and carbonatitic systems mobilize incompatible elements, such as Nb and REE (e.g., Elliott et al. 2018; Anenburg et al.

2020). Both solubility and mobility of such incompatible elements were previously thought to be enhanced by forming complexes with ligands in the metasomatic fluid (i.e., chloride-, fluoride-, sulfate-, phosphate-, and/or carbonate anions) as summarized by Elliott et al. (2018) and Anenburg et al. (2020).

Experiments by Anenburg et al. (2020) showed that such anionic ligands are not sufficient for REE mobilization in metasomatic fluids. Instead, they showed that the addition of alkali cations (i.e., sodium and potassium cations) to anionic ligands in a fluid is essential to increase solubility and mobility of REE which can allow for enhanced concentration of REE and migration of REE. These REE-bearing alkali-rich fluids can migrate through the source intrusion and host rocks and may become trapped in structural conduits within or away from the intrusion. Alternatively, Anenburg et al. (2020) found that the addition of silica to alkali-rich fluids negates the solubility of REE. The addition of silica to the system can be caused by the assimilation of silica-rich host into the source intrusion, or alkali-rich fluids reacting with silica-rich host or mixing with foreign fluids (e.g., meteoric water). Based on their experiments and evidence from the literature, Anenburg et al. (2020) state that the addition of silica to the magmatic system can trigger most of the REE to partition into early formed apatite in the intrusion, with the remaining REE partitioning into other phosphates and carbonates (e.g., bastnäsite and monazite). Alternatively, if alkali-rich fluids migrating from the intrusion interact with a silica-rich host rock, the addition of silica to the fluid can crystallize with the alkali cations to form silicate minerals (e.g., alkali feldspars, arfvedsonite, aegirine, phlogopite) followed by the precipitation of REE-phosphates or carbonates. This means that silica-rich fluids migrating through or from an intrusion or silica-rich host rocks interacting with alkali-rich fluids can inhibit the formation of extensive fenite aureoles around the source intrusion, thus most of the REE-bearing minerals will be found within the host intrusion.

An example of mineralization attributed to intrusion depth and host rock composition are silicate roof zone type deposits (see Beard et al. 2023). In these deposits, an alkaline-silicate intrusion is surrounded by silica-rich host rocks, where the interaction of residual melts and fenitizing fluids between the roof (shallower/top area of the intrusion) and the host rocks (*in situ* or as autoliths) may produce mineralized fenite aureoles, and Li, Be, U, Th, REE, Ti, Nb, Ta, Zr, and Zn

mineralization deposited as sills, and late-stage veins and pegmatites (Beard et al. 2023). Roof zones in alkali-silicate complexes are characteristically dominated by REE-Nb-Ta mineralization (Beard et al. 2023).

The minerals produced from fenitizing fluids and features such as zoning or rimming of minerals can provide us with a record of the compositional evolution of a metasomatic fluid (Elliott et al 2018; Anenburg et al. 2020; Sokół et al. 2022). For example, in experiments done by Anenburg et al. (2020) the fractionation of a Na-rich fluid led to the precipitation of Na-REE-rich apatite. In another experiment by Anenburg et al. (2020), fluid mixing destabilized Na minerals and led to the precipitation of REE phosphates, REE carbonates, and calcic REE fluorocarbonates.

Exploration

Exploration models for mineralization related to fenitization are not as well developed as those for other metasomatic-related mineralizing systems (e.g., Cu porphyry), however, recent literature is quickly advancing our understanding of the characteristics of fenitization, as REE-HFSE mineralization related to alkaline-silicate intrusions is of increasing economic interest (e.g., Elliott et al. 2018; Finch et al. 2019a; 2019b; Anenburg et al. 2020; Sokół et al. 2022; Beard et al. 2023). Elliott et al. (2018) suggested that brecciation around potassic fenites may be used as an exploration tool for Nb and REE mineralization in the source intrusion because brecciation is associated with the exsolution of fluids and volatiles of more evolved igneous phases. Anenburg et al. (2020) found that LREE tend to concentrate in the host intrusion, where HREE (e.g., Dy) are more soluble in alkali-rich fluids than LREE (e.g., La), and more so in potassic fluids compared to sodic fluids, indicating that potassic fenitization is associated with HREE mineralization. Anenburg et al. (2020) suggested that the HREE/LREE value can be used as a potential vector for REE mineralization in the host intrusion and its associated fenite aureole. Finch et al. (2019a) indicated that sulfur isotope techniques have the potential for REE prospecting in roof zones of alkaline-silicate systems because they can fingerprint the source of alkaline-carbonatite systems and are able to identify the evolution and characteristics (i.e., temperature and redox state) of early to late-stage magmatic fluids.

Geophysical methods are commonly used in exploring for critical element resources and have proven to be useful in exploring for HFSE- and REE-mineralization in alkaline-silicate systems (e.g., Shives 2015; Beard et al. 2023). Radiogenic elements such as potassium, uranium, and thorium are commonly associated with REE mineralization in alkaline-silicate systems, thus these elements are used as pathfinders to explore for REE mineralization (e.g., Shives 2015). Beard et al. (2023) suggested that magnetic surveys can be used to locate buried intrusions and gamma-ray surveys can be used to map K, U, and Th enrichment in fenites. Shives (2015) reviewed several examples in Canada where gamma-ray surveys have been used to map variable enrichments in K, U, and Th across rare metal deposits which proved to be useful in mapping geologic units (e.g., fenite, carbonatite, host rock, etc.) and indicating possible zones of critical element mineralization. Finch et al. (2019b) discussed that that careful petrological and mineralogical approaches should be conducted before interpreting airborne survey data for the exploration of critical elements in alkaline-silicate systems, as radiogenic elements are easily mobilized by hydrothermal fluids in contrast to REE and HFSE. A review of alkaline-silicate magmatic systems by Beard et al. (2023) presented a geologic model and recommendations for geophysical and geochemical approaches for exploring mineral resources hosted in these systems.

2 Geologic Background

Regional geology

The Canadian Cordillera is divided into five NW-SE trending belts, each characterized by their own combination of physiographic units, rock associations, metamorphic grade, and structural style (e.g., Monger & Price 2002). From west to east, they are the Insular Belt, Coast Plutonic Belt, Intermontane Belt, Omineca Belt, and Foreland Belt. In addition, there are two large strike-slip fault systems that extend through Yukon and British Columbia and are marked by physiographic features known as the Tintina Fault (or Tintina Trench) and the Rocky Mountain Fault (or Rocky Mountain Trench) (Roddick 1967). The Tintina Fault is the northern extension of the Rocky Mountain Fault; they are separated by an ancient structural transfer zone known as the Liard Transfer Fault (Cecile et al. 1997). Three distinct episodes of alkaline and associated carbonatite magmatic activity that are restricted to the Foreland and Omineca belts were summarized by Millonig et al. (2012) as occurring in the Neoproterozoic (~800–700 Ma), Late Cambrian (~500 Ma), and Upper Devonian to Lower Carboniferous (~360–340 Ma). These magmatic units are hosted in miogeoclinal strata that make up the Foreland and Omineca belts (e.g., Pell 1994; Cecile et al. 1997).

In British Columbia, carbonatite and associated alkaline rocks, such as nepheline/sodalite gneisses, and lamprophyres, and kimberlites, are known to occur along the eastern flank of the Cordillera within a broad zone that encompasses and is parallel to the Rocky Mountain Fault (e.g., Pell 1994). This zone extends to the east and west of the fault in the Omineca and Foreland belts, and hosts 17 known alkaline complexes, of which 14 have associated carbonatites (Pell 1994; Woolley & Kjarsgaard 2008). The zone of alkaline complexes along the fault has been previously subdivided into three NW-SE trending belts throughout British Columbia based on rock distribution and characteristics by Pell (1987), as summarized in Table 2.1.

Table 2.1. Summary of the NW-SE trending carbonatite and alkaline complex belts described by Pell (1987).

Belt	Location	Characteristics
Eastern belt	East of the Rocky Mountain Fault and within the Foreland Belt.	Alkaline and carbonatite intrusions have extensive fenitization halos, and intrusions appear as oval to ellipsoidal structures, or as sills, dikes and plugs that parallel the belt, all of which are hosted in Cambrian to Devonian metasedimentary miogeoclinal strata.
Central belt	Immediately west of the Rocky Mountain Fault within the Omineca Belt.	Amphibolite facies alkaline and carbonatite associated intrusions have minor amounts of fenitization, occur as foliated, sill-like bodies and are hosted in Late Proterozoic to Early Cambrian metasedimentary strata.
Western belt	Western area of the Omineca Belt associated with core gneiss complexes.	Amphibolite facies extrusive and intrusive units have extensive fenitization halos, form foliated sill-like bodies and are hosted in an Early Paleozoic to Late Proterozoic cover sequence of gneiss within Paleoproterozoic core complexes.

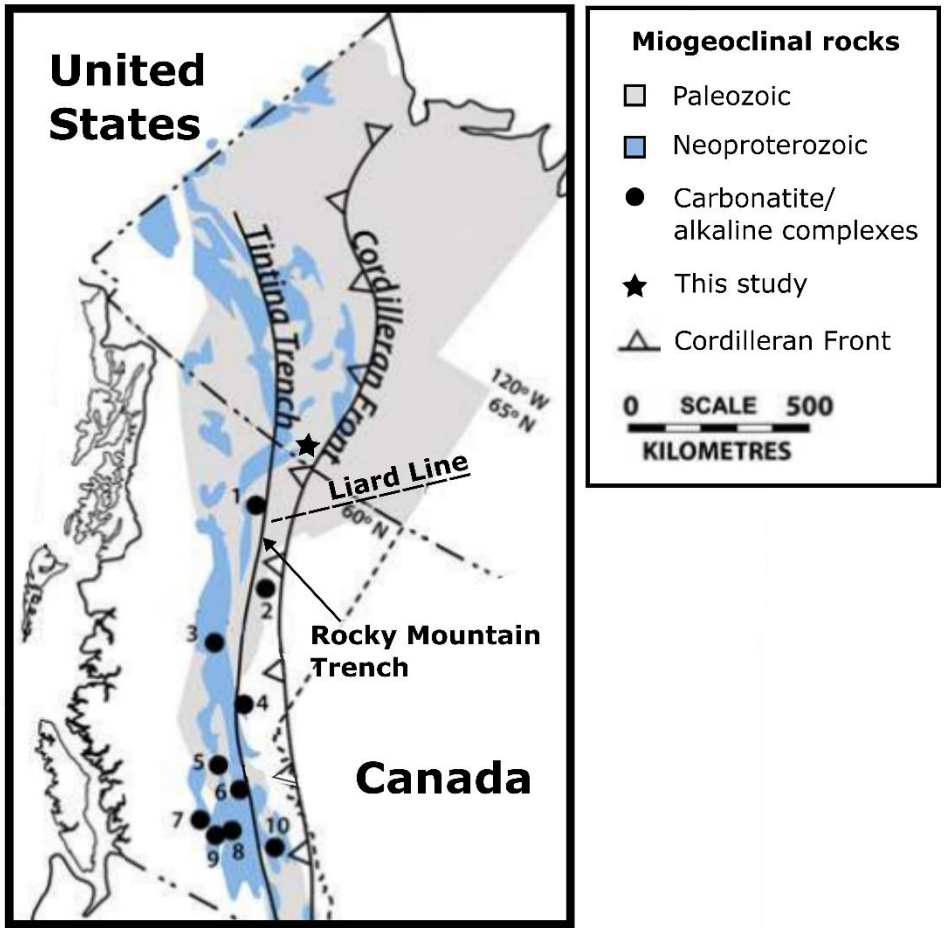

Figure 2.1. Distribution of carbonatite/alkaline complex occurrences in the Canadian Cordillera with respect to Neoproterozoic (pale blue) and Paleozoic (grey) miogeoclinal strata: black star: Pool Creek area (this study); black circles: 1 Kechika area, 2 Aley, 3 Lonnie and Vergil, 4 Wicheeda Lake, 5 Blue River area, 6 Trident Mountain, 7 Perry River and Mount Grace, 8 Mount Copeland, 9 Three Valley Gap, and 10 Ice River Complex; the approximate location of the Liard Line transfer fault (dashed line) is shown (Cecile et al. 1997); adapted from Millonig et al. (2012) and Chudy (2013).

The Canadian Cordilleran Miogeocline represents the ancient passive margin of western Laurentia that formed as the result of episodic rifting and extensional events, where rifting began in the Late Proterozoic (Cecile et al. 1997). The Canadian Cordilleran Miogeocline is divided into structural blocks by several northeast-trending crustal faults, the most prominent of which is the Liard Line (Figure 2.1; Cecile et al. 1997). The Liard Line is a dextral, Proterozoic transfer fault that divides the Cordilleran miogeocline through northeastern British Columbia into the Northwest Territories, east of the Pool Creek map area. North of the Liard Line, Paleozoic strata thicken and spread out toward the craton (characteristic of a lower plate margin) and south of the line the Paleozoic strata narrow (characteristic of an upper plate margin) and are confined to the previously mentioned deformation belts east of the Rocky Mountain Fault (Cecile et al. 1997; Lund 2008). In southeastern Yukon, the Macdonald Platform and Selwyn Basin units are deflected to the northeast by approximately 200 km (Pigage 2009), which are paralleled by the Liard Line. Is has been suggested by previous authors that is possible that the Liard Line controlled the northeast deflection of these units (Cecile et al. 1997; Pigage 2009; Hayward 2015) and may be the cause of the alkaline magmatism in the Pool Creek map area (Pigage & Mortensen 2004).

Morrows & Miles (2000) argued in favour of the existence of a near parallel and adjacent structure to the Liard Line in the Pool Creek map area. They described 10 to 20 km of displacement in the Pool Creek map area based on the residual total field magnetic geophysical maps and Bouguer gravity anomaly geophysical maps. They proposed that this displacement was caused by a second crustal dextral transfer fault which they named the Beaver River structure. Morrows & Miles (2000) further suggested that this structure is the northeast continuation of the Beaver Fault, mapped by Douglas (1976). Allen et al. (2001) refuted the suggestion of 10 to 20 km of displacement occurring in the Pool Creek map area after performing detailed mapping in 2000. They mapped the Beaver Fault across the area previously mapped by Douglas (1976) and concluded that a maximum of 2 km of sinistral displacement was possible in the area. Allen et al. (2001) interpreted the sinistral displacement to be an apparent feature caused by a north-plunging, anticline-syncline fold pair. Furthermore, Pigage (2009), in a report on the compilation of bedrock mapping in the southeastern Yukon between 1998 and 2005, completely rejected the idea of the Beaver Fault and the Beaver River structure based on several fold and fault structures

that are continuous across the proposed structure. Pigage (2009) attributed the apparent displacement of structures to be caused by the rapid facies change from the MacDonald carbonate rocks to the Selwyn basin shales and cherts, where the northeastern trend is likely inherited from fault scarps associated with the Liard Line.

In a more recent study, Hayward (2015) modelled and interpreted potential field and topographic data in conjunction with the interpretation of previously published geophysical, geochemical, and geological results. Hayward (2015) implied that the Beaver River structure exists based on the coincidence of the structure with a profound change in magnetic anomalies (due to changes in rock types) and the alignment of the structure with another lineament across the proto-Tintina Fault. Hayward (2015) suggested that the Beaver River structure is a subsidiary structure to the Liard Line that is related to either the lithospheric transfer zone of the Liard Line or a fracture zone. Based on the Bouguer gravity anomaly after reconstructing the displacement of the Tintina Fault, Hayward (2015) suggested that both the Liard Line and Beaver River structure extend westward and once formed continuous structures with east-west tending lineaments across the proto-Tintina Fault. Hayward (2015) suggested that these lithospheric faults are important influences on the development of upper crustal structure, intrusive rocks, rock exposure, and mineralization.

Pool Creek area

East of the Tintina Fault within the Foreland Belt in southeastern Yukon lies an area of alkaline magmatism (Figure 2.2; Harrison 1982; Stevens et al. 1982; Allen et al. 2001; Pigage & Mortensen 2004). These magmatic units intrude through Neoproterozoic to Triassic miogeoclinal continental margin platform and continental slope and basin terranes (e.g., Abbott et al. 1986; Cecile et al. 1997; Pigage 2008).

The history of bedrock geology and geophysical mapping conducted in southeastern Yukon by the Geological Survey of Canada and Yukon Geological Survey is summarized in Table 2.2. The bedrock geology of the Pool Creek map area was most recently summarized by Pigage (2009). The area is characterized by Proterozoic to Paleocene sedimentary strata which range from 5000 to 15,000 m in thickness. Structural features in the map area are related to pre-late Cambrian and

post-Trassic/pre-Paleocene contractional deformation events (Pigage 2009). The earlier deformation event is restricted to Proterozoic strata (Pigage 2009; MacNaughton et al. 2017). North to northeast trending reverse faults and open to tight folding are characteristic of the later deformation event (Pigage 2009).

Table 2.2. History of mapping of the Pool Creek area.

Map Area	**Type**	**Map scale/ column thickness**	**Reference**
Southeastern Yukon	Bedrock geology	1:253,440	Douglas & Norris (1959); Douglas (1976)
Pool Creek map sheet (NTS 95C/5)	Bedrock geology	1:100,000	Fallas et al. (2004)
Pool Creek map sheet (NTS 95C/5)	Bedrock geology	1:50,000	Pigage & Allen (2001); Pigage (2008; 2009)
La Biche River map area (NTS 95-C)	Bedrock geology	1:250,000	Fallas et al. (2014)
Northwest corner of the Pool Creek map sheet (NTS 95C/5)	Stratigraphic column	> 2900 m	Allen et al. (2001)
West area of the Pool Creek map sheet (NTS 95C/5)	Stratigraphic column	> 500 m	MacNaughton (2017) and MacNaughton et al. (2017)
Pool Creek map sheet (NTS 95C/5)	Gravity anomaly	1:1,000,000	Geological Survey of Canada (1993)
Pool Creek map sheet (NTS 95C/5)	Aeromagnetic anomaly	1:100,000	Stone (1999a; 1999b; 1999c; 1999d)
Pool Creek map sheet (NTS 95C/5)	Aeromagnetic anomaly	1:250,000	Aurora Geosciences Ltd. & Bruce (2017a; 2017b; 2017c; 2017d;)

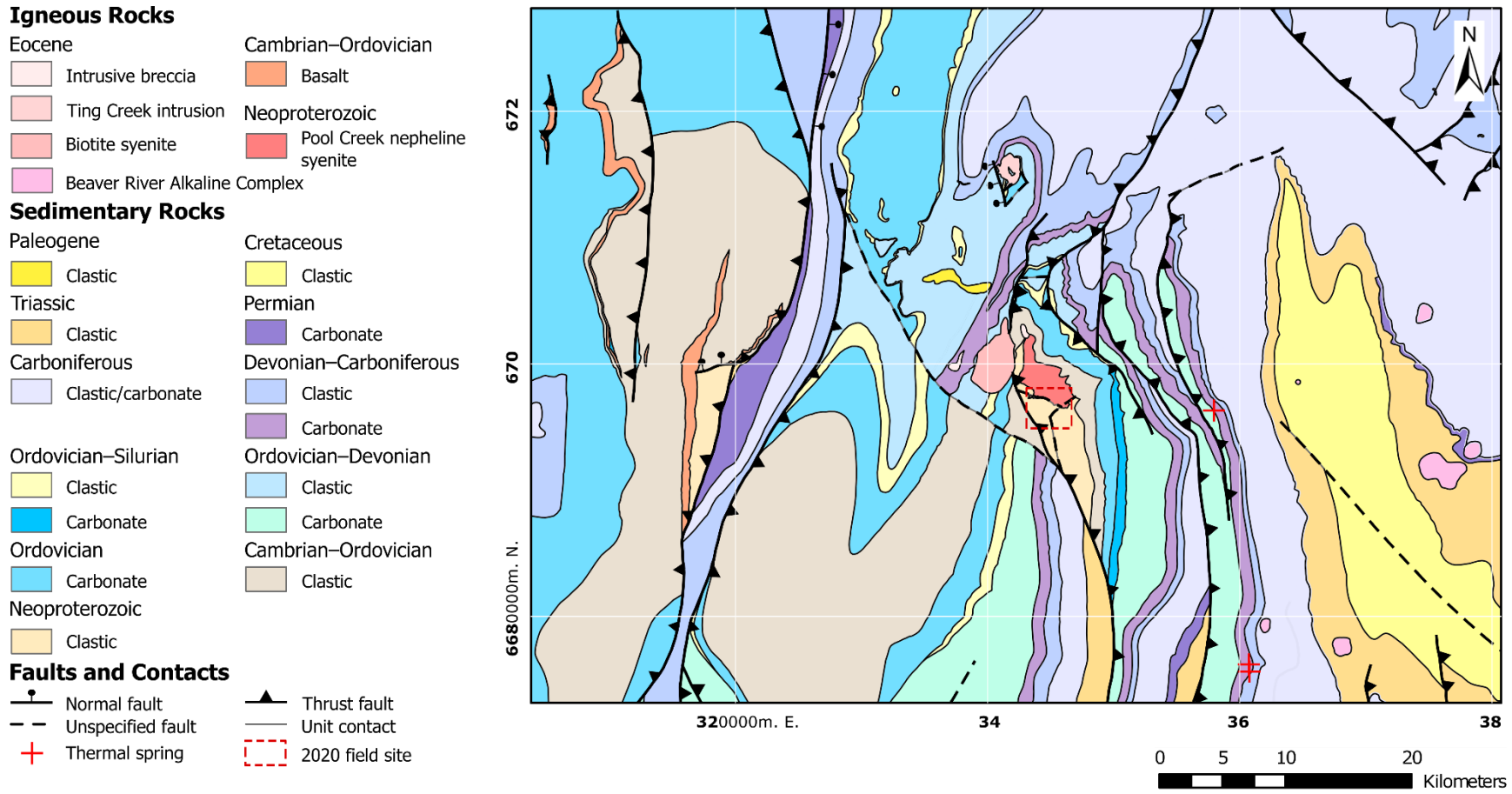

Figure 2.2. Location of alkaline magmatism in southeastern Yukon. Map data compiled from Swanton (2012), Fallas et al. (2014), and Yukon Geological Survey (2022). Thermal spring locations from Grasby et al. (2016). UTM Gridlines are NAD 1983 Zone 10N.

Multiple rifting events are recognized in the Pool Creek map area. Proterozoic rifting is evidenced by the presence of an alkaline Neoproterozoic syenite (Pool Creek nepheline syenite—Pigage & Mortensen 2004) and subrounded subalkaline basalt clasts in an unnamed Neoproterozoic volcaniclastic argillite unit (Pigage 2009; MacNaughton et al. 2017). Early Paleozoic rifting associated with reactivation of the Liard Line is evidenced by normal faulting and the presence of Ordovician alkaline basalts in rift-related strata (Goodfellow et al. 1995; Pigage 2009). Eocene alkaline magmatism in the area is prevalent, but of unknown provenance. An Eocene intrusion superimposed on a Neoproterozoic intrusion may be due to reactivation of the Liard Line through periodic extensional events (Pigage & Mortensen 2004). Small Eocene trachyte plugs known collectively as the Beaver River Alkaline Complex occur less than 55 km southeast and east of the superimposed intrusions (Douglas 1976; Harrison 1982; Fallas et al. 2004; 2014).

Three spatially close alkaline intrusions ranging from Neoproterozoic to Eocene in age [the Pool Creek nepheline syenite (Neoproterozoic), an unnamed biotite syenite (Eocene), and the Ting Creek intrusion (Eocene)] occur in the Pool Creek area (e.g., Stevens et al. 1982; Harrison 1982; Pigage & Mortensen 2004). The biotite syenite and Ting Creek intrusions are emplaced in Silurian-Devonian carbonates of the Macdonald Platform and siliciclastics of the Selwyn Basin (e.g., Cecile et al. 1997). The Pool Creek nepheline syenite is emplaced in a Neoproterozoic siliciclastic inlier unit from the lower Windermere Supergroup (Pigage 2009; MacNaughton 2017). The Pool Creek and biotite syenite intrusions occur less than 1 km apart and lie within claims called the Bandito property.

At the time of writing the Bandito property (outlined in Figure 2.3) consisted of a 3,700-hectare claim block made up of 179 quartz claims held by Endurance Gold Cooperation (Table 2.3). The property is located in southeastern Yukon (60.37° N, -125.80° W) on NTS map sheet 095C/5, approximately 43 km north of the Yukon-British Columbia border. This property lies within the traditional territory of the Kaska Nation. The nearest town is Fort Liard, 120 km southeast of the property. The Bandito property is only accessible by helicopter from Watson Lake (155 km southwest of the property) or the Smith River Airstrip (63 km southwest of the property). The physiography of the area is dominated by domes and valleys, and the Bandito property spans

Corundum Dome and Pyrochlore Dome. Alpine meadows are characteristic of the top of the domes, which descend into dense forest. The property is relatively snow-free from mid-June to mid-September.

Exploration of the Bandito property began in the mid-1970s after reports of radiometric anomalies from an airborne survey conducted by Eldorado Nuclear Ltd. Based on the anomalies reported, parts of the property were prospected and explored for U, Th, Nb, REE, Cu, and Ni from 1977 to 2014 (Swanton 2011; 2012; Endurance Gold Cooperation 2018a; 2018b; 2023). Exploration done during this timeframe included airborne radiometric geophysical surveys (most recently in 2006), grid-based ground scintillometer surveys, mapping of alteration zones, soil sampling, silt sampling, rock sampling (chip, pit, and grab), and diamond drilling. In-depth summaries of the exploration history of the property can be found in Swanton (2011; 2012). Endurance Gold Cooperation (2018a; 2018b; 2023) reported highlights of the elemental prospects and anomalies of the Bandito property.

Table 2.3. Bandito property quartz claims and their reported commodities. Data collected from Yukon Geological Survey (2023).

Grant Number	Claim Name	Recording Date	Expiry Date	Commodity
YA90928	MGM 8	April 18th, 1986	Dec 30th, 2024	REE, Y, Nb, U, Th
YC24964 – YC24971	AMIGO 1 – AMIGO 8	July 2nd, 2004	Dec 30th, 2024	Ni, Cu, REE, Y, Nb, U, Th, Be, Li
YC29447 – YC29518	BANDITO 1 – BANDITO 72	Jan 12th, 2006	Dec 30th, 2023	REE, Y, Nb, U, Th, Zr
YD14875 – YD14874	BANDITO 81 – BANDITO 136	Oct 20th, 2010	Dec 30th, 2023	REE, Y, Nb, U, Th
YE14595 – YE15034	BANDITO 205 – BANDITO 244	March 2nd, 2011	Dec 30th, 2024	REE, Y, Nb, U, Th

Diverse geology lies within the Bandito property (Figure 2.3). The local geology has experienced low-grade regional metamorphism (e.g., Allen et al. 2001). Sedimentary country rocks include Ordovician dolostone, Cambrian to Ordovician sandstone, and Proterozoic (late Cryogenian) clastic and volcaniclastic argillite miogeoclinal units (e.g., Pigage 2009; MacNaughton 2017; MacNaughton et al. 2017). The clastic and argillite units have been hornfelsed by the Pool Creek nepheline syenite (Pigage & Allen 2001; Pigage & Mortensen 2004; Pigage 2009). The clastic

unit predominantly composed of a laminated, non-calcareous, argillaceous quartz siltstone that is interbedded with sandstone, calc-silicate rock, and minor conglomerate lithofacies (e.g., Pigage 2009). The argillite unit is dominantly composed of a greenish laminated (i.e., thinly bedded) to massive argillite (i.e., siltstone and shale) that is interbedded with sandstone, and basalt-clast breccia lithofacies (e.g., Pigage 2009; MacNaughton et al. 2017). Igneous rocks include a Proterozoic basalt-clast conglomerate, various dikes, Eocene(?) rhyolitic breccia, the Neoproterozoic Pool Creek nepheline syenite intrusion, and part of the Eocene biotite syenite intrusion (e.g., Pigage & Mortensen 2004; Pigage 2009; Swanton 2012; MacNaughton 2017; Endurance Gold Corporation 2018a; 2018b; 2023). Dikes associated with the Pool Creek nepheline syenite cut through both the syenite and the country rock (Pigage & Mortensen 2004; Pigage 2009; Swanton 2012). The Proterozoic country rocks that host the Pool Creek nepheline syenite have experienced a variety of pervasive and localized metamorphic alterations, including metasomatism (i.e., quartz-sericite-pyrite and fenitization) and contact metamorphism (Allen et al. 2001; Pigage & Mortensen 2004; Pigage 2009; Swanton 2011; 2012). Detailed mapping of the alteration on the Bandito property is reported in Swanton (2012).

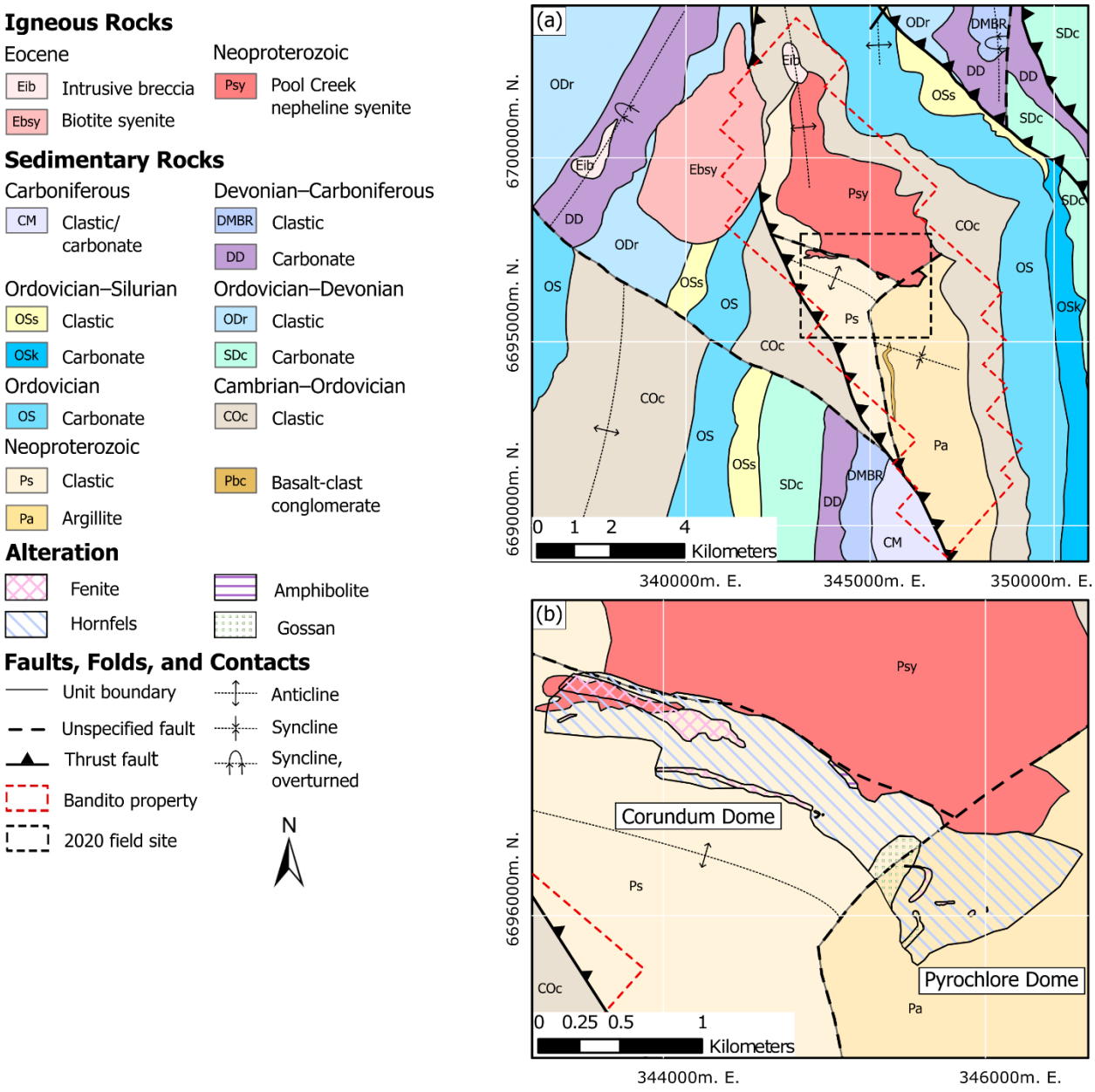

Figure 2.3. Geology of the northwestern section of the Pool Creek map area. (a) Geology of the Bandito property. (b) The 2020 field site area and previously mapped alteration on the Bandito property by Swanton (2012). The North Fenite Zone is hosted in unit Ps and South Fenite Zone in unit Pa. Map data from Pigage & Mortensen (2004), Swanton (2012), Fallas et al. (2014), MacNaughton (2017), and Yukon Geological Survey (2022). UTM Gridlines are NAD 1983 Zone 10N.

Neoproterozoic Pool Creek nepheline syenite

The Pool Creek nepheline syenite was informally named by Harrison (1982); it has also been referred to as the "Red Syenite" by Endurance Gold Corporation (2018a; 2018b; 2023). In general, the Pool Creek nepheline syenite is coarse to medium grained, equigranular, unfoliated, non-magnetic nepheline syenite intrusion whose main constituent is pink K-feldspar (Allen et al. 2001; Pigage & Mortensen 2004; Swanton 2011; 2012). The intrusion has been mildly to moderately altered (Pigage & Mortensen 2004; Swanton 2012). Pervasive sericite, hematite, and fluorite alteration occurs throughout the intrusion (Swanton 2012). Outcrops of the syenite weather to rounded, pink coloured knobs (Pigage & Mortensen 2004). Local linear, white-cream coloured clay-altered zones exist throughout the intrusion and occur up to 10 meters wide and extend for tens of meters (Allen et al. 2001; Pigage & Mortensen 2004). The Pool Creek nepheline syenite and its Proterozoic host rocks are cut by a few types of dikes (Pigage & Mortensen 2004; Swanton 2012). Contacts between the syenite and its host rocks have been observed (Pigage & Mortensen 2004; Pigage 2008; Swanton 2012). Pigage & Mortensen (2004) noted that the contact on the southern edge of the intrusion is obscured by faulting and adjacent strata are altered, and the contact on the eastern margin of the intrusion is unconformable and strata are unaltered. Swanton (2012) does not dispute the observations made by Pigage & Mortensen (2004).

The K-feldspar crystals are pink, euhedral, and randomly oriented and form laths that are typically 0.5 to 1 cm long but can attain 4 cm in length (Pigage & Mortensen 2004; Pigage 2009). Under plane-polarized light the crystals exhibit fine, disseminated, pinkish-opaque dust, perthitic texture, and coarse lamellar twinning (Pigage & Mortensen 2004; Pigage 2009). Modally, K-feldspar makes up approximately 50–60% (Pigage & Mortensen 2004; Pigage 2009) or 70% (Swanton 2012) of the syenite.

A pale green mineral that has been completely pseudomorphed by aggregates of sericite is thought to have been primary nepheline based on its hexagonal shape and the silica-undersaturated nature of the rock (Pigage & Mortensen 2004; Pigage 2009; Swanton 2012). The mineral is euhedral to subhedral and is 0.2 to 1.5 cm in size (Pigage & Mortensen 2004; Pigage

2009; Swanton 2012). This mineral makes up approximately 20–25% of the mode of the syenite and appears to have co-crystallized with K-feldspar (Pigage & Mortensen 2004; Pigage 2009; Swanton 2012).

Pigage & Mortensen (2004) and Pigage (2009) reported minor minerals in the syenite, including apatite, opaques, plagioclase, and biotite. These minor minerals form interstitial, symplectic aggregates and are suggested by the authors to be replacing an earlier unknown mafic mineral. Swanton (2012) reported that primary mafic minerals, such as sodium amphibole and biotite, are pseudomorphed by hematite, aegirine, and actinolite in the intrusion. Swanton (2012) mentioned that the intrusion lacks magnetite and suggests that if magnetite was present, then it has been replaced by hematite.

A detailed petrographic description of a thin section from one sample of the syenite was done at Vancouver Petrographics Ltd. and is reported in Appendix D of Swanton (2011). The sample (GD65) is described to be a nepheline syenite mainly composed of nepheline (strongly replaced by sericite) and potassium feldspar, with minor albite, acicular aegirine, skeletal magnesio-riebeckite, fluorite(?), relict biotite(?), hematite, ilmenite, and trace amounts of titanite.

Pigage & Mortensen (2004) reported on the geochemistry of six samples. Based on the total alkalis versus silica (TAS) diagram (Le Bas et al. 1986) and the Zr/TiO_2 versus Nb/Y diagram (Winchester & Floyd 1977; Pearce 1996), they classified the rocks as foid monzosyenite to foid syenite. Based on the shand index diagram, they described the rocks as peraluminous (Maniar & Piccoli 1989). There is a compositional change across the intrusion, where CaO increases towards the south and MgO increases towards the north. Based on a multi-element diagram normalized to the primitive mantle (Sun & McDonough 1989), Pigage & Mortensen (2004) noted that the rocks are enriched in incompatible elements, have a moderate negative Ti anomaly, and have minor positive Nd and Zr anomalies. The syenite plots in the within-plate field of the Ta versus Yb tectonic discrimination diagram for granites (Pearce et al. 1984). The geochemistry of nepheline syenite sample DG65 is reported in Appendix C of Swanton (2011).

The Pool Creek nepheline syenite was considered to be similar in age to nearby Eocene igneous activity of similar composition (Douglas 1976; Harrison 1982) until Pigage & Mortensen (2004)

reported Neoproterozoic U-Pb zircon ages for the syenite and its associated dikes that cluster around 640–650 Ma. They reported that the zircons analyzed have unusual U-Th-Pb systematics (low U, high Th).

Dikes

The Pool Creek nepheline syenite and its Proterozoic host rocks are both cut by dikes (Pigage & Mortensen 2004; Pigage 2009; Swanton 2012). Pigage & Mortensen (2004) described two sets of dikes: (1) altered, compositionally banded (mm-scale), purplish-pink coloured, near-vertical mafic dikes (<50 cm); (2) unaltered, banded dikes (m-scale). Based on their geochemistry and age Pigage & Mortensen (2004) associated these dikes with the Pool Creek nepheline syenite.

The mineralogies of the dike sets as reported by Pigage & Mortensen (2004) are as follows: (1) potassium feldspar, plagioclase, sericite pseudomorphs, minor opaques, and chlorite; and (2) plagioclase, potassium feldspar, aegirine and minor opaques, where all minerals in dike set (2) are reported to show no alteration.

Based on three samples reported in Pigage & Mortensen (2004), the composition of the dikes in set (1) is metaluminous to peraluminous, foidolite to foid syenite and rich in K_2O and significantly less Na_2O and CaO; SiO_2 ranges from 40% to 57%. Based on two samples, the dikes in set (2) are peraluminous to peralkaline, syenite to foid monzosyenite, and rich in CaO, Na_2O and significantly less K_2O; SiO_2 ranges from 61% to 68%. Based on a multi-element diagram normalized to the primitive mantle, these two sets of dikes are enriched in incompatible elements, have negligible to large negative Ti anomalies, and have minor positive anomalies of Nb and minor to major anomalies of Zr. Like the Pool Creek nepheline syenite, these dikes have a within-plate field signature.

Swanton (2012) discussed three sets of dikes: (1) Weakly magnetic, greenish-grey, carbonate amygdaloidal, pyroxene-phyric, mafic dikes that are nearly vertical and 1 cm to 40 cm in width. These dikes may be the compositionally banded mafic dikes that Pigage & Mortensen (2004) discussed, but it is hard to tell since they make no mention of phenocrysts or vesicles. (2) Dark pink syenite dikes that are NW striking and steeply NE to NNE dipping (which may be similar to

the orientation of the intrusion). These dikes may be the unaltered banded dikes that Pigage & Mortensen (2004) described. (3) A single white, unaltered, m-scale dike that Swanton (2012) interpreted to be from the biotite syenite, based on the description of the syenite from Pigage (2008).

Alteration

Previous work conducted on the altered rocks on the Bandito property has focused on exploration for commodities such as REE, U, Th, and Nd (e.g., Allen et al. 2001; Swanton 2011; 2012; Endurance Gold Corporation 2018a; 2018b; 2023). Swanton (2012) produced a detailed map of alteration on the south side of the Pool Creek nepheline syenite on the Bandito property consisting of hornfels, gossan, skarn, amphibolite, and fenite (Figure 2.3). Hornfels is associated with the Pool Creek nepheline syenite and extends several hundred meters from the syenite (Allen et al. 2001; Pigage & Mortensen 2004; Pigage 2009; Swanton 2012). Pigage (2009) reports a gossanous zone in the clastic unit that shows local orange-brown surface staining. Swanton (2012) describes the gossan zone as a red-orange coloured zone of quartz-sericite-pyrite alteration. The gossan zone is localized a few hundred meters south of the Pool Creek nepheline syenite in the Proterozoic sedimentary units and overprints some of the mapped fenite alteration. Swanton (2012) interpreted that the gossan is associated with later Cu and Ni mineralization (i.e., azurite, malachite, and annabergite) on the property, however, the provenance of the gossan zone is unknown.

Swanton (2012) mapped localized outcrops of fenite in the Proterozoic host rocks that extend up to 500 m away from the Pool Creek nepheline syenite. The fenite outcrops are grouped based on their positioning with respect to the Pool Creek nepheline syenite, generally referred to as the “North Fenite Zone” and “South Fenite Zone” by Swanton (2012). The “North Fenite Zone” is hosted in the Neoproterozoic clastic unit (that has locally been hornfelsed) and the “South Fenite Zone” in the Neoproterozoic argillite unit. The two fenite zones will be referred to as the “North Fenite Zone” and “South Fenite Zone” throughout this thesis. These fenite outcrops are linear in shape and typically parallel the local faults, suggesting a structural control with respect to fenitization (Swanton 2012). Soil sampling across the Bandito property revealed that the fenite is associated with elevated REE and Th concentrations (Swanton 2012). Based on the common

occurrence of fenite with alkaline-silicate intrusions in the literature, Swanton (2012) suggested that the fenite is associated with the Pool Creek nepheline syenite. The fenite and skarn units were interpreted to be non-magnetic based on aeromagnetic survey data from 2006 (Swanton 2012). However, magnetite veins cutting the fenite and "amphibolite" produced by sodium metasomatism are magnetic (Swanton 2012). Although industry reports provide some preliminary data (e.g., Swanton 2011; 2012), there has not been any academic investigation or interpretation of the source, petrogenesis, and timing of fenite or gossan alteration of the area.

Thin-section petrographic analysis of 18 samples from the Bandito property was conducted by Vancouver Petrographics Ltd. And is presented in Appendix D of Swanton (2011). The sample numbers, lithology, and rock constituents (i.e., mineralogy and clasts) are summarized in the Swanton (2011) report and are shown in Table 2.4. Seven of the samples were interpreted by Vancouver Petrographics Ltd. To be metasomatic in origin and are called fenite or albitite. The mineralogy of these seven samples is briefly summarized here. The fenite samples (478706, 478707, R4, GD7) are dominated by potassium feldspar, albite, and alkaline minerals (i.e., nepheline, arfvedsonite, aegirine) that have been partially to fully pseudomorphed by clays and/or hematite. A sample labelled as mafic laminated albitite (GD 69A) is mainly composed of fresh albite with minor sub-parallel laminae of biotite, hematized aegirine(?), and trace monzonite(?) and apatite. The fenite portion of the brecciated fenite and siltstone rock sample (478708) is dominantly composed of albite, with minor hematite, chlorite, cryptocrystalline material, and trace pyrite, tourmaline, and apatite. The silicified fenite sample (478712) is dominated by potassium feldspar, with minor quartz, microcrystalline material, sericite pseudomorphs, limonite, chlorite, and trace amounts of apatite, pyrite, and biotite(?).

Table 2.4. Petrographic descriptions of 18 polished thin sections of rock samples reported in Swanton (2011).

Sample Name	Lithology	Rock constituents
Abc	Altered porphyry	carbonate, chlorite(?), biotite, Fe oxides, pyrite
Pabc	Igneous breccia	plagioclase, quartz/chalcedony, chlorite, carbonate, sericite, Fe oxides
GD69A	Mafic laminae in albitite	albite, biotite, hematized aegirine(?), monazite(?), apatite
478704	Hornfelsed siltstone and Albite-quartz-monazite-zircon pyrite vein	host: clay, quartz, white mica, chlorite vein: albite, quartz, hematite, pyrite, monazite, zircon(?), fluorite

Sample Name	Lithology	Rock constituents
478706	Fenite	K-feldspar, albite, white mica (after nepheline?), cryptocrystalline material, kaolinite, quartz, hematite-limonite, zircon, pyrite
478707	Fenite	K-feldspar, cryptocrystalline material, white mica, albite, hematite-limonite, kaolinite, zircon, pyrite
478708	Brecciated fenite and siltstone	fenite: albite, chlorite, cryptocrystalline material, hematite, hematite (after pyrite), pyrite, tourmaline, apatite siltstone: quartz, unidentified fine-grained material
478711	Silicified brecciated mudstone(?)	quartz, hematite+limonite, pyrite, mudstone fragments
478712	Silicified fenite(?)	K-feldspar, quartz, high relief microgranular mineral, white mica, limonite, chlorite, biotite(?), pyrite, apatite
478713	Brecciated siltstone and quartz-sericite-hematite cataclasite	cataclasite: quartz, white mica, hematite, high relief microgranular mineral, fluorite, pyrite siltstone-fine sandstone: quartz, silt-sized materials
478714	Brecciated siltstone and quartz-rich cataclasite	siltstone-fine sandstone: quartz, silt-sized materials cataclasite: quartz, clay, annabergite(?), white mica, fine grained high relief material
G7	Quartz-niccolite granofels	quartz-niccolite-fluorite-granofels: quartz, cryptocrystalline material, niccolite, bismuth quartz-fluorite vein: quartz, bismuth, calcite
R4	Sericite-albite altered fenite	albite, K-feldspar, sericite, and albite (after aegirine), hematite, sericite, magnetite, apatite
GD4	Quartz-albite-hematite-monazite-xenotime cataclasite	quartz, albite, hematite, K-feldspar, monazite, xenotime, magnetite, rutile
GD7	Fenite	albite, K-feldspar, arfvedsonite, magnetite, sericite, epidote(?), fluorite
GD65	Nepheline syenite	nepheline, K-feldspar, albite, aegirine, magnesio-riebeckite, fluorite(?), white mica, aegirine and hematite (after biotite?), hematite (after ilmenite), sphene
GD72	Cataclasite	sandstone: fine grained material, quartz, calcite (and minor dolomite?) matrix: calcite (and minor dolomite?), hematite veins: calcite (and minor dolomite?), hematite, quartz, pyrite, micas
GD73	Cataclasite	quartz, clay, low-Ti biotite, plagioclase, hematite-geothite, white mica, zircon(?), pyrite

Geochemical analysis of the seven samples discussed in the previous paragraph (along with 49 other samples collected from various units on the property) was done by ALS Chemex Labs and is reported in Appendix C of Swanton (2011). Electron dispersive spectrometry analyses for samples 478706 and 478712 are reported in Swanton (2012). Geochemical analyses from the Swanton (2012) report reveal that metasomatic rocks on the property are enriched in Na with

respect to the host rock, the fenite varies in composition across the property, and REE-enriched zones in the fenite diminish in concentration more distally from the Pool Creek nepheline syenite.

Eocene biotite syenite

Pigage & Mortensen (2004) reported that the biotite syenite is a coarsely crystalline, unfoliated intrusion that occurs less than 1 km west of the Pool Creek nepheline syenite. Outcrops are best exposed as cliffs along a stream that runs east to west across the intrusion, where they weather to a crumbly grey-white with visible biotite. No dikes were reported to cut the biotite syenite and no marginal contacts with the host rocks were observed.

Pigage & Mortensen (2004) reported on the mineralogy, geochemistry, and geochronology of the biotite syenite. The biotite syenite has equant, equigranular crystals, made up of 40% moderately sericitized potassium-feldspar, which has incipient microcline grid twinning, 25% moderately sericitized plagioclase, 25% hornblende, and 10% biotite. Localized hornblende crystals are noted to have blue-green colour on their margins. Accessories include opaques, sphene, apatite, and clinopyroxene. Local mineral alteration was noted in the rock samples reported by Pigage & Mortensen (2004), where hornblende and clinopyroxene occurring as fine- to medium-grained aggregates.

Geochemistry and geochronology were reported by Pigage & Mortensen (2004) from one sample of the biotite syenite. Compositionally, the biotite syenite is monzonite based on the total alkalis versus silica diagram or foid monzosyenite based on the Zr/TiO_2 versus Nb/Y diagram. According to the shand index diagram, the rock is metaluminous. Based on a multi-element diagram normalized to the primitive mantle, the rock is enriched in incompatible elements and has a moderate negative Ti anomaly. Based on the Ta versus Yb tectonic discrimination diagram the rock plots in the within-plate field. Dating of six zircon crystals yielded a U-Pb age of 51.8 ± 0.2 Ma (Eocene) for the biotite syenite.

Eocene Ting Creek intrusion

The Ting Creek intrusion is an epizonal, syntectonic, unfoliated, multiphase-ring complex located 13 km north-northwest of the Bandito property (Harrison 1982). This composite complex has a metasomatic aureole, and units within the complex have been fenitized (Harrison 1982). According to Harrison (1982), the Ting Creek intrusion represents the salic low density, extreme differentiates of nepheline-normative alkali basalt. The order of emplacement of the rock units determined by Harrison (1982) was phonolite, igneous breccias → quartz syenite → titanite nepheline syenite → leucocratic nepheline syenite, tinguaite → foyaite, tinguaite → segregation veins → tuff breccia. An age of 53.1 ± 1.8 Ma was assigned for the Ting Creek intrusion based on K-Ar dating of three biotite separates from a rinkolite foyaite (Harrison 1982; Stevens et al. 1982).

Five magmatic suites were identified by Harrison (1982) based on the whole rock geochemistry and pyroxene mineral chemistry of 75 rock samples, which range from silica oversaturated to silica undersaturated, and miaskitic to agpaitic affinities. The miaskitic suite (titanite nepheline syenites and phonolites) is enriched in Mg, Ca, Fe^{2+}, Ti, P, and Sr. The "agpamiaskitic" suite (leucrocratic nepheline syenite and foyaite) have elevated Na, Si, and Al. The agpaitic suite (tinguaite and the segregation veins) show extreme enrichments in Zr, Rb, Y, Th, U, total loss on ignition, Mn, and Fe^{3+}.

Despite the extensive classification of the rock types, very little research has been done on the mineralogy of the Ting Creek intrusion. Unfortunately, all the rock samples Harrison used in his thesis were lost at some point after 1982, so further research on his samples cannot be conducted. In 2010, Prof. Lee Groat and Allison Brand (M.Sc.) revisited the Ting Creek intrusion to collect 29 samples in similar areas to Harrison (1982) so further work on the mineralogy and petrogenesis of the intrusion could be conducted. The whole rock geochemistry, Rietveld mineralogy, and thin section petrography of these samples are reported in B.Sc. thesis (Culligan 2011), where relevant data on the 2010 samples is compared to those reported in Harrison (1982). In addition, Culligan (2011) reported the occurrence of the REE-bearing minerals rinkite-

(Ce), $(Ca_3REE)Na(NaCa)Ti(Si_2O_7)_2(OF)F_2$, and britholite-(Ce), $(Ce,Ca)_5(SiO_4)_3(OH)$, in select samples through Electron Dispersive Spectrometry.

Eocene(?) intrusive breccia

Several outcrops of intrusive breccia have been reported to occur in the Pool Creek map area as dikes and plugs (i.e., outcrops west of the biotite syenite and immediately north and south of the Pool Creek nepheline syenite, Pigage & Mortensen 2004). Most of these outcrops are too small to map at a 1:50,000 scale (e.g., Pigage & Mortensen 2004; Pigage 2008; 2009). Numerous dikes are reported to occur around the breccias (Pigage 2009). No marginal contacts of this unit have been observed, but Culbert (1981) suggested it crosscuts the Pool Creek nepheline syenite.

As reported by Pigage & Mortensen (2004), the intrusive breccia adjacent to the Pool Creek nepheline syenite is aphanitic and has local devitrification and flow banding textures. Locally, the breccia weathers to a dark maroon colour. In the matrix, clasts up to pebble in size consist of quartz sandstone, siltstone, dark volcanics, and pink syenite, and crystals of plagioclase and sub-rounded quartz up to 1 mm across are common. Pigage & Mortensen (2004) further concluded that the breccia is likely a peraluminous syenite based on the shand index diagram and the Zr/TiO_2 versus Nb/Y diagram. The multi-element diagram normalized to the primitive mantle pattern shows large negative Ti anomalies and moderate negative Eu anomalies. Like the Pool Creek nepheline syenite and biotite syenite, this breccia plots in the within-plate field. The authors were unable to determine an age using U-Pb zircon dating. The unit is interpreted to be Eocene age based on the relationship with its surrounding units (Pigage & Mortensen 2004).

3 Sample Collection and Petrographic Descriptions

Fieldwork was carried out July 19–30, 2020. The field crew consisted of the author, Prof. Lee Groat, Lindsey Abdale (B.Sc.), and Mary Macquistan. Camp was made on Corundum Dome, and the Bandito property was examined July 19–24 and July 30. From July 24 to 30 we visited the Ting Creek alkalic intrusion. Due to time constraints, only the southern portion of the Bandito property was visited (Figure 3.1); in this area, the southern edge of the Pool Creek nepheline syenite and its altered and unaltered host rocks were sampled. This thesis focuses on rocks collected from the Bandito property; samples collected in 2020 from the Ting Creek intrusion will not be presented or discussed because it is beyond the scope of this thesis.

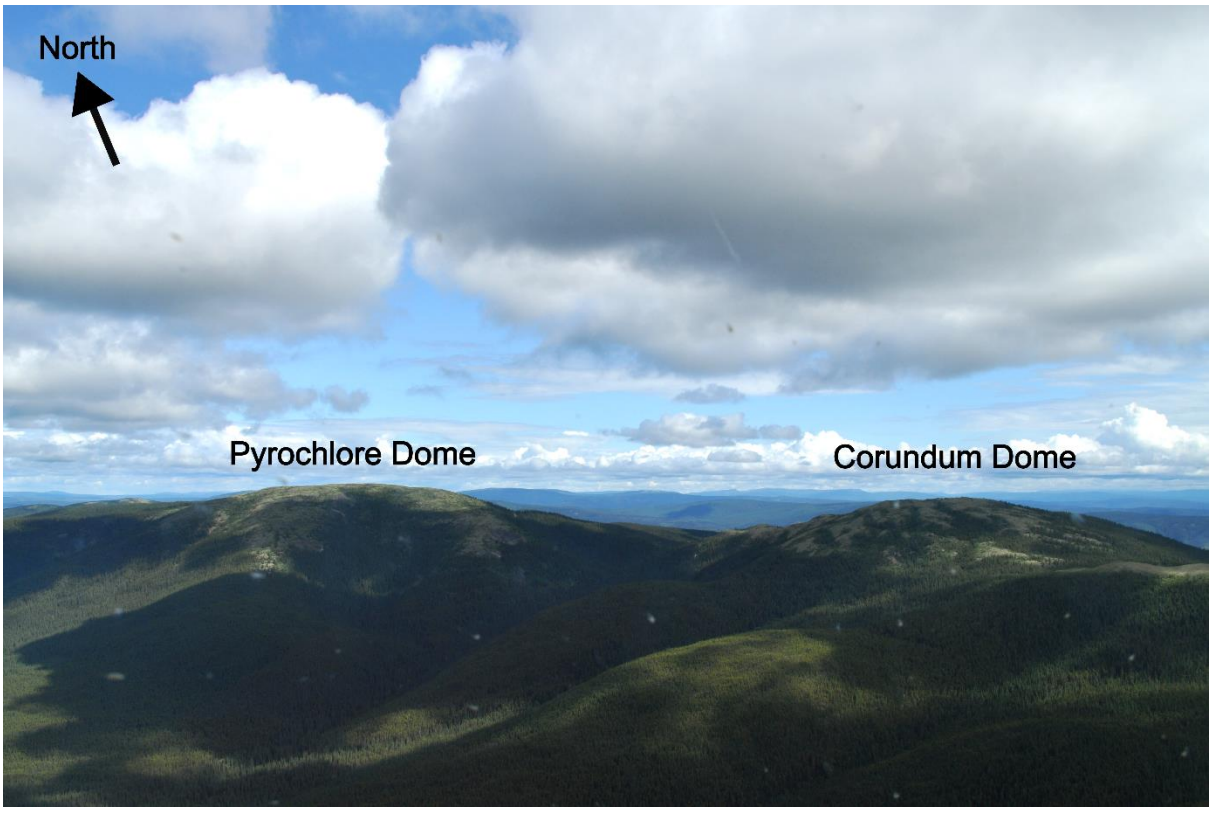

Figure 3.1. View of Corundum Dome and Pyrochlore Dome looking towards the northeast. Photo by author.

The 2020 camp on Corundum Dome was situated next to a small cold-water spring which was used as a water source. The top of the dome is just above treeline. The top of Pyrochlore Dome, which is also above treeline, can be seen clearly from Corundum Dome. To travel from

Corundum to Pyrochlore Dome the field party walked along the highest topography, where a low ridge with moderate to dense tree coverage connects the two domes. From July 19–24 water was observed in a small rocky pond on Pyrochlore Dome, however, when revisiting Pyrochlore Dome on July 30 the pond had dried up and all snow patches had melted. For future parties that return to either dome in late summer, the author recommends bringing a backup water source.

The petrography of the Pool Creek nepheline syenite and associated dikes was previously described by Pigage & Mortensen (2004). Swanton (2011; 2012) gave detailed petrographic descriptions of the Pool Creek nepheline syenite as well as several other units on the Bandito property, such as sedimentary units, breccias, cataclasite, granofels, porphyry, and fenites. Swanton (2012) referred to the mapped fenite on Corundum Dome as the "South Fenite Zone" and on Pyrochlore Dome as the "North Fenite Zone". Pigage (2009) and MacNaughton (2017) reported on the petrography of the Neoproterozoic clastic and argillite units.

This chapter will provide new information about the petrography of samples collected from the southern area of the Pool Creek nepheline syenite. Rock types that were sampled include argillite, quartzite, metaconglomerate, nepheline syenite, actinolite-altered syenite, altered arfvedsonite-aegirine syenite, layered fenites, porphyritic dikes, and volcanic breccias. The samples are described in context with the geographic area they were collected from, i.e., Corundum Dome (i.e., the South Fenite Zone) and Pyrochlore Dome (i.e., the North Fenite Zone). Samples with similar mineralogy and textures are grouped and described in a general sense. Respective thin section scans for each rock sample can be found in Appendix A. Rock names were assigned for the presented samples on the basis of modal mineralogy and textural modifiers. Grain sizes nomenclature (e.g., fine-grained, medium-grained, coarse-grained) are after those used by the International Union of Geological Sciences Subcommission on the Systematics of Metamorphic Rocks in Schmid et al. (2007). Measured mineral compositions of select mineral phases in select samples are reported in Chapter 4.

The characteristics and sources of metasomatic alteration, possible sources of deformation textures, and the implications of the variety of rock types observed in the sampling area are discussed at the end of the chapter. The discussion is focused on the syenitic and fenite samples

since those units are essential to answer the thesis questions presented at the beginning of Chapter 1.

Methods

Rock samples were collected from *in situ* outcrops when available. Grab samples (not *in situ* but directly adjacent to the outcrop) and float (an unknown distance from outcrop) were collected only if their apparent mineralogy and macrotexture(s) differed in comparison to the country rock. Samples were broken from outcrop using a hammer, then photos were taken of the samples on their outcrops and GPS coordinates were recorded. Each sample was then secured in its own cotton or plastic bag labelled with a unique sample number. Samples were approximately the size of two fists put together. Samples were stored in 2-gallon buckets upon return to camp each day.

Rock billets were cut using saws located in the EOS-M building at The University of British Columbia (UBC). Rock samples with obvious textures were cut in the orientation to best observe the textures (i.e., cut perpendicular to observed bedding, layering, and unit contacts). A Zeiss transmitted light microscope was used to conduct thin section petrography and imaging.

Thin sections were carbon coated prior to backscattered electron (BSE) imaging on the scanning electron microscope (SEM) in the Electron Microbeam & X-Ray Diffraction Facility at UBC. The backscattered electron imaging was used to assist in identifying mineral micro-textures (i.e., chemical zoning and mineral alteration) that are not visible with the petrographic microscope.

General field observations and sampling

Outcrops on the Bandito property are weathered and typically heavily to moderately covered by lichen, moss, and shrubs. The best outcrop exposures are along cliffs in areas mapped as faults, the ridge connecting Corundum Dome and Pyrochlore Dome, and on the top of the domes. Outcrops of the Proterozoic host units and of the Pool Creek nepheline syenite are commonly exposed as linear NE/SW trending knobs (Figure 3.2). A strike and dip of two outcrops of the argillite unit were taken, both measured 020/19.5, agreeing with those reported in Allen et al.

(2001). A map of rock sample locations collected in the study is shown in Figure 3.3. Sample numbers, collection method (*in situ*, grab, or float), and GPS coordinates are reported in Table 3.1

Figure 3.2. Arial view of NE/SW trending outcrops of Proterozoic host rock on the north face of Corundum Dome. Photo by author.

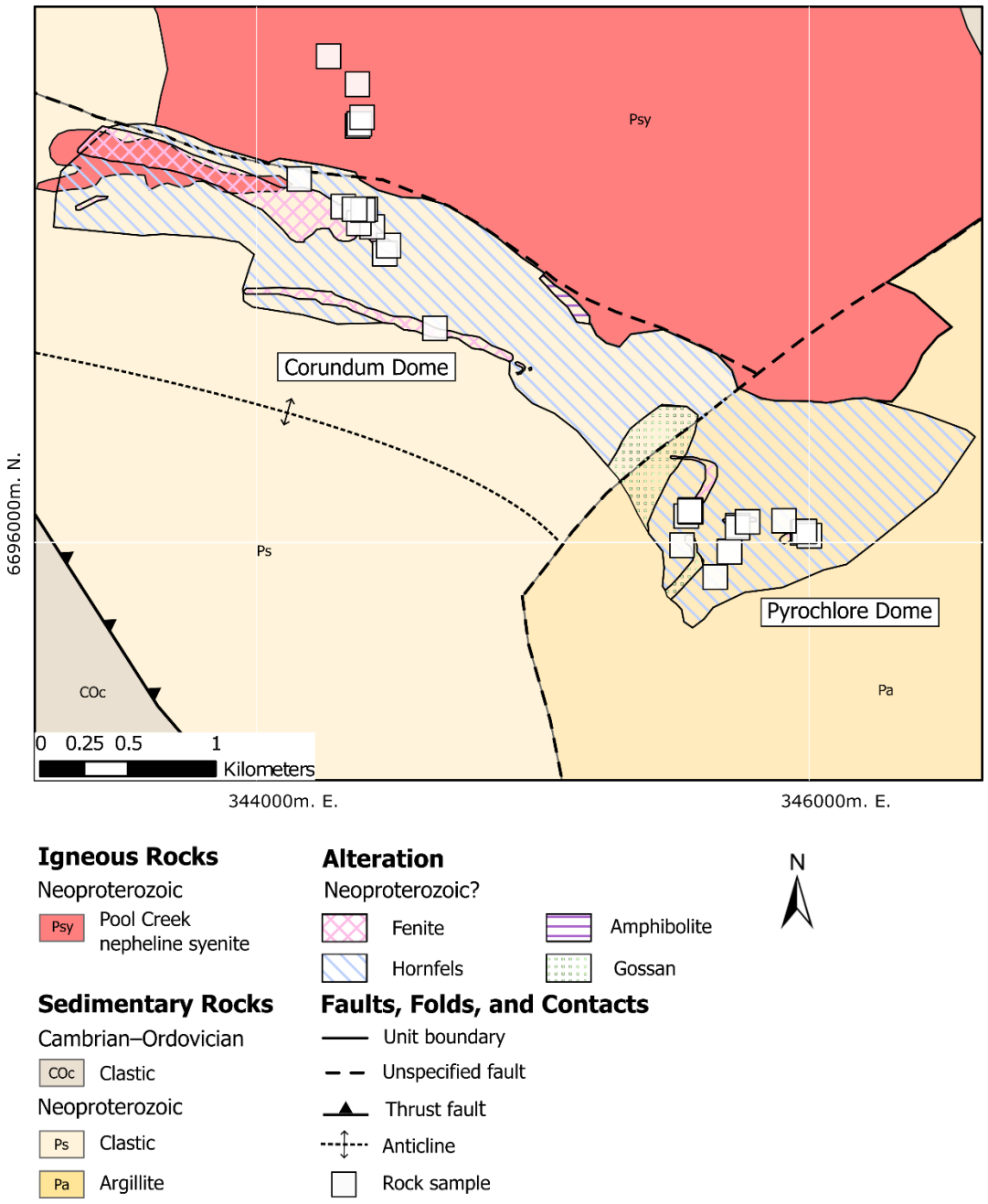

Figure 3.3. Map of 2020 rock samples collected from the Bandito property. UTM Gridlines are NAD 1983 Zone 10N. Map data from Pigage & Mortensen (2004), Swanton (2012), Fallas et al. (2014), and Yukon Geological Survey (2022). UTM Gridlines are NAD 1983 Zone 10.

Table 3.1. List of samples collected from the Bandito property in 2020. UTM Zone 10. Datum used is WGS 84. Locations: CD—Corundum Dome; PD—Pyrochlore Dome.

Field Sample Number	Sub-sample and Thin Section Number	Rock Type	Collection Type	Location	Easting (m)	Northing (m)
20TN1	20TN1	Altered feldspar microporphyritic syenite dike	Grab	CD	345659	6695876
20TN2	20TN2	Actinolite-altered	*In situ*	CD	345711	6695968
20TN3	20TN3-1	syenite dike in	*In situ*	CD	345711	6695967
	20TN3-2	contact with layered fenite				
20TN4	20TN4A	Layered	*In situ*	CD	345741	6696062
	20TN4B	arfvedsonite-albite				
	20TN4C	fenite				
	20TN4D	Actinolite-altered syenite in contact with layered fenite				
20TN5	20TN5	Bedded argillite	*In situ*	CD	345740	6696055
20TN6	20TN6-1	Actinolite-altered	*In situ*	CD	345554	6696096
	20TN6-2	syenite				
20TN7	20NTN7	Brecciated layered fenite	*In situ*	CD	345571	6696112
20TN8	20TN8A	Metallic veins	*In situ*	CD	345569	6696118
	20TN8B					
20TN9	20TN9	Actinolite-altered	*In situ*	CD	345571	6696116
20TN10	20TN10A	syenite	*In situ*	CD	345567	6696114
	20TN10B-1					
	20TN10B-2					
	20TN10C	Actinolite-altered syenite				
20TN11	20TN11	Volcanic breccia	*In situ*	CD	345539	6695991
20TN12	20TN12	Altered arfvedsonite-	*In situ*	PD	344645	6696774
20TN13	20TN13A	aegirine syenite	*In situ*	PD	344313	6697214
	20TN13B					
20TN14	20TN14		Grab	PD	344463	6697044
20TN15	20TN15A	Layered titanite-arfvedsonite syenite	Grab	PD	344477	6697073
	20TN15B	Altered layered				
	20TN15C	amphibole-diopside-phlogopite syenite				
20TN16	20TN16A-1	Altered arfvedsonite-	*In situ*	PD	344417	6697141
	20TN16A-2	aegirine syenite				
20TN17	20TN17A-1		*In situ*	PD	344369	6697154
	20TN17A-2					
	20TN17B	Calcite-quartz metaconglomerate				
	20TN17C	Quartzite				

Field Sample Number	Sub-sample and Thin Section Number	Rock Type	Collection Type	Location	Easting (m)	Northing (m)
20TN18	20TN18	Altered arfvedsonite-aegirine syenite	*In situ*	PD	344393	6697205
20TN19	20TN19	Zircon bearing quartz vein in altered arfvedsonite-aegirine syenite	*In situ*	PD	344384	6697201
20TN20	20TN20	Altered arfvedsonite-aegirine syenite	*In situ*	PD	344153	6697314
20TN22	20TN22A 20TN22B	Layered arfvedsonite-albite fenite	Float in rockfall	CD	345999	6696025
20TN23	20TN23	Layered arfvedsonite-albite fenite	Float in rockfall	CD	345982	6696041
20TN24	20TN24A 20TN24B	Bedded argillite Volcanic breccia	*In situ*	CD	345908	6696079
20TN25	20TN25A	Altered white syenite dikelets in contact with layered fenite	*In situ*	CD	345776	6696075
	20TN25B	Altered white syenite dikelets in contact with layered fenite				
	20TN25C 20TN25D	Layered phlogopite-potassium feldspar fenite				
	20TN25E 20TN25F	Actinolite-altered syenite				
20TN53	20TN53	Nepheline alkali feldspar syenite	*In situ*	PD	344365	6697505
20TN54	20TN54	Altered feldspar glomeroporphyritic syenite dike	*In situ*	PD	344371	6697512
20TN55A	20TN55A 20TN55B	Nepheline alkali feldspar syenite	*In situ*	PD	344381	6697536
20TN56	20TN56		*In situ*	PD	344364	6697656
20TN57	20TN57A 20TN57B 20TN57C-1 20TN57C-2	Altered porphyritic lamprophyre(?) dike	*In situ*	PD	344260	6697757
20TN58	20TN58A 20TN58B	Altered arfvedsonite-aegirine syenite	*In situ*	PD	344354	6697205

Corundum Dome sampling area

Samples collected on Corundum Dome are shown in Figure 3.4. Intrusive units in this area are hosted in a Neoproterozoic argillite unit. Outcrops are commonly poorly exposed and obscured by vegetation.

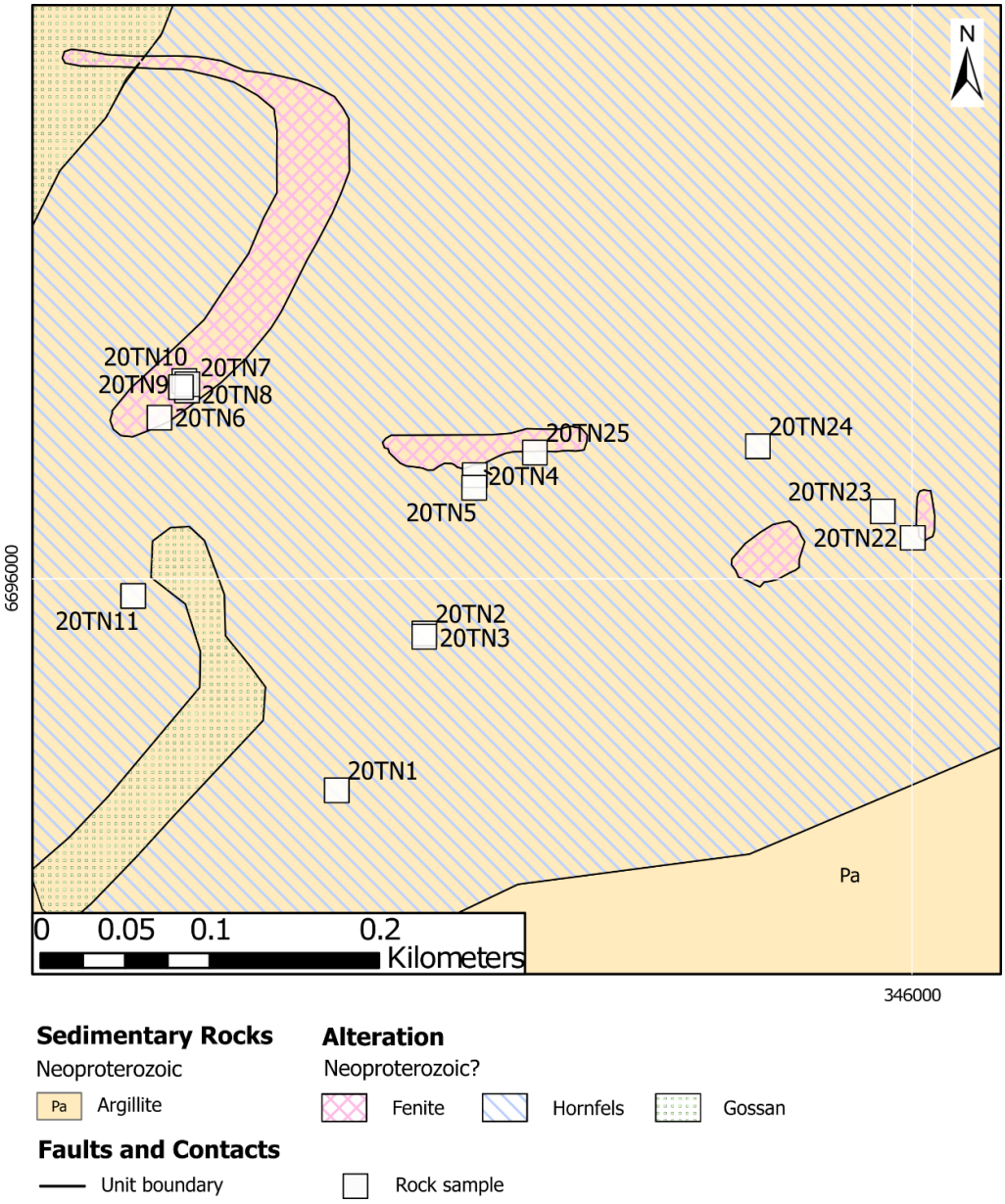

Figure 3.4. Map of samples collected from Corundum Dome in 2020. Map data from Pigage & Mortensen (2004), Swanton (2012), Fallas et al. (2014), and Yukon Geological Survey (2022). UTM Gridlines are NAD 1983 Zone 10.

Volcanic breccias

Two breccia samples (20TN11 and 20TN24B) were collected from outcrops in contact with the argillite unit. As discussed in Chapter 2, volcanic breccias are known to occur within and near the Bandito property (e.g., Pigage & Mortensen 2004; Swanton 2012). Based on the angularity and compositions of clasts, and alteration of the clasts and groundmass, the two samples are interpreted as volcanic breccias.

Sample 20TN11 is a volcanic breccia that was collected from an outcrop located between the South Fenite Zone and Gossan Zone. The outcrop is composed of a beige-coloured volcanic breccia unit in contact with a green-gray layered argillite unit (Figure 3.5). Weathered surfaces of the breccia unit are covered in patches of hematite. These patches occur within dark brown-red stained areas on the rock surface. Around these dark stained areas are random patches of greenish and beige coloured staining. Fresh surfaces are very fine grained with alternating layers of medium green to slightly darker green. The rock is nonmagnetic, moderately fractured, and is moderately porous.

Petrographic images of general textures observed in the rock sample are shown in Figure 3.6. Gravel to pebble (up to 4 cm) sized clasts make up 70% of the rock. The dominant clast type is subrounded feldspar porphyritic basalt and the less dominant clast type is an angular mudstone. The porphyritic basalt clasts have fine grained euhedral feldspar phenocrysts, felty microlites, and disseminated chlorite. Some clasts also have disseminated to clustered fine-grained blue-green amphibole. Porphyritic basalt clasts show alteration halos visible in hand sample and in transmitted light, where mudstone clasts don't exhibit alteration halos. The groundmass (30%) is made up of ultra fine to very fine-grained (< 0.1 mm) chlorite, clays, and very fine to fine grained, moderately altered, zoned feldspar crystals (Figure 3.6). Hematite is pervasive throughout the sample and occurs as fine to very fine-grained hematite disseminated throughout the clasts and groundmass. Hematite also occurs as medium-grained sheet-like fans in oval-shaped zones in cavities within the rock. Based on the angularity and compositions of clasts, and alteration of the clasts and groundmass, this sample is interpreted to be an altered mudstone-porphyritic basalt sub-angular to sub-rounded clast supported gravel-pebble volcanic breccia.

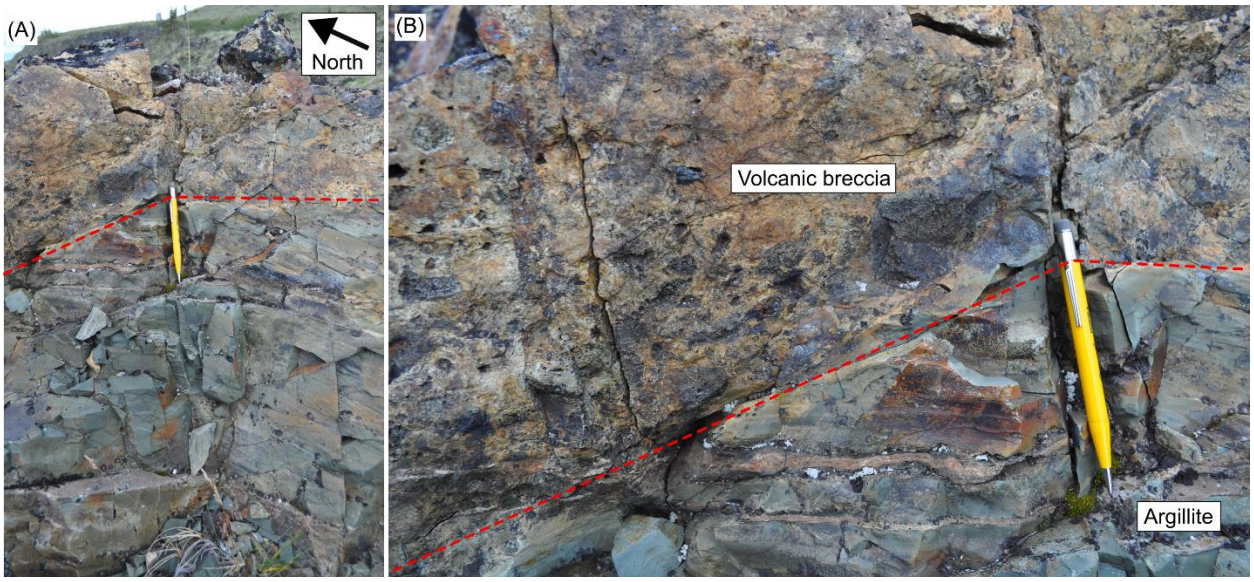

Figure 3.5. A volcanic breccia sample (20TN11) was collected from this outcrop. (A) and (B) show the contact between the volcanic breccia and argillite unit, outlined by the red dashed line.

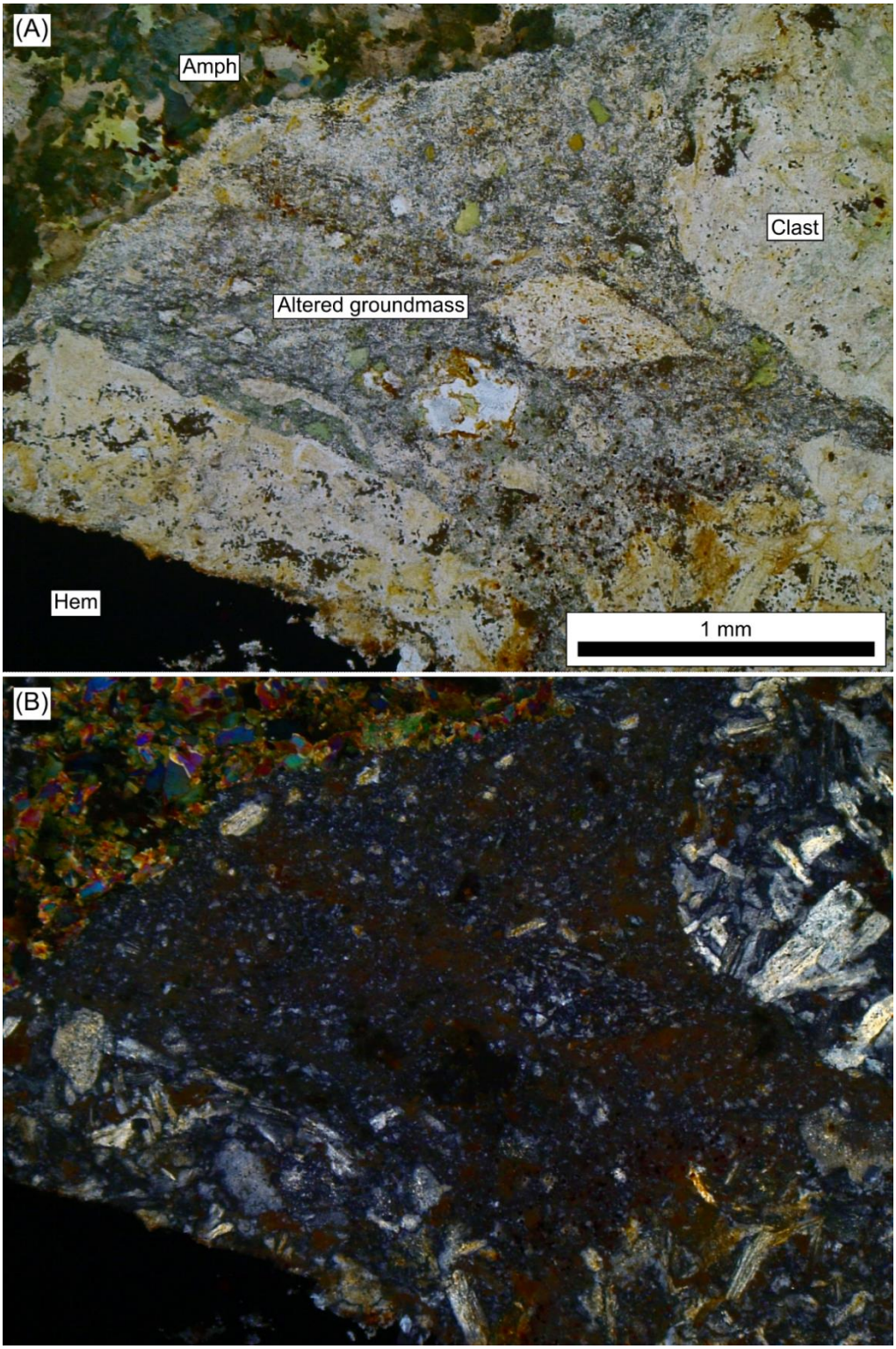

Figure 3.6. General textures of volcanic breccia sample 20TN11. (A, B) Rock clasts made up of fine-grained feldspar and sometimes amphibole. The groundmass is very to ultra-fine grained and strongly altered. (A) Plane polarized light. (B) Cross polarized light. Amph – amphibole, Hem – hematite.

Sample 20TN24B is a volcanic breccia that was collected from an outcrop located in the South Fenite Zone. The volcanic breccia is in contact with the argillite unit (Figure 3.7). Weathered surfaces of the breccia unit are pale gray to white with patches of red staining and are covered in white lichen and dark green-brown moss. Fresh surfaces are dark to medium blue-gray, crystalline, and vuggy. Weak layering and clast alignment are visible in the outcrop and under transmitted light.

Gravel and pebble sized clasts (up to 2 cm) make up 70% of the rock. Clasts are angular to subangular and gravel to pebble in size. The dominant clast types are a feldspar porphyritic rock (basalt?) and fine grained syenite. Some clasts are dominated by fine-grained clear amphibole. Other very fine-grained clasts are present but are too altered to reveal the protolith (possibly basalt or mud/siltstone?). The porphyritic basalt(?) clasts have fine grained euhedral, turbid feldspar phenocrysts, felty microlites, and disseminated opaque minerals and chlorite. Syenite clasts have fine grained turbid feldspar, zircon(?), opaque minerals, and disseminated chlorite and amphibole. The groundmass (30%) is strongly altered and composed of a grungy brown cryptocrystalline material, fine to very fine-grained (<0.5 mm) euhedral to subhedral feldspar, amphibole (tremolite?), chlorite, calcite, and opaques. Fine, elongate patches (infilled vugs or amygdules?) are lined with chlorite and commonly partially to fully infilled with calcite. Petrographic images of general textures observed in the rock sample are shown in Figure 3.8. Based on the angularity and compositions of clasts, and alteration of the clasts and groundmass, this sample is interpreted to be an altered limestone-syenite-porphyritic basalt, angular to sub-angular clast supported gravel-pebble volcanic breccia.

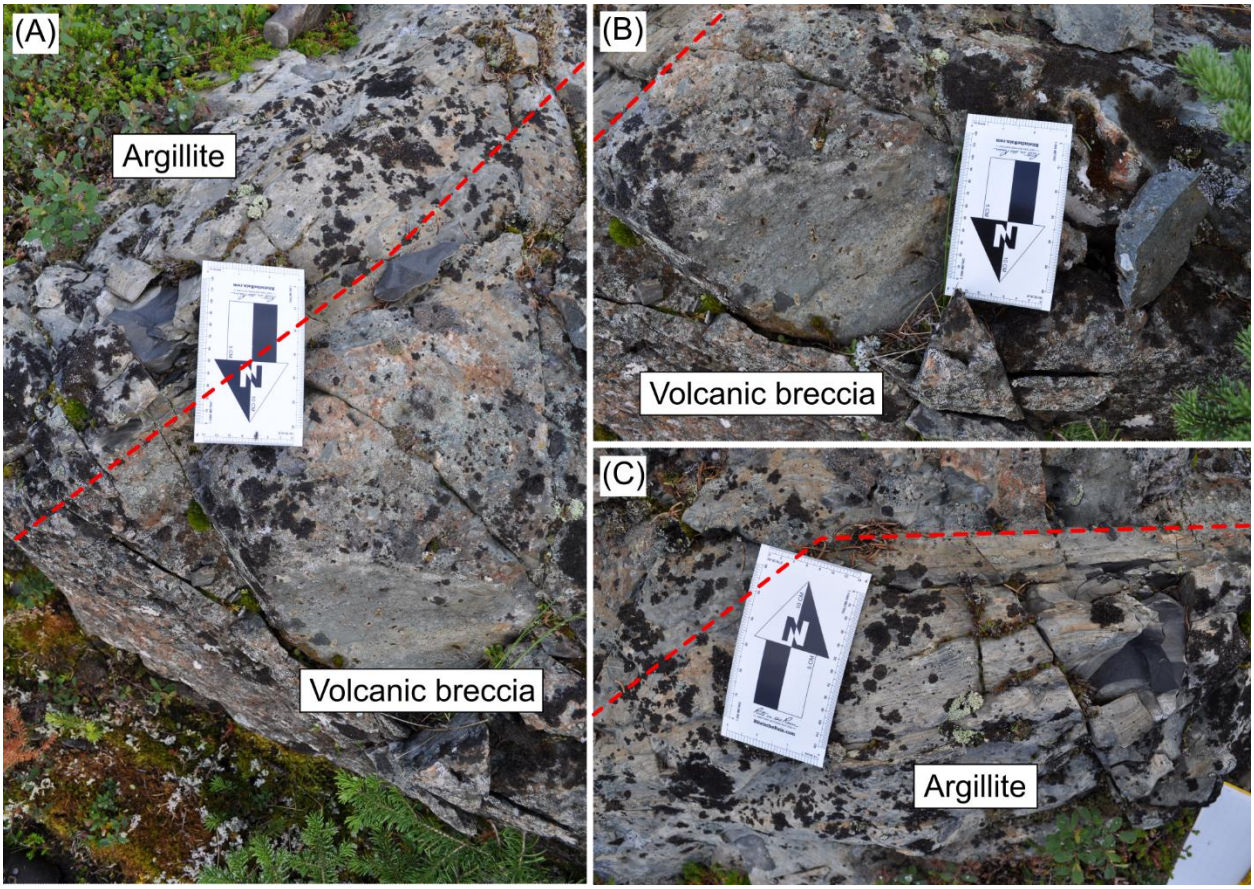

Figure 3.7. Outcrop providing volcanic breccia (20TN24B) and argillite (20TN24A) samples. The red dashed line outlines the contact between the two units. The north arrow card in the images is pointing north. (A) Outcrop photo. (B) Close up of the volcanic breccia. (C) Close up of the argillite unit.

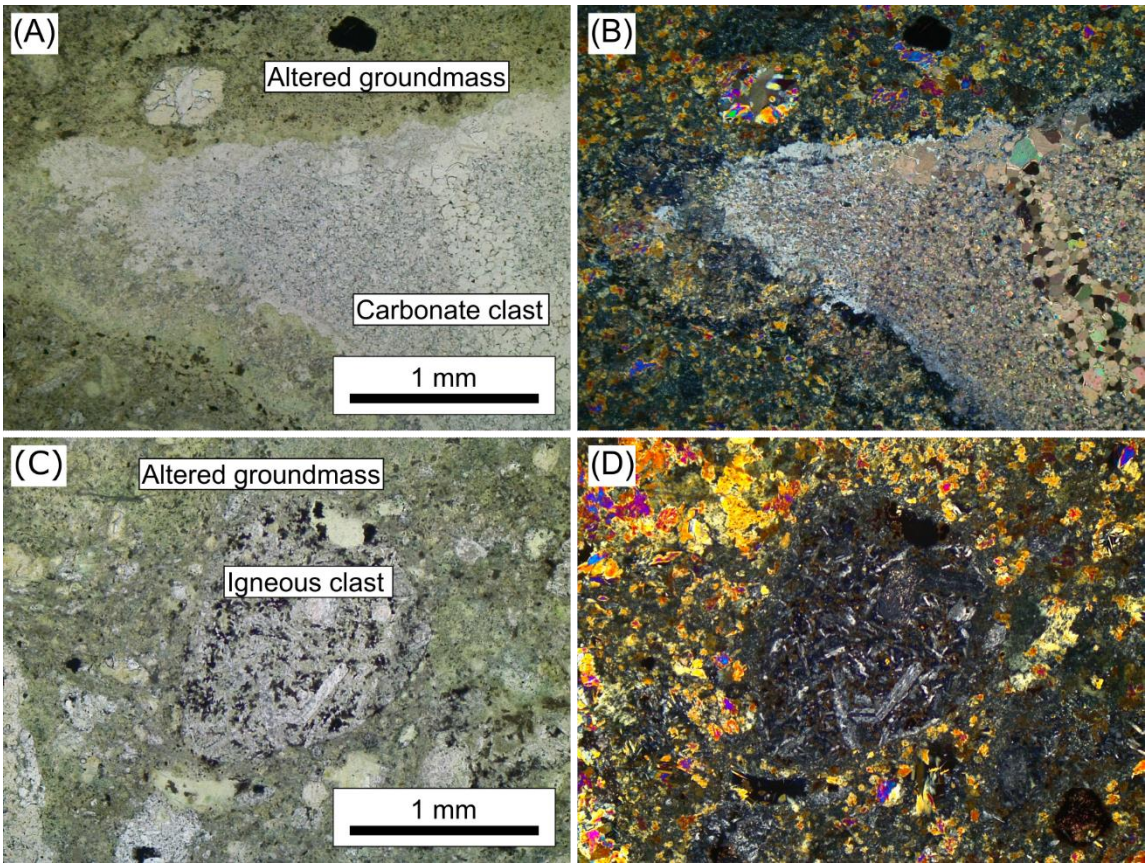

Figure 3.8. General textures from volcanic breccia sample 20TN24B. (A, B) Angular carbonate clast within the altered groundmass. (C, D) Igneous clast in the altered groundmass. (A, C) Plane polarized light. (B, D) Cross polarized light.

Altered feldspar microporphyritic dike

A strongly altered epidote-chlorite-sericite fine-grained feldspar microporphyritic dike (20TN1) crosscuts the host argillite unit just south of the South Fenite Zone at Corundum Dome. Weathered and nonweathered surfaces are weakly magnetic. Weathered surfaces of the dike are a dark rusty orange-brown colour. Freshly cut surfaces grade from a dark brown-green colour to a mottled mixture of brown-red with white colour.

Petrographic images of characteristic mineral textures of the sample are shown in Figure 3.9. Felspar phenocrysts (3%) are euhedral rectangular fine-grained (1 mm × <0.5 mm) laths that show carlsbad twinning. The groundmass is fine grained to very fine-grained and composed of euhedral fine-grained (<0.5 mm) feldspar (albite and K-feldspar) laths, and a former interstitial phase completely pseudomorphed by sericite. Minor amounts of euhedral, clear to green-yellow to yellow pleochroic epidote-allanite and euhedral opaques (pyrite and hematite) are present. Disseminated fibrous very fine-grained sericite and fibrous green to yellow-green pleochroic chlorite are common throughout the groundmass. Feldspars are moderately replaced by sericite. Chlorite alteration is more pervasive in the groundmass towards weathered surfaces and fracture-filled veins.

Multiple black fracture filled veins <1 mm thick composed of chlorite and epidote cut through the rock and are roughly perpendicular to weathered surfaces. These veins typically terminate 1 to 2 cm into the rock. A black and white vein lined with feldspar and filled with chlorite, epidote, and opaques, cuts through the rock and is crosscut by the black veins at roughly 60/120º angles. The rock is too altered to reveal the protolith, however based on the modal mineralogy of this rock, it is likely a porphyritic trachyte.

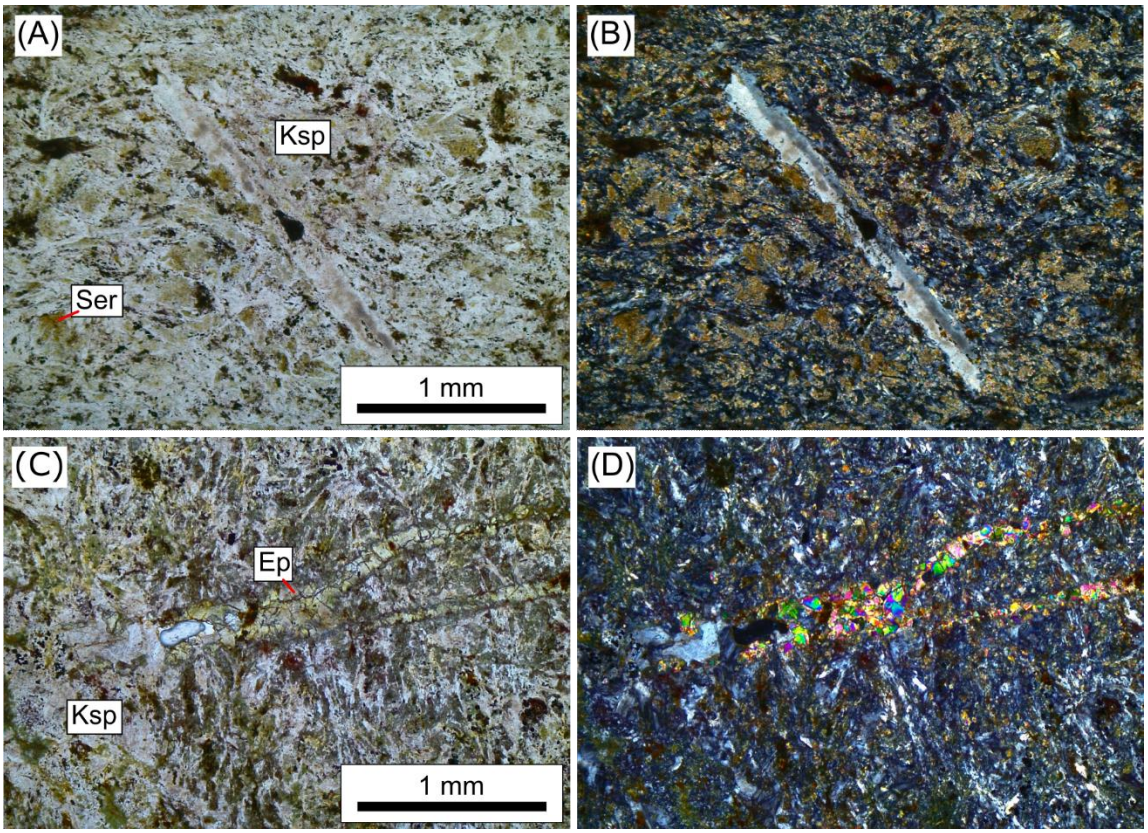

Figure 3.9. Mineral textures from sample 20TN1. (A, B) Feldspar phenocryst in a feldspar groundmass with interstitial sericite after a former phase. (C, D) Epidote-rich vein. (A, C) Plane polarized light. (B, D) Cross polarized light. Ksp – potassium feldspar, Ep – epidote, Ser – sericite.

Actinolite-altered syenite

Several samples of actinolite-altered syenite were collected from Corundum Dome. Outcrop photos and textures of select sampling sites are shown in Figure 3.10. Sampled outcrops show complex textures, such as layering, crosscutting relationships, and brecciation.

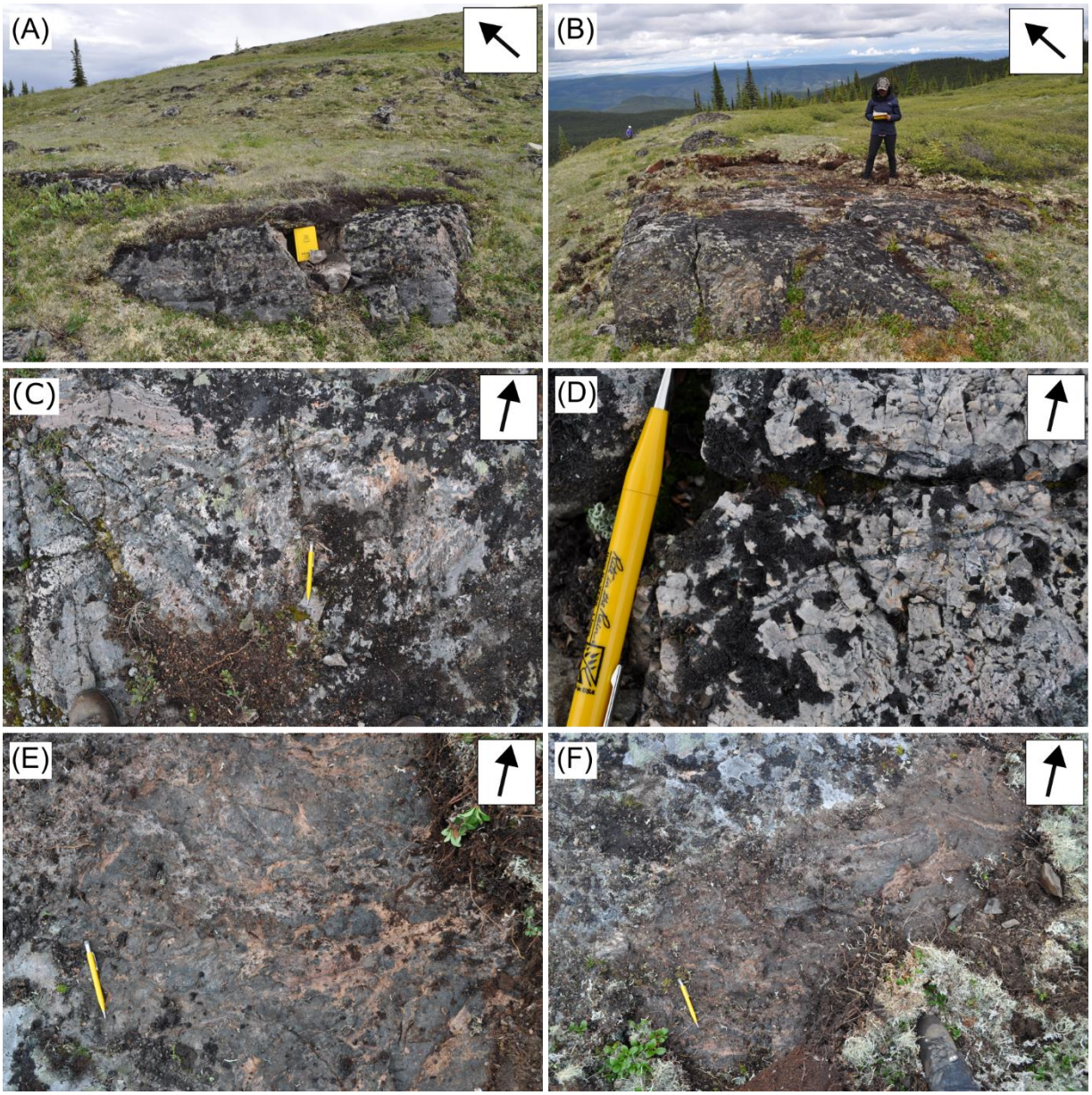

Figure 3.10. Outcrops where several actinolite-altered syenite samples were collected from. The outcrops tend to form long linear features. The arrow is pointing north. (A) 20TN3 outcrop. (B) Outcrop where samples 20TN6 to 20TN10 were collected. Variable textures (such as layering, brecciation, and crosscutting dikes and veins) occur in

the sampled outcrop, indicating that it has been affected by multiple geologic events. Throughout the outcrop, metallic grey hematite veins cut across all the observed units. (C) The west end and central part of the outcrop. On the west end (the left half of the image), millimetre to centimetre scale convolute layering between thin white, black, pink, and mottled pink layers occur adjacent to chaotic brecciation textures that continue towards the central part of the outcrop (the right half of the image). A coarse-grained white alkali feldspar dike crosscuts the fine-grained, mottled dark grey unit. On the central part of the outcrop, convoluted brecciation textures are prevalent and occur between black aggregates and a white phase. Black aggregates look stretched and aligned. (D) Metallic veins in the coarse-grained white alkali feldspar dike in the west end of the outcrop. Photos (E) and (F) are from the east end of the outcrop. In this area, the mottled dark grey unit looks brecciated by a pink feldspar intrusive unit. (E) The northern part of this the east end of the outcrop. Pale white veins or dikelets form a chaotic network that crosscuts the darker pink dark grey brecciated unit. (F) The southern part of the east end of the outcrop. The mottled dark grey unit is crosscut by white feldspar veins or dikelets that have halos of a black mineral phase, likely amphibole.

Moderately metasomatically altered amphibole-altered alkali feldspar syenites

Three samples (20TN4D, 20TN10C, 20TN25A) of coarse- to very coarse-grained, nonmagnetic, moderately altered alkali feldspar syenite were collected from discrete outcrops in the South Fenite Zone. All three samples are in contact with fine grained, strongly altered units (e.g., 20TN4A to C, 20TN10A to B, and 20TN25B to F). The zones and samples of the crosscut units are discussed in the next subsection of this chapter. One of the syenite samples (20TN10C) occurs as a centimeter scale dike (Figure 3.10C). The nature of emplacement (e.g., sill, dike, etc.) of the other two samples is undetermined due to minimal exposure of the units in the field. In hand sample, the syenites are dominated by white (20TN10C, 20TN25A) or pink (20TN4D) feldspar. The sample with the pink feldspar is mildly friable and more altered looking than the white alkali feldspar syenite samples.

Petrographic images of mineral textures characteristic of the sample suite are shown in Figure 3.11. Coarse grained (1.5 to 0.5 cm) potassium feldspar is the main constituent of the alkali feldspar syenites. Minor amounts of fine-grained (< 1 mm) phases such as albite and actinolite are common in the samples. Albite occurs as inclusions and becomes more prevalent and oriented towards (i.e., perpendicular to) contact boundaries with other units (i.e., fenites). Actinolite is fine grained green to green-yellow pleochroic, weakly zoned (best observed with BSE imaging), and occurs as discrete prismatic crystals and in acicular aggregates. Actinolite becomes more prevalent towards contact zones and is commonly altered and partially to completely replaced by opaque minerals, epidote-allanite, and other unidentified alteration phases. Fine grained aggregates of titanite were observed close to unit contacts in two of the samples (20TN4D and 20TN25A).

With respect to the pink alkali feldspar syenite (20TN4D), minor to trace amounts of fine grained (< 1 mm) andalusite, apatite, epidote-allanite, zircon, and opaques were observed and become prevalent with the presence of albite. Actinolite is sometimes intergrown with andalusite. Zircon is fractured, inclusion rich, and is commonly surrounded by opaque minerals. Trace amounts of very fine grained (< 0.1 mm) pyrochlore were observed with the SEM. Millimetre scale metallic veins of hematite were observed in hand sample. With respect to the white alkali feldspar

syenites samples (20TN10C and 20TN25A), aggregates of opaque minerals pseudomorph a former phase, possibly amphibole. Trace amounts of pyrochlore was observed in 20TN25A on the SEM. Veins of hematite cut through sample 20TN10C (Figure 3.10D).

Most of the minor mineralogy (actinolite, titanite, andalusite, apatite, epidote, allanite) is altered, occurs with albite, and become more prevalent towards contact boundaries. These mineral phases are common in contact metamorphic environments and therefore likely formed from contact metamorphism and metasomatic exchange processes between the syenites and the host rock. The white alkali feldspar syenite samples and pink alkali feldspar syenite sample may represent different magmatic phases from the same magmatic system. Notably, the white alkali feldspar syenite is different (is more altered and has different mineralogy) than the white alkali feldspar syenite that crosscuts the Pool Creek nepheline syenite that is described and attributed to the unnamed Eocene biotite syenite by Pigage & Mortensen (2004) and Swanton (2012). No nepheline was observed in the pink syenite, indicating that either nepheline has been completely altered, or that this syenite may be a different magmatic phase than the nepheline syenite.

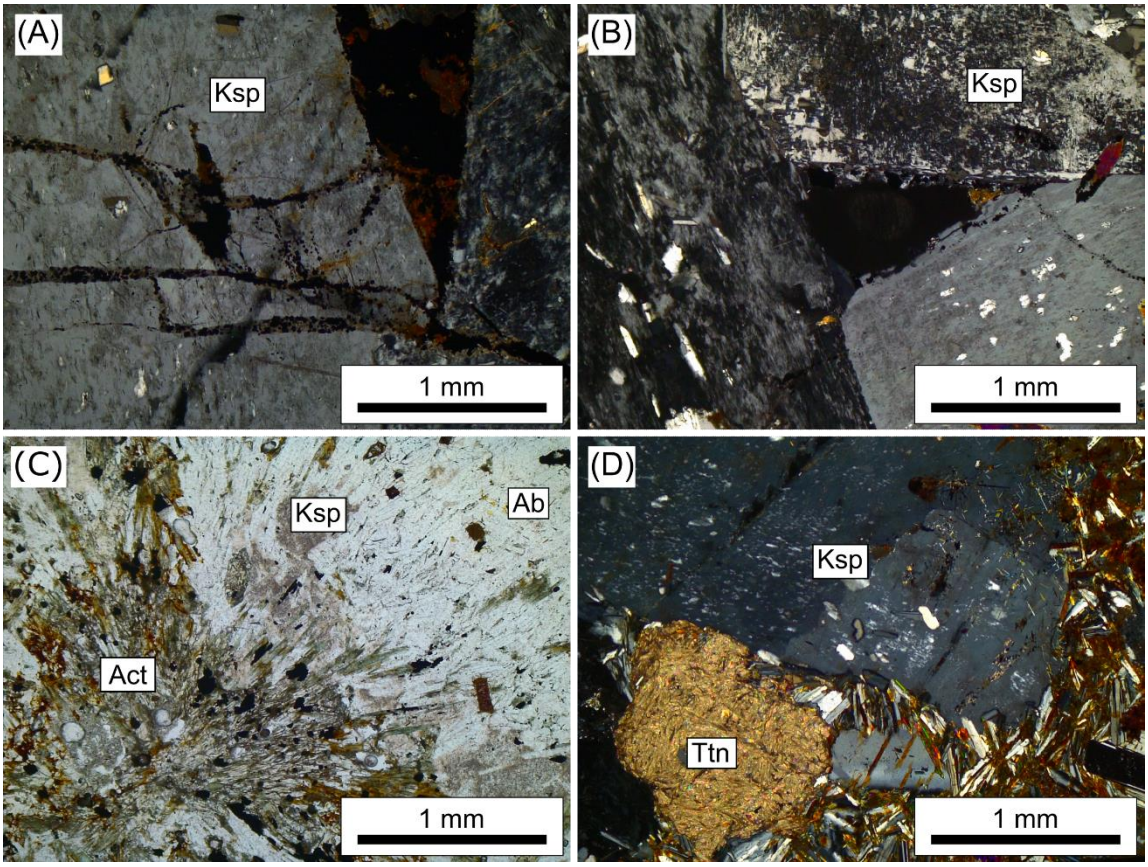

Figure 3.11. Mineral textures of select moderately actinolite-altered syenite samples. (A) Fractured, coarse grained potassium feldspar. Fractures contain abundant inclusions of hematite. (B) Coarse-grained potassium feldspar with chaotic twinning included with albite. (C) Acicular actinolite aggregate surrounded by fine grained potassium feldspar and albite. (D) Coarse grained potassium feldspar and titanite aggregate adjacent to a contact with the layered arfvedsonite-albite fenite. (C) Plane polarized light. (A, B, D) Cross polarized light. Ab – albite, Act – actinolite, Ksp – potassium feldspar, Ttn – titanite.

Strongly metasomatically altered actinolite-altered syenites

Nine samples (20TN2, 20TN3, 20TN6, 20TN9, 20TN10A, 20TN10B, 20TN10C, 20TN25E, and 20TN25F) of strongly altered, nonmagnetic to magnetic, fine grained, crystalline, feldspar and amphibole rich rocks were collected from several outcrops in the Corundum Dome sampling area. Samples and their outcrops are complex and have multiple zones showing variable mineralogy and textures (Figure 3.10). Weathered sample surfaces are commonly stained by a rusty dark orange-brown colour. Zones of dark purple fluorite crystals occur on some of the weathered sample surfaces (i.e., 20TN2 and 20TN3). Less altered surfaces are dark grey and covered in abundant black and grey lichen. Magnetism occurs in areas of some samples and appears to be associated with fine, back (opaque) crystals in alteration patches and along fractures (probably magnetite). Relicts of medium grained perthitic feldspar crystals that recrystallized to fine grained feldspars were observed in several of the samples. Samples with similar characteristics (i.e., mineral compositions and textures) are grouped and described in a general sense in the preceding paragraphs. Petrographic images of mineral textures characteristic of the sample suite are shown in Figure 3.12.

The hand specimen of sample 20TN2 is dark purple with light pink crystals and green patches. Sample 20TN3 has two zones, a dark purple and a white zone, which have different textures and mineralogy. The dark purple zone is similar to 20TN2; dark purple-grey in colour with pink patches and composed of fine grained turbid potassium feldspar, actinolite, zircon, opaques, epidote, allanite, calcite, and fluorite. The dark purple zone is outlined by dark green millimetre-scale rim of amphibole. The white zone occurs as small lenses at the edge of the dark purple zone in hand sample. This zone has a fine-grained albite groundmass, with disseminated arfvedsonite, lesser amounts of epidote and allanite, and fine grained strongly altered prismatic crystals. The minerals in the white zone are foliated and show crenulation cleavage.

Samples 20TN6, 20TN9, 20TN10A and 20TN10B were collected from the same outcrop as the white alkali feldspar dike described in sample 20TN10C. Notably, the coarse grained white syenite dike (20TN10C, discussed in the former subsection of this chapter) crosscuts the rock that samples 20TN10A and 20TN10B were collected from. Textures within these samples are

complex, such as mineral alignment, shearing, stretching, fracturing, and crosscutting. Pink zones are characterized by medium grained (5–1 mm), turbid-looking potassium feldspar crystals that commonly show mottled perthitic texture and carlsbad twinning. Pink and dark green zones are characterized by fine grained (< 1 mm) extremely turbid potassium feldspar crystals, and fine to medium grained (< 1.5 mm) amphibole crystals that occur either as discrete prismatic crystals or as acicular aggregates. White zones are characterized by fine grained (< 0.5 mm), oriented, albite laths. Sometimes the pink and dark green zone and white zone mix. Opaque minerals replacing former phases and infilling fractures are present in all three zones but are most prevalent in the pink and dark green zone. Minor to trace amounts of quartz, zircon, apatite, epidote-allanite, and pyrochlore were observed in these samples.

Samples 20TN25E and 20TN25F show similar zones, textures, and mineralogy as the previously described samples in this section (e.g., 20TN10A). However, potassium feldspars are so turbid that they are almost unrecognizable, and these samples are dominated by pervasive calcite, chlorite, and hematite alteration. In these samples, a former prismatic phase that occurs in a fine-grained feldspar groundmass and is preserved only by its relict crystal outline (lined by opaques) is completely replaced by the groundmass feldspars and opaques. Chlorite completely replaces former amphibole. Chlorite and hematite infilled fractures cut across the rock. The carbonate and chlorite alteration are likely from deuteric alteration.

Several of the actinolite-altered syenite samples show small, fine grained, strongly albitized zones. These zones are linear to lenticular and sometimes bear minor amounts of amphibole which are compositionally actinolite or arfvedsonite. These albite rich zones may represent completely altered zones of a crystallizing syenitic phase or possibly a former host rock.

Based on textures observed in hand sample and thin section, all of samples are interpreted to be of a strongly altered igneous phase or phases, likely of syenitic composition. Samples to 20TN2 and 20TN3 are interpreted to be strongly altered dikes or dikelets from a syenitic protolith (possibly the same unit as 20TN4D). Samples 20TN6, 20TN9, 20TN10A to 20TN10C, 20TN25E and 20TN25F, are composed of multiple altered zones, many of which show evidence of deformation. The pink zone and pink and green zone possibly represent different magmatic

phases or different degrees of metasomatic alteration. The white albite-rich zones observed in the samples are completely metasomatically altered, making it challenge whether these zones as albitized areas of a syenitic photolith or if they represent an alternative protolith.

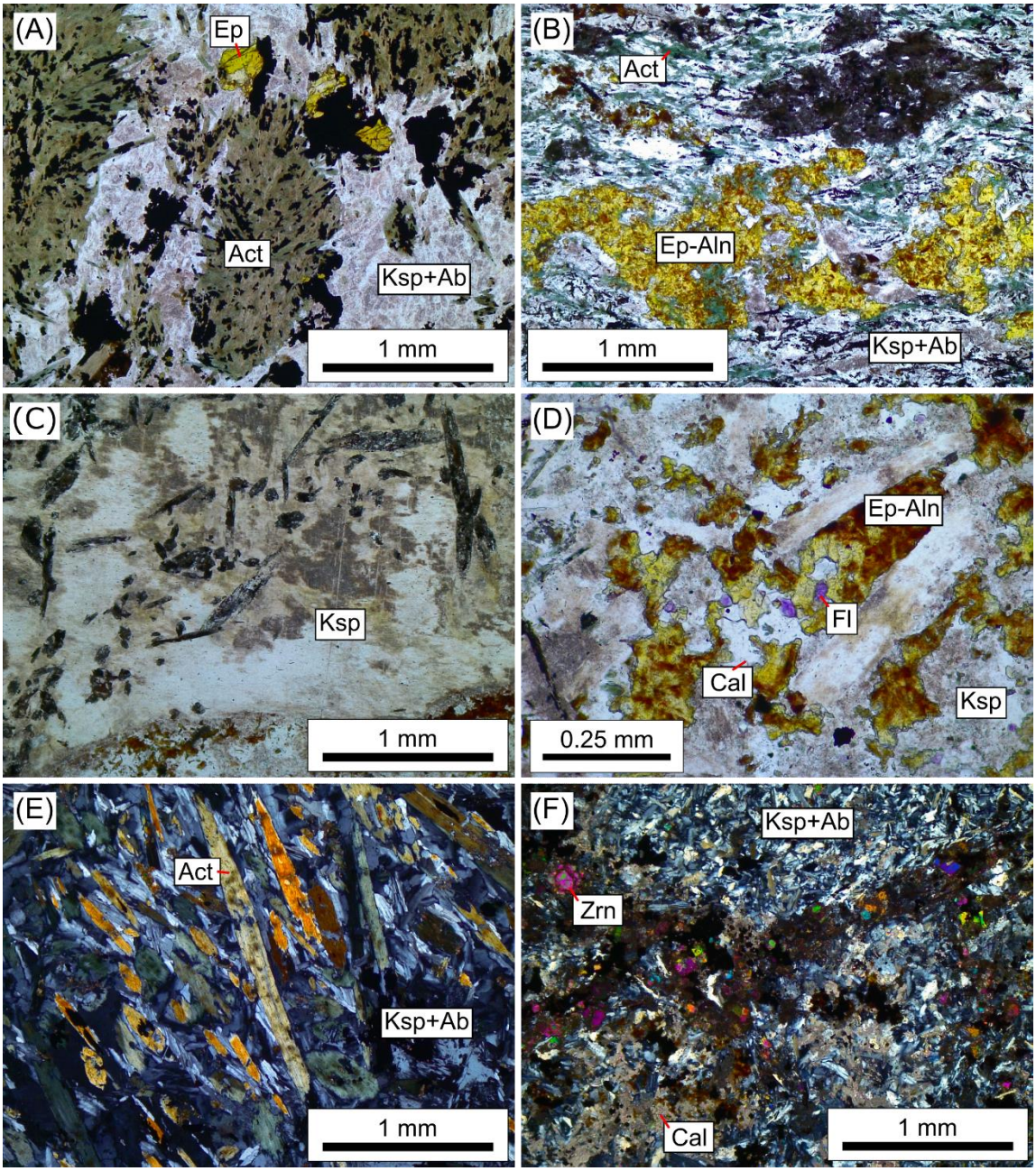

Figure 3.12. Mineral textures of select actinolite-altered syenite samples in plane and cross polarized light. (A) Acicular actinolite aggregates in an alkali feldspar groundmass. Fractured epidote crystals occur with opaque aggregates. (B) Epidote and allanite in an alkali feldspar and amphibole groundmass. (C) Altered coarse grained feldspar crystal with several altered actinolite inclusions. (D) Interstitial epidote, allanite, calcite, and fluorite alteration in a feldspar groundmass. (E) Aligned alkali feldspar and prismatic actinolite crystals. (F) Fine grained zircon, opaques, calcite, surrounded by fine grained alkali feldspar. (A – D) Plane polarized light. (E – D) Cross polarized light. Ep – epidote, Aln – allanite, Ksp – potassium feldspar, Cal – calcite, Fl – fluorite, Act – actinolite, Ab – albite, Zrn – zircon.

Fenites

Rock samples that have experienced extreme alkali metasomatic alteration (i.e., fenitization) are discussed in this section. Many samples show millimetre scale layering. Some of the layered samples show mild brecciation. One sample shows intense brecciation and no layering is visible.

Layered phlogopite-potassium feldspar fenite

Fine grained layered phlogopite-potassium feldspar fenite samples (20TN25C and 20TN25D) were collected from the same outcrop (Figure 3.13) as two of the layered arfvedsonite-albite fenite samples (20TN25A and 20TN25B). Layering in the phlogopite-potassium feldspar fenite samples is planar, millimeter scale, and defined on the basis of changing feldspar and phlogopite content. Petrographic images of characteristic mineral textures of the samples are shown in Figure 3.14. These samples are dominantly composed of fine to very fine alkali feldspars (< 0.1 mm) and fine to medium grained phlogopite poikiloblasts (3 × 0.5 mm to 0.1 × 0.1 mm). Phlogopite poikiloblasts commonly have lamellae of hematite ± rutile. Minor amounts of fine grained (< 0.3 mm) chlorite, calcite, fluorite, opaques, and trace amounts of bastnäsite, pyrochlore, and thorite are present throughout the groundmass in these samples. Two completely altered phases exist in the samples. One is a fine grained (< 3 mm × 0.5 mm) altered prismatic phase that is dominantly replaced by hematite, fluorite, thorite, and an undetermined Y-REE silicate phase. The other is a fine grained (< 3 mm × 3 mm) phase (possibly hexagonal) that is replaced by potassium feldspar, chlorite, hematite, bastnäsite, and pyrochlore. Aggregates of coarser grained feldspar are rare and exist within some of the albite-rich layers. Sample 20TN25D is cut by a fracture that parallels layering and is infilled with chlorite, feldspar, opaques, and calcite. Based on the prevalence of aluminum and hydrous phases, and presence of planar millimetre scale layers, the protolith is interpreted to be the argillite unit.

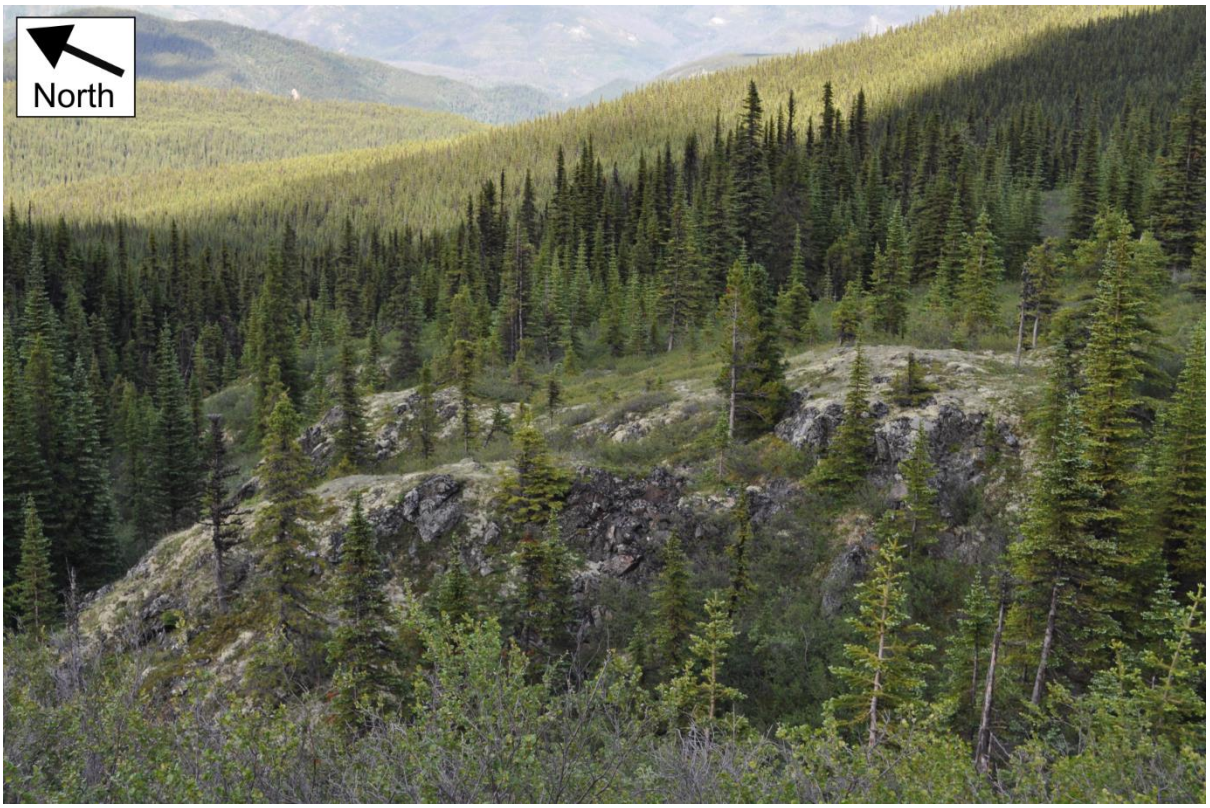

Figure 3.13. Outcrop generating samples 20TN25A to 20TN25F (layered phlogopite-potassium feldspar fenite, layered arfvedsonite-albite fenite, and actinolite-altered syenite).

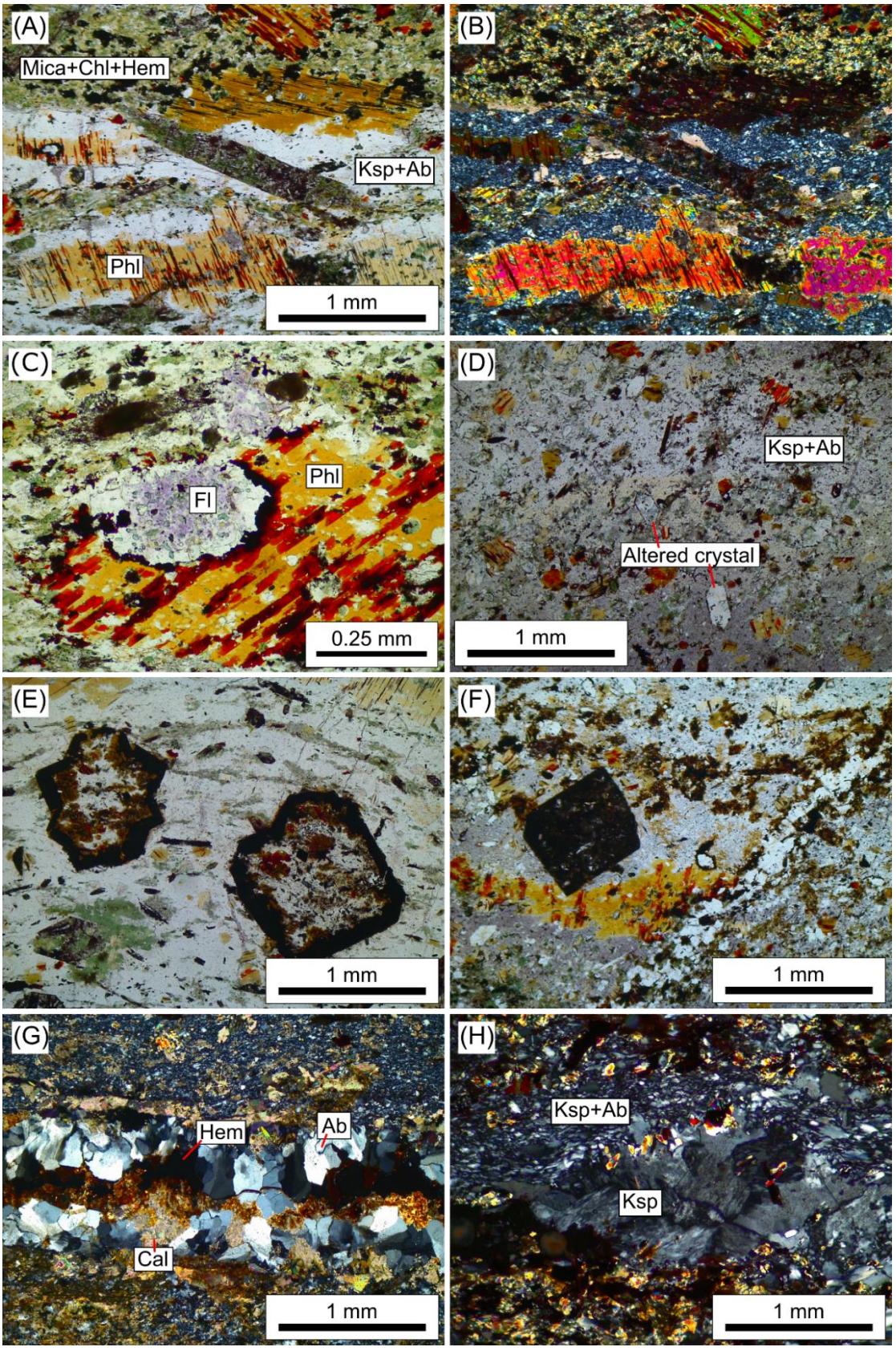
(A)
Mica+Chl+Hem
Ksp+Ab
Phl
1 mm
(B)
(C)
Fl
Phl
0.25 mm
(D)
Ksp+Ab
Altered crystal
1 mm
(E)
1 mm
(F)
1 mm
(G)
Hem
Ab
Cal
1 mm
(H)
Ksp+Ab
Ksp
1 mm

Figure 3.14. Mineral textures of layered phlogopite-potassium feldspar fenite samples. (A, B) show mica-rich and alkali feldspar-rich layers with phlogopite poikiloblasts and altered prismatic crystals. (C) Fluorite patches and included phlogopite with hematite and rutile lamellae. (D) Altered prismatic crystals replaced by alkali feldspar. (E, F) show completely altered crystals. (G) Calcite-hematite-albite vein. (H) Potassium feldspar aggregate. (A, C – F) Plane polarized light. (B, G, H) Cross polarized light. Ab – albite, Hem – hematite, Cal – calcite, Ksp – potassium feldspar, Fl – fluorite, Phl – phlogopite, Chl – chlorite.

Layered arfvedsonite-albite fenite

Select outcrops where layered arfvedsonite-albite fenite samples (20TN4A to 20TN4C, 20TN22A, 20TN22B, 20TN23, 20TN25A, and 20TN25B) were collected are shown in Figure 3.15. Samples 20TN4A to 20TN4C, 20TN25A and 20TN25B were in contact with the moderately actinolite-altered syenite samples (i.e., 20TN4D and 20TN25A, respectively) described in a former subsection of this chapter. Samples 20TN4A to 20TN4C show millimetre scale, planar to convolute layering. Thin sections show fractures that offset areas in the rocks. In samples 20TN22A, 20TN22B, and 20TN23, layering is convoluted and discontinuous (broken-up and apparently brecciated *in situ*) in hand sample and outcrop. Petrographic images of mineral textures characteristic of the sample suite are shown in Figure 3.16.

The groundmass in these samples is dominantly made up of very fine-grained albite (< 0.1 mm) and fine to medium grained arfvedsonite (2–0.1 mm). Minor amounts of very fine-grained apatite (< 0.1 mm) are present as discrete crystals throughout the groundmass. Fluorite is present as an alteration phase in minor to trace amounts. Fine-grained aggregates (up to 1 mm) of titanite are present along contact boundaries between the layered fenite and actinolite-altered syenite (e.g., 20TN25A). Two completely altered phases are common in the samples of the layered arfvedsonite-albite fenite. Thin, elongate, prismatic crystals (up to 1 cm × 0.5 mm) present throughout the groundmass are completely replaced by varying combinations of fine grained rutile, hematite, phlogopite, potassium feldspar, albite, and titanite. A former hexagonal crystal phase (~1 × 1 mm to 0.5 × 0.5 mm) visible in some samples is dominantly replaced by phlogopite and albite. Linear veins infilled with potassium feldspar and albite, and potassium feldspar and hematite are common across the samples. Potassium feldspar and hematite infill oval shaped patches (possibly a former mineral phase or voids) are also present in the samples.

Layering was observed in both the argillite and some altered syenitic units on Corundum Dome and Pyrochlore Dome. Unlike the altered syenitic samples, these layered fenite samples (20TN4A to 20TN4C, 20TN23, 20TN25A, and 20TN25B) have a prevalence of hydrous bearing phases, such as micas and amphiboles, indicating a protolith with high water content. Layers in samples (20TN4A to 20TN4C, and 20TN23, 20TN25A, and 20TN25B) are of a similar scale of

the fine beds observed in the argillite. Based on the prevalence of aluminum and hydrous-bearing mineral phases, and presence of planar millimetre scale layering, the protolith of these samples is interpreted to be the argillite unit.

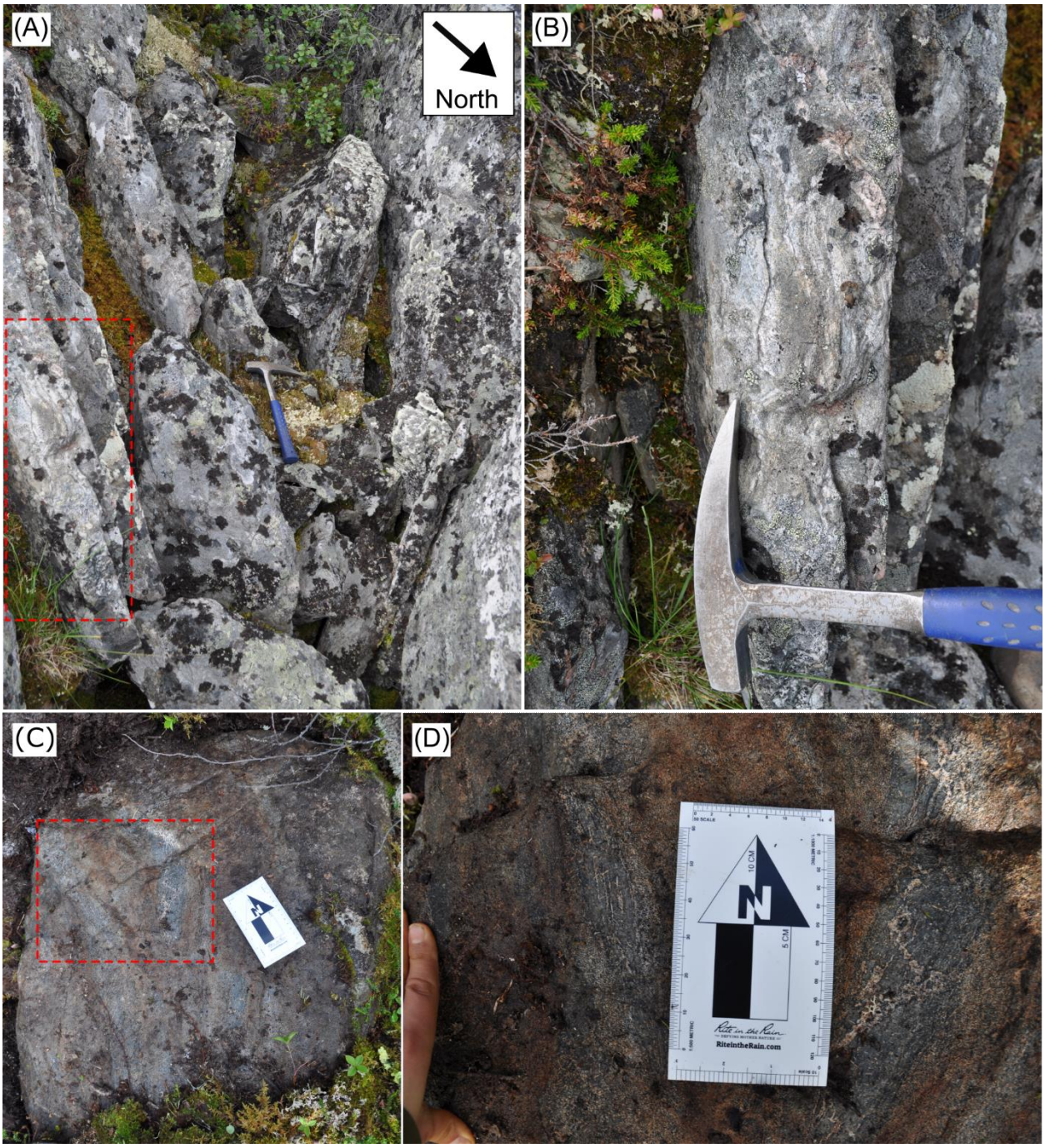

Figure 3.15. Outcrop photos of layered arfvedsonite-albite fenite samples. (A) Outcrop providing samples 20TN4A to 20TN4D. The red dashed box (B) shows a closeup of the layering visible in the outcrop. (C) Outcrop where sample 20TN23 was collected. The red dashed box (D) indicates a closeup of layering (black) that is weakly separated and broken up by an interstitial, light coloured phase.

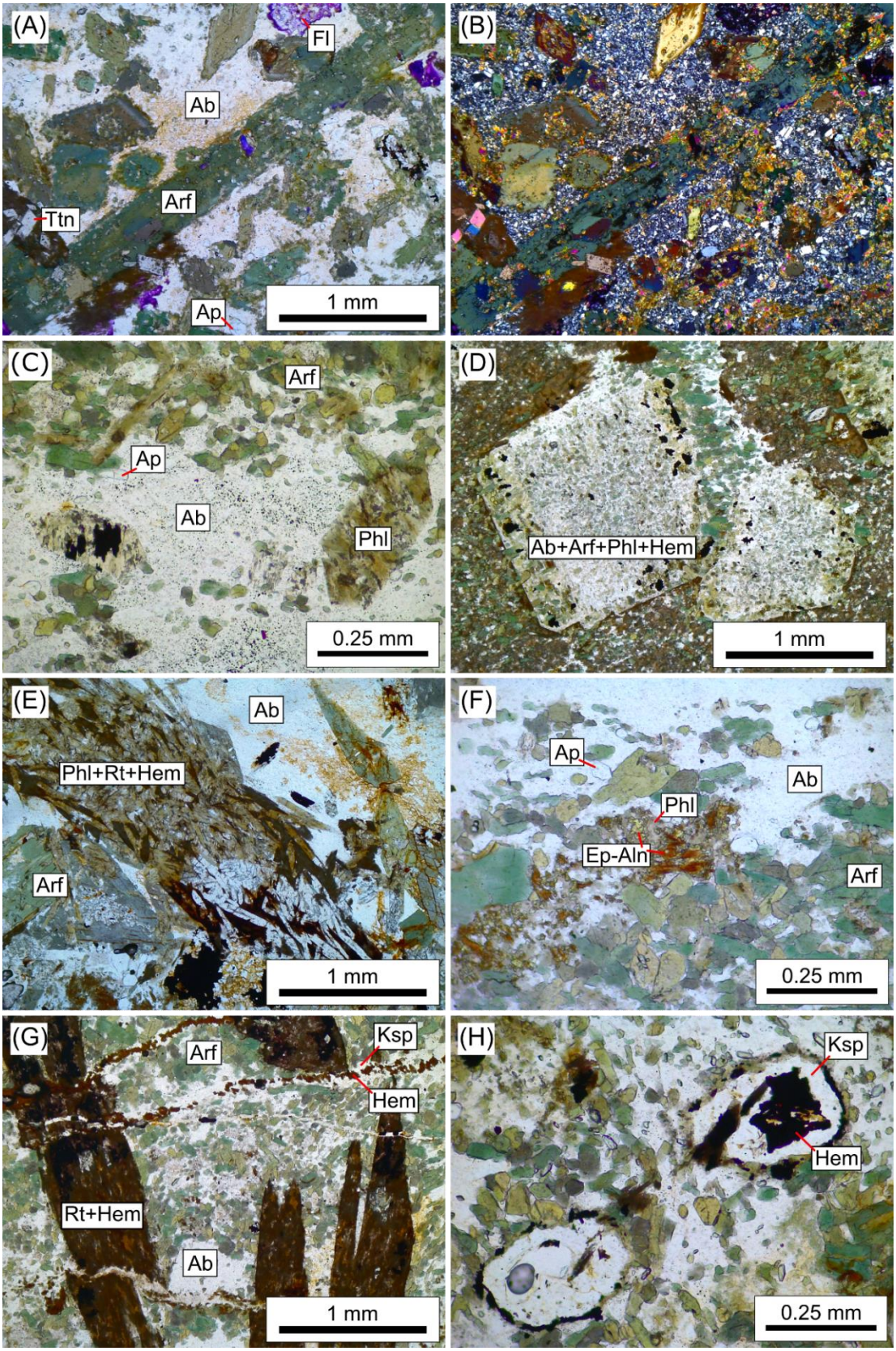
(A)
Fl
Ab
Arf
Ttn
Ap
1 mm
(B)
(C)
Arf
Ap
Ab
Phl
0.25 mm
(D)
Ab+Arf+Phl+Hem
1 mm
(E)
Ab
Phl+Rt+Hem
Arf
1 mm
(F)
Ap
Ab
Phl
Ep-Aln
Arf
0.25 mm
(G)
Arf
Ksp
Hem
Rt+Hem
Ab
1 mm
(H)
Ksp
Hem
0.25 mm

Figure 3.16. Mineral textures of layered arfvedsonite-albite fenite samples. (A, B) Included arfvedsonite in a very fine-grained albite groundmass. (C) Former prismatic phases completely replaced by phlogopite and hematite. (D) Former hexagonal phases completely replaced by albite, arfvedsonite, phlogopite, and hematite. (E) An elongate prismatic phase completely replaced by phlogopite, rutile, hematite, and alkali feldspar. (F) Epidote-allanite-phlogopite aggregate. (G) Veins of potassium feldspar and hematite cutting across the fine-grained groundmass and altered prismatic phases. (H) Ovoid phases completely replaced by potassium feldspar and hematite. (A, C, D, E, G, H) Plane polarized light. (B, F) Cross polarized light. Ab – albite, Arf – arfvedsonite, Ap – apatite, Aln – allanite, Ep – epidote, Ksp – potassium feldspar, Fl – fluorite, Phl – phlogopite, Ttn – titanite, Rt – rutile, Hem – hematite.

Brecciated arfvedsonite-potassium feldspar fenite

A brecciated arfvedsonite-potassium feldspar fenite (20TN7) was collected from the same outcrop as the actinolite-altered syenite (Figure 3.10C to 3.10F). Fresh surfaces are dominated by dark green to black patches interwoven with a white to pale pink groundmass (likely *in situ* brecciation). Sample 20TN7 is somewhat similar to sample 20TN23 from the layered arfvedsonite-albite fenite suite with respect to mineralogy and mineral textures, however, comparatively 20TN7 is pervasively brecciated by heavy fracturing, has significantly less albite and more potassium feldspar, and has discrete crystals of fractured fine grained andalusite and aggregates of fine-grained alkali feldspar that were not observed in the other layered fenite samples. Characteristic Mineral textures shown in Figure 3.17. Preserved fine grained feldspar aggregates in the brecciated arfvedsonite-potassium feldspar fenite provide evidence for a syenitic protolith (i.e., like the actinolite-altered syenite). However, the mineralogy is more similar to the two layered fenite suites, i.e., prevalent arfvedsonite, epidote-allanite, titanite, and rutile (like the layered arfvedsonite-albite fenite suite), and prevalent potassium feldspar and presence of feldspar aggregates (like the layered phlogopite-potassium feldspar fenite), suggesting an argillite protolith. The complicated nature of the brecciated arfvedsonite-potassium feldspar fenite suggests that it is a highly convoluted contact between the layered argillite and actinolite-altered syenite.

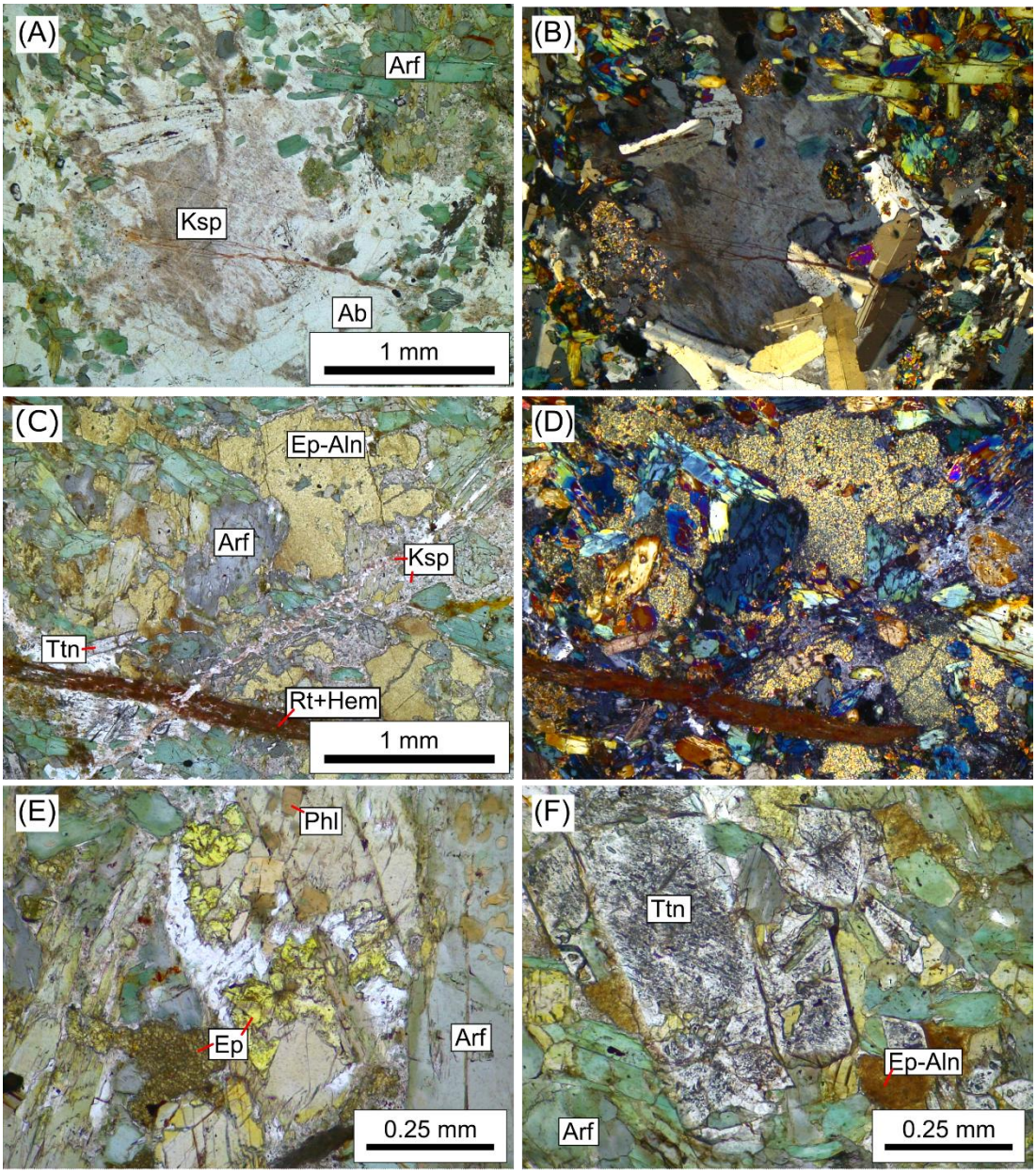

Figure 3.17. Mineral textures of brecciated arfvedsonite-potassium feldspar fenite. (A, B) Aggregate of fine-grained potassium feldspar and albite. (C, D) Potassium feldspar fracture-filled vein cutting across arfvedsonite, epidote pseudomorph, and an altered prismatic phase replaced by rutile and hematite. (E) Fine grained epidote. (F) Heavily included titanite crystals. (A, C, E, F) Plane polarized light. (B, D) Cross polarized light. Ab – albite, Arf – arfvedsonite, Aln – allanite, Ep – epidote, Ksp – potassium feldspar, Phl – phlogopite, Ttn – titanite, Rt – rutile, Hem – hematite.

Bedded argillite

Two nonmagnetic finely bedded argillite samples from the argillite unit were collected in the South Fenite Zone (20TN5, 20TN24A). Both samples were from outcrops with measured strikes/dips of 020/19.5. Strongly weathered surfaces of these rocks are oxidized to a dark red-brown rusty colour and surfaces with less weathering have a pale white colour. Exposed faces are also covered in green and black lichen. Outcrops of the argillite unit observed in the field are typically a pale to dark green-grey colour, massive, and have millimetre scale alternating beds (i.e., laminae) that have sharp and gradational contacts (Figure 3.18*).* Petrographic images of textures characteristic of the sample suite are shown in Figure 3.19.

Sample 20TN5 from the argillite unit is composed of dominantly clay- and silt-sized particles with up to fine-grained (<0.2 mm) sized particles. In hand sample, beds alternate from a pale to dark green-grey colour. Very fine-grained opaques are pervasive throughout the rocks. Most of the opaque minerals are hematite, with lesser amounts of pyrite and chalcopyrite. The mineralogy of lighter coloured layers is calcite mixed with clays, feldspar, and lesser quartz, and the darker layers are dominantly clays, amphibole, feldspars, and lesser quartz. Trace amounts of apatite and zircon crystals occur in the rock. Fractures in the rock are partially infilled with biotite and opaques. Sporadic fine grained feldspar clasts have been altered to clay (sericite?).

A contact of the argillite unit with a volcanic breccia (20TN24A and 20TN24B, respectively) was observed in the field (Figures 3.5 and 3.7). The thermally metamorphosed argillite is massive, finely bedded, and black-brown in colour. The beds are planar (some truncated by angular beds), nonplanar, and overturned. Similar to the unmetamorphosed argillite (20TN5), the groundmass is dominated by clays, amphibole, feldspars, and disseminated opaques (hematite, ilmenite, pyrite, and chalcopyrite). Minor to trace amounts of titanite, apatite, and zircon occur in the matrix. The sample also has small vugs infilled with fibrous and non-fibrous clear minerals (possibly a zeolite mineral or maybe quartz). Beds deform around rare coarser mineral clasts in the rock.

Figure 3.18. Outcrop of finely bedded argillite (sample 20TN5).

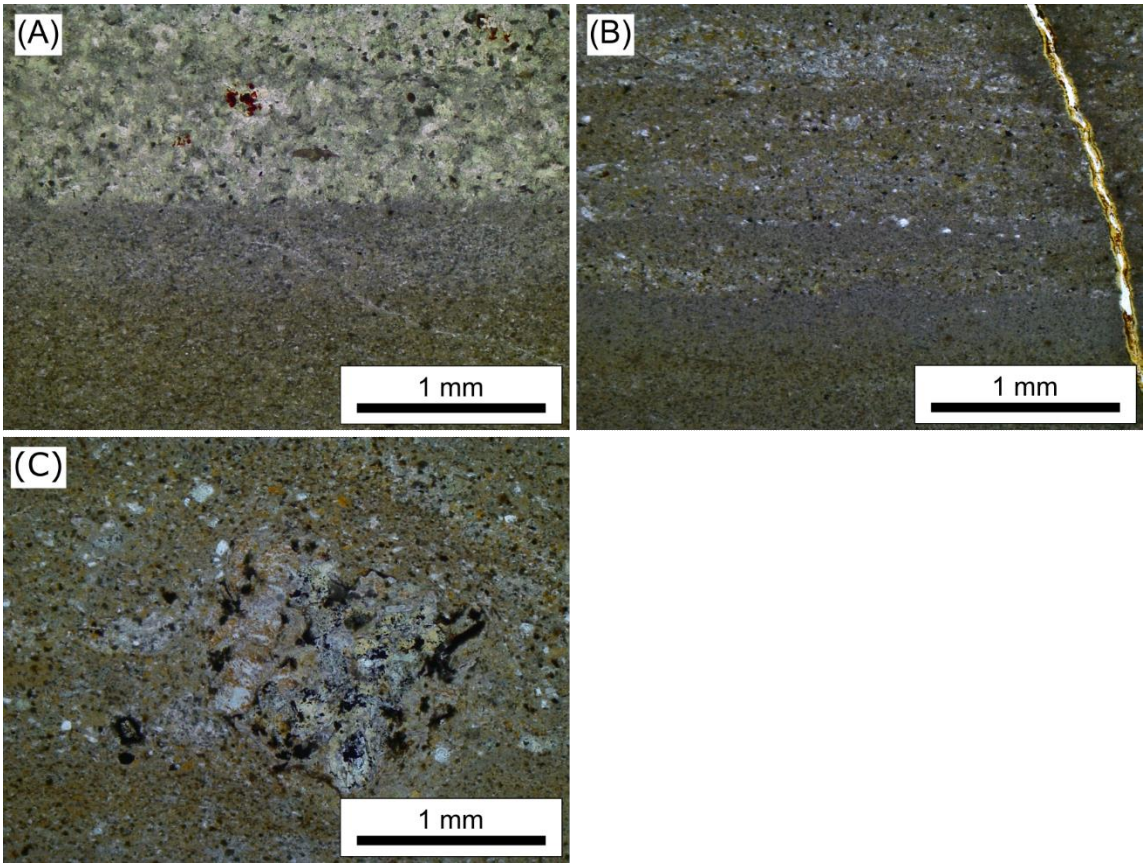

Figure 3.19. Characteristic textures in the bedded argillite samples 20TN5 and 20TN24A in plane polarized light. (A, B) Beds varying in mineral composition in the argillite. (C) A clast within the argillite.

Pyrochlore Dome sampling area

A map of the samples collected on Pyrochlore Dome is shown in Figure 3.20. A view of the sampling area on Pyrochlore Dome is shown in Figure 3.21. Units that are intrusive in this area are hosted in the Neoproterozoic clastic unit that has been locally contact metamorphosed to hornfels by the Pool Creek nepheline syenite (e.g., Pigage & Mortensen 2004). Outcrops of nepheline syenite are more pronounced than other units in the sampling area.

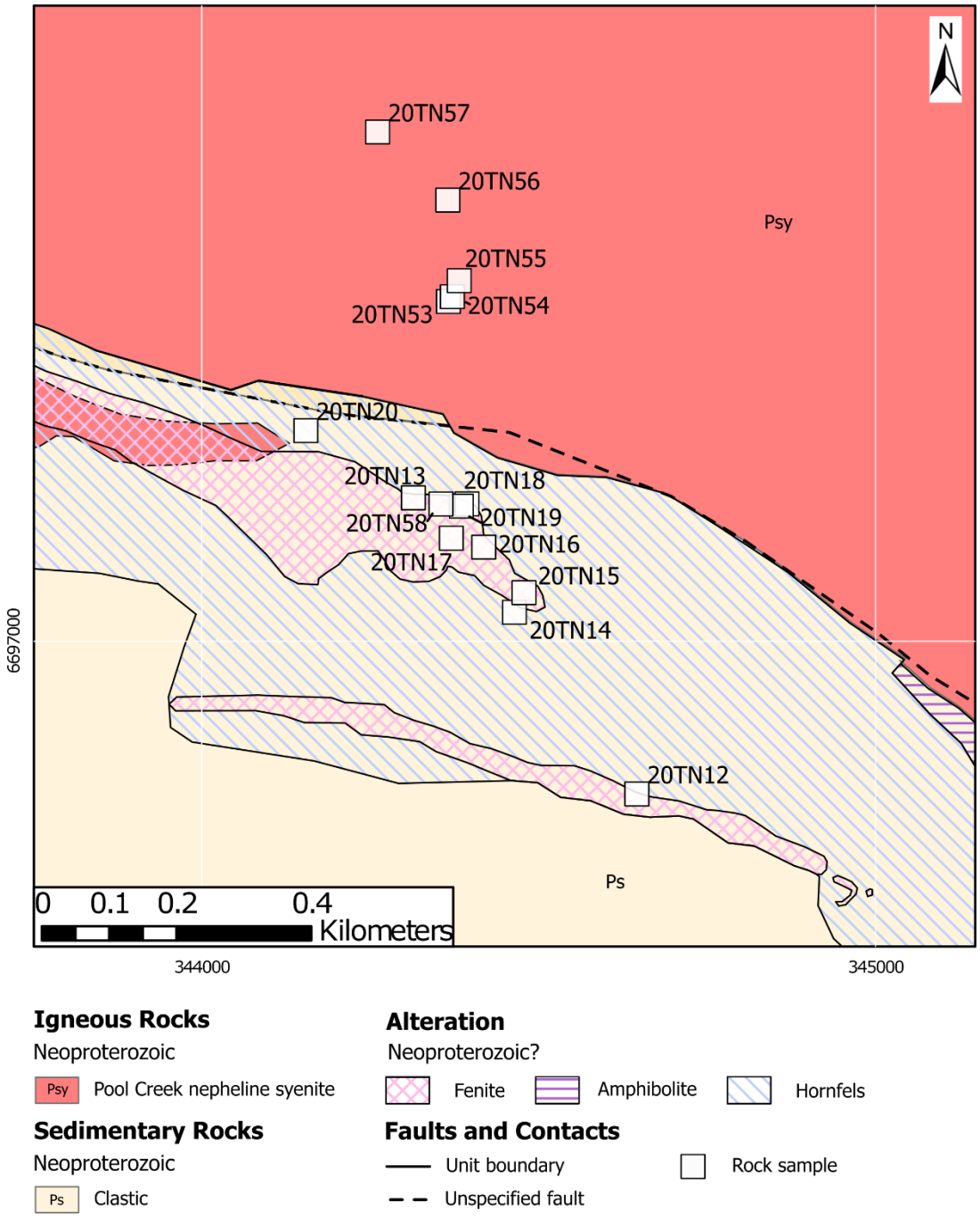

Figure 3.20. Map of samples collected from Pyrochlore Dome in 2020. Map data from Pigage & Mortensen (2004), Swanton (2012), Fallas et al. (2014), and Yukon Geological Survey (2022). UTM Gridlines are NAD 1983 Zone 10.

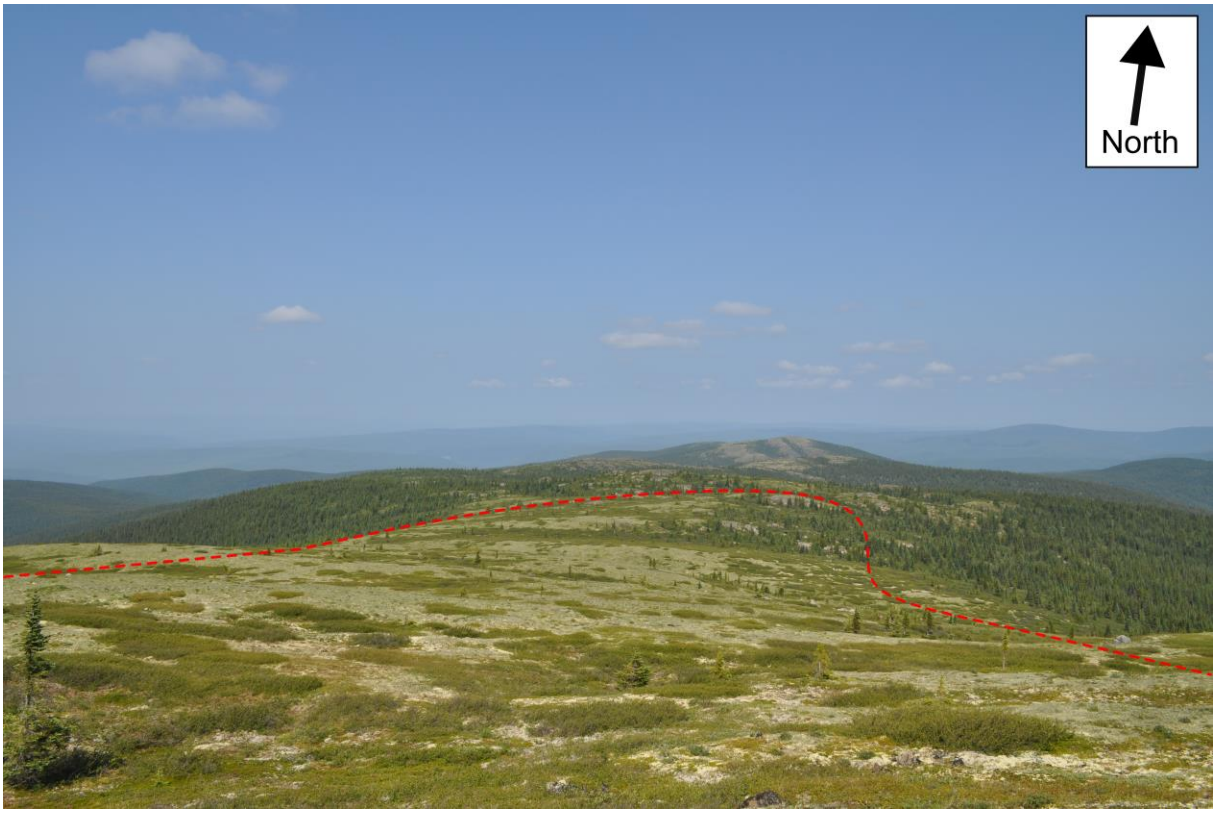

Figure 3.21. Image from the top of Pyrochlore Dome looking north. Sampling did not proceed north of the red dashed line. Image by author.

Dikes

Two compositionally and texturally different dikes were observed crosscutting the nepheline syenite.

Moderately altered feldspar glomeroporphyritic syenite dike

A nonmagnetic, moderately altered, columbite-rhodochrosite-bastnäsite bearing feldspar glomeroporphyritic syenite dike (20TN54) was observed to crosscut the nepheline syenite unit north of the North Fenite Zone (Figure 3.22). Weathered surfaces of the dike are dark grey with rusty orange staining and covered in lichen. Fresh surfaces of the dike are dark grey with a faint pink tint. Phenocrysts are visible in hand sample and are pink and clear to cloudy white in colour.

Petrographic images of characteristic textures of the sample are shown in Figure 3.23. Glomerophyre (up to 3.2 mm) are composed of fine to medium grained (~1.2 × 0.4 to 0.5 × 0.2 mm) euhedral albite crystals that show polysynthetic twins. The groundmass is dominantly composed of fine grained (< 1 × 0.3 mm), euhedral to subhedral laths of fine grained, turbid-looking, mild to moderately sericitized potassium feldspar. Potassium felspar crystals commonly show carlsbad twins. Fine grained (<0.5 mm) albite is present in the groundmass as discrete, subhedral, interstitial crystals. Zircon crystals are fine grained (<0.5 mm), subhedral, fractured, and are commonly obscured by opaques. Fine grained opaque minerals and very to ultra fine-grained white and brown micas are interstitial and pervasive throughout the groundmass (these phases may be replacing a previous interstitial phase). Carbonate minerals are very fine grained, subhedral to anhedral, and occur with opaque minerals. Carbonate minerals were analyzed with the electron microprobe and are compositionally rhodochrosite, calcite, and bastnäsite.

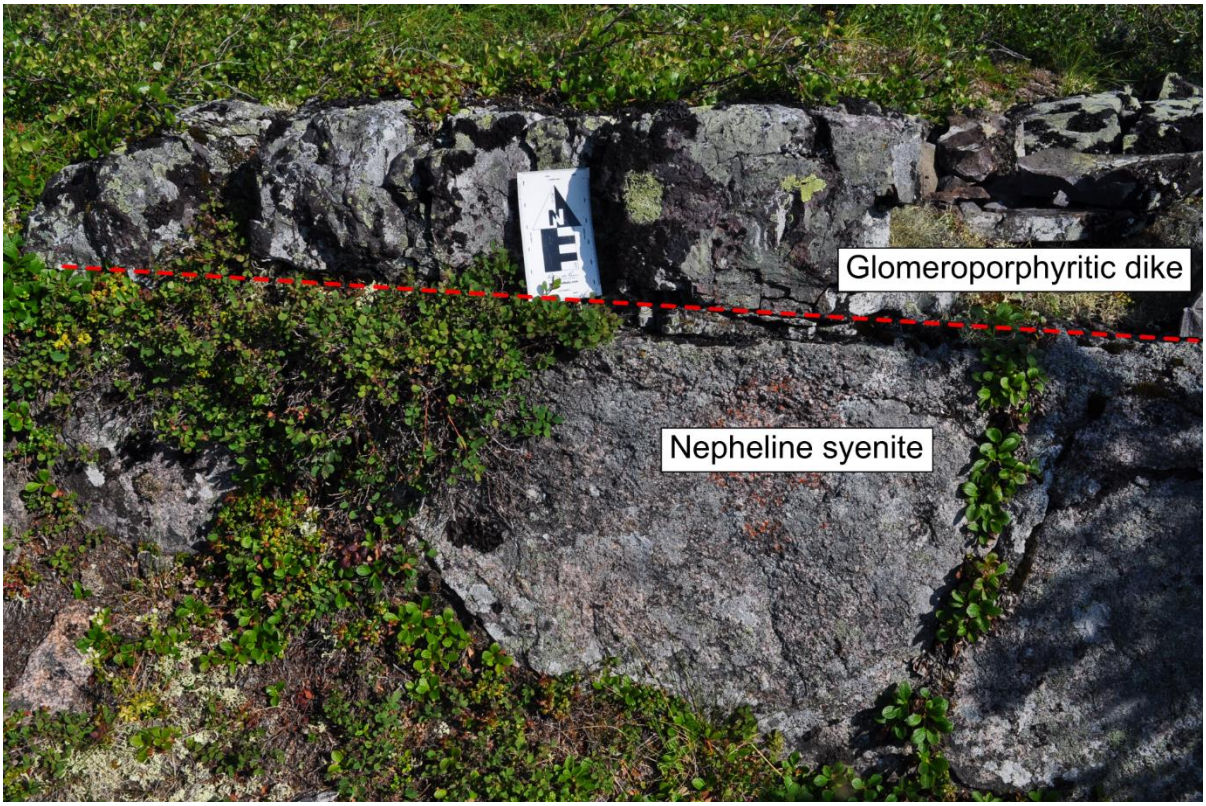

Figure 3.22. Outcrop where nepheline syenite and feldspar glomeroporphyritic syenite samples (20TN53 and 20TN54, respectively) were collected. The red dashed line outlines the contact between the two units. The arrow on the card is pointing north.

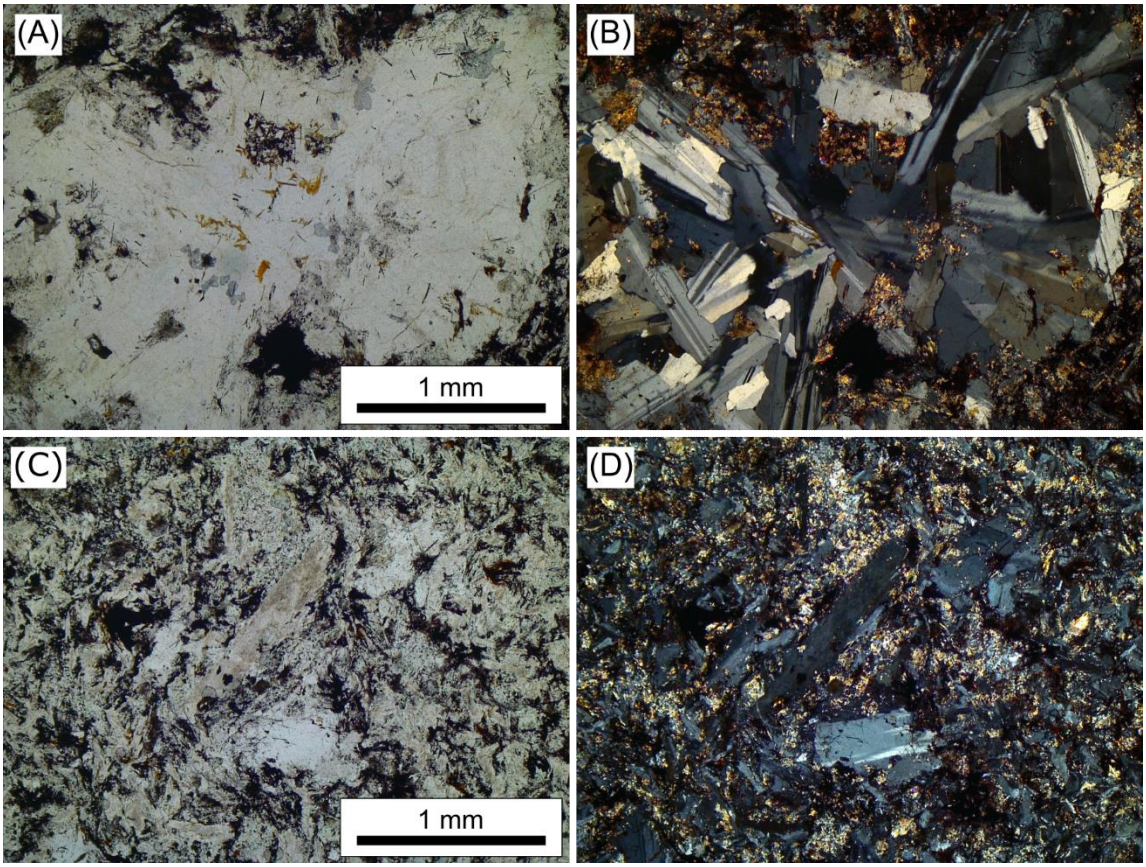

Figure 3.23. Characteristic textures of the feldspar glomeroporphyritic dike sample 20TN54. (A, B) Feldspar glomerophyre in plane polarized light and cross polarized light, respectively. (C, D) Fine-grained alkali feldspar groundmass with pervasive sericite and opaque minerals in plane polarized light and cross polarized light, respectively. (A, C) Plane polarized light. (B, D) Cross polarized light.

Strongly altered porphyritic apatite-carbonate-feldspar-phlogopite lamprophyre(?) dike

A small, broken-up, weathered dike crosscutting a nepheline syenite outcro*p* (Figure 3.24) *was* sampled (20TN57B and 20TN57C). The hand sample is fine grained, black, shimmery, and magnetic. Petrographic images of characteristic textures of the sample are shown in Figure 3.25. The sample is strongly altered to phlogopite and composed of completely altered phenocrysts. The phenocrysts are fine to medium grained (4–0.5 mm), hexagonal, prismatic, euhedral, and completely pseudomorphed by one or a combination of calcite, albite, phlogopite, chlorite, and opaque minerals. Phenocrysts that are dominantly replaced by sericite were likely nepheline, and phenocrysts that are dominantly replaced by phlogopite were likely hornblende. Some phenocrysts are surrounded by a halo of phlogopite. The groundmass is composed of fine grained (< 0.5 mm) phlogopite, albite, calcite, opaque minerals, and minor amounts of chlorite and sericite. Minor amounts of fine to very fine grained (< 1 mm), euhedral to subhedral apatite are disseminated in the groundmass. Trace amounts of a very fine-grained (< 0.1 mm) high relief phase (titanite or zircon?) is present in aggregates within the groundmass. Two types of veins were observed in the dike: a phlogopite fracture-filled vein, and an albite lined vein infilled with calcite and opaque minerals. The protolith of this altered dike is likely lamprophyre or lamproite based on the presence of phenocrysts and the high abundance of femic minerals.

Figure 3.24. Nepheline syenite outcrop where samples 20TN57A to 20TN57C were collected. The red arrow points to the location on the outcrop where the altered porphyritic dike was collected (dike not visible in the photo).

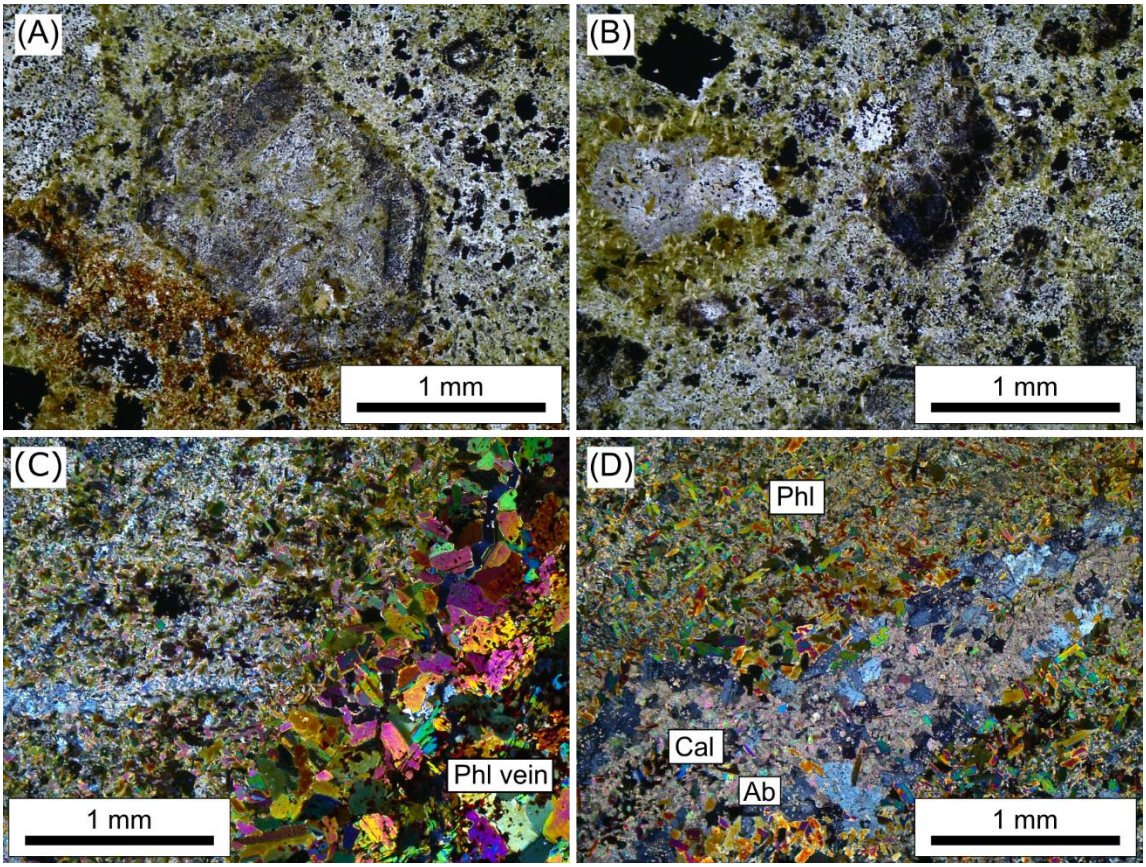

Figure 3.25. Characteristic textures of the porphyritic dike samples 20TN57B and 20TN57C. (A, B) Completely altered phenocrysts in a very fine grained groundmass. (C) Phlogopite fracture filled vein. (D) Calcite and albite vein. (A, B) Plane polarized light. (C, D) Cross polarized light. Ab – albite, Cal – calcite, Phl – phlogopite. (A, B) Plane polarized light. (C, D) Cross polarized light.

Nepheline alkali feldspar syenite

Samples of very coarse to coarse grained, phaneritic nepheline alkali feldspar syenite (20TN53, 20TN55, 20TN56, 20TN57A) were collected from distinct knobby outcrops on Pyrochlore Dome (Figure 3.26). Hand samples are moderately friable and nonmagnetic. Weathered surfaces are stained a red-brown oxidized colour. Nonweathered surfaces show euhedral red-pink coloured feldspar intergrown with euhedral to subhedral black (altered mafic) to pale green (sericitized nepheline) minerals.

Petrographic images of mineral textures characteristic of the sample suite are shown in Figure 3.27. Potassium feldspar (50–70%) is very coarse to coarse grained (0.5 to 4 cm), perthitic, turbid, euhedral-subhedral and fractured. Albite (5%) occurs as exsolution lamellae in potassium feldspar and as fine-grained (< 1 mm) rectangular laths along potassium feldspar grain boundaries. Nepheline (20–30%) is coarse to medium grained (0.5 to 1.5 cm), euhedral to subhedral, and completely pseudomorphed by very fine-grained sericite. An altered mafic phase (5%) is medium grained (~ 4 mm), euhedral to subhedral, and prismatic. The altered mafic phase is completely replaced by chlorite and biotite with lesser amounts of hematite, rutile, sericite, and albite. Zircon (1–2%) is fine to medium grained (up to 1.2 mm), subhedral, and fractured. More pristine looking zircon crystals are surrounded by potassium feldspar, and more altered looking zircon crystals occur within the altered mafic phase. Apatite (1%) is very fine grained (< 0.1 mm), euhedral, and occurs along grain boundaries between K-feldspar and nepheline or altered mafic minerals. Pyrochlore (<1%) and thorite (<1%) are very fine grained (< 0.1 mm) and occur with and are obscured by opaque minerals. Bastnäsite (<1%) and pyrochlore (<1%) are very fine grained, commonly occur with the altered mafic phase, and are obscured by opaque minerals. Pyrochlore is partially to completely altered to hematite. With respect to the observed mineralogy, the sample suite is miaskitic. Based on the modal mineralogy of the samples, they are altered foid (i.e., nepheline) alkali feldspar syenite.

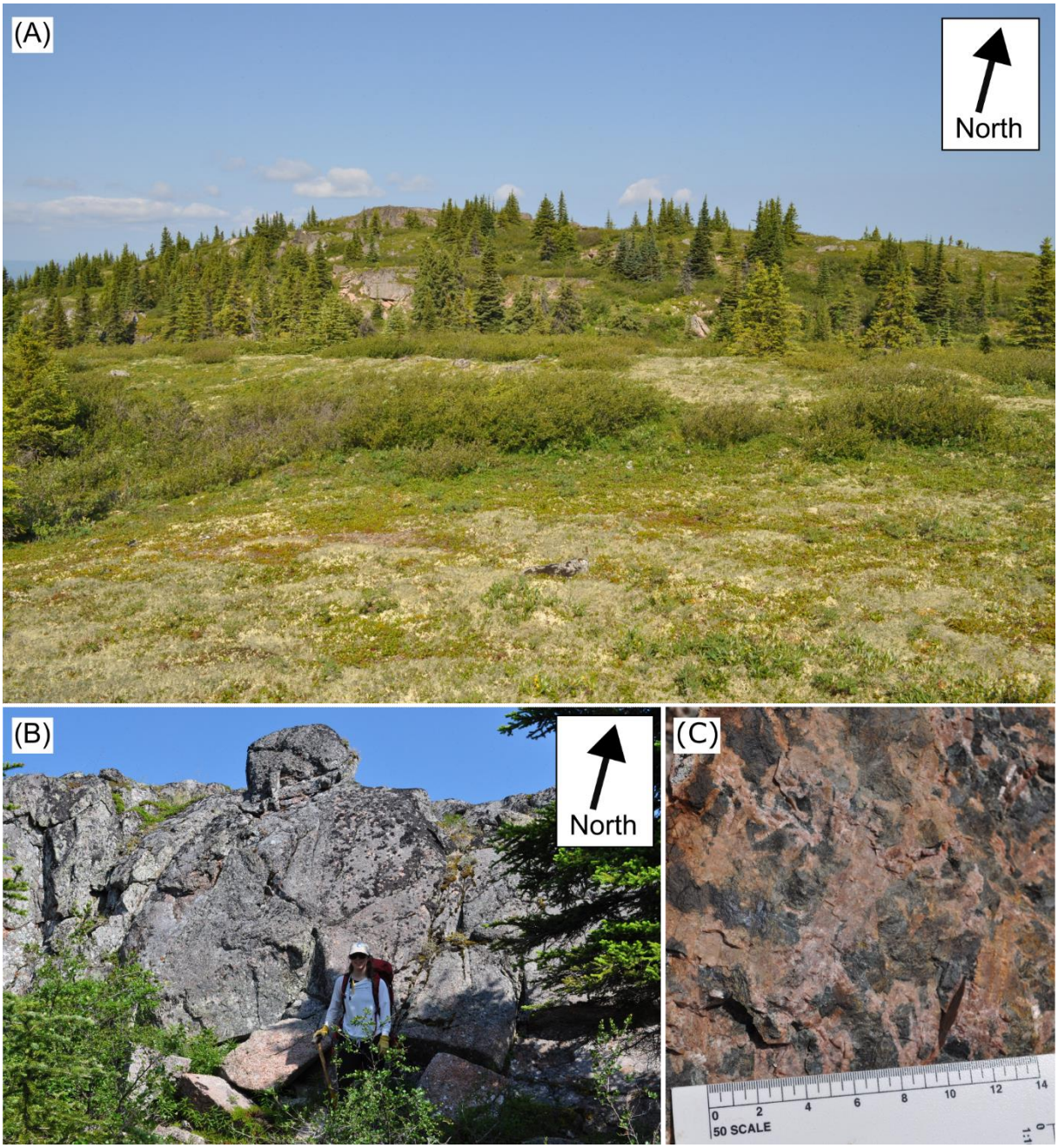

Figure 3.26. Outcrop photos from the nepheline syenite collection sites. (A) View looking approximately north towards nepheline syenite outcrops. (B) Outcrop where sample 20TN56 was collected. Author for scale. (C) Close up view of nepheline syenite outcrop where sample 20TN57A was collected.

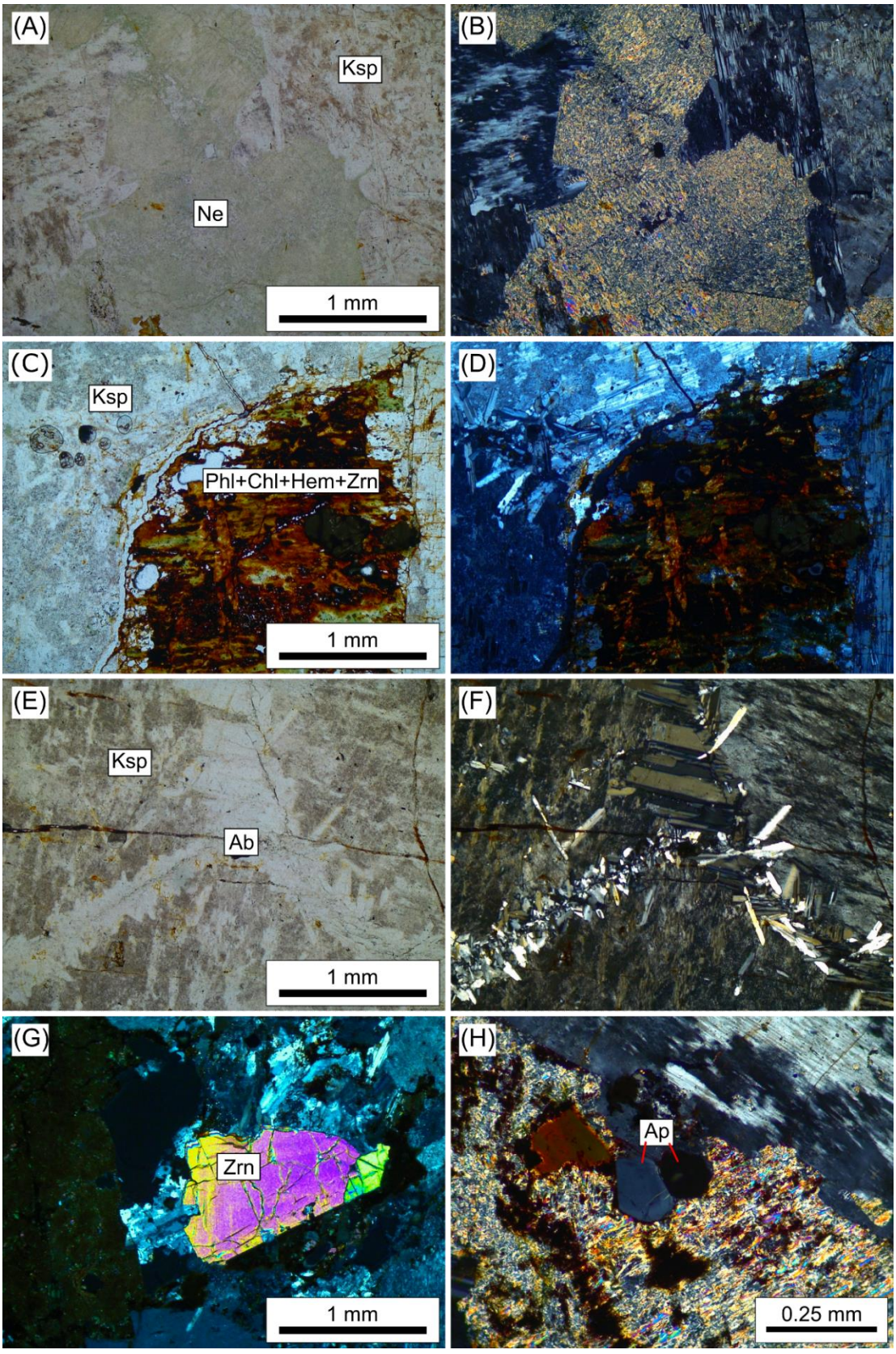
(A)
Ksp
Ne
1 mm
(B)
(C)
Ksp
Phl+Chl+Hem+Zrn
1 mm
(D)
(E)
Ksp
Ab
1 mm
(F)
(G)
Zrn
1 mm
(H)
Ap
0.25 mm

Figure 3.27. Mineral textures of select nepheline syenite samples. (A, B) Nepheline completely pseudomorphed by sericite. (C, D) A former mafic phase completely pseudomorphed by phlogopite, chlorite, and hematite. Note the altered zircon inclusion in the altered mafic phase. (E, F) Fine grained albite rimming coarse grained potassium feldspar. (G) Zircon in altered phase replaced by fine grained alkali feldspar, phlogopite, chlorite, and hematite. (H) Weakly zoned apatite in altered nepheline. (A, C, E) Plane polarized light. (B, D, F, G, H) Cross polarized light. Ab – albite Ksp – potassium feldspar, Phl – phlogopite, Chl – chlorite, Hem – hematite, Zrn – zircon.

Moderately to strongly altered arfvedsonite-aegirine alkali feldspar syenite

Samples of altered arfvedsonite-aegirine alkali feldspar syenite (20TN12, 20TN13, 20TN14, 20TN16, 20TN17A, 20TN18, 20TN19, 20TN20, 20TN58) were collected within a hornfelsed clastic unit (Figure 3.28). Only one contact was observed between an altered arfvedsonite-aegirine syenite (sample 20TN17A), a quartzite (20TN17C), and a quartz-carbonate conglomerate (20TN17B), shown in Figure 3.28C. Samples vary from mildly to moderately magnetic. Weathered surfaces in the field are stained dark red-brown and covered by green and black lichen. Freshly cut surfaces show a fine-grained groundmass that is either pale pink, white, or pale pink and white coloured with fine to coarse grained dark green to black minerals. In many samples the mafic crystals form graded layers with respect to crystal size. Some samples also have zones of coarse to medium grained pink crystals that form aggregates with the dark green to black mafic crystals. Quartz veins (mm to cm-scale) crosscut some of the samples. In hand samples where quartz veins are present, the directly adjacent feldspars are commonly a darker red-pink colour than the more distal pink or white feldspars.

Petrographic images of mineral textures characteristic of the sample suite are shown in Figure 3.29. Depending on the sample, minerals are randomly oriented or show alignment. Mineral alignment is interpreted to be caused by magmatic flow processes (i.e., trachytic texture). Very coarse to fine grained (4 × 1 cm to 1 × 0.5 mm) prismatic and euhedral crystals of partially to fully altered amphibole and pyroxene. Amphibole is green to blue-green pleochroic and is compositionally arfvedsonite. Pyroxene is green to yellow pleochroic, shows normal zoning (i.e, a gradient from core to rim), and is compositionally aegirine to aegirine-augite. Finer grained groundmass feldspars have a granoblastic texture. Fine grained (< 1 mm) groundmass albite and potassium feldspar crystals show polysynthetic twinning and tartan twinning (which sometimes looks chaotic), respectively. Coarser potassium feldspar crystals (5–3 mm) show perthitic texture and sometimes also show tartan twinning. Most groundmass and coarser grained potassium feldspar compositionally transition to albite towards their rims. All potassium feldspar crystals are turbid looking and become more turbid towards quartz veins. Minor to trace amounts of fine to very fine grained (< 1 mm) zircon, biotite, apatite, epidote, allanite, pyrochlore, columbite, and interstitial quartz were observed in the samples. Zircon occurs in the fine-grained feldspars,

in quartz veins and interstitial quartz, and in altered mafics. Zircon crystals vary from clear to being completely amorphous (metamict), and some crystals show visible zoning. Apatite was observed within the feldspar groundmass. Phlogopite, epidote, allanite, pyrochlore, and columbite occur with and directly adjacent to altered mafic minerals.

In the samples with randomly oriented feldspars, the groundmass is dominated by potassium feldspar with albite rims (e.g., 20TN13B). Depending on the sample, feldspars show orientation which vary from weak (e.g., 20TN14 and 20TN18) to moderate (e.g., 20TN20) to strong alignment (i.e., 20TN17A). In sample 20TN14, albite and potassium feldspar dominate the groundmass and both the groundmass and phenocrysts show moderate alignment. In sample 20TN17A, albite laths dominate the groundmass and bend around the less altered zones of coarser potassium feldspar and altered mafic minerals that do not show obvious alignment. In some areas of this sample, the feldspar laths create wavy and kinked textures. Notably, this sample was collected adjacent to a contact with the host rock.

The degree of alteration varies between samples, where primary phases and textures are mildly altered to completely replaced and destroyed. In general, fine-grained albite and fine to medium grained quartz partially to fully replace the coarser grained primary feldspars. Primary mafic minerals (i.e., pyroxene and amphibole) are replaced by hematite, quartz, albite, phlogopite, ± fluorite, and zircon. In the quartz veins and zones, quartz is fine to coarse grained, granoblastic, and commonly contains feldspar and zircon inclusions.

Unlike the nepheline syenite samples, these rocks do not appear to bear nepheline (and if they did there is no sign of it). Additionally, these syenite samples show some sort of systematic layering, are moderately to strongly metasomatized, and have late hematite and quartz alteration, where quartz occurs as veins and replacing mafic minerals. Therefore, these syenite samples are interpreted to be a different intrusive phase than the nepheline syenite. Alteration of the feldspars and phenocrysts has made it challenging to determine the unaltered composition of the samples, however, based on the mineralogy of the less altered zones and relict textures within the strongly altered zones, the samples are interpreted to be altered amphibole aegirine alkali feldspar syenite. Alteration is interpreted to be from late-stage alkali metasomatic fluids (i.e., autometasomatism).

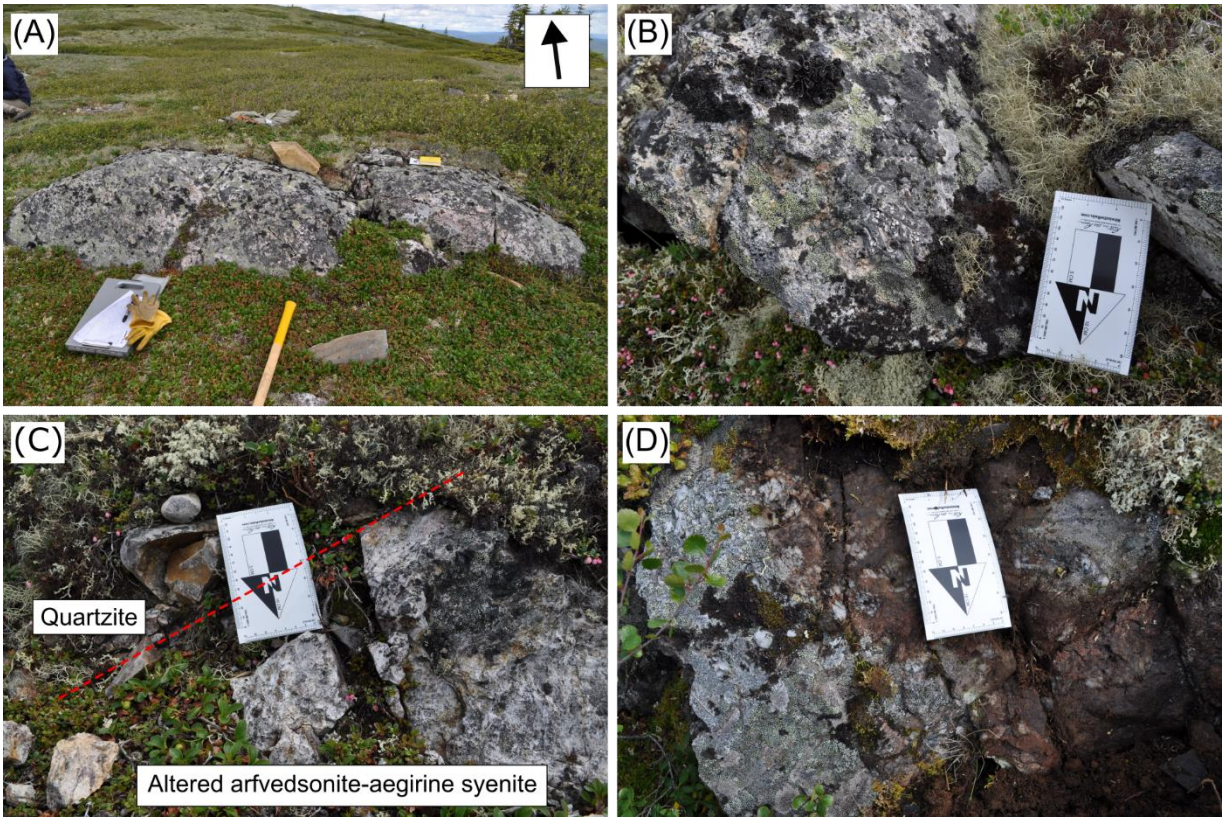

Figure 3.28. Select photos of outcrops sampled on Pyrochlore Dome. Arrows in the images are pointing north. (A) Outcrop from where 20TN12 was sampled. (B) Sample 20TN18 outcrop. Note that black crystals in the outcrop vary in size. (C) Outcrop from where samples 20TN17A to 20TN17C were collected. The red dashed line outlines a rough contact between the units. (D) Outcrop from where 20TN19 was sampled. Note the coarse-grained quartz vein in contact with a dark red altered arfvedsonite-aegirine syenite.

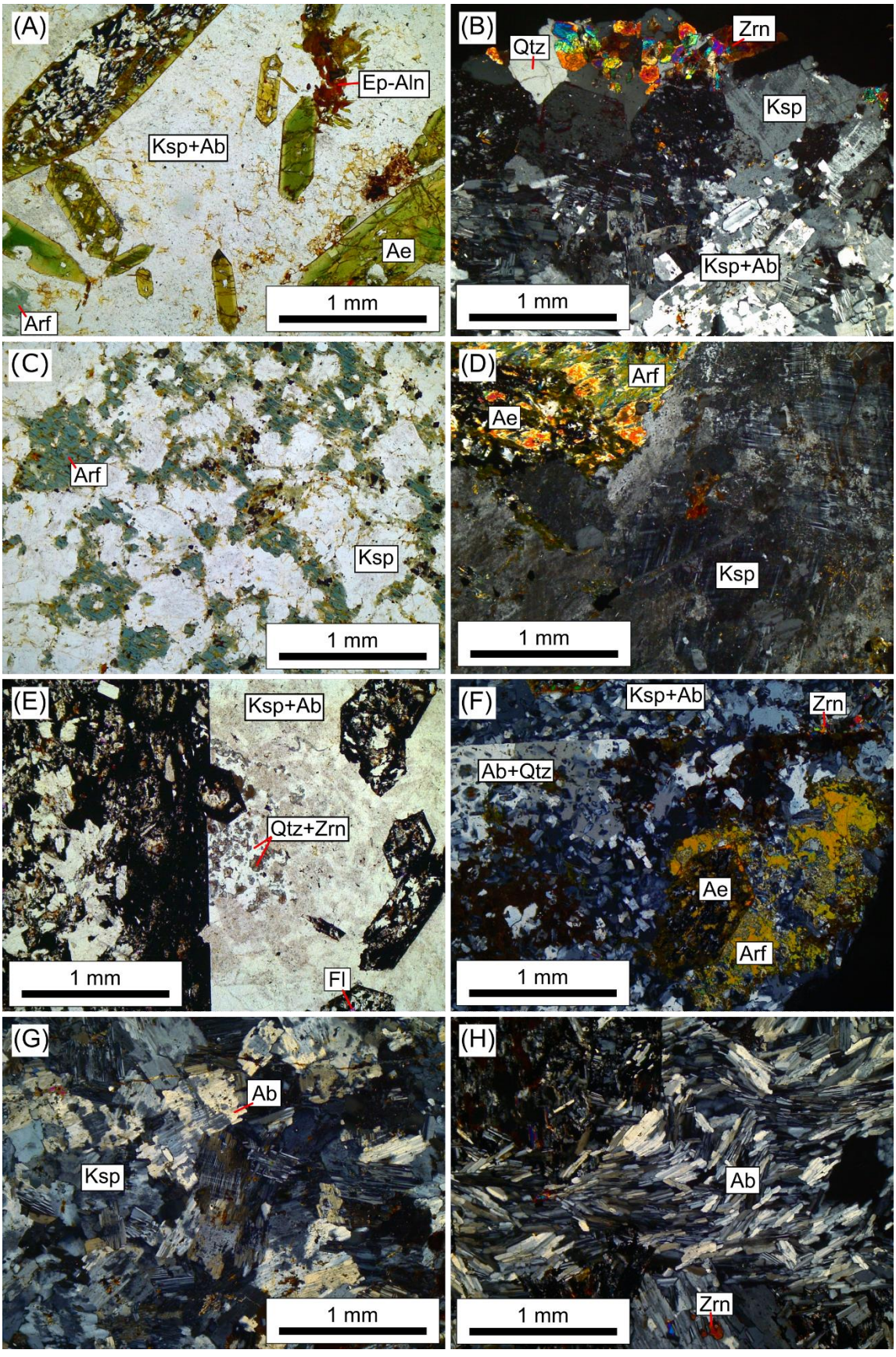
(A)
Ep-Aln
Ksp+Ab
Ae
Arf
1 mm
(B)
Qtz
Zrn
Ksp
Ksp+Ab
1 mm
(C)
Arf
Ksp
1 mm
(D)
Arf
Ae
Ksp
1 mm
(E)
Ksp+Ab
Qtz+Zrn
Fl
1 mm
(F)
Ksp+Ab
Zrn
Ab+Qtz
Ae
Arf
1 mm
(G)
Ab
Ksp
1 mm
(H)
Ab
Zrn
1 mm

Figure 3.29. Mineral textures of select altered arfvedsonite-aegirine syenite samples. (A) Fractured, zoned aegirine in a fine-grained groundmass of alkali feldspar. Some crystals of aegirine are partially included by fine grained feldspar. One crystal is also strongly altered to fine grained feldspars and an opaque phase. (B) Zircon in quartz vein at the edge of the thin section. Alkali feldspar crystals adjacent to the vein show chaotic twinning. (C) Arfvedsonite strongly replaced by fine grained potassium feldspar, phlogopite, and opaque minerals. (D) Turbid alkali feldspar crystals with chaotic twinning and arfvedsonite that is partially replaced by aegirine. (E) Coarse and fine-grained aegirine and arfvedsonite completely replaced by fine grained feldspars, quartz, opaque phases, and fluorite. (F) A coarse-grained crystal completely replaced by albite, quartz, aegirine, and arfvedsonite. (G) Potassium feldspar crystals partially altered to albite along the rims. (H) Strongly aligned albite. (A, C, E) Plane polarized light. (B, D, E, F – H) Cross polarized light. Ab – albite, Ae – aegirine, Aln – allanite, Arf – arfvedsonite, Ep – epidote, Fl – fluorite, Ksp – potassium feldspar, Qtz – quartz, Zrn – zircon.

Layered syenites

Three grab samples of fine to medium grained, layered syenite were collected from a poorly exposed, rubbly outcrop in the North Fenite Zone (Figure 3.30). No contacts were observed with the surrounding host units. Weathered surfaces of the samples are stained a dark brown colour. Fresh surfaces show alternating layers dominated by pink and dark coloured minerals. Due to the rubbly nature of the outcrop, the relationship between the samples from this outcrop is unknown.

Figure 3.30. Outcrop location of layered syenite samples. (A) Rubbly outcrop with Lindsey Abdale for scale. (B) Source boulder for sample 20TN15A. (C) Boulder providing samples 20TN15B and 20TN15C.

Layered titanite-arfvedsonite alkali feldspar syenite

One sample (20TN15A) of a weakly magnetic, layered titanite-arfvedsonite alkali feldspar syenite was collected from the rubbly outcrop (Figure 3.30). Fresh surfaces show alternating millimetre scale layers of pink feldspar and blue-black amphibole. Petrographic images of characteristic textures of the sample are shown in Figure 3.31. Crystals of fine to medium grained (up to 2 × 2 mm) potassium feldspar are turbid, subhedral, and commonly have tartan twinning or perthitic texture. Albite forms fine grained, euhedral to subhedral rectangular laths in the groundmass, commonly replacing edges of potassium feldspar. Arfvedsonite crystals are fine to medium grained (up to 2 × 0.5 mm) and blue to violet pleochroic. Titanite crystals are fine grained (< 1 × 0.2 mm), prismatic, and a pale pink-yellow. Arfvedsonite and titanite are mildly to moderately corroded and show moderate parallel alignment. Zircon occurs as fine grained to very fine grained (< 1 mm), subhedral to anhedral crystals that sometimes occur as aggregates. Very fine grained (< 0.1 mm), euhedral, pyrochlore is present throughout the feldspar groundmass. Crystals are commonly moderately included with feldspars and very fine, clear phases. Quartz is less common in the sample and occurs as a rare interstitial phase between feldspars and around some zircons.

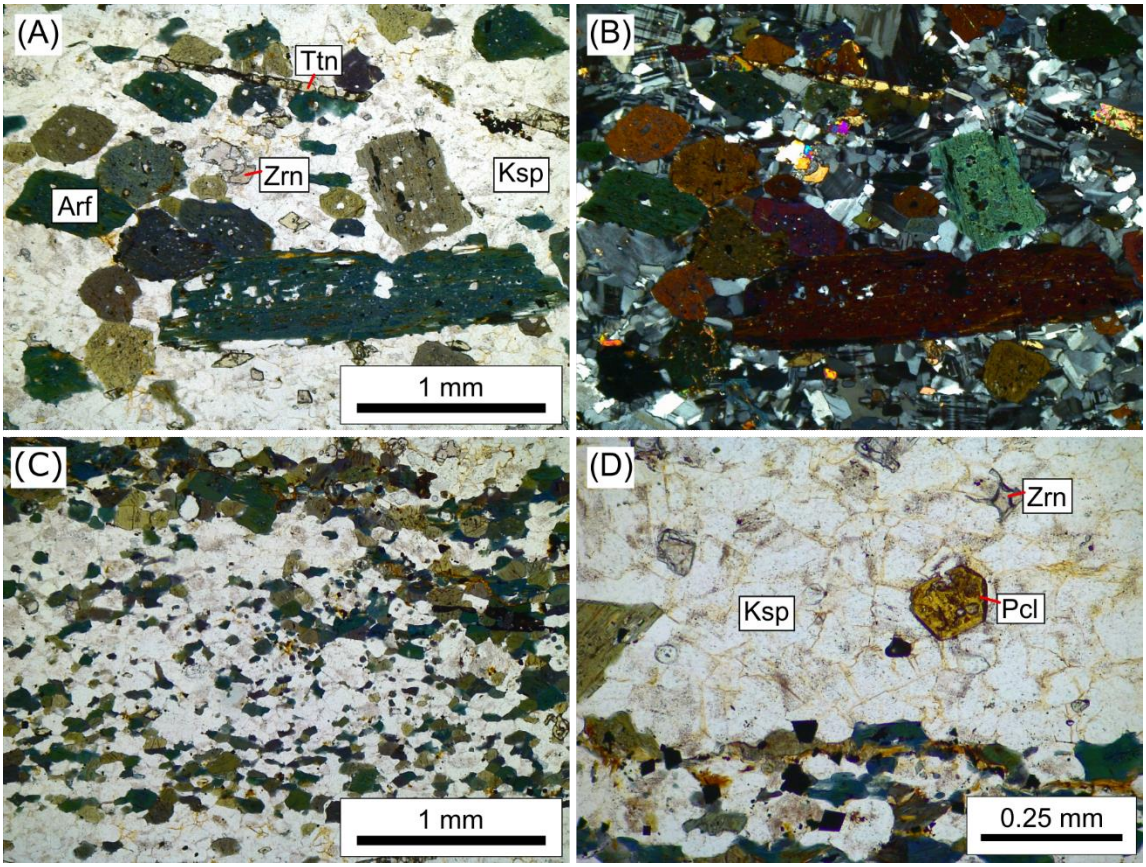

Figure 3.31. Characteristic textures in the layered titanite-arfvedsonite syenite sample 20TN15A. (A, B) show a coarser layer of potassium feldspar and arfvedsonite. (C) Finer layer of potassium feldspar and arfvedsonite. (D) Mildly altered pyrochlore in potassium feldspar. (A, C, D) Plane polarized light. (B) Cross polarized light. Arf – arfvedsonite, Ksp – potassium feldspar, Pcl – Pyrochlore, Ttn – titanite, Zrn – Zircon.

Altered and layered amphibole-diopside-biotite syenite

Two samples (20TN15B and 20TN15C) of altered, fine to very fine grained, layered amphibole-diopside-biotite syenite were collected from rubbly outcrop. Hand samples are almost indistinguishable from 20TN15A, however, the layers in these two samples are thicker (cm-scale) than those in 20TN15A. Layers are distinguished based on grain size and the dominance of phlogopite, diopside, and amphibole crystals. Petrographic images of mineral textures characteristic of the sample suite are shown in Figure 3.32.

The groundmass is composed of fine to very fine grained (< 0.5 mm) potassium feldspar that is partially to completely altered to albite. Feldspar in the phlogopite layers is dominated by albite. Phlogopite is fine grained (up to 1 mm), has irregular grain boundaries, is brown to brown-yellow pleochroic, commonly shows radiation damage halos from micro inclusions, and has lamellae of rutile and hematite. Diopside is fine to very fine grained (up to 0.5 mm), green, fractured, and commonly occurs as aggregates. Amphibole is fine grained (up to 0.5 mm) and has irregular grain boundaries, is green to pale brown-green pleochroic, and occurs in small aggregates in the phlogopite dominant layers. Fine grained (up to 0.5 mm) fluorite, calcite, apatite, titanite, zircon and monazite are common throughout the groundmass. Monazite is yellow to brown, commonly fractured, and partially to completely metamict. Hematite and rutile are common in biotite and a fine grained (up to 1 × 0.3 mm) altered prismatic phase present in all layers. The completely altered prismatic phase is replaced by an undetermined Y-rich alteration phase, and minor amounts of thorite, hematite, and groundmass feldspars. All phases are mildly to moderately included by a variety of very fine-grained phases. These samples show signs of heavy alteration based on the prevalence of inclusions, corroding phases, and albitization of the potassium feldspar.

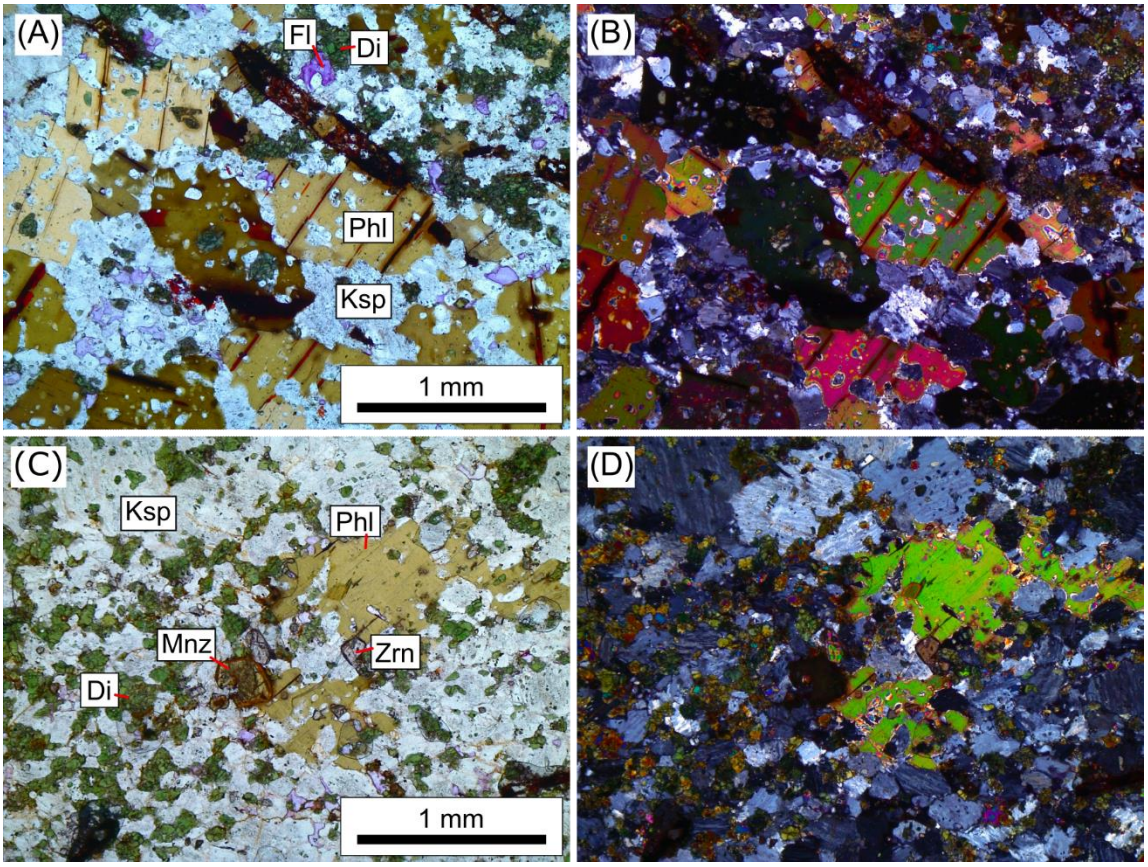

Figure 3.32. Characteristic textures in the layered titanite-arfvedsonite syenite samples 20TN15B and 20TN15C. (A, B) Strongly included phlogopite and a completely altered prismatic phase in plane polarized light and cross polarized light, respectively. (C, D) Zircon and a radially fractured, metamict monazite crystal. (A, C) Plane polarized light. (B, D) Cross polarized light. Di – diopside, Ksp – potassium feldspar, Fl – fluorite, Phl – phlogopite, Mnz – monazite, Zrn – zircon.

Quartzite

An upper fine to lower medium grained granoblastic quartzite sample from the hornfelsed clastic unit (20TN17C) was collected in the North Fenite Zone (Figure 3.28C). This sample was in contact with a conglomerate (20TN17B) and an altered arfvedsonite-aegirine syenite (20TN17A). Weathered surfaces are stained a rusty red-brown. Fresh surfaces have a homogenous creamy white colour. Quartz crystals (~97%) are on the boundary of fine to medium grained (~ 1 mm to 0.5 mm), have a granoblastic texture, have sutured boundaries and are mildly included (Figure 3.33). Inclusions and accessory minerals are very fine grained. Albite (<1%) forms euhedral rectangular laths with polysynthetic twinning and occurs as inclusions within quartz grains and along grain boundaries. Zircon (<<1%) is euhedral and very fine grained. Amphibole and biotite (<<1%) occur with opaque minerals (hematite; 1%) along grain boundaries and fractures in the rock. Trace amounts of monazite and a Pb-bearing mineral were observed with the scanning electron microscope. This quartzite is adjacent to a metasomatized syenite so this sample has likely experienced some degree of contact and metasomatic alteration.

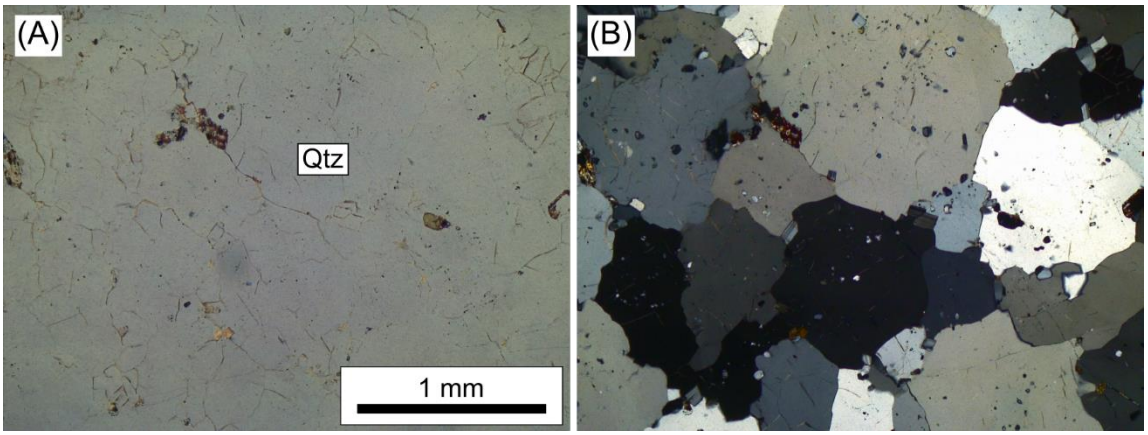

Figure 3.33. Characteristic textures in quartzite sample 20TN17C. (A, B) Granoblastic quartz included by albite and other undetermined phases. (A) Plane polarized light. (B) Cross polarized light. Qtz – quartz.

Monomictic calcite-quartz gravel-pebble ortho-metaconglomerate

A monomictic calcite-quartz gravel-pebble ortho-metaconglomerate sample was collected from the North Fenite Zone at a contact between metasomatized syenite (20TN17A) and quartzite (20TN17C). Weathered surfaces are stained a rusty brown-red and fresh surfaces are beige. Clasts are gravel to pebble sized (up to 1 cm), rounded to subrounded, and composed of very fine to fine grained quartz crystals with interstitial calcite cement (Figure 3.34). The matrix is composed of very fine to fine grained (up to 0.3 mm) interlocking calcite cement with disseminated very fine to fine-grained quartz crystals. Trace amounts of very fine-grained albite with polysynthetic twinning and potassium feldspar tartan twinning occur in the matrix. Fine to very fine-grained opaque minerals (hematite and pyrite) occur with trace amounts of very fine-grained biotite disseminated throughout the rock and along fractures and some grain boundaries. Hematite occurs along fractures within the rock. Interlocking crystals and triple junctions provide evidence that the sample has experienced some degree of recrystallization from contact metamorphism.

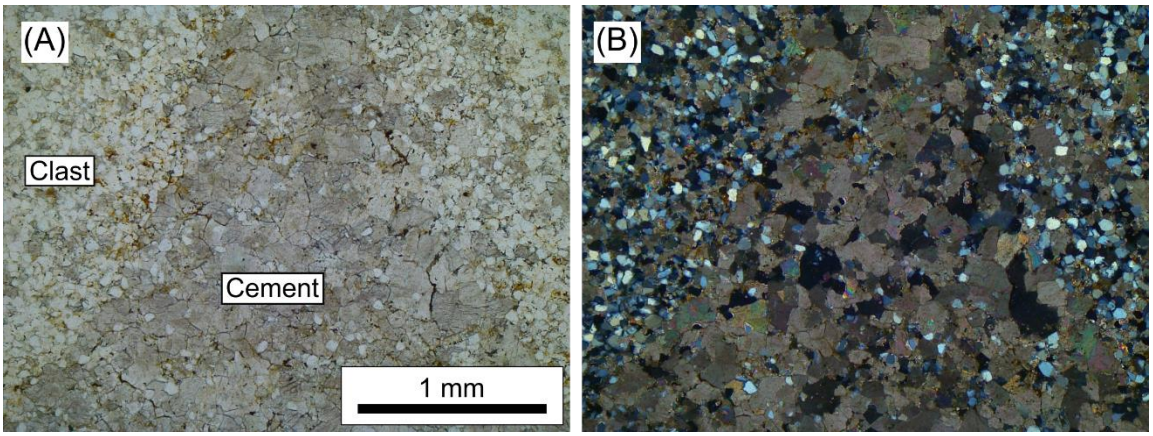

Figure 3.34. Characteristic textures in calcite-quartz metaconglomerate sample 20TN17B. (A, B) recrystallized calcite-quartz clasts cemented by recrystallized calcite. (A) Plane polarized light. (B) Cross polarized light.

Discussion

Variable rock types (syenites, dikes, fenites, volcanic breccias, quartzite, argillite) are described in this thesis. Several samples show evidence of alkali metasomatic alteration and textural evidence for deformation. Evidence for the source of metasomatic alteration, controls on incompatible element distribution, sources of deformation, and implications of the various rock types collected will be discussed below with respect to petrography.

Metasomatic alteration

As reviewed in Chapter 1, alkali metasomatic alteration is common in alkaline-silicate systems (e.g., syenitic intrusions) and occurs in the shallower levels of the intrusion during cooling (e.g., Zharikov et al. 2007; Elliott et al. 2018). Alkali metasomatism associated with syenitic and carbonatite intrusions is known as fenitization (e.g., Elliott et al. 2018). Characteristic mineralogy of alkali metasomatism in syenitic systems include alkali feldspars, sodic amphiboles and pyroxenes, phlogopite, and high field strength and rare earth element phases such as fluorapatite, titanite, and bastnäsite (e.g., Elliott et al. 2018). Evidence for alkali metasomatic alteration was observed in most of the samples reported on in this thesis.

Metasomatic alteration in the nepheline syenite is evidenced by fine grained albitization along potassium feldspar grain boundaries and the replacement of nepheline by sericite and a former mafic phase by hematite, ilmenite, phlogopite, chlorite, and bastnäsite. Two compositionally different dikes crosscut the nepheline syenite. In the altered porphyritic lamprophyre(?) dike, metasomatic alteration is evidenced by pervasive albite and phlogopite. Metasomatic alteration in the feldspar glomeroporphyritic syenite is evidenced by the alteration of former mafic minerals by hematite, ilmenite, rhodochrosite, and bastnäsite.

On Pyrochlore Dome, samples of altered arfvedsonite-aegirine syenite and layered syenites were collected. Metasomatic alteration in the amphibole-aegirine syenite is moderate to strong and is evidenced by recrystallization and replacement of coarse-grained phases to fine-grained alkali feldspars, albitization of potassium feldspar, and partial to complete replacement of pyroxene and amphibole by albite, hematite, rutile, chlorite, and lesser amounts of fluorite, quartz, and

zircon. Notably, late-stage zircon-bearing quartz areas and veins were observed in several of these samples. Metasomatic alteration in the layered syenite samples is evidenced by albitization of potassium feldspar, and abundant inclusions and irregular boundaries of many mineral phases (e.g., albite, fluorite, apatite, calcite). The amphibole-diopside-phlogopite syenite is more altered than the titanite-arfvedsonite syenite, as evidenced by recrystallization textures and the prevalence of fluorite, calcite, and an altered prismatic phase.

On Corundum Dome, actinolite-altered syenite, layered fenite, and brecciated fenite samples were collected. With respect to the actinolite-altered syenite samples, metasomatic alteration is moderate to strong, and is evidenced by albitization of potassium feldspar, altered actinolite aggregates, altered titanite, and the prevalence of epidote, allanite, apatite, hematite, rutile, and fluorite. With respect to the fenites, metasomatic alteration is evidenced by the prevalence of sodic and potassic phases, such as alkali feldspars, fluorite, phlogopite, and arfvedsonite.

Syenitic samples on Pyrochlore Dome and Corundum Dome commonly show potassium feldspar with perthitic texture (i.e., orthoclase) that is partially to completely transformed to tartan twinning (Figure 3.35). Tartan twinning is characteristic of microcline, and alteration of orthoclase to microcline is caused by hydrothermal alteration and tectonic strain (Vernon 2018). The transformation of orthoclase to microcline in this system is interpreted to be caused by hydrothermal alteration.

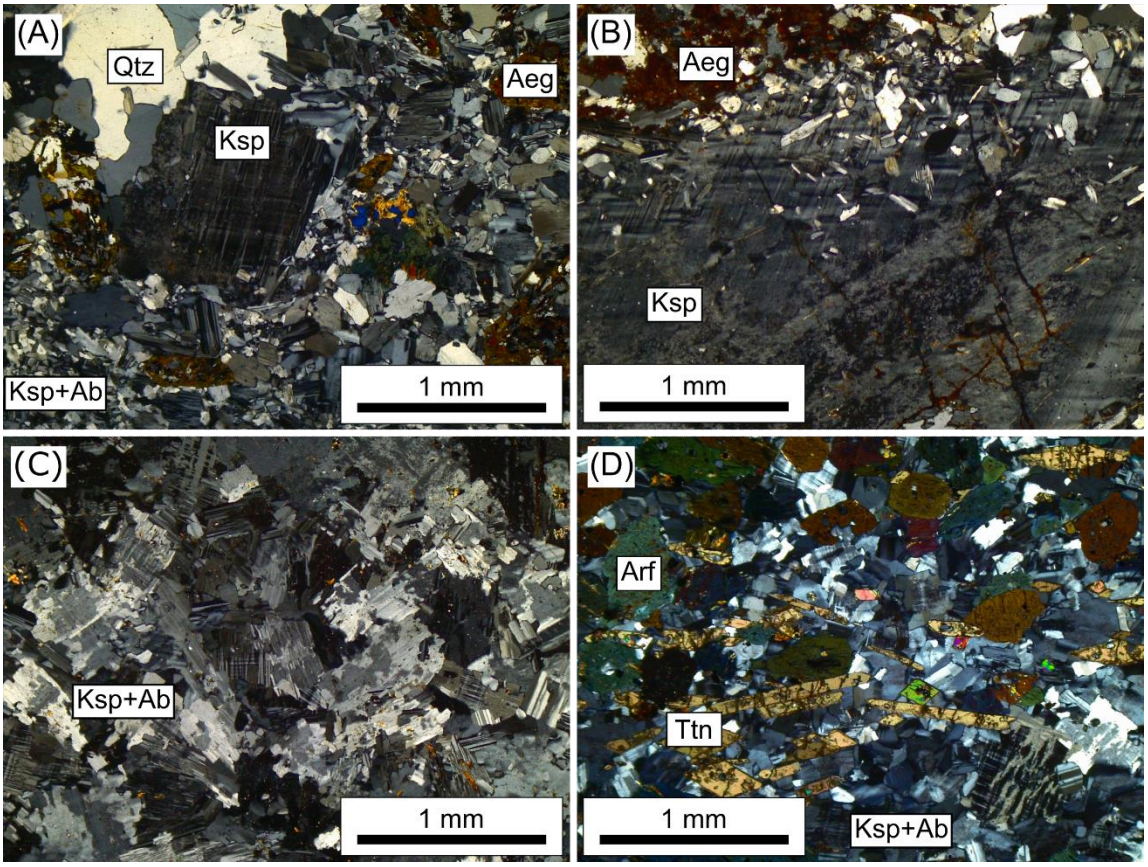

Figure 3.35. Tartan twinning in potassium feldspar from select samples of the arfvedsonite-aegirine syenite and layered titanite-arfvedsonite syenite. All images were taken under cross polarized light. (A, B) Patchy tartan twinning in potassium feldspar from sample 20TN20. (C) Patchy tartan twinning in sample 20TN13. (D) Patchy tartan twinning in sample 20TN15A.

Notably, similarities exist with respect to the primary mineralogy between the nepheline syenite and the altered arfvedsonite-aegirine syenite and actinolite-altered syenite. Similarities include the presence of coarse grained turbid-looking and perthitic potassium feldspar, and fine-grained zircon, apatite, and pyrochlore within these units. The primary mafic phase that has been completely altered in the nepheline syenite may have been amphibole (likely hornblende) based on the composition of its replacement mineralogy. The other altered syenites both have amphiboles that compositionally reflect their minor mineralogy (i.e., more sodic, and more calcic). The subtle similarities between the altered syenites and nepheline syenite indicate that the altered syenites may be autometasomatized nepheline syenite, of which, the mineralogy may be influenced by chemical exchanges between intruding syenitic phase and the adjacent host rock. More field mapping and petrographic investigations need to be conducted to confirm or refute this claim.

In summary, alkali metasomatic alteration observed in the samples across the sampling transect in this study is evidenced by the alkaline mineralogy, mineral textures, and rock textures. With respect to mineralogy and mineral textures, alkaline metasomatic alteration is represented by the partial to complete replacement of primary mineralogy by sodic and potassic phases (i.e., albite, sodic amphiboles, sodic pyroxene, and phlogopite), calcic phases (actinolite, apatite, titanite, epidote, allanite, calcite, fluorite, bastnäsite), and zircon, thorite, rutile, and hematite. With respect to textures observed in outcrop, alkali feldspar-rich zones appear to migrate and brecciate through the host rock or protolith (e.g., Figure 3.10E and Figure 3.13). These zones may be metasomatic fluid pathways.

Based on the interpretations made in this thesis, the sampled outcrops that were mapped as “fenite” by Swanton (2012) are fenitized syenitic phases on Pyrochlore Dome, and fenitized syenitic phases and bedded argillite on Corundum Dome. Notably, these outcrops were mapped as lenticular bodies by Swanton (2012). Are the syenitic phases intruding as lenticular bodies or is this an artifact due to the limit of mapping? If the former, what is controlling the lenticular shape? If the latter, what is the nature of emplacement of the syenitic units? Investigating the nature and controls of emplacement of these syenitic phases is beyond the scope of this thesis.

Distribution of incompatible elements

As reviewed in Chapter 1, Anenburg et al. (2020) discussed controls on the distribution of incompatible elements (i.e., high field strength and rare earth elements) by metasomatic fluids based on experiments with different ionic ligands. They concluded that alkali cations (i.e., K^+ and Na^+) to anionic ligands (i.e., F^- and Cl^-) in a fluid are essential to increase solubility and mobility of REEs which can allow for enhanced concentration of REEs and migration of REEs. They noted that the addition of silica to the system (by the assimilation of silica-rich host into the source intrusion, or alkali-rich fluids reacting with silica-rich host or mixing with foreign fluids) inhibits the migration of incompatible elements. Based on their experiments and evidence from the literature, Anenburg et al. (2020) stated that the addition of silica to the magmatic system can trigger most of the REEs to partition into early formed apatite in the intrusion, with the remaining REEs partitioning into other phosphates and carbonates (e.g., bastnäsite and monazite). Alternatively, if alkali-rich fluids migrating from the intrusion interact with a silica-rich host rock, silica added to the fluid can combine with the alkali cations to form silicate minerals (e.g., alkali feldspars, arfvedsonite, aegirine, phlogopite) followed by the precipitation of REE-phosphates or carbonates. This means that silica-rich fluids migrating through or from an intrusion or silica-rich host rocks interacting with alkali-rich fluids can inhibit the formation of extensive fenite aureoles around the source intrusion, thus most of the REE-bearing minerals will be found within the host intrusion.

The field and petrographic findings in this thesis support the conclusions of Anenburg et al. (2020). Minerals bearing Na, K, and F (e.g., albite, potassium feldspar, fluorite) are prevalent across all of the syenitic and fenite samples, indicating that Na^+, K^+, and F^- ions are the ligands that transported incompatible elements (HFSE and REE) in the metasomatic fluids that altered these rocks. Incompatible elements crystallized in phases such as pyrochlore, columbite, bastnäsite, apatite, monazite, epidote, allanite, titanite, zircon, and thorite, in the syenite and fenite samples. Metasomatic alteration observed by the author is restricted to the intrusion and immediately adjacent rocks in the argillite unit. Late quartz veining indicates that silica-rich fluids were present during metasomatism. Furthermore, the host rocks (clastic and argillite units) are rich in silica, which could be sources of silica to inhibit the transport of incompatible

elements outside of the intrusive phases and in turn, the extent of the fenite aureole. Based on the mineralogy, mineral textures, and distribution of HFSE and REE-bearing mineralization, the author suggests that the described syenitic intrusive phases are the sources of alkali-rich metasomatic (fenitizing) fluids and incompatible element (HFSE and REE) mineralization observed on the Bandito property.

Implications of multiple intrusive phases

As discussed in Chapter 1, alkaline-silicate intrusions commonly form complexes that are commonly composed of distinct ring-shaped intrusions made up of multiple intrusive phases and can have a variety of magmatic structures, for example, dikes, sills, and magmatic layering (e.g., Andersen et al. 2017; Marks & Markl 2017). Alkaline-silicate complexes occur locally to the Pool Creek nepheline syenite, such as the Eocene multiphase Ting Creek alkali intrusion (Harrison 1982), and regionally, to the south in the Canadian Cordillera (e.g., Pell 1994; Millonig et al. 2012), and to the northeast in the Northwest Territories (i.e., Nechalacho layered suite, Möller & Williams-Jones 2016).

The Pool Creek nepheline syenite is currently referred to as a single intrusive unit with localized hornfels and zones of fenite alteration (e.g., Pigage & Mortensen 2004; Swanton 2011, 2012). However, the variability in composition of magmatic rock types and structures over the sampling transect in the small sampling area of this thesis reveals more complex geology than previously described in the literature, indicating that the Pool Creek nepheline syenite is part of a multiphase (i.e., composite) system, composed of multiple types of syenites and dikes. Petrographic reports in Swanton (2011; 2012) and “rock sheets” in Swanton (2012) support this claim as they indicate multiple igneous phases. To clarify the nature of the system and distribution of geologic units making up what is known as the “Pool Creek nepheline syenite”, the author recommends that the Pool Creek nepheline syenite be referred as the Pool Creek alkaline-silicate complex. More detailed mapping of the igneous and metasomatic phases and host rocks should be conducted to gain a better understanding of the distribution and structure of magmatic phases and evolution of the magmatic system.

4 Mineral Composition

To date, no mineral chemistry on the Pool Creek nepheline syenite and alteration on the Bandito property has been publicly reported. This section will supplement the previous chapter on petrography and focus on the mineral chemistry of several silicate, phosphate, carbonate, oxide, and halide mineral groups in samples collected from the country rock, nepheline syenite, actinolite-altered syenite, altered arfvedsonite-aegirine syenite, fenites, and dikes. All electron microprobe (EMP) analyses and respective figures collected of known and unidentified minerals analyzed in this study can be found in Appendix B.

Methods

Quantitative analyses were acquired using a JEOL JXA-iHP200F electron microprobe at the University of British Columbia.

Feldspars, biotite, muscovite, chlorite, amphiboles, pyroxenes, hematite, and ilmenite

Analytical conditions were an accelerating voltage of 15 kV, a beam current of 20 nA, and a beam diameter of 5 microns for feldspars, amphiboles, and pyroxenes.

Feldspar

Elements were acquired using analyzing crystals LIFL for Fe *K*α and Ba *L*α, PETL for Ca *K*α and K *K*α, TAP for Si *K*α and Al *K*α, TAPL for Mg *K*α and Na *K*α, TAP for Si *K*α and Al *K*α, and TAPL for Mg *K*α and Na *K*α. The standards for feldspars were albite (Taylor), $NaAlSi_3O_8$, for Si *K*α, Na *K*a, barite (SPI), $BaSO_4$, for Ba *L*α, diopside (SPI), $MgCaSi_2O_6$, for Ca *K*α, and Mg Kα, hematite (SPI), Fe_2O_3, for Fe *K*α, and orthoclase (SPI), $KalSi_3O_8$, for Al *K*α and K *K*α. The on and off-peak counting time was 20 seconds for all elements.

Amphibole, biotite, muscovite, chlorite, and pyroxene

Elements were acquired using analyzing crystals LIFL for Fe *K*α, Ba *L*α, Mn *K*α, and Ti *K*α, PETL for Ca *K*α and K *K*α, TAP for Al *K*α and Si *K*α, TAPL for Na *K*α, Mg *K*α, and F *K*α, TAP

for Al *K*α and Si *K*α, and TAPL for Na *K*α, Mg *K*α, and F *K*α. The standards for amphiboles, micas, and pyroxene were albite (Taylor), $NaAlSi_3O_8$, for Si *K*α and Na *K*α, corundum (Taylor), Al_2O_3, for Al *K*α, spessartine (Taylor), $Mn_3Al_2Si_3O_{12}$, for Mn *K*α, barite (SPI), $BaSO_4$, for Ba *L*α, diopside (SPI), $MgCaSi_2O_6$, for Mg *K*α, fluorite (SPI), CaF_2, for Ca *K*α and F *K*α, hematite (SPI), Fe_2O_3, for Fe *K*α, rutile (SPI), TiO_2, for Ti *K*α, and orthoclase (SPI), $KalSi_3O_8$, for K *K*α. The counting time was 10 seconds for Mg *K*α, 15 seconds for Na *K*α, F *K*α, and 20 seconds for Ba *L*α, Ca *K*α, K *K*α, Al *K*α, Si *K*α, Mn *K*α, Ti *K*α, and Fe *K*α.

Unknown and standard intensities were corrected for deadtime. Standard intensities were corrected for standard drift over time. Oxygen was calculated by cation stoichiometry and included in the matrix correction. Oxygen equivalent from halogens (F/Cl), was subtracted in the matrix correction. Element H was calculated by difference from 100%. The Phi-Rho-Z matrix correction method utilized was Armstrong/Love Scott (CITZAF) (Armstrong 1988) and the mass absorption coefficients data set was FFAST (Chantler 2005).

Epidote, allanite, titanite, zircon, thorite, apatite, monazite, bastnäsite, rutile, pyrochlore, columbite, fluorite, and unknowns

Analytical conditions were an accelerating voltage of 15 kV, a beam current of 20 nA, and a beam diameter chosen between 1 and 10 microns depending on grain size and phase.

Elements were acquired using analyzing crystals LIFL for Fe *K*α, Mn *K*α, Ti *K*α, Hf *L*α, La *L*α, Ce *L*α, Nd *L*α, Ta *M*α, Sm *L*α, Gd *L*α, Pr *L*α, Eu *L*α, Tb *L*α, Dy *L*α, Ho *L*α, Er *L*α, Tm *L*α, Yb *L*α, and Lu *L*α, PETL for Zr *L*α, K *K*α, Ca *K*α, Th *M*α, Y *L*α, Nb *L*α, and U *M*β, PETJ for P *K*α, Pb *M*α, and Cl *K*α, PETL for Zr *L*α, K *K*α, Ca *K*α, Th *M*α, Y *L*α, Nb *L*α, and U *M*β, and TAPL for Si *K*α, F *K*α, Al *K*α, Na *K*α, and Mg *K*α. The standards were Hf (Astimex) for Hf *L*α, albite (Taylor), $NaAlSi_3O_8$, for Si *K*α, corundum (Taylor), Al_2O_3, for Al *K*α, spessartine (Taylor), $Mn_3Al_2Si_3O_{12}$, for Mn *K*α, columbite, $MnNb_2O_6$, for Nb *L*α, Ta (Astimex) for Ta *M*α, uranium oxide (Taylor), UO_2, for U *M*β, thorium oxide (Taylor), ThO_2, for Th *M*α, YPO_4 (NMNH168499) for Y *L*α, $LaPO_4$ (NMNH168490) for La *L*α, $CePO_4$ (NMNH168484) for Ce *L*α, $PrPO_4$ (NMNH168493) for Pr *L*α, $NdPO_4$ (NMNH168492) for Nd *L*α, $SmPO_4$ (NMNH168494) for Sm *L*α, $EuPO_4$ (NMNH168486) for Eu *L*α, $GdPO_4$ (NMNH168488) for Gd

*L*α, $TbPO_4$ (NMNH168496) for Tb *L*α, $DyPO_4$ (NMNH168485) for Dy *L*α, $HoPO_4$ (NMNH168489) for Ho *L*α, $ErPO_4$ (NMNH168486) for Er *L*α, $TmPO_4$ (NMNH168497) for Tm *L*α, $YbPO_4$ (NMNH168498) for Yb *L*α, $LuPO_4$ (NMNH168491) for Lu *L*α, apatite (SPI), $Ca_5(PO_4)_3F$, for Ca *K*α and P *K*α, crocoite (SPI), $PbCrO_4$, for Pb *M*α, diopside (SPI), $MgCaSi_2O_6$, for Mg *K*α, fluorite (SPI), CaF_2, for F *K*α (except for apatite, apatite (SPI), $Ca_5(PO4)_3F$, for F *K*α), hematite (SPI), Fe_2O_3, for Fe *K*α, rutile (SPI), TiO_2, for Ti *K*α, orthoclase (SPI), $KAlSi_3O_8$, for K *K*a, tugtupite (SPI), $Na_4BeAlSi_4O_{12}Cl$, for Na *K*α and Cl *K*α, and cubic zirconia (SPI), ZrO_2, for Zr *L*α.

The on peak counting time was 10 seconds for Ca *K*α, K *K*α, 20 seconds for Fe *K*α, Si *K*α, Mg *K*α, Al *K*α, Na *K*α, Mn *K*α, Ti *K*α, Hf *L*α, Ta *M*α, Th *M*α, U *M*β, P *K*α, Gd *L*α, Zr *L*α, Tb *L*α, Dy *L*α, Ho *L*α, Er *L*α, Tm *L*α, Yb *L*α, and Lu *L*α, 30 seconds for Pr *L*α, Eu *L*α, Ce *L*α, Nb *L*α, Cl *K*α, Y *L*α, Sm *L*α, F *K*α, and La *L*α, and 40 seconds for Nd *L*α and Pb *M*α. The off peak counting time was 10 seconds for Ca *K*α, K *K*α, Th *M*α, and U *M*β, 20 seconds for Mg *K*α, Al *K*α, Na *K*α, Mn *K*α, Ti *K*α, Hf *L*α, Fe *K*α, Si *K*α, P *K*α, Gd *L*α, Zr *L*α, Tb *L*α, Dy *L*α, Ho *L*α, Er *L*α, Tm *L*α, Yb *L*α, and Lu *L*α, 30 seconds for Pr *L*α, Eu *L*α, Ce *L*α, Nb *L*α, Cl *K*α, Y *L*α, Sm *L*α, F *K*α, and La *L*α, and 40 seconds for Nd *L*α and Pb *M*α. The off-peak background fitting method was Multi-Point for all WDS elements (see Allaz et al. 2019).

Unknown and standard intensities were corrected for deadtime. Standard intensities were corrected for standard drift over time. Interference corrections were applied to F for interference by P, Ce, and to Nd for interference by Ce, and to Cl for interference by Nd, and to Sm for interference by Ce, and to Gd for interference by La, Ce, and Nd, and to Eu for interference by Pr, and to Dy for interference by Eu and Yb, and to Ho for interference by Lu, and to Er for interference by Tb, and to Tm for interference by Dy, and to Yb for interference by Ho and Tb, and to Lu for interference by Ho, Dy, and Er (see Donovan et al. 1993). Oxygen was calculated by cation stoichiometry and was included in the matrix correction. Oxygen equivalent from halogens (F/Cl/Br/I), was subtracted in the matrix correction. The Phi-Rho-Z matrix correction method utilized was Armstrong/Love Scott (CITZAF) (see Armstrong 1988).

Silicate compositions

Silicate minerals are prevalent in all units within the 2020 sampling area on Pyrochlore Dome and Corundum Dome. To demonstrate the variation in silicate chemistry across the sampled suite of units, analyses from select samples are reported in this section. Silicate mineral compositions reported in this section include feldspar, mica, chlorite, amphibole, epidote, allanite, titanite, zircon, and thorite.

Feldspar

Feldspar-group minerals are present in all the sampled units in this study. Average feldspar compositions from select samples of the argillite, nepheline syenite, actinolite-altered syenite, altered arfvedsonite-aegirine syenite, fenites, and porphyritic dikes are shown in Table 4.1. All feldspar analyses are plotted on the feldspar composition ternary diagram in Figure 4.1.

Across all the analyzed feldspar samples, Si *apfu* range from 2.805 to 3.047, Al *apfu* from 0.914 to 1.232, Fe^{3+} *apfu* from 0.000 to 0.051, Fe^{2+} *apfu* from 0.000 to 0.042, Mg *apfu* from 0.000 to 0.087, Ba *apfu* from 0.000 to 0.009, Ca *apfu* from 0.000 to 0.190, Na *apfu* from 0.015 to 1.017, and K *apfu* from 0.001 to 1.044.

Most of the reported feldspars compositions are close to the two alkali feldspar endmembers, orthoclase ($KalSi_3O_8$) and albite ($NaAlSi_3O_8$). Potassic and sodic compositions range from $Or_{98.55}Ab_{1.45}$ to $Ab_{99.84}Or_{0.13}An_{0.03}$. The most calcic compositions are found in the argillite unit, where the most calcic composition analyzed is $Ab_{79.77}An_{18.32}Or_{1.91}$. Feldspars analysed with relatively higher calcic compositions (i.e., ≥ 0.39 CaO wt. %) have lower Si (2.805 *apfu*) and elevated Al (1.187 *apfu*) in comparison to the other analyses. In addition to albite and orthoclase end member compositions, the layered amphibole-diopside-phlogopite syenite sample (20TN15B) has compositions intermediate between orthoclase and albite, $Or_{53.85}Ab_{45.87}An_{0.28}$

As discussed in Chapter 3, albite, and orthoclase occur in minor amounts as discrete crystals or in lithic fragments in the argillite. In the syenite and fenite samples, albite is common and occurs as an exsolution phase in perthitic orthoclase and commonly replaces orthoclase from rim to core (Figure 4.2). The replacement of orthoclase by albite is indicative of sodic metasomatic alteration (e.g., Elliott et al. 2018).

Table 4.1. Average composition of feldspar from various rock types across the 2020 Corundum Dome and Pyrochlore Dome sampling area.

unit (sample)	argillite (20TN5, 20TN24A)		actinolite-altered syenite (20TN4D, 20TN6-2, 20TN10C)		altered arfvedsonite-aegirine syenite (20TN13B-2, 20TN20)		nepheline syenite (20TN55A, 20TN57A, 20TN53)		layered syenites (20TN15A, 20TN15B)		fenites (20TN3-2, 20TN4A, 20TN7, 20TN25D)		feldspar porphyritic lamprophyre(?) dike (20TN54)	
analysis	average	σ	average	σ	average	σ	average	σ	average	σ	average	σ	average	σ
n	7		12		8		31		12		14		3	
SiO_2 (wt. %)	64.77	0.29	65.01	0.63	64.40	0.61	64.91	0.96	65.38	0.52	64.34	0.68	63.40	0.82
Al_2O_3	17.85	0.16	17.65	0.22	17.25	0.52	17.66	0.37	17.75	0.44	17.87	0.29	17.20	0.15
Fe_2O_3*	0.28	0.05	0.07	0.06	0.61	0.45	0.18	0.16	0.34	0.33	0.25	0.20	0.46	0.32
FeO*	0.00	0.00	0.05	0.10	0.13	0.18	0.04	0.14	0.00	0.00	0.00	0.00	0.00	0.00
MgO	0.02	0.02	0.00	0.00	0.03	0.07	0.02	0.04	0.00	0.00	0.09	0.18	0.42	0.57
BaO	0.10	0.07	0.09	0.07	0.03	0.02	0.06	0.07	0.20	0.12	0.16	0.13	0.03	0.02
CaO	0.04	0.01	0.00	0.01	0.04	0.07	0.14	0.65	0.02	0.02	0.03	0.06	0.03	0.02
Na_2O	0.22	0.02	0.26	0.06	0.24	0.03	0.38	0.33	1.19	1.79	0.26	0.06	0.24	0.03
K_2O	17.17	0.06	17.34	0.12	17.19	0.11	16.89	0.54	15.80	2.72	17.10	0.25	16.78	0.34
Total	100.46	0.38	100.47	0.84	99.90	0.98	100.27	0.64	100.69	0.55	100.11	0.36	98.56	0.37
Si (*apfu*)	3.000	0.006	3.011	0.003	3.006	0.016	3.008	0.021	3.008	0.005	2.993	0.023	2.995	0.029
Al	0.975	0.007	0.964	0.005	0.949	0.025	0.964	0.017	0.963	0.017	0.980	0.018	0.958	0.007
Fe^{3+}	0.010	0.002	0.004	0.003	0.026	0.011	0.007	0.006	0.012	0.011	0.009	0.007	0.016	0.012
Fe^{2+}	0.000	0.000	0.000	0.000	0.000	0.000	0.000	0.000	0.000	0.000	0.000	0.000	0.000	0.000
Mg	0.002	0.001	0.000	0.000	0.002	0.005	0.001	0.003	0.000	0.000	0.006	0.013	0.029	0.041
Ba	0.002	0.001	0.002	0.001	0.001	0.000	0.001	0.001	0.004	0.002	0.003	0.002	0.001	0.000
Ca	0.002	0.001	0.000	0.000	0.002	0.003	0.007	0.033	0.001	0.001	0.001	0.003	0.002	0.001
Na	0.020	0.002	0.024	0.006	0.021	0.002	0.034	0.029	0.105	0.157	0.023	0.005	0.022	0.003
K	1.015	0.005	1.025	0.010	1.023	0.010	0.999	0.035	0.929	0.164	1.015	0.012	1.011	0.016
Cation sum	5.025	0.003	5.029	0.006	5.029	0.007	5.022	0.014	5.021	0.005	5.031	0.008	5.034	0.014
Or (mol %)	97.90	0.19	97.71	0.55	97.79	0.40	96.10	3.80	89.65	15.48	97.61	0.52	97.75	0.19
Ab	1.93	0.16	2.27	0.53	2.03	0.22	3.29	2.90	10.26	15.38	2.25	0.50	2.11	0.26
An	0.18	0.06	0.02	0.03	0.18	0.31	0.61	2.82	0.08	0.11	0.14	0.30	0.15	0.09

Note: Compositions were recalculated on the basis of 8 O *apfu*. * Determined by stoichiometry using Droop (1987) calculation method.

Table 4.1. Continued…

unit (sample)	argillite (20TN5, 20TN24A)		actinolite-altered syenite (20TN4D, 20TN6-2, 20TN10C)		altered arfvedsonite-aegirine syenite (20TN13B-2, 20TN20)		nepheline syenite (20TN55A, 20TN57A, 20TN53)		layered syenites (20TN15A, 20TN15B)		layered fenites (20TN3-2, 20TN4A, 20TN23, 20TN25D)		altered feldspar porphyritic dike (20TN54)		altered porphyritic lamprophyre(?) dike (20TN57C-1)	
analysis	average	σ	average	σ	average	σ	average	σ	average	σ	average	σ	average	σ	average	σ
n	11		10		16		30		9		15		2		5	
SiO_2 (wt. %)	66.24	18.39	69.26	0.30	68.32	0.69	68.99	0.50	68.51	0.52	68.61	0.43	68.43	0.18	68.87	0.26
Al_2O_3	20.24	5.74	19.01	0.37	18.66	0.63	19.02	0.26	18.74	0.44	19.02	0.30	18.80	0.13	19.09	0.15
Fe_2O_3*	0.39	0.35	0.03	0.05	0.22	0.31	0.07	0.12	0.38	0.42	0.11	0.11	0.11	0.11	0.19	0.11
FeO*	0.02	0.07	0.15	0.10	0.92	0.42	0.11	0.09	0.32	0.39	0.10	0.12	0.09	0.09	0.04	0.05
MgO	0.16	0.28	0.00	0.00	0.00	0.00	0.02	0.07	0.00	0.00	0.00	0.00	0.00	0.00	0.13	0.20
BaO	0.01	0.01	0.01	0.02	0.01	0.01	0.01	0.01	0.04	0.04	0.01	0.02	0.02	0.01	0.01	0.01
CaO	0.92	1.04	0.01	0.01	0.01	0.00	0.01	0.02	0.03	0.04	0.04	0.07	0.00	0.00	0.08	0.08
Na_2O	10.87	3.12	11.83	0.08	11.58	0.14	11.69	0.10	11.04	1.63	11.78	0.14	11.61	0.00	11.73	0.12
K_2O	0.53	0.66	0.13	0.05	0.15	0.05	0.18	0.08	1.03	2.46	0.13	0.03	0.26	0.08	0.12	0.09
Total	99.39	0.53	100.42	0.49	99.82	0.81	100.09	0.66	100.10	0.44	99.81	0.67	99.32	0.22	100.26	0.13
Si (*apfu*)	2.930	0.812	3.013	0.007	3.002	0.019	3.012	0.008	3.007	0.010	3.006	0.009	3.012	0.000	3.003	0.010
Al	1.056	0.301	0.975	0.014	0.966	0.027	0.979	0.010	0.969	0.018	0.982	0.013	0.975	0.004	0.981	0.007
Fe^{3+}	0.013	0.012	0.003	0.004	0.021	0.020	0.002	0.004	0.013	0.014	0.005	0.004	0.004	0.004	0.006	0.003
Fe^{2+}	0.001	0.003	0.003	0.003	0.017	0.016	0.004	0.003	0.012	0.014	0.002	0.003	0.003	0.003	0.001	0.002
Mg	0.010	0.018	0.000	0.000	0.000	0.000	0.001	0.005	0.000	0.000	0.000	0.000	0.000	0.000	0.008	0.013
Ba	0.000	0.000	0.000	0.000	0.000	0.000	0.000	0.000	0.001	0.001	0.000	0.000	0.000	0.000	0.000	0.000
Ca	0.044	0.050	0.000	0.000	0.000	0.000	0.000	0.001	0.002	0.002	0.002	0.003	0.000	0.000	0.004	0.004
Na	0.932	0.266	0.998	0.010	0.987	0.018	0.990	0.011	0.939	0.134	1.001	0.008	0.991	0.003	0.992	0.011
K	0.030	0.038	0.007	0.003	0.009	0.003	0.010	0.004	0.059	0.140	0.008	0.002	0.015	0.004	0.007	0.005
Cation sum	5.016	1.386	5.001	0.005	5.002	0.009	4.998	0.006	5.001	0.003	5.005	0.007	5.001	0.003	5.002	0.005
Or (mol %)	3.01	3.84	0.74	0.27	0.86	0.31	0.98	0.42	5.80	13.78	0.74	0.16	1.45	0.42	0.68	0.53
Ab	92.63	26.31	99.22	0.26	99.12	0.31	98.98	0.41	94.04	13.82	99.08	0.40	98.54	0.42	98.96	0.60
An	4.36	4.95	0.04	0.04	0.02	0.01	0.05	0.07	0.16	0.18	0.18	0.33	0.01	0.00	0.36	0.38

Note: Compositions were recalculated on the basis of 8 O *apfu*. * Determined by stoichiometry using Droop (1987) calculation method.

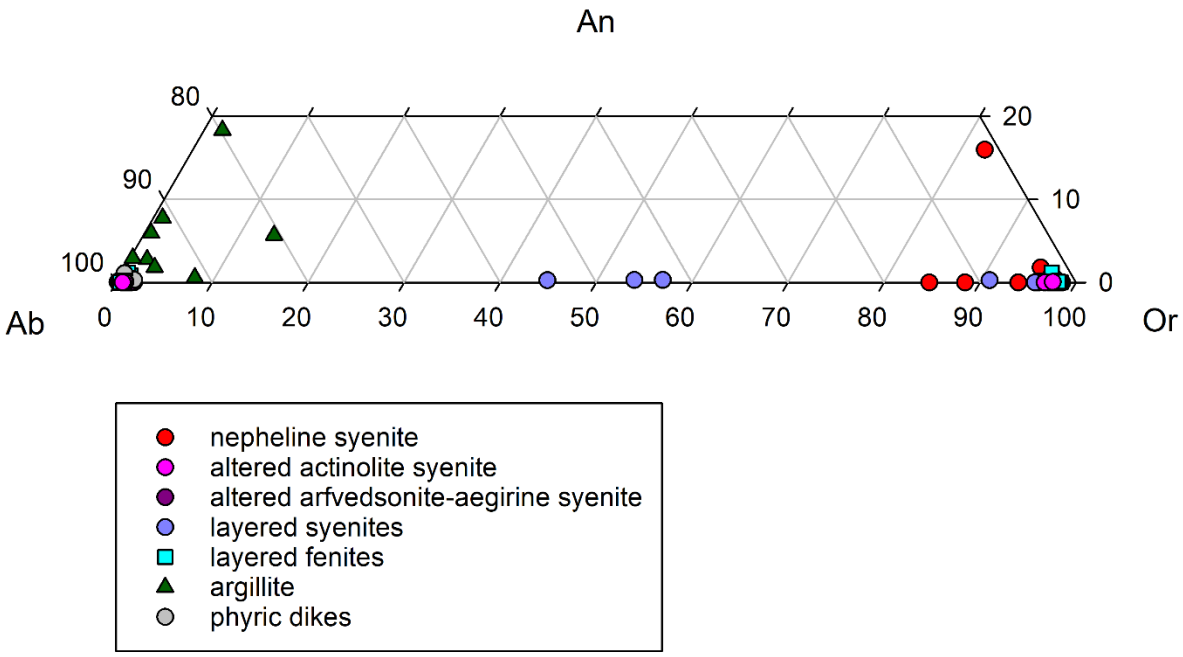

Figure 4.1. Individual feldspar analyses from select samples of various units on the Bandito property plotted on the An-Ab-Or classification ternary diagram. An – anorthite; Ab – albite; Or – orthoclase.

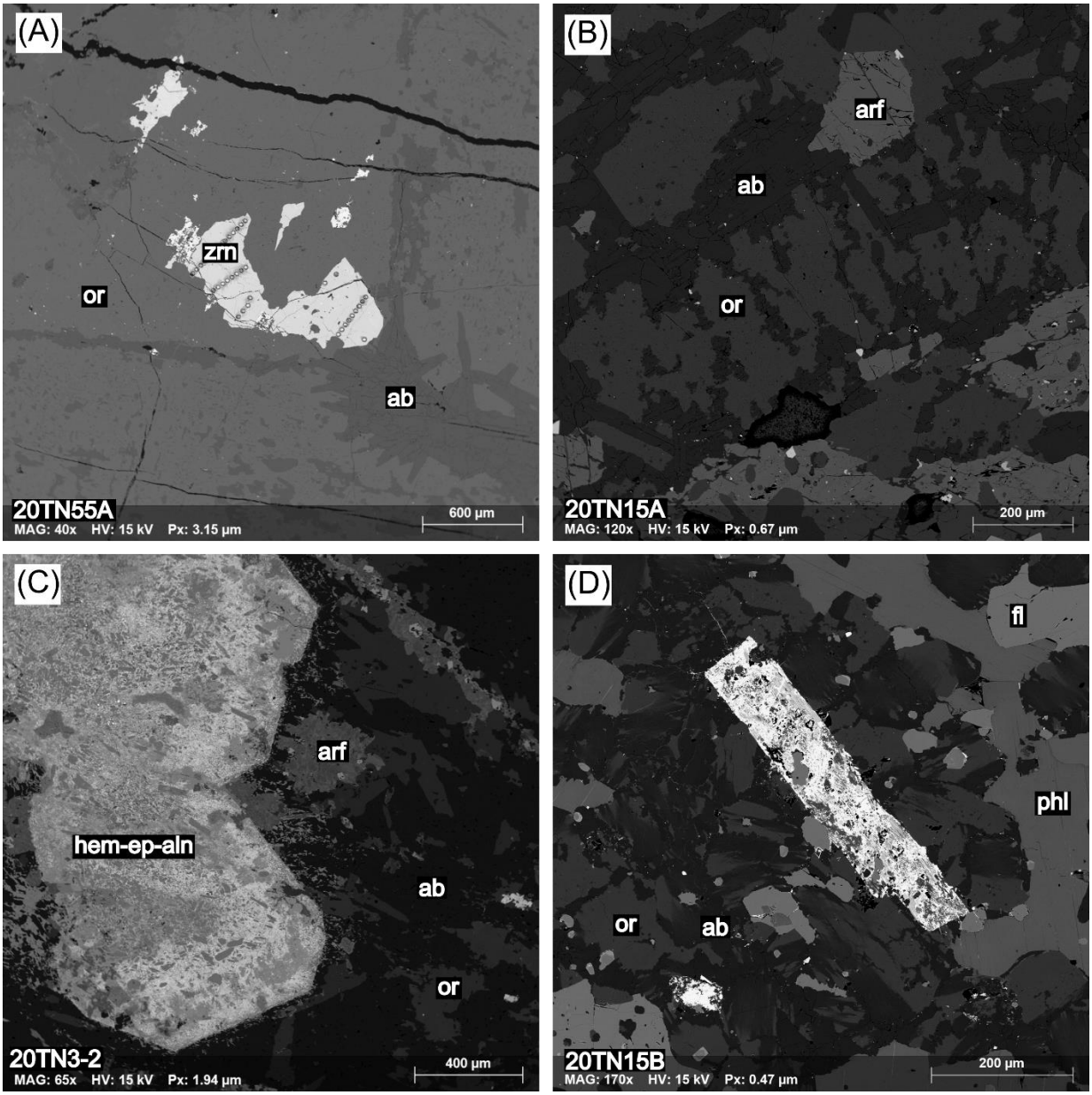

Figure 4.2. BSE images of albite and orthoclase in select samples. (A) perthitic orthoclase with albite exsolution and rims in a nepheline syenite sample (20TN55A). (B) orthoclase with extensive internal albite replacement in an altered titanite arfvedsonite syenite sample (20TN15A). (C) Albite replacing orthoclase in an arfvedsonite fenite sample (20TN3-2). (D) Feldspars showing transition from dark grey-black albite rim and lamellae to lighter orthoclase cores in a phlogopite fenite sample (20TN15B). ab – albite, or – orthoclase, hem – hematite, ep – epidote, aln – allanite, phl – phlogopite, fl – fluorite, zrn – zircon.

Mica and chlorite

Phyllosilicate minerals are present in all the sampled units within the Bandito property. As discussed in Chapter 3, phlogopite and chlorite replace mafics and sericite (i.e., very fine-grained muscovite) replaces nepheline in the nepheline syenite. Similarly, in the altered syenite suites sampled on Pyrochlore Dome and Corundum Dome, micas and chlorite occur in minor amounts with the breakdown of titanite, pyroxene, and amphibole phases. In the layered fenite samples from Corundum Dome, phlogopite occurs as discrete crystals (20TN25D) or in aggregates with titanite altered to Fe-Ti oxides (20TN4A-C). In some of the layered fenites (i.e., 20TN4A-C), muscovite completely replaces a tabular phase, possibly after K-feldspar or nepheline. In one the altered and layered amphibole-diopside-phlogopite syenite (20TN15B) on Pyrochlore Dome, phlogopite occur as pervasive discrete crystals. In the phlogopite altered porphyritic lamprophyre(?) dike (20TN57C-1), phlogopite is pervasive and occurs as discrete crystals throughout the groundmass.

Three phyllosilicate mineral groups were analyzed in this study: biotite, muscovite, and chlorite. Biotite and muscovite are part of the mica mineral group and chlorite is its own mineral group (chlorite group). The general formula for mica group minerals is $X_2Y_{4-6}Z_8O_{20}(OH,F)_4$, where X = K, Na, Ca, Ba, Rb, and Cs; Y = Al, Mg, Fe, Mn, Cr, Ti, and Li; and Z = Si, Al, Fe^{3+}, and Ti. The general formula for chlorite group minerals is $[R^{2+},R^{3+}]_{12}[Si_{8-x}R^{3+}]O_{20}(OH)_{16}$, where R^{2+} = Mg, Fe, Mn, Ni, Zn; R^{3+} = Al, Fe, and Cr; and $x \sim 1$ to 3.

Analyses from select samples of mica group minerals that are part of the biotite series, and that are muscovite and phengite in composition are reported in Table 4.2. Chlorite group minerals are reported in Table 4.3. Mica group minerals are plotted on compositional variation diagrams in Figure 4.3 and chlorite group minerals in Figure 4.4.

Biotite series minerals were analyzed from the nepheline syenite, altered syenites, fenites, and quartzite, argillite, and altered and porphyritic dikes. The main chemical variations in the biotite series observed across the samples are in the Si, Al, Mg, Fe, and F contents; where Si content ranges from 36.37 wt. % (2.789 *apfu*) to 47.85 wt. % (3.402 *apfu*) SiO_2, Al from 7.34 wt. % (0.622 *apfu*) to 14.94 wt. % (1.337 *apfu*) Al_2O_3, Mg from 11.11 wt. % (1.286 *apfu*) to 23.87 wt.

% (2.549 *apfu*) MgO, Fe from 3.48 wt. % (0.209 *apfu*) to 21.59 wt. % (1.402 *apfu*) FeO, and F from 0.61 wt. % (0.146 *apfu*) to 6.68 wt. % (1.570 *apfu*). The dominant species analyzed is phlogopite, with a few compositions of annite, where a transition between phlogopite to annite is observed in the nepheline syenite (Figure 4.3). Phlogopite in the feldspar porphyritic dike (sample 20TN54) has significantly higher Mg and F than all the other units. In general, phlogopite compositions from the altered syenites, fenites, quartzite, and argillite have elevated Mg and F contents with respect to the nepheline syenite and altered dike.

With respect to muscovite and phengite, the dominant species observed is muscovite, with a few compositions as phengite. The main chemical variations are in Si, Al, Mg, and Fe; where Si content ranges from 42.10 wt. % (2.882 *apfu*) to 54.54 wt. % (3.558 *apfu*) SiO_2, Al from 22.82 wt. % (1.858 *apfu*) to 38.56 wt. % (3.107 *apfu*) Al_2O_3, Mg from 0.07 wt. % (0.007 *apfu*) to 7.84 wt. % (0.817 *apfu*) MgO, and Fe from 0.41 wt. % (0.023 *apfu*) to 5.02 wt. % (0.293 *apfu*) FeO.

The nepheline syenite and altered porphyritic lamprophyre(?) dike (20TN57C-1) have both muscovite and phengite compositions. A single analysis from an altered syenite sample (20TN6-2) is muscovite in composition. The quartzite has only phengite compositions. The analyzed phengite compositions are notably higher in Si and F contents and have lower Al contents than the muscovite compositions.

The main chemical variations of the chlorite group minerals are with respect to the Si, Al, Mg, and Fe^{2+} contents; where Si contents range from 24.77 (5.426 *apfu*) to 34.84 wt. % (6.737 *apfu*) SiO_2, Al from 12.65 wt. % (3.024 *apfu*) to 19.39 wt. % (4.850 *apfu*) Al_2O_3, Mg from 12.24 wt. % (3.996 *apfu*) to 20.65 wt. % (6.438 *apfu*) MgO, and Fe^{2+} from 16.62 wt. % (2.798 *apfu*) to 30.40 wt. % (5.630 *apfu*) FeO.

Chlorite group minerals in the nepheline syenite, altered syenites, fenites, and argillite are clinochlore (Mg-dominant) and chamosite (Fe-dominant) compositions. The main variety is pycnochlorite, followed by ripidolite, brunsvigite, and diabantite. Clinochlore is present in the nepheline syenite, fenites, and argillite. The chlorite in the altered arfvedsonite-aegirine syenite is compositionally diabanite. One layered fenite sample (20TN25D) has compositions that transition between chamosite and clinochlore.

Table 4.2. Single and average compositions of micas from various rock types across the 2020 Corundum Dome and Pyrochlore Dome sampling area

unit (sample)	argillite (20TN24A)		quartzite (20TN17C)		nepheline syenite (20TN57A, 20TN53)		altered arfvedsonite-aegirine syenite (20TN13B-2)		layered phlogopite-potassium feldspar fenite (20TN25D)		layered arfvedsonite-albite (20TN4A)		brecciated arfvedsonite-potassium feldspar fenite (20TN7)		actinolite-altered syenite (20TN6-2)		altered and layered amphibole-diopside-phlogopite syenite (20TN15B)	
analysis	average	σ	average	σ	average	σ	average	σ	average	σ	average	σ	average	σ	average	σ	average	σ
n	6		4		19		11		15		10		2		4		11	
SiO_2 (wt. %)	39.02	0.89	41.17	2.17	38.91	1.29	40.89	1.69	42.83	1.92	39.77	2.00	40.02	0.68	39.75	1.20	40.77	2.19
TiO_2	2.08	0.28	0.56	0.05	3.22	0.81	0.24	0.20	1.15	0.65	0.16	0.07	0.27	0.13	0.58	0.24	0.92	0.67
Al_2O_3	13.29	0.80	11.15	0.33	10.53	0.48	10.43	0.43	9.49	1.16	12.38	1.02	11.72	1.10	12.29	0.63	10.77	1.53
MgO	14.41	0.79	16.14	0.33	14.03	2.17	15.89	0.82	18.53	1.23	19.52	0.45	18.04	0.78	17.35	1.47	17.67	2.00
CaO	0.10	0.07	0.03	0.03	0.02	0.02	0.02	0.01	0.15	0.35	0.05	0.03	0.04	0.00	0.08	0.03	0.09	0.21
MnO	0.07	0.02	0.02	0.01	0.32	0.08	0.20	0.04	1.17	0.80	1.47	0.61	1.72	0.36	0.66	0.06	1.05	0.69
FeO	15.62	0.74	14.98	0.92	17.62	2.70	16.72	1.21	9.89	2.51	10.88	1.71	12.27	0.85	13.22	1.56	12.66	3.75
Na_2O	0.08	0.03	0.03	0.01	0.06	0.02	0.04	0.02	0.05	0.05	0.06	0.03	0.02	0.01	0.04	0.01	0.07	0.04
K_2O	9.55	0.29	10.44	0.26	10.16	0.20	10.05	0.25	10.55	0.29	9.16	1.51	10.62	0.07	9.97	0.48	10.02	0.95
BaO	0.01	0.03	0.04	0.03	0.00	0.00	0.00	0.01	0.01	0.02	0.01	0.01	0.01	0.01	0.01	0.01	0.02	0.03
F	0.68	0.07	4.07	0.05	2.77	0.65	3.30	0.58	5.67	0.87	2.81	0.43	2.89	0.33	2.56	0.47	3.94	1.45
H_2O*	3.65	0.04	2.05	0.08	2.60	0.25	2.39	0.31	1.34	0.37	2.68	0.16	2.63	0.15	2.77	0.17	2.12	0.65
Total	98.55	0.25	100.67	0.63	100.26	0.50	100.16	0.36	100.85	0.71	98.93	1.58	100.25	0.09	99.29	0.92	100.10	1.25
Si (*apfu*)	2.949	0.052	3.095	0.106	2.977	0.058	3.103	0.086	3.182	0.103	2.973	0.103	3.002	0.045	2.993	0.050	3.063	0.122
Ti	0.118	0.016	0.031	0.003	0.186	0.046	0.014	0.012	0.064	0.036	0.009	0.004	0.015	0.007	0.033	0.014	0.052	0.038
Al	1.184	0.076	0.990	0.043	0.950	0.047	0.933	0.038	0.832	0.111	1.093	0.104	1.037	0.100	1.091	0.071	0.955	0.142
Mg	1.623	0.083	1.811	0.064	1.597	0.218	1.799	0.103	2.052	0.114	2.177	0.050	2.017	0.082	1.946	0.140	1.977	0.199
Ca	0.008	0.006	0.002	0.002	0.001	0.002	0.002	0.001	0.012	0.028	0.004	0.002	0.003	0.000	0.007	0.002	0.007	0.018
Mn	0.004	0.001	0.001	0.001	0.021	0.005	0.013	0.003	0.074	0.050	0.093	0.038	0.109	0.023	0.042	0.004	0.067	0.043
Fe^{2+}	0.988	0.051	0.944	0.073	1.130	0.183	1.063	0.090	0.617	0.165	0.682	0.118	0.770	0.055	0.834	0.110	0.800	0.249
Na	0.011	0.004	0.004	0.002	0.009	0.004	0.006	0.002	0.008	0.007	0.009	0.004	0.004	0.001	0.005	0.001	0.010	0.007
K	0.921	0.029	1.002	0.042	0.992	0.026	0.974	0.019	1.001	0.019	0.873	0.132	1.016	0.009	0.958	0.035	0.960	0.084
Ba	0.000	0.001	0.001	0.001	0.000	0.000	0.000	0.000	0.000	0.001	0.000	0.000	0.000	0.000	0.000	0.000	0.001	0.001
F^-	0.162	0.017	0.970	0.025	0.669	0.142	0.793	0.145	1.331	0.192	0.663	0.095	0.686	0.078	0.608	0.104	0.934	0.332
OH	1.838	0.017	1.030	0.025	1.331	0.142	1.207	0.145	0.669	0.192	1.337	0.095	1.314	0.078	1.392	0.104	1.066	0.332
O^{2-}	10.000	0.000	10.000	0.000	10.000	0.000	10.000	0.000	10.000	0.000	10.000	0.000	10.000	0.000	10.000	0.000	10.000	0.000
Anion sum	12.000	0.000	12.000	0.000	12.000	0.000	12.000	0.000	12.000	0.000	12.000	0.000	12.000	0.000	12.000	0.000	12.000	0.000
Cation sum	7.806	0.029	7.882	0.104	7.863	0.025	7.906	0.075	7.842	0.075	7.912	0.023	7.974	0.006	7.910	0.031	7.892	0.062
Mg/(Mg+Fe)	0.62	0.02	0.66	0.01	0.58	0.07	0.63	0.02	0.75	0.05	0.74	0.03	0.70	0.02	0.69	0.04	0.70	0.08

Note: Compositions were recalculated on the basis of 11 anions (O, F) *apfu*. * H_2O determined by stoichiometry.

Table 4.2. Continued…

unit (sample)	altered feldspar porphyritic dike (20TN54)		altered porphyritic lamprophyre(?) dike (20TN57C-1)		quartzite (20TN17C)		nepheline syenite (20TN55A, 20TN57A, 20TN53)		actinolite-altered syenite (20TN6-2)	altered porphyritic lamprophyre(?) dike (20TN57C-1)	
analysis	average	σ	average	σ	average	σ	average	σ	8621	average	σ
n	2		11		5		29		1	7	
SiO_2 (wt. %)	47.57	0.28	39.60	3.47	53.50	0.86	44.80	2.53	44.11	44.90	0.97
TiO_2	0.10	0.01	1.38	0.69	0.06	0.03	0.08	0.08	0.01	0.07	0.07
Al_2O_3	7.44	0.10	11.58	0.97	26.00	0.45	34.33	4.52	35.12	33.61	3.22
MgO	23.83	0.04	16.47	2.88	3.30	0.12	1.39	1.66	1.18	1.75	2.51
CaO	0.25	0.04	0.06	0.08	0.10	0.05	0.05	0.05	0.05	0.34	0.23
MnO	0.12	0.03	0.24	0.08	0.00	0.00	0.07	0.09	0.94	0.09	0.06
FeO	3.65	0.17	14.24	4.92	2.31	0.09	1.74	1.29	0.41	1.55	1.44
Na_2O	0.02	0.00	0.18	0.07	0.04	0.01	0.23	0.13	0.32	0.15	0.06
K_2O	10.16	0.04	10.05	0.27	9.81	0.27	11.08	0.53	11.18	11.64	0.38
BaO	0.00	0.00	0.27	0.25	0.06	0.04	0.04	0.04	0.62	0.04	0.05
F	6.59	0.02	3.79	1.36	1.14	0.07	0.39	0.38	0.25	0.63	0.78
H_2O*	1.07	0.01	2.16	0.53	3.99	0.06	4.21	0.19	4.27	4.10	0.41
Total	100.80	0.50	100.00	0.75	100.32	0.95	98.40	0.82	98.46	98.87	0.83
Si (*apfu*)	3.400	0.002	2.996	0.168	3.538	0.016	3.054	0.171	3.015	3.062	0.047
Ti	0.005	0.001	0.080	0.040	0.003	0.002	0.004	0.004	0.000	0.004	0.003
Al	0.627	0.005	1.037	0.113	2.026	0.023	2.758	0.359	2.829	2.700	0.241
Mg	2.540	0.009	1.853	0.264	0.326	0.015	0.141	0.170	0.121	0.181	0.262
Ca	0.019	0.003	0.004	0.006	0.007	0.004	0.004	0.003	0.004	0.025	0.017
Mn	0.007	0.002	0.015	0.006	0.000	0.000	0.004	0.005	0.054	0.005	0.003
Fe^{2+}	0.218	0.009	0.912	0.329	0.128	0.006	0.100	0.075	0.023	0.089	0.085
Na	0.003	0.000	0.026	0.011	0.005	0.001	0.030	0.017	0.043	0.019	0.008
K	0.927	0.008	0.972	0.018	0.828	0.029	0.963	0.043	0.974	1.013	0.023
Ba	0.000	0.000	0.008	0.008	0.002	0.001	0.001	0.001	0.017	0.001	0.001
F^-	1.490	0.003	0.899	0.290	0.239	0.014	0.084	0.082	0.054	0.137	0.173
OH	0.510	0.003	1.101	0.290	1.761	0.014	1.916	0.082	1.946	1.863	0.173
O^{2-}	10.000	0.000	10.000	0.000	10.000	0.000	10.000	0.000	10.000	10.000	0.000
Anion sum	12.000	0.000	12.000	0.000	12.000	0.000	12.000	0.000	12.000	12.000	0.000
Cation sum	7.746	0.008	7.905	0.092	6.863	0.029	7.059	0.045	7.079	7.100	0.100
Mg/(Mg+Fe)	0.92	0.00	0.67	0.11	0.72	0.00	0.46	0.17	0.61	0.55	0.13

Note: Compositions were recalculated on the basis of 11 anions (O, F) *apfu*. * H_2O determined by stoichiometry.

Table 4.3. Average chlorite compositions from various rock types across the Bandito property.

unit (sample)	argillite (20TN5, 20TN24A)		nepheline syenite (20TN55A, 20TN57A, 20TN53)		actinolite-altered syenite (20TN13B-2)		fenites (20TN7, 20TN23, 20TN25D)	
analysis	average	σ	average	σ	average	σ	average	σ
n	5		22		2		12	
SiO_2 (wt. %)	27.60	0.55	27.19	0.52	33.38	1.46	26.60	1.59
TiO_2	0.11	0.16	0.16	0.46	0.06	0.03	0.06	0.03
Al_2O_3	18.42	0.53	18.39	0.41	12.66	0.01	17.75	0.60
Fe_2O_3*	0.11	0.16	1.11	0.57	3.42	0.58	0.48	0.64
FeO*	19.84	0.49	22.49	0.88	20.07	2.05	25.65	4.54
MnO	0.31	0.08	0.48	0.11	0.29	0.01	0.82	0.58
MgO	19.76	0.70	16.36	0.82	14.86	0.03	15.01	2.25
CaO	0.14	0.08	0.05	0.03	0.15	0.01	0.07	0.04
Na_2O	0.03	0.06	0.02	0.01	0.04	0.00	0.01	0.02
K_2O	0.11	0.19	0.31	0.27	2.80	1.22	0.17	0.40
BaO	0.03	0.01	0.01	0.02	0.03	0.02	0.03	0.03
F	0.02	0.03	0.51	0.17	1.34	0.36	0.37	0.18
H_2O*	11.51	0.06	10.82	0.17	10.20	0.10	10.77	0.23
O=F,Cl	0.01	0.01	0.21	0.07	0.56	0.15	0.16	0.08
Total	97.98	0.54	97.66	0.45	98.73	1.25	97.63	0.56
Si (*apfu*)	5.730	0.099	5.678	0.078	6.658	0.079	5.669	0.190
Al iv	2.270	0.099	2.322	0.078	1.342	0.079	2.331	0.190
Al vi	2.245	0.078	2.254	0.135	1.752	0.009	2.167	0.087
Ti	0.017	0.025	0.024	0.073	0.009	0.004	0.009	0.005
Fe^{3+}	0.017	0.025	0.174	0.089	0.511	0.070	0.076	0.098
Fe^{2+}	3.460	0.084	3.930	0.184	3.364	0.450	4.607	0.911
Mn	0.055	0.015	0.084	0.019	0.049	0.004	0.146	0.098
Mg	6.115	0.230	5.093	0.247	4.424	0.149	4.758	0.598
Ca	0.031	0.018	0.011	0.007	0.033	0.004	0.016	0.009
Na	0.028	0.049	0.014	0.008	0.034	0.005	0.009	0.013
K	0.056	0.101	0.166	0.140	1.406	0.574	0.091	0.203
Ba	0.005	0.002	0.002	0.003	0.005	0.003	0.004	0.005
F^-	0.027	0.036	0.669	0.216	1.673	0.397	0.501	0.235
OH	15.973	0.036	15.331	0.216	14.327	0.397	15.499	0.235
Cation sum	20.030	0.033	19.752	0.132	19.587	0.043	19.883	0.135

Note: Oxide percentages based on 28 O *apfu*. Compositions were recalculated on the basis of 36 O *apfu*. * Fe^{2+}/Fe^{3+} and OH calculated assuming full site occupancy.

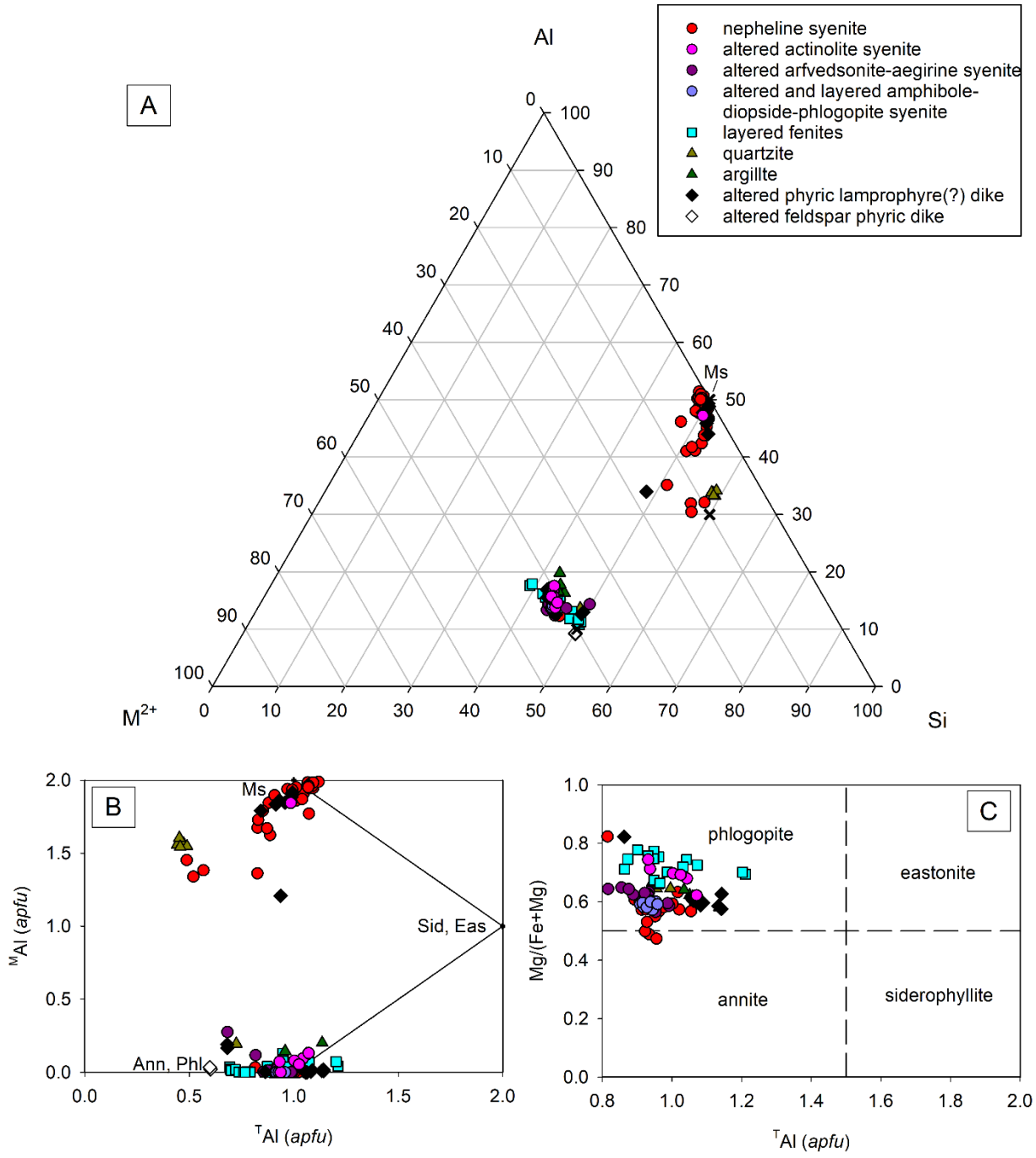

Figure 4.3. Individual analyses of mica group minerals from the Bandito property in compositional discrimination plots. (A) Si-Al-M^{2+} mica variation ternary diagram after Monier & Robert (1986). (B) ^{T}Al versus ^{M}Al bivariate mica classification diagram. (C) ^{T}Al vs. $Mg/(Mg+Fe^{2+})$ biotite classification bivariate diagram. Ann – annite; Phl – phlogopite; Eas – eastonite; Sid – siderophyllite, Ms – muscovite; Pg – phengite.

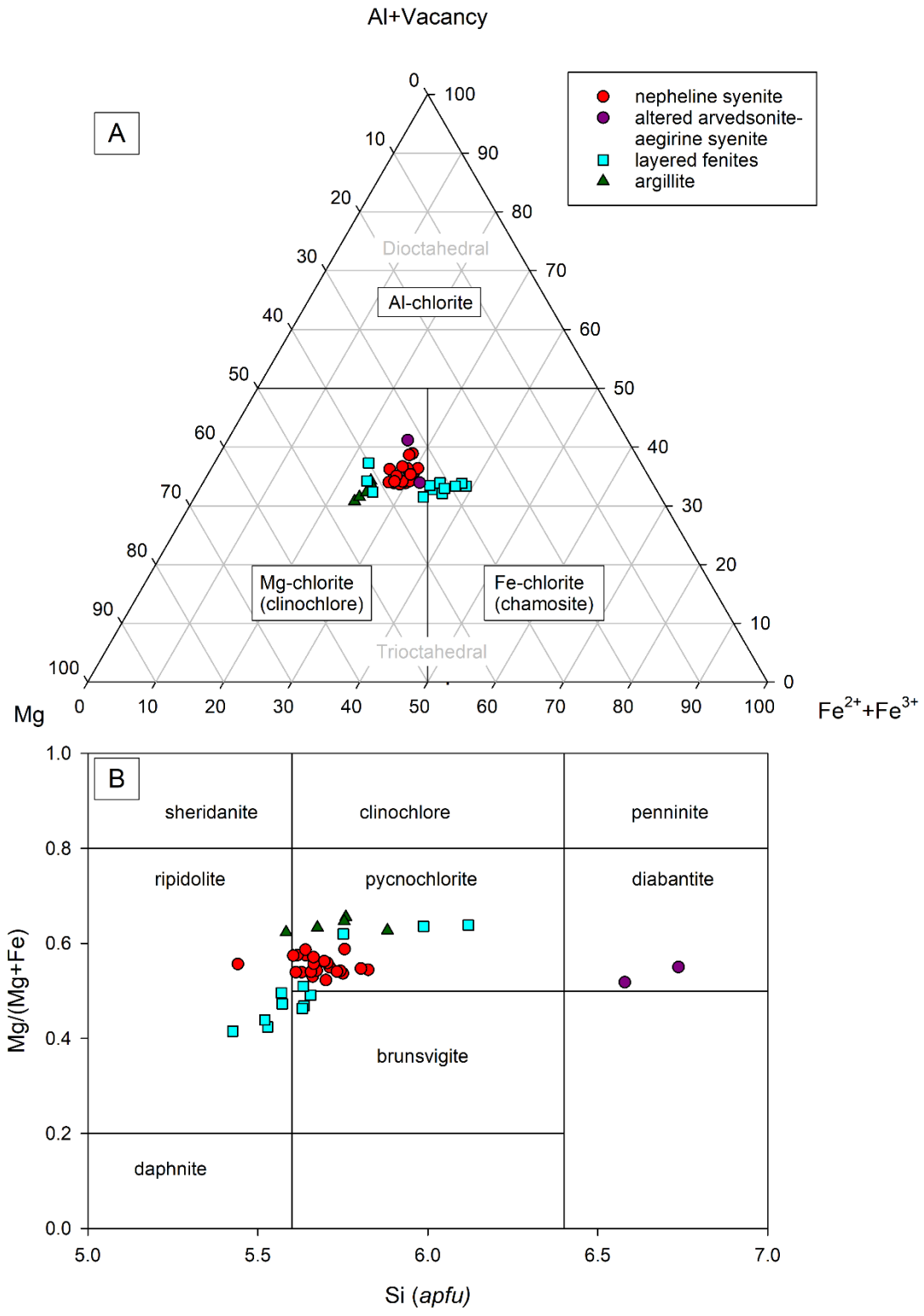

Figure 4.4. Chlorite analyses from units on the Bandito property plotted on chlorite classification diagrams. (A) Al-Mg-Fe ternary diagram after Zane & Weiss (1998). (B) Chlorite classification diagram after Hey (1954).

Amphibole

The general chemical formula of the minerals of the amphibole supergroup can be written as $AB_2C_5T_8O_{22}W_2$, where A = vacancy, Na, K, Ca, Pb, Li; B = Na, Ca, Mn^{2+}, Fe^{2+}, Mg, Li; C = Mg, Fe^{2+}, Mn^{2+}, Al, Fe^{3+}, Mn^{3+}, Cr^{3+}, Ti^{4+}, Li; T = Si, Al, Ti^{4+}, Be; and W = (OH), F, Cl, O^{2-}. Minor elements such as Zn, Ni^{2+}, Co^{2+}, V^{3+}, Sc, and Zr are also observed as C cations. The most recent amphibole classification scheme is Hawthorne et al. (2012). Notably, Locock (2014) created an Excel spreadsheet to classify chemical analyses of amphiboles following the recommendations in Hawthorne et al. (2012). The most recent version of the Locock spreadsheet was used to calculate amphibole compositions in this thesis.

Amphibole is present in the argillite, and common in altered syenite, and fenites. Amphibole compositions for select samples are reported in Table 4.4. All analyses are plotted on various amphibole compositional diagrams in Figure 4.5.

Amphibole is common in the altered syenites, fenites, and argillite units and are of calcic, sodic-calcic, and sodic compositions. According to the Locock (2014) recalculation sheet, amphibole compositions analysed in this thesis correspond to actinolite, ferro-actinolite, fluoro-arfvedsonite, magnesio-fluoro-arfvedsonite, ferri-fluoro-katophorite, fluoro-richterite, magnesio-ferri-hornblende, winchite, and riebeckite. Amphibole totals range from 96.38 wt. % to 100.08 wt. %. The Mg/(Fe + Mg) range from 0.261 to 0.787. The main chemical variations are in the Si, Fe, Mg, Ca, Na, and F contents; where SiO_2 from 49.83 wt. % (7.441 *apfu*) to 57.12 wt. % (8.382 *apfu*), Fe_2O_3 from 0.00 wt. % to 14.17 wt. % (1.601 *apfu*), FeO from 6.98 wt. % (0.845 *apfu*) to 23.40 wt. % (3.068 *apfu*), MgO from 5.20 wt. % (1.191 *apfu*) to 17.90 wt. % (3.818 *apfu*), CaO from 0.08 wt. % (0.013 *apfu*) to 12.99 wt. % (1.989 *apfu*), Na_2O from 0.07 wt. % (0.018 *apfu*) to 9.36 wt. % (2.779 *apfu*), and F from 0.00 wt. % to 3.99 wt. % (1.935 *apfu*).

Amphibole compositions in the argillite are dominantly actinolite. The actinolite-altered syenite on Corundum Dome contains actinolite. Arfvedsonite is the dominant amphibole composition in the altered arfvedsonite-aegirine syenite on Pyrochlore Dome. Fenite samples have sodic and sodic-calcic compositions, where the dominant species is arfvedsonite. Amphiboles show weak to strong chemical zoning in Ca compositions, Na compositions, and between Na and Na-Ca

compositions (Figure 4.5). Chemical zoning in some amphiboles is visible in SEM-BSE imaging (Figure 4.6). A strongly altered edge of an actinolite-altered syenite dikelet (20TN3-2) has both actinolite and arfvedsonite compositions, where actinolite compositions are characteristic of the syenite and the arfvedsonite of the completely metasomatized zone (see Chapter 3 for more detail).

As discussed in Chapter 3, in the argillite (e.g., 20TN5), actinolite occurs as uncommon discrete crystals. In the altered syenite (e.g., 20TN2, 20TN4D, 20TN6-2, 20TN10C), actinolite occurs as discrete crystals or in acicular aggregates. In the layered fenites and brecciated fenite (e.g., 20TN4A-C, 20TN23, 20TN7), arfvedsonite occurs as discrete crystals in an albite-dominated groundmass. In the layered titanite-arfvedsonite syenite (20TN15A), arfvedsonite crystals concentrate in alternating layers in an orthoclase-albite groundmass. The presence of sodic amphibole phases is indicative of sodic metasomatic alteration (e.g., Elliott et al. 2018). Similarly, the presence of calcic amphibole phases indicates calcic metasomatic alteration.

Table 4.4. Compositions of amphibole from various rock types across the 2020 Corundum Dome and Pyrochlore Dome sampling area.

mineral species	actinolite		ferro-actinolite		fluoro-arfvedsonite		magnesio-fluoro-arfvedsonite		ferri-fluoro-katophorite		fluoro-richterite		magnesio-ferri-hornblende	winchite	riebeckite
unit (sample)	argillite, altered syenite (20TN3-2, 20TN4D, 20TN5, 20TN6-2, 20TN10C, 20TN24A)		argillite, actinolite-altered syenite (20TN3-2, 20TN5, 20TN10C)		layered titanite-arfvedsonite syenite, altered arfvedsonite-aegirine syenite (20TN13B-2, 20TN15A, 20TN20)		fenites, actinolite-altered syenite, altered arfvedsonite-aegirine syenite (20TN3-2, 20TN4A, 20TN7, 20TN20, 20TN23)		fenites (20TN4A, 20TN7)		layered actinolite-albite fenite (20TN23)		argillite (20TN24A)	argillite (20TN5)	layered arfvedsonite-titanite syenite (20TN15A)
analysis	average	σ	average	σ	average	σ	average	σ	average	σ	average	σ	23-157-1	7-99-2	32-159-3
n	38		3		16		27		4		3		1	1	1
SiO_2 (wt. %)	53.62	1.09	50.86	1.19	53.28	1.09	53.74	0.49	53.11	0.90	54.15	0.11	51.04	57.12	53.31
TiO_2	0.10	0.13	0.05	0.06	0.58	0.52	0.47	0.16	0.26	0.04	0.24	0.04	0.62	0.07	0.48
Al_2O_3	1.52	0.89	2.16	1.10	0.25	0.11	1.03	0.34	1.66	0.58	1.01	0.06	4.13	7.24	0.48
Fe_2O_3**	0.80	0.46	1.19	0.47	5.21	1.77	5.43	1.24	4.42	0.44	2.94	0.06	1.98	0.00	14.17
FeO**	12.77	2.94	20.53	2.10	15.97	1.95	10.31	1.97	8.86	1.60	10.62	0.21	11.48	9.50	13.47
MnO	0.95	0.69	1.54	0.81	2.55	0.98	2.31	0.76	1.38	0.45	1.03	0.14	0.20	0.32	0.75
MgO	14.65	2.11	8.56	1.61	6.86	0.82	11.16	1.28	14.21	1.47	14.17	0.27	14.78	11.33	6.57
CaO	11.96	0.43	11.31	0.63	0.63	0.54	1.56	0.79	4.27	0.94	4.26	0.12	11.88	8.75	0.39
Na_2O	0.39	0.21	0.59	0.21	8.59	0.68	8.74	0.44	7.45	0.41	7.34	0.06	0.51	2.79	6.84
K_2O	0.17	0.09	0.23	0.02	1.98	0.40	1.87	0.23	1.48	0.31	1.61	0.05	0.30	0.16	0.42
H_2O+*	1.95	0.11	1.94	0.05	0.37	0.23	0.76	0.14	0.81	0.07	0.64	0.08	2.04	2.14	1.67
F	0.22	0.22	0.07	0.10	3.12	0.71	2.65	0.26	2.61	0.16	2.98	0.17	0.03	0.00	0.69
O=F	-0.09	0.09	-0.03	0.04	-1.31	0.30	-1.11	0.11	-1.10	0.07	-1.26	0.07	-0.01	0.00	-0.29
Total	99.01	0.50	99.01	0.87	98.07	0.82	98.92	0.84	99.40	0.16	99.72	0.16	98.97	99.42	98.95
Formula *(apfu)*															
T site															
Si	7.825	0.114	7.745	0.154	8.201	0.148	7.991	0.096	7.780	0.132	7.915	0.004	7.441	7.990	8.004
Al	0.175	0.114	0.255	0.154	0.004	0.000	0.043	0.033	0.221	0.132	0.085	0.004	0.559	0.010	0.000
Ti	0.001	0.000	0.000	0.000	0.000	0.000	0.000	0.000	0.000	0.000	0.000	0.000	0.000	0.000	0.000
Fe^{3+}	0.008	0.000	0.000	0.000	0.000	0.000	0.000	0.000	0.000	0.000	0.000	0.000	0.000	0.000	0.000
T subtotal	8.000	0.000	8.000	0.000	8.201	0.148	8.026	0.079	8.000	0.000	8.000	0.000	8.000	8.000	8.004
C site															
Ti	0.013	0.014	0.009	0.007	0.067	0.060	0.053	0.018	0.029	0.004	0.027	0.004	0.068	0.007	0.054
Al	0.088	0.047	0.131	0.042	0.044	0.020	0.146	0.057	0.066	0.043	0.089	0.014	0.151	1.183	0.085
Fe^{3+}	0.090	0.049	0.137	0.054	0.603	0.206	0.606	0.134	0.487	0.046	0.323	0.006	0.217	0.000	1.601
Mn^{2+}	0.128	0.077	0.168	0.107	0.332	0.129	0.292	0.099	0.171	0.057	0.127	0.018	0.000	0.038	0.096
Fe^{2+}	1.547	0.391	2.620	0.324	2.057	0.256	1.284	0.254	1.087	0.205	1.299	0.028	1.351	1.112	1.691
Mg	3.181	0.419	1.937	0.332	1.574	0.184	2.471	0.258	3.100	0.302	3.087	0.051	3.212	2.363	1.469
C subtotal	5.000	0.001	4.999	0.000	4.677	0.253	4.851	0.116	4.940	0.034	4.951	0.006	4.999	4.703	4.996
B site															
Mn^{2+}	0.030	0.013	0.031	0.013	0.000	0.000	0.000	0.000	0.000	0.000	0.000	0.000	0.024	0.000	0.000
Fe^{2+}	0.052	0.023	0.000	0.000	0.000	0.000	0.000	0.000	0.000	0.000	0.000	0.000	0.048	0.000	0.000
Mg	0.000	0.000	0.000	0.000	0.000	0.000	0.000	0.000	0.000	0.000	0.000	0.000	0.000	0.000	0.000
Ca	1.871	0.055	1.845	0.070	0.104	0.089	0.248	0.125	0.670	0.148	0.668	0.018	1.855	1.311	0.064
Na	0.082	0.054	0.124	0.065	1.896	0.089	1.752	0.125	1.330	0.148	1.332	0.018	0.072	0.689	1.936
B subtotal	1.999	0.004	2.000	0.000	2.000	0.000	2.000	0.000	2.000	0.000	2.000	0.000	1.999	2.000	2.000
A site															
Ca	0.000	0.000	0.000	0.000	0.000	0.000	0.000	0.000	0.000	0.000	0.000	0.000	0.000	0.000	0.000
Na	0.031	0.015	0.052	0.011	0.669	0.123	0.769	0.035	0.785	0.036	0.748	0.013	0.072	0.069	0.055

mineral species	actinolite		ferro-actinolite		fluoro-arfvedsonite		magnesio-fluoro-arfvedsonite		ferri-fluoro-katophorite		fluoro-richterite		magnesio-ferri-hornblende	winchite	riebeckite
unit (sample)	argillite, altered syenite (20TN3-2, 20TN4D, 20TN5, 20TN6-2, 20TN10C, 20TN24A)		argillite, actinolite-altered syenite (20TN3-2, 20TN5, 20TN10C)		layered titanite-arfvedsonite syenite, altered arfvedsonite-aegirine syenite (20TN13B-2, 20TN15A, 20TN20)		fenites, actinolite-altered syenite, altered arfvedsonite-aegirine syenite (20TN3-2, 20TN4A, 20TN7, 20TN20, 20TN23)		fenites (20TN4A, 20TN7)		layered actinolite-albite fenite (20TN23)		argillite (20TN24A)	argillite (20TN5)	layered arfvedsonite-titanite syenite (20TN15A)
analysis	average	σ	average	σ	average	σ	average	σ	average	σ	average	σ	23-157-1	7-99-2	32-159-3
n	38		3		16		27		4		3		1	1	1
K	0.032	0.017	0.045	0.005	0.389	0.078	0.354	0.044	0.276	0.058	0.300	0.008	0.056	0.028	0.080
A subtotal	0.062	0.025	0.098	0.014	1.058	0.192	1.123	0.049	1.061	0.034	1.048	0.006	0.128	0.097	0.135
O site	22.000	0.000	22.000	0.000	22.000	0.000	22.000	0.000	22.000	0.000	22.000	0.000	22.000	22.000	22.000
W site															
OH	1.898	0.101	1.966	0.048	0.379	0.238	0.754	0.134	0.793	0.069	0.620	0.078	1.987	2.000	1.673
F	0.121	0.099	0.102	0.000	1.517	0.341	1.246	0.134	1.207	0.069	1.380	0.078	0.013	0.000	0.327
O	0.000	0.000	0.000	0.000	0.277	0.029	0.000	0.000	0.000	0.000	0.000	0.000	0.000	0.000	0.000
W subtotal	2.000	0.000	2.000	0.000	2.000	0.000	2.000	0.000	2.000	0.000	2.000	0.000	2.000	2.000	2.000
Sum **T, C, B, A**	15.061	0.025	15.097	0.014	15.937	0.094	16.000	0.001	16.000	0.001	16.000	0.000	15.126	14.800	15.135

Note: Compositions were recalculated using the recommendations of Locock (2014). Actinolite species calculated using Si–Ca & Li=15 and Si–Na=15 *apfu* or Si–Ca & Li=15 Si–Mg & Li=13 *apfu* or Si–Ca & Li=15 Si–Mg & Li=13 Si–Na=15 *apfu*; arfvedsonite using Si–K=16 *apfu* or Si–Mg & Li=13 *apfu*; katophorite using Si–K=16 *apfu*; richterite using Si–K=16 *apfu*; hornblende using Si–Ca & Li=15 Si–Na=15 *apfu*; winchite using Si–Ca & Li=15 Si–Mg & Li=13 Si–Na=15 *apfu*; and riebeckite using Si–Mg & Li=13 *apfu*. * H_2O determined by stoichiometry. ** Ratio of Fe_2O_3 and FeO calculated to fit an electroneutral formula.

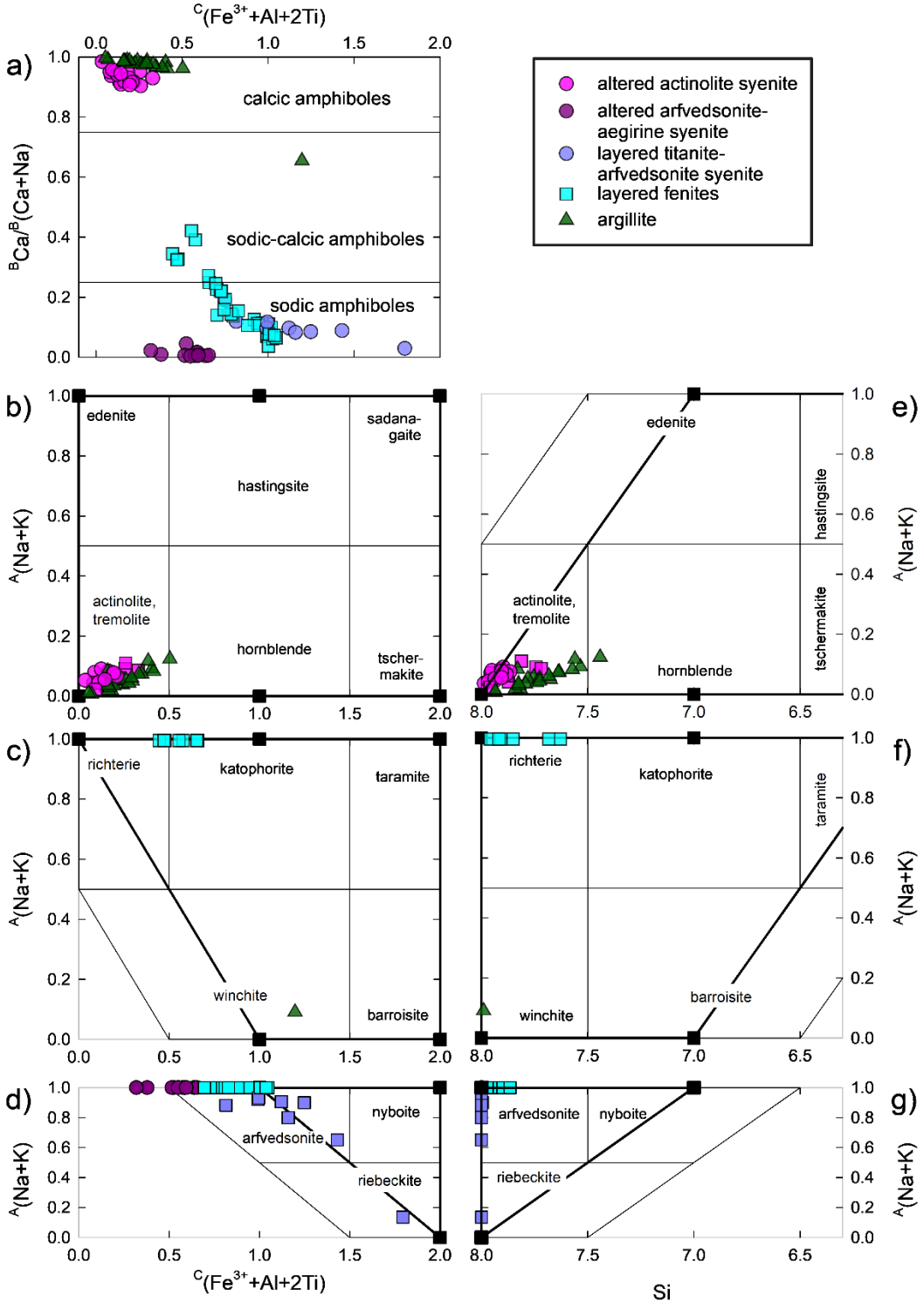

Figure 4.5. Classification diagrams for the individual amphibole assemblages from actinolite-altered syenite, altered arfvedsonite-aegirine syenite, layered titanite-arfvedsonite syenite, fenites, and argillite. (a–d after Hawthorne et al. 2012, and e–g after Leake et al. 1997). Note: compositions > 1 ^{A}(Na+K) *apfu* and > 8 have been automatically adjusted to 1 and 8 *apfu*, respectively.

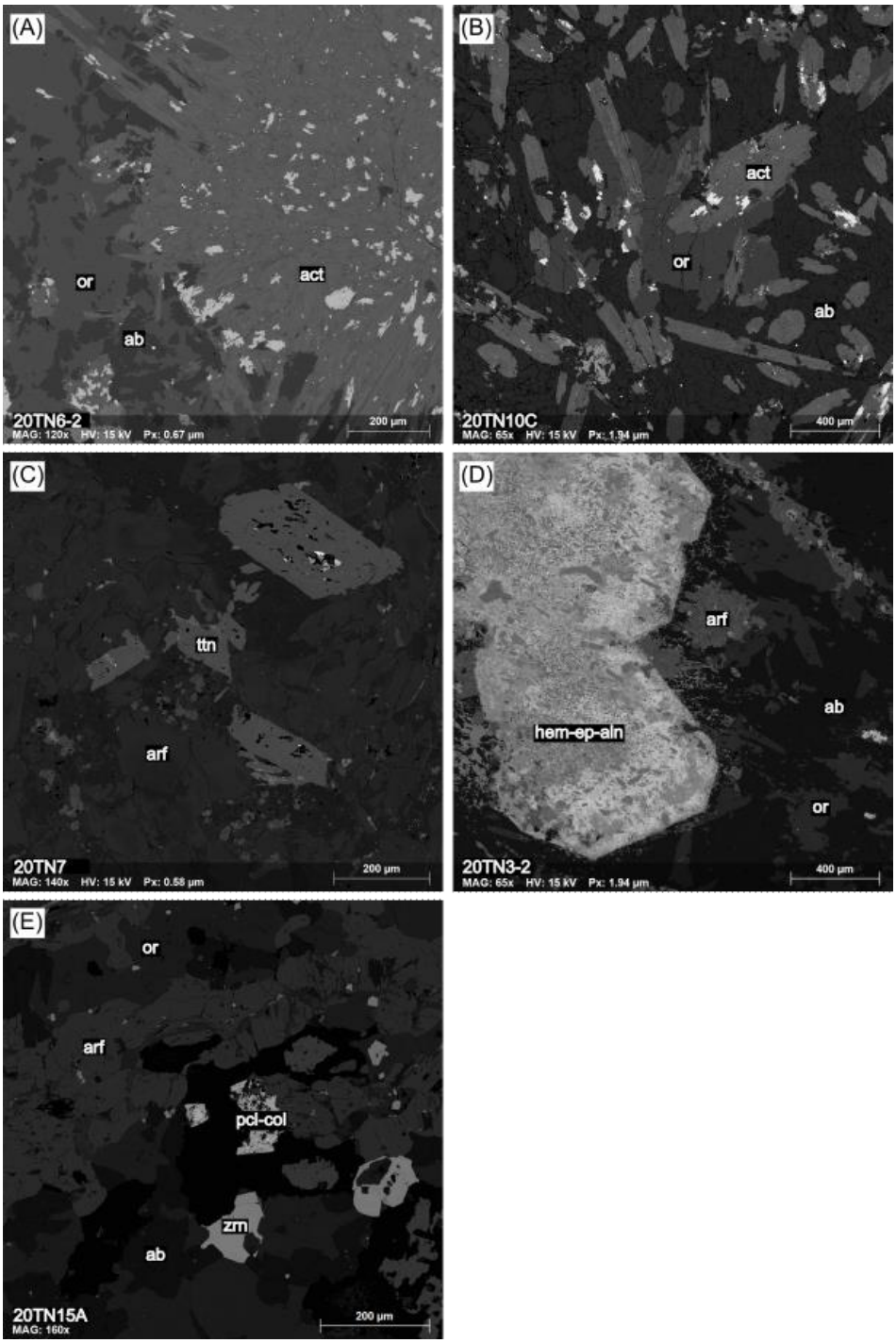

Figure 4.6. BSE images of chemical zoning in amphiboles from a variety of altered units on the Bandito property. (A) Patchy zoning in actinolite in altered syenite (20TN6-2). (B) Patchy zoning in actinolite in altered syenite (20TN10C). (C) Zoning in arfvedsonite in brecciated arfvedsonite-potassium feldspar fenite (20TN7). (D) Patchy zoning in arfvedsonite in layered arfvedsonite-albite fenite (20TN3-2). (E) Weak to no visible zoning in arfvedsonite in layered titanite arfvedsonite syenite (20TN15A). ab – albite, or – orthoclase, hem – hematite, ep – epidote, aln – allanite, pcl – pyrochlore, col – columbite, act – actinolite, arf – arfvedsonite, ttn – titanite, zrn – zircon.

Pyroxene

The general formula for pyroxene group minerals is $(W)_{1-p}(X,Y)_{1+p}Z_2O_6$, where W = Ca, Na; X = Mg, Fe^{2+}, Mn, Ni, Li; Y = Al, Fe^{3+}, Cr, Ti; and Z = Si, Al, where *p* represents parameters for W, X, and Y. Pyroxene is common in the altered arfvedsonite-aegirine syenite (20TN12, 20TN20) and the layered amphibole-diopside-phlogopite syenite (20TN15B). Pyroxene in the altered arfvedsonite-aegirine syenite is zoned and mildly to strongly altered. Average pyroxene compositions are reported in Table 4.5.

The sample analyzed from the altered arfvedsonite-aegirine syenite unit (e.g., 20TN20) contains Na-Fe rich clinopyroxene (aegirine-augite). From core to rim the most notable chemical changes observed from the EMP analyses are an increase in Na and Fe^{3+}, where Na-core = 10.33–11.08 wt. % (0.782–0.833 *apfu*), Na-rim = 11.79–12.97 wt. % (0.886–0.971 *apfu*); Fe^{3+}-core = 22.17–25.02 wt. % (0.651–0.729 *apfu*), Fe^{3+}-rim = 26.48–30.57 wt. % (0.770–0.888 *apfu*); and decrease in Ca and Fe^{2+}, where Ca-core = 3.78–4.98 wt. % (0.157–0.208 *apfu*), Ca-rim = 1.00–2.52 wt. % (0.027–0.105 *apfu*); Fe^{2+}-core = 5.49–7.27 wt. % (0.179–0.237 *apfu*), and Fe^{2+}-rim = 0.94–3.83 wt. % (0.030–0.124 *apfu*) concentrations. Chemical changes from core to rim of the altered pyroxene syenite sample are visible in BSE-SEM and SEM-X-ray map images (Figure 4.7). Chemical X-ray maps verify the EMP analyses and reveal more subtle zoning of Ti and Mg which decrease from core to rim.

The layered amphibole-diopside phlogopite syenite sample (20TN15B) contains Ca-Fe-Mg rich clinopyroxene (diopside) with minimal compositional variation, where Ca contents range from 20.05 wt. % (0.834 *apfu*) to 20.30 wt. % (0.841 *apfu*), Fe^{3+} contents range from 4.95 wt. % (0.144 *apfu*) to 5.89 wt. % (0.171 *apfu*), Fe^{2+} contents range from 11.05 wt. % (0.357 *apfu*) to 11.86 wt. % (0.384 *apfu*), and Mg contents range from 7.25 wt. % (0.420 *apfu*) to 7.50 wt. % (0.432 *apfu*).

Individual pyroxene analyses of the altered arfvedsonite-aegirine syenite and layered amphibole-diopside-phlogopite syenite are plotted on several compositional diagrams in Figure 4.8. According to the bivariate diagram and ternary plots, the pyroxenes in the altered syenite have

aegirine-augite cores and aegirine rims, and the pyroxene in the layered amphibole-diopside-phlogopite syenite is compositionally diopside (almost hedenbergite).

In the altered arfvedsonite aegirine syenite (20TN12, 20TN20), the aegirine-augite to aegirine crystals occur within arfvedsonite and in a groundmass of albite that has replaced orthoclase. The presence of aegirine and aegirine-augite phases associated with other sodic phases like arfvedsonite and albite is indicative of sodic metasomatic alteration (e.g., Elliott et al. 2018). The presence of diopside in an altered and layered amphibole-diopside-phlogopite syenite sample (20TN15B) may indicate calcic metasomatic alteration. Alternatively, the diopside could be a primary mineral phase.

Table 4.5. Average composition of pyroxene from an altered syenite samples from the 2020 Pyrochlore Dome sampling area.

mineral species	aegirine (rim)		aegirine-augite (core)		diopside	
unit (sample)	altered arfvedsonite-aegirine syenite (20TN20)		altered arfvedsonite-aegirine syenite (20TN20)		altered and layered amphibole-diopside-phlogopite syenite (20TN15B)	
analysis	average	σ	average	σ	average	σ
n	11		6		4	
SiO_2 (wt. %)	52.00	0.25	51.57	0.20	51.30	0.13
TiO_2	1.40	0.46	1.45	0.15	0.30	0.03
Al_2O_3	0.25	0.05	0.26	0.02	0.63	0.04
Fe_2O_3*	28.39	1.43	23.67	0.93	5.39	0.40
FeO*	2.04	1.06	6.24	0.58	11.52	0.33
MnO	0.84	0.33	0.66	0.04	0.88	0.02
MgO	0.35	0.06	0.40	0.06	7.41	0.09
CaO	1.35	0.60	4.37	0.44	20.18	0.09
BaO	0.00	0.00	0.00	0.00	0.03	0.02
Na_2O	12.55	0.36	10.73	0.26	2.06	0.08
K_2O	0.01	0.01	0.00	0.00	0.04	0.04
F	0.00	0.00	0.00	0.00	0.12	0.01
Total	99.17	0.49	99.35	0.24	99.86	0.22
Si (*apfu*)	2.011	0.006	2.010	0.005	1.984	0.006
Ti	0.041	0.013	0.042	0.004	0.009	0.001
Al	0.011	0.002	0.012	0.001	0.029	0.002
Fe^{3+}	0.826	0.040	0.694	0.026	0.157	0.011
Fe^{2+}	0.066	0.034	0.203	0.019	0.373	0.011
Mn	0.028	0.011	0.022	0.001	0.029	0.001
Mg	0.020	0.003	0.023	0.004	0.427	0.005
Ca	0.056	0.025	0.183	0.019	0.836	0.003
Ba	0.000	0.000	0.000	0.000	0.000	0.000
Na	0.941	0.026	0.810	0.018	0.155	0.006
K	0.000	0.000	0.000	0.000	0.002	0.002
F^-	0.000	0.000	0.000	0.000	0.014	0.002
O^{2-}	5.587	0.020	5.653	0.013	5.922	0.006
O^{2-} Corrected	6.000	0.000	6.000	0.000	6.000	0.000
Cation Sum	4.000	0.000	4.000	0.000	4.000	0.000

Note: Compositions were recalculated on the basis of the sum of 4 cation *apfu*; * – calculated from stoichiometry.

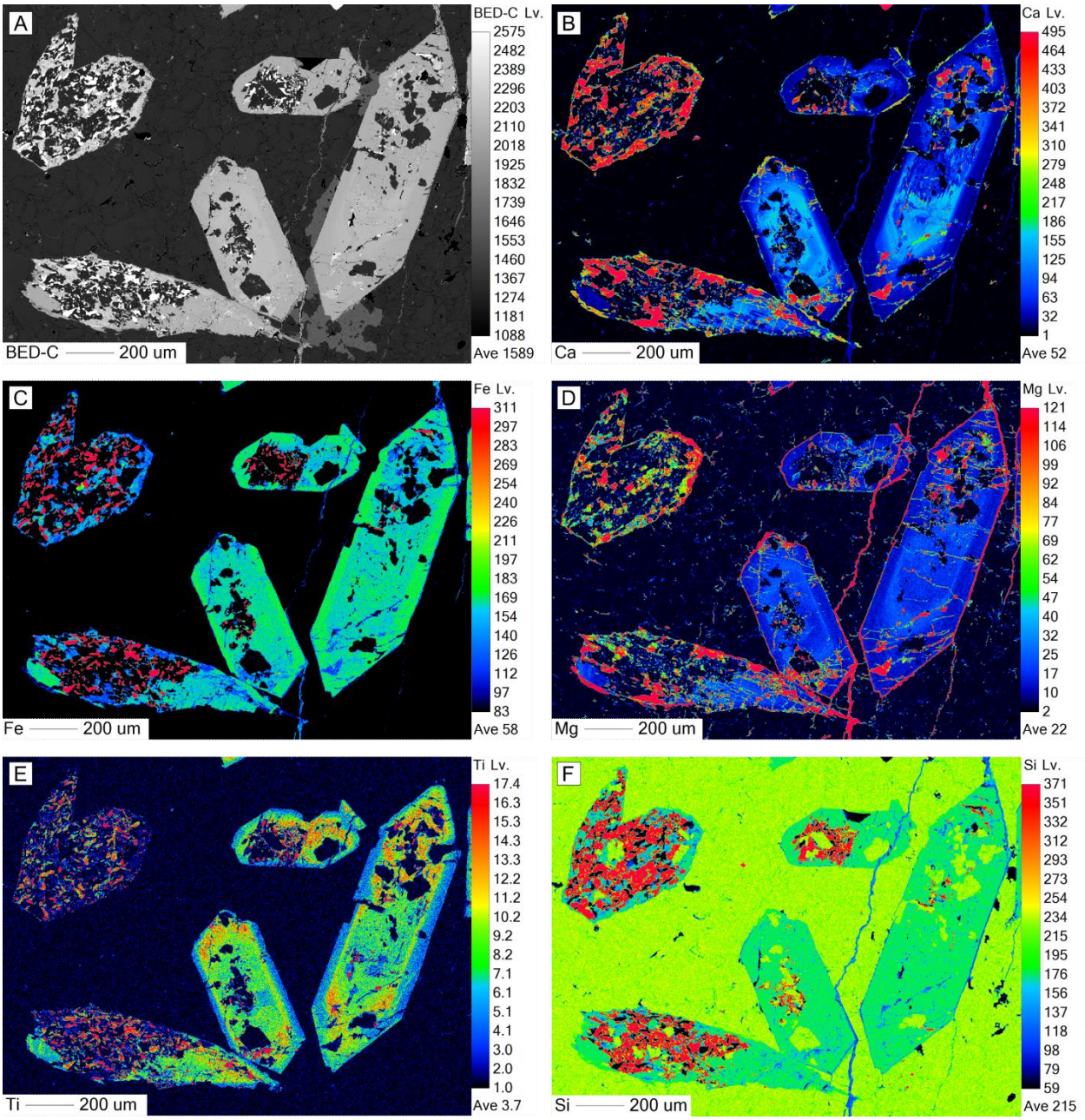

Figure 4.7. X-ray map images of zoned pyroxene crystals in altered arfvedsonite-aegirine syenite sample 20TN20. (A) BSE image; pyroxene is denoted by the lighter grey colour. (B) Ca X-ray level. (C) Fe X-ray level. (D) Mg X-ray level. (E) Ti X-ray level. (F) Si Z-ray level.

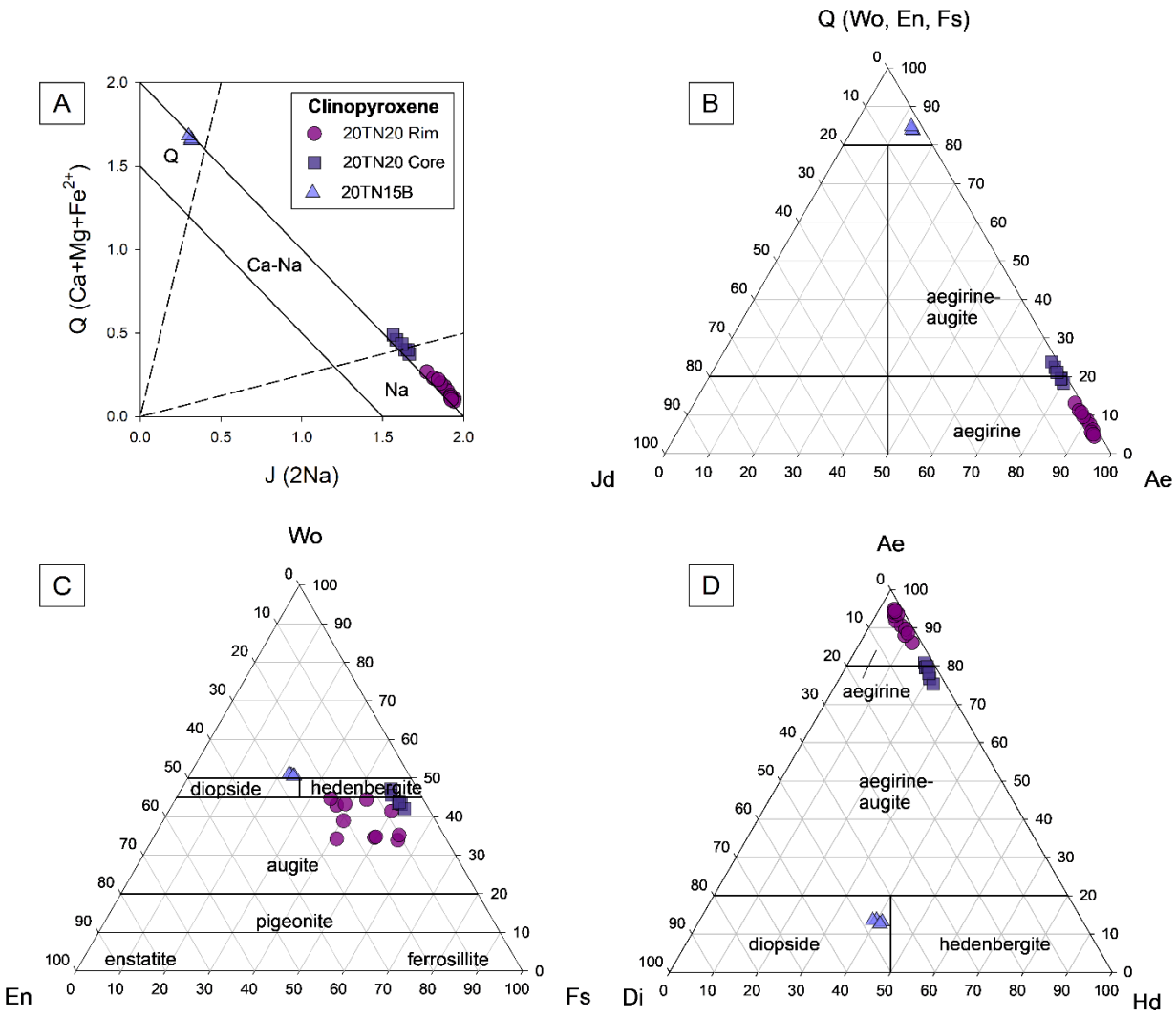

Figure 4.8. Pyroxene from the Bandito property plotted on compositional variation diagrams. (A) J vs. Q bivariate diagram. (B) Q-Jd-Ae ternary diagram (C) Wo-En-Fs ternary diagram. (D) Ae-Di-Hd ternary diagram. Wo – wollastonite ($Ca_2Si_2O_6$), En – enstatite ($Mg_2Si_2O_6$), Fs – ferrosilite ($Fe_2Si_2O_6$), Di – diopside ($MgCaSi_2O_6$), Ae – aegirine ($NaFeSi_2O_6$), Hd – hedenbergite ($FeCaSi_2O_6$).

Epidote-allanite

Epidote supergroup minerals have the general formula $A_2M_3(Si_2O_7)(SiO_4)O(OH)$ where A = large, high-coordination cations such as Ca, Mn^{2+}, Sr, Y, and REE^{3+}, and M = trivalent and sometimes divalent cations such as Al^{3+}, Fe^{3+}, Fe^{2+} and Mg^{2+}. The epidote supergroup includes species such as epidote and allanite, which were observed in the amphibole aegirine syenite, amphibole syenites, and fenites. Epidote and allanite commonly occur as discrete crystals, crystal clusters, and intergrowths with altered pyroxene, amphibole, and phlogopite. Average epidote compositions are shown in Table 4.6 and average allanite compositions are shown in Table 4.7.

With respect to epidote, Ca content is variable, where Ca from 18.97 wt. % (1.662 *apfu*) to 33.04 wt. % (2.857 *apfu*). Fe^{3+} content is variable, where Fe_2O_3 content ranges from 14.86 wt. % (0.867 *apfu*) to 24.09 wt. % (1.342 *apfu*). REE content ranges from 0.42 wt. % (0.011 *apfu*) to 5.02 wt. % (0.148 *apfu*). La content ranges from 0.01 wt. % to 1.28 wt. % (0.039 *apfu*). Ce content ranges from 0.00 wt. % to 2.04 wt. % (0.062 *apfu*).

With respect to allanite, Ca content is variable, where Ca from 8.71 wt. % (0.933 *apfu*) to 15.40 wt. % (1.428 *apfu*). Fe^{3+} content is variable, where Fe_2O_3 content ranges from 7.61 wt. % (0.515 *apfu*) to 28.81 wt. % (2.139 *apfu*). Fe^{2+} content is variable, where FeO content ranges from 0.00 wt. % to 8.99 wt. % (0.735 *apfu*). REE content ranges from 15.39 wt. % (0.485 *apfu*) to 28.73 wt. % (1.051 *apfu*). La content ranges from 2.96 wt. % (0.097 *apfu*) to 14.23 wt. % (0.493 *apfu*). Ce content ranges from 5.12 wt. % (0.169 *apfu*) to 12.64 wt. % (0.446 *apfu*).

According to the EMP analyses, REE-bearing epidote, allanite-(La), ferriallanite-(La), and ferriallanite-(Ce) compositions are present (Figure 4.9). Epidote and allanite compositions in the brecciated arfvedsonite-potassium feldspar fenite tend to have higher Al^{3+} content than compositions from the altered syenites. Ferriallanite from the altered syenites have higher Y+REE+Th *apfu* content than ferriallanite in the brecciated arfvedsonite-potassium feldspar fenite. In general, elemental substitutions between epidote and allanite compositions in the altered syenites can be explained by $Ca + Al^{3+} = Fe^{2+} + REE^{3+}$, and compositions in the layered fenite by $Ca + Fe^{3+} = Fe^{2+} + REE^{3+}$ based on discussions from Petrík et al. (1994).

Table 4.6. Average epidote compositions from various units from the 2020 Corundum Dome and Pyrochlore Dome sampling area.

unit (sample)	brecciated arfvedsonite-potassium feldspar fenite (20TN7)		actinolite-altered syenite (20TN4D)		actinolite-altered syenite (20TN6-2)		altered arfvedsonite-aegirine syenite (20TN20)	
analysis	average	σ	average	σ	average	σ	average	σ
n	8		4		6		4	
P_2O_5 (wt. %)	0.01	0.01	0.02	0.02	0.01	0.01	0.01	0.01
Nb_2O_5	0.00	0.01	0.00	0.00	0.01	0.01	0.01	0.01
SiO_2	37.28	0.10	36.64	0.18	36.47	0.25	37.41	0.19
TiO_2	0.02	0.02	0.02	0.01	0.07	0.06	0.05	0.03
ZrO_2	0.01	0.02	0.01	0.00	0.02	0.02	0.02	0.01
HfO_2	0.04	0.04	0.06	0.04	0.01	0.01	0.03	0.04
PbO	0.04	0.03	0.06	0.02	0.03	0.03	0.08	0.06
ThO_2	0.07	0.10	0.05	0.03	0.06	0.05	0.01	0.02
UO_2	0.04	0.02	0.04	0.02	0.04	0.04	0.03	0.02
$Al2O_3$	21.20	0.37	18.92	0.16	18.39	0.45	14.93	5.06
Fe_2O_3*	15.58	0.43	18.28	0.17	18.95	0.32	21.78	1.99
Y_2O_3	0.01	0.01	0.01	0.01	0.03	0.03	0.02	0.01
RE_2O_3	1.55	0.33	3.96	0.65	3.13	1.08	0.90	0.33
MgO	0.07	0.08	0.13	0.07	0.16	0.24	0.01	0.00
CaO	21.18	0.25	19.45	0.37	20.17	0.80	23.90	5.31
MnO	0.55	0.05	0.90	0.06	0.55	0.12	0.52	0.34
FeO*	0.00	0.00	0.00	0.00	0.00	0.00	0.00	0.00
Na_2O	0.01	0.02	0.01	0.00	0.01	0.01	0.01	0.00
K_2O	0.07	0.05	0.13	0.06	0.08	0.14	0.00	0.00
F	0.03	0.03	0.05	0.02	0.04	0.03	0.11	0.18
Cl	0.00	0.00	0.00	0.00	0.01	0.01	0.00	0.00
H_2O*	0.88	0.01	0.86	0.00	0.85	0.01	0.85	0.04
O=F,Cl	-0.01	0.01	-0.01	0.00	-0.01	0.01	-0.03	0.04
Total	98.65	0.21	99.57	0.19	99.05	0.38	100.64	1.91
P (*apfu*)	0.001	0.001	0.001	0.001	0.000	0.000	0.001	0.001
Nb	0.000	0.000	0.000	0.000	0.000	0.000	0.000	0.000
Si	3.000	0.000	3.000	0.000	3.000	0.000	3.000	0.000
Ti	0.001	0.001	0.001	0.001	0.004	0.004	0.003	0.002
Zr	0.001	0.001	0.000	0.000	0.001	0.001	0.001	0.000
Hf	0.001	0.001	0.001	0.001	0.000	0.000	0.001	0.001
Pb	0.001	0.001	0.001	0.001	0.001	0.001	0.002	0.001
Th	0.001	0.002	0.001	0.001	0.001	0.001	0.000	0.000
U	0.001	0.000	0.001	0.000	0.001	0.001	0.000	0.000
Al	2.010	0.032	1.826	0.011	1.782	0.041	1.409	0.474
Fe^{3+}	0.911	0.025	1.100	0.021	1.151	0.014	1.237	0.108
Y	0.000	0.000	0.000	0.000	0.001	0.001	0.001	0.000
REE	0.043	0.010	0.116	0.019	0.091	0.032	0.024	0.009
Mg	0.008	0.009	0.016	0.008	0.019	0.030	0.001	0.000
Ca	1.826	0.020	1.706	0.025	1.777	0.063	2.055	0.465
Mn	0.038	0.003	0.062	0.004	0.038	0.009	0.035	0.023
Fe^{2+}	0.000	0.000	0.000	0.000	0.000	0.000	0.000	0.000
Na	0.002	0.003	0.001	0.001	0.001	0.001	0.002	0.001
K	0.008	0.005	0.014	0.007	0.008	0.014	0.000	0.000
F^-	0.004	0.004	0.006	0.002	0.005	0.004	0.015	0.024
Cl^-	0.001	0.001	0.000	0.000	0.002	0.002	0.000	0.000
H	0.995	0.004	0.994	0.002	0.993	0.004	0.985	0.024
O (corrected)	12.000	0.000	12.000	0.000	12.000	0.000	12.000	0.000
Cation sum	7.858	0.022	7.855	0.014	7.886	0.018	7.787	0.100

Note: Compositions were recalculated on the basis of the sum of 3 Si cation *apfu*. * Calculated based on stoichiometry.

Table 4.7. Single and average allanite compositions from various units on the Bandito property.

unit (sample)	layered arfvedsonite-albite fenite (20TN23)	Brecciated arfvedsonite-potassium feldspar fenite (20TN7)		actinolite-altered syenite (20TN3-2)		actinolite-altered syenite(20TN6-2)		actinolite-altered syenite (20TN2)		actinolite-altered syenite (20TN4D)		altered arfvedsonite-aegirine syenite (20TN20)	
analysis	14-261-1	average	σ	average	σ	average	σ	average	σ	average	σ	average	σ
n	1	7		2		7		4		4		4	
P_2O_5 (wt. %)	0.02	0.01	0.01	0.01	0.01	0.04	0.02	0.02	0.01	0.03	0.04	0.01	0.00
Nb_2O_5	0.03	0.05	0.02	0.01	0.01	0.09	0.06	0.03	0.01	0.02	0.01	0.09	0.10
SiO_2	32.96	34.15	0.49	30.20	0.20	31.80	0.74	32.01	0.89	33.50	0.17	33.28	0.82
TiO_2	0.28	0.13	0.05	0.05	0.01	0.48	0.31	1.06	0.81	0.12	0.05	0.06	0.06
ZrO_2	0.04	0.03	0.02	0.01	0.01	0.02	0.02	0.00	0.00	0.01	0.02	0.00	0.00
HfO_2	0.00	0.04	0.03	0.01	0.01	0.04	0.05	0.06	0.04	0.03	0.04	0.05	0.05
PbO	0.06	0.04	0.04	0.02	0.02	0.05	0.03	0.09	0.04	0.03	0.03	0.05	0.05
ThO_2	0.30	0.08	0.06	0.03	0.02	0.03	0.04	0.14	0.05	0.02	0.02	0.01	0.02
UO_2	0.07	0.05	0.03	0.05	0.03	0.02	0.02	0.02	0.01	0.04	0.02	0.04	0.04
$Al2O_3$	17.70	19.54	0.82	4.76	0.78	13.25	1.45	11.81	1.69	16.50	1.18	15.04	0.95
Fe_2O_3*	8.33	9.90	1.88	25.67	3.14	11.48	2.53	15.24	2.45	13.06	2.53	16.47	1.15
Y_2O_3	0.07	0.01	0.02	0.04	0.04	0.08	0.03	0.03	0.01	0.02	0.01	0.03	0.01
RE_2O_3	20.75	16.98	1.10	27.86	0.87	23.90	2.36	22.87	2.72	20.16	1.86	18.85	2.62
MgO	0.42	0.19	0.08	0.25	0.02	0.49	0.16	0.21	0.05	0.31	0.04	0.15	0.10
CaO	12.72	14.45	0.47	8.78	0.07	11.04	0.93	11.51	1.27	12.97	0.39	13.57	1.18
MnO	1.81	1.68	0.30	0.62	0.06	1.54	0.36	1.31	0.47	1.93	0.34	1.34	1.00
FeO*	3.26	1.27	1.38	2.72	1.61	5.44	2.69	3.74	2.35	1.44	1.36	0.24	0.25
Na_2O	0.03	0.06	0.03	0.00	0.00	0.03	0.02	0.03	0.01	0.05	0.02	0.01	0.01
K_2O	0.06	0.04	0.02	0.00	0.00	0.03	0.02	0.04	0.07	0.09	0.03	0.00	0.00
F	0.07	0.06	0.03	0.03	0.03	0.08	0.10	0.02	0.02	0.06	0.05	0.01	0.01
Cl	0.00	0.02	0.01	0.01	0.01	0.01	0.01	0.02	0.01	0.04	0.01	0.00	0.00
H_2O*	0.80	0.82	0.01	0.69	0.00	0.76	0.02	0.76	0.02	0.79	0.00	0.79	0.02
O=F,Cl	-0.02	-0.02	0.00	-0.01	0.01	-0.02	0.02	-0.02	0.01	-0.03	0.01	0.00	0.00
Total	99.74	99.58	0.82	101.82	0.16	100.67	0.24	101.01	0.26	101.19	0.27	100.10	0.46
P (*apfu*)	0.001	0.001	0.001	0.001	0.001	0.003	0.002	0.002	0.001	0.002	0.003	0.000	0.000
Nb	0.001	0.002	0.001	0.001	0.001	0.004	0.003	0.001	0.001	0.001	0.001	0.004	0.004
Si	3.000	3.000	0.000	3.000	0.000	3.000	0.000	3.000	0.000	3.000	0.000	3.000	0.000
Ti	0.019	0.009	0.003	0.004	0.001	0.035	0.023	0.076	0.059	0.008	0.003	0.004	0.004
Zr	0.002	0.001	0.001	0.001	0.001	0.001	0.001	0.000	0.000	0.001	0.001	0.000	0.000
Hf	0.000	0.001	0.001	0.000	0.000	0.001	0.001	0.002	0.001	0.001	0.001	0.001	0.001
Pb	0.001	0.001	0.001	0.001	0.001	0.001	0.001	0.002	0.001	0.001	0.001	0.001	0.001
Th	0.006	0.002	0.001	0.001	0.000	0.001	0.001	0.003	0.001	0.000	0.000	0.000	0.000
U	0.001	0.001	0.001	0.001	0.001	0.000	0.001	0.000	0.000	0.001	0.000	0.001	0.001
Al	1.899	2.023	0.082	0.558	0.094	1.470	0.134	1.301	0.148	1.741	0.122	1.597	0.063
Fe^{3+}	0.571	0.647	0.114	1.917	0.222	0.813	0.169	1.072	0.153	0.880	0.171	1.111	0.053
Y	0.003	0.001	0.001	0.002	0.002	0.004	0.002	0.002	0.000	0.001	0.000	0.001	0.001
REE	0.690	0.544	0.041	1.012	0.039	0.823	0.097	0.785	0.113	0.658	0.064	0.622	0.101
Mg	0.056	0.025	0.010	0.037	0.003	0.069	0.023	0.030	0.008	0.041	0.005	0.021	0.014
Ca	1.240	1.360	0.032	0.934	0.001	1.115	0.069	1.153	0.094	1.244	0.033	1.309	0.084

unit (sample)	layered arfvedsonite-albite fenite (20TN23)	Brecciated arfvedsonite-potassium feldspar fenite (20TN7)		actinolite-altered syenite (20TN3-2)		actinolite-altered syenite(20TN6-2)		actinolite-altered syenite (20TN2)		actinolite-altered syenite (20TN4D)		altered arfvedsonite-aegirine syenite (20TN20)	
analysis	14-261-1	average	σ	average	σ	average	σ	average	σ	average	σ	average	σ
n	1	7		2		7		4		4		4	
Mn	0.139	0.125	0.022	0.052	0.004	0.123	0.029	0.104	0.037	0.147	0.026	0.104	0.079
Fe^{2+}	0.248	0.095	0.104	0.227	0.135	0.432	0.216	0.298	0.191	0.108	0.102	0.019	0.019
Na	0.005	0.010	0.005	0.001	0.001	0.006	0.003	0.006	0.002	0.009	0.004	0.001	0.001
K	0.007	0.004	0.002	0.000	0.000	0.004	0.003	0.005	0.008	0.011	0.004	0.000	0.000
F^-	0.010	0.009	0.005	0.005	0.005	0.014	0.016	0.004	0.004	0.009	0.008	0.001	0.002
Cl^-	0.000	0.005	0.003	0.005	0.002	0.003	0.003	0.007	0.002	0.012	0.002	0.001	0.001
H	0.989	0.986	0.003	0.990	0.007	0.983	0.018	0.989	0.004	0.980	0.009	0.997	0.002
O (corrected)	12.000	12.000	0.000	12.000	0.000	12.000	0.000	12.000	0.000	12.000	0.000	12.000	0.000
Cation sum	7.902	7.865	0.057	7.758	0.050	7.922	0.056	7.853	0.025	7.875	0.040	7.801	0.027

Note: Compositions were recalculated on the basis of the sum of 3 Si cation *apfu*. * Calculated based on stoichiometry.

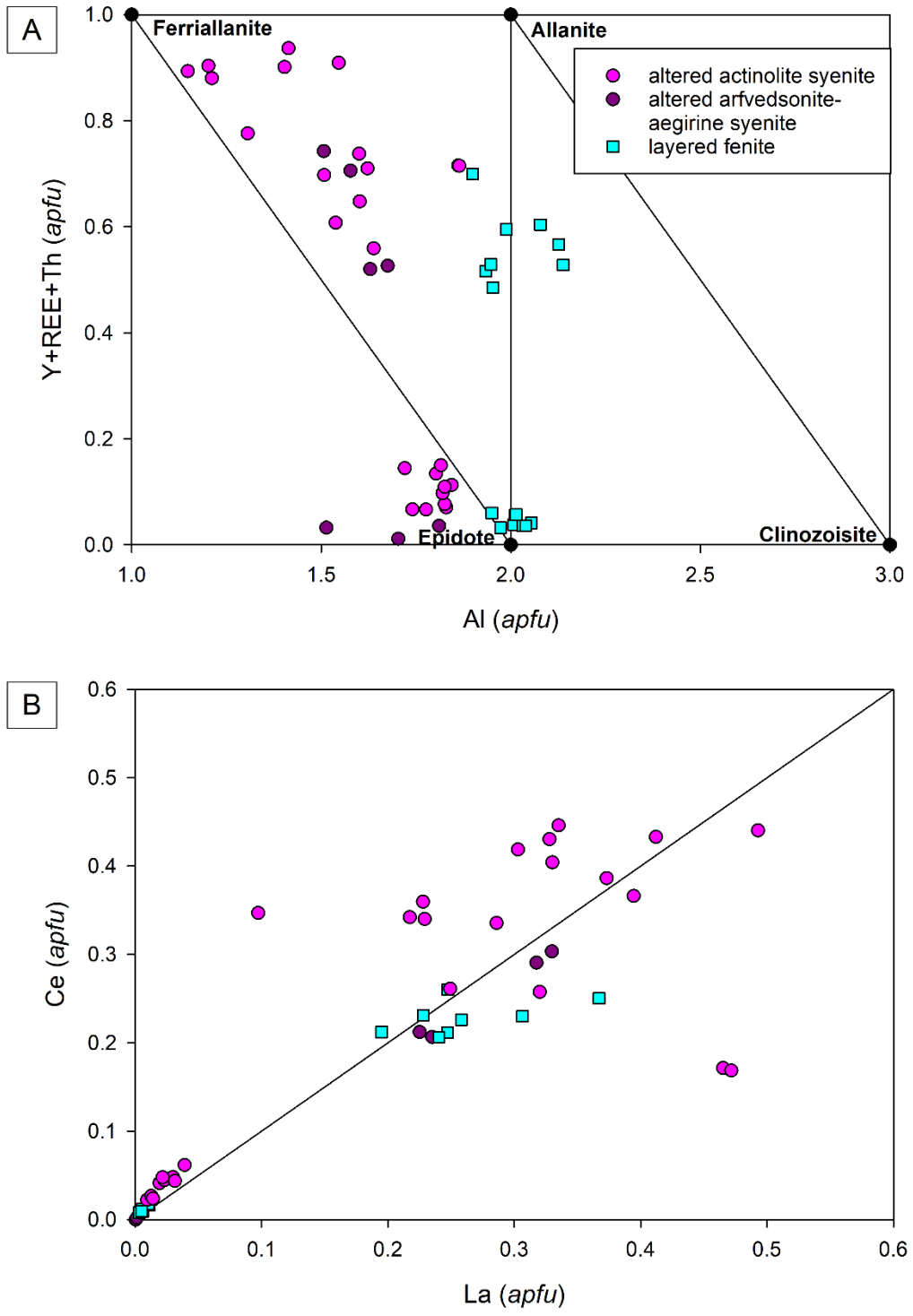

Figure 4.9. Chemical variation diagrams of epidote and ferriallanite in altered units on the Bandito property. (A) Y+REE +Th vs. Al_{tot} composition diagram after Petrík et al. (1995). (B) La *apfu* vs. Ce *apfu* bivariate diagram.

Titanite

Titanite, $CaTi[SiO_4](O,OH,F)$, is present in the actinolite-altered syenite, altered arfvedsonite-aegirine syenite, and layered titanite-arfvedsonite syenite samples and is common in the fenites. Titanite commonly occurs as discrete crystals and crystal clusters. Depending on the fenite sample, titanite crystals are moderately to strongly altered.

Titanite was analyzed from selected samples of the actinolite-altered syenite and fenites. Average titanite compositions are shown in Table 4.8. Titanite compositions from these units contain variable concentrations of Nb, Al, Fe, REE, Na, and F, where Nb range from 0.41 wt. % (0.006 *apfu*) to 7.29 wt. % (0.110 *apfu*) Nb_2O_5, Al ranges from 0.03 wt. % (0.001 *apfu*) to 9.41 wt. % (0.354 *apfu*) Al_2O_3, Fe ranges from 0.30 wt. % (0.007 *apfu*) to 3.70 wt. % (0.093 *apfu*) Fe_2O_3, REE range from 0.28 wt. % (0.003 *apfu*) to 4.81 wt. % (0.058 *apfu*) RE_2O_3, Na ranges from 0.01 wt. % (0.001 *apfu*) to 2.93 wt. % (0.191 *apfu*) Na_2O, and F range from 0.20 wt. % (0.021 *apfu*) to 2.37 (0.240 *apfu*) wt. %.

Titanite from the actinolite-altered syenite (20TN2) and layered arfvedsonite-albite fenite (20TN23) are strongly altered and have relatively higher Al, Fe, and F contents than the titanite in the layered titanite-arfvedsonite syenite (20TN15A) and brecciated arfvedsonite-potassium feldspar fenite (20TN7). Titanite from the layered titanite-arfvedsonite syenite has relatively high Y, REE, and Na, and low Ca contents with respect to the actinolite-altered syenite and layered arfvedsonite-albite fenite. The titanite in the brecciated arfvedsonite-potassium feldspar fenite has elevated Na content with respect to the titanite in the actinolite-altered syenite and layered arfvedsonite-albite fenite.

Table 4.8. Average composition of titanite from altered syenite and fenite units from the 2020 Corundum Dome and Pyrochlore Dome sampling area.

unit (sample)	actinolite-altered syenite (20TN2)		layered titanite-arfvedsonite syenite (20TN15A)		layered arfvedsonite-albite fenite (20TN23)		brecciated arfvedsonite-potassium feldspar fenite (20TN7)	
analysis	average	σ	average	σ	average	σ	average	σ
n	7		2		2		15	
P_2O_5 (wt. %)	0.01	0.01	0.02	0.02	0.12	0.03	0.02	0.01
Nb_2O_5	4.13	2.45	1.71	0.26	5.27	0.35	2.00	0.75
SiO_2	31.01	0.79	30.19	0.38	30.13	0.33	30.82	0.17
ZrO_2	0.05	0.03	0.07	0.07	0.47	0.04	0.21	0.24
HfO_2	0.05	0.05	0.03	0.03	0.08	0.01	0.03	0.03
TiO_2	26.85	1.83	38.13	0.49	22.79	0.28	37.88	1.00
PbO	0.04	0.04	0.01	0.01	0.06	0.06	0.02	0.03
ThO_2	0.03	0.04	0.01	0.01	0.84	0.41	0.05	0.05
UO_2	0.04	0.03	0.05	0.01	0.07	0.01	0.03	0.02
Al_2O_3	4.87	2.52	0.04	0.00	6.54	0.19	0.12	0.05
Fe_2O_3*	2.47	1.13	0.44	0.08	2.42	0.26	0.49	0.17
Y_2O_3	0.05	0.01	0.25	0.06	0.01	0.01	0.02	0.03
RE_2O_3	0.61	0.14	3.41	1.41	0.99	0.10	0.64	0.21
MgO	0.04	0.02	0.00	0.00	0.15	0.00	0.01	0.00
CaO	27.30	0.93	21.97	1.22	24.67	0.82	25.48	0.30
MnO	0.07	0.05	0.15	0.01	0.32	0.01	0.09	0.02
Na_2O	0.12	0.13	2.53	0.41	0.46	0.01	1.43	0.21
K_2O	0.15	0.16	0.01	0.00	0.10	0.03	0.04	0.04
F	1.38	0.68	0.66	0.03	1.60	0.07	0.36	0.11
Cl	0.05	0.03	0.01	0.01	0.10	0.04	0.00	0.01
O=F,Cl	-0.59	0.28	-0.28	0.01	-0.70	0.04	-0.15	0.04
Total	98.73	0.38	99.42	0.18	96.52	0.05	99.60	0.59
P (*apfu*)	0.000	0.000	0.001	0.001	0.003	0.001	0.000	0.000
Nb	0.062	0.037	0.026	0.004	0.081	0.006	0.030	0.011
Si	1.025	0.009	1.006	0.007	1.026	0.003	1.013	0.005
Zr	0.001	0.000	0.001	0.001	0.008	0.001	0.003	0.004
Hf	0.000	0.000	0.000	0.000	0.001	0.000	0.000	0.000
Ti	0.668	0.055	0.955	0.007	0.584	0.012	0.936	0.019
Pb	0.000	0.000	0.000	0.000	0.001	0.001	0.000	0.000
Th	0.000	0.000	0.000	0.000	0.007	0.003	0.000	0.000
U	0.000	0.000	0.000	0.000	0.001	0.000	0.000	0.000
Al	0.188	0.093	0.001	0.000	0.263	0.006	0.005	0.002
Fe^{3+}	0.062	0.029	0.011	0.002	0.062	0.007	0.012	0.004
Y	0.001	0.000	0.004	0.001	0.000	0.000	0.000	0.000
REE	0.007	0.002	0.041	0.017	0.011	0.001	0.007	0.002
Mg	0.002	0.001	0.000	0.000	0.008	0.000	0.000	0.000
Ca	0.967	0.015	0.784	0.039	0.900	0.023	0.897	0.013
Mn	0.002	0.001	0.004	0.000	0.009	0.000	0.003	0.001
Na	0.008	0.009	0.163	0.027	0.030	0.001	0.091	0.013
K	0.006	0.007	0.000	0.000	0.005	0.002	0.002	0.002
F^-	0.143	0.067	0.070	0.003	0.173	0.007	0.037	0.011
Cl	0.003	0.002	0.000	0.000	0.006	0.002	0.000	0.000
O	4.838	0.087	4.914	0.011	4.814	0.026	4.945	0.012
Sum	7.983	0.026	7.985	0.008	7.993	0.017	7.982	0.006

Note: Compositions were recalculated on the basis of the sum of 3 cation *apfu*. * All Fe assumed to be Fe_2O_3. Determined by stoichiometry using Droop (1987) calculation method.

Zircon

Zircon, $Zr(SiO_4)$, is present in all of the syenite and fenite samples. Notably, zircon in the fenite samples is very fine grained and were not analyzed. Zircon analyses from select samples are shown in Table 4.9. Zircon trace element chemistry collected by laser ablation inductively coupled mass spectrometry (LA-ICP-MS) can be found in Chapter 5 and Appendix C.

Across the analyzed suite of zircons, Zr ranges from 52.37 wt. % (0.818 *apfu*) to 63.63 wt. % (0.962 *apfu*), Hf ranges from 0.40 wt. % (0.004 *apfu*) to 1.25 wt. % (0.011 *apfu*), and REE range from 0.49 wt. % (0.005 *apfu*) to 1.50 wt. % (0.016 *apfu*). Zircon analyzed in the altered microsyenite (20TN2) has the highest Y_2O_3 of 1.39 wt. % (0.023 *apfu*). Zircon analyzed in the altered syenite (20TN12) has the highest RE_2O_3 of 1.50 wt. % (0.016 *apfu*).

The content wt. % totals of zircon in the nepheline syenite (20TN55A) are relatively low (95.93 to 98.13 wt. %) in comparison to the other units, likely due to missing elements and metamictization. Zircons in the actinolite-altered syenite sample (20TN4D) were analyzed for several elements but also report low totals (93.46 wt. % to 96.55 wt.%). The low content totals in the actinolite-altered syenite are likely due to alteration, which is supported by high Al up to 1.84 wt. % (0.069 *apfu*), Fe^{3+} up to 0.65 wt. % (0.017 *apfu*), and K up to 1.50 wt. % (0.061 *apfu*). The altered and layered amphibole-diopside-phlogopite syenite sample (20TN15B) has high totals (104.44 to 105.18 wt. %), where analyses have Al up to 0.30 wt. % (0.10 *apfu*), Fe^{3+} up to 0.32 wt. % (0.07 *apfu*), and Na up to 0.13 wt. % (0.007 *apfu*), indicating contaminated analyses. Micro inclusions were observed in the zircons in sample 20TN15B which are interpreted to be the cause of the contamination.

Table 4.9. Single and average compositions of zircon from various rock types from the 2020 Corundum Dome and Pyrochlore Dome sampling area.

unit (sample)	nepheline syenite (20TN55A)		actinolite-altered syenite (20TN4D)		altered arfvedsonite-aegirine syenite (20TN12)	actinolite-altered syenite (20TN2)		actinolite-altered syenite dikelet (20TN3-2)	layered titanite-arfvedsonite syenite (20TN15A)		layered arfvedsonite-diopside-phlogopite syenite (20TN15B)	
analysis	average	σ	average	σ	25-199-1	average	σ	53-293-3	average	σ	average	σ
n	5		3		1	10		1	2		3	
P_2O_5 (wt. %)	–	–	0.03	0.01	0.07	0.04	0.03	0.03	0.06	0.01	0.03	0.01
Nb_2O_5	–	–	1.19	1.39	0.20	0.07	0.03	0.09	0.08	0.01	0.06	0.01
SiO_2	33.30	0.23	30.49	2.78	34.76	33.40	0.28	33.30	32.92	0.08	38.97	0.28
ZrO_2	63.12	0.62	53.16	3.97	62.21	62.41	1.05	62.37	63.02	0.61	62.79	0.63
HfO_2	0.96	0.03	0.80	0.09	1.25	0.67	0.17	0.93	0.67	0.01	0.88	0.13
TiO_2	–	–	0.02	0.02	0.08	0.02	0.02	0.01	0.00	0.00	0.04	0.03
PbO	–	–	0.06	0.02	0.00	0.03	0.04	0.00	0.04	0.03	0.01	0.01
ThO_2	–	–	0.16	0.07	0.13	0.31	0.39	0.00	0.30	0.20	0.32	0.05
UO_2	–	–	0.36	0.08	0.03	0.04	0.03	0.06	0.08	0.05	0.11	0.06
Al_2O_3	–	–	0.75	0.77	0.00	0.01	0.01	0.01	0.02	0.00	0.11	0.13
Fe_2O_3*	–	–	0.50	0.17	0.10	0.09	0.08	0.50	0.08	0.02	0.27	0.05
Y_2O_3	–	–	0.43	0.02	0.09	0.70	0.33	0.70	0.03	0.01	0.22	0.08
RE_2O_3	–	–	0.71	0.12	1.50	0.76	0.18	0.83	0.88	0.32	0.74	0.10
MgO	0.00	0.00	0.03	0.01	0.01	0.00	0.00	0.00	0.00	0.00	0.00	0.00
CaO	–	–	0.25	0.23	0.02	0.06	0.03	0.08	0.01	0.01	0.02	0.02
MnO	–	–	0.04	0.01	0.02	0.02	0.02	0.01	0.01	0.01	0.03	0.01
Na_2O	–	–	0.04	0.01	0.03	0.02	0.01	0.01	0.02	0.00	0.06	0.05
K_2O	–	–	0.54	0.68	0.00	0.01	0.01	0.01	0.02	0.00	0.06	0.07
F	–	–	0.08	0.03	0.10	0.07	0.03	0.06	0.07	0.02	0.09	0.01
Cl	–	–	0.15	0.04	0.00	0.01	0.02	0.00	0.01	0.01	0.01	0.01
O=F,Cl	–	–	-0.07	0.02	-0.04	-0.03	0.01	-0.03	-0.03	0.01	-0.04	0.01
Total	97.38	0.77	89.70	7.60	100.56	98.72	0.48	98.97	98.26	0.04	104.80	0.30
P (*apfu*)	–	–	0.001	0.000	0.002	0.001	0.001	0.001	0.001	0.000	0.001	0.000
Nb	–	–	0.017	0.020	0.003	0.001	0.000	0.001	0.001	0.000	0.001	0.000
Si	1.035	0.004	1.033	0.032	1.050	1.032	0.003	1.027	1.024	0.001	1.105	0.006
Zr	0.957	0.004	0.881	0.044	0.917	0.940	0.009	0.938	0.956	0.006	0.868	0.010
Hf	0.008	0.000	0.008	0.000	0.011	0.006	0.002	0.008	0.006	0.000	0.007	0.001
Ti	–	–	0.000	0.000	0.002	0.001	0.000	0.000	0.000	0.000	0.001	0.001
Pb	–	–	0.001	0.000	0.000	0.000	0.000	0.000	0.000	0.000	0.000	0.000
Th	–	–	0.001	0.000	0.001	0.002	0.003	0.000	0.002	0.001	0.002	0.000
U	–	–	0.003	0.000	0.000	0.000	0.000	0.000	0.001	0.000	0.001	0.000
Al	–	–	0.029	0.029	0.000	0.000	0.000	0.000	0.001	0.000	0.004	0.004
Fe^{3+}	–	–	0.013	0.005	0.002	0.002	0.002	0.012	0.002	0.000	0.006	0.001
Y	–	–	0.008	0.001	0.001	0.012	0.006	0.012	0.000	0.000	0.003	0.001
REE	–	–	0.008	0.001	0.016	0.008	0.002	0.008	0.010	0.004	0.007	0.001
Mg	0.000	0.000	0.002	0.001	0.000	0.000	0.000	0.000	0.000	0.000	0.000	0.000
Ca	–	–	0.009	0.008	0.001	0.002	0.001	0.003	0.000	0.000	0.001	0.001
Mn	–	–	0.001	0.000	0.001	0.000	0.000	0.000	0.000	0.000	0.001	0.000
Na	–	–	0.003	0.000	0.002	0.001	0.001	0.001	0.001	0.000	0.003	0.003
K	–	–	0.022	0.028	0.000	0.001	0.000	0.000	0.001	0.000	0.002	0.002
F^-	–	–	0.008	0.003	0.009	0.007	0.003	0.006	0.007	0.002	0.008	0.001
Cl^-	–	–	0.009	0.003	0.000	0.000	0.001	0.000	0.000	0.000	0.001	0.000
Cation Sum	2.000	0.000	2.039	0.030	2.008	2.009	0.003	2.011	2.006	0.002	2.012	0.005

Note: Compositions were recalculated on the basis of 4 O *apfu*. * Determined by stoichiometry using Droop (1987) calculation method.

Thorite

Thorite, $Th(SiO_4)$, is present in trace amounts in the nepheline syenite, altered syenites, and fenites, commonly occurring with zircon, pyrochlore, allanite and as a replacement phase in areas of heavy alteration. Compositions of thorite in the altered arfvedsonite-aegirine syenite, actinolite-altered syenite, and fenites are reported in Table 4.10.

Overall, thorite totals and compositions measured are variable (91.25 to 103.43 wt. %), and cation sums are high (2.076 to 2.372 *apfu*), all of which indicate alteration and mixing with surrounding phases or micro inclusions. For example, thorite crystals in samples 20TN7 and 20TN15B have significantly higher F content than the other thorite analyses. The high F and REE content are attributed to mixing with an unknown Y-silicate phase (see Unidentified Phases subsection).

Table 4.10. Single and average compositions of thorite from various rock types from the 2020 Corundum Dome and Pyrochlore Dome sampling area.

unit (sample)	altered arfvedsonite-aegirine syenite (20TN12)	actinolite-altered syenite (20TN2)		actinolite-altered syenite dikelet (20TN3-2)		brecciated arfvedsonite-potassium feldspar fenite (20TN7)		altered and layered amphibole-diopside-phlogopite syenite (20TN15B)	
analysis	19-191-1	average	σ	average	σ	average	σ	average	σ
n	1	5		5		10		5	
P_2O_5 (wt. %)	0.32	0.06	0.04	0.19	0.21	1.09	0.42	1.08	0.85
Nb_2O_5	0.00	0.04	0.02	0.06	0.03	1.07	1.29	0.06	0.03
SiO_2	18.14	18.13	0.11	18.47	0.67	15.26	0.70	17.31	0.81
ZrO_2	0.24	0.14	0.08	0.24	0.18	0.28	0.09	0.19	0.22
HfO_2	0.16	0.16	0.09	0.03	0.02	0.09	0.10	0.10	0.07
TiO_2	0.06	0.12	0.09	0.03	0.04	2.16	1.41	0.16	0.11
PbO	0.90	1.09	0.69	0.68	0.21	0.20	0.11	0.34	0.12
ThO_2	65.98	66.43	1.12	66.42	2.37	66.51	3.03	64.29	9.33
UO_2	0.92	0.70	0.03	0.70	0.09	0.79	0.07	0.88	0.12
Al_2O_3	0.08	0.07	0.01	0.09	0.09	0.89	0.12	0.91	0.37
Fe_2O_3*	1.52	0.68	0.22	1.53	0.67	2.01	0.38	2.03	0.26
Y_2O_3	0.68	0.51	0.22	0.81	0.42	0.86	0.24	4.18	2.71
RE_2O_3	1.73	2.11	0.84	1.94	0.91	1.84	0.40	5.37	2.71
MgO	0.07	0.02	0.03	0.02	0.02	0.03	0.03	0.18	0.19
CaO	1.38	1.19	0.37	0.90	0.51	0.72	0.51	0.51	0.16
MnO	0.55	0.10	0.03	0.07	0.02	0.04	0.02	0.06	0.03
Na_2O	0.04	0.01	0.01	0.01	0.00	0.07	0.04	0.07	0.05
K_2O	0.10	0.06	0.00	0.05	0.01	0.09	0.02	0.22	0.11
F	0.70	0.83	0.16	0.70	0.36	3.43	0.32	4.64	0.35
Cl	0.00	0.11	0.14	0.02	0.02	0.00	0.01	0.01	0.01
O=F,Cl	-0.30	-0.38	0.09	-0.30	0.15	-1.45	0.13	-1.95	0.15
Total	93.27	92.20	0.90	92.66	0.95	96.00	1.61	100.63	2.78
P (*apfu*)	0.015	0.003	0.002	0.009	0.010	0.053	0.019	0.050	0.037
Nb	0.000	0.001	0.001	0.001	0.001	0.027	0.032	0.002	0.001
Si	1.003	1.034	0.012	1.026	0.020	0.882	0.029	0.977	0.025
Zr	0.006	0.004	0.002	0.007	0.005	0.008	0.003	0.005	0.005
Hf	0.003	0.003	0.001	0.000	0.000	0.002	0.002	0.002	0.001
Ti	0.002	0.005	0.004	0.001	0.002	0.092	0.058	0.007	0.005
Pb	0.013	0.017	0.011	0.010	0.003	0.003	0.002	0.005	0.002
Th	0.830	0.863	0.014	0.841	0.043	0.877	0.081	0.834	0.169
U	0.011	0.009	0.000	0.009	0.001	0.010	0.001	0.011	0.002
Al	0.005	0.005	0.001	0.006	0.006	0.061	0.009	0.059	0.021
Fe^{3+}	0.063	0.029	0.009	0.064	0.029	0.087	0.015	0.086	0.009
Y	0.020	0.016	0.007	0.024	0.012	0.027	0.008	0.121	0.075
REE	0.032	0.042	0.017	0.037	0.017	0.037	0.008	0.102	0.049
Mg	0.006	0.002	0.002	0.001	0.002	0.003	0.002	0.015	0.015
Ca	0.081	0.073	0.022	0.054	0.031	0.043	0.028	0.030	0.009
Mn	0.026	0.005	0.001	0.003	0.001	0.002	0.001	0.003	0.001
Na	0.004	0.001	0.001	0.001	0.001	0.008	0.004	0.007	0.005
K	0.007	0.005	0.000	0.004	0.001	0.006	0.001	0.015	0.007
F^-	0.123	0.151	0.029	0.124	0.065	0.631	0.088	0.833	0.105
Cl^-	0.000	0.011	0.014	0.002	0.002	0.000	0.000	0.001	0.001
Cation Sum	2.114	2.111	0.016	2.090	0.032	2.174	0.045	2.281	0.038

Note: Compositions were recalculated on the basis of 4 O *apfu*. * Determined by stoichiometry using Droop (1987) calculation method.

Phosphate compositions

Phosphate minerals are common in the syenite and fenite units within the Bandito property.

Apatite

Apatite, $Ca_5(PO_4)_3(OH,F,Cl)$, is present in the nepheline syenite, amphibole and pyroxene bearing syenites, fenites, and phlogopite altered porphyritic dike. With respect to the EMP analyses, most of the analyzed apatite crystals suffered moderate to high beam damage. Beam damage of apatite is indicated by gradual to sudden drops in recorded beam intensity for an analysis. The result of beam damage can significantly impact halogen variations, like F^- and Cl^- (Goldoff et al. 2012). Goldoff et al. (2012) discussed suboptimal and optimal operating conditions for EMP analyses of apatite crystals. Beam damage has resulted in high F content, and as a result, non-stoichiometric formulae calculated for most apatite crystals (i.e., F > 1 *apfu*); therefore, most apatite results are only semi-quantitative. Based on the suggested conditions of Goldoff et al. (2012), the biggest contributors to beam damage on apatite crystals were suboptimal beam sizes (i.e., less than 10 μm) due to small crystal sizes, measurements being conducted on crystallographic orientations close to the c-axis, using a beam current of 20 nA, and analysis of P and Ca later in the analytical scheme.

Single apatite analyses that are considered quantitative based on stoichiometry are reported in Table 4.11, and average apatite compositions of both quantitative and semi-quantitative analyses are shown in Table 4.12.

According to the EMP analyses, the apatite species present on the Bandito property is fluorapatite. Ca content ranges from 46.55 wt. % (4.551 *apfu*) to 54.40 wt. % (4.958 *apfu*), F content ranges 2.71 wt. % (0.713 *apfu*) to 4.97 wt. % (1.374 *apfu*), and Si contents range from 0.05 wt. % (0.004 *apfu*) to 4.09 wt. % (0.352 *apfu*). REE contents are variable and range from 0.57 wt. % (0.016 *apfu*) to 13.88 wt. % (0.465 *apfu*). Of the REE, Ce and La have the highest contents, where La contents range from 0.00 wt. % to 4.95 wt. % (0.168 *apfu*), and Ce contents range from 0.06 wt. % (0.002 *apfu*) to 6.45 wt. % (0.217 *apfu*). Zones with high REE contents

are visible in SEM-BSE images. The highest REE content in apatite crystals are in the layered titanite-arfvedsonite syenite (20TN15A) and nepheline syenite (20TN53).

Apatite crystals occur as discrete crystals in the observed units. Zoning in the analyzed apatite crystals is common and best observed under SEM-BSE (Figure 4.10). Zoning is normal (i.e., concentric) or blotchy depending on the crystal. REE content increases from darker regions to lighter regions (generally from core to rim).

Table 4.11. Quantitative apatite compositions from actinolite-altered syenite and layered amphibole-diopside-phlogopite syenite samples from the 2020 Corundum Dome and Pyrochlore Dome sampling area.

unit (sample)	actinolite-altered syenite (20TN4D)		layered amphibole-diopside-phlogopite syenite (20TN15B)			
analysis	17-231-5	17-2326	8-167-1	8-168-2	8-169-3	8-170-4
n	1	1	1	1	1	1
Nb_2O_5 (wt. %)	0.02	0.01	0.01	0.04	0.05	0.00
SiO_2	0.12	0.18	4.09	3.89	0.46	0.63
TiO_2	0.00	0.00	0.00	0.04	0.00	0.04
ZrO_2	0.09	0.13	0.08	1.19	0.14	0.14
HfO_2	0.10	0.04	0.14	0.24	0.00	0.06
PbO	0.04	0.03	0.00	0.03	0.09	0.00
ThO_2	0.00	0.01	0.61	0.29	0.14	0.23
UO_2	0.01	0.00	0.06	0.04	0.05	0.06
Al_2O_3	0.01	0.00	0.42	0.07	0.02	0.02
Y_2O_3	0.02	0.03	0.52	0.17	0.05	0.05
RE_2O_3	2.11	3.31	6.64	2.23	1.60	2.42
FeO	0.02	0.01	0.16	0.32	0.17	0.13
MnO	0.04	0.03	0.08	0.05	0.03	0.05
MgO	0.00	0.00	0.00	0.01	0.01	0.00
CaO	52.58	51.38	49.74	52.68	54.26	53.98
Na_2O	0.28	0.45	0.17	0.09	0.04	0.08
K_2O	0.00	0.00	0.40	0.03	0.09	0.04
P_2O_5	41.29	41.69	36.72	39.78	40.47	40.75
F	4.02	3.89	3.07	2.71	3.36	3.37
Cl	0.00	0.00	0.00	0.00	0.01	0.01
O=F,Cl	-1.69	-1.64	-1.29	-1.14	-1.41	-1.42
Total	99.07	99.57	101.62	102.76	99.61	100.64
Nb (*apfu*)	0.001	0.001	0.000	0.002	0.002	0.000
Si	0.011	0.015	0.352	0.323	0.039	0.053
Ti	0.000	0.000	0.000	0.003	0.000	0.003
Zr	0.004	0.006	0.003	0.048	0.006	0.006
Hf	0.002	0.001	0.003	0.006	0.000	0.001
Pb	0.001	0.001	0.000	0.001	0.002	0.000
Th	0.000	0.000	0.012	0.005	0.003	0.004
U	0.000	0.000	0.001	0.001	0.001	0.001
Al	0.001	0.000	0.043	0.007	0.002	0.002
Y	0.001	0.001	0.024	0.007	0.002	0.002
REE	0.065	0.103	0.206	0.066	0.047	0.071
Fe^{2+}	0.001	0.001	0.012	0.022	0.012	0.009
Mn	0.003	0.002	0.006	0.004	0.002	0.004
Mg	0.000	0.000	0.000	0.002	0.001	0.000
Ca	4.852	4.749	4.589	4.689	4.949	4.902
Na	0.046	0.076	0.029	0.014	0.006	0.012
K	0.000	0.000	0.044	0.003	0.010	0.005
P	3.011	3.044	2.677	2.798	2.917	2.924
F^-	1.095	1.062	0.837	0.713	0.904	0.903
Cl^-	0.000	0.000	0.000	0.000	0.001	0.002
O	11.998	12.073	12.069	12.260	11.991	12.032
Anion Sum	13.093	13.135	12.906	12.974	12.896	12.936

Note: Compositions were recalculated on the basis of the sum of 8 cation *apfu*.

Table 4.12. Average composition of apatite from various rock types from the 2020 Corundum Dome and Pyrochlore Dome sampling area. Averages were calculated using all data points.

unit (sample)	nepheline syenite (20TN53)		actinolite-altered syenite (20TN2, 20TN4D)		layered arfvedsonite-albite fenite (20TN25D)		layered arfvedsonite-albite fenite (20TN23)		layered amphibole-diopside-phlogopite syenite (20TN15B)		altered porphyritic lamprophyre(?) dike (20TN57C-1)	
analysis	average	σ	average	σ	average	σ	average	σ	average	σ	average	σ
n	17		9		8		6		8		11	
Nb_2O_5 (wt. %)	0.02	0.01	0.02	0.01	0.02	0.02	0.02	0.01	0.02	0.02	0.02	0.02
SiO_2	0.75	0.94	0.16	0.12	0.65	0.39	0.13	0.03	1.86	1.46	0.69	0.32
ZrO_2	0.11	0.04	0.12	0.03	0.12	0.02	0.13	0.02	0.36	0.41	0.11	0.02
HfO_2	0.04	0.04	0.05	0.04	0.03	0.03	0.05	0.10	0.09	0.07	0.03	0.03
TiO_2	0.02	0.02	0.02	0.02	0.02	0.03	0.04	0.03	0.01	0.02	0.04	0.02
PbO	0.03	0.03	0.03	0.03	0.05	0.03	0.03	0.02	0.04	0.04	0.04	0.04
ThO_2	0.05	0.04	0.03	0.06	0.04	0.04	0.04	0.04	0.29	0.18	0.05	0.04
UO_2	0.04	0.03	0.02	0.02	0.02	0.02	0.01	0.02	0.05	0.02	0.04	0.04
Al_2O_3	0.01	0.01	0.00	0.01	0.10	0.10	0.02	0.01	0.09	0.13	0.04	0.03
Y_2O_3	0.06	0.09	0.04	0.06	0.05	0.06	0.02	0.00	0.18	0.18	0.07	0.03
RE_2O_3	3.97	2.15	2.70	1.37	2.98	2.07	1.17	0.28	3.21	2.02	1.86	0.68
FeO	0.16	0.06	0.04	0.03	0.13	0.13	0.09	0.05	0.19	0.06	0.30	0.10
MnO	0.07	0.02	0.04	0.02	0.05	0.02	0.02	0.01	0.06	0.01	0.03	0.01
MgO	0.00	0.00	0.00	0.00	0.01	0.03	0.00	0.00	0.01	0.01	0.02	0.01
CaO	50.25	1.62	52.05	1.47	51.38	2.03	53.74	0.33	52.16	1.67	51.88	0.77
Na_2O	0.28	0.10	0.34	0.21	0.46	0.37	0.12	0.03	0.09	0.04	0.05	0.02
K_2O	0.03	0.04	0.00	0.00	0.00	0.00	0.02	0.01	0.12	0.12	0.14	0.10
P_2O_5	39.61	1.61	41.00	0.71	40.62	0.86	41.52	0.10	39.67	1.72	39.53	0.72
F	4.29	0.18	4.16	0.13	4.47	0.19	4.40	0.10	3.66	0.57	4.61	0.21
Cl	0.00	0.01	0.01	0.01	0.00	0.01	0.01	0.01	0.01	0.01	0.00	0.00
O=F,Cl	-1.81	0.07	-1.75	0.05	-1.88	0.08	-1.85	0.04	-1.54	0.24	-1.94	0.09
Total	97.98	1.38	99.08	0.52	99.33	0.39	99.72	0.35	100.63	1.00	97.61	0.70
Nb (*apfu*)	0.001	0.001	0.001	0.001	0.001	0.001	0.001	0.001	0.001	0.001	0.001	0.001
Si	0.067	0.086	0.014	0.011	0.056	0.034	0.011	0.003	0.159	0.125	0.061	0.028
Zr	0.005	0.002	0.005	0.001	0.005	0.001	0.005	0.001	0.015	0.017	0.005	0.001
Hf	0.001	0.001	0.001	0.001	0.001	0.001	0.001	0.002	0.002	0.002	0.001	0.001
Ti	0.001	0.001	0.001	0.002	0.001	0.002	0.003	0.002	0.001	0.001	0.002	0.001
Pb	0.001	0.001	0.001	0.001	0.001	0.001	0.001	0.000	0.001	0.001	0.001	0.001
Th	0.001	0.001	0.001	0.001	0.001	0.001	0.001	0.001	0.006	0.004	0.001	0.001
U	0.001	0.001	0.000	0.000	0.000	0.000	0.000	0.000	0.001	0.000	0.001	0.001
Al	0.001	0.001	0.001	0.001	0.010	0.011	0.002	0.001	0.009	0.013	0.004	0.003
Y	0.003	0.004	0.002	0.003	0.002	0.003	0.001	0.000	0.008	0.009	0.003	0.002
REE	0.127	0.072	0.084	0.044	0.093	0.067	0.035	0.009	0.099	0.064	0.057	0.022
Fe^{2+}	0.011	0.005	0.003	0.002	0.010	0.010	0.007	0.004	0.013	0.004	0.022	0.007
Mn	0.005	0.002	0.003	0.001	0.003	0.001	0.002	0.001	0.004	0.001	0.002	0.001
Mg	0.001	0.001	0.000	0.000	0.002	0.003	0.000	0.000	0.001	0.001	0.003	0.001
Ca	4.759	0.077	4.823	0.088	4.761	0.135	4.911	0.026	4.780	0.118	4.876	0.037
Na	0.049	0.018	0.058	0.036	0.078	0.063	0.019	0.005	0.015	0.006	0.009	0.004
K	0.004	0.004	0.000	0.000	0.001	0.000	0.002	0.001	0.013	0.013	0.015	0.011
P	2.963	0.087	3.002	0.023	2.974	0.034	2.998	0.008	2.872	0.110	2.936	0.032
F^-	1.200	0.045	1.137	0.036	1.222	0.040	1.187	0.029	0.992	0.163	1.280	0.051
Cl^-	0.001	0.001	0.001	0.001	0.001	0.001	0.001	0.001	0.001	0.001	0.000	0.001
O	11.960	0.032	11.972	0.040	11.930	0.031	11.935	0.012	12.042	0.089	11.856	0.033
Anion Sum	13.161	0.028	13.110	0.016	13.152	0.039	13.123	0.030	13.034	0.112	13.136	0.039

Note: Compositions were recalculated on the basis of the sum of 8 cation *apfu*.

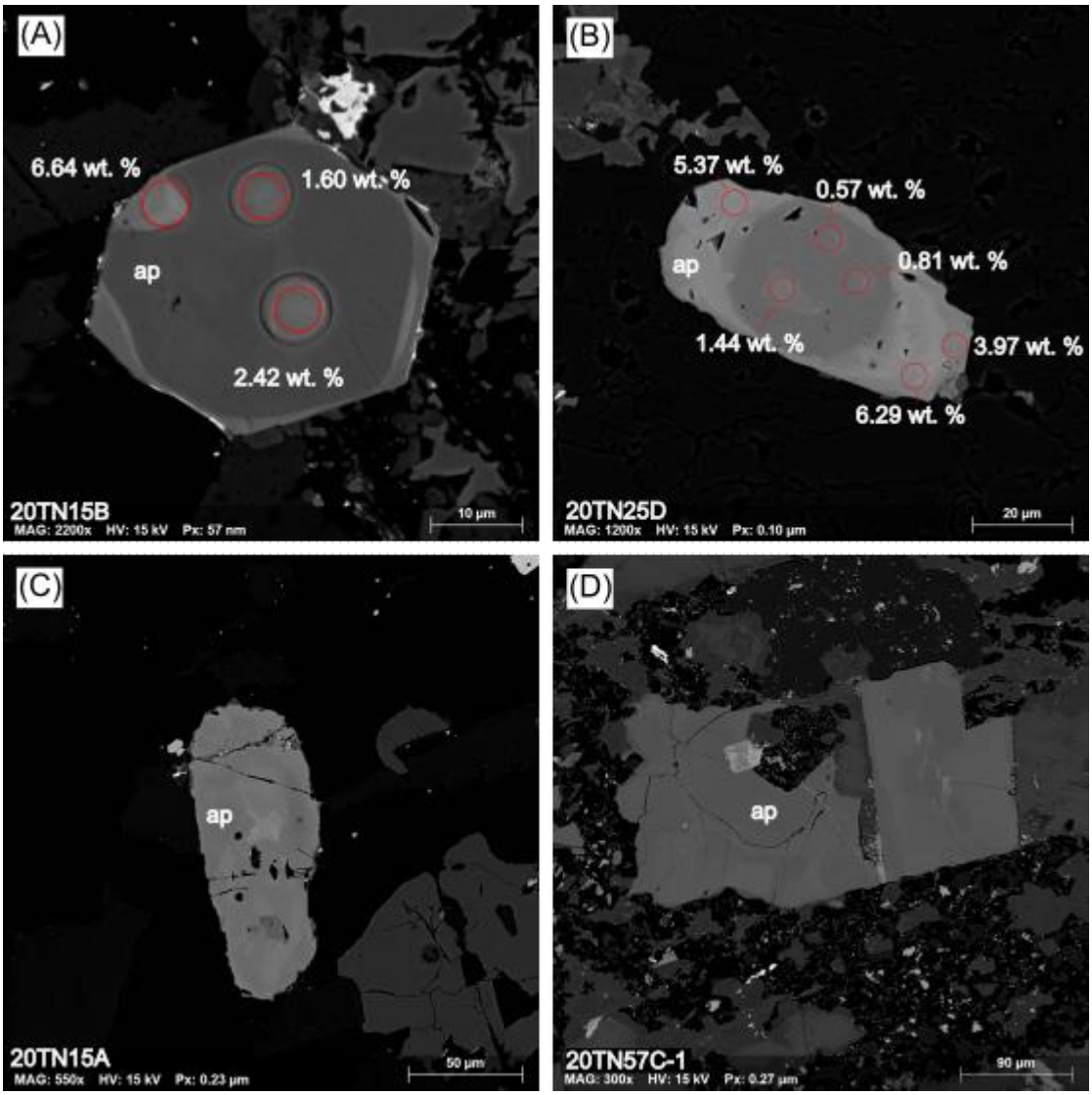

Figure 4.10. BSE images of zoning in fine-grained apatite crystals from a variety of altered units on the Bandito property. Examples of RE_2O_3 wt. % distribution from EMP analyses are shown in both (A) and (B). Red circles are to scale with the EMP beam diameter. (A) Zoned apatite in the altered and layered amphibole-diopside-phlogopite syenite (20TN15B). Beam damage from EMP analysis of the apatite is visible. (B) Zoned apatite in layered phlogopite-potassium feldspar fenite (20TN25D). (C) Blotchy zoning in an apatite crystal in layered titanite-arfvedsonite syenite (20TN15A). (D) Blotchy zoning in an apatite crystal in an altered porphyritic lamprophyre(?) dike (20TN57C-1). Both (A) and (B) show an increase in REE content from apatite core (darker area) to rim (lighter area).

Monazite

Monazite, $REE(PO_4)$, was observed in trace amounts in the quartzite, layered titanite-arfvedsonite syenite, altered arfvedsonite-aegirine syenite, and altered porphyritic lamprophyre(?) dike and occur as discrete crystals. Average monazite compositions from select samples are shown in Table 4.13.

According to the EMP analyses, most compositions are monazite-(Ce) and a few are monazite-(La). Ce content ranges from 26.89 wt. % (0.366 *apfu*) to 38.29 wt. % (0.549 *apfu*). La content ranges from 14.25 wt. % (0.203 *apfu*) to 34.17 wt. % (0.521 *apfu*). Compositions also contain relatively high concentrations of Pr and Nd, with Pr ranging from 3.38 wt. % (*apfu*) to 5.05 wt. % (*apfu*), and Nd from 2.46 wt. % (*apfu*) to 12.41 wt. % (*apfu*). Ca content is variable, where Ca ranges from 0.03 wt. % (0.001 *apfu*) to 7.73 wt. % (0.308 *apfu*).

Samples from the altered porphyritic lamprophyre(?) dike unit show the most Ce content, and crystals from the layered titanite-arfvedsonite syenite show the least. With the exception of one analysis from the quartzite, samples from the layered titanite-arfvedsonite syenite show the most La content, and crystals from the altered porphyritic lamprophyre(?) dike show the least. Samples from the altered porphyritic lamprophyre(?) dike shows the most Pr and Nd, and crystals from the layered titanite-arfvedsonite syenite show the least. Samples from the layered titanite-arfvedsonite syenite has the highest Ca, and crystals from the quartzite and altered porphyritic lamprophyre(?) dike show the least.

Table 4.13. Single and average composition of monazite from various units from the 2020 Corundum Dome and Pyrochlore Dome sampling area.

unit (sample)	altered arfvedsonite-aegirine syenite (20TN20)	quartzite (20TN17C)		layered titanite-arfvedsonite syenite (20TN15A)		altered porphyritic lamprophyre(?) dike (20TN57C-1)	
analysis	16-187-1	average	σ	average	σ	average	σ
n	1	5		5		3	
P_2O_5 (wt. %)	25.96	26.25	0.29	27.75	1.46	29.49	0.26
Nb_2O_5	0.00	0.01	0.01	0.01	0.01	0.02	0.02
SiO_2	0.44	0.45	0.13	0.73	0.31	0.35	0.06
TiO_2	0.04	0.03	0.02	0.02	0.03	0.43	0.28
ZrO_2	0.10	0.08	0.02	0.09	0.03	0.09	0.01
HfO_2	0.01	0.03	0.07	0.04	0.03	0.10	0.03
PbO	0.06	0.06	0.04	0.06	0.05	0.01	0.01
ThO_2	0.08	1.45	0.71	0.23	0.20	0.08	0.03
UO_2	0.09	0.11	0.05	0.07	0.02	0.06	0.02
Al_2O_3	0.02	0.01	0.02	0.03	0.02	0.07	0.01
Y_2O_3	0.08	0.16	0.07	0.08	0.06	0.04	0.00
La_2O_3	25.03	21.81	6.39	29.75	2.30	15.35	1.05
Ce_2O_3	34.38	34.01	2.08	29.48	1.31	38.07	0.17
Pr_2O_3	4.48	4.25	0.17	3.79	0.22	4.97	0.05
Nd_2O_3	6.15	7.16	2.32	3.53	0.93	11.25	1.00
Sm_2O_3	0.26	0.87	0.41	0.29	0.10	0.82	0.11
$HREE_2O_3$*	0.36	1.21	0.35	0.55	0.08	0.84	0.31
MgO	0.00	0.00	0.00	0.00	0.00	0.02	0.01
CaO	1.01	0.17	0.09	4.01	2.34	0.20	0.01
MnO	0.02	0.02	0.01	0.03	0.02	0.09	0.01
FeO	0.05	0.39	0.26	0.11	0.05	0.64	0.22
Na_2O	0.00	0.00	0.00	0.08	0.09	0.01	0.01
K_2O	0.00	0.02	0.01	0.07	0.04	0.10	0.02
F	0.00	0.00	0.00	0.09	0.18	0.00	0.00
Cl	0.00	0.01	0.01	0.01	0.01	0.03	0.01
O=F,Cl	0.00	0.00	0.00	-0.04	0.07	-0.01	0.00
Total	98.61	98.57	0.57	100.85	0.78	103.09	0.46
P (*apfu*)	0.915	0.926	0.004	0.921	0.018	0.960	0.003
Nb	0.000	0.000	0.000	0.000	0.000	0.000	0.000
Si	0.018	0.019	0.006	0.029	0.012	0.013	0.002
Ti	0.001	0.001	0.001	0.001	0.001	0.012	0.008
Zr	0.002	0.002	0.000	0.002	0.001	0.002	0.000
Hf	0.000	0.000	0.001	0.000	0.000	0.001	0.000
Pb	0.001	0.001	0.000	0.001	0.001	0.000	0.000
Th	0.001	0.014	0.007	0.002	0.002	0.001	0.000
U	0.001	0.001	0.000	0.001	0.000	0.001	0.000
Al	0.001	0.001	0.001	0.001	0.001	0.003	0.001
Y	0.002	0.004	0.002	0.002	0.001	0.001	0.000
La	0.384	0.335	0.096	0.431	0.044	0.218	0.014
Ce	0.524	0.519	0.033	0.424	0.032	0.536	0.001
Pr	0.068	0.065	0.003	0.054	0.004	0.070	0.001
Nd	0.091	0.107	0.035	0.050	0.013	0.155	0.015
Sm	0.004	0.012	0.006	0.004	0.001	0.011	0.002
HREE	0.005	0.016	0.005	0.007	0.001	0.010	0.004
Mg	0.000	0.000	0.000	0.000	0.000	0.001	0.001
Ca	0.045	0.008	0.004	0.165	0.092	0.008	0.000
Mn	0.001	0.001	0.000	0.001	0.001	0.003	0.000
Fe^{2+}	0.002	0.013	0.009	0.004	0.002	0.021	0.007
Na	0.000	0.000	0.000	0.006	0.006	0.000	0.001
K	0.000	0.001	0.001	0.003	0.002	0.005	0.001
F^-	0.000	0.000	0.000	0.010	0.021	0.000	0.000
Cl^-	0.000	0.001	0.001	0.001	0.001	0.002	0.001
Cation sum	2.065	2.046	0.004	2.108	0.031	2.031	0.007

Note: Compositions were recalculated on the basis of the sum of 4 O *apfu*. * Sum of Eu, Gd, Tb, Dy, Ho, Er, Tm, Yb, and Lu.

Carbonate compositions

Carbonate minerals are common in the argillite and altered units within the Bandito property. Calcite occurs as a replacement phase in the nepheline syenite and porphyritic dikes, and with epidote and fluorite in the actinolite-altered syenite and fenites on Corundum Dome. Rhodochrosite was observed as a replacement phase in a feldspar porphyritic dike. Bastnäsite, a REE carbonate mineral, is present as a replacement phase in the nepheline syenite, feldspar porphyritic dike, and fenites.

Calcite and rhodochrosite

Calcite ($CaCO_3$) is present in most units across the sampling area as an alteration product. Rhodochrosite (MnO_3) was identified in a single feldspar glomeroporphyritic dike sample (20TN54). Averages calcite and rhodochrosite analyses from select samples are shown in Table 4.14. In calcite, the Ca content ranges from wt. % (0.893 *apfu*) to wt. % (1.018 *apfu*). In rhodochrosite, Mn content ranges from 59.62 wt. % (0.951 *apfu*) to 60.33 wt. % (0.963 *apfu*), Mg from 1.25 wt. % (0.035 *apfu*) to 1.27 wt. % (0.036 *apfu*), and Fe^{2+} from 0.83 wt. % (0.013 *apfu*) to 1.35 wt. % (0.021 *apfu*).

Table 4.14. Compositions of calcite and rhodochrosite from samples of argillite, layered fenite, actinolite-altered syenite, and porphyritic dikes from the 2020 Corundum Dome and Pyrochlore Dome sampling area.

unit (sample)	argillite (20TN5)		actinolite-altered syenite dikelet (20TN3-2)		layered phlogopite-potassium feldspar fenite (20TN25D)		altered porphyritic lamprophyre(?) dike (20TN57C-1)		altered feldspar glomeroporphyritic dike (20TN54)	
analysis	average	σ	average	σ	average	σ	average	σ	average	σ
n	2		3		5		3		3	
CO_2* (wt%)	44.35	0.15	44.32	0.03	44.58	0.07	42.66	0.13	38.37	0.10
SiO_2	0.04	0.01	0.06	0.07	0.04	0.03	0.21	0.10	0.17	0.04
TiO_2	–	–	–	–	–	–	0.03	0.03	0.12	0.04
Al_2O_3	–	–	–	–	–	–	0.07	0.02	0.18	0.03
MgO	0.06	0.02	0.02	0.01	0.24	0.05	0.42	0.05	1.26	0.01
CaO	53.39	0.77	53.43	0.62	49.67	0.36	56.26	0.95	–	–
MnO	0.23	0.10	0.60	0.37	1.99	0.19	2.97	0.11	60.02	0.30
FeO	0.36	0.01	0.05	0.02	0.66	0.12	0.68	0.06	1.11	0.21
BaO	–	–	–	–	–	–	0.00	0.00	–	–
Na_2O	–	–	–	–	–	–	0.01	0.01	–	–
K_2O	–	–	–	–	–	–	0.22	0.02	–	–
F	–	–	–	–	–	–	0.06	0.04	–	–
O=F	–	–	–	–	–	–	-0.02	0.02	–	–
Total	98.43	0.48	98.49	0.12	97.18	0.20	103.55	0.59	101.23	0.26
C (*apfu*)	1.015	0.005	1.014	0.001	1.028	0.002	0.965	0.005	0.987	0.003
Si	0.001	0.000	0.001	0.001	0.001	0.000	0.004	0.002	0.003	0.001
Ti	–	–	–	–	–	–	0.000	0.000	0.002	0.001
Al	–	–	–	–	–	–	0.001	0.000	0.004	0.001
Mg	0.001	0.001	0.000	0.000	0.006	0.001	0.010	0.001	0.035	0.000
Ca	0.959	0.012	0.960	0.010	0.899	0.006	0.998	0.015	–	–
Mn	0.003	0.001	0.009	0.005	0.028	0.003	0.042	0.002	0.958	0.005
Fe^{2+}	0.005	0.000	0.001	0.000	0.009	0.002	0.009	0.001	0.017	0.003
Ba	–	–	–	–	–	–	0.000	0.000	–	–
Na	–	–	–	–	–	–	0.000	0.000	–	–
K	–	–	–	–	–	–	0.005	0.000	–	–
F^-	–	–	–	–	–	–	0.003	0.002	–	–

Note: Compositions were recalculated on the basis of 3 O *apfu*. All iron is assumed to be Fe^{2+}; – = not measured. * Determined by stoichiometry.

Bastnäsite

Bastnäsite, $(M)(CO_3)X$, where M = Y, REE, Th, and X = F, OH, was observed in trace amounts in the nepheline syenite, fenites, and altered dike as a replacement product. Average bastnäsite compositions from select samples are shown in Table 4.15. Bastnäsite is highly susceptible to beam damage. Some of the bastnäsite crystals became visibly damaged while selecting spots for EMP analysis (Figure 4.11). Total oxide wt. % values are generally over 100%, likely due to inclusions (evidenced by elevated content of non-formula elements, such as Si and Al), and beam damage.

According to the EMP analyses, most compositions are bastnäsite-(La) and bastnäsite-(Ce). REE content ranges from 64.01 wt. % (0.689 *apfu*) to 79.33 wt. % (1.217 *apfu*). F content ranges from 8.09 wt. % (0.760 *apfu*) to 13.46 wt. % (1.732 *apfu*). Of the REE, La and Ce are the most abundant, where La content ranges from 12.19 wt. % (0.144 *apfu*) to 45.10 wt. % (0.646 *apfu*), and Ce content ranges from 12.89 wt. % (0.170 *apfu*) to 40.23 wt. % (0.617 *apfu*). Compositions also contain relatively high concentrations of Pr and Nd, with Pr ranging from 3.87 wt. % (0.042 *apfu*) to 7.65 wt. % (0.104 *apfu*), and Nd from 1.15 wt. % (0.016 *apfu*) to 15.00 wt. % (0.173 *apfu*). Th contents range from 0.00 wt % to 7.32 wt. % (0.058 *apfu*).

Bastnäsite-(Ce) is the dominant variety in the layered phlogopite-potassium feldspar fenite (20TN25D) and altered and layered amphibole-diopside-phlogopite syenite (20TN15B). The nepheline syenite (20TN53 and 20TN57A) has both La and Ce species. The feldspar porphyritic dike and altered porphyritic lamprophyre(?) dike have bastnäsite-(Ce). The altered porphyritic lamprophyre(?) dike (20TN57C-1) and has the highest Nd content, and the layered titanite-arfvedsonite syenite (20TN15A) has the least. Bastnäsite crystals are tabular and commonly show lamellae visible under SEM-BSE imaging (Figure 4.11), where lighter lamellae have higher, and darker lamellae have lower REE contents. The darker lamellae with lower REE content have elevated Ca content in comparison to the lighter lamellae with higher REE content. The Ca versus REE+Y+Th bivariate diagram (Figure 4.12) shows a linear relationship, and that Ca substitutes for REE and other M site cations.

Table 4.15. Single and average compositions of bastnäsite from various units from the 2020 Corundum Dome and Pyrochlore Dome sampling area.

unit (sample)	layered titanite-arfvedsonite syenite(20TN15A)	altered and layered amphibole-diopside-phlogopite syenite (20TN15B)		layered phlogopite-potassium felspar fenite (20TN25D)		nepheline syenite (20TN53)		nepheline syenite (20TN57A)		feldspar glomeroporphyritic dike (20TN54)		altered porphyritic lamprophyre(?) dike (20TN57C-1)	
analysis	41-247-4	average	σ	average	σ	average	σ	average	σ	average	σ	average	σ
n	1	7		20		11		7		6		2	
P_2O_5 (wt. %)	0.00	0.05	0.08	0.01	0.01	0.06	0.05	–	–	0.03	0.03	0.02	0.02
Nb_2O_5	1.18	0.01	0.02	0.04	0.08	0.13	0.11	0.01	0.01	0.01	0.01	0.03	0.02
Ta_2O_5	–	–	–	–	–	–	–	0.20	0.03	–	–	–	–
CO_2*	17.87	19.15	2.38	17.96	1.26	19.38	1.79	18.60	1.00	18.51	1.12	21.81	0.56
SiO_2	0.18	1.44	0.82	0.31	0.40	0.83	0.87	0.69	0.79	0.71	0.57	1.59	1.00
ZrO_2	0.04	0.01	0.01	0.01	0.01	0.13	0.34	0.62	0.97	0.02	0.02	0.01	0.01
HfO_2	0.09	0.03	0.04	0.09	0.07	0.05	0.04	0.04	0.03	0.02	0.03	0.03	0.03
TiO_2	0.45	0.08	0.04	0.36	0.77	0.13	0.06	0.15	0.23	0.06	0.04	0.52	0.39
PbO	0.00	0.13	0.09	0.07	0.05	0.06	0.06	0.04	0.03	0.06	0.04	0.08	0.02
ThO_2	0.20	1.38	1.92	0.83	1.58	0.55	0.28	0.29	0.13	0.21	0.12	0.14	0.00
UO_2	0.09	0.07	0.03	0.06	0.04	0.05	0.04	0.13	0.10	0.05	0.03	0.03	0.03
Al_2O_3	0.01	0.29	0.26	0.06	0.13	0.30	0.35	0.11	0.12	0.25	0.19	0.36	0.23
Y_2O_3	0.00	0.59	0.51	0.04	0.03	0.20	0.06	0.15	0.07	0.09	0.05	0.08	0.04
RE_2O_3	77.81	73.28	4.95	74.93	3.43	71.69	4.77	73.12**	2.24**	77.58	1.83	67.22	0.73
MgO	0.00	0.18	0.30	0.00	0.00	0.09	0.27	–	–	0.02	0.02	0.02	0.00
CaO	0.41	2.71	3.29	1.42	2.15	2.76	3.62	1.77	1.90	1.90	2.37	6.99	0.17
MnO	0.12	0.04	0.02	0.04	0.02	0.19	0.09	0.00	0.00	0.02	0.01	0.06	0.01
FeO	0.29	0.48	0.36	0.11	0.10	1.34	0.71	0.00	0.00	0.24	0.19	0.55	0.04
Na_2O	0.13	0.13	0.20	0.06	0.11	0.05	0.13	0.00	0.00	0.13	0.18	0.20	0.20
K_2O	0.03	0.10	0.06	0.01	0.02	0.11	0.21	0.10	0.04	0.09	0.09	0.11	0.04
F	11.32	10.96	1.70	11.34	0.79	10.75	0.96	11.16	0.63	10.83	0.92	9.53	0.08
Cl	0.00	0.02	0.01	0.01	0.01	0.02	0.01	–	–	0.01	0.01	0.00	0.00
O=F,Cl	-4.77	-4.62	0.72	-4.78	0.33	-4.53	0.41	-4.70	0.26	-4.56	0.39	-4.01	0.03
Total	105.46	106.49	2.29	102.98	1.11	104.47	2.72	102.48	1.22	106.28	1.16	105.36	2.88
P (*apfu*)	0.000	0.002	0.003	0.000	0.000	0.002	0.002	–	–	0.001	0.001	0.000	0.000
Nb	0.021	0.000	0.000	0.001	0.001	0.002	0.002	0.000	0.000	0.000	0.000	0.000	0.000
Ta	–	–	–	–	–	–	–	0.002	0.000	–	–	–	–
C	0.947	0.939	0.020	0.970	0.010	0.957	0.026	0.976	0.012	0.940	0.010	0.949	0.026
Si	0.007	0.050	0.026	0.012	0.015	0.029	0.026	0.026	0.029	0.027	0.021	0.049	0.029
Zr	0.001	0.000	0.000	0.000	0.000	0.002	0.006	0.011	0.017	0.000	0.000	0.000	0.000
Hf	0.001	0.000	0.000	0.001	0.001	0.001	0.000	0.000	0.000	0.000	0.000	0.000	0.000
Ti	0.013	0.002	0.001	0.010	0.020	0.004	0.002	0.004	0.006	0.002	0.001	0.012	0.009
Pb	0.000	0.001	0.001	0.001	0.001	0.001	0.001	0.000	0.000	0.001	0.000	0.001	0.000
Th	0.002	0.012	0.018	0.007	0.013	0.005	0.003	0.003	0.001	0.002	0.001	0.001	0.000
U	0.001	0.001	0.000	0.001	0.000	0.000	0.000	0.001	0.001	0.000	0.000	0.000	0.000
Al	0.000	0.011	0.009	0.003	0.006	0.012	0.014	0.005	0.005	0.011	0.008	0.013	0.008
Y	0.000	0.011	0.010	0.001	0.001	0.004	0.001	0.003	0.001	0.002	0.001	0.001	0.001
REE	1.109	0.982	0.168	1.094	0.115	0.961	0.135	1.033	0.091	1.062	0.093	0.779	0.033
Mg	0.000	0.010	0.016	0.000	0.000	0.005	0.015	–	–	0.001	0.001	0.001	0.000
Ca	0.017	0.091	0.102	0.056	0.077	0.097	0.122	0.070	0.071	0.071	0.086	0.239	0.018
Mn	0.004	0.001	0.001	0.001	0.001	0.006	0.003	0.000	0.000	0.000	0.000	0.002	0.000
Fe^{2+}	0.009	0.015	0.013	0.004	0.003	0.042	0.024	0.000	0.000	0.008	0.006	0.015	0.002
Na	0.010	0.007	0.011	0.005	0.008	0.003	0.009	0.000	0.000	0.009	0.013	0.012	0.012
K	0.002	0.005	0.003	0.001	0.001	0.004	0.008	0.005	0.002	0.005	0.005	0.004	0.002
F^-	1.391	1.286	0.330	1.432	0.181	1.247	0.201	1.363	0.138	1.286	0.183	0.963	0.059
Cl^-	0.000	0.001	0.001	0.001	0.001	0.001	0.001	–	–	0.001	0.000	0.000	0.000
Cation Sum	2.144	2.141	0.075	2.167	0.045	2.136	0.037	2.139	0.035	2.141	0.040	2.079	0.024

Note: Compositions were recalculated on the basis of 3 O *apfu*. – = not measured. * Determined by stoichiometry. ** La, Ce, Pr, and Nd were the only REE contents analyzed.

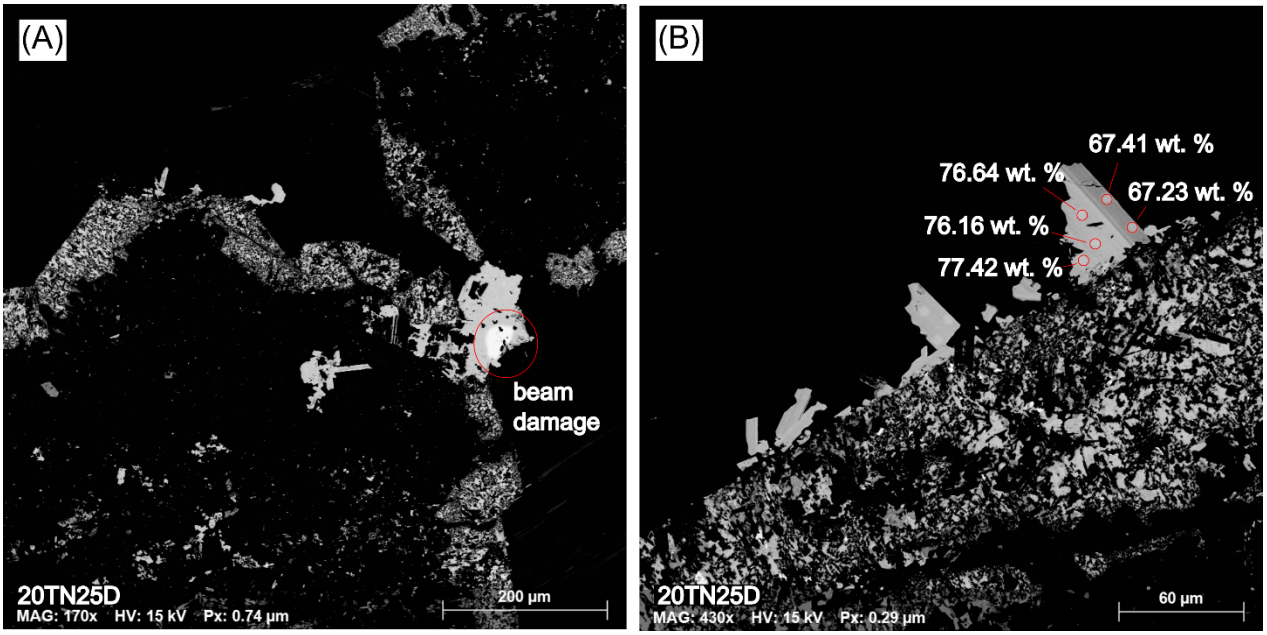

Figure 4.11. BSE images of bastnäsite from the layered phlogopite-potassium felspar fenite (sample 20TN25D). (A) Beam damage from EMP is outline in the red circle. (B) Tabular bastnäsite with lamellae. Examples of RE_2O_3 wt. % distribution from EMP analyses of light and darker lamellae. Red circles are to scale with the EMP beam diameter. REE content is higher in the lighter lamellae.

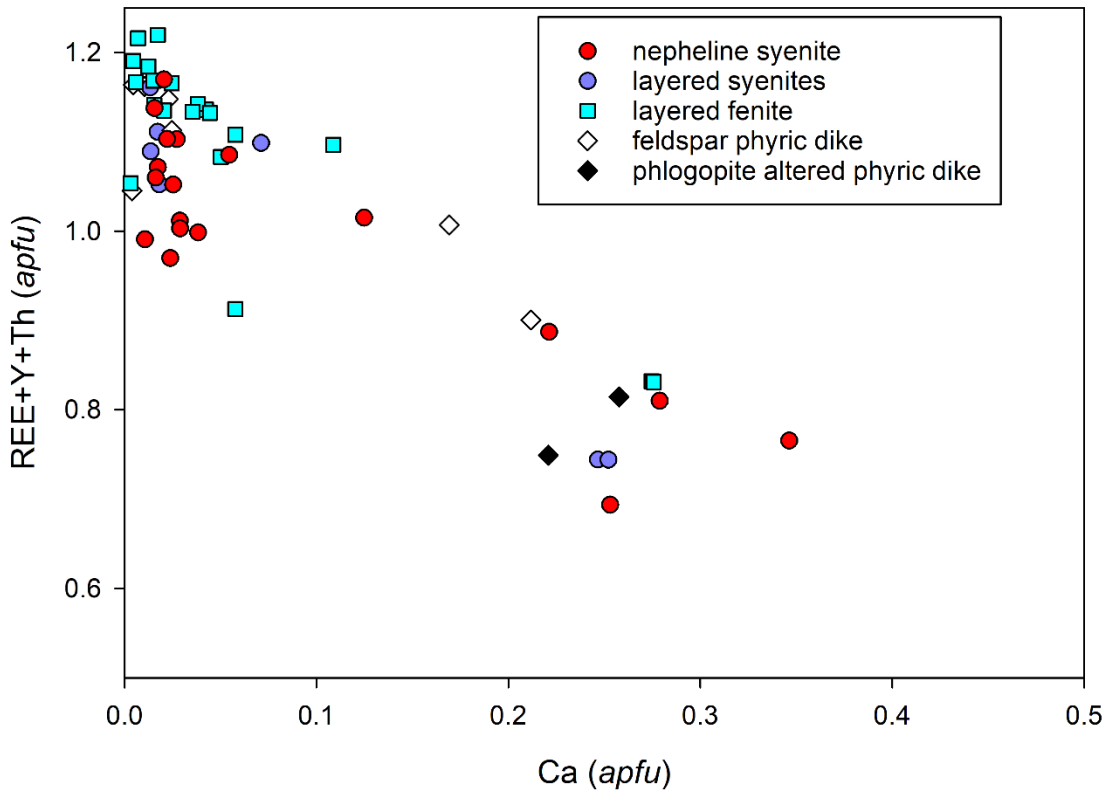

Figure 4.12. Ca versus REE+Y+Th bivariate diagram of bastnäsite analyses.

Oxide compositions

Oxide minerals are present in all of the units within the Bandito property. Fe, Ti, and Fe-Ti oxides are prevalent across all units. Niobium rich oxide minerals, such as pyrochlore and columbite are present in trace amounts in altered units.

Rutile, ilmenite, and hematite

Oxides such as rutile (TiO_2), ilmenite ($FeTiO_3$), and hematite (Fe_2O_3), are pervasive in units across the Bandito property. These oxides occur as discrete crystals, veins, and as symplectite intergrowths (see Chapter 3). Averages and single analyses from select samples for rutile are shown in Table 4.16 and ilmenite and hematite in Table 4.17.

Rutile was analyzed in nepheline syenite, altered syenite, and fenite samples. In these samples, Ti ranges from 90.35 wt. % (0.950 *apfu*) to 99.26 % (0.995 *apfu*), and Fe^{3+} from 0.43 wt. % (0.004 *apfu*) to 2.88 wt. % (0.031 *apfu*). In two samples (20TN15A and 20TN12), rutile was analyzed for Nb, REE, and other non-formula elements. In the two samples, Nb ranges from 0.96 wt. % (0.006 *apfu*) to 4.50 wt. % 0.027 *apfu*) and REE from 0.36 wt. % to 0.48 wt. % (0.002 *apfu*). Of the analyzed REE, Ce is the highest in concentration and ranges from 0.15 wt. % to 0.21 wt. % (0.001 *apfu*). Total wt. % contents are generally higher in rutile analyzed for Nb, REE, and other non-formula elements (99.97 wt. % to 100.84 wt. %) than rutile only analyzed for formula elements (94.44 wt. % to 100.21 wt. %), indicating that rutile analyses with relatively lower totals may also contain Nb, REE, and other non-formula elements.

Ilmenite in the argillite unit (20TN5) and altered porphyritic lamprophyre(?) dike (20TN57C-1) was analyzed. In these samples, Ti ranges from 51.68 wt. % (0.992 *apfu*) to 53.68 wt. % (1.068 *apfu*), Fe^{2+} from 38.35 wt. % (0.850 *apfu)* to 43.36 wt. % (0.926 *apfu*), and Fe^{3+} from 0.00 wt. % to 0.69 wt. % (0.013 *apfu*).

Hematite was analyzed from the nepheline syenite, fenite, dike, and quartzite samples. In hematite, Fe^{3+} content ranges from 75.52 wt. % (1.686 *apfu*) to 99.44 wt. % (1.999 *apfu*), Ti from 0.00 wt. % to 3.62 wt. % (0.073 *apfu*), and Si from 0.00 wt. % to 4.53 wt. % (0.134 *apfu*).

With respect to hematite analyses from the nepheline syenite and quartzite, Si contents are the highest and the total wt. % contents are the lowest. The elevated Si content and low totals likely represent micro inclusions and uncalculated H_2O.

Table 4.16. Compositions of rutile from units from the 2020 Corundum Dome and Pyrochlore Dome sampling area.

unit (sample)	layered titanite-arfvedsonite syenite (20TN15A)		altered arfvedsonite-aegirine syenite (20TN12)		nepheline syenite (20TN55A, 20TN57A)		altered arfvedsonite-aegirine syenite (20TN13A)		layered phlogopite-potassium feldspar fenite (20TN25D)
analysis	45-267-1	45-268-2	24-197-1	24-198-2	average	σ	average	σ	32-192-1
n	1		1		24		3		1
P_2O_5 (wt%)	0.04	0.03	0.00	0.02	–	–	–	–	–
Nb_2O_5	4.50	3.29	1.50	0.96	–	–	–	–	–
SiO_2	0.08	0.08	0.32	0.49	0.57	0.66	0.55	0.35	0.84
ZrO_2	0.00	0.03	0.01	0.01	–	–	–	–	–
HfO_2	0.09	0.07	0.01	0.01	–	–	–	–	–
TiO_2	94.64	94.40	96.44	96.87	95.67	2.75	92.47	2.36	93.07
ThO_2	0.00	0.02	0.00	0.07	–	–	–	–	–
UO_2	0.05	0.01	0.04	0.03	–	–	–	–	–
Al_2O_3	0.01	0.00	0.02	0.04	0.19	0.19	0.06	0.05	0.03
Fe_2O_3*	0.71	1.22	1.39	1.10	1.24	0.71	2.52	0.48	1.28
Y_2O_3	0.03	0.05	0.00	0.03	–	–	–	–	–
RE_2O_3	0.38	0.36	0.44	0.48	–	–	–	–	–
MgO	0.00	0.00	0.00	0.00	0.05	0.11	0.01	0.00	0.01
CaO	0.21	0.23	0.21	0.30	–	–	–	–	–
MnO	0.02	0.03	0.04	0.04	0.02	0.02	0.03	0.02	0.00
FeO*	0.00	0.00	0.00	0.00	0.00	0.00	0.00	0.00	0.00
PbO	0.00	0.01	0.00	0.00	–	–	–	–	–
Na_2O	0.01	0.01	0.07	0.10	–	–	–	–	–
K_2O	0.03	0.07	0.02	0.02	–	–	–	–	–
F	0.05	0.06	0.00	0.01	–	–	–	–	–
Cl	0.00	0.00	0.01	0.01	–	–	–	–	–
SUM	100.86	99.99	100.52	100.55	–	–	–	–	–
O=F,Cl	-0.02	-0.02	0.00	-0.01	–	–	–	–	–
Total	100.84	99.97	100.52	100.54	97.75	1.65	95.64	1.64	95.24
P (*apfu*)	0.000	0.000	0.000	0.000	–	–	–	–	–
Nb	0.027	0.020	0.009	0.006	–	–	–	–	–
Si	0.001	0.001	0.004	0.006	0.008	0.009	0.008	0.005	0.012
Zr	0.000	0.000	0.000	0.000	–	–	–	–	–
Hf	0.000	0.000	0.000	0.000	–	–	–	–	–
Ti	0.955	0.960	0.970	0.972	0.980	0.015	0.971	0.008	0.978
Th	0.000	0.000	0.000	0.000	–	–	–	–	–
U	0.000	0.000	0.000	0.000	–	–	–	–	–
Al	0.000	0.000	0.000	0.001	0.003	0.003	0.001	0.001	0.001
Fe^{3+}	0.007	0.012	0.014	0.011	0.013	0.008	0.027	0.005	0.013
Y	0.000	0.000	0.000	0.000	–	–	–	–	–
REE	0.002	0.002	0.002	0.002	–	–	–	–	–
Mg	0.000	0.000	0.000	0.000	0.001	0.002	0.000	0.000	0.000
Ca	0.003	0.003	0.003	0.004	–	–	–	–	–
Mn	0.000	0.000	0.000	0.000	0.000	0.000	0.000	0.000	0.000
Fe^{2+}	0.000	0.000	0.000	0.000	0.000	0.000	0.000	0.000	0.000
Pb	0.000	0.000	0.000	0.000	–	–	–	–	–
Na	0.000	0.000	0.002	0.003	–	–	–	–	–
K	0.001	0.001	0.000	0.000	–	–	–	–	–
F^-	0.002	0.002	0.000	0.001	–	–	–	–	–
Cl^-	0.000	0.000	0.000	0.000	–	–	–	–	–
Cation Sum	0.998	1.002	1.005	1.007	1.005	0.037	1.007	0.020	1.004

Note: Compositions were recalculated on the basis of 2 O *apfu*; – = not measured. * Determined by stoichiometry using Droop (1987) calculation method.

Table 4.17. Compositions of ilmenite, and hematite across the Bandito property.

unit (sample)	argillite (20TN24A)		altered porphyritic lamprophyre(?) dike (20TN57C-1)	nepheline syenite (20TN55A, 20TN57A, 20TN53)		layered fenite and actinolite-altered syenite (20TN4A, 20TN4D, 20TN6-2, 20TN10C)		quartzite and altered arfvedsonite-aegirine syenite (20TN17C, 20TN13B-2, 20TN20)		feldspar glomeroporphyritic dike (20TN54)		altered porphyritic lamprophyre(?) dike (20TN57C-1)	
analysis	average	σ	28-143-2	average	σ	average	σ	average	σ	average	σ	average	σ
n	3		1	10		17		7		2		4	
SiO_2 (wt%)	0.05	0.01	0.16	1.80	0.84	0.19	0.43	0.63	0.53	0.32	0.02	0.19	0.11
TiO_2	52.13	0.35	53.63	0.01	0.02	0.86	1.01	0.75	0.99	3.52	0.10	0.91	0.67
Al_2O_3	0.01	0.01	0.06	0.09	0.10	0.04	0.04	0.03	0.04	0.11	0.01	0.11	0.06
Fe_2O_3*	0.23	0.33	0.00	84.98	3.07	98.85	1.10	99.63	2.35	93.41	0.10	98.58	1.27
MgO	0.09	0.01	0.02	0.67	0.35	0.01	0.01	0.01	0.02	0.16	0.05	0.07	0.05
MnO	2.95	0.02	0.06	0.04	0.03	0.06	0.06	0.08	0.08	0.14	0.02	0.05	0.02
FeO*	42.84	0.36	38.35	0.00	0.00	0.00	0.00	0.00	0.00	0.00	0.00	0.00	0.00
Total	98.29	0.40	92.28	87.60	3.03	100.02	0.90	101.14	1.91	97.67	0.09	99.91	1.56
Si (*apfu*)	0.001	0.000	0.004	0.053	0.024	0.005	0.011	0.016	0.014	0.009	0.001	0.005	0.003
Ti	1.003	0.008	1.068	0.000	0.000	0.017	0.020	0.015	0.020	0.071	0.002	0.018	0.013
Al	0.000	0.000	0.002	0.003	0.003	0.001	0.001	0.001	0.001	0.004	0.000	0.004	0.002
Fe^{3+}	0.004	0.006	0.000	1.905	0.043	1.968	0.027	1.956	0.018	1.884	0.005	1.963	0.018
Mg	0.003	0.000	0.001	0.030	0.015	0.000	0.000	0.001	0.001	0.006	0.002	0.003	0.002
Mn	0.064	0.000	0.001	0.001	0.001	0.001	0.001	0.002	0.002	0.003	0.000	0.001	0.000
Fe	0.917	0.006	0.850	0.000	0.000	0.000	0.000	0.000	0.000	0.000	0.000	0.000	0.000
Cation sum	1.993	0.022	1.926	1.992	0.087	1.993	0.061	1.990	0.055	1.977	0.010	1.994	0.038

Note: Compositions were recalculated on the basis of 3 O *apfu*. * Determined by stoichiometry using Droop (1987) calculation method.

Pyrochlore

The Commission on New Minerals, Nomenclature, and Classification (CNMNC) review and revise the nomenclature of the pyrochlore supergroup minerals in Atencio et al. (2010), Christy and Atencio (2013), and Atencio (2021). The pyrochlore supergroup minerals have the general formula $A_{2-m}B_2X_{6-w}Y_{1-n}$, where the A site may host Na, Ca, Ag, Mn, Sr, Ba, Fe^{2+}, Pb^{2+}, Sn^{2+}, Sb^{3+}, Bi^{3+}, Y, REE, Sc, U, Th, □, or H_2O, B site may host Ta, Nb, Ti, Sb^{5+}, W, V^{5+}, Sn^{4+}, Zr, Hf, Fe^{3+}, Mg, Al, and Si, X site hosts O, and can include subordinate OH and F, and Y site hosts an anion (OH, F, O), vacancy (□), H_2O, or a large monovalent cation, for example, K, Cs, and Rb. Incomplete occupancy of the A, X, and Y sites are represented by parameters m, w, and n, respectively. In the nomenclature presented by the CNMNC, mineral groups (i.e., pyrochlore group, betafite group, microlite group, etc.) within the pyrochlore supergroup are defined by the dominant B site cation, and prefixes for mineral names within a group are based on the dominant A and Y site cations.

Pyrochlore group minerals are present in the actinolite-altered syenite, altered aegirine syenite, layered titanite-arfvedsonite syenite, and fenites. Pyrochlore analyses from select samples are shown in Table 4.18.

Across the analysed pyrochlore samples, Na, Ca, Fe, Ti, Nd, Ta, REE, and F contents are the most variable. Na content ranges 0.00 wt. % to 6.41 wt. % (0.814 *apfu*). Ca content ranges 6.84 wt. % (0.432 *apfu*) to 22.51 wt. % (1.520 *apfu*). Fe content ranges 0.05 wt. % (0.002 *apfu*) to 6.27 wt. % (0.305 *apfu*). Ti content ranges 0.67 wt. % (0.026 *apfu*) to 13.36 wt. % (0.585 *apfu*). Nb content ranges 43.43 wt. % (0.978 *apfu*) to 81.68 wt. % (1.955 *apfu*). In samples where Ta was analyzed, Ta content ranges from 0.18 wt. % (0.003 *apfu*) to 1.54 wt. % (0.026 *apfu*). REE content ranges 0.57 wt. % (0.011 *apfu*) to 17.95 wt. % (0.410 *apfu*). Of the REE, Ce is the highest in abundances, where Ce content ranges from 0.00 wt. % to 10.06 wt. % (0.232 *apfu*). F content ranges from 0.00 wt. % to 5.91 wt. % (1.134 *apfu*).

Based on the dominant components that make up the Y-site and A-site from EMP analyses, the variety of pyrochlore group minerals observed in this study are fluorcalciopyrochlore and kenopyrochlore (Figure 4.13). Relationships between A-site and Y-site vacancies in pyrochlore

are shown in the ternary diagram in Figure 4.13, and substitutions between Nb, Ti, Si, and Al at the B-site, and Na and F at the A-site in bivariate diagrams in Figure 4.14. There is a strong negative correlation between Nb and Ti content. In analyses where Nb contents are relatively low, Al contents are elevated. There is a positive correlation between REE+Y+Th and Ti content. There is a strong positive correlation between Na and F content.

Pyrochlore commonly shows alteration textures visible under the SEM (Figure 4.15). EMP analyses from zones of alteration show a decrease in Nb, Ca, Na, and F content, and increase in Al, Fe, Ti, REE, Y, and Th content. One of the altered areas in pyrochlore in sample 20TN6-2, has significantly elevated Pb content (up to 21.23 wt. %). The relative increase in A-site and Y-site vacancies, decrease in Nb, Ca, Na, and F content, and increase in Al, Fe, Ti, Pb, REE, Y, and Th content in pyrochlore is known to be driven by hydrothermal alteration of alkaline complexes (Nasraoui & Bilal 2000; Walter et al 2018). Therefore, alteration in pyrochlore in these samples is attributed to metasomatic alteration. Compositions that are fluorcalciopyrochlore are unaltered and igneous in origin, and compositions that are kenopyrochlore are altered or metasomatic in origin.

Table 4.18. Single and average compositions of pyrochlore from various units from the 2020 Corundum Dome and Pyrochlore Dome sampling area.

unit (sample)	actinolite-altered syenite (20TN2)		actinolite-altered syenite dikelet (20TN3-2)		actinolite-altered syenite (20TN4D)		actinolite-altered syenite (20TN6-2)		altered arfvedsonite-aegirine syenite (20TN12)	layered phlogopite-potassium feldspar fenite (20TN25D)		layered titanite-arfvedsonite syenite (20TN15A)		layered titanite-arfvedsonite syenite (20TN15A)		altered arfvedsonite-aegirine syenite (20TN20)		altered arfvedsonite-aegirine syenite (20TN20)	
analysis	avg.	σ	avg.	σ	avg.	σ	avg.	σ	23-196-1	avg.	σ	avg.	σ	avg.	σ	avg.	σ	avg.	σ
n	17		2		14		13		1	2		10		10		3		18	
Nb_2O_5 (wt. %)	64.89	13.39	69.68	2.25	69.96	8.52	73.51	10.12	53.41	46.48	1.19	51.23	2.11	55.27	0.71	57.91	0.93	63.99	2.43
Ta_2O_5	–	–	–	–	–	–	–	–	–	–	–	–	–	0.81	0.39	–	–	1.28	0.24
P_2O_5	0.02	0.02	0.02	0.01	0.03	0.02	0.05	0.10	0.00	0.01	0.01	0.02	0.02	–	–	0.02	0.01	–	–
SiO_2	0.55	0.84	0.62	0.30	4.54	4.77	1.30	2.40	0.17	2.87	0.02	1.10	2.06	0.02	0.04	0.44	0.06	0.09	0.08
TiO_2	5.62	3.69	3.93	0.78	2.31	1.89	2.03	0.78	7.78	12.73	0.48	9.56	1.26	9.22	1.42	4.55	0.43	4.36	0.51
ZrO_2	0.43	0.51	0.16	0.03	0.17	0.22	0.02	0.04	0.14	0.33	0.05	0.15	0.26	0.04	0.04	0.20	0.01	0.15	0.05
HfO_2	0.05	0.05	0.02	0.02	0.05	0.06	0.07	0.05	0.07	0.02	0.02	0.04	0.05	0.01	0.02	0.08	0.01	0.04	0.04
PbO	0.51	0.32	0.36	0.04	0.35	0.09	1.49	3.12	0.34	0.37	0.12	0.47	0.17	0.29	0.07	0.33	0.03	0.31	0.10
ThO_2	2.30	1.40	1.65	0.30	0.24	0.34	0.28	0.28	0.00	10.34	0.58	3.18	1.57	1.90	1.21	0.02	0.01	0.14	0.12
UO_2	0.13	0.07	0.26	0.00	0.33	0.32	0.30	0.48	0.31	0.24	0.04	0.42	0.14	0.67	0.18	0.50	0.05	0.72	0.20
Al_2O_3	0.06	0.08	0.02	0.00	1.39	1.44	0.41	0.67	0.00	0.23	0.07	0.24	0.58	0.00	0.00	0.02	0.00	0.01	0.01
Y_2O_3	0.41	0.20	1.18	0.20	0.21	0.09	0.72	0.37	0.15	0.24	0.04	0.14	0.09	0.10	0.11	0.07	0.02	0.06	0.03
RE_2O_3	3.30	3.49	2.82	0.08	2.26	1.15	1.48	0.59	9.22	9.16	0.93	7.74	4.46	7.36*	1.85*	9.43	0.90	3.54*	2.52*
MgO	0.00	0.01	0.01	0.01	0.06	0.18	0.36	0.93	0.00	0.09	0.03	0.02	0.03	–	–	0.01	0.01	–	–
CaO	17.32	3.65	12.37	1.45	15.58	2.15	15.72	2.12	18.24	5.11	1.73	14.15	2.93	15.81	1.85	17.07	0.32	19.53	1.37
MnO	0.14	0.06	0.63	0.22	0.27	0.15	0.15	0.04	0.32	1.35	0.92	0.38	0.31	0.22	0.12	0.31	0.02	0.17	0.06
FeO tot	0.67	0.61	2.63	1.17	1.24	1.71	1.85	1.23	0.14	4.35	1.38	0.85	0.89	0.30	0.20	0.20	0.10	0.14	0.10
Na_2O	0.79	0.99	0.03	0.01	0.90	1.41	0.42	0.98	2.48	0.04	0.01	4.51	2.33	5.36	1.76	2.22	0.14	3.12	0.87
K_2O	0.03	0.07	0.02	0.00	0.71	0.79	0.17	0.36	0.00	0.05	0.00	0.22	0.52	0.01	0.01	0.01	0.00	0.02	0.01
F	1.58	1.88	0.13	0.02	1.02	1.75	0.63	1.29	3.51	0.22	0.06	4.11	2.06	4.87	1.61	2.84	0.18	3.57	0.89
Cl	0.01	0.01	0.01	0.01	0.02	0.02	0.01	0.01	0.00	0.02	0.01	0.01	0.01	–	–	0.00	0.00	–	–
O=F,Cl	-0.67	0.79	-0.05	0.01	-0.43	0.74	-0.27	0.55	-1.48	-0.10	0.03	-1.73	0.86	-2.05	0.68	-1.19	0.07	-1.50	0.38
Total	98.16	3.06	96.51	0.61	101.19	2.13	100.71	2.28	94.81	94.14	0.41	96.80	1.35	100.23	1.09	95.01	0.11	99.74	0.59
Nb (*apfu*)	1.688	0.224	1.789	0.053	1.614	0.258	1.793	0.249	1.595	1.235	0.030	1.460	0.117	1.554	0.050	1.733	0.025	1.767	0.034
Ta	–	–	–	–	–	–	–	–	–	–	–	–	–	0.014	0.007	–	–	0.021	0.004
P	0.001	0.001	0.001	0.000	0.001	0.001	0.002	0.004	0.000	0.000	0.000	0.001	0.001	–	–	0.001	0.000	–	–
Si	0.034	0.051	0.035	0.017	0.206	0.208	0.067	0.120	0.011	0.168	0.001	0.062	0.109	0.002	0.002	0.029	0.004	0.005	0.005
Ti	0.259	0.182	0.168	0.034	0.096	0.095	0.083	0.034	0.387	0.563	0.022	0.454	0.068	0.429	0.053	0.227	0.022	0.201	0.026
Zr	0.013	0.016	0.004	0.001	0.004	0.005	0.000	0.001	0.004	0.010	0.001	0.005	0.008	0.001	0.001	0.007	0.000	0.004	0.002
Hf	0.001	0.001	0.000	0.000	0.001	0.001	0.001	0.001	0.001	0.000	0.000	0.001	0.001	0.000	0.000	0.001	0.000	0.001	0.001
Pb	0.008	0.006	0.006	0.001	0.005	0.001	0.021	0.042	0.006	0.006	0.002	0.008	0.003	0.005	0.001	0.006	0.001	0.005	0.002
Th	0.032	0.021	0.021	0.004	0.003	0.004	0.003	0.003	0.000	0.138	0.008	0.046	0.023	0.027	0.015	0.000	0.000	0.002	0.002
U	0.002	0.001	0.003	0.000	0.004	0.005	0.004	0.005	0.005	0.003	0.001	0.006	0.002	0.009	0.003	0.007	0.001	0.010	0.003
Al	0.004	0.005	0.001	0.000	0.074	0.075	0.025	0.039	0.000	0.016	0.005	0.016	0.036	0.000	0.000	0.002	0.000	0.000	0.000
Y	0.012	0.006	0.036	0.006	0.006	0.003	0.021	0.011	0.005	0.008	0.001	0.005	0.003	0.003	0.003	0.002	0.001	0.002	0.001
REE	0.070	0.079	0.054	0.002	0.042	0.025	0.027	0.010	0.221	0.193	0.021	0.178	0.103	0.167*	0.038*	0.227	0.022	0.080*	0.058*
Mg	0.000	0.000	0.001	0.001	0.004	0.014	0.028	0.069	0.000	0.008	0.002	0.001	0.002	–	–	0.001	0.001	–	–

unit (sample)	actinolite-altered syenite (20TN2)		actinolite-altered syenite dikelet (20TN3-2)		actinolite-altered syenite (20TN4D)		actinolite-altered syenite (20TN6-2)		altered arfvedsonite-aegirine syenite (20TN12)	layered phlogopite-potassium feldspar fenite (20TN25D)		layered titanite-arfvedsonite syenite (20TN15A)		layered titanite-arfvedsonite syenite (20TN15A)		altered arfvedsonite-aegirine syenite (20TN20)		altered arfvedsonite-aegirine syenite (20TN20)	
analysis	avg.	σ	avg.	σ	avg.	σ	avg.	σ	23-196-1	avg.	σ	avg.	σ	avg.	σ	avg.	σ	avg.	σ
n	17		2		14		13		1	2		10		10		3		18	
Ca	1.093	0.291	0.752	0.087	0.867	0.230	0.914	0.159	1.291	0.322	0.109	0.955	0.208	1.056	0.138	1.210	0.020	1.278	0.088
Mn	0.007	0.003	0.030	0.011	0.011	0.006	0.007	0.002	0.018	0.067	0.046	0.020	0.017	0.012	0.006	0.017	0.001	0.009	0.003
Fe^{2+}	0.033	0.032	0.125	0.056	0.058	0.084	0.082	0.053	0.008	0.214	0.068	0.045	0.047	0.015	0.010	0.011	0.005	0.007	0.005
Na	0.098	0.123	0.004	0.001	0.098	0.158	0.048	0.117	0.318	0.005	0.001	0.551	0.288	0.651	0.214	0.285	0.017	0.370	0.102
K	0.002	0.005	0.002	0.000	0.041	0.044	0.011	0.023	0.000	0.004	0.000	0.015	0.035	0.001	0.001	0.000	0.000	0.001	0.001
F^-	0.316	0.381	0.023	0.004	0.188	0.329	0.115	0.250	0.733	0.041	0.012	0.818	0.408	0.965	0.319	0.593	0.035	0.690	0.171
Cl^-	0.001	0.001	0.000	0.000	0.002	0.001	0.001	0.001	0.000	0.002	0.001	0.001	0.001	–	–	0.000	0.000	–	–
O^{2-}	6.064	0.070	5.978	0.031	5.765	0.353	5.937	0.273	6.260	5.773	0.032	5.999	0.190	6.042	0.039	6.314	0.021	6.180	0.062
Cation sum	3.358	0.390	3.033	0.009	3.134	0.384	3.137	0.209	3.872	2.959	0.027	3.828	0.351	3.946	0.295	3.766	0.007	3.765	0.143
Anion sum	6.382	0.447	6.002	0.028	5.954	0.553	6.052	0.312	6.993	5.816	0.020	6.818	0.408	7.007	0.345	6.908	0.015	6.871	0.163

Note: Compositions were recalculated on the basis of the sum of 2 B site cation *apfu*. * La, Ce, Pr, and Nd were the only REE contents analyzed.

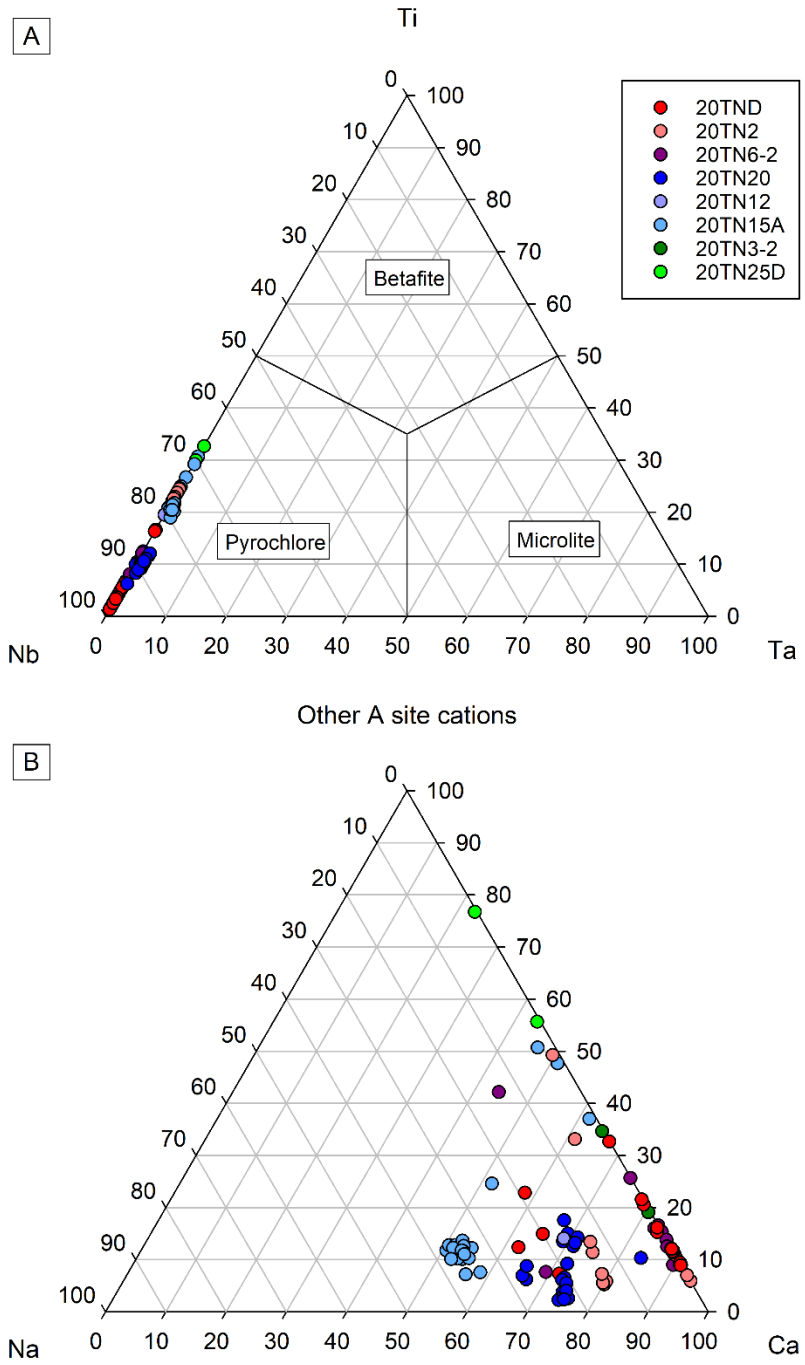
A
Ti
Nb
Ta
Other A site cations
B
Na
Ca
Betafite
Pyrochlore
Microlite
20TND
20TN2
20TN6-2
20TN20
20TN12
20TN15A
20TN3-2
20TN25D

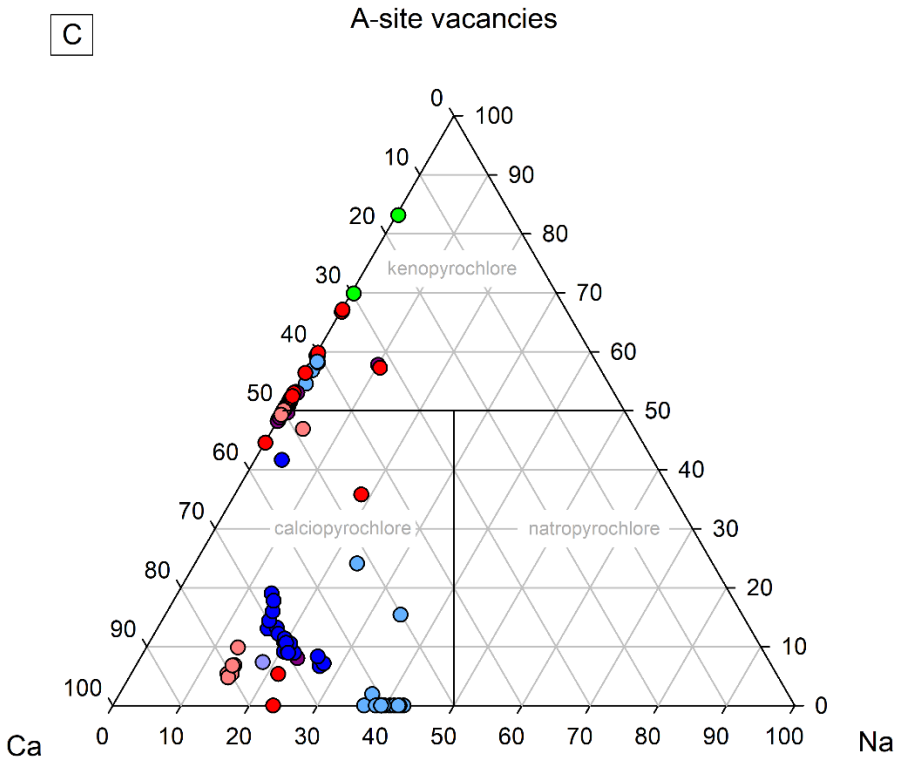

Figure 4.13. Pyrochlore group and composition ternary diagrams from select samples on the Bandito property. (A) Pyrochlore-supergroup minerals B-site composition ternary diagram modified from Hogarth (1977). (B) Pyrochlore-supergroup minerals, A-site composition ternary diagram modified from Atencio et al. (2010). (C) Ca-Na-A-site vacancies ternary diagram modified from Zurevinski & Mitchell (2004). Note, any negative *apfu* values that were calculated for the A-site vacancies were forced to zero.

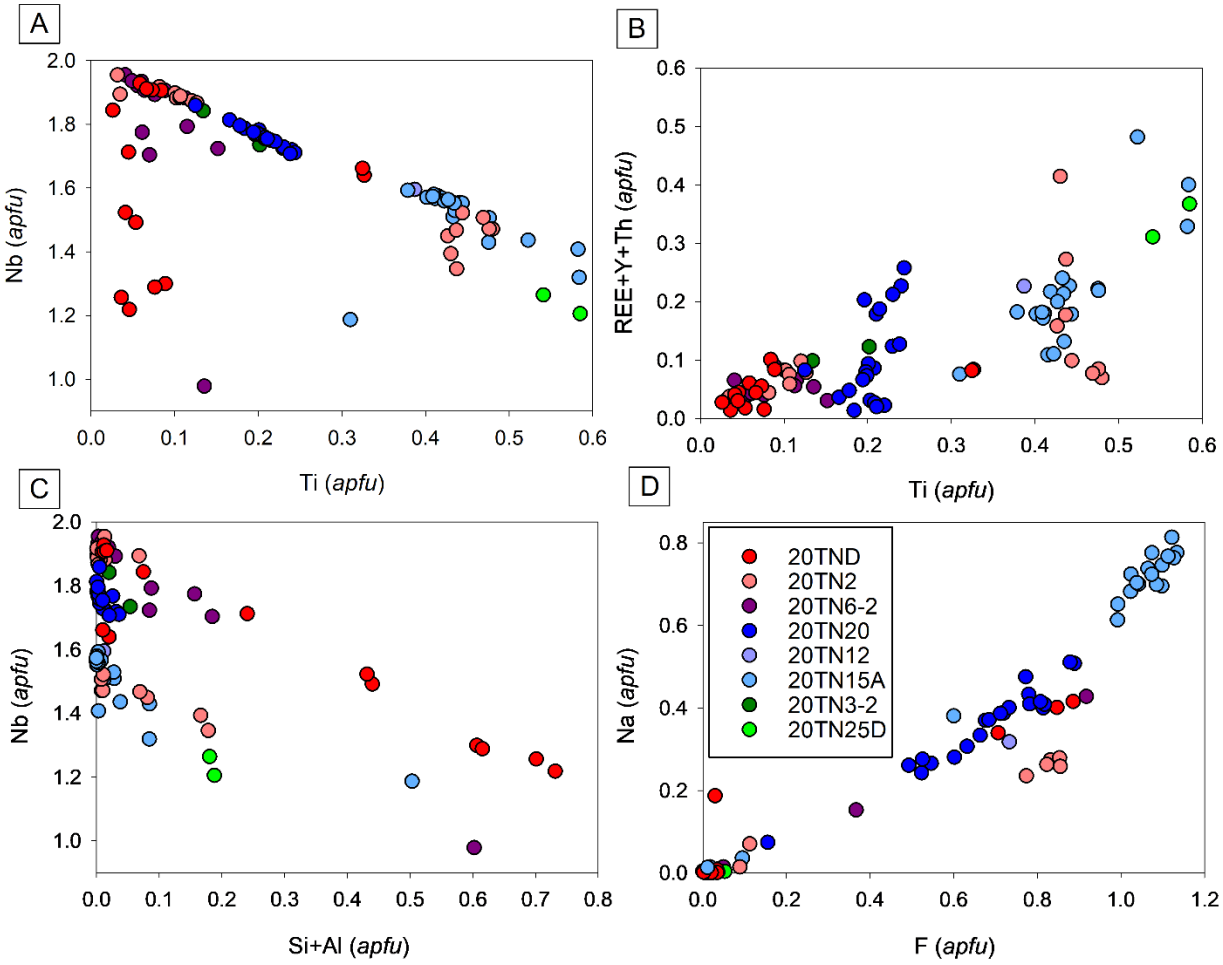

Figure 4.14. Pyrochlore bivariate diagrams of select elements. (A) Ti (*apfu*) versus Nb (*apfu*). Samples show a strong negative correlation between Ti and Nb content. (B) Ti (*apfu*) versus REE+Y+Th (*apfu*). Samples show a positive correlation between Ti and REE+Y+Th content. (C) Al (*apfu*) versus Nb (*apfu*). Samples that are outliers in (A) show a negative correlation between Si+Al and Nb content. (D) F (*apfu*) versus Na (*apfu*). Samples show a positive correlation between F and Na content.

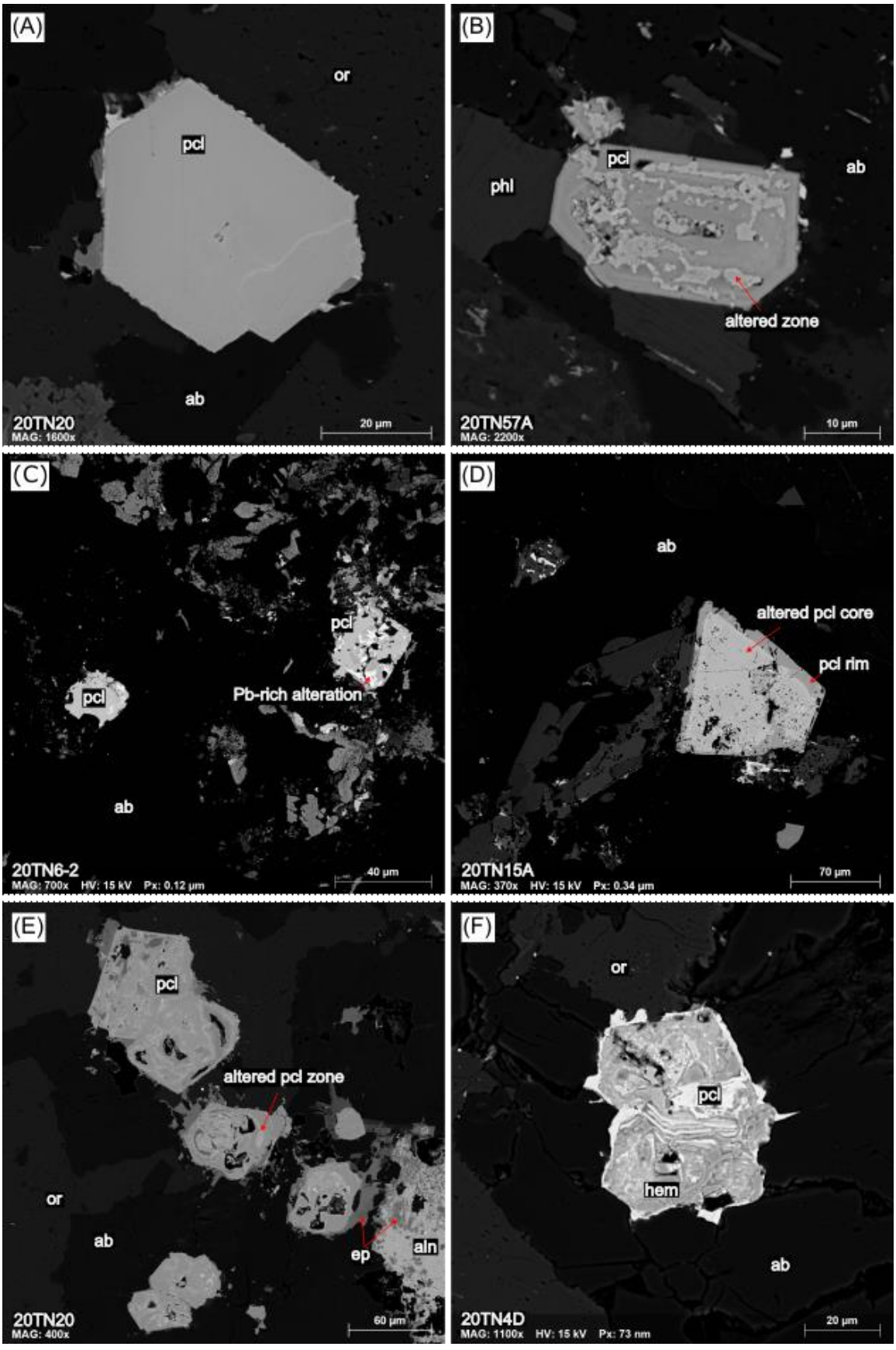
(A)
or
pcl
ab
20TN20
MAG: 1600x
20 µm
(B)
pcl
ab
phl
altered zone
20TN57A
MAG: 2200x
10 µm
(C)
pcl
pcl
Pb-rich alteration
ab
20TN6-2
MAG: 700x HV: 15 kV Px: 0.12 µm
40 µm
(D)
ab
altered pcl core
pcl rim
20TN15A
MAG: 370x HV: 15 kV Px: 0.34 µm
70 µm
(E)
pcl
altered pcl zone
or
ab
ep
aln
20TN20
MAG: 400x
60 µm
(F)
or
pcl
hem
ab
20TN4D
MAG: 1100x HV: 15 kV Px: 73 nm
20 µm

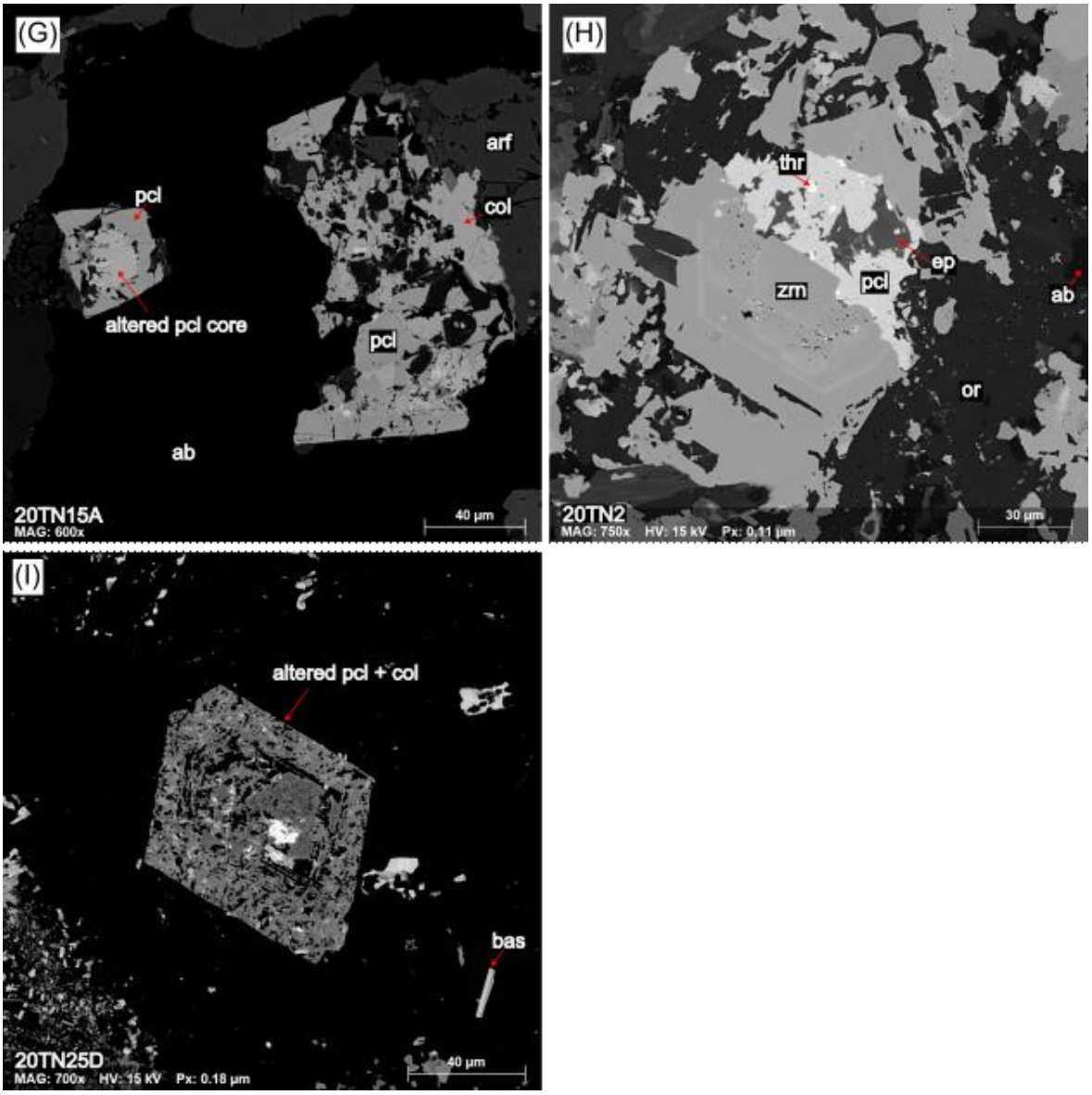

Figure 4.15. Pyrochlore textures in various units within the Bandito property. (A) Unaltered pyrochlore in 20TN20. (B) Altered pyrochlore with oscillatory zoning in 20TN57A. Heavy, Fe and Mn-enriched alteration occur along oscillatory boundaries. (C) Altered pyrochlore in 20TN6-2. Near-white zones have Pb-rich compositions. (D) Zoned and fractured pyrochlore in 20TN15A. The light gray pyrochlore core is enriched in REE and Th content and depleted in Na and F content with respect to the darker gray rim. (E) Patchy zoning in pyrochlore in 20TN20. (F) Strongly altered pyrochlore in 20TN4D. Pyrochlore is almost completely replaced by hematite. (G) Fractured pyrochlore with an altered, REE-enriched and Na-F depleted core (on the left) and pyrochlore occurring with columbite (on the right) in 20TN15A. (H) Patchy, altered pyrochlore occurring with an altered zircon, epidote, and thorite in 20TN2. (I) Strongly altered pyrochlore and columbite mixture in 20TN25D. ab – albite, or – orthoclase, hem – hematite, ep – epidote, aln – allanite, pcl – pyrochlore, col – columbite, bas – basnäsite, phl – phlogopite, arf – arfvedsonite, thr – thorite, zrn – zircon.

Columbite

Columbite, $(Fe^{2+}, Mn^{2+})Nb_2O_6$, was observed in trace amounts in the nepheline syenite, porphyritic dike, and fenite units. Columbite occurs as discrete crystals in the nepheline syenite and feldspar porphyritic dike and sometimes occurs intergrown with pyrochlore in the layered titanite-arfvedsonite syenite (Figure 4.16) and layered phlogopite-potassium feldspar fenite. Columbite compositions from select samples are shown in Table 4.19.

Nb content ranges from 59.45 wt. % (1.513 *apfu*) to 74.18 wt. % (1.876 *apfu*). Ta content ranges 0.54 wt. % (0.008 *apfu*) to 0.69 wt. % (0.011 *apfu*). Fe content ranges from 3.39 wt. % (0.160 *apfu*) to 11.47 wt. % (0.531 *apfu*). Mn content ranges 5.74 wt. % (0.274 *apfu*) to 17.61 wt. % (0.834 *apfu*). REE content ranges 0.15 wt. % (0.003 *apfu*) to 6.36 wt. % (0.126 *apfu*). Of the measured REE, Ce and Dy are the highest in abundance, where Ce content ranges from 0.08 wt. % (0.002 *apfu*) to 2.15 wt. % (0.044 *apfu*), and Dy content from 1.82 wt. % (0.033 *apfu*) to 4.44 wt. % (0.082 *apfu*).

According to the EMP analyses, columbite-(Mn) and columbite-(Fe) species are present in the analysed samples (Figure 4.17). Columbite-(Mn) occurs in the layered titanite-arfvedsonite syenite sample (20TN15A) and altered feldspar porphyritic dike (20TN54). Columbite-(Fe) occurs in the nepheline syenite (20TN53) and layered phlogopite-potassium feldspar fenite (20TN25D).

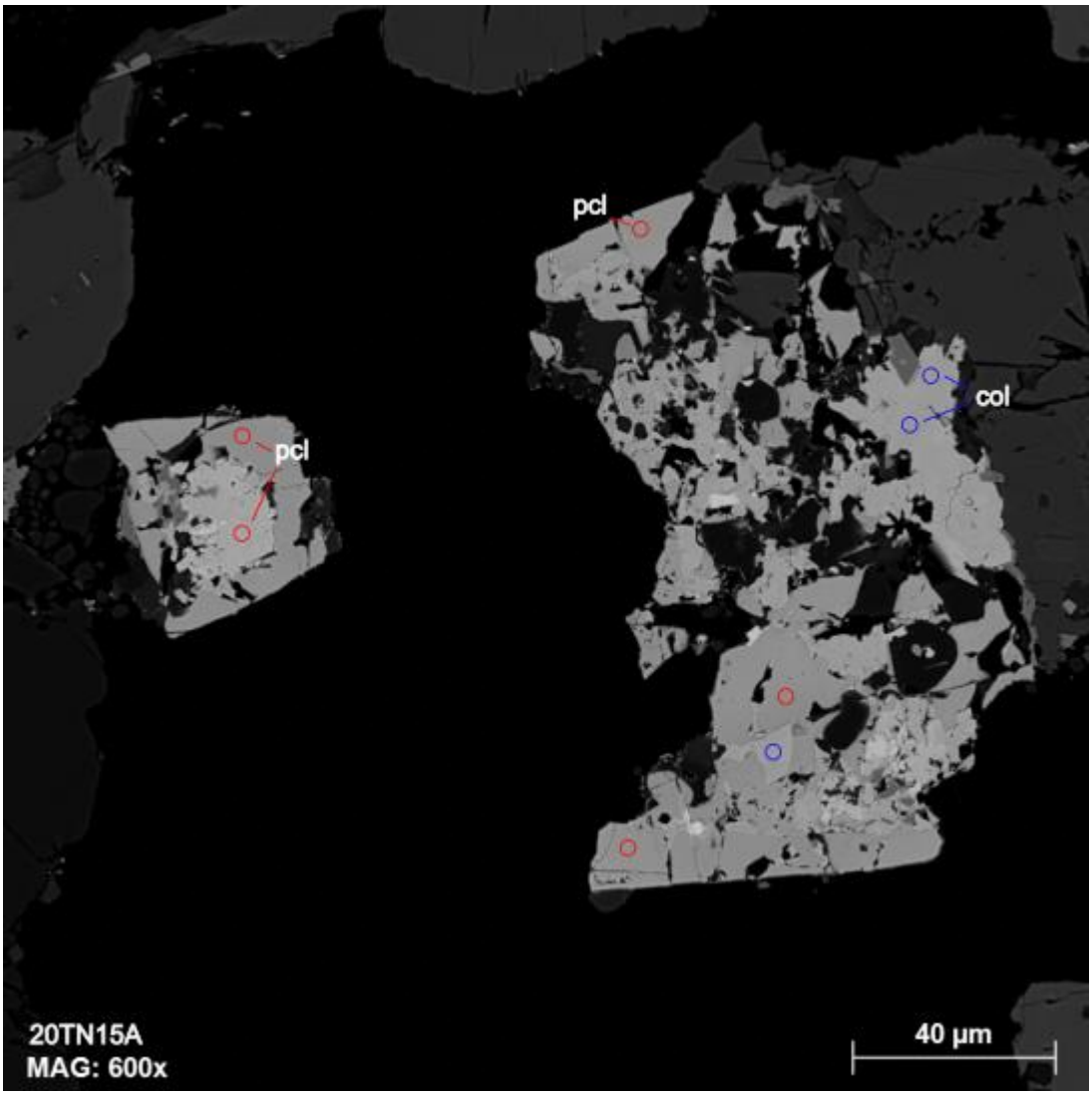

Figure 4.16. BSE image of columbite and pyrochlore in layered titanite-arfvedsonite syenite sample (20TN15A) from the Bandito property. Circles are to scale with the EMP beam diameter, where blue = columbite (col), and red = pyrochlore (pcl).

Table 4.19. Average composition of columbite from various units from the 2020 Corundum Dome and Pyrochlore Dome sampling area.

unit (sample)	layered phlogopite-potassium feldspar fenite (20TN25D)	layered titanite-arfvedsonite syenite (20TN15A)	layered titanite-arfvedsonite syenite (20TN15A)	layered titanite-arfvedsonite syenite (20TN15A)	layered titanite-arfvedsonite syenite (20TN15A)	nepheline syenite (20TN53)	nepheline syenite (20TN53)	nepheline syenite (20TN53)	feldspar glomeroporphyritic dike (20TN54)
analysis	15-195-1	7-165-4	7-167-6	7-168-7	40-243-1	33-290-2	33-291-3	33-292-4	48-274-1
Nb_2O_5 (wt. %)	59.45	72.38	74.18	73.40	62.41	62.25	64.72	70.01	67.84
Ta_2O_5	–	0.65	0.54	0.69	–	–	–	–	–
SiO_2	1.36	0.00	0.00	0.00	0.47	1.13	0.51	0.11	0.27
ZrO_2	0.83	0.01	0.00	0.02	0.01	0.10	0.11	0.10	0.11
HfO_2	0.13	0.10	0.05	0.13	0.02	0.00	0.07	0.00	0.02
TiO_2	9.90	3.52	2.88	3.20	8.10	7.55	8.93	6.07	4.59
PbO	0.18	0.31	0.32	0.42	0.51	0.29	0.32	0.18	0.29
ThO_2	1.05	1.12	0.34	0.54	2.21	1.05	0.51	0.20	0.02
UO_2	0.17	0.41	0.18	0.33	0.14	0.87	0.68	0.35	0.21
Al_2O_3	0.31	0.00	0.00	0.00	0.04	0.48	0.12	0.02	0.09
Y_2O_3	0.11	0.14	0.17	0.19	0.79	1.55	1.51	0.68	0.32
RE_2O_3	6.22	0.84*	0.15*	0.44*	6.36	4.58	5.21	3.86	5.54
FeO	10.09	3.39	3.67	3.82	4.88	10.50	10.49	11.47	6.14
MnO	5.74	16.62	17.61	17.01	8.32	6.81	6.94	8.15	12.86
MgO	0.31	–	–	–	0.02	0.32	0.09	0.10	0.07
CaO	2.99	0.63	0.15	0.42	3.27	0.90	0.98	0.43	0.73
Na_2O	0.06	0.00	0.00	0.00	0.05	0.06	0.04	0.01	0.10
K_2O	0.16	0.01	0.00	0.01	0.03	0.17	0.04	0.02	0.03
P_2O_5	0.02	–	–	–	0.04	0.04	0.05	0.00	0.04
F	0.47	0.00	0.00	0.00	0.08	0.06	0.00	0.00	0.00
Cl	0.02	–	–	–	0.01	0.03	0.02	0.01	0.00
O=F,Cl	-0.20	0.00	0.00	0.00	-0.04	-0.03	0.00	0.00	0.00
Total	99.37	100.14	100.24	100.61	97.73	98.69	101.32	101.77	99.26
Nb (*apfu*)	1.513	1.842	1.876	1.856	1.635	1.601	1.620	1.751	1.758
Ta	–	0.010	0.008	0.011	–	–	–	–	–
Si	0.076	0.000	0.000	0.000	0.027	0.064	0.028	0.006	0.015
Zr	0.023	0.000	0.000	0.001	0.000	0.003	0.003	0.003	0.003
Hf	0.002	0.002	0.001	0.002	0.000	0.000	0.001	0.000	0.000
Ti	0.419	0.149	0.121	0.135	0.353	0.323	0.372	0.252	0.198
Pb	0.003	0.005	0.005	0.006	0.008	0.004	0.005	0.003	0.004
Th	0.013	0.014	0.004	0.007	0.029	0.014	0.006	0.002	0.000
U	0.002	0.005	0.002	0.004	0.002	0.011	0.008	0.004	0.003
Al	0.020	0.000	0.000	0.000	0.002	0.032	0.008	0.001	0.006
Y	0.003	0.004	0.005	0.006	0.024	0.047	0.044	0.020	0.010
REE	0.123	0.017*	0.003*	0.009*	0.126	0.088	0.097	0.071	0.104
Fe^{2+}	0.475	0.160	0.172	0.179	0.237	0.499	0.486	0.531	0.294
Mn	0.274	0.793	0.834	0.806	0.408	0.328	0.325	0.382	0.625
Mg	0.026	–	–	–	0.002	0.027	0.007	0.008	0.006
Ca	0.180	0.038	0.009	0.025	0.203	0.055	0.058	0.025	0.045
Na	0.006	0.000	0.000	0.000	0.006	0.006	0.005	0.001	0.011
K	0.012	0.001	0.000	0.001	0.002	0.013	0.003	0.001	0.003
P	0.001	–	–	–	0.002	0.002	0.002	0.000	0.002
F^-	0.083	0.000	0.000	0.000	0.014	0.011	0.000	0.000	0.000
Cl^-	0.002	–	–	–	0.001	0.003	0.002	0.001	0.000
Cation Sum	3.172	3.041	3.041	3.046	3.067	3.115	3.078	3.062	3.087
Mn/(Mn+Fe)	0.365	0.832	0.829	0.818	0.633	0.397	0.401	0.418	0.680

Note: Compositions were recalculated on the basis of 6 O *apfu*. * La, Ce, Pr, and Nd were the only REE contents analyzed.

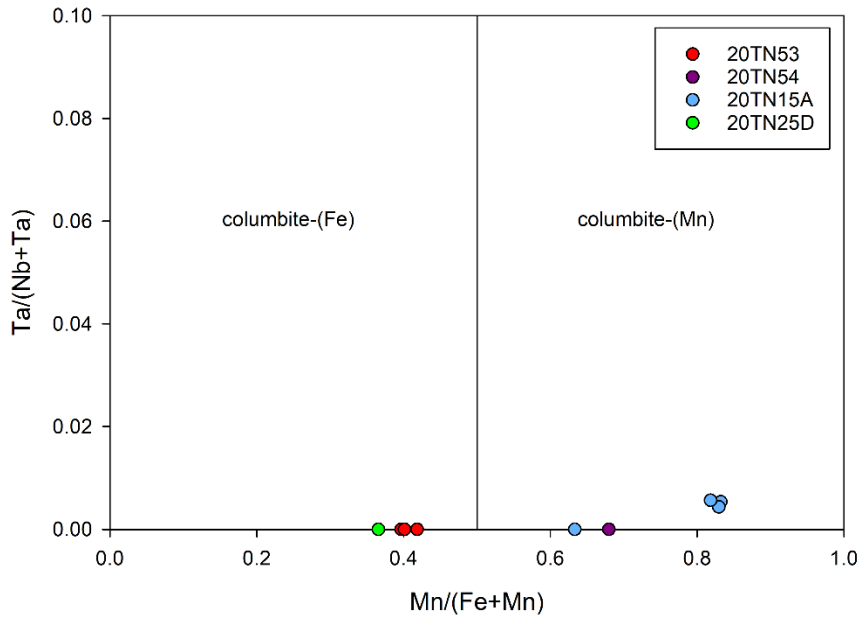

Figure 4.17. Ta/(Ta+Nb) versus Mn/(Mn+Fe) diagram of columbite from the Bandito property.

Halide compositions

Fluorite is the only halide that has been observed on the Bandito property.

Fluorite

Fluorite (CaF_2) was observed in the amphibole and pyroxene bearing syenites, and fenites across the Bandito property. Fluorite commonly occurs with calcite and epidote in the South Fenite Zone. In the North Fenite Zone, fluorite sometimes occurs as a replacement phase in altered mafics. Fluorite is pervasive throughout the layered amphibole-diopside-phlogopite syenite (20TN15B) in the North Fenite Zone.

Fluorite analyses from select samples of layered fenite, actinolite-altered syenite, and altered and layered amphibole-diopside-phlogopite syenite are reported in Table 4.20. Ca content range from 71.04 wt. % (0.982 *apfu*) to 77.20 wt. % (0.999 *apfu*) and F content from 45.43 wt. % (1.736 *apfu*) to 51.15 wt. % (2.075 *apfu)*. Only two analyses analyzed for REE, where REE content ranges from 0.48 wt. % (0.002 *apfu*) to 0.71 wt. % (0.003 *apfu*). Elevated concentrations of non-essential formula elements likely represent impurities or micro inclusions.

Table 4.20. Compositions of fluorite from various units from the 2020 Corundum Dome and Pyrochlore Dome sampling area.

unit (sample)	layered amphibole-diopside-phlogopite syenite (20TN15B)				actinolite-altered syenite dikelet (20TN3-2)			layered arfvedsonite-albite fenite (20TN23)	layered phlogopite-potassium feldspar fenite (20TN25D)		
analysis	8-171-5	8-172-6	18-104-1	18-105-2	11-63-1	11-64-2	17-84-1	34-174-4	37-217-1	37-218-2	37-219-3
P_2O_5 (wt. %)	0.03	0.00	–	–	–	–	–	–	–	–	–
Nb_2O_5	0.05	0.00	–	–	–	–	–	–	–	–	–
SiO_2	0.16	0.09	0.00	0.04	0.07	0.06	0.08	0.68	0.31	0.04	0.07
TiO_2	0.00	0.02	0.00	0.00	0.02	0.03	0.01	0.66	0.00	0.00	0.01
PbO	0.03	0.07	–	–	–	–	–	–	–	–	–
ThO_2	0.08	0.08	–	–	–	–	–	–	–	–	–
UO_2	0.01	0.00	–	–	–	–	–	–	–	–	–
Al_2O_3	0.04	0.02	0.02	0.02	0.02	0.02	0.01	0.12	0.03	0.02	0.02
Y_2O_3	0.05	0.04	–	–	–	–	–	–	–	–	–
RE_2O_3	0.71	0.48	–	–	–	–	–	–	–	–	–
MgO	0.01	0.02	0.00	0.00	0.00	0.00	0.01	0.01	0.09	0.00	0.00
CaO	71.04	71.95	73.12	73.33	77.20	76.04	76.76	76.44	74.58	72.64	72.44
MnO	0.03	0.05	0.01	0.00	0.00	0.00	0.00	0.01	0.00	0.00	0.00
FeO	0.05	0.22	0.01	0.04	0.05	0.14	0.08	0.11	0.11	0.26	0.49
BaO	–	–	0.00	0.00	0.00	0.00	0.00	0.00	0.00	0.00	0.01
Na_2O	0.04	0.04	0.01	0.02	0.01	0.03	0.00	0.03	0.03	0.00	0.02
K_2O	0.11	0.16	0.00	0.01	0.00	0.00	0.13	0.02	0.04	0.01	0.01
F	48.91	51.15	49.25	50.06	45.50	45.43	46.04	50.65	48.53	49.79	48.43
Cl	0.01	0.00	–	–	–	–	–	–	–	–	–
O=F,Cl	-20.60	-21.54	-20.74	-21.08	-19.16	-19.13	-19.39	-21.33	-20.44	-20.97	-20.39
Total	100.76	102.84	101.68	102.45	103.71	102.63	103.74	107.39	103.28	101.79	101.12
P (*apfu*)	0.000	0.000	–	–	–	–	–	–	–	–	–
Nb	0.000	0.000	–	–	–	–	–	–	–	–	–
Si	0.002	0.001	0.000	0.001	0.001	0.001	0.001	0.008	0.004	0.000	0.001
Ti	0.000	0.000	0.000	0.000	0.000	0.000	0.000	0.006	0.000	0.000	0.000
Pb	0.000	0.000	–	–	–	–	–	–	–	–	–
Th	0.000	0.000	–	–	–	–	–	–	–	–	–
U	0.000	0.000	–	–	–	–	–	–	–	–	–
Al	0.001	0.000	0.000	0.000	0.000	0.000	0.000	0.002	0.000	0.000	0.000
Y	0.000	0.000	–	–	–	–	–	–	–	–	–
REE	0.003	0.002	–	–	–	–	–	–	–	–	–
Mg	0.000	0.000	0.000	0.000	0.000	0.000	0.000	0.000	0.002	0.000	0.000
Ca	0.989	0.989	0.999	0.998	0.998	0.996	0.996	0.982	0.992	0.996	0.993
Mn	0.000	0.001	0.000	0.000	0.000	0.000	0.000	0.000	0.000	0.000	0.000
Fe^{2+}	0.001	0.002	0.000	0.000	0.000	0.001	0.001	0.001	0.001	0.003	0.005
Ba	–	–	0.000	0.000	0.000	0.000	0.000	0.000	0.000	0.000	0.000
Na	0.001	0.001	0.000	0.001	0.000	0.001	0.000	0.001	0.001	0.000	0.001
K	0.002	0.003	0.000	0.000	0.000	0.000	0.002	0.000	0.001	0.000	0.000
F^-	2.010	2.075	1.987	2.011	1.736	1.757	1.763	1.921	1.905	2.016	1.959
Cl^-	0.000	0.000	–	–	–	–	–	–	–	–	–
O^{2-}	-0.001	-0.036	0.007	-0.005	0.133	0.122	0.119	0.054	0.051	-0.007	0.022

Note: Compositions were recalculated on the basis of the sum of 1 cation *apfu*. ZrO_2 and HfO_2 were sought for but not detected. All iron is assumed to be Fe^{2+}; – = not detected.

Unidentified phase

The mineral chemistry analysis of an unidentified Y-Si-silicate alteration phase is reported in Appendix B. This unidentified phase replaces a prismatic mineral with thorite (Figure 4.18) in the altered and layered amphibole-diopside-phlogopite syenite (20TN15B).

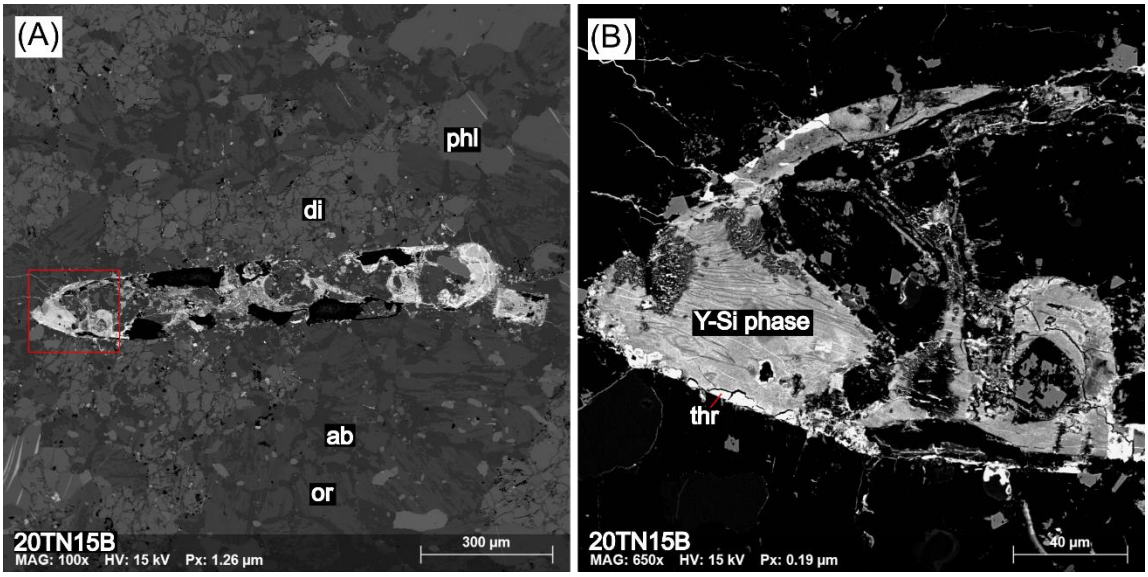

Figure 4.18. BSE images of an unidentified mineral phase from the altered and layered amphibole-diopside-phlogopite syenite (sample 20TN15B). (A) Zoomed out view of a completely altered prismatic phase that has been replaced by thorite and the unidentified Y-Si phase. The red box indicates the area of (B). ab – albite, or – orthoclase, phl – phlogopite, di – diopside, thr – thorite.

Concluding remarks

Mineral compositions were determined by EMP from select samples of the country rock, fenites, syenites, and dikes from Pyrochlore Dome and Corundum Dome within the Bandito property. The most significant mineralogical changes between the units are reflected in the presence and composition of phases bearing Na, K, Mg, Ca, Fe, Ti, Nb, REE, Th, and F. Silicate minerals that are common and show the most extreme change in composition across the sampled rock units are feldspar, amphibole, and pyroxene, where compositions change between potassic and sodic feldspar; Ca-Fe amphibole, Na-Ca, and Na amphibole; Ca pyroxene, and Na-Ca and Na pyroxene.

In the argillite unit, phases that were analyzed include albite, orthoclase, phlogopite, chlorite, actinolite, phlogopite, ilmenite, and calcite. Minerals that were analyzed in the fenite samples on Corundum Dome include albite, arfvedsonite, phlogopite, titanite, Fe-and Ti-oxides, and fluorite, and Nb and REE phases such as epidote, allanite, apatite, pyrochlore, bastnäsite, and other unidentified altered REE phases. In the actinolite-altered syenite on Corundum Dome, actinolite, epidote, allanite, zircon, thorite, pyrochlore, Fe-and Ti-oxides, calcite, and fluorite, and other unidentified altered REE phases were analyzed. Phases that were analyzed in the altered arfvedsonite-aegirine syenite, layered titanite-arfvedsonite syenite, and altered and layered amphibole-diopside-phlogopite syenite on Pyrochlore Dome include orthoclase, albite, arfvedsonite, phlogopite, aegirine-augite to aegirine, diopside, epidote, allanite, zircon, thorite, pyrochlore, columbite, Fe- and Ti-oxides, fluorite, and unidentified Pb-rich phases. Minerals analyzed in the nepheline syenite include orthoclase, albite, muscovite, phlogopite, chlorite, zircon, hematite, bastnäsite, as well as altered pyrochlore and columbite(?), and other unidentified altered REE phases.

As summarized by Elliott et al. (2018), alkali amphibole, sodic pyroxene, Na- and K-feldspars, and phlogopite are characteristic of rocks that have been altered by alkali metasomatism (i.e., fenitization). The presence of HFSE and REE phases in alkali altered units is common in alkaline-silicate systems (Elliott et al. 2018; Anenburg et al. 2020; Beard et al. 2023). Based on

the prevalence of sodic, HFSE, and REE phases within the sampled syenitic and fenitic units, these units are interpreted to have been altered by alkali metasomatism.

The two dikes that were sampled also show evidence for metasomatic alteration. The altered feldspar porphyritic dike (20TN54) is the only sample recorded to bear rhodochrosite which is indicative of high temperature metasomatism (Deer et al. 1992). The altered porphyritic lamprophyre(?) dike (20TN57C-1) is interpreted to have been altered by potassic metasomatism because the rock is dominated by phlogopite replacing most groundmass and phenocryst phases.

5 Zircon Trace Element Composition and Dating

Geochronological techniques and methods have greatly improved in the last few decades, as reviewed by Kolšer & Sylvester (2003) and Corfu (2013). The laser ablation inductively coupled mass spectrometry (LA-ICP-MS) technique is used for collecting U-Pb isotopes and trace element mineral chemistry of crystals *in situ*. Although the precision of LA-ICP-MS with respect to U-Pb dating is similar to secondary ion mass spectrometry (SIMS) and less than chemical abrasion thermal ionization mass spectrometry (CA-TIMS), it is less expensive and faster compared to these methods (e.g., Košler & Sylvester 2003). The U-Pb isotopic system in zircon is useful for dating the age of crystallization and timing of alteration/metamorphic events, as well as the age of detrital zircon populations (e.g., Mattinson et al. 1996; Mezger and Krogstad 1997; Geisler et al. 2003; Kolšer & Sylvester 2003; Wiemer et al. 2017). Similarly, zircon trace element chemistry is helpful in understanding the provenance and alteration history of crystals (e.g., Belousova et al. 2002; Geisler et al. 2003; Horie et al. 2006; Grimes et al. 2015; Wiemer et al. 2017).

With respect to trace element chemistry, chondrite normalized rare earth element patterns for unaltered igneous zircons are characteristically depleted in LREE and have a positive Ce anomaly, and have elevated MREE and HREE (e.g., Hinton & Upton 1991; Belousova 2002). In contrast, zircons that have experienced hydrothermal alteration tend to have elevated non-formula elements (e.g., Ca, Fe, REE), especially LREE (e.g., Geisler et al. 2003; Hoskin 2005; Horie et al. 2006; Utsunomiya et al. 2007; Wiemer et al. 2017).

The ratio Th/U is commonly reported in the literature for zircon chemistry because it can help to distinguish between environments of formation of zircons, where igneous zircons typically have ratios > 0.1 and metamorphic zircons typically have ratios < 0.1 (e.g., Belousova 2002; Kirkland et al. 2015; Yakymchuk et al. 2018). Despite this, the geologic processes that control the Th/U ratio in zircon are not fully understood, although it is generally agreed that Th concentrations in zircon is controlled by the presence of other Th-bearing phases (i.e., monazite and allanite) (e.g., Kirkland et al. 2015; Yakymchuk et al. 2018).

Belousova (2002) determined that trace element abundances in igneous zircon are characteristic of the igneous source rock type and can therefore be used to help determine the provenance of a zircon crystal. For example, zircon that crystallizes from a syenite, nepheline-syenite pegmatite, granitoid, and carbonatite have distinct trace element abundances. Hoskin (2005) defined a discrimination diagram that helps distinguish between magmatic and hydrothermal zircon. Furthermore, Grimes et al. (2015) produced discrimination diagrams that uses zircon trace element abundances to distinguish between tectonic environments of formation (e.g., continental arc, mid ocean ridge, and ocean island settings).

As briefly reviewed in Chapter 2, Pigage & Mortensen (2004) is the only study that has reported an age of crystallization for the Pool Creek nepheline syenite. They collected U-Pb zircon dates by isotope dilution thermal ionization mass spectrometry (ID-TIMS) from six different samples and concluded that the Pool Creek nepheline syenite and associated mafic and banded dikes were emplaced approximately 640 to 650 Mya. They also noted that complex U-Pb-Th systematics are characteristic of the Pool Creek nepheline syenite zircon grains.

The metasomatic alteration on the Bandito property has been associated with the Pool Creek nepheline syenite on the basis of mapping by Swanton (2011; 2012). This thesis will add a geochronologic and trace element chemistry study of zircon from the syenite and altered units on the Bandito property to the current knowledge and understanding of both the age of crystallization of the Pool Creek nepheline syenite and the age of metasomatic alteration that has been associated with it. Eight rock samples were selected for U-Pb zircon geochronology by LA-ICP-MS in order to compare age of crystallization and age of alteration events on the Bandito property and identify the relationship between these events.

Methods

Laser ablation inductively coupled mass spectrometry analyses were carried out using an 193 nm ArF excimer laser ablation system (Resolution M-50LR, Applied Spectra, USA) connected to a Quadrupole ICP-MS (Agilent 7700x) at the Pacific Centre for Isotopic and Geochemical Research at UBC. Measurements were performed at a repetition rate of 5 Hz and using a spot

size of 34 um. Energy density on the sample was ~2 J/cm^2. Ablation was carried out under a helium atmosphere. Argon served as the carrier gas and was admixed with N_2 for signal enhancement. The mass spectrometer was tuned for sensitivity, ThO/Th < 0.3% and a mass bias with 95% < 238/232 < 105%. Calibration for trace element analyses was carried out by standard-sample-bracketing using the silicate glass SRM NIST612 (Pearce et al. 1997) as external standard and Zr as internal standard using a default value of 49.5 wt.%. SRM NIST610 (Pearce et al. 1997) and USGS basalt reference material BCR2-G were cross-checked for quality control. $^{206}Pb/^{238}U$ dating was carried out using the zircon reference material Plešovice as primary calibration material (when calibrated to 91500, fractionation downhole was greater than Plešovice), crosschecked by the reference zircons Temora 2 and 91500 (Table 5.1). Data reduction was performed using the Iolite v.4 software (Paton et al. 2010; 2011). Ablation sweeps with mass 204 signals above background were rejected. Ablation point data were manually filtered; the rejected ablation data is not reported in this thesis. Isoplot software by Ludwig (2003) was used to construct standard concordia diagrams and calculate regression intercepts and weighted averages calculated. Unless otherwise noted, all errors are quoted at the 2 sigma or 95% level of confidence. Isotopic dates are calculated by the decay constants $\lambda^{238}U=1.55125E^{-10}$ and $\lambda^{235}U=9.8485E^{-10}$ (Jaffey et al. 1971).

Table 5.1. U-Pb dating zircon reference materials used in this study. Crosscheck and validation of standard ages were calculated in IsoPlot (Ludwig 2003). MSWD – mean squared weighted deviation. Standard ablation data are reported in Appendix D.

Reference material	Reference	Reference Age (Ma)	Crosscheck / validation (Ma; MSWD; n)
91500	Wiedenbeck et al. (1995)	1065	1037.04 ± 2.28; 17; 72
Temora 2	Black et al. (2004)	417	407.29 ± 1.40; 28; 38
Plešovice	Slama et al. (2008)	337	337.08 ± 0.57; 1.8; 68

Results

Eight samples collected from the Bandito property were analyzed for trace elements and U-Pb zircon geochronology using LA-ICP-MS. Of these eight samples, seven are from the unit mapped as fenite in Swanton (2012) and one is from the Pool Creek nepheline syenite. Zircon textures in transmitted light and scanning electron microscope cathodoluminescence (SEM-CL)

of each sample (except for 20TN16A-2) are shown in Figures 5.1–5.8. Zircon textures observed in SEM-CL were interpreted on the basis of zircon textures classified in Corfu et al. (2003). Chondrite normalized REE diagrams of the filtered zircon data of each of the eight samples are given in Figure 5.9. Weighted mean and Wetherill concordia diagrams displaying the filtered ablation data points for the samples are shown in Figures 5.10 and 5.11, respectively. For the complete trace element dataset of zircon see Appendix C, and for the complete dataset of U-Pb zircon see Appendix D.

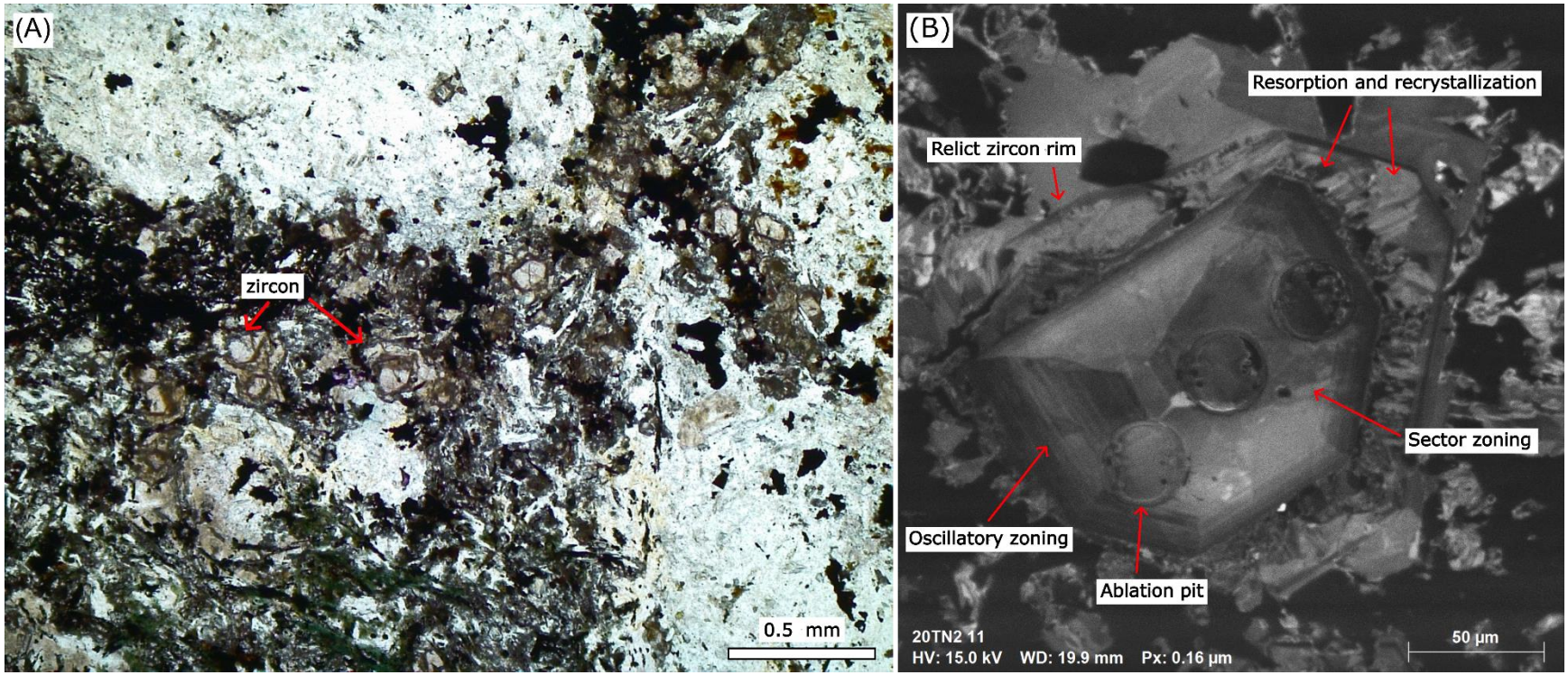

Figure 5.1. Zircon in 20TN2—actinolite-altered syenite. (A) Transmitted light in plane polarized light (PPL). Zircons have high relief and are clear with a pink-brown tint, euhedral to anhedral, sometimes mildly fractured, and mildly to moderately included. Irregular rims around subhedral to euhedral zircon cores are visible. (B) SEM-CL view. The zircon crystal shows oscillatory and sector zoning in the core. Ablation pits reveal inclusions of dark material (i.e., inclusions) or vacant space. The rim of the zircon core is still present, showing the high degree of resorption and secondary recrystallization (i.e., metasomatic zircon) that has affected the original zircon. Within and around the relict zircon rim is metasomatic zircon which is anhedral and varies in luminescence.

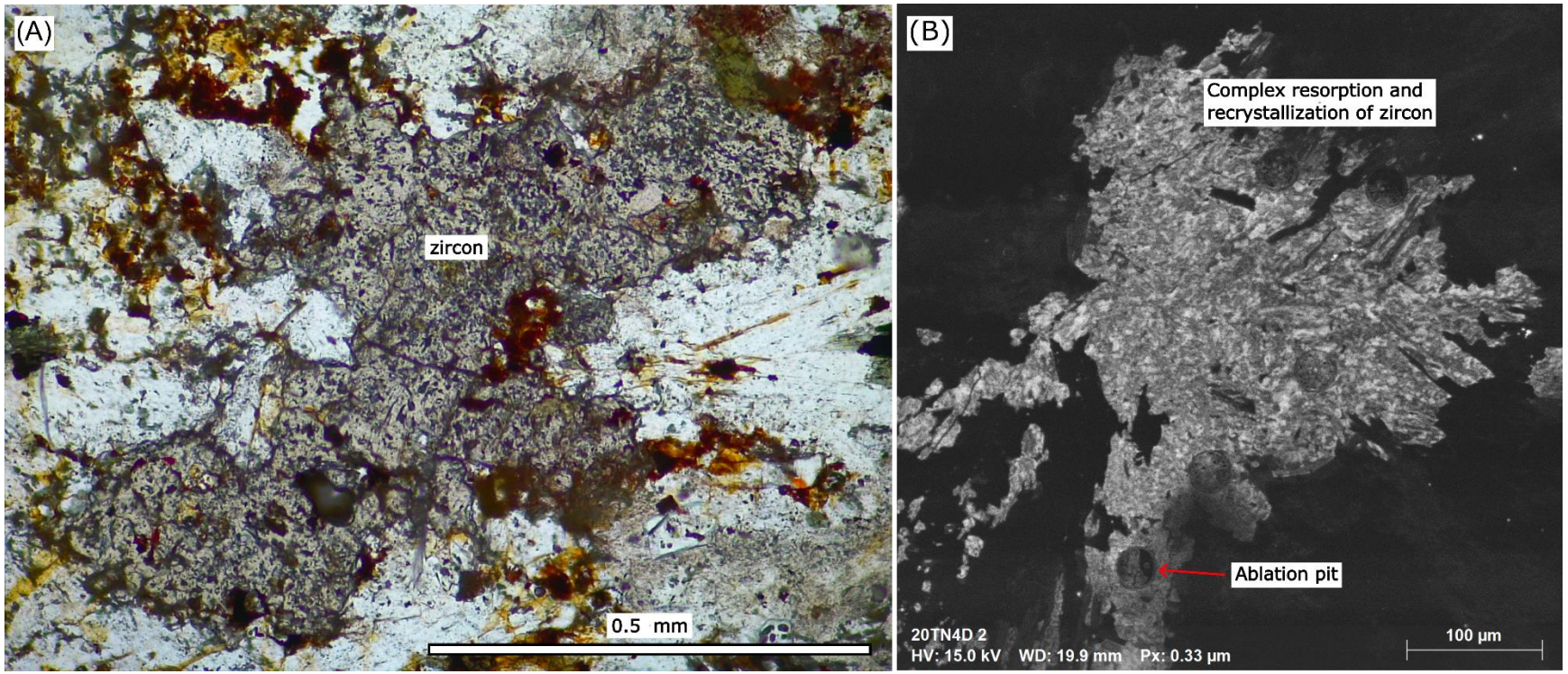

Figure 5.2. Zircon in 20TN4D—actinolite-altered syenite. (A) Transmitted light-PPL. Zircons have high relief and are fine grained, subhedral to anhedral, clear with a pink tint, strongly included (show sieve texture), and mildly fractured. (B) SEM-CL view. Zircons show complex patchy zoning and have irregular grain boundaries. Inclusions and micro veins lack luminescence.

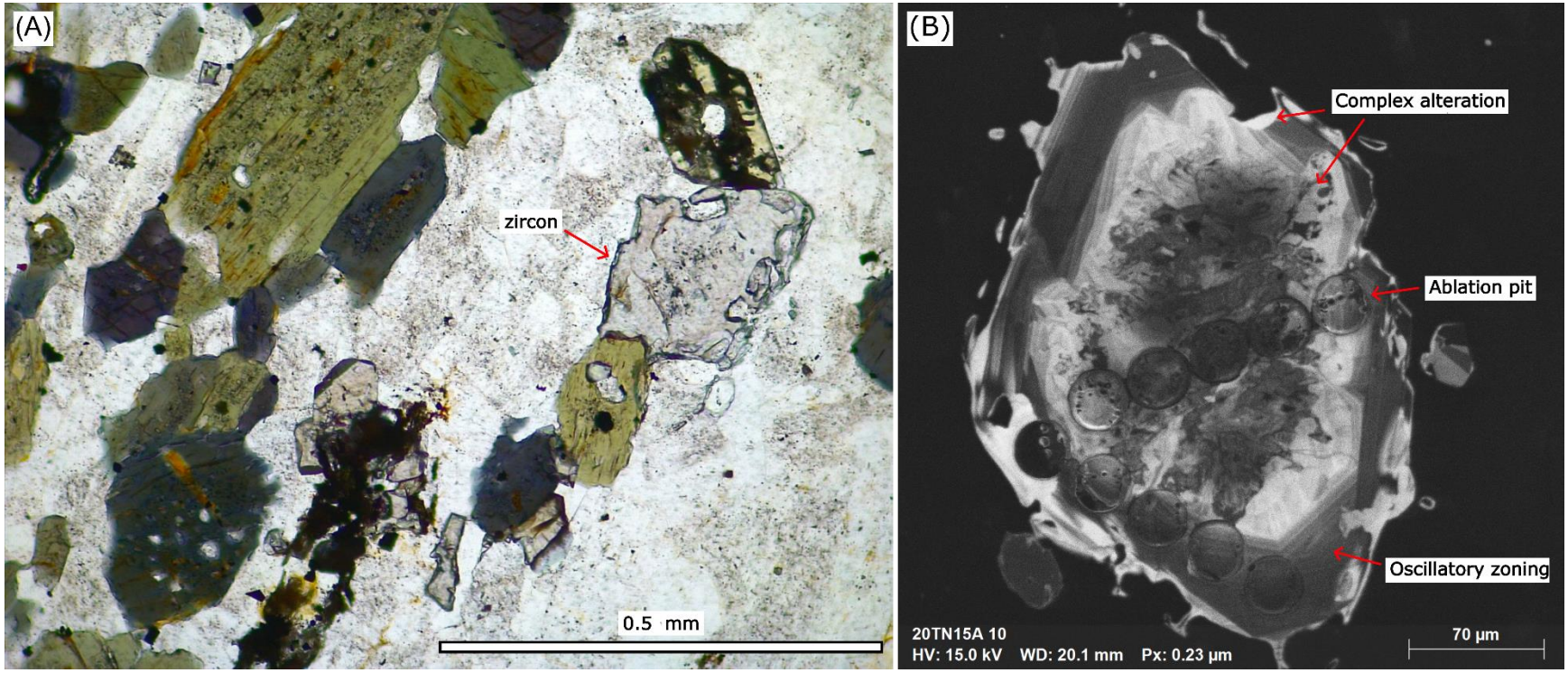

Figure 5.3. Zircon in sample 20TN15A—layered titanite-arfvedsonite syenite. (A) Transmitted light-PPL. Zircons have high relief and are clear, fine grained, euhedral to subhedral, sometimes mildly fractured, and mildly to moderately included. Inclusions are typically apatite. (B) SEM-CL view. The zircon crystal shows oscillatory zoned and inclusion-rich rims, convolute zoning near the core, complex alteration with U-rich (low luminescence) and U-poor (high luminescence) domains which are due to metamictization and secondary recrystallization, respectively. Ablation pits from an LA-ICP-MS experiment are visible across the crystal.

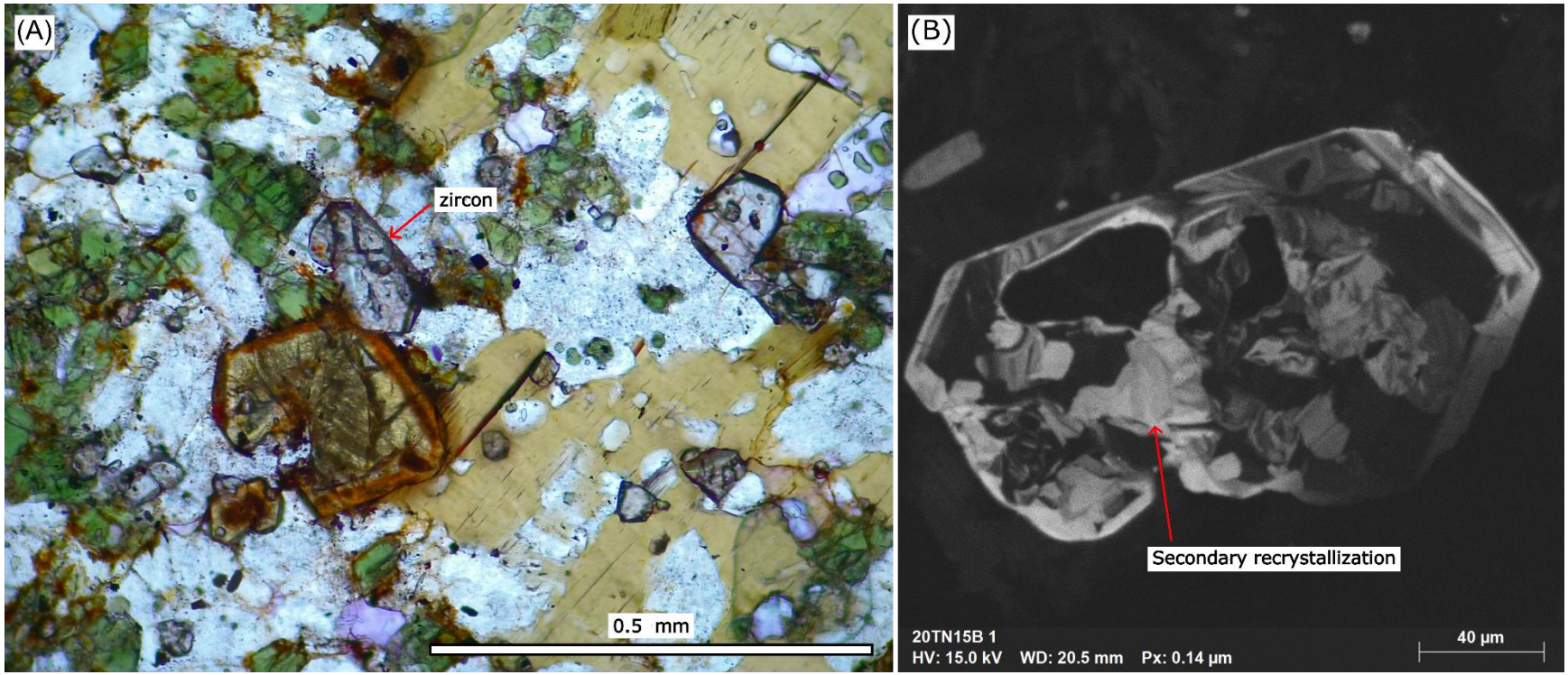

Figure 5.4. Zircon in sample 20TN15B—altered and layered amphibole-diopside-phlogopite syenite. (A) Transmitted light-PPL. Zircons have high relief and are clear, fine grained, euhedral to subhedral, mildly to moderately fractured, and mildly to moderately included. Inclusions are typically apatite. (B) SEM-CL view. The zircon crystal shows oscillatory zoned rims, complex alteration with U-rich (low luminescence) and U-poor (high luminescence) domains which are due to metamictization and secondary recrystallization, respectively.

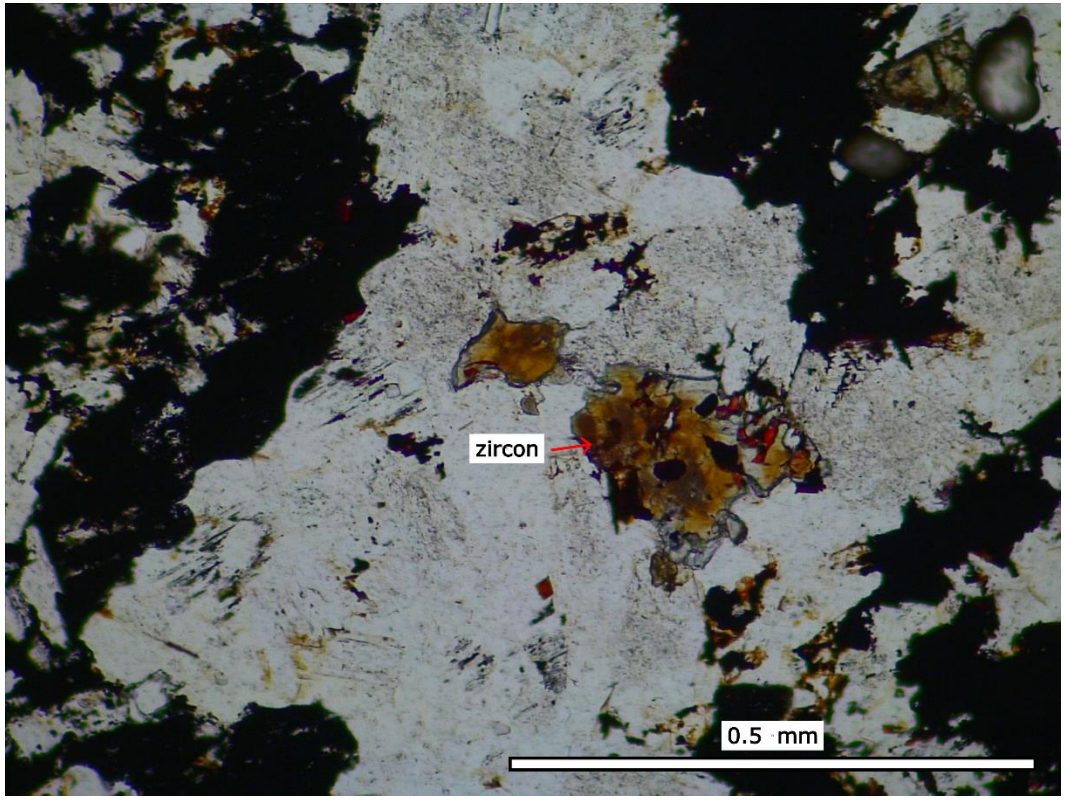

Figure 5.5. Zircon in 20TN16A-2—strongly altered arfvedsonite-aegirine syenite. Transmitted light-PPL. Zircons have high relief and are subhedral to anhedral, fine grained, clear to brown, and form in clusters in quartz and feldspar. No BSE-CL image is provided, however, zircons observed from this sample have low luminescence like 20TN17A-2 in Figure 5.6.

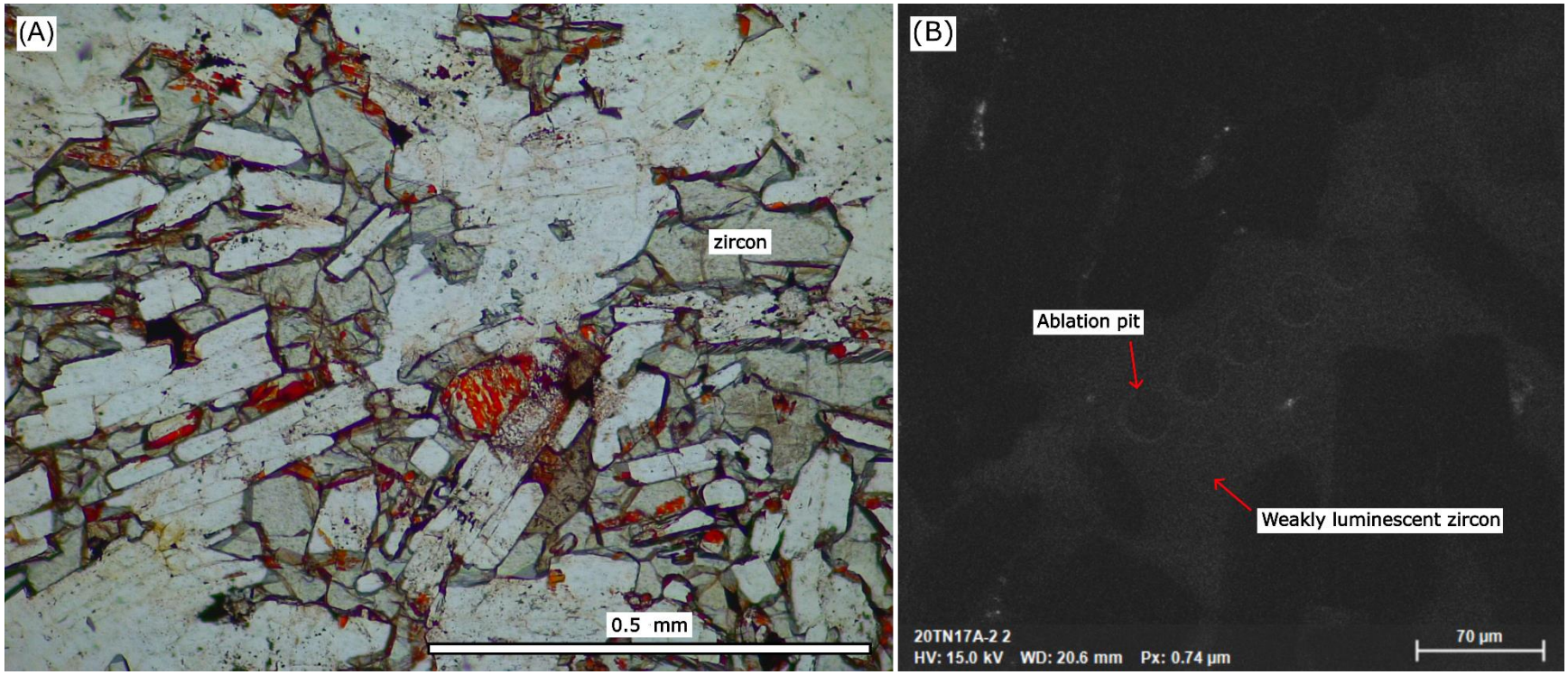

Figure 5.6. Zircon in 20TN17A-2—strongly altered arfvedsonite-aegirine syenite. (A) Transmitted light-PPL. Zircons are fine grained, subhedral to anhedral, lightly fractured, clear (sometimes with blotchy orange staining/inclusions), and interstitial between feldspars. (B) SEM-CL view. Zircons have low luminescence (have high U). Ablation pits from an LA-ICP-MS experiment are visible across the crystal.

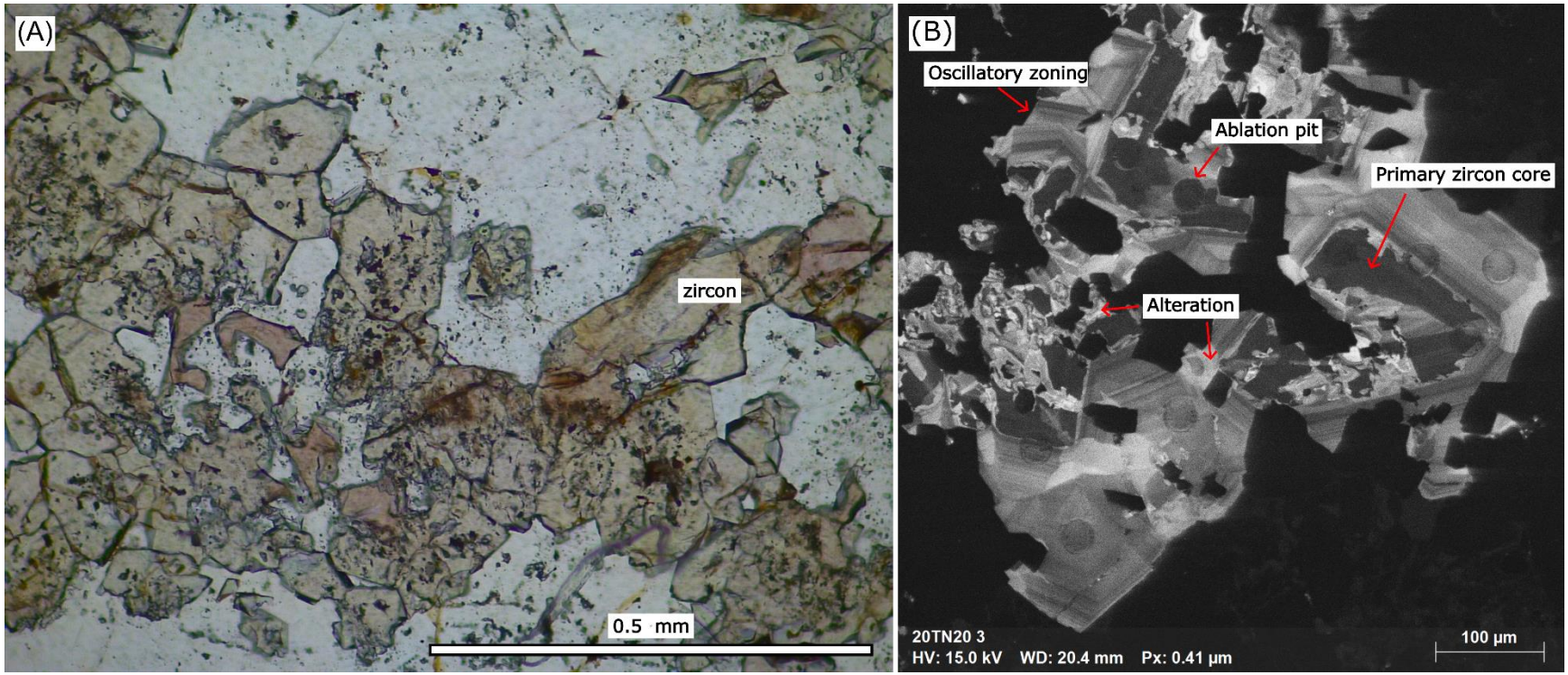

Figure 5.7. Zircon in sample 20TN20—altered arfvedsonite-aegirine syenite. (A) Transmitted light-PPL. Zircon has high relief, is clear with a pink tint, fine grained, euhedral to anhedral, and weakly to strongly included. Zircon is hosted in quartz veins and feldspar groundmass. In areas quartz, zircon crystals form anhedral aggregates. (B) SEM-CL view. Zircon crystals have U-rich cores (low luminescence) and U-poor rims (high luminescence). Rims show oscillatory zoning. Secondary alteration occurs in patches along fractures and grain boundaries in cores and rims. Grain boundaries are commonly irregularly shaped. Ablation pits from an LA-ICP-MS experiment are visible across the crystal.

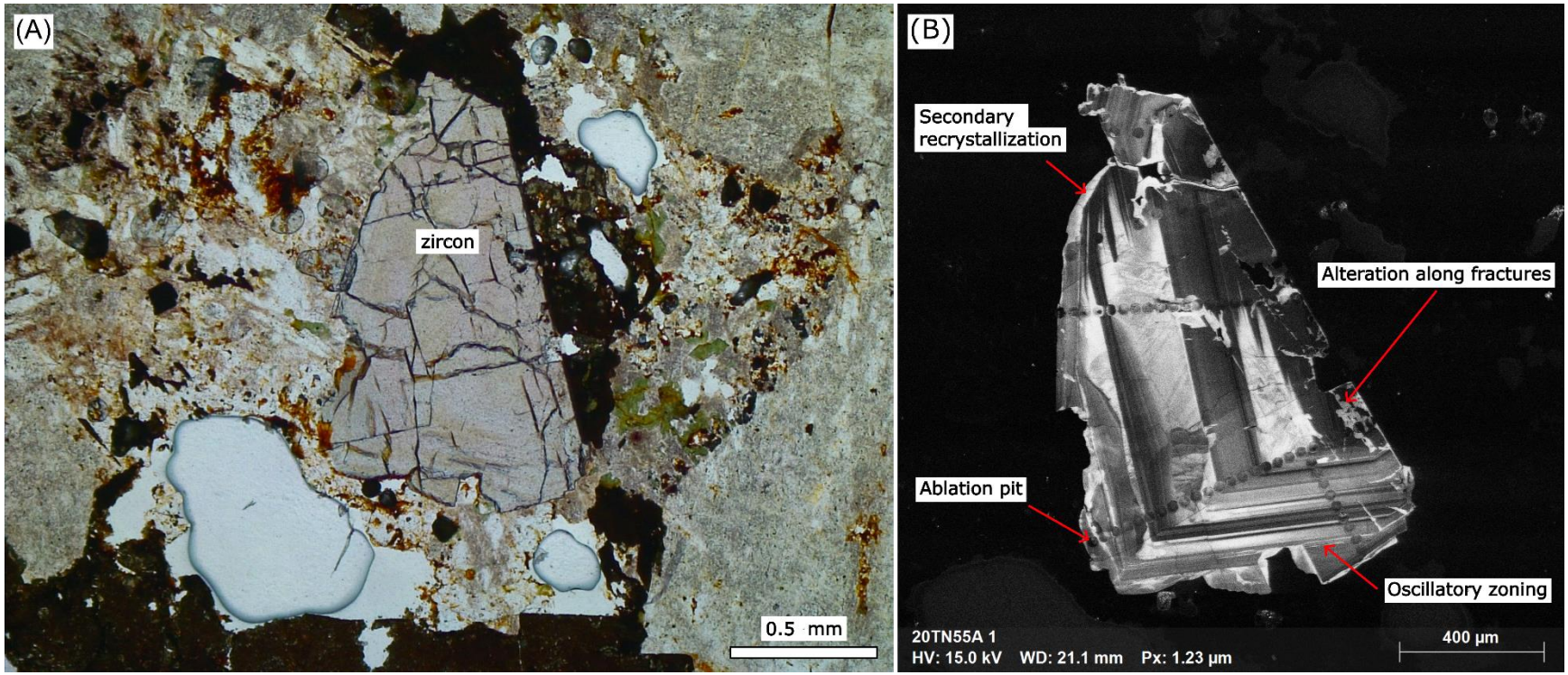

Figure 5.8. Zircon in 20TN55A—nepheline syenite. (A) Transmitted light-PPL. The zircon has a high relief and is clear, medium grained, subhedral, moderately fractured, and mildly resorbed along grain boundaries and fractures. (B) SEM-CL view. The zircon crystal shows oscillatory zoning along the rims and sector zoning in the core. Alteration and secondary recrystallization of the zircon crystal is evidenced by the luminescent rims along grain boundaries and fractures. Ablation pits from an LA-ICP-MS experiment are visible across the crystal.

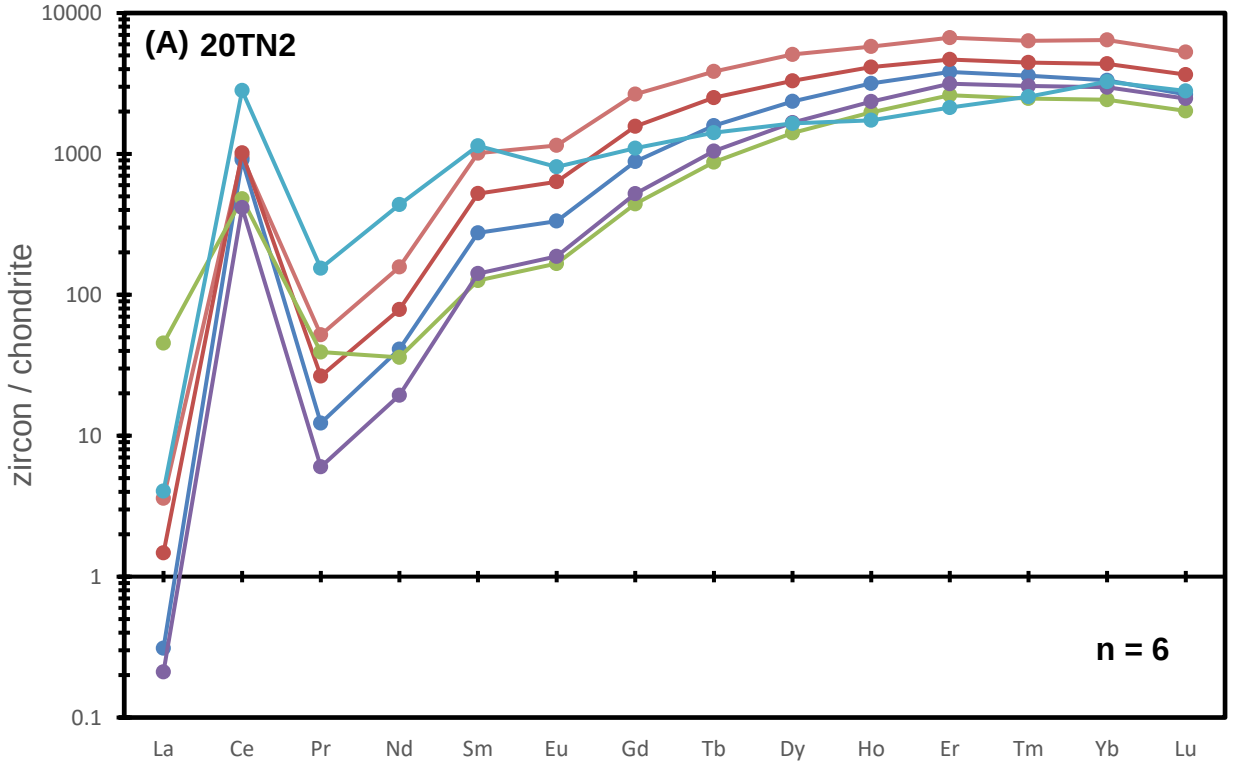
(A) 20TN2
zircon / chondrite
10000
1000
100
10
1
0.1
n = 6
La
Ce
Pr
Nd
Sm
Eu
Gd
Tb
Dy
Ho
Er
Tm
Yb
Lu

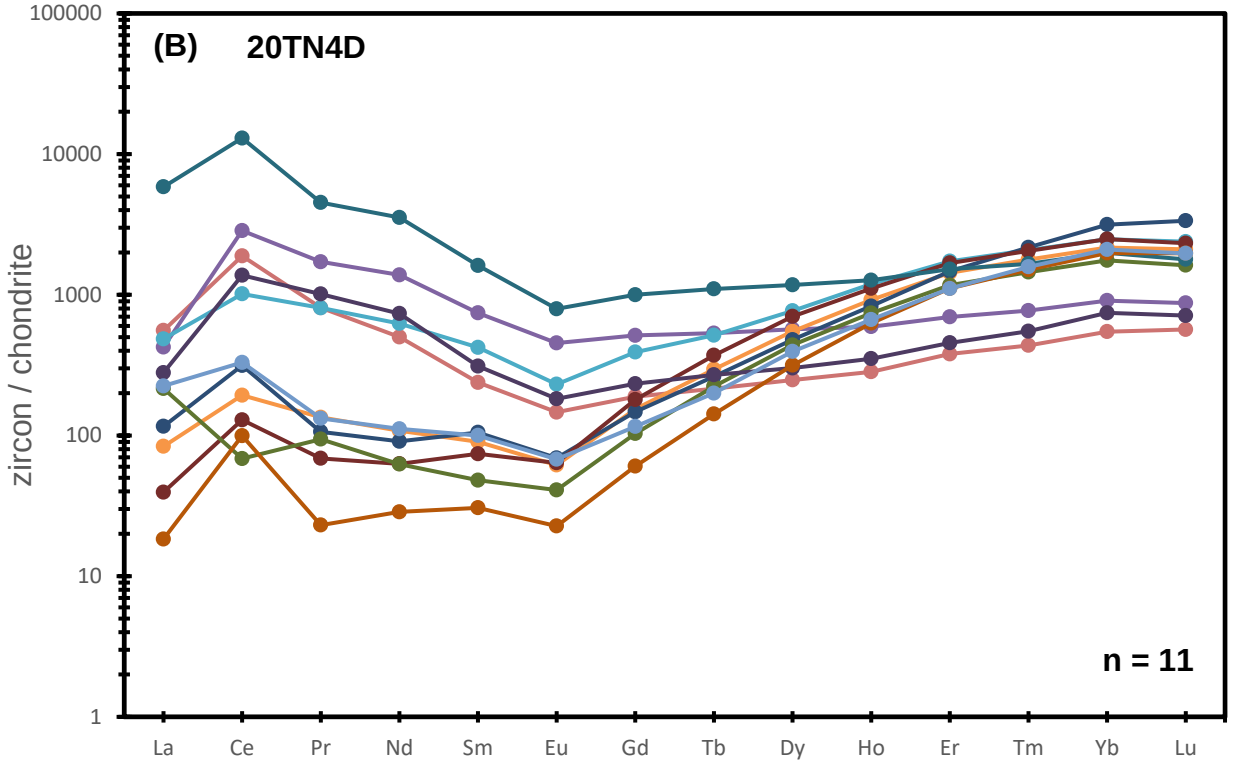
(B) 20TN4D
zircon / chondrite
100000
10000
1000
100
10
1
n = 11
La
Ce
Pr
Nd
Sm
Eu
Gd
Tb
Dy
Ho
Er
Tm
Yb
Lu

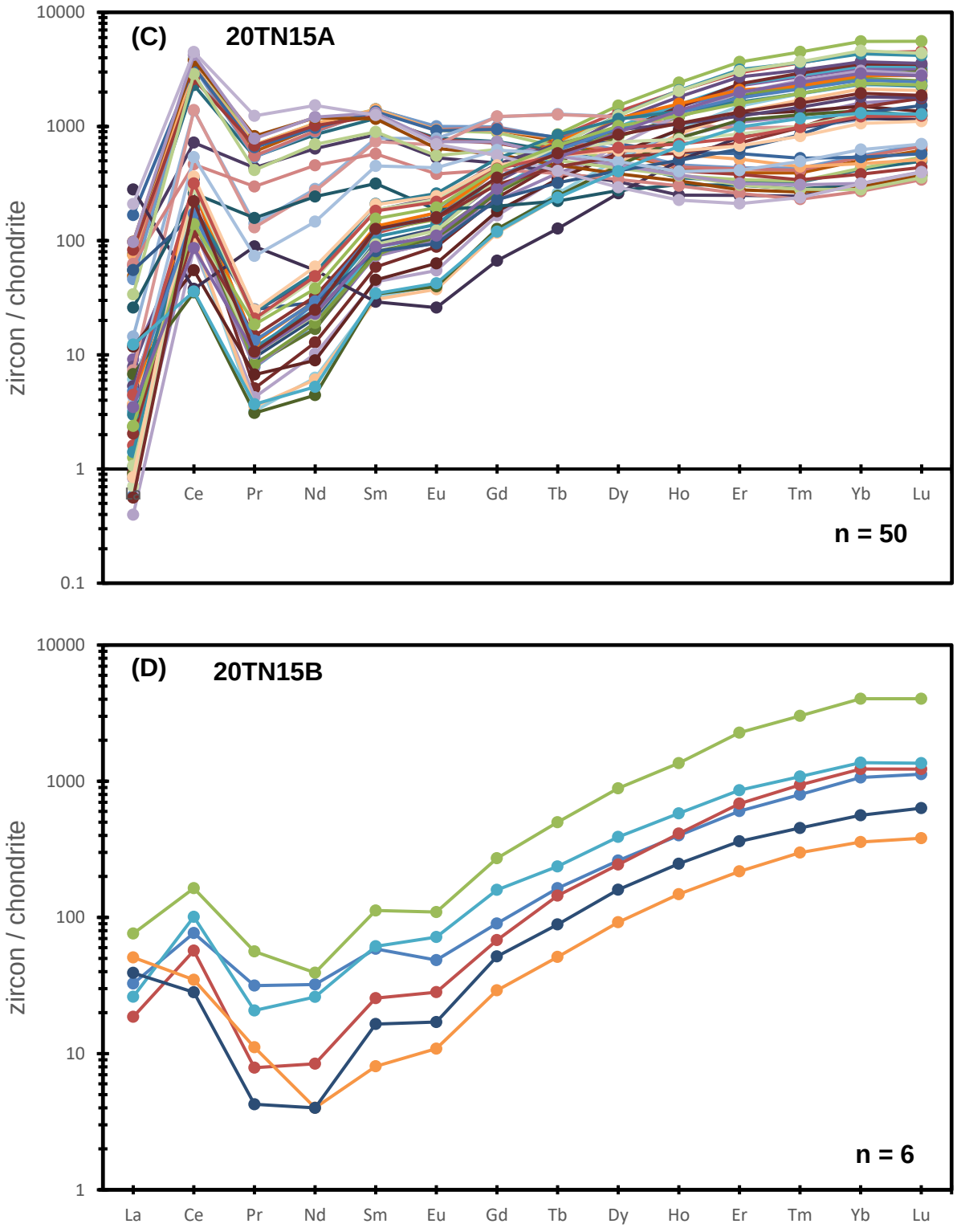
(C)
20TN15A
zircon / chondrite
10000
1000
100
10
1
0.1
La
Ce
Pr
Nd
Sm
Eu
Gd
Tb
Dy
Ho
Er
Tm
Yb
Lu
n = 50
(D)
20TN15B
zircon / chondrite
10000
1000
100
10
1
La
Ce
Pr
Nd
Sm
Eu
Gd
Tb
Dy
Ho
Er
Tm
Yb
Lu
n = 6

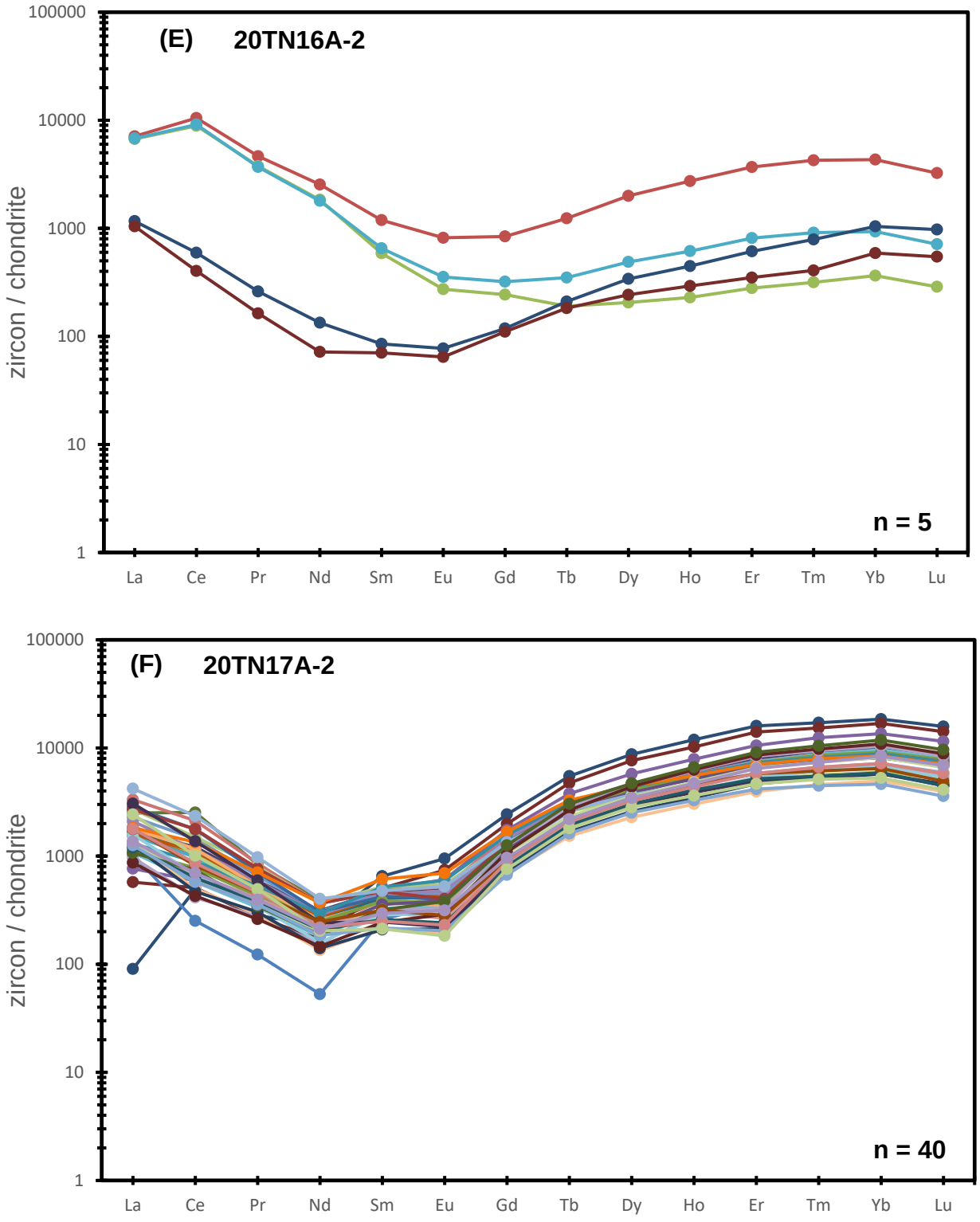
(E) 20TN16A-2
zircon / chondrite
100000
10000
1000
100
10
1
n = 5
La
Ce
Pr
Nd
Sm
Eu
Gd
Tb
Dy
Ho
Er
Tm
Yb
Lu
(F) 20TN17A-2
zircon / chondrite
100000
10000
1000
100
10
1
n = 40
La
Ce
Pr
Nd
Sm
Eu
Gd
Tb
Dy
Ho
Er
Tm
Yb
Lu

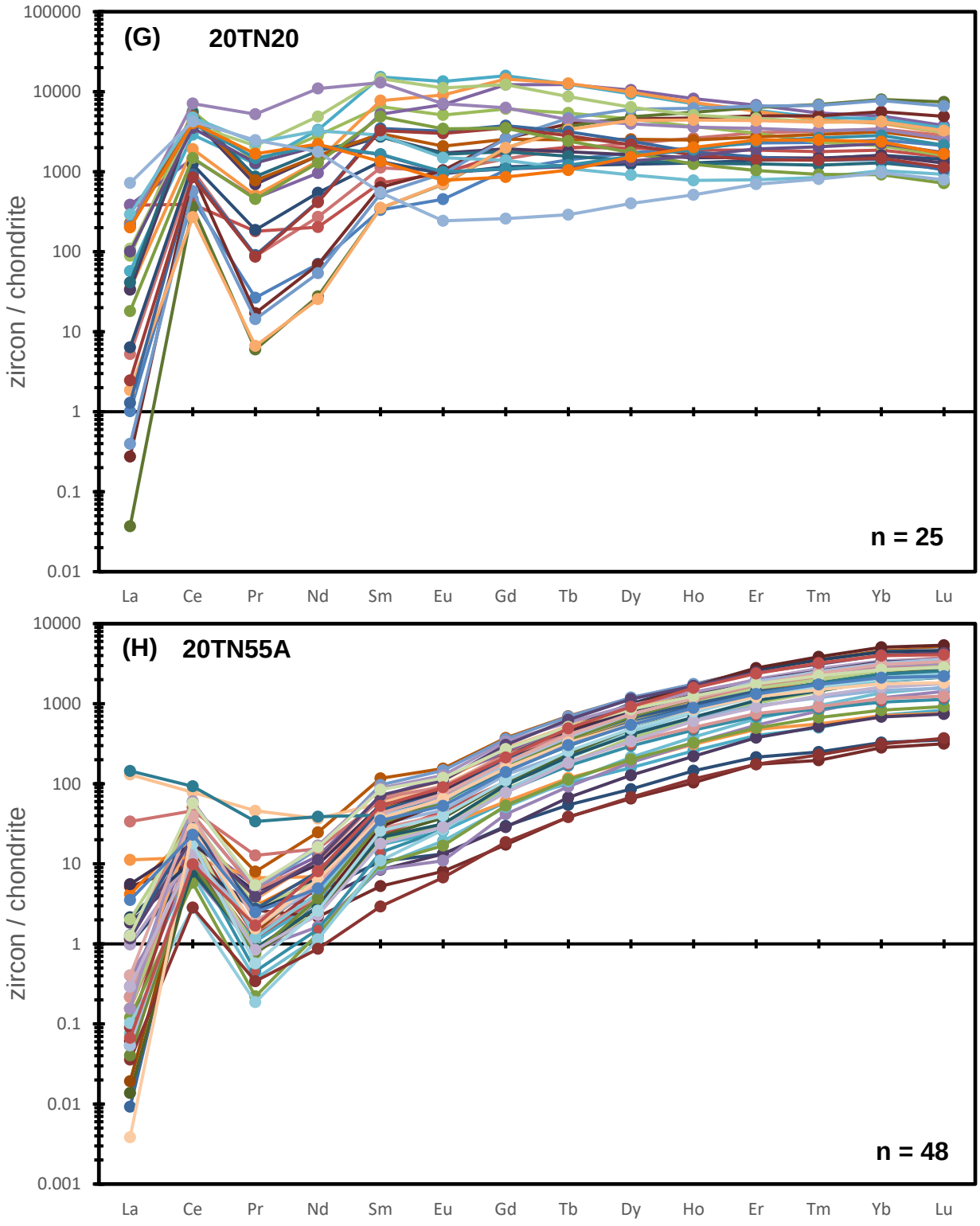

Figure 5.9. Chondrite normalized rare earth element diagrams of zircon ablations from eight rock samples. (A) 20TN2, (B) 20TN4D, (C) 20TN15A, (D) 20TN15B, (E) 20TN16A-2, (F) 20TN17A-2, (G) 20TN20, and (H) 20TN55A. Each line represents a single ablation point of a zircon (n). Values normalized to C1 chondrite values from McDonough & Sun (1995).

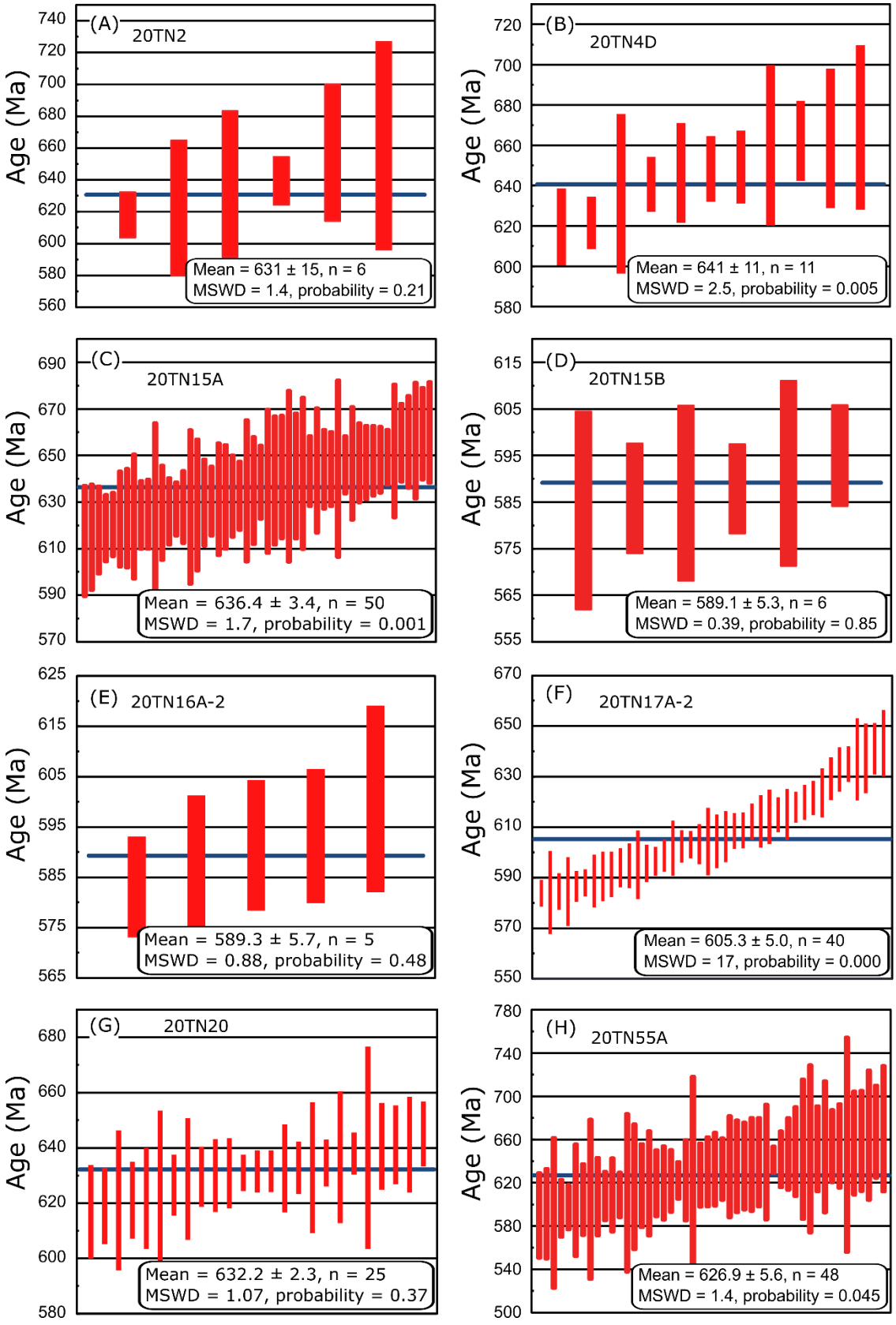

Figure 5.10. Weighted mean age diagrams of U-Pb zircon data from eight rock samples. (A) 20TN2, (B) 20TN4D, (C) 20TN15A, (D) 20TN15B, (E) 20TN16A-2, (F) 20TN17A-2, (G) 20TN20, and (H) 20TN55A. Each red box represents a single analysis (n) that is displayed on each respective diagram. Box heights are 2σ. The blue line represents the mean age of each analysis, weighted by data point errors only.

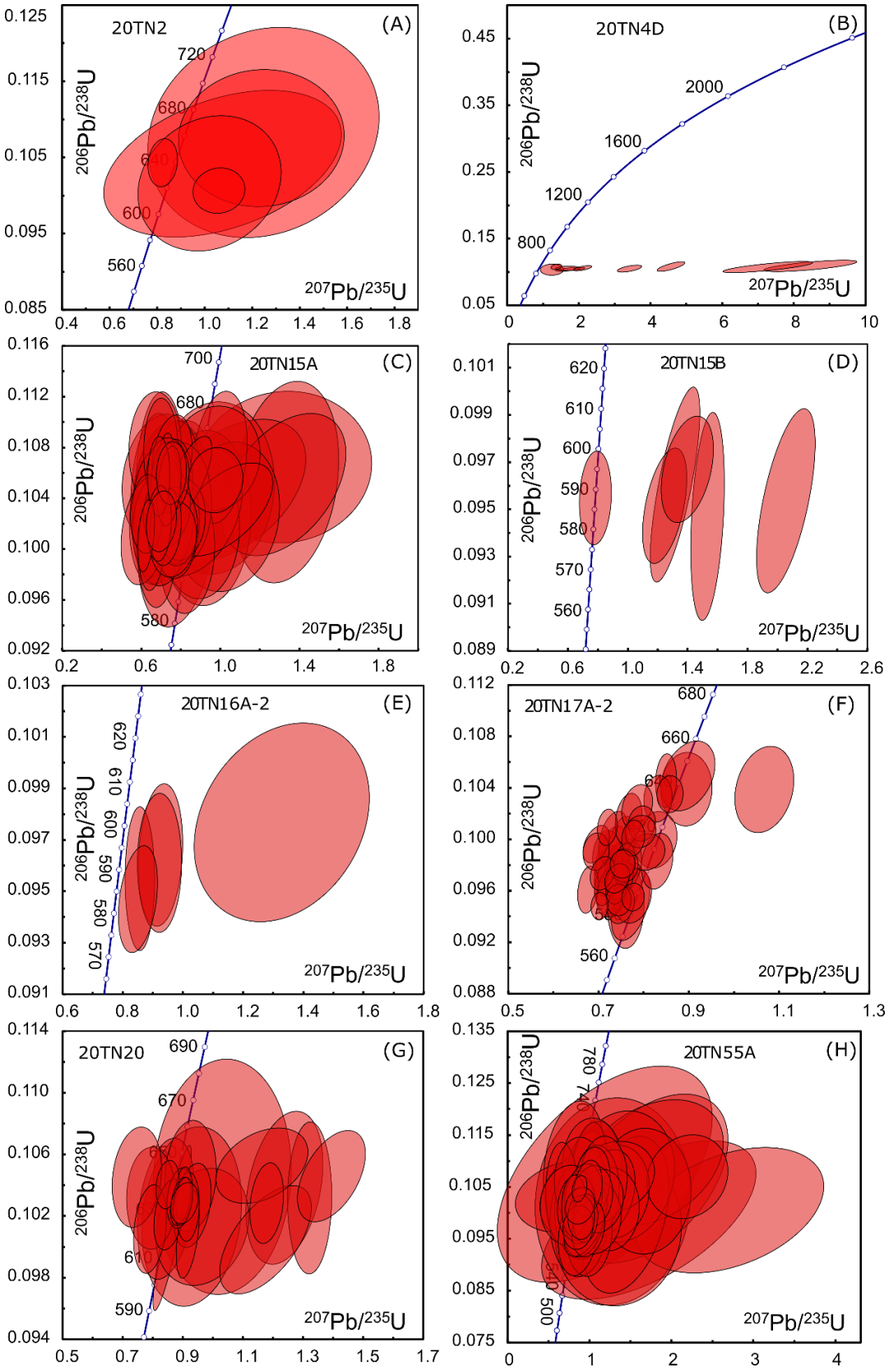
20TN2
(A)
720
680
640
600
560
$^{206}Pb/^{238}U$
$^{207}Pb/^{235}U$
20TN4D
(B)
2000
1600
1200
800
20TN15A
(C)
700
680
580
20TN15B
(D)
620
610
600
590
580
570
560
20TN16A-2
(E)
620
610
600
590
580
570
20TN17A-2
(F)
680
660
560
20TN20
(G)
690
670
610
590
20TN55A
(H)
780
500

Figure 5.11. Wetherill concordia diagrams of U-Pb zircon data from eight rock samples. Values along the concodria line represent $^{206}Pb/^{238}U$ dates. (A) 20TN2 dominantly shows concordant to near-concordant points. (B) 20TN4D shows discordant points which spread away from the concordia. (C) 20TN15A shows a tight cluster of concordant and near-concordant points where some are slightly discordant and reversely discordant. (D) 20TN15B shows points concordant to discordant. (E) 20TN16A-2 shows discordant to reverse discordant points that are near-concordant. (F) 20TN17A-2 points are mostly reverse discordant with two that are concordant. (G) 20TN20 shows several concordant points with a few near-concordant that are discordant and reverse discordant. (H) 20TN55A most points are concordant with a few that are discordant. Each ellipse represents a single analysis (n); refer to Figure 5.10 for the respective samples (n). Error ellipses are 2σ.

Zircon trace element chemistry

Based on the known relationship between LREE and hydrothermal alteration in zircon (e.g., Geisler et al. 2003; Hoskin 2005; Horie et al. 2006; Utsunomiya et al. 2007; Wiemer et al. 2017), typical REE patterns are interpreted to reflect unaltered areas of zircon crystals and atypical patterns with elevated LREE are interpreted to reflect alteration (i.e., metamictization, recrystallization, metasomatism, and inclusion). The zircons in this thesis show a variety of REE patterns, from typical (unaltered and LREE depleted) to atypical (altered and LREE enriched). Notably, some rock samples have zircon with typical and atypical REE patterns. This variability within discrete samples is clearly seen in SEM-CL images (Figures 5.1–5.8), which show a variety of primary igneous zircon that have been partially to completely altered. The variability of REE patterns within discrete samples highlights the conclusion that several zircons analyzed in this study have undergone varying degrees of alteration by metasomatic fluids.

According to the Th/U ratios (Figure 5.12), the zircon in this study are igneous. However, many zircon crystals in this study have experienced alteration (i.e., metamictization and secondary recrystallization) which has affected their Th and U contents. Zircon crystals that show minimal alteration based on cathodoluminescent imaging have low U values (> 10 ppm). All zircon crystals in 20TN17A-2 are highly metamict and plot along the boundary between the igneous and metamorphic fields on the Th/U diagram. Therefore, zircon with relatively high U values (>10 ppm) in this study are interpreted to have undergone some degree of alteration.

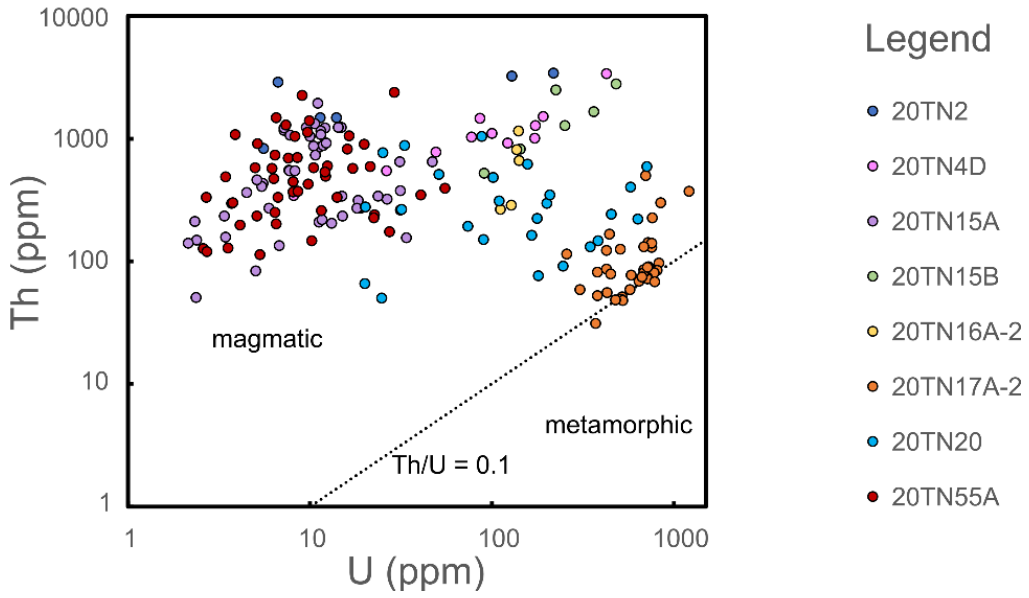

Figure 5.12. Uranium versus thorium bivariate diagram, where magmatic zircons plot >0.1 and metamorphic zircons plot <0.1. The less altered magmatic zircons in this study tend to have high Th and low U (<10 ppm) in comparison with the altered and metasomatic zircons which have high to moderate Th values and high U (>100 ppm). From top to bottom on the legend, n = 6, 11, 59, 6, 5, 40, 25, 48.

Zircon ablation data from eight rock samples reported in this thesis are plotted on several trace element discrimination diagrams for igneous rock sources (Figures 5.13–5.15 after Belousova 2002; Hoskin 2005; and Grimes et al. 2015) to assess the source rock type (e.g., syenite, pegmatite, etc.) of the zircons (as well as any alteration they may have undergone) and the tectono-magmatic environment they formed in.

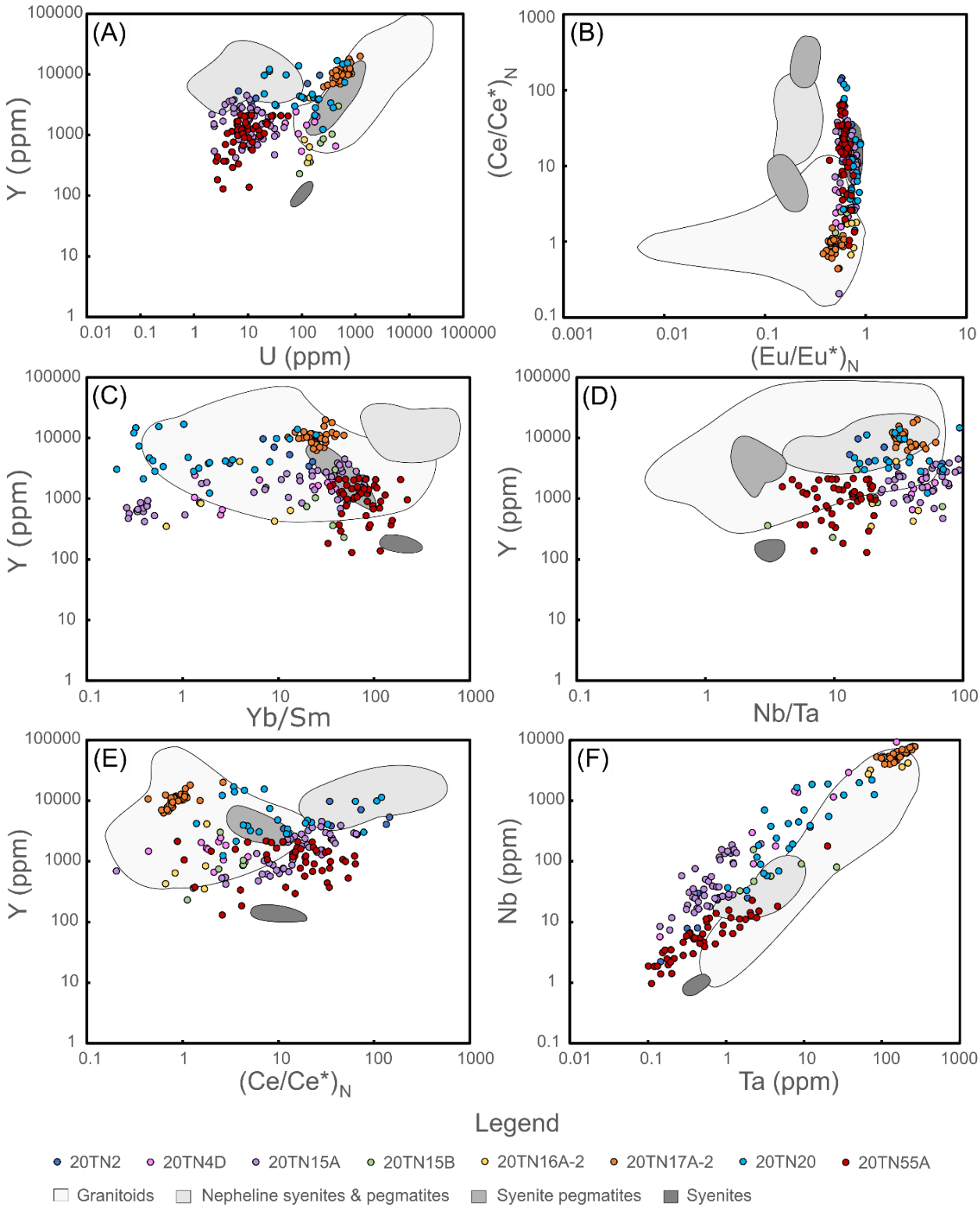

Figure 5.13. Source rock type discrimination diagrams. Shaded fields are after Belousova (2002). (A) U (ppm) versus Y (ppm). (B) $(Eu/Eu^*)_N$ versus $(Ce/Ce^*)_N$. (C) Yb/Sm versus Y (ppm). (D) Nb/Ta versus Y (ppm). (E)

$(Ce/Ce^*)_N$ versus Y (ppm). (F) Ta (ppm) versus Nb (ppm). In plots (B) and (E), $(Ce/Ce^*)_N$ is chondrite normalized Ce concentration divided by the average of the chondrite normalized La and Pr concentrations. In plot (B), $(Eu/Eu^*)_N$ is chondrite normalized Ce concentration divided by the average of the chondrite normalized Sm and Gd concentrations. From left to right on the legend, n = 6, 11, 59, 6, 5, 40, 25, 48.

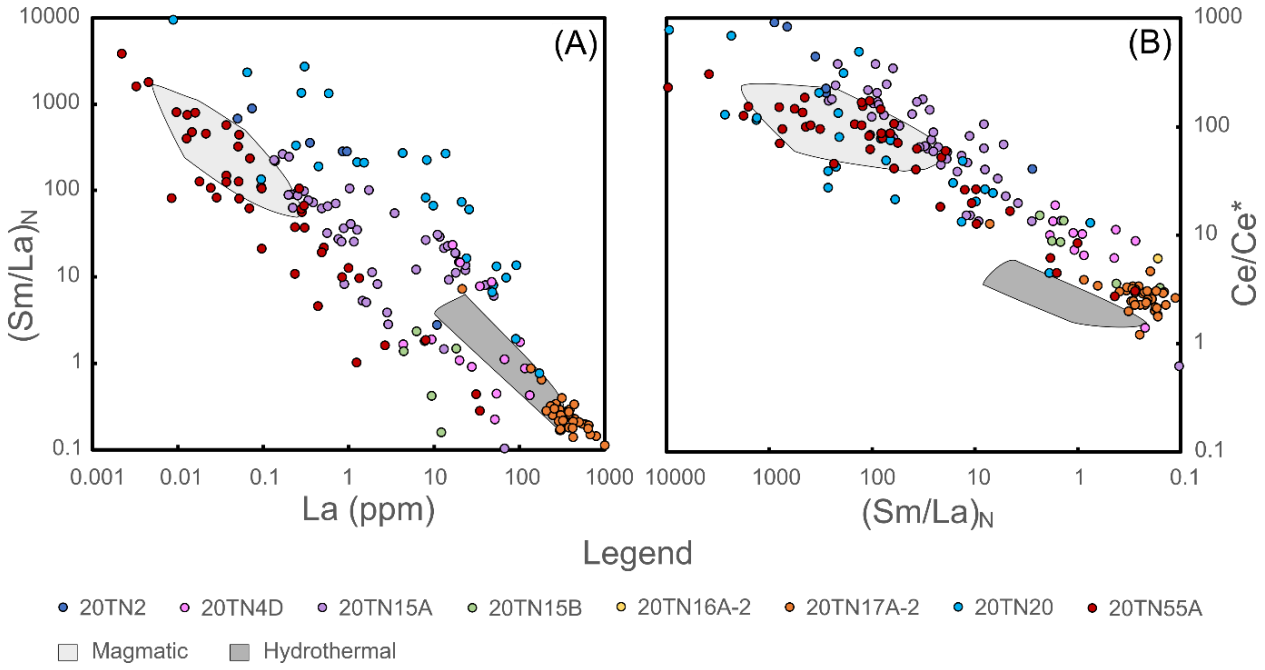

Figure 5.14. Magmatic versus hydrothermal zircon discrimination diagrams. (A) La (ppm) versus $(Sm/La)_N$. (B) $(Sm/La)_N$ versus Ce/Ce*. Less altered points plot in both the magmatic and hydrothermal fields, and more altered points typically plot in or near the hydrothermal field. Shaded fields are after Hoskin (2005). Less altered points dominantly plot in the magmatic field, and more altered points cluster near the hydrothermal field. From left to right on the legend, n = 6, 11, 59, 6, 5, 40, 25, 48.

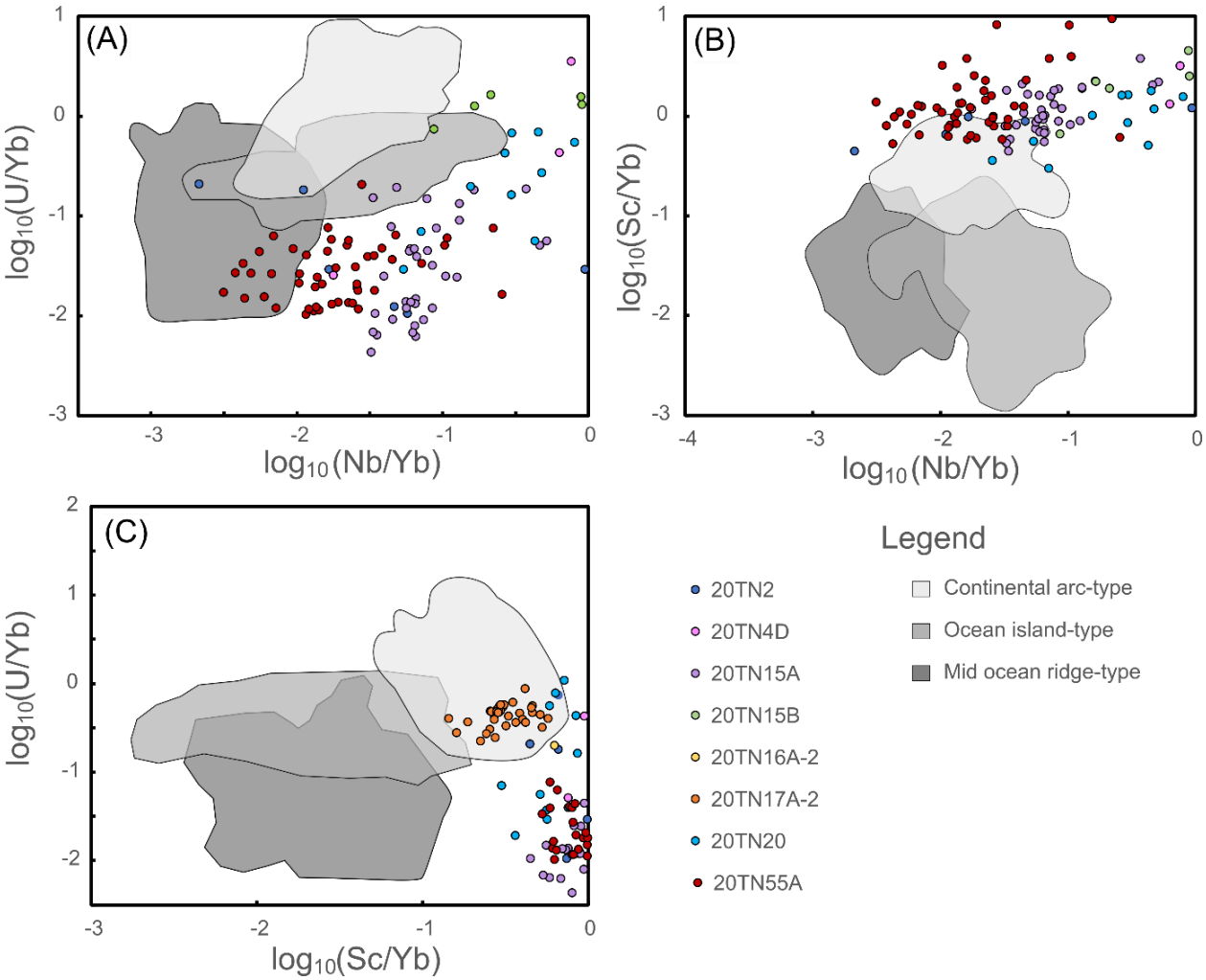

Figure 5.15. Tectono-magmatic discrimination diagrams. Shaded fields are approximate after those from Grimes et al. (2015). (A) Natural log of Nb/Yb versus natural log of U/Yb. Some of the less altered points plot within the mid ocean ridge-type and ocean island-type fields. (B) Natural log of Nb/Yb versus natural log of Sc/Yb. Some of the less altered points plot within the continental arc-type field. (C) Natural log of Sc/Yb versus natural log of U/Yb. Some of the more altered points plot within the continental arc-type field. Overall, sample points commonly do not plot within any of the fields, likely due to a combination of analytical error with the LA-ICP-MS experiment and the extent of the alteration of the zircon crystals.

According to the C1 chondrite normalized REE patterns of different sources of magmatic zircon from Belousova (2002), the REE patterns of zircon (Figure 5.9) in this study generally reflect the syenites, syenite pegmatites, and granitoids source rock compositions. Similarly, in the bivariate source rock type discrimination diagrams (Figure 5.13) after Belousova (2002), zircon crystals in this thesis plot within a mixture of source rock compositions; the most relevant include the syenite, nepheline syenite and pegmatite, syenite pegmatite, and granitoid compositions. The range of source rock compositions across the sample suite shown in the chondrite normalized REE diagrams and bivariate diagrams is due to altered zircon compositions. For example, in bivariate plot Eu/Eu* versus Ce/Ce* in Figure 5.13B, zircon crystals that have experienced minimal alteration (e.g., zircon in 20TN55A and 20TN15A) show higher Ce/Ce* than more altered zircon (e.g., zircon in 20TN17-2 and 20TN16A-2), where the less altered zircon analyses cluster tightly in the syenites field and zircon that are more altered plot in the granitoids field. The low Ce/Ce* in the more altered zircon crystals is due to the elevated La (ppm) with respect to Ce in the zircons, which is demonstrated in the chondrite normalized REE diagrams. Finally, in the bivariate magmatic versus hydrothermal zircon discrimination diagrams (Figure 5.14) after Hoskin (2005), zircon crystals from discrete rock samples plot within and between the magmatic and hydrothermal fields, supporting that the variability of zircon compositions observed in the sample suite is due to a mix of primary and altered compositions.

Zircon data plotted on the tectono-magmatic discrimination plots (Figure 5.15) after Grimes et al. (2015) are inconclusive. This result is not surprising because Grimes et al. (2015) warn that the accuracy and precision of data collection is key to meaningful results, and as previously discussed in this chapter, LA-ICP-MS is not as precise as other methods. The inaccuracy of the data plotted in this thesis is likely due to interferences with Sc that were recorded by the LA-ICP-MS when analyzing zircon (e.g., Regnery et al. 2010), as well as the degree of alteration and metasomatic nature of most of the zircons, which is reflected on the diagrams by the extremely high Nb values of most of the data points. Thus, the combination of these two factors is interpreted to be what is causing the large spread of points across and out of the diagram bounds.

Overall, elements that are not foundational to zircon's crystal structure (e.g., non-formula elements such as Ca, Nb, Ta, REE, and U) are generally lower in the less altered Pool Creek

nepheline syenite and higher in areas that underwent more intense alteration. This means that zircon analysed in this study with elevated LREE, Ta, Nb, U, and other non-formula elements reflect some degree of metamictization and hydrothermal alteration of primary igneous zircon, where hydrothermal alteration is interpreted to be caused by metasomatic fluids sourced from the Pool Creek nepheline syenite during the post-magmatic stage of the intrusion. This interpretation is supported by further evidence in Chapters 3, 4, 6, and 7, as well as by several studies in the literature that demonstrate post-magmatic alteration of zircon by late-stage alkali metasomatic fluids (e.g., autometasomatic or fenitizing) leading to enriched LREE and other non-formula elements in syenitic and granitic systems (e.g,, Belousova 2002; Soman et al. 2010; Walters et al. 2013; Vetrin & Skublov 2016; Sjöqvist et al. 2017; Kubeš et al. 2021).

Pigage & Mortensen (2004) reported that the primary igneous zircons from the Pool Creek nepheline syenite and associated dikes have unusual U-Th-Pb systematics (low U, high Th), the cause of which they stated was unclear. Metamictization and hydrothermal fluids interacting with partially metamict zircon can remove U and affect the U-Th-Pb system of a zircon (e.g., Mattinson et al. 1996; Geisler et al. 2002; 2003; McCreath et al. 2012). The unusual U-Th-Pb systematics of the zircons from the Neoproterozoic Pool Creek nepheline syenite and fenitized units are interpreted to be due to metamictization and post-magmatic hydrothermal alteration of the zircons.

U-Pb zircon geochronology

According to the weighted mean U-Pb zircon ages for the eight rock samples (Figure 5.10) from the Bandito property (which include select samples of nepheline syenite and altered syenites), these units are Neoproterozoic, which range from 589.1 ± 5.3 to 641 ± 11 Ma in age. The U-Pb ages reported in this thesis generally agree with the 640-650 Ma U-Pb zircon age for the Pool Creek nepheline syenite reported by Pigage & Mortensen (2004). Some of the ages of the unknowns (i.e., ablated zircons that are not standards) in this thesis are slightly younger or older than those reported by Pigage & Mortensen (2004), which may be due to analytical or natural factors such as bias during the data refinement process, instrumental error (known as "spectral effects"), the compositional differences between primary reference materials and the analyzed unknown materials (known as "matrix effects"), alteration of the unknowns, and later crystallization of the unknowns. The most applicable factors are summarized in bullet points below and are further discussed with respect to specific samples in the paragraphs that follow.

(1) The manual nature of the filtering and lack of corrections that can be applied to the LA-ICP-MS method may lead to skewed or biased ages of all samples in this study (see Methods: LA-ICP-MS for Zircon U-Pb Ages). There is no standard ^{206}Pb (i.e., common lead) correction for the LA-ICP-MS method (Paton et al. 2010; Paton et al. 2011). The author manually selected the average age of each unknown based on the flatness of the ablation pattern with respect to the $^{206}Pb/^{238}U$ age and the total beam counts in Iolite 4.0 to filter out any inclusions or obviously altered or metamict zones encountered during the ablation. Afterwards, the author further filtered the data by manually selecting unknowns that created the flattest plateau on the mean weighted diagram and discarded the remaining unknown analyses.

(2) Zircon standards used for the downhole fractionation correction (e.g., 91500, Plešovice, and Temora 2) of unknown materials in an LA-ICP-MS experiment can have a significant effect on the U-Pb geochronology results of the unknown materials if the primary reference material behaves differently than the unknown material during ablation (Ver Hoeve et al. 2018). For example, if the chosen primary reference material ablates similarly to an unknown (i.e., zircon) then the downhole fractionation correction will be

more appropriate and robust than if the primary reference material ablates differently than the unknown material (Ver Hoeve et al. 2018). The Plešovice standard was used as the primary calibration material in this thesis for the downhole correction because it appears to behave more similarly to the unknowns (due to its known heterogeneity in trace elements) than 91500, thereby providing a better downhole correction. However, the use of the Plešovice standard as the primary calibration material may have led to the output of slightly younger ages than what are true for the zircons ablated in this study. This possibility is supported by the other zircon reference materials (91500 and Temora 2) reported in this study having slightly lower ages than their known values when Plešovice was used as the primary calibration material for the experiment (see Methods: LA-ICP-MS for Zircon U-Pb Ages).

(3) The loss of radiogenic Pb or the addition of U can lead to younger ages in the U-Pb system than what is true for an unknown and may be represented by a discordant point on the Concordia diagram (Mattinson et al. 1996; Mezger and Krogstad 1997; Corfu 2013). Hydrothermal alteration and recrystallization of zircon can remove radiogenic Pb from the zircon crystal structure (e.g., Mattinson et al. 1996; Mezger and Krogstad 1997; Geisler et al. 2002; 2003). Smaller zircon crystals are more susceptible to Pb loss than larger zircons due to high surface area to volume ratios (Corfu 2013). Radiation damage (i.e., metamictization) is common in zircons due to alpha decay of radiogenic U and Th in the zircon crystal structure and leads to radiogenic Pb loss (e.g., Geisler et al. 2002; 2003; Horie et al. 2006). Zircons with high U experience more severe radiation damage than those with low U over time and are therefore more metamict and more susceptible to Pb loss (e.g., Mezger and Krogstad 1997; Geisler et al. 2002; 2003; Marsellos & Garver 2010). Metamict areas of zircon recrystallize at lower temperatures than crystalline zircon and are therefore more susceptible to Pb loss than crystalline zircons (e.g., Mezger and Krogstad 1997; Geisler et al. 2002; 2003; Marsellos & Garver 2010).

(4) The excess of Pb, the removal of U, and the internal redistribution of Pb or U in a zircon can lead to older ages in the U-Pb system and be represented by a reverse discordant point on the Concordia diagram (e.g., Mattinson et al. 1996; Corfu 2013). The addition of Pb or loss of U in zircon is rarely observed in nature (briefly summarized by Mattinson et

al. 1996 and Corfu 2013). Any apparent addition of Pb is commonly considered to be superficial and is commonly attributed to analytical artifacts and the redistribution of Pb within a zircon (e.g., Mattinson et al. 1996; Wiemer et al 2017). Metamict and annealed zircons can ablate differently than pristine zircon crystals in LA-ICP-MS experiments, which can result in an under- or overcorrected downhole fractionation correction and lead to an incorrect age (Steely et al. 2014; Marillo-Sailer et al. 2016). Inclusions bearing ^{206}Pb (i.e., common lead), such as apatite, monazite, titanite, and pyrochlore, can overprint the ^{206}Pb in an ablation analysis and lead to an increase in measured Pb (e.g., Morales et al. 2022). Loss of U from zircon is uncommon since U is well bound to the zircon crystal structure (e.g., Corfu 2013), however, in some instances the removal of U in zircon can be caused by hydrothermal alteration (e.g., Mattinson et al. 1996; Geisler et al. 2002; 2003).

As shown in the weighted mean diagrams (Figure 5.10), there is a large spread of ages between points within discrete samples as well as across the suite of samples. To visualize the overlap between the unknowns used to calculate the weighted mean age, the age ranges of the unknowns from each sample are plotted in Figure 5.16. As discussed earlier in this chapter, most (if not all) of the zircons analyzed in this thesis have experienced some degree of post-magmatic alteration based on textural evidence and elevated non-structural trace elements (e.g., LREE, Nb, Ta, and U). Additionally, several zircons are also included or intergrown with apatite, titanite, pyrochlore, thorite, and feldspar, and several of these minerals can overprint ^{206}Pb in zircon, which is elaborated on in bullet point (4). The large spread of U-Pb ages is interpreted to represent signals of the timing of crystallization and the timing of alteration of zircons. Regardless of the large spread of ages across the samples, ages still overlap between all of the samples, indicating that these zircons were crystallized and altered relatively closely in time.

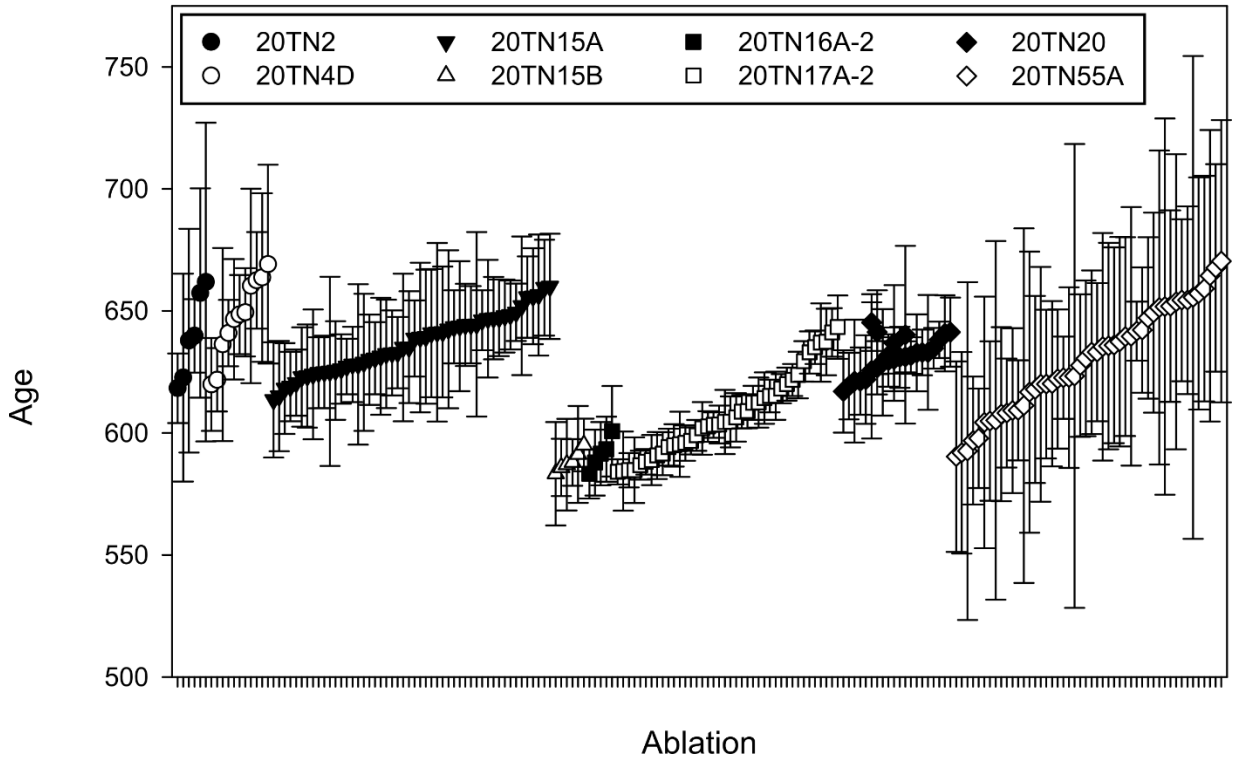

Figure 5.16. Weighted mean diagram comparing the U-Pb zircon age distribution of ablations across the eight samples analyzed in this thesis. The plot shows that sample ages occur relatively close in time and typically overlap. From left to right, n = 6, 11, 59, 6, 5, 40, 25, 48. Error bars represent 2σ.

Many zircon ablations across the suite of analyzed samples are concordant with a mix of discordant points, as shown in the Wetherill concodria diagrams (Figure 5.11). Samples that show a large spread of concordant to discordant points provide strong evidence for alteration of the affected samples (see points 3 and 4 above). Ages of samples with dominantly concordant to normal discordant points are considered to either represent the age of crystallization, age of alteration (see points 3 and 4 above), or a mix of the two, while those with dominantly reversely discordant data are inconclusive (see point 4 above) because they likely represent either a relatively high degree of alteration or analytical error, or both.

To check whether the weighted mean U-Pb zircon age of each of the analyzed zircon samples are mixed or not, ablation points of select zircons from samples of the nepheline syenite and altered syenites have been matched to their respective SEM-CL images. Figure 5.17 displays ablations versus age across a minimally altered zircon crystal from the nepheline syenite, and Figure 5.18 compares ablations of variously altered zircon crystals from four different altered syenite samples.

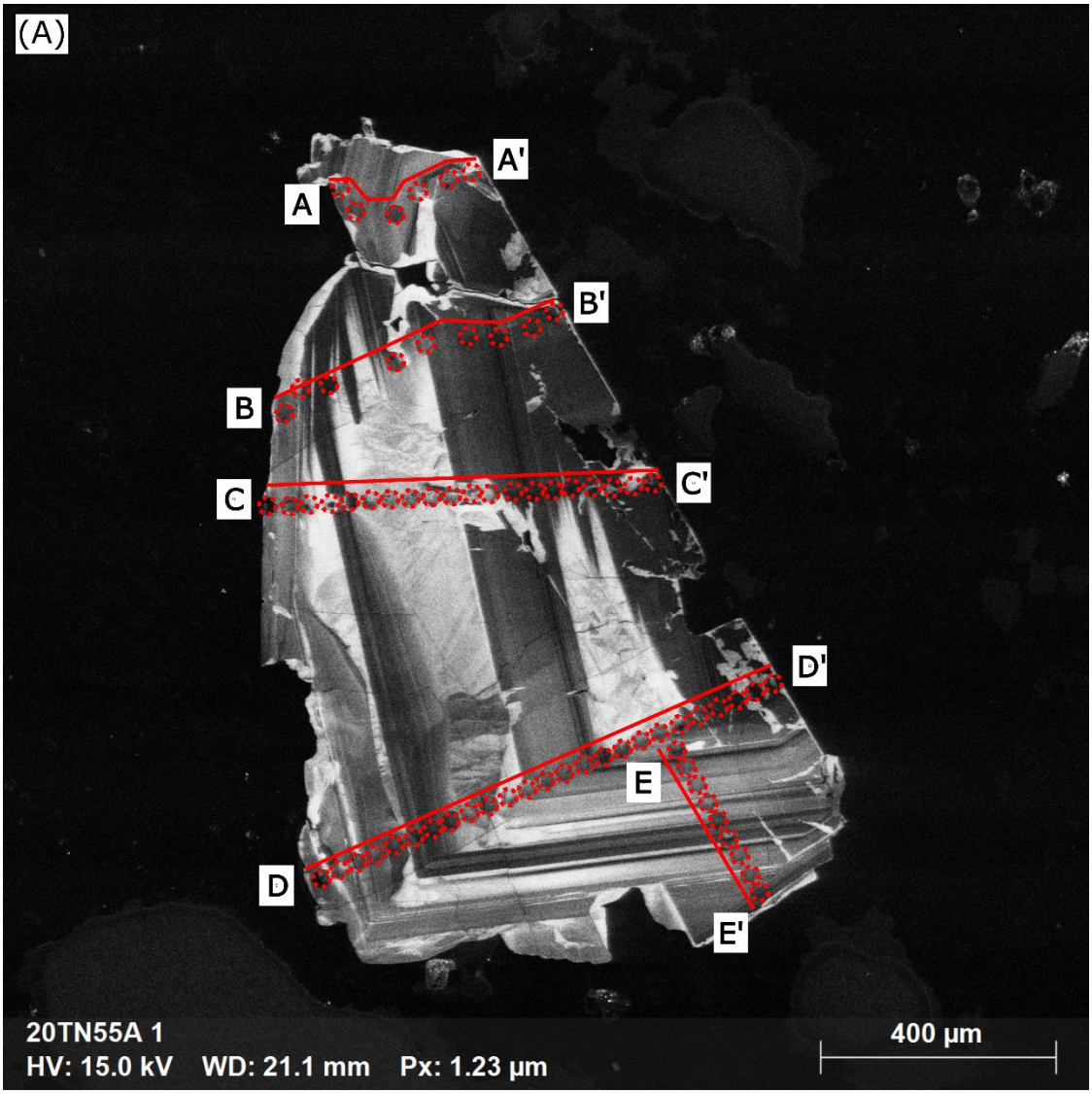
(A)
A
A'
B
B'
C
C'
D
D'
E
E'
20TN55A 1
HV: 15.0 kV WD: 21.1 mm Px: 1.23 µm
400 µm

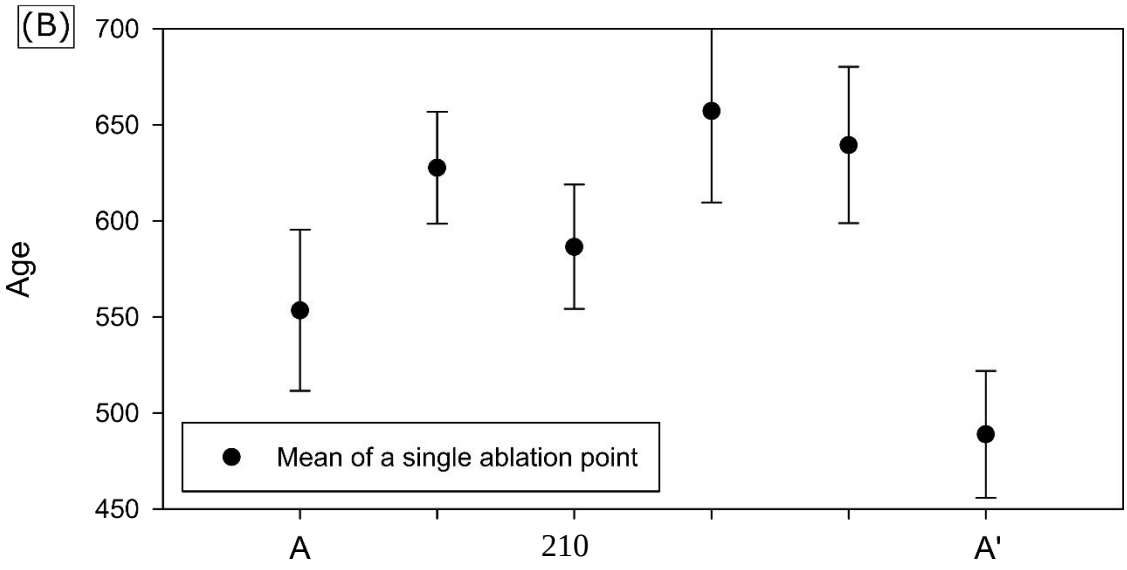
(B)
Age
700
650
600
550
500
450
Mean of a single ablation point
A
210
A'

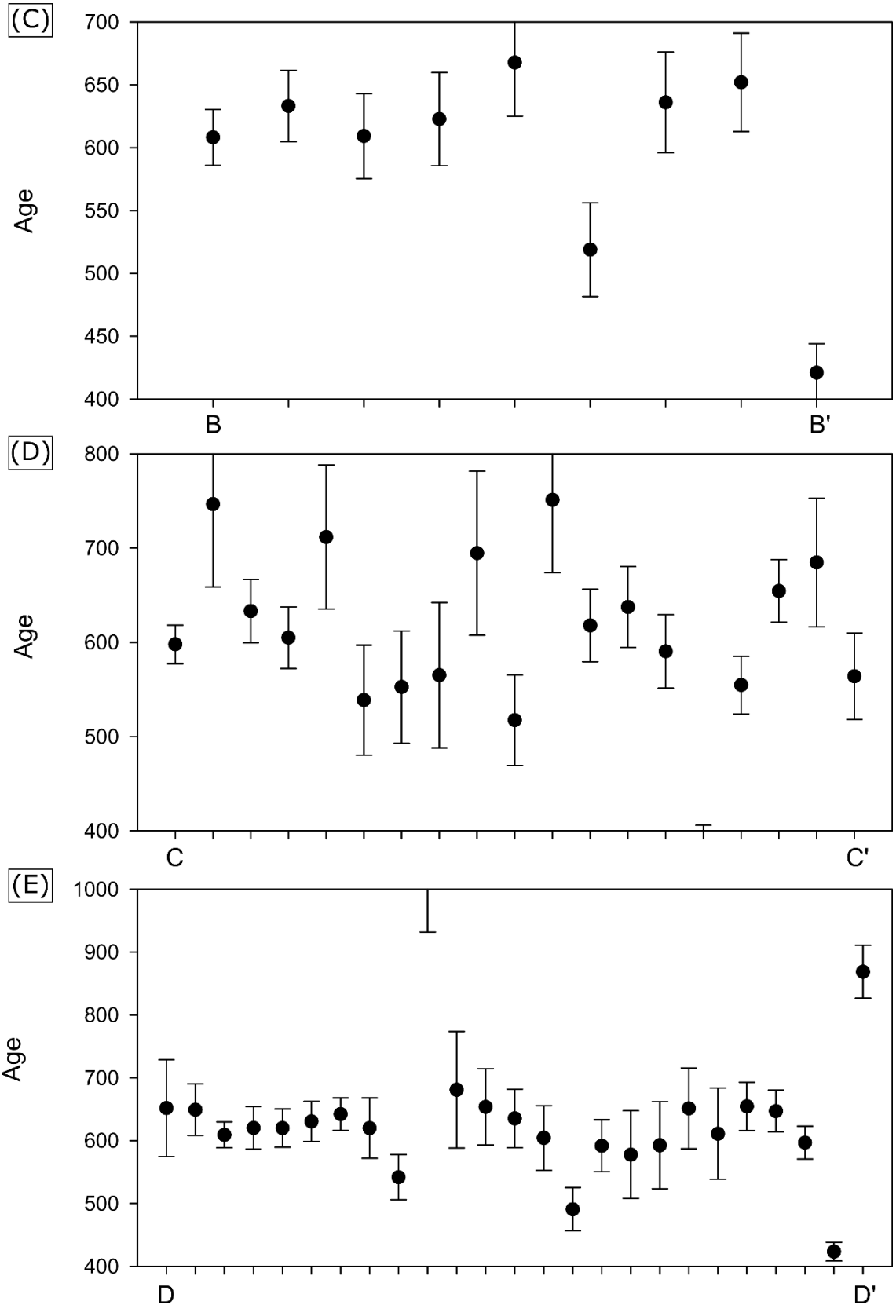
(C)
700
650
600
550
500
450
400
Age
B
B'
(D)
800
700
600
500
400
Age
C
C'
(E)
1000
900
800
700
600
500
400
Age
D
D'

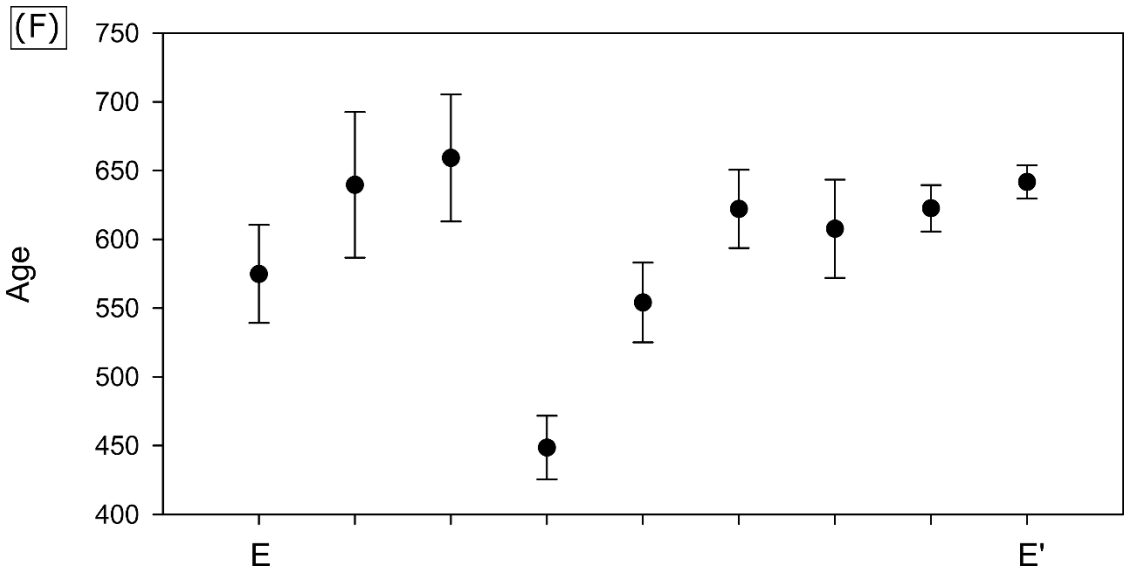

Figure 5.17. Ablations versus age of a minimally altered zircon from the Pool Creek nepheline syenite (sample 20TN55A). (A) SEM-CL image showing the locations of ablation line transects. (B) A-A'. (C) B-B'. (D) C-C'. (E) D-D'. (F) E-E'. Black circles represent the mean U-Pb age of a single ablation point. Error bars represent 2σ.

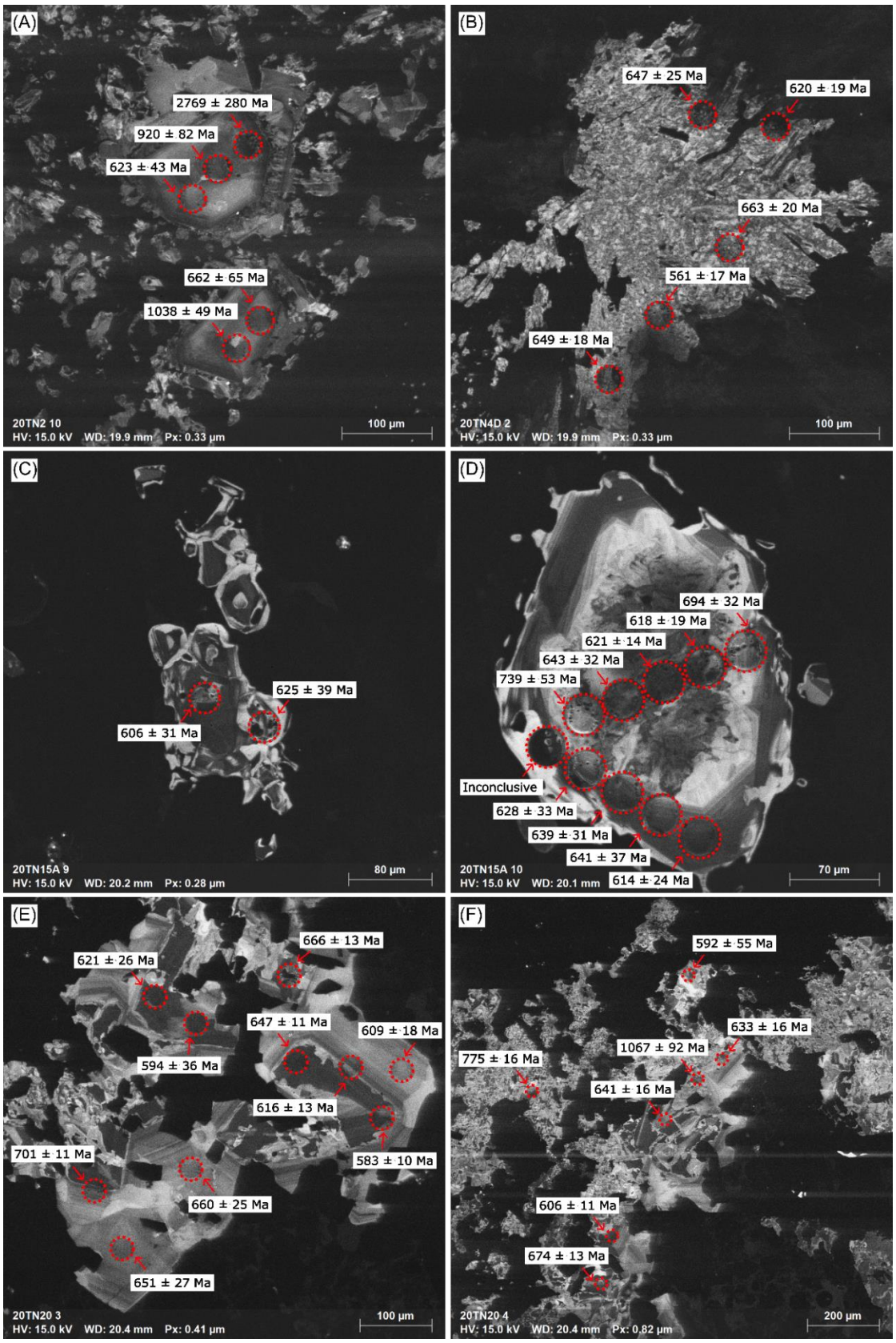

Figure 5.18. Ablation points and their respective ages across variously altered zircon crystals from four different samples. (A) 20TN2. (B) 20TN4D. (C–D) 20TN15A. (E) 20TN20. (F) 20TN55A. The red dashed circles represent the ablation point positions and sizes.

Based on the relationship between ablation ages and textures of zircons in Figure 5.17 and 5.18, ablations on areas with no obvious alteration range between roughly 600 and 660 Ma in age. In contrast, areas that show visible fractures and mineral inclusions typically report ages above this range (i.e., older) and areas that are recrystalized (highly luminescent rims or patches under SEM-CL) typically report ages below this range (i.e., younger). Based on the relationship between ablation ages and textures observed in the zircons from the five selected samples, the weighted mean ages of the nepheline syenite likely represent an age of crystallization and the four altered syenite samples represent a mixed age between crystallization and alteration. This finding likely applies to the other samples that have been dated in this study, as all samples show evidence of variable alteration (Figures 5.1–5.8).

Sample 20TN55A (Pool Creek nepheline syenite) shows a zircon impacted by the least amount of alteration (i.e., SEM-CL in Figure 5.8 and 5.17), and most ablation points are concordant on the Wetherill concordia diagram (Figures 5.11H). Based on the presence of alteration, the weighted mean age of 626.9 ± 5.6 Ma is interpreted to represent a mixed age of crystallization and alteration for this sample.

Samples 20TN2 (actinolite-altered syenite), 20TN4D (actinolite-altered syenite), 20TN15A (layered titanite-arfvedsonite syenite), and 20TN20 (altered arfvedsonite-aegirine syenite) show zircon cores with growth rims and complexly altered zircons (Figures 5.1, 5.2, 5.3, and 5.7, respectively). The weighted mean ages (631 ± 15 Ma, 641 ± 11 Ma, 632.2 ± 2.3 Ma, 636.4 ± 3.4 Ma, respectively) and mix of concordant and normal discordant points (on the Wetherill concordia diagrams in Figures 5.11A, B, C, and G, respectively) of these samples are interpreted to represent a mix between the age of crystallization and age of metasomatic alteration.

Samples 20TN15B (altered amphibole-diopside-phlogopite syenite), 20TN16A-2 (strongly altered arfvedsonite-aegirine syenite), and 20TN17A-2 (strongly altered arfvedsonite-aegirine syenite) are the most intensely altered samples (alteration is visible in SEM-CL images in Figures 5.4, 5.5, and 5.6, respectively, and are represented by a spread in concordant and normal to reverse discordant points on the Wetherill concordia diagram in Figures 5.10D, E, and F, respectively). The weighted mean ages of samples 20TN15B and 20TN16A-2 (589.1 ± 5.3 and

589.3 ± 5.7, respectively) are interpreted to represent a separate, alteration event unrelated to the crystallization or fenitization of the Pool Creek nepheline syenite. Due to the reversely discordant nature of several of the analyzed zircons from sample 20TN17A-2, the age for this sample (605.3 ± 5.0 Ma) is a mixture of crystallization and later alteration and therefore is inconclusive. The reverse discordance in this sample is most likely due to the highly metamict nature of the zircon, which probably caused analytical error [see points (2) and (4), above]. Regardless, the concordant analyses show a trend from older to younger ages, suggesting that the sample was affected by alteration.

A summary of the zircon weighted mean U-Pb ages and interpretations of each sample is given in Table 5.2. The U-Pb zircon ages from the Pool Creek nepheline syenite samples reported in this thesis overlap with the 640 to 650 Ma U-Pb zircon ages reported by Pigage & Mortensen (2004), supporting the interpretation that the Pool Creek nepheline syenite and associated dikes were emplaced during the Neoproterozoic. Furthermore, the U-Pb ages reported in this thesis provide strong evidence that the fenitization event previously associated with the Pool Creek nepheline syenite by Swanton (2011; 2012) occurred during the crystallization of the Pool Creek nepheline syenite, and therefore was driven by the post-magmatic crystallization of the Pool Creek nepheline syenite.

Table 5.2. Summary of zircon U-Pb ages of samples and their respective rock units in this study. Age calculation method is $^{206}Pb/^{238}U$ weighted mean age (error is 2σ).

Sample	Rock Unit	n analyses	Weighted Mean Age (Ma)	Comments	Conclusion
20TN2	Actinolite-altered syenite	6	631 ± 15	Zircon cores are surrounded by metasomatic rims.	Mixed age of crystallization and alteration.
20TN4D	Actinolite-altered syenite	11	641 ± 11	Most zircon is strongly altered and included. Unaltered zircon shows oscillatory and sector zoning.	Mixed age of crystallization and alteration.
20TN15A	Altered layered titanite-arfvedsonite syenite	50	636.4 ± 3.4	Zircon cores are commonly metamict and included and are surrounded by metasomatic rims.	Mixed age of crystallization and alteration.
20TN15B	Altered diopside-phlogopite syenite	6	589.1 ± 5.3	Zircons are commonly highly included and strongly recrystallized.	Age possibly represents a later alteration event?
20TN16A-2	Strongly altered arfvedsonite-aegirine syenite	5	589.3 ± 5.7	Zircon is mostly to completely metamict and has inclusions. Weighted mean age is young due to Pb loss from metamictization.	Age possibly represents a later alteration event?
20TN17A-2	Strongly altered arfvedsonite-aegirine syenite	40	605.3 ± 5.0	Zircon is completely metamict. Weighted mean age is young due to Pb loss from metamictization. Reverse discordance likely due to matrix effects.	Inconclusive age: zircons are too altered.
20TN20	Moderately altered arfvedsonite-aegirine syenite	25	632.2 ± 2.3	Zircon cores are surrounded by metasomatic rims.	Mixed age of crystallization and alteration.
20TN55A	Weakly altered nepheline syenite	48	626.9 ± 5.6	Zircon has oscillatory and sector zoning and patches of alteration and inclusions.	Mixed age of crystallization and alteration.

The approximate age of crystallization and fenitization of eight rock samples are compared to that of Pigage & Mortensen (2004) in Figure 5.19. Based on the earlier discussion, the age of crystallization and fenitization of these samples likely occurred between 620 to 660 Ma. Notably, visible in Figure 5.19 are steps in dates that overlap between samples. These may represent multiple geologic events, such as pulses of magma and alteration events. Syenites commonly form complexes involving multiple pulses of magmatism over time (e.g., Harrison 1982; McCreath et al. 2012; Andersen et al. 2017; Beard et al. 2023). In this thesis, multiple igneous rock types are described (see Chapter 3 and 6) and indicate that the Pool Creek nepheline syenite is a multiphase complex made up of multiple intrusive phases rather than a single nepheline syenite intrusion as previously discussed in the literature (Allen et al. 2001; Pigage & Mortensen 2004; Pigage 2009). A more thorough investigation of the syenites, dikes, and fenitized units across the property should be conducted to gain a deeper understanding the tectono-magmatic history of this area during the Neoproterozoic.

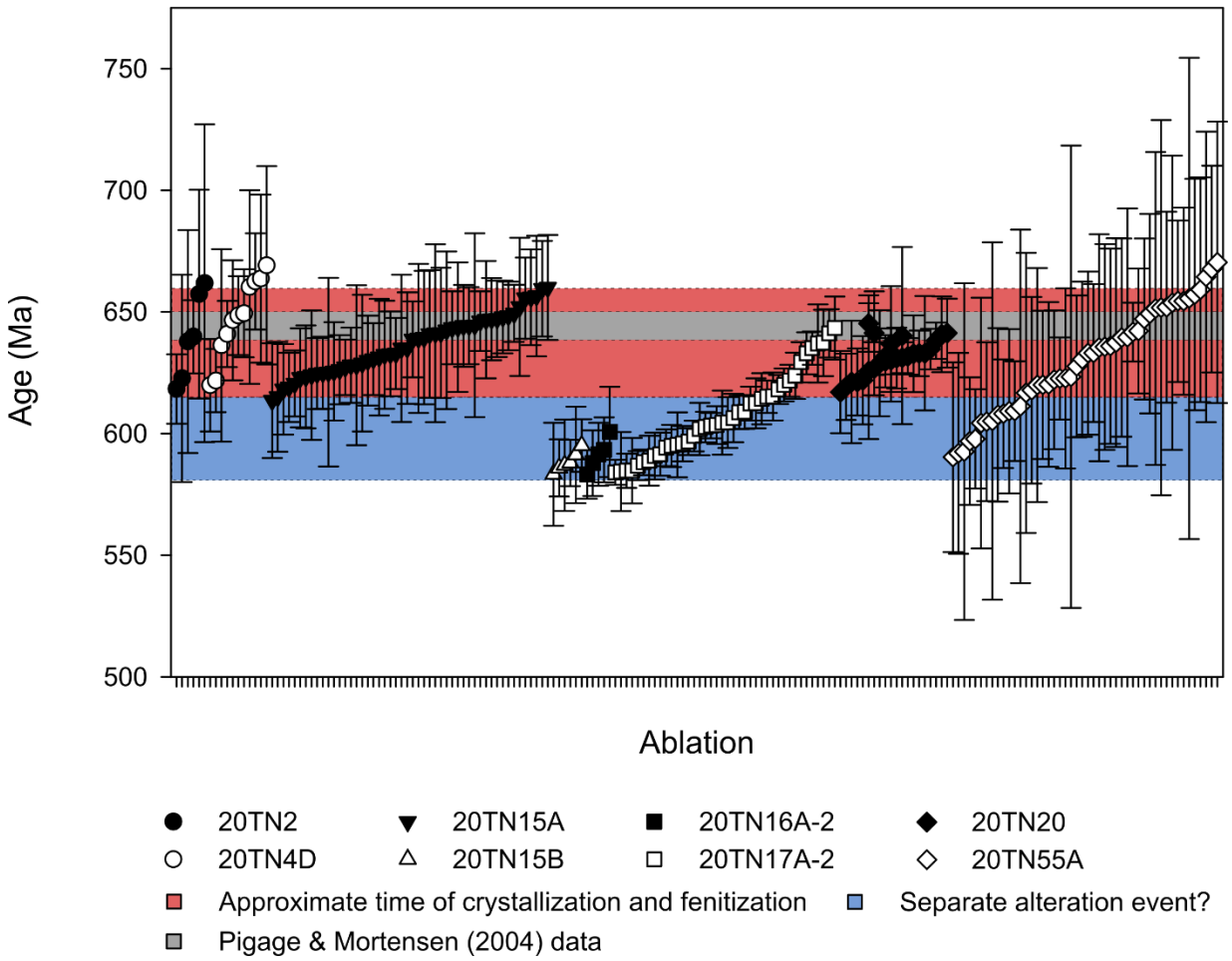

Figure 5.19. Approximate timing of crystallization and fenitization associated with the Pool Creek nepheline syenite. The age of crystallization of the Pool Creek nepheline syenite reported by Pigage & Mortensen (2004) is represented by the grey field. The approximate range timing of the crystallization and fenitization is represented by the red field. Later unrelated alteration is represented by the blue field. From left to right, n = 6, 11, 59, 6, 5, 40, 25, 48. Error bars represent 2σ.

The weighted mean U-Pb zircon dates reported in this study are considered mixed and therefore approximate because of the evidence for mixed ages from variable alteration across the suite of zircons (e.g., mineral inclusions, recrystallization, and metamictization), limitations of precision of the LA-ICP-MS method as discussed in points (1) to (4) above. The result of this study show that the combination of CL-imaging and LA-ICP-MS can be used to estimate end member ages, i.e., age of crystallization and age of alteration. Similar studies exist in the literature, for

example, McCreath et al. (2012) analyzed unaltered and altered areas of zircon and pyrochlore using LA-ICP-MS and determined independent age estimates of magmatic and hydrothermal episodes in the Motzfeldt Centre, Gardar Province, South Greenland.

If more research is to be conducted on the source and timing of emplacement and alteration of the magmatic and altered units (i.e., fenite, gossan, hornfels, skarn) on the Bandito property, the author recommends CL imaging be conducted to carefully plan ablation spots, and that ablation points be focused directly on zones within zircon that show no alteration and zones that show alteration so that end member ages are more accurately determined. Although CA-TIMS is a more robust dating method where more corrections can be applied to mitigate uncertainty within a zircon analysis, applying this method to the zircons in this study would report a degree of mixing which would be geologically meaningless.

6 Whole Rock Compositions

This chapter evaluates the major element oxide and trace element compositions of 21 samples collected from the Bandito property in 2020. The 21 analysed samples consist of argillite (×2), quartzite (×1), fenites (×6), actinolite-altered syenite (×4), altered arfvedsonite-aegirine syenite (×5), and nepheline syenite (×3).

Chemical comparison of the source rock, metasomatized rock, and the protolith of the altered rock useful in understanding the transfer of elements during metasomatic alteration and in turn the metasomatic fluid composition (e.g., Heinrich 1985; Le Bas 2008; Elliot et al. 2018; Anenburg 2020; Beard et a; 2023). Incompatible elements, such as REE, Zr, Nb, Ta, are associated with alkaline-silicate intrusions and their associated metasomatism (e.g., Elliott et al. 2018; Anenburg et al. 2020). Understanding the source of incompatible elements and processes and factors that control element mobilization and mineralization is essential to characterize the system (e.g., fluid source and mineralized host) as a whole and useful for exploration for potential critical element deposits (e.g., Finch et al. 2019b; Anenburg et al. 2020; Beard et al. 2023). To determine the source and composition of metasomatic fluids that have altered the samples in this study, the discussion will focus on chemical variations between the nepheline syenite, altered arfvedsonite-aegirine syenite, actinolite-altered syenite, fenites, and their respective host rocks. The factors contributing to the deposition and concentration of critical elements typically associated with syenitic rocks and fenite (i.e., REE, Y, Zr, Nb, Ta) will be discussed.

Methods

Of the suite of samples collected from the Bandito property in 2020, 29 were submitted to ALS Global - Geochemistry Analytical Lab in North Vancouver, BC, Canada for whole rock geochemical analysis. The analysed samples consist of argillite (×2), quartzite (×1), calcite-quartz metaconglomerate (×1), fenites (×6), actinolite-altered syenite (×4), altered arfvedsonite-aegirine syenite (×5), altered layered amphibole-diopside-phlogopite syenite (×2; one from a "light" coloured layer and one from a "dark" coloured layer), nepheline syenite (×3), altered dikes (×3), and volcanic breccias (×2). Although the calcite-quartz metaconglomerate, altered layered amphibole-diopside-phlogopite syenite, volcanic breccias, and altered dikes were analyzed, they will not be discussed in this chapter because they do not contribute to answering the questions posed in Chapter 1.

Samples were cut to ~6 × 6 × 6 cm blocks using the basement saws at UBC. Weathered surfaces of the samples were cut off the samples to minimize contamination. Samples were crushed at ALS using package PUL-51. Package CCP-PKG01 (suitable for samples that do not contain high concentrations of precious metals) and F-IC881 (KOH fusion and ion chromatography of F) were selected for major and trace elements.

Results

Whole rock compositions of samples from Pyrochlore Dome are reported in Table 6.1 and from Corundum Dome in Table 6.2. All sample compositions are plotted on various bivariate diagrams and multi element diagrams to observe trends within and between sample suites. Silica versus major element oxide bivariate diagrams are shown in Figure 6.1. Select major element oxide bivariate diagrams are shown in Figure 6.2. Select incompatible trace element bivariate diagrams are shown in Figure 6.3. To understand how incompatible elements fractionate in the sample suites, samples are plotted on the chondrite normalized rare earth element diagram and primitive mantle normalized incompatible element diagrams in Figure 6.4. Samples are plotted on the shand index [molar $Al_2O_3/(CaO+Na_2O+K_2O)$ versus molar $Al_2O_3/(Na_2O+K_2O)$] diagram after Shand (1927) in Figure 6.5 to assign alkalinity to each sample suite. Igneous samples are

plotted on the total alkalis versus silica (SiO_2 versus K_2O+Na_2O) diagram after Middlemost (1994) in Figure 6.6 to compare the chemical classification to petrographic observations. Igneous samples are plotted on the Yb versus Ta tectonic discrimination diagram after Pearce et al. (1984) in Figure 6.7 to interpret the tectonic origin of the samples.

Table 6.1. Bulk rock compositions of samples of nepheline syenite, altered arfvedsonite-aegirine syenite, and quartzite from Pyrochlore Dome.

Unit	nepheline syenite			altered arfvedsonite-aegirine syenite					quartzite
Sample	**20TN53**	**20TN55B**	**20TN57A**	**20TN12A**	**20TN13B**	**20TN16A**	**20TN17A**	**20TN18**	**20TN17C**
SiO_2 (wt. %)	55.60	60.70	55.50	64.60	67.60	67.30	64.80	65.10	99.20
Al_2O_3	20.50	18.70	21.80	15.65	16.50	13.70	12.20	10.25	0.99
Fe_2O_3	5.67	2.24	4.35	5.34	2.69	9.70	12.45	15.25	0.76
CaO	0.27	1.30	0.22	0.11	0.18	0.32	0.06	0.45	0.07
MgO	2.97	1.29	3.29	0.17	0.36	0.29	0.32	0.13	0.06
Na_2O	2.78	2.52	3.30	7.26	7.20	6.65	5.24	6.21	0.41
K_2O	8.98	10.90	8.06	4.43	5.56	2.83	3.45	0.26	0.20
Cr_2O_3	0.00	0.00	<0.002	<0.002	<0.002	0.00	0.00	0.00	0.01
TiO_2	0.61	0.67	0.57	0.19	0.06	0.24	0.45	0.38	0.06
MnO	0.17	0.18	0.10	0.13	0.08	0.11	0.14	0.35	0.02
P_2O_5	0.09	0.02	0.08	0.06	0.04	<0.01	0.01	0.01	<0.01
SrO	0.05	0.01	0.07	<0.01	<0.01	0.01	<0.01	0.01	0.01
BaO	0.02	0.03	0.07	0.01	<0.01	0.01	0.01	<0.01	<0.01
LOI	2.91	2.46	2.92	0.44	0.46	0.65	0.70	0.67	0.20
Total	100.62	101.02	100.33	98.39	100.73	101.81	99.83	99.07	101.99
C	0.06	0.28	0.03	0.05	0.04	0.04	0.07	0.04	0.03
S	0.01	0.01	0.01	0.01	0.01	0.02	0.01	0.01	<0.01
Ba (ppm)	226	286	517	127.5	28.6	61.2	80.5	30.4	29.4
Ce	413	297	290	436	98.6	54.6	200	181.5	39.8
Cr	<10	<10	<10	10	<10	10	10	10	30
Cs	5.95	1.38	2.65	1.02	4.3	1.51	1.17	0.21	0.25
Dy	8.34	7.71	8.94	6.25	2.09	1.96	3.13	6.44	0.71
Er	4.77	5.02	5.79	3.84	0.86	1.16	2.11	3.86	0.66
Eu	3.54	2.69	2.65	1.71	0.65	0.43	0.86	1.41	0.22
Ga	37	33.7	29.9	65.1	64	57.9	55.1	49.6	3.1
Gd	9.42	7.93	8.39	6.22	2.34	1.66	2.88	4.81	0.68
Ge	<5	<5	<5	<5	<5	<5	<5	<5	<5
Hf	17.8	36.6	10.8	39.3	5.3	34.8	17.4	29	6.4
Ho	1.69	1.74	1.97	1.31	0.35	0.39	0.68	1.39	0.17
La	269	187.5	160.5	320	71.1	38.2	138	103	21
Lu	0.74	0.79	0.8	0.59	0.1	0.23	0.39	0.46	0.16
Nb	471	659	302	783	236	199.5	430	242	52.2
Nd	114.5	72.8	81	84.7	24.9	11.6	33.9	39.7	8.6
Pr	40.1	25.7	27.3	32.9	8.81	4.38	14.15	13.8	2.87
Rb	286	261	198.5	333	358	167.5	168.5	11.8	8.8
Sm	15.15	10.5	11.65	9.95	3.35	1.77	4.15	6.26	1.21
Sn	7	10	5	21	9	47	10	55	2
Sr	379	82.1	384	19.6	35.7	30.5	19.4	42.4	5.6
Ta	23.4	22.2	14	12.8	3.7	5	13	2.2	1.6
Tb	1.53	1.31	1.51	1.03	0.38	0.3	0.51	1	0.12
Th	53.9	41.5	31.1	81.3	381	30.9	58.6	19.6	5.47
Tm	0.77	0.87	0.91	0.62	0.12	0.19	0.35	0.62	0.12
U	7.98	6.61	6.84	5.4	2.92	3.69	4.32	4.28	0.89
V	<5	7	<5	5	5	5	7	29	6
W	6	8	4	2	2	2	3	6	1
Y	51.8	54.2	54.3	43.9	12.2	14.1	20.4	46	5.5
Yb	4.83	5.79	5.69	3.91	0.61	1.32	2.66	3.42	0.94
Zr	1205	2050	768	2440	272	1715	1025	1385	344
As	3.7	3.8	1.7	5	1.3	3.1	9.9	3.5	1.5
Bi	0.2	0.13	0.08	0.61	0.19	0.5	0.61	0.36	0.11
Hg	<0.005	<0.005	<0.005	<0.005	<0.005	<0.005	0.006	<0.005	<0.005
In	0.033	0.033	0.029	0.005	0.007	0.008	0.022	0.027	<0.005
Re	<0.001	<0.001	<0.001	<0.001	<0.001	<0.001	<0.001	<0.001	<0.001
Sb	0.55	0.26	0.19	0.47	0.36	1.22	0.49	0.77	0.08
Se	0.3	<0.2	<0.2	<0.2	<0.2	<0.2	<0.2	<0.2	<0.2
Te	0.01	0.01	<0.01	0.01	<0.01	<0.01	<0.01	0.01	<0.01
Tl	0.2	0.03	0.14	0.04	0.13	0.05	0.04	0.03	<0.02
Ag	<0.5	<0.5	<0.5	<0.5	<0.5	<0.5	<0.5	<0.5	<0.5
Cd	<0.5	<0.5	<0.5	<0.5	<0.5	<0.5	<0.5	0.7	<0.5
Co	2	<1	1	7	2	1	7	1	<1
Cu	21	4	11	8	6	3	10	3	6
Li	190	40	230	40	60	90	80	30	10
Mo	1	3	1	6	1	30	41	15	4
Ni	<1	2	<1	4	5	<1	3	7	<1

Unit	nepheline syenite				altered arfvedsonite-aegirine syenite				quartzite
Sample	**20TN53**	**20TN55B**	**20TN57A**	**20TN12A**	**20TN13B**	**20TN16A**	**20TN17A**	**20TN18**	**20TN17C**
Pb (ppm)	13	11	8	14	28	31	41	40	3
Sc	<1	<1	<1	<1	<1	<1	1	1	<1
Zn	92	47	105	28	79	65	89	208	12
F	5310	1410	3940	700	880	2410	1160	3330	140

Table 6.2. Bulk rock compositions of samples of actinolite-altered syenite, fenites, and argillite from Corundum Dome.

Unit	actinolite-altered syenite					fenites					argillite	
Sample	**20TN2**	**20TN4D**	**20TN10A**	**20TN10B**	**20TN25F**	**20TN4A**	**20TN4B**	**20TN7**	**20TN25C**	**20TN25D**	**20TN5**	**20TN24A**
SiO_2 (wt. %)	55.80	53.40	61.20	57.90	50.40	57.70	58.90	52.50	52.10	53.80	51.80	53.30
Al_2O_3	13.20	14.65	14.80	13.25	14.10	12.85	13.20	11.35	13.50	12.30	13.15	14.45
Fe2O3	8.51	10.15	8.63	13.35	6.40	7.25	6.81	7.15	6.94	6.85	9.01	8.87
CaO	5.46	4.50	1.39	2.59	6.95	1.85	2.22	6.49	4.69	6.50	6.48	5.17
MgO	1.41	1.38	1.21	1.82	3.04	5.90	4.26	5.61	5.13	4.77	8.88	7.52
Na_2O	4.12	2.78	2.49	5.53	2.48	7.43	7.83	3.47	1.77	4.44	2.24	2.56
K_2O	5.14	6.48	9.94	3.60	5.61	2.84	2.12	6.79	7.52	3.20	4.27	5.01
Cr_2O_3	0.00	0.00	<0.002	<0.002	0.01	0.01	0.01	0.01	0.01	0.01	0.01	0.01
TiO_2	0.74	0.68	0.35	0.42	0.89	1.27	1.31	2.02	0.92	1.04	1.22	1.34
MnO	0.25	1.53	0.18	0.33	0.43	0.73	0.67	0.84	0.48	0.46	0.18	0.11
P_2O_5	0.16	0.27	0.04	0.06	0.15	0.24	0.28	0.80	0.21	0.15	0.17	0.17
SrO	0.03	0.05	0.01	0.04	0.01	0.04	0.04	0.05	0.01	0.01	0.02	0.02
BaO	0.05	0.06	0.05	0.02	0.01	0.03	0.02	0.12	0.03	0.01	0.07	0.07
LOI	2.47	1.19	0.75	0.73	7.92	1.85	1.44	2.79	5.48	6.45	2.65	1.62
Total	97.34	97.12	101.04	99.64	98.40	99.99	99.11	99.99	98.79	99.99	100.15	100.22
C	0.49	0.06	0.06	0.02	1.5	0.05	0.04	0.03	0.93	1.2	0.2	0.03
S	0.01	0.02	0.02	0.01	0.01	0.01	0.02	<0.01	0.01	0.02	0.01	0.02
Ba (ppm)	509	510	462	192	107.5	235	174.5	1075	261	108	678	653
Ce	1765	1915	399	1055	2060	275	925	465	1130	344	81.4	83.2
Cr	10	<10	10	<10	50	40	30	40	50	60	80	90
Cs	1.82	2.82	2.73	0.39	0.39	6.21	4.02	2.17	11.55	23.1	8.01	7.42
Dy	45.6	32.5	7.84	9.01	43.3	4.94	10.15	9.43	32.5	5.69	6.13	6.54
Er	32	21.6	4.77	6.21	24.8	3.15	5.7	5.31	15.8	3.24	3.79	4.02
Eu	10.3	7.58	2.02	3.11	10.7	1.66	3.26	2.5	8.35	1.47	1.54	1.65
Ga	68.2	76.4	55.5	69.4	73.2	64.1	71.1	50.6	70.4	69	21.8	23.5
Gd	38	29.1	7.51	9.89	42.7	5	10.55	10.1	33.9	6.28	6.51	6.79
Ge	<5	<5	<5	<5	<5	<5	<5	<5	<5	<5	<5	<5
Hf	216	221	65.2	127	96.8	65.8	78.6	28.6	59.4	27.7	6.8	7.1
Ho	10.3	6.92	1.64	1.94	8.94	1.04	1.96	1.97	6.17	1.14	1.28	1.42
La	1260	1680	308	677	1410	181.5	746	509	720	255	40.6	40.9
Lu	4.86	3.25	0.83	1.31	3.06	0.51	0.81	0.8	1.58	0.44	0.55	0.6
Nb	>2500	>2500	2080	>2500	903	1015	1530	>2500	1425	532	34.7	26.2
Nd	375	352	82	205	483	46.4	138.5	78.8	252	62.8	35.1	37.6
Pr	145	142	31.8	80.5	178.5	18.65	62	32.4	95	25.9	9.4	10.05
Rb	252	367	640	65.5	95.4	176.5	102	164.5	523	412	140	164.5
Sm	51.4	44.5	10.95	20.9	61.5	6.11	15.95	11.65	42.1	8.03	7.66	7.95
Sn	74	74	57	65	29	24	37	24	34	25	3	3
Sr	283	483	146	376	73.8	302	367	515	88.1	100	145.5	164.5
Ta	62.5	79.3	72	106	35	9.7	12.4	6.5	15.1	2.9	1.6	1.5
Tb	7.09	5.16	1.31	1.51	7.36	0.85	1.78	1.66	5.88	1.03	1.07	1.12
Th	252	713	98.5	178.5	298	82.8	718	>1000	309	142	13.55	12.65
Tm	5.3	3.55	0.8	1.13	3.77	0.5	0.86	0.8	2.2	0.45	0.56	0.61
U	11.9	40.6	47.5	61.9	17.3	7.39	13.1	12	24.9	5.69	2.5	2.69
V	27	44	17	24	128	87	84	176	108	132	203	242
W	48	49	11	16	18	7	17	17	23	20	2	2
Y	340	230	54.5	75.7	315	46.1	90.4	97.1	289	44.2	36.6	38.6

Unit	actinolite-altered syenite					fenites					argillite	
Sample	**20TN2**	**20TN4D**	**20TN10A**	**20TN10B**	**20TN25F**	**20TN4A**	**20TN4B**	**20TN7**	**20TN25C**	**20TN25D**	**20TN5**	**20TN24A**
Yb (ppm)	33.9	22.9	5.06	8.13	23	3.58	5.76	5.27	11.95	2.7	3.57	3.92
Zr	>10000	>10000	3410	7930	7660	4650	5770	3300	5150	2070	287	284
As	12.5	11.6	1.9	4	6.8	8.3	15.9	11.1	4.1	9.5	17.4	3.7
Bi	0.35	0.91	0.64	0.83	1.03	0.17	0.3	0.14	0.21	0.39	0.17	0.07
Hg	<0.005	0.013	<0.005	0.008	0.007	<0.005	0.007	<0.005	0.008	<0.005	<0.005	<0.005
In	<0.005	0.014	<0.005	<0.005	0.04	0.005	0.014	0.021	0.064	0.037	0.019	0.012
Re	0.001	<0.001	<0.001	<0.001	0.001	<0.001	<0.001	<0.001	0.001	<0.001	<0.001	<0.001
Sb	6.55	1.84	0.94	0.97	1.32	0.83	1.77	1.73	2.69	1.66	0.45	0.87
Se	0.4	0.2	<0.2	<0.2	<0.2	0.2	0.2	0.3	0.2	0.3	0.2	0.2
Te	0.1	0.15	0.06	0.04	0.14	0.07	0.1	0.06	0.1	0.09	0.15	0.06
Tl	0.04	0.08	0.09	0.04	0.03	0.45	0.25	0.16	1.07	1.18	0.51	0.44
Ag	0.5	4.6	<0.5	<0.5	1.7	2	4.3	5.1	1.9	0.8	<0.5	<0.5
Cd	0.7	1.3	<0.5	1.2	0.6	<0.5	0.7	1.4	0.6	0.5	0.5	<0.5
Co	<1	<1	9	16	3	11	5	<1	4	15	21	22
Cu	<1	5	13	15	10	<1	<1	11	1	50	95	32
Li	10	30	10	10	40	500	370	300	560	520	70	70
Mo	4	15	1	<1	28	6	5	3	8	28	<1	<1
Ni	5	<1	3	11	23	23	7	3	15	30	38	40
Pb	146	103	279	516	25	23	41	129	33	18	10	5
Sc	1	1	1	2	4	9	8	18	7	10	20	24
Zn	234	206	168	678	88	434	338	689	312	161	118	94
F	3140	1250	580	780	1560	10650	8220	>20000	8900	14850	1340	1710

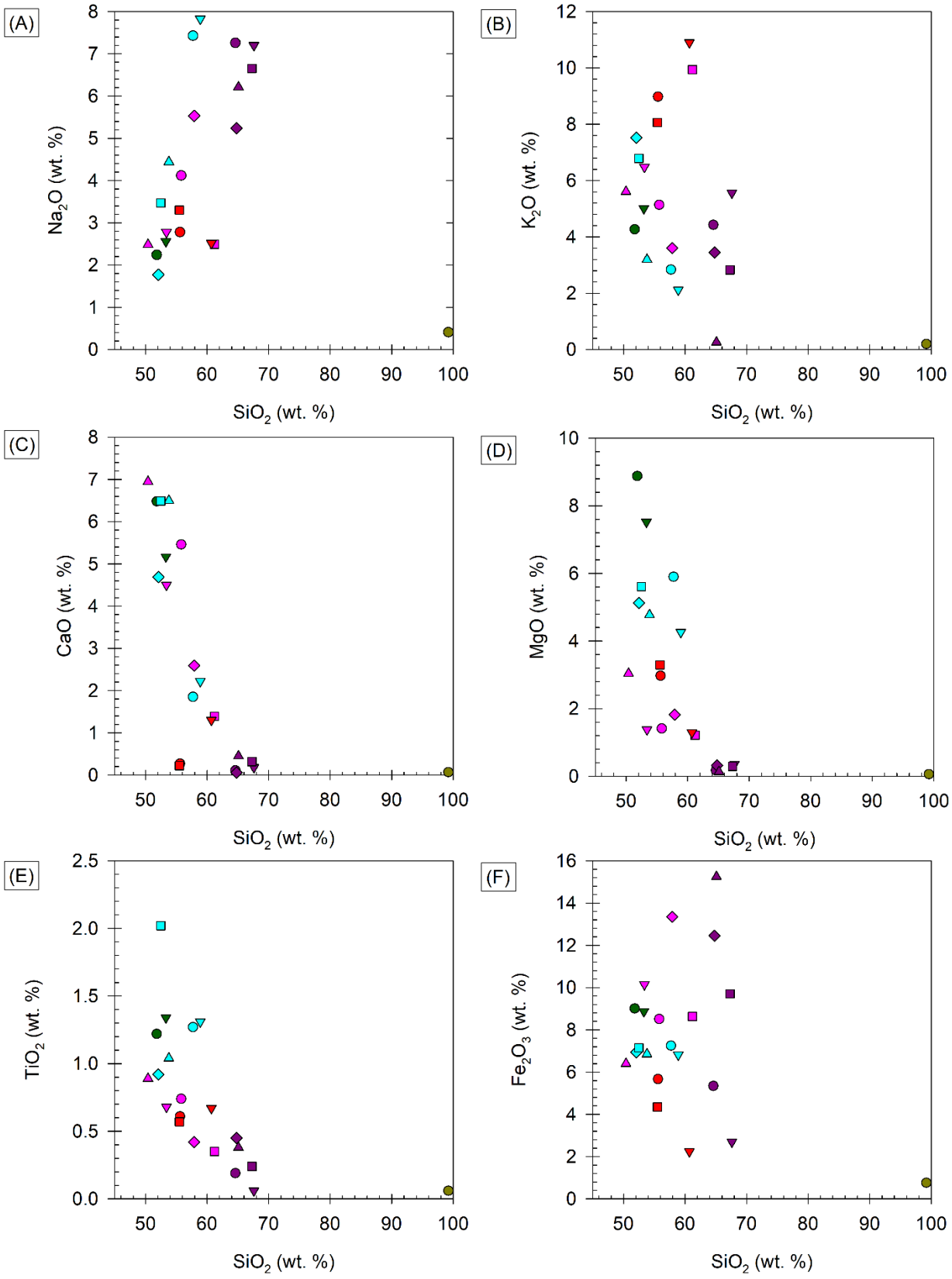
(A)
Na2O (wt. %)
SiO2 (wt. %)
(B)
K2O (wt. %)
SiO2 (wt. %)
(C)
CaO (wt. %)
SiO2 (wt. %)
(D)
MgO (wt. %)
SiO2 (wt. %)
(E)
TiO2 (wt. %)
SiO2 (wt. %)
(F)
Fe2O3 (wt. %)
SiO2 (wt. %)

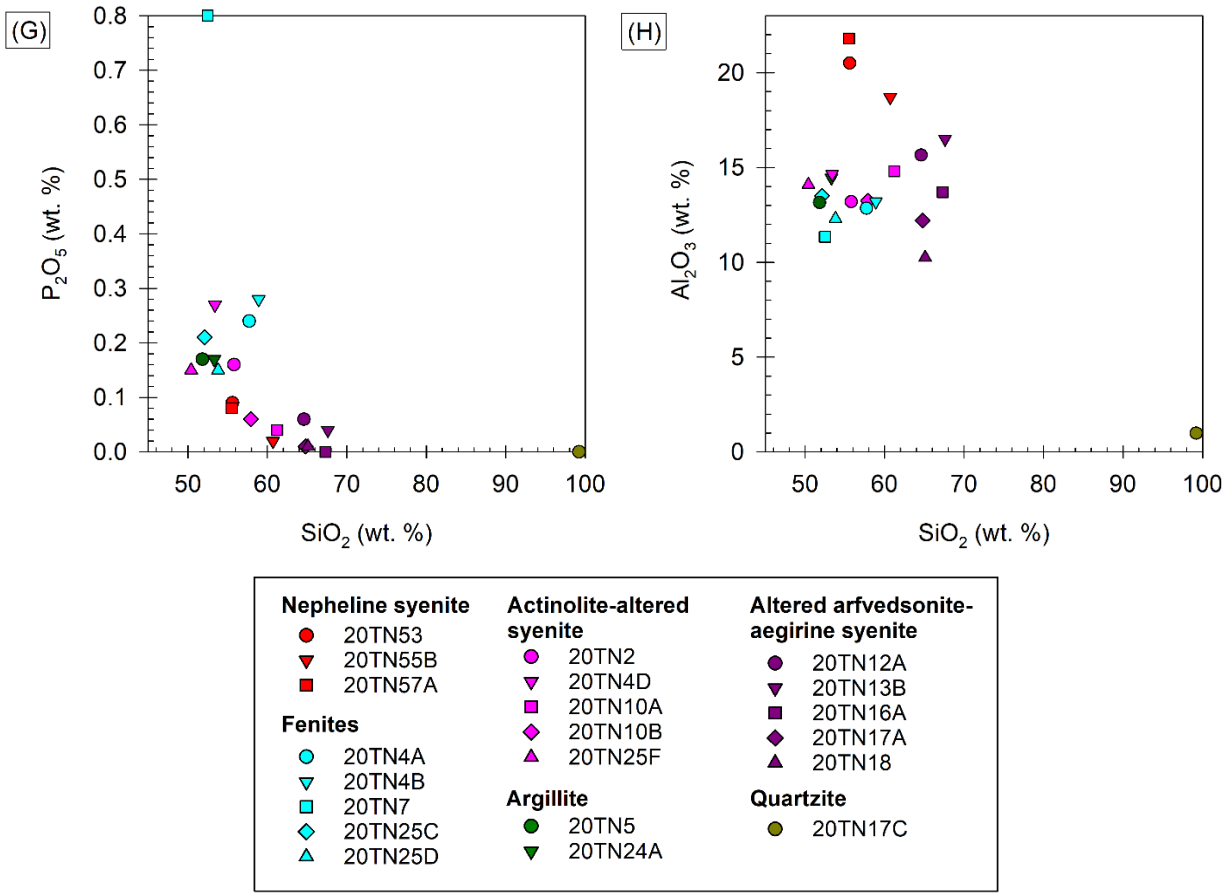

Figure 6.1. Bivariate diagrams of SiO_2 versus select major element oxides displaying samples of nepheline syenite, altered arfvedsonite-aegirine syenite, actinolite-altered syenite, fenites, argillite, and quartzite. (A) SiO_2 versus Na_2O. (B) SiO_2 versus K_2O. (C) SiO_2 versus CaO. (D) SiO_2 versus MgO. (E) SiO_2 versus TiO_2. (F) SiO_2 versus Fe_2O_3. (G) SiO_2 versus P_2O_5. (H) SiO_2 versus Al_2O_3.

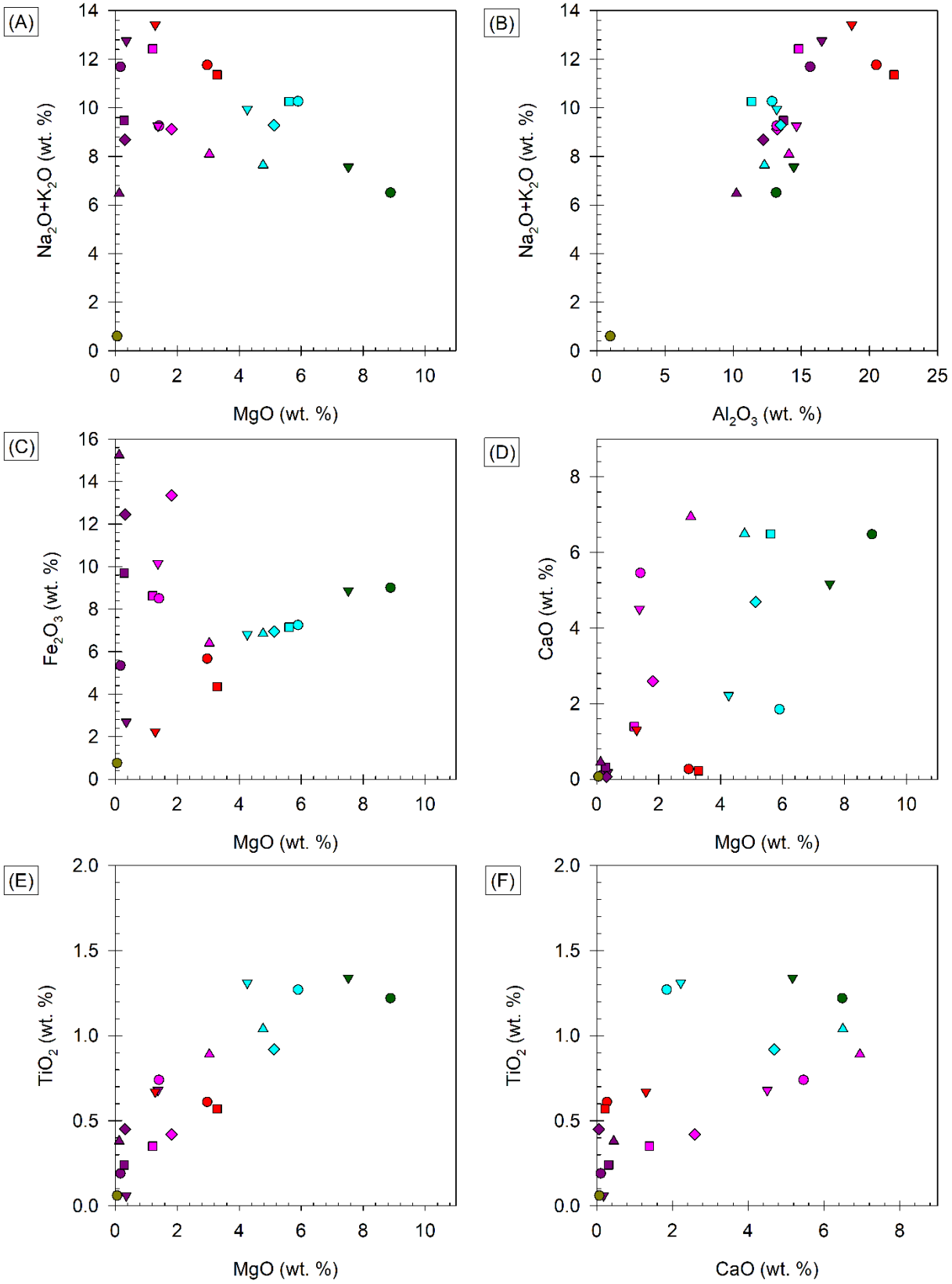
(A)
Na_2O+K_2O (wt. %)
MgO (wt. %)
(B)
Na_2O+K_2O (wt. %)
Al_2O_3 (wt. %)
(C)
Fe_2O_3 (wt. %)
MgO (wt. %)
(D)
CaO (wt. %)
MgO (wt. %)
(E)
TiO_2 (wt. %)
MgO (wt. %)
(F)
TiO_2 (wt. %)
CaO (wt. %)

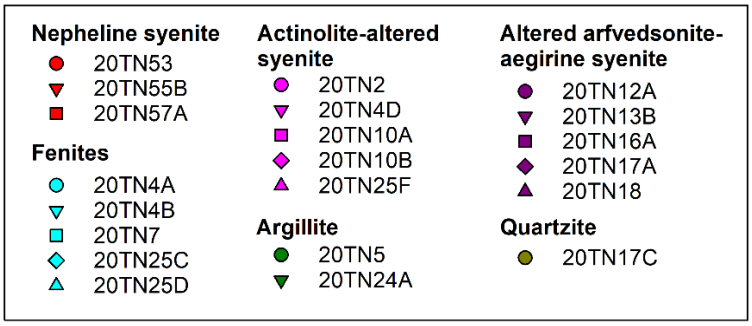

Figure 6.2. Bivariate diagrams of select major element oxides displaying samples of nepheline syenite, altered arfvedsonite-aegirine syenite, actinolite-altered syenite, fenites, argillite, and quartzite. (A) MgO versus Na_2O+K_2O. (B) Al_2O_3 versus Na_2O+K_2O. (C) MgO versus Fe_2O_3. (D) MgO versus CaO. (E) MgO versus TiO_2. (F) CaO versus TiO_2.

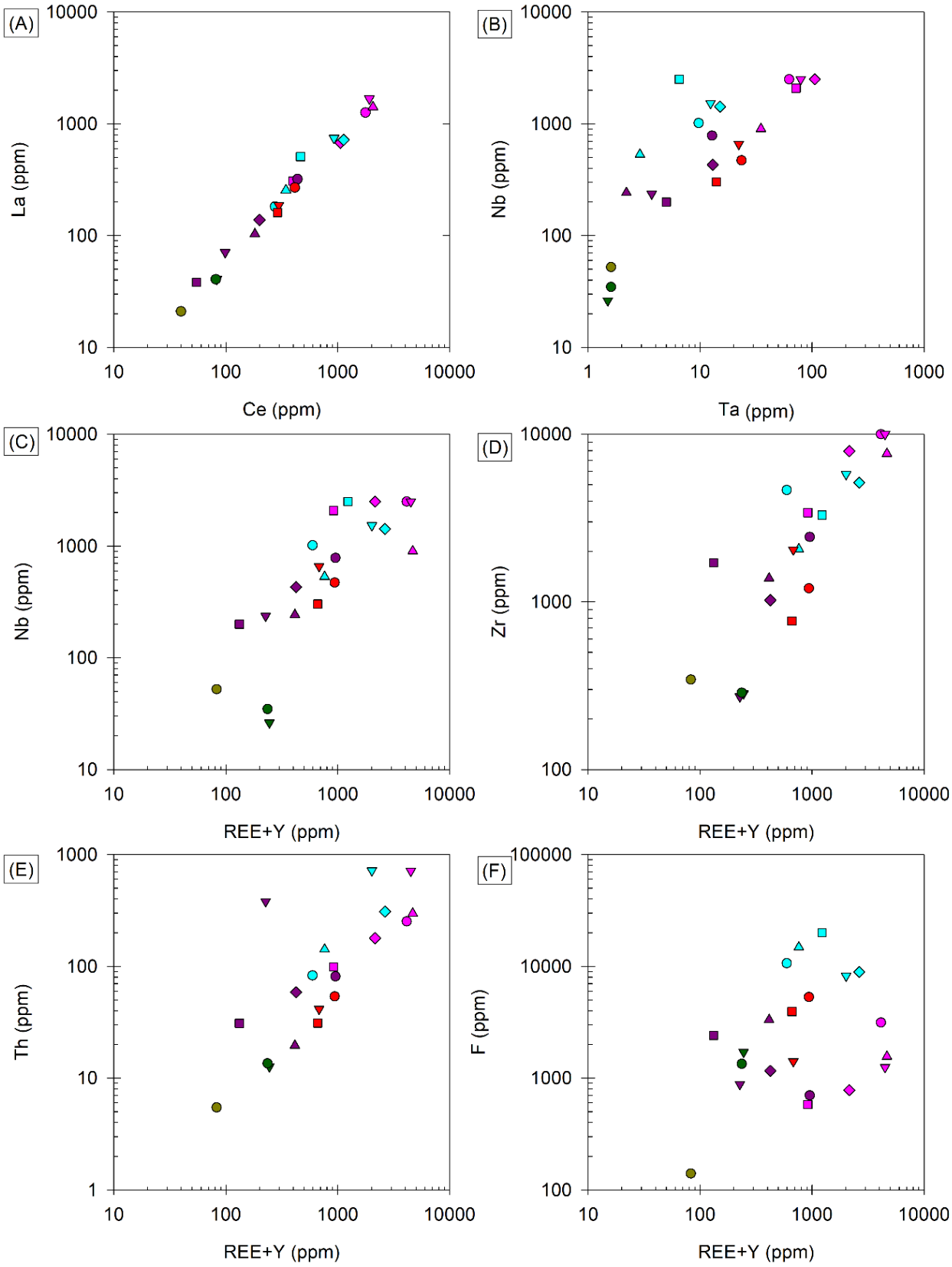
(A)
La (ppm)
Ce (ppm)
10000
1000
100
10
10
100
1000
10000
(B)
Nb (ppm)
Ta (ppm)
10000
1000
100
10
1
10
100
1000
(C)
Nb (ppm)
REE+Y (ppm)
10000
1000
100
10
10
100
1000
10000
(D)
Zr (ppm)
REE+Y (ppm)
10000
1000
100
10
100
1000
10000
(E)
Th (ppm)
REE+Y (ppm)
1000
100
10
1
10
100
1000
10000
(F)
F (ppm)
REE+Y (ppm)
100000
10000
1000
100
10
100
1000
10000

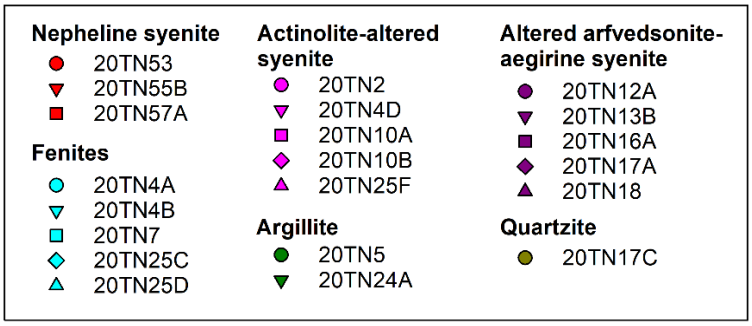

Figure 6.3. Bivariate diagrams of select trace elements displaying samples of nepheline syenite, altered arfvedsonite-aegirine syenite, actinolite-altered syenite, fenites, argillite, and quartzite. (A) Ce versus La. (B) Ta versus Nb. (C) REE+Y versus Nb. (D) REE+Y versus Zr. (E) REE+Y versus Th. (F) REE+Y versus F. Note, F values of sample 20TN7, Nb values of samples 20TN2, 20TN4D, 20TN7, 20TN10B, and Zr values of samples 20TN2 and 20TN4D are above the limit of detection and have been capped at their respective upper detection limits, >20,000 ppm, >2,500 ppm, and >10,000 ppm, respectively.

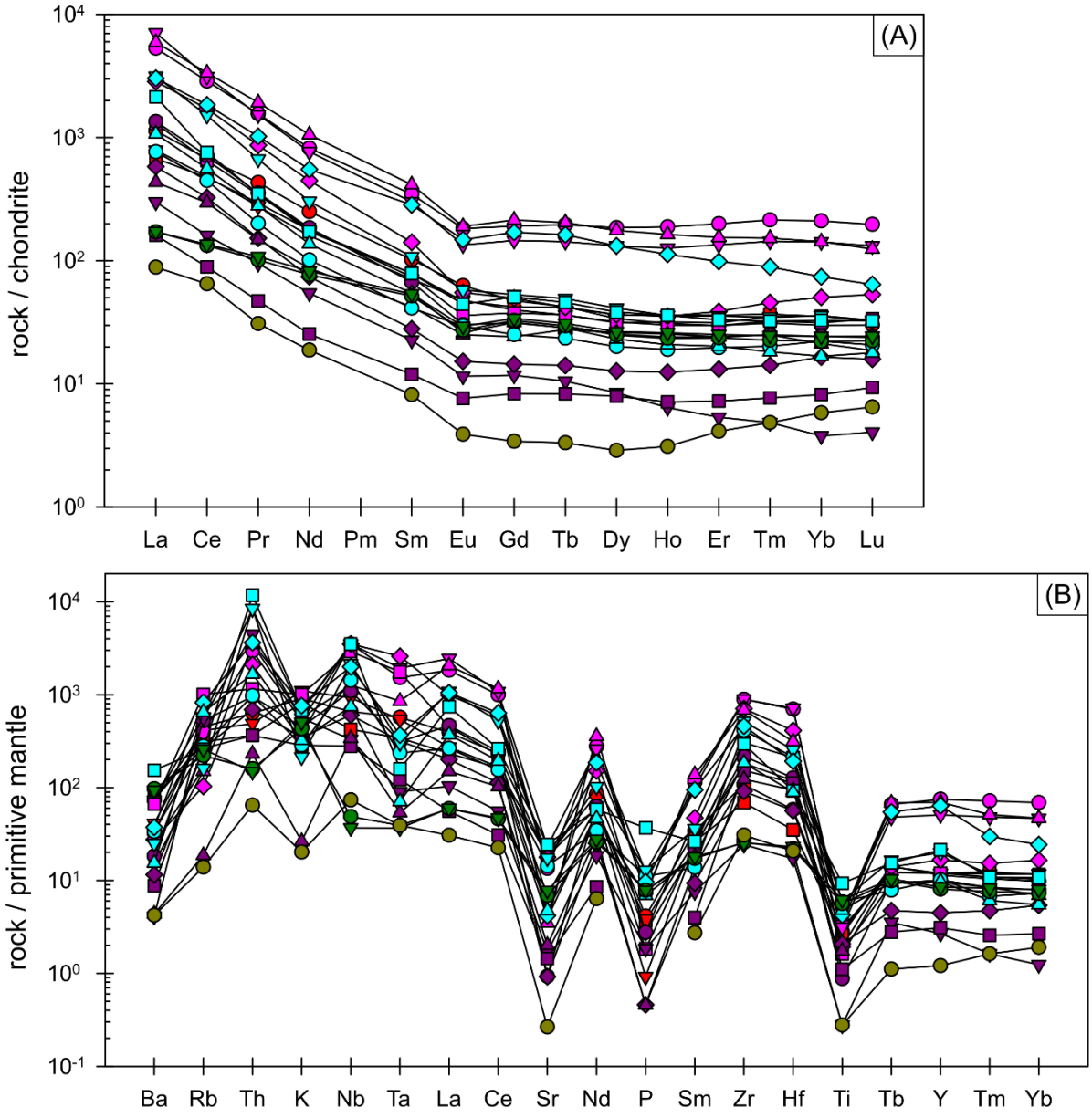

Nepheline syenite
- 20TN53
- 20TN55B
- 20TN57A

Fenites
- 20TN4A
- 20TN4B
- 20TN7
- 20TN25C
- 20TN25D

Actinolite-altered syenite
- 20TN2
- 20TN4D
- 20TN10A
- 20TN10B
- 20TN25F

Argillite
- 20TN5
- 20TN24A

Altered arfvedsonite-aegirine syenite
- 20TN12A
- 20TN13B
- 20TN16A
- 20TN17A
- 20TN18

Quartzite
- 20TN17C

Figure 6.4. Multi-element diagrams for select elements of whole rock compositions of nepheline syenite, altered arfvedsonite-aegirine syenite, actinolite-altered syenite, fenites, argillite, and quartzite. (A) Chondrite-normalized rare earth element diagram. Chondrite normalization values are from McDonough & Sun (1995). (B) Primitive mantle-normalized incompatible element diagram. Primitive mantle normalization values are from Sun & McDonough (1989). Note, Nb vales of samples 20TN2, 20TN4D, 20TN7, 20TN10B, Zr values of samples 20TN2 and 20TN4D, and Th value of sample 20TN7 are above the limit of detection and have been capped at their respective upper detection limits, >2,500 ppm, >10,000 ppm, and >1,000 ppm, respectively. P values of 20TN16A and 20TN17C are below the limit of detection and are not displayed on the respective diagram.

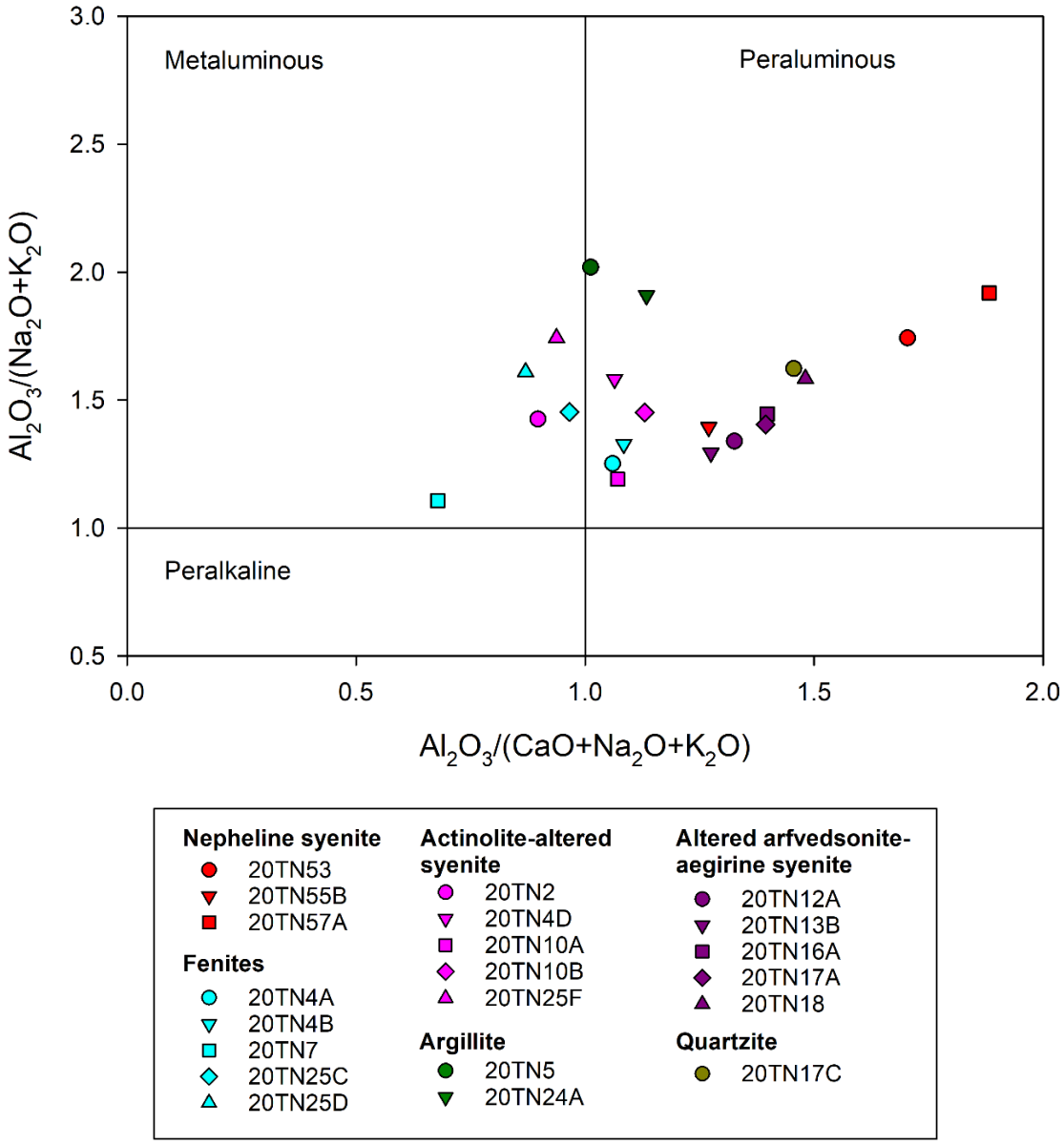

Figure 6.5. Shand index diagram after Shand (1927) displaying samples of nepheline syenite, altered arfvedsonite-aegirine syenite, actinolite-altered syenite, fenites, argillite, and quartzite.

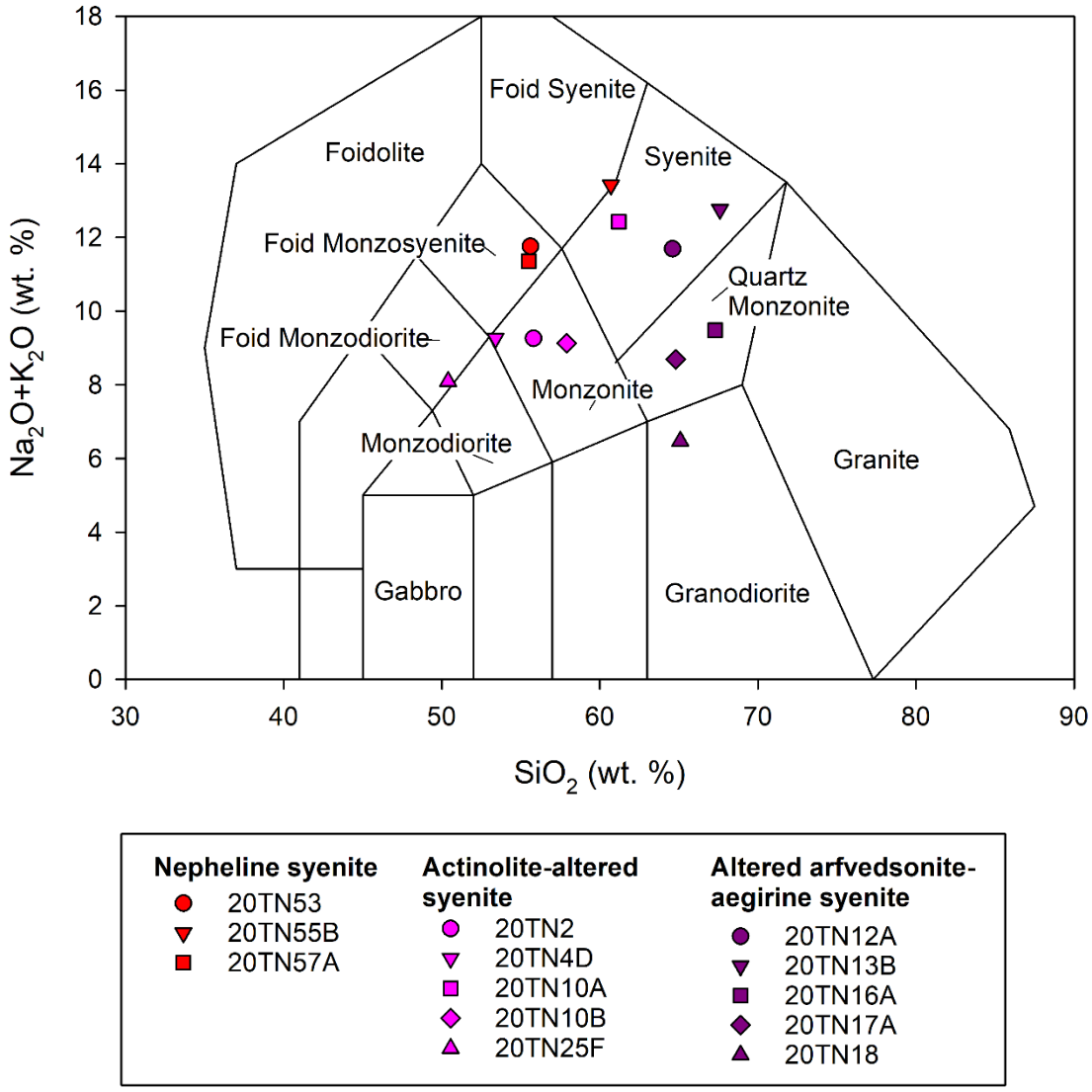

Figure 6.6. Total alkalis versus silica chemical classification diagram for plutonic rocks after Middlemost (1994) displaying samples of nepheline syenite, actinolite-altered syenite, and altered arfvedsonite-aegirine syenite.

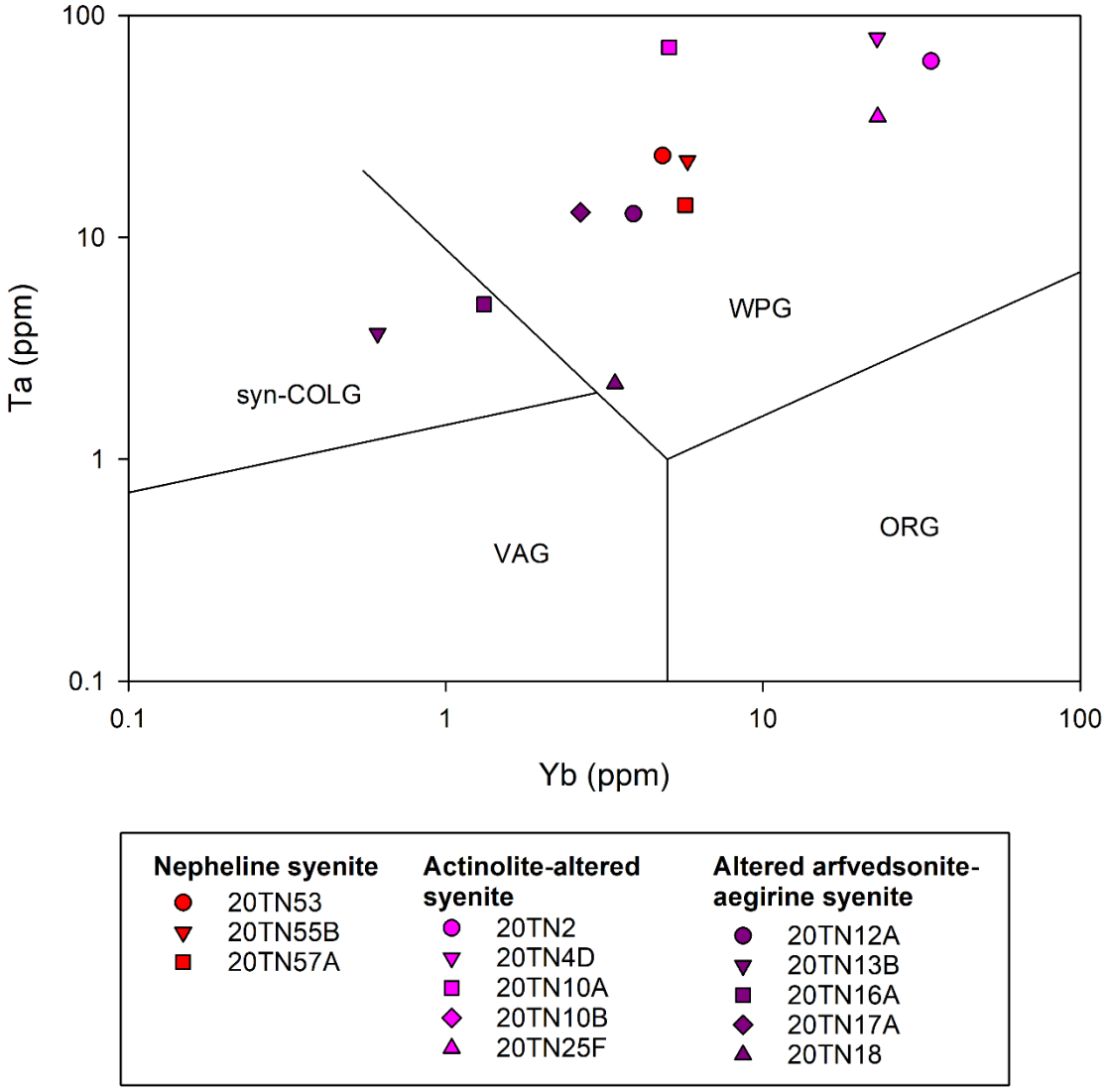

Figure 6.7. Yb versus Ta tectonic discrimination diagram for granites after Pearce et al. (1984) displaying samples of nepheline syenite, actinolite-altered syenite, and altered arfvedsonite-aegirine syenite.

General compositional trends

In general, major element oxides (Figure 6.1 and 6.2) and trace elements (Figure 6.3 and 6.4) show significant variation within and across the sample suites. Across all suites, the K_2O content is highest in the nepheline syenite > altered syenite, fenites, argillite > altered arfvedsonite-aegirine syenite > quartzite. Na_2O is highest in the altered arfvedsonite-aegirine syenite > altered syenite > nepheline syenite> quartzite. The MgO, CaO, and TiO_2 contents are highest in the argillite > fenites > actinolite-altered syenite > nepheline syenite > altered arfvedsonite-aegirine syenite > quartzite. The SiO_2 content is highest in the quartzite > altered arfvedsonite-aegirine syenite > nepheline syenite > altered syenite > argillite. In general, REE+Y, Zr, Nb, Ta, and Th contents are highest in the actinolite-altered syenite > fenite > nepheline syenite > argillite > quartzite.

The variation within and across the analyzed units reflects the varying degree of alteration within the altered units from petrographic observations (see Chapter 3). For example, elevated Na_2O content in the suites reflects increased sodic phases, such as albite, arfvedsonite, and aegirine. Potassic compositions such as potassium feldspar and phlogopite are indicated by elevated K_2O content. Elevated CaO content reflects increases calcic phases, such as actinolite, epidote, allanite, calcite, and fluorite. Titanite and rutile are associated with elevated TiO_2 content. Elevated P_2O_5 content indicates apatite. Zircon is indicated by elevated Zr content. Elevated Nb is indicative of pyrochlore and columbite. Elevated REE+Y is indicative of allanite and bastnäsite.

The compositional results in this thesis agree with those reported in previous rock and soil compositions collected by government surveys and industry reports. Whole rock geochemistry of Pool Creek nepheline syenite and associated dikes were reported by Pigage & Mortensen (2004). The nepheline syenite compositions in this thesis match those reported by Pigage & Mortensen (2004). Whole rock geochemistry and soil compositions have been reported by Swanton (2012). The results from this thesis agree with the soil sampling results from Swanton (2012), where HFSE and REE+Y content is higher within units on Corundum Dome (i.e., the South Fenite Zone) than units on Pyrochlore Dome (i.e., the North Fenite Zone).

Composition of the Pyrochlore Dome units

The nepheline syenite, altered arfvedsonite-aegirine syenite, and quartzite sample suites from Pyrochlore Dome (i.e., the North Fenite Zone) are discussed in this section.

Nepheline syenite

The nepheline syenite samples are characterized by high K_2O (8.06 to 10.9 wt. %) and Al_2O_3 (18.7 to 21. 8 wt. %) content and low Na_2O (2.52 to 3.3 wt. %) content. The high K_2O and Al_2O_3 composition in the nepheline syenite reflects the prevalence of orthoclase, nepheline (pseudomorphed after sericite), and phlogopite that replaces a former mafic phase observed in the samples (Chapter 3). The low Na_2O content reflects the lack of sodic phases (i.e., albite) and the minor presence of albite observed in comparison to the other syenite suites.

The nepheline syenite samples have Zr (up to 2050 ppm), Ta (up to 23.4 ppm), Nb (up to 659 ppm), and REE+Y (up to 939.18 ppm). Based on petrographic observations (Chapter 3) and measured mineral compositions (Chapter 4), Zr is in zircon, Ta and Nb are in pyrochlore, and REE in bastnäsite. With respect to the chondrite normalized rare earth element (REE) diagram (Figure 6.4), the light REE (LREE; La to Ho) are enriched in comparison to the middle REE (MREE; Sm to Tb) and heavy REE (HREE; Er to Lu), and MREE and HREE form a flat pattern. On the primitive mantle normalized diagram, the nepheline syenite samples show negative anomalies in Ba, Sr, P, and Ti

On the Shand index diagram (Figure 6.5), the nepheline syenite plots in the peraluminous field that trend towards the peralkaline field. On the total alkalis versus silica diagram (Figure 6.6), the nepheline syenite samples plot in the foid syenite and foid monzosyenite fields, agreeing with the observed modal mineralogy. The sample that plots in the foid syenite field (20TN55B) is the least altered and best represents the primary composition of the suite. The samples that plot in the monzosyenite fields have more albite present. On the tectonic discrimination diagram, the nepheline syenite plots in the within plate granites field (Figure 6.7).

Altered arfvedsonite-aegirine syenite

The altered arfvedsonite-aegirine syenite samples are characterized by high SiO_2 (64.6 to 67.6 wt. %) and Na_2O (5.24 to 7.26 wt. %) content, low to moderate K_2O content (0.26 to 5.56 wt. %), and a large spread in Fe_2O_3 (2.69 to 15.25 wt. %) and Al_2O_3 (10.25 to 16.5 wt. %) content. The sum of Na_2O+K_2O show a positive correlation with Al_2O_3 and a negative correlation with Fe_2O_3. Based on petrographic observations, elevated SiO_2 content reflect the abundance of quartz veining and quartz replacement of phases in the suite. The samples with high Na_2O+K_2O and Al_2O_3 and low Fe_2O_3 have arfvedsonite and aegirine that have not been completely replaced by hematite. In contrast, the samples with low Na_2O+K_2O and Al_2O_3 and high Fe_2O_3 have aegirine and arfvedsonite completely replaced by hematite. Therefore, the negative correlation between Na_2O+K_2O, Al_2O_3, and Fe_2O_3 in the sample suite reflects the degree of replacement of aegirine and arfvedsonite by hematite.

With respect to minor elements, the altered arfvedsonite-aegirine syenite samples have 272 to 2440 ppm Zr, 2.2 to 13 ppm Ta, 199.5 to 783 ppm Nb, and 132.29 to 952.93 ppm REE+Y. Based on petrographic observations (Chapter 3) and measured mineral compositions (Chapter 4), the Zr is in zircon, Ta and Nb are in pyrochlore and REE in epidote, allanite, and apatite. With respect to the chondrite normalized REE diagram (Figure 6.4), the LREE are enriched in comparison to the MREE and HREE. In most of the samples, the MREE and HREE form a flat pattern. In one sample, HREE are mildly depleted with respect to MREE. On the primitive mantle normalized diagram, the altered arfvedsonite-aegirine syenite samples show negative anomalies in Ba, Sr, P, and Ti. One sample has a large negative K and Rb anomaly.

On the Shand index diagram, the altered arfvedsonite-aegirine syenite samples plot plots in the peraluminous field that trend towards the peralkaline field (Figure 6.5). On the total alkalis versus silica diagram (Figure 6.6), the altered arfvedsonite-aegirine syenite samples plot in the syenite, quartz monzonite, and granodiorite fields. This composition does not accurately reflect the primary composition of the rock. Based on petrographic observations, the decrease in alkalis is due to increasing Fe_2O_3 content from hematite replacement of arfvedsonite and aegirine, and the increase in SiO_2 is due to quartz veining and replacement. A sample that plots in the syenite

field (20TN12) is the least altered of the suite and therefore more accurately represents the unaltered protolith composition. On the tectonic discrimination diagram, the altered arfvedsonite-aegirine syenite samples plot in the within plate granites and syn-collisional granites fields. The least of the altered samples plot well within the within plate granites field. The more altered samples plot in the syn-collisional granites field as they trend towards the compositions of the host rocks. Metasomatic alteration of fluids that have interacted between the syenite and the host rock is interpreted to have caused this trend.

Quartzite

The quartzite has simple composition of 99.2 wt. % SiO_2 and trace amounts of Al_2O_3, Na_2O_3, and Fe_2O_3. The chemistry represents the abundance of quartz and trace amounts of albite and hematite observed in the sample (see Chapter 3). The quartzite contains detectible amounts of Zr (trace zircon), Nb and Ta (trace pyrochlore), and REE+Y (trace monazite). The chondrite normalized REE pattern of the quartzite show that LREE are slightly elevated with respect to MREE and HREE which form a relatively flat pattern (Figure 6.4). The primitive mantle normalized multi element diagram of the quartzite shows a positive K anomaly, and a negative Sr and Ti anomaly. The quartzite is peraluminous based on the alkalinity index diagram (Figure 6.5).

Source of metasomatism on Pyrochlore Dome

The altered arfvedsonite-aegirine syenite is hosted in a clastic unit which contains abundant quartzite. Samples in the altered arfvedsonite-aegirine syenite suite show variable alteration mineralogy and textures, where metasomatic alteration is represented by albitization of former potassium feldspar, complete replacement of arfvedsonite and aegirine by hematite, and prevalent quartz veining (see Chapter 3). This metasomatic alteration in the sample suite is represented compositionally, where increasing alteration is represented by an increase in SiO_2, Na_2O, and Fe_2O_3 content and decrease in K_2O, Al_2O_3, HFSE (Zr, Ta, Nb), and REE+Y content (Figure 6.1 to 6.4). A correlation exists between the composition of the arfvedsonite-aegirine syenite sample suite and the quartzite with respect to major element oxides and trace elements, where the more altered samples (e.g., 20TN16A and 20TN17A) trend towards the composition

of the quartzite. Based on the correlation between the composition of the altered arfvedsonite-aegirine syenite suite and quartzite, the altered arfvedsonite-aegirine syenite is interpreted to be the source of the metasomatic fluid and was autometasomatized by the fluid that was buffered to a more silica-rich composition through fluid-rock interactions with the host quartzite. The quartz veins therefore likely represent the crystallization of the late stage, silica-saturated autometasomatic fluids.

As discussed by Anenburg et al. (2020), alkali elements are ligands to REE and HFSE in metasomatic fluids. The interaction between alkali-rich metasomatic fluids and a quartz-rich host can increase the silica content in the fluid through chemical buffering. The addition of silica to alkali-rich metasomatic fluids force crystallization of alkali silicate phases (such as pyroxenes and amphiboles) and REE and HFSE phases. Anenburg et al.'s (2020) study supports the petrographic and chemical observations between the rocks in the North Fenite Zone, where samples with preserved arfvedsonite and aegirine occur with pyrochlore, epidote, allanite, and apatite, and quartz veins in the samples commonly bear zoned zircons. This indicates that the original metasomatic fluid composition of the altered arfvedsonite-aegirine syenite was alkali-rich (i.e., Na and K) and silica-poor.

Chemical relationships also exist between the nepheline syenite and the altered arfvedsonite-aegirine syenite. Of the altered arfvedsonite-aegirine syenite samples, 20TN12 is the least altered based on petrographic observations (see Chapter 3). This less-altered sample has textures and geochemical compositions similar to the nepheline syenite samples. For example, combined alkali oxides (Na_2O+K_2O) (Figure 6.2), and HFSE and REE content show overlap between the nepheline syenite and altered arfvedsonite-aegirine syenite samples (Figure 6.3 and 6.4). Major element oxides and trace element compositions of the altered arfvedsonite-aegirine syenite overlap with the nepheline syenite and are transitional between the nepheline syenite and the quartzite. The similarities and transitional relationship between the altered arfvedsonite-aegirine syenite and nepheline syenite indicate that the protolith of the altered arfvedsonite-aegirine syenite is the nepheline syenite. If this is true, then the altered arfvedsonite-aegirine syenite would be an endofenite phase of the nepheline syenite. More investigation with respect to field relationships and petrographic textures needs to be conducted to confidently interpret this claim.

If the altered arfvedsonite-aegirine syenite is in fact endofenite of the nepheline syenite, then the source of the metasomatic fluids that metasomatized the altered arfvedsonite-aegirine syenite is the nepheline syenite.

Composition of the Corundum Dome units

The actinolite-altered syenite, fenites, and argillite sample suites from the South Fenite Zone are discussed in this section.

Actinolite-altered syenite

The actinolite-altered syenite suite shows a large spread between Na_2O (2.48 to wt. 5.53 %), K_2O (3.6 to 9.94 wt. %), CaO (1.39 to 6.95 wt. %), and Fe_2O_3 (6.4 to 13.35 wt. %) content (Figure 6.1 and 6.2). The samples show a moderate negative correlation between Na_2O and K_2O. A moderate negative correlation exists between CaO and Fe_2O_3. A weak positive correlation occurs between Na_2O and Fe_2O_3. A strong positive correlation occurs between CaO, TiO_2, and P_2O_5, all of which have a strong negative correlation with SiO_2. Based on petrographic observations, the correlation between Na_2O and K_2O reflects the alteration of potassium feldspar to albite. The replacement of actinolite by epidote, hematite, and ~phlogopite is represented by the correlation between CaO and Fe_2O_3. The correlation between Na_2O and Fe_2O_3 reflects albite and hematite alteration throughout the samples. The alteration of former phases by calcite, fluorite, apatite, titanite, and rutile is represented by correlation between CaO, TiO_2, and P_2O_5 and their correlation with SiO_2. The large spread reflects degree of sodic, calcic, and potassic alteration (by albite, actinolite, titanite, epidote, allanite, apatite, calcite, and hematite) within each sample suite based on petrographic observations.

With respect to minor elements, the actinolite-altered syenite samples have 3410 to >10000 ppm Zr, 35 to 106 ppm Ta, 903 to >2500 ppm Nb, and 918.03 to 4675.63 ppm REE+Y. These elements have strong positive correlations with each other within the sample suite (Figure 6.3). Based on petrographic observations (Chapter 3) and measured mineral compositions (Chapter 4), the Zr is in zircon, Ta and Nb are in pyrochlore, and REE in epidote, allanite, and apatite. With respect to the chondrite-normalized REE diagram (Figure 6.4), the LREE are enriched in comparison to the MREE and HREE. The samples show a relatively flat MREE and HREE pattern. Between some of the samples there is a shift in the entire REE pattern by 1/4 to 3/4 of a magnitude. The samples that are lower in total REE (i.e., 20TN10A and 20TN10B) are the finer-

grained actinolite-altered syenites with chaotic deformation textures and notably contain less epidote, allanite, and apatite than the other samples in this suite. The samples with higher REE (20TN2, 20TN4D, 20TN25F) have prevalent epidote, allanite, and apatite, and are notably coarser grained and are in contact with the fenites. On the primitive mantle normalized diagram, the actinolite-altered syenite samples show negative anomalies in Ba, Sr, P, and Ti.

On the shand index diagram (Figure 6.5), the actinolite-altered syenite samples plot in the peraluminous and metaluminous fields. On the total alkalis versus silica diagram (Figure 6.6), the actinolite-altered syenite samples plot in the syenite, monzonite, and foid monzodiorite fields. This range of compositions do not accurately reflect the primary composition of the rock. The least altered sample in this suite (20TN4D) plots in the syenite field and more accurately represents the original unaltered composition of the protolith. On the tectonic discrimination diagram (Figure 6.7), the actinolite-altered syenite plots in the within-plate granites field.

Fenites

The fenites (from the South Fenite Zone) show a large spread Na_2O (1.77 to 7.38 wt. %), K_2O (2.12 to 7.52 wt. %), and CaO (1.85 to 6.5 wt. %), and have consistent Fe_2O_3 (6.81 to 7.25 wt. %) (Figure 6.1). The spread in Na_2O and K_2O content reflects changes in albite and potassium feldspar, arfvedsonite, and phlogopite content. The spread in CaO is from variations in apatite, epidote, allanite, titanite, and carbonates. With respect to minor elements, the samples have 8220 to >20000 ppm F, 82.8 >1000 ppm Th, 2070 to 5770 ppm Zr, 2.9 to 15.1 ppm Ta, 532 to >2500 ppm Nb, and 594.99 to 2646.43 ppm REE+Y. Notably, the fenites have high Li contents that range from 300 to 560 ppm. These elements have strong positive correlations with each other within the sample suite (Figure 6.3). Based on petrographic observations (Chapter 3) and measured mineral compositions (Chapter 4), the F is in fluorite, bastnäsite, and phlogopite, Th in thorite, Zr is in zircon, Ta and Nb are in pyrochlore and columbite, and REE in epidote, allanite, and apatite.

With respect to the chondrite normalized REE diagram (Figure 6.4), the LREE are enriched in comparison to the MREE and HREE. The samples show a relatively flat MREE and HREE pattern. Between some of the samples there is a shift in the entire REE pattern by 1/4 to 1/2 of a

magnitude. On the primitive mantle normalized diagram, the samples show strong positive Th, Nb, Nd, and Zr anomalies, and strong negative K, Ta, Sr, P and Ti anomalies.

Argillite

The argillite composition is dominated by SiO_2 (51.8 to 53.3 wt. %), Al_2O_3 (13.15 to 14.45 wt. %), Fe_2O_3 (8.87 to 9.01 wt. %), MgO (5.17 to 8.88 wt. %), CaO (5.17 to 6.48 wt. %), K_2O (4.27 to 5.01 wt. %), and N_2O (2.24 to 2.56 wt. %) content. The argillite samples contain up to 287 ppm Zr, 34.7 ppm Nb, 1.6 ppm Ta, and 244.97 ppm REE+Y. The chondrite normalized REE pattern shows that LREE are slightly elevated with respect to MREE and HREE which form a relatively flat pattern (Figure 6.4). The primitive mantle normalized multi element diagram show positive K anomaly, and negative Th, Sr, P, and Ti anomalies. The argillite is peraluminous based on the Shand index diagram (Figure 6.5).

Source of metasomatism on Corundum Dome

The actinolite-altered syenite is hosted in an argillite unit. The actinolite-altered syenite is in contact with fenitized argillite that vary in texture, mineralogy, and composition (i.e., fenites; see Chapter 3). Samples in the actinolite-altered syenite suite also show variable alteration mineralogy and textures, where metasomatic alteration is represented by albitization of former potassium feldspar, chemical zoning in actinolite, partial to complete replacement of former prismatic phases by titanite, rutile, phlogopite, epidote-allanite, and hematite, an increase in abundance in apatite, epidote-allanite, calcite, and fluorite, and prevalent alkali feldspar and hematite replacement and veining (see Chapter 3). The metasomatic alteration textures and mineralogy observed in Chapter 3 in the actinolite-altered syenite and fenite sample suites are also represented in the whole rock compositions. Different degrees of alteration in the actinolite syenite suite is represented by strong to moderate variations in Na_2O, K_2O, SiO_2, Fe_2O_3, MgO, CaO, TiO_2, P_2O_5, F, HFSE (Zr, Ta, Nb, Th, U), and REE+Y content (Figure 6.1 to 6.4). For example, increased albite content is associated with an increase in Na_2O and decrease in K_2O content, and increased titanite and rutile content is associated with an increase in CaO and TiO_2 content. Different degrees of alteration in the suite of fenites is represented by strong to moderate variations in Na_2O, K_2O, CaO, SiO_2, MgO, TiO_2, P_2O_5, F, HFSE (Zr, Ta, Nb, Th, U), and

REE+Y content. For example, the layered arfvedsonite-albite fenite samples have elevated Na_2O content and the layered phlogopite-potassium feldspar and brecciated arfvedsonite-potassium feldspar fenites have elevated K_2O content.

Strong chemical correlations exist between the major and trace element compositions of the actinolite-altered syenite, fenites, and argillite sample suites (Figure 6.1 to 6.4). The suite of fenites has compositions intermediate between the argillite and the actinolite-altered syenite, and the composition of samples within the suites of the actinolite-altered syenite and the fenites trend towards the argillite. These trends indicate chemical exchange between units that would be explained by metasomatic fluid and rock interactions (e.g., Anenburg et al. 2020). Based on the correlation between the composition of the actinolite-altered syenite, fenites, and argillite, the actinolite-altered syenite is interpreted to be the source of the metasomatic fluid.

Since the argillite has chemically reactive mineralogy (see Chapter 3), the protolith of the fenites is interpreted to have been argillite that became buffered (i.e., fenitized) by metasomatic fluids. The metasomatic fluid that reacted with the argillite protolith is interpreted to have been rich in Na, K, F, Nb, Zr, Th, and REE+Y content because the fenites are elevated in these elements with respect to the argillite (Figure 6.3 and 6.4). The enriched content of these incompatible elements is reflected in minerals such as alkali feldspars, phlogopite, pyrochlore, bastnäsite, and fluorite (see Chapter 3). The fenites have lower Mg, Ca, Ti content than the argillite, indicating that these elements were exchanged between the rock and the metasomatic fluid. Within the altered actinolite suite, sample content are elevated in Mg, Ca, and Ti content. The compositional trend observed within the actinolite syenite suite is interpreted to be from autometasomatism with the metasomatic fluid that was buffered by fluid-rock interactions with the argillite to a more Mg-Ca-Ti rich composition.

Chemical relationships also exist between the nepheline syenite, actinolite-altered syenite, and the fenites. Compositions the actinolite-altered syenite and the fenites overlap with and are enriched with respect to the nepheline syenite. The similarities and transitional relationship between the actinolite-altered syenite and nepheline syenite indicate that the protolith of the actinolite-altered syenite is the nepheline syenite. If this is true, then the actinolite-altered syenite

would be an endofenite phase of the nepheline syenite. More investigation with respect to field relationships and petrographic textures needs to be conducted to confidently interpret this claim. If the actinolite-altered syenite is in fact endofenite of the nepheline syenite, then the source of the metasomatic fluids that metasomatized the actinolite-altered syenite is the nepheline syenite.

Nepheline syenite: Protolith of the altered syenite suites?

It is well documented in the literature that host rock compositions change the metasomatic fluid composition through buffering (e.g., Elliott et al. 2018). The chemical compositions of fenite are extremely variable between different complexes in the literature because metasomatic fluid and fenite protolith compositions can vary significantly (e.g., Elliott et al. 2018). In general, alkali metasomatism (i.e., fenitization) is considered to remove silica and adds alkalis, however, it depends on the composition of the fluid and host rock (e.g., Elliott et al. 2018, Anenburg et al. 2020). As reviewed by Elliott et al. (2018), if the protolith is poor in alkali content then an alkali-rich fluid would add alkalis through fluid-rock interactions (i.e., buffering), and if the protolith is already rich in alkalis then alkalis could be subtracted from the protolith through buffering. The same process is true for silica, where if the rock is initially silica poor, then silica would be added, and if the rock is silica rich then silica would be subtracted.

As discussed in the previous sections, the less altered samples from the nepheline syenite, altered arfvedsonite-aegirine syenite, and actinolite-altered syenite suites generally share similar major oxide content (e.g., Na_2O+K_2O and SiO_2) and show similar patterns on the normalized multi element compositional diagrams (Figure 6.1 to 6.4). The geochemical compositional overlap and similarity in rock and mineral textures (see Chapter 3) indicate that the nepheline syenite is the protolith of these two altered syenite suites. The actinolite-altered syenite and altered arfvedsonite-aegirine syenite are hosted in chemically different rock types (i.e., quartzite and argillite). Since the host rock types are compositionally different (i.e., SiO_2 rich in the North Fenite Zone and Fe_2O_3-MgO-CaO-SiO_2 rich in the South Fenite Zone), a metasomatic fluid buffering with the respective host would reflect the respective host rock composition (i.e., become more SiO2 rich in quartzite and more Mg-Ca-Ti rich in argillite). If the source intrusion is nearly adjacent to the host rock and buffered metasomatic fluid, the fluid could interact with

the source intrusion and buffer it to compositionally trend towards the composition of the fluid. This chemical exchange process between the source intrusions and host rocks is evidenced by the increased silica content in the altered arfvedsonite-aegirine syenite (e.g., late-stage quartz veining and replacement) and Mg-Ca-Ti content in the actinolite-altered syenite (e.g., actinolite, titanite, rutile, epidote, calcite, fluorite).

The argument could be made that the nepheline syenite is the protolith of the altered arfvedsonite-aegirine syenite and actinolite-altered syenite based on the petrographic observations and bulk rock compositions. However, since syenites commonly occur in alkali-silicate complexes, it is possible that the nepheline syenite, actinolite-altered syenite, and altered arfvedsonite-aegirine syenite could be completely different syenitic phases from the same parental melt. More field mapping, sampling, and petrographic studies are needed to confidently answer whether the actinolite-altered syenites are endofenite of the nepheline syenite or if these three syenitic phases are distinct phases.

Mineralization implications

Mineralization in alkaline-silicate systems is attributed to intrusion depth and host rock composition. An example of mineralization that occurs in alkaline-silicate intrusions are silicate roof zone deposits (Beard et al. 2023). In these deposits, an alkaline-silicate intrusion is surrounded by silica-rich host rocks, where the interaction of residual melts and fenitizing fluids between the roof (shallower/top area of the intrusion) and the host rocks may form fenites, lenses, sills, late-stage veins, and pegmatites enriched in Li, Be, U, Th, REE, Ti, Nb, Ta, Zr, and Zn mineralization (Beard et al. 2023).

The suites of syenites and fenites discussed in this chapter on the property contain high REE, Nb, and Zr content relative to the unaltered host rocks, that occur in phases such as pyrochlore, columbite, zircon, titanite, apatite, epidote, allanite, and bastnäsite. The HFSE and REE contents are the highest in the actinolite-altered syenite and fenites in the South Fenite Zone, and comparatively are up to approximately 15x and 10x greater than the altered arfvedsonite-aegirine syenite and nepheline syenite, respectively, in the North Fenite Zone (see Figure 6.4). Notably,

the fenites have high Li contents (300 to 560 ppm). The combination of brecciation and potassic fenitization is characteristic of shallow depths in alkali-silicate intrusions (Elliott et al. 2018). Potassium content is more elevated in the fenite units and brecciation and potassic-rich mineralogy was observed in several actinolite-altered syenite and fenite outcrops in the South Fenite Zone (see Chapter 3). The combination of the high HFSE- REE content along with observed brecciation and elevated potassium content of the South Fenite Zone indicates that the actinolite-altered syenite and fenites are part of a silicate roof top zone. The close spatial relationship between these rocks and the arfvedsonite-aegirine syenite suggests that the rocks in the North Fenie Zone are also part of a silicate roof top zone. If the former statements are true, this would provide insight to the orientation of the magmatic system. However, more work needs to be conducted across all the intrusive units and their interactions with the host rocks to understand the system as a whole before making interpretations about the orientation of the magmatic system.

7 Geophysical Surveys: Handheld Gamma Ray Spectrometry and Magnetic Susceptibility

Two geophysical methods were conducted to investigate the radiation and magnetic characteristics of the sampled rock suites on Corundum Dome and Pyrochlore Dome within the Bandito property. A handheld gamma ray spectrometry survey was conducted along the sampling route during 2020 fieldwork. After fieldwork, hand samples that were collected were analyzed using a magnetic susceptibility meter.

This chapter will compare the handheld gamma ray survey and magnetic survey results reported in this thesis to the literature and industry reports from the units on the Bandito property. The gamma ray survey results in this chapter will also be compared to measured bulk rock compositions reported in Chapter 6 to see if a correlation exists between elevated K, U, Th concentrations from the survey and elevated REE content in the bulk rock samples. If a correlation exists between elevated radiogenic contents in the survey and the REE content in the bulk rock samples, then radiometric surveys could be used to map REE mineralization associated with the Pool Creek nepheline syenite and associated igneous and metasomatic units.

Methods

Radiation spectrometry

A hand-held Radiation Solutions Incorporated RS-230 spectrometer (Radiation Solutions Inc. 2015) was used to conduct a radiation spectrometry survey simultaneously with rock sample collection. The instrument measures the average radiation intensity of the circular area of a uniform material approximately 90 cm in diameter and penetrates to a depth of up to 30 cm (Shives 2017). The spectrometer was carried at the hip by the same person throughout field work in an effort to keep it at the same height from the ground to minimize variables during data collection. The spectrometer was kept several meters away from collected rock samples to prevent its recordings from being skewed. Data points were collected at 30-second intervals. The instrument was only shut off during breaks, if it needed a reboot, or if it ran out of battery. The survey line was relatively straight while travelling to rock sampling locations and formed a rough

zigzag pattern through the area where rock sampling was being conducted. When high readings relative to the unaltered host rock were observed, zigzag spacing was intentionally made tighter. The data are reported in counts per second (cps) for K, U, Th and Total Count, or percent (%) for K since it is a major element and parts per million (ppm) for the trace elements, U and Th, and Total Count. Note, uranium and thorium will be discussed in terms of equivalent values, such as equivalent uranium (eU) and equivalent thorium (eTh) due to natural disequilibrium that can occur in their decay series (Erdi-Krausz et al. 2003).

Magnetic susceptibility

Hand samples of rock with dimensions larger than or equal to 60 × 30 mm were measured at UBC using a KT-6 Magnetic Susceptibility Meter. Measurements were taken from fresh surfaces with minimal surface unevenness. Sample measurement and correction methods follow that of the KT-6 Manual (SatisGeo 2007).

Results

The spectrometer measurements across the sampling area at the Bandito property range from K = 0.5 to 4.6 %, eU = 0.3 to 16.8 ppm, eTh = 3.6 to 286.3 ppm, and Total Count = 5.5 to 146.7 ppm. The spectrometry transect with respect to the measured intensities of K, eU, eTh, and Total Counts are shown in map view in Figure 7.1 and measured intensities over the duration of the field season are shown in Figure 7.2. Sample numbers, rock type, collection method (*in situ*, grab, or float), GPS coordinates, and magnetic susceptibility of representative samples is reported in Table 7.1. The handheld magnetic susceptibility measurements from the rock samples collected at the Bandito property range from 0.03×10^{-3} to 20.94×10^{-3} SI.

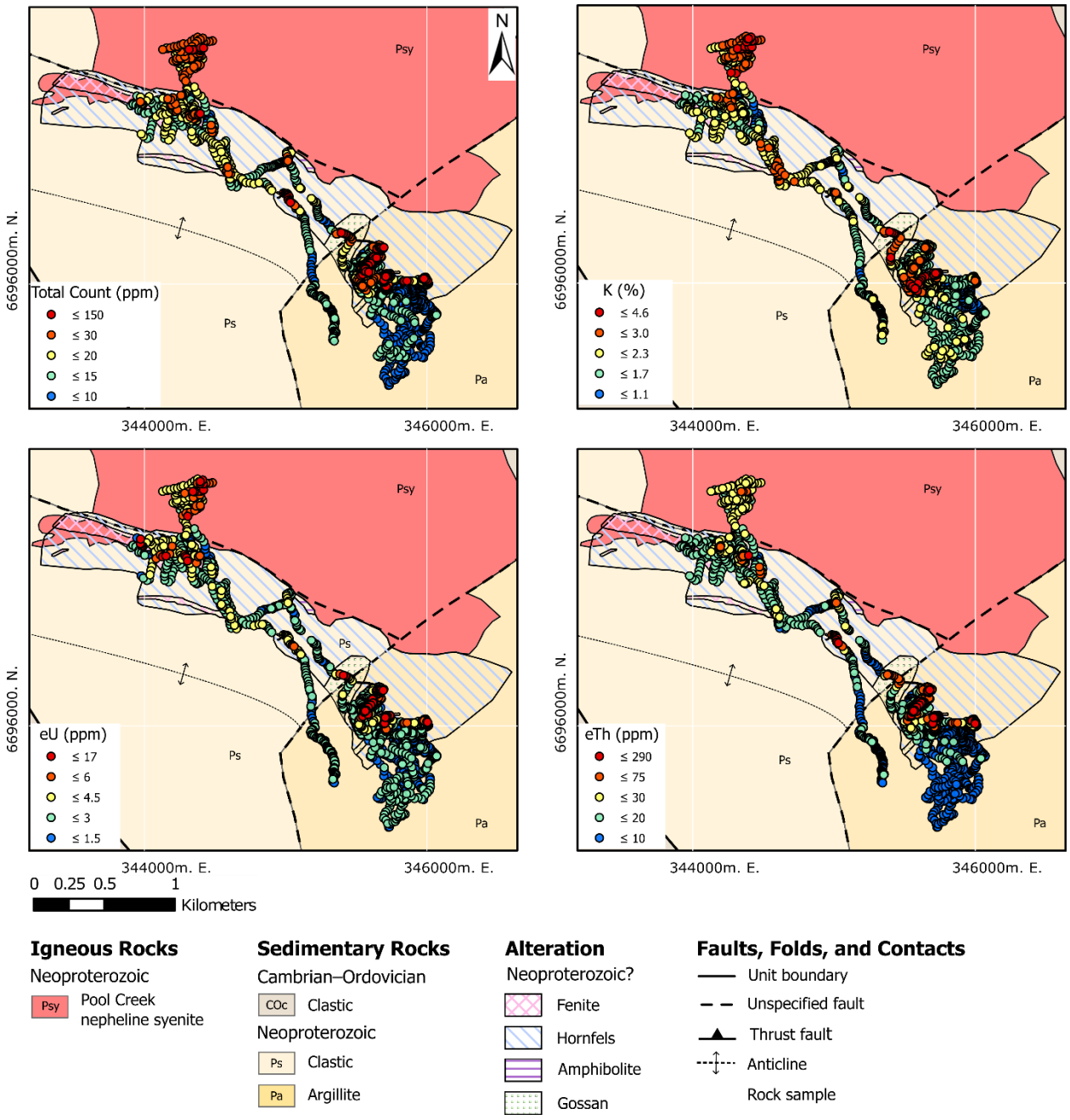

Figure 7.1. Spectrometry tracks across Corundum Dome and Pyrochlore Dome. Survey data show Total Count (ppm), K (%), eU (ppm), and eTh (ppm).

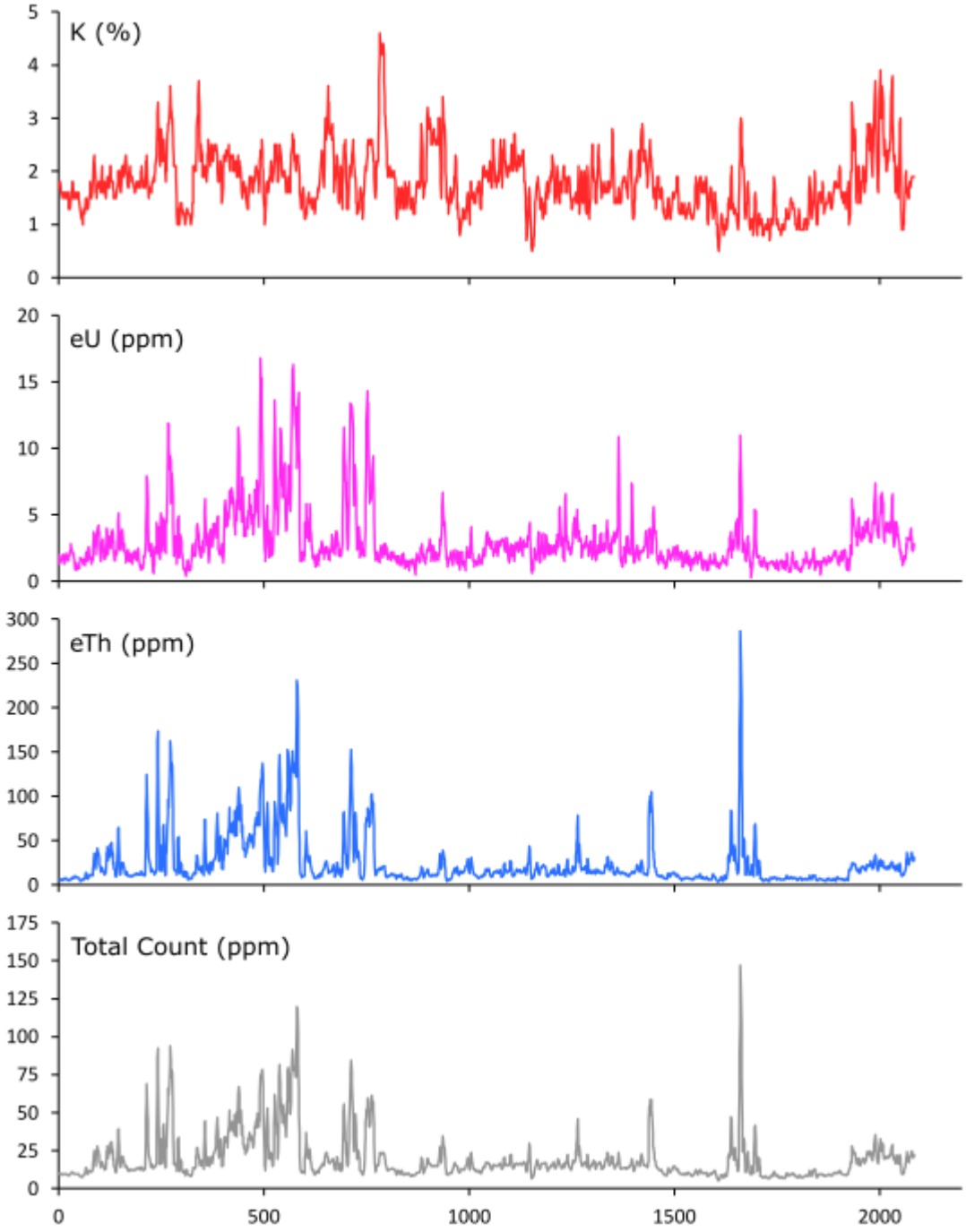

Figure 7.2. Spectrometry trace over the field duration versus K (%), eU (ppm), eTh (ppm), and Total Counts (ppm).

Radiation intensity of K, eU, and eTh with respect to the mapped geology on the Bandito property are summarized in Table 7.2. Geologic units are with respect to those in the Swanton (2012) report. The overall K, eU, eTh, and Total Count intensity across the transect was the lowest in the unaltered host rock and hornfels, moderate in the gossan, Pyrochlore Dome (i.e., the North Fenite Zone) and Pool Creek nepheline syenite, and the highest on Corundum Dome (i.e., the South Fenite Zone).

Table 7.2. Relative radiation measurements of the geology on the Bandito property. L = low; ML = moderately low; M = moderate; MH = moderately high; H = high.

Geologic Unit	**K**	**eU**	**eTh**	**Total Count**
Unaltered host (clastic unit, argillite unit)	ML	L to ML	L	L to ML
Hornfels zone	ML to M	ML	L to ML	ML
Gossan zone	MH	ML to M	ML to MH	M to MH
Pyrochlore Dome (North Fenite Zone)	ML to MH	ML	ML	ML to MH
Corundum Dome (South Fenite Zone)	M to H	M to H	MH to H	M to H
Pool Creek nepheline syenite	M to H	ML to M	M	M to MH

With respect to the magnetic susceptibility of samples collected from the Bandito property, the country rock (argillite, siltstone, metaconglomerate, and quartzite) values range from 0.03×10^{-3} to 0.29×10^{-3} SI with an average of 0.19×10^{-3} SI. Values from the Pool Creek nepheline syenite range from 0.13×10^{-3} to 0.44×10^{-3} SI with an average value of 0.22×10^{-3} SI. Fenites range from 0.20×10^{-3} to 1.10×10^{-3} SI with an average of 0.44×10^{-3} SI. Other more altered igneous rocks (actinolite-altered syenite and altered arfvedsonite-aegirine syenite) that range from 0.15×10^{-3} to 4.94×10^{-3} SI with an average of 1.35×10^{-3} SI. Notably, only six samples of the syenite have values above 1.00×10^{-3} SI. A volcanic breccia has a value of 0.34×10^{-3} SI. Dikes range from 0.27×10^{-3} to 20.94×10^{-3} SI. The feldspar glomeroporphyritic syenite dike (sample 20TN54) is the least altered dike and is the only one of the dikes that has a low magnetic susceptibility of 0.27×10^{-3} SI that is comparable to the Pool Creek nepheline syenite. The feldspar microporphyritic dike (sample 20TN1) and porphyritic lamprophyre(?) dike (sample 20TN57C) have the highest magnetic susceptibility values on the Bandito property (6.87×10^{-3} SI and 20.94×10^{-3} SI, respectively) and are also the most altered of the dikes.

Table 7.1. List of samples collected from the Bandito property in 2020 and their respective magnetic susceptibility measurements. UTM Zone 10. Datum used is WGS 84. Locations: CD—corundum dome; PD—pyrochlore dome. Magnetic susceptibility is reported in SI units.

Sample Number	Sub-sample Number	Unit	Collection Type	Location	Easting (m)	Northing (m)	Magnetic Susceptibility ($\times 10^{-3}$ SI)
20TN1		Altered feldspar microporphyritic syenite dike	Grab	CD	345659	6695876	6.87
20TN2		Actinolite-altered syenite	*In situ*	CD	345711	6695968	2.82
20TN3	20TN3-1 20TN3-2	dike in contact with layered fenite	*In situ*	CD	345711	6695967	4.28
20TN4	20TN4A 20TN4B 20TN4C	Layered arfvedsonite-albite fenite	*In situ*	CD	345741	6696062	0.25
	20TN4D	Actinolite-altered syenite in contact with layered fenite					0.17
20TN5		Bedded argillite	*In situ*	CD	345740	6696055	0.24*
20TN6	20TN6-1 20TN6-2	Actinolite-altered syenite	*In situ*	CD	345554	6696096	0.75
20TN7		Brecciated layered fenite	*In situ*	CD	345571	6696112	0.58
20TN8	20TN8A 20TN8B	Metallic veins	*In situ*	CD	345569	6696118	N/A
20TN9		Actinolite-altered syenite	*In situ*	CD	345571	6696116	4.94
20TN10	20TN10A 20TN10B 20TN10C	Actinolite-altered syenite Actinolite-altered syenite	*In situ*	CD	345567	6696114	0.30
20TN11		Volcanic breccia	*In situ*	CD	345539	6695991	0.17
20TN12		Altered arfvedsonite-aegirine syenite	*In situ*	PC	344645	6696774	0.17
20TN13	20TN13A 20TN13B		*In situ*	PD	344313	6697214	0.32
20TN14	20TN14		Grab	PD	344463	6697044	0.40

Sample Number	Sub-sample Number	Unit	Collection Type	Location	Easting (m)	Northing (m)	Magnetic Susceptibility ($\times 10^{-3}$ SI)
20TN15	20TN15A	Layered titanite-arfvedsonite syenite	Grab	PD	344477	6697073	4.33
	20TN15B	Altered layered amphibole-diopside-phlogopite syenite					
	20TN15C						
20TN16	20TN16A-1	Altered arfvedsonite-aegirine syenite	*In situ*	PD	344417	6697141	0.15
	20TN16A-2						
20TN17	20TN17A-1		*In situ*	PD	344369	6697154	1.01
	20TN17A-2						
	20TN17B	Calcite-quartz metaconglomerate					0.03*
	20TN17C	Quartzite					0.24*
20TN18		Altered arfvedsonite-aegirine syenite	*In situ*	PD	344393	6697205	2.05
20TN19		Zircon bearing quartz vein in altered arfvedsonite-aegirine syenite	*In situ*	PD	344384	6697201	2.08
20TN20		Altered arfvedsonite-aegirine syenite	*In situ*	PD	344153	6697314	0.78
20TN22	20TN22A	Layered arfvedsonite-albite fenite	Float; rockfall	CD	345999	6696025	0.21
	20TN22B						
20TN23		Layered arfvedsonite-albite fenite	Float; rock	CD	345982	6696041	1.10
20TN24	20TN24A	Bedded argillite	*In situ*	CD	345908	6696079	0.29
	20TN24B	Volcanic breccia					0.34
20TN25	20TN25A	Altered white syenite dikelets in contact with layered fenite	*In situ*	CD	345776	6696075	0.25
	20TN25B						

Sample Number	Sub-sample Number	Unit	Collection Type	Location	Easting (m)	Northing (m)	Magnetic Susceptibility ($\times 10^{-3}$ SI)
		Altered white syenite dikelets in contact with layered fenite					
	20TN25C	Layered phlogopite-potassium feldspar fenite					0.20
	20TN25D						
	20TN25E	Actinolite-altered syenite					0.25
	20TN25F						
20TN53		Nepheline alkali feldspar syenite	*In situ*	PD	344365	6697505	0.23
20TN54		Altered feldspar glomeroporphyritic syenite dike	*In situ*	PD	344371	6697512	0.27
20TN55A	20TN55A	Nepheline alkali feldspar syenite	*In situ*	PD	344381	6697536	0.14
	20TN55B						
20TN56		Pool Creek nepheline syenite	*In situ*	PD	344364	6697656	0.44
20TN57	20TN57A	Pool Creek nepheline syenite	*In situ*	PD	344260	6697757	0.13
	20TN57B	Altered porphyritic lamprophyre(?) dike					20.94*
	20TN57C-1						
	20TN57C-2						
20TN58	20TN58A	Altered arfvedsonite-aegirine syenite	*In situ*	PD	344354	6697205	3.53
	20TN58B						

** = Sample measurement may be affected by small sample size and/or weathering. A small sample size leads to a smaller measured value. Weathered surfaces on a sample may lead to a higher measured value.*

Implications of gamma ray spectrometry survey

Gamma ray spectrometry is a geophysical technique that measures naturally occurring radioactive isotopes of K, U, and Th across geologic surfaces. Since all rocks emit some degree of radiation, this method is useful in mapping geologic units and alteration associated with LILE, HFSE, and REE mineralization (e.g., Shives 2015; 2017). Combining gamma ray spectrometry with other methods such as magnetic susceptibility measurements, mineralogical, and whole rock geochemical information is optimal for mapping systems associated with mineralization (e.g., Beard et al. 2023).

In Figures 7.1 and 7.2, eU and eTh show a positive correlation with each other. Potassium has a positive correlation with eU and eTh, though it is not as obvious. Based on these observations, eU and eTh have a strong positive correlation, and both have a moderate positive correlation with K on the Bandito property. The overall trend from the lowest to highest radiogenic values across the units on the Bandito property is argillite and quartzite < hornfels zone < Pyrochlore Dome < gossan zone < Pool Creek nepheline syenite < Corundum Dome. Based on the Total Count results, K-, Th-, and U-bearing minerals are typically concentrating in areas that have experienced metasomatic alteration, such as the nepheline syenite, altered arfvedsonite-aegirine syenite, actinolite-altered syenite, and the fenites.

Bulk rock compositions reported in Chapter 6 are consistent with the gamma ray results, where a strong correlation exists between U and Th whole rock content. Whole rock compositions highest in Th and U are the layered syenites and actinolite-altered syenite on Corundum Dome > nepheline syenite > altered arfvedsonite-aegirine syenite > argillite and quartzite. Furthermore, a strong positive correlation exists between Th, U, and REE, where Th and U content increase with REE content (Figure 7.3). Relationships between K_2O-Th, K_2O-U, and K_2O-REE are variable. The strong correlation between Th, U, and REE content indicates that elevated eTh and eU concentrations measured by gamma ray surveys on the Bandito property can be used to map REE mineralization and in turn, as vectors to explore for REE mineralization. Soil sampling from an exploration report by Swanton (2012) agree with the gamma ray survey results reported

in this chapter, where Th and U concentrations are the highest in the zones mapped as fenite (particularly on Corundum Dome) and the Pool Creek nepheline syenite.

The spectrometer track along Corundum Dome (the South Fenite Zone) (Figure 7.4) dominantly has high variation between K, eU, and eTh and hosts the areas highest in K, eU, and eTh on the property. In contrast, Pyrochlore Dome (the North Fenite Zone) (Figure 7.5) has relatively lower values with moderate variation across the distinct units. Based on the rock types reported on and discussed in this thesis, these chemical variations are interpreted to be controlled by the composition and fluid rock interactions between the host rock and the intrusive syenitic units (see Chapter 6 discussion). Similar variations between the two zones are reflected in soil survey results reported by Swanton (2012). Swanton (2012) speculated that these variations in the soil surveys are due to the change in topography between the two zones which may reflect different depths of the intrusion , zoning in the transition, or proximity to the intrusion.

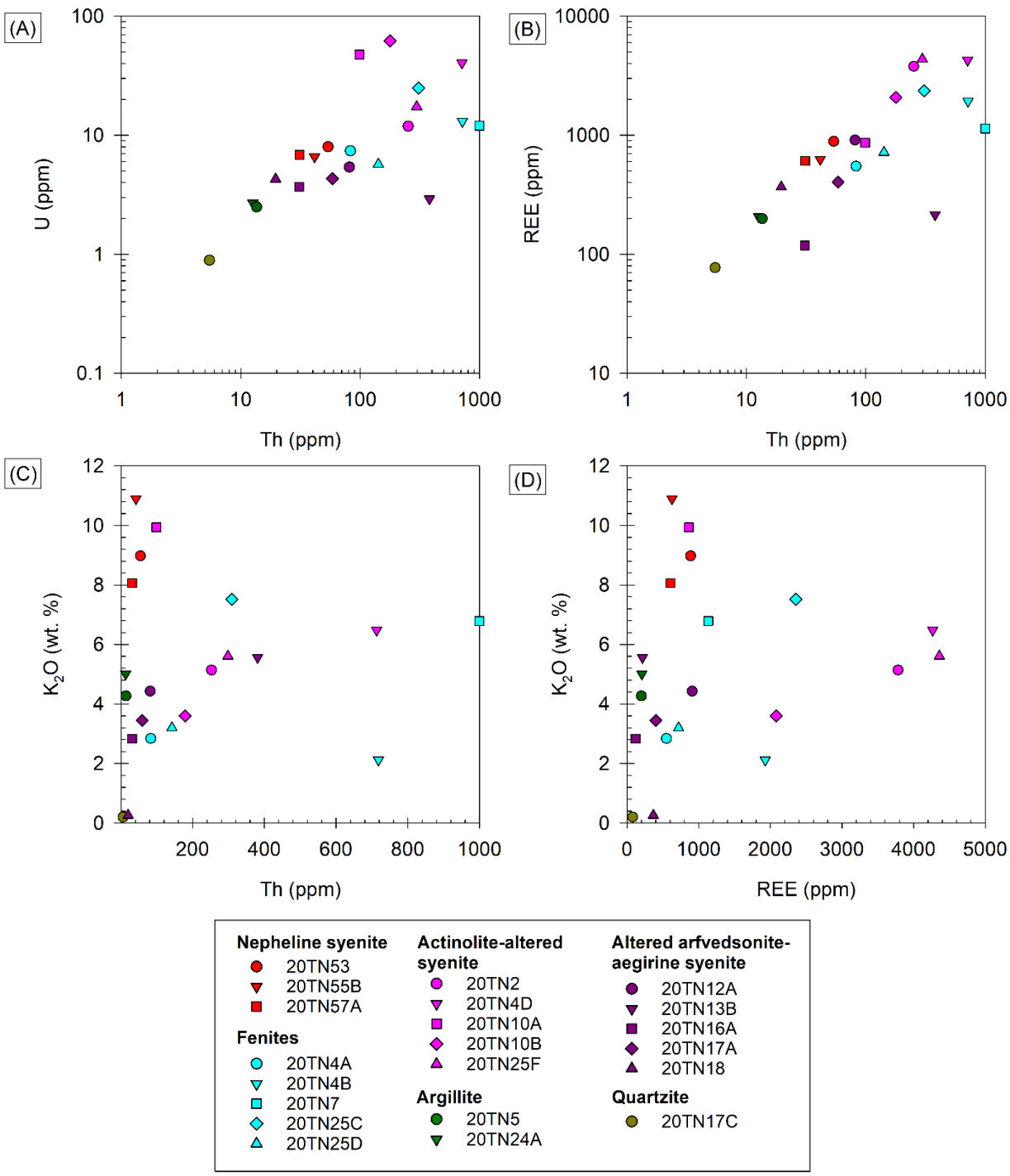

Figure 7.3. Bulk rock bivariate compositional diagrams displaying samples collected from Corundum Dome (argillite, actinolite-altered syenite, and fenites) and Pyrochlore Dome (quartzite, altered arfvedsonite-aegirine syenite, nepheline syenite). (A) Th versus U. (B) Th versus REE. (C) K_2O versus Th. (D) K_2O versus REE.

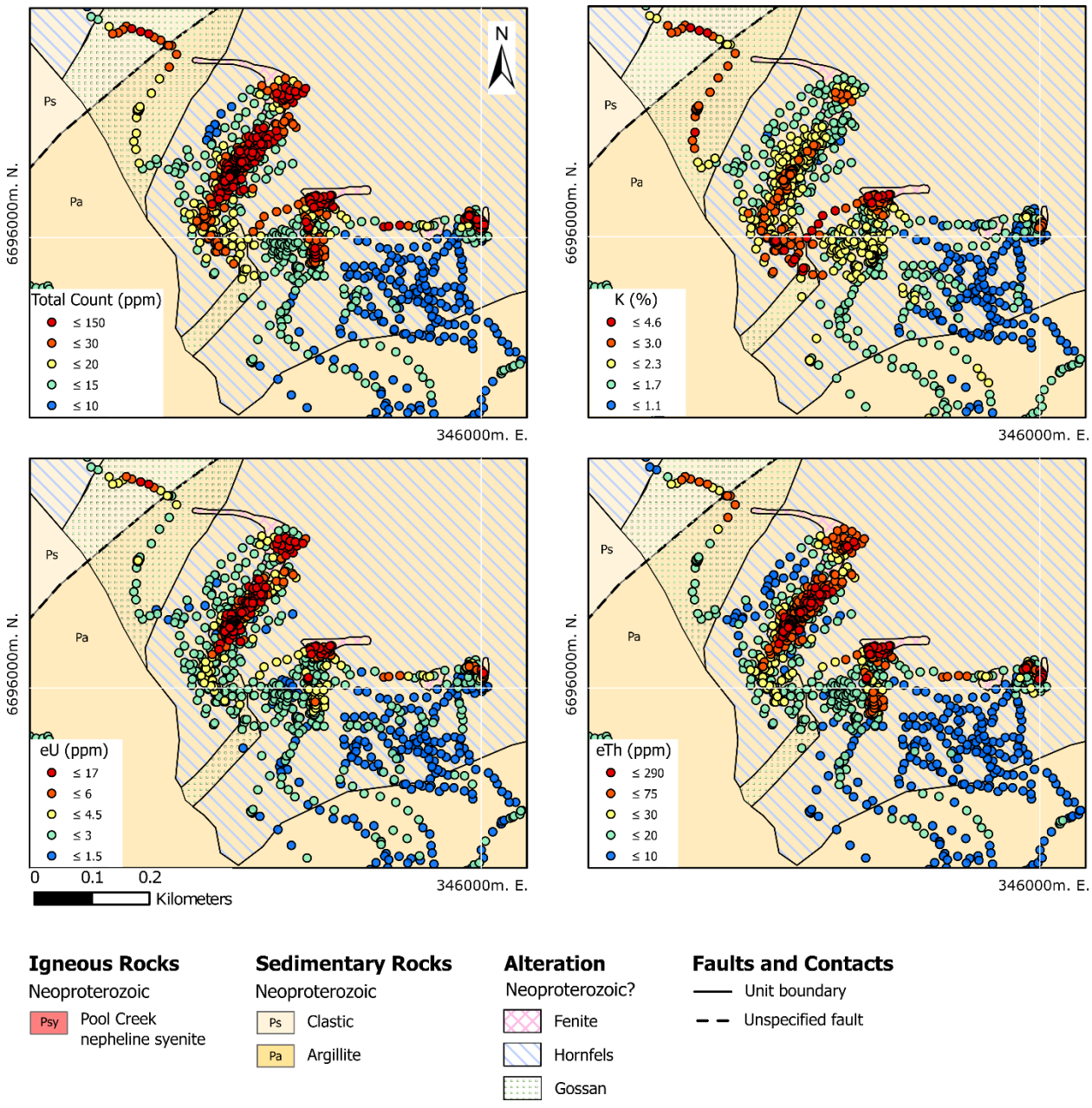

Figure 7.4. Gamma ray spectrometer track on Corundum Dome over the South Fenite Zone and gossan zone.

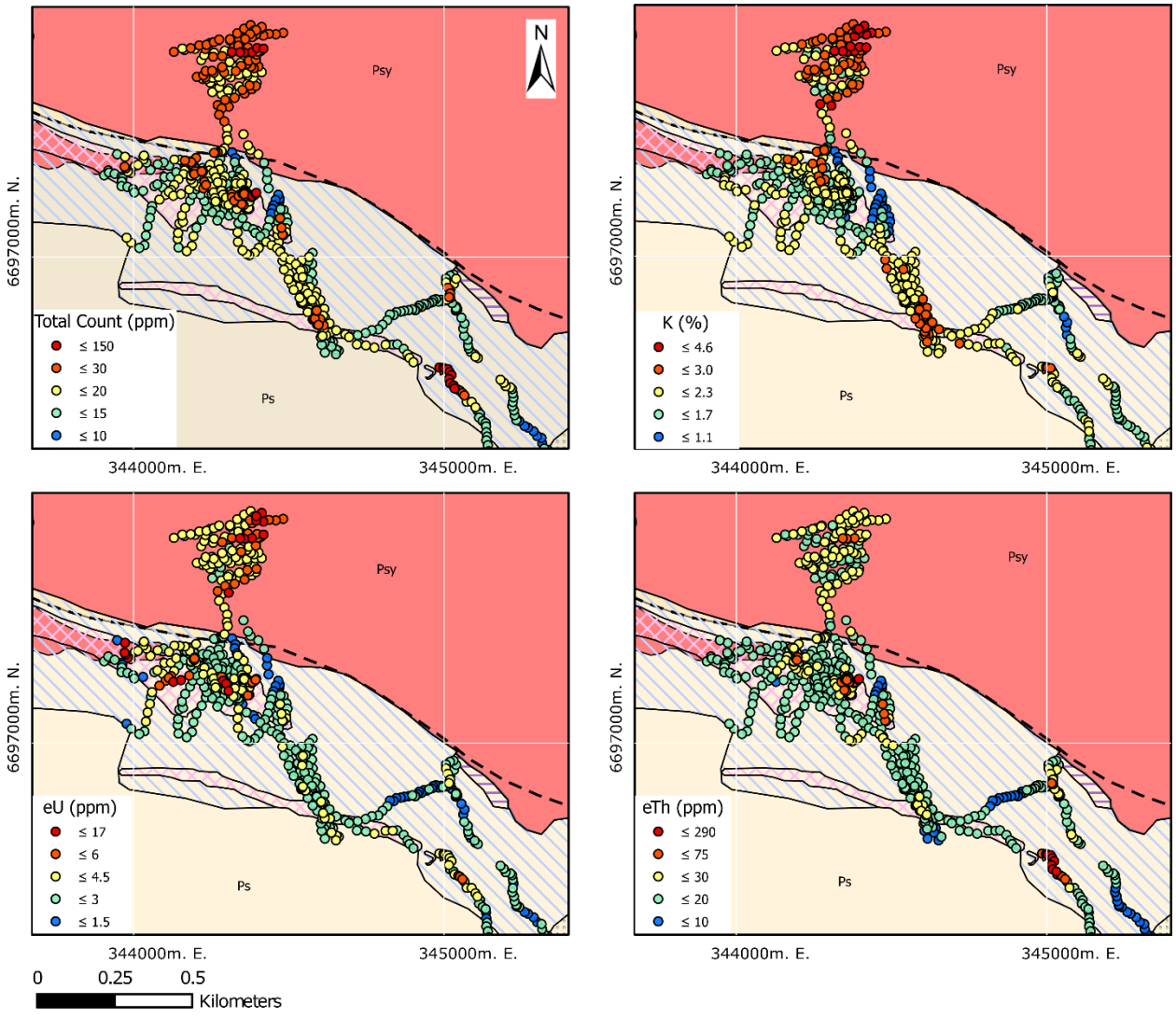

Figure 7.5. Gamma ray spectrometer track on Pyrochlore Dome over the North Fenite Zone and southwestern edge of the Pool Creek nepheline syenite.

Gamma ray spectrometry survey considerations

Several considerations need to be made when measuring and interpreting radiometric data, such as unit exposure, precipitation, soil moisture, element mobility, and temperature and pressure (Erdi-Krausz et al. 2003). There is moderate to high variation in radiation measurements with respect to K, eU, eTh, and Total Counts, within most of the mapped units that were traversed on the Bandito property (Figure 7.1). There are several factors that could be contributing to this variation, however, poor outcrop exposure due to heavy vegetation coverage across the property made it challenging to visually observe distinct changes in lithology that may have contributed to variable measurements. The variation observed within units along the transect is likely due by one or some combination of the following:

(1) Unmapped, miss-mapped, or overlapping units. For example, Swanton (2012) mentioned "windows" of the Pool Creek nepheline syenite outcropping in areas of the South Fenite Zone (on Corundum Dome) that are not mapped within the report. Swanton (2012) also reports the overlapping of units occurs on the property, where the gossan zone overprints some of the South Fenite Zone.

(2) Variable outcrop exposure due to vegetation or overburden. Since the spectrometer detects radiation from depths of up to 35 cm (Erdi-Krausz et al. 2003), areas covered in thick vegetation, soil, or glacial debris, may have contributed to a lower measured value that is representative of the covered rock unit on the Bandito property. Similarly, weathering and erosion possibly causing apparent higher or lower measurement values. For example, a rockfall of a unit higher in radiogenic minerals depositing on a unit lower in radiogenic minerals could create an apparent high zone in that unit, or the liberation or concentration of radiogenic minerals in soil or runoff could create zones of radiogenic highs surrounded by radiogenic lows. The 2020 transect recorded on the Bandito property occurred across heavily vegetated steep domes where several rockfalls and scree slopes were observed. Furthermore, gossan, a weathering product of sulphide mineralization (Haldar 2018) that occurs on the property provides evidence that weathering has affected rock units.

(3) Changes in topography. Variability in terrane can impact measurements, leading to measured zones with higher (e.g., walking directly next to a steep feature) or lower (e.g.,

walking atop a narrow feature) values than are characteristic of the units being measured (e.g., Erdi-Krausz et al. 2003; Shives 2017). Areas that were traversed on the Bandito property were commonly relatively even or with a gentle slope, and very few areas were extremely steep. It is possible that traversing steep slopes or next to steep outcrop faces lead to apparent high values.

(4) Precipitation or soil moisture. Precipitation and saturated soils can lead to apparent increases in radiation levels, particularly with respect to uranium (Erdi-Krausz et al. 2003). During the 2020 field season, there were sporadic and brief thunderstorms and rain showers that covered the surveying area of the Bandito property. Rainfall only occurred once during surveying. Surveying with the spectrometer was paused during the period of precipitation and conducted upon the end of a rainfall. It is recommended that surveying should not be conducted until at least three hours after rainfall (Erdi-Krausz et al. 2003), so it is possible that the measured uranium values in the survey after a rainfall are apparently higher than what they truly are.

(5) Structurally controlled distribution of radiogenic minerals within units. For example, metasomatic fluids migrating along fracture or fault surfaces may precipitate radiogenic K-, U-, or Th-bearing minerals (e.g., Decrée et al. 2015). Thus, veining along fault and fracture surfaces in different units across the property may bear a higher concentration of radiogenic minerals than typically observed in the respective unit.

(6) Remobilization of radiogenic elements by low temperature fluids from units typically high in radiogenic minerals to units low in radiogenic minerals. For example, U and Th can become mobilized during low-temperature alteration (e.g., Beard et al. 2023). The gossan exposure reported by Swanton (2012) provides evidence for low temperature alteration on the Bandito property. Furthermore, deep circulating thermal springs hosted in deformed sedimentary rocks occur a few kilometers east the Bandito property (Grasby et al. 2016; Figure 2.2). Therefore, it is possible that low-temperature fluids migrating through permeable structures could have remobilized U and Th in units not typically associated with U- and Th-mineralization within the Bandito property.

The unaltered host rock and hornfels zone typically have low to moderate values of K and low to moderately low radiogenic values of eU and eTh. The values recorded from these units indicate

that radiogenic K is common, and that U and Th mineralization is not associated with these units, which agrees with the soil survey results reported in Swanton (2012). Very low concentrations in the unaltered host and honfelsed units is likely due to vegetation coverage. Elevated concentrations in the radiogenic elements in the unaltered host rock may indicate areas of unmapped alteration, variable outcrop exposure, or uneven topography. Similarly, elevated values in the hornfels may indicate unmapped areas of more intense alteration (i.e., gossan or fenite) or of the Pool Creek nepheline syenite, variable outcrop exposure, or uneven topography. For example, there is a notable area adjacent to one of the outcrops of the in the South Fenite Zone in Figure 7.4 as well asl the North Fenite Zone in Figure 7.5 that have relatively high values of K, eU, and eTh in the unit mapped as hornfels. In the field, these areas consist of exposed boulder-sized rockfall surrounded by thick brush on moderately steep terrane. Due to the proximity to the mapped fenite outcrops and that the highest radiation values on the property are associated with the fenite unit, it is likely that these areas are either an unmapped part of the fenite or are fenite rockfall covering the hornfels unit.

Significant variations in recorded radiogenic values occurs over the gossan zone. According to Swanton (2012), the gossan zone is related to an unknown source that came after fenitization because gossan alteration is not associated with syenite magmatism in the literature and the gossan zone overprints areas of the fenite. The elevated K, eU, and eTh values recorded in the gossan zone may be derived from a primary or secondary source. Potential primary sources for this alteration may be fluids migrating from a nearby Eocene biotite syenite, buried/unmapped granitoid intrusion, or other local geothermal sources. The secondary source for the elevated radiogenic values may be Neoproterozoic fenite. Since the gossan zone alteration occurred after fenitization, it is possible that the elevated radiometric values represent areas of unmapped fenite (or erosion of fenite-material) that may or may not have been overprinted by gossan alteration. Alternatively, since gossan alteration is associated with alteration in a low temperature environment (Velasco et al 2013; Haldar 2018; Dunn & Heyden 2022), it is possible that the elevated radiation values within the gossan were caused by the remobilization of U and Th from the fenite by low temperature fluids.

The area of the Pool Creek nepheline syenite covered in the spectrometer survey has significant variation in recorded radiogenic values. Alkaline-silicate intrusions are associated with K, U, and Th mineralization (e.g., Shives 2015, Elliott et al. 2018; Beard et al. 2023). The variation in the radiogenic values over the syenite likely indicate variable outcrop exposure, and may also indicate zoning in the intrusion, variable alteration within the intrusion, dikes or veining cutting the intrusion.

As discussed in earlier chapters of this thesis (Chapter 3, 4, 5, 6), the intrusive units associated with the Pool Creek nepheline syenite are interpreted to be the cause of fenitization on the Bandito property. Notably, high values in the north and South Fenite Zone follow the shape of the mapped outcrop areas in Swanton (2012) which parallel local faults, suggesting that mineralization may concentrate along factures associated with faulting. Based on the variability in location and small zones with high eU and eTh values along the spectrometer survey, alteration may be focused along unit contact boundaries, fractures, other structural traps that the metasomatic fluids travelled through. However, more field mapping needs to be conducted to clarify the nature and distribution of the mineralization system.

If an effort is made in future studies or exploration projects to conduct a larger radiation spectrometry survey and assign a characteristic range of radiometric values to each rock type on the property, then radiation survey results could aid with mapping unexposed units and mapping mineralization associated with radiogenic K, U, and Th. With respect to exploration recommendations made by Beard et al. (2023), the combination of using methods such as geophysical surveys and geochemical sampling over the entire intrusion and the adjacent host rock can improve our understanding of the petrogenesis, and extent and controls of mineralization across the intrusion and its host which can be helpful for exploration models in alkaline-silicate systems.

Implications of magnetic susceptibility measurements

Magnetic susceptibility is a geophysical method that measures the degree to which a rock can be magnetized in an external magnetic field (Hinze et al. 2013). Magnetic susceptibility is a dimensionless quality commonly reported as SI. Handheld magnetometers are commonly used to measure the magnetic susceptibility of drill core or used in smaller-scale surveys that are conducted on foot and measurements. Large scale magnetic surveys are conducted via aircraft (i.e., aeromagnetic surveys) and produce magnetic anomaly maps of the surveyed area; these maps show local anomalies of rock units with respect to the earths magnetic field. Magnetic anomaly data can be positive or negative values and are commonly reported as nanotesla (nT). Positive magnetic anomalies indicate magnetic rocks with respect to the Earth's magnetic field, where negative anomalies indicate rocks that are comparatively less magnetic. Magnetic susceptibility and anomaly maps are used to distinguish between different rock units and is commonly used for exploration for various types of economic deposits (e.g., Hart et al. 2004; Swanton 2011; 2012; Hinze et al. 2013).

The magnetic susceptibility measurements across the sampling area at the Bandito property range from 0.03×10^{-3} to 20.94×10^{-3} SI. On average, the altered host rocks (0.44×10^{-3} SI) and the more altered-looking igneous rocks (1.35×10^{-3} SI) have higher magnetic susceptibility values in comparison to the less altered host rocks (0.19×10^{-3} SI) and the less altered igneous samples (0.22×10^{-3} SI), respectively. Similarly, the more altered dikes (6.87×10^{-3} SI and 20.94×10^{-3} SI) have higher magnetic susceptibility values than the less to moderately altered dikes (0.27×10^{-3} SI, 2.82×10^{-3} SI, and 4.28×10^{-3} SI). Therefore, in general, increased magnetic susceptibility on the property is associated with increasing degrees of alteration. The increased susceptibility of an altered rock likely depends on the parameters of alteration, such as the type of alteration (e.g., metasomatic) and composition and temperature of alteration-related fluids, as well as the composition of the rock that is experiencing alteration.

Hart et al. (2004) summarized the redox state of several calc-alkaline plutons of the North Cordilleran mid-Cretaceous Plutonic Province throughout the Yukon. Further work was done on characterizing on the mid-Cretaceous plutons in southeast Yukon by Heffernan (2004),

Rasmussen et al. (2007), Rasmussen (2013), and Pigage et al. (2014). The nearest of the mid-Cretaceous plutonic suites reported in the region are located approximately 40 km west to northwest of the Pool Creek nepheline syenite in the Coal River map area (NST 95D) and include the Hyland plutonic suite (2.3×10^{-3} SI; Hart et al. 2004), Tungsten plutonic suite (0.16×10^{-3} SI; Hart et al. 2004), and Tay River plutonic suite (0.2×10^{-3} to 17.8×10^{-3} SI; Pigage et al. 2014). The closest mid-Cretaceous plutons with respect to the Bandito property belong to the Tay River suite, which comprises the Gusty tonalite (0.4×10^{-3} SI), Oudder granodiorite (14.0×10^{-3} SI), Powers quartz monzodiorite (0.4×10^{-3} SI), Jorgensen quartz monzodiorite (0.2×10^{-3} SI), and Lookout granodiorite (0.2×10^{-3} SI). Furthermore, Pigage et al. (2014) reported that the sedimentary rocks in the map area have magnetic susceptibilities $<1 \times 10^{-3}$ SI. It is worth mentioning that the local Eocene intrusions (i.e., Ting Creek intrusion, biotite syenite, Beaver River Alkaline Complex) have no published magnetic susceptibility data.

The least-altered areas sampled from the main body of the Pool Creek nepheline syenite have an average magnetic susceptibility of approximately 0.22×10^{-3} SI. With respect to the regional mid-Cretaceous intrusions, the magnetic susceptibility of the Pool Creek nepheline syenite is comparable with the Tungsten plutonic suite and is slightly lower than the Hyland plutonic suite. With respect to the nearest plutons of the Tay River suite, the magnetic susceptibility of the Pool Creek nepheline syenite is comparable to the Gusty, Powers, Jorgensen, and Lookout plutons, and is much lower than the Oudder pluton. With respect to the sedimentary rocks in the Coal River map area, the host rocks on the Bandito property have a similarly low values of approximately 0.19×10^{-3} SI.

Beard et al. (2023) stated that magnetic surveys are effective tools for mapping structural lineaments and poorly to unexposed magmatic systems. Magnetic anomalies associate with the Tay River suite (Pigage et al. 2014) trend from the east of the Coal River map area towards the western edge of the Bandito property (Figure 7.6). Pigage et al. (2014) speculated that, although the anomalies don’t always centre around the exposed intrusions, the high positive anomalies likely represent a magnetic portion of the plutons that have been buried or magnetic mineralization in hornfels or skarn; the rapid change in magnetic intensity from high to low in the lateral direction from these high positive anomalies implies steep intrusive contacts.

There are two high positive magnetic anomalies on the Bandito property, one is NW tending and the other is EW trending. The NW tending anomaly overlaps with the Cu-Ni associated gossan zone discussed in Chapter 2 (Swanton 2011; 2012). Swanton (2012) interpreted the magnetic anomalies on the Bandito property to be associated with a buried magnetic intrusive body or magnetite-bearing host rocks at depth and not with fenitization since fenite outcrops are nonmagnetic. Swanton (2012) made this interpretation based on the observation that outcrops with magnetic minerals overlap with the high positive anomaly. Dikes associated with the Pool Creek nepheline syenite that cut through the host units and the syenite itself are magnetic (Pigage & Mortensen 2004; Swanton 2011; 2012), so it is possible that these reflect the more magnetic nature of the pluton at depth. Could the high positive anomalies adjacent to the southern edge of the syenites on the Bandito property belong to more magnetic buried parts of either of the syenite intrusions or a different buried intrusion such as the mid-Cretaceous Tay River suite?

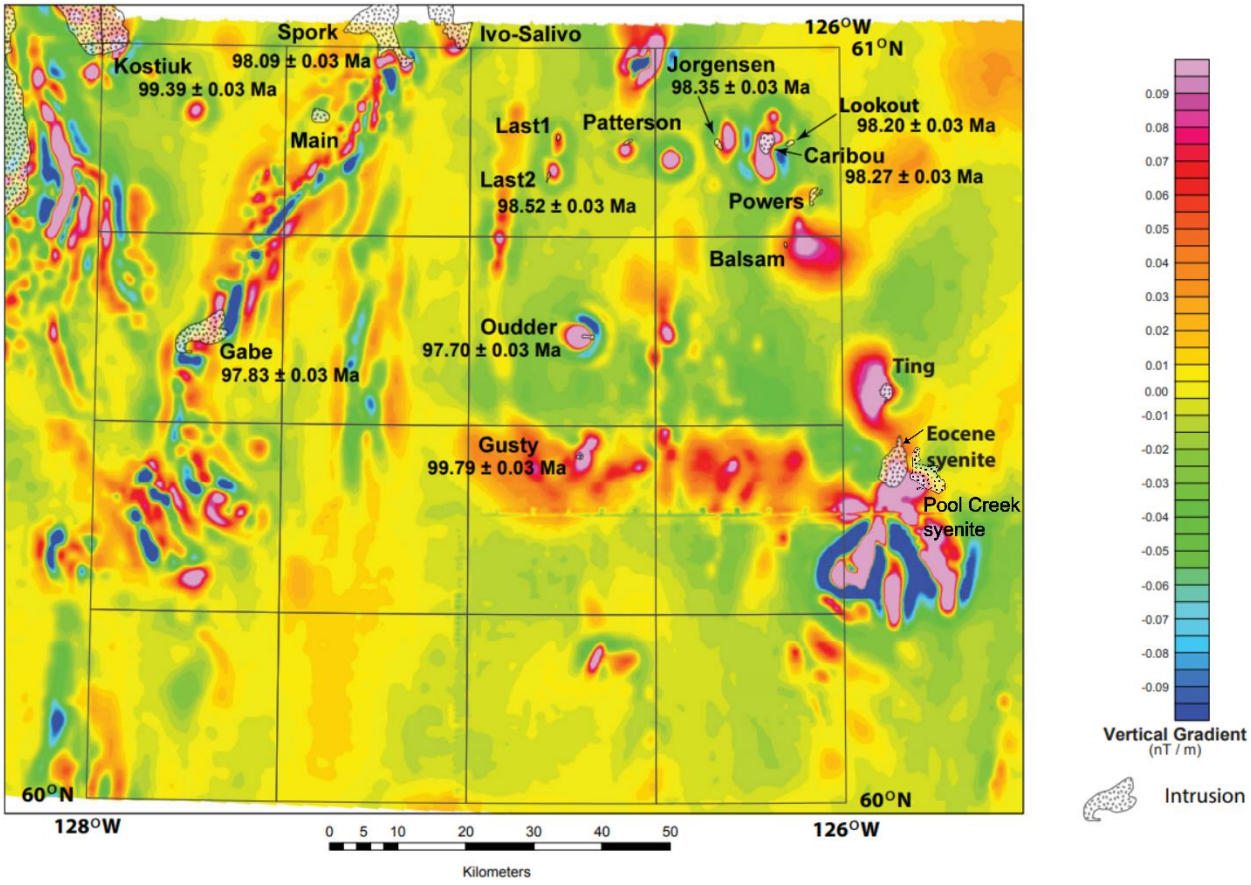

Figure 7.6. First vertical derivative of regional aeromagnetic survey of the Coal River map area and the west of the Pool Creek map area in Yukon, Canada, modified after Pigage et al. (2014). High positive magnetic anomalies (i.e., pink) are characteristic of magnetic sources (e.g., magnetite-bearing rocks), and low (negative) magnetic anomalies (i.e., blue) are characteristic of non-magnetic sources.

If there is an unmapped or buried pluton of a more granitic composition within or adjacent to the property, that could explain the peculiar Cu-Ni associated gossan alteration (which is atypical for foid syenites) that occurred sometime after the fenitization that is associated with the Pool Creek nepheline syenite. For example, the granitic mid-Cretaceous Plutonic Province in Yukon hosts Cu mineralization, amongst several other commodities (e.g., Hart et al. 2004; Rasmussen 2013). However, other sources of mineralization occur in Yukon that could be responsible for the Cu-Ni mineralization. Sedimentary exhalative (SEDEX) deposits associated with Pb-Zn mineralization occur in the Selwyn Basin in Yukon, where pyrite hosts a variety of elements such as Cu and Ni (Gadd et al. 2016). There are three sites with evidence Pb-Zn mineralization occur near the Bandito property. West of the property on the SW edge of the Eocene biotite syenite is a Pb-Zn soil anomaly in a skarn deposit hosted in limestone reported by Culbert (1981). Cathro (1983) and Gregory (2008) reported Pb-Zn soil anomalies approximately 10 km northwest of the Biotite syenite. Approximately 10 km north of the Pool Creek nepheline syenite is a showing of galena and sphalerite associated with Zn-Pb-Ag SEDEX mineralization reported by Burt (1983). Hyper-enriched black shales that host Ni-Mo-Zn-Pt-Pd-Au-Re mineralization occur in the Selwyn Basin (Gadd et al. 2019). Copper-nickel-platinum group element mineralization occurs in Yukon but is associated with the Triassic Wrangellia flood basalts (Greene et al. 2005). However, mid-Cretaceous granitoids, Wrangellian basalts, and SEDEX and hyper-enriched black shale deposits have yet to be identified on or directly adjacent to the Bandito property. Based on the geophysical evidence presented by Swanton (2011; 2012) and Pigage et al. (2014), it is likely that the source of the Cu-Ni mineralization and gossan on the Bandito property is related to a buried intrusion. More concrete investigations need to be conducted on the gossan zone identified by Swanton (2012) to confirm the source of alteration; however, this is out of the scope of this thesis.

8 Concluding Remarks

The objectives of this dissertation were to determine:

(1) the source(s) of alkali metasomatic (i.e., fenitizing) fluids and the timing of the associated metasomatic alteration of the sampled fenitized units on Pyrochlore Dome and Corundum Dome on the Bandito property,
(2) the distribution of rare earth element and high field strength element mineralization across the sampled area on Pyrochlore Dome and Corundum Dome, and
(3) the mechanisms responsible for rare earth element and high field strength element mineralization across the sampled area on Pyrochlore Dome and Corundum Dome.

A combination of petrography, mineral chemistry compositions, zircon dating, whole rock compositions, and gamma ray surveys contributed to the understanding of the source of alkali metasomatism and the controls on metasomatic mineralogy and critical element (i.e., REE, Nb, and Zr) mineralization on Pyrochlore Dome and Corundum Dome on the Bandito property.

With respect to objective (1), the alkali metasomatic (i.e., fenitizing) fluids are interpreted to be sourced from Neoproterozoic magmatism associated with the Pool Creek nepheline syenite. This interpretation is based on the similar mineral textures observed across the nepheline syenite and metasomatically altered syenite suites, the mineral and bulk rock geochemical compositional relationships between the nepheline syenite, altered syenite suites, and their respective host rocks, and the overlapping Neoproterozoic U-Pb zircon ages between the nepheline syenite and altered syenite suites. This interpretation confirms Swanton's (2012) claim that the alkali metasomatic alteration on the Bandito property is associated with the Pool Creek nepheline syenite.

The differences between metasomatic alteration mineralogy and bulk rock compositions observed across the nepheline syenite and altered syenite suites on Pyrochlore Dome and Corundum Dome are interpreted to be dictated by the intrusive and host rock compositions and the spatial distribution between intrusive units and the respective host (i.e., closer, more reflective of host rock composition; further, more reflective of primary igneous composition).

Autometasomatism of the nepheline syenite is indicated by Na-alteration of potassium feldspar to albite; sericite replacement of nepheline; replacement of a formerly mafic mineralogy by phlogopite, chlorite, rutile, and bastnäsite; and alteration of pyrochlore to hematite. Metasomatic alteration of other igneous units on Pyrochlore Dome is reflected by Na-Si-Fe rich mineralogy (i.e., prevalence of albite, arfvedsonite, aegirine, quartz, and hematite). Metasomatic alteration is strong in the syenites and weak in the quartzite. Metasomatic alteration on Corundum Dome is reflected in Ca-K-Na rich mineralogy (e.g., actinolite, epidote, phlogopite, albite). Metasomatic alteration is strong in the actinolite syenite and the fenites (i.e., layered phlogopite-feldspar fenite, layered arfvedsonite-albite fenite, and brecciated arfvedsonite-potassium feldspar fenite). Metasomatic mineralogy reflects the chemical nature of the intrusive and host units, implying contact metasomatism (i.e., metasomatic fluid interactions between an intruding phase and the respective host rock). Based on the relationship between metasomatic alteration and host rock composition, it is possible that the actinolite-altered syenite and altered arfvedsonite-aegirine syenite represent the metasomatized contact of the nepheline syenite between the argillite and the quartzite.

With respect to objective (2), the characteristics of metasomatic alteration and REE and HFSE content is different on Corundum Dome and Pyrochlore Dome. Mineralogical and compositional differences are summarized in Table 8.1. On Corundum Dome, the mineralization occurs in the actinolite-altered syenite and the fenites. Based on petrographic observations and bulk rock compositions, the REE and HFSE content is highest in the actinolite-altered syenite, closely followed by the fenites. On Pyrochlore Dome, mineralization occurs within the nepheline syenite, layered titanite-arfvedsonite syenite, layered amphibole-diopside-phlogopite syenite, and the altered arfvedsonite-aegirine syenite. Based on petrographic observations and bulk rock compositions, the REE and HFSE mineral content is greatest in the nepheline syenite and the least altered arfvedsonite-aegirine syenite and lowest in the most altered samples of the arfvedsonite-aegirine syenite. From greatest to lowest content across the sampled suites on Pyrochlore Dome and Corundum Dome, the REE and HFSE content is actinolite-altered syenite > fenites > nepheline syenite > altered arfvedsonite-aegirine syenite > argillite > quartzite.

Table 8.1. Summary of metasomatism and observed REE and HFSE mineralogy and content from the sampled units on the Bandito property.

Rock Type	Location	Type of Metasomatism	REE, Ti, Nb, Zr Mineralogy	Bulk Rock REE+Y, Nb and Zr Content
Nepheline syenite	Pyrochlore Dome	Na auto-metasomatism	bastnäsite, pyrochlore, columbite, apatite, zircon	**REE+Y:** 661.4 to 939.18 ppm **Nb:** 302 to 659 ppm **Zr:** 768 to 2050 ppm
Altered arfvedsonite-aegirine syenite		Na auto-metasomatism and Si contact metasomatism	epidote, allanite, apatite, pyrochlore, columbite, niobian rutile, zircon	**REE+Y:** 132.29 to 952.93 ppm **Nb:** 199.5 to 783 ppm **Zr:** 272 to 2440 ppm
Layered titanite-arfvedsonite syenite		Na auto-metasomatism	bastnäsite, pyrochlore, columbite, niobian titanite, niobian rutile, zircon	Not measured
Layered amphibole-diopside-phlogopite syenite		Na auto-metasomatism	bastnäsite, monazite, apatite, titanite, zircon, unidentified REE-bearing silicate	Not measured
Quartzite		Na contact metasomatism	zircon, monazite, pyrochlore	**REE+Y:** 82.76 ppm **Nb:** 52.2 ppm **Zr:** 344 ppm
Actinolite-altered syenite	Corundum Dome	K-Na-Ca contact metasomatism	epidote, allanite, apatite, pyrochlore, niobian titanite, niobian rutile, and zircon	**REE+Y:** 918.03 to 4675.63 ppm **Nb:** 903 to >2500 ppm **Zr:** 3410 to >10000 ppm
Fenites		K-Na-Ca contact metasomatism	bastnäsite, apatite, titanite, epidote, allanite, pyrochlore, columbite	**REE+Y:** 594.99 to 2646.43 ppm **Nb:** 532 to >2500 ppm **Zr:** 2070 to 5770 ppm
Argillite		N.A.	apatite, titanite, zircon	**REE+Y:** 235.76 to 244.97 ppm **Nb:** 26.2 to 34.7 ppm **Zr:** 284 to 287 ppm

In the nepheline syenite, altered syenites, and fenites, REE, Nb, Zr bearing minerals commonly occur with thorite (see Chapter 3), and REE, Nb, and Zr content increases with Th content (see Chapter 6). The high Th and U content are reflected in the handheld gamma ray survey results (see Chapter 7). The positive correlation between Th, U, and REE content indicates that elevated eTh and eU concentrations measured by gamma ray surveys can be used to map REE mineralization and, in turn, as vectors to explore for REE mineralization on the Bandito property.

With respect to objective (3), the mechanisms controlling REE and HFSE mineralization are interpreted to be controlled by chemical reactions from autometasomatism and contact metasomatism. Within the nepheline syenite, where no nearby host contacts were observed, the REE and HFSE mineralization is associated with the altered mafic mineralogy. When hosted in quartzite, the REE and HFSE mineralization is restricted to the intrusive phases. When hosted in argillite, the REE and HFSE mineralization occurs in the both the intrusive phases and adjacent fenitized argillite (i.e., layered fenites).

General implications

The variability in composition of magmatic rock types (see Chapter 3, 4, and 6) and overlapping ages of units (see Chapter 5) indicate that the Pool Creek nepheline syenite forms a composite alkaline-silicate complex. These factors indicate that the Pool Creek nepheline syenite is a multiphase complex, i.e., it is made up of multiple intrusive phases rather than a single nepheline syenite intrusion as previously discussed in the literature (Allen et al. 2001; Pigage & Mortensen 2004; Pigage 2009). To clarify the nature of the magmatic system making up what is known as the “Pool Creek nepheline syenite”, the author recommends that the Pool Creek nepheline syenite be referred as the Pool Creek alkaline-silicate complex.

Roof zones in alkaline-silicate systems may produce Li, Be, U, Th, REE, Ti, Nb, Ta, Zr, and Zn mineralization deposited in fenite aureoles, and as lenses, sills, and late-stage veins and pegmatites (Beard et al. 2023). The nepheline syenite, altered syenite suites, and fenites discussed in Chapter 6 contain high REE, Nb, and Zr content that occur in phases such as pyrochlore, columbite, zircon, niobian titanite, niobian rutile, apatite, epidote, allanite, and bastnäsite. The petrology and mineralogy of the sample area on Pyrochlore Dome and Corundum Dome is consistent with that of a roof zone and mineralization observed in silicate roof zone type deposits. If the former statement is true, this would provide insight to the orientation of the magmatic system and the style of critical element mineralization. However, more work needs to be conducted across all the intrusive units and the host rocks to understand the magmatic and alteration system as a whole before making conclusions about the orientation of the magmatic system.

Whole rock content from the sample suite shows that REE, Nb, and Zr contents positively correlate with Th and U content, and eU and eTh measurements in the gamma ray survey match the Th and U content of the samples. These findings show that gamma ray surveys could be used to map the Neoproterozoic metasomatic alteration associated with increased REE, Nb, and Zr content within the Bandito property. Similarly, radiometric gamma ray surveys could be useful in exploring for REE, Nb, Zr mineralization in other alkaline-silicate complexes. Notably, Th and U are easily mobilized by hydrothermal alteration, therefore gamma ray surveys should not be the only method used to explore for REE, Nb, and Zr mineralization in a system that has undergone metasomatic alteration. The results of this thesis support the exploration recommendations for alkaline-silicate systems made by authors like Finch et al. (2019b) and Beard et al. (2023), where combining methods such as geophysical surveys, geochemical sampling, and petrographic studies over the entire intrusion and the adjacent host rock can be used to understand the petrogenesis and extent and controls of mineralization across the intrusion and its host, and to generate relevant models for exploration.

Future work

Field mapping, petrographic and geochemical investigations, and an airborne gamma ray geophysical survey should be conducted across the entire property to gain a more thorough understanding of the magmatic system, extent of metasomatic alteration, and the controls and distribution of REE, Nb, and Zr mineralization. A more thorough understanding of this magmatic system will contribute to the understanding of the variety of igneous phases, orientation of the magmatic system, and style of critical element mineralization and provide further insight into the tectono-magmatic history of southeast Yukon during the Neoproterozoic.

Some of the altered syenitic rock types (i.e., the actinolite-altered syenite and the altered arfvedsonite-aegirine syenite) discussed in this thesis may represent the contact metasomatism of the nepheline syenite and the respective host units (see Chapter 6 discussion). More detailed field mapping and petrographic studies should be conducted to determine whether or not the altered syenites are contact metasomatized phases of the nepheline syenite (i.e., endofenite) or if they

are distinct igneous phases that are likely genetically related to the nepheline syenite (i.e., share a common parent melt).

Bibliography

Abbott, J.G., Gordey, S.P., & Tempelman-Kluit, D.J. (1986) Setting of strati-form, sediment-hosted lead-zinc deposits in Yukon and northeastern British Columbia. *In* Mineral Deposits of Northern Cordillera (J.A. Morin ed.). Canadian Institute of Mining and Metallurgy Special Volume 37, 1–18.

Allaz, J.M., Williams, M.L., Jercinovic, M.J., Goemann, K., & Donovan, J. (2019) Multipoint background analysis: Gaining precision and accuracy in microprobe trace element analysis. *Microscopy and Microanalysis* **25**(1), 30–46.

Allen, T.L., Pigage, L.C., & MacNaughton, R.B. (2001) Preliminary geology of the Pool Creek map area (95C/5), southeastern Yukon. *In* Yukon Exploration and Geology 2000 (D.S. Emond, & L.H. Weston, eds.). Exploration and Geological Services Division, Yukon, Indian and Northern Affairs Canada, 53–72.

Andersen, T., Elburg, M., & Erambert, M. (2018) Contrasting trends of agpaitic crystallization in nepheline syenite in the Pilanesberg Alkaline Complex, South Africa. *Lithos* **312–313**, 375–388. DOI: https://doi.org/10.1016/j.lithos.2018.05.015

Andersen, T., Elburg, M., & Erambert, M. (2017) The miaskitic-to-agpaitic transition in peralkaline nepheline syenite (white foyaite) from the Pilanesberg Complex, South Africa. *Chemical Geology* **455**, 166–181. DOI: https://doi.org/10.1016/j.chemgeo.2016.08.020

Anenburg, M., Mavrogenes, J.A., Frigo, C., & Wall, F. (2020) Rare earth element mobility in and around carbonatites controlled by sodium, potassium, and silica. *Science Advances* **6**(41). DOI: https://doi.org/10.1126/sciadv.abb6570

Armstrong, J.T. (1988) Quantitative analysis of silicate and oxide materials: Comparison of Monte Carlo, ZAP, and φ(ρz) procedures. *In* Microbeam Analysis (E. Newbury, ed.). San Francisco Press, 239–246.

Atencio, D. (2021) Pyrochlore-Supergroup Minerals Nomenclature: An Update. *Frontiers in Chemistry* **9**. DOI: https://doi.org/10.3389/fchem.2021.713368

Atencio, D., Gieré, R., Andrade, M.B., Christy, A.G., & Kartashov, P.M. (2010) The pyrochlore supergroup of minerals: Nomenclature. *Canadian Mineralogist* **48**(3), 673–678. https://doi.org/10.3749/canmin.48.3.673

Aurora Geosciences Ltd. & Bruce, J.O. (2017a) Residual total magnetic field, shaded colour contour map (NTS 095C). *In* Reprocessing of Yukon magnetic data for NTS 095C. Yukon Geological Survey, Open File 2017-6, scale 1:250000, sheet 1 of 4.

Aurora Geosciences Ltd. & Bruce, J.O. (2017b) Reduced-to-pole magnetic field, shaded colour contour map (NTS 095C). *In* Reprocessing of Yukon magnetic data for NTS 095C. Yukon Geological Survey, Open File 2017-6, scale 1:250000, sheet 2 of 4.

Aurora Geosciences Ltd. & Bruce, J.O. (2017c) First vertical derivative of the reduced-to-pole magnetic field, shaded colour contour map (NTS 095C). *In* Reprocessing of Yukon magnetic data for NTS 095C. Yukon Geological Survey, Open File 2017-6, scale 1:250000, sheet 3 of 4.

Aurora Geosciences Ltd. & Bruce, J.O., (2017d) Tilt derivative of the reduced-to-pole magnetic field, shaded colour contour map (NTS 095C). *In* Reprocessing of Yukon magnetic data for NTS 095C. Yukon Geological Survey, Open File 2017-6, scale 1:250000, sheet 4 of 4.

Balashov, Y.A. & Glaznev, V.N. (2006) Cycles of alkaline magmatism. *Geochemistry International* **44**(3), 274–285. DOI: https://doi.org/10.1134/S0016702906030050

Beard, C.D., Goodenough, K.M., Borst, A.M., Wall, F., Siegfried, P.R., Deady, E.A., Pohl, C., Hutchison, W., Finch, A.A., Walter, B.F., Elliott, H.A.L., & Brauch, K. (2023) Alkaline-Silicate REE-HFSE Systems. *Economic Geology* **118**(1), 177–208. DOI: https://doi.org/10.5382/econgeo.4956

Bell, K. & Simonetti, A. (1996) Carbonatite Magmatism and Plume Activity: Implications from the Nd, Pb and Sr Isotope Systematics of Oldoinyo Lengai. *Journal of Petrology* **37**(6), 1321–1339.

Belousova, E.A., Griffin, W.L., O'Reilly, S.Y., & Fisher, N.I. (2002) Igneous zircon: Trace element composition as an indicator of source rock type. *Contributions to Mineralogy and Petrology* **143**(5), 602–622. DOI: https://doi.org/10.1007/s00410-002-0364-7

Black, L.P., Kamo, S.L., Allen, C.M., Davis, D.W., Aleinikoff, J.N., Valley, J.W., Mundil, R., Campbell, I.H., Korsch, R.J., Williams, I.S., & Foudoulis, C. (2004) Improved 206Pb/238U microprobe geochronology by the monitoring of a trace-element-related matrix effect; SHRIMP, ID-TIMS, ELA-ICP-MS and oxygen isotope documentation for a series of zircon standards. *Chemical Geology* **205**(1–2), 115–140. DOI: https://doi.org/10.1016/j.chemgeo.2004.01.003

Brögger, W.G. (1921) Die Eruptivgesteine des Kristianiagebietes, IV. Das fengebiet in Telemark, Norvegen. *Naturv. Klasse* **9**, 150–167.

Burt, P. (1983) Geological, geochemical and geophysical report on work performed during June and July of 1983 on the BEAV 1 to 180 claims. Mineral assessment report #091486. *Energy, Mines and Resources, Yukon Government*, 46 p. Available from https://yma.gov.yk.ca/091486.pdf

Byrne, K., Lesage, G., Gleeson, S.A., Piercey, S.J., Lypaczewski, P., & Kyser, K. (2020) Linking mineralogy to lithogeochemistry in the Highland Valley Copper District: Implications for porphyry copper footprints. *Economic Geology* **115**(4), 871–901. DOI: https://doi.org/10.5382/econgeo.4733

Cathro, R.J. (1983) Report on geological and geochemical surveys conducted July 12-August 17, 1982, TRANZ 1-14 claims – YA68631-YA68644, Watson Lake M.D., Yukon, claim sheet 95C/5, Latitude 60°28'N; Longitude 125°56'W. Mineral assessment report #091459. *Energy, Mines and Resources, Yukon Government*, 9 p.

Cecile, M.P., Morrow, D.W., & Williams, G.K. (1997) Early Paleozoic (Cambrian to Early Devonian) tectonic framework, Canadian Cordillera. *Bulletin of Canadian Petroleum Geology* **45**, 54–74.

Chakhmouradian, A.R. & Zaitsev, A.N. (2012) Rare Earth Mineralization in Igneous Rocks: Sources and Processes. Elements 8(5), 347–353. DOI: https://doi.org/10.2113/gselements.8.5.347

Chakhmouradian, A.R., Reguir, E.P., Kressall, R.D., Crozier, J., Pisiak, L.K., Sidhu, R., & Yang, P. (2015) Carbonatite-hosted niobium deposit at Aley, northern British Columbia (Canada): Mineralogy, geochemistry and petrogenesis. *Ore Geology Reviews* **64**, 642–666. DOI: https://doi.org/10.1016/j.oregeorev.2014.04.020

Chantler, C.T., Olsen, K., Dragoset, R.A., Chang, J., Kishore, A.R., Kotochigova, S.A., & Zucker, D.S. (2005) Detailed tabulation of atomic form factors, photoelectric absorption and scattering cross section, and mass attenuation coefficients for Z= 1-92 from E= 1-10 eV to E= 0.4-1.0 MeV. *NIST, Physical Measurement Laboratory*. DOI: https://dx.doi.org/10.18434/T4HS32

Christy, A. G. & Atencio, D. (2013) Clarification of status of species in the pyrochlore supergroup. *Mineralogical Magazine* **77**(1), 13–20. DOI: https://doi.org/10.1180/minmag.2013.077.1.02

Chudy, T. C. (2013) The petrogenesis of the Ta-bearing Fir carbonatite system, east-central British Columbia, Canada. Ph.D. Thesis, University of British Columbia. Available from https://open.library.ubc.ca/collections/ubctheses/24/items/1.0072150

Corfu, F. (2013) A century of U-pb geochronology: The long quest towards concordance. In *Bulletin of the Geological Society of America* **125**(1–2), 33–47. DOI: https://doi.org/10.1130/B30698.1

Corfu, F., Hanchar, J.M., Hoskin, P.W. O., & Kinny, P. (2003) Atlas of Zircon Textures. *Reviews in Mineralogy and Geochemistry* **53**(1), 469–500. Retrieved from http://pubs.geoscienceworld.org/msa/rimg/article- pdf/53/1/469/2946246/468. Chapter16FINAL-OCT.pdf

Culbert, R.R. (1981) Geochemical report on the THOR 1 – 22 mineral claims, Watson Lake mining district. E&B Explorations Ltd. *Yukon Department of Energy, Mines and Resources*, report #090846. Retrieved from https://yma.gov.yk.ca/090846.pdf

Culligan, K. (2011) The Geochemistry and Mineralogy of the Ting Creek Alkalic Intrusion, Yukon Territory. B.Sc. thesis, University of British Columbia.

Decrée, S., Boulvais, P., Cobert, C., Baele, J.M., Midende, G., Gardien, V., Tack, L., Nimpagaritse, G., & Demaiffe, D. (2015) Structurally-controlled hydrothermal alteration in the syntectonic Neoproterozoic Upper Ruvubu Alkaline Plutonic Complex (Burundi): Implications for REE and HFSE mobilities. *Precambrian Research* **269**, 281–295. DOI: https://doi.org/10.1016/j.precamres.2015.08.016

Howie, R.A., Zussman, J., & Deer, W. (1992) *An introduction to the rock-forming minerals (second edition)*. Longman, London, UK. 696 p.

Donovan, J.J., Snyder, D.A., & Rivers, M.L. (1993) An improved interference correction for trace element analysis. *Microbeam Analysis* **2**, 23–28.

Douglas, R.J.W. & Norris, D.K. (1959) Fort Liard and La Biche map Areas, Northwest Territories and Yukon, 095b and 095c. *Geological Survey of Canada* 59-6, 28 p. (2 sheets). DOI: doi.org/10.4095/101240

Douglas, R.J.W. (1976) Geology, La Biche River, Yukon Territory-District of Mackenzie. Geological Survey of Canada, Map 1380A, scale 1:250 000.

Droop, G.T.R. (1987) A general equation for estimating Fe3+ concentrations in ferromagnesian silicates and oxides from microprobe analyses, using stoichiometric criteria. *Mineralogical magazine* **51**(361), 431–435.

Dunn, S.C., & von der Heyden, B.P. (2022) Proterozoic – Paleozoic orogenic gold mineralization along the southwestern margin of the Tanzania Craton: A review. *Journal of African Earth Sciences* **185**. DOI: https://doi.org/10.1016/j.jafrearsci.2021.104400

Dyhr, C.T. & Holm, P.M. (2010) A volcanological and geochemical investigation of Boa Vista, Cape Verde Islands; 40Ar/39Ar geochronology and field constraints. *Journal of Volcanology and Geothermal Research* **189**(1–2), 19–32. DOI: https://doi.org/10.1016/j.jvolgeores.2009.10.010

Eby, G.N. (1990). The A-type granitoids: A review of their occurrence and chemical characteristics and speculations on their petrogenesis. *Lithos* **26**(1–2), 115–134. DOI: https://doi.org/10.1016/0024-4937(90)90043-Z

Elburg, M.A. & Cawthorn, R.G. (2017) Source and evolution of the alkaline Pilanesberg Complex, South Africa. *Chemical Geology* **455**, 148–165. DOI: https://doi.org/10.1016/j.chemgeo.2016.10.007

Elliott, H.A.L., Wall, F., Chakhmouradian, A.R., Siegfried, P.R., Dahlgren, S., Weatherley, S., Finch, A.A., Marks, M.AW., Dowman, E., & Deady, E. (2018) Fenites associated with carbonatite complexes: A review. Ore Geology Reviews 93, 38–59, DOI: doi.org/10.1016/j.oregeorev.2017.12.003

Endurance Gold Corporation (2018a) Bandito, Yukon Territory, Canada, Syenite Hosted Heavy Rare Earth-Niobium & Sediment Hosted Nickel-Copper (Cobalt). Technical report. Available online: http://www.endurancegold.com/Bandito/Technical/Bandito%20Executive%20Summary%20Feb%202018.pdf [accessed on 10 September, 2020].

Endurance Gold Corporation (2018b) The Bandito Intrusive Related Rare Earth-Niobium (Nickel-Copper) Project, Yukon. Presentation. Available online: http://www.endurancegold.com/Bandito/EDG_Bandito_May_2018.pdf [accessed on 10 September, 2020].

Endurance Gold Corporation (2023) The Bandito Intrusive Related Rare Earth-Niobium (Nickel-Copper) Project, Yukon. Presentation. Available online: https://endurancegold.com/site/assets/files/7813/edgpp_bandito_jan17_2023.pdf [accessed on 31 March, 2023].

Erdi-Krausz, G., Matolin, M., Minty, B., Nicolet, J.P., Reford, W.S., & Schetselaar, E.M. (2003) Guidelines for radioelement mapping using gamma ray spectrometry data. *International Atomic Energy Agency* **1363**. Available online: http://www-pub.iaea.org/MTCD/publications/PDF/te_1363_web.pdf

Estrade, G., Béziat, D., Salvi, S., Tiepolo, M., Paquette, J.L., & Rakotovao, S. (2014) Unusual evolution of silica-under- and -oversaturated alkaline rocks in the Cenozoic Ambohimirahavavy Complex (Madagascar): Mineralogical and geochemical evidence. *Lithos* **206–207**(1), 361–383. https://doi.org/10.1016/j.lithos.2014.08.008

Fallas, K.M., Pigage, L.C., & MacNaughton, R.B. (2004) Geology, southwest La Biche River (95C/SW), Yukon Territory and British Columbia. Geological Survey of Canada, Open File 4664 (scale 1:100 000, 2 sheets).

Fallas, K.M., Lane, L.S., & Pigage, L.C. (2014) Geology, La Biche River, Yukon–Northwest Territories; Geological Survey of Canada, Canadian Geoscience Map 144, scale 1:250 000. DOI: doi:10.4095/29460

Finch, A.A., Hutchison, W., Borst, A.M., Horsburgh, N.J., & Stüecken, E.E. (2019) The architecture and geochemistry of magmatic roof zones: implications for mineralization and exploration. *In* Life with Ore Deposits on Earth – 15th SGA Biennial Meeting **1-4**, 1712–1715.

Finch, A.A., McCreath, J.A., Reekie, C.D.J., Hutchison, W., Ismaila, A., Armour-Brown, A., Andersen, T., & Simonsen, S.L. (2019) From Mantle to Motzfeldt: A genetic model for syenite-hosted Ta, Nb-mineralisation. *Ore Geology Reviews* **107**, 402–416. DOI: https://doi.org/10.1016/j.oregeorev.2019.02.032

Frost, B.R. & Frost, C.D. (2008) A geochemical classification for feldspathic igneous rocks. *Journal of Petrology* **49**(11), 1955–1969. DOI: https://doi.org/10.1093/petrology/egn054

Frost, C.D. & Frost, B.R. (2011) On ferroan (A-type) granitoids: Their compositional variability and modes of origin. *Journal of Petrology* **52**(1), 39–53. DOI: https://doi.org/10.1093/petrology/egq070

Gadd, M.G., Layton-Matthews, D., Peter, J.M., & Paradis, S.J. (2016) The world-class Howard's Pass SEDEX Zn-Pb district, Selwyn Basin, Yukon. Part I: trace element compositions of pyrite record input of hydrothermal, diagenetic, and metamorphic fluids to mineralization. *Mineralium Deposita* **51**(3), 319–342.

Gadd, M.G., Peter, J.M., Jackson, S.E., Yang, Z., & Petts, D. (2019) Platinum, Pd, Mo, Au and Re deportment in hyper-enriched black shale Ni-Zn-Mo-PGE mineralization, Peel River, Yukon, Canada. *Ore Geology Reviews* **107**, 600–614.

Geisler, T., Pidgeon, R.T., van Bronswijk, W., & Kurtz, R. (2002) Transport of uranium, thorium, and lead in metamict zircon under low-temperature hydrothermal conditions. *Chemical Geology* **191**, 141–154.

Geisler, T., Pidgeon, R.T., Kurtz, R., van Bronswijk, W., & Schleicher, H. (2003) Experimental hydrothermal alteration of partially metamict zircon. *American Mineralogist* **88**(10), 1496–1513. DOI: https://doi.org/10.2138/am-2003-1013

Geological Survey of Canada (1993) Yukon and Northwest Territories. *Geological Survey of Canada*, Open File 2733 (1 sheet). DOI: https://doi.org/10.4095/183958

Goldoff, B., Webster, J.D., & Harlov, D.E. (2012) Characterization of fluor-chlorapatites by electron probe microanalysis with a focus on time-dependent intensity variation of halogens. *American Mineralogist* **97**(7), 1103–1115. DOI: https://doi.org/10.2138/am.2012.3812

Goodfellow, W.D., Cecile, M.P., & Leybourne, M.I. (1995) Geochemistry, petrogenesis, and tectonic setting of lower Paleozoic alkalic and potassic volcanic rocks, Northern Canadian Cordilleran Miogeocline. *Canadian Journal of Earth Sciences* **32**, 1236–1254.

Grasby, S., Ferguson, G., Brady, A., Sharp, C., Dunfield, P., & McMechan, M. (2016) Deep Groundwater Circulation through Gas Shales in Mountain Belts. *Procedia Earth and Planetary Science* **17**, 532–533. DOI: https://doi.org/10.1016/j.proeps.2016.12.134

Greene, A.R., Scoates, J.S., Weis, D. and Israel, S., (2005) Flood basalts of the Wrangellia Terrane, southwest Yukon: Implications for the formation of oceanic plateaus, continental crust and Ni-CuPGE mineralization. *In* Yukon Exploration and Geology 2004 (D.S. Emond, L.L. Lewis and G.D. Bradshaw, eds.), Yukon Geological Survey, 109–120. Available from https://publications.gc.ca/collections/Collection/R71-41-2004E(11).pdf

Gregory, D. (2008) Assessment Report Describing Prospecting, Mapping and Geochemical Sampling at the Trani Property. Strategic Metals Ltd. Report #094903. Available from https://data.geology.gov.yk.ca/AssessmentReport/094903#InfoTab

Grimes, C.B., Wooden, J.L., Cheadle, M.J., & John, B.E. (2015) "Fingerprinting" tectono-magmatic provenance using trace elements in igneous zircon. *Contributions to Mineralogy and Petrology* **170**(5–6), 1–26. DOI: https://doi.org/10.1007/s00410-015-1199-3

Haldar, S.K. (2018) *Mineral Exploration: principles and applications*. Elsevier, Amsterdam, The Netherlands. DOI: https://doi.org/10.1016/b978-0-12-814022-2.00005-8

Harrison, J.C. (1982) Petrology of the 'Ting Creek' alkalic intrusion, southeast Yukon. Unpublished M.Sc. thesis, University of Toronto, Ontario, 299 p.

Hart, C.J., Goldfarb, R.J., Lewis, L.L., & Mair, J.L. (2004) The Northern Cordilleran Mid-Cretaceous plutonic province: Ilmenite/magnetite-series granitoids and intrusion-related mineralisation. *Resource Geology* **54**(3), 253–280.

Hawthorne, F.C., Oberti, R., Harlow, G.E., Maresch, W.v., Martin, R.F., Schumacher, J.C., & Welch, M. D. (2012) IMA Report: Nomenclature of the amphibole supergroup. *American Mineralogist* **97**(11–12), 2031–2048. DOI: https://doi.org/10.2138/am.2012.4276

Hayward, N. (2015) Geophysical investigation and reconstruction of lithosphericstructure and its control on geology, structure, and mineralization in the Cordillera of northernCanada and eastern Alaska. *AGU Publications* **10**, 2165–2189. DOI: doi.org/10.1002/2015TC003871

Heffernan, R.S. (2004) Temporal, geochemical, isotopic, and metallogenic studies of mid-Cretaceous magmatism in the Tintina Gold Province, southeastern Yukon and southwestern Northwest Territories, Canada. M.Sc. thesis, University of British Columbia, 83 p.

Heinrich, E.W. (1966) *The geology of carbonatites*. Rand McNally & Co., Chicago, Illinois.

Heinrich, E.W. (1985) Infinite variations on a fenite theme. *The Indian Mineralogist*, 151–162.

Hey, M.H. (1954) A new review of the chlorites. Mineralogical Magazine and Journal of the *Mineralogical Society* **30**(224), 277–292.

Hinton, R.W. & Upton, B.G.J. (1991) The chemistry of zircon: Variations within and between large crystals from syenite and alkali basalt xenoliths. *Geochimica Et Cosmochimica Acta* **55**(11), 3287–3302. DOI: https://doi.org/10.1016/0016-7037(91)90489-R

Hinze, W.J., Von Frese, R.R.B., and Saad, A.H. (2013) *Gravity and Magnetic Exploration: Principles, Practices and Applications*. Cambrige Univsersity Press.

Hogarth, D. D. (1977). Classification and nomenclature of the pyrochlore group. *American Mineralogist* **62**(5-6), 403–410.

Horie, K., Hidaka, H., & Gauthier-Lafaye, F. (2006) Elemental distribution in zircon: Alteration and radiation-damage effects. *Physics and Chemistry of the Earth* **31**(10–14), 587–592. DOI: https://doi.org/10.1016/j.pce.2006.01.001

Hoskin, P.W.O. (2005) Trace-element composition of hydrothermal zircon and the alteration of Hadean zircon from the Jack Hills, Australia. *Geochimica et Cosmochimica Acta* **69**(3), 637–648. DOI: https://doi.org/10.1016/j.gca.2004.07.006

Iddings, J.P. (1892). The origin of igneous rocks. *Bulletin of the Philosophical Society of Washington* **12**, 89–214.

Irvine, T.N. & Baragar, W.R.A. (1971) A Guide to the Chemical Classification of the Common Volcanic Rocks. *Canadian Journal of Earth Science* **8**, 523–548.

Jaffey A.H., Flynn K.F., Glendenin L.E., Bentley W.C., & Essling A.M. (1971) Precision measurement of half-lives and specific activities of 235U and 238U. *Physical Review C* **4**(5),1889–1906. DOI: doi:http:// dx.doi.org/10.1103/PhysRevC.4.1889

Khomyakov, A. (1995) *Mineralogy of Hyperagpaitic Alkaline Rocks*. Oxford Scientific Publications. Clarendon Press, Oxford, 222 p.

Kirkland, C.L., Smithies, R.H., Taylor, R.J. M., Evans, N., & McDonald, B. (2015) Zircon Th/U ratios in magmatic environs. *Lithos* **212–215**, 397–414. DOI: https://doi.org/10.1016/ j.lithos.2014.11.021

Košler, J. & Sylvester P.J. (2003) Present Trends and the Future of Zircon in Geochronology: Laser Ablation ICPMS. *Reviews in Mineralogy and Geochemistry* **53**(1): 243–275. DOI: https://doi.org/10.2113/0530243

Kramm, U. & Kogarko, L.N. (1994) Nd and Sr isotope signatures of the Khibina and Lovozero agpaitic centres, Kola Alkaline province, Russia. *Lithos* **32**(3–4), 225–242. DOI: https://doi.org/10.1016/0024-4937(94)90041-8

Krishnamurthy, P. (2019) Carbonatites of India. *Journal of the Geological Society of India* **94**(2), 117–138. DOI https://doi.org/10.1007/s12594-019-1281-y

Kubeš, M., Leichmann, J., Wertich, V., Mozola, J., Holá, M., Kanický, V., & Škoda, R. (2021) Metamictization and fluid-driven alteration triggering massive HFSE and REE mobilization from zircon and titanite: Direct evidence from EMPA imaging and LA-ICP-MS analyses. *Chemical Geology* **586**. DOI: https://doi.org/10.1016/j.chemgeo.2021.120593

Le Bas, M.J. (2008) Fenites Associated with Carbonatites. *The Canadian Mineralogist* **46**(4), 915–932. DOI: https://doi.org/10.3749/canmin.46.4.915

Le Bas, M.J., le Maitre, R.W., Streckeisen, A., & Zanettin, B. (1986) A chemical classification of volcanic rocks based on the total alkali-silica diagram. *Journal of Petrology* **27**(3), 745–750. DOI: https://doi.org/10.1093/petrology/27.3.745

Le Maitre, R.W (2002) *Igneous Rocks: A Classification and Glossary of Terms: Recommendations of the International Union of Geological Sciences Subcommission on the Systematics of Igneous Rocks*. Cambridge, Cambridge University Press. DOI: 10.1017/CBO9780511535581.

Leake, B.E., Woolley, A.R., Arps, C.E.S, Birch, W.D., Gilbert, M.C., Grice, J.D., Hawthorne, F.C., Kato, A., Kisch, H.J., Krivovichev, V.G., Linthout, K., Laird, J., Mandarino, J.A., Maresch, W.V., Nickel, E.H., Rock, N.M.S., Schumacher, J.C., Smith, D.C., Stephenson, N.C.N., Ungaretti, L., Whittaker, E.J.W., & Youzhi, G. (1997) Nomenclature of amphiboles; report of the subcommittee on amphiboles of the International Mineralogical Association, Commission on New Minerals and Mineral Names. *The Canadian Mineralogist* **35**(1), 219–246. DOI: doi: 10.1180/minmag.1997.061.405.13.

Lee, W.-J. & Wyllie, P.J. (1998) Processes of Crustal Carbonatite Formation by Liquid Immiscibility and Differentiation, Elucidated by Model Systems. *Journal of Petrology* **39**, 2005–2013. DOI: https://doi.org/10.1093/petroj/39.11-12.2005

Locock, A.J. (2014) An Excel spreadsheet to classify chemical analyses of amphiboles following the IMA 2012 recommendations. *Computers & Geosciences* **62**, 1–11.

Ludwig, K.R. (2003) User's manual for IsoPlot 3.0. A geochronological toolkit for Microsoft Excel, 71.

Lund, K. (2008) Geometry of the Neoproterozoic and Paleozoic rift margin of western Laurentia: Implications for mineral deposit settings. *Geological Society of America* **4**, 429–444. DOI: https://doi.org/10.1130/GES00121.1

MacDonald, G.A. (1968) Composition and Origin of Hawaii Lavas. *Geological Society of America Memoir*s **116**, 477–522. DOI: http://dx.doi.org/10.1130/MEM116-p477

MacNaughton, R.B. (2017) An unnamed Proterozoic map unit, Pool Creek map area (NTS 95C/5), southeasternmost Yukon. *In* Central Foreland NATMAP Project: Proterozoic to

Devonian stratigraphic sections in British Columbia and Yukon (L.S. Lane & R.B. MacNaughton, eds.) Geological Survey of Canada, Bulletin 603, 205–222. DOI: https://doi.org/10.4095/299867

Macnaughton, R.B., Pigage, L.C., & Allen, T.L. (2017) Sedimentology and regional significance of the 'argillite unit', a probable Cryogenian map unit in southeast Yukon, Canada. *Geological Journal* **52**, 369–393. DOI: https://doi.org/10.1002/gj.2765

Maniar, P.D. & Piccoli, P.M (1989) Tectonic discrimination of granitoids. *Geological Society of America Bulletin* **101**, 635–643.

Marillo-Sialer, E., Woodhead, J., Hanchar, J.M., Reddy, S.M., Greig, A., Hergt, J., & Kohn, B. (2016) An investigation of the laser-induced zircon "matrix effect." *Chemical Geology* **438**, 11–24. DOI: https://doi.org/10.1016/j.chemgeo.2016.05.014

Marks, M.A.W. & Markl, G., (2015) The Ilímaussaq alkaline complex, South Greenland. *In* Layered Intrusions (Charlier, B., Namur, O., Latypov, R., Tegner, C., eds.). Springer Geology, Dordrecht, 649–691.

Marks, M.A.W. & Markl, G. (2017) A global review on agpaitic rocks. *Earth-Science Reviews* **173**, 229–258. DOI: https://doi.org/10.1016/j.earscirev.2017.06.002

Markl, G., Marks, M.A.W., & Frost, B.R. (2010) On the controls of oxygen fugacity in the generation and crystallization of peralkaline rocks. *Journal of Petrology* **51**, 1831–1847.

Marks, M.A.W., Hettmann, K., Schilling, J., Frost, B.R., & Markl, G. (2011) The mineralogical diversity of alkaline igneous rocks: Critical factors for the transition from miaskitic to agpaitic phase assemblages. *Journal of Petrology* **52**(3), 439–455. DOI: https://doi.org/10.1093/petrology/egq086

Marsellos, A.E. & Garver, J.I. (2010) Radiation damage and uranium concentration in zircon as assessed by Raman spectroscopy and neutron irradiation. *American Mineralogist* **95**(8–9), 1192–1201. DOI: https://doi.org/10.2138/am.2010.3264

Mattinson, J.M., Graubard, C.M., Parkinson, D.L., & McClelland, W.C. (1996) U-Pb reverse discordance in zircons: the role of fine-scale oscillatory zoning and sub-micron transport of Pb. *Geophysical Monograph-American Geophysical Union* **95**, 355–370.

McCreath, J.A., Finch, A.A., Simonsen, S.L., Donaldson, C.H., & Armour-Brown, A. (2012) Independent ages of magmatic and hydrothermal activity in alkaline igneous rocks: The Motzfeldt Centre, Gardar Province, South Greenland. *Contributions to Mineralogy and Petrology* **163**(6), 967–982. DOI: https://doi.org/10.1007/s00410-011-0709-1

McDonough, W. & Sun, S.S. (1995) The composition of the Earth. *Chemical Geology* **120**, 223–253.

Mezger, K. & Krogstad, E.J. (1997) Interpretation of discordant U-Pb zircon ages: An evaluation. *Journal of metamorphic Geology* **15**(1), 127–140.

Middlemost, E.A.K. (1994) Naming materials in the magma/igneous rock system. *Earth-Science Reviews* **37**, 215–224.

Millonig, L.J., Gerdes, A., & Groat, L.A. (2012) U-Th-Pb geochronology of meta-carbonatites and meta-alkaline rocks in the southern Canadian Cordillera: A geodynamic perspective. *Lithos* **152**, 202–217.

Mitchell, R. H. (2005) Carbonatites and carbonatites and carbonatites. *Canadian Mineralogist* **43**(6), 2049–2068. DOI: https://doi.org/10.2113/gscanmin.43.6.2049

Möller, V. & Williams-Jones, A. E. (2016) Petrogenesis of the Nechalacho Layered Suite, Canada: Magmatic Evolution of a REE-Nb-rich Nepheline Syenite Intrusion. *Journal of Petrology* **57**(2), 229–276. DOI: https://doi.org/10.1093/petrology/egw003

Monger, J. & Price, R. (2002) The Canadian Cordillera: geology and tectonic evolution. *Canadian Society of Exploration Geophysicists Recorder*, 17–36.

Monier, G. & Robert, J.L. (1986) Muscovite solid solutions in the system K_2O–MgO–FeO–Al_2O_3–SiO_2–H_2O: an experimental study at 2 kbar P_{H2O} and comparison with natural Li-free white micas. *Mineralogical Magazine* **50**, 257–266.

Morales, I., Molina, J.F., Cambeses, A., Montero, P., & Bea, F. (2022) Experimental Annealing of Zircon: Influence of Inclusions on Stability, Intracrystalline Melt Migration, Common Lead Leaching, and Permeability to Fluids. *ACS Earth and Space Chemistry* **6**(2), 288–307. DOI: https://doi.org/10.1021/acsearthspacechem.1c00212

Morogan, V. (1994) Ijolite versus carbonatite as sources of fenitization. *Terra Nova* **6**(2), 166–176. DOI: https://doi.org/10.1111/j.1365-3121.1994.tb00650.x

Morrow, D.W. & Miles, W.C. (2000) The Beaver River Structure: a cross-strike discontinuity of possible crustal dimensions in the southern Mackenzie Fold Belt, Yukon and Northwest territories, Canada. *Bulletin of Canadian Petroleum Geology* **47**, 19–29.

Nasraoui, M. & Bilal, E. (2000) Pyrochlores from the Lueshe carbonatite complex (Democratic Republic of Congo): a geochemical record of different alteration stages. *Journal of Asian Earth Sciences* **18**(2), 237–251.

Nielsen, T.F.D. and Rosing, M.T., 1990. The Archaean Skjoldungen alkaline province, South-East Greenland. *Rapport Grønlands Geologiske Undersøgelse* **148**, 93–100.

Parker, D.F., Ren, M., Adams, D.T., Tsai, H., & Long, L.E. (2012) Mid-Tertiary magmatism in western Big Bend National Park, Texas, U.S.A.: Evolution of basaltic source regions and

generation of peralkaline rhyolite. *Lithos* **144–145**, 161–176. DOI: https://doi.org/10.1016/j.lithos.2012.04.019

Paton, C., Woodhead, J.D., Hellstrom, J.C., Hergt, J.M., Greig, A., & Maas, R. (2010) Improved laser ablation U-Pb zircon geochronology through robust downhole fractionation correction. *Geochemistry, Geophysics, Geosystems* **11**(3).

Paton, C., Hellstrom, J., Paul, B., Woodhead, J., & Hergt, J. (2011) Iolite: Freeware for the visualisation and processing of mass spectrometric data. *Journal of Analytical Atomic Spectrometry* **26**(12), 2508–2518.

Peacock, M.A. (1931) Classification of igneous rock series. *Journal of Geology* **39**(1), 54–67. DOI: https://doi.org/10.1086/623788.

Pearce, J.A. (1996) A user's guide to basalt discrimination diagrams. *In* Trace element geochemistry of volcanic rocks: applications for massive sulphide exploration (D.A. Wyman, ed.). Geological Association of Canada, Short Course Notes **12**, 79–113.

Pearce, J.A., Harris, N.B.W., & Tindle, A.G. (1984) Trace element discrimination diagrams for the tectonic interpretation of granitic rocks. *Journal of Petrology* **25**, 956–983.

Pearce, N.J., Perkins, W.T., Westgate, J.A., Gorton, M.P., Jackson, S.E., Neal, C.R., & Chenery, S.P. (1997) A compilation of new and published major and trace element data for NIST SRM 610 and NIST SRM 612 glass reference materials. *Geostandards Newsletter* **21**(1), 115–144.

Pell, J. (1987) Alkaline Ultrabasic Rocks in British Columbia: Carbonatites, Nepheline Syenites, Kimberlites and Related Rocks. B.C. *Ministry of Energy, Mines and Petroleum Resources*. Open File, 109.

Pell, J. (1994) Carbonatites, nepheline syenites, kimberlites and related rocks in British Columbia. *Ministry of Energy, Mines and Petroleum Resources*, Bulletin **88**. Available from https://cmscontent.nrs.gov.bc.ca/geoscience/publicationcatalogue/Bulletin/BCGS_B088.pdf

Petrík, I., Broska, I., Lipka, J., & Siman, P. (1995) Granitoid allanite-(Ce): substitution relations, redox conditions and REE distributions (on an example of I-type granitoids, western Carpathians, Slovakia). *Geologica Carpathica* **46**, 79–94.

Pfaff, K., Krumrei, T., Marks, M., Wenzel, T., Rudolf, T., & Markl, G. (2008) Chemical and physical evolution of the 'lower layered sequence' from the nepheline syenitic Ilímaussaq intrusion, South Greenland: implications for the origin of magmatic layering in peralkaline felsic liquids. *Lithos* **106**, 280–296.

Pigage, L.C. & Allen T.L. (2001) Geological map of Pool Creek (NTS 95C/5), southeastern Yukon (1:50 000 scale). Exploration and Geological Services Division, Yukon Region, Indian and Northern Affairs Canada, Open File 2001-32.

Pigage, L.C. & Mortensen, J.K. (2004) Superimposed Neoproterozoic and Early Tertiary alkaline magmatism in the La Biche River area, southeast Yukon Territory. *Bulletin of Canadian Petroleum Geology* **52**, 325–342.

Pigage, L. (2008) Geological map of the Pool Creek area (NTS 95C/5), southeast Yukon. *Yukon Geological Survey*, Geoscience Map 2008-1.

Pigage, L.C. (2009) Bedrock geology of NTS95C/5 (Pool Creek) and NTS95D/8 map sheets, southeast Yukon. *Yukon Geological Survey*, Bulletin **16**, 150 p.

Pigage, L.C., Crowley, J.L., Roots, C.F., & Abbott, J.G. (2014) Geochemistry and U-Pb zircon geochronology of mid-Cretaceous Tay River suite intrusions in southeast Yukon. *In* Yukon Exploration and Geology 2014, (K.E. MacFarlane, M.G. Nordling, & P.J. Sack, eds.), Yukon Geological Survey, Canada, 169–194.

Radiation Solutions Inc. (2015) RS-125/230 User Manual – Revision 1.05. Available from https://www.aseg.org.au/sites/default/files/RS-125%20RS-230_User_Manual%20%28GR%29.pdf

Rasmussen, K.L. (2013) The timing, composition, and petrogenesis of syn- to post-accretionary magmatism in the northern Cordilleran miogeocline, eastern Yukon and southwestern Northwest Territories. Ph.D. thesis, University of British Columbia, 788 p.

Rasmussen, K.L., Mortensen, J.K., Falck, H., & Ullrich, T.D. (2007) The potential for intrusion-related mineralization within the South Nahanni MERA area, Selwyn and Mackenzie Mountains, Northwest Territories. *In* Mineral and energy resource assessment of the Greater Nahanni Ecosystem under consideration for the expansion of the Nahanni National Park Reserve, Northwest Territories. Geological Survey of Canada, Open File 5344, 203–278.

Regnery, J., Stoll, B., & Peter Jochum, K. (2010) High-resolution LA-ICP-MS for accurate determination of low abundances of K, Sc and other trace elements in geological samples. *Geostandards and Geoanalytical Research* **34**(1), 19–38. DOI: https://doi.org/10.1111/j.1751-908X.2009.00025.x

Roddick, J.A. (1967) Tintina Trench. *Journal of Geology* **75**, 23–33, DOI: https://doi.org/10.1086/627228.

SatisGeo (2007). Kappameter KT-6 Intrusction Manual. Available from https://manualzz.com/doc/12227954/kt--6-table-of-contents-kappameter

Schmid, R., Fettes, D., Harte, B., Davis, E., & Desmons, J. (2007) How to name a metamorphic rock. *In* Metamorphic Rocks: A Classification and Glossary of Terms: Recommendations of the International Union of Geological Sciences Subcommission on the Systematics of Metamorphic Rocks (D. Fettes & J. Desmons, eds.). Cambridge University Press, Cambridge, 3–15.

Shand, S.J. (1927) *Eruptive Rocks*. Thomas Murby & Co., London.

Shives, R.B.K., 2015. Using gamma ray spectrometry to fi nd rare metals. *In* Symposium on Strategic and Critical Materials Proceedings, November 13-14, 2015, Victoria, British Columbia (G.J. Simandl, & M. Neetz, eds.). British Columbia Ministry of Energy and Mines, British Columbia Geological Survey Paper 2015-3, 199–209. Available from https://cmscontent.nrs.gov.bc.ca/geoscience/PublicationCatalogue/Paper/BCGS_P2015-03-23_Shives.pdf

Shives, R. (2017) Gamma Ray Spectrometry: Exploration, Environment, Health and Safety. Minerals North Conference, Prince George Conference and Civic Centre, April 26, 2017. Available from http://mineralsnorth.ca/images/uploads/pdf/2017_Shives_Gamma_Ray_Spectrometry.pdf

Sindern, S. & Kramm, U. (2000) Volume characteristics and element transfer of fenite aureoles: A case study from the Iivaara alkaline complex, Finland. *Lithos* **51**(1–2), 75–93. DOI: https://doi.org/10.1016/S0024-4937(99)00075-4

Sjöqvist, A.S.L., Cornell, D.H., Andersen, T., Christensson, U.I., & Berg, J.T. (2017) Magmatic age of rare-earth element and zirconium mineralisation at the Norra Kärr alkaline complex, southern Sweden, determined by U–Pb and Lu–Hf isotope analyses of metasomatic zircon and eudialyte. *Lithos* **294–295**, 73–86. DOI: https://doi.org/10.1016/j.lithos.2017.09.023

Sokół, K., Finch, A. A., Hutchison, W., Cloutier, J., Borst, A. M., & Humphreys, M. C. (2022) Quantifying metasomatic high-field-strength and rare-earth element transport from alkaline magmas. *Geology* **50**(3), 305–310. DOI: https://doi.org/10.1130/G49471.1

Sláma, J., Košler, J., Condon, D.J., Crowley, J.L., Gerdes, A., Hanchar, J.M., Horstwood, M.S. A., Morris, G.A., Nasdala, L., Norberg, N., Schaltegger, U., Schoene, B., Tubrett, M.N., & Whitehouse, M.J. (2008) Plešovice zircon - A new natural reference material for U-Pb and Hf isotopic microanalysis. *Chemical Geology* **249**(1–2), 1–35. DOI: https://doi.org/10.1016/j.chemgeo.2007.11.005

Soman, A., Geisler, T., Tomaschek, F., Grange, M., & Berndt, J. (2010) Alteration of crystalline zircon solid solutions: A case study on zircon from an alkaline pegmatite from Zomba-Malosa, Malawi. *Contributions to Mineralogy and Petrology* **160**(6), 909–930. DOI: https://doi.org/10.1007/s00410-010-0514-2

Sørensen, H. (1997) The agpaitic rocks - an overview. *Mineralogical Magazine* **61**(407), 485–498. DOI: https://doi.org/10.1180/minmag.1997.061.407.02

Steely, A.N., Hourigan, J.K., & Juel, E. (2014) Discrete multi-pulse laser ablation depth profiling with a single-collector ICP-MS: Sub-micron U-Pb geochronology of zircon and the effect of radiation damage on depth-dependent fractionation. *Chemical Geology* **372**, 92–108. DOI: https://doi.org/10.1016/j.chemgeo.2014.02.021

Stevens, R.D., Delabio, R.N., & Lachance, G.R. (1982) Age determinations and geological studies K-Ar isotopic ages, report 15. *Geological Survey of Canada* **81-2**, 56 p. DOI: https://doi.org/10.4095/119043

Stone, P. (1999a) Aeromagnetic Total Field Map, Yukon; NTS 95 C/NW scale 1:100,000. Geological Survey of Canada Open File 3199, 1 sheet. DOI https://doi.org/10.4095/211424

Stone, P. (1999b) Aeromagnetic Total Field Map, Yukon; NTS 95 C/NE scale 1:100,000. Geological Survey of Canada Open File 3199, 1 sheet. DOI: https://doi.org/10.4095/211425

Stone, P. (1999c) Aeromagnetic Total Field Map, Yukon; NTS 95 C/SW scale 1:100,000. Geological Survey of Canada Open File 3199, 1 sheet. DOI: https://doi.org/10.4095/211430

Stone, P. (1999d) Aeromagnetic Total Field Map, Yukon; NTS 95 C/SE scale 1:100,000. Geological Survey of Canada Open File 3199, 1 sheet. DOI: https://doi.org/10.4095/211431

Sun, S.S. & McDonough, W.F. (1989) Chemical and isotopic systematics of oceanic basalts; implications for mantle composition and processes. *Geological Society Special Publications* **42**, 313 – 345.

Sun, S. & McDonough, W.F. (1989) Chemical and isotopic systematics of oceanic basalts: implications for mantle composition and processes. *In* Magmatism in the Ocean Basins (A.D. Saunders & M.J. Norry, eds.). Geological Society of London, Special Publications Number 42, 313–345.

Swanton, D. (2011) 2010 Geochemical Work Report on the Bandito Project. Endurance Gold Corporation. Yukon Energy, Mines, and Resources assessment report #095303.

Swanton, D. (2012) 2011 Geological and Geochemical Work Report on the Bandito Project. Endurance Gold Corporation. Yukon Energy, Mines, and Resources assessment report #095454.

Tilley, C.E. (1950) Some aspects of magmatic evolution. Quarterly Journal of the Geological Society of London. 106, 37–61.

Upton, B.G.J., Emeleus, C.H., Heaman, L.M., Goodenough, K.M., & Finch, A.A. (2003). Magmatism of the mid-Proterozoic Gardar Province, South Greenland: Chronology, petrogenesis and geological setting. *Lithos* **68**(1–2), 43–65. DOI: https://doi.org/10.1016/S0024-4937(03)00030-6

Ussing, N.V., (1912) Geology of the country around Julianehaab, Greenland. Meddelelser om Grønland. *Kjøbehavn* **38**, 1–426.

Utsunomiya, S., Valley, J.W., Cavosie, A.J., Wilde, S.A., & Ewing, R.C. (2007) Radiation damage and alteration of zircon from a 3.3 Ga porphyritic granite from the Jack Hills, Western Australia. Chemical *Geology* **236**(1–2), 92–111. DOI: https://doi.org/10.1016/j.chemgeo.2006.09.003

Velasco, F., Herrero, J. M., Suárez, S., Yusta, I., Alvaro, A., & Tornos, F. (2013) Supergene features and evolution of gossans capping massive sulphide deposits in the Iberian Pyrite Belt. *Ore Geology Reviews* **53**, 181–203. DOI: https://doi.org/10.1016/j.oregeorev.2013.01.008

ver Hoeve, T.J., Scoates, J.S., Wall, C.J., Weis, D., & Amini, M. (2018) A temperature-composition framework for crystallization of fractionated interstitial melt in the Bushveld Complex from trace element systematics of zircon and rutile. *Journal of Petrology* **59**(7), 1383–1416. DOI: https://doi.org/10.1093/petrology/egy066

Vernon, R.H. (2018) *A practical guide to rock microstructure (second edition)*. Cambridge University Press. DOI: https://doi.org/10.1017/9781108654609

Verwoerd, W.J., (1966) South African carbonatites and their probable mode of origin. *Annale van die Uniwersiteit van Stellenbosch. Reeks A* **41**(2) 121–233.

Vetrin, V.R. & Skublov, S.G. (2016) Trace elements in various genetic types of zircon from syenite of the Sakharjok massif, Kola Peninsula. *Geology of Ore Deposits* **58**(7), 542–550. DOI: https://doi.org/10.1134/S1075701516070126

von Eckermann, H. (1948) *The alkaline district of Alnö Island (Alnö alkalina område)*. No. 36 in Sveriges Geologiska Undersökning. Esselte, Stockholm.

Walter, B.F., Parsapoor, A., Braunger, S., Marks, M.A.W., Wenzel, T., Martin, M., & Markl, G. (2018) Pyrochlore as a monitor for magmatic and hydrothermal processes in carbonatites from the Kaiserstuhl volcanic complex (SW Germany). *Chemical Geology* **498**, 1–16. DOI: https://doi.org/10.1016/j.chemgeo.2018.08.008

Walters, A.S., Goodenough, K.M., Hughes, H.S.R., Roberts, N.M.W., Gunn, A.G., Rushton, J., & Lacinska, A. (2013) Enrichment of Rare Earth Elements during magmatic and post-magmatic processes: A case study from the Loch Loyal Syenite Complex, northern Scotland. *Contributions to Mineralogy and Petrology* **166**(4), 1177–1202. DOI: https://doi.org/10.1007/s00410-013-0916-z

Wiedenbeck, M., Allé, P., Corfu, F., Griffin, W.L., Meier, M., Oberli, F., Quadt, A.V., Roddick, J.C., & Spiegel, W. (1995) Three natural zircon standards for U-Th-Pb, Lu-Hf, trace element and REE analyses. *Geostandards Newsletter* **19**(1), 1–23.

Wiemer, D., Allen, C.M., Murphy, D.T., & Kinaev, I. (2017) Effects of thermal annealing and chemical abrasion on ca. 3.5 Ga metamict zircon and evidence for natural reverse discordance: Insights for U–Pb LA-ICP-MS dating. *Chemical Geology* **466**, 285–302. DOI: https://doi.org/10.1016/j.chemgeo.2017.06.019

Winchester, J.A. & Floyd, P.A. (1977) Geochemical discrimination of different magma series and their differentiation products using immobile elements. *Chemical Geology* **20**, 325–343.

Winter, J.D. (2010) *Principles of Igneous and Metamorphic Petrology (second edition)*. Prentice Hall, New Jersey.

Woolley, A.R. & Bailey, D.K. (2012). The crucial role of lithospheric structure in the generation and release of carbonatites: geological evidence. *Mineralogical Magazine* **76**(2), 259–270. DOI: https://doi.org/10.1180/minmag.2012.076.2.02

Woolley, A.R. & Kempe, D.R.C. (1989) Carbonatites: nomenclature, average chemical compositions, and element distribution. *In* Carbonatites: Genesis and Evolution (Bell, K. ed.). Unwin Hyman Ltd, 1–14.

Woolley, A.R. & Kjarsgaard, B.A. (2008) Paragenetic types of carbonatite as indicated by the diversity and relative abundances of associated silicate rocks: evidence from a global database. *The Canadian Mineralogist* **46**, 741–752. DOI: 10.3749/canmin.46.4.741.

Wu, B., Wen, H.J., Bonnetti, C., Wang, R.C., Yang, J.H., & Wu, F.Y. (2019) Rinkite-(Ce) in the nepheline syenite pegmatite from the Saima alkaline complex, northeastern China: ITS occurrence, alteration, and implications for REE mineralization. *Canadian Mineralogist* **57**, 903–924. DOI: https://doi.org/10.3749/CANMIN.1900042

Yakymchuk, C., Kirkland, C. L., & Clark, C. (2018) Th/U ratios in metamorphic zircon. *Journal of Metamorphic Geology* **36**(6), 715–737. DOI: https://doi.org/10.1111/jmg.12307

Yoder, H.S., Jr., & Tilley C.E., (1962) Origin of basaltic maGMAS: An experimental study of natural and synthetic rock systems. *Journal of Petrology* **3**, 342–532.

Yukon Geological Survey (2022) Yukon digital bedrock geology. Government of Yukon, Available from https://data.geology.gov.yk.ca/Compilation/3 [accessed April 05, 2022].

Yukon Geological Survey (2023) List of all mineral occurrences. Government of Yukon, Available from https://data.geology.gov.yk.ca/Occurrences/ [accessed March 06, 2023]

Zane, A. & Weiss, Z. (1998) A procedure for classifying rock-forming chlorites based on microprobe data. *Rendiconti Lincei-scienze Fisiche E Naturali Rendiconti* **9**, 51–56.

Zharikov, V.A., Pertsev, N.N., Rusinov, V.L., Callegari, E., Fettes, D.J., (2007) Metasomatism and metasomatic rocks. *In* Recommendations by the IUGS Subcommision of the Systematics of Metamorphic Rocks (D. Fettes & J. Desmons, eds.). Cambridge University Press, New York.

Zurevinski, S.E. & Mitchell, R.H. (2004) Extreme compositional variation of pyrochlore-group minerals at the Oka carbonatite complex, Quebec: evidence of magma mixing? *The Canadian Mineralogist* **42**(4), 1159–1168. DOI: https://doi.org/10.2113/gscanmin.42.4.1159

Appendix A: Thin Section Scans

This appendix contains thin section scans from samples collected on Corundum Dome and Pyrochlore Dome.

Corundum Dome

The following section has thin section scans from samples collected on Pyrochlore Dome.

Bedded argillite

Hand specimens: 20TN5, 20TN24A

Thin sections: 20TN5, 20TN24A

This section includes thin section scans from two bedded argillite samples.

Sample 20TN5

Rock name: Bedded argillite

20TN5

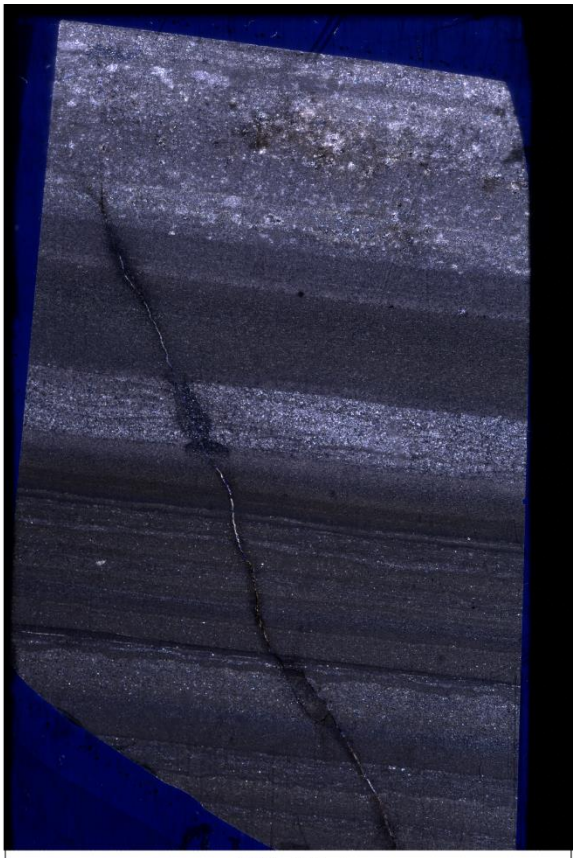
20TN5

Sample 20TN24A

Rock name: Bedded argillite

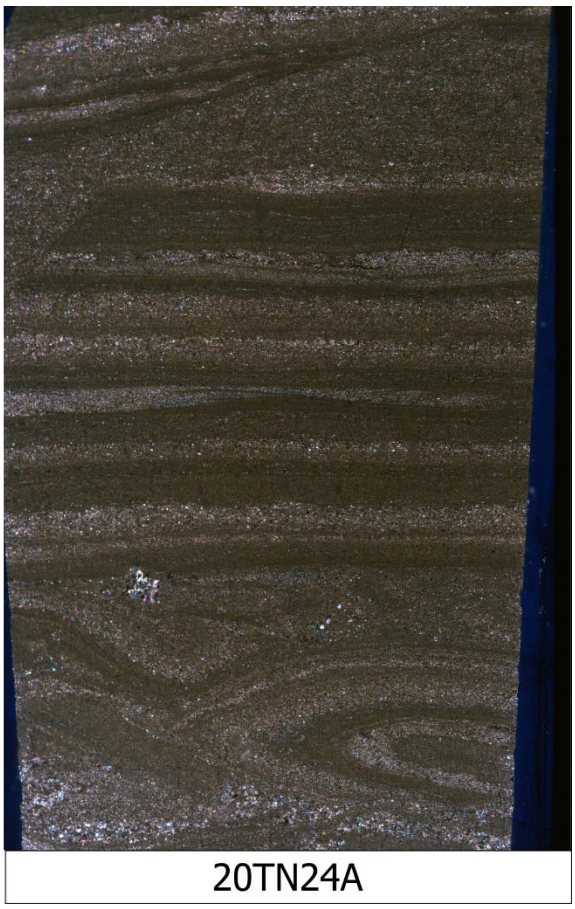

Fenites

Hand specimens: 20TN4A, 20TN4B, 20TN4C, 20TN22A, 20TN22B, 20TN23, 20TN7, 20TN 25C, 20TN25D

Thin sections: 20TN4A, 20TN4B, 20TN4C-1, 20TN4C-2, 20TN22A, 20TN22B, 20TN23, 20TN7, 20TN 25C, 20TN25D

This section includes thin section scans from the layered arfvedsonite-albite fenite, layered phlogopite-potassium feldspar fenite, and brecciated arfvedsonite-potassium feldspar fenite.

Note, samples 20TN25A and 20TN25B in the actinolite-altered syenite section have layered arfvedsonite-albite fenite zones.

Layered phlogopite-potassium feldspar fenite

Sample 20TN25C

Rock name: Layered phlogopite-potassium feldspar fenite

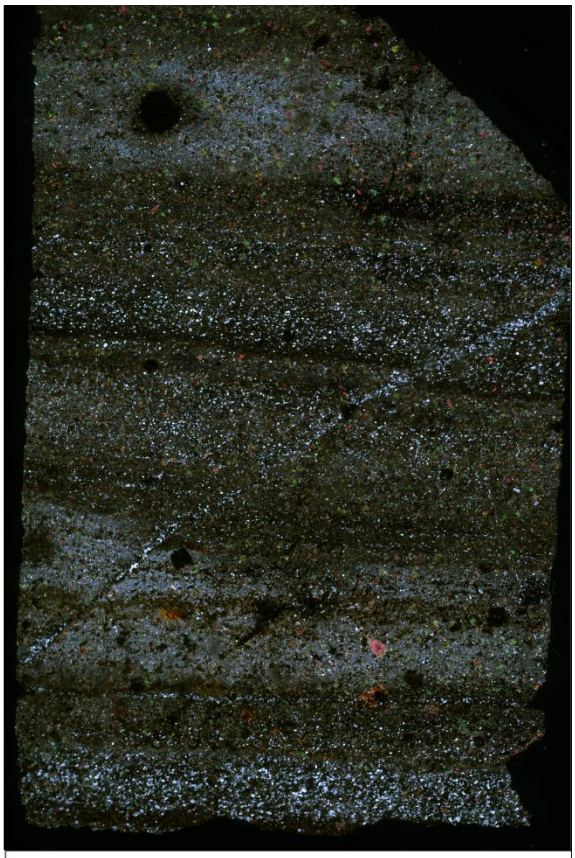

Sample 20TN25C

Rock name: Layered phlogopite-potassium feldspar fenite

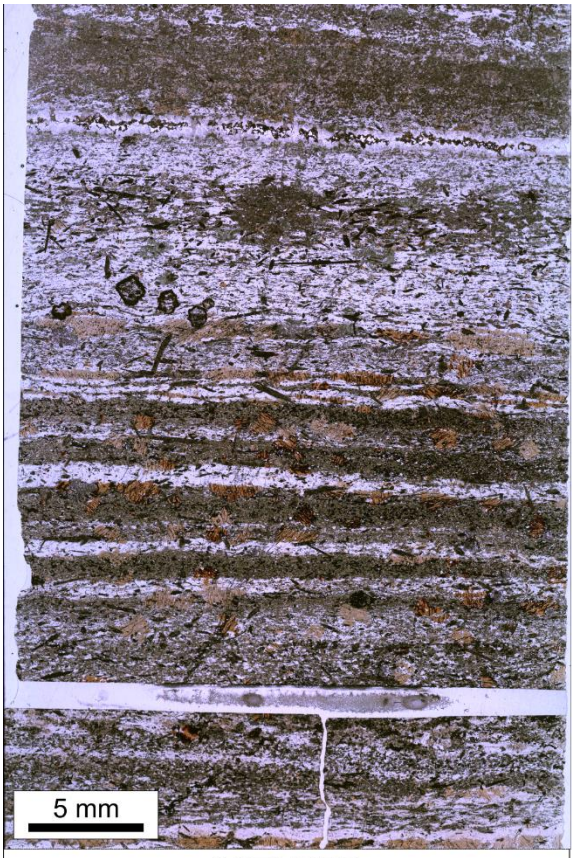

20TN25D

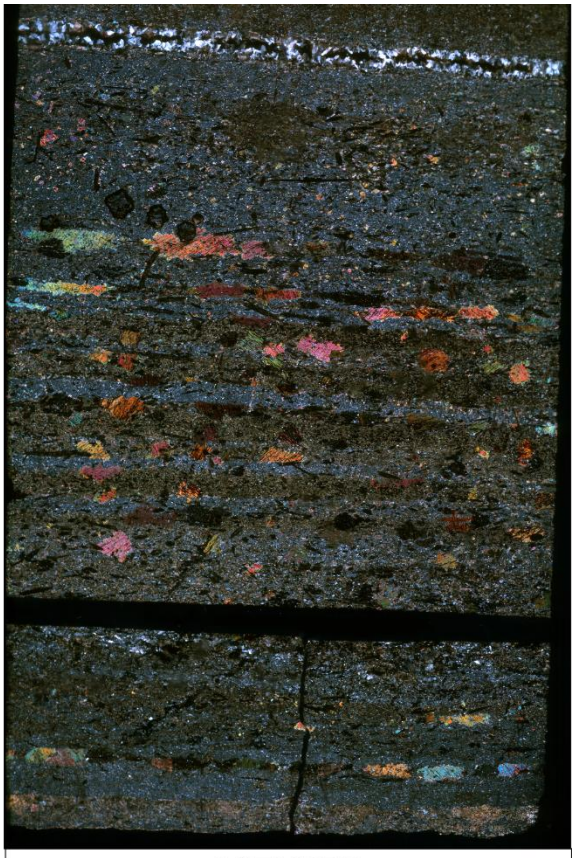

20TN25D

Layered arfvedsonite-albite fenite

Sample *20TN4*A

Rock name: Layered arfvedsonite-albite fenite

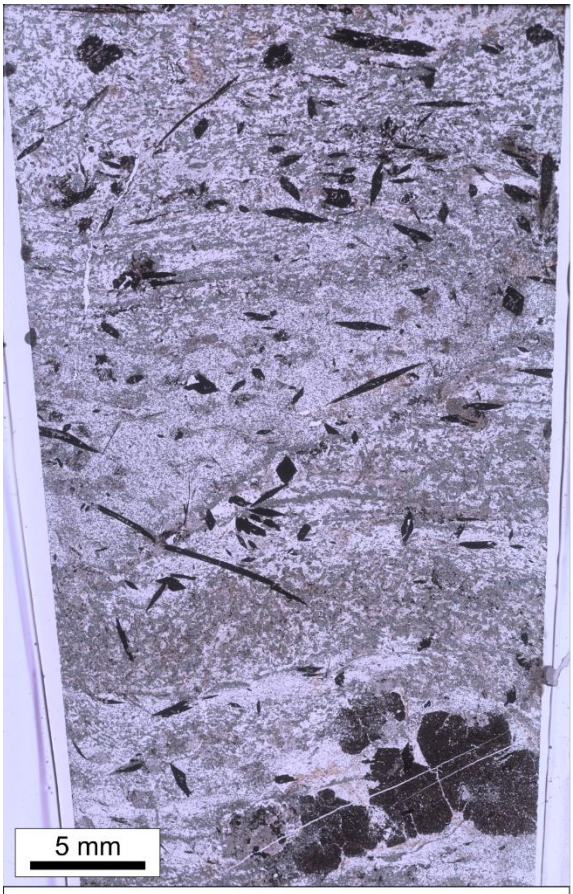

20TN4A

20TN4A

Sample 20TN4B

Rock name: Layered arfvedsonite-albite fenite

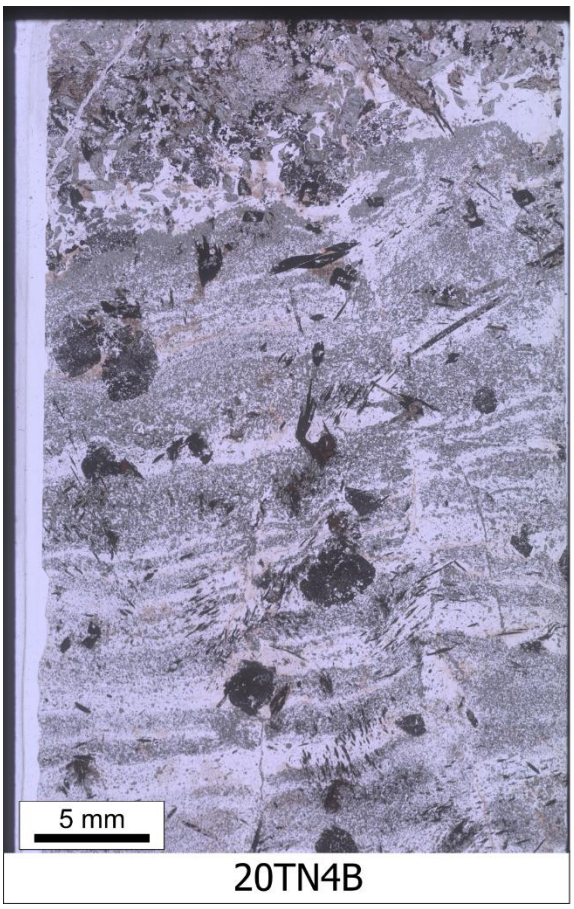

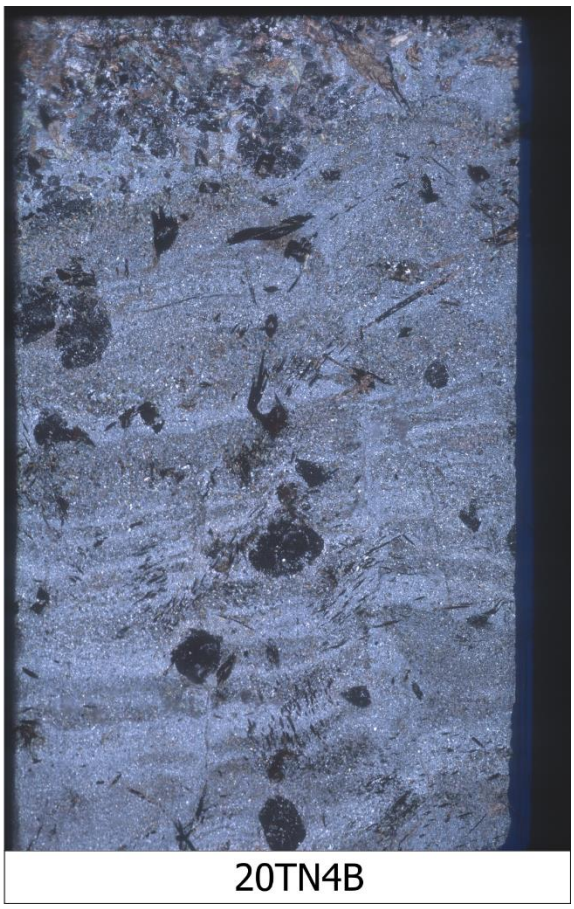

Sample 20TN4C

Rock name: Layered arfvedsonite-albite fenite

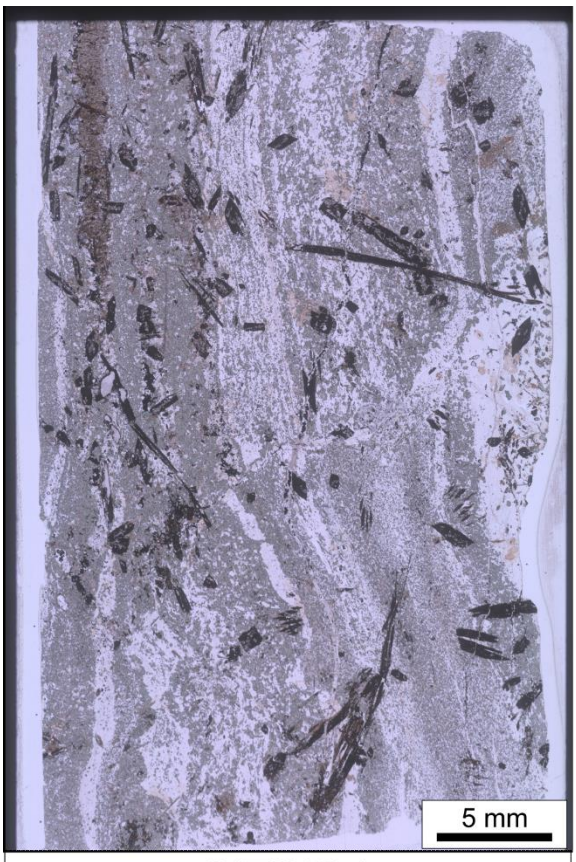

20TN4C-1

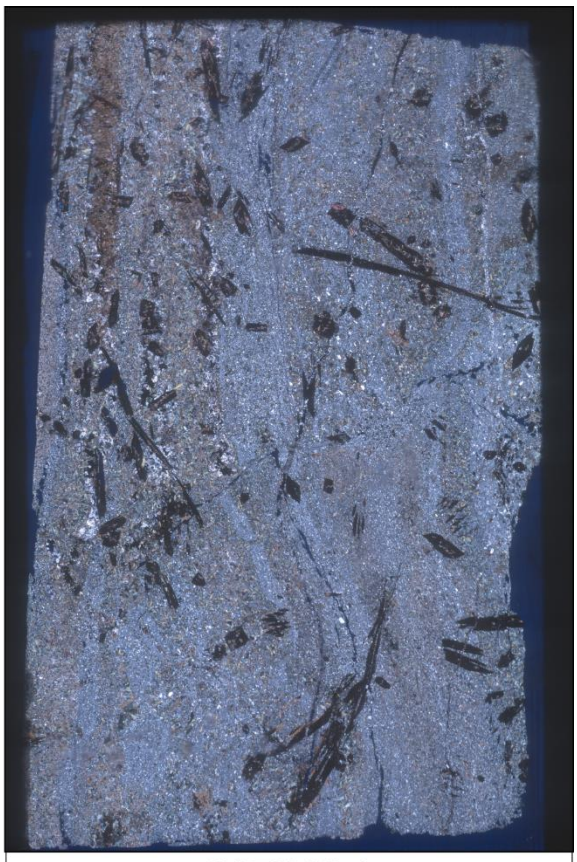

20TN4C-1

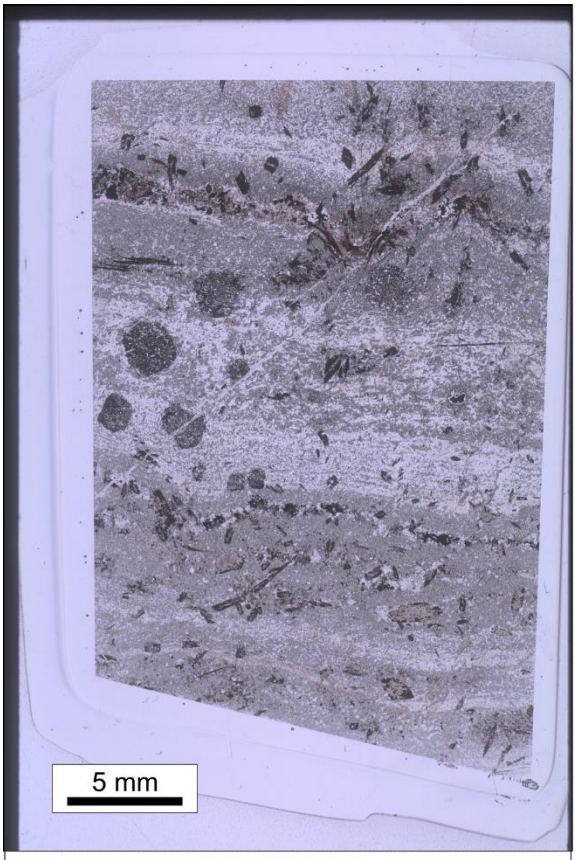

20TN4C-2

20TN4C-2

Sample 20TN22A

Rock name: Layered arfvedsonite-albite fenite

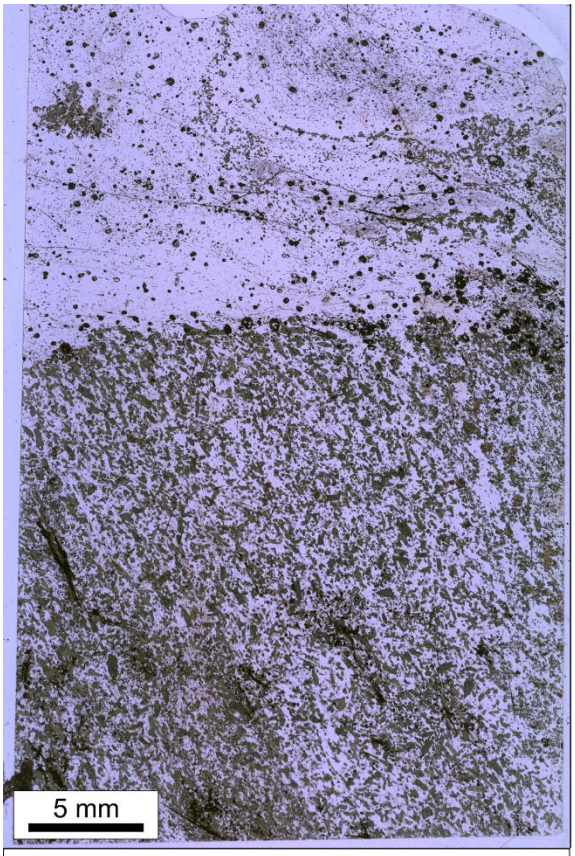

20TN22A

20TN22A

Sample 20TN22B

Rock name: Layered arfvedsonite-albite fenite

20TN22B

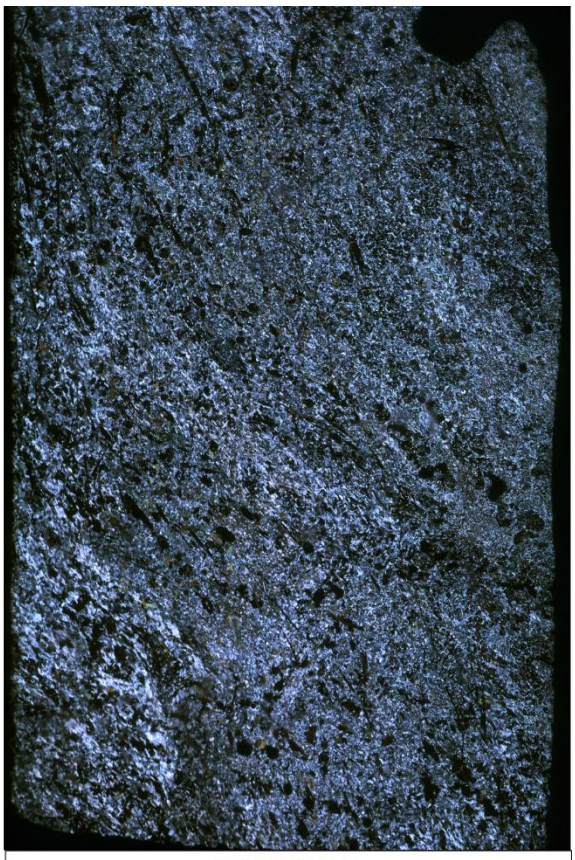

20TN22B

Sample 20TN23

Rock name: Layered arfvedsonite-albite fenite

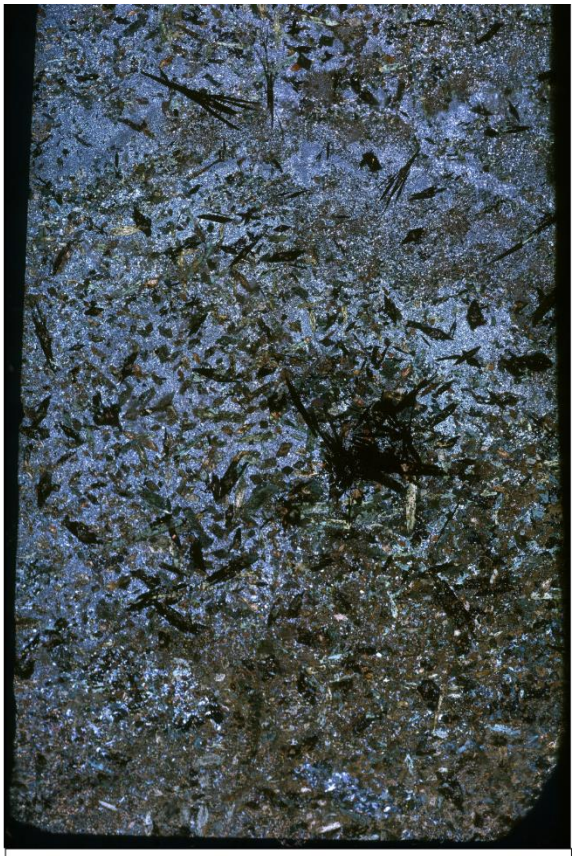

Brecciated arfvedsonite-potassium feldspar fenite

Sample 20TN7

Rock name: Brecciated arfvedsonite-potassium feldspar fenite

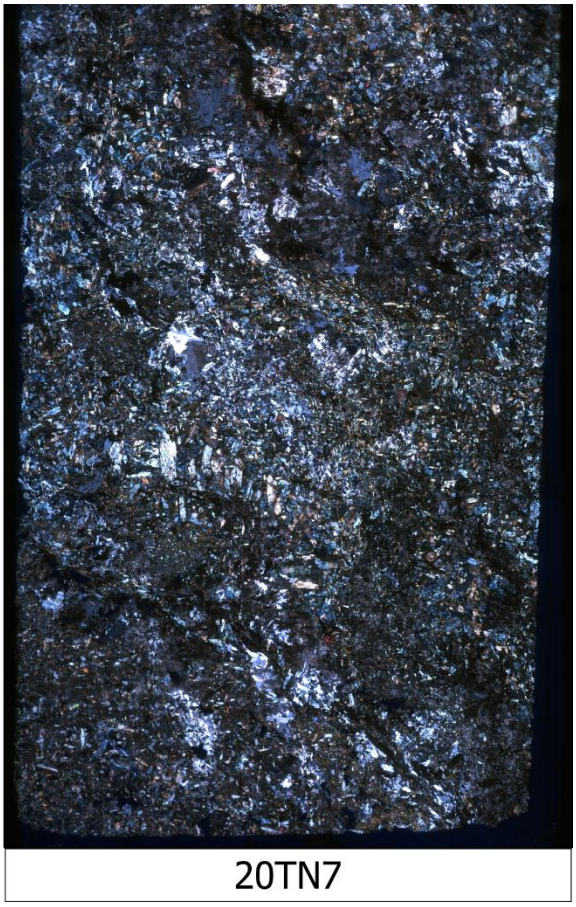

Metasomatically altered actinolite-altered syenite

Hand specimens: 20TN2, 20TN3, 20TN4D, 20TN6, 20TN9, 20TN10A, 20TN10B, 20TN10C, 20TN25A, 20TN25B, 20TN25E, 20TN25F

Thin sections: 20TN2, 20TN3-1, 20TN3-2, 20TN4D, 20TN6-1, 20TN6-2, 20TN9, 20TN10A, 20TN10B-1, 20TN10B-2, 20TN10C, 20TN25A, 20TN25B, 20TN25E, 20TN25F

This section includes thin section scans from actinolite-altered syenite samples.

Note, samples 20TN25A and 20TN25B have layered arfvedsonite-albite fenite zones.

Sample 20TN2

Rock name: Moderately altered actinolite-altered syenite

20TN2

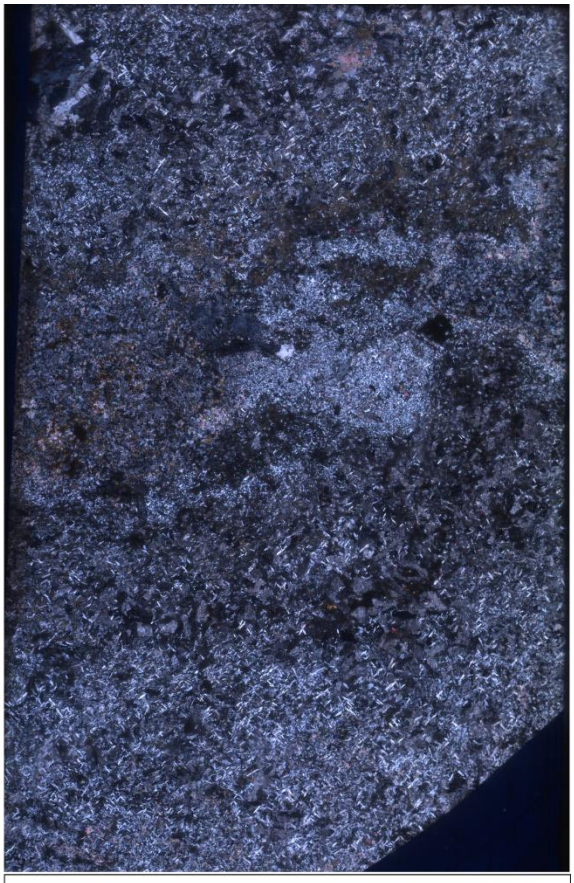

20TN2

Sample 20TN3

Thin Section(s): 20TN3-1, 20TN3-2

Rock name: Moderately altered actinolite-altered syenite dikelet

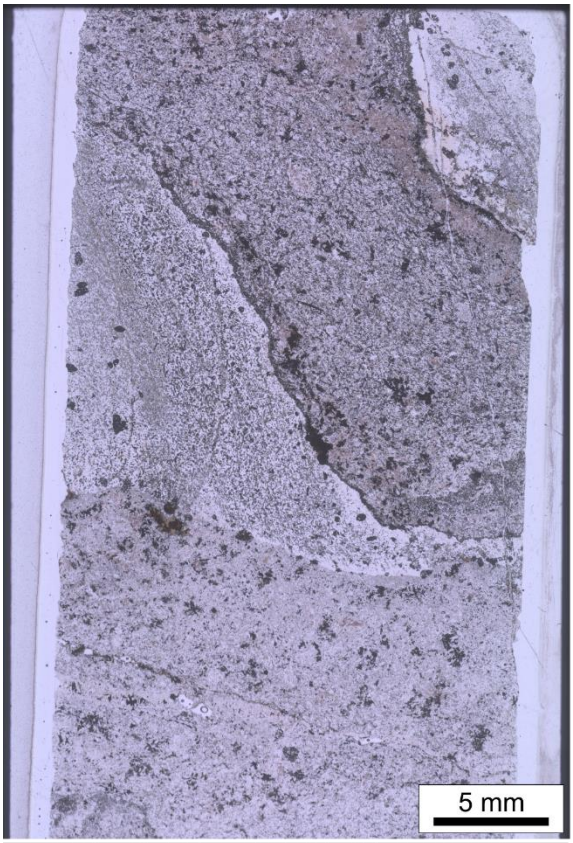

20TN3-1

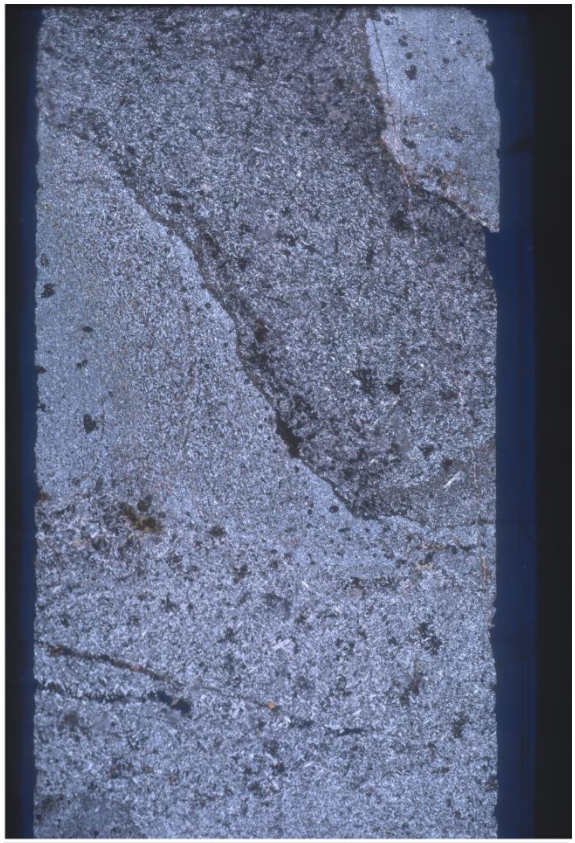

20TN3-1

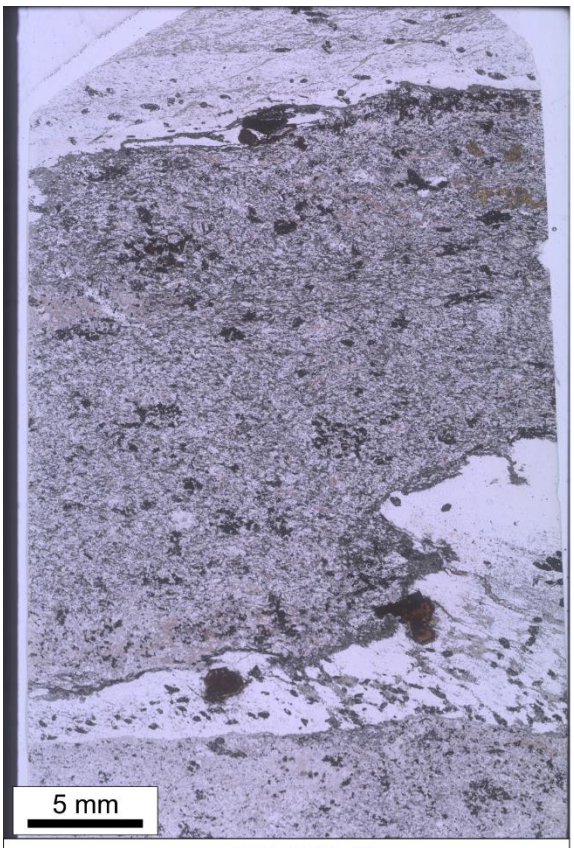

20TN3-2

20TN3-2

Sample 20TN4D

Rock name: Moderately altered actinolite-altered syenite

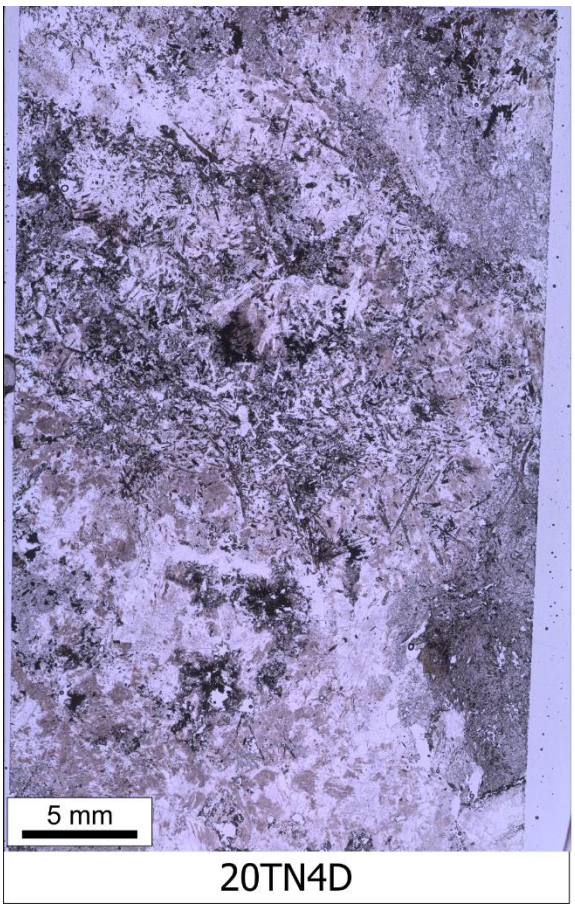

Sample 20TN6

Thin Section(s): 20TN6-1, 20TN6-2

Rock name: Strongly altered actinolite-altered syenite

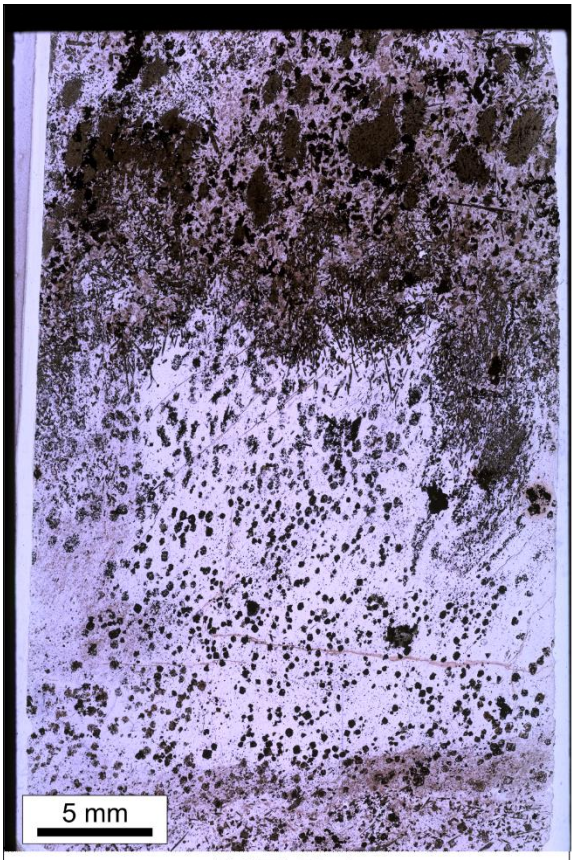

20TN6-1

20TN6-1

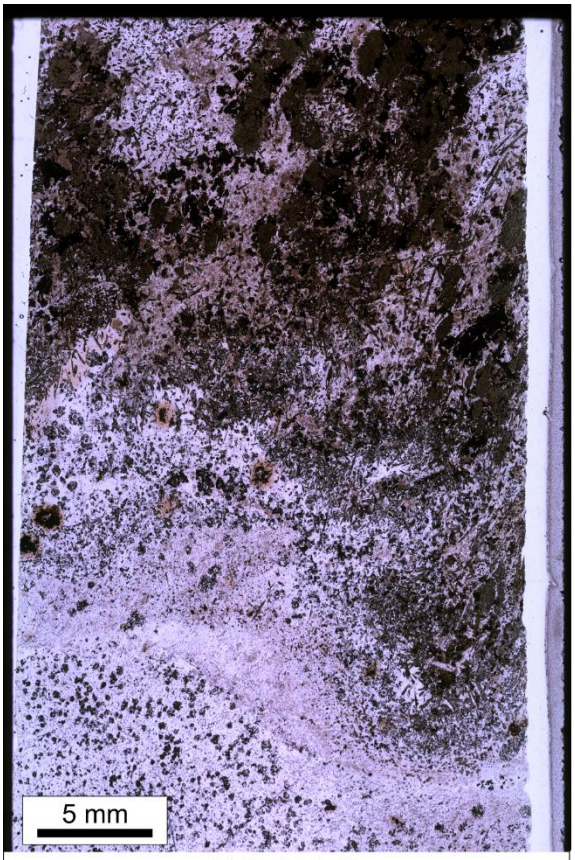

20TN6-2

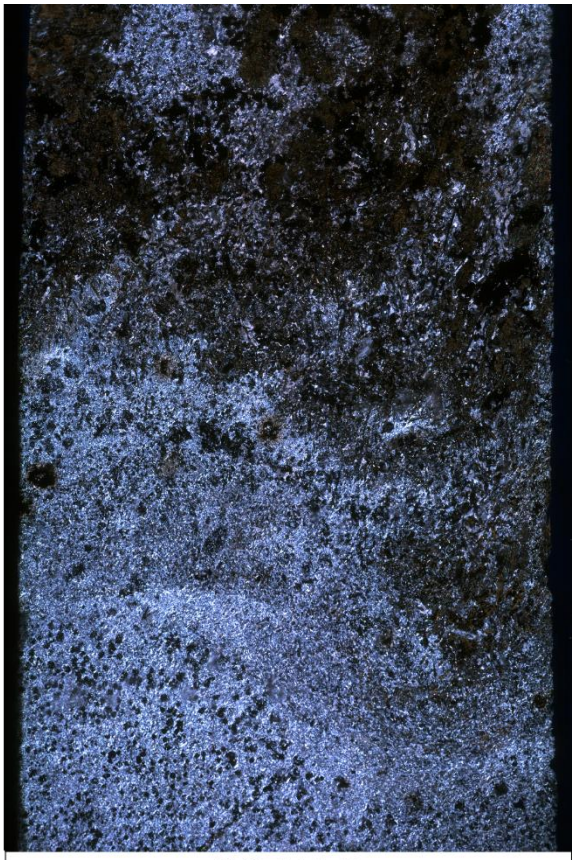

20TN6-2

Sample 20TN9

Rock name: Strongly altered actinolite-altered syenite

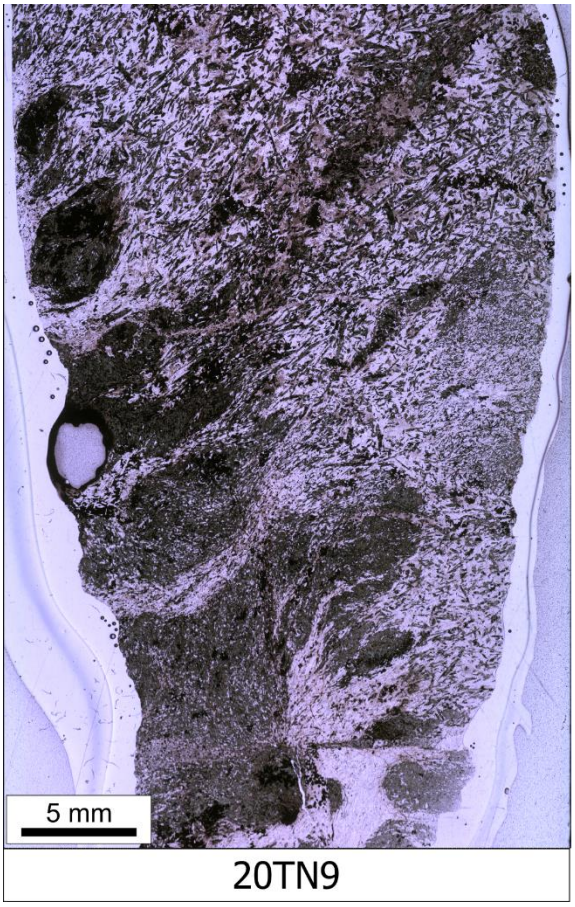

20TN9

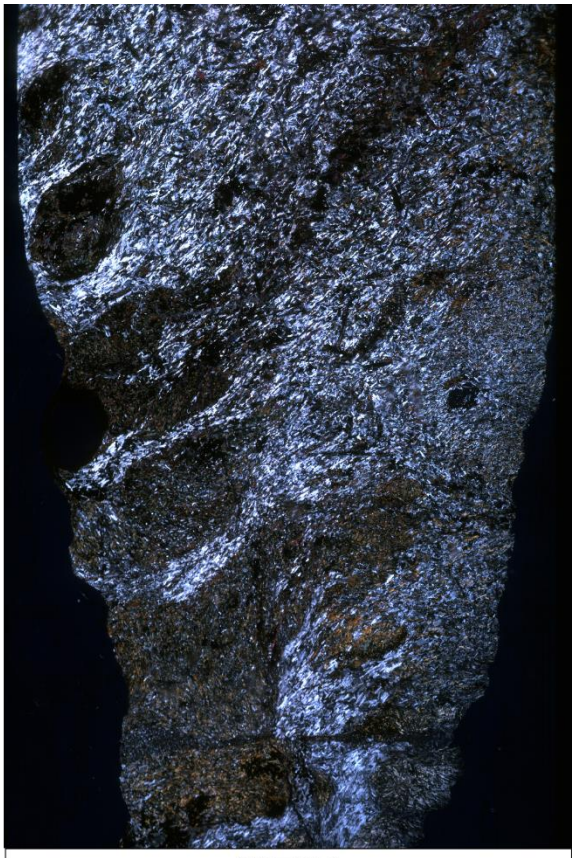

20TN9

Sample 20TN10A

Rock name: Strongly altered actinolite-altered syenite

20TN10A

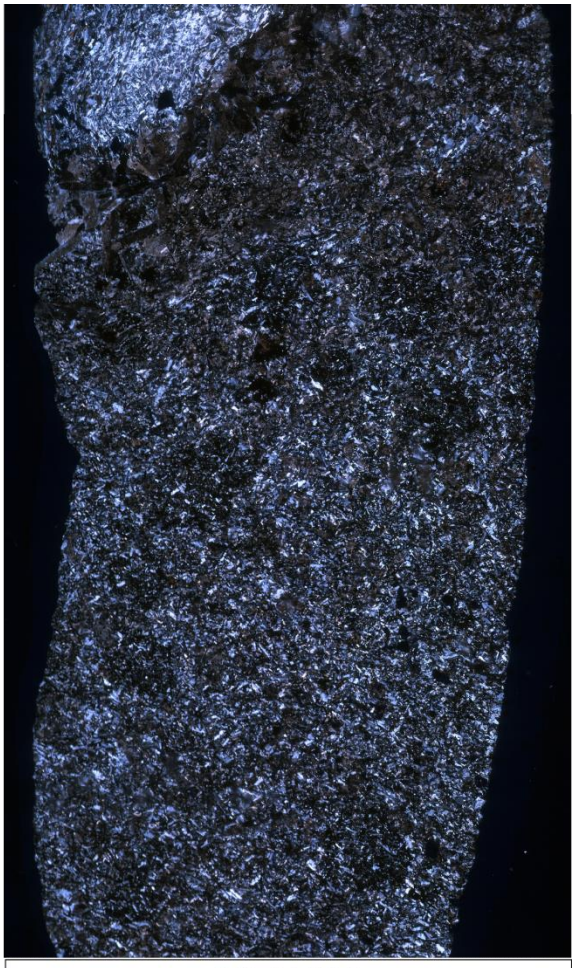

20TN10A

Sample 20TN10B

Thin Section(s): 20TN10B-1, 20TNB-2

Rock name: Strongly altered actinolite-altered syenite

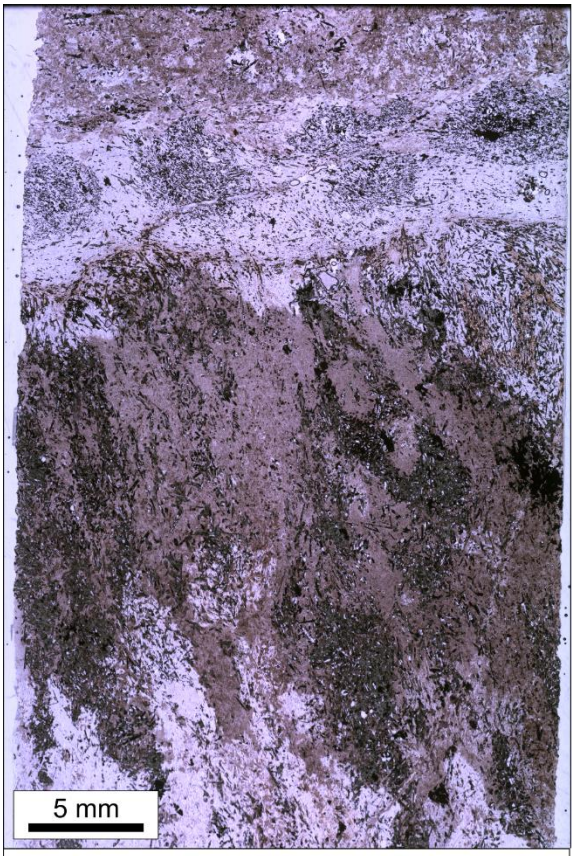

20TN10B-1

20TN10B-1

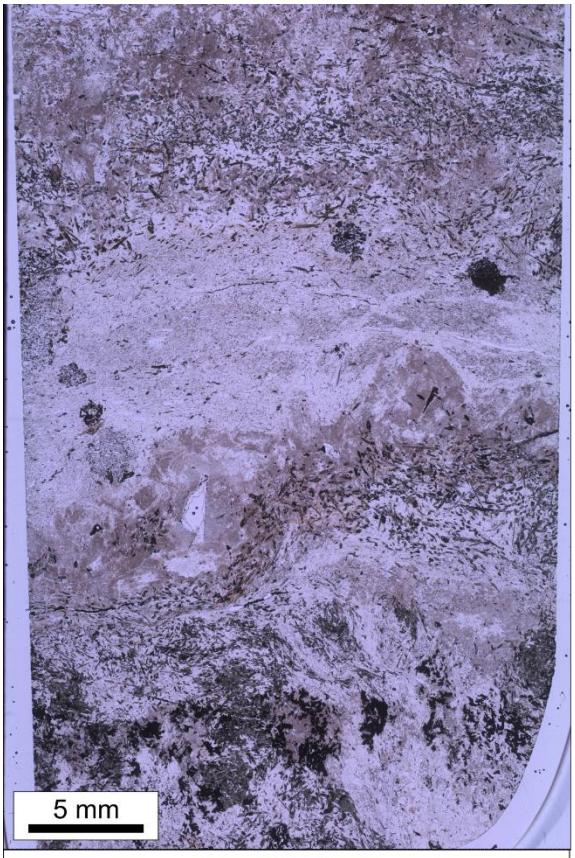

20TN10B-2

20TN10B-2

Sample 20TN10C

Rock name 1: Fine grained strongly altered actinolite-altered syenite (upper half)

Rock name 2: Coarse grained moderately altered actinolite-altered syenite dike (lower half)

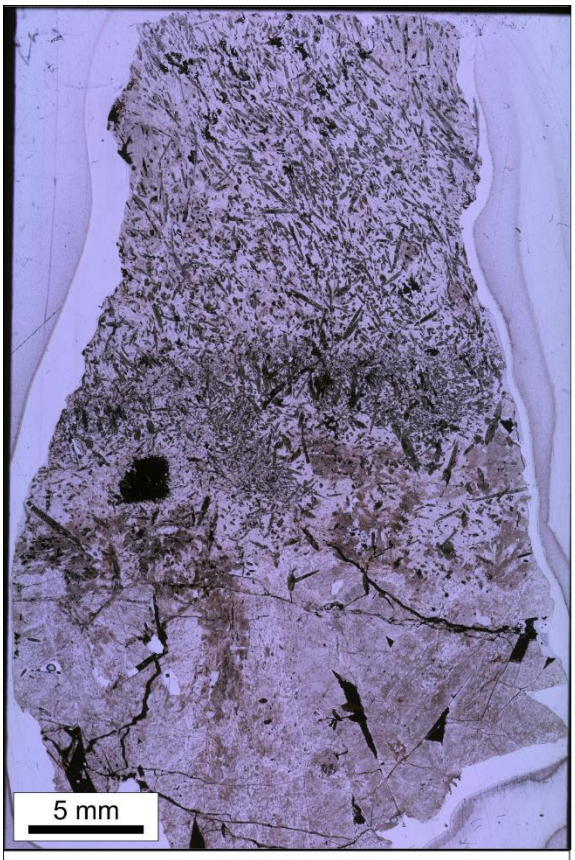

20TN10C

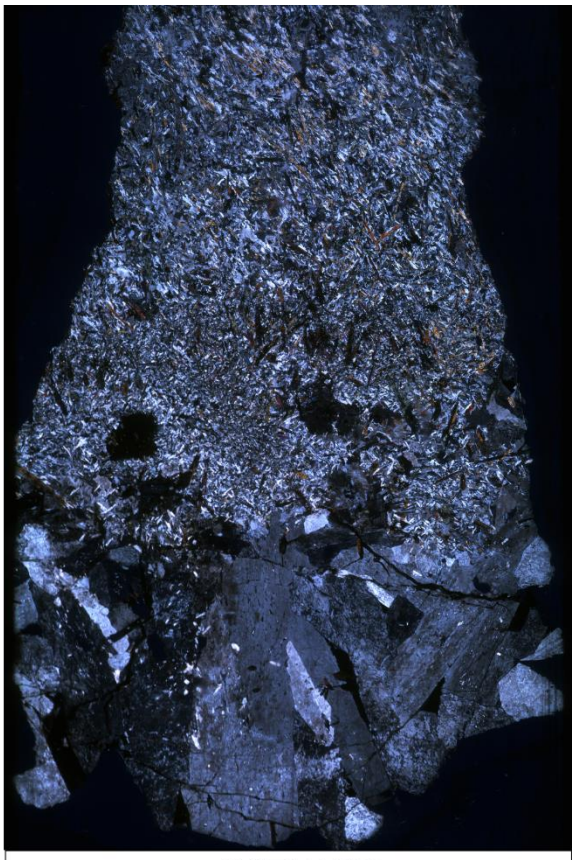

20TN10C

Sample 20TN25A

Rock name 1: Strongly altered actinolite-altered syenite (upper half)

Rock name 2: layered arfvedsonite-albite fenite (lower half)

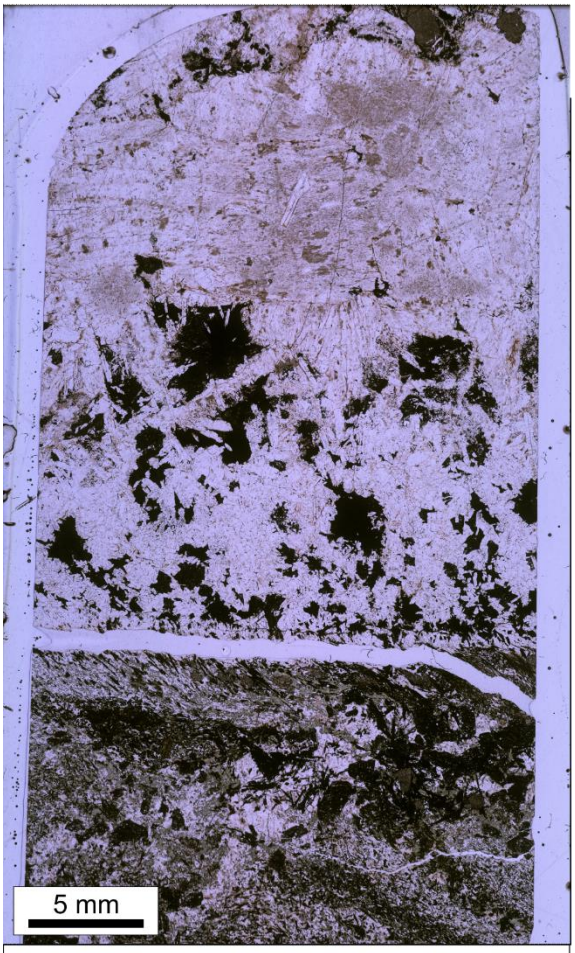

20TN25A

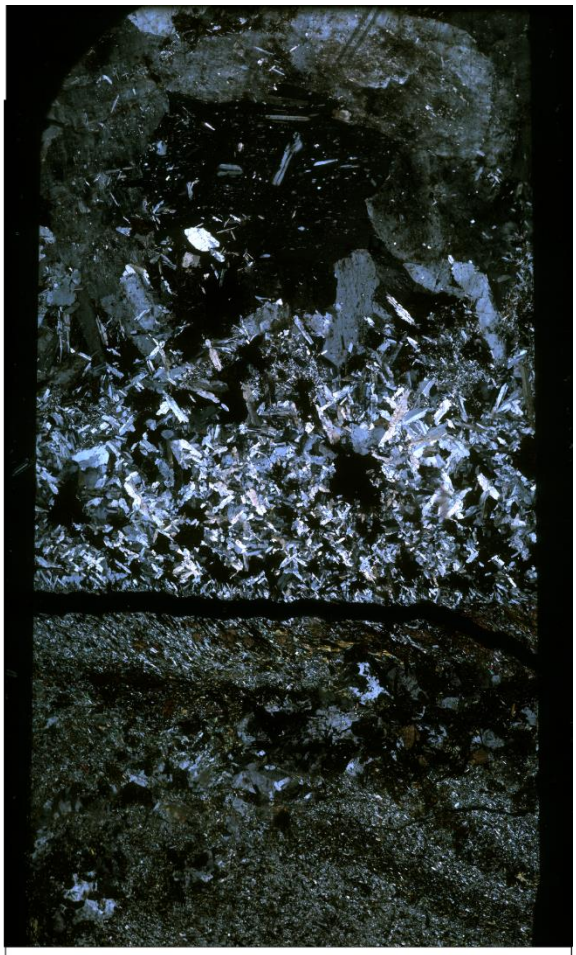

20TN25A

Sample 20TN25B

Rock name 1: Strongly altered actinolite-altered syenite dikelet (centre)

Rock name 2: layered arfvedsonite-albite fenite (above and below the actinolite-altered syenite dikelet)

Sample 20TN25E

Rock name: Strongly altered actinolite-altered syenite

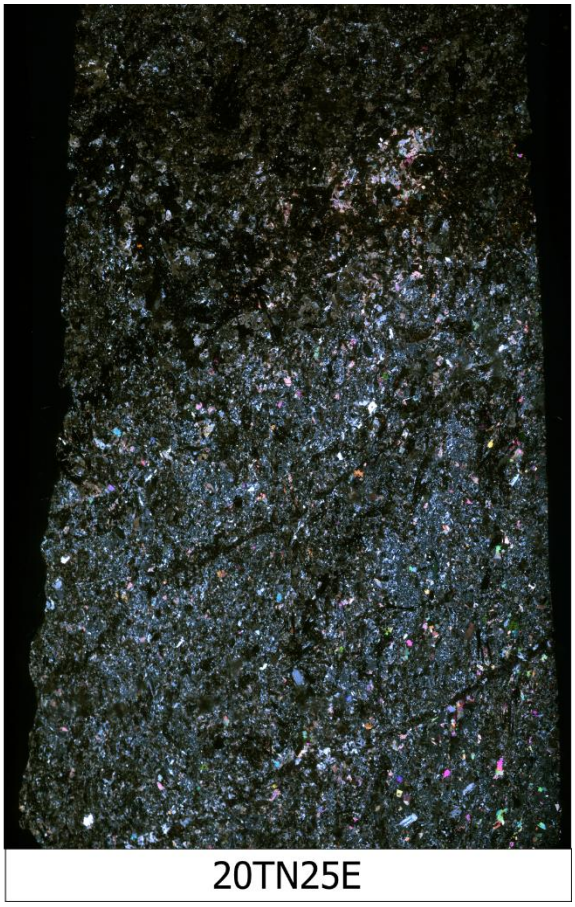

Sample 20TN25F

Rock name: Strongly altered actinolite-altered syenite

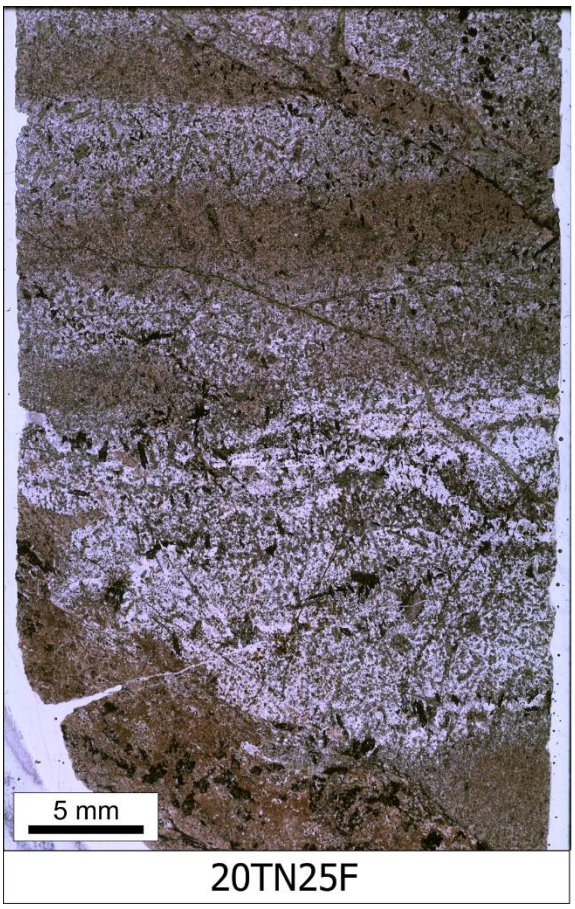

20TN25F

20TN25F

Volcanic breccias

Hand specimens: 20TN11, 20TN24B

Thin sections: 20TN11, 20TN24B

This section includes thin section scans from two different volcanic breccia samples. Sample 20TN11 is an altered mudstone-porphyritic basalt sub-angular to sub-rounded clast supported gravel-pebble volcanic breccia. Sample 20TN24B is an altered limestone-syenite-porphyritic basalt, angular to sub-angular clast supported gravel-pebble volcanic breccia.

Sample 20TN11

Rock name: Altered limestone-syenite-porphyritic basalt, angular to sub-angular clast supported gravel-pebble volcanic breccia

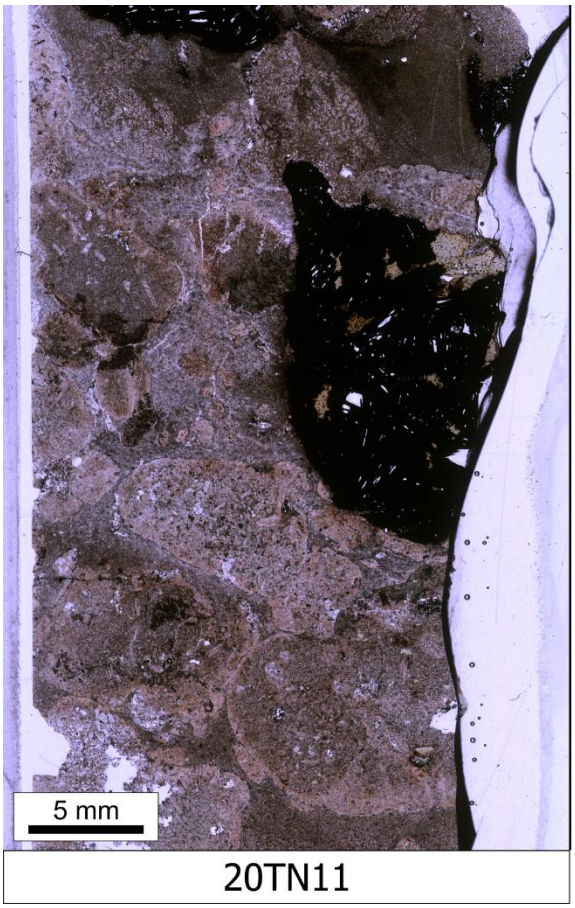

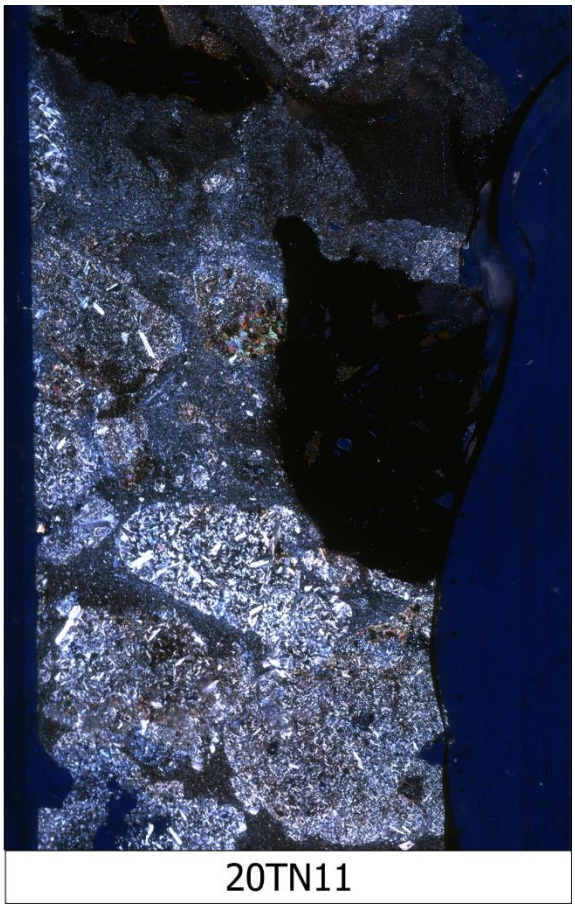

Sample 20TN24B

Rock name: Altered limestone-syenite-porphyritic basalt, angular to sub-angular clast supported gravel-pebble volcanic breccia

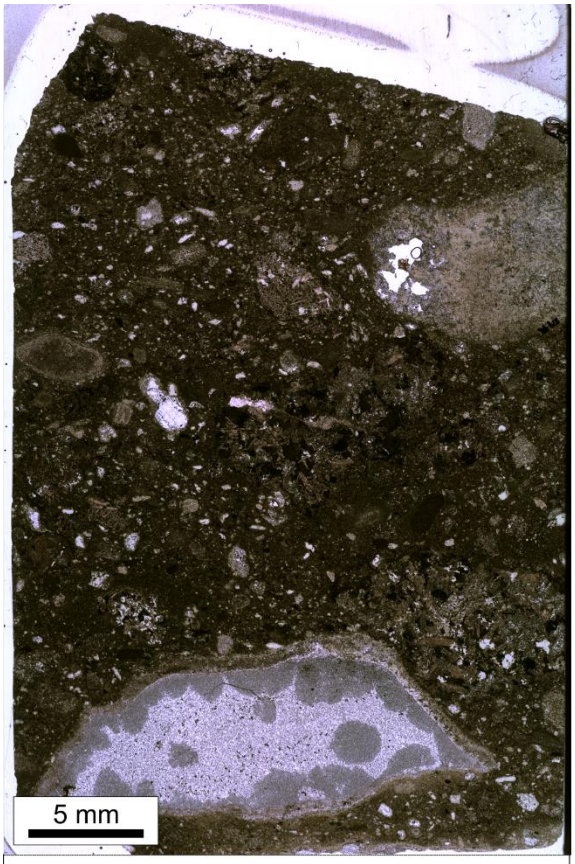

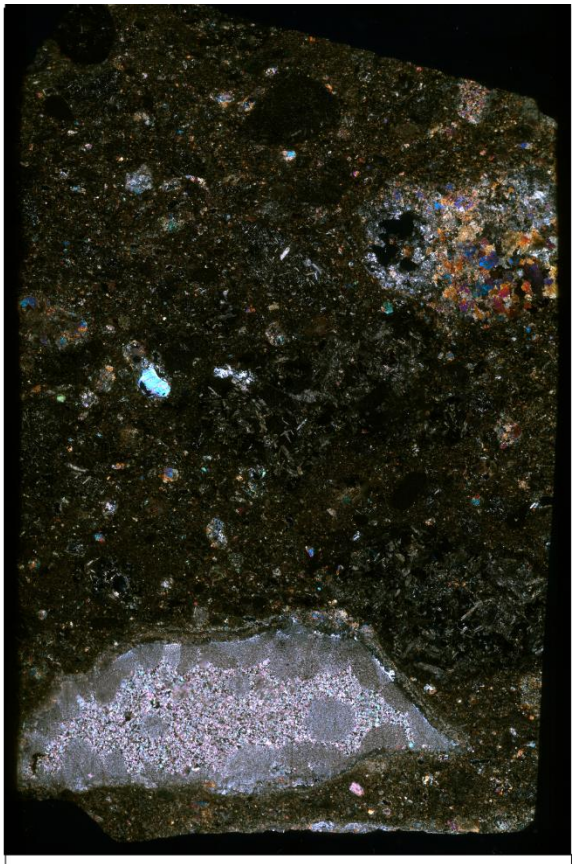

Altered feldspar microporphyritic dike

Hand specimens: 20TN1

Thin section: 20TN1

Sample 20TN1

Rock name: Altered feldspar microporphyritic dike

20TN1

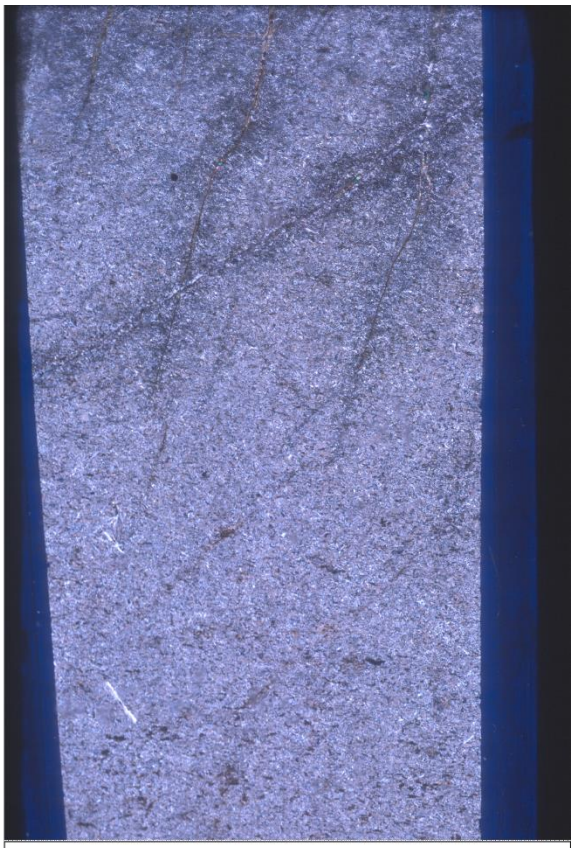

20TN1

Pyrochlore Dome

The following section has thin section scans from samples collected on Pyrochlore Dome.

Calcite-quartz metaconglomerate

Hand specimens: 20TN17B

Thin sections: 20TN17B

Sample 20TN17B

Rock name: Monomictic calcite-quartz gravel-pebble ortho-metaconglomerate

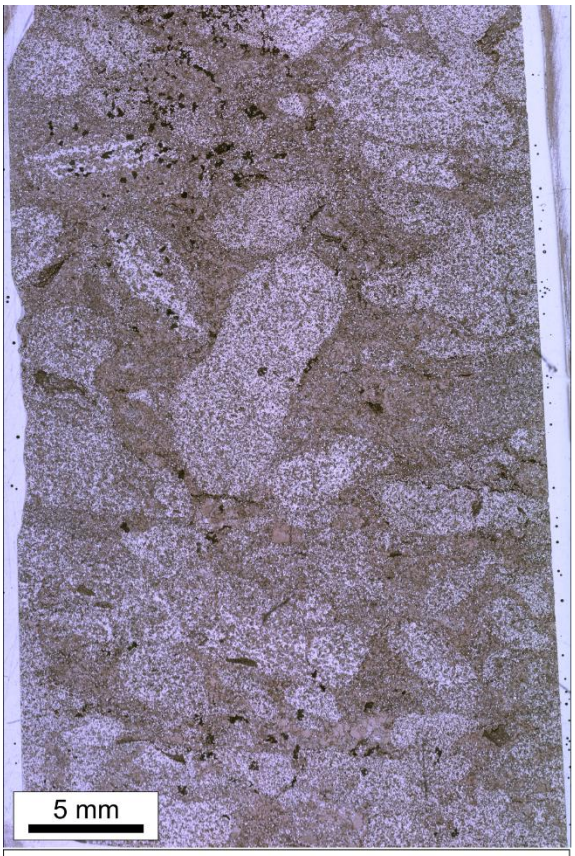

20TN17B

20TN17B

Quartzite

Hand specimens: 20TN17C

Thin sections: 20TN17C

Sample 20TN17C

Rock name: Upper fine to lower medium grained granoblastic quartzite

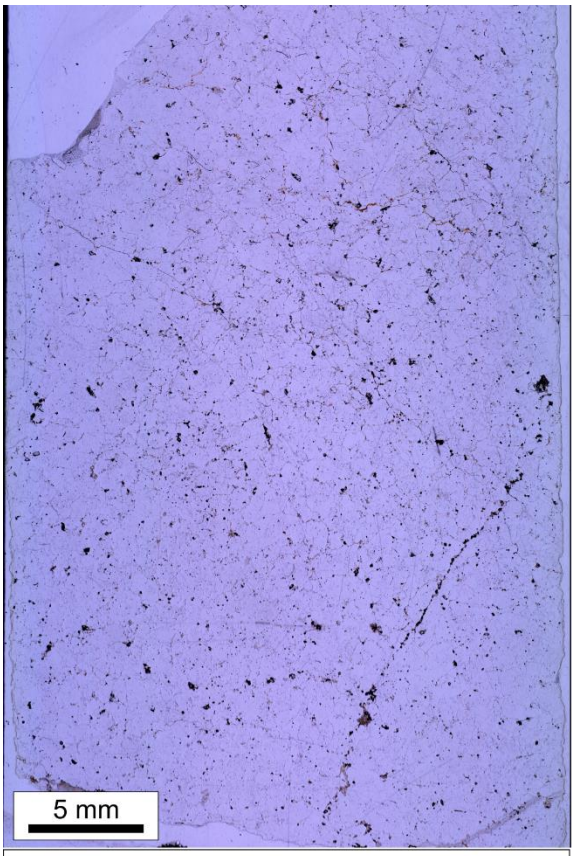

20TN17C

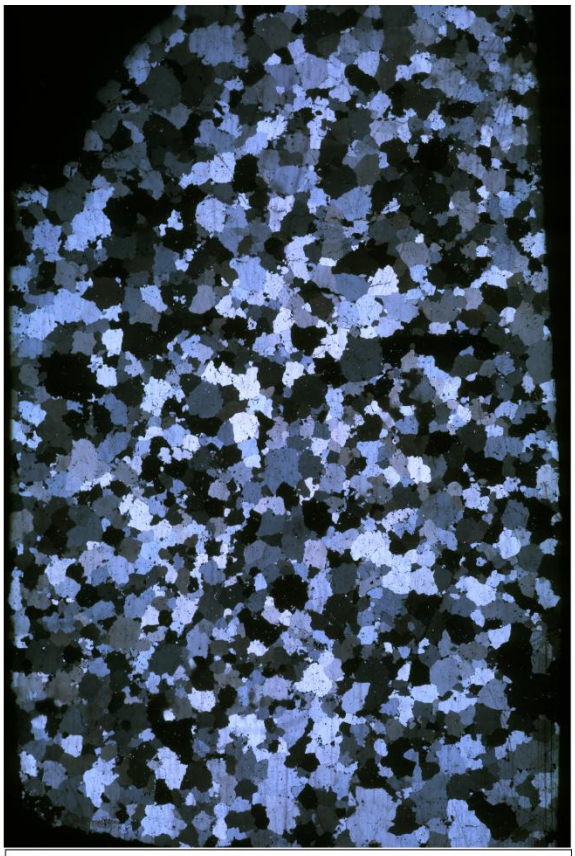

20TN17C

Metasomatically altered arfvedsonite-aegirine syenite

Hand Specimen: 20TN12A, 20TN13A, 20TN13B, 20TN14A, 20TN16A, 20TN17A, 20TN18, 20TN19, 20TN20, 20TN58A, 20TN58B

Thin Section(s): 20TN12A, 20TN13A, 20TN13B-1, 20TN13B-2, 20TN14A, 20TN16A-1, 20TN16A-2, 20TN17A-1, 20TN17A-2, 20TN18, 20TN19, 20TN20, 20TN58A, 20TN58B

This section includes thin section scans from altered arfvedsonite-aegirine syenite samples.

Sample 20TN12A

Rock name: Moderately altered arfvedsonite-aegirine syenite

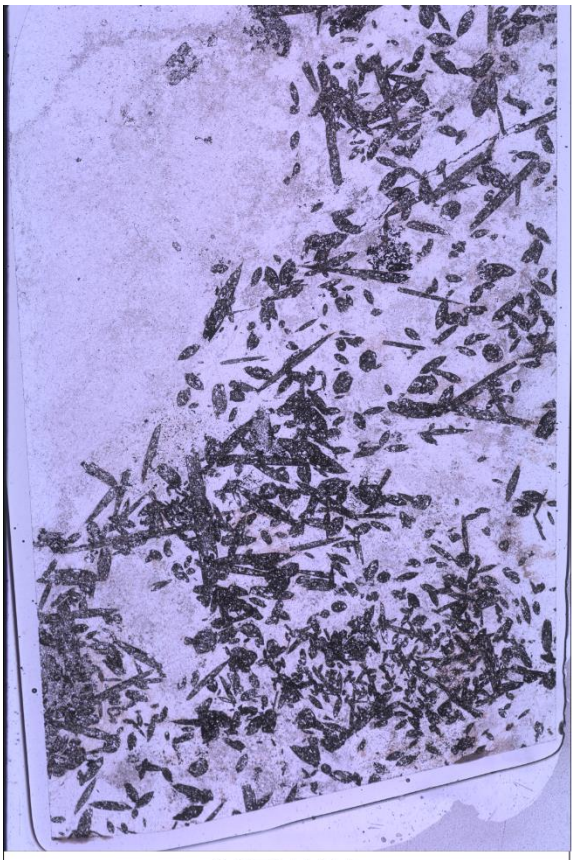

20TN12A

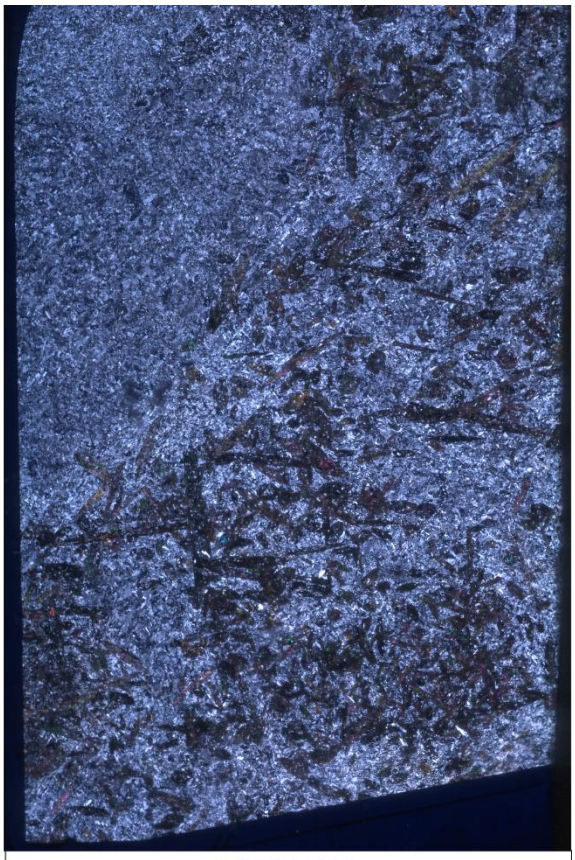

20TN12A

Sample 20TN13A

Rock name: Strongly altered arfvedsonite-aegirine syenite

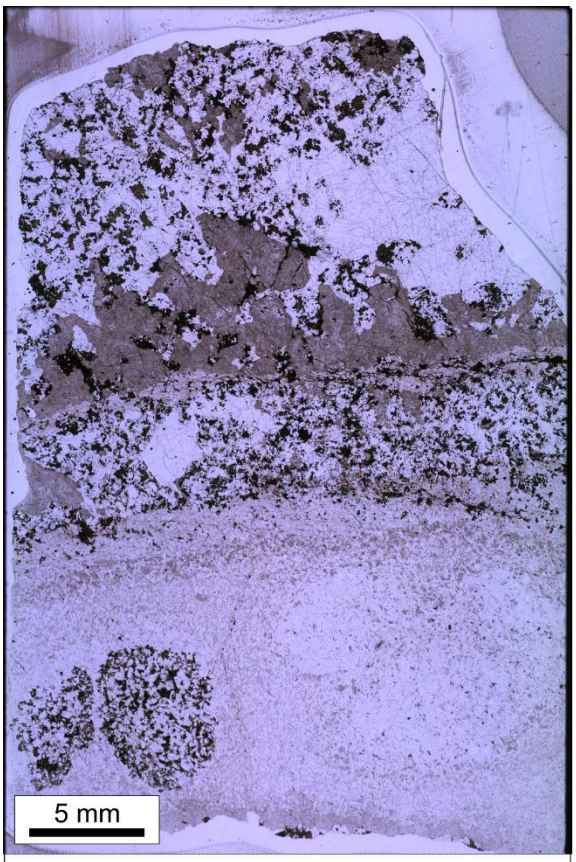

20TN13A

20TN13A

Sample 20TN13B

Thin sections: 20TN13B-1, 20TN13B-2

Rock name: Strongly altered arfvedsonite-aegirine syenite

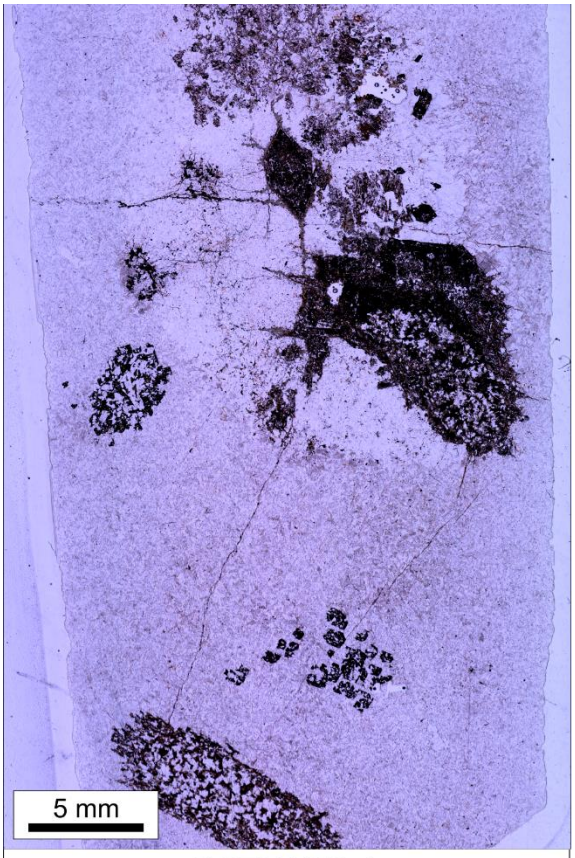

20TN13B-1

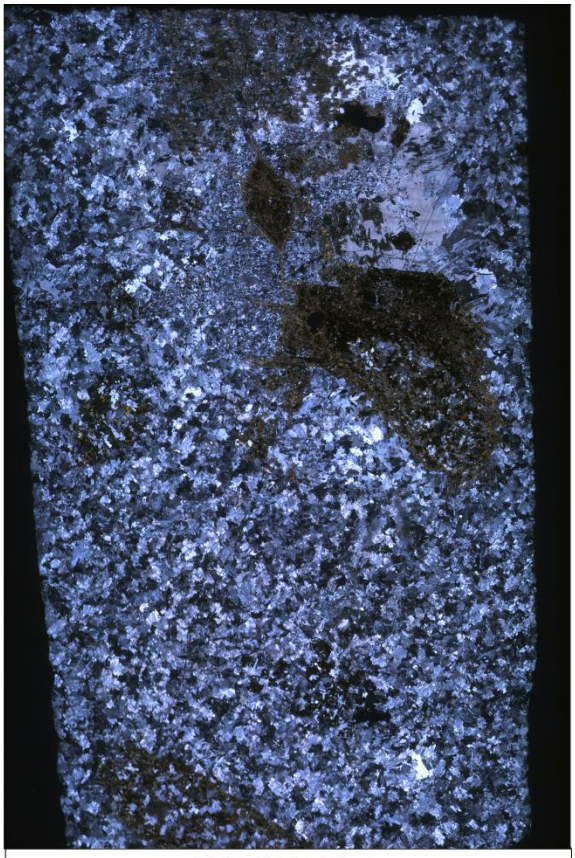

20TN13B-1

20TN13B-2

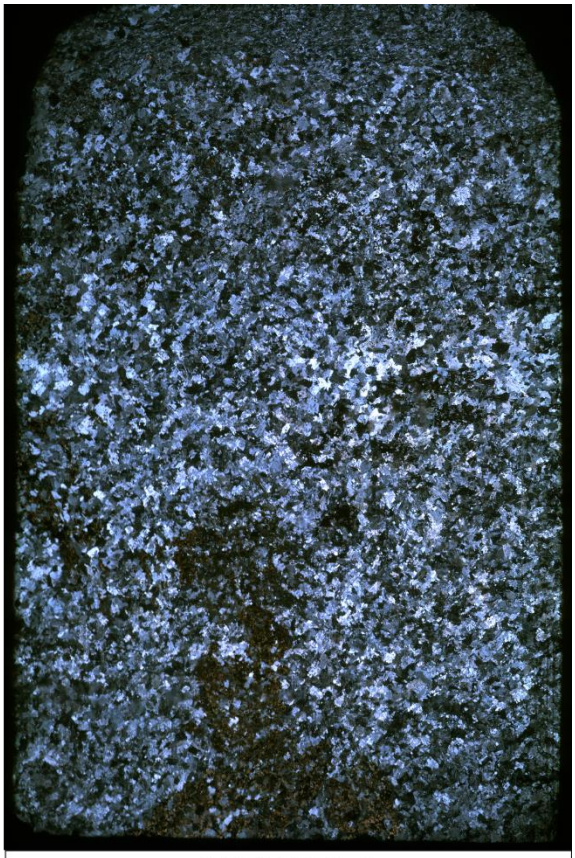

20TN13B-2

Sample 20TN14

Thin Section: 20TN14A

Rock name: Strongly altered arfvedsonite-aegirine syenite

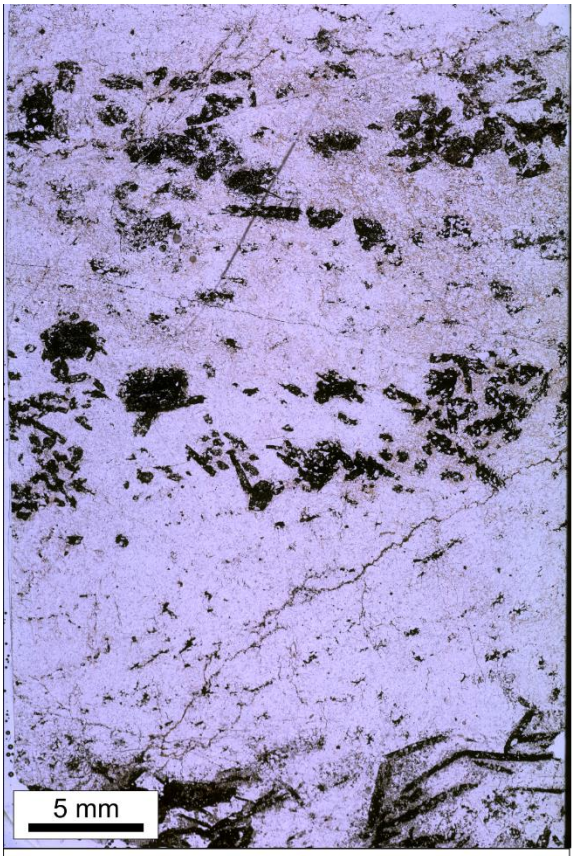

20TN14B

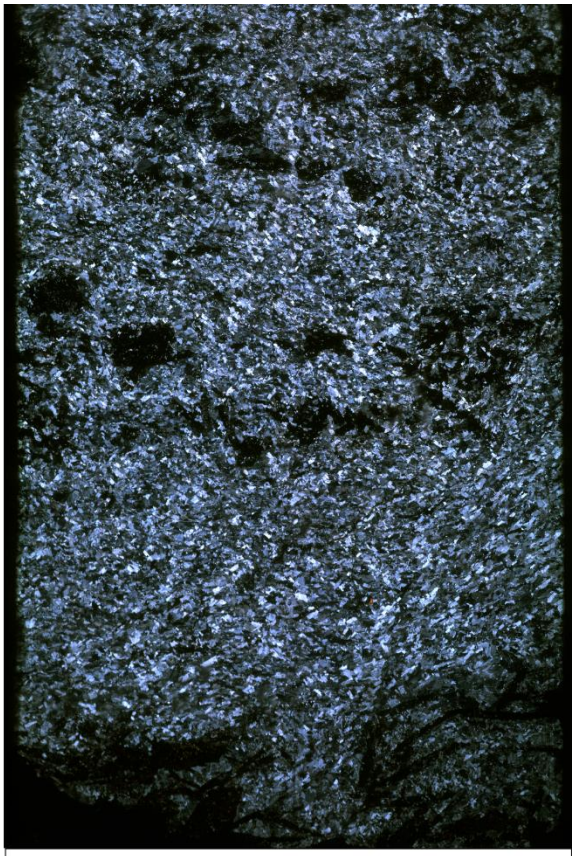

20TN14B

Sample 20TN16A

Thin Section(s): 20TN16A-1, 20TN16A-2

Rock name: Strongly altered arfvedsonite-aegirine syenite

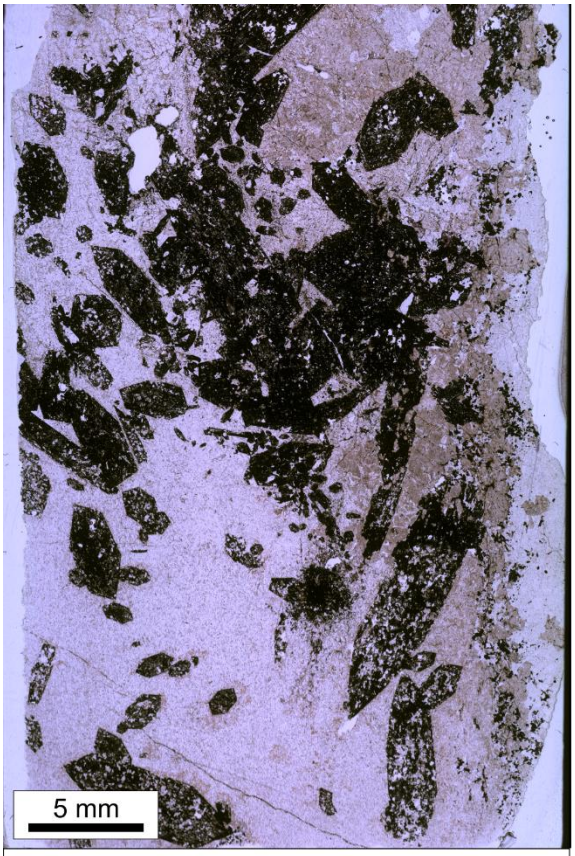

20TN16A-1

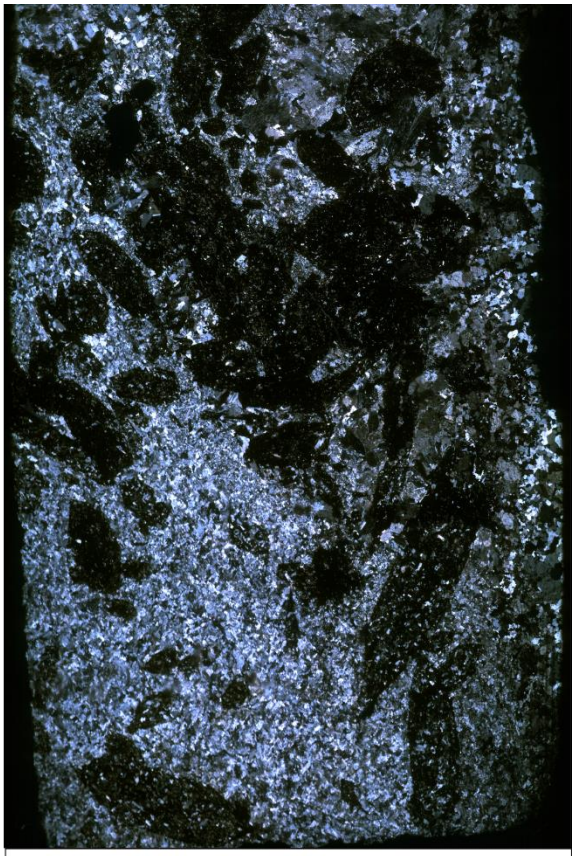

20TN16A-1

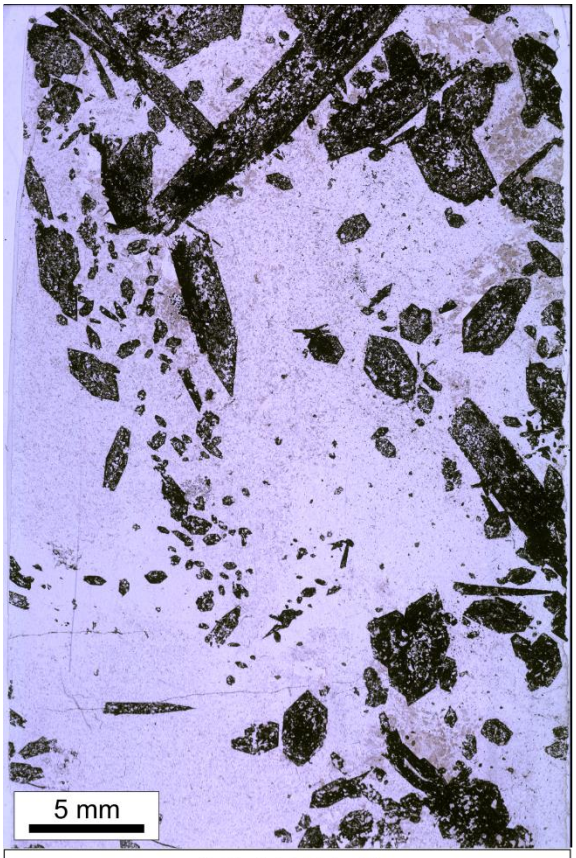

20TN16A-2

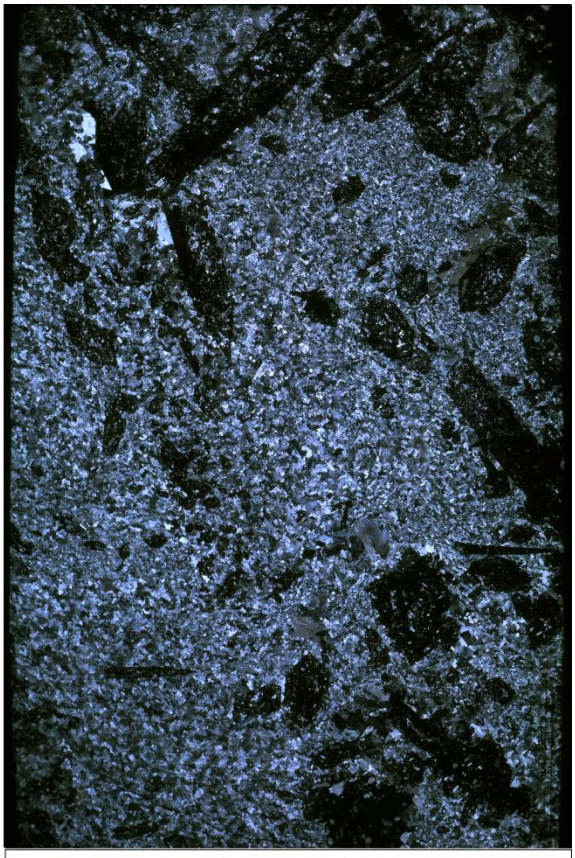

20TN16A-2

Sample 20TN17A

Thin Sections: 20TN17A-1, 20TN17A-2

Rock name: Strongly altered arfvedsonite-aegirine syenite

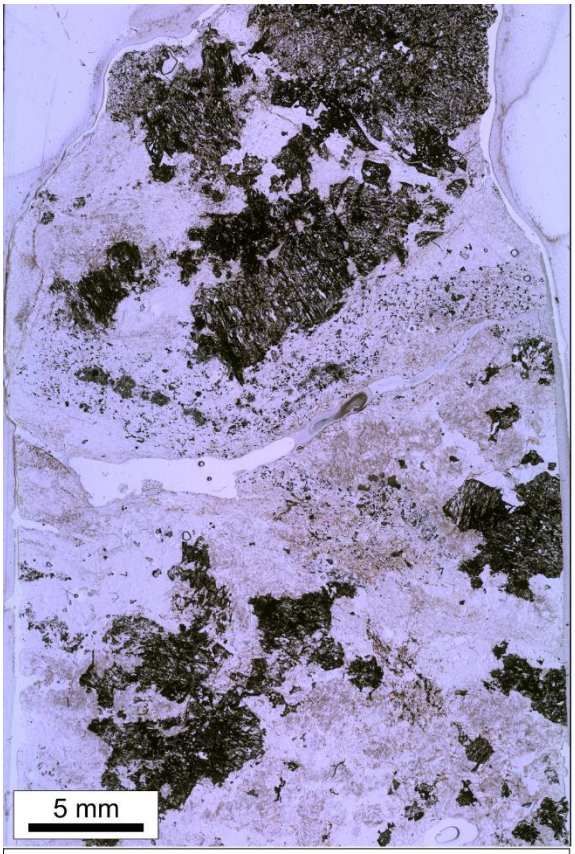

20TN17A-1

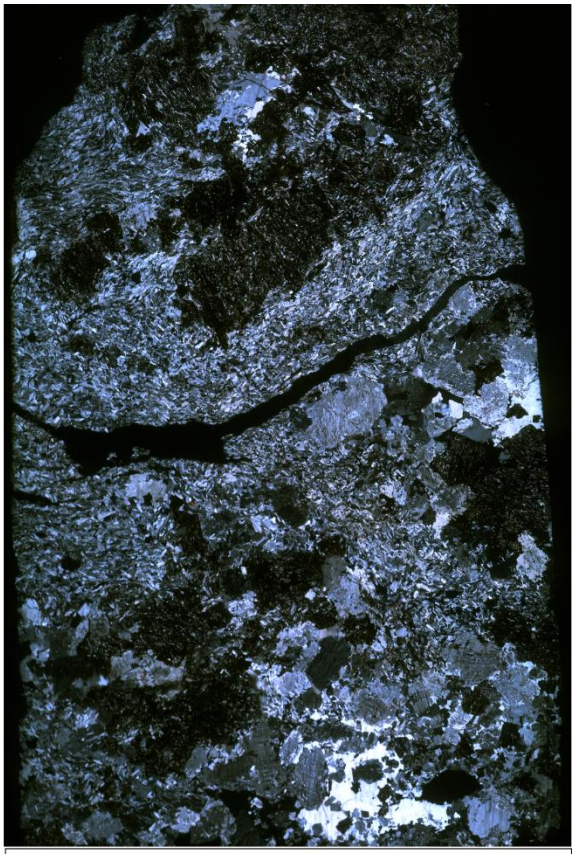

20TN17A-1

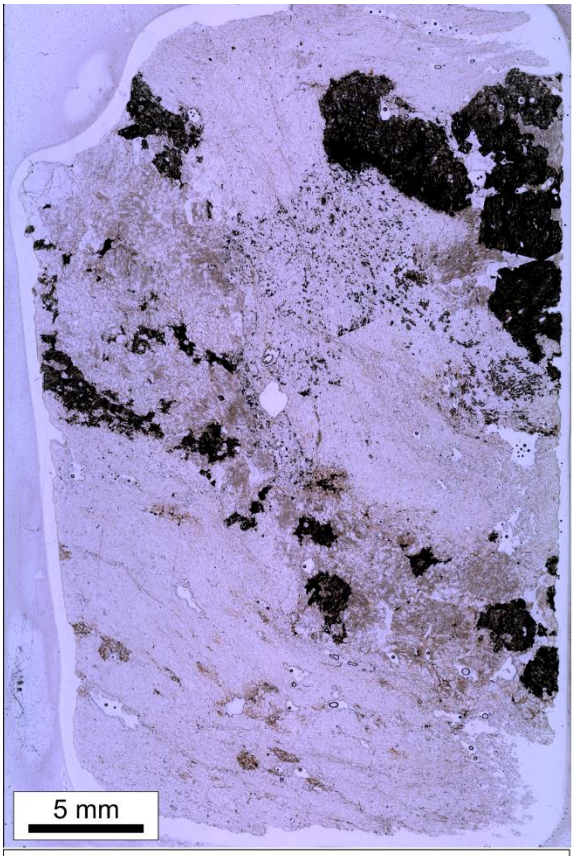

20TN17A-2

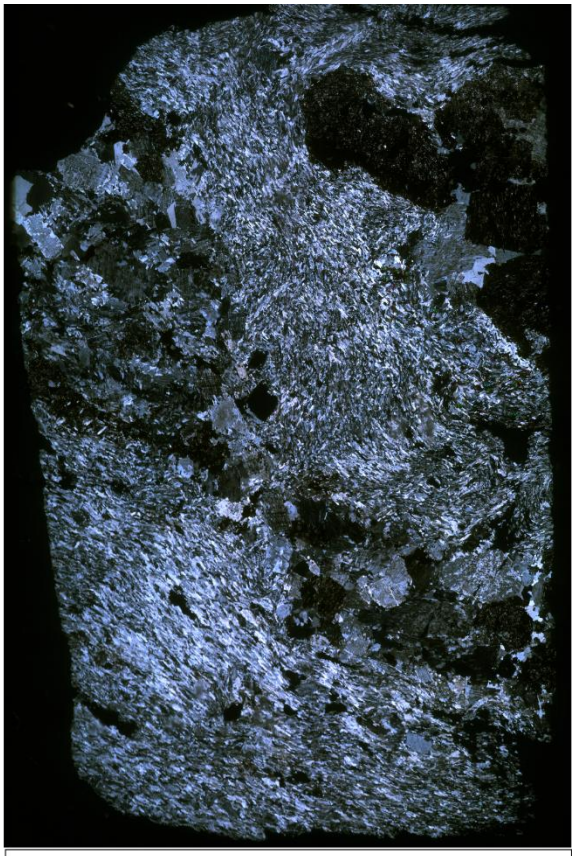

20TN17A-2

Sample 20TN18

Rock name: Strongly altered arfvedsonite-aegirine syenite

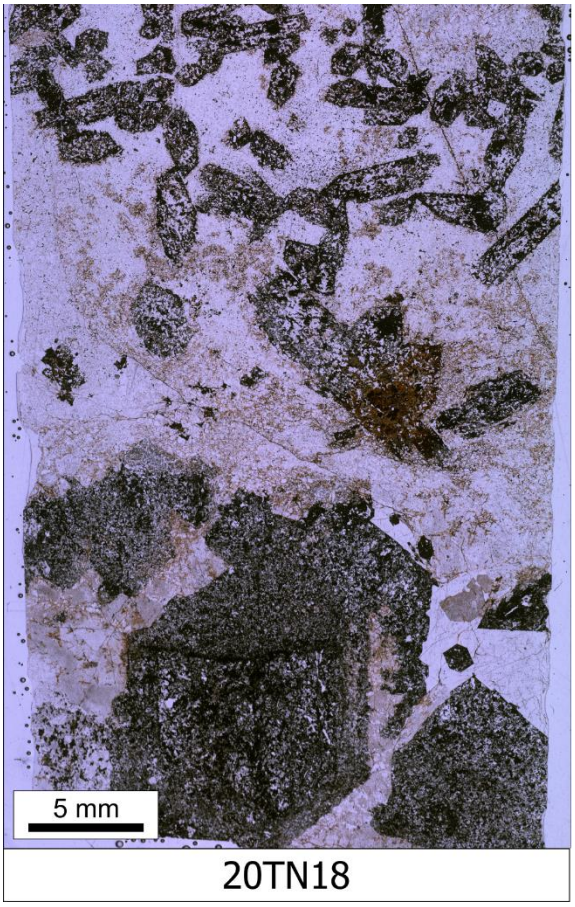

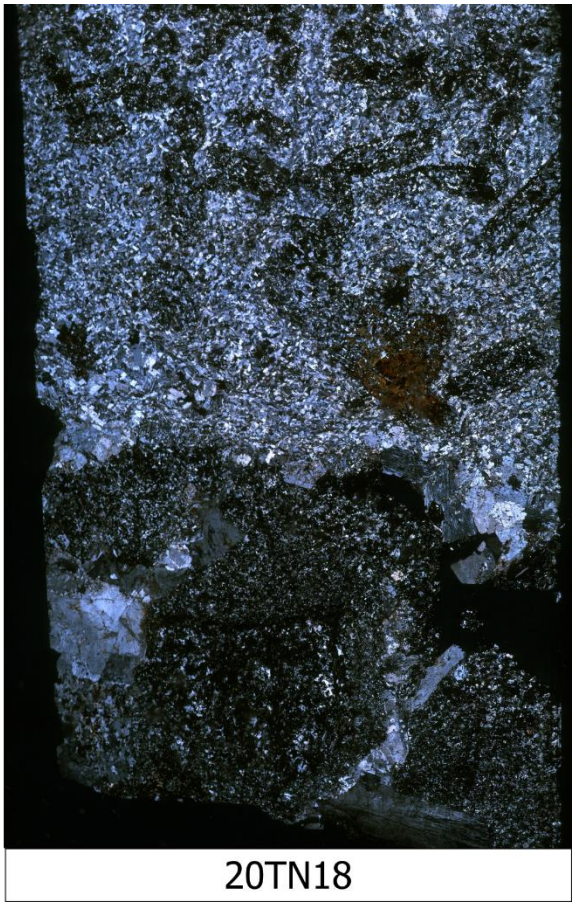

Sample 20TN19

Rock name: zircon-potassium feldspar-quartz vein

This vein is in contact with the strongly altered arfvedsonite-aegirine syenite

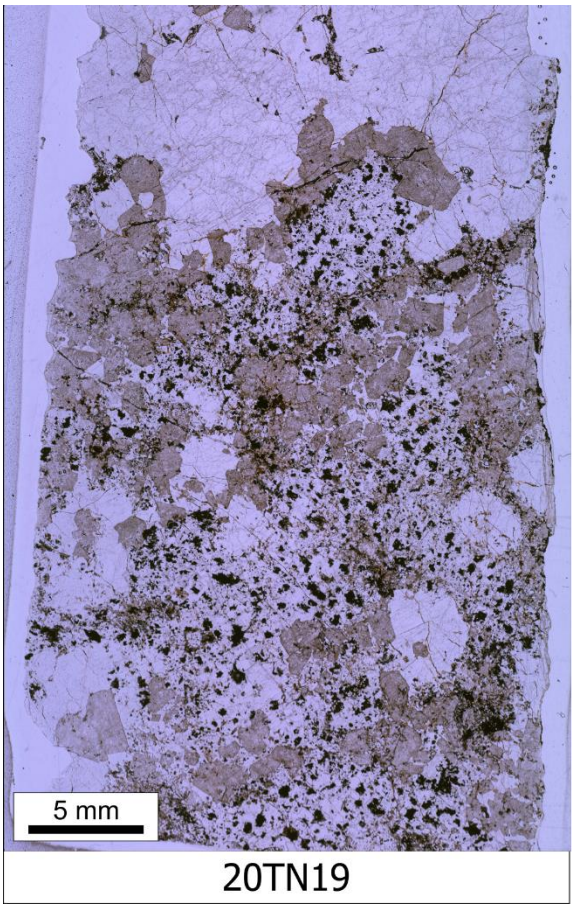

Sample 20TN20

Rock name: Moderately altered arfvedsonite-aegirine syenite

20TN20

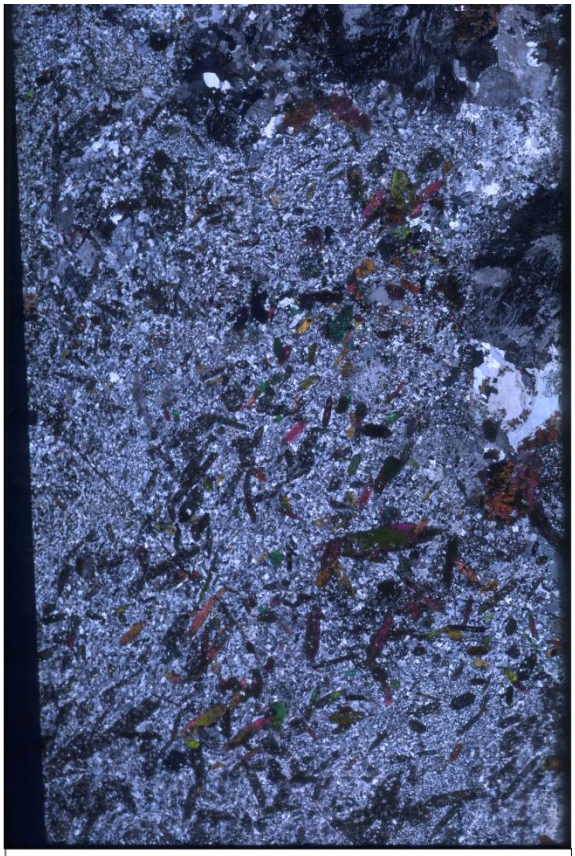

20TN20

Sample 20TN58A

Rock name: Strongly altered arfvedsonite-aegirine syenite

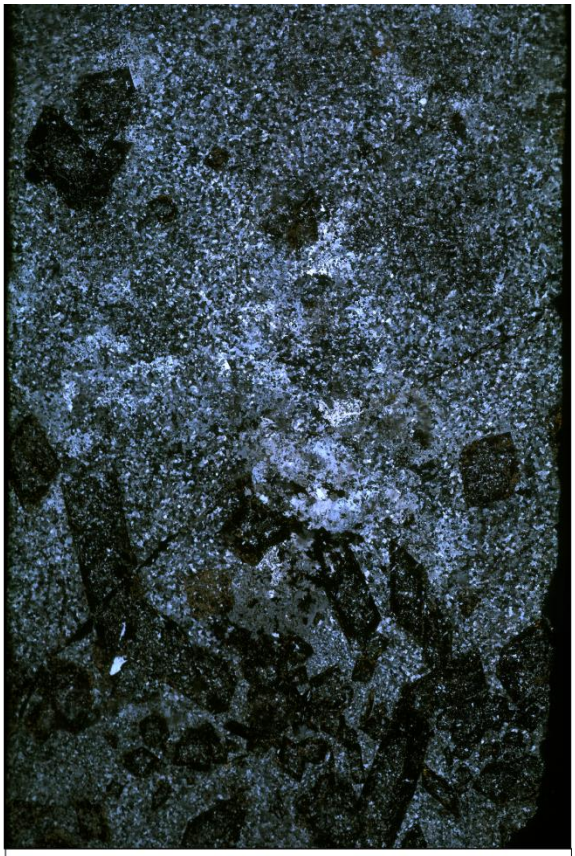

Sample 20TN58B

Rock name: Strongly altered arfvedsonite-aegirine syenite

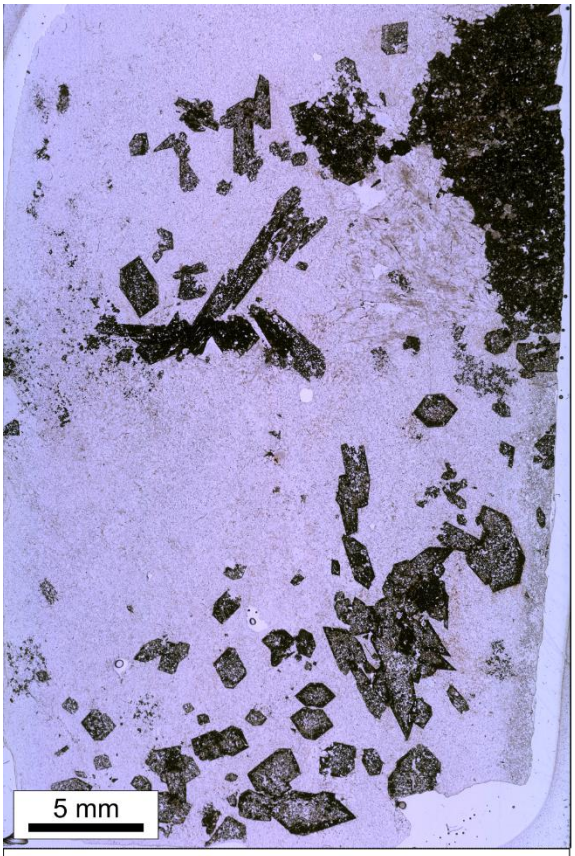

20TN58B

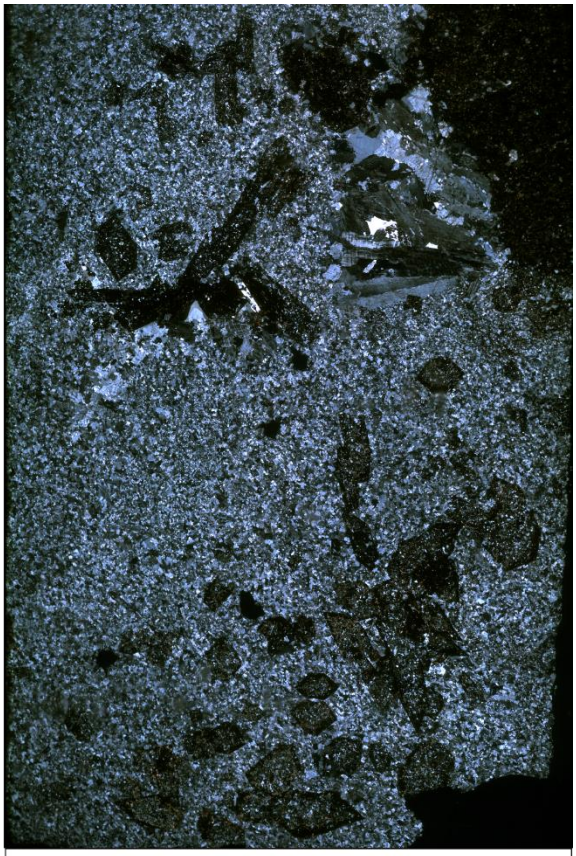

20TN58B

Layered titanite-arfvedsonite syenite

Hand specimens: 20TN15A

Thin sections: 20TN15A

Sample 20TN15A

Rock name: Layered titanite-arfvedsonite syenite

20TN15A

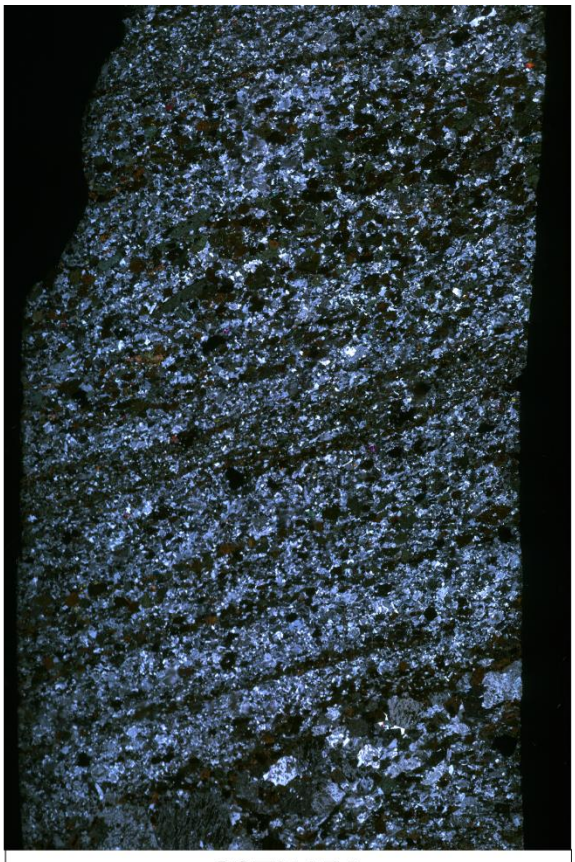

20TN15A

Altered layered amphibole-diopside-phlogopite syenite

Hand specimens: 20TN15B, 20TN15C

Thin sections: 20TN15B, 20TN15C

Sample 20TN15B

Rock name: Altered layered amphibole-diopside-phlogopite syenite

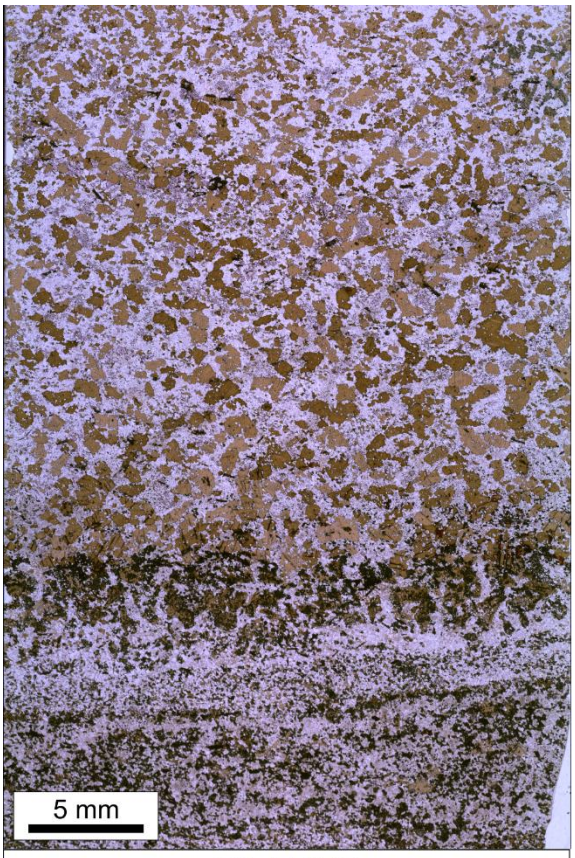

20TN15B

20TN15B

Sample 20TN15C

Rock name: Altered layered amphibole-diopside-phlogopite syenite

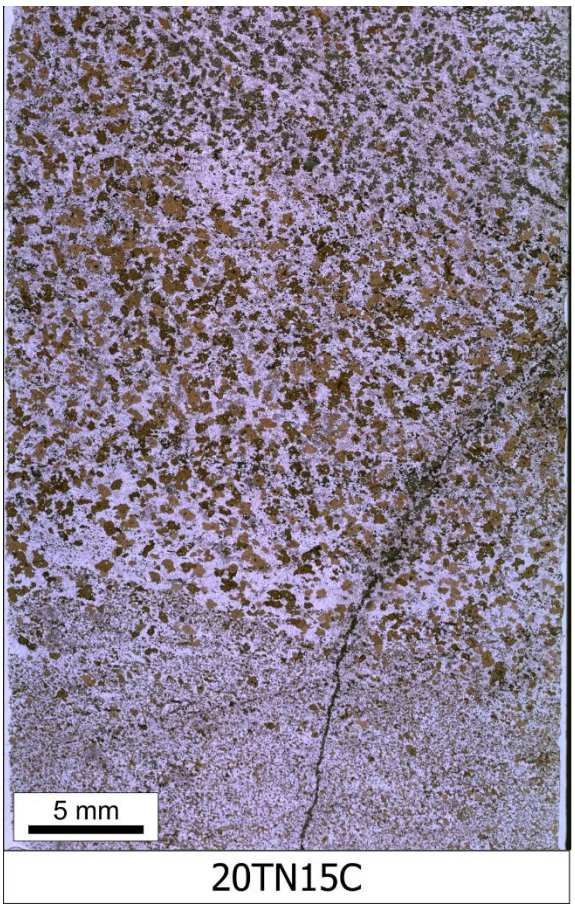

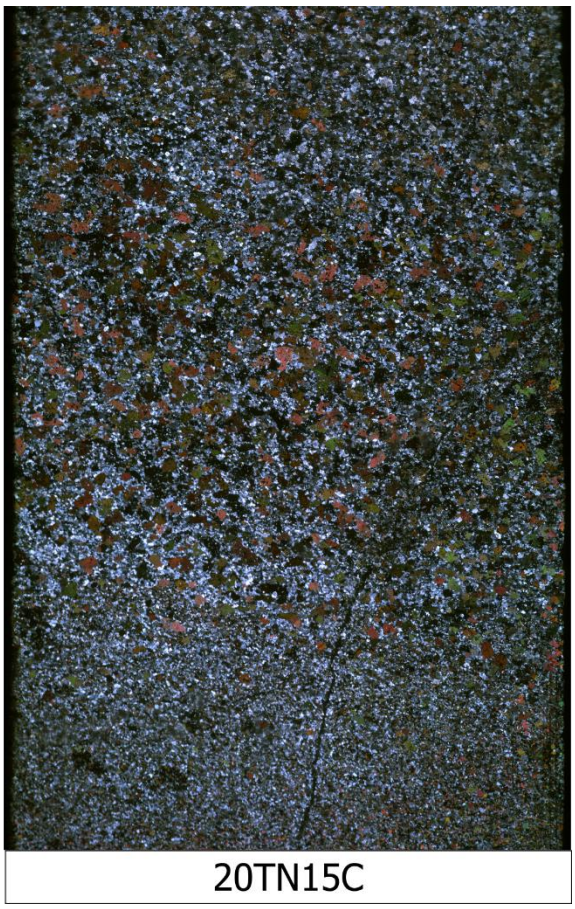

Nepheline alkali feldspar syenite

Hand Specimen: 20TN53, 20TN55A, 20TN55B, 20TN56, 20TN57A

Thin Section(s): 20TN53, 20TN55A, 20TN55B, 20TN56, 20TN57A

These samples were collected form the unit known as the “Pool Creek nepheline syenite”. The rocks are coarse to very coarse grained. In these samples, nepheline has been completely replaced by sericite. A former mafic mineral has been completely replaced by chlorite and phlogopite. Potassium feldspar is perthitic and turbid looking. Potassium feldspar boundaries are commonly lined with fine grained albite.

Sample 20TN53

Rock name: Mildly altered nepheline alkali feldspar syenite

20TN53


20TN53

Sample 20TN55A

Rock name: Mildly altered nepheline alkali feldspar syenite

Note the second order interference colours of the fine grained zircon crystals (right image).

20TN55A

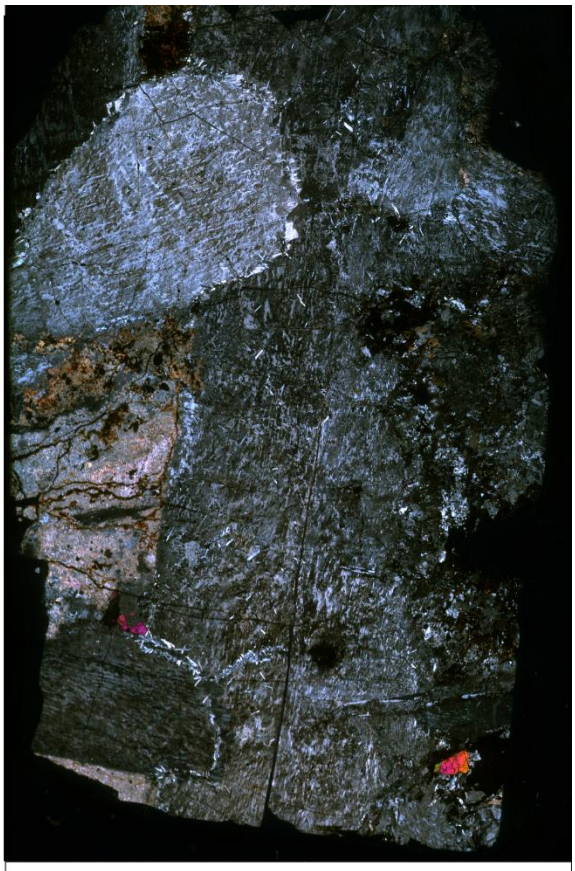

20TN55A

Sample 20TN55B

Rock name: Mildly altered nepheline alkali feldspar syenite

Sample 20TN56

Rock name: Mildly altered nepheline alkali feldspar syenite

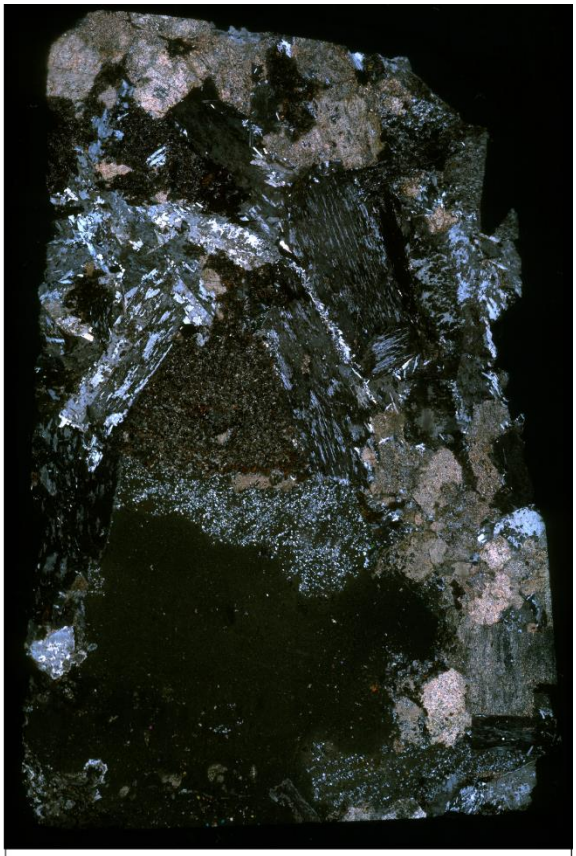

Sample 20TN57A

Rock name: Mildly altered nepheline alkali feldspar syenite

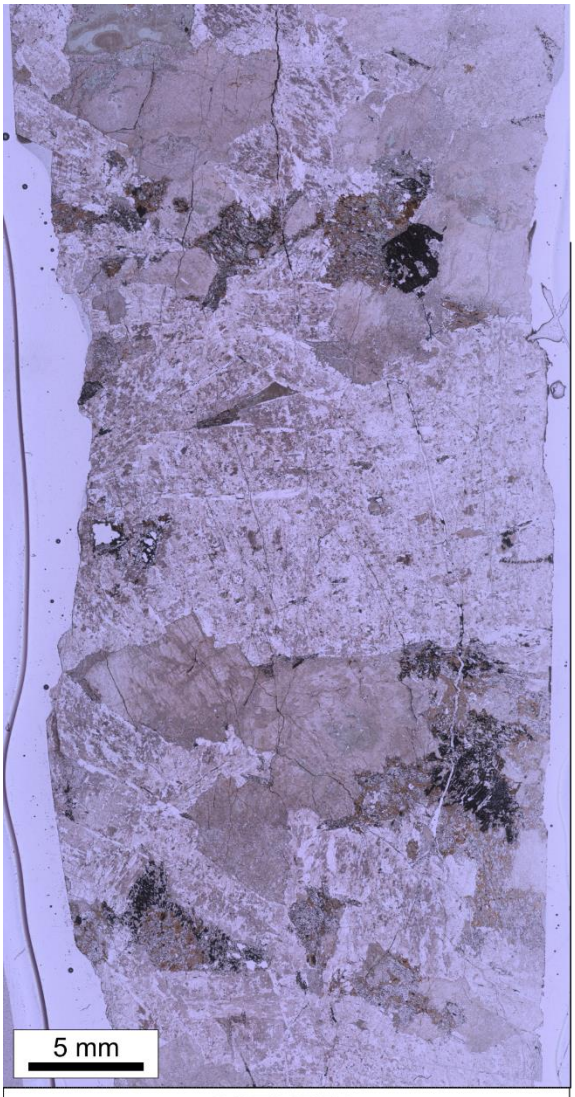

20TN57A

20TN57A

Altered porphyritic lamprophyre(?) dike

Hand specimens: 20TN57B, 20TN57C

Thin sections: 20TN57B, 20TN57C-1, 20TN57C-2

Note, 20TN57C-2 shows a contact with nepheline alkali feldspar syenite.

Sample 20TN57B

Rock name: Strongly altered porphyritic lamprophyre(?) dike

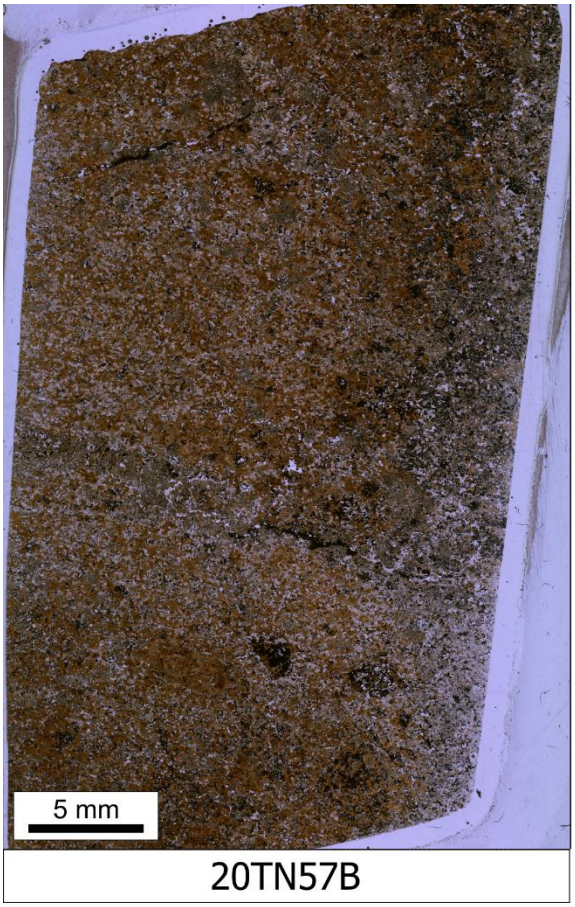

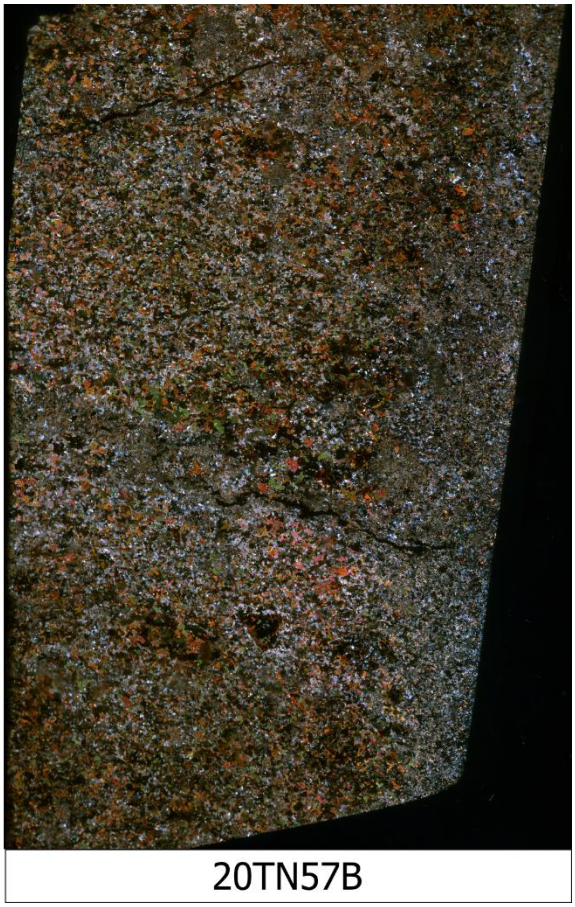

Sample 20TN57C-1

Rock name: Strongly altered porphyritic lamprophyre(?) dike

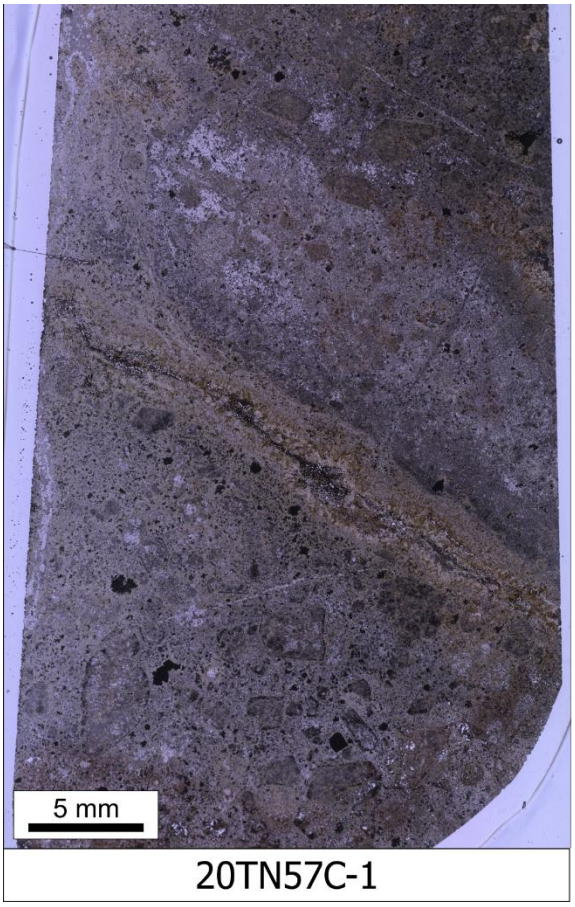

20TN57C-1

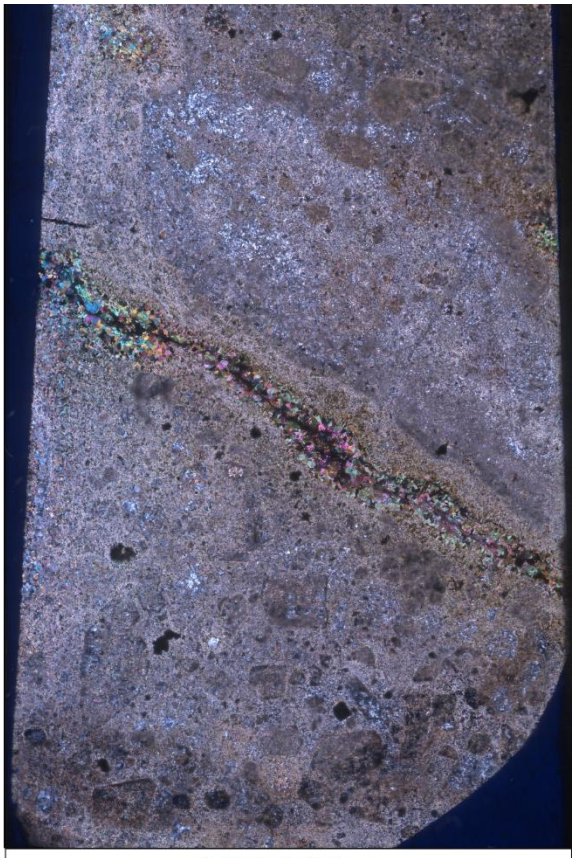

20TN57C-1

Sample 20TN57C-2

Rock name: Strongly altered porphyritic lamprophyre(?) dike

Note, this sample is in contact with the nepheline syenite (upper left corner).

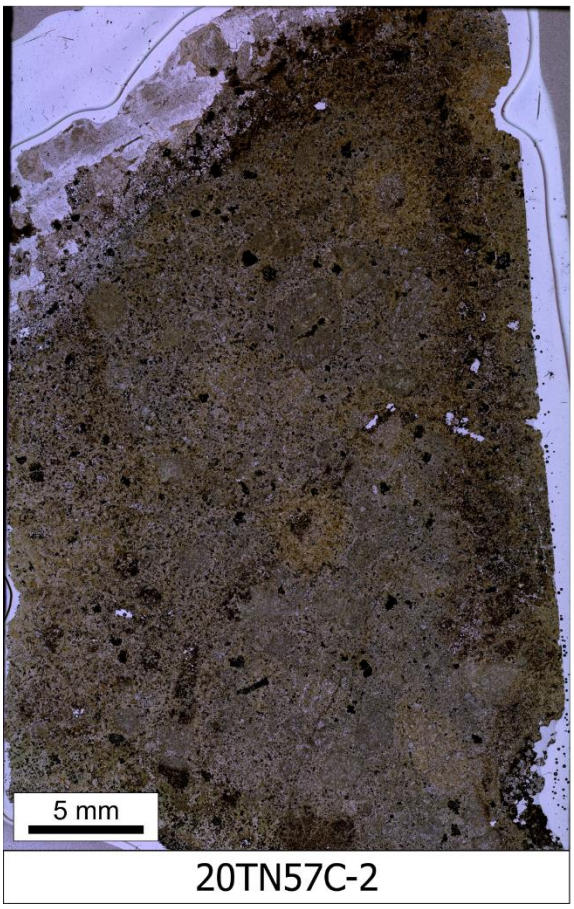

Altered feldspar glomeroporphyritic syenite dike

Hand specimens: 20TN54

Thin sections: 20TN54

20TN54

Rock name: Altered feldspar glomeroporphyritic syenite dike

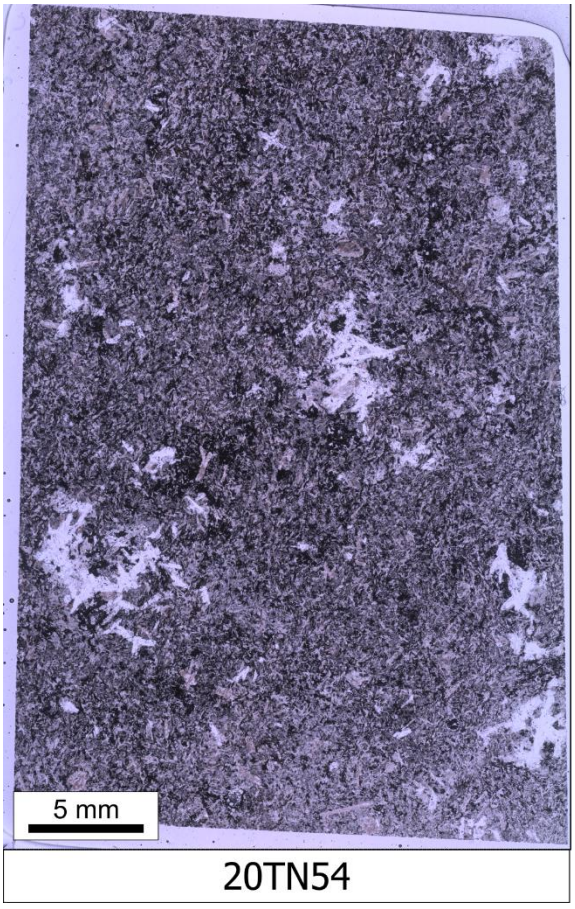

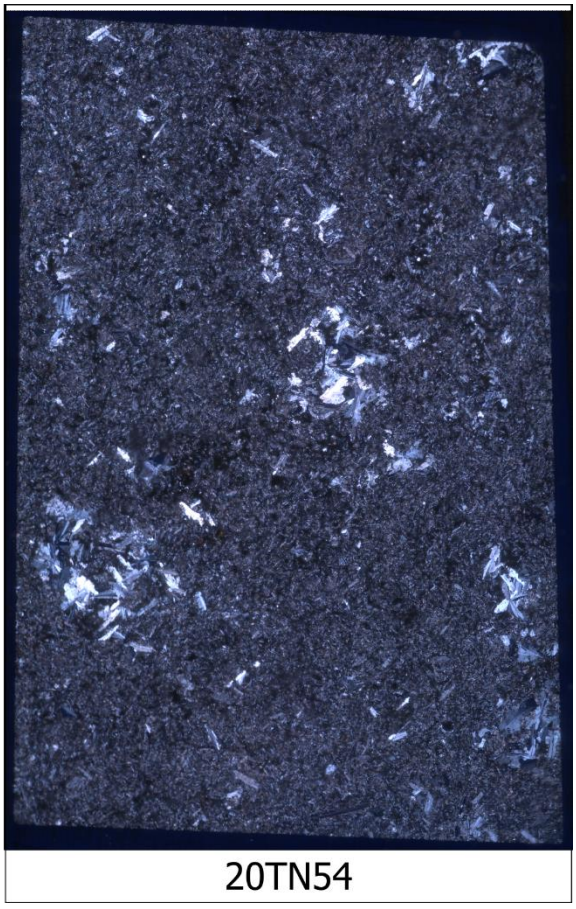

Appendix B: Complete Electron Microprobe Dataset

Table B.1. Composition of feldspar from various rock types across the 2020 Corundum Dome and Pyrochlore Dome sampling area.

Sample	20TN55A	20TN55A	20TN55A	20TN55A	20TN55A	20TN55A	20TN55A	20TN55A	20TN55A	20TN55A	20TN55A	20TN55A	20TN55A
Analysis	9-51-1	9-52-2	9-53-3	9-54-4	9-55-5	9-56-6	9-57-7	9-58-8	9-59-9	9-60-10	9-61-11	9-62-12	15-82-1
Comment	Ab	Ab	Ksp	Ksp	Ab	Ksp	Ksp	Ab	Ab	Ksp	Ab	Ksp	Ab
SiO_2 (wt. %)	68.46	68.24	64.87	64.95	68.35	63.95	64.27	68.15	67.84	64.51	68.07	64.50	69.17
Al_2O_3	19.23	18.68	17.58	17.57	18.93	17.39	17.50	18.48	18.59	17.62	18.70	17.64	19.28
Fe_2O_3*	0.24	0.22	0.03	0.01	0.26	0.42	0.32	0.17	0.15	0.14	0.08	0.16	0.00
MgO	0.00	0.00	0.00	0.00	0.00	0.13	0.07	0.00	0.07	0.01	0.00	0.00	0.00
CaO	0.01	0.00	0.00	0.00	0.00	0.00	0.00	0.01	0.02	0.00	0.01	0.02	0.00
FeO*	0.00	0.00	0.00	0.00	0.00	0.00	0.00	0.00	0.00	0.00	0.00	0.00	0.18
BaO	0.01	0.00	0.00	0.10	0.00	0.07	0.14	0.06	0.00	0.01	0.00	0.05	0.00
Na_2O	11.66	11.66	0.32	0.28	11.70	0.16	0.24	11.75	11.58	0.21	11.86	0.21	11.64
K_2O	0.25	0.24	17.06	17.03	0.22	16.98	17.05	0.04	0.25	17.09	0.05	17.21	0.24
Total	99.85	99.04	99.85	99.95	99.47	99.10	99.60	98.66	98.50	99.60	98.77	99.80	100.51
Si (*apfu*)	2.998	3.013	3.016	3.018	3.005	3.004	3.005	3.019	3.011	3.010	3.012	3.007	3.007
Al	0.993	0.972	0.963	0.962	0.981	0.963	0.964	0.965	0.972	0.969	0.975	0.969	0.988
Fe^{3+}	0.008	0.007	0.001	0.000	0.009	0.015	0.011	0.006	0.005	0.005	0.003	0.006	0.000
Mg	0.000	0.000	0.000	0.000	0.000	0.009	0.005	0.000	0.005	0.001	0.000	0.000	0.000
Ca	0.000	0.000	0.000	0.000	0.000	0.000	0.000	0.000	0.001	0.000	0.000	0.001	0.000
Fe^{2+}	0.000	0.000	0.000	0.000	0.000	0.000	0.000	0.000	0.000	0.000	0.000	0.000	0.007
Ba	0.000	0.000	0.000	0.002	0.000	0.001	0.003	0.001	0.000	0.000	0.000	0.001	0.000
Na	0.990	0.998	0.029	0.026	0.998	0.015	0.022	1.009	0.997	0.019	1.017	0.019	0.981
K	0.014	0.013	1.012	1.010	0.012	1.017	1.017	0.002	0.014	1.017	0.003	1.024	0.013
Cation sum	5.003	5.004	5.021	5.018	5.005	5.023	5.027	5.002	5.005	5.022	5.010	5.027	4.996
% Ca	0.03	0.00	0.00	0.00	0.01	0.00	0.02	0.04	0.09	0.00	0.03	0.08	0.00
% Na	98.60	98.67	2.75	2.48	98.75	1.45	2.13	99.72	98.54	1.87	99.67	1.86	98.69
% K	1.37	1.33	97.25	97.52	1.24	98.55	97.84	0.24	1.37	98.13	0.30	98.06	1.31
Total	100	100	100	100	100	100	100	100	100	100	100	100	100

Note: Compositions were recalculated on the basis of 8 O apfu. * Calculated by stoichiometry using Droop (1987) calculation method.

Table B.1. (Continued) Composition of feldspar from various rock types across the 2020 Corundum Dome and Pyrochlore Dome sampling area.

Sample	20TN55A	20TN55A	20TN55A	20TN55A	20TN55A	20TN55A	20TN55A	20TN55A	20TN55A	20TN55A	20TN55A	20TN55A	20TN55A
Analysis	15-83-2	15-85-4	15-86-5	15-87-6	15-88-7	15-89-8	15-90-9	15-91-10	15-92-11	19-104-1	19-105-2	19-106-3	19-107-4
Comment	Ab	Ab	Ab	Ksp	Ksp	Ksp	Ksp	Ksp	Ksp	Ab	Ksp	Ksp	Ab
SiO_2 (wt. %)	69.03	69.06	69.01	64.76	64.93	64.42	64.99	65.43	66.35	69.19	64.99	65.48	69.64
Al_2O_3	19.19	19.39	19.48	17.49	17.72	17.45	17.61	17.48	17.22	18.68	17.58	17.75	18.88
Fe_2O_3*	0.17	0.00	0.00	0.17	0.01	0.26	0.13	0.06	0.00	0.00	0.09	0.04	0.00
MgO	0.00	0.00	0.00	0.00	0.00	0.00	0.00	0.00	0.01	0.00	0.00	0.00	0.00
CaO	0.00	0.00	0.00	0.38	0.00	0.01	0.00	0.00	0.00	0.02	0.01	0.01	0.01
FeO*	0.07	0.22	0.20	0.00	0.00	0.00	0.00	0.00	0.07	0.16	0.00	0.00	0.01
BaO	0.00	0.00	0.01	0.00	0.03	0.03	0.03	0.03	0.02	0.00	0.00	0.02	0.00
Na_2O	11.71	11.60	11.60	0.33	0.29	0.24	0.29	0.21	0.25	11.69	0.23	0.27	11.90
K_2O	0.24	0.17	0.20	17.10	17.21	17.20	17.28	17.15	16.87	0.27	17.14	17.25	0.02
Total	100.41	100.44	100.50	100.23	100.19	99.60	100.32	100.37	100.78	100.01	100.04	100.83	100.46
Si (*apfu*)	3.005	3.003	3.000	3.008	3.012	3.010	3.013	3.026	3.047	3.024	3.017	3.016	3.024
Al	0.985	0.994	0.998	0.957	0.969	0.961	0.962	0.953	0.932	0.962	0.962	0.964	0.966
Fe^{3+}	0.006	0.000	0.000	0.006	0.000	0.009	0.004	0.002	0.000	0.000	0.003	0.001	0.000
Mg	0.000	0.000	0.000	0.000	0.000	0.000	0.000	0.000	0.001	0.000	0.000	0.000	0.000
Ca	0.000	0.000	0.000	0.019	0.000	0.001	0.000	0.000	0.000	0.001	0.000	0.001	0.000
Fe^{2+}	0.002	0.008	0.007	0.000	0.000	0.000	0.000	0.000	0.003	0.006	0.000	0.000	0.000
Ba	0.000	0.000	0.000	0.000	0.000	0.000	0.001	0.001	0.000	0.000	0.000	0.000	0.000
Na	0.988	0.978	0.978	0.030	0.026	0.022	0.026	0.019	0.022	0.990	0.020	0.024	1.002
K	0.013	0.009	0.011	1.013	1.018	1.025	1.022	1.012	0.988	0.015	1.015	1.014	0.001
Cation sum	5.000	4.993	4.995	5.032	5.026	5.028	5.028	5.012	4.993	4.998	5.018	5.020	4.994
% Ca	0.00	0.00	0.02	1.79	0.00	0.05	0.00	0.00	0.00	0.07	0.04	0.06	0.03
% Na	98.69	99.04	98.87	2.79	2.51	2.09	2.45	1.84	2.22	98.43	1.97	2.33	99.84
% K	1.31	0.96	1.10	95.42	97.49	97.86	97.55	98.15	97.78	1.49	97.99	97.61	0.13
Total	100	100	100	100	100	100	100	100	100	100	100	100	100

Table B.1. (Continued) Composition of feldspar from various rock types across the 2020 Corundum Dome and Pyrochlore Dome sampling area.

Sample	20TN55A	20TN55A	20TN57A	20TN57A	20TN57A	20TN57A	20TN57A	20TN57A	20TN57A	20TN57A	20TN57A	20TN57A	20TN57A
Analysis	19-108-5	19-109-6	22-130-1	22-131-2	22-132-3	22-133-4	22-134-5	22-135-6	22-136-7	22-137-8	22-138-9	22-139-10	22-140-11
Comment	Ksp	Ab	Ab	Ab	Ab	Ab	Ab	Ab	Ab	Ab	Ksp	Ksp	Ksp
SiO_2 (wt. %)	65.31	69.03	69.09	68.86	69.19	68.94	69.11	69.63	68.70	69.55	64.80	63.64	65.34
Al_2O_3	17.74	18.57	19.48	19.20	19.21	19.00	19.29	19.09	18.91	19.14	17.99	19.12	17.79
Fe_2O_3*	0.36	0.07	0.00	0.00	0.00	0.00	0.00	0.00	0.52	0.00	0.16	0.32	0.18
MgO	0.00	0.01	0.01	0.00	0.00	0.01	0.00	0.02	0.42	0.02	0.02	0.17	0.00
CaO	0.00	0.01	0.00	0.00	0.01	0.00	0.01	0.06	0.05	0.06	0.05	0.00	0.00
FeO*	0.00	0.00	0.12	0.12	0.30	0.14	0.11	0.31	0.00	0.13	0.00	0.00	0.00
BaO	0.08	0.00	0.00	0.00	0.00	0.00	0.00	0.00	0.02	0.02	0.03	0.09	0.03
Na_2O	0.27	11.89	11.59	11.50	11.55	11.70	11.49	11.76	11.68	11.76	0.34	0.29	0.70
K_2O	17.12	0.03	0.25	0.27	0.22	0.18	0.25	0.07	0.27	0.10	17.02	16.63	16.61
Total	100.89	99.61	100.52	99.95	100.48	99.97	100.25	100.94	100.58	100.77	100.41	100.26	100.65
Si (*apfu*)	3.010	3.025	3.002	3.009	3.009	3.013	3.009	3.014	2.993	3.014	2.999	2.950	3.011
Al	0.963	0.959	0.997	0.989	0.985	0.978	0.990	0.974	0.971	0.978	0.981	1.044	0.966
Fe^{3+}	0.013	0.002	0.000	0.000	0.000	0.000	0.000	0.000	0.017	0.000	0.006	0.011	0.006
Mg	0.000	0.001	0.000	0.000	0.000	0.000	0.000	0.001	0.027	0.002	0.001	0.011	0.000
Ca	0.000	0.001	0.000	0.000	0.001	0.000	0.000	0.003	0.002	0.003	0.003	0.000	0.000
Fe^{2+}	0.000	0.000	0.004	0.004	0.011	0.005	0.004	0.011	0.000	0.005	0.000	0.000	0.000
Ba	0.001	0.000	0.000	0.000	0.000	0.000	0.000	0.000	0.000	0.000	0.001	0.002	0.000
Na	0.024	1.011	0.976	0.974	0.974	0.992	0.970	0.987	0.987	0.988	0.031	0.026	0.063
K	1.006	0.001	0.014	0.015	0.012	0.010	0.014	0.004	0.015	0.005	1.005	0.983	0.976
Cation sum	5.018	5.000	4.994	4.991	4.991	4.999	4.987	4.994	5.013	4.994	5.025	5.028	5.022
% Ca	0.00	0.05	0.00	0.00	0.06	0.02	0.03	0.27	0.23	0.26	0.25	0.02	0.00
% Na	2.36	99.80	98.62	98.47	98.72	99.00	98.56	99.33	98.25	99.19	2.95	2.61	6.03
% K	97.64	0.15	1.38	1.53	1.22	0.98	1.41	0.40	1.51	0.54	96.80	97.37	93.97
Total	100	100	100	100	100	100	100	100	100	100	100	100	100

Table B.1. (Continued) Composition of feldspar from various rock types across the 2020 Corundum Dome and Pyrochlore Dome sampling area.

Sample	20TN57A	20TN57A	20TN57A	20TN57A	20TN57A	20TN57A	20TN57A	20TN57A	20TN57A	20TN57A	20TN53	20TN53	20TN53
Analysis	22-141-12	22-142-13	29-181-1	29-182-2	29-183-3	29-184-4	29-185-5	29-186-6	29-187-7	29-188-8	33-202-1	33-203-2	33-204-3
Comment	Ksp	Ksp	Ab	Ab	Ab	Ksp	Ksp	Ksp	Ksp	Ksp	Ab	Ab	Ksp
SiO_2 (wt. %)	64.96	65.44	68.58	69.04	69.05	65.31	65.65	65.29	66.00	66.06	69.02	69.26	65.56
Al_2O_3	17.71	17.76	18.76	19.05	18.88	17.46	17.70	17.91	17.91	18.01	19.08	19.02	17.78
Fe_2O_3*	0.21	0.21	0.12	0.00	0.00	0.22	0.12	0.21	0.23	0.30	0.06	0.00	0.02
MgO	0.01	0.01	0.00	0.01	0.00	0.02	0.01	0.02	0.01	0.01	0.00	0.00	0.00
CaO	0.00	0.00	0.00	0.00	0.00	0.00	0.00	0.00	0.00	0.00	0.00	0.00	0.00
FeO*	0.00	0.00	0.00	0.16	0.16	0.00	0.00	0.00	0.00	0.00	0.19	0.17	0.00
BaO	0.02	0.07	0.00	0.01	0.01	0.13	0.05	0.01	0.31	0.19	0.03	0.00	0.00
Na_2O	0.32	0.41	11.77	11.77	11.76	0.32	0.45	0.69	1.33	1.77	11.73	11.77	0.22
K_2O	17.03	16.86	0.13	0.13	0.13	17.06	16.78	16.42	15.43	14.88	0.17	0.19	17.22
Total	100.25	100.76	99.35	100.17	99.99	100.52	100.76	100.55	101.21	101.23	100.27	100.42	100.80
Si (*apfu*)	3.010	3.014	3.015	3.012	3.017	3.020	3.020	3.008	3.014	3.010	3.009	3.014	3.018
Al	0.967	0.964	0.972	0.979	0.972	0.952	0.960	0.972	0.964	0.967	0.980	0.976	0.965
Fe^{3+}	0.007	0.007	0.004	0.000	0.000	0.008	0.004	0.007	0.008	0.010	0.002	0.000	0.001
Mg	0.000	0.001	0.000	0.001	0.000	0.001	0.001	0.001	0.001	0.001	0.000	0.000	0.000
Ca	0.000	0.000	0.000	0.000	0.000	0.000	0.000	0.000	0.000	0.000	0.000	0.000	0.000
Fe^{2+}	0.000	0.000	0.000	0.006	0.006	0.000	0.000	0.000	0.000	0.000	0.007	0.006	0.000
Ba	0.000	0.001	0.000	0.000	0.000	0.002	0.001	0.000	0.006	0.003	0.001	0.000	0.000
Na	0.029	0.037	1.003	0.995	0.997	0.028	0.040	0.062	0.118	0.156	0.991	0.993	0.020
K	1.007	0.990	0.007	0.007	0.007	1.006	0.985	0.965	0.899	0.865	0.010	0.011	1.011
Cation sum	5.021	5.014	5.002	5.000	4.999	5.018	5.010	5.016	5.008	5.012	5.000	5.000	5.015
% Ca	0.00	0.01	0.02	0.01	0.00	0.01	0.00	0.00	0.00	0.00	0.00	0.00	0.00
% Na	2.80	3.56	99.28	99.28	99.28	2.75	3.90	6.01	11.56	15.29	99.05	98.94	1.91
% K	97.20	96.43	0.70	0.71	0.72	97.24	96.10	93.99	88.44	84.71	0.95	1.06	98.09
Total	100	100	100	100	100	100	100	100	100	100	100	100	100

Table B.1. (Continued) Composition of feldspar from various rock types across the 2020 Corundum Dome and Pyrochlore Dome sampling area.

Sample	20TN53	20TN53	20TN53	20TN53	20TN53	20TN53	20TN53	20TN53	20TN53	20TN10C	20TN10C	20TN10C	20TN10C
Analysis	33-205-4	33-206-5	35-214-1	35-215-2	35-216-3	35-218-5	35-219-6	39-231-1	39-232-2	15-80-1	15-81-2	15-82-3	15-83-4
Comment	Ksp	Ab	Ksp	Ab	Ab	Ab	Ksp	Ksp	Ksp	Ksp	Ksp	Ksp	Ab
SiO_2 (wt. %)	65.65	69.13	65.80	69.80	69.68	69.81	61.04	63.82	64.10	65.69	65.62	64.87	69.67
Al_2O_3	17.67	19.07	17.65	19.22	19.15	18.96	16.64	17.53	17.37	17.76	17.74	17.54	19.42
Fe_2O_3*	0.10	0.00	0.14	0.00	0.00	0.00	0.79	0.07	0.03	0.17	0.18	0.11	0.00
MgO	0.00	0.01	0.00	0.00	0.00	0.00	0.01	0.03	0.00	0.00	0.00	0.00	0.00
CaO	0.00	0.01	0.01	0.00	0.00	0.00	3.69	0.03	0.12	0.00	0.00	0.00	0.00
FeO*	0.00	0.17	0.00	0.10	0.11	0.10	0.00	0.73	0.30	0.00	0.00	0.00	0.05
BaO	0.03	0.00	0.04	0.00	0.01	0.00	0.12	0.07	0.12	0.07	0.05	0.04	0.00
Na_2O	0.21	11.68	0.23	11.72	11.62	11.69	0.19	0.23	0.25	0.23	0.21	0.23	11.81
K_2O	17.27	0.13	17.42	0.15	0.21	0.20	16.01	17.14	17.24	17.41	17.46	17.45	0.11
Total	100.93	100.20	101.28	100.99	100.80	100.76	98.48	99.58	99.49	101.34	101.25	100.23	101.07
Si (*apfu*)	3.020	3.013	3.020	3.016	3.018	3.024	2.928	2.991	3.005	3.014	3.014	3.013	3.009
Al	0.958	0.980	0.955	0.979	0.977	0.968	0.941	0.968	0.960	0.961	0.960	0.960	0.989
Fe^{3+}	0.004	0.000	0.005	0.000	0.000	0.000	0.028	0.026	0.011	0.006	0.006	0.004	0.000
Mg	0.000	0.001	0.000	0.000	0.000	0.000	0.000	0.002	0.000	0.000	0.000	0.000	0.000
Ca	0.000	0.000	0.000	0.000	0.000	0.000	0.190	0.001	0.006	0.000	0.000	0.000	0.000
Fe^{2+}	0.000	0.006	0.000	0.004	0.004	0.004	0.000	0.000	0.000	0.000	0.000	0.000	0.002
Ba	0.001	0.000	0.001	0.000	0.000	0.000	0.002	0.001	0.002	0.001	0.001	0.001	0.000
Na	0.019	0.987	0.020	0.982	0.976	0.982	0.018	0.021	0.022	0.021	0.018	0.020	0.989
K	1.013	0.007	1.020	0.008	0.012	0.011	0.980	1.025	1.031	1.019	1.023	1.034	0.006
Cation sum	5.015	4.994	5.021	4.989	4.987	4.988	5.087	5.035	5.037	5.022	5.023	5.032	4.995
% Ca	0.00	0.04	0.02	0.00	0.02	0.02	15.97	0.14	0.55	0.01	0.00	0.00	0.00
% Na	1.83	99.22	1.95	99.14	98.78	98.88	1.51	1.97	2.11	1.99	1.77	1.94	99.38
% K	98.17	0.74	98.02	0.86	1.20	1.10	82.51	97.89	97.33	98.00	98.23	98.06	0.62
Total	100	100	100	100	100	100	100	100	100	100	100	100	100

Table B.1. (Continued) Composition of feldspar from various rock types across the 2020 Corundum Dome and Pyrochlore Dome sampling area.

Sample	20TN10C	20TN10C	20TN10C	20TN4A	20TN4A	20TN4A	20TN4A	20TN4A	20TN4A	20TN4A	20TN4D	20TN4D	20TN4D
Analysis	15-84-5	15-85-6	17-92-3	29-121-6	29-122-7	31-128-1	31-129-2	36-149-4	37-151-1	37-152-2	39-157-1	39-158-2	39-159-3
Comment	Ab	Ab	Ab	Ksp	Ksp	Ab	Ab	Ksp	Ab	Ab	Ab	Ab	Ksp
SiO_2 (wt. %)	69.26	69.19	69.69	63.89	63.35	68.95	68.97	62.54	68.91	68.90	69.14	69.11	65.52
Al_2O_3	19.44	18.86	18.96	18.09	18.16	18.71	18.92	18.50	18.92	19.12	18.66	18.77	17.63
Fe_2O_3*	0.00	0.12	0.00	0.27	0.46	0.30	0.31	0.80	0.04	0.03	0.01	0.03	0.01
MgO	0.00	0.00	0.00	0.20	0.35	0.00	0.01	0.66	0.01	0.01	0.00	0.00	0.00
CaO	0.00	0.00	0.03	0.01	0.00	0.01	0.01	0.03	0.01	0.17	0.01	0.01	0.00
FeO*	0.04	0.00	0.10	0.00	0.00	0.00	0.00	0.00	0.36	0.31	0.09	0.28	0.11
BaO	0.00	0.02	0.00	0.26	0.30	0.00	0.00	0.18	0.00	0.00	0.02	0.00	0.16
Na_2O	11.83	11.80	11.95	0.28	0.27	11.98	11.96	0.27	12.00	11.87	11.98	11.88	0.23
K_2O	0.09	0.21	0.03	17.23	16.93	0.17	0.13	16.42	0.11	0.21	0.15	0.12	17.42
Total	100.66	100.19	100.75	100.22	99.82	100.11	100.31	99.40	100.32	100.59	100.02	100.18	101.06
Si (*apfu*)	3.004	3.018	3.020	2.976	2.964	3.013	3.008	2.934	3.006	2.999	3.021	3.016	3.017
Al	0.994	0.969	0.968	0.993	1.001	0.964	0.972	1.023	0.973	0.981	0.961	0.965	0.957
Fe^{3+}	0.000	0.004	0.000	0.010	0.016	0.010	0.010	0.028	0.012	0.010	0.003	0.009	0.004
Mg	0.000	0.000	0.000	0.014	0.024	0.000	0.001	0.046	0.001	0.001	0.000	0.000	0.000
Ca	0.000	0.000	0.001	0.000	0.000	0.001	0.001	0.002	0.000	0.008	0.000	0.000	0.000
Fe^{2+}	0.001	0.000	0.004	0.000	0.000	0.000	0.000	0.000	0.000	0.000	0.000	0.000	0.000
Ba	0.000	0.000	0.000	0.005	0.005	0.000	0.000	0.003	0.000	0.000	0.000	0.000	0.003
Na	0.995	0.997	1.004	0.025	0.025	1.015	1.011	0.025	1.015	1.002	1.015	1.005	0.020
K	0.005	0.012	0.001	1.024	1.010	0.009	0.007	0.983	0.006	0.012	0.008	0.007	1.023
Cation sum	4.999	5.000	4.998	5.047	5.045	5.012	5.010	5.044	5.013	5.012	5.008	5.003	5.024
% Ca	0.02	0.00	0.13	0.03	0.02	0.05	0.06	0.16	0.03	0.79	0.03	0.03	0.00
% Na	99.48	98.82	99.73	2.39	2.40	99.04	99.23	2.46	99.37	98.07	99.17	99.29	1.95
% K	0.50	1.18	0.14	97.58	97.58	0.91	0.71	97.38	0.60	1.14	0.80	0.69	98.05
Total	100	100	100	100	100	100	100	100	100	100	100	100	100

Table B.1. (Continued) Composition of feldspar from various rock types across the 2020 Corundum Dome and Pyrochlore Dome sampling area.

Sample	20TN4D	20TN4D	20TN4D	20TN4D	20TN4D	20TN4D	20TN4D	20TN20	20TN20	20TN20	20TN20	20TN20	20TN20
Analysis	39-160-4	39-161-5	44-180-1	44-181-2	44-182-3	46-187-3	46-188-4	49-193-1	49-194-2	49-195-3	49-197-5	49-198-6	52-214-1
Comment	Ksp	Ksp	Ksp	Ksp	Ab	Ksp	Ksp	Ab	Ab	Ab	Ksp	Ksp	Ab
SiO_2 (wt. %)	65.40	65.12	64.22	64.42	68.63	63.87	64.22	67.78	67.41	67.89	63.53	63.46	67.27
Al_2O_3	17.91	17.78	17.42	17.43	18.30	17.37	17.34	17.62	17.31	18.33	17.12	17.10	19.27
Fe_2O_3*	0.00	0.00	0.03	0.01	0.03	0.09	0.09	0.13	0.15	0.04	0.02	0.04	0.16
MgO	0.01	0.00	0.00	0.00	0.00	0.00	0.01	0.00	0.00	0.00	0.00	0.02	0.00
CaO	0.00	0.00	0.00	0.01	0.01	0.02	0.00	0.01	0.01	0.00	0.06	0.01	0.00
FeO*	0.04	0.01	0.33	0.14	0.31	0.00	0.00	1.35	1.50	0.39	0.19	0.38	1.55
BaO	0.13	0.15	0.04	0.28	0.05	0.02	0.01	0.00	0.01	0.00	0.02	0.01	0.00
Na_2O	0.27	0.26	0.21	0.23	11.89	0.41	0.25	11.78	11.71	11.68	0.25	0.19	11.79
K_2O	17.37	17.32	17.49	17.23	0.18	17.07	17.36	0.10	0.17	0.16	17.16	17.24	0.10
Total	101.13	100.64	99.71	99.75	99.38	98.86	99.27	98.63	98.12	98.45	98.34	98.41	99.98
Si (*apfu*)	3.008	3.010	3.005	3.011	3.023	3.008	3.013	3.017	3.020	3.017	3.011	3.007	2.959
Al	0.971	0.969	0.960	0.960	0.950	0.964	0.959	0.924	0.914	0.960	0.956	0.955	0.999
Fe^{3+}	0.001	0.000	0.012	0.005	0.010	0.003	0.003	0.045	0.050	0.013	0.007	0.014	0.051
Mg	0.001	0.000	0.000	0.000	0.000	0.000	0.001	0.000	0.000	0.000	0.000	0.001	0.000
Ca	0.000	0.000	0.000	0.000	0.000	0.001	0.000	0.000	0.000	0.000	0.003	0.000	0.000
Fe^{2+}	0.000	0.000	0.000	0.000	0.000	0.000	0.000	0.000	0.000	0.000	0.000	0.000	0.000
Ba	0.002	0.003	0.001	0.005	0.001	0.000	0.000	0.000	0.000	0.000	0.000	0.000	0.000
Na	0.024	0.023	0.019	0.021	1.015	0.037	0.022	1.017	1.017	1.006	0.023	0.017	1.006
K	1.019	1.021	1.044	1.027	0.010	1.025	1.039	0.006	0.010	0.009	1.038	1.042	0.005
Cation sum	5.027	5.027	5.040	5.030	5.010	5.040	5.037	5.009	5.011	5.005	5.038	5.038	5.021
% Ca	0.00	0.00	0.00	0.04	0.04	0.11	0.00	0.03	0.03	0.01	0.29	0.04	0.02
% Na	2.28	2.23	1.75	2.02	98.95	3.50	2.11	99.41	99.01	99.08	2.19	1.64	99.45
% K	97.72	97.77	98.25	97.93	1.01	96.40	97.88	0.56	0.95	0.91	97.52	98.32	0.54
Total	100	100	100	100	100	100	100	100	100	100	100	100	100

Table B.1. (Continued) Composition of feldspar from various rock types across the 2020 Corundum Dome and Pyrochlore Dome sampling area.

Sample	20TN20	20TN20	20TN20	20TN3-2	20TN3-2	20TN3-2	20TN3-2	20TN3-2	20TN3-2	20TN3-2	20TN3-2	20TN15A	20TN15A
Analysis	52-215-2	52-216-3	52-218-5	8-53-1	8-54-2	14-70-1	14-71-2	14-72-3	14-73-4	14-74-5	14-75-6	22-98-1	22-99-2
Comment	Ab	Ab	Ksp	Ab	Ab	Ksp	Ab	Ab	Ksp	Ksp	Ksp	Ksp	Ksp
SiO_2 (wt. %)	67.72	66.99	64.44	68.89	68.26	64.74	69.13	67.79	64.98	64.83	64.74	65.44	64.37
Al_2O_3	19.42	19.11	18.59	19.15	18.73	17.55	18.90	18.41	17.49	17.54	17.56	17.00	16.79
Fe_2O_3*	0.10	0.14	0.05	0.04	0.19	0.15	0.00	0.00	0.02	0.04	0.02	1.12	0.99
MgO	0.00	0.00	0.00	0.00	0.00	0.00	0.00	0.00	0.00	0.00	0.00	0.00	0.00
CaO	0.00	0.01	0.21	0.02	0.01	0.01	0.00	0.00	0.01	0.02	0.00	0.00	0.00
FeO*	0.96	1.43	0.47	0.20	0.07	0.00	0.09	0.22	0.00	0.00	0.00	0.00	0.00
BaO	0.01	0.04	0.05	0.00	0.01	0.13	0.00	0.01	0.03	0.00	0.24	0.06	0.07
Na_2O	11.63	11.61	0.24	11.74	11.66	0.18	11.70	11.54	0.23	0.21	0.24	0.27	0.27
K_2O	0.24	0.13	17.24	0.11	0.12	17.46	0.13	0.14	17.23	17.33	17.04	17.16	17.02
Total	99.98	99.32	101.24	100.15	99.04	100.22	99.95	98.10	99.98	99.99	99.85	101.06	99.50
Si (*apfu*)	2.972	2.965	2.967	3.006	3.012	3.010	3.019	3.020	3.020	3.015	3.016	3.018	3.017
Al	1.004	0.997	1.009	0.985	0.974	0.962	0.973	0.966	0.958	0.962	0.964	0.924	0.927
Fe^{3+}	0.032	0.048	0.016	0.001	0.006	0.005	0.000	0.000	0.001	0.002	0.001	0.039	0.035
Mg	0.000	0.000	0.000	0.000	0.000	0.000	0.000	0.000	0.000	0.000	0.000	0.000	0.000
Ca	0.000	0.000	0.010	0.001	0.000	0.000	0.000	0.000	0.001	0.001	0.000	0.000	0.000
Fe^{2+}	0.000	0.000	0.000	0.007	0.003	0.000	0.003	0.008	0.000	0.000	0.000	0.000	0.000
Ba	0.000	0.001	0.001	0.000	0.000	0.002	0.000	0.000	0.001	0.000	0.004	0.001	0.001
Na	0.990	0.996	0.021	0.993	0.998	0.017	0.991	0.997	0.020	0.019	0.022	0.024	0.025
K	0.013	0.008	1.013	0.006	0.007	1.036	0.007	0.008	1.021	1.028	1.013	1.010	1.018
Cation sum	5.011	5.015	5.038	5.000	5.000	5.032	4.993	4.999	5.022	5.027	5.019	5.017	5.023
% Ca	0.01	0.05	0.97	0.09	0.04	0.05	0.01	0.02	0.05	0.12	0.02	0.00	0.00
% Na	98.68	99.19	2.05	99.33	99.31	1.58	99.27	99.21	1.97	1.85	2.10	2.33	2.36
% K	1.31	0.76	96.98	0.59	0.66	98.38	0.72	0.77	97.99	98.04	97.88	97.67	97.64
Total	100	100	100	100	100	100	100	100	100	100	100	100	100

Table B.1. (Continued) Composition of feldspar from various rock types across the 2020 Corundum Dome and Pyrochlore Dome sampling area.

Sample	20TN15A	20TN15A	20TN54	20TN54	20TN54	20TN54	20TN54	20TN5	20TN5	20TN5	20TN5	20TN5	20TN5
Analysis	22-100-3	22-101-4	25-108-1	25-109-2	25-110-3	25-111-4	28-119-4	9-102-1	9-103-2	12-106-1	12-107-2	12-108-3	16-131-1
Comment	Ab	Ab	Ab	Ab	Ksp	Ksp	Ksp	Ab	Ab	Ksp	Ksp	Ab	Ab
SiO_2 (wt. %)	67.85	68.31	68.25	68.61	64.13	63.83	62.25	65.67	67.02	65.08	64.65	66.58	66.94
Al_2O_3	18.70	18.44	18.67	18.92	17.34	17.00	17.26	18.78	19.44	17.98	17.88	19.63	20.19
Fe_2O_3*	1.17	0.75	0.21	0.00	0.09	0.40	0.88	1.07	0.31	0.29	0.35	1.11	0.22
MgO	0.01	0.00	0.00	0.00	0.02	0.00	1.23	0.64	0.03	0.01	0.02	0.87	0.01
CaO	0.01	0.00	0.00	0.00	0.04	0.00	0.05	0.13	0.60	0.03	0.06	0.22	1.28
FeO*	0.00	0.34	0.00	0.18	0.00	0.00	0.00	0.00	0.00	0.00	0.00	0.00	0.00
BaO	0.01	0.06	0.01	0.03	0.04	0.00	0.05	0.00	0.00	0.18	0.23	0.03	0.04
Na_2O	11.57	11.64	11.61	11.61	0.21	0.28	0.23	10.79	11.38	0.24	0.25	11.23	11.13
K_2O	0.18	0.06	0.34	0.18	17.20	16.78	16.36	1.42	0.33	17.12	17.10	0.12	0.12
Total	99.49	99.60	99.09	99.54	99.08	98.29	98.31	98.50	99.12	100.94	100.52	99.80	99.94
Si (*apfu*)	2.992	3.008	3.013	3.012	3.013	3.019	2.955	2.948	2.967	3.000	2.996	2.933	2.941
Al	0.972	0.957	0.972	0.979	0.960	0.948	0.965	0.994	1.014	0.977	0.977	1.019	1.045
Fe^{3+}	0.039	0.025	0.007	0.000	0.003	0.014	0.031	0.036	0.010	0.010	0.012	0.037	0.007
Mg	0.000	0.000	0.000	0.000	0.001	0.000	0.087	0.043	0.002	0.001	0.001	0.057	0.001
Ca	0.000	0.000	0.000	0.000	0.002	0.000	0.002	0.006	0.028	0.001	0.003	0.010	0.060
Fe^{2+}	0.000	0.012	0.000	0.007	0.000	0.000	0.000	0.000	0.000	0.000	0.000	0.000	0.000
Ba	0.000	0.001	0.000	0.001	0.001	0.000	0.001	0.000	0.000	0.003	0.004	0.001	0.001
Na	0.989	0.994	0.994	0.988	0.019	0.026	0.021	0.939	0.977	0.022	0.022	0.959	0.948
K	0.010	0.003	0.019	0.010	1.031	1.012	0.991	0.081	0.019	1.007	1.011	0.007	0.007
Cation sum	5.003	5.000	5.004	4.997	5.030	5.019	5.053	5.047	5.018	5.021	5.026	5.023	5.010
% Ca	0.02	0.00	0.01	0.01	0.18	0.02	0.23	0.59	2.78	0.13	0.28	1.07	5.94
% Na	98.96	99.67	98.12	98.95	1.82	2.46	2.04	91.51	95.39	2.10	2.13	98.22	93.38
% K	1.02	0.33	1.87	1.03	98.00	97.52	97.72	7.89	1.83	97.77	97.59	0.71	0.68
Total	100	100	100	100	100	100	100	100	100	100	100	100	100

Table B.1. (Continued) Composition of feldspar from various rock types across the 2020 Corundum Dome and Pyrochlore Dome sampling area.

Sample	20TN5	20TN24A	20TN24A	20TN24A	20TN24A	20TN24A	20TN24A	20TN24A	20TN24A	20TN24A	20TN24A	20TN24A	20TN25D
Analysis	16-132-2	20-143-1	20-144-2	20-145-3	20-146-4	20-147-5	20-148-6	20-149-7	20-150-8	26-173-1	26-174-2	26-175-3	29-181-1
Comment	Ab	Ab	Ab	Ab	Ksp	Ksp	Ab	Ksp	Ab	Ksp	Ksp	Ab	Ab
SiO_2 (wt. %)	67.54	62.88	66.40	62.40	64.44	64.78	67.83	64.59	68.21	65.31	64.57	67.20	68.15
Al_2O_3	19.57	23.37	20.37	22.40	17.90	17.49	19.23	17.77	19.26	17.97	17.96	20.43	19.04
Fe_2O_3*	0.25	0.24	0.12	0.23	0.23	0.22	0.33	0.32	0.00	0.24	0.35	0.37	0.00
MgO	0.01	0.04	0.01	0.02	0.07	0.03	0.01	0.02	0.03	0.00	0.02	0.05	0.00
CaO	0.63	1.15	1.67	3.84	0.03	0.05	0.08	0.02	0.14	0.03	0.04	0.39	0.01
FeO*	0.00	0.00	0.00	0.00	0.00	0.00	0.00	0.00	0.26	0.00	0.00	0.00	0.17
BaO	0.03	0.01	0.00	0.02	0.02	0.03	0.02	0.10	0.00	0.05	0.06	0.00	0.03
Na_2O	11.57	8.98	10.85	9.24	0.19	0.21	11.78	0.21	11.42	0.23	0.23	11.21	11.54
K_2O	0.05	2.30	0.17	0.34	17.25	17.21	0.12	17.12	0.26	17.23	17.17	0.56	0.15
Total	99.65	98.96	99.58	98.50	100.13	100.02	99.42	100.16	99.57	101.06	100.40	100.21	99.09
Si (*apfu*)	2.970	2.814	2.929	2.805	2.995	3.013	2.987	3.001	2.997	3.004	2.994	2.943	3.005
Al	1.014	1.232	1.059	1.187	0.981	0.959	0.998	0.973	0.997	0.974	0.981	1.054	0.990
Fe^{3+}	0.008	0.008	0.004	0.008	0.008	0.008	0.011	0.011	0.000	0.008	0.012	0.012	0.000
Mg	0.001	0.002	0.000	0.001	0.005	0.002	0.001	0.001	0.002	0.000	0.001	0.004	0.000
Ca	0.030	0.055	0.079	0.185	0.001	0.003	0.004	0.001	0.006	0.001	0.002	0.018	0.000
Fe^{2+}	0.000	0.000	0.000	0.000	0.000	0.000	0.000	0.000	0.009	0.000	0.000	0.000	0.006
Ba	0.000	0.000	0.000	0.000	0.000	0.000	0.000	0.002	0.000	0.001	0.001	0.000	0.001
Na	0.986	0.779	0.928	0.805	0.017	0.019	1.006	0.019	0.972	0.020	0.021	0.952	0.987
K	0.003	0.131	0.010	0.019	1.023	1.021	0.007	1.015	0.015	1.011	1.015	0.031	0.009
Cation sum	5.013	5.022	5.009	5.010	5.031	5.024	5.015	5.024	4.998	5.020	5.027	5.015	4.998
% Ca	2.93	5.70	7.76	18.32	0.13	0.24	0.39	0.11	0.65	0.12	0.21	1.83	0.04
% Na	96.79	80.71	91.28	79.77	1.64	1.80	98.93	1.87	97.87	1.98	1.98	95.07	99.11
% K	0.27	13.59	0.96	1.91	98.23	97.96	0.68	98.02	1.48	97.90	97.81	3.10	0.85
Total	100	100	100	100	100	100	100	100	100	100	100	100	100

Table B.1. (Continued) Composition of feldspar from various rock types across the 2020 Corundum Dome and Pyrochlore Dome sampling area.

Sample	20TN25D	20TN25D	20TN25D	20TN25D	20TN25D	20TN25D	20TN25D	20TN25D	20TN13B-2	20TN13B-2	20TN13B-2	20TN13B-2	20TN13B-2
Analysis	29-182-2	33-195-3	36-211-1	36-212-2	36-213-3	36-214-4	36-215-5	36-216-6	7-51-1	7-52-2	7-53-3	7-54-4	7-55-5
Comment	Ab	Ksp	Ab	Ab	Ksp	Ksp	Ksp	Ab	Ab	Ab	Ab	Ksp	Ksp
SiO_2 (wt. %)	68.18	64.66	68.47	68.28	64.50	64.40	64.62	68.12	69.23	68.85	69.12	65.08	64.03
Al_2O_3	19.13	17.92	19.63	18.85	17.71	17.74	17.85	19.23	19.13	18.39	19.10	17.19	17.12
Fe_2O_3*	0.24	0.13	0.05	0.18	0.27	0.24	0.14	0.17	0.00	0.00	0.00	0.86	1.03
MgO	0.01	0.00	0.00	0.01	0.01	0.01	0.00	0.01	0.00	0.00	0.00	0.00	0.20
CaO	0.01	0.25	0.01	0.26	0.00	0.00	0.01	0.02	0.00	0.01	0.01	0.00	0.02
FeO*	0.00	0.00	0.00	0.00	0.00	0.00	0.00	0.00	0.95	1.15	0.88	0.00	0.00
BaO	0.00	0.03	0.00	0.04	0.09	0.09	0.06	0.00	0.00	0.00	0.00	0.06	0.05
Na_2O	11.73	0.23	11.86	11.85	0.37	0.38	0.20	11.69	11.49	11.22	11.37	0.22	0.22
K_2O	0.16	17.13	0.13	0.12	16.97	17.04	17.17	0.15	0.19	0.29	0.14	17.29	16.91
Total	99.46	100.34	100.15	99.58	99.92	99.91	100.05	99.38	100.98	99.90	100.62	100.71	99.59
Si (*apfu*)	2.998	2.998	2.988	3.002	3.003	3.000	3.003	2.996	3.005	3.022	3.007	3.013	2.998
Al	0.991	0.979	1.010	0.977	0.971	0.974	0.978	0.997	0.978	0.952	0.980	0.938	0.945
Fe^{3+}	0.008	0.004	0.002	0.006	0.009	0.009	0.005	0.006	0.000	0.000	0.000	0.030	0.036
Mg	0.000	0.000	0.000	0.000	0.001	0.001	0.000	0.000	0.000	0.000	0.000	0.000	0.014
Ca	0.000	0.012	0.000	0.012	0.000	0.000	0.000	0.001	0.000	0.000	0.000	0.000	0.001
Fe^{2+}	0.000	0.000	0.000	0.000	0.000	0.000	0.000	0.000	0.034	0.042	0.032	0.000	0.000
Ba	0.000	0.001	0.000	0.001	0.002	0.002	0.001	0.000	0.000	0.000	0.000	0.001	0.001
Na	1.000	0.020	1.004	1.010	0.034	0.034	0.018	0.997	0.967	0.955	0.959	0.019	0.020
K	0.009	1.013	0.007	0.007	1.008	1.013	1.018	0.008	0.010	0.016	0.008	1.021	1.010
Cation sum	5.007	5.027	5.011	5.015	5.028	5.032	5.023	5.005	4.995	4.988	4.986	5.023	5.026
% Ca	0.05	1.19	0.04	1.17	0.00	0.02	0.03	0.09	0.01	0.03	0.02	0.00	0.09
% Na	99.04	1.93	99.25	98.19	3.23	3.26	1.71	99.09	98.92	98.33	99.18	1.86	1.98
% K	0.91	96.87	0.72	0.64	96.77	96.72	98.26	0.82	1.07	1.64	0.79	98.14	97.93
Total	100	100	100	100	100	100	100	100	100	100	100	100	100

Table B.1. (Continued) Composition of feldspar from various rock types across the 2020 Corundum Dome and Pyrochlore Dome sampling area.

Sample	20TN13B-2	20TN13B-2	20TN13B-2	20TN13B-2	20TN13B-2	20TN13B-2	20TN13B-2	20TN13B-2	20TN13B-2	20TN13B-2	20TN15B	20TN15B	20TN15B
Analysis	12-72-1	12-73-2	12-74-3	14-80-1	14-81-2	14-82-3	14-83-4	14-84-5	14-85-6	14-86-7	17-97-1	17-98-2	17-99-3
Comment	Ab	Ab	Ab	Ab	Ab	Ab	Ksp	Ksp	Ksp	Ab	Ksp	Ab	Ab
SiO_2 (wt. %)	68.65	68.76	68.94	68.50	68.35	68.65	64.90	64.80	64.97	69.01	65.19	69.03	67.40
Al_2O_3	19.08	18.84	19.44	18.55	17.88	18.22	16.92	16.85	17.07	18.88	17.89	19.49	18.43
Fe_2O_3*	0.11	0.41	0.00	1.09	0.88	0.32	0.98	0.99	0.94	0.00	0.31	0.00	0.18
MgO	0.00	0.00	0.00	0.00	0.00	0.00	0.00	0.00	0.00	0.00	0.00	0.00	0.00
CaO	0.00	0.01	0.00	0.01	0.00	0.01	0.00	0.00	0.00	0.00	0.02	0.10	0.05
FeO*	0.49	0.93	0.24	0.26	0.49	0.96	0.00	0.00	0.00	1.16	0.00	0.13	0.00
BaO	0.01	0.02	0.00	0.00	0.03	0.02	0.00	0.01	0.03	0.00	0.31	0.00	0.12
Na_2O	11.65	11.52	11.67	11.62	11.56	11.56	0.23	0.25	0.28	11.44	0.47	11.66	6.44
K_2O	0.07	0.15	0.10	0.16	0.19	0.10	17.22	17.19	17.23	0.16	16.83	0.20	7.98
Total	100.07	100.64	100.39	100.19	99.38	99.83	100.25	100.09	100.54	100.65	101.02	100.63	100.61
Si (*apfu*)	3.003	3.000	3.000	3.001	3.020	3.018	3.018	3.019	3.014	3.008	3.003	2.999	3.012
Al	0.983	0.969	0.997	0.958	0.931	0.944	0.927	0.925	0.933	0.970	0.971	0.998	0.971
Fe^{3+}	0.004	0.013	0.000	0.036	0.029	0.010	0.034	0.035	0.033	0.000	0.011	0.000	0.006
Mg	0.000	0.000	0.000	0.000	0.000	0.000	0.000	0.000	0.000	0.000	0.000	0.000	0.000
Ca	0.000	0.000	0.000	0.000	0.000	0.000	0.000	0.000	0.000	0.000	0.001	0.005	0.003
Fe^{2+}	0.018	0.034	0.009	0.010	0.018	0.035	0.000	0.000	0.000	0.042	0.000	0.005	0.000
Ba	0.000	0.000	0.000	0.000	0.001	0.000	0.000	0.000	0.001	0.000	0.006	0.000	0.002
Na	0.988	0.974	0.984	0.987	0.990	0.985	0.020	0.022	0.026	0.966	0.042	0.982	0.558
K	0.004	0.008	0.006	0.009	0.010	0.006	1.022	1.022	1.020	0.009	0.989	0.011	0.455
Cation sum	5.000	5.000	4.996	5.000	5.000	5.000	5.022	5.023	5.026	4.995	5.022	4.999	5.007
% Ca	0.02	0.03	0.02	0.02	0.02	0.04	0.01	0.02	0.00	0.02	0.10	0.49	0.26
% Na	99.60	99.12	99.41	99.09	98.93	99.38	1.95	2.15	2.44	99.08	4.04	98.39	54.96
% K	0.38	0.85	0.57	0.88	1.05	0.58	98.04	97.83	97.56	0.89	95.86	1.12	44.78
Total	100	100	100	100	100	100	100	100	100	100	100	100	100

Table B.1. (Continued) Composition of feldspar from various rock types across the 2020 Corundum Dome and Pyrochlore Dome sampling area.

Sample	20TN15 B	20TN15 B	20TN15 B	20TN15 B	20TN15 B	20TN15 B	20TN15 B	20TN15 B	20TN57C-1	20TN57C-1	20TN57C-1	20TN57C-1	20TN57C-1
Analysis	17-100-4	17-101-5	17-102-6	17-103-7	21-115-1	21-116-2	21-117-3	21-118-4	26-133-1	26-134-2	26-135-3	29-144-1	29-145-2
Comment	Ksp	Ksp	Ksp	Ab	Ksp	Ksp	Ab	Ksp	Ab	Ab	Ab	Ab	Ab
SiO_2 (wt. %)	66.11	64.97	65.21	68.72	64.90	66.43	68.99	65.57	69.05	69.02	68.91	68.37	69.03
Al_2O_3	18.13	17.76	17.72	19.10	17.85	18.50	19.40	17.80	18.98	18.96	18.95	19.28	19.26
Fe_2O_3*	0.20	0.10	0.31	0.29	0.18	0.19	0.16	0.31	0.18	0.31	0.20	0.26	0.00
MgO	0.00	0.00	0.00	0.01	0.00	0.00	0.00	0.00	0.00	0.08	0.01	0.52	0.03
CaO	0.06	0.00	0.00	0.06	0.01	0.06	0.08	0.05	0.02	0.03	0.03	0.06	0.24
FeO*	0.00	0.00	0.00	0.07	0.00	0.00	0.00	0.00	0.07	0.00	0.00	0.00	0.14
BaO	0.25	0.36	0.33	0.02	0.26	0.18	0.08	0.34	0.02	0.00	0.00	0.00	0.02
Na_2O	4.98	0.30	0.49	11.66	0.38	5.34	11.64	1.03	11.83	11.78	11.86	11.52	11.66
K_2O	10.01	17.19	16.77	0.19	17.10	9.52	0.28	16.04	0.06	0.11	0.08	0.31	0.06
Total	99.74	100.68	100.85	100.11	100.68	100.22	100.64	101.14	100.21	100.28	100.04	100.31	100.43
Si (*apfu*)	3.007	3.007	3.008	3.003	3.002	3.000	2.999	3.008	3.011	3.008	3.010	2.984	3.003
Al	0.972	0.969	0.963	0.984	0.973	0.985	0.994	0.962	0.975	0.974	0.976	0.992	0.988
Fe^{3+}	0.007	0.003	0.011	0.009	0.006	0.007	0.005	0.011	0.006	0.010	0.007	0.009	0.000
Mg	0.000	0.000	0.000	0.000	0.000	0.000	0.000	0.000	0.000	0.005	0.001	0.034	0.002
Ca	0.003	0.000	0.000	0.003	0.000	0.003	0.004	0.003	0.001	0.001	0.002	0.003	0.011
Fe^{2+}	0.000	0.000	0.000	0.002	0.000	0.000	0.000	0.000	0.003	0.000	0.000	0.000	0.005
Ba	0.004	0.007	0.006	0.000	0.005	0.003	0.001	0.006	0.000	0.000	0.000	0.000	0.000
Na	0.439	0.027	0.044	0.988	0.034	0.467	0.981	0.092	1.000	0.995	1.004	0.975	0.984
K	0.581	1.015	0.987	0.011	1.009	0.548	0.016	0.939	0.003	0.006	0.004	0.017	0.003
Cation sum	5.013	5.027	5.020	5.000	5.030	5.013	5.000	5.021	5.000	5.000	5.003	5.012	4.996
% Ca	0.29	0.01	0.00	0.26	0.03	0.28	0.35	0.26	0.10	0.13	0.15	0.30	1.10
% Na	42.91	2.55	4.29	98.68	3.25	45.87	98.08	8.88	99.55	99.27	99.43	97.98	98.58
% K	56.80	97.44	95.71	1.05	96.72	53.85	1.57	90.86	0.34	0.60	0.42	1.72	0.32
Total	100	100	100	100	100	100	100	100	100	100	100	100	100

Table B.1. (Continued) Composition of feldspar from various rock types across the 2020 Corundum Dome and Pyrochlore Dome sampling area.

Sample	20TN15A	20TN15A	20TN15A	20TN15A	20TN15A	20TN15A	20TN23	20TN23	20TN7	20TN7	20TN7	20TN6-2	20TN6-2
Analysis	31-151-1	31-152-2	31-153-3	31-154-4	31-155-5	31-156-6	35-177-1	35-178-2	41-199-1	41-200-2	41-201-3	5-52-2	5-53-3
Comment	Ksp	Ksp	Ksp	Ab	Ab	Ab	Ab	Ab	Ksp	Ksp	Ksp	Ab	Ab
SiO_2 (wt. %)	65.47	65.42	65.46	68.74	68.80	68.73	68.89	69.20	65.00	64.66	63.84	69.35	69.03
Al_2O_3	17.95	17.74	17.91	18.25	18.35	18.50	19.56	19.01	17.89	17.93	18.24	19.16	18.99
Fe_2O_3*	0.14	0.11	0.15	0.00	0.00	0.91	0.11	0.00	0.28	0.30	0.43	0.00	0.14
MgO	0.00	0.00	0.00	0.00	0.00	0.00	0.00	0.00	0.01	0.01	0.03	0.00	0.00
CaO	0.00	0.01	0.00	0.00	0.00	0.00	0.00	0.04	0.02	0.02	0.01	0.02	0.02
FeO*	0.00	0.00	0.00	1.06	0.95	0.29	0.00	0.10	0.00	0.00	0.00	0.15	0.20
BaO	0.06	0.06	0.10	0.00	0.00	0.07	0.05	0.07	0.18	0.21	0.51	0.00	0.00
Na_2O	0.27	0.26	0.24	11.55	11.51	11.66	11.86	11.78	0.26	0.21	0.30	11.76	11.74
K_2O	17.29	17.32	17.38	0.11	0.16	0.15	0.07	0.13	17.26	17.35	16.90	0.17	0.15
Total	101.19	100.92	101.26	99.71	99.76	100.31	100.55	100.33	100.90	100.69	100.27	100.59	100.27
Si (*apfu*)	3.008	3.014	3.008	3.023	3.023	3.007	2.994	3.014	3.000	2.995	2.974	3.012	3.010
Al	0.972	0.963	0.970	0.946	0.950	0.954	1.002	0.976	0.973	0.978	1.001	0.981	0.976
Fe^{3+}	0.005	0.004	0.005	0.000	0.000	0.030	0.004	0.000	0.010	0.011	0.015	0.000	0.005
Mg	0.000	0.000	0.000	0.000	0.000	0.000	0.000	0.000	0.000	0.001	0.002	0.000	0.000
Ca	0.000	0.000	0.000	0.000	0.000	0.000	0.000	0.002	0.001	0.001	0.001	0.001	0.001
Fe^{2+}	0.000	0.000	0.000	0.039	0.035	0.011	0.000	0.004	0.000	0.000	0.000	0.005	0.007
Ba	0.001	0.001	0.002	0.000	0.000	0.001	0.001	0.001	0.003	0.004	0.009	0.000	0.000
Na	0.024	0.024	0.022	0.985	0.980	0.989	1.000	0.994	0.023	0.019	0.027	0.990	0.993
K	1.013	1.018	1.019	0.006	0.009	0.008	0.004	0.007	1.016	1.025	1.004	0.009	0.008
Cation sum	5.023	5.024	5.025	4.999	4.997	5.000	5.005	4.999	5.028	5.033	5.033	4.998	5.000
% Ca	0.00	0.03	0.00	0.02	0.00	0.00	0.01	0.19	0.12	0.07	0.06	0.08	0.09
% Na	2.33	2.26	2.09	99.37	99.09	99.18	99.58	99.08	2.21	1.83	2.62	98.99	99.08
% K	97.67	97.71	97.91	0.60	0.91	0.82	0.41	0.72	97.67	98.09	97.31	0.92	0.84
Total	100	100	100	100	100	100	100	100	100	100	100	100	100

Table B.1. (Continued) Composition of feldspar from various rock types across the 2020 Corundum Dome and Pyrochlore Dome sampling area.

Sample	20TN6-2	20TN6-2	20TN6-2
Analysis	5-54-4	14-72-1	14-73-2
Comment	Ksp	Ab	Ksp
SiO_2 (wt. %)	65.61	69.49	65.56
Al_2O_3	17.98	19.52	17.91
Fe_2O_3*	0.03	0.00	0.06
MgO	0.00	0.00	0.00
CaO	0.00	0.00	0.01
FeO*	0.00	0.24	0.00
BaO	0.09	0.00	0.03
Na_2O	0.38	11.72	0.28
K_2O	17.24	0.12	17.25
Total	101.34	101.10	101.11
Si (*apfu*)	3.009	3.003	3.012
Al	0.972	0.994	0.970
Fe^{3+}	0.001	0.000	0.002
Mg	0.000	0.000	0.000
Ca	0.000	0.000	0.001
Fe^{2+}	0.000	0.009	0.000
Ba	0.002	0.000	0.001
Na	0.034	0.982	0.025
K	1.008	0.007	1.011
Cation sum	5.026	4.994	5.020
% Ca	0.00	0.01	0.05
% Na	3.27	99.32	2.41
% K	96.73	0.67	97.54
Total	100	100	100

Table B.2. Composition of mica from various rock types across the 2020 Corundum Dome and Pyrochlore Dome sampling area.

Sample	20TN55A	20TN55A	20TN55A	20TN55A	20TN55A	20TN55A	20TN55A	20TN55A	20TN57A	20TN57A	20TN57A	20TN57A
Analysis	13753	13731	13742	13764	16931	16942	16953	16964	261641	261652	261663	261674
Mineral	Ms	Ph	Ph	Ph	Ms	Ms	Ms	Ms	Ms	Ph	Ms	Ms
SiO_2 (wt. %)	44.65	49.60	50.36	51.87	43.45	43.85	43.39	43.58	46.82	46.23	47.04	44.85
TiO_2	0.17	0.24	0.31	0.21	0.17	0.13	0.10	0.01	0.04	0.10	0.10	0.00
Al_2O_3	30.53	23.91	22.82	24.30	35.46	35.68	36.81	38.45	31.29	27.04	32.19	37.71
MgO	1.96	4.51	4.92	3.93	0.36	0.44	0.30	0.07	2.63	6.53	1.95	0.35
CaO	0.03	0.02	0.13	0.07	0.01	0.02	0.01	0.02	0.13	0.12	0.16	0.02
MnO	0.14	0.12	0.47	0.03	0.05	0.03	0.02	0.02	0.03	0.11	0.00	0.02
FeO	4.87	4.50	4.47	3.38	2.25	1.74	1.62	0.54	2.42	3.42	1.91	0.50
BaO	0.09	0.00	0.00	0.02	0.06	0.05	0.16	0.02	0.08	0.00	0.17	0.01
Na_2O	0.07	0.03	0.04	0.04	0.13	0.12	0.19	0.22	0.24	0.14	0.24	0.15
K_2O	10.87	10.19	9.37	10.29	11.79	11.72	11.72	11.68	10.76	10.78	11.08	11.88
F	0.50	0.92	1.34	1.23	0.10	0.21	0.11	0.17	0.54	1.50	0.38	0.09
H_2O*	4.06	3.89	3.70	3.84	4.31	4.28	4.35	4.37	4.17	3.66	4.27	4.46
Total	97.94	97.93	97.94	99.22	98.14	98.28	98.77	99.15	99.16	99.60	99.49	100.05
Si (*apfu*)	3.114	3.433	3.481	3.513	2.987	3.001	2.954	2.933	3.174	3.174	3.171	2.989
Ti	0.009	0.012	0.016	0.011	0.009	0.007	0.005	0.000	0.002	0.005	0.005	0.000
Al	2.510	1.950	1.858	1.940	2.873	2.878	2.954	3.051	2.500	2.188	2.557	2.962
Mg	0.204	0.465	0.507	0.397	0.037	0.045	0.031	0.007	0.266	0.668	0.196	0.035
Ca	0.002	0.002	0.010	0.005	0.001	0.002	0.001	0.001	0.009	0.009	0.011	0.001
Mn	0.008	0.007	0.027	0.002	0.003	0.002	0.001	0.001	0.002	0.006	0.000	0.001
Fe^{2+}	0.284	0.261	0.259	0.191	0.130	0.100	0.092	0.030	0.137	0.196	0.108	0.028
Ba	0.002	0.000	0.000	0.001	0.002	0.001	0.004	0.001	0.002	0.000	0.004	0.000
Na	0.010	0.004	0.005	0.006	0.018	0.016	0.026	0.029	0.032	0.019	0.032	0.020
K	0.967	0.899	0.826	0.889	1.035	1.023	1.018	1.003	0.930	0.944	0.953	1.009
F	0.110	0.202	0.292	0.263	0.022	0.045	0.024	0.037	0.115	0.325	0.081	0.020
OH	1.890	1.798	1.708	1.737	1.978	1.955	1.976	1.963	1.885	1.675	1.919	1.980
O	10.000	10.000	10.000	10.000	10.000	10.000	10.000	10.000	10.000	10.000	10.000	10.000
Anion sum	12.000	12.000	12.000	12.000	12.000	12.000	12.000	12.000	12.000	12.000	12.000	12.000
Cation sum	7.111	7.031	6.990	6.954	7.093	7.073	7.086	7.057	7.055	7.208	7.038	7.045
Mg/(Mg+Fe)	0.411	0.635	0.640	0.673	0.218	0.307	0.249	0.176	0.656	0.767	0.644	0.548

Note: Compositions were recalculated on the basis of 11 anions (O, F) *apfu*. * H_2O determined by stoichiometry.

Table B.2. (Continued) Composition of mica from various rock types across the 2020 Corundum Dome and Pyrochlore Dome sampling area.

Sample	20TN57A	20TN57A	20TN57A	20TN53	20TN53	20TN53	20TN53	20TN53	20TN53	20TN53	20TN53	20TN53
Analysis	261685	311951	311962	342091	342102	342113	342124	342135	362201	362212	362223	392333
Mineral	Ms	Ms	Ms	Ms	Ms	Ms	Ms	Ms	Ms	Ms	Ms	Ms
SiO_2 (wt. %)	46.14	42.52	43.26	44.68	46.45	46.23	44.39	46.74	42.66	42.61	42.68	42.23
TiO_2	0.06	0.05	0.03	0.02	0.03	0.00	0.00	0.00	0.09	0.13	0.02	0.08
Al_2O_3	31.82	35.04	36.09	36.37	34.44	35.57	36.65	33.27	38.06	37.29	37.93	37.47
MgO	2.60	2.15	0.98	0.25	1.09	0.61	0.40	1.87	0.20	0.35	0.20	0.45
CaO	0.20	0.04	0.02	0.03	0.05	0.03	0.02	0.05	0.04	0.03	0.04	0.03
MnO	0.05	0.07	0.05	0.00	0.01	0.00	0.03	0.00	0.04	0.05	0.01	0.05
FeO	2.70	2.84	1.55	0.65	1.06	0.83	0.71	0.94	0.74	1.05	0.77	1.04
BaO	0.08	0.07	0.00	0.02	0.02	0.00	0.00	0.02	0.00	0.05	0.00	0.01
Na_2O	0.27	0.14	0.09	0.22	0.11	0.10	0.30	0.26	0.43	0.37	0.30	0.33
K_2O	10.87	10.74	11.73	11.44	11.42	11.55	11.35	11.15	10.97	10.97	11.19	11.02
F	0.55	0.27	0.25	0.11	0.47	0.32	0.19	0.49	0.13	0.12	0.14	0.26
H_2O*	4.16	4.23	4.26	4.37	4.24	4.33	4.34	4.22	4.33	4.31	4.32	4.23
Total	99.50	98.17	98.31	98.15	99.39	99.57	98.38	99.00	97.69	97.34	97.58	97.20
Si (*apfu*)	3.129	2.928	2.960	3.031	3.120	3.092	3.008	3.149	2.912	2.926	2.919	2.907
Ti	0.003	0.002	0.001	0.001	0.002	0.000	0.000	0.000	0.005	0.007	0.001	0.004
Al	2.542	2.843	2.911	2.908	2.726	2.804	2.927	2.641	3.062	3.018	3.057	3.040
Mg	0.263	0.221	0.100	0.025	0.109	0.061	0.040	0.188	0.021	0.035	0.020	0.046
Ca	0.015	0.003	0.002	0.002	0.003	0.002	0.002	0.004	0.003	0.002	0.003	0.003
Mn	0.003	0.004	0.003	0.000	0.001	0.000	0.002	0.000	0.002	0.003	0.001	0.003
Fe^{2+}	0.153	0.164	0.088	0.037	0.060	0.047	0.040	0.053	0.042	0.060	0.044	0.060
Ba	0.002	0.002	0.000	0.000	0.001	0.000	0.000	0.000	0.000	0.001	0.000	0.000
Na	0.035	0.019	0.012	0.029	0.014	0.012	0.039	0.034	0.057	0.050	0.039	0.044
K	0.940	0.943	1.024	0.990	0.978	0.986	0.981	0.958	0.956	0.961	0.976	0.968
F	0.118	0.060	0.055	0.024	0.101	0.068	0.040	0.104	0.028	0.025	0.030	0.057
OH	1.882	1.940	1.945	1.976	1.899	1.932	1.960	1.896	1.972	1.975	1.970	1.943
O	10.000	10.000	10.000	10.000	10.000	10.000	10.000	10.000	10.000	10.000	10.000	10.000
Anion sum	12.000	12.000	12.000	12.000	12.000	12.000	12.000	12.000	12.000	12.000	12.000	12.000
Cation sum	7.085	7.130	7.101	7.024	7.012	7.005	7.039	7.027	7.059	7.064	7.059	7.075
Mg/(Mg+Fe)	0.628	0.568	0.522	0.405	0.644	0.567	0.488	0.781	0.318	0.360	0.310	0.424

Table B.2. (Continued) Composition of mica from various rock types across the 2020 Corundum Dome and Pyrochlore Dome sampling area.

Sample	20TN53	20TN53	20TN53	20TN53	20TN53	20TN17C	20TN17C	20TN17C	20TN17C	20TN17C	20TN57C-1	20TN57C-1
Analysis	392344	392355	392366	392377	392399	9571	9582	9593	9604	9615	251291	251302
Mineral	Ms	Ms	Ms	Ms	Ms	Ph	Ph	Ph	Ph	Ph	Ms	Ms
SiO_2 (wt. %)	42.39	42.15	42.52	42.84	42.92	54.49	52.85	52.46	54.54	53.17	46.60	44.44
TiO_2	0.06	0.08	0.05	0.04	0.09	0.07	0.01	0.07	0.04	0.10	0.03	0.08
Al_2O_3	37.67	38.56	38.15	37.61	37.51	25.97	25.91	25.82	26.83	25.47	32.97	35.95
MgO	0.26	0.13	0.16	0.22	0.35	3.39	3.29	3.37	3.07	3.40	1.34	0.59
CaO	0.03	0.04	0.03	0.02	0.05	0.05	0.11	0.05	0.09	0.18	0.08	0.02
MnO	0.03	0.05	0.21	0.16	0.15	0.00	0.01	0.00	0.00	0.01	0.21	0.03
FeO	1.07	0.70	0.62	0.74	0.82	2.29	2.39	2.38	2.15	2.35	1.02	1.25
BaO	0.00	0.03	0.02	0.02	0.03	0.08	0.05	0.12	0.02	0.03	0.00	0.02
Na_2O	0.37	0.50	0.43	0.34	0.40	0.03	0.04	0.05	0.04	0.06	0.11	0.25
K_2O	10.96	10.85	10.79	11.22	10.95	9.96	9.66	10.22	9.43	9.76	11.87	11.75
F	0.23	0.10	0.18	0.11	0.22	1.14	1.13	1.06	1.14	1.26	0.50	0.13
H_2O*	4.26	4.34	4.30	4.33	4.28	4.05	3.96	3.98	4.07	3.90	4.19	4.36
Total	97.32	97.54	97.47	97.65	97.77	101.52	99.41	99.56	101.43	99.69	98.92	98.88
Si (*apfu*)	2.912	2.882	2.908	2.930	2.931	3.558	3.528	3.511	3.548	3.544	3.158	3.012
Ti	0.003	0.004	0.003	0.002	0.004	0.004	0.001	0.004	0.002	0.005	0.002	0.004
Al	3.049	3.107	3.075	3.032	3.020	1.999	2.039	2.037	2.057	2.000	2.633	2.872
Mg	0.027	0.014	0.016	0.023	0.035	0.330	0.328	0.336	0.298	0.338	0.135	0.060
Ca	0.002	0.003	0.003	0.001	0.004	0.003	0.008	0.004	0.007	0.013	0.006	0.002
Mn	0.002	0.003	0.012	0.009	0.008	0.000	0.000	0.000	0.000	0.000	0.012	0.002
Fe^{2+}	0.062	0.040	0.036	0.042	0.047	0.125	0.133	0.133	0.117	0.131	0.058	0.071
Ba	0.000	0.001	0.001	0.001	0.001	0.002	0.001	0.003	0.000	0.001	0.000	0.001
Na	0.049	0.066	0.056	0.045	0.053	0.004	0.005	0.006	0.005	0.008	0.015	0.033
K	0.960	0.947	0.942	0.979	0.954	0.830	0.823	0.873	0.783	0.829	1.026	1.016
F	0.049	0.021	0.039	0.024	0.048	0.234	0.238	0.224	0.235	0.265	0.106	0.028
OH	1.951	1.979	1.961	1.976	1.952	1.766	1.762	1.776	1.765	1.735	1.894	1.972
O	10.000	10.000	10.000	10.000	10.000	10.000	10.000	10.000	10.000	10.000	10.000	10.000
Anion sum	12.000	12.000	12.000	12.000	12.000	12.000	12.000	12.000	12.000	12.000	12.000	12.000
Cation sum	7.065	7.067	7.051	7.064	7.058	6.855	6.866	6.906	6.815	6.869	7.044	7.073
Mg/(Mg+Fe)	0.296	0.242	0.256	0.307	0.391	0.725	0.710	0.716	0.718	0.720	0.659	0.452

Table B.2. (Continued) Composition of mica from various rock types across the 2020 Corundum Dome and Pyrochlore Dome sampling area.

Sample	20TN57C-1	20TN57C-1	20TN57C-1	20TN57C-1	20TN57C-1	20TN6-2	20TN57A	20TN57A	20TN57A	20TN57A	20TN57A	20TN57A
Analysis	251313	251324	271383	271394	271416	8621	231431	231442	231453	231464	231475	231486
Mineral	Ms	Ms	Ms	Ms	Ph	Ms	Phl	Phl	Phl	Phl	Phl	Phl
SiO_2 (wt. %)	45.57	45.45	43.63	44.74	43.85	44.11	39.06	38.68	38.94	38.91	38.43	38.88
TiO_2	0.06	0.07	0.03	0.02	0.23	0.01	3.46	3.51	3.62	2.96	3.06	2.78
Al_2O_3	35.18	34.32	35.81	34.98	26.06	35.12	10.31	10.68	10.66	10.17	11.34	10.44
MgO	0.60	0.76	0.17	0.98	7.84	1.18	14.76	13.55	14.52	14.23	15.65	14.38
CaO	0.39	0.26	0.71	0.57	0.31	0.05	0.02	0.01	0.00	0.01	0.01	0.01
MnO	0.12	0.06	0.08	0.03	0.13	0.94	0.32	0.30	0.32	0.33	0.26	0.30
FeO	0.97	1.33	0.47	0.79	5.02	0.41	16.45	18.18	17.00	17.38	15.91	17.32
BaO	0.14	0.07	0.00	0.02	0.02	0.62	0.00	0.00	0.00	0.00	0.00	0.00
Na_2O	0.10	0.18	0.14	0.07	0.18	0.32	0.12	0.04	0.04	0.07	0.04	0.03
K_2O	11.87	11.78	11.61	11.87	10.74	11.18	9.79	10.43	10.40	10.26	9.71	10.35
F	0.28	0.33	0.29	0.34	2.53	0.25	2.98	2.58	2.89	2.89	2.89	2.91
H_2O*	4.32	4.26	4.21	4.25	3.09	4.27	2.51	2.70	2.58	2.52	2.57	2.52
Total	99.61	98.87	97.14	98.65	100.00	98.46	99.78	100.67	100.96	99.72	99.86	99.92
Si (*apfu*)	3.068	3.087	3.007	3.042	3.063	3.015	2.984	2.957	2.955	2.995	2.924	2.986
Ti	0.003	0.004	0.001	0.001	0.012	0.000	0.199	0.202	0.206	0.171	0.175	0.161
Al	2.791	2.747	2.908	2.804	2.146	2.829	0.929	0.962	0.953	0.923	1.017	0.945
Mg	0.061	0.077	0.018	0.100	0.817	0.121	1.682	1.545	1.643	1.634	1.774	1.647
Ca	0.028	0.019	0.052	0.042	0.023	0.004	0.002	0.001	0.000	0.000	0.001	0.000
Mn	0.007	0.003	0.004	0.002	0.008	0.054	0.020	0.020	0.020	0.021	0.017	0.019
Fe^{2+}	0.055	0.076	0.027	0.045	0.293	0.023	1.051	1.163	1.079	1.119	1.012	1.113
Ba	0.004	0.002	0.000	0.000	0.001	0.017	0.000	0.000	0.000	0.000	0.000	0.000
Na	0.013	0.024	0.019	0.009	0.024	0.043	0.017	0.006	0.005	0.011	0.006	0.005
K	1.020	1.020	1.021	1.030	0.957	0.974	0.954	1.017	1.006	1.007	0.942	1.014
F	0.060	0.071	0.063	0.073	0.558	0.054	0.719	0.623	0.693	0.705	0.696	0.707
OH	1.940	1.929	1.937	1.927	1.442	1.946	1.281	1.377	1.307	1.295	1.304	1.293
O	10.000	10.000	10.000	10.000	10.000	10.000	10.000	10.000	10.000	10.000	10.000	10.000
Anion sum	12.000	12.000	12.000	12.000	12.000	12.000	12.000	12.000	12.000	12.000	12.000	12.000
Cation sum	7.050	7.058	7.057	7.074	7.343	7.079	7.838	7.872	7.868	7.881	7.867	7.890
Mg/(Mg+Fe)	0.497	0.492	0.359	0.681	0.731	0.608	0.611	0.566	0.599	0.589	0.633	0.593

Table B.2. (Continued) Composition of mica from various rock types across the 2020 Corundum Dome and Pyrochlore Dome sampling area.

Sample	20TN57A	20TN57A	20TN57A	20TN57A	20TN57A	20TN57A	20TN57A	20TN57A	20TN57A	20TN57A	20TN53	20TN53
Analysis	231497	231508	281731	281742	281753	281764	281775	281786	281797	281808	372231	372242
Mineral	Phl	Phl	Phl	Phl	Phl	Phl	Phl	Phl	Phl	Phl	Phl	Phl
SiO_2 (wt. %)	37.45	37.51	39.08	39.28	38.17	38.34	38.53	38.90	39.06	38.59	38.70	38.87
TiO_2	3.53	3.73	3.50	3.26	2.78	3.14	3.05	3.78	3.46	3.46	4.03	3.85
Al_2O_3	11.61	11.21	10.12	9.92	10.42	10.19	10.44	10.16	10.29	10.23	10.84	11.17
MgO	13.51	13.62	13.73	14.83	13.39	11.64	11.11	11.63	13.89	12.72	13.59	13.90
CaO	0.03	0.04	0.01	0.01	0.00	0.00	0.00	0.01	0.00	0.00	0.06	0.07
MnO	0.26	0.26	0.45	0.32	0.41	0.48	0.43	0.34	0.39	0.35	0.25	0.25
FeO	18.09	17.79	17.78	16.76	19.09	21.20	21.59	20.45	18.00	19.68	17.21	16.73
BaO	0.00	0.00	0.00	0.00	0.00	0.00	0.00	0.01	0.00	0.00	0.00	0.00
Na_2O	0.07	0.07	0.09	0.10	0.03	0.07	0.07	0.06	0.05	0.04	0.03	0.03
K_2O	9.95	10.01	10.22	10.22	10.42	10.19	10.17	10.12	10.36	10.32	10.11	9.98
F	2.32	2.40	2.65	2.95	2.69	2.24	2.21	2.26	2.71	2.43	2.72	2.65
H_2O*	2.79	2.74	2.66	2.53	2.59	2.79	2.81	2.82	2.65	2.74	2.63	2.69
Total	99.61	99.37	100.30	100.19	99.99	100.27	100.42	100.53	100.86	100.56	100.18	100.18
Si (*apfu*)	2.887	2.899	2.992	3.000	2.959	2.981	2.992	2.999	2.978	2.972	2.955	2.955
Ti	0.205	0.217	0.202	0.187	0.162	0.184	0.178	0.219	0.199	0.201	0.232	0.220
Al	1.055	1.021	0.913	0.893	0.952	0.934	0.956	0.923	0.925	0.928	0.975	1.001
Mg	1.553	1.569	1.567	1.688	1.547	1.349	1.286	1.336	1.578	1.461	1.548	1.576
Ca	0.002	0.004	0.001	0.001	0.000	0.000	0.000	0.001	0.000	0.000	0.005	0.006
Mn	0.017	0.017	0.029	0.021	0.027	0.032	0.028	0.022	0.025	0.023	0.016	0.016
Fe^{2+}	1.167	1.150	1.139	1.071	1.238	1.379	1.402	1.318	1.148	1.268	1.099	1.064
Ba	0.000	0.000	0.000	0.000	0.000	0.000	0.000	0.000	0.000	0.000	0.000	0.000
Na	0.011	0.011	0.013	0.015	0.005	0.010	0.011	0.009	0.007	0.007	0.005	0.005
K	0.978	0.987	0.998	0.996	1.030	1.010	1.008	0.996	1.008	1.014	0.985	0.968
F	0.566	0.586	0.642	0.712	0.659	0.552	0.542	0.550	0.654	0.591	0.658	0.637
OH	1.434	1.414	1.358	1.288	1.341	1.448	1.458	1.450	1.346	1.409	1.342	1.363
O	10.000	10.000	10.000	10.000	10.000	10.000	10.000	10.000	10.000	10.000	10.000	10.000
Anion sum	12.000	12.000	12.000	12.000	12.000	12.000	12.000	12.000	12.000	12.000	12.000	12.000
Cation sum	7.875	7.873	7.855	7.872	7.920	7.879	7.861	7.823	7.868	7.873	7.820	7.810
Mg/(Mg+Fe)	0.568	0.573	0.573	0.607	0.550	0.489	0.474	0.499	0.574	0.531	0.581	0.593

Table B.2. (Continued) Composition of mica from various rock types across the 2020 Corundum Dome and Pyrochlore Dome sampling area.

Sample	20TN53	20TN17C	20TN17C	20TN17C	20TN17C	20TN13A	20TN13A	20TN13A	20TN4A	20TN4A	20TN4A	20TN4A
Analysis	372264	8522	8533	8544	8555	261131	261142	261153	291161	291172	291183	291194
Mineral	Phl	Phl	Phl	Phl	Phl	Phl	Phl	Phl	Phl	Phl	Phl	Phl
SiO_2 (wt. %)	43.99	44.86	40.30	39.28	40.23	39.46	40.39	39.78	36.37	39.51	36.58	42.23
TiO_2	0.13	0.52	0.58	0.62	0.49	0.60	0.49	1.07	0.11	0.16	0.12	0.28
Al_2O_3	9.94	10.70	11.05	11.28	11.59	10.57	10.34	10.67	13.88	12.30	14.15	10.72
MgO	21.92	15.72	16.61	16.25	15.97	15.19	15.07	14.03	19.41	19.95	19.31	20.38
CaO	0.05	0.03	0.00	0.01	0.08	0.01	0.12	0.02	0.03	0.02	0.11	0.03
MnO	0.15	0.01	0.04	0.01	0.01	0.23	0.21	0.17	1.66	1.05	1.46	2.58
FeO	8.23	13.56	14.79	15.92	15.64	18.37	17.84	19.07	13.55	11.13	13.19	7.81
BaO	0.01	0.05	0.07	0.06	0.00	0.00	0.02	0.00	0.01	0.00	0.01	0.00
Na_2O	0.05	0.03	0.02	0.02	0.05	0.03	0.03	0.03	0.02	0.03	0.05	0.14
K_2O	10.05	10.02	10.69	10.63	10.39	10.38	9.66	10.18	6.69	9.32	6.65	10.62
F	5.32	4.03	4.16	4.05	4.05	2.96	3.05	3.00	2.17	2.93	2.01	3.46
H_2O*	1.62	2.20	1.98	2.00	2.04	2.50	2.47	2.49	2.88	2.61	2.97	2.44
Total	101.45	101.73	100.29	100.13	100.55	100.30	99.69	100.51	96.78	99.03	96.61	100.70
Si (*apfu*)	3.185	3.275	3.056	3.004	3.045	3.027	3.092	3.047	2.789	2.958	2.797	3.099
Ti	0.007	0.029	0.033	0.036	0.028	0.035	0.028	0.062	0.006	0.009	0.007	0.016
Al	0.848	0.920	0.987	1.017	1.034	0.956	0.933	0.963	1.255	1.085	1.276	0.927
Mg	2.365	1.711	1.878	1.853	1.802	1.738	1.719	1.603	2.219	2.227	2.201	2.230
Ca	0.004	0.002	0.000	0.001	0.006	0.001	0.010	0.002	0.003	0.001	0.009	0.003
Mn	0.009	0.001	0.002	0.001	0.001	0.015	0.013	0.011	0.108	0.067	0.095	0.160
Fe^{2+}	0.498	0.828	0.938	1.018	0.990	1.179	1.142	1.222	0.869	0.697	0.844	0.479
Ba	0.000	0.002	0.002	0.002	0.000	0.000	0.001	0.000	0.000	0.000	0.000	0.000
Na	0.007	0.004	0.003	0.003	0.007	0.005	0.005	0.005	0.003	0.004	0.007	0.020
K	0.928	0.933	1.035	1.037	1.004	1.016	0.944	0.995	0.654	0.890	0.649	0.995
F	1.218	0.931	0.998	0.981	0.970	0.719	0.738	0.727	0.525	0.694	0.485	0.804
OH	0.782	1.069	1.002	1.019	1.030	1.281	1.262	1.273	1.475	1.306	1.515	1.196
O	10.000	10.000	10.000	10.000	10.000	10.000	10.000	10.000	10.000	10.000	10.000	10.000
Anion sum	12.000	12.000	12.000	12.000	12.000	12.000	12.000	12.000	12.000	12.000	12.000	12.000
Cation sum	7.852	7.705	7.935	7.972	7.916	7.970	7.888	7.909	7.906	7.937	7.886	7.929
Mg/(Mg+Fe)	0.823	0.674	0.666	0.645	0.645	0.593	0.598	0.565	0.694	0.745	0.701	0.777

Table B.2. (Continued) Composition of mica from various rock types across the 2020 Corundum Dome and Pyrochlore Dome sampling area.

Sample	20TN4A	20TN4A	20TN4A	20TN4A	20TN4A	20TN4A	20TN54	20TN54	20TN24A	20TN24A	20TN24A	20TN24A
Analysis	291205	291238	351446	351457	361461	361483	281161	281172	241631	241642	241653	241675
Mineral	Phl	Phl	Phl	Phl	Phl	Phl	Phl	Phl	Phl	Phl	Phl	Phl
SiO_2 (wt. %)	40.87	38.48	41.34	41.95	41.04	39.30	47.29	47.85	38.95	38.94	40.68	39.24
TiO_2	0.25	0.08	0.06	0.12	0.22	0.15	0.11	0.09	2.47	2.20	1.60	2.05
Al_2O_3	11.09	12.67	12.17	12.56	11.79	12.42	7.34	7.54	13.04	13.32	12.53	12.60
MgO	20.00	19.39	18.96	19.71	19.12	18.95	23.79	23.87	14.48	14.34	15.44	15.22
CaO	0.01	0.05	0.03	0.08	0.04	0.07	0.28	0.21	0.09	0.06	0.05	0.02
MnO	2.56	1.30	1.10	0.70	0.95	1.29	0.15	0.09	0.11	0.05	0.05	0.06
FeO	9.03	11.77	10.30	9.59	10.57	11.82	3.48	3.82	15.55	15.75	14.38	15.17
BaO	0.02	0.02	0.00	0.02	0.05	0.00	0.00	0.00	0.00	0.00	0.00	0.00
Na_2O	0.05	0.07	0.07	0.05	0.06	0.07	0.03	0.02	0.07	0.11	0.05	0.03
K_2O	10.42	8.04	10.72	10.61	9.97	8.61	10.20	10.12	9.01	9.66	9.47	9.78
F	3.30	2.76	2.95	2.93	3.01	2.57	6.57	6.61	0.82	0.62	0.68	0.72
H_2O*	2.47	2.63	2.67	2.73	2.60	2.75	1.06	1.08	3.57	3.68	3.69	3.63
Total	100.08	97.27	100.37	101.06	99.41	97.99	100.30	101.30	98.16	98.72	98.61	98.52
Si (*apfu*)	3.038	2.927	3.051	3.052	3.053	2.968	3.399	3.402	2.949	2.941	3.041	2.966
Ti	0.014	0.005	0.003	0.007	0.012	0.008	0.006	0.005	0.141	0.125	0.090	0.116
Al	0.972	1.136	1.059	1.077	1.034	1.105	0.622	0.632	1.164	1.185	1.104	1.122
Mg	2.216	2.199	2.086	2.138	2.120	2.134	2.549	2.530	1.635	1.614	1.721	1.715
Ca	0.001	0.004	0.002	0.006	0.004	0.006	0.022	0.016	0.007	0.005	0.004	0.002
Mn	0.161	0.084	0.069	0.043	0.060	0.083	0.009	0.005	0.007	0.003	0.003	0.004
Fe^{2+}	0.561	0.749	0.636	0.584	0.657	0.747	0.209	0.227	0.985	0.995	0.899	0.959
Ba	0.001	0.001	0.000	0.001	0.001	0.000	0.000	0.000	0.000	0.000	0.000	0.000
Na	0.007	0.010	0.010	0.007	0.008	0.010	0.003	0.003	0.010	0.016	0.007	0.005
K	0.988	0.780	1.009	0.985	0.946	0.829	0.935	0.918	0.871	0.931	0.903	0.943
F	0.776	0.664	0.687	0.674	0.708	0.613	1.493	1.487	0.196	0.148	0.160	0.172
OH	1.224	1.336	1.313	1.326	1.292	1.387	0.507	0.513	1.804	1.852	1.840	1.828
O	10.000	10.000	10.000	10.000	10.000	10.000	10.000	10.000	10.000	10.000	10.000	10.000
Anion sum	12.000	12.000	12.000	12.000	12.000	12.000	12.000	12.000	12.000	12.000	12.000	12.000
Cation sum	7.959	7.895	7.926	7.899	7.895	7.890	7.754	7.738	7.769	7.815	7.772	7.831
Mg/(Mg+Fe)	0.754	0.725	0.748	0.773	0.747	0.720	0.921	0.916	0.622	0.618	0.656	0.640

Table B.2. (Continued) Composition of mica from various rock types across the 2020 Corundum Dome and Pyrochlore Dome sampling area.

Sample	20TN24A	20TN24A	20TN25D	20TN25D	20TN25D	20TN25D	20TN25D	20TN25D	20TN25D	20TN25D	20TN25D	20TN25D
Analysis	271761	271772	311861	311872	311883	311894	311905	311916	352033	352066	352099	3521010
Mineral	Phl	Phl	Phl	Phl	Phl	Phl	Phl	Phl	Phl	Phl	Phl	Phl
SiO_2 (wt. %)	37.71	38.62	43.97	45.31	45.16	45.14	44.91	42.14	41.44	42.15	40.23	39.96
TiO_2	1.90	2.25	1.49	1.32	1.31	1.43	1.45	1.89	0.31	0.17	0.37	0.41
Al_2O_3	14.94	13.33	9.05	8.49	8.30	8.27	8.59	9.85	11.01	10.44	11.44	11.22
MgO	13.08	13.88	18.98	19.74	19.65	19.78	19.22	17.48	19.66	19.30	16.61	16.82
CaO	0.13	0.24	0.01	0.01	0.01	0.01	0.00	0.00	0.08	0.09	0.41	0.14
MnO	0.09	0.06	1.79	0.53	1.15	1.23	1.87	2.34	0.09	0.14	0.18	0.28
FeO	16.72	16.16	8.56	7.55	7.39	7.16	7.41	10.29	11.15	11.58	14.11	14.90
BaO	0.07	0.00	0.00	0.00	0.04	0.04	0.00	0.01	0.03	0.00	0.02	0.01
Na_2O	0.11	0.09	0.02	0.02	0.04	0.03	0.02	0.02	0.03	0.05	0.13	0.16
K_2O	9.92	9.45	10.83	10.81	10.71	10.75	10.95	10.49	10.82	10.27	10.12	10.07
F	0.63	0.61	6.03	6.38	6.46	6.53	6.60	5.17	5.30	4.77	4.11	4.44
H_2O*	3.65	3.66	1.23	1.09	1.03	1.00	0.98	1.58	1.53	1.78	2.01	1.85
Total	98.94	98.34	101.98	101.24	101.26	101.39	102.00	101.26	101.45	100.74	99.73	100.25
Si (*apfu*)	2.864	2.934	3.222	3.307	3.305	3.299	3.280	3.134	3.069	3.127	3.052	3.034
Ti	0.108	0.129	0.082	0.072	0.072	0.079	0.079	0.106	0.017	0.009	0.021	0.023
Al	1.337	1.193	0.782	0.730	0.715	0.713	0.739	0.864	0.961	0.913	1.023	1.004
Mg	1.481	1.571	2.073	2.147	2.144	2.155	2.093	1.938	2.170	2.135	1.879	1.904
Ca	0.010	0.019	0.001	0.001	0.001	0.001	0.000	0.000	0.006	0.007	0.033	0.011
Mn	0.006	0.004	0.111	0.033	0.071	0.076	0.116	0.147	0.006	0.009	0.012	0.018
Fe^{2+}	1.062	1.026	0.525	0.461	0.452	0.438	0.453	0.640	0.690	0.719	0.896	0.946
Ba	0.002	0.000	0.000	0.000	0.001	0.001	0.000	0.000	0.001	0.000	0.001	0.000
Na	0.016	0.013	0.004	0.003	0.005	0.005	0.003	0.003	0.004	0.008	0.020	0.023
K	0.961	0.916	1.012	1.006	1.000	1.003	1.020	0.995	1.022	0.972	0.979	0.976
F	0.151	0.146	1.397	1.472	1.495	1.510	1.525	1.216	1.242	1.118	0.985	1.065
OH	1.849	1.854	0.603	0.528	0.505	0.490	0.475	0.784	0.758	0.882	1.015	0.935
O	10.000	10.000	10.000	10.000	10.000	10.000	10.000	10.000	10.000	10.000	10.000	10.000
Anion sum	12.000	12.000	12.000	12.000	12.000	12.000	12.000	12.000	12.000	12.000	12.000	12.000
Cation sum	7.847	7.805	7.813	7.761	7.768	7.769	7.783	7.827	7.947	7.898	7.915	7.940
Mg/(Mg+Fe)	0.581	0.604	0.765	0.813	0.804	0.807	0.786	0.711	0.757	0.746	0.674	0.664

Table B.2. (Continued) Composition of mica from various rock types across the 2020 Corundum Dome and Pyrochlore Dome sampling area.

Sample	20TN25D	20TN25D	20TN25D	20TN25D	20TN25D	20TN13B-2	20TN13B-2	20TN13B-2	20TN13B-2	20TN13B-2	20TN13B-2	20TN13B-2
Analysis	382201	382212	382223	382234	382245	10663	10674	10685	10696	13761	13772	13783
Mineral	Phl	Phl	Phl	Phl	Phl	Phl	Phl	Phl	Phl	Phl	Phl	Phl
SiO_2 (wt. %)	43.18	39.12	43.91	42.92	42.89	40.82	41.61	40.08	41.10	40.19	39.67	39.02
TiO_2	0.74	0.70	1.32	2.17	2.23	0.25	0.17	0.30	0.04	0.15	0.16	0.67
Al_2O_3	9.03	10.95	8.43	8.57	8.67	10.04	9.64	10.41	9.93	10.37	10.28	10.93
MgO	20.06	17.46	19.12	17.07	17.01	16.02	16.87	16.58	16.61	16.38	16.27	14.91
CaO	0.07	1.40	0.02	0.03	0.01	0.02	0.02	0.01	0.00	0.03	0.01	0.05
MnO	1.55	0.36	1.96	2.09	2.03	0.20	0.16	0.19	0.16	0.20	0.14	0.19
FeO	7.57	12.84	7.55	10.07	10.15	16.97	16.10	16.94	16.27	17.22	17.45	18.62
BaO	0.00	0.00	0.00	0.06	0.00	0.01	0.00	0.00	0.00	0.00	0.00	0.02
Na_2O	0.01	0.02	0.03	0.08	0.13	0.02	0.04	0.04	0.02	0.06	0.05	0.03
K_2O	10.88	10.51	10.67	10.21	10.22	9.81	9.74	10.04	10.01	10.05	10.12	10.06
F	6.48	4.40	6.68	5.87	5.87	3.68	3.60	3.59	3.73	4.01	3.81	3.37
H_2O*	0.96	1.84	0.87	1.21	1.21	2.19	2.26	2.24	2.18	2.03	2.10	2.30
Total	100.53	99.59	100.55	100.36	100.44	100.03	100.21	100.42	100.05	100.70	100.07	100.16
Si (*apfu*)	3.209	2.990	3.263	3.222	3.216	3.112	3.145	3.051	3.124	3.061	3.046	3.005
Ti	0.041	0.040	0.074	0.123	0.126	0.014	0.010	0.017	0.002	0.009	0.009	0.039
Al	0.791	0.986	0.738	0.758	0.766	0.902	0.858	0.934	0.890	0.930	0.931	0.992
Mg	2.222	1.989	2.119	1.910	1.902	1.820	1.901	1.881	1.882	1.860	1.862	1.711
Ca	0.006	0.114	0.001	0.002	0.001	0.001	0.002	0.001	0.000	0.003	0.001	0.004
Mn	0.097	0.023	0.123	0.133	0.129	0.013	0.010	0.012	0.011	0.013	0.009	0.013
Fe^{2+}	0.470	0.821	0.469	0.632	0.636	1.082	1.018	1.078	1.034	1.097	1.121	1.199
Ba	0.000	0.000	0.000	0.002	0.000	0.000	0.000	0.000	0.000	0.000	0.000	0.001
Na	0.002	0.003	0.005	0.012	0.019	0.003	0.006	0.006	0.003	0.009	0.007	0.005
K	1.031	1.025	1.012	0.977	0.978	0.954	0.939	0.975	0.970	0.977	0.991	0.988
F	1.524	1.064	1.570	1.394	1.393	0.887	0.860	0.864	0.897	0.966	0.925	0.821
OH	0.476	0.936	0.430	0.606	0.607	1.113	1.140	1.136	1.103	1.034	1.075	1.179
O	10.000	10.000	10.000	10.000	10.000	10.000	10.000	10.000	10.000	10.000	10.000	10.000
Anion sum	12.000	12.000	12.000	12.000	12.000	12.000	12.000	12.000	12.000	12.000	12.000	12.000
Cation sum	7.870	7.991	7.803	7.771	7.773	7.902	7.888	7.955	7.916	7.958	7.978	7.956
Mg/(Mg+Fe)	0.796	0.702	0.782	0.714	0.713	0.624	0.649	0.633	0.643	0.626	0.622	0.586

Table B.2. (Continued) Composition of mica from various rock types across the 2020 Corundum Dome and Pyrochlore Dome sampling area.

Sample	20TN25D	20TN25D	20TN25D	20TN25D	20TN25D	20TN13B-2	20TN13B-2	20TN13B-2	20TN13B-2	20TN13B-2	20TN13B-2	20TN13B-2
Analysis	382201	382212	382223	382234	382245	10663	10674	10685	10696	13761	13772	13783
Mineral	Phl	Phl	Phl	Phl	Phl	Phl	Phl	Phl	Phl	Phl	Phl	Phl
SiO_2 (wt. %)	43.18	39.12	43.91	42.92	42.89	40.82	41.61	40.08	41.10	40.19	39.67	39.02
TiO_2	0.74	0.70	1.32	2.17	2.23	0.25	0.17	0.30	0.04	0.15	0.16	0.67
Al_2O_3	9.03	10.95	8.43	8.57	8.67	10.04	9.64	10.41	9.93	10.37	10.28	10.93
MgO	20.06	17.46	19.12	17.07	17.01	16.02	16.87	16.58	16.61	16.38	16.27	14.91
CaO	0.07	1.40	0.02	0.03	0.01	0.02	0.02	0.01	0.00	0.03	0.01	0.05
MnO	1.55	0.36	1.96	2.09	2.03	0.20	0.16	0.19	0.16	0.20	0.14	0.19
FeO	7.57	12.84	7.55	10.07	10.15	16.97	16.10	16.94	16.27	17.22	17.45	18.62
BaO	0.00	0.00	0.00	0.06	0.00	0.01	0.00	0.00	0.00	0.00	0.00	0.02
Na_2O	0.01	0.02	0.03	0.08	0.13	0.02	0.04	0.04	0.02	0.06	0.05	0.03
K_2O	10.88	10.51	10.67	10.21	10.22	9.81	9.74	10.04	10.01	10.05	10.12	10.06
F	6.48	4.40	6.68	5.87	5.87	3.68	3.60	3.59	3.73	4.01	3.81	3.37
H_2O*	0.96	1.84	0.87	1.21	1.21	2.19	2.26	2.24	2.18	2.03	2.10	2.30
Total	100.53	99.59	100.55	100.36	100.44	100.03	100.21	100.42	100.05	100.70	100.07	100.16
Si (*apfu*)	3.209	2.990	3.263	3.222	3.216	3.112	3.145	3.051	3.124	3.061	3.046	3.005
Ti	0.041	0.040	0.074	0.123	0.126	0.014	0.010	0.017	0.002	0.009	0.009	0.039
Al	0.791	0.986	0.738	0.758	0.766	0.902	0.858	0.934	0.890	0.930	0.931	0.992
Mg	2.222	1.989	2.119	1.910	1.902	1.820	1.901	1.881	1.882	1.860	1.862	1.711
Ca	0.006	0.114	0.001	0.002	0.001	0.001	0.002	0.001	0.000	0.003	0.001	0.004
Mn	0.097	0.023	0.123	0.133	0.129	0.013	0.010	0.012	0.011	0.013	0.009	0.013
Fe^{2+}	0.470	0.821	0.469	0.632	0.636	1.082	1.018	1.078	1.034	1.097	1.121	1.199
Ba	0.000	0.000	0.000	0.002	0.000	0.000	0.000	0.000	0.000	0.000	0.000	0.001
Na	0.002	0.003	0.005	0.012	0.019	0.003	0.006	0.006	0.003	0.009	0.007	0.005
K	1.031	1.025	1.012	0.977	0.978	0.954	0.939	0.975	0.970	0.977	0.991	0.988
F	1.524	1.064	1.570	1.394	1.393	0.887	0.860	0.864	0.897	0.966	0.925	0.821
OH	0.476	0.936	0.430	0.606	0.607	1.113	1.140	1.136	1.103	1.034	1.075	1.179
O	10.000	10.000	10.000	10.000	10.000	10.000	10.000	10.000	10.000	10.000	10.000	10.000
Anion sum	12.000	12.000	12.000	12.000	12.000	12.000	12.000	12.000	12.000	12.000	12.000	12.000
Cation sum	7.870	7.991	7.803	7.771	7.773	7.902	7.888	7.955	7.916	7.958	7.978	7.956
Mg/(Mg+Fe)	0.796	0.702	0.782	0.714	0.713	0.624	0.649	0.633	0.643	0.626	0.622	0.586

Table B.2. (Continued) Composition of mica from various rock types across the 2020 Corundum Dome and Pyrochlore Dome sampling area.

Sample	20TN13B-2	20TN13B-2	20TN13B-2	20TN13B-2	20TN15B	20TN15B	20TN15B	20TN15B	20TN15B	20TN15B	20TN15B	20TN15B
Analysis	13794	15871	15882	15893	16901	16912	16923	16934	16945	16956	16967	201101
Mineral	Phl	Phl	Phl	Phl	Phl	Phl	Phl	Phl	Phl	Phl	Phl	Phl
SiO_2 (wt. %)	39.14	40.40	42.45	45.24	39.02	39.26	39.86	39.70	39.54	39.58	39.21	39.49
TiO_2	0.59	0.15	0.05	0.07	1.67	1.77	1.52	1.56	1.51	1.34	1.66	1.46
Al_2O_3	10.90	10.59	10.56	11.08	10.42	10.45	10.27	10.07	10.15	10.14	10.25	10.46
MgO	15.13	16.17	15.77	14.03	14.39	14.31	14.96	14.88	14.75	15.15	14.74	15.31
CaO	0.02	0.02	0.02	0.02	0.00	0.02	0.01	0.02	0.10	0.07	0.10	0.05
MnO	0.15	0.24	0.28	0.25	0.51	0.57	0.57	0.49	0.55	0.54	0.62	0.51
FeO	18.22	16.71	15.28	14.11	18.53	18.51	18.09	17.77	18.28	17.75	18.33	17.45
BaO	0.02	0.00	0.00	0.00	0.03	0.00	0.01	0.02	0.00	0.00	0.03	0.02
Na_2O	0.06	0.07	0.02	0.06	0.12	0.11	0.09	0.13	0.14	0.18	0.12	0.07
K_2O	10.16	9.79	10.13	10.70	9.93	10.15	10.27	10.11	9.62	9.83	9.81	10.00
F	3.21	2.65	2.43	2.19	3.44	3.43	3.66	3.86	3.69	3.67	3.52	2.87
H_2O*	2.37	2.68	2.84	3.05	2.26	2.28	2.21	2.08	2.16	2.17	2.24	2.56
Total	99.99	99.46	99.84	100.80	100.33	100.87	101.52	100.69	100.48	100.42	100.64	100.26
Si (*apfu*)	3.012	3.078	3.183	3.318	3.005	3.008	3.030	3.041	3.033	3.034	3.008	3.016
Ti	0.034	0.009	0.003	0.004	0.097	0.102	0.087	0.090	0.087	0.077	0.096	0.084
Al	0.988	0.951	0.934	0.958	0.946	0.944	0.920	0.909	0.918	0.916	0.927	0.942
Mg	1.736	1.837	1.763	1.534	1.653	1.635	1.695	1.699	1.686	1.731	1.686	1.743
Ca	0.002	0.002	0.002	0.001	0.000	0.001	0.001	0.001	0.008	0.006	0.008	0.004
Mn	0.010	0.015	0.018	0.015	0.033	0.037	0.036	0.032	0.036	0.035	0.040	0.033
Fe^{2+}	1.173	1.065	0.958	0.865	1.193	1.186	1.150	1.138	1.172	1.138	1.176	1.114
Ba	0.001	0.000	0.000	0.000	0.001	0.000	0.000	0.001	0.000	0.000	0.001	0.001
Na	0.009	0.011	0.003	0.008	0.018	0.016	0.014	0.020	0.021	0.027	0.018	0.011
K	0.997	0.951	0.969	1.001	0.976	0.992	0.996	0.988	0.941	0.961	0.960	0.974
F	0.781	0.639	0.577	0.507	0.839	0.832	0.881	0.936	0.896	0.890	0.855	0.694
OH	1.219	1.361	1.423	1.493	1.161	1.168	1.119	1.064	1.104	1.110	1.145	1.306
O	10.000	10.000	10.000	10.000	10.000	10.000	10.000	10.000	10.000	10.000	10.000	10.000
Anion sum	12.000	12.000	12.000	12.000	12.000	12.000	12.000	12.000	12.000	12.000	12.000	12.000
Cation sum	7.962	7.919	7.833	7.704	7.922	7.922	7.929	7.919	7.902	7.925	7.921	7.921
Mg/(Mg+Fe)	0.595	0.630	0.644	0.635	0.574	0.572	0.588	0.592	0.583	0.596	0.581	0.603

Table B.2. (Continued) Composition of mica from various rock types across the 2020 Corundum Dome and Pyrochlore Dome sampling area.

Sample	20TN15B	20TN15B	20TN15B	20TN57C-1	20TN57C-1	20TN57C-1	20TN57C-1	20TN57C-1	20TN57C-1	20TN57C-1	20TN57C-1	20TN57C-1
Analysis	201112	201123	201134	231201	231212	231223	231234	231245	271361	271372	271405	301461
Mineral	Phl	Phl	Phl	Phl	Phl	Phl	Phl	Phl	Phl	Phl	Phl	Phl
SiO_2 (wt. %)	39.13	39.36	39.25	37.88	37.50	38.15	37.57	38.07	37.01	42.98	36.89	46.19
TiO_2	1.43	1.53	1.45	1.60	1.62	1.61	1.90	1.66	2.21	0.26	1.79	0.31
Al_2O_3	10.48	10.40	10.60	11.69	12.05	11.63	11.63	12.03	12.74	10.05	12.48	10.04
MgO	14.98	15.16	14.82	15.23	14.52	15.19	14.97	14.53	13.87	21.90	14.23	20.86
CaO	0.03	0.03	0.06	0.00	0.00	0.01	0.01	0.00	0.01	0.04	0.02	0.19
MnO	0.53	0.55	0.51	0.25	0.27	0.34	0.32	0.30	0.27	0.16	0.30	0.09
FeO	17.25	17.50	17.71	16.80	17.24	16.79	17.15	17.84	17.99	8.27	17.66	5.43
BaO	0.07	0.01	0.15	0.15	0.26	0.18	0.20	0.26	0.64	0.00	0.80	0.00
Na_2O	0.05	0.05	0.05	0.19	0.22	0.28	0.22	0.16	0.23	0.10	0.16	0.06
K_2O	9.71	10.11	10.06	10.03	9.94	9.76	9.86	10.21	9.63	10.56	9.86	10.32
F	2.75	2.76	2.77	3.12	3.01	3.12	2.84	3.05	2.56	5.86	2.90	6.04
H_2O*	2.58	2.60	2.59	2.40	2.43	2.41	2.52	2.46	2.67	1.33	2.48	1.31
Total	98.98	100.07	100.04	99.34	99.06	99.47	99.18	100.57	99.83	101.51	99.57	100.84
Si (*apfu*)	3.022	3.014	3.012	2.925	2.911	2.938	2.909	2.918	2.858	3.137	2.866	3.318
Ti	0.083	0.088	0.084	0.093	0.095	0.093	0.110	0.096	0.128	0.014	0.105	0.017
Al	0.954	0.939	0.959	1.064	1.102	1.055	1.061	1.087	1.159	0.865	1.143	0.850
Mg	1.724	1.731	1.695	1.753	1.681	1.744	1.728	1.660	1.597	2.383	1.649	2.234
Ca	0.002	0.002	0.005	0.000	0.000	0.000	0.001	0.000	0.001	0.003	0.001	0.015
Mn	0.034	0.036	0.033	0.016	0.018	0.022	0.021	0.019	0.017	0.010	0.020	0.005
Fe^{2+}	1.114	1.121	1.137	1.085	1.119	1.082	1.111	1.143	1.162	0.505	1.148	0.326
Ba	0.002	0.000	0.005	0.005	0.008	0.006	0.006	0.008	0.020	0.000	0.024	0.000
Na	0.007	0.007	0.008	0.029	0.034	0.042	0.033	0.024	0.034	0.015	0.024	0.008
K	0.956	0.987	0.985	0.988	0.984	0.958	0.974	0.998	0.948	0.983	0.977	0.946
F	0.671	0.670	0.673	0.763	0.740	0.761	0.697	0.740	0.625	1.353	0.712	1.373
OH	1.329	1.330	1.327	1.237	1.260	1.239	1.303	1.260	1.375	0.647	1.288	0.627
O	10.000	10.000	10.000	10.000	10.000	10.000	10.000	10.000	10.000	10.000	10.000	10.000
Anion sum	12.000	12.000	12.000	12.000	12.000	12.000	12.000	12.000	12.000	12.000	12.000	12.000
Cation sum	7.900	7.926	7.921	7.958	7.952	7.941	7.953	7.954	7.925	7.915	7.958	7.718
Mg/(Mg+Fe)	0.600	0.600	0.592	0.614	0.597	0.612	0.604	0.588	0.575	0.822	0.585	0.871

Table B.2. (Continued) Composition of mica from various rock types across the 2020 Corundum Dome and Pyrochlore Dome sampling area.

Sample	20TN57C-1	20TN57C-1	20TN7	20TN7	20TN6-2	20TN6-2	20TN6-2	20TN6-2
Analysis	301472	301505	401976	401987	12681	13691	13702	13713
Mineral	Phl	Phl	Phl	Phl	Phl	Phl	Phl	Phl
SiO_2 (wt. %)	46.12	37.28	40.70	39.33	38.09	39.93	39.52	41.46
TiO_2	0.30	1.89	0.40	0.15	0.97	0.41	0.60	0.35
Al_2O_3	10.27	12.74	10.62	12.83	13.26	12.22	12.16	11.51
MgO	20.52	15.38	18.81	17.26	15.00	17.70	17.66	19.06
CaO	0.23	0.11	0.04	0.04	0.12	0.06	0.07	0.08
MnO	0.10	0.23	2.08	1.36	0.72	0.67	0.69	0.57
FeO	5.31	16.11	11.42	13.12	15.51	13.01	13.28	11.10
BaO	0.00	0.43	0.00	0.03	0.01	0.00	0.01	0.01
Na_2O	0.05	0.26	0.03	0.02	0.04	0.02	0.04	0.05
K_2O	10.31	10.12	10.54	10.69	9.15	10.26	10.25	10.24
F	6.05	3.07	3.22	2.56	1.84	2.72	2.53	3.15
H_2O*	1.30	2.46	2.48	2.78	3.02	2.71	2.78	2.56
Total	100.56	100.08	100.35	100.16	97.73	99.69	99.58	100.14
Si (*apfu*)	3.319	2.858	3.047	2.957	2.929	2.998	2.975	3.068
Ti	0.016	0.109	0.023	0.008	0.056	0.023	0.034	0.019
Al	0.871	1.151	0.937	1.137	1.202	1.081	1.079	1.004
Mg	2.201	1.757	2.100	1.935	1.720	1.980	1.982	2.103
Ca	0.018	0.009	0.003	0.003	0.010	0.004	0.006	0.007
Mn	0.006	0.015	0.132	0.087	0.047	0.042	0.044	0.035
Fe^{2+}	0.320	1.033	0.715	0.825	0.997	0.817	0.836	0.687
Ba	0.000	0.013	0.000	0.001	0.000	0.000	0.000	0.000
Na	0.007	0.038	0.005	0.002	0.006	0.003	0.005	0.007
K	0.946	0.990	1.007	1.025	0.897	0.982	0.984	0.967
F	1.378	0.745	0.763	0.608	0.449	0.645	0.602	0.737
OH	0.622	1.255	1.237	1.392	1.551	1.355	1.398	1.263
O	10.000	10.000	10.000	10.000	10.000	10.000	10.000	10.000
Anion sum	12.000	12.000	12.000	12.000	12.000	12.000	12.000	12.000
Cation sum	7.705	7.972	7.968	7.980	7.865	7.932	7.946	7.898
Mg/(Mg+Fe)	0.871	0.626	0.713	0.680	0.622	0.697	0.692	0.744

Table B.3. Composition of chlorite from various rock types across the 2020 Corundum Dome and Pyrochlore Dome sampling area.

Sample	20TN55A	20TN55A	20TN55A	20TN55A	20TN55A	20TN55A	20TN55A	20TN55A	20TN55A	20TN55A	20TN57A	20TN57A
Analysis	12691	12702	12713	12724	171004	171015	201101	201112	201123	201134	241531	241542
Species	pycno-chlorite	pycno-chlorite	pycno-chlorite	pycno-chlorite	pycno-chlorite	pycno-chlorite	pycno-chlorite	pycno-chlorite	pycno-chlorite	ripid-olite	pycno-chlorite	pycno-chlorite
SiO_2 (wt. %)	26.79	27.16	27.21	27.25	27.78	28.09	27.49	27.84	27.45	25.95	28.24	27.02
TiO_2	0.17	0.00	0.06	0.08	0.03	0.05	0.07	0.08	0.06	2.27	0.06	0.02
Al_2O_3	18.34	18.71	17.72	18.07	18.84	18.93	17.93	17.93	18.02	17.47	17.98	18.53
Fe_2O_3*	0.94	1.40	1.19	1.05	2.43	2.26	1.72	1.87	1.30	1.50	0.96	0.52
FeO*	23.34	23.36	23.04	23.08	20.89	20.69	22.35	21.67	22.95	22.23	20.96	22.49
MnO	0.75	0.42	0.43	0.50	0.82	0.40	0.38	0.37	0.43	0.46	0.46	0.49
MgO	15.32	15.13	16.50	16.00	15.00	15.24	15.87	15.81	15.93	16.60	17.47	17.44
CaO	0.03	0.04	0.03	0.02	0.12	0.08	0.10	0.13	0.09	0.03	0.02	0.04
Na_2O	0.01	0.00	0.00	0.02	0.02	0.01	0.03	0.04	0.03	0.01	0.01	0.02
K_2O	0.49	0.33	0.07	0.67	0.45	0.57	0.21	0.36	0.33	0.02	1.20	0.13
BaO	0.05	0.00	0.01	0.00	0.00	0.00	0.01	0.00	0.01	0.00	0.00	0.03
F	0.48	0.48	0.59	0.72	0.75	0.50	0.69	0.64	0.59	0.58	0.76	0.39
H_2O*	10.72	10.78	10.67	10.59	10.58	10.86	10.58	10.65	10.71	10.69	10.76	11.00
O=F,Cl	0.20	0.20	0.25	0.30	0.32	0.21	0.29	0.27	0.25	0.25	0.32	0.16
Total	97.22	97.61	97.27	97.74	97.39	97.47	97.13	97.12	97.65	97.57	98.59	97.97
Si (*apfu*)	5.661	5.700	5.712	5.673	5.750	5.824	5.743	5.803	5.732	5.441	5.755	5.640
Al iv	2.339	2.300	2.288	2.327	2.250	2.176	2.257	2.197	2.268	2.559	2.245	2.360
Al vi	2.277	2.380	2.143	2.172	2.428	2.521	2.222	2.276	2.224	1.808	2.149	2.230
Ti	0.027	0.000	0.010	0.013	0.005	0.007	0.011	0.012	0.009	0.357	0.010	0.003
Fe^{3+}	0.150	0.220	0.187	0.165	0.379	0.352	0.270	0.293	0.204	0.237	0.148	0.082
Fe^{2+}	4.125	4.100	4.044	4.017	3.615	3.588	3.905	3.778	4.009	3.899	3.572	3.927
Mn	0.135	0.074	0.076	0.087	0.144	0.070	0.067	0.065	0.076	0.082	0.079	0.086
Mg	4.824	4.733	5.161	4.965	4.627	4.708	4.942	4.914	4.960	5.189	5.307	5.427
Ca	0.007	0.010	0.006	0.005	0.026	0.017	0.021	0.030	0.019	0.007	0.005	0.009
Na	0.007	0.002	0.000	0.013	0.013	0.009	0.027	0.029	0.026	0.009	0.011	0.019
K	0.263	0.176	0.036	0.354	0.238	0.302	0.109	0.190	0.176	0.008	0.623	0.071
Ba	0.008	0.000	0.002	0.000	0.000	0.000	0.002	0.000	0.002	0.000	0.001	0.005
F	0.642	0.643	0.787	0.946	0.988	0.661	0.917	0.847	0.784	0.774	0.981	0.513
OH*	15.358	15.357	15.213	15.054	15.012	15.339	15.083	15.153	15.216	15.226	15.019	15.487
Cation sum	19.822	19.696	19.665	19.792	19.474	19.575	19.578	19.587	19.705	19.595	19.904	19.860

Note: Oxide percentages based on 28 O *apfu*. Compositions were recalculated on the basis of 36 O *apfu*. *Fe^{2+}/Fe^{3+} and OH calculated assuming full site occupancy.

Table B.3. (Continued) Composition of chlorite from various rock types across the 2020 Corundum Dome and Pyrochlore Dome sampling area.

Sample	20TN57A	20TN57A	20TN57A	20TN57A	20TN57A	20TN57A	20TN57A	20TN57A	20TN57A	20TN53	20TN5	20TN5
Analysis	241553	241564	241575	241586	241597	301912	301923	301934	301945	372253	81001	81012
Species	pycno-chlorite	pycno-chlorite	pycno-chlorite	pycno-chlorite	pycno-chlorite	pycno-chlorite	pycno-chlorite	pycno-chlorite	pycno-chlorite	pycno-chlorite	pycno-chlorite	pycno-chlorite
SiO_2 (wt. %)	27.49	26.43	26.54	26.89	27.02	27.24	26.88	27.42	26.92	26.96	28.46	27.53
TiO_2	0.03	0.06	0.01	0.03	0.04	0.10	0.09	0.06	0.02	0.03	0.08	0.02
Al_2O_3	19.03	18.72	18.50	18.55	18.27	18.34	18.65	18.71	18.72	18.58	18.19	17.80
Fe_2O_3*	1.06	0.50	0.37	0.42	0.71	0.64	0.59	0.97	0.54	1.42	0.41	0.00
FeO*	21.93	23.72	23.90	22.57	21.64	23.02	23.05	22.09	22.56	23.18	19.54	19.12
MnO	0.48	0.38	0.38	0.43	0.49	0.48	0.49	0.49	0.47	0.50	0.36	0.32
MgO	16.26	15.88	15.96	17.43	17.75	17.01	16.63	17.15	17.44	16.07	18.80	20.65
CaO	0.03	0.05	0.06	0.03	0.02	0.03	0.04	0.04	0.01	0.05	0.12	0.05
Na_2O	0.02	0.02	0.03	0.02	0.02	0.01	0.01	0.03	0.02	0.01	0.16	0.01
K_2O	0.62	0.17	0.20	0.26	0.19	0.11	0.08	0.26	0.16	0.02	0.49	0.01
BaO	0.00	0.00	0.00	0.00	0.00	0.04	0.05	0.05	0.00	0.00	0.04	0.02
F	0.39	0.24	0.22	0.42	0.52	0.30	0.22	0.49	0.44	0.71	0.04	0.00
H_2O*	11.02	10.95	10.97	10.94	10.82	11.08	11.09	10.97	10.96	10.63	11.51	11.45
O=F,Cl	0.17	0.10	0.09	0.18	0.22	0.13	0.09	0.21	0.19	0.30	0.02	0.00
Total	98.18	97.02	97.05	97.81	97.27	98.27	97.77	98.51	98.09	97.86	98.17	96.96
Si (*apfu*)	5.704	5.628	5.656	5.616	5.640	5.695	5.664	5.663	5.604	5.611	5.881	5.758
Al iv	2.296	2.372	2.344	2.384	2.360	2.305	2.336	2.337	2.396	2.389	2.119	2.242
Al vi	2.408	2.350	2.325	2.217	2.178	2.242	2.318	2.264	2.232	2.226	2.333	2.153
Ti	0.005	0.010	0.002	0.005	0.006	0.015	0.015	0.009	0.004	0.005	0.012	0.003
Fe^{3+}	0.165	0.081	0.060	0.066	0.112	0.100	0.093	0.151	0.085	0.222	0.064	0.000
Fe^{2+}	3.805	4.224	4.259	3.943	3.778	4.025	4.061	3.817	3.927	4.035	3.376	3.381
Mn	0.084	0.068	0.068	0.076	0.086	0.085	0.087	0.086	0.083	0.088	0.063	0.057
Mg	5.028	5.039	5.071	5.428	5.525	5.300	5.222	5.279	5.412	4.985	5.791	6.438
Ca	0.006	0.012	0.013	0.007	0.005	0.006	0.009	0.009	0.003	0.012	0.025	0.011
Na	0.017	0.016	0.024	0.017	0.012	0.007	0.009	0.023	0.014	0.012	0.125	0.009
K	0.326	0.094	0.110	0.137	0.099	0.059	0.043	0.135	0.087	0.013	0.257	0.005
Ba	0.000	0.000	0.000	0.000	0.000	0.007	0.007	0.007	0.000	0.000	0.006	0.003
F	0.518	0.317	0.294	0.559	0.691	0.397	0.293	0.646	0.581	0.931	0.047	0.000
OH*	15.482	15.683	15.706	15.441	15.309	15.603	15.707	15.354	15.419	15.069	15.953	16.000
Cation sum	19.844	19.894	19.932	19.895	19.802	19.845	19.864	19.780	19.848	19.598	20.053	20.059

Table B.3. (Continued) Composition of chlorite from various rock types across the 2020 Corundum Dome and Pyrochlore Dome sampling area.

Sample	20TN5	20TN5	20TN24A	20TN25D	20TN25D	20TN25D	20TN25D	20TN25D	20TN25D	20TN25D	20TN25D	20TN25D
Analysis	151281	151292	241664	301831	301842	301853	352011	352022	352044	352055	352077	352088
Species	ripidolite	pycnochlorite	pycnochlorite	brunsvigite	ripidolite	ripidolite	brunsvigite	ripidolite	ripidolite	pycnochlorite	ripidolite	brunsvigite
SiO_2 (wt. %)	26.83	27.88	27.31	26.11	24.77	25.27	26.53	25.35	26.25	26.18	25.94	25.67
TiO_2	0.04	0.00	0.43	0.00	0.07	0.03	0.03	0.04	0.07	0.07	0.09	0.09
Al_2O_3	19.39	18.32	18.38	17.38	18.71	18.60	17.52	18.36	17.77	17.29	18.22	17.51
Fe_2O_3*	0.00	0.00	0.14	0.20	0.00	0.00	0.62	0.00	0.78	0.00	0.42	0.19
FeO*	20.51	19.81	20.21	28.36	30.40	29.84	26.84	29.39	26.44	26.63	27.43	27.84
MnO	0.39	0.34	0.15	0.44	0.66	0.61	0.40	0.64	0.35	0.44	0.49	0.43
MgO	19.19	20.43	19.71	14.13	12.24	12.35	14.83	12.93	14.97	15.53	13.99	13.55
CaO	0.29	0.11	0.13	0.03	0.08	0.12	0.03	0.06	0.03	0.05	0.08	0.10
Na_2O	0.01	0.00	0.00	0.00	0.00	0.00	0.00	0.01	0.00	0.00	0.02	0.03
K_2O	0.01	0.00	0.02	0.02	0.00	0.02	0.01	0.06	0.04	0.03	0.03	0.05
BaO	0.02	0.03	0.04	0.00	0.00	0.01	0.03	0.01	0.02	0.00	0.08	0.08
F	0.00	0.00	0.07	0.42	0.16	0.13	0.52	0.23	0.71	0.38	0.40	0.28
H_2O*	11.51	11.62	11.45	10.60	10.73	10.80	10.60	10.72	10.42	10.68	10.67	10.58
O=F,Cl	0.00	0.00	0.03	0.18	0.07	0.05	0.22	0.10	0.30	0.16	0.17	0.12
Total	98.19	98.54	98.02	97.52	97.75	97.74	97.74	97.69	97.55	97.12	97.70	96.27
Si (*apfu*)	5.583	5.754	5.675	5.636	5.426	5.529	5.655	5.521	5.570	5.633	5.572	5.631
Al iv	2.417	2.246	2.325	2.364	2.574	2.471	2.345	2.479	2.430	2.367	2.428	2.369
Al vi	2.342	2.214	2.184	2.085	2.276	2.335	2.091	2.251	2.062	2.039	2.213	2.179
Ti	0.006	0.000	0.067	0.000	0.012	0.005	0.004	0.006	0.011	0.011	0.014	0.014
Fe^{3+}	0.000	0.000	0.022	0.032	0.000	0.000	0.099	0.000	0.124	0.000	0.069	0.032
Fe^{2+}	3.597	3.433	3.513	5.121	5.630	5.470	4.784	5.370	4.691	4.793	4.927	5.107
Mn	0.069	0.059	0.027	0.081	0.122	0.113	0.073	0.118	0.064	0.081	0.089	0.080
Mg	5.953	6.286	6.107	4.546	3.996	4.028	4.712	4.198	4.735	4.982	4.477	4.431
Ca	0.066	0.025	0.028	0.008	0.020	0.029	0.007	0.013	0.006	0.011	0.019	0.025
Na	0.005	0.000	0.001	0.000	0.000	0.000	0.000	0.004	0.000	0.000	0.019	0.022
K	0.006	0.001	0.013	0.012	0.002	0.013	0.005	0.033	0.021	0.018	0.018	0.025
Ba	0.003	0.005	0.007	0.000	0.000	0.001	0.004	0.001	0.004	0.000	0.013	0.014
F	0.000	0.000	0.089	0.568	0.220	0.181	0.706	0.321	0.959	0.517	0.540	0.395
OH*	16.000	16.000	15.911	15.432	15.780	15.819	15.294	15.679	15.041	15.483	15.460	15.605
Cation sum	20.047	20.022	19.967	19.884	20.058	19.995	19.779	19.994	19.718	19.935	19.858	19.929

Table B.3. (Continued) Composition of chlorite from various rock types across the 2020 Corundum Dome and Pyrochlore Dome sampling area.

Sample	20TN13B-2	20TN13B-2	20TN23	20TN7	20TN7
Analysis	10641	10652	371811	401943	401954
Species	diabantite	diabantite	pycnochlorite	pycnochlorite	pycnochlorite
SiO_2 (wt. %)	31.92	34.84	30.40	29.15	27.59
TiO_2	0.03	0.09	0.10	0.09	0.00
Al_2O_3	12.67	12.65	16.74	17.00	17.86
Fe_2O_3*	2.84	3.99	1.77	1.83	0.00
FeO*	22.12	18.02	16.62	17.49	20.52
MnO	0.30	0.28	2.05	1.61	1.74
MgO	14.88	14.83	18.04	18.74	18.82
CaO	0.17	0.14	0.09	0.13	0.02
Na_2O	0.05	0.04	0.06	0.02	0.01
K_2O	1.58	4.01	1.47	0.13	0.23
BaO	0.05	0.01	0.01	0.00	0.07
F	0.98	1.69	0.62	0.47	0.16
H_2O*	10.30	10.09	11.04	11.04	11.30
O=F,Cl	0.41	0.71	0.26	0.20	0.07
Total	97.48	99.98	98.75	97.50	98.23
Si (*apfu*)	6.580	6.737	6.119	5.987	5.751
Al iv	1.420	1.263	1.881	2.013	2.249
Al vi	1.743	1.761	2.167	2.150	2.153
Ti	0.005	0.013	0.014	0.014	0.000
Fe^{3+}	0.441	0.581	0.268	0.283	0.000
Fe^{2+}	3.814	2.913	2.798	3.004	3.585
Mn	0.053	0.045	0.349	0.280	0.307
Mg	4.573	4.275	5.413	5.737	5.848
Ca	0.037	0.029	0.020	0.029	0.004
Na	0.039	0.029	0.044	0.014	0.005
K	0.832	1.980	0.755	0.066	0.121
Ba	0.008	0.002	0.002	0.000	0.012
F	1.276	2.070	0.786	0.615	0.210
OH*	14.724	13.930	15.214	15.385	15.790
Cation sum	19.544	19.630	19.830	19.578	20.033

Table B.4. Composition of amphibole from various rock types across the 2020 Corundum Dome and Pyrochlore Dome sampling area.

Sample	20TN10C	20TN10C	20TN10C	20TN10C	20TN10C	20TN4A	20TN4A
Analysis	20981	20992	201003	221031	221042	301241	301252
Mineral	actinolite	actinolite	actinolite	ferro-actinolite	actinolite	magnesio-fluoro-arfvedsonite	magnesio-fluoro-arfvedsonite
SiO_2 (wt. %)	54.41	53.65	54.04	52.53	54.84	53.53	53.60
TiO_2	0.02	0.00	0.09	0.00	0.03	0.75	0.73
Al_2O_3	0.96	0.63	0.45	1.27	0.69	1.12	1.22
MnO	1.15	1.47	1.61	2.39	1.28	2.14	2.36
FeO	13.76	16.13	16.90	19.72	13.97	10.26	9.21
Fe_2O_3	0.89	1.44	0.43	0.54	0.59	6.26	6.33
MgO	14.08	12.43	11.88	9.19	14.06	10.69	11.18
CaO	11.66	11.40	11.40	11.37	11.51	1.42	1.28
Na_2O	0.72	0.67	0.62	0.65	0.70	9.01	9.10
K_2O	0.22	0.12	0.13	0.23	0.29	1.88	1.81
H_2O+	1.83	1.91	1.90	1.89	1.83	0.98	0.93
F	0.49	0.27	0.26	0.21	0.51	2.19	2.31
O=F,Cl	-0.21	-0.12	-0.11	-0.09	-0.21	-0.92	-0.97
Total	99.97	100.01	99.60	99.91	100.08	99.30	99.09
T *(apfu)*							
Si	7.903	7.897	7.988	7.892	7.957	7.943	7.938
Al	0.097	0.103	0.012	0.108	0.043	0.057	0.062
Ti	0.000	0.000	0.000	0.000	0.000	0.000	0.000
Fe^{3+}	0.000	0.000	0.000	0.000	0.000	0.000	0.000
T subtotal	8.000	8.000	8.000	8.000	8.000	8.000	8.000
C							
Ti	0.002	0.001	0.010	0.000	0.003	0.083	0.082
Al	0.068	0.006	0.067	0.117	0.074	0.139	0.150
Fe^{3+}	0.097	0.160	0.048	0.061	0.064	0.699	0.705
Mn^{2+}	0.114	0.121	0.169	0.286	0.123	0.270	0.296
Fe^{2+}	1.671	1.985	2.089	2.477	1.695	1.274	1.141
Mg	3.048	2.728	2.617	2.058	3.041	2.365	2.468
C subtotal	5.000	5.001	5.000	4.999	5.000	4.830	4.842
B							
Mn^{2+}	0.028	0.063	0.032	0.017	0.034	0.000	0.000
Fe^{2+}	0.000	0.000	0.000	0.000	0.000	0.000	0.000
Mg	0.000	0.000	0.000	0.000	0.000	0.000	0.000
Ca	1.814	1.798	1.806	1.831	1.789	0.225	0.203
Na	0.158	0.140	0.162	0.152	0.177	1.775	1.797
B subtotal	2.000	2.001	2.000	2.000	2.000	2.000	2.000
A							
Ca	0.000	0.000	0.000	0.000	0.000	0.000	0.000
Na	0.045	0.052	0.016	0.037	0.021	0.816	0.816
K	0.040	0.023	0.025	0.045	0.054	0.355	0.342
A subtotal	0.085	0.075	0.041	0.082	0.075	1.171	1.158
O (non-W)	22.000	22.000	22.000	22.000	22.000	22.000	22.000
W							
OH	1.774	1.872	1.878	1.898	1.767	0.970	0.919
F	0.226	0.128	0.122	0.102	0.233	1.030	1.081
O	0.000	0.000	0.000	0.000	0.000	0.000	0.000
W subtotal	2.000	2.000	2.000	2.000	2.000	2.000	2.000
Sum T, C, B, A	15.085	15.077	15.041	15.081	15.075	16.001	16.000
Mg/(Mg+Fe)	0.633	0.560	0.550	0.448	0.634	0.545	0.572

Note: Compositions were recalculated using the recommendations of Locock (2014). Actinolite species calculated using Si–Ca & Li=15 and Si–Na=15 *apfu* or Si–Ca & Li=15 Si–Mg & Li=13 *apfu* or Si–Ca & Li=15 Si–Mg &

Li=13 Si–Na=15 *apfu*; arfvedsonite using Si–K=16 *apfu* or Si–Mg & Li=13 *apfu*; katophorite using Si–K=16 *apfu*; richterite using Si–K=16 *apfu*; hornblende using Si–Ca & Li=15 Si–Na=15 *apfu*; winchite using Si–Ca & Li=15 Si–Mg & Li=13 Si–Na=15 *apfu*; and riebeckite using Si–Mg & Li=13 *apfu*. * H_2O determined by stoichiometry. ** Ratio of Fe_2O_3 and FeO calculated to fit an electroneutral formula.

Table B.4. (Continued) Composition of amphibole from various rock types across the 2020 Corundum Dome and Pyrochlore Dome sampling area.

Sample	20TN4A	20TN4A	20TN4A	20TN4A	20TN4A	20TN4A	20TN4A
Analysis	301263	301274	351391	351402	351413	351424	351435
Mineral	magnesio-fluoro-arfvedsonite	magnesio-fluoro-arfvedsonite	magnesio-fluoro-arfvedsonite	ferri-fluoro-katophorite	magnesio-fluoro-arfvedsonite	magnesio-fluoro-arfvedsonite	magnesio-fluoro-arfvedsonite
SiO_2 (wt. %)	53.83	53.92	53.79	53.80	54.93	54.45	53.90
TiO_2	0.59	0.56	0.62	0.29	0.30	0.32	0.60
Al_2O_3	0.98	1.02	1.09	1.04	1.06	1.28	1.12
MnO	2.07	2.22	2.00	2.05	2.26	2.07	1.89
FeO	10.66	9.47	10.64	11.40	7.14	7.56	11.14
Fe_2O_3	5.74	6.18	5.64	4.07	6.91	6.59	5.54
MgO	10.93	11.25	10.87	11.74	12.70	12.59	10.60
CaO	1.61	1.47	1.44	3.16	0.99	0.90	1.37
Na_2O	8.91	9.06	8.95	7.90	9.18	9.13	9.03
K_2O	1.78	1.80	1.83	1.85	2.13	2.01	1.82
H_2O+	0.90	0.85	0.80	0.91	0.77	0.82	0.83
F	2.37	2.49	2.57	2.35	2.72	2.59	2.51
O=F,Cl	-1.00	-1.05	-1.08	-0.99	-1.15	-1.09	-1.06
Total	99.36	99.25	99.17	99.58	99.94	99.23	99.29
T *(apfu)*							
Si	7.976	7.973	7.982	7.959	7.991	7.975	7.996
Al	0.024	0.027	0.018	0.041	0.009	0.025	0.004
Ti	0.000	0.000	0.000	0.000	0.000	0.000	0.000
Fe^{3+}	0.000	0.000	0.000	0.000	0.000	0.000	0.000
T subtotal	8.000	8.000	8.000	8.000	8.000	8.000	8.000
C							
Ti	0.066	0.063	0.069	0.032	0.033	0.035	0.067
Al	0.147	0.151	0.173	0.140	0.172	0.197	0.192
Fe^{3+}	0.640	0.687	0.630	0.454	0.757	0.726	0.619
Mn^{2+}	0.260	0.278	0.252	0.257	0.279	0.256	0.237
Fe^{2+}	1.321	1.171	1.320	1.411	0.869	0.926	1.382
Mg	2.413	2.479	2.404	2.589	2.753	2.748	2.345
C subtotal	4.847	4.829	4.848	4.883	4.863	4.888	4.842
B							
Mn^{2+}	0.000	0.000	0.000	0.000	0.000	0.000	0.000
Fe^{2+}	0.000	0.000	0.000	0.000	0.000	0.000	0.000
Mg	0.000	0.000	0.000	0.000	0.000	0.000	0.000
Ca	0.256	0.233	0.229	0.501	0.154	0.142	0.217
Na	1.744	1.767	1.771	1.499	1.846	1.858	1.783
B subtotal	2.000	2.000	2.000	2.000	2.000	2.000	2.000
A							
Ca	0.000	0.000	0.000	0.000	0.000	0.000	0.000
Na	0.816	0.831	0.805	0.768	0.743	0.735	0.813
K	0.336	0.339	0.347	0.350	0.395	0.376	0.345
A subtotal	1.152	1.170	1.152	1.118	1.138	1.111	1.158
O (non-W)	22.000	22.000	22.000	22.000	22.000	22.000	22.000
W							
OH	0.891	0.833	0.794	0.901	0.747	0.802	0.821
F	1.109	1.167	1.206	1.099	1.253	1.198	1.179
O	0.000	0.000	0.000	0.000	0.000	0.000	0.000
W subtotal	2.000	2.000	2.000	2.000	2.000	2.000	2.000
Sum T, C, B, A	15.999	15.999	16.000	16.001	16.001	15.999	16.000
Mg/(Mg+Fe)	0.552	0.572	0.552	0.581	0.629	0.625	0.540

Table B.4. (Continued) Composition of amphibole from various rock types across the 2020 Corundum Dome and Pyrochlore Dome sampling area.

Sample	20TN4D	20TN4D	20TN4D	20TN4D	20TN4D	20TN4D	20TN20
Analysis	421681	421692	421703	421714	461851	461862	512101
Mineral	actinolite	actinolite	actinolite	actinolite	actinolite	actinolite	magnesio-fluoro-arfvedsonite
SiO_2 (wt. %)	55.05	54.29	55.01	54.76	55.47	53.68	54.24
TiO_2	0.03	0.04	0.03	0.09	0.00	0.01	0.26
Al_2O_3	0.50	0.84	0.34	0.62	0.40	0.76	0.18
MnO	2.30	2.08	1.98	1.99	1.24	2.37	3.81
FeO	9.49	9.59	8.34	9.05	8.40	10.20	12.65
Fe_2O_3	0.41	0.96	0.44	0.45	0.28	0.83	4.27
MgO	16.25	15.87	17.05	16.55	17.90	15.29	7.90
CaO	12.05	11.61	12.17	12.19	12.79	11.80	0.23
Na_2O	0.53	0.72	0.45	0.42	0.23	0.59	9.29
K_2O	0.31	0.23	0.11	0.15	0.13	0.21	2.22
H_2O+	1.70	1.74	1.82	1.86	1.80	1.76	0.33
F	0.79	0.66	0.53	0.45	0.62	0.59	3.44
O=F,Cl	-0.33	-0.28	-0.22	-0.19	-0.26	-0.25	-1.45
Total	99.09	98.34	98.06	98.37	98.99	97.84	97.36
T *(apfu)*							
Si	7.952	7.907	7.968	7.934	7.938	7.897	8.303
Al	0.048	0.093	0.032	0.066	0.062	0.103	0.000
Ti	0.000	0.000	0.000	0.000	0.000	0.000	0.000
Fe^{3+}	0.000	0.000	0.000	0.000	0.000	0.000	0.000
T subtotal	8.000	8.000	8.000	8.000	8.000	8.000	8.303
C							
Ti	0.003	0.004	0.003	0.010	0.000	0.001	0.030
Al	0.037	0.050	0.027	0.040	0.004	0.029	0.032
Fe^{3+}	0.044	0.105	0.047	0.049	0.030	0.092	0.492
Mn^{2+}	0.269	0.227	0.230	0.231	0.142	0.269	0.494
Fe^{2+}	1.147	1.168	1.011	1.097	1.006	1.255	1.620
Mg	3.500	3.445	3.682	3.574	3.818	3.354	1.803
C subtotal	5.000	4.999	5.000	5.001	5.000	5.000	4.471
B							
Mn^{2+}	0.013	0.030	0.013	0.014	0.008	0.026	0.000
Fe^{2+}	0.000	0.000	0.000	0.000	0.000	0.000	0.000
Mg	0.000	0.000	0.000	0.000	0.000	0.000	0.000
Ca	1.865	1.811	1.889	1.893	1.962	1.859	0.037
Na	0.123	0.159	0.098	0.093	0.030	0.115	1.963
B subtotal	2.001	2.000	2.000	2.000	2.000	2.000	2.000
A							
Ca	0.000	0.000	0.000	0.000	0.000	0.000	0.000
Na	0.027	0.045	0.028	0.024	0.034	0.055	0.794
K	0.057	0.043	0.020	0.027	0.023	0.040	0.433
A subtotal	0.084	0.088	0.048	0.051	0.057	0.095	1.227
O (non-W)	22.000	22.000	22.000	22.000	22.000	22.000	22.000
W							
OH	1.638	1.695	1.757	1.796	1.719	1.724	0.334
F	0.362	0.305	0.243	0.204	0.281	0.276	1.666
O	0.000	0.000	0.000	0.000	0.000	0.000	0.000
W subtotal	2.000	2.000	2.000	2.000	2.000	2.000	2.000
Sum T, C, B, A	15.085	15.087	15.048	15.052	15.057	15.095	16.001
Mg/(Mg+Fe)	0.746	0.730	0.777	0.757	0.787	0.713	0.461

Table B.4. (Continued) Composition of amphibole from various rock types across the 2020 Corundum Dome and Pyrochlore Dome sampling area.

Sample	20TN20	20TN20	20TN20	20TN3-2	20TN3-2	20TN3-2	20TN3-2
Analysis	512112	512123	512134	9551	9562	9573	18862
Mineral	magnesio-fluoro-arfvedsonite	fluoro-arfvedsonite	fluoro-arfvedsonite	magnesio-fluoro-arfvedsonite	magnesio-fluoro-arfvedsonite	magnesio-fluoro-arfvedsonite	actinolite
SiO_2 (wt. %)	53.81	53.22	54.31	53.28	52.29	53.63	54.41
TiO_2	0.19	0.20	0.28	0.52	0.54	0.46	0.00
Al_2O_3	0.15	0.24	0.19	1.47	1.90	1.27	0.63
MnO	3.65	3.88	3.84	3.39	3.36	3.90	1.13
FeO	12.62	14.29	14.77	9.31	9.43	9.76	14.34
Fe_2O_3	4.46	3.70	2.38	5.50	5.57	3.31	0.24
MgO	7.79	7.07	7.39	10.25	10.27	11.06	13.90
CaO	0.23	0.57	0.14	0.49	0.78	1.77	12.11
Na_2O	9.21	8.96	9.06	9.36	9.02	8.60	0.32
K_2O	2.23	2.00	2.18	1.65	1.59	1.60	0.10
H_2O+	0.36	0.45	0.40	0.69	0.61	0.69	1.91
F	3.34	3.12	3.25	2.74	2.87	2.76	0.30
O=F,Cl	-1.40	-1.31	-1.37	-1.15	-1.21	-1.16	-0.13
Total	96.64	96.38	96.84	97.50	96.99	97.64	99.26
T *(apfu)*							
Si	8.303	8.289	8.382	8.024	7.931	8.055	7.960
Al	0.000	0.000	0.000	0.000	0.069	0.000	0.040
Ti	0.000	0.000	0.000	0.000	0.000	0.000	0.000
Fe^{3+}	0.000	0.000	0.000	0.000	0.000	0.000	0.000
T subtotal	8.303	8.289	8.382	8.024	8.000	8.055	8.000
C							
Ti	0.022	0.023	0.033	0.059	0.061	0.052	0.000
Al	0.026	0.045	0.035	0.261	0.270	0.225	0.068
Fe^{3+}	0.518	0.433	0.277	0.623	0.635	0.374	0.026
Mn^{2+}	0.476	0.512	0.502	0.432	0.431	0.496	0.119
Fe^{2+}	1.629	1.861	1.906	1.173	1.196	1.226	1.755
Mg	1.793	1.641	1.699	2.302	2.321	2.476	3.032
C subtotal	4.464	4.515	4.452	4.850	4.914	4.849	5.000
B							
Mn^{2+}	0.000	0.000	0.000	0.000	0.000	0.000	0.020
Fe^{2+}	0.000	0.000	0.000	0.000	0.000	0.000	0.000
Mg	0.000	0.000	0.000	0.000	0.000	0.000	0.000
Ca	0.038	0.095	0.024	0.078	0.127	0.284	1.898
Na	1.962	1.905	1.976	1.922	1.873	1.716	0.082
B subtotal	2.000	2.000	2.000	2.000	2.000	2.000	2.000
A							
Ca	0.000	0.000	0.000	0.000	0.000	0.000	0.000
Na	0.794	0.800	0.736	0.810	0.778	0.789	0.008
K	0.438	0.396	0.429	0.317	0.307	0.307	0.020
A subtotal	1.232	1.196	1.165	1.127	1.085	1.096	0.028
O (non-W)	22.000	22.000	22.000	22.000	22.000	22.000	22.000
W							
OH	0.372	0.463	0.412	0.695	0.622	0.691	1.862
F	1.628	1.537	1.588	1.305	1.378	1.309	0.138
O	0.000	0.000	0.000	0.000	0.000	0.000	0.000
W subtotal	2.000	2.000	2.000	2.000	2.000	2.000	2.000
Sum T, C, B, A	15.999	16.000	15.999	16.001	15.999	16.000	15.028
Mg/(Mg+Fe)	0.455	0.417	0.438	0.562	0.559	0.607	0.630

Table B.4. (Continued) Composition of amphibole from various rock types across the 2020 Corundum Dome and Pyrochlore Dome sampling area.

Sample	20TN3-2	20TN3-2	20TN3-2	20TN3-2	20TN3-2	20TN15A	20TN15A
Analysis	18873	18884	19901	19912	19923	21951	21962
Mineral	actinolite	actinolite	actinolite	actinolite	ferro-actinolite	fluoro-arfvedsonite	fluoro-arfvedsonite
SiO_2 (wt. %)	51.79	52.98	52.08	53.03	49.83	51.94	52.09
TiO_2	0.03	0.07	0.01	0.00	0.02	1.25	1.05
Al_2O_3	1.77	1.14	2.09	1.24	1.50	0.34	0.26
MnO	1.14	1.23	0.91	1.09	1.80	1.45	1.52
FeO	15.73	15.22	14.53	16.55	23.40	17.73	18.15
Fe_2O_3	1.72	0.90	2.19	1.11	1.42	6.59	6.00
MgO	12.13	12.60	12.63	11.77	6.35	6.54	6.56
CaO	11.50	11.81	11.52	11.42	10.52	1.20	1.19
Na_2O	0.54	0.41	0.62	0.63	0.82	8.00	8.02
K_2O	0.17	0.16	0.26	0.25	0.26	1.55	1.60
H_2O+	1.87	1.88	1.89	1.91	1.91	0.56	0.51
F	0.28	0.29	0.28	0.23	0.00	2.32	2.50
O=F,Cl	-0.12	-0.12	-0.12	-0.10	0.00	-0.98	-1.05
Total	98.54	98.57	98.89	99.12	97.83	98.50	98.40
T *(apfu)*							
Si	7.743	7.872	7.718	7.878	7.811	8.033	8.067
Al	0.257	0.128	0.282	0.122	0.189	0.000	0.000
Ti	0.000	0.000	0.000	0.000	0.000	0.000	0.000
Fe^{3+}	0.000	0.000	0.000	0.000	0.000	0.000	0.000
T subtotal	8.000	8.000	8.000	8.000	8.000	8.033	8.067
C							
Ti	0.004	0.007	0.001	0.000	0.002	0.146	0.122
Al	0.054	0.071	0.083	0.095	0.088	0.062	0.048
Fe^{3+}	0.193	0.100	0.244	0.124	0.167	0.767	0.699
Mn^{2+}	0.080	0.138	0.081	0.118	0.191	0.190	0.199
Fe^{2+}	1.966	1.891	1.801	2.056	3.068	2.293	2.350
Mg	2.703	2.792	2.790	2.606	1.483	1.509	1.514
C subtotal	5.000	4.999	5.000	4.999	4.999	4.967	4.932
B							
Mn^{2+}	0.065	0.016	0.034	0.020	0.048	0.000	0.000
Fe^{2+}	0.000	0.000	0.000	0.000	0.000	0.000	0.000
Mg	0.000	0.000	0.000	0.000	0.000	0.000	0.000
Ca	1.842	1.880	1.829	1.817	1.766	0.199	0.198
Na	0.093	0.104	0.137	0.163	0.186	1.801	1.802
B subtotal	2.000	2.000	2.000	2.000	2.000	2.000	2.000
A							
Ca	0.000	0.000	0.000	0.000	0.000	0.000	0.000
Na	0.064	0.014	0.041	0.018	0.063	0.599	0.605
K	0.032	0.031	0.049	0.048	0.052	0.307	0.316
A subtotal	0.096	0.045	0.090	0.066	0.115	0.906	0.921
O (non-W)	22.000	22.000	22.000	22.000	22.000	22.000	22.000
W							
OH	1.869	1.862	1.869	1.892	2.000	0.574	0.530
F	0.131	0.138	0.131	0.108	0.000	1.135	1.226
O	0.000	0.000	0.000	0.000	0.000	0.292	0.244
W subtotal	2.000	2.000	2.000	2.000	2.000	2.001	2.000
Sum T, C, B, A	15.096	15.044	15.090	15.065	15.114	15.906	15.920
Mg/(Mg+Fe)	0.556	0.584	0.577	0.545	0.314	0.330	0.332

Table B.4. (Continued) Composition of amphibole from various rock types across the 2020 Corundum Dome and Pyrochlore Dome sampling area.

Sample	20TN15A	20TN15A	20TN15A	20TN5	20TN5	20TN5	20TN5
Analysis	21973	241061	241072	7981	7992	131241	131252
Mineral	fluoro-arfvedsonite	fluoro-arfvedsonite	fluoro-arfvedsonite	actinolite	winchite	actinolite	actinolite
SiO_2 (wt. %)	51.29	52.21	52.77	52.96	57.12	53.86	54.17
TiO_2	1.35	1.09	0.86	0.11	0.07	0.15	0.16
Al_2O_3	0.54	0.32	0.28	2.32	7.24	2.05	1.86
MnO	1.52	1.39	1.38	0.45	0.32	0.32	0.32
FeO	17.49	16.49	17.06	13.55	9.50	9.69	10.39
Fe_2O_3	7.11	5.89	4.95	0.70	0.00	0.86	0.71
MgO	6.16	7.75	8.39	14.26	11.33	17.04	16.68
CaO	1.05	1.45	1.48	12.32	8.75	12.25	12.37
Na_2O	7.99	8.04	7.92	0.17	2.79	0.25	0.25
K_2O	1.55	1.47	1.56	0.10	0.16	0.17	0.17
H_2O+	0.56	0.56	0.80	2.03	2.14	2.04	2.07
F	2.24	2.41	2.47	0.05	0.00	0.08	0.05
O=F,Cl	-0.94	-1.02	-1.04	-0.02	0.00	-0.04	-0.02
Total	97.92	98.06	98.87	99.00	99.42	98.72	99.19
T *(apfu)*							
Si	7.996	8.044	8.031	7.740	7.990	7.753	7.781
Al	0.004	0.000	0.000	0.260	0.010	0.247	0.219
Ti	0.000	0.000	0.000	0.000	0.000	0.000	0.000
Fe^{3+}	0.000	0.000	0.000	0.000	0.000	0.000	0.000
T subtotal	8.000	8.044	8.031	8.000	8.000	8.000	8.000
C							
Ti	0.159	0.127	0.099	0.012	0.007	0.016	0.017
Al	0.095	0.058	0.050	0.140	1.183	0.100	0.096
Fe^{3+}	0.835	0.683	0.566	0.077	0.000	0.093	0.077
Mn^{2+}	0.200	0.182	0.178	0.009	0.038	0.000	0.000
Fe^{2+}	2.281	2.125	2.171	1.657	1.112	1.134	1.237
Mg	1.431	1.781	1.904	3.106	2.363	3.656	3.572
C subtotal	5.001	4.956	4.968	5.001	4.703	4.999	4.999
B							
Mn^{2+}	0.000	0.000	0.000	0.047	0.000	0.039	0.039
Fe^{2+}	0.000	0.000	0.000	0.000	0.000	0.032	0.011
Mg	0.000	0.000	0.000	0.000	0.000	0.000	0.000
Ca	0.175	0.239	0.242	1.929	1.311	1.889	1.904
Na	1.825	1.761	1.758	0.024	0.689	0.041	0.045
B subtotal	2.000	2.000	2.000	2.000	2.000	2.001	1.999
A							
Ca	0.000	0.000	0.000	0.000	0.000	0.000	0.000
Na	0.591	0.641	0.578	0.024	0.069	0.030	0.025
K	0.309	0.290	0.303	0.019	0.028	0.032	0.031
A subtotal	0.900	0.931	0.881	0.043	0.097	0.062	0.056
O (non-W)	22.000	22.000	22.000	22.000	22.000	22.000	22.000
W							
OH	0.577	0.571	0.813	1.977	2.000	1.961	1.978
F	1.106	1.176	1.187	0.023	0.000	0.039	0.022
O	0.317	0.254	0.000	0.000	0.000	0.000	0.000
W subtotal	2.000	2.001	2.000	2.000	2.000	2.000	2.000
Sum T, C, B, A	15.901	15.931	15.880	15.044	14.800	15.062	15.054
Mg/(Mg+Fe)	0.315	0.388	0.410	0.642	0.680	0.744	0.729

Table B.4. (Continued) Composition of amphibole from various rock types across the 2020 Corundum Dome and Pyrochlore Dome sampling area.

Sample	20TN5	20TN5	20TN5	20TN5	20TN5	20TN5	20TN5
Analysis	131263	151303	171341	171352	171363	171374	171385
Mineral	actinolite	actinolite	actinolite	actinolite	actinolite	actinolite	ferro-actinolite
SiO_2 (wt. %)	53.19	55.79	52.30	52.75	51.81	55.52	50.21
TiO_2	0.18	0.00	0.07	0.04	0.06	0.01	0.14
Al_2O_3	2.43	0.69	3.15	1.76	1.57	0.33	3.71
MnO	0.32	0.28	0.41	0.70	0.55	0.28	0.45
FeO	12.95	9.80	14.16	16.26	18.87	9.26	18.45
Fe_2O_3	0.73	0.18	0.56	0.40	0.96	0.58	1.62
MgO	14.90	17.67	13.44	12.43	10.76	17.89	10.15
CaO	12.05	12.90	12.45	12.31	12.01	12.99	12.05
Na_2O	0.25	0.09	0.22	0.13	0.17	0.07	0.31
K_2O	0.18	0.03	0.09	0.04	0.08	0.02	0.20
H_2O+	2.04	2.09	2.04	2.02	1.99	2.08	2.00
F	0.06	0.04	0.00	0.00	0.00	0.03	0.00
O=F,Cl	-0.02	-0.02	0.00	0.00	0.00	-0.01	0.00
Total	99.24	99.53	98.88	98.85	98.82	99.03	99.29
T *(apfu)*							
Si	7.726	7.936	7.675	7.818	7.792	7.935	7.533
Al	0.274	0.064	0.325	0.182	0.208	0.055	0.467
Ti	0.000	0.000	0.000	0.000	0.000	0.001	0.000
Fe^{3+}	0.000	0.000	0.000	0.000	0.000	0.008	0.000
T subtotal	8.000	8.000	8.000	8.000	8.000	7.999	8.000
C							
Ti	0.020	0.000	0.007	0.005	0.007	0.000	0.016
Al	0.142	0.051	0.220	0.126	0.071	0.000	0.189
Fe^{3+}	0.079	0.019	0.062	0.045	0.109	0.054	0.183
Mn^{2+}	0.000	0.017	0.033	0.063	0.029	0.029	0.027
Fe^{2+}	1.532	1.165	1.738	2.015	2.373	1.106	2.315
Mg	3.226	3.747	2.941	2.746	2.412	3.811	2.269
C subtotal	4.999	4.999	5.001	5.000	5.001	5.000	4.999
B							
Mn^{2+}	0.039	0.017	0.017	0.024	0.041	0.005	0.029
Fe^{2+}	0.041	0.000	0.000	0.000	0.000	0.000	0.000
Mg	0.000	0.000	0.000	0.000	0.000	0.000	0.000
Ca	1.875	1.966	1.957	1.955	1.935	1.989	1.937
Na	0.045	0.017	0.025	0.021	0.024	0.006	0.034
B subtotal	2.000	2.000	1.999	2.000	2.000	2.000	2.000
A							
Ca	0.000	0.000	0.000	0.000	0.000	0.000	0.000
Na	0.026	0.006	0.038	0.015	0.024	0.012	0.057
K	0.032	0.005	0.016	0.008	0.015	0.003	0.039
A subtotal	0.058	0.011	0.054	0.023	0.039	0.015	0.096
O (non-W)	22.000	22.000	22.000	22.000	22.000	22.000	22.000
W							
OH	1.973	1.982	2.000	2.000	2.000	1.987	2.000
F	0.027	0.018	0.000	0.000	0.000	0.013	0.000
O	0.000	0.000	0.000	0.000	0.000	0.000	0.000
W subtotal	2.000	2.000	2.000	2.000	2.000	2.000	2.000
Sum T, C, B, A	15.057	15.010	15.054	15.023	15.040	15.014	15.095
Mg/(Mg+Fe)	0.661	0.760	0.620	0.571	0.493	0.767	0.476

Table B.4. (Continued) Composition of amphibole from various rock types across the 2020 Corundum Dome and Pyrochlore Dome sampling area.

Sample	20TN5	20TN24A	20TN24A	20TN24A	20TN24A	20TN24A	20TN24A
Analysis	171396	231571	231582	231593	231615	231626	251681
Mineral	actinolite	magnesio-ferri-hornblende	actinolite	actinolite	actinolite	actinolite	actinolite
SiO_2 (wt. %)	52.34	51.04	52.70	52.07	53.12	52.32	52.66
TiO_2	0.03	0.62	0.42	0.46	0.33	0.05	0.44
Al_2O_3	1.56	4.13	2.90	3.45	2.39	3.69	2.67
MnO	0.76	0.20	0.24	0.24	0.24	0.20	0.30
FeO	18.04	11.48	11.74	11.59	11.86	9.88	11.49
Fe_2O_3	0.38	1.98	1.16	1.37	0.63	1.70	1.29
MgO	11.28	14.78	15.53	15.18	15.53	16.33	15.62
CaO	12.06	11.88	11.80	11.76	12.00	11.75	11.98
Na_2O	0.15	0.51	0.37	0.44	0.26	0.45	0.33
K_2O	0.05	0.30	0.20	0.21	0.13	0.33	0.17
H_2O+	2.00	2.04	2.05	2.03	2.06	2.02	2.04
F	0.00	0.03	0.04	0.06	0.00	0.12	0.06
O=F,Cl	0.00	-0.01	-0.02	-0.03	0.00	-0.05	-0.03
Total	98.65	98.97	99.12	98.82	98.56	98.79	99.02
T *(apfu)*							
Si	7.840	7.441	7.634	7.572	7.726	7.560	7.638
Al	0.160	0.559	0.366	0.428	0.274	0.440	0.362
Ti	0.000	0.000	0.000	0.000	0.000	0.000	0.000
Fe^{3+}	0.000	0.000	0.000	0.000	0.000	0.000	0.000
T subtotal	8.000	8.000	8.000	8.000	8.000	8.000	8.000
C							
Ti	0.004	0.068	0.046	0.051	0.036	0.005	0.048
Al	0.115	0.151	0.130	0.163	0.135	0.189	0.095
Fe^{3+}	0.043	0.217	0.126	0.149	0.069	0.185	0.141
Mn^{2+}	0.060	0.000	0.000	0.000	0.000	0.000	0.000
Fe^{2+}	2.260	1.351	1.344	1.345	1.393	1.103	1.339
Mg	2.518	3.212	3.354	3.292	3.367	3.518	3.378
C subtotal	5.000	4.999	5.000	5.000	5.000	5.000	5.001
B							
Mn^{2+}	0.036	0.024	0.029	0.029	0.029	0.025	0.037
Fe^{2+}	0.000	0.048	0.078	0.065	0.051	0.091	0.054
Mg	0.000	0.000	0.000	0.000	0.000	0.000	0.000
Ca	1.935	1.855	1.831	1.832	1.870	1.819	1.862
Na	0.029	0.072	0.061	0.074	0.050	0.065	0.046
B subtotal	2.000	1.999	1.999	2.000	2.000	2.000	1.999
A							
Ca	0.000	0.000	0.000	0.000	0.000	0.000	0.000
Na	0.014	0.072	0.041	0.049	0.023	0.061	0.046
K	0.009	0.056	0.038	0.038	0.025	0.060	0.031
A subtotal	0.023	0.128	0.079	0.087	0.048	0.121	0.077
O (non-W)	22.000	22.000	22.000	22.000	22.000	22.000	22.000
W							
OH	2.000	1.987	1.982	1.971	2.000	1.945	1.972
F	0.000	0.013	0.018	0.029	0.000	0.055	0.028
O	0.000	0.000	0.000	0.000	0.000	0.000	0.000
W subtotal	2.000	2.000	2.000	2.000	2.000	2.000	2.000
Sum T, C, B, A	15.023	15.126	15.078	15.087	15.048	15.121	15.077
Mg/(Mg+Fe)	0.522	0.665	0.684	0.679	0.690	0.718	0.688

Table B.4. (Continued) Composition of amphibole from various rock types across the 2020 Corundum Dome and Pyrochlore Dome sampling area.

Sample	20TN24A	20TN24A	20TN24A	20TN24A	20TN13B-2	20TN13B-2	20TN13B-2
Analysis	251692	251703	251714	251725	9571	9582	9593
Mineral	actinolite	actinolite	actinolite	actinolite	fluoro-arfvedsonite	fluoro-arfvedsonite	fluoro-arfvedsonite
SiO_2 (wt. %)	54.56	54.65	52.85	53.82	54.50	54.25	54.21
TiO_2	0.11	0.11	0.34	0.22	0.07	0.06	0.04
Al_2O_3	1.64	1.45	2.36	1.64	0.16	0.16	0.16
MnO	0.29	0.25	0.29	0.14	3.75	3.07	2.97
FeO	10.29	9.20	11.21	12.85	13.92	13.94	13.66
Fe_2O_3	0.46	0.64	1.21	0.00	4.08	5.16	5.33
MgO	17.15	17.88	15.88	15.30	7.24	7.12	7.22
CaO	12.20	12.22	11.99	12.27	0.10	0.09	0.11
Na_2O	0.16	0.18	0.28	0.10	9.22	9.29	9.34
K_2O	0.09	0.09	0.14	0.48	2.41	2.50	2.45
H_2O+	2.06	2.08	2.06	2.04	0.14	0.10	0.08
F	0.06	0.04	0.00	0.05	3.84	3.91	3.95
O=F,Cl	-0.03	-0.02	0.00	-0.02	-1.62	-1.65	-1.66
Total	99.04	98.77	98.60	98.88	97.81	98.00	97.87
T *(apfu)*							
Si	7.823	7.825	7.682	7.830	8.346	8.303	8.300
Al	0.177	0.175	0.318	0.170	0.000	0.000	0.000
Ti	0.000	0.000	0.000	0.000	0.000	0.000	0.000
Fe^{3+}	0.000	0.000	0.000	0.000	0.000	0.000	0.000
T subtotal	8.000	8.000	8.000	8.000	8.346	8.303	8.300
C							
Ti	0.011	0.012	0.037	0.024	0.008	0.007	0.005
Al	0.100	0.069	0.086	0.111	0.029	0.029	0.028
Fe^{3+}	0.049	0.069	0.132	0.000	0.470	0.595	0.615
Mn^{2+}	0.000	0.000	0.000	0.000	0.487	0.398	0.385
Fe^{2+}	1.174	1.033	1.305	1.547	1.783	1.784	1.749
Mg	3.665	3.816	3.441	3.319	1.653	1.625	1.648
C subtotal	4.999	4.999	5.001	5.001	4.430	4.438	4.430
B							
Mn^{2+}	0.036	0.030	0.035	0.018	0.000	0.000	0.000
Fe^{2+}	0.061	0.069	0.058	0.017	0.000	0.000	0.000
Mg	0.000	0.000	0.000	0.000	0.000	0.000	0.000
Ca	1.875	1.875	1.867	1.913	0.017	0.014	0.018
Na	0.029	0.026	0.040	0.028	1.983	1.986	1.982
B subtotal	2.001	2.000	2.000	1.976	2.000	2.000	2.000
A							
Ca	0.000	0.000	0.000	0.000	0.000	0.000	0.000
Na	0.016	0.023	0.040	0.000	0.754	0.770	0.792
K	0.017	0.017	0.025	0.088	0.471	0.488	0.478
A subtotal	0.033	0.040	0.065	0.088	1.225	1.258	1.270
O (non-W)	22.000	22.000	22.000	22.000	22.000	22.000	22.000
W							
OH	1.971	1.983	2.000	1.978	0.139	0.106	0.086
F	0.029	0.017	0.000	0.022	1.861	1.894	1.914
O	0.000	0.000	0.000	0.000	0.000	0.000	0.000
W subtotal	2.000	2.000	2.000	2.000	2.000	2.000	2.000
Sum T, C, B, A	15.033	15.039	15.066	15.065	16.001	15.999	16.000
Mg/(Mg+Fe)	0.741	0.765	0.697	0.680	0.423	0.406	0.411

Table B.4. (Continued) Composition of amphibole from various rock types across the 2020 Corundum Dome and Pyrochlore Dome sampling area.

Sample	20TN13B-2	20TN13B-2	20TN13B-2	20TN13B-2	20TN15A	20TN15A	20TN15A
Analysis	9604	9615	9626	9637	321571	321582	321593
Mineral	fluoro-arfvedsonite	fluoro-arfvedsonite	fluoro-arfvedsonite	fluoro-arfvedsonite	fluoro-arfvedsonite	fluoro-arfvedsonite	riebeckite
SiO_2 (wt. %)	54.15	54.54	54.38	53.99	52.23	52.41	53.31
TiO_2	0.09	0.11	0.05	0.32	1.33	1.08	0.48
Al_2O_3	0.18	0.16	0.14	0.11	0.41	0.28	0.48
MnO	3.12	2.94	3.36	3.51	1.54	1.52	0.75
FeO	14.34	14.73	13.51	18.19	17.75	19.55	13.47
Fe_2O_3	4.54	4.31	4.84	1.92	9.07	7.43	14.17
MgO	7.25	7.24	7.29	6.02	5.33	5.20	6.57
CaO	0.10	0.08	0.11	0.30	1.11	1.03	0.39
Na_2O	9.17	9.30	9.36	8.73	7.28	7.81	6.84
K_2O	2.41	2.33	2.38	2.27	1.54	1.52	0.42
H_2O+	0.06	0.08	0.11	0.31	0.59	0.58	1.67
F	3.99	3.96	3.89	3.42	2.23	2.38	0.69
O=F,Cl	-1.68	-1.67	-1.64	-1.44	-0.94	-1.00	-0.29
Total	97.71	98.12	97.77	97.65	99.47	99.80	98.95
T *(apfu)*							
Si	8.311	8.330	8.324	8.378	8.023	8.060	8.004
Al	0.000	0.000	0.000	0.000	0.000	0.000	0.000
Ti	0.000	0.000	0.000	0.000	0.000	0.000	0.000
Fe^{3+}	0.000	0.000	0.000	0.000	0.000	0.000	0.000
T subtotal	8.311	8.330	8.324	8.378	8.023	8.060	8.004
C							
Ti	0.010	0.013	0.006	0.037	0.154	0.124	0.054
Al	0.032	0.028	0.025	0.020	0.074	0.051	0.085
Fe^{3+}	0.524	0.495	0.557	0.224	1.048	0.860	1.601
Mn^{2+}	0.406	0.381	0.436	0.462	0.201	0.198	0.096
Fe^{2+}	1.841	1.882	1.729	2.360	2.281	2.515	1.691
Mg	1.660	1.649	1.663	1.392	1.221	1.191	1.469
C subtotal	4.473	4.448	4.416	4.495	4.979	4.939	4.996
B							
Mn^{2+}	0.000	0.000	0.000	0.000	0.000	0.000	0.000
Fe^{2+}	0.000	0.000	0.000	0.000	0.000	0.000	0.000
Mg	0.000	0.000	0.000	0.000	0.000	0.000	0.000
Ca	0.016	0.013	0.017	0.049	0.182	0.170	0.064
Na	1.984	1.987	1.983	1.951	1.818	1.830	1.936
B subtotal	2.000	2.000	2.000	2.000	2.000	2.000	2.000
A							
Ca	0.000	0.000	0.000	0.000	0.000	0.000	0.000
Na	0.744	0.768	0.796	0.675	0.350	0.500	0.055
K	0.471	0.454	0.464	0.450	0.301	0.299	0.080
A subtotal	1.215	1.222	1.260	1.125	0.651	0.799	0.135
O (non-W)	22.000	22.000	22.000	22.000	22.000	22.000	22.000
W							
OH	0.065	0.085	0.117	0.322	0.607	0.595	1.673
F	1.935	1.915	1.883	1.678	1.085	1.156	0.327
O	0.000	0.000	0.000	0.000	0.307	0.249	0.000
W subtotal	2.000	2.000	2.000	2.000	1.999	2.000	2.000
Sum T, C, B, A	15.999	16.000	16.000	15.998	15.653	15.798	15.135
Mg/(Mg+Fe)	0.412	0.410	0.421	0.350	0.268	0.261	0.309

Table B.4. (Continued) Composition of amphibole from various rock types across the 2020 Corundum Dome and Pyrochlore Dome sampling area.

Sample	20TN23	20TN23	20TN23	20TN23	20TN23	20TN23	20TN23
Analysis	331601	331612	331623	331634	331645	331656	331667
Mineral	magnesio-fluoro-arfvedsonite	magnesio-fluoro-arfvedsonite	magnesio-fluoro-arfvedsonite	magnesio-fluoro-arfvedsonite	fluoro-richterite	magnesio-fluoro-arfvedsonite	magnesio-fluoro-arfvedsonite
SiO_2 (wt. %)	53.30	53.24	53.93	53.77	53.99	53.33	53.29
TiO_2	0.64	0.56	0.65	0.67	0.25	0.46	0.49
Al_2O_3	1.21	1.15	1.04	0.99	1.08	1.22	1.25
MnO	1.63	1.70	1.51	1.64	1.19	1.54	1.67
FeO	12.76	12.34	12.48	12.73	10.81	12.08	12.32
Fe_2O_3	4.05	4.29	4.26	4.27	2.89	4.27	4.28
MgO	11.07	11.11	11.17	11.02	13.80	11.75	11.32
CaO	2.42	2.43	1.76	1.83	4.18	2.87	2.80
Na_2O	8.19	8.19	8.53	8.48	7.41	7.98	8.06
K_2O	1.70	1.71	1.79	1.74	1.56	1.67	1.68
H_2O+	0.83	0.78	0.79	0.84	0.70	0.79	0.82
F	2.49	2.60	2.60	2.48	2.83	2.60	2.52
O=F,Cl	-1.05	-1.09	-1.09	-1.04	-1.19	-1.10	-1.06
Total	99.23	99.02	99.43	99.42	99.50	99.45	99.43
T *(apfu)*							
Si	7.938	7.943	7.995	7.986	7.919	7.907	7.916
Al	0.062	0.057	0.005	0.014	0.081	0.093	0.084
Ti	0.000	0.000	0.000	0.000	0.000	0.000	0.000
Fe^{3+}	0.000	0.000	0.000	0.000	0.000	0.000	0.000
T subtotal	8.000	8.000	8.000	8.000	8.000	8.000	8.000
C							
Ti	0.072	0.063	0.072	0.075	0.027	0.052	0.055
Al	0.150	0.145	0.177	0.159	0.106	0.121	0.135
Fe^{3+}	0.454	0.481	0.476	0.477	0.319	0.476	0.479
Mn^{2+}	0.205	0.215	0.189	0.206	0.148	0.193	0.210
Fe^{2+}	1.589	1.540	1.547	1.581	1.326	1.498	1.530
Mg	2.458	2.471	2.469	2.439	3.018	2.597	2.507
C subtotal	4.928	4.915	4.930	4.937	4.944	4.937	4.916
B							
Mn^{2+}	0.000	0.000	0.000	0.000	0.000	0.000	0.000
Fe^{2+}	0.000	0.000	0.000	0.000	0.000	0.000	0.000
Mg	0.000	0.000	0.000	0.000	0.000	0.000	0.000
Ca	0.386	0.389	0.279	0.291	0.657	0.455	0.446
Na	1.614	1.611	1.721	1.709	1.343	1.545	1.554
B subtotal	2.000	2.000	2.000	2.000	2.000	2.000	2.000
A							
Ca	0.000	0.000	0.000	0.000	0.000	0.000	0.000
Na	0.750	0.759	0.731	0.733	0.764	0.748	0.767
K	0.322	0.326	0.339	0.330	0.292	0.315	0.318
A subtotal	1.072	1.085	1.070	1.063	1.056	1.063	1.085
O (non-W)	22.000	22.000	22.000	22.000	22.000	22.000	22.000
W							
OH	0.828	0.773	0.781	0.837	0.688	0.779	0.815
F	1.172	1.227	1.219	1.163	1.312	1.221	1.185
O	0.000	0.000	0.000	0.000	0.000	0.000	0.000
W subtotal	2.000	2.000	2.000	2.000	2.000	2.000	2.000
Sum T, C, B, A	16.000	16.000	16.000	16.000	16.000	16.000	16.001
Mg/(Mg+Fe)	0.546	0.550	0.550	0.542	0.647	0.568	0.555

Table B.4. (Continued) Composition of amphibole from various rock types across the 2020 Corundum Dome and Pyrochlore Dome sampling area.

Sample	20TN23	20TN23	20TN23	20TN23	20TN7	20TN7	20TN7
Analysis	331678	331689	3316910	3317011	391841	391852	391863
Mineral	fluoro-richterite	magnesio-fluoro-arfvedsonite	fluoro-richterite	magnesio-fluoro-arfvedsonite	magnesio-fluoro-arfvedsonite	magnesio-fluoro-arfvedsonite	magnesio-fluoro-arfvedsonite
SiO_2 (wt. %)	54.22	53.59	54.23	53.16	53.98	53.90	54.18
TiO_2	0.19	0.53	0.29	0.47	0.30	0.43	0.24
Al_2O_3	0.95	1.11	0.99	1.25	0.83	0.70	0.72
MnO	1.04	1.72	0.85	1.61	2.56	3.20	2.65
FeO	10.33	13.08	10.73	12.29	7.79	9.29	7.51
Fe_2O_3	3.02	3.99	2.90	4.34	7.65	5.90	7.63
MgO	14.44	10.90	14.26	11.24	11.51	11.03	11.95
CaO	4.44	2.01	4.17	2.78	0.84	1.36	1.00
Na_2O	7.27	8.38	7.34	8.08	9.21	8.68	8.98
K_2O	1.60	1.61	1.67	1.66	2.07	2.20	2.24
H_2O+	0.68	0.84	0.53	0.76	0.76	0.76	0.72
F	2.90	2.47	3.22	2.64	2.68	2.65	2.78
O=F,Cl	-1.22	-1.04	-1.36	-1.11	-1.13	-1.12	-1.17
Total	99.85	99.20	99.82	99.17	99.06	99.00	99.44
T *(apfu)*							
Si	7.909	7.983	7.918	7.919	7.983	8.021	7.980
Al	0.091	0.017	0.082	0.081	0.017	0.000	0.020
Ti	0.000	0.000	0.000	0.000	0.000	0.000	0.000
Fe^{3+}	0.000	0.000	0.000	0.000	0.000	0.000	0.000
T subtotal	8.000	8.000	8.000	8.000	8.000	8.021	8.000
C							
Ti	0.021	0.060	0.032	0.052	0.034	0.048	0.027
Al	0.071	0.177	0.089	0.139	0.128	0.123	0.105
Fe^{3+}	0.332	0.447	0.318	0.486	0.851	0.661	0.846
Mn^{2+}	0.128	0.217	0.105	0.203	0.321	0.403	0.331
Fe^{2+}	1.260	1.629	1.311	1.532	0.963	1.156	0.925
Mg	3.140	2.421	3.103	2.497	2.538	2.447	2.625
C subtotal	4.952	4.951	4.958	4.909	4.835	4.838	4.859
B							
Mn^{2+}	0.000	0.000	0.000	0.000	0.000	0.000	0.000
Fe^{2+}	0.000	0.000	0.000	0.000	0.000	0.000	0.000
Mg	0.000	0.000	0.000	0.000	0.000	0.000	0.000
Ca	0.693	0.321	0.653	0.444	0.134	0.217	0.158
Na	1.307	1.679	1.347	1.556	1.866	1.783	1.842
B subtotal	2.000	2.000	2.000	2.000	2.000	2.000	2.000
A							
Ca	0.000	0.000	0.000	0.000	0.000	0.000	0.000
Na	0.749	0.742	0.731	0.777	0.774	0.722	0.721
K	0.298	0.307	0.311	0.315	0.390	0.418	0.421
A subtotal	1.047	1.049	1.042	1.092	1.164	1.140	1.142
O (non-W)	22.000	22.000	22.000	22.000	22.000	22.000	22.000
W							
OH	0.662	0.836	0.511	0.754	0.748	0.751	0.703
F	1.338	1.164	1.489	1.246	1.252	1.249	1.297
O	0.000	0.000	0.000	0.000	0.000	0.000	0.000
W subtotal	2.000	2.000	2.000	2.000	2.000	2.000	2.000
Sum T, C, B, A	15.999	16.000	16.000	16.001	15.999	15.999	16.001
Mg/(Mg+Fe)	0.664	0.538	0.656	0.553	0.583	0.574	0.597

Table B.4. (Continued) Composition of amphibole from various rock types across the 2020 Corundum Dome and Pyrochlore Dome sampling area.

Sample	20TN7	20TN7	20TN7	20TN7	20TN7	20TN7	20TN6-2
Analysis	391874	391885	391896	391907	391918	401965	6551
Mineral	ferri-fluoro-katophorite	ferri-fluoro-katophorite	magnesio-fluoro-arfvedsonite	magnesio-fluoro-arfvedsonite	magnesio-fluoro-arfvedsonite	ferri-fluoro-katophorite	actinolite
SiO_2 (wt. %)	52.35	54.19	53.73	54.15	54.24	52.10	53.48
TiO_2	0.27	0.20	0.31	0.27	0.23	0.29	0.05
Al_2O_3	2.03	1.16	1.05	0.79	0.75	2.42	1.21
MnO	1.24	0.80	1.13	2.00	2.66	1.42	1.57
FeO	8.63	6.98	8.18	8.33	7.36	8.42	14.52
Fe_2O_3	4.38	5.15	5.28	6.11	7.95	4.06	0.95
MgO	14.61	15.62	14.39	12.94	11.84	14.85	13.12
CaO	4.99	3.53	3.16	1.99	0.95	5.40	11.56
Na_2O	7.18	7.79	7.87	8.60	8.96	6.92	0.59
K_2O	1.16	1.71	1.76	1.79	2.43	1.17	0.24
H_2O+	0.82	0.78	0.79	0.75	0.77	0.74	1.88
F	2.58	2.72	2.65	2.72	2.67	2.77	0.33
O=F,Cl	-1.09	-1.15	-1.11	-1.14	-1.13	-1.17	-0.14
Total	99.15	99.48	99.18	99.28	99.69	99.37	99.36
T *(apfu)*							
Si	7.682	7.850	7.865	7.956	7.974	7.627	7.865
Al	0.318	0.150	0.135	0.044	0.026	0.373	0.135
Ti	0.000	0.000	0.000	0.000	0.000	0.000	0.000
Fe^{3+}	0.000	0.000	0.000	0.000	0.000	0.000	0.000
T subtotal	8.000	8.000	8.000	8.000	8.000	8.000	8.000
C							
Ti	0.030	0.022	0.034	0.030	0.026	0.032	0.006
Al	0.033	0.048	0.047	0.093	0.104	0.044	0.074
Fe^{3+}	0.484	0.562	0.581	0.675	0.880	0.447	0.105
Mn^{2+}	0.154	0.098	0.140	0.250	0.331	0.176	0.153
Fe^{2+}	1.060	0.845	1.002	1.023	0.905	1.030	1.786
Mg	3.196	3.373	3.140	2.833	2.595	3.242	2.876
C subtotal	4.957	4.948	4.944	4.904	4.841	4.971	5.000
B							
Mn^{2+}	0.000	0.000	0.000	0.000	0.000	0.000	0.043
Fe^{2+}	0.000	0.000	0.000	0.000	0.000	0.000	0.000
Mg	0.000	0.000	0.000	0.000	0.000	0.000	0.000
Ca	0.784	0.548	0.495	0.313	0.150	0.846	1.822
Na	1.216	1.452	1.505	1.687	1.850	1.154	0.135
B subtotal	2.000	2.000	2.000	2.000	2.000	2.000	2.000
A							
Ca	0.000	0.000	0.000	0.000	0.000	0.000	0.000
Na	0.826	0.735	0.728	0.761	0.704	0.810	0.035
K	0.218	0.316	0.328	0.335	0.456	0.219	0.045
A subtotal	1.044	1.051	1.056	1.096	1.160	1.029	0.080
O (non-W)	22.000	22.000	22.000	22.000	22.000	22.000	22.000
W							
OH	0.801	0.752	0.775	0.736	0.756	0.719	1.847
F	1.199	1.248	1.225	1.264	1.244	1.281	0.153
O	0.000	0.000	0.000	0.000	0.000	0.000	0.000
W subtotal	2.000	2.000	2.000	2.000	2.000	2.000	2.000
Sum T, C, B, A	16.001	15.999	16.000	16.000	16.001	16.000	15.080
Mg/(Mg+Fe)	0.674	0.706	0.665	0.625	0.592	0.687	0.603

Table B.4. (Continued) Composition of amphibole from various rock types across the 2020 Corundum Dome and Pyrochlore Dome sampling area.

Sample	20TN6-2	20TN6-2	20TN6-2
Analysis	6562	6573	6584
Mineral	actinolite	actinolite	actinolite
SiO_2 (wt. %)	53.58	52.91	54.63
TiO_2	0.06	0.03	0.03
Al_2O_3	1.39	1.07	0.95
MnO	1.49	2.16	1.18
FeO	14.87	17.69	12.84
Fe_2O_3	0.67	0.84	0.65
MgO	12.90	10.64	14.75
CaO	11.35	11.09	12.07
Na_2O	0.66	0.73	0.51
K_2O	0.25	0.27	0.14
H_2O+	1.90	1.94	1.92
F	0.30	0.15	0.33
O=F,Cl	-0.13	-0.06	-0.14
Total	99.28	99.46	99.84
T *(apfu)*			
Si	7.882	7.904	7.905
Al	0.118	0.096	0.095
Ti	0.000	0.000	0.000
Fe^{3+}	0.000	0.000	0.000
T subtotal	8.000	8.000	8.000
C			
Ti	0.006	0.004	0.003
Al	0.123	0.092	0.066
Fe^{3+}	0.074	0.094	0.071
Mn^{2+}	0.137	0.230	0.125
Fe^{2+}	1.830	2.210	1.553
Mg	2.829	2.370	3.181
C subtotal	4.999	5.000	4.999
B			
Mn^{2+}	0.048	0.044	0.020
Fe^{2+}	0.000	0.000	0.000
Mg	0.000	0.000	0.000
Ca	1.789	1.776	1.872
Na	0.163	0.181	0.108
B subtotal	2.000	2.001	2.000
A			
Ca	0.000	0.000	0.000
Na	0.024	0.031	0.034
K	0.047	0.051	0.026
A subtotal	0.071	0.082	0.060
O (non-W)	22.000	22.000	22.000
W			
OH	1.862	1.931	1.851
F	0.138	0.069	0.149
O	0.000	0.000	0.000
W subtotal	2.000	2.000	2.000
Sum T, C, B, A	15.070	15.083	15.059
Mg/(Mg+Fe)	0.598	0.507	0.662

Table B.5. Composition of pyroxene from various rock types across the 2020 Corundum Dome and Pyrochlore Dome sampling area.

Sample	20TN20	20TN20	20TN20	20TN20	20TN20	20TN20	20TN20	20TN20	20TN20	20TN20	20TN20	20TN20	20TN20
Analysis	552303	552314	552325	552336	552347	552358	501991	502002	5020810	5020911	542211	542233	542266
Mineral	Ag	Ag	Ag	Ag	Ag	Ag	Ag	Ag	Ag	Ag	Ag	Ag	Ag
Comment	Core	Core	Core	Core	Core	Core	Rim	Rim	Rim	Rim	Rim	Rim	Rim
SiO_2 (wt. %)	51.89	51.25	51.46	51.68	51.62	51.55	51.59	51.47	52.34	52.03	52.29	52.15	52.09
TiO_2	1.21	1.39	1.43	1.40	1.66	1.61	1.76	1.86	1.18	1.51	0.67	1.09	1.37
Al_2O_3	0.28	0.22	0.24	0.25	0.28	0.28	0.17	0.16	0.18	0.31	0.29	0.30	0.29
Fe_2O_3*	25.02	24.58	23.27	22.16	23.72	23.26	27.04	28.05	29.22	29.19	26.80	29.82	27.41
FeO*	5.67	5.49	6.44	7.27	6.16	6.43	2.18	1.28	0.98	0.99	3.83	1.62	2.83
MnO	0.61	0.67	0.73	0.64	0.64	0.65	1.28	1.40	1.25	1.08	0.72	0.49	0.64
MgO	0.33	0.38	0.48	0.48	0.34	0.40	0.39	0.39	0.33	0.33	0.37	0.28	0.47
CaO	3.78	4.35	4.84	4.98	3.89	4.41	1.21	1.18	1.00	0.65	2.52	0.90	2.33
BaO	0.00	0.00	0.00	0.00	0.00	0.00	0.00	0.00	0.00	0.00	0.00	0.00	0.00
Na_2O	11.08	10.81	10.48	10.33	10.96	10.70	12.41	12.57	12.84	12.96	11.79	12.83	12.12
K_2O	0.00	0.00	0.00	0.01	0.00	0.00	0.00	0.00	0.00	0.00	0.01	0.02	0.01
F	0.00	0.00	0.00	0.00	0.00	0.00	0.00	0.00	0.00	0.00	0.00	0.00	0.00
Total	99.87	99.13	99.37	99.19	99.27	99.29	98.03	98.36	99.31	99.03	99.27	99.51	99.56
Si (*apfu*)	2.010	2.002	2.007	2.019	2.011	2.010	2.017	2.006	2.018	2.010	2.026	2.009	2.009
Ti	0.035	0.041	0.042	0.041	0.049	0.047	0.052	0.054	0.034	0.044	0.019	0.032	0.040
Al	0.013	0.010	0.011	0.011	0.013	0.013	0.008	0.007	0.008	0.014	0.013	0.014	0.013
Fe^{3+}	0.729	0.722	0.683	0.651	0.695	0.683	0.795	0.822	0.848	0.849	0.781	0.865	0.796
Fe^{2+}	0.184	0.179	0.210	0.237	0.201	0.210	0.071	0.042	0.032	0.032	0.124	0.052	0.091
Mn	0.020	0.022	0.024	0.021	0.021	0.022	0.042	0.046	0.041	0.035	0.024	0.016	0.021
Mg	0.019	0.022	0.028	0.028	0.020	0.023	0.023	0.023	0.019	0.019	0.021	0.016	0.027
Ca	0.157	0.182	0.202	0.208	0.163	0.184	0.051	0.049	0.041	0.027	0.105	0.037	0.096
Ba	0.000	0.000	0.000	0.000	0.000	0.000	0.000	0.000	0.000	0.000	0.000	0.000	0.000
Na	0.833	0.819	0.792	0.782	0.828	0.809	0.941	0.950	0.960	0.970	0.886	0.959	0.906
K	0.000	0.000	0.000	0.000	0.000	0.000	0.000	0.000	0.000	0.000	0.000	0.001	0.000
F^-	0.000	0.000	0.000	0.000	0.000	0.000	0.000	0.000	0.000	0.000	0.000	0.000	0.000
O^{2-}	5.635	5.639	5.658	5.674	5.652	5.659	5.602	5.589	5.576	5.576	5.609	5.568	5.602
O^{2-} Corrected	6.000	6.000	6.000	6.000	6.000	6.000	6.000	6.000	6.000	6.000	6.000	6.000	6.000

Note: Compositions were recalculated on the basis of the sum of 4 cation apfu; * – calculated from stoichiometry.

Table B.5. (Continued) Composition of pyroxene from various rock types across the 2020 Corundum Dome and Pyrochlore Dome sampling area.

Sample	20TN20	20TN20	20TN20	20TN20	20TN15B	20TN15B	20TN15B	20TN15B
Analysis	552281	552292	552369	5523710	191061	191072	191083	191094
Mineral	Ag	Ag	Ag	Ag	Di	Di	Di	Di
Comment	Rim	Rim	Rim	Rim				
SiO_2 (wt. %)	52.11	52.11	51.93	51.91	51.41	51.11	51.26	51.43
TiO_2	0.97	1.87	2.22	0.93	0.31	0.34	0.31	0.27
Al_2O_3	0.29	0.24	0.23	0.28	0.65	0.66	0.65	0.56
Fe_2O_3*	30.44	27.30	26.48	30.57	5.65	5.89	5.06	4.95
FeO*	0.94	3.14	3.52	1.08	11.37	11.05	11.81	11.86
MnO	0.67	0.61	0.59	0.50	0.90	0.86	0.88	0.90
MgO	0.27	0.35	0.36	0.28	7.42	7.50	7.25	7.45
CaO	0.72	1.54	1.80	0.96	20.15	20.23	20.05	20.30
BaO	0.00	0.00	0.00	0.00	0.01	0.04	0.01	0.05
Na_2O	12.97	12.43	12.30	12.85	2.14	2.10	2.09	1.93
K_2O	0.01	0.00	0.01	0.00	0.01	0.01	0.02	0.11
F	0.00	0.00	0.00	0.00	0.12	0.11	0.14	0.10
Total	99.39	99.60	99.42	99.39	100.13	99.90	99.51	99.89
Si^{4+} (*apfu*)	2.009	2.009	2.006	2.003	1.982	1.975	1.990	1.989
Ti^{4+}	0.028	0.054	0.065	0.027	0.009	0.010	0.009	0.008
Al^{3+}	0.013	0.011	0.010	0.013	0.030	0.030	0.030	0.025
Fe^{3+}	0.883	0.792	0.770	0.888	0.164	0.171	0.148	0.144
Fe^{2+}	0.030	0.101	0.114	0.035	0.367	0.357	0.383	0.384
Mn^{2+}	0.022	0.020	0.019	0.016	0.029	0.028	0.029	0.029
Mg^{2+}	0.015	0.020	0.021	0.016	0.426	0.432	0.420	0.429
Ca^{2+}	0.030	0.063	0.074	0.040	0.832	0.838	0.834	0.841
Ba^{2+}	0.000	0.000	0.000	0.000	0.000	0.001	0.000	0.001
Na^{+}	0.969	0.929	0.921	0.961	0.160	0.157	0.157	0.144
K^{+}	0.000	0.000	0.000	0.000	0.001	0.001	0.001	0.005
F^{-}	0.000	0.000	0.000	0.000	0.015	0.013	0.017	0.013
O^{2-}	5.559	5.604	5.615	5.556	5.918	5.914	5.926	5.928
O^{2-} Corrected	6.000	6.000	6.000	6.000	6.000	6.000	6.000	6.000

Table B.6. Composition of epidote and allanite from various rock types across the 2020 Corundum Dome and Pyrochlore Dome sampling area.

Sample	20TN3-2	20TN3-2	20TN20	20TN20	20TN20	20TN20	20TN20	20TN20
Analysis	302221	302232	111721	111732	111743	111754	141821	141832
Mineral	Allanite-(La)	Allanite-(Ce)	Allanite-(La)	Allanite-(La)	Allanite-(La)	Allanite-(La)	Epidote	Epidote
P_2O_5 (wt. %)	0.00	0.01	0.01	0.00	0.01	0.00	0.03	0.00
Nb_2O_5	0.03	0.00	0.23	0.12	0.00	0.00	0.00	0.02
SiO_2	30.01	30.40	32.37	32.60	33.80	34.34	37.69	37.45
TiO_2	0.06	0.04	0.02	0.00	0.13	0.10	0.04	0.04
ZrO_2	0.03	0.00	0.00	0.01	0.00	0.00	0.01	0.00
HfO_2	0.01	0.00	0.03	0.12	0.00	0.03	0.00	0.00
ThO_2	0.06	0.01	0.01	0.04	0.00	0.00	0.00	0.04
UO_2	0.02	0.09	0.00	0.00	0.08	0.10	0.00	0.03
Al_2O_3	5.54	3.99	13.79	14.54	15.57	16.27	18.16	19.18
Fe_2O_3*	22.53	28.81	15.35	15.31	17.71	17.52	20.57	19.16
Y_2O_3	0.00	0.08	0.04	0.02	0.01	0.04	0.02	0.01
La_2O_3	13.37	11.32	9.65	9.36	7.18	6.98	0.01	0.18
Ce_2O_3	12.03	11.98	8.94	8.63	6.35	6.63	0.00	0.26
Pr_2O_3	1.57	1.43	1.21	1.13	0.89	0.96	0.00	0.02
Nd_2O_3	1.22	1.43	0.89	0.91	0.99	1.05	0.00	0.05
Sm_2O_3	0.07	0.08	0.03	0.00	0.12	0.15	0.01	0.06
Eu_2O_3	0.00	0.00	0.00	0.00	0.00	0.00	0.01	0.04
Gd_2O_3	0.03	0.06	0.17	0.07	0.13	0.10	0.02	0.05
Tb_2O_3	0.05	0.11	0.06	0.02	0.08	0.09	0.04	0.08
Dy_2O_3	0.18	0.24	0.84	0.75	0.15	0.13	0.07	0.35
Ho_2O_3	0.02	0.14	0.05	0.01	0.05	0.07	0.07	0.05
Er_2O_3	0.00	0.19	0.02	0.08	0.07	0.13	0.10	0.07
Tm_2O_3	0.00	0.02	0.06	0.00	0.04	0.04	0.07	0.04
Yb_2O_3	0.04	0.00	0.01	0.01	0.00	0.10	0.00	0.00
Lu_2O_3	0.15	0.00	0.00	0.00	0.00	0.02	0.02	0.02
MgO	0.27	0.23	0.23	0.28	0.04	0.06	0.01	0.01
CaO	8.71	8.85	12.36	12.42	14.79	14.72	21.65	20.03
MnO	0.56	0.67	2.49	2.17	0.36	0.34	0.09	0.81
FeO*	4.33	1.11	0.42	0.00	0.56	0.00	0.00	0.00
PbO	0.04	0.00	0.05	0.12	0.03	0.00	0.06	0.00
Na_2O	0.00	0.01	0.02	0.00	0.00	0.00	0.01	0.01
K_2O	0.00	0.00	0.00	0.00	0.00	0.01	0.00	0.00
F	0.06	0.00	0.00	0.02	0.02	0.00	0.01	0.00
Cl	0.02	0.01	0.01	0.01	0.00	0.00	0.00	0.00
H_2O	0.69	0.69	0.77	0.77	0.80	0.81	0.87	0.87
-(O=F,Cl)	-0.02	0.00	0.00	-0.01	-0.01	0.00	0.00	0.00
Total	101.66	101.99	100.13	99.53	99.94	100.81	99.64	98.93
P (*apfu*)	0.000	0.001	0.001	0.000	0.001	0.000	0.002	0.000
Nb	0.001	0.000	0.010	0.005	0.000	0.000	0.000	0.001
Si	3.000	3.000	3.000	3.000	3.000	3.000	3.000	3.000
Ti	0.004	0.003	0.001	0.000	0.009	0.007	0.003	0.003
Zr	0.001	0.000	0.000	0.000	0.000	0.000	0.000	0.000
Hf	0.000	0.000	0.001	0.003	0.000	0.001	0.000	0.000
Th	0.001	0.000	0.000	0.001	0.000	0.000	0.000	0.001
U	0.000	0.002	0.000	0.000	0.002	0.002	0.000	0.001
Al	0.653	0.464	1.506	1.577	1.629	1.675	1.703	1.811
Fe^{3+}	1.695	2.139	1.071	1.051	1.183	1.140	1.171	1.094
Y	0.000	0.004	0.002	0.001	0.000	0.002	0.001	0.000
La	0.493	0.412	0.330	0.318	0.235	0.225	0.000	0.005
Ce	0.440	0.433	0.303	0.291	0.206	0.212	0.000	0.008

Sample	20TN3-2	20TN3-2	20TN20	20TN20	20TN20	20TN20	20TN20	20TN20
Analysis	302221	302232	111721	111732	111743	111754	141821	141832
Mineral	Allanite-(La)	Allanite-(Ce)	Allanite-(La)	Allanite-(La)	Allanite-(La)	Allanite-(La)	Epidote	Epidote
Pr (*apfu*)	0.057	0.051	0.041	0.038	0.029	0.031	0.000	0.000
Nd	0.044	0.050	0.029	0.030	0.031	0.033	0.000	0.001
Sm	0.003	0.003	0.001	0.000	0.004	0.005	0.000	0.002
Eu	0.000	0.000	0.000	0.000	0.000	0.000	0.000	0.001
Gd	0.001	0.002	0.005	0.002	0.004	0.003	0.001	0.001
Tb	0.002	0.004	0.002	0.001	0.002	0.003	0.001	0.002
Dy	0.006	0.008	0.025	0.022	0.004	0.004	0.002	0.009
Ho	0.001	0.004	0.001	0.000	0.001	0.002	0.002	0.001
Er	0.000	0.006	0.001	0.002	0.002	0.004	0.003	0.002
Tm	0.000	0.001	0.002	0.000	0.001	0.001	0.002	0.001
Yb	0.001	0.000	0.000	0.000	0.000	0.003	0.000	0.000
Lu	0.004	0.000	0.000	0.000	0.000	0.000	0.000	0.000
Mg	0.040	0.034	0.032	0.039	0.006	0.008	0.001	0.001
Ca	0.933	0.936	1.228	1.224	1.406	1.378	1.846	1.719
Mn	0.047	0.056	0.196	0.169	0.027	0.025	0.006	0.055
Fe^{2+}	0.362	0.091	0.032	0.000	0.042	0.000	0.000	0.000
Pb	0.001	0.000	0.001	0.003	0.001	0.000	0.001	0.000
Na	0.000	0.001	0.004	0.001	0.000	0.000	0.001	0.002
K	0.000	0.000	0.000	0.000	0.000	0.001	0.000	0.000
F	0.010	0.000	0.000	0.003	0.003	0.000	0.001	0.000
Cl	0.007	0.003	0.002	0.003	0.000	0.001	0.000	0.000
H	0.983	0.997	0.998	0.994	0.997	0.999	0.999	1.000
O (corrected)	12.000	12.000	12.000	12.000	12.000	12.000	12.000	12.000
Cation sum	7.809	7.708	7.826	7.784	7.828	7.764	7.748	7.721

Note: Compositions were recalculated on the basis of the sum of 3 Si cation *apfu*. * Calculated based on stoichiometry.

Table B.6. (Continued) Composition of epidote and allanite from various rock types across the 2020 Corundum Dome and Pyrochlore Dome sampling area.

Sample	20TN20	20TN20	20TN7	20TN7	20TN7	20TN7	20TN7	20TN7
Analysis	141843	141854	52251	52262	52273	52284	62313	62324
Mineral	Epidote	Epidote	Allanite-(La)	Allanite-(La)	Allanite-(Ce)	Allanite-(Ce)	Epidote	Epidote
P_2O_5 (wt. %)	0.01	0.01	0.00	0.00	0.02	0.02	0.01	0.00
Nb_2O_5	0.01	0.00	0.07	0.06	0.06	0.06	0.00	0.00
SiO_2	37.17	37.34	34.15	34.67	33.10	34.06	37.08	37.39
TiO_2	0.00	0.10	0.18	0.21	0.13	0.09	0.04	0.02
ZrO_2	0.02	0.03	0.03	0.07	0.00	0.00	0.03	0.00
HfO_2	0.09	0.04	0.00	0.06	0.08	0.00	0.00	0.02
ThO_2	0.00	0.01	0.11	0.17	0.14	0.12	0.33	0.00
UO_2	0.06	0.01	0.02	0.02	0.01	0.04	0.05	0.06
Al_2O_3	6.39	15.98	20.66	18.96	18.61	18.76	20.45	20.86
Fe_2O_3*	24.09	23.28	8.31	11.47	7.61	12.00	15.89	16.33
Y_2O_3	0.03	0.02	0.04	0.05	0.00	0.00	0.01	0.03
La_2O_3	0.05	0.16	7.63	7.53	7.40	7.02	0.33	0.12
Ce_2O_3	0.07	0.25	6.58	6.51	7.84	7.17	0.72	0.30
Pr_2O_3	0.03	0.03	0.87	0.73	0.97	0.85	0.10	0.03
Nd_2O_3	0.03	0.07	0.36	0.39	0.69	0.57	0.16	0.09
Sm_2O_3	0.00	0.05	0.07	0.03	0.09	0.01	0.02	0.06
Eu_2O_3	0.00	0.01	0.00	0.00	0.00	0.00	0.00	0.03
Gd_2O_3	0.00	0.07	0.01	0.00	0.00	0.05	0.04	0.00
Tb_2O_3	0.07	0.08	0.06	0.09	0.12	0.04	0.13	0.05
Dy_2O_3	0.40	0.11	0.58	0.68	0.52	0.54	0.22	0.21
Ho_2O_3	0.02	0.03	0.08	0.04	0.04	0.00	0.02	0.08
Er_2O_3	0.05	0.11	0.09	0.15	0.16	0.05	0.04	0.07
Tm_2O_3	0.00	0.11	0.04	0.02	0.01	0.09	0.05	0.09
Yb_2O_3	0.06	0.01	0.00	0.00	0.12	0.02	0.05	0.00
Lu_2O_3	0.01	0.08	0.00	0.05	0.00	0.00	0.00	0.00
MgO	0.01	0.01	0.18	0.29	0.16	0.34	0.26	0.03
CaO	33.04	20.88	14.39	14.75	13.99	14.17	20.79	20.93
MnO	0.89	0.28	1.93	2.02	1.48	1.51	0.53	0.65
FeO*	0.00	0.00	1.54	0.00	4.15	0.00	0.00	0.00
PbO	0.16	0.10	0.02	0.10	0.11	0.00	0.06	0.00
Na_2O	0.02	0.01	0.06	0.11	0.03	0.09	0.07	0.00
K_2O	0.00	0.01	0.03	0.04	0.02	0.07	0.07	0.16
F	0.42	0.01	0.12	0.06	0.05	0.02	0.09	0.00
Cl	0.00	0.00	0.00	0.02	0.03	0.03	0.00	0.01
H_2O	0.78	0.86	0.82	0.82	0.80	0.81	0.87	0.88
-(O=F,Cl)	-0.09	0.00	-0.03	-0.02	-0.02	-0.02	-0.02	0.00
Total	103.87	100.12	99.00	100.13	98.48	98.56	98.48	98.51
P (*apfu*)	0.000	0.000	0.000	0.000	0.001	0.002	0.001	0.000
Nb	0.001	0.000	0.003	0.002	0.002	0.002	0.000	0.000
Si	3.000	3.000	3.000	3.000	3.000	3.000	3.000	3.000
Ti	0.000	0.006	0.012	0.014	0.009	0.006	0.003	0.001
Zr	0.001	0.001	0.001	0.003	0.000	0.000	0.001	0.000
Hf	0.002	0.001	0.000	0.001	0.002	0.000	0.000	0.001
Th	0.000	0.000	0.002	0.003	0.003	0.003	0.006	0.000
U	0.001	0.000	0.000	0.000	0.000	0.001	0.001	0.001
Al	0.608	1.513	2.138	1.934	1.988	1.948	1.950	1.972
Fe^{3+}	1.341	1.342	0.550	0.720	0.519	0.778	0.927	0.942
Y	0.001	0.001	0.002	0.002	0.000	0.000	0.000	0.001
La	0.001	0.005	0.247	0.240	0.247	0.228	0.010	0.004
Ce	0.002	0.007	0.212	0.206	0.260	0.231	0.021	0.009

Sample	20TN20	20TN20	20TN7	20TN7	20TN7	20TN7	20TN7	20TN7
Analysis	141843	141854	52251	52262	52273	52284	62313	62324
Mineral	Epidote	Epidote	Allanite-(La)	Allanite-(La)	Allanite-(Ce)	Allanite-(Ce)	Epidote	Epidote
Pr (*apfu*)	0.001	0.001	0.028	0.023	0.032	0.027	0.003	0.001
Nd	0.001	0.002	0.011	0.012	0.022	0.018	0.005	0.003
Sm	0.000	0.002	0.002	0.001	0.003	0.000	0.001	0.002
Eu	0.000	0.000	0.000	0.000	0.000	0.000	0.000	0.001
Gd	0.000	0.002	0.000	0.000	0.000	0.001	0.001	0.000
Tb	0.002	0.002	0.002	0.002	0.004	0.001	0.003	0.001
Dy	0.010	0.003	0.016	0.019	0.015	0.015	0.006	0.005
Ho	0.000	0.001	0.002	0.001	0.001	0.000	0.001	0.002
Er	0.001	0.003	0.002	0.004	0.005	0.001	0.001	0.002
Tm	0.000	0.003	0.001	0.001	0.000	0.003	0.001	0.002
Yb	0.001	0.000	0.000	0.000	0.003	0.000	0.001	0.000
Lu	0.000	0.002	0.000	0.001	0.000	0.000	0.000	0.000
Mg	0.001	0.001	0.024	0.037	0.021	0.045	0.032	0.004
Ca	2.857	1.797	1.354	1.367	1.358	1.337	1.802	1.799
Mn	0.061	0.019	0.144	0.148	0.114	0.113	0.036	0.044
Fe^{2+}	0.000	0.000	0.113	0.000	0.315	0.000	0.000	0.000
Pb	0.004	0.002	0.000	0.002	0.003	0.000	0.001	0.000
Na	0.003	0.002	0.010	0.018	0.005	0.016	0.011	0.000
K	0.000	0.001	0.003	0.005	0.002	0.008	0.007	0.016
F	0.057	0.002	0.018	0.009	0.007	0.003	0.013	0.000
Cl	0.000	0.000	0.000	0.006	0.008	0.008	0.000	0.002
H	0.943	0.998	0.981	0.985	0.985	0.989	0.987	0.998
O (corrected)	12.000	12.000	12.000	12.000	12.000	12.000	12.000	12.000
Cation sum	7.958	7.720	7.900	7.783	7.951	7.793	7.844	7.815

Table B.6. (Continued) Composition of epidote and allanite from various rock types across the 2020 Corundum Dome and Pyrochlore Dome sampling area.

Sample	20TN7	20TN7	20TN7	20TN7	20TN7	20TN7	20TN7	20TN7
Analysis	62346	82371	82382	82393	92401	92412	92423	92434
Mineral	Epidote	Allanite-(La)	Allanite-(La)	Allanite-(Ce)	Epidote	Epidote	Epidote	Epidote
P_2O_5 (wt. %)	0.01	0.01	0.00	0.00	0.00	0.01	0.04	0.01
Nb_2O_5	0.02	0.04	0.02	0.03	0.00	0.00	0.00	0.01
SiO_2	37.30	34.37	34.06	34.65	37.23	37.24	37.32	37.42
TiO_2	0.00	0.06	0.12	0.13	0.03	0.07	0.00	0.01
ZrO_2	0.01	0.04	0.05	0.01	0.01	0.04	0.02	0.00
HfO_2	0.02	0.05	0.00	0.07	0.01	0.07	0.11	0.03
ThO_2	0.06	0.00	0.05	0.00	0.02	0.05	0.00	0.06
UO_2	0.03	0.07	0.09	0.08	0.06	0.00	0.02	0.06
Al_2O_3	21.19	20.66	20.02	19.13	21.19	21.22	21.45	21.59
Fe_2O_3*	15.83	7.84	9.74	12.34	15.69	15.57	15.29	15.20
Y_2O_3	0.01	0.00	0.01	0.00	0.01	0.00	0.01	0.01
La_2O_3	0.20	8.02	9.43	6.10	0.37	0.35	0.11	0.17
Ce_2O_3	0.31	7.07	7.13	6.69	0.55	0.59	0.27	0.32
Pr_2O_3	0.07	0.92	1.00	0.90	0.07	0.16	0.05	0.03
Nd_2O_3	0.09	0.54	0.37	0.91	0.21	0.16	0.09	0.11
Sm_2O_3	0.01	0.10	0.06	0.08	0.03	0.07	0.01	0.02
Eu_2O_3	0.01	0.00	0.00	0.00	0.00	0.04	0.04	0.03
Gd_2O_3	0.00	0.03	0.00	0.02	0.04	0.04	0.04	0.01
Tb_2O_3	0.03	0.06	0.04	0.00	0.04	0.11	0.07	0.07
Dy_2O_3	0.21	0.61	0.63	0.40	0.21	0.27	0.20	0.25
Ho_2O_3	0.05	0.06	0.00	0.07	0.14	0.07	0.18	0.06
Er_2O_3	0.21	0.15	0.04	0.07	0.16	0.06	0.13	0.09
Tm_2O_3	0.05	0.18	0.00	0.01	0.16	0.04	0.04	0.03
Yb_2O_3	0.04	0.05	0.00	0.13	0.02	0.00	0.02	0.08
Lu_2O_3	0.03	0.06	0.00	0.00	0.00	0.02	0.06	0.00
MgO	0.09	0.14	0.13	0.12	0.03	0.02	0.05	0.04
CaO	21.40	14.54	13.94	15.40	21.03	21.07	21.60	21.35
MnO	0.58	1.92	1.79	1.11	0.60	0.55	0.51	0.51
FeO*	0.00	1.97	0.16	1.10	0.00	0.00	0.00	0.00
PbO	0.05	0.00	0.01	0.02	0.00	0.05	0.05	0.02
Na_2O	0.01	0.03	0.05	0.03	0.01	0.00	0.00	0.01
K_2O	0.01	0.03	0.01	0.06	0.03	0.05	0.05	0.12
F	0.02	0.04	0.08	0.04	0.02	0.04	0.05	0.00
Cl	0.00	0.03	0.01	0.01	0.01	0.00	0.01	0.01
H_2O	0.88	0.83	0.82	0.83	0.88	0.88	0.88	0.89
-(O=F,Cl)	-0.01	-0.02	-0.02	-0.01	-0.01	-0.01	-0.01	0.00
Total	98.86	100.49	99.85	100.54	98.84	98.92	98.74	98.60
P (*apfu*)	0.001	0.001	0.000	0.000	0.000	0.001	0.003	0.000
Nb	0.001	0.002	0.001	0.001	0.000	0.000	0.000	0.001
Si	3.000	3.000	3.000	3.000	3.000	3.000	3.000	3.000
Ti	0.000	0.004	0.008	0.009	0.002	0.004	0.000	0.000
Zr	0.000	0.002	0.002	0.001	0.000	0.002	0.001	0.000
Hf	0.000	0.001	0.000	0.002	0.000	0.002	0.002	0.001
Th	0.001	0.000	0.001	0.000	0.000	0.001	0.000	0.001
U	0.001	0.001	0.002	0.002	0.001	0.000	0.000	0.001
Al	2.008	2.126	2.078	1.952	2.012	2.014	2.032	2.040
Fe^{3+}	0.933	0.515	0.646	0.804	0.923	0.915	0.898	0.882
Y	0.001	0.000	0.000	0.000	0.000	0.000	0.000	0.000
La	0.006	0.258	0.306	0.195	0.011	0.011	0.003	0.005
Ce	0.009	0.226	0.230	0.212	0.016	0.017	0.008	0.010

Sample	20TN7	20TN7	20TN7	20TN7	20TN7	20TN7	20TN7	20TN7
Analysis	62346	82371	82382	82393	92401	92412	92423	92434
Mineral	Epidote	Allanite-(La)	Allanite-(La)	Allanite-(Ce)	Epidote	Epidote	Epidote	Epidote
Pr (*apfu*)	0.002	0.029	0.032	0.028	0.002	0.005	0.001	0.001
Nd	0.003	0.017	0.012	0.028	0.006	0.005	0.002	0.003
Sm	0.000	0.003	0.002	0.002	0.001	0.002	0.000	0.001
Eu	0.000	0.000	0.000	0.000	0.000	0.001	0.001	0.001
Gd	0.000	0.001	0.000	0.001	0.001	0.001	0.001	0.000
Tb	0.001	0.002	0.001	0.000	0.001	0.003	0.002	0.002
Dy	0.005	0.017	0.018	0.011	0.005	0.007	0.005	0.006
Ho	0.001	0.002	0.000	0.002	0.003	0.002	0.004	0.002
Er	0.005	0.004	0.001	0.002	0.004	0.002	0.003	0.002
Tm	0.001	0.005	0.000	0.000	0.004	0.001	0.001	0.001
Yb	0.001	0.001	0.000	0.003	0.000	0.000	0.001	0.002
Lu	0.001	0.001	0.000	0.000	0.000	0.001	0.002	0.000
Mg	0.011	0.019	0.017	0.015	0.004	0.002	0.006	0.004
Ca	1.844	1.360	1.316	1.428	1.816	1.818	1.860	1.834
Mn	0.040	0.142	0.133	0.082	0.041	0.037	0.034	0.035
Fe^{2+}	0.000	0.144	0.012	0.080	0.000	0.000	0.000	0.000
Pb	0.001	0.000	0.000	0.001	0.000	0.001	0.001	0.000
Na	0.001	0.005	0.009	0.004	0.002	0.000	0.000	0.001
K	0.001	0.003	0.001	0.007	0.003	0.005	0.005	0.013
F	0.003	0.007	0.013	0.007	0.002	0.006	0.007	0.000
Cl	0.000	0.007	0.003	0.002	0.002	0.000	0.002	0.001
H	0.997	0.986	0.984	0.991	0.995	0.994	0.991	0.999
O (corrected)	12.000	12.000	12.000	12.000	12.000	12.000	12.000	12.000
Cation sum	7.883	7.904	7.844	7.880	7.866	7.865	7.889	7.849

Table B.6. (Continued) Composition of epidote and allanite from various rock types across the 2020 Corundum Dome and Pyrochlore Dome sampling area.

Sample	20TN6-2	20TN6-2	20TN6-2	20TN6-2	20TN6-2	20TN6-2	20TN6-2	20TN6-2
Analysis	162671	162682	162693	172701	172712	172723	192801	192812
Mineral	Epidote	Epidote	Epidote	Allanite-(Ce)	Allanite-(La)	Allanite-(Ce)	Epidote	Epidote
P_2O_5 (wt. %)	0.01	0.00	0.02	0.03	0.01	0.03	0.00	0.00
Nb_2O_5	0.01	0.00	0.00	0.05	0.10	0.01	0.01	0.01
SiO_2	36.73	36.59	36.62	32.30	31.52	32.50	36.58	35.97
TiO_2	0.02	0.01	0.07	0.31	1.03	0.25	0.15	0.00
ZrO_2	0.04	0.02	0.05	0.02	0.04	0.04	0.00	0.03
HfO_2	0.00	0.03	0.00	0.00	0.02	0.14	0.00	0.00
ThO_2	0.06	0.01	0.13	0.00	0.12	0.01	0.00	0.12
UO_2	0.00	0.09	0.02	0.00	0.07	0.02	0.10	0.00
Al_2O_3	18.45	18.93	18.90	14.61	13.78	14.91	18.00	18.34
Fe_2O_3*	19.19	18.78	18.97	9.31	8.38	11.15	19.44	18.43
Y_2O_3	0.00	0.02	0.00	0.09	0.09	0.02	0.06	0.06
La_2O_3	0.35	0.31	0.42	6.65	11.24	6.73	0.46	0.63
Ce_2O_3	0.78	0.74	0.89	10.58	10.50	10.06	0.79	1.35
Pr_2O_3	0.10	0.12	0.19	1.28	1.50	1.27	0.13	0.21
Nd_2O_3	0.30	0.37	0.32	1.95	1.38	1.99	0.28	0.82
Sm_2O_3	0.05	0.09	0.09	0.21	0.13	0.23	0.04	0.24
Eu_2O_3	0.07	0.04	0.03	0.00	0.00	0.05	0.05	0.05
Gd_2O_3	0.10	0.14	0.07	0.10	0.02	0.02	0.05	0.15
Tb_2O_3	0.05	0.08	0.07	0.09	0.12	0.07	0.08	0.10
Dy_2O_3	0.25	0.20	0.23	0.43	0.64	0.49	0.14	0.28
Ho_2O_3	0.00	0.08	0.08	0.05	0.06	0.01	0.03	0.22
Er_2O_3	0.09	0.15	0.09	0.15	0.15	0.16	0.09	0.22
Tm_2O_3	0.01	0.12	0.03	0.15	0.03	0.00	0.06	0.10
Yb_2O_3	0.15	0.00	0.07	0.09	0.17	0.00	0.00	0.01
Lu_2O_3	0.00	0.00	0.01	0.00	0.07	0.00	0.00	0.01
MgO	0.13	0.05	0.03	0.25	0.77	0.33	0.01	0.03
CaO	20.50	20.49	20.45	12.08	10.64	12.02	21.27	19.51
MnO	0.69	0.53	0.57	1.23	2.12	1.31	0.30	0.54
FeO*	0.00	0.00	0.00	8.11	4.76	5.81	0.00	0.00
PbO	0.00	0.01	0.02	0.05	0.04	0.09	0.01	0.04
Na_2O	0.01	0.00	0.00	0.01	0.06	0.02	0.01	0.01
K_2O	0.02	0.01	0.03	0.02	0.01	0.04	0.00	0.02
F	0.05	0.03	0.00	0.00	0.31	0.01	0.04	0.02
Cl	0.01	0.00	0.01	0.01	0.03	0.00	0.02	0.00
H_2O	0.86	0.86	0.87	0.78	0.72	0.79	0.85	0.85
-(O=F,Cl)	-0.02	-0.01	0.00	0.00	-0.08	0.00	-0.02	0.00
Total	99.04	98.87	99.31	100.96	100.54	100.56	99.07	98.38
P (*apfu*)	0.001	0.000	0.001	0.002	0.000	0.002	0.000	0.000
Nb	0.000	0.000	0.000	0.002	0.004	0.000	0.000	0.001
Si	3.000	3.000	3.000	3.000	3.000	3.000	3.000	3.000
Ti	0.001	0.001	0.004	0.021	0.073	0.017	0.009	0.000
Zr	0.001	0.001	0.002	0.001	0.002	0.002	0.000	0.001
Hf	0.000	0.001	0.000	0.000	0.001	0.004	0.000	0.000
Th	0.001	0.000	0.002	0.000	0.003	0.000	0.000	0.002
U	0.000	0.002	0.000	0.000	0.001	0.000	0.002	0.000
Al	1.776	1.829	1.825	1.600	1.546	1.622	1.740	1.803
Fe^{3+}	1.150	1.141	1.158	0.651	0.600	0.775	1.179	1.137
Y	0.000	0.001	0.000	0.004	0.005	0.001	0.003	0.003
La	0.010	0.009	0.013	0.228	0.395	0.229	0.014	0.019
Ce	0.023	0.022	0.027	0.360	0.366	0.340	0.024	0.041

Sample	20TN6-2	20TN6-2	20TN6-2	20TN6-2	20TN6-2	20TN6-2	20TN6-2	20TN6-2
Analysis	162671	162682	162693	172701	172712	172723	192801	192812
Mineral	Epidote	Epidote	Epidote	Allanite-(Ce)	Allanite-(La)	Allanite-(Ce)	Epidote	Epidote
Pr (*apfu*)	0.003	0.004	0.006	0.043	0.052	0.043	0.004	0.006
Nd	0.009	0.011	0.009	0.065	0.047	0.066	0.008	0.024
Sm	0.001	0.003	0.003	0.007	0.004	0.008	0.001	0.007
Eu	0.002	0.001	0.001	0.000	0.000	0.002	0.002	0.002
Gd	0.003	0.004	0.002	0.003	0.001	0.001	0.001	0.004
Tb	0.001	0.002	0.002	0.003	0.004	0.002	0.002	0.003
Dy	0.007	0.005	0.006	0.013	0.020	0.015	0.004	0.008
Ho	0.000	0.002	0.002	0.002	0.002	0.000	0.001	0.006
Er	0.002	0.004	0.002	0.004	0.005	0.005	0.002	0.006
Tm	0.000	0.003	0.001	0.004	0.001	0.000	0.002	0.003
Yb	0.004	0.000	0.002	0.002	0.005	0.000	0.000	0.000
Lu	0.000	0.000	0.000	0.000	0.002	0.000	0.000	0.000
Mg	0.016	0.006	0.003	0.034	0.109	0.046	0.002	0.004
Ca	1.794	1.800	1.795	1.202	1.085	1.189	1.870	1.743
Mn	0.048	0.037	0.040	0.097	0.171	0.103	0.021	0.038
Fe^{2+}	0.000	0.000	0.000	0.630	0.379	0.448	0.000	0.000
Pb	0.000	0.000	0.000	0.001	0.001	0.002	0.000	0.001
Na	0.002	0.000	0.000	0.001	0.012	0.004	0.001	0.002
K	0.002	0.001	0.003	0.003	0.002	0.004	0.000	0.002
F	0.006	0.004	0.000	0.000	0.050	0.002	0.006	0.003
Cl	0.003	0.000	0.003	0.001	0.008	0.000	0.006	0.000
H	0.991	0.996	0.997	0.999	0.942	0.998	0.988	0.997
O (corrected)	12.000	12.000	12.000	12.000	12.000	12.000	12.000	12.000
Cation sum	7.868	7.893	7.912	7.984	7.953	7.930	7.904	7.869

Table B.6. (Continued) Composition of epidote and allanite from various rock types across the 2020 Corundum Dome and Pyrochlore Dome sampling area.

Sample	20TN6-2	20TN6-2	20TN6-2	20TN6-2	20TN2	20TN2	20TN2	20TN2
Analysis	202832	212841	212852	222861	41762	61842	61853	61864
Mineral	Allanite-(Ce)	Allanite-(Ce)	Allanite-(La)	Epidote	Allanite-(Ce)	Allanite-(Ce)	Allanite-(Ce)	Allanite-(Ce)
P_2O_5 (wt. %)	0.06	0.04	0.04	0.01	0.02	0.01	0.02	0.03
Nb_2O_5	0.15	0.08	0.03	0.00	0.02	0.02	0.05	0.04
SiO_2	31.18	31.43	32.94	36.34	33.36	31.28	31.14	32.24
TiO_2	0.33	0.34	0.22	0.15	0.44	1.96	1.76	0.08
ZrO_2	0.01	0.00	0.00	0.00	0.01	0.00	0.00	0.00
HfO_2	0.00	0.02	0.08	0.03	0.00	0.12	0.04	0.07
ThO_2	0.02	0.00	0.08	0.04	0.10	0.09	0.23	0.13
UO_2	0.05	0.02	0.00	0.02	0.03	0.00	0.02	0.04
Al_2O_3	12.37	12.56	14.04	17.68	14.51	10.72	10.11	11.91
Fe_2O_3*	10.67	12.83	16.77	18.88	16.89	12.05	13.78	18.24
Y_2O_3	0.11	0.13	0.05	0.04	0.02	0.04	0.02	0.03
La_2O_3	9.31	10.60	9.53	0.98	7.51	9.27	9.43	8.33
Ce_2O_3	11.47	11.05	7.72	1.59	7.93	12.26	12.64	9.85
Pr_2O_3	1.47	1.52	1.20	0.22	1.05	1.43	1.37	1.48
Nd_2O_3	1.95	1.91	1.26	0.63	0.97	1.07	0.99	1.95
Sm_2O_3	0.23	0.22	0.17	0.27	0.10	0.06	0.07	0.17
Eu_2O_3	0.01	0.00	0.00	0.03	0.00	0.00	0.00	0.00
Gd_2O_3	0.11	0.24	0.09	0.28	0.00	0.04	0.09	0.14
Tb_2O_3	0.12	0.09	0.02	0.11	0.07	0.09	0.06	0.14
Dy_2O_3	0.58	0.69	0.53	0.28	0.51	0.54	0.42	0.19
Ho_2O_3	0.05	0.12	0.17	0.13	0.03	0.09	0.04	0.09
Er_2O_3	0.14	0.17	0.12	0.10	0.04	0.05	0.04	0.20
Tm_2O_3	0.10	0.03	0.06	0.06	0.14	0.12	0.05	0.15
Yb_2O_3	0.00	0.09	0.00	0.08	0.04	0.01	0.00	0.09
Lu_2O_3	0.00	0.04	0.04	0.10	0.05	0.00	0.00	0.00
MgO	0.57	0.49	0.53	0.70	0.14	0.26	0.27	0.17
CaO	10.22	10.22	12.16	18.79	13.54	10.57	10.32	11.61
MnO	1.65	1.95	1.43	0.66	1.72	1.69	1.28	0.56
FeO*	6.66	3.12	0.60	0.00	0.43	6.24	5.65	2.63
PbO	0.00	0.02	0.09	0.09	0.10	0.04	0.14	0.09
Na_2O	0.05	0.03	0.03	0.02	0.03	0.03	0.05	0.02
K_2O	0.00	0.05	0.07	0.38	0.16	0.01	0.00	0.00
F	0.08	0.06	0.05	0.09	0.06	0.04	0.00	0.00
Cl	0.00	0.01	0.03	0.00	0.03	0.02	0.02	0.03
H_2O	0.74	0.75	0.77	0.84	0.78	0.75	0.74	0.76
-(O=F,Cl)	-0.02	-0.02	-0.02	-0.02	-0.03	-0.02	-0.01	-0.01
Total	100.45	100.90	100.93	99.60	100.80	100.93	100.84	101.46
P (*apfu*)	0.005	0.003	0.003	0.000	0.002	0.001	0.001	0.003
Nb	0.006	0.004	0.001	0.000	0.001	0.001	0.002	0.002
Si	3.000	3.000	3.000	3.000	3.000	3.000	3.000	3.000
Ti	0.024	0.025	0.015	0.009	0.029	0.141	0.127	0.005
Zr	0.000	0.000	0.000	0.000	0.000	0.000	0.000	0.000
Hf	0.000	0.000	0.002	0.001	0.000	0.003	0.001	0.002
Th	0.000	0.000	0.002	0.001	0.002	0.002	0.005	0.003
U	0.001	0.000	0.000	0.000	0.001	0.000	0.000	0.001
Al	1.403	1.413	1.507	1.720	1.538	1.212	1.148	1.306
Fe^{3+}	0.772	0.922	1.149	1.142	1.143	0.870	0.999	1.277
Y	0.006	0.007	0.002	0.002	0.001	0.002	0.001	0.002

Sample	20TN6-2	20TN6-2	20TN6-2	20TN6-2	20TN2	20TN2	20TN2	20TN2
Analysis	202832	212841	212852	222861	41762	61842	61853	61864
Mineral	Allanite-(Ce)	Allanite-(Ce)	Allanite-(La)	Epidote	Allanite-(Ce)	Allanite-(Ce)	Allanite-(Ce)	Allanite-(Ce)
La (*apfu*)	0.330	0.373	0.320	0.030	0.249	0.328	0.335	0.286
Ce	0.404	0.386	0.258	0.048	0.261	0.430	0.446	0.336
Pr	0.052	0.053	0.040	0.007	0.034	0.050	0.048	0.050
Nd	0.067	0.065	0.041	0.019	0.031	0.037	0.034	0.065
Sm	0.008	0.007	0.005	0.008	0.003	0.002	0.003	0.006
Eu	0.000	0.000	0.000	0.001	0.000	0.000	0.000	0.000
Gd	0.003	0.008	0.003	0.008	0.000	0.001	0.003	0.004
Tb	0.004	0.003	0.001	0.003	0.002	0.003	0.002	0.004
Dy	0.018	0.021	0.015	0.007	0.015	0.017	0.013	0.006
Ho	0.001	0.004	0.005	0.004	0.001	0.003	0.001	0.003
Er	0.004	0.005	0.003	0.003	0.001	0.002	0.001	0.006
Tm	0.003	0.001	0.002	0.001	0.004	0.004	0.001	0.004
Yb	0.000	0.003	0.000	0.002	0.001	0.000	0.000	0.002
Lu	0.000	0.001	0.001	0.002	0.001	0.000	0.000	0.000
Mg	0.082	0.070	0.072	0.086	0.019	0.037	0.039	0.024
Ca	1.054	1.045	1.187	1.662	1.304	1.086	1.065	1.157
Mn	0.134	0.157	0.110	0.046	0.131	0.137	0.104	0.044
Fe^{2+}	0.536	0.249	0.046	0.000	0.032	0.501	0.456	0.205
Pb	0.000	0.001	0.002	0.002	0.002	0.001	0.004	0.002
Na	0.009	0.006	0.005	0.003	0.005	0.006	0.009	0.004
K	0.001	0.006	0.009	0.040	0.018	0.001	0.000	0.000
F	0.012	0.010	0.008	0.013	0.009	0.006	0.000	0.000
Cl	0.001	0.003	0.009	0.000	0.009	0.006	0.005	0.009
H	0.987	0.988	0.983	0.987	0.983	0.988	0.995	0.991
O (corrected)	12.000	12.000	12.000	12.000	12.000	12.000	12.000	12.000
Cation sum	7.942	7.851	7.824	7.870	7.851	7.887	7.854	7.818

Table B.6. (Continued) Composition of epidote and allanite from various rock types across the 2020 Corundum Dome and Pyrochlore Dome sampling area.

Sample	20TN4D	20TN4D	20TN4D	20TN4D	20TN4D	20TN4D	20TN4D	20TN4D
Analysis	162191	162202	162213	162224	162235	162246	162257	162268
Mineral	Allanite-(La)	Allanite-(La)	Epidote	Epidote	Epidote	Allanite-(Ce)	Epidote	Allanite-(Ce)
P_2O_5 (wt. %)	0.01	0.09	0.00	0.04	0.00	0.00	0.03	0.02
Nb_2O_5	0.02	0.00	0.00	0.01	0.00	0.04	0.00	0.03
SiO_2	33.67	33.38	36.82	36.62	36.76	33.67	36.36	33.30
TiO_2	0.06	0.08	0.01	0.03	0.02	0.14	0.00	0.18
ZrO_2	0.05	0.00	0.01	0.01	0.00	0.00	0.00	0.01
HfO_2	0.00	0.01	0.10	0.00	0.05	0.09	0.07	0.00
ThO_2	0.00	0.04	0.00	0.06	0.05	0.00	0.09	0.04
UO_2	0.00	0.05	0.00	0.04	0.06	0.04	0.05	0.05
Al_2O_3	17.73	17.60	18.95	19.09	18.98	15.60	18.67	15.08
Fe_2O_3*	11.84	9.60	18.08	18.16	18.39	14.64	18.48	16.16
Y_2O_3	0.03	0.01	0.02	0.01	0.00	0.01	0.00	0.01
La_2O_3	14.16	14.23	0.76	0.72	1.04	2.96	1.28	6.54
Ce_2O_3	5.25	5.12	1.49	1.59	1.46	10.63	2.04	10.37
Pr_2O_3	1.25	1.28	0.16	0.19	0.22	1.05	0.30	1.22
Nd_2O_3	0.14	0.11	0.35	0.40	0.33	1.34	0.55	0.61
Sm_2O_3	0.06	0.06	0.06	0.09	0.04	0.08	0.07	0.00
Eu_2O_3	0.00	0.00	0.08	0.03	0.01	0.02	0.01	0.00
Gd_2O_3	0.00	0.09	0.00	0.07	0.07	0.08	0.04	0.00
Tb_2O_3	0.06	0.00	0.00	0.16	0.00	0.10	0.03	0.01
Dy_2O_3	0.56	0.51	0.35	0.31	0.31	0.57	0.28	0.72
Ho_2O_3	0.03	0.11	0.00	0.11	0.08	0.05	0.06	0.00
Er_2O_3	0.09	0.01	0.03	0.05	0.08	0.12	0.15	0.17
Tm_2O_3	0.14	0.14	0.00	0.03	0.00	0.04	0.06	0.00
Yb_2O_3	0.11	0.03	0.00	0.00	0.03	0.10	0.04	0.06
Lu_2O_3	0.09	0.00	0.00	0.07	0.03	0.17	0.09	0.00
MgO	0.32	0.33	0.23	0.08	0.06	0.33	0.16	0.25
CaO	12.90	12.84	19.71	19.58	19.69	13.60	18.82	12.54
MnO	1.69	1.65	0.99	0.87	0.85	1.91	0.87	2.49
FeO*	0.17	2.81	0.00	0.00	0.00	2.80	0.00	0.00
PbO	0.07	0.04	0.10	0.06	0.04	0.00	0.04	0.00
Na_2O	0.08	0.08	0.01	0.00	0.00	0.03	0.01	0.03
K_2O	0.10	0.04	0.12	0.04	0.17	0.10	0.20	0.13
F	0.12	0.09	0.07	0.02	0.05	0.02	0.04	0.00
Cl	0.04	0.06	0.00	0.00	0.00	0.04	0.00	0.04
H_2O	0.79	0.79	0.86	0.86	0.86	0.80	0.86	0.79
-(O=F,Cl)	-0.04	-0.04	-0.02	-0.01	-0.01	-0.02	-0.01	-0.02
Total	101.58	101.24	99.36	99.40	99.73	101.15	99.78	100.81
P (*apfu*)	0.001	0.007	0.000	0.003	0.000	0.000	0.002	0.001
Nb	0.001	0.000	0.000	0.000	0.000	0.001	0.000	0.001
Si	3.000	3.000	3.000	3.000	3.000	3.000	3.000	3.000
Ti	0.004	0.006	0.001	0.002	0.001	0.010	0.000	0.012
Zr	0.002	0.000	0.000	0.000	0.000	0.000	0.000	0.000
Hf	0.000	0.000	0.002	0.000	0.001	0.002	0.002	0.000
Th	0.000	0.001	0.000	0.001	0.001	0.000	0.002	0.001
U	0.000	0.001	0.000	0.001	0.001	0.001	0.001	0.001
Al	1.861	1.864	1.820	1.844	1.825	1.638	1.815	1.601
Fe^{3+}	0.794	0.649	1.071	1.096	1.101	0.982	1.129	1.094
Y	0.002	0.001	0.001	0.000	0.000	0.000	0.000	0.001
La	0.465	0.472	0.023	0.022	0.031	0.097	0.039	0.217
Ce	0.171	0.169	0.044	0.048	0.044	0.347	0.062	0.342

Sample	20TN4D	20TN4D	20TN4D	20TN4D	20TN4D	20TN4D	20TN4D	20TN4D
Analysis	162191	162202	162213	162224	162235	162246	162257	162268
Mineral	Allanite-(La)	Allanite-(La)	Epidote	Epidote	Epidote	Allanite-(Ce)	Epidote	Allanite-(Ce)
Pr (*apfu*)	0.041	0.042	0.005	0.006	0.007	0.034	0.009	0.040
Nd	0.004	0.004	0.010	0.012	0.010	0.043	0.016	0.020
Sm	0.002	0.002	0.002	0.003	0.001	0.002	0.002	0.000
Eu	0.000	0.000	0.002	0.001	0.000	0.001	0.000	0.000
Gd	0.000	0.003	0.000	0.002	0.002	0.002	0.001	0.000
Tb	0.002	0.000	0.000	0.004	0.000	0.003	0.001	0.000
Dy	0.016	0.015	0.009	0.008	0.008	0.016	0.007	0.021
Ho	0.001	0.003	0.000	0.003	0.002	0.001	0.002	0.000
Er	0.002	0.000	0.001	0.001	0.002	0.003	0.004	0.005
Tm	0.004	0.004	0.000	0.001	0.000	0.001	0.002	0.000
Yb	0.003	0.001	0.000	0.000	0.001	0.003	0.001	0.002
Lu	0.002	0.000	0.000	0.002	0.001	0.005	0.002	0.000
Mg	0.042	0.045	0.028	0.010	0.007	0.044	0.020	0.033
Ca	1.232	1.237	1.720	1.718	1.722	1.299	1.663	1.211
Mn	0.127	0.126	0.069	0.060	0.059	0.144	0.061	0.190
Fe^{2+}	0.013	0.211	0.000	0.000	0.000	0.208	0.000	0.000
Pb	0.002	0.001	0.002	0.001	0.001	0.000	0.001	0.000
Na	0.013	0.013	0.002	0.000	0.000	0.005	0.001	0.006
K	0.012	0.005	0.012	0.004	0.017	0.012	0.022	0.015
F	0.018	0.014	0.010	0.003	0.007	0.003	0.005	0.000
Cl	0.010	0.016	0.000	0.001	0.000	0.010	0.000	0.010
H	0.972	0.970	0.990	0.996	0.993	0.987	0.995	0.990
O (corrected)	12.000	12.000	12.000	12.000	12.000	12.000	12.000	12.000
Cation sum	7.847	7.909	7.835	7.857	7.853	7.918	7.873	7.824

Table B.7. Composition of titanite from various rock types across the 2020 Corundum Dome and Pyrochlore Dome sampling area.

Sample	20TN15A	20TN15A	20TN7	20TN7	20TN7	20TN7	20TN7	20TN7	20TN7	20TN7	20TN7	20TN7	20TN7	20TN7
Analysis	462691	462702	32111	32122	32133	32144	32155	32166	32177	32188	32199	322010	62291	62302
P_2O_5 (wt. %)	0.04	0.00	0.02	0.02	0.01	0.01	0.02	0.00	0.01	0.01	0.04	0.02	0.04	0.01
Nb_2O_5	1.96	1.45	3.10	1.57	1.88	2.04	1.35	1.39	0.97	2.72	2.52	2.55	2.33	3.58
SiO_2	29.81	30.57	30.89	31.11	30.96	30.85	30.97	30.96	30.96	30.88	30.83	30.76	30.52	30.42
TiO_2	37.64	38.62	38.02	38.62	38.01	37.65	38.91	38.66	38.87	38.00	37.87	36.30	36.16	35.82
ZrO_2	0.13	0.00	0.03	0.12	0.23	0.38	0.25	0.05	0.02	0.15	0.05	0.24	0.90	0.57
HfO_2	0.07	0.00	0.01	0.05	0.09	0.06	0.02	0.02	0.02	0.11	0.00	0.00	0.02	0.02
ThO_2	0.02	0.00	0.11	0.00	0.02	0.15	0.00	0.02	0.03	0.00	0.06	0.17	0.10	0.05
UO_2	0.06	0.04	0.06	0.06	0.01	0.04	0.00	0.00	0.04	0.04	0.06	0.04	0.06	0.03
Al_2O_3	0.03	0.04	0.08	0.10	0.08	0.10	0.10	0.08	0.09	0.10	0.09	0.19	0.18	0.25
Fe_2O_3*	0.52	0.37	0.34	0.35	0.36	0.45	0.37	0.30	0.44	0.42	0.42	0.79	0.72	0.87
Y_2O_3	0.19	0.32	0.00	0.00	0.02	0.01	0.03	0.01	0.01	0.00	0.01	0.02	0.11	0.06
La_2O_3	0.91	0.02	0.00	0.00	0.00	0.00	0.00	0.00	0.00	0.00	0.00	0.00	0.00	0.00
Ce_2O_3	2.31	0.77	0.13	0.13	0.18	0.15	0.15	0.12	0.16	0.19	0.12	0.28	0.26	0.35
Pr_2O_3	0.29	0.11	0.00	0.00	0.00	0.00	0.01	0.00	0.00	0.00	0.00	0.00	0.00	0.01
Nd_2O_3	0.68	0.46	0.04	0.01	0.02	0.00	0.01	0.00	0.00	0.01	0.00	0.05	0.12	0.13
Sm_2O_3	0.16	0.07	0.00	0.04	0.00	0.05	0.01	0.00	0.00	0.01	0.01	0.00	0.01	0.04
Eu_2O_3	0.03	0.04	0.02	0.00	0.03	0.00	0.02	0.01	0.02	0.04	0.00	0.02	0.01	0.04
Gd_2O_3	0.11	0.13	0.05	0.06	0.01	0.03	0.02	0.03	0.02	0.05	0.06	0.04	0.05	0.00
Tb_2O_3	0.05	0.04	0.06	0.11	0.02	0.03	0.00	0.00	0.09	0.09	0.03	0.01	0.08	0.06
Dy_2O_3	0.12	0.16	0.03	0.08	0.06	0.09	0.03	0.05	0.03	0.03	0.05	0.02	0.06	0.05
Ho_2O_3	0.07	0.12	0.09	0.14	0.06	0.10	0.07	0.04	0.10	0.05	0.06	0.16	0.08	0.05
Er_2O_3	0.05	0.07	0.07	0.04	0.14	0.03	0.04	0.00	0.00	0.15	0.09	0.05	0.03	0.02
Tm_2O_3	0.01	0.02	0.10	0.05	0.09	0.06	0.01	0.06	0.05	0.09	0.05	0.07	0.01	0.03
Yb_2O_3	0.03	0.00	0.13	0.11	0.10	0.16	0.04	0.02	0.00	0.03	0.03	0.00	0.07	0.00
Lu_2O_3	0.00	0.00	0.07	0.18	0.15	0.09	0.07	0.04	0.00	0.07	0.06	0.02	0.06	0.00
MgO	0.00	0.00	0.01	0.01	0.00	0.01	0.00	0.00	0.00	0.01	0.00	0.00	0.00	0.01
CaO	20.75	23.19	24.97	25.63	25.32	24.95	25.55	25.41	25.82	25.30	25.16	25.53	25.89	25.48
MnO	0.16	0.14	0.09	0.10	0.10	0.14	0.10	0.10	0.10	0.12	0.10	0.07	0.06	0.06
PbO	0.03	0.00	0.11	0.00	0.03	0.00	0.00	0.00	0.06	0.02	0.01	0.02	0.00	0.03
Na_2O	2.93	2.12	1.71	1.48	1.60	1.69	1.51	1.50	1.34	1.68	1.60	1.12	0.99	1.17
K_2O	0.01	0.01	0.03	0.01	0.01	0.00	0.01	0.01	0.01	0.12	0.05	0.02	0.14	0.06
F	0.69	0.64	0.34	0.28	0.30	0.34	0.29	0.40	0.41	0.59	0.50	0.20	0.28	0.20
Cl	0.01	0.00	0.00	0.00	0.00	0.00	0.02	0.00	0.02	0.00	0.00	0.02	0.00	0.00
O=F,Cl	-0.29	-0.27	-0.14	-0.12	-0.13	-0.14	-0.13	-0.17	-0.18	-0.25	-0.21	-0.09	-0.12	-0.09
Total	99.60	99.24	100.56	100.34	99.76	99.51	99.88	99.10	99.50	100.81	99.73	98.69	99.20	99.38

Sample	20TN15A	20TN15A	20TN7	20TN7	20TN7	20TN7	20TN7	20TN7	20TN7	20TN7	20TN7	20TN7	20TN7	20TN7
Analysis	462691	462702	32111	32122	32133	32144	32155	32166	32177	32188	32199	322010	62291	62302
P (*apfu*)	0.001	0.000	0.000	0.001	0.000	0.000	0.000	0.000	0.000	0.000	0.001	0.001	0.001	0.000
Nb	0.030	0.022	0.046	0.023	0.028	0.030	0.020	0.021	0.014	0.040	0.037	0.038	0.035	0.054
Si	0.999	1.013	1.010	1.013	1.015	1.015	1.010	1.016	1.014	1.005	1.012	1.024	1.015	1.011
Ti	0.949	0.962	0.934	0.946	0.937	0.931	0.955	0.955	0.957	0.930	0.935	0.909	0.904	0.895
Zr	0.002	0.000	0.000	0.002	0.004	0.006	0.004	0.001	0.000	0.002	0.001	0.004	0.015	0.009
Hf	0.001	0.000	0.000	0.001	0.001	0.001	0.000	0.000	0.000	0.001	0.000	0.000	0.000	0.000
Th	0.000	0.000	0.001	0.000	0.000	0.001	0.000	0.000	0.000	0.000	0.000	0.001	0.001	0.000
U	0.000	0.000	0.000	0.000	0.000	0.000	0.000	0.000	0.000	0.000	0.000	0.000	0.000	0.000
Al	0.001	0.002	0.003	0.004	0.003	0.004	0.004	0.003	0.003	0.004	0.004	0.007	0.007	0.010
Fe^{3+}	0.013	0.009	0.008	0.008	0.009	0.011	0.009	0.007	0.011	0.010	0.010	0.020	0.018	0.022
Y	0.003	0.006	0.000	0.000	0.000	0.000	0.001	0.000	0.000	0.000	0.000	0.000	0.002	0.001
La	0.011	0.000	0.000	0.000	0.000	0.000	0.000	0.000	0.000	0.000	0.000	0.000	0.000	0.000
Ce	0.028	0.009	0.002	0.002	0.002	0.002	0.002	0.001	0.002	0.002	0.001	0.003	0.003	0.004
Pr	0.004	0.001	0.000	0.000	0.000	0.000	0.000	0.000	0.000	0.000	0.000	0.000	0.000	0.000
Nd	0.008	0.005	0.000	0.000	0.000	0.000	0.000	0.000	0.000	0.000	0.000	0.001	0.001	0.002
Sm	0.002	0.001	0.000	0.000	0.000	0.001	0.000	0.000	0.000	0.000	0.000	0.000	0.000	0.000
Eu	0.000	0.000	0.000	0.000	0.000	0.000	0.000	0.000	0.000	0.000	0.000	0.000	0.000	0.000
Gd	0.001	0.001	0.001	0.001	0.000	0.000	0.000	0.000	0.000	0.001	0.001	0.000	0.001	0.000
Tb	0.001	0.000	0.001	0.001	0.000	0.000	0.000	0.000	0.001	0.001	0.000	0.000	0.001	0.001
Dy	0.001	0.002	0.000	0.001	0.001	0.001	0.000	0.001	0.000	0.000	0.001	0.000	0.001	0.001
Ho	0.001	0.001	0.001	0.001	0.001	0.001	0.001	0.000	0.001	0.000	0.001	0.002	0.001	0.001
Er	0.000	0.001	0.001	0.000	0.001	0.000	0.000	0.000	0.000	0.002	0.001	0.001	0.000	0.000
Tm	0.000	0.000	0.001	0.000	0.001	0.001	0.000	0.001	0.001	0.001	0.000	0.001	0.000	0.000
Yb	0.000	0.000	0.001	0.001	0.001	0.002	0.000	0.000	0.000	0.000	0.000	0.000	0.001	0.000
Lu	0.000	0.000	0.001	0.002	0.001	0.001	0.001	0.000	0.000	0.001	0.001	0.000	0.001	0.000
Mg	0.000	0.000	0.000	0.000	0.000	0.000	0.000	0.000	0.000	0.000	0.000	0.000	0.000	0.001
Ca	0.745	0.823	0.874	0.895	0.889	0.879	0.893	0.894	0.906	0.883	0.885	0.911	0.922	0.907
Mn	0.005	0.004	0.003	0.003	0.003	0.004	0.003	0.003	0.003	0.003	0.003	0.002	0.002	0.002
Pb	0.000	0.000	0.001	0.000	0.000	0.000	0.000	0.000	0.001	0.000	0.000	0.000	0.000	0.000
Na	0.191	0.136	0.108	0.093	0.102	0.108	0.096	0.095	0.085	0.106	0.102	0.073	0.064	0.075
K	0.001	0.000	0.001	0.000	0.000	0.000	0.000	0.000	0.000	0.005	0.002	0.001	0.006	0.003
F	0.073	0.067	0.035	0.029	0.031	0.035	0.030	0.041	0.042	0.061	0.051	0.021	0.030	0.022
Cl	0.001	0.000	0.000	0.000	0.000	0.000	0.001	0.000	0.001	0.000	0.000	0.001	0.000	0.000
O	4.903	4.926	4.953	4.948	4.942	4.940	4.945	4.942	4.939	4.926	4.939	4.967	4.957	4.969
Sum	7.977	7.993	7.988	7.977	7.973	7.976	7.977	7.983	7.982	7.986	7.991	7.989	7.987	7.990

Note: Compositions were recalculated on the basis of the sum of 3 cation *apfu*. * All Fe assumed to be Fe_2O_3. Determined by stoichiometry using Droop (1987) calculation method.

Table B.7. (Continued) Composition of titanite from various rock types across the 2020 Corundum Dome and Pyrochlore Dome sampling area.

Sample	20TN7	20TN7	20TN7	20TN23	20TN23	20TN2	20TN2	20TN2	20TN2	20TN2	20TN2	20TN2	20TN7	20TN7
Analysis	102441	102452	102463	132571	132604	31711	31722	31733	31744	61886	102076	152181	102441	102452
P_2O_5 (wt. %)	0.03	0.00	0.02	0.09	0.16	0.00	0.01	0.01	0.03	0.00	0.00	0.02	0.03	0.00
Nb_2O_5	1.16	1.31	1.51	4.92	5.62	0.41	1.09	3.84	7.29	3.83	6.44	6.00	1.16	1.31
SiO_2	30.72	30.76	30.77	30.46	29.79	32.17	31.79	31.71	30.68	30.27	30.20	30.26	30.72	30.76
TiO_2	39.14	38.42	37.77	22.51	23.07	24.99	25.76	26.22	25.21	30.70	27.63	27.47	39.14	38.42
ZrO_2	0.05	0.06	0.05	0.51	0.44	0.01	0.06	0.04	0.04	0.04	0.11	0.04	0.05	0.06
HfO_2	0.00	0.00	0.06	0.07	0.08	0.13	0.10	0.03	0.00	0.02	0.06	0.00	0.00	0.00
ThO_2	0.01	0.02	0.03	0.44	1.25	0.00	0.02	0.00	0.00	0.08	0.04	0.09	0.01	0.02
UO_2	0.05	0.00	0.03	0.08	0.06	0.01	0.05	0.09	0.06	0.04	0.00	0.04	0.05	0.00
Al_2O_3	0.12	0.10	0.11	6.74	6.35	9.41	7.81	4.76	3.62	2.45	2.40	3.65	0.12	0.10
Fe_2O_3*	0.41	0.53	0.59	2.16	2.68	0.48	1.03	2.80	3.70	2.92	3.31	3.02	0.41	0.53
Y_2O_3	0.01	0.00	0.01	0.02	0.00	0.03	0.07	0.04	0.04	0.05	0.04	0.04	0.01	0.00
La_2O_3	0.00	0.00	0.00	0.08	0.04	0.00	0.00	0.00	0.00	0.00	0.00	0.00	0.00	0.00
Ce_2O_3	0.05	0.10	0.16	0.24	0.21	0.05	0.05	0.10	0.11	0.21	0.28	0.08	0.05	0.10
Pr_2O_3	0.00	0.02	0.00	0.04	0.00	0.00	0.00	0.02	0.00	0.01	0.00	0.00	0.00	0.02
Nd_2O_3	0.00	0.00	0.04	0.05	0.04	0.01	0.00	0.02	0.04	0.04	0.08	0.02	0.00	0.00
Sm_2O_3	0.00	0.00	0.00	0.00	0.00	0.01	0.04	0.08	0.00	0.05	0.02	0.00	0.00	0.00
Eu_2O_3	0.00	0.01	0.02	0.03	0.03	0.04	0.01	0.02	0.03	0.03	0.01	0.03	0.00	0.01
Gd_2O_3	0.07	0.04	0.03	0.03	0.08	0.00	0.02	0.01	0.00	0.02	0.00	0.00	0.07	0.04
Tb_2O_3	0.03	0.11	0.00	0.02	0.15	0.06	0.02	0.05	0.04	0.11	0.08	0.03	0.03	0.11
Dy_2O_3	0.06	0.02	0.02	0.13	0.14	0.05	0.11	0.03	0.01	0.01	0.12	0.00	0.06	0.02
Ho_2O_3	0.00	0.00	0.00	0.11	0.05	0.02	0.05	0.05	0.08	0.00	0.06	0.06	0.00	0.00
Er_2O_3	0.00	0.00	0.10	0.00	0.07	0.07	0.10	0.08	0.10	0.04	0.09	0.01	0.00	0.00
Tm_2O_3	0.05	0.00	0.13	0.05	0.12	0.00	0.02	0.12	0.10	0.07	0.00	0.01	0.05	0.00
Yb_2O_3	0.01	0.00	0.02	0.03	0.09	0.19	0.08	0.07	0.09	0.01	0.08	0.09	0.01	0.00
Lu_2O_3	0.00	0.00	0.05	0.09	0.07	0.07	0.00	0.00	0.12	0.06	0.00	0.02	0.00	0.00
MgO	0.00	0.01	0.02	0.15	0.16	0.01	0.03	0.07	0.03	0.03	0.03	0.05	0.00	0.01
CaO	25.97	25.70	25.57	25.49	23.84	28.90	28.27	27.30	27.01	26.35	26.06	27.23	25.97	25.70
MnO	0.06	0.11	0.11	0.33	0.31	0.03	0.06	0.09	0.05	0.09	0.18	0.01	0.06	0.11
PbO	0.00	0.08	0.00	0.00	0.12	0.09	0.06	0.00	0.00	0.09	0.05	0.00	0.00	0.08
Na_2O	1.33	1.38	1.42	0.46	0.47	0.02	0.05	0.07	0.09	0.23	0.40	0.01	1.33	1.38
K_2O	0.01	0.02	0.05	0.07	0.14	0.07	0.19	0.50	0.24	0.02	0.03	0.02	0.01	0.02
F	0.52	0.39	0.35	1.68	1.53	2.37	2.26	1.60	0.64	0.84	0.65	1.28	0.52	0.39
Cl	0.00	0.00	0.00	0.14	0.07	0.02	0.09	0.06	0.02	0.09	0.08	0.01	0.00	0.00
O=F,Cl	-0.22	-0.17	-0.15	-0.74	-0.66	-1.00	-0.97	-0.69	-0.27	-0.37	-0.29	-0.54	-0.22	-0.17
Total	99.65	99.02	98.88	96.46	96.57	98.74	98.29	99.17	99.18	98.40	98.26	99.03	99.65	99.02

Sample	20TN7	20TN7	20TN7	20TN23	20TN23	20TN2	20TN2	20TN2	20TN2	20TN2	20TN2	20TN2	20TN7	20TN7
Analysis	102441	102452	102463	132571	132604	31711	31722	31733	31744	61886	102076	152181	102441	102452
P (*apfu*)	0.001	0.000	0.001	0.002	0.005	0.000	0.000	0.000	0.001	0.000	0.000	0.000	0.001	0.000
Nb	0.017	0.019	0.022	0.075	0.087	0.006	0.016	0.057	0.110	0.058	0.099	0.091	0.017	0.019
Si	1.004	1.011	1.014	1.030	1.023	1.027	1.029	1.041	1.025	1.017	1.023	1.012	1.004	1.011
Ti	0.962	0.950	0.936	0.572	0.596	0.600	0.627	0.647	0.633	0.775	0.704	0.691	0.962	0.950
Zr	0.001	0.001	0.001	0.008	0.007	0.000	0.001	0.001	0.001	0.001	0.002	0.001	0.001	0.001
Hf	0.000	0.000	0.001	0.001	0.001	0.001	0.001	0.000	0.000	0.000	0.001	0.000	0.000	0.000
Th	0.000	0.000	0.000	0.003	0.010	0.000	0.000	0.000	0.000	0.001	0.000	0.001	0.000	0.000
U	0.000	0.000	0.000	0.001	0.000	0.000	0.000	0.001	0.000	0.000	0.000	0.000	0.000	0.000
Al	0.005	0.004	0.004	0.268	0.257	0.354	0.298	0.184	0.143	0.097	0.096	0.144	0.005	0.004
Fe^{3+}	0.010	0.013	0.015	0.055	0.069	0.012	0.025	0.069	0.093	0.074	0.084	0.076	0.010	0.013
Y	0.000	0.000	0.000	0.000	0.000	0.001	0.001	0.001	0.001	0.001	0.001	0.001	0.000	0.000
La	0.000	0.000	0.000	0.001	0.001	0.000	0.000	0.000	0.000	0.000	0.000	0.000	0.000	0.000
Ce	0.001	0.001	0.002	0.003	0.003	0.001	0.001	0.001	0.001	0.003	0.003	0.001	0.001	0.001
Pr	0.000	0.000	0.000	0.000	0.000	0.000	0.000	0.000	0.000	0.000	0.000	0.000	0.000	0.000
Nd	0.000	0.000	0.001	0.001	0.000	0.000	0.000	0.000	0.000	0.000	0.001	0.000	0.000	0.000
Sm	0.000	0.000	0.000	0.000	0.000	0.000	0.000	0.001	0.000	0.001	0.000	0.000	0.000	0.000
Eu	0.000	0.000	0.000	0.000	0.000	0.000	0.000	0.000	0.000	0.000	0.000	0.000	0.000	0.000
Gd	0.001	0.000	0.000	0.000	0.001	0.000	0.000	0.000	0.000	0.000	0.000	0.000	0.001	0.000
Tb	0.000	0.001	0.000	0.000	0.002	0.001	0.000	0.000	0.000	0.001	0.001	0.000	0.000	0.001
Dy	0.001	0.000	0.000	0.001	0.002	0.001	0.001	0.000	0.000	0.000	0.001	0.000	0.001	0.000
Ho	0.000	0.000	0.000	0.001	0.001	0.000	0.001	0.000	0.001	0.000	0.001	0.001	0.000	0.000
Er	0.000	0.000	0.001	0.000	0.001	0.001	0.001	0.001	0.001	0.000	0.001	0.000	0.000	0.000
Tm	0.000	0.000	0.001	0.001	0.001	0.000	0.000	0.001	0.001	0.001	0.000	0.000	0.000	0.000
Yb	0.000	0.000	0.000	0.000	0.001	0.002	0.001	0.001	0.001	0.000	0.001	0.001	0.000	0.000
Lu	0.000	0.000	0.000	0.001	0.001	0.001	0.000	0.000	0.001	0.001	0.000	0.000	0.000	0.000
Mg	0.000	0.001	0.001	0.007	0.008	0.001	0.001	0.004	0.001	0.002	0.001	0.003	0.000	0.001
Ca	0.910	0.905	0.903	0.923	0.877	0.988	0.981	0.960	0.967	0.949	0.946	0.976	0.910	0.905
Mn	0.002	0.003	0.003	0.009	0.009	0.001	0.002	0.003	0.001	0.003	0.005	0.000	0.002	0.003
Pb	0.000	0.001	0.000	0.000	0.001	0.001	0.001	0.000	0.000	0.001	0.000	0.000	0.000	0.001
Na	0.084	0.088	0.091	0.030	0.031	0.001	0.003	0.004	0.006	0.015	0.026	0.001	0.084	0.088
K	0.001	0.001	0.002	0.003	0.006	0.003	0.008	0.021	0.010	0.001	0.001	0.001	0.001	0.001
F	0.053	0.041	0.037	0.179	0.166	0.240	0.232	0.166	0.067	0.089	0.069	0.135	0.053	0.041
Cl	0.000	0.000	0.000	0.008	0.004	0.001	0.005	0.003	0.001	0.005	0.005	0.000	0.000	0.000
O	4.935	4.936	4.934	4.789	4.840	4.701	4.725	4.809	4.905	4.916	4.922	4.885	4.935	4.936
Sum	7.988	7.977	7.971	7.976	8.010	7.941	7.961	7.978	7.974	8.010	7.996	8.020	7.988	7.977

Table B.8. Composition of zircon from various rock types across the 2020 Corundum Dome and Pyrochlore Dome sampling area.

Sample	20TN55A	20TN55A	20TN55A	20TN55A	20TN55A	20TN15A	20TN15A	20TN3-2	20TN12	20TN15B	20TN15B	20TN15B	20TN2
Analysis	14771	14782	14793	14804	14815	372361	372372	532933	251991	41621	91731	91742	51771
P_2O_5 (wt. %)	–	–	–	–	–	0.05	0.07	0.03	0.07	0.04	0.02	0.04	0.04
Nb_2O_5	–	–	–	–	–	0.09	0.07	0.09	0.20	0.07	0.05	0.06	0.06
SiO_2	33.57	33.24	33.11	33.00	33.57	32.84	33.00	33.30	34.76	39.33	38.92	38.66	33.61
TiO_2	–	–	–	–	–	0.00	0.00	0.01	0.08	0.01	0.04	0.08	0.03
ZrO_2	63.12	63.68	63.23	61.96	63.61	62.41	63.63	62.37	62.21	61.92	63.42	63.04	63.56
HfO_2	0.94	0.93	1.00	0.97	0.94	0.66	0.67	0.93	1.25	1.05	0.83	0.74	0.51
ThO_2	–	–	–	–	–	0.50	0.09	0.00	0.13	0.38	0.26	0.32	0.06
UO_2	–	–	–	–	–	0.13	0.03	0.06	0.03	0.09	0.05	0.19	0.02
Al_2O_3	–	–	–	–	–	0.02	0.02	0.01	0.00	0.30	0.02	0.02	0.01
Fe_2O_3*	–	–	–	–	–	0.10	0.07	0.50	0.10	0.21	0.28	0.32	0.03
Y_2O_3	–	–	–	–	–	0.04	0.01	0.70	0.09	0.13	0.32	0.21	0.47
La_2O_3	–	–	–	–	–	0.02	0.00	0.00	0.02	0.06	0.00	0.02	0.02
Ce_2O_3	–	–	–	–	–	0.67	0.11	0.06	0.79	0.06	0.00	0.04	0.10
Pr_2O_3	–	–	–	–	–	0.06	0.03	0.02	0.04	0.03	0.00	0.02	0.00
Nd_2O_3	–	–	–	–	–	0.22	0.05	0.00	0.21	0.05	0.03	0.02	0.05
Sm_2O_3	–	–	–	–	–	0.00	0.00	0.02	0.09	0.07	0.03	0.04	0.00
Eu_2O_3	–	–	–	–	–	0.03	0.01	0.03	0.03	0.08	0.03	0.04	0.05
Gd_2O_3	–	–	–	–	–	0.03	0.04	0.06	0.10	0.09	0.02	0.04	0.02
Tb_2O_3	–	–	–	–	–	0.03	0.08	0.02	0.07	0.08	0.09	0.00	0.00
Dy_2O_3	–	–	–	–	–	0.01	0.00	0.09	0.04	0.09	0.02	0.00	0.07
Ho_2O_3	–	–	–	–	–	0.06	0.06	0.14	0.06	0.03	0.10	0.10	0.09
Er_2O_3	–	–	–	–	–	0.06	0.03	0.17	0.03	0.05	0.15	0.15	0.12
Tm_2O_3	–	–	–	–	–	0.00	0.11	0.05	0.01	0.06	0.20	0.06	0.16
Yb_2O_3	–	–	–	–	–	0.00	0.03	0.17	0.01	0.07	0.13	0.06	0.01
Lu_2O_3	–	–	–	–	–	0.00	0.00	0.00	0.00	0.00	0.00	0.00	0.00
MgO	0.01	0.00	0.00	0.00	0.01	0.00	0.00	0.00	0.01	0.01	0.00	0.00	0.00
CaO	–	–	–	–	–	0.02	0.00	0.08	0.02	0.01	0.02	0.05	0.03
MnO	–	–	–	–	–	0.00	0.01	0.01	0.02	0.04	0.05	0.02	0.00
PbO	–	–	–	–	–	0.07	0.02	0.00	0.00	0.00	0.02	0.00	0.06
Na_2O	–	–	–	–	–	0.01	0.02	0.01	0.03	0.13	0.02	0.02	0.02
K_2O	–	–	–	–	–	0.02	0.01	0.01	0.00	0.16	0.02	0.02	0.01
F	–	–	–	–	–	0.09	0.05	0.06	0.10	0.10	0.07	0.09	0.08
Cl	–	–	–	–	–	0.00	0.01	0.00	0.00	0.03	0.01	0.00	0.01
O=F,Cl	–	–	–	–	–	-0.04	-0.02	-0.03	-0.04	-0.05	-0.03	-0.04	-0.03
Total	97.64	97.85	97.34	95.93	98.13	98.22	98.30	98.97	100.56	104.78	105.18	104.44	99.25

Sample	20TN55A	20TN55A	20TN55A	20TN55A	20TN55A	20TN15A	20TN15A	20TN3-2	20TN12	20TN15B	20TN15B	20TN15B	20TN2
Analysis	14771	14782	14793	14804	14815	372361	372372	532933	251991	41621	91731	91742	51771
P (*apfu*)	–	–	–	–	–	0.001	0.002	0.001	0.002	0.001	0.000	0.001	0.001
Nb	–	–	–	–	–	0.001	0.001	0.001	0.003	0.001	0.001	0.001	0.001
Si	1.039	1.030	1.031	1.040	1.035	1.025	1.023	1.027	1.050	1.112	1.101	1.100	1.031
Ti	–	–	–	–	–	0.000	0.000	0.000	0.002	0.000	0.001	0.002	0.001
Zr	0.953	0.962	0.960	0.952	0.956	0.950	0.962	0.938	0.917	0.854	0.875	0.875	0.950
Hf	0.008	0.008	0.009	0.009	0.008	0.006	0.006	0.008	0.011	0.009	0.007	0.006	0.004
Th	–	–	–	–	–	0.004	0.001	0.000	0.001	0.002	0.002	0.002	0.000
U	–	–	–	–	–	0.001	0.000	0.000	0.000	0.001	0.000	0.001	0.000
Al	–	–	–	–	–	0.001	0.001	0.000	0.000	0.010	0.001	0.001	0.000
Fe^{3+}	–	–	–	–	–	0.002	0.002	0.012	0.002	0.004	0.006	0.007	0.001
Y	–	–	–	–	–	0.001	0.000	0.012	0.001	0.002	0.005	0.003	0.008
La	–	–	–	–	–	0.000	0.000	0.000	0.000	0.001	0.000	0.000	0.000
Ce	–	–	–	–	–	0.008	0.001	0.001	0.009	0.001	0.000	0.000	0.001
Pr	–	–	–	–	–	0.001	0.000	0.000	0.000	0.000	0.000	0.000	0.000
Nd	–	–	–	–	–	0.002	0.001	0.000	0.002	0.000	0.000	0.000	0.000
Sm	–	–	–	–	–	0.000	0.000	0.000	0.001	0.001	0.000	0.000	0.000
Eu	–	–	–	–	–	0.000	0.000	0.000	0.000	0.001	0.000	0.000	0.001
Gd	–	–	–	–	–	0.000	0.000	0.001	0.001	0.001	0.000	0.000	0.000
Tb	–	–	–	–	–	0.000	0.001	0.000	0.001	0.001	0.001	0.000	0.000
Dy	–	–	–	–	–	0.000	0.000	0.001	0.000	0.001	0.000	0.000	0.001
Ho	–	–	–	–	–	0.001	0.001	0.001	0.001	0.000	0.001	0.001	0.001
Er	–	–	–	–	–	0.001	0.000	0.002	0.000	0.000	0.001	0.001	0.001
Tm	–	–	–	–	–	0.000	0.001	0.000	0.000	0.001	0.002	0.001	0.002
Yb	–	–	–	–	–	0.000	0.000	0.002	0.000	0.001	0.001	0.001	0.000
Lu	–	–	–	–	–	0.000	0.000	0.000	0.000	0.000	0.000	0.000	0.000
Mg	0.000	0.000	0.000	0.000	0.000	0.000	0.000	0.000	0.000	0.000	0.000	0.000	0.000
Ca	–	–	–	–	–	0.001	0.000	0.003	0.001	0.000	0.001	0.001	0.001
Mn	–	–	–	–	–	0.000	0.000	0.000	0.001	0.001	0.001	0.000	0.000
Pb	–	–	–	–	–	0.001	0.000	0.000	0.000	0.000	0.000	0.000	0.001
Na	–	–	–	–	–	0.001	0.001	0.001	0.002	0.007	0.001	0.001	0.001
K	–	–	–	–	–	0.001	0.000	0.000	0.000	0.006	0.001	0.001	0.000
F	–	–	–	–	–	0.009	0.005	0.006	0.009	0.009	0.007	0.008	0.008
Cl	–	–	–	–	–	0.000	0.001	0.000	0.000	0.001	0.000	0.000	0.000
Cation Sum	2.000	2.000	2.000	2.000	2.000	2.008	2.004	2.011	2.008	2.019	2.008	2.008	2.007

Note: Compositions were recalculated on the basis of 4 O *apfu*. * Determined by stoichiometry using Droop (1987) calculation method.

Table B.8. (Continued) Composition of zircon from various rock types across the 2020 Corundum Dome and Pyrochlore Dome sampling area.

Sample	20TN2	20TN2	20TN2	20TN2	20TN2	20TN2	20TN2	20TN2	20TN2	20TN4D	20TN4D
Analysis	51782	51793	51804	51815	51826	122091	122102	122113	122124	222542	222553
P_2O_5 (wt. %)	0.07	0.01	0.04	0.02	0.13	0.04	0.00	0.03	0.06	0.03	0.05
Nb_2O_5	0.10	0.03	0.12	0.05	0.09	0.10	0.04	0.06	0.07	0.27	3.14
SiO_2	33.71	33.51	32.98	33.58	32.78	33.42	33.40	33.54	33.45	33.48	31.20
TiO_2	0.00	0.05	0.00	0.04	0.03	0.02	0.00	0.01	0.03	0.05	0.00
ZrO_2	63.55	62.80	60.52	63.35	60.70	63.08	62.24	62.45	61.84	52.37	58.37
HfO_2	0.63	0.83	0.95	0.47	0.74	0.40	0.79	0.79	0.60	0.86	0.86
ThO_2	0.11	0.06	1.01	0.04	1.13	0.19	0.15	0.00	0.37	0.20	0.21
UO_2	0.04	0.07	0.05	0.08	0.00	0.07	0.06	0.04	0.00	0.47	0.35
Al_2O_3	0.02	0.01	0.02	0.01	0.01	0.01	0.00	0.00	0.05	1.84	0.10
Fe_2O_3*	0.01	0.04	0.29	0.03	0.18	0.05	0.08	0.06	0.09	0.65	0.26
Y_2O_3	0.50	0.36	0.83	0.48	1.39	0.37	0.56	1.11	0.94	0.39	0.44
La_2O_3	0.00	0.00	0.00	0.02	0.00	0.03	0.00	0.01	0.00	0.02	0.02
Ce_2O_3	0.04	0.20	0.04	0.11	0.09	0.10	0.12	0.05	0.09	0.10	0.13
Pr_2O_3	0.02	0.01	0.00	0.03	0.04	0.07	0.06	0.03	0.00	0.04	0.04
Nd_2O_3	0.02	0.04	0.00	0.02	0.06	0.01	0.08	0.03	0.03	0.01	0.03
Sm_2O_3	0.04	0.02	0.00	0.06	0.09	0.00	0.00	0.00	0.06	0.02	0.04
Eu_2O_3	0.02	0.03	0.03	0.01	0.01	0.00	0.04	0.03	0.02	0.04	0.01
Gd_2O_3	0.06	0.00	0.06	0.08	0.12	0.04	0.00	0.05	0.10	0.04	0.05
Tb_2O_3	0.02	0.04	0.04	0.08	0.08	0.01	0.08	0.01	0.08	0.00	0.04
Dy_2O_3	0.06	0.09	0.15	0.10	0.21	0.02	0.09	0.15	0.18	0.14	0.08
Ho_2O_3	0.07	0.11	0.00	0.09	0.11	0.08	0.05	0.14	0.13	0.10	0.00
Er_2O_3	0.10	0.14	0.05	0.05	0.15	0.15	0.16	0.16	0.20	0.11	0.10
Tm_2O_3	0.03	0.02	0.07	0.03	0.00	0.00	0.03	0.09	0.08	0.07	0.06
Yb_2O_3	0.00	0.06	0.10	0.16	0.10	0.08	0.00	0.12	0.06	0.18	0.11
Lu_2O_3	0.00	0.00	0.00	0.00	0.00	0.00	0.00	0.00	0.00	0.00	0.00
MgO	0.00	0.00	0.00	0.00	0.00	0.00	0.00	0.00	0.00	0.03	0.01
CaO	0.04	0.06	0.15	0.05	0.09	0.07	0.05	0.05	0.05	0.10	0.58
MnO	0.00	0.02	0.05	0.02	0.05	0.01	0.01	0.00	0.01	0.04	0.05
PbO	0.01	0.00	0.08	0.00	0.10	0.04	0.00	0.00	0.00	0.08	0.04
Na_2O	0.02	0.02	0.03	0.03	0.03	0.01	0.01	0.01	0.01	0.05	0.04
K_2O	0.00	0.00	0.04	0.02	0.01	0.01	0.01	0.02	0.00	1.50	0.04
F	0.09	0.01	0.09	0.10	0.05	0.03	0.05	0.08	0.11	0.10	0.04
Cl	0.00	0.00	0.05	0.02	0.00	0.00	0.00	0.00	0.00	0.17	0.08
O=F,Cl	-0.04	0.00	-0.05	-0.05	-0.02	-0.01	-0.02	-0.03	-0.05	-0.08	-0.04
Total	99.36	98.62	97.81	99.18	98.54	98.54	98.16	99.11	98.65	93.46	96.55

Sample	20TN2	20TN2	20TN2	20TN2	20TN2	20TN2	20TN2	20TN2	20TN2	20TN4D	20TN4D
Analysis	51782	51793	51804	51815	51826	122091	122102	122113	122124	222542	222553
P (*apfu*)	0.002	0.000	0.001	0.000	0.003	0.001	0.000	0.001	0.001	0.001	0.001
Nb	0.001	0.000	0.002	0.001	0.001	0.001	0.001	0.001	0.001	0.004	0.045
Si	1.032	1.033	1.034	1.031	1.024	1.031	1.036	1.033	1.035	1.072	0.994
Ti	0.000	0.001	0.000	0.001	0.001	0.000	0.000	0.000	0.001	0.001	0.000
Zr	0.948	0.944	0.925	0.949	0.924	0.949	0.941	0.937	0.933	0.818	0.907
Hf	0.006	0.007	0.008	0.004	0.007	0.004	0.007	0.007	0.005	0.008	0.008
Th	0.001	0.000	0.007	0.000	0.008	0.001	0.001	0.000	0.003	0.001	0.002
U	0.000	0.001	0.000	0.001	0.000	0.000	0.000	0.000	0.000	0.003	0.002
Al	0.001	0.000	0.001	0.000	0.000	0.000	0.000	0.000	0.002	0.069	0.004
Fe^{3+}	0.000	0.001	0.007	0.001	0.004	0.001	0.002	0.001	0.002	0.016	0.006
Y	0.008	0.006	0.014	0.008	0.023	0.006	0.009	0.018	0.015	0.007	0.008
La	0.000	0.000	0.000	0.000	0.000	0.000	0.000	0.000	0.000	0.000	0.000
Ce	0.000	0.002	0.000	0.001	0.001	0.001	0.001	0.001	0.001	0.001	0.001
Pr	0.000	0.000	0.000	0.000	0.000	0.001	0.001	0.000	0.000	0.000	0.000
Nd	0.000	0.000	0.000	0.000	0.001	0.000	0.001	0.000	0.000	0.000	0.000
Sm	0.000	0.000	0.000	0.001	0.001	0.000	0.000	0.000	0.001	0.000	0.000
Eu	0.000	0.000	0.000	0.000	0.000	0.000	0.000	0.000	0.000	0.000	0.000
Gd	0.001	0.000	0.001	0.001	0.001	0.000	0.000	0.000	0.001	0.000	0.001
Tb	0.000	0.000	0.000	0.001	0.001	0.000	0.001	0.000	0.001	0.000	0.000
Dy	0.001	0.001	0.002	0.001	0.002	0.000	0.001	0.001	0.002	0.001	0.001
Ho	0.001	0.001	0.000	0.001	0.001	0.001	0.000	0.001	0.001	0.001	0.000
Er	0.001	0.001	0.001	0.000	0.001	0.001	0.002	0.002	0.002	0.001	0.001
Tm	0.000	0.000	0.001	0.000	0.000	0.000	0.000	0.001	0.001	0.001	0.001
Yb	0.000	0.001	0.001	0.002	0.001	0.001	0.000	0.001	0.001	0.002	0.001
Lu	0.000	0.000	0.000	0.000	0.000	0.000	0.000	0.000	0.000	0.000	0.000
Mg	0.000	0.000	0.000	0.000	0.000	0.000	0.000	0.000	0.000	0.002	0.001
Ca	0.001	0.002	0.005	0.002	0.003	0.002	0.002	0.002	0.002	0.003	0.020
Mn	0.000	0.000	0.001	0.001	0.001	0.000	0.000	0.000	0.000	0.001	0.001
Pb	0.000	0.000	0.001	0.000	0.001	0.000	0.000	0.000	0.000	0.001	0.000
Na	0.001	0.001	0.002	0.002	0.002	0.001	0.001	0.001	0.000	0.003	0.002
K	0.000	0.000	0.002	0.001	0.000	0.000	0.000	0.001	0.000	0.061	0.002
F	0.009	0.001	0.009	0.010	0.004	0.003	0.005	0.008	0.011	0.010	0.004
Cl	0.000	0.000	0.003	0.001	0.000	0.000	0.000	0.000	0.000	0.009	0.005
Cation Sum	2.006	2.006	2.015	2.010	2.014	2.006	2.008	2.011	2.011	2.080	2.011

Table B.9. Composition of thorite from various rock types across the 2020 Corundum Dome and Pyrochlore Dome sampling area.

Sample	20TN3-2	20TN3-2	20TN3-2	20TN3-2	20TN3-2	20TN12	20TN7	20TN7	20TN7	20TN7	20TN7	20TN7	20TN7
Analysis	312293	312304	522881	522892	522903	191911	42211	42222	42233	42244	72351	72362	112471
P_2O_5 (wt. %)	0.57	0.05	0.00	0.06	0.28	0.32	1.35	1.66	1.46	1.19	1.47	1.42	0.48
Nb_2O_5	0.06	0.02	0.05	0.09	0.08	0.00	4.79	1.07	0.77	0.62	0.58	0.47	1.42
SiO_2	19.06	19.44	18.20	17.97	17.67	18.14	15.13	16.74	15.72	15.45	15.36	14.82	15.00
TiO_2	0.00	0.00	0.02	0.05	0.11	0.06	2.07	3.26	2.38	1.94	1.87	1.65	5.74
ZrO_2	0.60	0.16	0.11	0.14	0.20	0.24	0.24	0.36	0.21	0.16	0.22	0.19	0.34
HfO_2	0.02	0.02	0.03	0.00	0.07	0.16	0.06	0.20	0.28	0.03	0.00	0.14	0.00
ThO_2	62.71	67.01	65.87	70.11	66.40	65.98	62.07	64.32	67.78	66.76	68.17	68.83	60.57
UO_2	0.65	0.71	0.77	0.82	0.55	0.92	0.83	0.71	0.80	0.77	0.91	0.83	0.69
Al_2O_3	0.06	0.28	0.05	0.02	0.05	0.08	0.80	0.85	0.81	0.89	0.79	0.80	0.99
Fe_2O_3*	0.71	1.36	1.85	1.09	2.64	1.52	2.16	2.29	2.33	1.80	2.05	1.49	2.28
Y_2O_3	1.57	0.35	0.63	0.60	0.89	0.68	0.86	0.80	0.97	0.76	0.76	0.63	0.65
La_2O_3	0.23	0.20	0.08	0.03	0.11	0.00	0.10	0.06	0.02	0.04	0.00	0.01	0.04
Ce_2O_3	1.00	0.54	0.32	0.32	0.34	0.20	0.83	0.63	0.74	0.59	0.57	0.43	0.50
Pr_2O_3	0.39	0.08	0.06	0.06	0.07	0.02	0.09	0.05	0.05	0.07	0.08	0.11	0.04
Nd_2O_3	0.70	0.24	0.18	0.13	0.21	0.18	0.28	0.28	0.29	0.21	0.24	0.17	0.22
Sm_2O_3	0.16	0.03	0.08	0.13	0.08	0.25	0.13	0.13	0.08	0.08	0.14	0.02	0.00
Eu_2O_3	0.04	0.02	0.01	0.01	0.02	0.04	0.02	0.05	0.03	0.05	0.05	0.04	0.01
Gd_2O_3	0.30	0.02	0.14	0.06	0.14	0.21	0.13	0.15	0.18	0.02	0.07	0.06	0.02
Tb_2O_3	0.00	0.06	0.02	0.02	0.14	0.16	0.03	0.00	0.06	0.01	0.07	0.11	0.00
Dy_2O_3	0.24	0.23	0.17	0.18	0.22	0.40	0.10	0.23	0.14	0.14	0.07	0.13	0.08
Ho_2O_3	0.14	0.17	0.09	0.12	0.12	0.14	0.09	0.22	0.18	0.03	0.22	0.11	0.05
Er_2O_3	0.16	0.03	0.06	0.08	0.01	0.07	0.11	0.17	0.15	0.03	0.06	0.12	0.06
Tm_2O_3	0.25	0.09	0.09	0.12	0.01	0.03	0.12	0.19	0.00	0.00	0.09	0.00	0.13
Yb_2O_3	0.02	0.09	0.00	0.00	0.00	0.02	0.00	0.14	0.23	0.00	0.08	0.00	0.19
Lu_2O_3	0.09	0.07	0.00	0.02	0.06	0.00	0.00	0.01	0.06	0.00	0.04	0.08	0.06
MgO	0.00	0.05	0.03	0.00	0.00	0.07	0.05	0.05	0.01	0.03	0.01	0.02	0.03
CaO	0.85	0.83	1.87	0.54	0.44	1.38	1.01	1.78	0.46	0.63	0.43	0.52	1.51
MnO	0.06	0.07	0.03	0.09	0.07	0.55	0.06	0.08	0.02	0.02	0.03	0.00	0.03
PbO	0.85	0.74	0.30	0.65	0.88	0.90	0.45	0.22	0.12	0.13	0.23	0.12	0.31
Na_2O	0.01	0.00	0.01	0.01	0.01	0.04	0.06	0.11	0.05	0.08	0.02	0.03	0.16
K_2O	0.04	0.06	0.04	0.06	0.04	0.10	0.10	0.10	0.09	0.09	0.07	0.08	0.08
F	0.23	0.41	1.19	1.00	0.65	0.70	3.00	2.79	3.38	3.51	3.44	3.34	3.60
Cl	0.04	0.05	0.00	0.00	0.00	0.00	0.00	0.01	0.01	0.00	0.01	0.00	0.00
O=F,Cl	-0.10	-0.18	-0.50	-0.42	-0.28	-0.30	-1.26	-1.18	-1.43	-1.48	-1.45	-1.41	-1.51
Total	91.70	93.30	91.82	94.19	92.28	93.27	95.86	98.56	98.45	94.64	96.76	95.37	93.75

Sample	20TN3-2	20TN3-2	20TN3-2	20TN3-2	20TN3-2	20TN12	20TN7	20TN7	20TN7	20TN7	20TN7	20TN7	20TN7
Analysis	312293	312304	522881	522892	522903	191911	42211	42222	42233	42244	72351	72362	112471
P (*apfu*)	0.026	0.002	0.000	0.003	0.013	0.015	0.063	0.073	0.069	0.059	0.072	0.072	0.023
Nb	0.001	0.001	0.001	0.002	0.002	0.000	0.119	0.025	0.019	0.016	0.015	0.013	0.036
Si	1.034	1.053	1.032	1.022	0.993	1.003	0.831	0.870	0.876	0.907	0.886	0.880	0.841
Ti	0.000	0.000	0.001	0.002	0.005	0.002	0.085	0.127	0.100	0.086	0.081	0.074	0.242
Zr	0.016	0.004	0.003	0.004	0.006	0.006	0.007	0.009	0.006	0.004	0.006	0.005	0.009
Hf	0.000	0.000	0.000	0.000	0.001	0.003	0.001	0.003	0.004	0.001	0.000	0.002	0.000
Th	0.774	0.826	0.850	0.907	0.849	0.830	0.776	0.761	0.859	0.892	0.895	0.930	0.773
U	0.008	0.009	0.010	0.010	0.007	0.011	0.010	0.008	0.010	0.010	0.012	0.011	0.009
Al	0.004	0.018	0.003	0.002	0.003	0.005	0.052	0.052	0.053	0.062	0.054	0.056	0.066
Fe^{3+}	0.029	0.056	0.079	0.047	0.112	0.063	0.089	0.090	0.098	0.079	0.089	0.067	0.096
Y	0.045	0.010	0.019	0.018	0.027	0.020	0.025	0.022	0.029	0.024	0.023	0.020	0.019
La	0.005	0.004	0.002	0.001	0.002	0.000	0.002	0.001	0.000	0.001	0.000	0.000	0.001
Ce	0.020	0.011	0.007	0.007	0.007	0.004	0.017	0.012	0.015	0.013	0.012	0.009	0.010
Pr	0.008	0.001	0.001	0.001	0.001	0.000	0.002	0.001	0.001	0.001	0.002	0.002	0.001
Nd	0.014	0.005	0.004	0.003	0.004	0.004	0.006	0.005	0.006	0.004	0.005	0.004	0.004
Sm	0.003	0.001	0.002	0.003	0.002	0.005	0.002	0.002	0.001	0.002	0.003	0.000	0.000
Eu	0.001	0.000	0.000	0.000	0.000	0.001	0.000	0.001	0.001	0.001	0.001	0.001	0.000
Gd	0.005	0.000	0.003	0.001	0.003	0.004	0.002	0.003	0.003	0.000	0.001	0.001	0.000
Tb	0.000	0.001	0.000	0.000	0.003	0.003	0.000	0.000	0.001	0.000	0.001	0.002	0.000
Dy	0.004	0.004	0.003	0.003	0.004	0.007	0.002	0.004	0.003	0.003	0.001	0.003	0.001
Ho	0.002	0.003	0.002	0.002	0.002	0.002	0.002	0.004	0.003	0.001	0.004	0.002	0.001
Er	0.003	0.001	0.001	0.001	0.000	0.001	0.002	0.003	0.003	0.001	0.001	0.002	0.001
Tm	0.004	0.001	0.002	0.002	0.000	0.001	0.002	0.003	0.000	0.000	0.002	0.000	0.002
Yb	0.000	0.002	0.000	0.000	0.000	0.000	0.000	0.002	0.004	0.000	0.001	0.000	0.003
Lu	0.002	0.001	0.000	0.000	0.001	0.000	0.000	0.000	0.001	0.000	0.001	0.001	0.001
Mg	0.000	0.004	0.002	0.000	0.000	0.006	0.005	0.004	0.001	0.003	0.001	0.001	0.003
Ca	0.049	0.048	0.113	0.033	0.026	0.081	0.060	0.099	0.027	0.039	0.027	0.033	0.091
Mn	0.003	0.003	0.002	0.005	0.003	0.026	0.003	0.003	0.001	0.001	0.002	0.000	0.001
Pb	0.012	0.011	0.005	0.010	0.013	0.013	0.007	0.003	0.002	0.002	0.004	0.002	0.005
Na	0.001	0.000	0.001	0.001	0.001	0.004	0.007	0.011	0.005	0.009	0.002	0.004	0.017
K	0.003	0.004	0.003	0.004	0.003	0.007	0.007	0.007	0.007	0.007	0.005	0.006	0.006
F	0.039	0.070	0.213	0.180	0.116	0.123	0.520	0.458	0.596	0.651	0.628	0.627	0.638
Cl	0.004	0.004	0.000	0.000	0.000	0.000	0.000	0.001	0.001	0.000	0.001	0.000	0.000
Cation Sum	2.076	2.084	2.148	2.094	2.093	2.129	2.183	2.210	2.207	2.226	2.208	2.204	2.264

Note: Compositions were recalculated on the basis of 4 O *apfu*. * Determined by stoichiometry using Droop (1987) calculation method.

Table B.9. (Continued) Composition of thorite from various rock types across the 2020 Corundum Dome and Pyrochlore Dome sampling area.

Sample	20TN7	20TN7	20TN7	20TN15B	20TN15B	20TN15B	20TN15B	20TN15B	20TN2	20TN2	20TN2	20TN2	20TN2
Analysis	112482	112493	112504	42001	42012	42023	121834	121845	71891	71902	71913	71924	71935
P_2O_5 (wt. %)	0.67	0.56	0.69	2.53	1.28	1.16	0.30	0.13	0.10	0.08	0.10	0.00	0.04
Nb_2O_5	0.36	0.59	0.07	0.08	0.11	0.03	0.04	0.05	0.03	0.07	0.05	0.00	0.06
SiO_2	15.75	13.96	14.73	17.96	17.15	18.42	16.95	16.10	18.15	18.31	18.13	18.09	17.95
TiO_2	1.06	1.30	0.31	0.21	0.26	0.27	0.05	0.00	0.13	0.28	0.14	0.00	0.08
ZrO_2	0.38	0.47	0.24	0.62	0.12	0.08	0.10	0.01	0.17	0.10	0.26	0.02	0.13
HfO_2	0.03	0.20	0.00	0.12	0.18	0.05	0.16	0.00	0.10	0.07	0.17	0.13	0.32
ThO_2	68.08	67.78	70.77	59.43	56.93	54.33	72.99	77.80	65.96	65.07	65.99	68.40	66.73
UO_2	0.66	0.83	0.85	0.90	0.77	0.73	1.06	0.93	0.68	0.71	0.71	0.75	0.67
Al_2O_3	1.20	0.84	0.92	1.16	0.96	1.43	0.51	0.49	0.08	0.09	0.07	0.06	0.06
Fe_2O_3*	2.27	2.27	1.16	1.91	2.12	2.49	1.78	1.83	0.62	0.59	0.50	0.57	1.11
Y_2O_3	1.00	0.71	1.48	7.58	5.57	5.74	1.49	0.51	0.72	0.68	0.64	0.13	0.40
La_2O_3	0.14	0.07	0.14	0.23	0.79	1.45	0.02	0.00	0.14	0.15	0.12	0.00	0.00
Ce_2O_3	0.64	0.55	0.76	2.05	2.08	3.10	1.42	0.26	0.97	1.03	0.77	0.08	0.20
Pr_2O_3	0.04	0.09	0.09	0.14	0.19	0.28	0.05	0.04	0.11	0.17	0.15	0.03	0.00
Nd_2O_3	0.29	0.26	0.32	0.43	0.55	0.66	0.16	0.07	0.61	0.66	0.43	0.05	0.13
Sm_2O_3	0.09	0.15	0.20	0.29	0.30	0.27	0.10	0.11	0.14	0.10	0.10	0.03	0.08
Eu_2O_3	0.05	0.00	0.04	0.12	0.04	0.06	0.05	0.00	0.04	0.08	0.02	0.00	0.09
Gd_2O_3	0.17	0.08	0.12	0.54	0.39	0.51	0.19	0.09	0.25	0.27	0.26	0.10	0.22
Tb_2O_3	0.08	0.10	0.09	0.07	0.16	0.22	0.05	0.10	0.05	0.01	0.07	0.11	0.01
Dy_2O_3	0.18	0.13	0.07	0.99	0.70	0.74	0.32	0.08	0.22	0.18	0.23	0.05	0.13
Ho_2O_3	0.13	0.06	0.18	0.50	0.34	0.34	0.12	0.24	0.07	0.11	0.14	0.16	0.12
Er_2O_3	0.12	0.04	0.17	0.60	0.58	0.48	0.20	0.19	0.00	0.03	0.01	0.08	0.15
Tm_2O_3	0.00	0.00	0.13	0.23	0.12	0.07	0.29	0.10	0.08	0.06	0.11	0.11	0.15
Yb_2O_3	0.09	0.00	0.11	0.61	0.42	0.38	0.18	0.03	0.01	0.03	0.13	0.09	0.00
Lu_2O_3	0.00	0.00	0.00	0.18	0.02	0.16	0.00	0.01	0.04	0.00	0.20	0.01	0.01
MgO	0.09	0.00	0.00	0.14	0.13	0.55	0.03	0.06	0.00	0.00	0.00	0.04	0.06
CaO	0.36	0.24	0.29	0.57	0.73	0.58	0.30	0.34	0.79	1.03	0.91	1.75	1.50
MnO	0.00	0.06	0.05	0.02	0.05	0.06	0.09	0.09	0.09	0.07	0.07	0.14	0.11
PbO	0.24	0.05	0.12	0.21	0.48	0.46	0.20	0.33	0.52	0.52	0.57	2.09	1.77
Na_2O	0.09	0.07	0.03	0.15	0.06	0.09	0.01	0.03	0.00	0.00	0.02	0.01	0.02
K_2O	0.12	0.09	0.06	0.16	0.28	0.40	0.11	0.14	0.06	0.06	0.06	0.07	0.07
F	3.76	3.86	3.68	4.66	4.85	4.09	4.46	5.13	1.00	0.84	0.71	1.01	0.61
Cl	0.00	0.00	0.00	0.02	0.02	0.00	0.00	0.00	0.36	0.18	0.02	0.00	0.00
O=F,Cl	-1.58	-1.63	-1.55	-1.97	-2.05	-1.72	-1.88	-2.16	-0.50	-0.39	-0.30	-0.42	-0.26
Total	96.57	93.75	96.30	103.43	96.66	97.98	101.92	103.14	91.78	91.25	91.54	93.72	92.70

Sample	20TN7	20TN7	20TN7	20TN15B	20TN15B	20TN15B	20TN15B	20TN15B	20TN2	20TN2	20TN2	20TN2	20TN2
Analysis	112482	112493	112504	42001	42012	42023	121834	121845	71891	71902	71913	71924	71935
P (*apfu*)	0.033	0.030	0.036	0.111	0.062	0.053	0.015	0.007	0.005	0.004	0.005	0.000	0.002
Nb	0.009	0.017	0.002	0.002	0.003	0.001	0.001	0.001	0.001	0.002	0.001	0.000	0.001
Si	0.927	0.883	0.917	0.929	0.984	0.984	1.000	0.991	1.047	1.045	1.034	1.032	1.014
Ti	0.047	0.062	0.014	0.008	0.011	0.011	0.002	0.000	0.006	0.012	0.006	0.000	0.004
Zr	0.011	0.014	0.007	0.016	0.003	0.002	0.003	0.000	0.005	0.003	0.007	0.000	0.003
Hf	0.001	0.004	0.000	0.002	0.003	0.001	0.003	0.000	0.002	0.001	0.003	0.002	0.005
Th	0.912	0.975	1.002	0.699	0.744	0.660	0.980	1.089	0.866	0.845	0.856	0.888	0.857
U	0.009	0.012	0.012	0.010	0.010	0.009	0.014	0.013	0.009	0.009	0.009	0.010	0.008
Al	0.083	0.062	0.067	0.071	0.065	0.090	0.036	0.036	0.005	0.006	0.005	0.004	0.004
Fe^{3+}	0.101	0.108	0.054	0.074	0.092	0.100	0.079	0.085	0.027	0.025	0.021	0.025	0.047
Y	0.031	0.024	0.049	0.209	0.170	0.163	0.047	0.017	0.022	0.021	0.019	0.004	0.012
La	0.003	0.002	0.003	0.004	0.017	0.029	0.000	0.000	0.003	0.003	0.003	0.000	0.000
Ce	0.014	0.013	0.017	0.039	0.044	0.061	0.031	0.006	0.020	0.022	0.016	0.002	0.004
Pr	0.001	0.002	0.002	0.003	0.004	0.005	0.001	0.001	0.002	0.004	0.003	0.001	0.000
Nd	0.006	0.006	0.007	0.008	0.011	0.013	0.003	0.002	0.013	0.014	0.009	0.001	0.003
Sm	0.002	0.003	0.004	0.005	0.006	0.005	0.002	0.002	0.003	0.002	0.002	0.001	0.002
Eu	0.001	0.000	0.001	0.002	0.001	0.001	0.001	0.000	0.001	0.002	0.000	0.000	0.002
Gd	0.003	0.002	0.003	0.009	0.007	0.009	0.004	0.002	0.005	0.005	0.005	0.002	0.004
Tb	0.001	0.002	0.002	0.001	0.003	0.004	0.001	0.002	0.001	0.000	0.001	0.002	0.000
Dy	0.003	0.003	0.001	0.016	0.013	0.013	0.006	0.002	0.004	0.003	0.004	0.001	0.002
Ho	0.002	0.001	0.003	0.008	0.006	0.006	0.002	0.005	0.001	0.002	0.003	0.003	0.002
Er	0.002	0.001	0.003	0.010	0.010	0.008	0.004	0.004	0.000	0.001	0.000	0.001	0.003
Tm	0.000	0.000	0.003	0.004	0.002	0.001	0.005	0.002	0.001	0.001	0.002	0.002	0.003
Yb	0.002	0.000	0.002	0.010	0.007	0.006	0.003	0.001	0.000	0.001	0.002	0.002	0.000
Lu	0.000	0.000	0.000	0.003	0.000	0.003	0.000	0.000	0.001	0.000	0.003	0.000	0.000
Mg	0.008	0.000	0.000	0.011	0.011	0.044	0.003	0.006	0.000	0.000	0.000	0.003	0.005
Ca	0.023	0.016	0.019	0.031	0.045	0.033	0.019	0.023	0.049	0.063	0.055	0.107	0.091
Mn	0.000	0.003	0.003	0.001	0.003	0.003	0.004	0.004	0.004	0.003	0.004	0.007	0.005
Pb	0.004	0.001	0.002	0.003	0.007	0.007	0.003	0.005	0.008	0.008	0.009	0.032	0.027
Na	0.010	0.008	0.003	0.015	0.007	0.009	0.001	0.004	0.000	0.000	0.002	0.001	0.002
K	0.009	0.007	0.005	0.010	0.020	0.027	0.009	0.011	0.004	0.004	0.004	0.005	0.005
F	0.699	0.772	0.724	0.763	0.880	0.690	0.832	0.998	0.183	0.152	0.127	0.182	0.109
Cl	0.000	0.000	0.000	0.001	0.002	0.000	0.000	0.000	0.035	0.017	0.002	0.000	0.000
Cation Sum	2.260	2.260	2.245	2.324	2.372	2.359	2.282	2.319	2.114	2.109	2.094	2.137	2.117

Table B.10. Composition of apatite from various rock types across the 2020 Corundum Dome and Pyrochlore Dome sampling area.

Sample	20TN15A	20TN23	20TN23	20TN23	20TN23	20TN23	20TN23	20TN15B	20TN15B	20TN15B	20TN15B	20TN15B	20TN15B
Analysis	42-258-4	12-251-1	12-252-2	12-253-3	12-254-4	12-255-5	12-256-6	5-163-1	5-164-2	6-165-1	6-166-2	8-167-1	8-168-2
P_2O_5 (wt. %)	33.91	41.51	41.51	41.64	41.35	41.47	41.65	37.07	39.72	41.72	41.13	36.72	39.78
Nb_2O_5	0.01	0.00	0.02	0.04	0.01	0.02	0.00	0.03	0.01	0.00	0.03	0.01	0.04
SiO_2	0.05	0.13	0.11	0.11	0.14	0.11	0.20	2.98	1.69	0.51	0.65	4.09	3.89
TiO_2	0.00	0.06	0.06	0.00	0.05	0.00	0.07	0.02	0.01	0.00	0.00	0.00	0.04
ZrO_2	0.17	0.12	0.14	0.16	0.11	0.16	0.11	0.14	0.93	0.14	0.13	0.08	1.19
HfO_2	0.06	0.00	0.00	0.26	0.00	0.00	0.04	0.05	0.04	0.08	0.13	0.14	0.24
ThO_2	0.01	0.00	0.04	0.10	0.07	0.00	0.00	0.55	0.32	0.09	0.13	0.61	0.29
UO_2	0.04	0.00	0.00	0.01	0.02	0.01	0.05	0.07	0.05	0.06	0.00	0.06	0.04
Al_2O_3	0.00	0.01	0.01	0.01	0.02	0.01	0.04	0.07	0.05	0.03	0.03	0.42	0.07
Y_2O_3	0.09	0.03	0.02	0.03	0.02	0.03	0.02	0.46	0.16	0.02	0.06	0.52	0.17
La_2O_3	4.95	0.54	0.60	0.56	0.40	0.31	0.57	2.40	1.07	0.50	0.64	2.45	0.79
Ce_2O_3	6.45	0.27	0.23	0.24	0.18	0.11	0.40	2.51	0.98	0.45	0.61	2.44	0.78
Pr_2O_3	0.78	0.10	0.08	0.09	0.07	0.02	0.12	0.41	0.16	0.11	0.13	0.38	0.12
Nd_2O_3	1.06	0.06	0.04	0.05	0.02	0.00	0.08	0.46	0.12	0.10	0.11	0.39	0.12
Sm_2O_3	0.18	0.01	0.02	0.02	0.02	0.02	0.08	0.10	0.04	0.02	0.05	0.07	0.03
Eu_2O_3	0.00	0.01	0.02	0.05	0.00	0.01	0.03	0.03	0.02	0.03	0.04	0.01	0.05
Gd_2O_3	0.07	0.04	0.00	0.01	0.01	0.00	0.05	0.06	0.05	0.04	0.08	0.19	0.00
Tb_2O_3	0.05	0.02	0.00	0.03	0.00	0.00	0.08	0.00	0.03	0.06	0.00	0.13	0.00
Dy_2O_3	0.11	0.06	0.00	0.02	0.00	0.03	0.12	0.10	0.07	0.08	0.06	0.07	0.09
Ho_2O_3	0.03	0.00	0.01	0.03	0.05	0.04	0.03	0.15	0.07	0.01	0.06	0.15	0.05
Er_2O_3	0.02	0.05	0.01	0.11	0.02	0.00	0.00	0.13	0.00	0.02	0.06	0.05	0.08
Tm_2O_3	0.00	0.13	0.04	0.02	0.07	0.08	0.00	0.13	0.02	0.01	0.06	0.17	0.01
Yb_2O_3	0.07	0.01	0.05	0.04	0.04	0.08	0.00	0.13	0.00	0.06	0.07	0.04	0.11
Lu_2O_3	0.10	0.00	0.00	0.04	0.14	0.00	0.03	0.06	0.00	0.03	0.00	0.08	0.00
MgO	0.00	0.00	0.00	0.00	0.00	0.00	0.00	0.00	0.03	0.00	0.00	0.00	0.01
CaO	47.27	53.62	53.88	53.46	53.62	54.40	53.43	49.56	51.33	52.93	52.82	49.74	52.68
MnO	0.11	0.03	0.03	0.04	0.00	0.01	0.04	0.07	0.06	0.05	0.05	0.08	0.05
FeO	0.05	0.18	0.14	0.13	0.04	0.03	0.06	0.16	0.23	0.17	0.14	0.16	0.32
PbO	0.01	0.04	0.00	0.04	0.00	0.03	0.06	0.08	0.01	0.00	0.09	0.00	0.03
Na_2O	1.18	0.12	0.13	0.11	0.11	0.06	0.15	0.10	0.11	0.06	0.08	0.17	0.09
K_2O	0.00	0.04	0.01	0.02	0.01	0.01	0.02	0.22	0.03	0.08	0.05	0.40	0.03
F	4.20	4.49	4.44	4.47	4.36	4.19	4.46	4.04	4.06	4.36	4.31	3.07	2.71
Cl	0.02	0.00	0.01	0.02	0.00	0.00	0.00	0.00	0.01	0.00	0.01	0.00	0.00
O=F,Cl	-1.77	-1.89	-1.87	-1.89	-1.83	-1.76	-1.88	-1.70	-1.71	-1.83	-1.82	-1.29	-1.14
Total	99.29	99.79	99.78	100.05	99.09	99.49	100.13	100.64	99.78	100.00	99.99	101.62	102.76

Sample	20TN15A	20TN23	20TN23	20TN23	20TN23	20TN23	20TN23	20TN15B	20TN15B	20TN15B	20TN15B	20TN15B	20TN15B
Analysis	42-258-4	12-251-1	12-252-2	12-253-3	12-254-4	12-255-5	12-256-6	5-163-1	5-164-2	6-165-1	6-166-2	8-167-1	8-168-2
P (*apfu*)	2.638	2.998	2.992	3.009	3.000	2.986	3.004	2.755	2.908	3.017	2.983	2.677	2.798
Nb	0.000	0.000	0.001	0.002	0.000	0.001	0.000	0.001	0.000	0.000	0.001	0.000	0.002
Si	0.005	0.011	0.009	0.010	0.012	0.010	0.017	0.262	0.146	0.044	0.056	0.352	0.323
Ti	0.000	0.004	0.004	0.000	0.003	0.000	0.005	0.001	0.001	0.000	0.000	0.000	0.003
Zr	0.008	0.005	0.006	0.007	0.004	0.006	0.004	0.006	0.039	0.006	0.005	0.003	0.048
Hf	0.001	0.000	0.000	0.006	0.000	0.000	0.001	0.001	0.001	0.002	0.003	0.003	0.006
Th	0.000	0.000	0.001	0.002	0.001	0.000	0.000	0.011	0.006	0.002	0.003	0.012	0.005
U	0.001	0.000	0.000	0.000	0.000	0.000	0.001	0.001	0.001	0.001	0.000	0.001	0.001
Al	0.000	0.001	0.001	0.001	0.002	0.001	0.004	0.007	0.005	0.003	0.003	0.043	0.007
Y	0.005	0.001	0.001	0.001	0.001	0.001	0.001	0.022	0.007	0.001	0.003	0.024	0.007
La	0.168	0.017	0.019	0.017	0.013	0.010	0.018	0.078	0.034	0.016	0.020	0.078	0.024
Ce	0.217	0.008	0.007	0.008	0.006	0.003	0.013	0.081	0.031	0.014	0.019	0.077	0.024
Pr	0.026	0.003	0.003	0.003	0.002	0.001	0.004	0.013	0.005	0.003	0.004	0.012	0.004
Nd	0.035	0.002	0.001	0.002	0.001	0.000	0.002	0.014	0.004	0.003	0.003	0.012	0.004
Sm	0.006	0.000	0.000	0.000	0.000	0.001	0.002	0.003	0.001	0.001	0.001	0.002	0.001
Eu	0.000	0.000	0.001	0.001	0.000	0.000	0.001	0.001	0.001	0.001	0.001	0.000	0.001
Gd	0.002	0.001	0.000	0.000	0.000	0.000	0.001	0.002	0.001	0.001	0.002	0.006	0.000
Tb	0.002	0.001	0.000	0.001	0.000	0.000	0.002	0.000	0.001	0.002	0.000	0.004	0.000
Dy	0.003	0.002	0.000	0.001	0.000	0.001	0.003	0.003	0.002	0.002	0.002	0.002	0.002
Ho	0.001	0.000	0.000	0.001	0.001	0.001	0.001	0.004	0.002	0.000	0.002	0.004	0.001
Er	0.001	0.001	0.000	0.003	0.001	0.000	0.000	0.004	0.000	0.000	0.002	0.001	0.002
Tm	0.000	0.003	0.001	0.000	0.002	0.002	0.000	0.004	0.001	0.000	0.002	0.005	0.000
Yb	0.002	0.000	0.001	0.001	0.001	0.002	0.000	0.003	0.000	0.002	0.002	0.001	0.003
Lu	0.003	0.000	0.000	0.001	0.004	0.000	0.001	0.002	0.000	0.001	0.000	0.002	0.000
Mg	0.000	0.000	0.000	0.000	0.000	0.000	0.000	0.001	0.003	0.000	0.000	0.000	0.002
Ca	4.653	4.901	4.916	4.890	4.923	4.958	4.878	4.661	4.756	4.844	4.849	4.589	4.689
Mn	0.009	0.002	0.002	0.003	0.000	0.001	0.003	0.005	0.005	0.004	0.003	0.006	0.004
Fe^{2+}	0.004	0.013	0.010	0.009	0.003	0.002	0.004	0.012	0.016	0.012	0.010	0.012	0.022
Pb	0.000	0.001	0.000	0.001	0.000	0.001	0.001	0.002	0.000	0.000	0.002	0.000	0.001
Na	0.211	0.020	0.022	0.019	0.018	0.011	0.026	0.017	0.018	0.010	0.013	0.029	0.014
K	0.000	0.004	0.001	0.002	0.001	0.001	0.002	0.024	0.004	0.009	0.005	0.044	0.003
F	1.220	1.212	1.195	1.206	1.181	1.127	1.202	1.123	1.109	1.177	1.168	0.837	0.713
Cl	0.003	0.000	0.001	0.003	0.000	0.000	0.000	0.001	0.002	0.000	0.001	0.000	0.000
O^{2-}	11.490	11.920	11.917	11.947	11.939	11.939	11.947	11.954	12.038	12.007	11.983	12.069	12.260
Anion Sum	12.713	13.132	13.113	13.156	13.120	13.065	13.149	13.078	13.149	13.183	13.153	12.906	12.974

Note: Compositions were recalculated on the basis of the sum of 8 cation *apfu*.

Table B.10. (Continued) Composition of apatite from various rock types across the 2020 Corundum Dome and Pyrochlore Dome sampling area.

Sample	20TN15B	20TN15B	20TN25D	20TN25D	20TN25D	20TN25D	20TN25D	20TN25D	20TN25D	20TN25D	20TN57C-1	20TN57C-1	20TN57C-1
Analysis	8-169-3	8-170-4	14-187-1	14-188-2	14-189-3	14-190-4	14-191-5	14-192-6	14-193-7	14-194-8	20-222-1	20-223-2	20-224-3
P_2O_5 (wt. %)	40.47	40.75	39.83	42.19	40.41	40.12	41.84	39.79	40.75	40.00	39.14	38.98	39.69
Nb_2O_5	0.05	0.00	0.00	0.03	0.03	0.03	0.07	0.01	0.02	0.00	0.05	0.03	0.02
SiO_2	0.46	0.63	0.99	0.14	0.50	1.36	0.14	0.52	0.70	0.84	0.96	0.98	0.48
TiO_2	0.00	0.04	0.00	0.02	0.04	0.00	0.00	0.08	0.02	0.00	0.04	0.07	0.03
ZrO_2	0.14	0.14	0.15	0.07	0.08	0.14	0.13	0.11	0.11	0.13	0.14	0.10	0.11
HfO_2	0.00	0.06	0.00	0.05	0.00	0.00	0.00	0.10	0.05	0.03	0.00	0.00	0.08
ThO_2	0.14	0.23	0.00	0.06	0.01	0.05	0.00	0.13	0.04	0.07	0.10	0.11	0.04
UO_2	0.05	0.06	0.02	0.00	0.00	0.02	0.01	0.01	0.03	0.07	0.06	0.01	0.04
Al_2O_3	0.02	0.02	0.19	0.02	0.01	0.31	0.02	0.02	0.05	0.16	0.11	0.04	0.04
Y_2O_3	0.05	0.05	0.02	0.02	0.18	0.06	0.02	0.02	0.10	0.00	0.09	0.09	0.01
La_2O_3	0.39	0.69	2.01	0.06	0.20	1.04	0.00	2.19	0.15	1.17	0.40	0.53	0.21
Ce_2O_3	0.39	0.54	2.11	0.06	0.42	1.65	0.08	2.30	0.29	1.85	0.69	0.79	0.20
Pr_2O_3	0.05	0.09	0.38	0.05	0.12	0.25	0.03	0.38	0.08	0.31	0.12	0.13	0.05
Nd_2O_3	0.07	0.13	0.43	0.01	0.20	0.38	0.05	0.51	0.16	0.39	0.26	0.27	0.06
Sm_2O_3	0.00	0.06	0.04	0.01	0.05	0.02	0.02	0.13	0.08	0.05	0.04	0.06	0.07
Eu_2O_3	0.00	0.05	0.03	0.00	0.00	0.01	0.02	0.00	0.04	0.00	0.04	0.00	0.00
Gd_2O_3	0.08	0.08	0.06	0.05	0.05	0.08	0.06	0.04	0.09	0.03	0.14	0.05	0.00
Tb_2O_3	0.02	0.03	0.02	0.10	0.00	0.07	0.09	0.16	0.03	0.00	0.00	0.02	0.04
Dy_2O_3	0.04	0.02	0.06	0.03	0.11	0.07	0.04	0.07	0.10	0.08	0.04	0.07	0.02
Ho_2O_3	0.11	0.07	0.08	0.03	0.11	0.13	0.08	0.13	0.13	0.00	0.07	0.09	0.08
Er_2O_3	0.11	0.06	0.08	0.12	0.06	0.04	0.14	0.08	0.02	0.00	0.08	0.06	0.07
Tm_2O_3	0.15	0.21	0.04	0.05	0.05	0.15	0.09	0.10	0.08	0.06	0.10	0.05	0.05
Yb_2O_3	0.03	0.21	0.03	0.00	0.07	0.08	0.09	0.06	0.09	0.07	0.00	0.11	0.06
Lu_2O_3	0.15	0.17	0.02	0.01	0.00	0.00	0.02	0.14	0.01	0.03	0.07	0.08	0.08
MgO	0.01	0.00	0.00	0.00	0.02	0.00	0.00	0.00	0.08	0.00	0.05	0.01	0.02
CaO	54.26	53.98	48.83	53.88	52.62	49.94	53.82	48.88	52.99	50.10	51.56	51.15	52.40
MnO	0.03	0.05	0.06	0.01	0.07	0.05	0.03	0.06	0.05	0.05	0.02	0.06	0.04
FeO	0.17	0.13	0.06	0.04	0.42	0.07	0.04	0.04	0.29	0.10	0.54	0.23	0.25
PbO	0.09	0.00	0.10	0.04	0.04	0.06	0.02	0.09	0.00	0.04	0.07	0.01	0.00
Na_2O	0.04	0.08	0.94	0.01	0.20	0.75	0.03	0.87	0.15	0.72	0.06	0.04	0.03
K_2O	0.09	0.04	0.01	0.00	0.01	0.01	0.00	0.00	0.00	0.00	0.38	0.19	0.13
F	3.36	3.37	4.23	4.70	4.56	4.32	4.76	4.35	4.56	4.26	4.29	4.35	4.65
Cl	0.01	0.01	0.00	0.01	0.01	0.00	0.01	0.00	0.01	0.00	0.00	0.01	0.00
O=F,Cl	-1.41	-1.42	-1.78	-1.98	-1.92	-1.82	-2.01	-1.83	-1.92	-1.79	-1.81	-1.84	-1.96

Sample	20TN15B	20TN15B	20TN25D	20TN25D	20TN25D	20TN25D	20TN25D	20TN25D	20TN25D	20TN25D	20TN57C-1	20TN57C-1	20TN57C-1
Analysis	8-169-3	8-170-4	14-187-1	14-188-2	14-189-3	14-190-4	14-191-5	14-192-6	14-193-7	14-194-8	20-222-1	20-223-2	20-224-3
Total	99.61	100.64	99.02	99.89	98.74	99.44	99.75	99.54	99.41	98.84	97.89	96.92	97.07
P (*apfu*)	2.917	2.924	2.956	3.041	2.954	2.943	3.023	2.966	2.957	2.955	2.896	2.920	2.946
Nb	0.002	0.000	0.000	0.001	0.001	0.001	0.003	0.000	0.001	0.000	0.002	0.001	0.001
Si	0.039	0.053	0.087	0.012	0.043	0.118	0.012	0.046	0.060	0.073	0.084	0.087	0.042
Ti	0.000	0.003	0.000	0.001	0.003	0.000	0.000	0.005	0.001	0.000	0.003	0.005	0.002
Zr	0.006	0.006	0.006	0.003	0.004	0.006	0.005	0.005	0.005	0.006	0.006	0.004	0.005
Hf	0.000	0.001	0.000	0.001	0.000	0.000	0.000	0.002	0.001	0.001	0.000	0.000	0.002
Th	0.003	0.004	0.000	0.001	0.000	0.001	0.000	0.003	0.001	0.001	0.002	0.002	0.001
U	0.001	0.001	0.000	0.000	0.000	0.000	0.000	0.000	0.001	0.001	0.001	0.000	0.001
Al	0.002	0.002	0.020	0.002	0.001	0.032	0.002	0.002	0.005	0.016	0.011	0.004	0.004
Y	0.002	0.002	0.001	0.001	0.008	0.003	0.001	0.001	0.005	0.000	0.004	0.004	0.000
La	0.012	0.022	0.065	0.002	0.006	0.033	0.000	0.071	0.005	0.038	0.013	0.017	0.007
Ce	0.012	0.017	0.068	0.002	0.013	0.052	0.002	0.074	0.009	0.059	0.022	0.026	0.006
Pr	0.002	0.003	0.012	0.002	0.004	0.008	0.001	0.012	0.002	0.010	0.004	0.004	0.002
Nd	0.002	0.004	0.014	0.000	0.006	0.012	0.002	0.016	0.005	0.012	0.008	0.008	0.002
Sm	0.000	0.002	0.001	0.000	0.002	0.001	0.001	0.004	0.002	0.002	0.001	0.002	0.002
Eu	0.000	0.001	0.001	0.000	0.000	0.000	0.001	0.000	0.001	0.000	0.001	0.000	0.000
Gd	0.002	0.002	0.002	0.001	0.001	0.002	0.002	0.001	0.003	0.001	0.004	0.001	0.000
Tb	0.001	0.001	0.000	0.003	0.000	0.002	0.003	0.005	0.001	0.000	0.000	0.001	0.001
Dy	0.001	0.001	0.002	0.001	0.003	0.002	0.001	0.002	0.003	0.002	0.001	0.002	0.001
Ho	0.003	0.002	0.002	0.001	0.003	0.004	0.002	0.004	0.003	0.000	0.002	0.003	0.002
Er	0.003	0.002	0.002	0.003	0.002	0.001	0.004	0.002	0.001	0.000	0.002	0.002	0.002
Tm	0.004	0.006	0.001	0.001	0.001	0.004	0.002	0.003	0.002	0.002	0.003	0.001	0.001
Yb	0.001	0.006	0.001	0.000	0.002	0.002	0.002	0.002	0.002	0.002	0.000	0.003	0.002
Lu	0.004	0.004	0.001	0.000	0.000	0.000	0.000	0.004	0.000	0.001	0.002	0.002	0.002
Mg	0.001	0.000	0.000	0.000	0.002	0.000	0.000	0.000	0.011	0.001	0.006	0.001	0.003
Ca	4.949	4.902	4.586	4.914	4.869	4.636	4.921	4.611	4.865	4.684	4.827	4.849	4.923
Mn	0.002	0.004	0.005	0.001	0.005	0.004	0.002	0.004	0.004	0.003	0.002	0.004	0.003
Fe^{2+}	0.012	0.009	0.005	0.003	0.031	0.005	0.003	0.003	0.021	0.007	0.039	0.017	0.018
Pb	0.002	0.000	0.002	0.001	0.001	0.001	0.000	0.002	0.000	0.001	0.002	0.000	0.000
Na	0.006	0.012	0.160	0.002	0.033	0.125	0.005	0.149	0.025	0.122	0.010	0.006	0.005
K	0.010	0.005	0.001	0.000	0.001	0.001	0.000	0.000	0.001	0.000	0.042	0.022	0.015
F	0.904	0.903	1.173	1.265	1.247	1.183	1.286	1.211	1.235	1.175	1.185	1.219	1.290
Cl	0.001	0.002	0.000	0.002	0.001	0.000	0.001	0.000	0.001	0.000	0.000	0.001	0.000
O^{2-}	11.991	12.032	11.957	11.956	11.869	11.966	11.923	11.932	11.898	11.939	11.862	11.896	11.834
Anion Sum	12.896	12.936	13.130	13.223	13.116	13.148	13.209	13.143	13.134	13.115	13.047	13.116	13.124

Table B.10. (Continued) Composition of apatite from various rock types across the 2020 Corundum Dome and Pyrochlore Dome sampling area.

Sample	20TN57C-1	20TN57C-1	20TN57C-1	20TN57C-1	20TN57C-1	20TN57C-1	20TN57C-1	20TN57C-1	20TN2	20TN4D	20TN4D	20TN4D	20TN4D
Analysis	24-229-1	24-230-2	24-231-3	24-232-4	24-233-5	24-234-6	24-235-7	24-236-8	6-187-5	17-227-1	17-228-2	17-229-3	17-230-4
P_2O_5 (wt. %)	39.85	38.54	39.73	39.08	39.94	41.15	38.64	40.10	39.35	41.76	40.75	41.16	40.48
Nb_2O_5	0.02	0.03	0.00	0.00	0.05	0.00	0.00	0.03	0.05	0.02	0.00	0.00	0.00
SiO_2	0.62	1.00	0.45	1.15	0.37	0.14	1.00	0.49	0.46	0.05	0.10	0.08	0.19
TiO_2	0.01	0.04	0.03	0.04	0.07	0.01	0.03	0.01	0.08	0.00	0.03	0.00	0.02
ZrO_2	0.12	0.10	0.14	0.12	0.11	0.11	0.09	0.08	0.17	0.14	0.13	0.10	0.12
HfO_2	0.00	0.00	0.00	0.06	0.05	0.00	0.06	0.08	0.01	0.06	0.10	0.00	0.00
ThO_2	0.01	0.08	0.04	0.04	0.02	0.00	0.12	0.01	0.20	0.00	0.01	0.00	0.00
UO_2	0.09	0.12	0.05	0.00	0.02	0.01	0.10	0.00	0.00	0.02	0.00	0.02	0.04
Al_2O_3	0.04	0.02	0.01	0.02	0.03	0.05	0.01	0.04	0.00	0.00	0.00	0.00	0.00
Y_2O_3	0.10	0.08	0.05	0.10	0.03	0.03	0.12	0.09	0.20	0.04	0.03	0.00	0.01
La_2O_3	0.45	0.50	0.32	0.58	0.14	0.02	0.51	0.28	0.96	0.20	0.69	0.64	1.39
Ce_2O_3	0.70	0.85	0.54	0.99	0.20	0.12	0.86	0.54	2.62	0.25	0.70	0.57	1.45
Pr_2O_3	0.10	0.14	0.09	0.20	0.07	0.02	0.17	0.10	0.36	0.10	0.14	0.11	0.22
Nd_2O_3	0.22	0.31	0.22	0.35	0.08	0.07	0.27	0.17	0.88	0.04	0.12	0.12	0.22
Sm_2O_3	0.06	0.04	0.04	0.11	0.05	0.07	0.10	0.03	0.08	0.00	0.04	0.03	0.05
Eu_2O_3	0.04	0.04	0.05	0.03	0.03	0.02	0.03	0.04	0.09	0.05	0.02	0.00	0.03
Gd_2O_3	0.05	0.07	0.11	0.12	0.06	0.00	0.09	0.06	0.12	0.00	0.03	0.03	0.00
Tb_2O_3	0.06	0.12	0.06	0.05	0.12	0.04	0.05	0.15	0.03	0.12	0.05	0.08	0.01
Dy_2O_3	0.07	0.05	0.08	0.08	0.00	0.03	0.05	0.11	0.05	0.03	0.07	0.01	0.07
Ho_2O_3	0.04	0.07	0.08	0.10	0.00	0.03	0.08	0.10	0.08	0.02	0.08	0.04	0.03
Er_2O_3	0.00	0.09	0.05	0.07	0.05	0.08	0.02	0.01	0.11	0.05	0.00	0.06	0.00
Tm_2O_3	0.00	0.06	0.07	0.13	0.07	0.14	0.01	0.02	0.15	0.03	0.06	0.07	0.05
Yb_2O_3	0.07	0.17	0.07	0.09	0.01	0.10	0.00	0.04	0.00	0.00	0.01	0.08	0.00
Lu_2O_3	0.14	0.08	0.00	0.14	0.05	0.11	0.03	0.06	0.03	0.00	0.06	0.07	0.00
MgO	0.02	0.02	0.01	0.02	0.02	0.03	0.02	0.03	0.00	0.00	0.00	0.00	0.00
CaO	51.57	51.50	51.72	51.11	52.64	53.87	51.39	51.77	49.05	54.05	52.54	52.61	50.93
MnO	0.01	0.01	0.03	0.04	0.03	0.04	0.03	0.05	0.09	0.02	0.04	0.05	0.06
FeO	0.19	0.27	0.22	0.30	0.29	0.24	0.30	0.43	0.11	0.04	0.03	0.03	0.03
PbO	0.01	0.07	0.00	0.00	0.11	0.00	0.09	0.05	0.04	0.03	0.01	0.08	0.10
Na_2O	0.11	0.04	0.06	0.05	0.03	0.04	0.03	0.08	0.76	0.07	0.23	0.22	0.50
K_2O	0.03	0.09	0.06	0.06	0.09	0.11	0.09	0.25	0.01	0.00	0.00	0.00	0.00
F	4.66	4.42	4.64	4.48	4.97	4.94	4.69	4.64	4.15	4.20	4.14	4.17	4.23
Cl	0.01	0.00	0.00	0.01	0.00	0.00	0.00	0.00	0.00	0.00	0.03	0.01	0.00

Sample	20TN57C-1	20TN57C-1	20TN57C-1	20TN57C-1	20TN57C-1	20TN57C-1	20TN57C-1	20TN57C-1	20TN2	20TN4D	20TN4D	20TN4D	20TN4D
Analysis	24-229-1	24-230-2	24-231-3	24-232-4	24-233-5	24-234-6	24-235-7	24-236-8	6-187-5	17-227-1	17-228-2	17-229-3	17-230-4
O=F,Cl	-1.96	-1.86	-1.96	-1.89	-2.09	-2.08	-1.98	-1.95	-1.75	-1.77	-1.75	-1.76	-1.78
Total	97.51	97.17	97.07	97.82	97.70	99.52	97.12	97.97	98.51	99.64	98.51	98.71	98.45
P (*apfu*)	2.967	2.887	2.967	2.917	2.953	2.978	2.898	2.964	2.952	3.010	2.991	3.012	2.997
Nb	0.001	0.001	0.000	0.000	0.002	0.000	0.000	0.001	0.002	0.001	0.000	0.000	0.000
Si	0.055	0.088	0.040	0.101	0.032	0.012	0.088	0.043	0.041	0.004	0.009	0.007	0.016
Ti	0.001	0.003	0.002	0.003	0.004	0.001	0.002	0.001	0.005	0.000	0.002	0.000	0.001
Zr	0.005	0.005	0.006	0.005	0.005	0.005	0.004	0.004	0.007	0.006	0.005	0.004	0.005
Hf	0.000	0.000	0.000	0.002	0.001	0.000	0.002	0.002	0.000	0.001	0.002	0.000	0.000
Th	0.000	0.002	0.001	0.001	0.000	0.000	0.002	0.000	0.004	0.000	0.000	0.000	0.000
U	0.002	0.002	0.001	0.000	0.000	0.000	0.002	0.000	0.000	0.000	0.000	0.000	0.001
Al	0.004	0.003	0.001	0.002	0.003	0.005	0.001	0.004	0.000	0.000	0.000	0.000	0.000
Y	0.005	0.004	0.002	0.005	0.001	0.001	0.006	0.004	0.009	0.002	0.002	0.000	0.001
La	0.015	0.016	0.011	0.019	0.004	0.001	0.017	0.009	0.031	0.006	0.022	0.021	0.045
Ce	0.023	0.027	0.017	0.032	0.006	0.004	0.028	0.017	0.085	0.008	0.022	0.018	0.046
Pr	0.003	0.004	0.003	0.006	0.002	0.001	0.006	0.003	0.012	0.003	0.005	0.003	0.007
Nd	0.007	0.010	0.007	0.011	0.003	0.002	0.009	0.005	0.028	0.001	0.004	0.004	0.007
Sm	0.002	0.001	0.001	0.003	0.002	0.002	0.003	0.001	0.002	0.000	0.001	0.001	0.002
Eu	0.001	0.001	0.001	0.001	0.001	0.000	0.001	0.001	0.003	0.002	0.001	0.000	0.001
Gd	0.002	0.002	0.003	0.003	0.002	0.000	0.003	0.002	0.004	0.000	0.001	0.001	0.000
Tb	0.002	0.004	0.002	0.002	0.003	0.001	0.001	0.004	0.001	0.003	0.001	0.002	0.000
Dy	0.002	0.001	0.002	0.002	0.000	0.001	0.002	0.003	0.001	0.001	0.002	0.000	0.002
Ho	0.001	0.002	0.002	0.003	0.000	0.001	0.002	0.003	0.002	0.000	0.002	0.001	0.001
Er	0.000	0.002	0.001	0.002	0.001	0.002	0.001	0.000	0.003	0.001	0.000	0.002	0.000
Tm	0.000	0.002	0.002	0.004	0.002	0.004	0.000	0.001	0.004	0.001	0.002	0.002	0.001
Yb	0.002	0.005	0.002	0.002	0.000	0.003	0.000	0.001	0.000	0.000	0.000	0.002	0.000
Lu	0.004	0.002	0.000	0.004	0.001	0.003	0.001	0.001	0.001	0.000	0.001	0.002	0.000
Mg	0.002	0.002	0.001	0.003	0.003	0.003	0.002	0.004	0.000	0.000	0.000	0.000	0.000
Ca	4.859	4.883	4.889	4.828	4.926	4.933	4.878	4.844	4.656	4.931	4.880	4.872	4.772
Mn	0.001	0.001	0.002	0.003	0.002	0.003	0.002	0.004	0.006	0.002	0.003	0.004	0.004
Fe^{2+}	0.014	0.020	0.016	0.022	0.021	0.017	0.023	0.031	0.008	0.003	0.002	0.002	0.002
Pb	0.000	0.002	0.000	0.000	0.003	0.000	0.002	0.001	0.001	0.001	0.000	0.002	0.002
Na	0.019	0.007	0.009	0.008	0.004	0.007	0.005	0.013	0.130	0.012	0.039	0.036	0.085
K	0.003	0.011	0.007	0.007	0.011	0.012	0.010	0.028	0.001	0.001	0.000	0.000	0.000
F	1.295	1.236	1.296	1.250	1.374	1.335	1.314	1.282	1.163	1.131	1.135	1.140	1.171
Cl	0.001	0.000	0.000	0.001	0.000	0.000	0.000	0.000	0.000	0.000	0.005	0.001	0.000
O^{2-}	11.891	11.849	11.874	11.903	11.797	11.822	11.822	11.866	11.934	11.971	11.948	11.972	11.948
Anion Sum	13.187	13.085	13.170	13.155	13.171	13.157	13.136	13.148	13.097	13.101	13.088	13.112	13.120

Table B.10. (Continued) Composition of apatite from various rock types across the 2020 Corundum Dome and Pyrochlore Dome sampling area.

Sample	20TN4D	20TN4D	20TN4D	20TN4D	20TN53	20TN53	20TN53	20TN53	20TN53	20TN53	20TN53	20TN53	20TN53
Analysis	17-231-5	17-232-6	17-233-7	17-234-8	27-266-1	27-267-2	27-268-3	27-269-4	27-270-5	27-271-6	27-272-7	27-273-8	27-274-9
P_2O_5 (wt. %)	41.29	41.69	40.96	41.57	41.31	40.68	38.98	39.44	40.17	39.76	39.54	39.80	40.41
Nb_2O_5	0.02	0.01	0.02	0.02	0.03	0.00	0.01	0.00	0.02	0.01	0.00	0.02	0.03
SiO_2	0.12	0.18	0.19	0.05	0.50	0.20	0.40	0.38	0.31	0.28	0.34	0.33	0.43
TiO_2	0.00	0.00	0.01	0.00	0.00	0.02	0.03	0.03	0.00	0.01	0.03	0.03	0.02
ZrO_2	0.09	0.13	0.11	0.07	0.15	0.09	0.11	0.09	0.10	0.19	0.10	0.12	0.14
HfO_2	0.10	0.04	0.10	0.06	0.02	0.04	0.00	0.00	0.00	0.11	0.00	0.01	0.01
ThO_2	0.00	0.01	0.04	0.02	0.02	0.07	0.06	0.01	0.02	0.03	0.00	0.06	0.00
UO_2	0.01	0.00	0.05	0.05	0.04	0.02	0.10	0.00	0.04	0.01	0.00	0.01	0.02
Al_2O_3	0.01	0.00	0.02	0.01	0.00	0.00	0.01	0.00	0.02	0.01	0.00	0.02	0.01
Y_2O_3	0.02	0.03	0.03	0.02	0.04	0.00	0.02	0.05	0.02	0.03	0.02	0.03	0.04
La_2O_3	0.75	1.24	1.31	0.21	0.83	0.98	1.32	1.39	1.06	0.96	1.18	1.12	0.99
Ce_2O_3	0.78	1.27	1.26	0.27	1.06	0.95	1.46	1.46	1.04	1.08	1.14	1.14	1.04
Pr_2O_3	0.16	0.19	0.22	0.03	0.12	0.14	0.22	0.24	0.19	0.17	0.18	0.15	0.17
Nd_2O_3	0.10	0.17	0.19	0.09	0.18	0.16	0.26	0.27	0.18	0.17	0.17	0.19	0.20
Sm_2O_3	0.02	0.03	0.02	0.01	0.01	0.06	0.06	0.02	0.01	0.03	0.04	0.02	0.05
Eu_2O_3	0.01	0.01	0.04	0.06	0.00	0.02	0.04	0.00	0.04	0.00	0.03	0.00	0.00
Gd_2O_3	0.01	0.00	0.07	0.01	0.08	0.03	0.08	0.10	0.06	0.00	0.07	0.04	0.02
Tb_2O_3	0.04	0.03	0.06	0.04	0.06	0.04	0.03	0.04	0.00	0.01	0.00	0.05	0.10
Dy_2O_3	0.05	0.05	0.10	0.06	0.04	0.04	0.03	0.06	0.07	0.00	0.05	0.00	0.04
Ho_2O_3	0.05	0.04	0.04	0.10	0.09	0.10	0.11	0.08	0.06	0.02	0.05	0.15	0.10
Er_2O_3	0.05	0.12	0.12	0.05	0.14	0.00	0.08	0.06	0.06	0.19	0.16	0.08	0.09
Tm_2O_3	0.00	0.00	0.14	0.01	0.08	0.08	0.03	0.11	0.09	0.14	0.12	0.01	0.11
Yb_2O_3	0.08	0.02	0.06	0.13	0.09	0.15	0.07	0.03	0.09	0.13	0.05	0.03	0.10
Lu_2O_3	0.03	0.14	0.09	0.13	0.01	0.00	0.00	0.00	0.07	0.13	0.07	0.06	0.13
MgO	0.00	0.00	0.00	0.00	0.00	0.00	0.01	0.01	0.00	0.01	0.00	0.01	0.01
CaO	52.58	51.38	51.37	53.91	52.55	51.39	49.43	49.28	49.82	50.40	49.56	50.02	51.57
MnO	0.04	0.03	0.05	0.02	0.05	0.08	0.07	0.07	0.07	0.04	0.06	0.06	0.05
FeO	0.02	0.01	0.04	0.03	0.08	0.07	0.19	0.10	0.24	0.15	0.24	0.21	0.20
PbO	0.04	0.03	0.00	0.00	0.04	0.00	0.05	0.03	0.00	0.00	0.04	0.02	0.00
Na_2O	0.28	0.45	0.49	0.08	0.18	0.31	0.39	0.42	0.31	0.32	0.34	0.32	0.23
K_2O	0.00	0.00	0.00	0.00	0.00	0.01	0.03	0.01	0.03	0.03	0.05	0.03	0.01
F	4.02	3.89	4.25	4.36	4.51	4.29	4.30	4.25	4.46	4.33	4.36	4.45	4.47
Cl	0.00	0.00	0.01	0.01	0.01	0.01	0.00	0.00	0.00	0.01	0.01	0.00	0.00
O=F,Cl	-1.69	-1.64	-1.79	-1.84	-1.90	-1.81	-1.81	-1.79	-1.88	-1.82	-1.84	-1.88	-1.88
Total	99.07	99.57	99.68	99.62	100.42	98.22	96.18	96.25	96.77	96.92	96.15	96.68	98.90

Sample	20TN4D	20TN4D	20TN4D	20TN4D	20TN53	20TN53	20TN53	20TN53	20TN53	20TN53	20TN53	20TN53	20TN53
Analysis	17-231-5	17-232-6	17-233-7	17-234-8	27-266-1	27-267-2	27-268-3	27-269-4	27-270-5	27-271-6	27-272-7	27-273-8	27-274-9
P (*apfu*)	3.011	3.044	3.001	3.005	2.996	3.011	2.970	3.000	3.030	2.991	3.004	3.004	2.980
Nb	0.001	0.001	0.001	0.001	0.001	0.000	0.000	0.000	0.001	0.000	0.000	0.001	0.001
Si	0.011	0.015	0.016	0.004	0.042	0.017	0.036	0.034	0.028	0.025	0.030	0.029	0.037
Ti	0.000	0.000	0.001	0.000	0.000	0.001	0.002	0.002	0.000	0.001	0.002	0.002	0.001
Zr	0.004	0.006	0.004	0.003	0.006	0.004	0.005	0.004	0.005	0.008	0.004	0.005	0.006
Hf	0.002	0.001	0.002	0.002	0.001	0.001	0.000	0.000	0.000	0.003	0.000	0.000	0.000
Th	0.000	0.000	0.001	0.000	0.000	0.001	0.001	0.000	0.000	0.001	0.000	0.001	0.000
U	0.000	0.000	0.001	0.001	0.001	0.000	0.002	0.000	0.001	0.000	0.000	0.000	0.000
Al	0.001	0.000	0.002	0.001	0.000	0.000	0.002	0.000	0.002	0.001	0.000	0.002	0.002
Y	0.001	0.001	0.001	0.001	0.002	0.000	0.001	0.002	0.001	0.002	0.001	0.001	0.002
La	0.024	0.040	0.042	0.006	0.026	0.032	0.044	0.046	0.035	0.031	0.039	0.037	0.032
Ce	0.025	0.040	0.040	0.008	0.033	0.030	0.048	0.048	0.034	0.035	0.037	0.037	0.033
Pr	0.005	0.006	0.007	0.001	0.004	0.004	0.007	0.008	0.006	0.005	0.006	0.005	0.005
Nd	0.003	0.005	0.006	0.003	0.005	0.005	0.008	0.009	0.006	0.006	0.005	0.006	0.006
Sm	0.001	0.001	0.001	0.000	0.000	0.002	0.002	0.001	0.000	0.001	0.001	0.001	0.001
Eu	0.000	0.000	0.001	0.002	0.000	0.001	0.001	0.000	0.001	0.000	0.001	0.000	0.000
Gd	0.000	0.000	0.002	0.000	0.002	0.001	0.002	0.003	0.002	0.000	0.002	0.001	0.001
Tb	0.001	0.001	0.002	0.001	0.002	0.001	0.001	0.001	0.000	0.000	0.000	0.002	0.003
Dy	0.001	0.001	0.003	0.002	0.001	0.001	0.001	0.002	0.002	0.000	0.001	0.000	0.001
Ho	0.001	0.001	0.001	0.003	0.002	0.003	0.003	0.002	0.002	0.001	0.001	0.004	0.003
Er	0.001	0.003	0.003	0.001	0.004	0.000	0.002	0.002	0.002	0.005	0.004	0.002	0.003
Tm	0.000	0.000	0.004	0.000	0.002	0.002	0.001	0.003	0.003	0.004	0.003	0.000	0.003
Yb	0.002	0.000	0.002	0.003	0.002	0.004	0.002	0.001	0.002	0.003	0.001	0.001	0.003
Lu	0.001	0.004	0.002	0.003	0.000	0.000	0.000	0.000	0.002	0.003	0.002	0.001	0.003
Mg	0.000	0.000	0.001	0.000	0.000	0.000	0.001	0.001	0.000	0.001	0.000	0.001	0.002
Ca	4.852	4.749	4.764	4.932	4.824	4.813	4.766	4.743	4.756	4.799	4.764	4.778	4.814
Mn	0.003	0.002	0.004	0.001	0.004	0.006	0.005	0.005	0.006	0.003	0.005	0.004	0.004
Fe^{2+}	0.001	0.001	0.003	0.002	0.006	0.005	0.014	0.007	0.018	0.011	0.018	0.016	0.015
Pb	0.001	0.001	0.000	0.000	0.001	0.000	0.001	0.001	0.000	0.000	0.001	0.000	0.000
Na	0.046	0.076	0.083	0.013	0.029	0.053	0.068	0.073	0.054	0.055	0.058	0.055	0.038
K	0.000	0.000	0.000	0.000	0.000	0.001	0.003	0.002	0.003	0.004	0.006	0.003	0.001
F	1.095	1.062	1.163	1.177	1.223	1.186	1.225	1.207	1.256	1.216	1.236	1.256	1.231
Cl	0.000	0.000	0.002	0.001	0.001	0.002	0.000	0.000	0.000	0.002	0.001	0.000	0.000
O^{2-}	11.998	12.073	11.964	11.941	11.963	11.963	11.916	11.964	11.973	11.935	11.945	11.939	11.933
Anion Sum	13.093	13.135	13.129	13.118	13.187	13.151	13.141	13.171	13.229	13.153	13.182	13.195	13.164

Table B.10. (Continued) Composition of apatite from various rock types across the 2020 Corundum Dome and Pyrochlore Dome sampling area.

Sample	20TN53	20TN53	20TN53	20TN53	20TN53	20TN53	20TN53	20TN53
Analysis	28-275-1	28-276-2	28-277-3	28-278-4	29-279-1	29-280-2	29-281-3	31-285-1
P_2O_5 (wt. %)	39.82	40.15	35.64	40.33	40.98	41.16	39.76	35.38
Nb_2O_5	0.01	0.04	0.02	0.03	0.02	0.00	0.03	0.02
SiO_2	0.47	0.72	3.18	0.39	0.50	0.47	0.35	3.44
TiO_2	0.06	0.01	0.04	0.03	0.00	0.00	0.01	0.02
ZrO_2	0.06	0.06	0.17	0.11	0.08	0.13	0.11	0.09
HfO_2	0.07	0.07	0.06	0.00	0.07	0.02	0.10	0.07
ThO_2	0.03	0.02	0.09	0.07	0.03	0.06	0.06	0.15
UO_2	0.05	0.09	0.05	0.04	0.02	0.03	0.10	0.03
Al_2O_3	0.05	0.02	0.02	0.03	0.01	0.01	0.00	0.01
Y_2O_3	0.02	0.02	0.32	0.06	0.03	0.00	0.04	0.28
La_2O_3	1.03	0.96	2.14	1.00	0.83	0.76	1.49	2.43
Ce_2O_3	1.48	1.15	4.22	1.53	0.99	0.95	1.51	4.61
Pr_2O_3	0.23	0.18	0.56	0.23	0.16	0.08	0.21	0.66
Nd_2O_3	0.34	0.23	1.49	0.31	0.16	0.18	0.21	1.57
Sm_2O_3	0.05	0.04	0.23	0.02	0.02	0.02	0.06	0.21
Eu_2O_3	0.00	0.05	0.04	0.01	0.02	0.06	0.01	0.06
Gd_2O_3	0.04	0.06	0.08	0.12	0.03	0.07	0.04	0.15
Tb_2O_3	0.07	0.06	0.07	0.06	0.11	0.00	0.03	0.05
Dy_2O_3	0.09	0.05	0.11	0.09	0.06	0.08	0.02	0.10
Ho_2O_3	0.06	0.09	0.07	0.01	0.13	0.06	0.07	0.07
Er_2O_3	0.03	0.08	0.05	0.03	0.08	0.06	0.06	0.01
Tm_2O_3	0.06	0.07	0.06	0.09	0.07	0.07	0.00	0.14
Yb_2O_3	0.12	0.02	0.11	0.00	0.03	0.02	0.06	0.01
Lu_2O_3	0.00	0.00	0.15	0.00	0.19	0.04	0.15	0.04
MgO	0.01	0.01	0.00	0.00	0.00	0.00	0.00	0.00
CaO	49.95	51.87	47.45	50.62	52.32	52.34	49.18	46.55
MnO	0.07	0.07	0.12	0.02	0.08	0.06	0.08	0.09
FeO	0.26	0.21	0.16	0.15	0.08	0.08	0.12	0.09
PbO	0.00	0.05	0.00	0.06	0.01	0.08	0.00	0.07
Na_2O	0.34	0.16	0.18	0.38	0.16	0.16	0.49	0.15
K_2O	0.16	0.09	0.04	0.07	0.01	0.00	0.02	0.00
F	4.30	4.44	4.05	4.54	4.13	4.18	3.99	3.94
Cl	0.00	0.00	0.01	0.02	0.01	0.00	0.01	0.00
O=F,Cl	-1.81	-1.87	-1.71	-1.91	-1.74	-1.76	-1.68	-1.66
Total	97.49	99.26	99.28	98.51	99.68	99.48	96.67	98.85

Sample	20TN53	20TN53	20TN53	20TN53	20TN53	20TN53	20TN53	20TN53
Analysis	28-275-1	28-276-2	28-277-3	28-278-4	29-279-1	29-280-2	29-281-3	31-285-1
P (*apfu*)	2.986	2.949	2.725	2.995	2.990	3.003	3.012	2.733
Nb	0.000	0.002	0.001	0.001	0.001	0.000	0.001	0.001
Si	0.041	0.062	0.287	0.034	0.043	0.041	0.031	0.314
Ti	0.004	0.000	0.003	0.002	0.000	0.000	0.001	0.001
Zr	0.003	0.003	0.008	0.005	0.003	0.006	0.005	0.004
Hf	0.002	0.002	0.002	0.000	0.002	0.000	0.003	0.002
Th	0.001	0.000	0.002	0.001	0.001	0.001	0.001	0.003
U	0.001	0.002	0.001	0.001	0.000	0.001	0.002	0.001
Al	0.005	0.002	0.002	0.003	0.001	0.001	0.000	0.001
Y	0.001	0.001	0.016	0.003	0.002	0.000	0.002	0.013
La	0.033	0.031	0.071	0.032	0.026	0.024	0.049	0.082
Ce	0.048	0.037	0.139	0.049	0.031	0.030	0.049	0.154
Pr	0.007	0.006	0.018	0.007	0.005	0.002	0.007	0.022
Nd	0.011	0.007	0.048	0.010	0.005	0.006	0.007	0.051
Sm	0.001	0.001	0.007	0.001	0.000	0.001	0.002	0.007
Eu	0.000	0.001	0.001	0.000	0.001	0.002	0.000	0.002
Gd	0.001	0.002	0.002	0.004	0.001	0.002	0.001	0.005
Tb	0.002	0.002	0.002	0.002	0.003	0.000	0.001	0.002
Dy	0.003	0.001	0.003	0.003	0.002	0.002	0.001	0.003
Ho	0.002	0.002	0.002	0.000	0.004	0.002	0.002	0.002
Er	0.001	0.002	0.002	0.001	0.002	0.002	0.002	0.000
Tm	0.002	0.002	0.002	0.002	0.002	0.002	0.000	0.004
Yb	0.003	0.000	0.003	0.000	0.001	0.000	0.002	0.000
Lu	0.000	0.000	0.004	0.000	0.005	0.001	0.004	0.001
Mg	0.001	0.002	0.000	0.000	0.000	0.000	0.000	0.000
Ca	4.741	4.822	4.592	4.758	4.831	4.833	4.715	4.551
Mn	0.005	0.005	0.009	0.002	0.006	0.005	0.006	0.007
Fe^{2+}	0.020	0.015	0.012	0.011	0.006	0.006	0.009	0.007
Pb	0.000	0.001	0.000	0.001	0.000	0.002	0.000	0.002
Na	0.058	0.027	0.032	0.064	0.027	0.027	0.085	0.026
K	0.018	0.010	0.005	0.008	0.001	0.000	0.002	0.000
F	1.203	1.217	1.158	1.258	1.126	1.140	1.130	1.136
Cl	0.000	0.000	0.001	0.002	0.002	0.000	0.001	0.000
O^{2-}	11.951	11.917	11.954	11.930	12.002	12.007	12.017	12.020
Anion Sum	13.155	13.134	13.114	13.191	13.130	13.147	13.148	13.156

Table B.11. Composition of monazite from various rock types across the 2020 Corundum Dome and Pyrochlore Dome sampling area.

Sample	20TN15A	20TN15A	20TN15A	20TN15A	20TN15A	20TN17C	20TN17C	20TN17C	20TN17C
Analysis	362341	4125310	4125411	432602	432613	71641	71652	71663	71674
P_2O_5 (wt. %)	28.21	26.76	26.09	27.38	30.33	26.34	26.41	25.88	25.97
Nb_2O_5	0.00	0.00	0.02	0.04	0.00	0.00	0.00	0.00	0.03
SiO_2	0.58	0.79	0.64	1.27	0.35	0.51	0.52	0.63	0.35
TiO_2	0.02	0.00	0.00	0.01	0.08	0.00	0.00	0.02	0.05
ZrO_2	0.07	0.11	0.10	0.04	0.11	0.04	0.10	0.08	0.10
HfO_2	0.09	0.00	0.03	0.06	0.05	0.00	0.17	0.00	0.00
ThO_2	0.12	0.14	0.62	0.08	0.19	1.43	1.21	2.28	2.04
UO_2	0.09	0.05	0.06	0.10	0.05	0.19	0.04	0.10	0.11
Al_2O_3	0.04	0.04	0.06	0.00	0.01	0.05	0.01	0.00	0.00
Y_2O_3	0.18	0.10	0.03	0.02	0.08	0.19	0.20	0.22	0.18
La_2O_3	25.71	31.38	31.99	30.94	28.73	21.21	17.87	16.42	19.36
Ce_2O_3	29.81	30.21	30.49	29.99	26.89	34.55	36.18	34.81	34.48
Pr_2O_3	3.98	3.76	3.93	3.92	3.38	4.12	4.42	4.44	4.27
Nd_2O_3	5.19	3.43	3.70	2.89	2.46	7.08	8.63	9.57	7.69
Sm_2O_3	0.46	0.28	0.32	0.24	0.17	0.81	1.20	1.27	0.96
Eu_2O_3	0.00	0.00	0.00	0.00	0.00	0.00	0.00	0.01	0.00
Gd_2O_3	0.15	0.11	0.24	0.31	0.07	0.71	0.83	0.77	0.61
Tb_2O_3	0.05	0.00	0.06	0.08	0.11	0.19	0.01	0.09	0.06
Dy_2O_3	0.03	0.02	0.00	0.00	0.01	0.07	0.08	0.04	0.09
Ho_2O_3	0.04	0.06	0.05	0.09	0.07	0.21	0.16	0.24	0.20
Er_2O_3	0.01	0.06	0.00	0.01	0.06	0.00	0.05	0.03	0.05
Tm_2O_3	0.11	0.08	0.08	0.07	0.12	0.12	0.18	0.19	0.20
Yb_2O_3	0.12	0.03	0.01	0.09	0.02	0.06	0.08	0.03	0.09
Lu_2O_3	0.04	0.14	0.00	0.02	0.14	0.02	0.08	0.00	0.00
MgO	0.00	0.00	0.00	0.00	0.00	0.00	0.00	0.00	0.00
CaO	5.35	2.84	0.91	3.21	7.73	0.23	0.09	0.26	0.25
MnO	0.05	0.00	0.03	0.02	0.03	0.02	0.03	0.03	0.04
FeO	0.05	0.14	0.11	0.07	0.18	0.38	0.46	0.28	0.80
PbO	0.06	0.00	0.00	0.10	0.12	0.11	0.08	0.03	0.07
Na_2O	0.02	0.04	0.02	0.06	0.25	0.00	0.00	0.00	0.00
K_2O	0.13	0.08	0.08	0.03	0.02	0.03	0.04	0.03	0.02
F	0.00	0.00	0.00	0.00	0.44	0.00	0.00	0.00	0.00
Cl	0.04	0.00	0.02	0.00	0.00	0.04	0.01	0.01	0.00
O=F,Cl	-0.01	0.00	0.00	0.00	-0.18	-0.01	0.00	0.00	0.00
Total	100.80	100.64	99.66	101.11	102.06	98.69	99.10	97.75	98.07
P (*apfu*)	0.925	0.906	0.910	0.909	0.955	0.927	0.927	0.922	0.923
Nb	0.000	0.000	0.000	0.001	0.000	0.000	0.000	0.000	0.001
Si	0.023	0.032	0.026	0.050	0.013	0.021	0.021	0.026	0.015
Ti	0.001	0.000	0.000	0.000	0.002	0.000	0.000	0.001	0.002
Zr	0.001	0.002	0.002	0.001	0.002	0.001	0.002	0.002	0.002
Hf	0.001	0.000	0.000	0.001	0.001	0.000	0.002	0.000	0.000
Th	0.001	0.001	0.006	0.001	0.002	0.014	0.011	0.022	0.019
U	0.001	0.000	0.001	0.001	0.000	0.002	0.000	0.001	0.001
Al	0.002	0.002	0.003	0.000	0.000	0.002	0.000	0.000	0.000
Y	0.004	0.002	0.001	0.000	0.002	0.004	0.004	0.005	0.004
La	0.367	0.463	0.486	0.447	0.394	0.325	0.273	0.255	0.300
Ce	0.423	0.442	0.460	0.430	0.366	0.526	0.549	0.537	0.530
Pr	0.056	0.055	0.059	0.056	0.046	0.062	0.067	0.068	0.065
Nd	0.072	0.049	0.054	0.040	0.033	0.105	0.128	0.144	0.115
Sm	0.006	0.004	0.004	0.003	0.002	0.012	0.017	0.018	0.014
Eu	0.000	0.000	0.000	0.000	0.000	0.000	0.000	0.000	0.000

Sample	20TN15A	20TN15A	20TN15A	20TN15A	20TN15A	20TN17C	20TN17C	20TN17C	20TN17C
Analysis	362341	4125310	4125411	432602	432613	71641	71652	71663	71674
Gd (*apfu*)	0.002	0.001	0.003	0.004	0.001	0.010	0.011	0.011	0.009
Tb	0.001	0.000	0.001	0.001	0.001	0.003	0.000	0.001	0.001
Dy	0.000	0.000	0.000	0.000	0.000	0.001	0.001	0.001	0.001
Ho	0.000	0.001	0.001	0.001	0.001	0.003	0.002	0.003	0.003
Er	0.000	0.001	0.000	0.000	0.001	0.000	0.001	0.000	0.001
Tm	0.001	0.001	0.001	0.001	0.001	0.002	0.002	0.003	0.003
Yb	0.001	0.000	0.000	0.001	0.000	0.001	0.001	0.000	0.001
Lu	0.000	0.002	0.000	0.000	0.002	0.000	0.001	0.000	0.000
Mg	0.000	0.000	0.000	0.000	0.000	0.000	0.000	0.000	0.000
Ca	0.222	0.122	0.040	0.135	0.308	0.010	0.004	0.012	0.011
Mn	0.002	0.000	0.001	0.001	0.001	0.001	0.001	0.001	0.001
Fe^{2+}	0.002	0.005	0.004	0.002	0.006	0.013	0.016	0.010	0.028
Pb	0.001	0.000	0.000	0.001	0.001	0.001	0.001	0.000	0.001
Na	0.002	0.003	0.001	0.004	0.018	0.000	0.000	0.000	0.000
K	0.007	0.004	0.004	0.001	0.001	0.002	0.002	0.002	0.001
F	0.000	0.000	0.000	0.000	0.051	0.000	0.000	0.000	0.000
Cl	0.002	0.000	0.001	0.000	0.000	0.003	0.000	0.001	0.000
Cation Sum	2.123	2.098	2.067	2.093	2.159	2.047	2.045	2.044	2.052

Note: Compositions were recalculated on the basis of the sum of 4 O *apfu*. * Sum of Eu, Gd, Tb, Dy, Ho, Er, Tm, Yb, and Lu.

Table B.11. (Continued) Composition of monazite from various rock types across the 2020 Corundum Dome and Pyrochlore Dome sampling area.

Sample	20TN17C	20TN20	20TN57C-1	20TN57C-1	20TN57C-1
Analysis	81681	161871	192191	192202	192213
P_2O_5 (wt. %)	26.66	25.96	29.23	29.39	29.85
Nb_2O_5	0.00	0.00	0.00	0.00	0.04
SiO_2	0.26	0.44	0.31	0.43	0.30
TiO_2	0.05	0.04	0.22	0.25	0.82
ZrO_2	0.10	0.10	0.10	0.09	0.08
HfO_2	0.01	0.01	0.14	0.10	0.05
ThO_2	0.26	0.08	0.10	0.09	0.04
UO_2	0.12	0.09	0.09	0.03	0.07
Al_2O_3	0.00	0.02	0.06	0.09	0.05
Y_2O_3	0.03	0.08	0.04	0.04	0.04
La_2O_3	34.18	25.03	14.25	15.04	16.76
Ce_2O_3	30.03	34.38	38.04	37.87	38.29
Pr_2O_3	4.01	4.48	5.05	4.93	4.93
Nd_2O_3	2.85	6.15	12.41	11.38	9.97
Sm_2O_3	0.11	0.26	0.96	0.80	0.69
Eu_2O_3	0.00	0.00	0.10	0.11	0.01
Gd_2O_3	0.24	0.22	0.16	0.06	0.00
Tb_2O_3	0.11	0.03	0.11	0.09	0.05
Dy_2O_3	0.00	0.00	0.00	0.01	0.00
Ho_2O_3	0.00	0.02	0.22	0.12	0.18
Er_2O_3	0.04	0.01	0.11	0.03	0.10
Tm_2O_3	0.06	0.06	0.24	0.11	0.16
Yb_2O_3	0.01	0.00	0.10	0.10	0.01
Lu_2O_3	0.04	0.02	0.20	0.12	0.00
MgO	0.00	0.00	0.03	0.00	0.02
CaO	0.03	1.01	0.19	0.20	0.20
MnO	0.00	0.02	0.09	0.09	0.07
FeO	0.01	0.05	0.83	0.76	0.34
PbO	0.00	0.06	0.03	0.00	0.00
Na_2O	0.00	0.00	0.00	0.02	0.00
K_2O	0.00	0.00	0.11	0.07	0.11
F	0.00	0.00	0.00	0.00	0.00
Cl	0.01	0.00	0.01	0.03	0.04
O=F,Cl	0.00	0.00	0.00	-0.01	-0.01
Total	99.22	98.61	103.54	102.45	103.27
P (*apfu*)	0.933	0.915	0.956	0.962	0.964
Nb	0.000	0.000	0.000	0.000	0.001
Si	0.011	0.018	0.012	0.017	0.012
Ti	0.002	0.001	0.006	0.007	0.024
Zr	0.002	0.002	0.002	0.002	0.001
Hf	0.000	0.000	0.002	0.001	0.001
Th	0.002	0.001	0.001	0.001	0.000
U	0.001	0.001	0.001	0.000	0.001
Al	0.000	0.001	0.003	0.004	0.002
Y	0.001	0.002	0.001	0.001	0.001
La	0.521	0.384	0.203	0.214	0.236
Ce	0.455	0.524	0.538	0.536	0.534
Pr	0.060	0.068	0.071	0.069	0.068
Nd	0.042	0.091	0.171	0.157	0.136
Sm	0.002	0.004	0.013	0.011	0.009
Eu	0.000	0.000	0.001	0.001	0.000

Sample	20TN17C	20TN20	20TN57C-1	20TN57C-1	20TN57C-1
Analysis	81681	161871	192191	192202	192213
Gd (*apfu*)	0.003	0.003	0.002	0.001	0.000
Tb	0.001	0.000	0.001	0.001	0.001
Dy	0.000	0.000	0.000	0.000	0.000
Ho	0.000	0.000	0.003	0.001	0.002
Er	0.000	0.000	0.001	0.000	0.001
Tm	0.001	0.001	0.003	0.001	0.002
Yb	0.000	0.000	0.001	0.001	0.000
Lu	0.001	0.000	0.002	0.001	0.000
Mg	0.000	0.000	0.002	0.000	0.001
Ca	0.001	0.045	0.008	0.008	0.008
Mn	0.000	0.001	0.003	0.003	0.002
Fe^{2+}	0.000	0.002	0.027	0.025	0.011
Pb	0.000	0.001	0.000	0.000	0.000
Na	0.000	0.000	0.000	0.001	0.000
K	0.000	0.000	0.006	0.003	0.005
F	0.000	0.000	0.000	0.000	0.000
Cl	0.001	0.000	0.001	0.002	0.002
Cation Sum	2.040	2.065	2.039	2.032	2.023

Table B.12. Composition of rhodochrosite and calcite from various rock types across the 2020 Corundum Dome and Pyrochlore Dome sampling area.

Sample	20TN54	20TN54	20TN54	20TN3-2	20TN3-2	20TN3-2	20TN5	20TN5
Analysis	30-122-1	30-123-2	30-124-3	12-65-1	12-66-2	15-82-1	19-141-1	19-142-2
Mineral	Rhodochrosite	Rhodochrosite	Rhodochrosite	Calcite	Calcite	Calcite	Calcite	Calcite
SiO_2 (wt. %)	0.22	0.12	0.18	0.01	0.02	0.15	0.03	0.05
TiO_2	0.14	0.16	0.07	–	–	–	–	–
Al_2O_3	0.16	0.16	0.23	–	–	–	–	–
FeO	1.15	1.35	0.83	0.04	0.03	0.08	0.35	0.37
MnO	59.62	60.33	60.10	0.33	0.35	1.13	0.14	0.33
MgO	1.27	1.27	1.25	0.02	0.00	0.03	0.03	0.08
CaO	–	–	–	53.89	53.85	52.56	54.16	52.62
CO_2	38.47	38.23	38.43	44.30	44.31	44.36	44.20	44.50
O	0.00	0.00	0.00	0.00	0.00	0.00	0.00	0.00
Total	101.01	101.60	101.09	98.58	98.56	98.32	98.91	97.95
Si (*apfu*)	0.004	0.002	0.003	0.000	0.000	0.003	0.000	0.001
Ti	0.002	0.002	0.001	–	–	–	–	–
Al	0.004	0.003	0.005	–	–	–	–	–
Fe	0.018	0.021	0.013	0.001	0.000	0.001	0.005	0.005
Mn	0.951	0.963	0.959	0.005	0.005	0.016	0.002	0.005
Mg	0.036	0.036	0.035	0.000	0.000	0.001	0.001	0.002
Ca	–	–	–	0.967	0.967	0.945	0.971	0.946
C	0.989	0.983	0.988	1.013	1.014	1.016	1.010	1.020

Note: Compositions were recalculated on the basis of 3 O *apfu*. All iron is assumed to be Fe^{2+}; – = not measured. * Determined by stoichiometry.

Table B.12. (Continued) Composition of rhodochrosite and calcite from various rock types across the 2020 Corundum Dome and Pyrochlore Dome sampling area.

Sample	20TN25D	20TN25D	20TN25D	20TN25D	20TN25D	20TN57C-1	20TN57C-1	20TN57C-1
Analysis	28-178-1	28-179-2	34-198-1	34-200-3	39-225-1	23-125-6	30-148-3	30-149-4
Mineral	Calcite	Calcite	Calcite	Calcite	Calcite	Calcite	Calcite	Calcite
SiO_2 (wt. %)	0.02	0.03	0.06	0.00	0.09	0.35	0.12	0.17
TiO_2	–	–	–	–	–	0.07	0.01	0.00
Al_2O_3	–	–	–	–	–	0.09	0.05	0.06
FeO	0.78	0.78	0.70	0.52	0.50	0.76	0.64	0.63
MnO	2.03	2.08	2.11	2.09	1.62	3.12	2.92	2.85
MgO	0.25	0.23	0.27	0.30	0.15	0.49	0.39	0.37
CaO	49.29	49.37	49.96	49.51	50.23	55.38	55.82	57.57
BaO	–	–	–	–	–	0.00	0.00	0.00
Na_2O	–	–	–	–	–	0.02	0.01	0.01
K_2O	–	–	–	–	–	0.20	0.24	0.21
F	–	–	–	–	–	0.07	0.10	0.00
CO_2	44.62	44.59	44.45	44.62	44.62	42.77	42.73	42.48
O	0.00	0.00	0.00	0.00	0.00	-0.03	-0.04	0.00
Total	96.99	97.08	97.56	97.05	97.21	103.29	102.99	104.36
Si (*apfu*)	0.000	0.001	0.001	0.000	0.001	0.006	0.002	0.003
Ti	–	–	–	–	–	0.001	0.000	0.000
Al	–	–	–	–	–	0.002	0.001	0.001
Fe	0.011	0.011	0.010	0.007	0.007	0.011	0.009	0.009
Mn	0.029	0.030	0.030	0.030	0.023	0.044	0.041	0.040
Mg	0.006	0.006	0.007	0.008	0.004	0.012	0.010	0.009
Ca	0.893	0.894	0.903	0.896	0.908	0.983	0.994	1.018
Ba	–	–	–	–	–	0.000	0.000	0.000
Na	–	–	–	–	–	0.001	0.000	0.000
K	–	–	–	–	–	0.004	0.005	0.004
F	–	–	–	–	–	0.004	0.005	0.000
C		1.029	1.024	1.029	1.028	0.967	0.970	0.957

Table B.13. Composition of bastnäsite from various rock types across the 2020 Corundum Dome and Pyrochlore Dome sampling area.

Sample	20TN15A	20TN54	20TN54	20TN54	20TN54	20TN54	20TN54	20TN15B	20TN15B	20TN15B	20TN15B	20TN15B	20TN15B
Analysis	41-247-4	47-271-1	47-273-3	49-276-1	49-277-2	49-279-4	49-281-6	2-193-1	2-194-2	2-196-4	2-197-5	2-198-6	3-199-1
P_2O_5 (wt. %)	0.00	0.05	0.05	0.00	0.06	0.00	0.00	0.03	0.00	0.00	0.01	0.04	0.02
Nb_2O_5	1.18	0.01	0.01	0.03	0.01	0.00	0.00	0.00	0.02	0.04	0.00	0.01	0.00
SiO_2	0.18	0.49	0.76	0.30	0.41	1.94	0.37	0.37	0.47	2.71	1.63	0.96	2.25
TiO_2	0.45	0.03	0.06	0.04	0.08	0.02	0.14	0.10	0.03	0.01	0.11	0.06	0.14
ZrO_2	0.04	0.00	0.02	0.00	0.04	0.00	0.04	0.03	0.00	0.03	0.00	0.00	0.00
HfO_2	0.09	0.00	0.08	0.04	0.00	0.03	0.00	0.00	0.11	0.01	0.02	0.00	0.06
ThO_2	0.20	0.35	0.00	0.29	0.32	0.19	0.12	0.71	0.60	0.53	0.43	0.58	0.70
UO_2	0.09	0.03	0.04	0.02	0.04	0.03	0.12	0.07	0.09	0.08	0.00	0.07	0.10
Al_2O_3	0.01	0.22	0.26	0.08	0.16	0.66	0.10	0.05	0.05	0.81	0.47	0.12	0.38
Y_2O_3	0.00	0.16	0.01	0.07	0.10	0.15	0.05	0.16	0.16	0.69	1.18	0.33	0.14
La_2O_3	45.10	30.50	29.55	30.61	25.86	29.72	25.04	30.52	30.67	23.45	22.27	29.40	31.83
Ce_2O_3	27.10	36.40	37.75	35.19	36.71	36.03	38.98	36.52	37.07	30.80	30.12	36.39	36.87
Pr_2O_3	3.87	4.60	4.92	5.19	4.55	4.75	4.59	4.45	4.42	4.12	3.91	4.38	4.53
Nd_2O_3	1.15	5.74	6.01	6.64	6.38	6.22	5.66	4.84	5.11	6.76	6.87	5.32	4.51
Sm_2O_3	0.03	0.39	0.36	0.44	0.44	0.38	0.27	0.26	0.15	0.98	1.06	0.22	0.12
Eu_2O_3	0.00	0.00	0.00	0.00	0.00	0.00	0.00	0.00	0.00	0.03	0.12	0.00	0.00
Gd_2O_3	0.20	0.50	0.57	0.84	0.57	0.74	0.64	0.14	0.27	0.86	1.06	0.30	0.26
Tb_2O_3	0.07	0.12	0.06	0.08	0.09	0.09	0.01	0.00	0.06	0.11	0.15	0.14	0.13
Dy_2O_3	0.02	0.05	0.00	0.00	0.02	0.00	0.06	0.00	0.00	0.13	0.18	0.04	0.00
Ho_2O_3	0.03	0.09	0.02	0.10	0.07	0.08	0.00	0.00	0.00	0.36	0.48	0.06	0.00
Er_2O_3	0.04	0.00	0.04	0.02	0.00	0.05	0.00	0.10	0.07	0.11	0.10	0.14	0.10
Tm_2O_3	0.15	0.06	0.00	0.12	0.09	0.13	0.05	0.04	0.10	0.19	0.16	0.00	0.08
Yb_2O_3	0.02	0.00	0.00	0.00	0.04	0.05	0.00	0.18	0.00	0.08	0.10	0.00	0.01
Lu_2O_3	0.04	0.06	0.00	0.11	0.00	0.00	0.01	0.02	0.13	0.09	0.23	0.07	0.06
MgO	0.00	0.05	0.02	0.00	0.00	0.02	0.01	0.02	0.07	0.00	0.00	0.23	0.88
CaO	0.41	0.60	0.10	0.24	6.03	0.10	4.33	0.53	0.31	7.82	7.92	0.33	0.46
MnO	0.12	0.00	0.01	0.04	0.02	0.02	0.01	0.04	0.00	0.06	0.05	0.02	0.05
FeO	0.29	0.22	0.57	0.09	0.07	0.10	0.41	0.33	0.29	0.21	0.23	0.42	0.54
PbO	0.00	0.09	0.09	0.09	0.02	0.04	0.01	0.17	0.05	0.10	0.13	0.05	0.08
Na_2O	0.13	0.10	0.05	0.01	0.04	0.54	0.06	0.00	0.00	0.54	0.32	0.00	0.00
K_2O	0.03	0.04	0.27	0.03	0.05	0.01	0.17	0.07	0.06	0.06	0.04	0.09	0.21
F	11.32	10.95	11.96	11.14	8.93	11.20	10.80	11.48	11.52	8.95	8.09	11.20	12.02
Cl	0.00	0.01	0.02	0.01	0.02	0.01	0.00	0.02	0.01	0.00	0.02	0.02	0.00
CO_2*	17.87	18.04	17.24	17.51	20.65	18.74	18.86	17.47	17.38	22.69	23.01	18.20	18.35
-(O=F)	-4.77	-4.61	-5.04	-4.69	-3.77	-4.72	-4.55	-4.84	-4.85	-3.77	-3.41	-4.72	-5.06

Sample	20TN15A	20TN54	20TN54	20TN54	20TN54	20TN54	20TN54	20TN15B	20TN15B	20TN15B	20TN15B	20TN15B	20TN15B
Analysis	41-247-4	47-271-1	47-273-3	49-276-1	49-277-2	49-279-4	49-281-6	2-193-1	2-194-2	2-196-4	2-197-5	2-198-6	3-199-1
Total	105.46	105.35	105.84	104.68	108.11	107.34	106.34	103.87	104.43	109.63	107.05	104.45	109.83
P (*apfu*)	0.000	0.002	0.002	0.000	0.002	0.000	0.000	0.001	0.000	0.000	0.000	0.001	0.001
Nb	0.021	0.000	0.000	0.000	0.000	0.000	0.000	0.000	0.000	0.001	0.000	0.000	0.000
Si	0.007	0.019	0.031	0.012	0.014	0.071	0.014	0.015	0.019	0.080	0.048	0.037	0.082
Ti	0.013	0.001	0.002	0.001	0.002	0.001	0.004	0.003	0.001	0.000	0.003	0.002	0.004
Zr	0.001	0.000	0.000	0.000	0.001	0.000	0.001	0.001	0.000	0.000	0.000	0.000	0.000
Hf	0.001	0.000	0.001	0.000	0.000	0.000	0.000	0.000	0.001	0.000	0.000	0.000	0.001
Th	0.002	0.003	0.000	0.003	0.002	0.002	0.001	0.007	0.006	0.004	0.003	0.005	0.006
U	0.001	0.000	0.000	0.000	0.000	0.000	0.001	0.001	0.001	0.000	0.000	0.001	0.001
Al	0.000	0.010	0.012	0.004	0.006	0.028	0.004	0.002	0.002	0.028	0.016	0.005	0.016
Y	0.000	0.003	0.000	0.002	0.002	0.003	0.001	0.003	0.003	0.011	0.019	0.007	0.003
La	0.646	0.433	0.437	0.451	0.313	0.399	0.337	0.454	0.456	0.254	0.244	0.418	0.426
Ce	0.385	0.513	0.554	0.514	0.440	0.480	0.521	0.539	0.547	0.332	0.328	0.513	0.490
Pr	0.055	0.065	0.072	0.075	0.054	0.063	0.061	0.065	0.065	0.044	0.042	0.061	0.060
Nd	0.016	0.079	0.086	0.095	0.075	0.081	0.074	0.070	0.074	0.071	0.073	0.073	0.059
Sm	0.000	0.005	0.005	0.006	0.005	0.005	0.003	0.004	0.002	0.010	0.011	0.003	0.001
Eu	0.000	0.000	0.000	0.000	0.000	0.000	0.000	0.000	0.000	0.000	0.001	0.000	0.000
Gd	0.003	0.006	0.008	0.011	0.006	0.009	0.008	0.002	0.004	0.008	0.010	0.004	0.003
Tb	0.001	0.002	0.001	0.001	0.001	0.001	0.000	0.000	0.001	0.001	0.001	0.002	0.001
Dy	0.000	0.001	0.000	0.000	0.000	0.000	0.001	0.000	0.000	0.001	0.002	0.001	0.000
Ho	0.000	0.001	0.000	0.001	0.001	0.001	0.000	0.000	0.000	0.003	0.005	0.001	0.000
Er	0.000	0.000	0.000	0.000	0.000	0.001	0.000	0.001	0.001	0.001	0.001	0.002	0.001
Tm	0.002	0.001	0.000	0.001	0.001	0.002	0.001	0.000	0.001	0.002	0.001	0.000	0.001
Yb	0.000	0.000	0.000	0.000	0.000	0.001	0.000	0.002	0.000	0.001	0.001	0.000	0.000
Lu	0.000	0.001	0.000	0.001	0.000	0.000	0.000	0.000	0.002	0.001	0.002	0.001	0.001
Mg	0.000	0.003	0.001	0.000	0.000	0.001	0.000	0.001	0.004	0.000	0.000	0.013	0.048
Ca	0.017	0.025	0.004	0.010	0.212	0.004	0.169	0.023	0.013	0.247	0.252	0.014	0.018
Mn	0.004	0.000	0.000	0.001	0.001	0.000	0.000	0.001	0.000	0.001	0.001	0.001	0.002
Fe^{2+}	0.009	0.007	0.019	0.003	0.002	0.003	0.012	0.011	0.010	0.005	0.006	0.014	0.016
Pb	0.000	0.001	0.001	0.001	0.000	0.000	0.000	0.002	0.001	0.001	0.001	0.001	0.001
Na	0.010	0.008	0.004	0.001	0.003	0.038	0.004	0.000	0.000	0.031	0.019	0.000	0.000
K	0.002	0.002	0.014	0.001	0.002	0.000	0.008	0.004	0.003	0.002	0.001	0.004	0.010
F	1.391	1.333	1.516	1.407	0.926	1.289	1.246	1.464	1.469	0.833	0.760	1.364	1.380
Cl	0.000	0.001	0.001	0.001	0.001	0.000	0.000	0.001	0.001	0.000	0.001	0.001	0.000
C*	0.947	0.948	0.944	0.954	0.924	0.931	0.939	0.962	0.957	0.911	0.933	0.956	0.910
Cation sum	2.144	2.138	2.199	2.152	2.068	2.123	2.164	2.174	2.173	2.052	2.025	2.137	2.160

Note: Compositions were recalculated on the basis of 3 O *apfu*. – = not measured. * Determined by stoichiometry. ** La, Ce, Pr, and Nd were the only REE contents analyzed.

Table B.13. (Continued) Composition of bastnäsite from various rock types across the 2020 Corundum Dome and Pyrochlore Dome sampling area.

Sample	20TN15B	20TN25D	20TN25D	20TN25D	20TN25D	20TN25D	20TN25D	20TN25D	20TN25D	20TN25D	20TN25D	20TN25D	20TN25D
Analysis	10-176-2	16-198-1	16-199-2	16-200-3	16-201-4	16-202-5	17-203-1	17-204-2	17-205-3	17-206-4	17-207-5	17-208-6	17-209-7
P_2O_5 (wt. %)	0.26	0.03	0.03	0.00	0.00	0.03	0.00	0.00	0.01	0.03	0.00	0.01	0.02
Nb_2O_5	0.01	0.08	0.03	0.38	0.05	0.02	0.00	0.00	0.01	0.06	0.06	0.02	0.00
SiO_2	1.69	1.94	0.37	0.11	0.18	0.41	0.18	0.75	0.26	0.15	0.34	0.12	0.19
TiO_2	0.08	0.31	0.38	3.70	0.34	0.22	0.24	0.36	0.40	0.05	0.10	0.19	0.10
ZrO_2	0.02	0.00	0.00	0.00	0.00	0.02	0.02	0.00	0.01	0.05	0.00	0.00	0.00
HfO_2	0.00	0.11	0.12	0.09	0.12	0.13	0.20	0.00	0.09	0.02	0.01	0.00	0.13
ThO_2	6.09	0.20	0.36	7.32	1.16	0.44	0.29	0.17	0.67	0.31	0.36	0.56	0.12
UO_2	0.10	0.09	0.07	0.14	0.03	0.09	0.12	0.03	0.04	0.05	0.07	0.00	0.12
Al_2O_3	0.19	0.59	0.06	0.00	0.00	0.07	0.02	0.17	0.03	0.02	0.08	0.02	0.03
Y_2O_3	1.50	0.05	0.02	0.06	0.03	0.04	0.00	0.07	0.06	0.01	0.06	0.00	0.00
La_2O_3	25.36	30.09	31.65	25.66	34.57	31.66	31.65	30.74	31.43	31.44	30.36	31.37	24.56
Ce_2O_3	30.32	36.97	36.20	31.96	33.06	35.80	36.57	36.62	36.64	36.89	36.00	36.05	33.64
Pr_2O_3	4.24	4.63	4.55	4.15	4.07	4.63	4.51	4.59	4.43	4.36	4.40	4.44	4.11
Nd_2O_3	5.91	4.34	3.80	3.99	1.97	3.68	3.76	4.04	3.03	3.82	3.92	3.75	4.52
Sm_2O_3	0.60	0.15	0.10	0.16	0.07	0.16	0.15	0.09	0.15	0.14	0.12	0.14	0.19
Eu_2O_3	0.00	0.00	0.00	0.00	0.00	0.00	0.00	0.00	0.00	0.00	0.00	0.00	0.00
Gd_2O_3	0.71	0.00	0.00	0.17	0.03	0.00	0.00	0.00	0.00	0.00	0.00	0.00	0.00
Tb_2O_3	0.13	0.11	0.04	0.02	0.05	0.06	0.05	0.14	0.11	0.01	0.14	0.07	0.00
Dy_2O_3	0.25	0.00	0.00	0.02	0.01	0.00	0.00	0.00	0.00	0.00	0.00	0.02	0.00
Ho_2O_3	0.14	0.05	0.00	0.08	0.11	0.00	0.01	0.00	0.00	0.09	0.09	0.14	0.16
Er_2O_3	0.05	0.00	0.09	0.04	0.06	0.00	0.18	0.00	0.08	0.00	0.07	0.07	0.04
Tm_2O_3	0.12	0.07	0.00	0.00	0.19	0.08	0.09	0.01	0.04	0.07	0.05	0.08	0.00
Yb_2O_3	0.14	0.04	0.14	0.08	0.00	0.02	0.03	0.04	0.01	0.02	0.08	0.00	0.00
Lu_2O_3	0.00	0.04	0.15	0.13	0.00	0.01	0.00	0.08	0.13	0.17	0.13	0.04	0.00
MgO	0.05	0.00	0.00	0.00	0.00	0.00	0.00	0.00	0.00	0.00	0.00	0.00	0.00
CaO	1.63	0.08	0.36	1.53	2.54	0.55	0.10	0.47	0.13	0.98	1.20	1.36	7.59
MnO	0.05	0.08	0.03	0.05	0.04	0.03	0.03	0.05	0.01	0.05	0.04	0.03	0.02
FeO	1.32	0.19	0.23	0.39	0.12	0.12	0.09	0.18	0.06	0.03	0.05	0.09	0.05
PbO	0.33	0.05	0.03	0.14	0.10	0.17	0.05	0.00	0.00	0.10	0.04	0.05	0.06
Na_2O	0.03	0.45	0.04	0.04	0.28	0.02	0.01	0.11	0.03	0.02	0.07	0.00	0.02
K_2O	0.14	0.02	0.08	0.01	0.01	0.01	0.00	0.00	0.00	0.01	0.02	0.00	0.00
F	13.46	11.91	11.61	10.37	11.78	12.05	11.87	11.97	11.80	11.26	10.92	11.04	9.44
Cl	0.04	0.01	0.01	0.05	0.01	0.00	0.01	0.03	0.01	0.00	0.00	0.00	0.00
CO_2*	16.93	18.39	17.52	19.66	17.68	17.14	17.00	17.53	17.26	17.67	18.27	17.98	21.18

Sample	20TN15B	20TN25D	20TN25D	20TN25D	20TN25D	20TN25D	20TN25D	20TN25D	20TN25D	20TN25D	20TN25D	20TN25D	20TN25D
Analysis	10-176-2	16-198-1	16-199-2	16-200-3	16-201-4	16-202-5	17-203-1	17-204-2	17-205-3	17-206-4	17-207-5	17-208-6	17-209-7
-(O=F)	-5.68	-5.02	-4.89	-4.38	-4.96	-5.08	-5.00	-5.05	-4.97	-4.74	-4.60	-4.65	-3.98
Total	106.19	106.06	103.18	106.14	103.69	102.59	102.23	103.20	101.94	103.14	102.47	102.99	102.33
P (*apfu*)	0.009	0.001	0.001	0.000	0.000	0.001	0.000	0.000	0.000	0.001	0.000	0.000	0.001
Nb	0.000	0.001	0.000	0.006	0.001	0.000	0.000	0.000	0.000	0.001	0.001	0.000	0.000
Si	0.069	0.073	0.015	0.004	0.007	0.017	0.008	0.030	0.011	0.006	0.013	0.005	0.006
Ti	0.002	0.009	0.012	0.098	0.010	0.007	0.008	0.011	0.013	0.001	0.003	0.006	0.002
Zr	0.000	0.000	0.000	0.000	0.000	0.000	0.000	0.000	0.000	0.001	0.000	0.000	0.000
Hf	0.000	0.001	0.001	0.001	0.001	0.002	0.002	0.000	0.001	0.000	0.000	0.000	0.001
Th	0.056	0.002	0.003	0.058	0.011	0.004	0.003	0.002	0.006	0.003	0.003	0.005	0.001
U	0.001	0.001	0.001	0.001	0.000	0.001	0.001	0.000	0.000	0.000	0.001	0.000	0.001
Al	0.009	0.026	0.003	0.000	0.000	0.004	0.001	0.008	0.002	0.001	0.004	0.001	0.001
Y	0.032	0.001	0.000	0.001	0.001	0.001	0.000	0.001	0.001	0.000	0.001	0.000	0.000
La	0.381	0.416	0.473	0.332	0.509	0.486	0.491	0.459	0.482	0.466	0.438	0.457	0.306
Ce	0.452	0.508	0.536	0.410	0.483	0.545	0.564	0.542	0.558	0.542	0.515	0.522	0.416
Pr	0.063	0.063	0.067	0.053	0.059	0.070	0.069	0.068	0.067	0.064	0.063	0.064	0.051
Nd	0.086	0.058	0.055	0.050	0.028	0.055	0.057	0.058	0.045	0.055	0.055	0.053	0.054
Sm	0.008	0.002	0.001	0.002	0.001	0.002	0.002	0.001	0.002	0.002	0.002	0.002	0.002
Eu	0.000	0.000	0.000	0.000	0.000	0.000	0.000	0.000	0.000	0.000	0.000	0.000	0.000
Gd	0.010	0.000	0.000	0.002	0.000	0.000	0.000	0.000	0.000	0.000	0.000	0.000	0.000
Tb	0.002	0.001	0.000	0.000	0.001	0.001	0.001	0.002	0.001	0.000	0.002	0.001	0.000
Dy	0.003	0.000	0.000	0.000	0.000	0.000	0.000	0.000	0.000	0.000	0.000	0.000	0.000
Ho	0.002	0.001	0.000	0.001	0.001	0.000	0.000	0.000	0.000	0.001	0.001	0.002	0.002
Er	0.001	0.000	0.001	0.000	0.001	0.000	0.002	0.000	0.001	0.000	0.001	0.001	0.000
Tm	0.002	0.001	0.000	0.000	0.002	0.001	0.001	0.000	0.001	0.001	0.001	0.001	0.000
Yb	0.002	0.000	0.002	0.001	0.000	0.000	0.000	0.000	0.000	0.000	0.001	0.000	0.000
Lu	0.000	0.000	0.002	0.001	0.000	0.000	0.000	0.001	0.002	0.002	0.002	0.000	0.000
Mg	0.003	0.000	0.000	0.000	0.000	0.000	0.000	0.000	0.000	0.000	0.000	0.000	0.000
Ca	0.071	0.003	0.015	0.058	0.109	0.025	0.004	0.021	0.006	0.042	0.050	0.058	0.275
Mn	0.002	0.003	0.001	0.001	0.001	0.001	0.001	0.002	0.000	0.002	0.001	0.001	0.001
Fe^{2+}	0.045	0.006	0.008	0.011	0.004	0.004	0.003	0.006	0.002	0.001	0.001	0.003	0.001
Pb	0.004	0.000	0.000	0.001	0.001	0.002	0.001	0.000	0.000	0.001	0.000	0.001	0.001
Na	0.002	0.033	0.003	0.003	0.021	0.002	0.001	0.009	0.002	0.001	0.005	0.000	0.002
K	0.007	0.001	0.004	0.001	0.001	0.000	0.000	0.000	0.000	0.001	0.001	0.000	0.000
F	1.732	1.413	1.487	1.150	1.487	1.586	1.581	1.531	1.552	1.429	1.350	1.380	1.008
Cl	0.002	0.000	0.001	0.003	0.001	0.000	0.000	0.002	0.001	0.000	0.000	0.000	0.000
C*	0.941	0.942	0.968	0.941	0.963	0.974	0.977	0.968	0.980	0.969	0.975	0.970	0.976
Cation sum	2.264	2.154	2.175	2.039	2.217	2.205	2.198	2.189	2.184	2.165	2.139	2.152	2.100

Table B.13. (Continued) Composition of bastnäsite from various rock types across the 2020 Corundum Dome and Pyrochlore Dome sampling area.

Sample	20TN25D	20TN25D	20TN25D	20TN25D	20TN25D	20TN25D	20TN25D	20TN25D	20TN57C -1	20TN57C -1	20TN53	20TN53	20TN53
Analysis	17-210-8	17-211-9	17-212-10	17-213-11	17-214-12	18-215-1	18-217-3	18-218-4	21-225-1	22-227-2	24-257-1	24-258-2	24-259-3
P_2O_5 (wt. %)	0.02	0.01	0.00	0.00	0.00	0.02	0.00	0.00	0.03	0.00	0.09	0.13	0.04
Nb_2O_5	0.00	0.01	0.06	0.02	0.00	0.04	0.02	0.02	0.02	0.05	0.15	0.22	0.10
SiO_2	0.20	0.10	0.08	0.12	0.19	0.13	0.16	0.20	0.59	2.58	0.79	0.51	0.24
TiO_2	0.08	0.11	0.16	0.25	0.07	0.12	0.09	0.01	0.14	0.91	0.18	0.22	0.10
ZrO_2	0.00	0.00	0.03	0.00	0.00	0.00	0.01	0.00	0.00	0.02	1.20	0.00	0.05
HfO_2	0.06	0.12	0.12	0.00	0.13	0.26	0.00	0.00	0.05	0.00	0.11	0.13	0.00
ThO_2	0.26	0.15	0.26	0.49	0.20	0.44	0.26	2.51	0.14	0.14	0.82	0.62	0.78
UO_2	0.02	0.05	0.08	0.01	0.03	0.08	0.05	0.03	0.00	0.06	0.08	0.07	0.03
Al_2O_3	0.05	0.02	0.01	0.02	0.00	0.03	0.02	0.01	0.13	0.59	0.14	0.17	0.17
Y_2O_3	0.00	0.00	0.05	0.03	0.02	0.08	0.07	0.10	0.04	0.12	0.33	0.11	0.16
La_2O_3	24.94	30.53	31.27	32.23	32.58	33.89	32.07	32.76	13.28	12.91	32.34	31.17	41.32
Ce_2O_3	33.20	37.01	36.37	36.51	35.96	34.99	36.56	33.60	31.79	32.51	27.19	22.54	14.54
Pr_2O_3	4.09	4.56	4.46	4.42	4.52	4.45	4.30	4.22	5.00	5.18	5.52	5.13	7.40
Nd_2O_3	4.40	3.99	3.72	3.72	3.34	3.12	3.68	2.99	14.39	15.00	8.08	7.35	8.65
Sm_2O_3	0.24	0.19	0.08	0.17	0.11	0.16	0.19	0.16	1.20	1.13	0.73	0.60	0.67
Eu_2O_3	0.00	0.00	0.00	0.00	0.00	0.00	0.00	0.00	0.21	0.23	0.00	0.00	0.00
Gd_2O_3	0.06	0.00	0.00	0.00	0.00	0.00	0.10	0.00	0.11	0.52	0.49	0.44	0.30
Tb_2O_3	0.03	0.04	0.08	0.03	0.03	0.15	0.08	0.12	0.04	0.08	0.15	0.07	0.08
Dy_2O_3	0.00	0.00	0.02	0.00	0.00	0.00	0.00	0.02	0.04	0.00	0.14	0.06	0.07
Ho_2O_3	0.06	0.06	0.12	0.02	0.13	0.03	0.18	0.12	0.10	0.16	0.14	0.04	0.14
Er_2O_3	0.12	0.11	0.03	0.07	0.04	0.00	0.02	0.11	0.06	0.00	0.10	0.00	0.11
Tm_2O_3	0.16	0.12	0.01	0.09	0.15	0.02	0.14	0.10	0.22	0.18	0.08	0.13	0.22
Yb_2O_3	0.05	0.00	0.01	0.05	0.11	0.04	0.05	0.12	0.05	0.01	0.05	0.01	0.12
Lu_2O_3	0.04	0.03	0.00	0.11	0.18	0.13	0.01	0.00	0.00	0.05	0.09	0.04	0.21
MgO	0.00	0.00	0.00	0.00	0.00	0.00	0.00	0.00	0.02	0.02	0.00	0.00	0.00
CaO	7.66	0.88	1.02	0.15	0.37	0.28	0.34	0.81	7.16	6.82	0.62	0.25	0.42
MnO	0.08	0.07	0.01	0.03	0.03	0.00	0.04	0.04	0.06	0.07	0.25	0.21	0.35
FeO	0.04	0.03	0.08	0.09	0.31	0.03	0.05	0.05	0.59	0.51	1.38	1.34	1.55
PbO	0.08	0.08	0.00	0.05	0.17	0.07	0.12	0.03	0.06	0.10	0.04	0.10	0.00
Na_2O	0.02	0.00	0.00	0.00	0.00	0.01	0.00	0.08	0.00	0.39	0.01	0.05	0.01
K_2O	0.00	0.00	0.00	0.00	0.04	0.00	0.02	0.02	0.15	0.07	0.02	0.03	0.03
F	9.36	11.33	11.31	12.11	12.30	11.73	11.43	11.26	9.61	9.46	11.39	11.15	10.80
Cl	0.02	0.01	0.02	0.01	0.02	0.00	0.01	0.02	0.00	0.00	0.03	0.03	0.02

Sample	20TN25D	20TN25D	20TN25D	20TN25D	20TN25D	20TN25D	20TN25D	20TN25D	20TN57C-1	20TN57C-1	20TN53	20TN53	20TN53
Analysis	17-210-8	17-211-9	17-212-10	17-213-11	17-214-12	18-215-1	18-217-3	18-218-4	21-225-1	22-227-2	24-257-1	24-258-2	24-259-3
CO_2*(wt. %)	21.21	17.58	17.68	16.74	16.58	17.11	17.36	17.57	21.25	22.37	18.21	18.93	18.26
-(O=F)	-3.95	-4.77	-4.77	-5.10	-5.18	-4.94	-4.82	-4.75	-4.05	-3.98	-4.81	-4.70	-4.55
Total	102.63	102.42	102.36	102.46	102.44	102.47	102.63	102.34	102.47	108.24	106.16	97.12	103.91
P (*apfu*)	0.000	0.000	0.000	0.000	0.000	0.001	0.000	0.000	0.001	0.000	0.003	0.004	0.001
Nb	0.000	0.000	0.001	0.000	0.000	0.001	0.000	0.000	0.000	0.001	0.003	0.004	0.002
Si	0.007	0.004	0.003	0.005	0.008	0.005	0.007	0.008	0.020	0.078	0.030	0.020	0.009
Ti	0.002	0.003	0.005	0.008	0.002	0.004	0.003	0.000	0.003	0.021	0.005	0.006	0.003
Zr	0.000	0.000	0.001	0.000	0.000	0.000	0.000	0.000	0.000	0.000	0.022	0.000	0.001
Hf	0.001	0.001	0.001	0.000	0.002	0.003	0.000	0.000	0.001	0.000	0.001	0.001	0.000
Th	0.002	0.001	0.002	0.005	0.002	0.004	0.002	0.023	0.001	0.001	0.007	0.006	0.007
U	0.000	0.000	0.001	0.000	0.000	0.001	0.001	0.000	0.000	0.000	0.001	0.001	0.000
Al	0.002	0.001	0.000	0.001	0.000	0.001	0.001	0.000	0.005	0.021	0.006	0.008	0.008
Y	0.000	0.000	0.001	0.001	0.000	0.002	0.001	0.002	0.001	0.002	0.007	0.002	0.003
La	0.309	0.458	0.466	0.507	0.518	0.522	0.486	0.492	0.165	0.144	0.451	0.457	0.588
Ce	0.409	0.551	0.538	0.570	0.567	0.535	0.550	0.501	0.391	0.360	0.377	0.328	0.205
Pr	0.050	0.068	0.066	0.069	0.071	0.068	0.064	0.063	0.061	0.057	0.076	0.074	0.104
Nd	0.053	0.058	0.054	0.057	0.051	0.047	0.054	0.043	0.173	0.162	0.109	0.104	0.140
Sm	0.003	0.003	0.001	0.003	0.002	0.002	0.003	0.002	0.014	0.012	0.010	0.008	0.009
Eu	0.000	0.000	0.000	0.000	0.000	0.000	0.000	0.000	0.002	0.002	0.000	0.000	0.000
Gd	0.001	0.000	0.000	0.000	0.000	0.000	0.001	0.000	0.001	0.005	0.006	0.006	0.004
Tb	0.000	0.001	0.001	0.000	0.000	0.002	0.001	0.002	0.000	0.001	0.002	0.001	0.001
Dy	0.000	0.000	0.000	0.000	0.000	0.000	0.000	0.000	0.000	0.000	0.002	0.001	0.001
Ho	0.001	0.001	0.002	0.000	0.002	0.000	0.002	0.002	0.001	0.002	0.002	0.000	0.002
Er	0.001	0.001	0.000	0.001	0.001	0.000	0.000	0.001	0.001	0.000	0.001	0.000	0.001
Tm	0.002	0.001	0.000	0.001	0.002	0.000	0.002	0.001	0.002	0.002	0.001	0.002	0.003
Yb	0.001	0.000	0.000	0.001	0.001	0.001	0.001	0.002	0.000	0.000	0.001	0.000	0.001
Lu	0.000	0.000	0.000	0.001	0.002	0.002	0.000	0.000	0.000	0.000	0.001	0.000	0.002
Mg	0.000	0.000	0.000	0.000	0.000	0.000	0.000	0.000	0.001	0.001	0.000	0.000	0.000
Ca	0.276	0.038	0.044	0.007	0.017	0.012	0.015	0.035	0.258	0.221	0.025	0.011	0.017
Mn	0.002	0.002	0.000	0.001	0.001	0.000	0.001	0.001	0.002	0.002	0.008	0.007	0.011
Fe^{2+}	0.001	0.001	0.003	0.003	0.011	0.001	0.002	0.002	0.017	0.013	0.044	0.045	0.050
Pb	0.001	0.001	0.000	0.001	0.002	0.001	0.001	0.000	0.001	0.001	0.000	0.001	0.000
Na	0.001	0.000	0.000	0.000	0.000	0.001	0.000	0.006	0.000	0.023	0.001	0.004	0.001
K	0.000	0.000	0.000	0.000	0.002	0.000	0.001	0.001	0.006	0.003	0.001	0.002	0.002
F	0.995	1.456	1.447	1.634	1.675	1.548	1.485	1.449	1.021	0.904	1.364	1.404	1.317
Cl	0.001	0.001	0.001	0.001	0.001	0.000	0.001	0.001	0.000	0.000	0.002	0.002	0.002
C*	0.973	0.975	0.976	0.975	0.975	0.975	0.973	0.976	0.975	0.923	0.941	1.029	0.961
Cation sum	2.098	2.171	2.168	2.218	2.241	2.190	2.174	2.165	2.103	2.056	2.143	2.133	2.138

Table B.13. (Continued) Composition of bastnäsite from various rock types across the 2020 Corundum Dome and Pyrochlore Dome sampling area.

Sample	20TN53	20TN53	20TN53	20TN53	20TN53	20TN53	20TN53	20TN53	20TN57A	20TN57A	20TN57A	20TN57A	20TN57A
Analysis	24-260-4	24-261-5	24-262-6	24-263-7	32-286-1	32-287-2	32-288-3	36-300-4	12-192-1	12-193-2	13-195-1	13-196-2	13-197-3
P_2O_5 (wt. %)	0.17	0.01	0.09	0.06	0.00	0.05	0.01	0.01	–	–	–	–	–
Nb_2O_5	0.34	0.27	0.14	0.20	0.00	0.00	0.00	0.01	0.00	0.02	0.02	0.00	0.02
Ta_2O_5	–	–	–	–	–	–	–	–	0.22	0.22	0.15	0.20	0.19
SiO_2	0.41	0.46	0.17	1.72	0.29	1.22	0.18	3.16	0.10	0.08	1.69	2.09	0.60
TiO_2	0.22	0.11	0.15	0.13	0.04	0.01	0.09	0.15	0.01	0.00	0.00	0.02	0.45
ZrO_2	0.11	0.00	0.00	0.00	0.00	0.00	0.03	0.00	0.00	0.01	2.22	2.08	0.00
HfO_2	0.05	0.03	0.00	0.04	0.09	0.07	0.05	0.00	0.06	0.00	0.06	0.07	0.01
ThO_2	0.98	0.62	0.77	0.59	0.18	0.29	0.09	0.32	0.42	0.28	0.18	0.09	0.21
UO_2	0.01	0.02	0.00	0.03	0.02	0.04	0.09	0.14	0.00	0.24	0.09	0.27	0.15
Al_2O_3	0.08	0.13	0.06	0.60	0.03	0.90	0.00	1.02	0.00	0.03	0.14	0.36	0.18
Y_2O_3	0.21	0.23	0.24	0.22	0.19	0.14	0.18	0.16	0.10	0.12	0.25	0.25	0.12
La_2O_3	36.33	38.53	37.48	43.84	18.92	22.78	17.52	19.17	23.68	20.89	21.51	21.02	21.42
Ce_2O_3	20.61	20.51	22.77	12.89	32.67	36.43	31.25	31.06	39.91	38.13	38.52	38.29	39.52
Pr_2O_3	6.24	6.69	6.48	7.65	4.34	4.79	4.36	4.50	4.83	4.64	4.65	4.78	4.92
Nd_2O_3	9.17	9.68	9.37	10.39	8.50	7.65	8.97	8.05	7.38	7.96	8.18	8.05	8.41
Sm_2O_3	0.61	0.65	0.60	0.61	0.88	0.51	1.15	0.62	–	–	–	–	–
Eu_2O_3	0.00	0.00	0.00	0.00	0.15	0.00	0.08	0.00	–	–	–	–	–
Gd_2O_3	0.27	0.37	0.29	0.18	0.42	0.15	0.65	0.31	–	–	–	–	–
Tb_2O_3	0.09	0.09	0.00	0.07	0.07	0.02	0.13	0.07	–	–	–	–	–
Dy_2O_3	0.07	0.02	0.06	0.00	0.16	0.12	0.12	0.03	–	–	–	–	–
Ho_2O_3	0.08	0.10	0.11	0.18	0.24	0.02	0.20	0.11	–	–	–	–	–
Er_2O_3	0.10	0.06	0.09	0.07	0.10	0.00	0.01	0.00	–	–	–	–	–
Tm_2O_3	0.13	0.04	0.08	0.01	0.17	0.11	0.13	0.06	–	–	–	–	–
Yb_2O_3	0.03	0.01	0.13	0.00	0.00	0.07	0.06	0.00	–	–	–	–	–
Lu_2O_3	0.01	0.01	0.02	0.00	0.02	0.24	0.00	0.06	–	–	–	–	–
MgO	0.00	0.00	0.00	0.00	0.01	0.93	0.00	0.00	–	–	–	–	–
CaO	0.39	0.65	0.53	0.74	7.85	0.96	9.99	8.01	0.36	3.02	0.72	0.61	1.28
MnO	0.15	0.13	0.03	0.10	0.18	0.25	0.30	0.14	–	–	–	–	–
FeO	2.83	1.91	1.14	1.93	0.79	1.34	0.45	0.12	–	–	–	–	–
PbO	0.18	0.02	0.04	0.02	0.14	0.11	0.00	0.00	0.01	0.05	0.04	0.05	0.04
Na_2O	0.01	0.00	0.01	0.45	0.00	0.00	0.00	0.01	–	–	–	–	–
K_2O	0.07	0.06	0.03	0.04	0.05	0.02	0.03	0.77	0.09	0.09	0.09	0.10	0.19
F	11.48	11.45	10.79	11.50	9.25	11.91	9.18	9.35	11.10	10.72	11.55	11.47	11.71
Cl	0.03	0.02	0.02	0.03	0.00	0.01	0.00	0.01	–	–	–	–	–

Sample	20TN53	20TN53	20TN53	20TN53	20TN53	20TN53	20TN53	20TN53	20TN57A	20TN57A	20TN57A	20TN57A	20TN57A
Analysis	24-260-4	24-261-5	24-262-6	24-263-7	32-286-1	32-287-2	32-288-3	36-300-4	12-192-1	12-193-2	13-195-1	13-196-2	13-197-3
CO_2*(wt. %)	18.00	17.76	18.05	18.73	21.38	18.71	21.89	23.26	17.72	18.84	18.83	19.23	17.97
-(O=F)	-4.84	-4.83	-4.55	-4.85	-3.90	-5.02	-3.86	-3.94	-4.68	-4.51	-4.86	-4.83	-4.93
Total	104.62	105.83	105.21	108.16	103.23	104.83	103.31	106.74	101.30	100.82	104.03	104.22	102.44
P (*apfu*)	0.006	0.000	0.003	0.002	0.000	0.002	0.000	0.000	–	–	–	–	–
Nb	0.006	0.005	0.002	0.003	0.000	0.000	0.000	0.000	0.000	0.000	0.000	0.000	0.000
Ta	–	–	–	–	–	–	–	–	0.002	0.002	0.002	0.002	0.002
Si	0.016	0.018	0.007	0.062	0.010	0.046	0.006	0.093	0.004	0.003	0.063	0.076	0.024
Ti	0.007	0.003	0.004	0.004	0.001	0.000	0.002	0.003	0.000	0.000	0.000	0.001	0.013
Zr	0.002	0.000	0.000	0.000	0.000	0.000	0.000	0.000	0.000	0.000	0.040	0.037	0.000
Hf	0.001	0.000	0.000	0.000	0.001	0.001	0.000	0.000	0.001	0.000	0.001	0.001	0.000
Th	0.009	0.006	0.007	0.005	0.001	0.002	0.001	0.002	0.004	0.002	0.002	0.001	0.002
U	0.000	0.000	0.000	0.000	0.000	0.000	0.001	0.001	0.000	0.002	0.001	0.002	0.001
Al	0.003	0.006	0.003	0.026	0.001	0.039	0.000	0.035	0.000	0.001	0.006	0.016	0.009
Y	0.004	0.005	0.005	0.004	0.003	0.003	0.003	0.002	0.002	0.002	0.005	0.005	0.003
La	0.521	0.553	0.533	0.584	0.231	0.314	0.209	0.208	0.356	0.297	0.297	0.283	0.314
Ce	0.293	0.292	0.321	0.170	0.397	0.498	0.370	0.335	0.596	0.538	0.527	0.512	0.576
Pr	0.088	0.095	0.091	0.101	0.052	0.065	0.051	0.048	0.072	0.065	0.063	0.064	0.071
Nd	0.127	0.135	0.129	0.134	0.101	0.102	0.104	0.085	0.107	0.110	0.109	0.105	0.120
Sm	0.008	0.009	0.008	0.008	0.010	0.007	0.013	0.006	–	–	–	–	–
Eu	0.000	0.000	0.000	0.000	0.002	0.000	0.001	0.000	–	–	–	–	–
Gd	0.003	0.005	0.004	0.002	0.005	0.002	0.007	0.003	–	–	–	–	–
Tb	0.001	0.001	0.000	0.001	0.001	0.000	0.001	0.001	–	–	–	–	–
Dy	0.001	0.000	0.001	0.000	0.002	0.001	0.001	0.000	–	–	–	–	–
Ho	0.001	0.001	0.001	0.002	0.002	0.000	0.002	0.001	–	–	–	–	–
Er	0.001	0.001	0.001	0.001	0.001	0.000	0.000	0.000	–	–	–	–	–
Tm	0.002	0.000	0.001	0.000	0.002	0.001	0.001	0.001	–	–	–	–	–
Yb	0.000	0.000	0.001	0.000	0.000	0.001	0.001	0.000	–	–	–	–	–
Lu	0.000	0.000	0.000	0.000	0.000	0.003	0.000	0.001	–	–	–	–	–
Mg	0.000	0.000	0.000	0.000	0.001	0.052	0.000	0.000	–	–	–	–	–
Ca	0.016	0.027	0.022	0.029	0.279	0.038	0.346	0.253	0.016	0.125	0.029	0.024	0.054
Mn	0.005	0.004	0.001	0.003	0.005	0.008	0.008	0.004	–	–	–	–	–
Fe^{2+}	0.092	0.062	0.037	0.058	0.022	0.042	0.012	0.003	–	–	–	–	–
Pb	0.002	0.000	0.000	0.000	0.001	0.001	0.000	0.000	0.000	0.001	0.000	0.000	0.000
Na	0.000	0.000	0.001	0.031	0.000	0.000	0.000	0.000	–	–	–	–	–
K	0.004	0.003	0.001	0.002	0.002	0.001	0.001	0.029	0.005	0.005	0.004	0.004	0.010
F	1.410	1.410	1.315	1.314	0.970	1.406	0.939	0.872	1.433	1.308	1.366	1.326	1.474
Cl	0.002	0.001	0.001	0.002	0.000	0.001	0.000	0.001	–	–	–	–	–
C*	0.955	0.944	0.950	0.924	0.968	0.953	0.967	0.936	0.987	0.992	0.961	0.959	0.976
Cation sum	2.175	2.177	2.135	2.155	2.100	2.181	2.110	2.051	2.152	2.146	2.111	2.093	2.175

Table B.13. (Continued) Composition of bastnäsite from various rock types across the 2020 Corundum Dome and Pyrochlore Dome sampling area.

Sample	20TN57A	20TN57A
Analysis	13-198-4	13-199-5
Nb_2O_5 (wt. %)	0.03	0.00
Ta_2O_5	0.19	0.25
SiO_2	0.08	0.17
TiO_2	0.57	0.03
ZrO_2	0.03	0.01
HfO_2	0.06	0.01
ThO_2	0.44	0.42
UO_2	0.00	0.17
Al_2O_3	0.00	0.03
Y_2O_3	0.09	0.10
La_2O_3	20.76	23.20
Ce_2O_3	36.52	40.23
Pr_2O_3	4.49	4.83
Nd_2O_3	7.42	7.69
CaO	5.92	0.46
PbO	0.09	0.01
K_2O	0.05	0.07
F	9.86	11.72
CO_2*	20.43	17.21
-(O=F)	-4.15	-4.94
Total	102.87	101.68
Nb (*apfu*)	0.000	0.000
Ta	0.002	0.003
Si	0.003	0.007
Ti	0.015	0.001
Zr	0.000	0.000
Hf	0.001	0.000
Th	0.003	0.004
U	0.000	0.002
Al	0.000	0.002
Y	0.002	0.002
La	0.267	0.358
Ce	0.466	0.617
Pr	0.057	0.074
Nd	0.092	0.115
Ca	0.221	0.020

Sample	20TN57A	20TN57A
Analysis	13-198-4	13-199-5
Pb (*apfu*)	0.001	0.000
K	0.002	0.004
F	1.087	1.552
C*	0.972	0.983
Cation sum	2.105	2.192

Table B.14. Composition of niobian rutile from sampled 20TN15A and 20TN12 from the 2020 Pyrochlore Dome sampling area.

Sample	20TN15A	20TN15A	20TN12	20TN12
Analysis	452671	452682	241971	241982
Mineral	Nb-rutile	Nb-rutile	Nb-rutile	Nb-rutile
P_2O_5 (wt. %)	0.04	0.03	0.00	0.02
Nb_2O_5	4.50	3.29	1.50	0.96
SiO_2	0.08	0.08	0.32	0.49
TiO_2	94.64	94.40	96.44	96.87
ZrO_2	0.00	0.03	0.01	0.01
HfO_2	0.09	0.07	0.01	0.01
ThO_2	0.00	0.02	0.00	0.07
UO_2	0.05	0.01	0.04	0.03
Al_2O_3	0.01	0.00	0.02	0.04
Fe_2O_3*	0.71	1.22	1.39	1.10
Y_2O_3	0.03	0.05	0.00	0.03
La_2O_3	0.00	0.00	0.00	0.00
Ce_2O_3	0.16	0.15	0.21	0.18
Pr_2O_3	0.00	0.00	0.00	0.00
Nd_2O_3	0.00	0.00	0.03	0.01
Sm_2O_3	0.01	0.01	0.00	0.00
Eu_2O_3	0.00	0.02	0.01	0.06
Gd_2O_3	0.00	0.03	0.00	0.02
Tb_2O_3	0.00	0.01	0.03	0.03
Dy_2O_3	0.00	0.03	0.04	0.00
Ho_2O_3	0.03	0.01	0.08	0.03
Er_2O_3	0.05	0.02	0.00	0.01
Tm_2O_3	0.03	0.02	0.05	0.00
Yb_2O_3	0.09	0.03	0.00	0.08
Lu_2O_3	0.01	0.02	0.00	0.06
MgO	0.00	0.00	0.00	0.00
CaO	0.21	0.23	0.21	0.30
MnO	0.02	0.03	0.04	0.04
PbO	0.00	0.01	0.00	0.00
Na_2O	0.01	0.01	0.07	0.10
K_2O	0.03	0.07	0.02	0.02
F	0.05	0.06	0.00	0.01
Cl	0.00	0.00	0.01	0.01
-(O=F,Cl)	0.05	0.10	0.14	0.10
Total	100.84	99.97	100.52	100.54
P (*apfu*)	0.000	0.000	0.000	0.000
Nb	0.027	0.020	0.009	0.006
Si	0.001	0.001	0.004	0.006
Ti	0.955	0.960	0.970	0.972
Zr	0.000	0.000	0.000	0.000
Hf	0.000	0.000	0.000	0.000
Th	0.000	0.000	0.000	0.000
U	0.000	0.000	0.000	0.000
Al	0.000	0.000	0.000	0.001
Fe^{3+}	0.007	0.012	0.014	0.011
Y	0.000	0.000	0.000	0.000
La	0.000	0.000	0.000	0.000
Ce	0.001	0.001	0.001	0.001
Pr	0.000	0.000	0.000	0.000
Nd	0.000	0.000	0.000	0.000

Sample	20TN15A	20TN15A	20TN12	20TN12
Analysis	452671	452682	241971	241982
Mineral	Nb-rutile	Nb-rutile	Nb-rutile	Nb-rutile
Sm (*apfu*)	0.000	0.000	0.000	0.000
Eu	0.000	0.000	0.000	0.000
Gd	0.000	0.000	0.000	0.000
Tb	0.000	0.000	0.000	0.000
Dy	0.000	0.000	0.000	0.000
Ho	0.000	0.000	0.000	0.000
Er	0.000	0.000	0.000	0.000
Tm	0.000	0.000	0.000	0.000
Yb	0.000	0.000	0.000	0.000
Lu	0.000	0.000	0.000	0.000
Mg	0.000	0.000	0.000	0.000
Ca	0.003	0.003	0.003	0.004
Mn	0.000	0.000	0.000	0.000
Pb	0.000	0.000	0.000	0.000
Na	0.000	0.000	0.002	0.003
K	0.001	0.001	0.000	0.000
F	0.002	0.002	0.000	0.001
Cl	0.000	0.000	0.000	0.000
O	2.000	2.000	2.000	2.000
Cation Sum	0.998	1.002	1.005	1.007

Note: Compositions were recalculated on the basis of 2 O *apfu*. * Determined by stoichiometry using Droop (1987) calculation method.

Table B.15. Composition of rutile, ilmenite, and hematite from various rock types across the 2020 Corundum Dome and Pyrochlore Dome sampling area.

Sample	20TN55A	20TN55A	20TN55A	20TN55A	20TN55A	20TN55A	20TN55A	20TN55A	20TN55A	20TN55A	20TN55A	20TN55A
Analysis	10631	10642	10653	10664	11682	211151	211162	211173	211184	211195	211206	211217
Mineral	Rutile	Rutile	Rutile	Rutile	Rutile	Rutile	Rutile	Rutile	Rutile	Rutile	Rutile	Rutile
SiO_2 (wt. %)	0.04	0.11	0.02	0.08	1.34	0.15	0.33	0.70	1.23	1.56	2.12	1.92
TiO_2	98.17	98.18	98.77	98.17	94.98	97.41	98.48	92.11	91.07	92.03	92.47	92.83
Al_2O_3	0.03	0.05	0.02	0.03	0.59	0.04	0.07	0.24	0.43	0.33	0.44	0.56
Fe_2O_3*	1.01	0.64	0.57	0.76	0.43	1.03	0.71	2.64	2.85	1.91	1.52	1.63
MgO	0.01	0.02	0.02	0.04	0.00	0.00	0.00	0.05	0.34	0.02	0.39	0.26
MnO	0.03	0.01	0.00	0.02	0.00	0.03	0.02	0.03	0.01	0.04	0.03	0.00
-(O=F,Cl)	0.10	0.06	0.06	0.08	0.04	0.10	0.07	0.26	0.29	0.19	0.15	0.16
Total	99.30	99.00	99.39	99.09	97.34	98.66	99.61	95.77	95.93	95.89	96.96	97.21
Si *(apfu)*	0.001	0.001	0.000	0.001	0.018	0.002	0.004	0.010	0.017	0.022	0.029	0.026
Ti	0.991	0.993	0.995	0.992	0.971	0.989	0.989	0.966	0.952	0.959	0.950	0.952
Al	0.000	0.001	0.000	0.000	0.009	0.001	0.001	0.004	0.007	0.005	0.007	0.009
Fe^{3+}	0.010	0.006	0.006	0.008	0.004	0.010	0.007	0.028	0.030	0.020	0.016	0.017
Mg	0.000	0.000	0.000	0.001	0.000	0.000	0.000	0.001	0.007	0.000	0.008	0.005
Mn	0.000	0.000	0.000	0.000	0.000	0.000	0.000	0.000	0.000	0.000	0.000	0.000
O	2.000	2.000	2.000	2.000	2.000	2.000	2.000	2.000	2.000	2.000	2.000	2.000
Cation Sum	1.003	1.002	1.002	1.003	1.003	1.003	1.002	1.009	1.013	1.007	1.010	1.009

Note: Compositions were recalculated on the basis of 2 O *apfu*; – = not measured. * Determined by stoichiometry using Droop (1987) calculation method.

Table B.15. (Continued) Composition of rutile, ilmenite, and hematite from various rock types across the 2020 Corundum Dome and Pyrochlore Dome sampling area.

Sample	20TN55A	20TN55A	20TN55A	20TN55A	20TN55A	20TN55A	20TN55A	20TN55A	20TN57A	20TN57A	20TN57A	20TN57A
Analysis	211228	211239	2112410	2112511	2112612	2112713	2112814	2112915	271691	271702	271713	271724
Mineral	Rutile	Rutile	Rutile	Rutile	Rutile	Rutile	Rutile	Rutile	Rutile	Rutile	Rutile	Rutile
SiO_2 (wt. %)	0.18	0.72	0.42	1.67	0.37	0.03	0.00	0.01	0.03	0.27	0.11	0.31
TiO_2	99.26	96.96	97.41	92.61	99.09	97.86	97.26	97.55	94.33	92.18	94.59	92.35
Al_2O_3	0.23	0.49	0.28	0.32	0.17	0.01	0.01	0.00	0.01	0.04	0.02	0.07
Fe_2O_3*	0.49	0.44	0.49	1.71	0.47	1.02	0.94	0.92	1.99	2.18	1.76	1.76
MgO	0.01	0.01	0.04	0.02	0.04	0.00	0.00	0.00	0.00	0.02	0.00	0.02
MnO	0.03	0.02	0.01	0.05	0.03	0.01	0.00	0.05	0.01	0.00	0.00	0.01
-(O=F,Cl)	0.05	0.04	0.05	0.17	0.05	0.10	0.09	0.09	0.20	0.22	0.18	0.18
Total	100.21	98.64	98.65	96.38	100.17	98.94	98.22	98.53	96.37	94.69	96.48	94.51
Si *(apfu)*	0.002	0.010	0.006	0.023	0.005	0.000	0.000	0.000	0.000	0.004	0.002	0.004
Ti	0.991	0.981	0.987	0.959	0.989	0.992	0.993	0.993	0.984	0.978	0.984	0.981
Al	0.004	0.008	0.005	0.005	0.003	0.000	0.000	0.000	0.000	0.001	0.000	0.001
Fe^{3+}	0.005	0.004	0.005	0.018	0.005	0.010	0.010	0.009	0.021	0.023	0.018	0.019
Mg	0.000	0.000	0.001	0.000	0.001	0.000	0.000	0.000	0.000	0.000	0.000	0.000
Mn	0.000	0.000	0.000	0.001	0.000	0.000	0.000	0.001	0.000	0.000	0.000	0.000
O	2.000	2.000	2.000	2.000	2.000	2.000	2.000	2.000	2.000	2.000	2.000	2.000
Cation Sum	1.002	1.003	1.003	1.006	1.002	1.003	1.002	1.003	1.005	1.006	1.005	1.005

Table B.15. (Continued) Composition of rutile, ilmenite, and hematite from various rock types across the 2020 Corundum Dome and Pyrochlore Dome sampling area.

Sample	20TN13A	20TN13A	20TN13A	20TN25D	20TN24A	20TN24A	20TN24A	20TN57C-1	20TN55A	20TN57A	20TN57A	20TN57A
Analysis	251101	251112	251123	321921	211511	211522	211533	281432	11671	251601	251612	251623
Mineral	Rutile	Rutile	Rutile	Rutile	Ilmenite	Ilmenite	Ilmenite	Ilmenite	Hematite	Hematite	Hematite	Hematite
SiO_2 (wt. %)	0.31	0.29	1.04	0.84	0.04	0.06	0.03	0.16	2.09	2.11	2.47	2.58
TiO_2	95.77	91.29	90.35	93.07	52.52	52.19	51.68	53.63	0.06	0.04	0.01	0.02
Al_2O_3	0.03	0.03	0.13	0.03	0.00	0.01	0.02	0.06	0.33	0.08	0.07	0.10
Fe_2O_3*	1.84	2.88	2.85	1.28	0.00	0.00	0.69	0.00	83.36	83.93	84.77	82.53
MgO	0.01	0.00	0.01	0.01	0.09	0.08	0.10	0.02	0.53	1.14	0.84	0.96
MnO	0.00	0.03	0.06	0.00	2.97	2.93	2.94	0.06	0.06	0.05	0.05	0.04
-(O=F,Cl)	0.18	0.29	0.29	0.13	0.00	0.00	0.07	0.00				
Total	97.96	94.52	94.44	95.24	98.23	97.85	98.81	92.28	86.43	87.35	88.21	86.22
Si *(apfu)*	0.004	0.004	0.015	0.012	0.001	0.002	0.001	0.004	0.063	0.063	0.072	0.077
Ti	0.981	0.972	0.961	0.978	1.010	1.008	0.992	1.068	0.001	0.001	0.000	0.000
Al	0.000	0.000	0.002	0.001	0.000	0.000	0.001	0.002	0.012	0.003	0.003	0.004
Fe^{3+}	0.019	0.031	0.030	0.013	0.000	0.000	0.013	0.000	1.886	1.878	1.875	1.863
Mg	0.000	0.000	0.000	0.000	0.003	0.003	0.004	0.001	0.024	0.051	0.037	0.043
Mn	0.000	0.000	0.001	0.000	0.064	0.064	0.064	0.001	0.001	0.001	0.001	0.001
O	2.000	2.000	2.000	2.000	3.000	3.000	3.000	3.000	3.000	3.000	3.000	3.000
Cation Sum	1.005	1.008	1.009	1.004	1.989	1.991	2.000	1.926	1.987	1.996	1.988	1.989

Table B.15. (Continued) Composition of rutile, ilmenite, and hematite from various rock types across the 2020 Corundum Dome and Pyrochlore Dome sampling area.

Sample	20TN57A	20TN53	20TN53	20TN53	20TN53	20TN53	20TN17C	20TN17C	20TN10C	20TN10C	20TN10C	20TN10C
Analysis	251634	321971	321982	321993	322004	322015	13711	13722	14761	14772	14783	14794
Mineral	Hematite	Hematite	Hematite	Hematite	Hematite	Hematite	Hematite	Hematite	Hematite	Hematite	Hematite	Hematite
SiO_2 (wt. %)	2.45	0.87	0.78	0.64	3.01	0.98	1.59	1.14	0.03	0.04	0.00	0.00
TiO_2	0.00	0.01	0.00	0.00	0.00	0.00	0.03	0.01	1.22	1.43	0.34	0.27
Al_2O_3	0.14	0.00	0.00	0.01	0.00	0.18	0.00	0.00	0.05	0.06	0.00	0.02
Fe_2O_3*	83.75	83.34	83.51	84.32	86.66	93.65	99.99	101.17	98.88	98.51	99.37	99.03
MgO	1.01	0.35	0.18	0.55	1.04	0.15	0.01	0.01	0.00	0.00	0.00	0.00
MnO	0.07	0.00	0.00	0.00	0.09	0.02	0.21	0.19	0.03	0.04	0.00	0.02
-(O=F,Cl)												
Total	87.42	84.57	84.48	85.52	90.79	94.98	101.83	102.53	100.21	100.08	99.71	99.33
Si *(apfu)*	0.073	0.027	0.024	0.020	0.086	0.027	0.041	0.029	0.001	0.001	0.000	0.000
Ti	0.000	0.000	0.000	0.000	0.000	0.000	0.001	0.000	0.024	0.028	0.007	0.005
Al	0.005	0.000	0.000	0.000	0.000	0.006	0.000	0.000	0.001	0.002	0.000	0.001
Fe^{3+}	1.867	1.953	1.962	1.956	1.855	1.953	1.941	1.957	1.965	1.958	1.991	1.992
Mg	0.045	0.016	0.008	0.025	0.044	0.006	0.001	0.001	0.000	0.000	0.000	0.000
Mn	0.002	0.000	0.000	0.000	0.002	0.000	0.005	0.004	0.001	0.001	0.000	0.000
O	3.000	3.000	3.000	3.000	3.000	3.000	3.000	3.000	3.000	3.000	3.000	3.000
Cation Sum	1.991	1.996	1.995	2.002	1.987	1.993	1.988	1.992	1.992	1.990	1.998	1.998

Table B.15. (Continued) Composition of rutile, ilmenite, and hematite from various rock types across the 2020 Corundum Dome and Pyrochlore Dome sampling area.

Sample	20TN10C	20TN10C	20TN4A	20TN4A	20TN4D	20TN4D	20TN4D	20TN4D	20TN6-2	20TN6-2	20TN6-2	20TN20
Analysis	18941	18952	341371	341382	411661	411672	471891	471902	7591	7602	7613	532191
Mineral	Hematite	Hematite	Hematite	Hematite	Hematite	Hematite	Hematite	Hematite	hematite	hematite	hematite	Hematite
SiO_2 (wt. %)	0.08	0.00	0.01	0.06	0.05	0.03	0.01	0.04	0.08	0.06	0.06	0.03
TiO_2	0.04	1.41	0.98	3.27	0.00	0.05	0.00	0.03	1.86	2.93	0.72	2.92
Al_2O_3	0.13	0.02	0.03	0.08	0.12	0.06	0.02	0.03	0.11	0.00	0.03	0.04
Fe_2O_3*	99.18	98.33	98.99	96.54	99.26	99.03	99.82	98.82	96.94	97.21	99.44	96.17
MgO	0.00	0.00	0.03	0.02	0.00	0.01	0.00	0.00	0.03	0.02	0.02	0.00
MnO	0.02	0.05	0.09	0.08	0.03	0.04	0.00	0.00	0.08	0.08	0.06	0.06
-(O=F,Cl)												
Total	99.45	99.81	100.14	100.06	99.45	99.21	99.86	98.92	99.09	100.30	100.32	99.22
Si *(apfu)*	0.002	0.000	0.000	0.002	0.001	0.001	0.000	0.001	0.002	0.002	0.001	0.001
Ti	0.001	0.028	0.019	0.065	0.000	0.001	0.000	0.001	0.037	0.058	0.014	0.058
Al	0.004	0.001	0.001	0.002	0.004	0.002	0.001	0.001	0.003	0.000	0.001	0.001
Fe^{3+}	1.992	1.961	1.970	1.908	1.994	1.995	1.999	1.997	1.942	1.919	1.977	1.919
Mg	0.000	0.000	0.001	0.001	0.000	0.000	0.000	0.000	0.001	0.001	0.001	0.000
Mn	0.001	0.001	0.002	0.002	0.001	0.001	0.000	0.000	0.002	0.002	0.001	0.001
O	3.000	3.000	3.000	3.000	3.000	3.000	3.000	3.000	3.000	3.000	3.000	3.000
Cation Sum	1.999	1.991	1.994	1.979	2.000	2.000	2.000	1.999	1.988	1.981	1.995	1.981

Table B.15. (Continued) Composition of rutile, ilmenite, and hematite from various rock types across the 2020 Corundum Dome and Pyrochlore Dome sampling area.

Sample	20TN20	20TN54	20TN54	20TN13B-2	20TN13B-2	20TN15B	20TN57C-1	20TN57C-1	20TN57C-1	20TN57C-1
Analysis	532202	271141	271152	11701	11712	221191	241261	241272	241283	281421
Mineral	Hematite	Hematite	Hematite	hematite	hematite	hematite	hematite	hematite	hematite	hematite
SiO_2 (wt. %)	0.07	0.30	0.34	0.57	0.78	0.27	0.30	0.30	0.08	0.09
TiO_2	1.36	3.42	3.62	0.31	0.01	0.63	1.19	0.51	0.10	1.85
Al_2O_3	0.00	0.10	0.13	0.02	0.00	0.12	0.14	0.20	0.06	0.04
Fe_2O_3*	97.12	93.52	93.31	102.24	102.62	98.13	97.22	97.83	98.68	100.58
MgO	0.00	0.12	0.21	0.00	0.01	0.06	0.11	0.13	0.03	0.01
MnO	0.00	0.12	0.16	0.04	0.00	0.07	0.08	0.05	0.02	0.04
-(O=F,Cl)										
Total	98.56	97.58	97.76	103.17	103.41	99.28	99.04	99.02	98.97	102.62
Si *(apfu)*	0.002	0.008	0.009	0.015	0.020	0.007	0.008	0.008	0.002	0.002
Ti	0.028	0.069	0.073	0.006	0.000	0.013	0.024	0.010	0.002	0.036
Al	0.000	0.003	0.004	0.000	0.000	0.004	0.004	0.006	0.002	0.001
Fe^{3+}	1.961	1.889	1.879	1.971	1.973	1.967	1.949	1.965	1.992	1.947
Mg	0.000	0.005	0.008	0.000	0.000	0.002	0.004	0.005	0.001	0.000
Mn	0.000	0.003	0.004	0.001	0.000	0.002	0.002	0.001	0.000	0.001
O	3.000	3.000	3.000	3.000	3.000	3.000	3.000	3.000	3.000	3.000
Cation Sum	1.990	1.977	1.977	1.993	1.993	1.995	1.991	1.996	1.999	1.988

Table B.16. Composition of pyrochlore from various rock types across the 2020 Corundum Dome and Pyrochlore Dome sampling area.

Sample	20TN3-2	20TN3-2	20TN3-2	20TN3-2	20TN15A	20TN15A	20TN15A	20TN15A	20TN15A
Analysis	292201	292212	322311	322322	392411	392422	412441	412452	412463
Species	keno-pyrochlore	keno-pyrochlore	keno-pyrochlore	fluoro-calcio-pyrochlore	fluoro-calcio-pyrochlore	fluoro-calcio-pyrochlore	keno-pyrochlore	fluoro-calcio-pyrochlore	fluoro-calcio-pyrochlore
P_2O_5 (wt. %)	0.02	0.00	0.01	0.00	0.04	0.00	0.04	0.03	0.06
Nb_2O_5	67.43	52.63	71.93	52.84	52.49	51.28	50.45	50.42	53.59
SiO_2	0.92	2.39	0.32	1.74	0.00	0.43	0.56	1.06	0.34
TiO_2	4.71	8.28	3.15	8.16	8.95	8.84	11.04	10.08	9.16
ZrO_2	0.19	0.37	0.12	0.22	0.06	0.89	0.03	0.06	0.02
HfO_2	0.05	0.04	0.00	0.00	0.00	0.07	0.00	0.00	0.00
ThO_2	1.96	0.80	1.35	0.84	1.51	1.98	4.02	4.54	2.75
UO_2	0.27	1.73	0.26	1.45	0.31	0.32	0.34	0.35	0.59
Al_2O_3	0.02	0.12	0.02	0.17	0.01	0.00	0.04	0.24	0.07
Y_2O_3	1.38	0.44	0.98	0.47	0.10	0.13	0.41	0.14	0.08
La_2O_3	0.04	2.20	0.04	0.49	2.70	2.67	3.65	1.31	0.45
Ce_2O_3	0.34	6.21	0.33	2.47	4.39	4.47	10.06	3.60	2.20
Pr_2O_3	0.04	0.73	0.14	0.14	0.48	0.48	1.07	0.39	0.20
Nd_2O_3	0.42	1.61	0.32	0.42	0.57	0.61	2.04	0.67	0.39
Sm_2O_3	0.23	0.25	0.17	0.12	0.00	0.05	0.20	0.07	0.04
Eu_2O_3	0.09	0.06	0.03	0.00	0.00	0.00	0.05	0.03	0.04
Gd_2O_3	0.29	0.07	0.15	0.07	0.05	0.03	0.11	0.11	0.07
Tb_2O_3	0.09	0.08	0.12	0.01	0.00	0.09	0.05	0.04	0.00
Dy_2O_3	0.69	0.23	0.66	0.05	0.07	0.09	0.25	0.46	0.35
Ho_2O_3	0.20	0.16	0.25	0.08	0.01	0.04	0.17	0.00	0.07
Er_2O_3	0.14	0.17	0.15	0.07	0.09	0.07	0.08	0.06	0.03
Tm_2O_3	0.13	0.14	0.14	0.08	0.02	0.02	0.11	0.00	0.07
Yb_2O_3	0.12	0.13	0.19	0.02	0.04	0.09	0.11	0.00	0.08
Lu_2O_3	0.09	0.01	0.02	0.05	0.00	0.00	0.00	0.00	0.00
MgO	0.03	0.02	0.00	0.01	0.00	0.00	0.00	0.08	0.05
CaO	10.92	9.27	13.83	17.08	15.63	15.36	8.28	12.44	15.88
MnO	0.85	0.31	0.41	0.23	0.18	0.21	0.28	1.12	0.79
FeO	3.80	3.15	1.46	0.99	0.10	0.13	1.82	1.70	0.72
PbO	0.32	0.52	0.41	2.23	0.41	0.37	0.52	0.80	0.75
Na_2O	0.03	0.06	0.04	1.68	6.41	6.15	0.29	3.13	5.33
K_2O	0.03	0.03	0.02	0.04	0.01	0.01	0.06	0.10	0.10
F	0.15	0.13	0.11	2.93	5.42	5.22	0.48	3.03	4.97
Cl	0.00	0.00	0.01	0.03	0.00	0.00	0.01	0.00	0.03
-(O=F,Cl)	-0.06	-0.06	-0.05	-1.24	-2.28	-2.20	-0.20	-1.27	-2.10
Total	95.90	92.29	97.12	93.94	97.75	97.90	96.41	94.80	97.15
P (*apfu*)	0.001	0.000	0.001	0.000	0.002	0.000	0.002	0.002	0.003
Nb	1.735	1.452	1.842	1.489	1.554	1.510	1.436	1.429	1.529
Si	0.052	0.146	0.018	0.108	0.000	0.028	0.035	0.067	0.022
Ti	0.202	0.380	0.134	0.383	0.441	0.433	0.523	0.475	0.435

Sample	20TN3-2	20TN3-2	20TN3-2	20TN3-2	20TN15A	20TN15A	20TN15A	20TN15A	20TN15A
Analysis	292201	292212	322311	322322	392411	392422	412441	412452	412463
Species	keno-pyrochlore	keno-pyrochlore	keno-pyrochlore	fluoro-calcio-pyrochlore	fluoro-calcio-pyrochlore	fluoro-calcio-pyrochlore	keno-pyrochlore	fluoro-calcio-pyrochlore	fluoro-calcio-pyrochlore
Zr (*apfu*)	0.005	0.011	0.003	0.007	0.002	0.028	0.001	0.002	0.001
Hf	0.001	0.001	0.000	0.000	0.000	0.001	0.000	0.000	0.000
Th	0.025	0.011	0.017	0.012	0.023	0.029	0.058	0.065	0.039
U	0.003	0.024	0.003	0.020	0.005	0.005	0.005	0.005	0.008
Al	0.001	0.009	0.001	0.012	0.000	0.000	0.003	0.018	0.006
Y	0.042	0.014	0.030	0.016	0.003	0.005	0.014	0.005	0.003
La	0.001	0.050	0.001	0.011	0.065	0.064	0.085	0.030	0.011
Ce	0.007	0.139	0.007	0.056	0.105	0.107	0.232	0.083	0.051
Pr	0.001	0.016	0.003	0.003	0.011	0.011	0.025	0.009	0.004
Nd	0.009	0.035	0.007	0.009	0.013	0.014	0.046	0.015	0.009
Sm	0.004	0.005	0.003	0.003	0.000	0.001	0.004	0.002	0.001
Eu	0.002	0.001	0.001	0.000	0.000	0.000	0.001	0.001	0.001
Gd	0.005	0.001	0.003	0.001	0.001	0.001	0.002	0.002	0.001
Tb	0.002	0.002	0.002	0.000	0.000	0.002	0.001	0.001	0.000
Dy	0.013	0.005	0.012	0.001	0.001	0.002	0.005	0.009	0.007
Ho	0.004	0.003	0.005	0.002	0.000	0.001	0.003	0.000	0.001
Er	0.003	0.003	0.003	0.001	0.002	0.001	0.002	0.001	0.001
Tm	0.002	0.003	0.002	0.002	0.000	0.000	0.002	0.000	0.001
Yb	0.002	0.002	0.003	0.000	0.001	0.002	0.002	0.000	0.002
Lu	0.001	0.000	0.000	0.001	0.000	0.000	0.000	0.000	0.000
Mg	0.002	0.002	0.000	0.001	0.000	0.000	0.000	0.007	0.005
Ca	0.666	0.606	0.839	1.140	1.097	1.071	0.559	0.836	1.073
Mn	0.041	0.016	0.020	0.012	0.010	0.011	0.015	0.060	0.042
Fe	0.181	0.161	0.069	0.052	0.005	0.007	0.096	0.089	0.038
Pb	0.005	0.009	0.006	0.037	0.007	0.006	0.009	0.013	0.013
Na	0.003	0.007	0.004	0.203	0.814	0.776	0.036	0.381	0.652
K	0.002	0.003	0.002	0.003	0.001	0.001	0.005	0.008	0.008
F	0.027	0.026	0.019	0.578	1.122	1.074	0.095	0.600	0.993
Cl	0.000	0.000	0.001	0.004	0.000	0.000	0.001	0.000	0.003
O	5.950	5.991	6.011	6.014	6.105	6.086	6.128	5.967	5.991
Cation Sum	3.023	3.115	3.042	3.586	4.166	4.118	3.205	3.614	3.966
Sum B	2.000	2.000	2.000	2.000	2.000	2.000	2.000	2.000	2.000
Sum A	1.023	1.115	1.042	1.586	2.166	2.118	1.205	1.614	1.966
Anions (X+Y)	5.977	6.017	6.031	6.596	7.227	7.161	6.225	6.568	6.986
A-vacancies	0.977	0.885	0.958	0.414	-0.166	-0.118	0.795	0.386	0.034

Note: Compositions were recalculated on the basis of the sum of 2 B site cation *apfu*. * La, Ce, Pr, and Nd were the only REE contents analyzed.

Table B.16. (Continued) Composition of pyrochlore from various rock types across the 2020 Corundum Dome and Pyrochlore Dome sampling area.

Sample	20TN15A	20TN15A	20TN15A	20TN15A	20TN15A	20TN15A	20TN15A	20TN3-2	20TN3-2
Analysis	412507	412518	442621	442632	442643	442654	442665	542941	542952
Species	fluoro-calcio-pyrochlore	fluoro-calcio-pyrochlore	keno-pyrochlore	keno-pyrochlore	fluoro-calcio-pyrochlore	fluoro-calcio-pyrochlore	keno-pyrochlore	keno-pyrochlore	fluoro-calcio-pyrochlore
P_2O_5 (wt. %)	0.03	0.00	0.00	0.00	0.00	0.04	0.03	0.03	0.00
Nb_2O_5	54.21	49.48	46.58	45.00	52.79	50.97	46.58	53.23	49.99
SiO_2	0.04	7.14	1.29	1.69	0.00	0.15	1.55	2.16	0.09
TiO_2	8.60	7.77	12.39	12.75	9.07	9.68	12.07	8.47	8.19
ZrO_2	0.06	0.00	0.33	0.28	0.07	0.02	0.11	0.24	0.09
HfO_2	0.09	0.00	0.03	0.06	0.07	0.17	0.06	0.03	0.00
ThO_2	2.50	1.83	7.05	6.79	2.46	3.19	5.48	1.08	0.12
UO_2	0.56	0.68	0.23	0.28	0.39	0.40	0.20	1.03	0.79
Al_2O_3	0.03	1.98	0.05	0.09	0.01	0.02	0.09	0.08	0.00
Y_2O_3	0.08	0.09	0.19	0.44	0.09	0.14	0.52	0.67	0.12
La_2O_3	0.22	0.22	3.36	2.67	1.07	1.51	2.64	1.45	0.00
Ce_2O_3	1.95	1.68	6.66	7.06	3.33	3.80	7.07	4.77	0.29
Pr_2O_3	0.15	0.17	0.72	0.76	0.32	0.43	0.87	0.59	0.02
Nd_2O_3	0.26	0.26	1.22	1.71	0.57	0.68	1.89	1.55	0.08
Sm_2O_3	0.01	0.04	0.14	0.25	0.10	0.11	0.27	0.30	0.00
Eu_2O_3	0.00	0.00	0.03	0.07	0.05	0.01	0.02	0.04	0.04
Gd_2O_3	0.03	0.02	0.08	0.23	0.07	0.06	0.21	0.30	0.07
Tb_2O_3	0.08	0.00	0.05	0.06	0.10	0.05	0.06	0.04	0.00
Dy_2O_3	0.10	0.04	0.26	0.26	0.12	0.13	0.30	0.40	0.04
Ho_2O_3	0.02	0.11	0.06	0.09	0.11	0.05	0.16	0.30	0.04
Er_2O_3	0.00	0.01	0.10	0.01	0.01	0.09	0.10	0.11	0.08
Tm_2O_3	0.03	0.07	0.10	0.09	0.02	0.01	0.15	0.10	0.11
Yb_2O_3	0.13	0.03	0.10	0.06	0.00	0.07	0.04	0.00	0.00
Lu_2O_3	0.05	0.04	0.01	0.00	0.05	0.03	0.00	0.05	0.05
MgO	0.00	0.00	0.02	0.03	0.00	0.00	0.01	0.03	0.00
CaO	17.28	15.68	9.36	8.73	16.57	15.03	8.87	10.47	22.00
MnO	0.15	0.11	0.46	0.36	0.27	0.23	0.42	0.32	0.11
FeO	0.28	0.20	2.82	3.19	0.18	0.52	2.94	2.83	0.30
PbO	0.36	0.27	0.46	0.49	0.33	0.40	0.34	0.37	0.42
Na_2O	6.24	5.96	0.12	0.14	6.06	5.38	0.09	0.02	2.80
K_2O	0.06	1.76	0.03	0.03	0.01	0.01	0.02	0.07	0.00
F	5.58	5.91	0.09	0.10	5.48	4.95	0.09	0.00	4.42
Cl	0.00	0.01	0.01	0.00	0.00	0.00	0.02	0.02	0.00
-(O=F,Cl)	-2.35	-2.49	-0.04	-0.04	-2.31	-2.08	-0.04	0.00	-1.86
Total	96.84	99.07	94.35	93.75	97.44	96.26	93.22	91.14	88.41
P (*apfu*)	0.002	0.000	0.000	0.000	0.000	0.002	0.002	0.002	0.000
Nb	1.574	1.187	1.319	1.274	1.553	1.507	1.320	1.464	1.564
Si	0.003	0.379	0.081	0.106	0.000	0.010	0.097	0.131	0.006

Sample	20TN15A	20TN15A	20TN15A	20TN15A	20TN15A	20TN15A	20TN15A	20TN3-2	20TN3-2
Analysis	412507	412518	442621	442632	442643	442654	442665	542941	542952
Species	fluoro-calcio-pyrochlore	fluoro-calcio-pyrochlore	keno-pyrochlore	keno-pyrochlore	fluoro-calcio-pyrochlore	fluoro-calcio-pyrochlore	keno-pyrochlore	keno-pyrochlore	fluoro-calcio-pyrochlore
Ti (*apfu*)	0.415	0.310	0.584	0.600	0.444	0.476	0.569	0.388	0.426
Zr	0.002	0.000	0.010	0.009	0.002	0.001	0.003	0.007	0.003
Hf	0.002	0.000	0.001	0.001	0.001	0.003	0.001	0.000	0.000
Th	0.037	0.022	0.100	0.097	0.036	0.048	0.078	0.015	0.002
U	0.008	0.008	0.003	0.004	0.006	0.006	0.003	0.014	0.012
Al	0.002	0.124	0.003	0.007	0.000	0.001	0.007	0.006	0.000
Y	0.003	0.003	0.006	0.015	0.003	0.005	0.017	0.022	0.004
La	0.005	0.004	0.078	0.062	0.026	0.036	0.061	0.032	0.000
Ce	0.046	0.033	0.153	0.162	0.079	0.091	0.162	0.106	0.007
Pr	0.003	0.003	0.016	0.017	0.007	0.010	0.020	0.013	0.001
Nd	0.006	0.005	0.027	0.038	0.013	0.016	0.042	0.034	0.002
Sm	0.000	0.001	0.003	0.005	0.002	0.002	0.006	0.006	0.000
Eu	0.000	0.000	0.001	0.001	0.001	0.000	0.000	0.001	0.001
Gd	0.001	0.000	0.002	0.005	0.001	0.001	0.004	0.006	0.002
Tb	0.002	0.000	0.001	0.001	0.002	0.001	0.001	0.001	0.000
Dy	0.002	0.001	0.005	0.005	0.002	0.003	0.006	0.008	0.001
Ho	0.000	0.002	0.001	0.002	0.002	0.001	0.003	0.006	0.001
Er	0.000	0.000	0.002	0.000	0.000	0.002	0.002	0.002	0.002
Tm	0.001	0.001	0.002	0.002	0.000	0.000	0.003	0.002	0.002
Yb	0.003	0.000	0.002	0.001	0.000	0.001	0.001	0.000	0.000
Lu	0.001	0.001	0.000	0.000	0.001	0.001	0.000	0.001	0.001
Mg	0.000	0.000	0.002	0.003	0.000	0.000	0.001	0.002	0.000
Ca	1.189	0.892	0.628	0.586	1.155	1.053	0.595	0.682	1.632
Mn	0.008	0.005	0.024	0.019	0.015	0.013	0.022	0.017	0.006
Fe	0.015	0.009	0.148	0.167	0.010	0.028	0.154	0.144	0.017
Pb	0.006	0.004	0.008	0.008	0.006	0.007	0.006	0.006	0.008
Na	0.777	0.613	0.014	0.017	0.764	0.682	0.011	0.003	0.376
K	0.005	0.119	0.002	0.002	0.001	0.001	0.001	0.006	0.000
F	1.134	0.992	0.017	0.019	1.127	1.023	0.017	0.000	0.969
Cl	0.000	0.001	0.001	0.000	0.000	0.000	0.002	0.002	0.000
O	6.027	5.452	6.120	6.088	6.078	6.049	6.086	5.997	6.213
Cation Sum	4.117	3.726	3.228	3.217	4.134	4.010	3.201	3.126	4.078
Sum B	2.000	2.000	2.000	2.000	2.000	2.000	2.000	2.000	2.000
Sum A	2.117	1.726	1.228	1.217	2.134	2.010	1.201	1.126	2.078
Anions (X+Y)	7.161	6.444	6.138	6.107	7.204	7.072	6.106	6.000	7.182
A-vacancies	-0.117	0.274	0.772	0.783	-0.134	-0.010	0.799	0.874	-0.078

Table B.16. (Continued) Composition of pyrochlore from various rock types across the 2020 Corundum Dome and Pyrochlore Dome sampling area.

Sample	20TN3-2	20TN3-2	20TN3-2	20TN20	20TN20	20TN20	20TN12	20TN6-2	20TN6-2
Analysis	542963	542974	542985	121761	121772	121783	231961	182731	182742
Species	keno-pyrochlore	fluoro-calcio-pyrochlore	calcio-pyrochlore	fluoro-calcio-pyrochlore	fluoro-calcio-pyrochlore	fluoro-calcio-pyrochlore	fluoro-calcio-pyrochlore	keno-pyrochlore	keno-pyrochlore
P_2O_5 (wt. %)	0.00	0.01	0.01	0.01	0.03	0.03	0.00	0.03	0.04
Nb_2O_5	43.98	47.50	48.94	57.57	59.19	56.98	53.41	80.59	79.59
SiO_2	3.33	1.06	1.62	0.44	0.36	0.51	0.17	0.02	0.25
TiO_2	9.65	7.75	9.76	4.83	3.95	4.88	7.78	1.51	1.38
ZrO_2	0.21	0.13	0.13	0.22	0.19	0.19	0.14	0.00	0.00
HfO_2	0.11	0.05	0.00	0.07	0.09	0.06	0.07	0.06	0.07
ThO_2	1.28	0.30	0.93	0.02	0.02	0.01	0.00	0.21	0.10
UO_2	1.78	0.77	1.28	0.53	0.43	0.52	0.31	0.02	0.05
Al_2O_3	0.12	0.04	0.07	0.03	0.02	0.02	0.00	0.03	0.09
Y_2O_3	1.31	0.15	0.43	0.09	0.04	0.07	0.15	0.75	0.66
La_2O_3	2.24	0.04	1.94	2.81	2.60	3.19	1.84	0.00	0.00
Ce_2O_3	7.87	0.48	5.62	4.68	4.16	5.30	4.92	0.02	0.08
Pr_2O_3	1.03	0.03	0.62	0.53	0.48	0.57	0.61	0.00	0.00
Nd_2O_3	2.81	0.09	1.22	0.67	0.50	0.85	1.23	0.10	0.10
Sm_2O_3	0.60	0.05	0.25	0.00	0.04	0.03	0.13	0.16	0.14
Eu_2O_3	0.13	0.00	0.00	0.01	0.00	0.01	0.03	0.06	0.04
Gd_2O_3	0.46	0.03	0.09	0.08	0.07	0.09	0.07	0.15	0.13
Tb_2O_3	0.16	0.08	0.01	0.03	0.07	0.10	0.03	0.02	0.01
Dy_2O_3	0.72	0.13	0.24	0.15	0.16	0.16	0.19	0.24	0.29
Ho_2O_3	0.35	0.05	0.10	0.11	0.04	0.04	0.05	0.14	0.05
Er_2O_3	0.07	0.05	0.03	0.07	0.06	0.03	0.00	0.23	0.09
Tm_2O_3	0.12	0.09	0.10	0.09	0.07	0.11	0.05	0.10	0.04
Yb_2O_3	0.02	0.08	0.05	0.06	0.12	0.06	0.03	0.01	0.00
Lu_2O_3	0.08	0.11	0.00	0.02	0.03	0.05	0.03	0.00	0.08
MgO	0.04	0.06	0.04	0.00	0.01	0.01	0.00	0.00	0.02
CaO	6.75	20.46	16.34	17.34	17.26	16.61	18.24	16.50	16.35
MnO	0.39	0.19	0.33	0.31	0.28	0.33	0.32	0.14	0.16
FeO	3.67	0.86	2.02	0.13	0.13	0.33	0.14	1.20	1.05
PbO	0.25	0.39	0.34	0.36	0.33	0.29	0.34	0.27	0.31
Na_2O	0.02	2.66	0.77	2.19	2.40	2.07	2.48	0.02	0.02
K_2O	0.05	0.07	0.05	0.01	0.00	0.01	0.00	0.02	0.08
F	0.14	4.55	0.46	2.88	3.03	2.60	3.51	0.06	0.09
Cl	0.00	0.00	0.00	0.01	0.00	0.00	0.00	0.01	0.01
-(O=F,Cl)	-0.06	-1.92	-0.19	-1.21	-1.27	-1.10	-1.48	-0.03	-0.04
Total	89.67	86.40	93.58	95.13	94.88	95.02	94.81	102.63	101.33
P (*apfu*)	0.000	0.001	0.000	0.001	0.002	0.001	0.000	0.001	0.002
Nb	1.291	1.502	1.414	1.719	1.768	1.711	1.595	1.935	1.922
Si	0.216	0.074	0.104	0.029	0.024	0.034	0.011	0.001	0.013

Sample	20TN3-2	20TN3-2	20TN3-2	20TN20	20TN20	20TN20	20TN12	20TN6-2	20TN6-2
Analysis	542963	542974	542985	121761	121772	121783	231961	182731	182742
Species	keno-pyrochlore	fluoro-calcio-pyrochlore	calcio-pyrochlore	fluoro-calcio-pyrochlore	fluoro-calcio-pyrochlore	fluoro-calcio-pyrochlore	fluoro-calcio-pyrochlore	keno-pyrochlore	keno-pyrochlore
Ti (*apfu*)	0.471	0.408	0.469	0.240	0.196	0.244	0.387	0.060	0.055
Zr	0.007	0.004	0.004	0.007	0.006	0.006	0.004	0.000	0.000
Hf	0.002	0.001	0.000	0.001	0.002	0.001	0.001	0.001	0.001
Th	0.019	0.005	0.013	0.000	0.000	0.000	0.000	0.003	0.001
U	0.026	0.012	0.018	0.008	0.006	0.008	0.005	0.000	0.001
Al	0.009	0.004	0.005	0.002	0.002	0.002	0.000	0.002	0.006
Y	0.045	0.006	0.015	0.003	0.001	0.002	0.005	0.021	0.019
La	0.054	0.001	0.046	0.068	0.063	0.078	0.045	0.000	0.000
Ce	0.187	0.012	0.132	0.113	0.101	0.129	0.119	0.000	0.002
Pr	0.024	0.001	0.014	0.013	0.011	0.014	0.015	0.000	0.000
Nd	0.065	0.002	0.028	0.016	0.012	0.020	0.029	0.002	0.002
Sm	0.013	0.001	0.005	0.000	0.001	0.001	0.003	0.003	0.002
Eu	0.003	0.000	0.000	0.000	0.000	0.000	0.001	0.001	0.001
Gd	0.010	0.001	0.002	0.002	0.002	0.002	0.002	0.003	0.002
Tb	0.003	0.002	0.000	0.001	0.001	0.002	0.001	0.000	0.000
Dy	0.015	0.003	0.005	0.003	0.003	0.003	0.004	0.004	0.005
Ho	0.007	0.001	0.002	0.002	0.001	0.001	0.001	0.002	0.001
Er	0.001	0.001	0.001	0.001	0.001	0.001	0.000	0.004	0.002
Tm	0.002	0.002	0.002	0.002	0.001	0.002	0.001	0.002	0.001
Yb	0.000	0.002	0.001	0.001	0.002	0.001	0.001	0.000	0.000
Lu	0.002	0.002	0.000	0.000	0.001	0.001	0.001	0.000	0.001
Mg	0.004	0.006	0.004	0.000	0.001	0.001	0.000	0.000	0.001
Ca	0.469	1.533	1.118	1.227	1.222	1.182	1.291	0.939	0.935
Mn	0.021	0.011	0.018	0.017	0.016	0.019	0.018	0.006	0.007
Fe	0.199	0.050	0.108	0.007	0.007	0.018	0.008	0.053	0.047
Pb	0.004	0.007	0.006	0.006	0.006	0.005	0.006	0.004	0.005
Na	0.002	0.361	0.096	0.281	0.307	0.266	0.318	0.002	0.002
K	0.004	0.006	0.004	0.001	0.000	0.001	0.000	0.001	0.006
F	0.029	1.007	0.093	0.602	0.632	0.547	0.733	0.011	0.015
Cl	0.000	0.000	0.000	0.001	0.000	0.000	0.000	0.001	0.000
O	6.058	6.115	6.395	6.312	6.289	6.341	6.261	6.035	6.008
Cation Sum	3.178	4.023	3.633	3.774	3.767	3.756	3.872	3.051	3.041
Sum B	2.000	2.000	2.000	2.000	2.000	2.000	2.000	2.000	2.000
Sum A	1.178	2.023	1.633	1.774	1.767	1.756	1.872	1.051	1.041
Anions (X+Y)	6.086	7.121	6.488	6.915	6.922	6.887	6.995	6.046	6.023
A-vacancies	0.822	-0.023	0.367	0.226	0.233	0.244	0.128	0.949	0.959

Table B.16. (Continued) Composition of pyrochlore from various rock types across the 2020 Corundum Dome and Pyrochlore Dome sampling area.

Sample	20TN6-2	20TN6-2	20TN6-2	20TN6-2	20TN6-2	20TN6-2	20TN6-2	20TN6-2	20TN6-2
Analysis	182753	182764	182775	182786	182797	232871	242881	252891	262901
Species	calcio-pyrochlore	keno-pyrochlore	calcio-pyrochlore	calcio-pyrochlore	calcio-pyrochlore	keno-pyrochlore	keno-pyrochlore	keno-pyrochlore	keno-pyrochlore
P_2O_5 (wt. %)	0.00	0.02	0.04	0.00	0.03	0.05	0.07	0.02	0.00
Nb_2O_5	80.56	71.74	79.30	78.03	79.87	73.12	74.43	77.24	77.03
SiO_2	0.02	2.73	0.19	0.40	0.10	1.13	1.86	0.04	0.01
TiO_2	1.01	1.77	1.60	1.88	1.21	2.81	1.54	2.15	2.77
ZrO_2	0.00	0.02	0.00	0.01	0.00	0.02	0.00	0.00	0.04
HfO_2	0.03	0.00	0.14	0.03	0.02	0.04	0.15	0.00	0.11
ThO_2	0.10	0.22	0.20	0.18	0.18	1.04	0.18	0.48	0.68
UO_2	0.02	0.19	0.14	0.17	0.10	0.30	0.11	0.09	0.11
Al_2O_3	0.03	0.66	0.08	0.13	0.05	0.41	0.94	0.04	0.02
Y_2O_3	0.90	0.78	0.90	0.57	0.68	0.63	0.73	1.60	1.00
La_2O_3	0.04	0.04	0.00	0.00	0.02	0.14	0.04	0.02	0.02
Ce_2O_3	0.10	0.08	0.05	0.11	0.07	0.62	0.14	0.10	0.11
Pr_2O_3	0.05	0.05	0.02	0.04	0.02	0.05	0.05	0.05	0.03
Nd_2O_3	0.12	0.06	0.05	0.07	0.05	0.13	0.10	0.14	0.08
Sm_2O_3	0.12	0.06	0.06	0.10	0.00	0.05	0.04	0.11	0.06
Eu_2O_3	0.06	0.02	0.01	0.04	0.00	0.03	0.06	0.07	0.03
Gd_2O_3	0.35	0.12	0.14	0.06	0.13	0.17	0.09	0.33	0.09
Tb_2O_3	0.00	0.00	0.04	0.10	0.06	0.05	0.10	0.02	0.05
Dy_2O_3	0.43	0.25	0.30	0.14	0.25	0.22	0.19	0.63	0.24
Ho_2O_3	0.26	0.10	0.15	0.13	0.06	0.09	0.11	0.31	0.12
Er_2O_3	0.25	0.16	0.03	0.16	0.05	0.06	0.08	0.23	0.06
Tm_2O_3	0.22	0.10	0.10	0.16	0.15	0.07	0.06	0.09	0.07
Yb_2O_3	0.17	0.04	0.00	0.12	0.04	0.13	0.07	0.00	0.10
Lu_2O_3	0.01	0.05	0.00	0.00	0.08	0.06	0.02	0.00	0.00
MgO	0.01	0.51	0.13	0.00	0.06	0.02	0.03	0.00	0.00
CaO	16.38	14.82	16.37	16.44	16.45	14.66	16.27	15.60	16.30
MnO	0.11	0.11	0.14	0.11	0.12	0.19	0.16	0.10	0.16
FeO	2.16	4.88	2.75	2.68	2.13	1.19	0.75	0.61	0.45
PbO	0.32	0.37	0.32	0.29	0.37	2.05	0.49	0.40	0.55
Na_2O	0.02	0.01	0.00	0.01	0.01	0.09	0.04	0.06	0.14
K_2O	0.01	0.26	0.09	0.00	0.07	0.03	0.01	0.02	0.03
F	0.09	0.14	0.10	0.02	0.07	0.23	0.00	0.14	0.29
Cl	0.00	0.00	0.01	0.01	0.00	0.01	0.00	0.03	0.00
-(O=F,Cl)	-0.04	-0.06	-0.04	-0.01	-0.03	-0.10	0.00	-0.06	-0.12
Total	103.93	100.32	103.41	102.18	102.47	99.81	98.92	100.67	100.62
P (*apfu*)	0.000	0.001	0.002	0.000	0.001	0.002	0.003	0.001	0.000
Nb	1.955	1.704	1.907	1.893	1.936	1.793	1.775	1.906	1.883
Si	0.001	0.144	0.010	0.022	0.005	0.061	0.098	0.002	0.000

Sample	20TN6-2	20TN6-2	20TN6-2	20TN6-2	20TN6-2	20TN6-2	20TN6-2	20TN6-2	20TN6-2
Analysis	182753	182764	182775	182786	182797	232871	242881	252891	262901
Species	calcio-pyrochlore	keno-pyrochlore	calcio-pyrochlore	calcio-pyrochlore	calcio-pyrochlore	keno-pyrochlore	keno-pyrochlore	keno-pyrochlore	keno-pyrochlore
Ti (*apfu*)	0.041	0.070	0.064	0.076	0.049	0.115	0.061	0.088	0.113
Zr	0.000	0.001	0.000	0.000	0.000	0.001	0.000	0.000	0.001
Hf	0.000	0.000	0.002	0.000	0.000	0.001	0.002	0.000	0.002
Th	0.001	0.003	0.002	0.002	0.002	0.013	0.002	0.006	0.008
U	0.000	0.002	0.002	0.002	0.001	0.004	0.001	0.001	0.001
Al	0.002	0.041	0.005	0.008	0.003	0.026	0.058	0.002	0.001
Y	0.026	0.022	0.025	0.016	0.019	0.018	0.021	0.047	0.029
La	0.001	0.001	0.000	0.000	0.000	0.003	0.001	0.000	0.000
Ce	0.002	0.001	0.001	0.002	0.001	0.012	0.003	0.002	0.002
Pr	0.001	0.001	0.000	0.001	0.000	0.001	0.001	0.001	0.001
Nd	0.002	0.001	0.001	0.001	0.001	0.003	0.002	0.003	0.002
Sm	0.002	0.001	0.001	0.002	0.000	0.001	0.001	0.002	0.001
Eu	0.001	0.000	0.000	0.001	0.000	0.001	0.001	0.001	0.001
Gd	0.006	0.002	0.002	0.001	0.002	0.003	0.002	0.006	0.002
Tb	0.000	0.000	0.001	0.002	0.001	0.001	0.002	0.000	0.001
Dy	0.008	0.004	0.005	0.002	0.004	0.004	0.003	0.011	0.004
Ho	0.004	0.002	0.003	0.002	0.001	0.002	0.002	0.005	0.002
Er	0.004	0.003	0.000	0.003	0.001	0.001	0.001	0.004	0.001
Tm	0.004	0.002	0.002	0.003	0.002	0.001	0.001	0.001	0.001
Yb	0.003	0.001	0.000	0.002	0.001	0.002	0.001	0.000	0.002
Lu	0.000	0.001	0.000	0.000	0.001	0.001	0.000	0.000	0.000
Mg	0.001	0.040	0.010	0.000	0.005	0.002	0.003	0.000	0.000
Ca	0.942	0.835	0.933	0.946	0.945	0.852	0.920	0.912	0.944
Mn	0.005	0.005	0.006	0.005	0.006	0.009	0.007	0.005	0.007
Fe	0.097	0.214	0.122	0.120	0.096	0.054	0.033	0.028	0.020
Pb	0.005	0.005	0.005	0.004	0.005	0.030	0.007	0.006	0.008
Na	0.002	0.001	0.000	0.001	0.001	0.010	0.004	0.006	0.014
K	0.001	0.018	0.006	0.000	0.005	0.002	0.001	0.002	0.002
F	0.016	0.023	0.017	0.004	0.011	0.039	0.000	0.024	0.049
Cl	0.000	0.000	0.001	0.001	0.000	0.001	0.000	0.002	0.000
O	6.118	5.921	6.074	6.081	6.073	5.927	5.895	6.035	5.995
Cation Sum	3.117	3.124	3.119	3.118	3.097	3.027	3.016	3.050	3.053
Sum B	2.000	2.000	2.000	2.000	2.000	2.000	2.000	2.000	2.000
Sum A	1.117	1.124	1.119	1.118	1.097	1.027	1.016	1.050	1.053
Anions (X+Y)	6.134	5.945	6.091	6.085	6.084	5.967	5.895	6.061	6.044
A-vacancies	0.883	0.876	0.881	0.882	0.903	0.973	0.984	0.950	0.947

Table B.16. (Continued) Composition of pyrochlore from various rock types across the 2020 Corundum Dome and Pyrochlore Dome sampling area.

Sample	20TN6-2	20TN6-2	20TN6-2	20TN2	20TN2	20TN2	20TN2	20TN2	20TN2
Analysis	262912	272921	272932	21691	21702	81941	81952	81963	81974
Species	fluoro-calcio-pyrochlore	keno-pyrochlore	keno-pyrochlore	keno-pyrochlore	keno-pyrochlore	keno-pyrochlore	keno-pyrochlore	calcio-pyrochlore	keno-pyrochlore
P_2O_5 (wt. %)	0.02	0.51	0.39	0.02	0.01	0.00	0.03	0.03	0.02
Nb_2O_5	60.69	48.35	43.43	81.68	79.72	76.97	76.23	75.60	76.13
SiO_2	0.98	3.24	9.11	0.19	0.91	0.00	0.02	0.23	0.09
TiO_2	3.21	3.74	3.61	0.79	0.88	2.44	2.94	2.46	2.58
ZrO_2	0.00	0.10	0.14	0.00	0.00	0.03	0.02	0.00	0.05
HfO_2	0.07	0.18	0.14	0.00	0.17	0.00	0.13	0.03	0.06
ThO_2	0.03	0.00	0.06	0.48	0.82	0.99	0.99	1.62	1.94
UO_2	0.78	2.14	1.81	0.08	0.11	0.02	0.05	0.16	0.12
Al_2O_3	0.31	0.67	2.52	0.05	0.32	0.02	0.01	0.01	0.02
Y_2O_3	0.09	0.06	0.06	0.35	0.35	0.53	0.51	0.67	0.59
La_2O_3	0.03	0.18	0.13	0.00	0.04	0.01	0.15	0.08	0.05
Ce_2O_3	0.31	2.97	1.68	0.07	0.00	0.88	1.30	0.23	0.15
Pr_2O_3	0.00	0.06	0.03	0.00	0.04	0.17	0.17	0.04	0.03
Nd_2O_3	0.06	0.13	0.13	0.09	0.12	0.84	0.86	0.29	0.23
Sm_2O_3	0.01	0.00	0.07	0.06	0.04	0.18	0.22	0.20	0.18
Eu_2O_3	0.05	0.04	0.02	0.03	0.07	0.04	0.03	0.03	0.07
Gd_2O_3	0.04	0.00	0.12	0.11	0.06	0.02	0.21	0.29	0.27
Tb_2O_3	0.06	0.00	0.11	0.05	0.09	0.06	0.02	0.21	0.12
Dy_2O_3	0.13	0.09	0.14	0.12	0.15	0.15	0.12	0.19	0.27
Ho_2O_3	0.04	0.02	0.07	0.07	0.09	0.13	0.16	0.24	0.14
Er_2O_3	0.08	0.04	0.19	0.12	0.11	0.18	0.12	0.21	0.04
Tm_2O_3	0.18	0.07	0.18	0.13	0.14	0.15	0.12	0.10	0.15
Yb_2O_3	0.11	0.16	0.08	0.05	0.09	0.02	0.10	0.12	0.05
Lu_2O_3	0.18	0.00	0.02	0.08	0.00	0.08	0.17	0.04	0.07
MgO	0.40	0.02	3.53	0.00	0.01	0.00	0.00	0.00	0.00
CaO	19.03	5.64	9.24	16.85	16.36	15.77	15.52	15.93	15.96
MnO	0.16	0.15	0.24	0.08	0.12	0.08	0.06	0.11	0.12
FeO	0.99	2.41	3.21	0.33	0.46	0.46	0.43	0.69	0.71
PbO	1.51	21.23	12.16	0.45	0.40	0.31	0.25	0.29	0.34
Na_2O	3.51	0.82	1.58	0.00	0.00	0.01	0.01	0.00	0.02
K_2O	0.17	0.05	1.41	0.03	0.32	0.01	0.00	0.00	0.01
F	4.62	1.19	2.33	0.12	0.05	0.17	0.13	0.13	0.13
Cl	0.01	0.04	0.02	0.00	0.01	0.01	0.01	0.01	0.00
-(O=F,Cl)	-1.95	-0.51	-0.99	-0.05	-0.03	-0.07	-0.06	-0.06	-0.06
Total	95.95	93.81	96.99	102.42	102.03	100.66	101.03	100.19	100.68
P (*apfu*)	0.001	0.030	0.016	0.001	0.001	0.000	0.001	0.001	0.001
Nb	1.724	1.494	0.978	1.955	1.894	1.898	1.874	1.883	1.884
Si	0.062	0.222	0.454	0.010	0.048	0.000	0.001	0.013	0.005

Sample	20TN6-2	20TN6-2	20TN6-2	20TN2	20TN2	20TN2	20TN2	20TN2	20TN2
Analysis	262912	272921	272932	21691	21702	81941	81952	81963	81974
Species	fluoro-calcio-pyrochlore	keno-pyrochlore	keno-pyrochlore	keno-pyrochlore	keno-pyrochlore	keno-pyrochlore	keno-pyrochlore	calcio-pyrochlore	keno-pyrochlore
Ti (*apfu*)	0.152	0.192	0.135	0.032	0.035	0.100	0.120	0.102	0.106
Zr	0.000	0.003	0.003	0.000	0.000	0.001	0.001	0.000	0.001
Hf	0.001	0.004	0.002	0.000	0.003	0.000	0.002	0.001	0.001
Th	0.000	0.000	0.001	0.006	0.010	0.012	0.012	0.020	0.024
U	0.011	0.033	0.020	0.001	0.001	0.000	0.001	0.002	0.001
Al	0.023	0.054	0.148	0.003	0.020	0.001	0.001	0.001	0.001
Y	0.003	0.002	0.002	0.010	0.010	0.015	0.015	0.020	0.017
La	0.001	0.005	0.002	0.000	0.001	0.000	0.003	0.002	0.001
Ce	0.007	0.074	0.031	0.001	0.000	0.018	0.026	0.005	0.003
Pr	0.000	0.002	0.001	0.000	0.001	0.003	0.003	0.001	0.001
Nd	0.001	0.003	0.002	0.002	0.002	0.016	0.017	0.006	0.005
Sm	0.000	0.000	0.001	0.001	0.001	0.003	0.004	0.004	0.003
Eu	0.001	0.001	0.000	0.000	0.001	0.001	0.000	0.001	0.001
Gd	0.001	0.000	0.002	0.002	0.001	0.000	0.004	0.005	0.005
Tb	0.001	0.000	0.002	0.001	0.002	0.001	0.000	0.004	0.002
Dy	0.003	0.002	0.002	0.002	0.003	0.003	0.002	0.003	0.005
Ho	0.001	0.000	0.001	0.001	0.002	0.002	0.003	0.004	0.002
Er	0.002	0.001	0.003	0.002	0.002	0.003	0.002	0.004	0.001
Tm	0.004	0.001	0.003	0.002	0.002	0.002	0.002	0.002	0.003
Yb	0.002	0.003	0.001	0.001	0.001	0.000	0.002	0.002	0.001
Lu	0.003	0.000	0.000	0.001	0.000	0.001	0.003	0.001	0.001
Mg	0.038	0.002	0.263	0.000	0.000	0.000	0.000	0.000	0.000
Ca	1.281	0.413	0.493	0.956	0.921	0.922	0.904	0.940	0.936
Mn	0.008	0.009	0.010	0.004	0.005	0.004	0.003	0.005	0.006
Fe	0.052	0.138	0.134	0.014	0.020	0.021	0.020	0.032	0.033
Pb	0.026	0.391	0.163	0.006	0.006	0.005	0.004	0.004	0.005
Na	0.428	0.109	0.153	0.000	0.000	0.001	0.001	0.000	0.002
K	0.014	0.004	0.090	0.002	0.022	0.001	0.000	0.000	0.001
F	0.917	0.257	0.367	0.021	0.009	0.029	0.022	0.022	0.022
Cl	0.001	0.004	0.002	0.000	0.001	0.001	0.001	0.001	0.000
O	6.010	5.816	5.019	6.001	5.959	6.016	6.011	6.048	6.039
Cation Sum	3.851	3.191	3.117	3.016	3.013	3.036	3.030	3.065	3.058
Sum B	2.000	2.000	2.000	2.000	2.000	2.000	2.000	2.000	2.000
Sum A	1.851	1.191	1.117	1.016	1.013	1.036	1.030	1.065	1.058
Anions (X+Y)	6.928	6.078	5.388	6.022	5.969	6.046	6.034	6.071	6.061
A-vacancies	0.149	0.809	0.883	0.984	0.987	0.964	0.970	0.935	0.942

Table B.16. (Continued) Composition of pyrochlore from various rock types across the 2020 Corundum Dome and Pyrochlore Dome sampling area.

Sample	20TN2	20TN2	20TN2	20TN2	20TN2	20TN2	20TN2	20TN2	20TN2
Analysis	91981	91992	92003	92014	102021	102032	102043	102054	102065
Species	keno-pyrochlore	fluoro-calcio-pyrochlore	calcio-pyrochlore	keno-pyrochlore	fluoro-calcio-pyrochlore	fluoro-calcio-pyrochlore	fluoro-calcio-pyrochlore	fluoro-calcio-pyrochlore	fluoro-calcio-pyrochlore
P_2O_5 (wt. %)	0.02	0.05	0.00	0.06	0.03	0.01	0.02	0.00	0.01
Nb_2O_5	49.39	51.89	49.55	49.09	51.65	52.68	48.34	49.30	53.80
SiO_2	2.45	0.10	2.80	2.52	0.15	0.10	1.13	0.96	0.15
TiO_2	9.16	10.17	9.67	9.01	10.04	9.85	8.55	8.82	9.44
ZrO_2	0.26	1.20	1.22	0.96	1.25	0.48	1.27	0.82	0.67
HfO_2	0.00	0.09	0.06	0.03	0.08	0.05	0.01	0.00	0.12
ThO_2	4.30	2.48	4.55	4.22	2.28	2.33	4.85	4.73	2.10
UO_2	0.03	0.27	0.15	0.19	0.14	0.18	0.17	0.25	0.08
Al_2O_3	0.18	0.02	0.14	0.13	0.01	0.02	0.08	0.08	0.02
Y_2O_3	0.49	0.12	0.40	0.49	0.14	0.11	0.28	0.34	0.14
La_2O_3	1.47	0.03	0.98	1.06	0.02	0.01	0.55	0.66	0.08
Ce_2O_3	7.17	0.46	4.35	4.92	1.02	0.84	0.91	1.50	1.55
Pr_2O_3	1.06	0.09	0.61	0.76	0.11	0.07	0.15	0.29	0.16
Nd_2O_3	3.22	0.15	1.89	2.09	0.42	0.30	0.69	0.82	0.65
Sm_2O_3	0.48	0.00	0.34	0.31	0.02	0.05	0.17	0.14	0.06
Eu_2O_3	0.14	0.04	0.07	0.05	0.02	0.06	0.04	0.04	0.05
Gd_2O_3	0.41	0.07	0.24	0.23	0.00	0.05	0.06	0.03	0.01
Tb_2O_3	0.11	0.04	0.07	0.10	0.08	0.08	0.10	0.01	0.04
Dy_2O_3	0.25	0.12	0.22	0.25	0.08	0.09	0.07	0.10	0.15
Ho_2O_3	0.18	0.09	0.10	0.24	0.09	0.11	0.11	0.05	0.06
Er_2O_3	0.09	0.07	0.03	0.02	0.07	0.13	0.08	0.16	0.08
Tm_2O_3	0.21	0.13	0.12	0.18	0.10	0.02	0.15	0.10	0.00
Yb_2O_3	0.10	0.12	0.00	0.11	0.01	0.00	0.09	0.00	0.00
Lu_2O_3	0.14	0.00	0.12	0.01	0.09	0.00	0.04	0.11	0.00
MgO	0.01	0.00	0.02	0.02	0.00	0.00	0.00	0.00	0.00
CaO	8.69	22.28	11.97	10.72	22.51	22.32	20.23	19.08	21.99
MnO	0.27	0.13	0.28	0.25	0.16	0.16	0.15	0.10	0.16
FeO	2.38	0.23	2.16	2.09	0.19	0.19	0.61	0.63	0.40
PbO	1.26	0.33	0.93	1.86	0.39	0.37	0.84	1.23	0.34
Na_2O	0.12	2.25	0.60	0.46	2.17	2.27	2.01	1.84	2.17
K_2O	0.03	0.01	0.05	0.04	0.00	0.01	0.01	0.03	0.01
F	0.45	4.19	0.59	0.75	4.26	4.26	4.07	3.72	4.16
Cl	0.01	0.00	0.00	0.03	0.00	0.00	0.01	0.04	0.03
-(O=F,Cl)	-0.19	-1.76	-0.25	-0.32	-1.79	-1.79	-1.72	-1.57	-1.76
Total	94.34	95.46	94.04	92.91	95.79	95.39	94.11	94.41	96.90
P (*apfu*)	0.001	0.002	0.000	0.003	0.002	0.000	0.001	0.000	0.000
Nb	1.394	1.471	1.346	1.378	1.472	1.507	1.450	1.468	1.522
Si	0.153	0.006	0.168	0.157	0.009	0.006	0.075	0.063	0.009

Sample	20TN2	20TN2	20TN2	20TN2	20TN2	20TN2	20TN2	20TN2	20TN2
Analysis	91981	91992	92003	92014	102021	102032	102043	102054	102065
Species	keno-pyrochlore	fluoro-calcio-pyrochlore	calcio-pyrochlore	keno-pyrochlore	fluoro-calcio-pyrochlore	fluoro-calcio-pyrochlore	fluoro-calcio-pyrochlore	fluoro-calcio-pyrochlore	fluoro-calcio-pyrochlore
Ti (*apfu*)	0.430	0.480	0.437	0.421	0.476	0.469	0.426	0.437	0.444
Zr	0.008	0.037	0.036	0.029	0.039	0.015	0.041	0.026	0.021
Hf	0.000	0.002	0.001	0.001	0.002	0.001	0.000	0.000	0.002
Th	0.061	0.035	0.062	0.060	0.033	0.034	0.073	0.071	0.030
U	0.000	0.004	0.002	0.003	0.002	0.002	0.003	0.004	0.001
Al	0.013	0.001	0.010	0.010	0.000	0.002	0.006	0.006	0.001
Y	0.016	0.004	0.013	0.016	0.005	0.004	0.010	0.012	0.005
La	0.034	0.001	0.022	0.024	0.001	0.000	0.014	0.016	0.002
Ce	0.164	0.011	0.096	0.112	0.024	0.019	0.022	0.036	0.036
Pr	0.024	0.002	0.013	0.017	0.003	0.002	0.004	0.007	0.004
Nd	0.072	0.003	0.041	0.046	0.009	0.007	0.016	0.019	0.015
Sm	0.010	0.000	0.007	0.007	0.000	0.001	0.004	0.003	0.001
Eu	0.003	0.001	0.001	0.001	0.001	0.001	0.001	0.001	0.001
Gd	0.009	0.001	0.005	0.005	0.000	0.001	0.001	0.001	0.000
Tb	0.002	0.001	0.001	0.002	0.002	0.002	0.002	0.000	0.001
Dy	0.005	0.002	0.004	0.005	0.002	0.002	0.002	0.002	0.003
Ho	0.004	0.002	0.002	0.005	0.002	0.002	0.002	0.001	0.001
Er	0.002	0.001	0.001	0.000	0.001	0.002	0.002	0.003	0.002
Tm	0.004	0.003	0.002	0.003	0.002	0.000	0.003	0.002	0.000
Yb	0.002	0.002	0.000	0.002	0.000	0.000	0.002	0.000	0.000
Lu	0.003	0.000	0.002	0.000	0.002	0.000	0.001	0.002	0.000
Mg	0.001	0.000	0.002	0.002	0.000	0.000	0.000	0.000	0.000
Ca	0.581	1.497	0.771	0.713	1.520	1.513	1.438	1.346	1.474
Mn	0.014	0.007	0.014	0.013	0.008	0.009	0.008	0.006	0.009
Fe	0.124	0.012	0.109	0.108	0.010	0.010	0.034	0.035	0.021
Pb	0.021	0.006	0.015	0.031	0.007	0.006	0.015	0.022	0.006
Na	0.014	0.274	0.070	0.055	0.266	0.279	0.258	0.235	0.263
K	0.003	0.001	0.004	0.003	0.000	0.001	0.001	0.002	0.001
F	0.089	0.831	0.112	0.147	0.849	0.853	0.855	0.774	0.823
Cl	0.001	0.000	0.000	0.003	0.000	0.000	0.001	0.005	0.003
O	6.046	6.110	5.999	5.998	6.138	6.142	6.198	6.177	6.154
Cation Sum	3.172	3.870	3.257	3.232	3.898	3.898	3.915	3.827	3.873
Sum B	2.000	2.000	2.000	2.000	2.000	2.000	2.000	2.000	2.000
Sum A	1.172	1.870	1.257	1.232	1.898	1.898	1.915	1.827	1.873
Anions (X+Y)	6.136	6.941	6.112	6.147	6.986	6.995	7.053	6.956	6.980
A-vacancies	0.828	0.130	0.743	0.768	0.102	0.102	0.085	0.173	0.127

Table B.16. (Continued) Composition of pyrochlore from various rock types across the 2020 Corundum Dome and Pyrochlore Dome sampling area.

Sample	20TN2	20TN2	20TN2	20TN25D	20TN25D	20TN4D	20TN4D	20TN4D	20TN4D
Analysis	132131	132142	132153	151962	151973	182362	182406	192411	192422
Species	keno-pyrochlore	keno-pyrochlore	calcio-pyrochlore	keno-pyrochlore	keno-pyrochlore	calcio-pyrochlore	keno-pyrochlore	fluoro-calcio-pyrochlore	fluoro-calcio-pyrochlore
P_2O_5 (wt. %)	0.06	0.03	0.00	0.02	0.00	0.01	0.04	0.03	0.01
Nb_2O_5	76.92	76.01	77.30	45.29	47.67	72.59	64.00	58.27	56.29
SiO_2	0.03	0.04	0.01	2.85	2.88	0.09	9.75	0.27	0.12
TiO_2	2.61	3.09	1.98	13.20	12.25	1.93	2.63	6.97	6.61
ZrO_2	0.02	0.02	0.01	0.38	0.29	0.00	0.02	0.28	0.11
HfO_2	0.00	0.12	0.00	0.00	0.04	0.04	0.07	0.17	0.00
ThO_2	1.46	2.05	1.18	10.92	9.76	0.97	1.12	0.05	0.00
UO_2	0.11	0.18	0.16	0.29	0.20	0.11	0.12	1.08	1.07
Al_2O_3	0.00	0.01	0.00	0.29	0.16	0.05	3.18	0.04	0.02
Y_2O_3	0.64	0.80	0.51	0.20	0.28	0.30	0.23	0.10	0.08
La_2O_3	0.02	0.04	0.00	1.57	0.77	0.31	0.29	0.35	0.35
Ce_2O_3	0.12	0.14	0.12	4.90	3.41	1.67	1.45	1.99	1.71
Pr_2O_3	0.04	0.09	0.03	0.66	0.56	0.28	0.25	0.19	0.16
Nd_2O_3	0.18	0.20	0.10	1.71	1.46	0.80	0.84	0.36	0.38
Sm_2O_3	0.06	0.09	0.06	0.31	0.35	0.12	0.14	0.04	0.06
Eu_2O_3	0.04	0.02	0.00	0.12	0.07	0.06	0.06	0.00	0.04
Gd_2O_3	0.09	0.19	0.12	0.22	0.22	0.04	0.10	0.10	0.07
Tb_2O_3	0.04	0.04	0.08	0.11	0.05	0.03	0.03	0.08	0.03
Dy_2O_3	0.19	0.24	0.11	0.26	0.84	0.11	0.31	0.13	0.11
Ho_2O_3	0.08	0.20	0.01	0.09	0.16	0.05	0.22	0.12	0.21
Er_2O_3	0.04	0.17	0.06	0.07	0.07	0.14	0.16	0.11	0.12
Tm_2O_3	0.10	0.09	0.08	0.02	0.19	0.12	0.15	0.14	0.09
Yb_2O_3	0.15	0.13	0.04	0.05	0.08	0.08	0.19	0.00	0.09
Lu_2O_3	0.08	0.00	0.01	0.00	0.00	0.00	0.05	0.00	0.00
MgO	0.00	0.00	0.00	0.11	0.06	0.00	0.03	0.00	0.00
CaO	16.27	16.07	16.61	6.84	3.39	14.02	11.87	20.40	19.34
MnO	0.14	0.09	0.12	0.43	2.27	0.17	0.73	0.25	0.22
FeO	0.52	0.71	0.36	2.96	5.73	6.27	2.76	0.36	3.56
PbO	0.29	0.36	0.33	0.49	0.25	0.48	0.36	0.32	0.21
Na_2O	0.01	0.00	0.00	0.05	0.03	0.01	2.15	3.32	3.28
K_2O	0.01	0.03	0.00	0.05	0.05	0.01	0.06	0.03	0.03
F	0.16	0.10	0.11	0.15	0.28	0.19	0.21	4.30	4.29
Cl	0.02	0.02	0.01	0.01	0.03	0.01	0.07	0.01	0.00
-(O=F,Cl)	-0.07	-0.05	-0.05	-0.07	-0.13	-0.08	-0.10	-1.81	-1.81
Total	100.47	101.34	99.45	94.55	93.72	100.98	103.55	98.04	96.87
P (*apfu*)	0.003	0.001	0.000	0.001	0.000	0.001	0.001	0.002	0.000
Nb	1.888	1.867	1.917	1.206	1.265	1.906	1.300	1.640	1.662
Si	0.001	0.002	0.001	0.168	0.169	0.005	0.438	0.017	0.008

Sample	20TN2	20TN2	20TN2	20TN25D	20TN25D	20TN4D	20TN4D	20TN4D	20TN4D
Analysis	132131	132142	132153	151962	151973	182362	182406	192411	192422
Species	keno-pyrochlore	keno-pyrochlore	calcio-pyrochlore	keno-pyrochlore	keno-pyrochlore	calcio-pyrochlore	keno-pyrochlore	fluoro-calcio-pyrochlore	fluoro-calcio-pyrochlore
Ti (*apfu*)	0.107	0.126	0.082	0.585	0.541	0.084	0.089	0.327	0.325
Zr	0.001	0.001	0.000	0.011	0.008	0.000	0.000	0.008	0.003
Hf	0.000	0.002	0.000	0.000	0.001	0.001	0.001	0.003	0.000
Th	0.018	0.025	0.015	0.146	0.130	0.013	0.011	0.001	0.000
U	0.001	0.002	0.002	0.004	0.003	0.001	0.001	0.015	0.016
Al	0.000	0.000	0.000	0.020	0.011	0.003	0.168	0.003	0.002
Y	0.018	0.023	0.015	0.006	0.009	0.009	0.006	0.003	0.003
La	0.000	0.001	0.000	0.034	0.017	0.007	0.005	0.008	0.008
Ce	0.002	0.003	0.002	0.106	0.073	0.036	0.024	0.045	0.041
Pr	0.001	0.002	0.001	0.014	0.012	0.006	0.004	0.004	0.004
Nd	0.004	0.004	0.002	0.036	0.031	0.017	0.014	0.008	0.009
Sm	0.001	0.002	0.001	0.006	0.007	0.002	0.002	0.001	0.001
Eu	0.001	0.000	0.000	0.002	0.001	0.001	0.001	0.000	0.001
Gd	0.002	0.003	0.002	0.004	0.004	0.001	0.002	0.002	0.001
Tb	0.001	0.001	0.001	0.002	0.001	0.001	0.000	0.002	0.001
Dy	0.003	0.004	0.002	0.005	0.016	0.002	0.004	0.003	0.002
Ho	0.001	0.003	0.000	0.002	0.003	0.001	0.003	0.002	0.004
Er	0.001	0.003	0.001	0.001	0.001	0.003	0.002	0.002	0.002
Tm	0.002	0.002	0.001	0.000	0.004	0.002	0.002	0.003	0.002
Yb	0.003	0.002	0.001	0.001	0.001	0.001	0.003	0.000	0.002
Lu	0.001	0.000	0.000	0.000	0.000	0.000	0.001	0.000	0.000
Mg	0.000	0.000	0.000	0.010	0.005	0.000	0.002	0.000	0.000
Ca	0.947	0.936	0.976	0.432	0.213	0.872	0.572	1.360	1.353
Mn	0.007	0.004	0.006	0.021	0.113	0.008	0.028	0.013	0.012
Fe	0.024	0.032	0.016	0.146	0.281	0.305	0.104	0.019	0.194
Pb	0.004	0.005	0.005	0.008	0.004	0.007	0.004	0.005	0.004
Na	0.001	0.000	0.000	0.006	0.003	0.001	0.187	0.401	0.416
K	0.001	0.002	0.000	0.003	0.004	0.001	0.004	0.002	0.003
F	0.028	0.017	0.020	0.029	0.053	0.036	0.029	0.847	0.886
Cl	0.002	0.002	0.001	0.001	0.003	0.000	0.005	0.001	0.000
O	6.014	6.037	6.030	5.810	5.745	6.288	5.484	6.150	6.314
Cation Sum	3.044	3.060	3.050	2.986	2.931	3.297	2.983	3.900	4.079
Sum B	2.000	2.000	2.000	2.000	2.000	2.000	2.000	2.000	2.000
Sum A	1.044	1.060	1.050	0.986	0.931	1.297	0.983	1.900	2.079
Anions (X+Y)	6.043	6.057	6.050	5.840	5.800	6.324	5.519	6.999	7.200
A-vacancies	0.956	0.940	0.950	1.014	1.069	0.703	1.017	0.100	-0.079

Table B.16. (Continued) Composition of pyrochlore from various rock types across the 2020 Corundum Dome and Pyrochlore Dome sampling area.

Sample	20TN4D	20TN4D	20TN4D	20TN4D	20TN4D	20TN4D	20TN4D	20TN4D	20TN4D
Analysis	202431	202442	202453	202464	202475	212481	212492	212503	212514
Species	keno-pyrochlore	keno-pyrochlore	fluoro-calcio-pyrochlore	keno-pyrochlore	keno-pyrochlore	keno-pyrochlore	keno-pyrochlore	keno-pyrochlore	keno-pyrochlore
P_2O_5 (wt. %)	0.04	0.02	0.01	0.00	0.03	0.02	0.05	0.06	0.02
Nb_2O_5	67.58	72.12	57.56	62.65	79.40	81.00	79.08	73.20	76.17
SiO_2	12.69	7.15	9.10	12.64	1.06	0.16	0.13	6.67	3.55
TiO_2	1.17	1.55	2.04	1.41	0.67	1.47	1.82	1.18	1.19
ZrO_2	0.20	0.64	0.68	0.00	0.00	0.02	0.14	0.11	0.03
HfO_2	0.02	0.00	0.17	0.00	0.06	0.00	0.06	0.00	0.05
ThO_2	0.00	0.02	0.00	0.10	0.09	0.10	0.35	0.21	0.11
UO_2	0.42	0.28	0.27	0.30	0.19	0.06	0.17	0.27	0.22
Al_2O_3	3.69	2.08	2.81	3.70	0.33	0.05	0.08	2.29	1.09
Y_2O_3	0.16	0.14	0.08	0.13	0.25	0.23	0.35	0.31	0.22
La_2O_3	0.10	0.11	0.01	0.06	0.06	0.10	0.03	0.05	0.00
Ce_2O_3	0.23	0.36	0.21	1.03	0.14	0.67	0.42	0.32	0.23
Pr_2O_3	0.02	0.03	0.05	0.23	0.02	0.19	0.09	0.06	0.04
Nd_2O_3	0.06	0.05	0.06	0.86	0.08	0.77	0.49	0.41	0.40
Sm_2O_3	0.00	0.03	0.00	0.10	0.00	0.09	0.23	0.11	0.13
Eu_2O_3	0.02	0.00	0.02	0.05	0.03	0.05	0.10	0.08	0.04
Gd_2O_3	0.04	0.03	0.00	0.03	0.03	0.15	0.16	0.15	0.14
Tb_2O_3	0.07	0.02	0.06	0.00	0.05	0.06	0.11	0.05	0.10
Dy_2O_3	0.07	0.09	0.10	0.12	0.14	0.15	0.18	0.15	0.17
Ho_2O_3	0.00	0.03	0.00	0.00	0.07	0.15	0.15	0.11	0.02
Er_2O_3	0.01	0.02	0.07	0.00	0.06	0.14	0.09	0.10	0.00
Tm_2O_3	0.10	0.05	0.14	0.02	0.28	0.11	0.11	0.14	0.07
Yb_2O_3	0.05	0.01	0.05	0.01	0.07	0.09	0.01	0.11	0.00
Lu_2O_3	0.00	0.08	0.04	0.15	0.16	0.20	0.09	0.14	0.00
MgO	0.00	0.00	0.00	0.06	0.69	0.01	0.00	0.00	0.00
CaO	13.81	15.34	15.78	13.03	16.30	16.16	15.71	15.05	15.43
MnO	0.23	0.26	0.16	0.15	0.16	0.22	0.38	0.19	0.39
FeO	0.18	0.19	0.93	0.47	0.46	0.26	0.85	0.32	0.25
PbO	0.25	0.31	0.53	0.22	0.38	0.43	0.31	0.30	0.32
Na_2O	0.04	0.09	3.54	0.03	0.01	0.00	0.02	0.04	0.01
K_2O	2.35	1.63	1.50	1.70	0.40	0.09	0.02	1.30	0.77
F	0.00	0.23	4.51	0.08	0.21	0.09	0.02	0.04	0.13
Cl	0.01	0.02	0.03	0.01	0.01	0.02	0.01	0.04	0.00
-(O=F,Cl)	0.00	-0.10	-1.91	-0.04	-0.09	-0.04	-0.01	-0.03	-0.06
Total	103.60	102.88	98.63	99.30	101.80	103.26	101.78	103.55	101.24
P (*apfu*)	0.001	0.001	0.001	0.000	0.001	0.001	0.002	0.002	0.001
Nb	1.257	1.492	1.289	1.219	1.844	1.928	1.908	1.523	1.713
Si	0.522	0.327	0.451	0.544	0.054	0.008	0.007	0.307	0.176

Sample	20TN4D	20TN4D	20TN4D	20TN4D	20TN4D	20TN4D	20TN4D	20TN4D	20TN4D
Analysis	202431	202442	202453	202464	202475	212481	212492	212503	212514
Species	keno-pyrochlore	keno-pyrochlore	fluoro-calcio-pyrochlore	keno-pyrochlore	keno-pyrochlore	keno-pyrochlore	keno-pyrochlore	keno-pyrochlore	keno-pyrochlore
Ti (*apfu*)	0.036	0.053	0.076	0.046	0.026	0.058	0.073	0.041	0.045
Zr	0.004	0.014	0.016	0.000	0.000	0.000	0.004	0.002	0.001
Hf	0.000	0.000	0.002	0.000	0.001	0.000	0.001	0.000	0.001
Th	0.000	0.000	0.000	0.001	0.001	0.001	0.004	0.002	0.001
U	0.004	0.003	0.003	0.003	0.002	0.001	0.002	0.003	0.002
Al	0.179	0.112	0.164	0.188	0.020	0.003	0.005	0.124	0.064
Y	0.004	0.003	0.002	0.003	0.007	0.006	0.010	0.008	0.006
La	0.002	0.002	0.000	0.001	0.001	0.002	0.001	0.001	0.000
Ce	0.003	0.006	0.004	0.016	0.003	0.013	0.008	0.005	0.004
Pr	0.000	0.001	0.001	0.004	0.000	0.004	0.002	0.001	0.001
Nd	0.001	0.001	0.001	0.013	0.002	0.015	0.009	0.007	0.007
Sm	0.000	0.000	0.000	0.001	0.000	0.002	0.004	0.002	0.002
Eu	0.000	0.000	0.000	0.001	0.001	0.001	0.002	0.001	0.001
Gd	0.001	0.001	0.000	0.000	0.000	0.003	0.003	0.002	0.002
Tb	0.001	0.000	0.001	0.000	0.001	0.001	0.002	0.001	0.002
Dy	0.001	0.001	0.002	0.002	0.002	0.002	0.003	0.002	0.003
Ho	0.000	0.000	0.000	0.000	0.001	0.002	0.003	0.002	0.000
Er	0.000	0.000	0.001	0.000	0.001	0.002	0.001	0.001	0.000
Tm	0.001	0.001	0.002	0.000	0.004	0.002	0.002	0.002	0.001
Yb	0.001	0.000	0.001	0.000	0.001	0.001	0.000	0.002	0.000
Lu	0.000	0.001	0.001	0.002	0.003	0.003	0.001	0.002	0.000
Mg	0.000	0.000	0.000	0.004	0.053	0.000	0.000	0.000	0.000
Ca	0.609	0.752	0.838	0.601	0.897	0.912	0.898	0.742	0.822
Mn	0.008	0.010	0.007	0.006	0.007	0.010	0.017	0.008	0.016
Fe	0.006	0.007	0.039	0.017	0.020	0.011	0.038	0.012	0.011
Pb	0.003	0.004	0.007	0.003	0.005	0.006	0.004	0.004	0.004
Na	0.004	0.008	0.340	0.002	0.001	0.000	0.002	0.004	0.001
K	0.123	0.095	0.095	0.093	0.026	0.006	0.002	0.076	0.049
F	0.000	0.034	0.707	0.011	0.034	0.014	0.004	0.006	0.020
Cl	0.001	0.001	0.002	0.001	0.001	0.002	0.001	0.003	0.000
O	5.258	5.530	5.345	5.252	5.831	5.990	5.998	5.569	5.743
Cation Sum	2.771	2.897	3.344	2.768	2.986	3.007	3.019	2.889	2.935
Sum B	2.000	2.000	2.000	2.000	2.000	2.000	2.000	2.000	2.000
Sum A	0.771	0.897	1.344	0.768	0.986	1.007	1.019	0.889	0.935
Anions (X+Y)	5.258	5.565	6.054	5.264	5.866	6.006	6.003	5.579	5.764
A-vacancies	1.229	1.103	0.656	1.232	1.014	0.993	0.981	1.111	1.065

Table B.16. (Continued) Composition of pyrochlore from various rock types across the 2020 Corundum Dome and Pyrochlore Dome sampling area.

Sample	20TN4D	20TN15A	20TN15A	20TN15A	20TN15A	20TN15A	20TN15A	20TN15A	20TN15A
Analysis	212525	51571	51582	51593	61601	61612	71621	71632	71643
Species	keno-pyrochlore	fluoro-calcio-pyrochlore	fluoro-calcio-pyrochlore	fluoro-calcio-pyrochlore	fluoro-calcio-pyrochlore	fluoro-calcio-pyrochlore	keno-pyrochlore	fluoro-calcio-pyrochlore	fluoro-calcio-pyrochlore
P_2O_5 (wt. %)	0.07	–	–	–	–	–	–	–	–
Nb_2O_5	79.50	55.08	55.44	55.93	54.69	55.34	53.72	55.35	56.57
Ta_2O_5	–	1.49	0.68	1.50	0.65	0.75	0.18	0.84	0.57
SiO_2	0.22	0.00	0.00	0.03	0.01	0.12	0.05	0.04	0.00
TiO_2	1.65	8.47	8.89	7.99	9.19	8.73	13.36	9.01	8.82
ZrO_2	0.09	0.01	0.02	0.00	0.04	0.03	0.14	0.06	0.00
HfO_2	0.05	0.06	0.00	0.00	0.00	0.00	0.00	0.00	0.03
ThO_2	0.20	1.12	1.34	1.29	1.36	1.59	5.46	1.63	1.63
UO_2	0.03	0.78	0.79	0.66	0.39	0.90	0.40	0.90	0.58
Al_2O_3	0.07	0.01	0.00	0.01	0.01	0.00	0.00	0.00	0.00
Y_2O_3	0.35	0.03	0.07	0.04	0.06	0.08	0.43	0.07	0.09
La_2O_3	0.08	2.23	2.99	2.38	2.76	1.92	3.25	0.68	2.08
Ce_2O_3	0.38	3.81	4.33	3.77	4.47	3.86	5.78	2.42	3.44
Pr_2O_3	0.09	0.44	0.57	0.42	0.56	0.44	0.87	0.19	0.41
Nd_2O_3	0.47	0.52	0.64	0.47	0.57	0.54	1.58	0.46	0.53
Sm_2O_3	0.18	–	–	–	–	–	–	–	–
Eu_2O_3	0.04	–	–	–	–	–	–	–	–
Gd_2O_3	0.12	–	–	–	–	–	–	–	–
Tb_2O_3	0.04	–	–	–	–	–	–	–	–
Dy_2O_3	0.22	–	–	–	–	–	–	–	–
Ho_2O_3	0.05	–	–	–	–	–	–	–	–
Er_2O_3	0.06	–	–	–	–	–	–	–	–
Tm_2O_3	0.00	–	–	–	–	–	–	–	–
Yb_2O_3	0.00	–	–	–	–	–	–	–	–
Lu_2O_3	0.00	–	–	–	–	–	–	–	–
MgO	0.00	–	–	–	–	–	–	–	–
CaO	15.92	16.15	15.66	15.81	16.13	16.60	10.57	17.86	16.84
MnO	0.20	0.05	0.08	0.03	0.37	0.28	0.32	0.18	0.32
FeO	0.56	0.15	0.22	0.15	0.26	0.55	0.76	0.30	0.15
PbO	0.44	0.41	0.27	0.25	0.17	0.27	0.38	0.32	0.22
Na_2O	0.01	6.10	6.08	6.29	5.75	5.96	0.11	5.76	5.84
K_2O	0.06	0.02	0.01	0.02	0.04	0.01	0.02	0.01	0.00
F	0.01	5.51	5.38	5.58	5.25	5.17	0.06	5.57	5.55
Cl	0.02	–	–	–	–	–	–	–	–
-(O=F,Cl)	-0.01	-2.32	-2.26	-2.35	-2.21	-2.18	-0.03	-2.35	-2.34
Total	101.17	100.10	101.20	100.26	100.50	100.97	97.44	99.31	101.33
P (*apfu*)	0.003	–	–	–	–	–	–	–	–
Nb	1.911	1.571	1.569	1.593	1.553	1.567	1.408	1.559	1.580

Sample	20TN4D	20TN15A	20TN15A	20TN15A	20TN15A	20TN15A	20TN15A	20TN15A	20TN15A
Analysis	212525	51571	51582	51593	61601	61612	71621	71632	71643
Species	keno-pyrochlore	fluoro-calcio-pyrochlore	fluoro-calcio-pyrochlore	fluoro-calcio-pyrochlore	fluoro-calcio-pyrochlore	fluoro-calcio-pyrochlore	keno-pyrochlore	fluoro-calcio-pyrochlore	fluoro-calcio-pyrochlore
Ta (*apfu*)	–	0.026	0.012	0.026	0.011	0.013	0.003	0.014	0.010
Si	0.012	0.000	0.000	0.002	0.000	0.008	0.003	0.002	0.000
Ti	0.066	0.402	0.419	0.379	0.434	0.411	0.582	0.422	0.410
Zr	0.002	0.000	0.001	0.000	0.001	0.001	0.004	0.002	0.000
Hf	0.001	0.001	0.000	0.000	0.000	0.000	0.000	0.000	0.001
Th	0.002	0.016	0.019	0.019	0.019	0.023	0.072	0.023	0.023
U	0.000	0.011	0.011	0.009	0.005	0.013	0.005	0.013	0.008
Al	0.004	0.001	0.000	0.001	0.000	0.000	0.000	0.000	0.000
Y	0.010	0.001	0.002	0.001	0.002	0.003	0.013	0.002	0.003
La	0.001	0.052	0.069	0.055	0.064	0.044	0.069	0.016	0.047
Ce	0.007	0.088	0.099	0.087	0.103	0.088	0.123	0.055	0.078
Pr	0.002	0.010	0.013	0.010	0.013	0.010	0.018	0.004	0.009
Nd	0.009	0.012	0.014	0.011	0.013	0.012	0.033	0.010	0.012
Sm	0.003	–	–	–	–	–	–	–	–
Eu	0.001	–	–	–	–	–	–	–	–
Gd	0.002	–	–	–	–	–	–	–	–
Tb	0.001	–	–	–	–	–	–	–	–
Dy	0.004	–	–	–	–	–	–	–	–
Ho	0.001	–	–	–	–	–	–	–	–
Er	0.001	–	–	–	–	–	–	–	–
Tm	0.000	–	–	–	–	–	–	–	–
Yb	0.000	–	–	–	–	–	–	–	–
Lu	0.000	–	–	–	–	–	–	–	–
Mg	0.000	–	–	–	–	–	–	–	–
Ca	0.907	1.091	1.051	1.067	1.086	1.114	0.657	1.193	1.114
Mn	0.009	0.003	0.004	0.002	0.019	0.015	0.015	0.010	0.017
Fe	0.025	0.008	0.012	0.008	0.014	0.029	0.037	0.016	0.008
Pb	0.006	0.007	0.005	0.004	0.003	0.005	0.006	0.005	0.004
Na	0.001	0.747	0.738	0.768	0.701	0.724	0.013	0.695	0.699
K	0.004	0.002	0.001	0.001	0.003	0.001	0.001	0.001	0.000
F	0.002	1.099	1.065	1.113	1.043	1.024	0.011	1.098	1.085
Cl	0.001	–	–	–	–	–	–	–	–
O	5.971	6.029	6.057	6.019	6.075	6.110	5.961	6.012	6.029
Cation Sum	2.997	4.047	4.039	4.042	4.045	4.080	3.063	4.043	4.022
Sum B	2.000	2.000	2.000	2.000	2.000	2.000	2.000	2.000	2.000
Sum A	0.997	2.047	2.039	2.042	2.045	2.080	1.063	2.043	2.022
Anions (X+Y)	5.975	7.128	7.121	7.132	7.118	7.134	5.972	7.110	7.115
A-vacancies	1.003	-0.047	-0.039	-0.042	-0.045	-0.080	0.937	-0.043	-0.022

Table B.16. (Continued) Composition of pyrochlore from various rock types across the 2020 Corundum Dome and Pyrochlore Dome sampling area.

Sample	20TN15A	20TN15A	20TN20	20TN20	20TN20	20TN20	20TN20	20TN20	20TN20
Analysis	71665	71698	81701	81712	81723	91731	91742	91753	101761
Species	fluoro-calcio-pyrochlore	fluoro-calcio-pyrochlore	fluoro-calcio-pyrochlore	fluoro-calcio-pyrochlore	fluoro-calcio-pyrochlore	fluoro-calcio-pyrochlore	fluoro-calcio-pyrochlore	calcio-pyrochlore	fluoro-calcio-pyrochlore
Nb_2O_5 (wt. %)	55.52	55.11	63.09	64.28	61.56	60.95	61.66	61.77	65.32
Ta_2O_5	0.51	0.94	1.43	0.87	1.52	1.46	1.35	1.34	1.52
SiO_2	0.00	0.00	0.11	0.00	0.19	0.15	0.08	0.11	0.04
TiO_2	9.12	8.60	4.49	4.35	4.92	4.87	4.44	4.54	4.04
ZrO_2	0.02	0.05	0.21	0.07	0.19	0.18	0.20	0.17	0.05
HfO_2	0.00	0.01	0.00	0.00	0.07	0.03	0.09	0.00	0.04
ThO_2	1.83	1.77	0.23	0.41	0.22	0.15	0.33	0.20	0.00
UO_2	0.58	0.74	0.64	0.83	0.68	0.48	0.85	0.36	0.89
Al_2O_3	0.00	0.00	0.00	0.01	0.02	0.01	0.00	0.00	0.00
Y_2O_3	0.08	0.07	0.06	0.05	0.06	0.06	0.02	0.04	0.05
La_2O_3	2.56	2.11	0.81	0.98	1.26	2.86	2.50	2.72	0.03
Ce_2O_3	3.97	3.53	2.13	2.21	3.01	4.84	3.94	4.19	0.38
Pr_2O_3	0.41	0.44	0.21	0.25	0.34	0.60	0.46	0.40	0.05
Nd_2O_3	0.58	0.59	0.47	0.41	0.63	0.76	0.61	0.67	0.12
CaO	16.01	16.51	18.95	18.66	18.21	17.62	18.14	17.87	20.83
MnO	0.32	0.28	0.22	0.22	0.31	0.17	0.13	0.18	0.12
FeO	0.10	0.30	0.07	0.10	0.12	0.09	0.15	0.23	0.05
PbO	0.27	0.31	0.25	0.43	0.24	0.16	0.49	0.25	0.36
Na_2O	5.82	5.91	4.26	4.30	3.96	1.99	2.26	2.15	3.69
K_2O	0.01	0.01	0.02	0.01	0.02	0.03	0.03	0.06	0.01
F	5.27	5.38	4.57	4.53	3.94	2.64	2.64	2.49	4.07
-(O=F,Cl)	-2.22	-2.26	-1.92	-1.91	-1.66	-1.11	-1.11	-1.05	-1.71
Total	100.77	100.38	100.29	101.05	99.81	99.00	99.26	98.69	99.93
Nb (*apfu*)	1.563	1.574	1.755	1.782	1.725	1.729	1.754	1.751	1.787
Ta	0.009	0.016	0.024	0.014	0.026	0.025	0.023	0.023	0.025
Si	0.000	0.000	0.007	0.000	0.012	0.009	0.005	0.007	0.002
Ti	0.427	0.409	0.208	0.201	0.230	0.230	0.210	0.214	0.184
Zr	0.001	0.001	0.006	0.002	0.006	0.006	0.006	0.005	0.001
Hf	0.000	0.000	0.000	0.000	0.001	0.001	0.002	0.000	0.001
Th	0.026	0.025	0.003	0.006	0.003	0.002	0.005	0.003	0.000
U	0.008	0.010	0.009	0.011	0.009	0.007	0.012	0.005	0.012
Al	0.000	0.000	0.000	0.001	0.001	0.001	0.000	0.000	0.000
Y	0.003	0.002	0.002	0.002	0.002	0.002	0.001	0.001	0.001
La	0.059	0.049	0.018	0.022	0.029	0.066	0.058	0.063	0.001

Sample	20TN15A	20TN15A	20TN20	20TN20	20TN20	20TN20	20TN20	20TN20	20TN20
Analysis	71665	71698	81701	81712	81723	91731	91742	91753	101761
Species	fluoro-calcio-pyrochlore	fluoro-calcio-pyrochlore	fluoro-calcio-pyrochlore	fluoro-calcio-pyrochlore	fluoro-calcio-pyrochlore	fluoro-calcio-pyrochlore	fluoro-calcio-pyrochlore	calcio-pyrochlore	fluoro-calcio-pyrochlore
Ce (*apfu*)	0.090	0.082	0.048	0.050	0.068	0.111	0.091	0.096	0.008
Pr	0.009	0.010	0.005	0.006	0.008	0.014	0.011	0.009	0.001
Nd	0.013	0.013	0.010	0.009	0.014	0.017	0.014	0.015	0.003
Ca	1.069	1.118	1.250	1.226	1.209	1.185	1.223	1.200	1.350
Mn	0.017	0.015	0.012	0.011	0.016	0.009	0.007	0.009	0.006
Fe	0.005	0.016	0.003	0.005	0.006	0.005	0.008	0.012	0.002
Pb	0.005	0.005	0.004	0.007	0.004	0.003	0.008	0.004	0.006
Na	0.703	0.724	0.508	0.511	0.476	0.243	0.276	0.261	0.433
K	0.001	0.001	0.002	0.001	0.002	0.002	0.002	0.005	0.001
F	1.038	1.074	0.889	0.879	0.772	0.523	0.526	0.493	0.779
O	6.044	6.080	6.118	6.130	6.169	6.272	6.305	6.292	6.143
Cation Sum	4.008	4.070	3.874	3.866	3.847	3.665	3.715	3.684	3.825
Sum B	2.000	2.000	2.000	2.000	2.000	2.000	2.000	2.000	2.000
Sum A	2.008	2.070	1.874	1.866	1.847	1.665	1.715	1.684	1.825
Anions (X+Y)	7.082	7.154	7.007	7.009	6.941	6.795	6.830	6.784	6.923
A-vacancies	-0.008	-0.070	0.126	0.134	0.153	0.335	0.285	0.316	0.175

Table B.16. (Continued) Composition of pyrochlore from various rock types across the 2020 Corundum Dome and Pyrochlore Dome sampling area.

Sample	20TN20	20TN20	20TN20	20TN20	20TN20	20TN20	20TN20	20TN20	20TN20
Analysis	101772	101783	101794	101805	101816	101827	101838	101849	1018510
Species	fluoro-calcio-pyrochlore	fluoro-calcio-pyrochlore	fluoro-calcio-pyrochlore	calcio-pyrochlore	fluoro-calcio-pyrochlore	fluoro-calcio-pyrochlore	fluoro-calcio-pyrochlore	fluoro-calcio-pyrochlore	fluoro-calcio-pyrochlore
Nb_2O_5 (wt. %)	63.42	61.00	64.57	71.82	63.75	66.27	64.17	64.29	64.69
Ta_2O_5	1.45	1.54	1.34	0.59	1.32	1.06	1.38	1.37	1.15
SiO_2	0.05	0.33	0.05	0.08	0.06	0.00	0.07	0.08	0.04
TiO_2	4.26	5.11	4.46	2.90	4.30	3.64	4.86	4.58	4.25
ZrO_2	0.07	0.24	0.18	0.08	0.12	0.10	0.19	0.20	0.18
HfO_2	0.07	0.07	0.07	0.00	0.00	0.00	0.06	0.00	0.14
ThO_2	0.18	0.00	0.08	0.08	0.32	0.03	0.04	0.21	0.09
UO_2	1.22	0.57	0.65	0.52	0.81	0.80	0.63	1.00	0.76
Al_2O_3	0.00	0.00	0.00	0.00	0.00	0.00	0.01	0.00	0.01
Y_2O_3	0.07	0.11	0.10	0.13	0.07	0.07	0.06	0.05	0.08
La_2O_3	0.71	1.09	0.19	0.32	0.52	0.31	0.11	0.13	0.58
Ce_2O_3	1.93	3.16	0.73	1.78	1.83	0.85	0.54	0.58	1.65
Pr_2O_3	0.22	0.44	0.10	0.35	0.18	0.13	0.05	0.08	0.20
Nd_2O_3	0.46	0.76	0.20	1.30	0.45	0.21	0.22	0.22	0.39
CaO	19.77	19.27	20.96	16.62	20.17	20.48	21.31	20.92	20.21
MnO	0.21	0.27	0.11	0.10	0.22	0.16	0.11	0.11	0.17
FeO	0.08	0.10	0.10	0.52	0.17	0.16	0.13	0.13	0.10
PbO	0.30	0.51	0.22	0.40	0.32	0.26	0.17	0.27	0.40
Na_2O	3.09	2.78	3.49	0.66	3.25	3.41	3.43	3.48	3.15
K_2O	0.02	0.02	0.02	0.00	0.02	0.00	0.01	0.00	0.01
F	3.46	3.39	4.09	0.86	3.70	3.83	4.28	4.27	3.56
-(O=F,Cl)	-1.46	-1.43	-1.72	-0.36	-1.56	-1.61	-1.80	-1.80	-1.50
Total	99.58	99.32	99.97	98.74	100.01	100.18	100.03	100.17	100.33
Nb (*apfu*)	1.771	1.707	1.766	1.859	1.772	1.814	1.746	1.759	1.776
Ta	0.024	0.026	0.022	0.009	0.022	0.017	0.023	0.023	0.019
Si	0.003	0.020	0.003	0.005	0.004	0.000	0.004	0.005	0.002
Ti	0.198	0.238	0.203	0.125	0.199	0.166	0.220	0.208	0.194
Zr	0.002	0.007	0.005	0.002	0.004	0.003	0.006	0.006	0.005
Hf	0.001	0.001	0.001	0.000	0.000	0.000	0.001	0.000	0.002
Th	0.003	0.000	0.001	0.001	0.005	0.000	0.001	0.003	0.001
U	0.017	0.008	0.009	0.007	0.011	0.011	0.008	0.013	0.010
Al	0.000	0.000	0.000	0.000	0.000	0.000	0.001	0.000	0.001
Y	0.002	0.004	0.003	0.004	0.002	0.002	0.002	0.002	0.002
La	0.016	0.025	0.004	0.007	0.012	0.007	0.003	0.003	0.013

Sample	20TN20	20TN20	20TN20	20TN20	20TN20	20TN20	20TN20	20TN20	20TN20
Analysis	101772	101783	101794	101805	101816	101827	101838	101849	1018510
Species	fluoro-calcio-pyrochlore	fluoro-calcio-pyrochlore	fluoro-calcio-pyrochlore	calcio-pyrochlore	fluoro-calcio-pyrochlore	fluoro-calcio-pyrochlore	fluoro-calcio-pyrochlore	fluoro-calcio-pyrochlore	fluoro-calcio-pyrochlore
Ce (*apfu*)	0.044	0.072	0.016	0.037	0.041	0.019	0.012	0.013	0.037
Pr	0.005	0.010	0.002	0.007	0.004	0.003	0.001	0.002	0.005
Nd	0.010	0.017	0.004	0.027	0.010	0.005	0.005	0.005	0.009
Ca	1.308	1.279	1.359	1.020	1.328	1.328	1.374	1.356	1.315
Mn	0.011	0.014	0.006	0.005	0.011	0.008	0.006	0.005	0.009
Fe	0.004	0.005	0.005	0.025	0.009	0.008	0.007	0.007	0.005
Pb	0.005	0.008	0.004	0.006	0.005	0.004	0.003	0.004	0.007
Na	0.370	0.334	0.410	0.074	0.387	0.401	0.400	0.409	0.371
K	0.001	0.002	0.002	0.000	0.002	0.000	0.001	0.000	0.001
F	0.676	0.664	0.782	0.155	0.720	0.733	0.814	0.818	0.685
O	6.228	6.215	6.146	6.088	6.220	6.175	6.117	6.128	6.197
Cation Sum	3.796	3.777	3.824	3.219	3.827	3.797	3.821	3.822	3.784
Sum B	2.000	2.000	2.000	2.000	2.000	2.000	2.000	2.000	2.000
Sum A	1.796	1.777	1.824	1.219	1.827	1.797	1.821	1.822	1.784
Anions (X+Y)	6.904	6.879	6.928	6.243	6.939	6.907	6.932	6.945	6.881
A-vacancies	0.204	0.223	0.176	0.781	0.173	0.203	0.179	0.178	0.216

Table B.16. (Continued) Composition of pyrochlore from various rock types across the 2020 Corundum Dome and Pyrochlore Dome sampling area.

Sample	20TN20	20TN20
Analysis	1018611	1018712
Species	fluoro-calcio-pyrochlore	fluoro-calcio-pyrochlore
Nb_2O_5 (wt. %)	65.15	64.17
Ta_2O_5	1.17	1.24
SiO_2	0.02	0.14
TiO_2	3.88	4.63
ZrO_2	0.12	0.13
HfO_2	0.04	0.05
ThO_2	0.00	0.00
UO_2	0.67	0.66
Al_2O_3	0.01	0.02
Y_2O_3	0.06	0.02
La_2O_3	0.34	0.15
Ce_2O_3	1.26	0.52
Pr_2O_3	0.19	0.03
Nd_2O_3	0.28	0.19
CaO	20.44	21.08
MnO	0.13	0.08
FeO	0.11	0.08
PbO	0.20	0.36
Na_2O	3.27	3.54
K_2O	0.00	0.00
F	3.69	4.22
-(O=F,Cl)	-1.55	-1.78
Total	99.48	99.52
Nb (*apfu*)	1.796	1.755
Ta	0.019	0.020
Si	0.001	0.008
Ti	0.178	0.211
Zr	0.004	0.004
Hf	0.001	0.001
Th	0.000	0.000
U	0.009	0.009
Al	0.001	0.001
Y	0.002	0.001
La	0.008	0.003

Sample	20TN20	20TN20
Analysis	1018611	1018712
Species	fluoro-calcio-pyrochlore	fluoro-calcio-pyrochlore
Ce (*apfu*)	0.028	0.012
Pr	0.004	0.001
Nd	0.006	0.004
Ca	1.335	1.366
Mn	0.007	0.004
Fe	0.006	0.004
Pb	0.003	0.006
Na	0.387	0.415
K	0.000	0.000
F	0.712	0.808
O	6.186	6.119
Cation Sum	3.795	3.824
Sum B	2.000	2.000
Sum A	1.795	1.824
Anions (X+Y)	6.898	6.926
A-vacancies	0.205	0.176

Table B.17. Unidentified mineral compositions from various rock types across the 2020 Corundum Dome and Pyrochlore Dome sampling area.

Sample	20TN15B	20TN15B	20TN15B	20TN15B	20TN15B	20TN15B
Analysis	52053	52031	52042	21571	21593	21582
Comment	Y-Si-silicate	Y-Si-silicate	Y-Si-silicate	Y-Si-silicate	Y-Si-silicate	Y-Si-silicate
P_2O_5 (wt. %)	0.08	0.08	0.08	0.08	0.09	0.11
Nb_2O_5	0.04	0.00	0.02	0.00	0.05	0.02
SiO_2	24.31	29.82	26.40	31.57	32.58	30.84
TiO_2	0.16	0.11	0.13	0.15	0.10	0.14
ZrO_2	0.01	0.01	0.00	0.03	0.00	0.00
HfO_2	0.03	0.01	0.11	0.07	0.20	0.15
ThO_2	5.39	5.84	6.91	6.56	5.46	7.08
UO_2	0.22	0.15	0.10	0.08	0.11	0.15
Al_2O_3	0.82	0.73	0.61	0.63	0.60	0.87
Y_2O_3	12.77	15.93	14.02	15.90	17.71	15.14
La_2O_3	3.55	1.09	2.32	0.86	1.20	0.71
Ce_2O_3	6.16	3.16	4.37	3.41	3.51	3.44
Pr_2O_3	0.94	0.61	0.74	0.69	0.66	0.68
Nd_2O_3	2.56	2.40	2.45	2.83	2.33	2.95
Sm_2O_3	0.85	0.97	0.85	1.09	0.95	1.05
Eu_2O_3	0.21	0.27	0.26	0.29	0.31	0.30
Gd_2O_3	1.17	1.30	1.08	1.21	1.24	1.26
Tb_2O_3	0.10	0.35	0.38	0.35	0.32	0.09
Dy_2O_3	1.55	1.83	1.68	1.90	1.95	1.84
Ho_2O_3	0.76	0.88	0.89	0.76	0.86	0.85
Er_2O_3	0.97	0.98	1.04	1.10	1.37	1.02
Tm_2O_3	0.24	0.15	0.16	0.18	0.29	0.25
Yb_2O_3	0.45	0.66	0.61	0.74	0.75	0.58
Lu_2O_3	0.00	0.00	0.04	0.00	0.00	0.00
MgO	0.76	0.34	0.22	0.16	0.09	0.36
CaO	6.52	7.69	6.90	7.91	8.30	7.41
MnO	0.20	0.23	0.21	0.20	0.21	0.20
FeO	4.88	5.14	4.74	5.10	5.34	5.66
PbO	1.67	2.13	1.81	1.86	1.93	2.03
Na_2O	0.15	0.16	0.16	0.21	0.17	0.14
K_2O	0.49	0.25	0.26	0.12	0.06	0.23
F	3.32	2.27	2.22	2.12	1.69	1.53
Cl	0.07	0.07	0.05	0.07	0.05	0.07
O=F,Cl	-1.41	-0.97	-0.95	-0.91	-0.73	-0.66
Total	80.01	84.61	80.88	87.32	89.76	86.48

Appendix C: Complete Zircon Trace Element Dataset

Table C.1. Zircon trace element results determined by LA-ICP-MS for zircon crystals in samples 20TN2, 20TN4D, 20TN13A, 20TN15A, 20TN15B, 20TN16A-2, 20TN17A-2, 20TN20, and 20TN55A from Corundum Dome and Pyrochlore Dome, Pool Creek area, southeast Yukon, Canada. Th and U values are from the U-Pb selections. b.d.l = below detection limit.

Sample and Spot Number	Note	Li (ppm)	±2σ	Si (ppm)	±2σ	P (ppm)	±2σ	Ca (ppm)	±2σ	Sc (ppm)	±2σ	Ti (ppm)	±2σ
20TN2_2	June	1.43	0.41	174435	3686	429	111	2	74	461	12	1.76	1.01
20TN2_4	June	9.19	0.94	167160	5625	334	184	22	98	476	15	0.98	0.74
20TN2_7	June	13.05	0.97	171565	3708	281	181	52	78	461	11	2.72	1.25
20TN2_21	June	5.66	1.05	165200	4291	28.9	21.2	67	84	470	11	55.35	28.89
20TN2_25	June	3.29	0.86	164459	3936	44.5	18.2	5	82	469	11	1.77	1.21
20TN2_44	July	3.12	0.64	150388	2709	8.6	12.7	17	63	388	8	0.83	0.65
20TN4D_2	June	47.12	2.19	170603	4744	47.8	31.7	357	125	457	10	50.96	6.77
20TN4D_6	June	68.23	2.47	164349	4939	10.2	32.0	615	221	463	12	61.83	24.59
20TN4D_9	June	47.11	5.22	183211	7358	130	36	24049	6393	500	18	26501	7630
20TN4D_10	June	47.27	1.87	166752	4243	38.7	20.5	971	325	463	12	293.19	71.68
20TN4D_11	July	7.19	1.04	175829	7190	19.4	13.0	1843	752	383	8	127.53	48.70
20TN4D_12	July	40.07	1.82	159197	3584	21.5	16.9	496	125	377	9	46.13	5.36
20TN4D_13	July	40.74	1.62	148427	4344	88.2	42.9	217	92	375	9	22.62	10.30
20TN4D_19	July	99.58	4.01	153477	3297	79.4	27.3	271	96	383	11	32.14	4.42
20TN4D_20	July	4.93	0.72	157188	3958	26.0	14.8	3741	274	376	8	62.14	5.29
20TN4D_27	July	9.37	1.12	151266	3349	b.d.l.		59	61	378	9	0.05	0.55
20TN4D_28	July	6.63	1.10	156261	6106	51.4	18.0	4355	799	366	10	3459	208
20TN15A_231_1	March	21.12	1.14	140138	2020	52.5	14.4	b.d.l.		394	7	4.03	2.19
20TN15A_231_2	March	13.36	0.90	137879	2148	63.9	13.1	b.d.l.		396	7	3.66	1.42
20TN15A_231_3	March	5.02	0.50	139399	2939	63.4	13.0	17	54	399	7	3.76	0.96
20TN15A_231_4	March	25.08	1.20	138523	2418	71.1	15.8	15	62	391	5	3.32	1.56
20TN15A_231_5	March	26.01	1.19	137497	3110	70.4	14.0	51	62	395	8	3.87	1.51
20TN15A_232	March	44.69	18.59	132952	5625	37.9	19.4	123	99	404	12	114	59
20TN15A_233	March	13.40	0.92	138381	2793	40.1	11.3	106	58	394	10	3.13	1.30
20TN15A_234	March	10.70	0.65	138996	2873	42.5	12.6	26	54	397	7	3.27	1.31
20TN15A_247_1	March	4.50	0.61	147412	3992	123	25	b.d.l.		412	6	7.91	1.76
20TN15A_247_2	March	0.68	0.27	148186	3299	57.4	22.2	19	72	416	7	19.18	2.92
20TN15A_247_3	March	3.36	0.54	141927	2478	13.2	19.9	b.d.l.		420	9	22.64	3.09
20TN15A_247_4	March	23.31	1.24	146474	2759	24.1	22.4	24	69	421	6	18.99	3.04
20TN15A_247_5	March	35.06	1.85	143246	2715	9.4	21.2	69	64	409	7	28.72	3.63
20TN15A_247_6	March	43.52	3.18	144251	2188	43.1	17.5	b.d.l.		414	8	23.07	3.01
20TN15A_248	March	13.80	2.34	147126	5689	41.4	25.5	33	66	409	7	7.83	5.12
20TN15A_250	March	24.89	2.08	143559	2277	68.5	19.4	b.d.l.		414	6	24.00	3.55
20TN15A_251	March	25.37	1.87	148375	6482	145	39	584	393	415	10	25.05	5.43
20TN15A_252	March	3.10	0.86	144900	3127	102	21	133	90	408	9	19.33	2.69
20TN15A_253_1	March	19.40	1.79	140792	6251	40.7	19.4	8	85	398	12	14.27	5.48
20TN15A_253_2	March	23.33	1.52	144106	3421	44.3	24.6	24	63	403	7	21.70	13.10
20TN15A_253_3	March	11.60	1.03	142278	2816	87.8	23.4	38	78	406	8	1.54	1.30
20TN15A_253_4	March	27.53	1.51	140470	2125	67.8	20.5	b.d.l.		401	8	4.32	1.37
20TN15A_254	March	16.62	1.50	146942	2444	49.5	20.4	94	95	404	9	13.76	2.57

Sample and Spot Number	^{56}Fe (ppm)	±2σ	^{57}Fe (ppm)	±2σ	Y (ppm)	±2σ	Zr (ppm)	±2σ	Nb (ppm)	±2σ	Mo (ppm)	±2σ
20TN2_2	4.6	4.0	3.3	3.0	9679	184	510677	8367	2.21	0.23	2.65	0.51
20TN2_4	b.d.l.		0.7	3.4	5365	126	500934	11373	24.76	0.89	2.06	0.35
20TN2_7	4.9	3.3	2.1	2.5	7103	155	502905	10915	7.78	0.37	2.03	0.41
20TN2_21	3.4	3.2	0.3	2.5	3476	102	500062	11107	367	180	1.86	0.37
20TN2_25	b.d.l.		0.0	2.3	4055	77	503183	7406	7.95	0.68	1.70	0.30
20TN2_44	2.1	2.5	b.d.l.		3824	66	493769	7527	29.89	3.10	0.61	0.22
20TN4D_2	21199	4322	9352	2196	541	22	500970	11019	295	22	28.77	10.11
20TN4D_6	1137	534	524	244	1057	51	498191	7261	1374	581	2.01	0.32
20TN4D_9	2292	337	1025	170	2054	182	515417	26618	19654	2626	13.36	2.21
20TN4D_10	727	130	341	58	1645	51	506233	8379	2904	1870	14.39	2.85
20TN4D_11	909	159	707	124	1828	39	490251	6679	9246	3707	14.12	6.37
20TN4D_12	599	77	441	59	2117	148	491402	9010	1155	178	6.65	1.58
20TN4D_13	1080	614	627	349	1475	42	498452	8136	178	113	8.04	1.51
20TN4D_19	1052	181	680	96	662	11	509639	10350	90.65	10.38	0.96	0.32
20TN4D_20	892	88	638	72	2425	39	507276	7417	1441	62	2.55	0.47
20TN4D_27	13.8	3.9	12.5	5.4	1186	37	512777	8013	5.66	0.81	133.82	41.90
20TN4D_28	2399	520	1630	334	1584	117	498906	10265	5390	2304	17.17	3.77
20TN15A_231_1	2.3	2.8	0.0	2.7	2922	39	498344	5409	50.33	1.14	0.57	0.24
20TN15A_231_2	6.7	3.3	1.4	2.2	3878	52	495491	6052	46.67	0.87	0.49	0.19
20TN15A_231_3	4.8	2.7	1.4	3.6	4508	63	501765	5054	30.83	0.71	0.25	0.15
20TN15A_231_4	3.8	2.3	4.7	3.2	2813	328	493873	7494	29.13	1.18	0.54	0.24
20TN15A_231_5	6.3	2.7	4.6	3.3	2993	106	496286	7887	35.13	1.06	0.45	0.21
20TN15A_232	2717	1793	1646	1113	2749	67	501074	10747	56.13	6.31	0.27	0.21
20TN15A_233	b.d.l.		b.d.l.		2832	128	494697	6161	34.38	1.52	0.33	0.17
20TN15A_234	13.1	3.1	3.7	3.0	2321	64	497128	5238	25.67	1.27	0.43	0.22
20TN15A_247_1	27.1	3.2	21.7	4.9	424	6	466168	7214	57.57	1.71	0.53	0.23
20TN15A_247_2	11.2	4.0	6.8	4.2	609	12	470193	5510	134	3	0.38	0.19
20TN15A_247_3	11.6	3.4	15.6	4.5	705	11	470032	7181	142	2	0.30	0.19
20TN15A_247_4	15.8	1.9	6.4	4.1	766	12	465385	6316	141	3	0.75	0.31
20TN15A_247_5	51.8	12.0	29.6	7.2	757	13	472139	9479	136	2	0.36	0.16
20TN15A_247_6	49.8	13.6	33.5	11.2	628	9	470939	5797	143	3	0.51	0.22
20TN15A_248	195	56	119	36	1403	248	460365	8918	19.09	2.16	0.63	0.28
20TN15A_250	21.2	3.4	13.1	4.0	867	13	470808	7837	185	4	0.33	0.21
20TN15A_251	665	350	433	239	939	32	469037	6731	155	5	0.37	0.25
20TN15A_252	11.9	2.9	9.4	4.2	615	7	464526	7817	117	3	0.53	0.25
20TN15A_253_1	264	123	181	92	2415	70	465559	11870	27.30	0.97	0.20	0.13
20TN15A_253_2	29.1	11.4	19.0	9.9	3211	61	467894	7355	38.76	2.41	0.85	0.44
20TN15A_253_3	b.d.l.		b.d.l.		3622	68	465390	6451	24.65	0.58	0.25	0.15
20TN15A_253_4	97.7	16.0	64.7	10.8	2798	40	466029	4911	38.02	0.85	0.58	0.31
20TN15A_254	16.2	4.0	17.5	6.3	1776	30	465513	6749	95.35	1.94	0.50	0.26

Sample and Spot Number	La (ppm)	±2σ	Ce (ppm)	±2σ	Pr (ppm)	±2σ	Nd (ppm)	±2σ	Sm (ppm)	±2σ	Eu (ppm)	±2σ	Gd (ppm)	±2σ
20TN2_2	0.85	0.64	586	11	4.82	0.28	72.00	3.07	150	5	64.66	1.64	527.5	12.5
20TN2_4	0.07	0.03	556	18	1.14	0.10	18.79	1.27	40.72	1.92	18.79	0.82	175.6	6.5
20TN2_7	0.35	0.18	622	12	2.45	0.17	35.94	1.89	77.43	3.11	35.74	1.17	312.1	9.4
20TN2_21	10.76	5.59	295	31	3.64	1.66	16.44	5.30	18.68	1.17	9.37	0.44	87.9	2.5
20TN2_25	0.05	0.02	255	14	0.56	0.07	8.85	0.56	20.93	1.63	10.55	0.70	103.8	4.0
20TN2_44	0.96	0.13	1726	64	14.33	1.46	200	14	169	4	45.58	1.43	218.4	3.7
20TN4D_2	132	18	1158	148	75.11	9.93	229	28	35.25	2.78	8.24	0.46	37.6	2.0
20TN4D_6	101	10	1751	92	159	13	632	40	110	4	25.56	1.10	102.3	3.6
20TN4D_9	115	24	622	117	74.87	16.42	286	56	62.56	6.40	13.01	1.30	77.9	6.4
20TN4D_10	19.83	6.93	118	41	12.49	6.27	49.33	24.19	13.35	3.07	3.47	0.53	30.7	2.2
20TN4D_11	27.51	12.35	193	47	9.86	3.37	41.52	12.75	15.54	4.03	3.90	0.79	29.3	3.8
20TN4D_12	9.37	0.71	79.07	4.64	6.38	0.72	28.74	2.75	10.97	0.89	3.60	0.27	35.7	2.9
20TN4D_13	51.09	27.62	42.00	6.19	8.74	3.69	28.58	12.15	7.12	1.62	2.30	0.32	20.5	2.1
20TN4D_19	66.24	5.71	844	19	93.95	2.37	336	9	46.06	1.71	10.26	0.57	46.4	1.8
20TN4D_20	1387	98	7965	194	420	8	1618	30	239	6	44.74	1.40	198.9	4.7
20TN4D_27	4.35	0.43	61.06	4.39	2.14	0.25	13.08	1.40	4.53	0.64	1.28	0.16	12.0	0.9
20TN4D_28	53.28	11.27	203	37	12.27	2.35	50.93	7.89	14.79	2.76	3.81	0.55	23.0	2.5
20TN15A_231_1	0.14	0.06	217	3	1.01	0.10	12.91	0.99	18.67	1.32	9.92	0.39	88.5	3.4
20TN15A_231_2	0.38	0.08	172	2	1.01	0.10	11.32	1.07	17.26	1.19	9.00	0.51	81.2	2.8
20TN15A_231_3	0.30	0.06	125	3	1.23	0.12	13.39	0.76	18.23	1.42	8.62	0.48	84.0	2.6
20TN15A_231_4	2.16	0.26	93.79	6.29	0.78	0.13	7.75	1.10	11.11	1.97	5.44	0.93	52.1	6.7
20TN15A_231_5	0.76	0.08	105	4	0.72	0.11	8.62	0.89	13.00	0.92	6.12	0.51	56.9	2.8
20TN15A_232	0.25	0.10	213	4	0.88	0.23	9.58	0.85	14.24	2.03	7.17	0.56	68.8	4.2
20TN15A_233	0.22	0.05	120	5	0.47	0.06	5.86	0.67	8.72	0.96	4.97	0.40	47.1	3.3
20TN15A_234	0.21	0.08	99.86	2.12	0.76	0.08	7.68	0.83	11.88	1.23	5.83	0.35	52.3	2.6
20TN15A_247_1	17.97	0.67	442	8	40.35	1.39	292	7	125	4	29.94	1.21	95.4	3.7
20TN15A_247_2	13.01	0.36	1409	37	50.48	1.36	387	9	174	5	44.58	1.60	146.8	5.0
20TN15A_247_3	11.61	0.46	2112	29	56.00	1.38	452	10	209	5	55.42	1.64	185.0	5.8
20TN15A_247_4	10.89	0.44	2018	39	50.06	1.17	409	9	209	7	56.45	1.84	197.4	4.7
20TN15A_247_5	14.32	0.32	2134	29	51.37	0.92	417	7	204	4	52.83	1.54	194.3	3.8
20TN15A_247_6	17.93	0.55	2409	45	64.25	1.01	486	11	209	5	52.08	1.65	176.3	4.1
20TN15A_248	0.20	0.05	78.03	11.51	0.73	0.16	8.78	1.75	10.83	2.00	5.57	1.10	44.5	8.3
20TN15A_250	17.67	0.69	2064	98	63.96	2.19	485	18	208	8	52.64	1.52	184.6	4.8
20TN15A_251	39.71	9.60	2028	50	61.03	2.01	443	10	199	6	51.85	2.00	187.8	6.2
20TN15A_252	19.64	0.36	1592	44	63.18	1.47	465	9	182	5	43.24	1.54	142.5	4.3
20TN15A_253_1	0.55	0.09	118	5	0.76	0.08	8.68	1.05	11.13	1.37	6.50	0.58	55.2	3.3
20TN15A_253_2	1.87	0.17	118	4	1.01	0.11	10.55	0.85	13.20	0.69	7.16	0.31	65.4	2.5
20TN15A_253_3	0.33	0.07	90.16	3.90	1.08	0.12	11.40	0.99	16.03	1.22	7.82	0.52	69.2	2.6
20TN15A_253_4	0.87	0.08	175	4	1.19	0.13	13.63	0.95	19.81	1.56	9.87	0.60	81.8	2.4
20TN15A_254	3.43	0.22	842	18	13.12	0.59	129	5	117	4	44.13	1.22	241.7	6.6

Sample and Spot Number	Tb (ppm)	±2σ	Dy (ppm)	±2σ	Ho (ppm)	±2σ	Er (ppm)	±2σ	Tm (ppm)	±2σ	Yb (ppm)	±2σ	Lu (ppm)	±2σ
20TN2_2	138.8	2.6	1249	20	315.6	6.2	1069	22	156.6	3.5	1036	29	130	3
20TN2_4	57.24	1.79	580.3	18.0	172.7	4.6	610.7	18.2	88.7	2.9	535	18	64.99	2.92
20TN2_7	90.47	2.19	811.7	15.7	225.5	5.7	748.0	21.1	110.0	2.9	702	16	89.87	2.38
20TN2_21	31.55	0.99	346.3	12.1	107.8	3.9	417.5	15.6	61.1	2.8	390	22	49.66	2.63
20TN2_25	37.80	1.21	410.0	11.4	128.3	2.9	503.9	9.1	75.0	1.5	478	14	60.81	2.45
20TN2_44	51.08	1.02	405.1	7.0	94.5	1.8	340.9	6.6	62.9	1.3	524	8	68.82	1.36
20TN4D_2	7.76	0.32	61.0	3.0	15.5	0.7	60.8	2.9	10.8	0.6	88	4	13.93	0.65
20TN4D_6	19.26	0.85	139.9	6.7	32.4	2.1	111.4	6.6	19.1	1.3	146	9	21.50	1.31
20TN4D_9	18.61	1.57	189.0	16.7	65.2	6.9	277.0	21.5	51.3	5.3	400	37	58.66	5.40
20TN4D_10	10.67	0.41	135.0	4.9	50.3	1.8	229.1	7.0	44.0	1.6	349	13	51.84	2.11
20TN4D_11	9.47	0.64	117.9	4.8	45.4	1.3	234.9	4.4	53.6	1.2	508	9	82.64	2.90
20TN4D_12	13.40	0.94	172.5	12.2	60.6	4.3	269.2	18.8	50.6	3.5	401	27	57.17	4.25
20TN4D_13	8.07	0.40	108.2	3.1	40.4	1.0	187.4	5.3	35.8	1.1	283	9	39.91	1.25
20TN4D_19	9.73	0.36	74.1	3.1	19.2	0.7	72.9	1.8	13.6	0.5	120	5	17.51	0.55
20TN4D_20	39.72	0.87	288.9	6.8	69.3	1.4	243.4	4.7	41.0	1.0	320	8	43.95	0.86
20TN4D_27	5.12	0.34	77.7	3.5	34.3	1.3	177.6	7.0	37.3	1.3	319	8	48.57	1.38
20TN4D_28	7.22	0.67	97.3	7.0	36.4	2.2	177.2	13.8	39.0	2.0	338	26	48.44	4.41
20TN15A_231_1	28.04	0.51	280.3	5.0	83.0	1.6	318.1	6.0	57.8	1.2	481	8	79.61	1.44
20TN15A_231_2	28.93	0.67	332.0	5.6	111.7	2.0	473.7	7.3	89.0	1.3	714	10	111	2
20TN15A_231_3	30.80	0.76	374.9	8.1	132.2	1.8	587.4	12.4	111.1	1.9	895	15	137	2
20TN15A_231_4	18.79	2.53	222.8	28.3	80.5	9.6	363.9	41.4	67.1	7.7	520	58	78.09	8.15
20TN15A_231_5	20.24	0.76	244.7	8.9	85.0	3.5	373.6	10.4	69.5	1.8	542	16	82.54	2.00
20TN15A_232	21.66	0.90	238.8	6.7	74.5	2.2	300.7	7.1	54.8	1.7	448	8	72.58	1.84
20TN15A_233	17.45	1.12	219.8	12.2	81.0	3.8	378.2	15.9	72.4	3.3	567	25	86.06	3.68
20TN15A_234	17.95	0.69	200.6	6.8	66.3	2.5	285.0	9.4	53.9	1.7	457	13	74.39	2.08
20TN15A_247_1	14.38	0.54	80.6	1.8	13.7	0.6	39.9	1.4	6.1	0.4	50	2	9.66	0.39
20TN15A_247_2	21.80	0.70	119.2	3.7	19.5	0.5	52.9	1.6	8.0	0.4	68	2	12.22	0.47
20TN15A_247_3	26.85	0.62	140.4	3.6	23.8	0.7	62.7	1.9	9.7	0.4	81	3	15.19	0.48
20TN15A_247_4	28.53	0.61	153.2	4.1	25.1	0.6	69.5	2.7	10.7	0.4	90	2	17.07	0.59
20TN15A_247_5	27.76	0.57	146.6	3.5	24.1	0.7	68.0	2.2	10.2	0.4	87	2	16.45	0.74
20TN15A_247_6	23.94	0.56	123.7	3.3	20.3	0.7	54.6	1.6	8.2	0.3	69	2	13.22	0.43
20TN15A_248	14.09	2.33	146.2	24.7	44.0	6.9	174.4	27.0	30.5	4.8	259	41	42.75	7.29
20TN15A_250	28.59	0.70	174.9	4.1	31.0	0.9	82.8	2.0	11.0	0.4	76	3	12.61	0.45
20TN15A_251	29.05	1.05	171.9	4.6	32.5	1.0	92.5	3.7	13.0	0.9	87	4	14.19	0.53
20TN15A_252	20.82	0.48	118.8	3.0	22.3	0.6	60.8	1.7	8.4	0.4	61	2	10.79	0.38
20TN15A_253_1	18.95	0.67	230.0	6.7	74.6	1.5	307.2	10.2	54.4	1.7	426	12	61.75	1.56
20TN15A_253_2	22.49	0.70	282.2	6.2	99.1	2.2	434.6	10.2	76.7	1.5	593	10	87.84	2.14
20TN15A_253_3	24.81	0.79	309.0	9.0	113.2	2.9	504.0	10.9	89.5	1.8	697	11	103	2
20TN15A_253_4	26.69	0.69	290.1	6.0	86.1	2.0	334.0	5.4	55.8	1.1	449	9	68.69	1.17
20TN15A_254	46.38	1.06	300.5	7.2	55.0	1.6	155.8	4.2	24.0	0.7	185	5	30.75	0.80

Sample and Spot Number	Hf (ppm)	±2σ	Ta (ppm)	±2σ	Pb (ppm)	±2σ	Hf (wt. %)	U (ppm)	Th (ppm)	Pb (ppm)
20TN2_2	3508	69	0.14	0.03	99.92	2.26	0.35	217	3425	2312
20TN2_4	4240	106	1.89	0.16	74.36	2.38	0.42	6.64	2878	1941
20TN2_7	3501	96	0.32	0.05	101	2	0.35	128	3244	3222
20TN2_21	3773	81	11.97	5.88	67.26	17.78	0.38	11.39	1484	1357
20TN2_25	3692	69	0.43	0.08	24.13	2.45	0.37	13.93	1485	958
20TN2_44	6340	99	0.44	0.07	19.95	1.04	0.63	5.53	835	813
20TN4D_2	4664	106	2.16	0.20	58.36	2.41	0.47	99.47	1106	655
20TN4D_6	4428	138	8.33	2.71	71.83	2.80	0.44	85.85	1467	1186
20TN4D_9	4058	137	418	72	82.31	5.13	0.41	191	1510	1147
20TN4D_10	4072	75	37.47	21.40	43.54	0.98	0.41	172	1008	985
20TN4D_11	8234	217	153	61	66.70	20.71	0.82	26.19	545	640
20TN4D_12	3612	93	23.99	2.36	66.51	4.30	0.36	173	1277	1356
20TN4D_13	3354	74	4.32	1.75	38.16	2.60	0.34	122	919	946
20TN4D_19	4394	122	2.25	0.40	117	3	0.44	426	3386	2798
20TN4D_20	5367	230	7.62	0.58	44.06	1.63	0.54	77.25	1032	1155
20TN4D_27	4787	98	0.14	0.03	10.09	0.61	0.48	8.14	343	321
20TN4D_28	5522	184	102	40	21.48	5.64	0.55	48.96	776	781
20TN15A_231_1	4350	55	0.55	0.07	62.56	0.89	0.44	12.07	1217	810
20TN15A_231_2	3340	46	0.60	0.08	74.23	1.19	0.33	10.61	1314	881
20TN15A_231_3	3158	45	0.34	0.06	75.32	1.29	0.32	9.49	1239	828
20TN15A_231_4	3278	55	0.39	0.06	68.60	3.21	0.33	7.21	1172	794
20TN15A_231_5	3292	55	0.38	0.07	74.47	2.22	0.33	7.18	1216	795
20TN15A_232	4219	145	0.65	0.14	106	3	0.42	10.97	1932	1207
20TN15A_233	3087	53	0.52	0.07	70.56	2.58	0.31	7.77	1065	704
20TN15A_234	3600	60	0.37	0.05	43.60	1.43	0.36	5.51	430	370
20TN15A_247_1	5016	91	0.27	0.06	46.21	1.49	0.50	5.94	272	209
20TN15A_247_2	4921	70	0.97	0.11	125	4	0.49	11.21	852	560
20TN15A_247_3	4798	78	1.12	0.14	177	3	0.48	14.81	1241	813
20TN15A_247_4	4725	83	1.10	0.11	175	3	0.47	14.27	1233	806
20TN15A_247_5	4813	81	1.16	0.15	163	4	0.48	11.47	1152	750
20TN15A_247_6	4830	69	1.27	0.13	157	3	0.48	11.44	1075	708
20TN15A_248	4337	370	0.32	0.06	28.89	3.73	0.43	2.38	149	115
20TN15A_250	5081	108	1.20	0.11	134	6	0.51	11.81	881	576
20TN15A_251	5585	296	1.26	0.18	111	2	0.56	12.24	921	553
20TN15A_252	5178	153	0.82	0.07	81.12	2.42	0.52	7.66	555	360
20TN15A_253_1	3268	69	0.53	0.11	49.79	0.90	0.33	3.39	234	187
20TN15A_253_2	2906	54	0.67	0.10	65.90	2.37	0.29	3.71	297	243
20TN15A_253_3	2793	49	0.42	0.07	58.20	1.34	0.28	4.49	364	254
20TN15A_253_4	3466	50	0.75	0.08	64.61	1.33	0.35	5.40	407	273
20TN15A_254	5404	195	1.24	0.14	145.13	3	0.54	10.46	869	588

Sample and Spot Number	Note	Li (ppm)	±2σ	Si (ppm)	±2σ	P (ppm)	±2σ	Ca (ppm)	±2σ	Sc (ppm)	±2σ	Ti (ppm)	±2σ
20TN15A_258	March	9.16	0.71	146723	2705	67.6	39.7	b.d.l.		401	7	11.50	1.63
20TN15A_259_1	March	8.90	0.78	146995	2079	167	34	12	51	396	8	1.96	0.98
20TN15A_259_2	March	7.10	0.72	146462	2725	86.6	44.8	16	59	394	6	2.33	1.07
20TN15A_259_3	March	17.82	1.07	144436	2547	90.7	40.6	29	46	403	6	3.10	1.21
20TN15A_259_4	March	20.31	1.48	147446	2666	156	44	7	65	397	7	3.56	1.14
20TN15A_260_2	March	27.19	1.54	155331	3149	261	55	b.d.l.		402	6	8.74	2.64
20TN15A_260_3	March	24.65	1.74	150144	2861	263	49	b.d.l.		400	8	1.38	1.27
20TN15A_260_4	March	14.13	1.44	146739	2393	506	159	19	89	399	7	14.24	5.39
20TN15A_261	March	6.14	0.69	148020	2597	145	38	4	59	403	6	14.78	5.00
20TN15A_262	March	2.39	0.67	151080	3043	85.8	44.0	22	54	411	8	30.55	3.17
20TN15A_264	March	14.63	0.86	149355	3847	186	50	32	68	412	8	520	277
20TN15A_265	March	0.43	0.24	147103	2876	85.3	39.9	b.d.l.		398	7	20.68	2.44
20TN15A_266	March	10.86	0.96	148268	2619	63.4	36.8	b.d.l.		401	7	29.31	4.26
20TN15A_267_3	March	11.94	1.04	147188	3323	116	54	47	53	395	6	4.10	1.13
20TN15A_273_2	March	2.21	0.67	140852	2076	24.8	13.1	33	52	385	8	2.54	1.31
20TN15A_274_1	March	18.03	1.07	146123	3252	36.2	12.0	b.d.l.		381	6	3.08	1.30
20TN15A_274_2	March	13.52	0.87	143994	2759	50.4	13.2	b.d.l.		387	7	4.08	1.32
20TN15A_276	March	10.02	0.83	142794	2919	25.2	12.9	b.d.l.		383	6	6.55	1.66
20TN15A_278	March	2.34	0.44	142103	2978	27.0	16.7	b.d.l.		388	6	4.00	1.46
20TN15A_279	March	4.93	0.64	151124	2989	32.8	12.7	b.d.l.		392	7	40.20	3.97
20TN15A_281	March	0.19	0.20	140564	2549	34.5	14.5	9	53	387	8	4.91	1.44
20TN15A_282	March	7.76	0.56	142157	2540	35.1	17.1	b.d.l.		387	7	3.41	0.89
20TN15A_283	March	19.22	1.68	139369	2363	52.7	15.8	81	65	384	6	5.68	1.62
20TN15A_284_1	March	6.72	0.89	140582	2151	55.0	14.2	b.d.l.		386	7	2.16	1.16
20TN15A_284_2	March	4.06	0.46	140343	2336	35.7	13.2	b.d.l.		382	6	1.85	1.11
20TN15A_284_3	March	8.83	1.01	142227	2440	80.5	15.1	26	49	381	8	10.21	3.63
20TN15A_284_6	March	7.99	0.74	138228	3015	40.2	9.7	b.d.l.		377	7	2.93	1.40
20TN15B_132	March	34.25	2.23	148398	5112	17.7	53.3	352	160	433	7	29.30	12.31
20TN15B_133	March	37.67	2.57	149078	7642	42.3	65.5	130	185	442	12	8.35	3.70
20TN15B_140	March	72.15	3.34	152594	8093	38.5	18.2	244	161	428	28	47.98	41.96
20TN15B_156	March	32.67	4.53	148852	7190	0.2	18.9	117	77	420	14	10.99	2.42
20TN15B_157	March	2.38	0.73	144744	3145	10.6	9.5	b.d.l.		397	9	11.45	2.26
20TN15B_158	March	1.44	0.35	146503	1914	16.0	13.7	36	71	409	7	46.26	10.83
20TN16A-2_101	March	7.49	0.93	158825	7118	381	35	907	191	433	15	1902	72
20TN16A-2_104	March	11.83	0.94	159240	3640	831	44	1691	237	418	5	2538	106
20TN16A-2_106	March	14.27	1.23	157878	2765	804	28	1331	220	420	11	2130	61
20TN16A-2_115	March	33.73	2.09	161515	4036	281	27	1182	439	420	9	811	98
20TN16A-2_117	March	28.35	3.00	147489	5280	274	30	716	193	421	18	753	46
20TN17A-2_70	March	5.00	0.65	158737	2655	725	45	148	129	428	7	987	23
20TN17A-2_71	March	4.28	0.38	153159	2676	679	33	289	94	430	9	1025	19
20TN17A-2_72	March	3.69	0.43	158021	3271	610	32	128	91	434	8	1025	27

Sample and Spot Number	^{56}Fe (ppm)	±2σ	^{57}Fe (ppm)	±2σ	Y (ppm)	±2σ	Zr (ppm)	±2σ	Nb (ppm)	±2σ	Mo (ppm)	±2σ
20TN15A_258	b.d.l.		1.2	4.1	1876	23	498126	6551	90.79	1.54	0.51	0.19
20TN15A_259_1	5.8	2.0	3.4	3.0	3733	60	501867	6784	24.62	0.72	0.35	0.15
20TN15A_259_2	1.6	1.9	3.3	2.9	2206	31	499527	5534	16.01	0.55	0.48	0.17
20TN15A_259_3	3.0	2.0	6.9	5.0	1702	28	503256	6190	16.85	0.51	0.53	0.23
20TN15A_259_4	27.8	5.0	31.0	8.2	1534	91	498294	9879	21.28	1.07	0.37	0.17
20TN15A_260_2	62.1	9.4	45.3	9.6	1335	145	503402	5556	11.72	0.96	1.57	0.46
20TN15A_260_3	1650	509	1332	409	1016	33	496370	7801	7.33	0.42	0.79	0.38
20TN15A_260_4	22.9	6.2	22.4	8.3	691	41	499541	6022	8.41	1.02	0.47	0.24
20TN15A_261	328	163	254	143	542	14	496113	6139	76.07	3.96	0.40	0.20
20TN15A_262	23.4	2.9	17.1	5.0	570	8	502483	4703	156	3	0.35	0.20
20TN15A_264	61.6	26.0	49.4	24.5	530	9	498662	6951	138	18	0.47	0.22
20TN15A_265	5.2	2.8	5.0	3.1	666	8	499933	4691	106	2	0.63	0.22
20TN15A_266	17.3	2.8	9.9	5.4	715	9	505205	6503	147	3	0.46	0.21
20TN15A_267_3	39.1	13.4	34.4	13.8	856	25	502178	7800	17.88	0.63	0.56	0.25
20TN15A_273_2	0.9	2.3	7.0	4.3	1046	91	508447	6440	14.19	1.06	0.42	0.22
20TN15A_274_1	12.7	3.4	6.1	3.9	2063	56	498413	5677	22.90	0.61	0.45	0.16
20TN15A_274_2	4.0	2.6	b.d.l.		2586	44	507444	8641	25.27	0.64	0.42	0.21
20TN15A_276	5.7	2.8	6.0	3.0	859	14	499423	6405	37.62	0.62	0.43	0.23
20TN15A_278	5.8	3.3	2.7	3.0	1535	46	504657	6537	26.45	0.64	0.43	0.16
20TN15A_279	72.9	6.5	49.9	9.4	476	6	505572	6656	196	3	0.46	0.21
20TN15A_281	b.d.l.		3.7	2.9	1273	29	508227	5356	28.10	0.74	0.38	0.20
20TN15A_282	8.0	2.7	7.5	4.1	2373	51	504226	7138	24.12	0.63	0.44	0.19
20TN15A_283	2.9	3.0	2.9	2.9	1421	29	496741	5859	25.50	0.65	0.28	0.13
20TN15A_284_1	2.6	2.4	0.6	3.3	2332	40	503081	7883	24.52	0.70	0.17	0.11
20TN15A_284_2	0.3	3.1	2.2	2.8	2312	46	504314	7675	18.52	0.84	0.47	0.16
20TN15A_284_3	55.5	14.4	41.6	11.9	962	53	501983	6714	16.43	2.39	0.97	0.51
20TN15A_284_6	1.9	1.9	0.1	3.8	1989	28	499901	7564	28.44	0.69	0.35	0.18
20TN15B_132	646	433	413	269	743	100	497632	9905	155	71	0.69	0.35
20TN15B_133	701	116	441	71	871	57	492236	8789	32.73	10.73	0.46	0.31
20TN15B_140	4656	3171	2486	1734	3035	249	505396	9856	56.44	14.62	1.89	1.49
20TN15B_156	2073	307	1337	284	1040	105	474728	18308	46.91	3.81	0.93	0.70
20TN15B_157	177	32	110	19	230	4	473684	6168	90.06	6.98	0.48	0.24
20TN15B_158	276	71	178	47	363	9	476580	6357	80.02	22.44	0.57	0.19
20TN16A-2_101	1090	41	956	72	4140	128	508179	15313	4240	84	1.08	0.72
20TN16A-2_104	2119	85	1837	73	351	60	515625	9549	4183	97	0.59	0.25
20TN16A-2_106	1947	238	1729	213	836	61	515763	8920	3587	137	0.67	0.22
20TN16A-2_115	2435	365	1785	256	641	23	507329	9503	3193	147	0.52	0.25
20TN16A-2_117	1424	178	1066	206	425	23	500109	14788	2741	262	0.41	0.42
20TN17A-2_70	901	22	571	31	10396	94	510313	6002	6162	102	0.67	0.24
20TN17A-2_71	871	15	554	20	10311	158	515858	7263	5808	73	0.73	0.28
20TN17A-2_72	988	22	592	23	11351	132	516334	5603	6492	176	1.56	0.40

Sample and Spot Number	La (ppm)	±2σ	Ce (ppm)	±2σ	Pr (ppm)	±2σ	Nd (ppm)	±2σ	Sm (ppm)	±2σ	Eu (ppm)	±2σ	Gd (ppm)	±2σ
20TN15A_258	1.73	0.15	852	13	12.12	0.42	124	4	109	3	38.79	1.04	243.7	7.0
20TN15A_259_1	0.25	0.05	96.04	2.22	0.95	0.12	10.20	0.74	13.71	0.88	6.89	0.38	68.8	2.9
20TN15A_259_2	0.09	0.03	53.25	1.27	0.39	0.06	4.66	0.58	6.46	0.88	3.08	0.20	33.0	1.6
20TN15A_259_3	1.44	0.12	59.51	1.26	0.30	0.05	2.88	0.27	4.75	0.60	2.30	0.21	24.2	1.3
20TN15A_259_4	0.88	0.11	63.62	3.61	0.33	0.07	2.77	0.42	4.54	0.74	2.11	0.30	23.3	2.0
20TN15A_260_2	2.79	0.67	33.73	3.48	0.62	0.14	4.08	1.04	6.71	1.15	3.56	0.56	36.0	5.0
20TN15A_260_3	1.60	0.33	21.58	1.75	0.29	0.05	2.03	0.40	5.04	0.73	2.24	0.24	25.2	1.9
20TN15A_260_4	66.44	25.18	23.17	3.04	8.25	3.13	25.11	9.64	4.30	1.11	1.46	0.26	13.3	1.6
20TN15A_261	6.15	0.38	159	8	14.65	0.83	111	7	46.80	2.32	10.50	0.53	39.9	2.4
20TN15A_262	23.14	0.79	2315	59	76.33	2.53	544	15	172	6	36.21	1.32	113.0	4.2
20TN15A_264	14.84	2.49	285	6	27.62	0.93	209	6	85.19	2.65	21.60	0.77	83.4	3.0
20TN15A_265	8.01	0.32	1768	25	38.50	0.84	319	7	133	5	31.26	0.88	125.0	3.5
20TN15A_266	23.05	0.81	2591	43	72.67	1.63	552	11	194	6	41.48	1.09	146.1	3.1
20TN15A_267_3	13.07	7.22	105	7	2.32	0.94	13.18	3.13	11.93	1.23	5.31	0.56	45.6	2.8
20TN15A_273_2	0.48	0.09	72.55	5.11	1.36	0.17	14.93	1.59	18.66	2.05	8.81	0.91	61.6	5.1
20TN15A_274_1	1.26	0.14	113	4	2.20	0.14	22.32	1.26	27.33	1.56	13.35	0.60	93.2	3.8
20TN15A_274_2	0.71	0.11	122	2	2.20	0.16	23.85	1.16	31.04	1.71	14.57	0.69	104.0	2.9
20TN15A_276	1.02	0.10	330	13	6.81	0.39	66.98	2.01	66.69	2.69	24.49	0.83	123.5	3.1
20TN15A_278	0.17	0.04	176	4	1.85	0.24	21.19	1.40	27.57	1.78	12.92	0.73	88.7	3.5
20TN15A_279	49.65	1.96	2750	90	115	4	699	19	186	7	39.31	0.93	111.1	3.8
20TN15A_281	0.20	0.05	223	4	2.29	0.16	27.07	1.51	30.69	1.16	13.81	0.55	90.8	3.1
20TN15A_282	1.14	0.14	105	3	1.23	0.14	13.42	0.87	18.11	1.37	9.13	0.47	71.1	2.8
20TN15A_283	1.06	0.15	194	3	1.92	0.13	22.31	0.99	26.98	1.71	12.30	0.59	84.8	3.1
20TN15A_284_1	0.56	0.11	85.47	3.91	1.71	0.15	17.36	0.96	23.07	1.19	10.97	0.51	83.8	2.4
20TN15A_284_2	0.82	0.08	52.75	1.07	0.96	0.09	10.44	1.17	13.05	1.00	6.23	0.48	56.5	2.2
20TN15A_284_3	2.91	0.60	21.98	0.92	0.34	0.06	2.39	0.48	5.09	0.53	2.38	0.24	23.8	1.5
20TN15A_284_6	0.13	0.05	135	4	0.99	0.12	11.31	1.11	18.71	1.17	9.01	0.48	70.9	2.7
20TN15B_132	7.75	1.80	47.07	7.22	2.93	0.88	14.71	3.77	8.69	1.87	2.74	0.51	18.0	2.6
20TN15B_133	4.41	0.35	34.96	1.79	0.73	0.14	3.85	1.46	3.78	1.00	1.59	0.34	13.6	1.5
20TN15B_140	18.04	6.33	100	17	5.22	1.77	17.95	5.30	16.63	3.80	6.17	2.29	54.1	8.1
20TN15B_156	6.20	1.16	61.96	6.71	1.92	0.26	11.91	1.83	9.09	2.25	4.04	0.57	31.7	4.2
20TN15B_157	12.05	1.05	21.36	1.10	1.03	0.10	1.83	0.27	1.19	0.33	0.61	0.12	5.8	0.6
20TN15B_158	9.28	1.19	17.31	1.02	0.39	0.08	1.83	0.51	2.44	0.41	0.96	0.13	10.3	1.2
20TN16A-2_101	1682	155	6431	242	432	12	1163	35	176	9	46.05	1.71	167.3	8.3
20TN16A-2_104	1589	57	5451	109	349	8	840	28	86.92	4.45	15.38	1.18	48.5	4.2
20TN16A-2_106	1608	57	5594	114	343	9	820	21	96.75	3.65	19.97	0.69	63.9	3.1
20TN16A-2_115	276	43	364	40	24.19	3.43	61.14	6.77	12.61	1.47	4.36	0.74	23.6	2.6
20TN16A-2_117	247	14	247	21	15.16	1.63	32.81	3.58	10.42	1.47	3.63	0.61	22.0	2.5
20TN17A-2_70	387	9	636	10	44.91	0.92	106	3	56.83	2.70	19.57	0.82	241.8	5.6
20TN17A-2_71	403	7	647	11	45.67	0.75	110	3	58.68	2.22	20.57	0.66	248.4	4.8
20TN17A-2_72	364	14	600	23	42.75	1.38	107	3	63.73	2.61	22.22	0.60	263.3	5.1

Sample and Spot Number	Tb (ppm)	±2σ	Dy (ppm)	±2σ	Ho (ppm)	±2σ	Er (ppm)	±2σ	Tm (ppm)	±2σ	Yb (ppm)	±2σ	Lu (ppm)	±2σ
20TN15A_258	45.83	0.75	299.5	4.9	57.2	0.8	154.1	3.4	24.5	0.8	196	6	31.69	0.85
20TN15A_259_1	24.70	0.72	306.6	8.1	111.6	2.5	488.7	8.9	91.2	1.6	741	12	108	2
20TN15A_259_2	12.70	0.47	168.8	4.2	69.1	1.2	314.4	6.8	62.5	1.3	495	9	71.11	1.28
20TN15A_259_3	9.38	0.39	128.2	3.8	51.6	1.4	241.3	5.1	47.7	1.0	373	8	55.40	1.38
20TN15A_259_4	8.60	0.54	117.0	5.5	46.7	2.1	214.6	7.2	42.1	1.5	343	14	50.79	1.99
20TN15A_260_2	12.47	1.64	143.3	15.7	51.0	4.5	204.7	13.9	33.6	1.8	242	10	33.28	1.38
20TN15A_260_3	8.88	0.46	111.8	5.7	43.0	1.4	182.2	5.3	31.2	0.7	221	5	30.40	0.62
20TN15A_260_4	4.60	0.42	63.8	5.2	27.5	1.8	128.9	6.0	24.1	1.1	190	8	28.05	1.14
20TN15A_261	8.02	0.41	67.7	2.7	16.9	0.8	49.0	1.9	7.0	0.4	49	2	9.04	0.30
20TN15A_262	16.60	0.56	94.7	2.1	18.2	0.6	44.6	1.4	6.6	0.3	48	2	9.32	0.38
20TN15A_264	14.00	0.45	84.5	2.1	16.5	0.7	41.4	1.6	5.7	0.3	44	2	8.40	0.33
20TN15A_265	18.22	0.52	106.2	2.9	20.3	0.4	49.3	1.3	7.0	0.2	45	2	8.76	0.30
20TN15A_266	19.90	0.47	112.7	3.1	20.6	0.5	50.7	1.4	7.6	0.4	51	2	9.84	0.31
20TN15A_267_3	11.58	0.73	100.6	4.5	27.6	0.9	101.3	3.2	20.9	0.6	211	5	37.52	1.27
20TN15A_273_2	16.03	1.26	134.5	9.6	31.9	2.1	114.7	7.2	24.2	1.2	238	12	43.45	1.71
20TN15A_274_1	25.27	0.83	230.2	6.9	57.8	1.8	196.5	6.1	36.5	1.3	292	10	44.21	1.74
20TN15A_274_2	30.38	0.80	286.0	8.1	74.2	1.5	261.7	6.1	48.0	1.3	381	8	55.63	1.56
20TN15A_276	21.02	0.47	121.2	2.9	22.0	0.5	66.1	1.9	12.2	0.4	101	3	17.25	0.69
20TN15A_278	22.41	0.59	180.8	4.2	42.0	1.3	137.4	5.0	24.8	1.1	204	7	30.33	1.12
20TN15A_279	14.72	0.61	72.1	2.2	12.4	0.4	33.8	1.4	5.9	0.3	51	2	9.76	0.36
20TN15A_281	20.22	0.56	151.2	4.1	33.4	0.9	108.2	3.1	20.3	0.7	171	5	27.33	0.86
20TN15A_282	22.38	0.52	237.3	5.2	72.6	2.2	284.8	8.2	52.6	1.4	410	11	60.23	1.66
20TN15A_283	20.19	0.63	160.1	3.5	38.3	1.0	127.1	3.2	24.4	0.6	197	6	30.42	0.91
20TN15A_284_1	24.71	0.67	248.1	4.5	67.8	1.9	255.2	6.1	48.0	1.3	384	12	56.73	1.80
20TN15A_284_2	19.14	0.60	219.0	5.4	75.4	1.6	317.9	6.1	60.4	1.6	468	10	68.53	1.62
20TN15A_284_3	8.59	0.45	99.7	3.7	36.7	1.0	158.3	4.8	29.0	0.6	211	5	31.50	0.90
20TN15A_284_6	21.00	0.52	207.9	4.4	58.1	1.2	214.5	5.7	39.5	1.3	314	8	46.01	1.08
20TN15B_132	5.92	0.79	64.3	9.2	21.9	2.8	96.5	11.8	19.7	2.2	172	15	27.71	2.90
20TN15B_133	5.22	0.29	60.1	3.9	22.5	0.8	109.5	5.5	23.2	1.2	198	6	30.20	1.46
20TN15B_140	18.04	1.82	218.2	28.8	74.2	6.6	363.8	25.5	74.5	3.1	649	36	99.26	3.58
20TN15B_156	8.55	0.82	96.0	12.5	31.7	2.7	137.4	11.4	26.7	2.4	220	20	33.38	2.70
20TN15B_157	1.85	0.14	22.7	1.1	8.1	0.3	34.9	1.4	7.4	0.3	58	2	9.38	0.35
20TN15B_158	3.21	0.19	39.3	1.3	13.5	0.4	57.9	1.8	11.2	0.5	91	2	15.60	0.62
20TN16A-2_101	44.62	1.73	491.4	12.9	149.4	4.4	590.8	22.9	105.3	4.3	696	26	79.84	3.98
20TN16A-2_104	6.88	0.93	50.6	9.2	12.5	2.8	44.7	10.0	7.8	1.6	59	12	7.08	1.22
20TN16A-2_106	12.63	0.73	120.2	9.4	33.6	2.9	129.9	11.0	22.5	2.1	150	11	17.54	1.30
20TN16A-2_115	7.59	0.61	83.8	5.1	24.4	1.2	97.9	5.6	19.5	1.1	168	8	23.96	1.08
20TN16A-2_117	6.59	0.59	59.7	4.0	16.0	1.1	56.0	5.2	10.1	0.7	95	8	13.44	0.78
20TN17A-2_70	96.12	1.62	986.5	16.8	294.1	3.8	1179	20	205.3	3.9	1466	29	191	2
20TN17A-2_71	97.95	1.84	1016	14	299.7	4.9	1199	17	202.7	3.1	1486	22	190	3
20TN17A-2_72	103.5	1.2	1086	18	320.3	4.9	1271	18	218.9	3.3	1570	18	205	3

Sample and Spot Number	Hf (ppm)	±2σ	Ta (ppm)	±2σ	Pb (ppm)	±2σ	Hf (wt. %)	U (ppm)	Th (ppm)	Pb (ppm)
20TN15A_258	5297	174	1.25	0.14	152	2	0.53	9.95	1044	662
20TN15A_259_1	3067	43	0.40	0.06	54.99	0.76	0.31	5.11	461	286
20TN15A_259_2	2912	43	0.31	0.05	27.41	0.72	0.29	2.14	140	114
20TN15A_259_3	3106	53	0.43	0.08	35.37	0.83	0.31	3.43	157	142
20TN15A_259_4	3117	68	0.44	0.09	33.54	2.71	0.31	2.33	212	153
20TN15A_260_2	3276	78	0.20	0.05	102	17	0.33	46.73	648	397
20TN15A_260_3	3225	41	0.19	0.05	92.96	30.33	0.32	33.70	155	136
20TN15A_260_4	3767	55	0.14	0.04	60.41	4.15	0.38	14.91	340	224
20TN15A_261	5485	176	0.40	0.06	10.44	0.48	0.55	2.35	50.7	40.9
20TN15A_262	4957	165	0.88	0.10	93.97	3.95	0.50	7.70	549	362
20TN15A_264	5464	208	1.36	0.41	18.33	0.49	0.55	5.00	83.6	66.6
20TN15A_265	5116	169	0.84	0.10	78.85	1.38	0.51	8.23	549	351
20TN15A_266	4914	160	1.05	0.11	107	2	0.49	10.65	736	481
20TN15A_267_3	3811	62	0.62	0.10	30.57	2.34	0.38	6.77	134	104
20TN15A_273_2	3641	67	0.39	0.07	24.22	1.25	0.36	11.17	208	157
20TN15A_274_1	3733	45	0.77	0.08	39.43	1.22	0.37	13.11	205	167
20TN15A_274_2	3597	35	0.81	0.09	41.22	1.27	0.36	15.06	233	184
20TN15A_276	4605	147	0.81	0.12	39.62	1.29	0.46	18.93	271	213
20TN15A_278	3920	72	0.91	0.14	34.86	0.70	0.39	18.53	274	214
20TN15A_279	4867	184	2.81	0.18	88.04	3.83	0.49	31.05	651	430
20TN15A_281	3929	76	1.22	0.12	44.94	0.68	0.39	31.26	377	290
20TN15A_282	3170	54	0.77	0.07	38.91	0.87	0.32	18.30	315	251
20TN15A_283	3796	68	1.08	0.11	46.31	2.19	0.38	26.38	323	262
20TN15A_284_1	3501	50	0.72	0.09	33.32	0.96	0.35	18.04	272	218
20TN15A_284_2	2941	45	0.57	0.07	25.88	0.63	0.29	11.65	217	183
20TN15A_284_3	3219	59	0.45	0.08	38.43	1.64	0.32	31.28	262	227
20TN15A_284_6	3448	75	1.08	0.10	32.69	0.78	0.34	23.70	340	279
20TN15B_132	7975	336	2.25	0.66	127	48	0.80	225	2499	970
20TN15B_133	7971	121	1.51	0.22	88.97	7.02	0.80	251	1278	551
20TN15B_140	6112	441	3.77	0.36	223	15	0.61	481	2792	798
20TN15B_156	4620	369	2.27	0.36	155	6	0.46	362	1654	775
20TN15B_157	4545	89	9.25	0.65	54.42	2.28	0.45	90.60	525	335
20TN15B_158	6069	290	26.30	7.88	66.89	2.74	0.61	143	821	462
20TN16A-2_101	10133	375	141	9	63.93	5.69	1.01	140	664	400
20TN16A-2_104	13277	313	217	8	29.50	1.08	1.33	127	286	160
20TN16A-2_106	13304	276	182	5	34.24	0.70	1.33	111	264	152
20TN16A-2_115	7636	250	71.32	3.62	93.04	3.57	0.76	140	1157	572
20TN16A-2_117	8151	220	66.94	5.71	67.86	4.06	0.82	137	814	488
20TN17A-2_70	7748	220	187	3	78.23	1.63	0.77	824	96.9	94.0
20TN17A-2_71	8337	118	178	3	74.64	1.55	0.83	710	82.6	77.3
20TN17A-2_72	9092	127	199	7	77.18	1.32	0.91	723	90.4	84.7

Sample and Spot Number	Note	Li (ppm)	±2σ	Si (ppm)	±2σ	P (ppm)	±2σ	Ca (ppm)	±2σ	Sc (ppm)	±2σ	Ti (ppm)	±2σ
20TN17A-2_75	March	2.37	0.39	164007	3415	1367	54	89	119	426	8	202	20
20TN17A-2_76	March	3.20	0.84	148693	3800	873	58	202	186	434	17	610	31
20TN17A-2_83	March	2.67	0.49	146572	6915	1087	104	1050	172	413	14	1413	32
20TN17A-2_85	March	4.02	0.60	156442	2987	1097	60	111	105	408	7	745	16
20TN17A-2_86	March	5.40	0.62	157960	2995	1083	63	98	98	399	8	974	24
20TN17A-2_88	March	4.87	0.46	150847	2586	1063	68	199	88	401	6	889	23
20TN17A-2_89_1	March	3.59	0.45	152523	2717	886	49	144	90	404	8	918	24
20TN17A-2_89_2	March	4.18	0.40	151578	2791	934	63	95	65	405	5	898	23
20TN17A-2_89_3	March	4.17	0.52	155257	3731	981	66	b.d.l.		399	10	939	18
20TN17A-2_89_4	March	3.34	0.50	152276	2548	916	53	227	103	398	6	949	25
20TN17A-2_89_5	March	3.95	0.60	162449	4585	1213	71	208	126	400	6	937	26
20TN17A-2_90_1	March	7.83	0.70	152477	3003	1702	93	136	97	399	4	945	21
20TN17A-2_90_2	March	6.65	0.65	162063	5177	2757	164	126	94	415	10	945	28
20TN17A-2_90_3	March	5.70	0.71	148556	3357	870	59	11	77	401	11	905	25
20TN17A-2_90_4	March	5.61	0.46	152821	2327	1070	52	118	85	404	6	927	24
20TN17A-2_90_5	March	5.21	0.42	155704	3602	1741	226	378	122	405	9	1063	19
20TN17A-2_92_1	March	4.66	0.64	157290	3300	1490	71	209	107	396	10	1011	28
20TN17A-2_92_2	March	5.53	0.51	158002	2900	904	59	64	93	396	7	869	24
20TN17A-2_92_3	March	6.40	0.71	151330	3210	840	50	233	57	393	5	925	17
20TN17A-2_92_4	March	5.89	0.57	157803	2779	957	46	82	73	405	10	793	16
20TN17A-2_92_5	March	4.16	0.45	151588	2666	820	36	114	85	400	7	822	28
20TN17A-2_92_6	March	4.03	0.41	156358	3766	1107	49	239	82	404	8	1053	29
20TN17A-2_96_3	March	4.16	0.72	155705	6432	278	28	565	185	428	9	1339	38
20TN17A-2_96_4	March	3.91	0.56	160298	3353	321	18	445	160	433	7	1494	32
20TN17A-2_96_5	March	2.29	0.47	163246	4195	330	20	438	103	427	5	1774	66
20TN17A-2_97_1	March	4.78	0.83	152906	6058	371	41	678	228	435	8	1457	59
20TN17A-2_97_2	March	3.15	0.89	147290	6197	304	20	1121	310	419	15	1561	53
20TN17A-2_97_3	March	2.52	0.49	154379	6924	270	28	712	236	426	13	1664	49
20TN17A-2_97_4	March	2.81	0.52	158318	5434	337	23	488	108	426	12	1688	51
20TN17A-2_97_5	March	4.27	0.54	160291	5468	350	22	82	112	424	8	913	30
20TN17A-2_98_2	March	7.06	0.94	155421	4820	406	28	189	128	428	14	1134	49
20TN17A-2_98_4	March	2.73	0.51	143566	3600	318	34	703	216	431	15	1696	33
20TN17A-2_98_6	March	3.87	0.79	154471	5027	439	23	539	236	436	11	1619	29
20TN17A-2_98_7	March	3.50	0.77	147972	4514	332	17	809	308	426	20	1690	53
20TN17A-2_99_2	March	8.11	0.95	164193	3049	353	21	140	80	421	9	1015	23
20TN17A-2_99_3	March	5.13	0.83	154560	5661	365	22	360	114	436	10	1385	49
20TN17A-2_99_5	March	7.62	0.65	161911	4652	316	17	182	94	428	8	953	22
20TN20_5	June	1.96	0.68	169808	3864	107	42	b.d.l.		473	15	2.00	1.06
20TN20_11	June	6.80	0.95	164114	3176	73	23	26	78	470	14	1.97	0.99
20TN20_14	June	3.19	0.66	164297	5135	112	25	61	98	467	12	9.35	2.28
20TN20_15	June	5.20	0.64	165148	4328	37	21	74	106	466	11	17.83	1.70

Sample and Spot Number	^{56}Fe (ppm)	±2σ	^{57}Fe (ppm)	±2σ	Y (ppm)	±2σ	Zr (ppm)	±2σ	Nb (ppm)	±2σ	Mo (ppm)	±2σ
20TN17A-2_75	509	59	333	41	20132	237	508673	6961	5313	103	2.42	0.67
20TN17A-2_76	867	28	542	48	18006	575	509867	12499	6482	145	2.65	0.90
20TN17A-2_83	2088	44	1115	39	10595	273	482153	13490	4030	159	0.81	0.38
20TN17A-2_85	658	15	351	19	15695	168	482126	6696	7893	147	0.55	0.19
20TN17A-2_86	997	21	533	22	10689	150	486162	7405	6018	91	0.37	0.18
20TN17A-2_88	973	112	535	66	10046	96	473026	4778	4611	115	0.65	0.31
20TN17A-2_89_1	775	12	419	19	11868	135	478577	4393	6350	87	0.69	0.29
20TN17A-2_89_2	796	16	417	23	11111	158	476912	5236	6262	88	0.53	0.27
20TN17A-2_89_3	820	13	434	18	11081	120	474138	7037	6323	101	0.66	0.31
20TN17A-2_89_4	885	18	486	19	11200	111	479002	5750	5612	98	0.43	0.17
20TN17A-2_89_5	1767	323	972	181	11138	156	478271	8200	4681	106	0.74	0.22
20TN17A-2_90_1	1083	31	595	22	10353	144	479519	5836	6229	105	0.98	0.36
20TN17A-2_90_2	3223	350	1717	187	11828	202	478030	8501	6353	118	1.53	0.55
20TN17A-2_90_3	900	18	468	18	11454	159	482935	8573	7776	109	0.56	0.23
20TN17A-2_90_4	972	22	524	23	10846	132	480541	5876	6117	143	0.66	0.27
20TN17A-2_90_5	1389	34	758	33	10200	177	481513	6543	4601	101	0.41	0.20
20TN17A-2_92_1	1279	41	708	32	10296	113	484389	6333	4471	65	0.38	0.21
20TN17A-2_92_2	771	14	402	29	11035	151	484508	6567	6966	104	0.64	0.29
20TN17A-2_92_3	2068	180	1123	106	11201	147	475955	6918	7747	102	0.56	0.23
20TN17A-2_92_4	2502	249	1360	149	12828	184	483470	6277	7480	136	0.44	0.21
20TN17A-2_92_5	716	8	396	20	12631	204	478562	5276	6379	100	0.48	0.24
20TN17A-2_92_6	1309	34	701	37	9888	202	487584	9708	4464	117	0.34	0.17
20TN17A-2_96_3	1468	33	1278	35	8366	171	516129	10230	5235	143	0.70	0.30
20TN17A-2_96_4	1525	27	1331	49	9823	143	523132	5729	6548	121	0.67	0.24
20TN17A-2_96_5	1769	72	1573	79	12338	159	521894	7890	6868	79	0.39	0.15
20TN17A-2_97_1	1694	56	1483	82	7773	192	524094	13595	5185	194	0.70	0.27
20TN17A-2_97_2	2202	85	1855	102	6322	90	515943	10775	3992	98	1.01	0.54
20TN17A-2_97_3	2235	64	1966	85	7034	181	505323	13829	4257	96	0.49	0.25
20TN17A-2_97_4	1658	31	1400	49	11235	175	517538	8212	6209	125	0.52	0.26
20TN17A-2_97_5	713	14	622	34	11597	155	518689	7776	7022	161	0.55	0.29
20TN17A-2_98_2	1220	34	1028	72	7386	146	511971	11258	5400	171	0.79	0.30
20TN17A-2_98_4	1861	61	1628	28	7947	301	509631	15682	5957	332	0.33	0.31
20TN17A-2_98_6	1798	35	1575	61	8506	187	521618	15933	5225	133	0.90	0.41
20TN17A-2_98_7	2131	85	1843	75	6652	164	514298	10588	5047	117	0.53	0.24
20TN17A-2_99_2	916	22	785	35	8490	176	519755	8311	7004	101	0.55	0.23
20TN17A-2_99_3	1569	42	1410	71	7089	143	526688	11394	5037	142	0.61	0.28
20TN17A-2_99_5	896	12	747	29	9507	145	519399	6356	7512	206	0.96	0.29
20TN20_5	b.d.l.		3.7	3.4	4420	142	508159	8460	164	9	1.32	0.28
20TN20_11	2.7	2.7	1.9	2.5	4055	118	495265	10836	191	13	1.56	0.34
20TN20_14	27.0	14.3	17.1	8.7	4226	89	490500	9923	241	28	1.42	0.34
20TN20_15	33.6	4.0	19.6	4.4	7476	138	484740	9560	704	11	1.54	0.31

Sample and Spot Number	La (ppm)	±2σ	Ce (ppm)	±2σ	Pr (ppm)	±2σ	Nd (ppm)	±2σ	Sm (ppm)	±2σ	Eu (ppm)	±2σ	Gd (ppm)	±2σ
20TN17A-2_75	21.41	1.95	303	8	26.13	1.26	105	4	96.45	2.60	53.36	1.47	483.7	8.8
20TN17A-2_76	136	3	312	9	25.29	0.70	77.80	3.34	74.42	5.16	41.80	2.24	394.9	11.5
20TN17A-2_83	245	4	154	5	11.40	0.41	24.17	1.90	38.57	2.03	20.45	1.38	221.8	8.5
20TN17A-2_85	181	3	364	8	32.05	0.96	93.46	3.28	72.75	2.47	34.06	1.14	346.5	7.9
20TN17A-2_86	441	7	733	15	51.58	1.10	125	4	62.17	2.05	23.54	0.77	268.2	5.5
20TN17A-2_88	593	19	1551	41	77.31	1.91	177	4	73.20	2.33	25.25	0.74	284.1	5.4
20TN17A-2_89_1	387	8	746	15	54.68	1.51	143	4	70.56	2.45	28.44	0.83	303.9	5.9
20TN17A-2_89_2	378	12	723	21	48.89	1.25	124	4	60.46	2.47	23.56	0.93	275.9	4.6
20TN17A-2_89_3	378	9	676	18	49.18	1.50	125	2	64.93	2.13	24.07	0.77	279.1	7.0
20TN17A-2_89_4	543	12	884	19	60.73	1.12	141	3	67.42	2.68	25.40	0.73	289.6	7.2
20TN17A-2_89_5	789	23	1301	39	79.63	2.50	166	5	71.15	2.60	29.18	1.00	299.9	8.7
20TN17A-2_90_1	642	22	918	30	73.94	2.35	167	4	76.60	1.87	30.83	0.99	263.6	7.4
20TN17A-2_90_2	496	16	700	20	54.32	1.46	132	4	64.71	2.71	26.89	1.00	287.0	8.0
20TN17A-2_90_3	256	5	354	7	31.06	0.89	81.94	3.58	48.54	2.32	19.18	0.75	236.9	6.9
20TN17A-2_90_4	420	14	713	27	48.85	1.62	117	5	55.43	2.80	19.52	0.80	248.7	4.7
20TN17A-2_90_5	672	10	1083	29	65.65	1.18	139	3	62.50	2.73	22.44	0.91	267.0	7.4
20TN17A-2_92_1	639	6	1086	15	71.20	1.32	168	5	69.47	3.70	22.58	1.07	262.5	6.0
20TN17A-2_92_2	267	4	475	7	39.58	1.05	114	4	56.47	1.89	20.77	0.62	249.6	5.5
20TN17A-2_92_3	294	4	408	7	36.27	0.71	95.36	3.19	52.77	2.09	21.71	0.64	236.7	5.3
20TN17A-2_92_4	311	4	543	7	49.00	0.96	134	3	76.62	3.02	33.49	0.95	311.8	9.5
20TN17A-2_92_5	433	6	824	18	65.46	1.20	169	4	90.61	2.59	39.12	1.53	334.7	8.6
20TN17A-2_92_6	998	23	1440	47	90.36	1.76	184	7	70.55	3.28	29.51	1.39	267.1	7.1
20TN17A-2_96_3	326	6	416	10	37.67	1.08	104	3	45.08	2.55	14.91	0.92	179.3	5.8
20TN17A-2_96_4	303	6	381	7	33.71	0.85	90.56	2.95	47.12	3.04	17.23	0.91	212.6	6.9
20TN17A-2_96_5	230	3	253	7	25.81	0.63	70.30	3.17	46.16	1.88	18.55	0.74	247.5	5.4
20TN17A-2_97_1	376	9	408	10	31.84	1.15	72.76	4.51	42.42	4.34	16.49	1.06	178.1	6.3
20TN17A-2_97_2	305	4	306	9	26.89	1.09	61.56	3.67	31.87	2.75	10.80	0.90	137.4	5.8
20TN17A-2_97_3	297	6	289	7	28.24	0.97	64.22	3.28	30.94	2.75	11.96	1.23	141.5	5.3
20TN17A-2_97_4	206	3	262	6	24.24	0.68	66.82	2.85	36.10	1.58	16.30	0.76	217.4	5.9
20TN17A-2_97_5	254	8	455	17	31.96	1.28	85.48	4.10	47.16	2.84	21.51	0.94	250.6	8.5
20TN17A-2_98_2	725	18	841	23	55.15	2.07	110	4	36.35	2.91	12.46	0.73	153.6	4.1
20TN17A-2_98_4	286	25	385	58	35.44	3.75	95.04	13.09	38.32	5.40	13.60	1.80	161.1	4.3
20TN17A-2_98_6	420	9	501	14	42.29	1.65	112	6	46.79	2.37	15.89	0.83	184.7	6.6
20TN17A-2_98_7	298	13	353	14	33.03	1.18	84.28	4.96	32.02	2.09	11.45	0.89	133.3	5.1
20TN17A-2_99_2	423	6	527	10	42.77	1.04	99.78	4.39	36.99	2.39	12.97	0.58	176.2	4.4
20TN17A-2_99_3	575	15	617	23	45.97	1.18	92.89	2.80	31.47	2.34	10.30	0.75	150.9	6.7
20TN17A-2_99_5	322	17	426	19	36.66	1.39	97.06	3.23	43.67	2.26	17.70	0.64	192.0	5.2
20TN20_5	1.25	0.09	632	42	8.16	0.79	124	8	166	11	57.53	3.64	288.2	14.6
20TN20_11	0.24	0.05	278	27	2.47	0.48	32.16	5.46	49.17	4.21	25.50	1.38	207.6	8.0
20TN20_14	90.16	31.89	241	14	16.70	4.23	92.76	12.15	107	5	53.66	2.27	340.8	13.8
20TN20_15	21.08	0.47	3495	59	122	3	1292	26	964	18	287.4	6.3	1212	22

Sample and Spot Number	Tb (ppm)	±2σ	Dy (ppm)	±2σ	Ho (ppm)	±2σ	Er (ppm)	±2σ	Tm (ppm)	±2σ	Yb (ppm)	±2σ	Lu (ppm)	±2σ
20TN17A-2_75	198.3	3.4	2148	27	650.2	8.9	2559	46	422.9	6.4	2972	42	389	6
20TN17A-2_76	171.3	1.9	1881	49	558.0	16.4	2248	69	378.5	9.4	2714	85	348	12
20TN17A-2_83	93.23	3.36	1004	30	303.3	8.3	1167	35	211.1	5.4	1505	33	188	5
20TN17A-2_85	136.3	2.7	1416	23	429.9	5.5	1687	23	307.2	4.4	2182	35	283	4
20TN17A-2_86	103.2	1.8	1032	13	297.8	5.1	1131	20	204.1	3.5	1414	23	181	3
20TN17A-2_88	105.5	1.8	1003	15	281.1	3.5	1063	17	189.0	2.7	1311	21	167	2
20TN17A-2_89_1	114.5	2.4	1138	21	327.9	5.3	1265	17	226.1	3.5	1581	19	200	3
20TN17A-2_89_2	104.9	2.2	1067	16	308.9	4.8	1193	15	213.9	3.5	1504	27	191	3
20TN17A-2_89_3	107.7	2.4	1070	16	312.0	3.4	1193	17	213.8	4.2	1476	24	188	3
20TN17A-2_89_4	110.4	1.8	1096	17	314.1	4.9	1204	17	214.8	4.2	1486	24	192	4
20TN17A-2_89_5	111.0	1.9	1088	16	310.6	6.0	1195	21	215.5	4.2	1489	26	192	3
20TN17A-2_90_1	93.63	1.66	849.4	15.0	226.1	4.7	813.7	13.9	139.0	2.6	963	24	128	3
20TN17A-2_90_2	111.1	3.1	1096	21	307.4	5.6	1124	21	198.5	3.5	1406	19	190	4
20TN17A-2_90_3	97.27	1.88	993.1	16.7	303.0	5.3	1194	19	216.9	3.1	1548	26	198	4
20TN17A-2_90_4	99.19	1.73	1013	15	300.1	4.7	1158	20	208.2	3.9	1450	26	189	3
20TN17A-2_90_5	99.46	1.96	979.1	18.4	284.0	5.7	1067	20	186.8	4.5	1311	20	168	4
20TN17A-2_92_1	103.2	2.1	1015	17	295.7	5.9	1118	21	199.2	3.2	1378	22	174	3
20TN17A-2_92_2	97.98	2.03	1004	17	299.8	4.2	1175	21	211.6	3.1	1471	22	192	4
20TN17A-2_92_3	95.19	1.73	952.0	16.6	283.5	4.0	1107	18	199.2	3.8	1411	23	184	3
20TN17A-2_92_4	113.7	2.3	1074	23	308.0	6.1	1167	19	201.9	3.9	1423	27	183	4
20TN17A-2_92_5	118.5	2.4	1099	20	303.6	5.8	1125	20	196.6	3.5	1358	28	174	4
20TN17A-2_92_6	96.39	2.32	908.0	19.6	252.2	6.2	931.3	23.8	163.5	3.6	1156	20	146	3
20TN17A-2_96_3	72.50	1.53	728.7	14.8	217.3	4.3	841.0	13.8	153.3	2.8	1114	25	136	3
20TN17A-2_96_4	84.28	1.56	874.8	15.0	263.9	6.4	1051	17	181.9	4.7	1317	23	162	4
20TN17A-2_96_5	101.8	1.7	1094	15	336.0	4.1	1338	25	233.0	3.0	1676	32	208	4
20TN17A-2_97_1	69.91	2.22	735.6	19.2	217.7	5.6	854.8	35.8	151.6	5.6	1083	41	131	4
20TN17A-2_97_2	55.35	2.11	562.4	10.4	165.4	6.4	632.8	19.6	113.3	2.7	798	8	97.33	3.96
20TN17A-2_97_3	60.60	2.21	635.6	23.2	189.3	7.9	746.9	21.0	129.1	4.5	927	33	115	4
20TN17A-2_97_4	96.24	1.98	1079	16	342.9	5.9	1379	21	241.8	4.1	1754	31	218	5
20TN17A-2_97_5	109.8	2.5	1156	24	362.1	7.4	1457	31	258.8	5.1	1905	37	237	5
20TN17A-2_98_2	68.87	2.72	732.9	19.9	212.4	5.1	788.5	28.4	136.0	5.5	932	28	110	5
20TN17A-2_98_4	69.61	3.26	747.2	26.8	222.6	4.7	829.9	16.0	135.1	3.9	949	29	110	2
20TN17A-2_98_6	78.61	2.35	847.3	24.3	248.8	8.0	925.4	25.6	151.7	3.4	1041	29	121	4
20TN17A-2_98_7	58.32	1.54	618.8	10.1	179.0	6.0	665.8	22.2	110.4	2.6	746	37	88.25	4.00
20TN17A-2_99_2	75.69	1.60	797.2	20.5	238.2	4.4	929.9	19.1	163.9	3.1	1158	27	143	3
20TN17A-2_99_3	65.29	1.73	695.3	15.6	197.6	5.3	745.5	26.1	126.8	4.5	849	31	101	3
20TN17A-2_99_5	79.17	1.41	847.5	12.4	256.9	4.2	1033	21	182.3	3.6	1349	25	170	4
20TN20_5	70.26	3.21	556.4	24.5	143.1	5.0	492.4	17.0	79.2	2.8	553	20	69.70	2.38
20TN20_11	50.96	2.04	424.1	13.3	108.1	3.1	366.4	9.6	57.4	1.7	401	12	52.09	1.53
20TN20_14	73.06	2.03	486.1	10.7	101.6	2.2	298.5	6.5	44.0	0.9	300	6	37.60	1.03
20TN20_15	195.5	3.3	1120	16	200.2	4.4	485.4	9.1	57.5	1.5	338	8	39.42	1.20

Sample and Spot Number	Hf (ppm)	±2σ	Ta (ppm)	±2σ	Pb (ppm)	±2σ	Hf (wt. %)	U (ppm)	Th (ppm)	Pb (ppm)
20TN17A-2_75	7867	196	121	3	142	3	0.79	1208	373	333
20TN17A-2_76	8601	202	158	5	96.68	3.50	0.86	757	227	224
20TN17A-2_83	6569	111	125	3	66.93	2.42	0.66	370	31.3	45.3
20TN17A-2_85	8963	113	249	4	90.23	1.50	0.90	807	84.8	70.6
20TN17A-2_86	8782	184	187	3	80.47	1.50	0.88	729	140	86.9
20TN17A-2_88	8905	115	153	3	79.29	1.47	0.89	723	78.1	75.5
20TN17A-2_89_1	9332	146	180	3	78.60	0.95	0.93	778	81.0	62.1
20TN17A-2_89_2	9132	139	196	3	76.29	1.44	0.91	712	73.3	56.8
20TN17A-2_89_3	9072	157	187	3	78.46	2.16	0.91	644	69.1	54.5
20TN17A-2_89_4	9591	145	160	3	78.04	1.34	0.96	713	72.1	54.0
20TN17A-2_89_5	9674	203	148	3	84.23	2.29	0.97	717	142	97.7
20TN17A-2_90_1	9084	139	203	5	95.17	2.06	0.91	842	300	170
20TN17A-2_90_2	9296	192	215	5	95.47	2.71	0.93	699	499	270
20TN17A-2_90_3	8658	142	267	4	74.73	1.55	0.87	750	129	116
20TN17A-2_90_4	8482	141	209	6	78.76	1.46	0.85	683	85.5	66.3
20TN17A-2_90_5	9497	155	155	3	83.06	2.80	0.95	754	141	78.4
20TN17A-2_92_1	7917	211	147	2	80.71	1.69	0.79	684	132	71.2
20TN17A-2_92_2	7395	199	234	4	79.77	1.52	0.74	582	77.0	47.5
20TN17A-2_92_3	9080	154	264	4	79.17	1.59	0.91	680	80.4	60.3
20TN17A-2_92_4	8653	192	229	4	94.79	1.18	0.87	668	74.1	56.4
20TN17A-2_92_5	9155	143	182	4	89.27	1.38	0.92	785	67.7	45.4
20TN17A-2_92_6	10009	219	143	4	84.94	2.32	1.00	715	89.7	54.1
20TN17A-2_96_3	12511	310	171	5	60.35	2.24	1.25	517	51.2	38.9
20TN17A-2_96_4	9738	159	217	5	71.05	2.47	0.97	570	59.1	42.0
20TN17A-2_96_5	9192	146	243	4	72.31	1.42	0.92	509	49.0	39.8
20TN17A-2_97_1	9011	345	106	5	69.27	3.69	0.90	425	123	89.3
20TN17A-2_97_2	8724	235	108	3	61.88	2.79	0.87	257	114	90.6
20TN17A-2_97_3	8424	325	143	4	56.37	2.22	0.84	523	48.0	45.6
20TN17A-2_97_4	7962	158	203	4	66.87	2.35	0.80	477	48.6	39.5
20TN17A-2_97_5	8512	213	207	6	76.40	2.19	0.85	430	55.3	36.0
20TN17A-2_98_2	7757	219	126	5	81.27	2.98	0.78	441	166	96.4
20TN17A-2_98_4	8338	262	139	47	67.67	4.07	0.83	507	125	82.5
20TN17A-2_98_6	7188	156	85.29	2.42	73.00	2.54	0.72	378	52.5	32.9
20TN17A-2_98_7	7651	188	98.37	3.07	65.07	1.60	0.77	303	58.9	46.9
20TN17A-2_99_2	7085	329	181	4	83.58	2.08	0.71	423	86.2	52.5
20TN17A-2_99_3	8921	172	128	3	77.20	7.86	0.89	380	81.4	50.6
20TN17A-2_99_5	7479	243	228	7	81.22	2.50	0.75	448	78.6	34.6
20TN20_5	8286	145	6.44	0.31	13.85	0.38	0.83	89.9	151	94.3
20TN20_11	6101	119	7.19	0.48	31.07	0.73	0.61	109	310	246
20TN20_14	6944	160	4.42	0.42	57.54	9.82	0.69	165	162	169
20TN20_15	4953	92	3.13	0.17	101	3	0.50	631	221	202

Sample and Spot Number	Note	Li (ppm)	±2σ	Si (ppm)	±2σ	P (ppm)	±2σ	Ca (ppm)	±2σ	Sc (ppm)	±2σ	Ti (ppm)	±2σ
20TN20_18	June	1.69	0.57	166792	3976	166	22	301	113	468	11	114	8
20TN20_19	June	2.36	0.75	167341	4934	190	29	149	115	464	9	52.26	11.26
20TN20_20	June	1.44	0.61	165199	4073	274	29	18	94	462	11	35.00	2.68
20TN20_21	June	4.84	0.70	163676	2916	42	32	6	77	466	13	3.03	1.41
20TN20_23	June	0.52	0.51	165556	3930	147	43	85	94	463	9	2.75	1.12
20TN20_24	June	0.46	0.55	167210	3480	222	29	b.d.l.		465	8	1.36	1.14
20TN20_25	June	16.96	1.32	168544	4195	44	33	36	116	465	14	8.85	2.45
20TN20_26	June	30.49	1.48	167915	3835	39	28	46	96	455	11	18.64	7.94
20TN20_4	July	3.71	0.50	152188	3192	40	15	441	215	381	8	193	58
20TN20_9	July	3.11	0.57	150577	2846	46	10	27	62	376	8	1.17	0.72
20TN20_19	July	0.25	0.36	154697	3511	215	19	17	63	374	8	1.56	0.92
20TN20_21	July	0.71	0.36	165054	4128	178	19	177	156	377	8	105	37
20TN20_24	July	32.18	1.80	152035	3302	51	13	b.d.l.		374	7	30.89	3.32
20TN20_25	July	0.85	0.31	154876	3288	86	15	b.d.l.		382	10	0.58	0.62
20TN20_26	July	34.09	1.79	153237	3772	29	12	24	53	375	7	0.23	0.63
20TN20_27	July	39.90	3.03	153172	3326	42	11	21	58	382	11	0.40	0.51
20TN20_28	July	54.54	2.90	151051	2736	29	12	b.d.l.		380	8	2.29	0.68
20TN20_29	July	22.26	2.03	158975	4962	60	11	44	63	393	10	26.38	5.09
20TN20_30	July	16.05	1.17	160622	4744	91	13	172	104	384	10	108	19
20TN20_31	July	24.06	4.17	156657	3414	72	14	106	58	385	7	94.99	7.31
20TN20_33	July	3.58	0.56	151308	4069	63	15	103	80	380	9	51.83	3.77
20TN55A_9_9	March	5.70	0.61	141871	2310	1	16	5	59	438	7	0.89	0.99
20TN55A_11	March	8.17	0.72	143286	2375	b.d.l.		b.d.l.		443	7	10.30	9.82
20TN55A_14	March	5.14	1.19	139010	3696	b.d.l.		b.d.l.		434	9	1.27	0.93
20TN55A_16_1	March	6.36	0.79	143647	2570	26	24	90	72	433	9	2.70	1.04
20TN55A_16_2	March	3.43	0.66	139062	2244	14	22	b.d.l.		432	9	1.29	0.93
20TN55A_16_7	March	2.24	0.22	139240	3174	1	21	b.d.l.		433	10	6.01	2.40
20TN55A_21_1	March	2.93	0.41	151234	3578	25	22	23	83	439	10	2.12	1.62
20TN55A_23_3	March	24.39	1.19	149336	3584	35	23	57	50	433	10	2.79	0.91
20TN55A_23_4	March	14.26	1.44	149248	2512	36	29	110	68	435	7	1.77	1.08
20TN55A_23_5	March	5.74	0.57	152281	3109	25	29	705	357	433	6	3.03	1.06
20TN55A_23_6	March	5.10	0.51	147322	2710	28	28	b.d.l.		438	7	1.60	1.21
20TN55A_23_7	March	2.89	0.40	146961	2493	b.d.l.		b.d.l.		435	7	0.70	0.90
20TN55A_23_8	March	2.09	0.32	145213	2751	34	23	b.d.l.		430	10	b.d.l.	
20TN55A_23_10	March	8.28	1.57	144524	2824	50	25	b.d.l.		426	8	1.15	0.89
20TN55A_23_12	March	1.76	0.45	144269	2540	b.d.l.		54	64	427	6	0.71	0.73
20TN55A_23_13	March	0.78	0.30	146131	2867	59	36	b.d.l.		434	12	0.16	1.22
20TN55A_23_14	March	0.50	0.20	145548	2634	17	23	b.d.l.		432	7	1.50	1.07
20TN55A_23_18	March	6.35	0.56	145372	2942	36	25	25	70	429	7	1.37	0.96
20TN55A_23_19	March	11.63	0.93	143534	2594	58	20	129	84	421	4	1.78	1.13
20TN55A_23_20	March	6.79	0.71	143784	2169	30	29	b.d.l.		424	7	1.35	0.87

Sample and Spot Number	^{56}Fe (ppm)	±2σ	^{57}Fe (ppm)	±2σ	Y (ppm)	±2σ	Zr (ppm)	±2σ	Nb (ppm)	±2σ	Mo (ppm)	±2σ
20TN20_18	73.1	6.4	32.6	5.3	17115	279	489508	8558	1659	58	1.04	0.30
20TN20_19	1207	892	427	304	14755	352	491943	12174	1888	334	1.13	0.29
20TN20_20	6.4	3.2	4.3	2.9	15643	221	487444	9386	1863	31	1.25	0.29
20TN20_21	25.5	13.8	16.0	9.2	2848	179	493919	6679	117	6	1.15	0.32
20TN20_23	b.d.l.		0.0	2.6	9867	184	486152	10388	388	14	1.50	0.32
20TN20_24	1.7	3.6	b.d.l.		11304	190	493173	10695	33.1	0.8	1.11	0.33
20TN20_25	b.d.l.		1.4	3.3	3409	66	491935	9722	421	24	1.38	0.33
20TN20_26	7.4	3.9	1.5	3.0	2834	95	491279	10501	699	28	1.26	0.31
20TN20_4	0.2	2.3	3.8	2.2	4838	87	495035	8228	1977	543	0.64	0.26
20TN20_9	1.8	2.6	1.3	2.5	3022	67	490498	6188	57.4	4.8	0.60	0.17
20TN20_19	b.d.l.		1.3	2.3	14060	203	492894	7712	88.8	9.3	0.58	0.20
20TN20_21	77.8	10.8	51.7	8.2	12292	278	495183	8264	2199	329	0.63	0.18
20TN20_24	9.8	2.9	12.8	3.7	2129	53	493558	6921	379	15	0.49	0.18
20TN20_25	2.7	3.7	2.2	3.2	9803	154	496024	6001	36.68	1.24	0.40	0.20
20TN20_26	1.8	2.4	0.2	2.1	4740	91	497253	6975	68.59	2.70	0.23	0.11
20TN20_27	2.9	2.8	0.4	2.4	4256	120	496248	9430	63.05	1.93	0.62	0.20
20TN20_28	5.6	2.7	4.7	2.5	3066	156	490581	6853	183	8	0.72	0.20
20TN20_29	14.5	3.4	18.7	4.6	3204	77	498481	11650	551	47	0.68	0.20
20TN20_30	556	178	432	138	3857	61	485457	9767	1253	184	0.84	0.23
20TN20_31	49.1	4.2	37.3	7.9	3955	445	488403	7156	1233	47	0.42	0.15
20TN20_33	24.5	2.8	18.7	3.8	1242	47	485819	9270	448	13	0.45	0.19
20TN55A_9_9	b.d.l.		b.d.l.		1154	20	491003	8606	5.79	0.32	0.94	0.21
20TN55A_11	7.9	4.6	4.3	3.8	2171	25	493460	6584	8.18	0.29	0.80	0.24
20TN55A_14	b.d.l.		2.1	3.9	294	56	488765	7744	1.86	0.43	0.94	0.34
20TN55A_16_1	20.2	5.9	11.6	5.3	374	12	490406	5739	8.21	0.49	0.89	0.33
20TN55A_16_2	21.1	4.6	11.8	4.4	184	11	490936	7107	5.43	0.67	0.93	0.29
20TN55A_16_7	366	163	162	69	130	2	496791	6981	10.12	1.71	6.46	2.65
20TN55A_21_1	39.0	14.2	29.5	7.1	335	77	541272	5777	11.79	3.13	1.03	0.33
20TN55A_23_3	12.1	4.8	6.4	3.9	2113	38	544305	7849	22.54	0.92	0.71	0.29
20TN55A_23_4	0.3	3.4	b.d.l.		2109	49	544415	8575	13.73	0.86	0.83	0.23
20TN55A_23_5	329	33	180	16	1469	20	542801	6356	14.27	0.47	2.45	0.60
20TN55A_23_6	13.6	3.8	6.0	3.4	705	12	547121	8104	4.64	0.25	0.95	0.27
20TN55A_23_7	23.0	4.8	10.0	4.7	376	16	545947	7437	4.33	0.22	0.84	0.27
20TN55A_23_8	13.3	4.4	8.1	3.4	437	14	537153	7314	2.99	0.26	0.68	0.21
20TN55A_23_10	4.5	3.7	0.5	3.0	1667	85	538878	8177	6.30	0.46	0.72	0.22
20TN55A_23_12	1.1	3.2	b.d.l.		1066	24	544314	7140	2.45	0.14	0.99	0.32
20TN55A_23_13	b.d.l.		1.3	3.8	1406	37	545051	8503	2.49	0.22	0.75	0.24
20TN55A_23_14	25.9	3.4	10.4	4.4	371	74	548693	9438	1.39	0.28	0.73	0.28
20TN55A_23_18	b.d.l.		0.5	3.0	529	24	545864	6464	3.13	0.30	0.72	0.27
20TN55A_23_19	132	26	71.4	16.9	1271	31	537747	7359	15.21	0.57	0.71	0.26
20TN55A_23_20	b.d.l.		b.d.l.		773	108	544157	7971	5.23	0.37	0.64	0.22

Sample and Spot Number	La (ppm)	±2σ	Ce (ppm)	±2σ	Pr (ppm)	±2σ	Nd (ppm)	±2σ	Sm (ppm)	±2σ	Eu (ppm)	±2σ	Gd (ppm)	±2σ
20TN20_18	91.44	8.30	895	23	43.44	2.14	440	16	775	26	388.3	8.9	2434.6	50.6
20TN20_19	13.53	1.20	1778	47	116	3	1520	42	2260	41	757.5	18.7	3152.4	66.7
20TN20_20	8.14	0.50	1174	46	46.87	2.85	620	33	1144	55	512.0	18.0	2861.2	68.3
20TN20_21	1.51	0.16	755	48	17.32	1.32	249	19	198	14	52.99	3.39	229.1	14.5
20TN20_23	0.07	0.02	567	13	1.58	0.11	31.48	1.84	94.62	2.87	58.62	1.87	516.9	12.9
20TN20_24	0.01	0.01	221	3	0.56	0.09	12.64	1.01	51.80	1.94	39.18	0.80	388.7	10.1
20TN20_25	7.94	1.19	2814	128	64.70	6.37	723	54	407	17	96.51	3.25	383.8	13.4
20TN20_26	9.76	0.66	3376	67	80.53	2.54	833	25	405	13	93.19	3.38	353.0	10.6
20TN20_4	53.63	15.31	3027	89	72.33	4.04	719	24	443	12	117.4	2.8	506.3	13.4
20TN20_9	0.28	0.09	162	21	2.53	0.56	46.50	9.54	65.39	9.04	21.69	2.45	115.9	9.6
20TN20_19	0.09	0.03	351	16	1.33	0.14	24.60	1.52	78.35	3.47	53.33	2.13	514.2	14.9
20TN20_21	25.76	0.80	2364	67	196	6	2237	73	2158	67	626.6	15.0	2438.5	54.9
20TN20_24	69.29	2.02	2911	98	216	6	1480	55	425	16	84.12	3.25	276.7	11.4
20TN20_25	0.44	0.23	166	3	0.61	0.06	11.63	0.88	52.06	2.03	39.63	1.05	395.8	6.5
20TN20_26	0.31	0.07	565	12	8.40	0.53	195	7	514	9	180.6	2.5	749.1	11.4
20TN20_27	0.58	0.14	521	14	8.02	0.35	190	7	484	12	169.6	3.9	700.9	15.4
20TN20_28	4.29	0.32	909	68	42.14	3.28	590	45	721	33	193.6	4.0	696.7	25.3
20TN20_29	23.76	1.51	2160	68	119	3	951	28	243	9	55.01	2.86	215.4	10.5
20TN20_30	48.91	4.07	2465	92	137	9	970	47	245	7	56.05	2.09	216.4	7.8
20TN20_31	47.66	2.72	2482	255	156	21	1011	145	198	24	44.04	3.61	170.9	8.6
20TN20_33	171	4	2599	66	230	5	808	17	81.35	2.98	13.70	0.58	51.5	1.8
20TN55A_9_9	0.04	0.02	7.27	0.39	0.10	0.02	1.79	0.35	3.41	0.42	2.57	0.24	21.2	1.3
20TN55A_11	0.07	0.02	12.52	0.50	0.48	0.07	5.73	0.76	10.24	0.95	6.75	0.34	49.4	1.8
20TN55A_14	0.05	0.02	5.92	1.45	0.10	0.04	1.57	0.56	2.57	0.72	1.44	0.45	11.7	3.2
20TN55A_16_1	2.65	0.48	7.38	0.75	0.62	0.12	3.17	0.40	2.66	0.52	1.69	0.25	11.9	1.2
20TN55A_16_2	0.24	0.06	5.13	0.57	0.28	0.07	2.05	0.43	1.59	0.35	0.75	0.13	5.9	1.0
20TN55A_16_7	1.23	0.52	6.20	0.74	0.24	0.11	1.00	0.49	0.78	0.30	0.45	0.10	3.4	0.5
20TN55A_21_1	0.43	0.18	5.94	0.90	0.28	0.11	1.58	0.53	1.25	0.42	0.75	0.18	5.7	1.2
20TN55A_23_3	0.26	0.09	31.32	1.03	0.74	0.09	11.31	0.91	17.30	1.32	8.73	0.32	74.3	2.4
20TN55A_23_4	0.05	0.02	24.66	1.46	0.44	0.07	7.08	0.60	14.31	1.17	8.27	0.58	72.0	2.8
20TN55A_23_5	8.00	4.09	28.24	7.75	1.18	0.54	7.06	1.77	9.23	0.86	5.19	0.36	46.7	2.5
20TN55A_23_6	0.04	0.02	9.44	0.34	0.09	0.03	1.12	0.28	2.86	0.40	1.80	0.25	16.9	1.1
20TN55A_23_7	0.10	0.03	4.55	0.34	0.08	0.03	0.75	0.20	1.27	0.26	0.62	0.12	8.3	0.8
20TN55A_23_8	0.02	0.01	4.37	0.23	0.03	0.02	0.56	0.16	1.42	0.35	1.09	0.19	10.2	1.0
20TN55A_23_10	0.05	0.03	18.42	1.25	0.33	0.06	5.22	0.87	10.15	1.33	6.19	0.65	55.3	4.4
20TN55A_23_12	0.00	0.01	10.69	0.46	0.07	0.02	1.60	0.42	5.24	0.80	3.15	0.24	32.3	1.5
20TN55A_23_13	0.02	0.02	12.54	0.64	0.11	0.04	2.33	0.51	6.02	0.68	4.90	0.40	46.3	2.8
20TN55A_23_14	0.03	0.02	3.55	0.98	0.02	0.01	0.61	0.26	1.48	0.50	0.95	0.32	10.6	2.7
20TN55A_23_18	b.d.l.		7.46	0.50	0.04	0.02	0.70	0.24	2.05	0.46	1.50	0.22	15.9	1.2
20TN55A_23_19	0.99	0.11	16.58	0.64	0.28	0.04	3.47	0.47	7.80	0.68	4.10	0.28	39.4	1.9
20TN55A_23_20	b.d.l.		8.39	0.97	0.07	0.03	1.68	0.45	4.62	0.77	2.64	0.41	25.8	3.6

Sample and Spot Number	Tb (ppm)	±2σ	Dy (ppm)	±2σ	Ho (ppm)	±2σ	Er (ppm)	±2σ	Tm (ppm)	±2σ	Yb (ppm)	±2σ	Lu (ppm)	±2σ
20TN20_18	444.4	9.5	2579	61	447.2	9.7	1089	21	133.5	4.2	801	22	92.94	2.19
20TN20_19	448.5	8.5	2304	58	385.6	9.0	934.7	25.8	117.9	3.0	735	15	86.67	2.28
20TN20_20	458.2	9.9	2432	49	401.2	6.4	911.1	18.7	109.2	2.4	647	11	74.90	1.81
20TN20_21	43.10	2.78	305.1	20.0	70.1	4.6	222.1	14.7	36.0	2.2	259	15	35.10	2.08
20TN20_23	143.8	3.0	1119	25	256.2	5.4	800.2	20.0	123.4	2.6	904	22	121	3
20TN20_24	133.1	2.7	1192	28	302.5	6.2	1017	24	170.9	3.0	1287	26	183	4
20TN20_25	64.13	1.76	399.8	9.6	81.5	1.8	240.6	4.9	36.5	0.9	256	6	31.58	0.82
20TN20_26	56.30	1.85	341.7	11.6	69.4	2.5	200.6	8.4	29.8	1.0	208	8	26.85	1.15
20TN20_4	90.64	2.08	624.9	13.8	135.8	3.3	434.6	8.3	72.3	1.3	506	9	61.86	1.30
20TN20_9	30.18	1.67	288.3	9.8	82.0	2.2	307.6	5.4	51.6	1.0	370	8	47.13	0.88
20TN20_19	168.2	3.7	1484	25	339.1	5.7	1056	16	166.7	3.1	1248	28	163	4
20TN20_21	313.7	6.1	1579	37	278.0	7.6	739.1	18.8	103.9	2.9	673	20	76.51	1.71
20TN20_24	39.63	1.46	223.8	6.7	42.5	0.9	126.9	3.2	20.9	0.5	166	4	22.85	0.47
20TN20_25	121.2	3.1	1077	23	242.0	4.8	696.8	14.3	102.9	2.2	680	18	80.24	1.38
20TN20_26	114.1	1.8	593.1	13.0	96.3	2.0	244.5	4.6	34.3	0.8	230	5	25.87	0.73
20TN20_27	101.6	2.4	534.6	16.1	87.3	2.8	226.6	5.5	34.4	0.8	237	6	27.80	0.80
20TN20_28	87.38	4.09	427.5	19.9	67.7	3.1	165.8	9.3	22.8	1.2	148	6	17.66	1.06
20TN20_29	41.82	2.09	334.8	13.4	86.3	2.4	308.2	7.0	50.5	1.2	361	10	42.55	1.29
20TN20_30	43.68	1.61	382.2	11.0	102.7	2.5	383.1	9.4	65.2	1.7	457	11	52.94	1.40
20TN20_31	37.78	2.16	375.9	37.1	110.0	12.4	397.9	46.5	61.5	6.8	381	39	41.04	4.47
20TN20_33	10.46	0.38	98.7	2.9	28.1	1.0	111.7	4.3	20.0	1.0	156	10	19.48	0.71
20TN55A_9_9	9.05	0.31	115.6	3.3	47.3	1.2	235.2	6.3	48.3	1.3	446	11	74.47	1.81
20TN55A_11	18.84	0.46	229.7	4.8	88.1	1.6	412.4	9.6	81.8	1.7	708	14	115	3
20TN55A_14	3.65	0.89	39.0	8.0	14.1	2.6	64.0	10.6	12.4	1.7	115	13	20.41	2.08
20TN55A_16_1	4.25	0.28	46.5	1.4	17.0	0.6	76.5	2.4	13.8	0.6	115	5	18.73	0.85
20TN55A_16_2	1.96	0.21	21.1	1.8	7.9	0.7	34.4	1.3	6.2	0.4	53	3	8.70	0.45
20TN55A_16_7	1.39	0.13	16.1	1.1	5.6	0.3	28.0	1.4	4.8	0.3	46	2	7.78	0.44
20TN55A_21_1	2.43	0.42	31.4	6.2	12.0	2.4	60.2	13.1	12.8	2.9	110	25	18.28	3.92
20TN55A_23_3	25.24	0.65	289.1	8.0	95.3	1.8	419.9	9.4	87.3	2.3	738	18	123	3
20TN55A_23_4	24.92	0.87	294.1	6.7	96.2	2.5	417.2	8.4	85.9	1.9	716	16	117	3
20TN55A_23_5	16.10	0.55	200.8	4.8	67.0	1.0	299.9	5.1	62.3	1.2	543	10	92.49	1.66
20TN55A_23_6	6.64	0.25	90.9	2.7	34.2	0.7	163.1	3.0	35.0	1.1	327	7	57.31	1.54
20TN55A_23_7	3.32	0.23	45.4	2.7	17.6	0.9	86.4	4.4	20.1	1.0	191	10	35.06	1.44
20TN55A_23_8	3.86	0.19	52.8	2.1	21.0	0.9	103.5	3.6	23.4	0.9	220	9	39.43	1.30
20TN55A_23_10	18.90	1.47	223.0	14.2	74.8	3.9	319.4	14.7	63.2	2.8	524	18	84.71	3.03
20TN55A_23_12	11.96	0.37	149.0	2.9	51.1	0.8	221.0	3.7	42.4	0.7	342	6	55.53	1.39
20TN55A_23_13	16.21	0.64	194.2	5.7	63.7	2.3	269.9	10.1	51.7	1.4	418	12	68.46	3.04
20TN55A_23_14	4.07	0.96	49.5	11.6	17.8	3.7	79.7	16.1	16.6	2.9	134	21	22.69	3.45
20TN55A_23_18	6.06	0.37	73.1	3.9	25.6	1.3	110.5	5.7	21.4	1.2	169	7	27.92	1.38
20TN55A_23_19	14.52	0.70	169.0	5.2	56.2	1.7	231.2	6.6	43.2	1.2	338	8	52.67	1.37
20TN55A_23_20	8.87	1.23	105.7	15.1	36.3	5.0	150.0	19.0	29.5	3.6	237	28	38.40	4.45

Sample and Spot Number	Hf (ppm)	±2σ	Ta (ppm)	±2σ	Pb (ppm)	±2σ	Hf (wt. %)	U (ppm)	Th (ppm)	Pb (ppm)
20TN20_18	3971	75	8.17	0.32	65.85	1.53	0.40	453	243	237
20TN20_19	5376	99	20.21	2.93	74.53	4.66	0.54	579	405	448
20TN20_20	4285	148	12.70	0.65	89.21	2.66	0.43	707	590	549
20TN20_21	8458	207	2.51	0.26	20.06	1.61	0.85	179	76.2	81.7
20TN20_23	11785	252	12.05	0.52	16.93	0.45	1.18	50.9	511	484
20TN20_24	12472	216	1.85	0.15	3.85	0.16	1.25	24.8	50.3	50.0
20TN20_25	7952	218	6.29	0.34	38.44	1.82	0.80	347	132	134
20TN20_26	7629	187	10.09	0.65	42.41	1.34	0.76	382	147	146
20TN20_4	7198	137	51.06	15.08	49.93	3.30	0.72	20.1	277	955
20TN20_9	6469	109	3.36	0.29	12.00	0.35	0.65	73.6	194	189
20TN20_19	12144	247	2.77	0.24	21.86	2.44	1.21	87.7	1046	96.1
20TN20_21	10695	175	74.26	11.22	34.13	1.78	1.07	25.1	765	1705
20TN20_24	7362	126	3.75	0.20	52.68	1.05	0.74	177	224	155
20TN20_25	5753	181	1.05	0.10	11.74	0.36	0.58	20.0	65.6	1324
20TN20_26	8232	145	4.77	0.43	88.56	1.90	0.82	156	616	167
20TN20_27	7839	147	3.05	0.19	89.06	1.95	0.78	101	484	503
20TN20_28	5937	117	2.61	0.16	98.42	2.03	0.59	33.11	877	361
20TN20_29	8586	179	20.85	0.66	35.90	1.88	0.86	31.86	266	4748
20TN20_30	8257	162	79.49	27.25	311	120	0.83	199	298	354
20TN20_31	7970	154	32.32	2.40	33.37	2.35	0.80	208	346	701
20TN20_33	11219	182	8.49	0.43	10.60	0.43	1.12	246	90.9	3327
20TN55A_9_9	6887	164	0.36	0.06	18.39	0.47	0.69	5.00	578	540
20TN55A_11	8999	133	0.58	0.10	32.14	0.93	0.90	7.34	1292	1279
20TN55A_14	6472	266	0.10	0.04	9.54	2.46	0.65	5.15	907	748
20TN55A_16_1	6260	160	1.51	0.16	11.56	1.65	0.63	3.87	1077	938
20TN55A_16_2	5255	141	0.46	0.07	13.23	2.18	0.53	2.68	332	338
20TN55A_16_7	6840	179	0.57	0.10	15.76	1.20	0.68	3.44	487	438
20TN55A_21_1	7855	151	1.15	0.30	10.79	0.28	0.79	6.65	331	286
20TN55A_23_3	7621	133	2.18	0.18	86.17	3.11	0.76	29.03	2391	1976
20TN55A_23_4	7659	143	0.74	0.13	49.48	3.74	0.77	9.89	1401	1196
20TN55A_23_5	7329	210	2.04	0.11	24.40	0.58	0.73	6.33	474	467
20TN55A_23_6	7851	128	0.52	0.09	12.89	0.43	0.79	3.77	301	287
20TN55A_23_7	8249	116	0.73	0.10	6.13	0.44	0.82	2.59	126	124
20TN55A_23_8	7939	163	0.38	0.07	5.67	0.22	0.79	2.72	119	115
20TN55A_23_10	7116	143	0.50	0.12	31.69	2.98	0.71	6.17	573	563
20TN55A_23_12	7247	123	0.18	0.04	9.62	0.29	0.72	4.11	198	184
20TN55A_23_13	7276	142	0.22	0.07	10.67	0.50	0.73	6.51	201	193
20TN55A_23_14	6204	168	0.15	0.05	3.29	0.93	0.62	3.54	128	116
20TN55A_23_18	5978	149	0.15	0.04	12.28	0.84	0.60	5.10	233	215
20TN55A_23_19	6126	218	2.66	0.19	30.06	0.67	0.61	12.44	595	557
20TN55A_23_20	7467	141	0.39	0.06	20.18	1.40	0.75	12.13	494	455

Sample and Spot Number	Note	Li (ppm)	±2σ	Si (ppm)	±2σ	P (ppm)	±2σ	Ca (ppm)	±2σ	Sc (ppm)	±2σ	Ti (ppm)	±2σ
20TN55A_23_21	March	12.54	0.90	145425	3078	23	26	b.d.l.		432	10	0.62	1.02
20TN55A_23_22	March	8.98	0.83	143968	2678	32	17	37	70	430	9	1.01	1.11
20TN55A_23_23	March	1.44	0.25	142860	2681	16	26	65	50	427	9	0.61	0.76
20TN55A_23_24	March	3.02	1.09	142025	2336	66	25	24	63	435	8	b.d.l.	
20TN55A_23_25	March	0.54	0.19	147911	3445	73	39	24	57	431	8	41.51	17.34
20TN55A_24_1	March	5.64	0.45	143517	3108	63	27	b.d.l.		421	9	1.50	1.02
20TN55A_24_2	March	0.32	0.17	145213	3400	103	28	b.d.l.		429	11	b.d.l.	
20TN55A_24_3	March	0.54	0.18	140523	2299	1	24	46	51	419	7	0.90	0.92
20TN55A_24_4	March	4.41	0.49	145135	3496	29	26	b.d.l.		425	7	2.63	1.39
20TN55A_24_7	March	0.36	0.15	141527	2239	73	27	136	74	422	8	0.58	1.10
20TN55A_24_8	March	1.33	0.26	141708	2919	24	21	b.d.l.		419	8	0.11	0.73
20TN55A_25_3	March	14.60	1.02	142210	2073	31	25	21	61	423	7	1.59	1.15
20TN55A_25_6	March	12.36	1.01	142373	3254	20	30	62	87	416	7	2.75	1.08
20TN55A_25_7	March	16.59	0.98	142494	2428	36	21	17	79	418	8	2.19	0.84
20TN55A_25_8	March	10.55	0.72	141147	2607	31	23	39	73	418	9	2.06	0.91
20TN55A_25_16	March	19.94	1.37	142451	2369	b.d.l.		18	65	422	7	1.34	1.33
20TN55A_25_17	March	2.24	1.02	138938	2445	35	18	b.d.l.		416	7	b.d.l.	
20TN55A_25_19	March	0.85	0.18	140868	2208	38	26	23	77	421	9	1.38	0.94
20TN55A_27	March	3.39	0.49	140798	3373	23	24	48	80	417	8	1.31	0.88
20TN55A_28	March	0.94	0.21	140334	2742	16	13	1409	694	411	7	0.93	1.06
20TN55A_30	March	0.72	0.22	137253	2465	b.d.l.		b.d.l.		417	8	b.d.l.	
20TN55A_39	March	10.47	1.11	152864	2086	10	14	13	67	418	6	0.91	0.97
20TN55A_40	March	18.09	1.23	150161	2627	12	15	28	56	416	7	2.49	1.20
20TN55A_42	March	2.77	0.94	150913	2407	26	14	b.d.l.		413	6	1.59	1.01
20TN55A_43	March	2.84	0.37	152519	3147	35	13	54	69	415	8	0.003	1.221
20TN55A_44	March	13.73	1.76	149892	2410	9	11	49	50	415	9	1.31	1.03
20TN55A_46	March	9.64	0.74	149891	3471	11	17	84	63	416	8	0.85	1.08
20TN55A_47	March	0.44	0.26	152721	3455	12	17	34	70	415	10	0.12	0.79

Sample and Spot Number	^{56}Fe (ppm)	±2σ	^{57}Fe (ppm)	±2σ	Y (ppm)	±2σ	Zr (ppm)	±2σ	Nb (ppm)	±2σ	Mo (ppm)	±2σ
20TN55A_23_21	8.4	4.2	3.0	2.7	572	21	548486	7993	8.86	0.31	0.78	0.24
20TN55A_23_22	b.d.l.		1.4	2.3	1217	21	544540	8515	5.44	0.30	0.87	0.30
20TN55A_23_23	22.0	8.4	14.1	4.0	1663	45	543715	5078	6.41	0.32	0.58	0.18
20TN55A_23_24	48.2	13.0	25.8	6.6	959	158	549011	7875	3.42	0.54	0.85	0.33
20TN55A_23_25	711	308	387	170	2124	35	548102	10125	178	72	1.07	0.41
20TN55A_24_1	9.3	4.7	0.7	3.2	2073	25	542795	5949	11.72	1.12	0.96	0.27
20TN55A_24_2	76.1	30.2	46.8	18.7	2064	53	541844	7005	3.48	0.18	0.80	0.24
20TN55A_24_3	b.d.l.		2.5	2.0	906	21	541392	6731	1.83	0.18	0.70	0.21
20TN55A_24_4	2.4	3.4	2.9	3.0	1592	28	545005	10005	18.05	1.57	0.60	0.24
20TN55A_24_7	2.8	3.2	1.8	2.1	765	14	541138	6827	0.96	0.10	0.55	0.23
20TN55A_24_8	2.1	4.6	b.d.l.		1218	32	545254	7880	1.86	0.16	0.53	0.22
20TN55A_25_3	414	185	230	103	1316	55	545302	7482	15.49	0.81	0.74	0.27
20TN55A_25_6	363	26	190	19	1226	28	542417	6747	10.98	0.41	0.90	0.34
20TN55A_25_7	4.5	3.9	b.d.l.		1691	41	546032	6382	11.62	0.72	0.65	0.22
20TN55A_25_8	2.3	3.0	b.d.l.		990	30	539929	5862	4.59	0.22	0.39	0.18
20TN55A_25_16	1.9	4.4	0.8	3.5	1179	74	548042	8537	12.78	1.54	0.61	0.21
20TN55A_25_17	11.3	4.6	4.8	3.5	137	52	545275	5883	1.41	0.35	0.34	0.15
20TN55A_25_19	3.8	3.5	3.1	3.2	1500	25	546960	7578	2.80	0.23	0.76	0.25
20TN55A_27	16.2	3.9	5.4	3.5	2028	154	537169	6861	11.28	1.14	0.60	0.26
20TN55A_28	191	52	110	31	1056	76	538068	5122	3.90	0.51	0.63	0.22
20TN55A_30	b.d.l.		b.d.l.		1431	21	542595	7156	1.95	0.15	0.56	0.32
20TN55A_39	3.0	2.8	0.1	3.3	1465	37	509249	5675	6.65	0.38	0.73	0.20
20TN55A_40	6.6	2.9	5.6	3.4	1606	59	509611	5419	11.12	0.97	0.92	0.25
20TN55A_42	15.2	2.7	8.2	3.8	684	25	507023	5094	6.51	0.27	0.58	0.23
20TN55A_43	5.4	3.0	1.4	4.0	909	18	511759	6438	2.17	0.19	0.49	0.28
20TN55A_44	5.6	2.8	8.1	3.3	990	67	510101	5932	6.46	0.62	0.61	0.24
20TN55A_46	6.1	2.6	6.4	4.0	1068	43	508151	7398	5.86	0.37	0.44	0.18
20TN55A_47	1.2	3.0	b.d.l.		2099	36	510605	8899	4.41	0.23	0.81	0.31

Sample and Spot Number	La (ppm)	±2σ	Ce (ppm)	±2σ	Pr (ppm)	±2σ	Nd (ppm)	±2σ	Sm (ppm)	±2σ	Eu (ppm)	±2σ	Gd (ppm)	±2σ
20TN55A_23_21	0.05	0.04	9.56	0.38	0.13	0.04	1.78	0.25	4.08	0.64	2.31	0.28	20.6	1.5
20TN55A_23_22	0.00	0.00	13.74	0.55	0.07	0.02	1.67	0.33	4.65	0.50	3.22	0.24	34.8	1.9
20TN55A_23_23	0.23	0.05	7.77	0.40	0.15	0.04	2.36	0.33	5.48	0.65	3.95	0.34	34.9	1.6
20TN55A_23_24	0.02	0.01	1.72	0.22	0.02	0.01	0.52	0.23	1.62	0.57	1.50	0.38	16.1	2.9
20TN55A_23_25	30.90	13.31	47.94	17.62	4.26	1.86	16.79	6.15	8.48	1.42	5.43	0.58	44.7	2.9
20TN55A_24_1	0.51	0.11	6.80	0.32	0.23	0.06	3.06	0.46	6.91	0.61	4.44	0.27	44.0	2.1
20TN55A_24_2	0.01	0.01	6.36	0.37	0.08	0.04	1.33	0.32	4.30	0.70	3.26	0.35	32.7	2.1
20TN55A_24_3	0.00	0.00	5.79	0.23	0.07	0.03	1.10	0.33	3.24	0.46	2.11	0.16	21.1	1.1
20TN55A_24_4	1.32	0.11	10.99	0.53	0.42	0.06	4.48	0.55	7.98	0.90	4.45	0.34	42.4	1.9
20TN55A_24_7	0.01	0.01	4.86	0.32	0.08	0.03	1.33	0.30	3.17	0.47	1.77	0.17	19.1	1.3
20TN55A_24_8	0.00	0.01	8.42	0.37	0.13	0.03	2.89	0.48	5.08	0.62	3.38	0.28	31.6	1.4
20TN55A_25_3	0.28	0.12	25.33	0.93	0.43	0.08	4.98	0.56	9.87	1.08	5.19	0.37	44.8	2.6
20TN55A_25_6	0.48	0.09	22.26	0.44	0.27	0.06	2.74	0.45	5.76	0.64	3.56	0.30	35.3	1.7
20TN55A_25_7	0.04	0.02	36.95	1.71	0.47	0.07	7.73	1.23	13.02	1.50	7.19	0.50	67.1	3.5
20TN55A_25_8	b.d.l.		18.31	0.55	0.11	0.05	1.97	0.35	5.10	0.64	3.20	0.23	29.4	1.8
20TN55A_25_16	0.30	0.05	17.52	1.15	0.25	0.06	3.65	0.62	6.97	0.93	4.16	0.44	39.5	2.9
20TN55A_25_17	0.01	0.01	1.74	0.79	0.03	0.02	0.40	0.21	0.43	0.29	0.38	0.20	3.7	1.8
20TN55A_25_19	0.01	0.01	6.20	0.35	0.07	0.03	1.69	0.36	4.78	0.56	3.36	0.26	32.6	1.9
20TN55A_27	0.28	0.06	13.11	0.94	0.36	0.05	5.14	0.85	10.63	1.19	6.20	0.69	60.9	6.1
20TN55A_28	34.27	24.96	56.99	34.25	3.14	1.95	17.75	10.45	6.01	1.41	3.57	0.42	28.6	2.1
20TN55A_30	0.01	0.01	7.59	0.30	0.15	0.03	2.57	0.37	5.92	0.45	3.47	0.36	35.3	1.8
20TN55A_39	0.10	0.04	24.03	0.84	0.18	0.05	2.56	0.43	6.32	0.67	4.21	0.39	36.9	1.4
20TN55A_40	0.30	0.08	35.06	2.07	0.50	0.07	7.41	0.98	12.46	1.21	6.67	0.59	54.0	3.4
20TN55A_42	0.07	0.02	7.89	1.06	0.08	0.03	1.05	0.26	2.65	0.55	1.63	0.22	15.4	1.7
20TN55A_43	b.d.l.		10.94	0.56	0.05	0.02	1.19	0.29	3.82	0.59	2.25	0.22	21.8	1.5
20TN55A_44	0.00	0.00	16.66	1.32	0.14	0.04	2.93	0.41	5.48	0.72	3.65	0.35	31.2	2.7
20TN55A_46	0.84	0.50	14.14	0.79	0.23	0.09	2.25	0.45	5.16	0.63	2.98	0.25	27.8	1.5
20TN55A_47	0.02	0.01	6.03	0.25	0.16	0.05	3.67	0.49	7.83	0.77	5.08	0.35	42.4	1.9

Sample and Spot Number	Tb (ppm)	±2σ	Dy (ppm)	±2σ	Ho (ppm)	±2σ	Er (ppm)	±2σ	Tm (ppm)	±2σ	Yb (ppm)	±2σ	Lu (ppm)	±2σ
20TN55A_23_21	6.74	0.38	82.2	3.4	27.7	1.2	120.6	5.0	22.7	1.0	187	8	30.58	1.52
20TN55A_23_22	12.42	0.43	157.7	5.4	55.7	1.7	251.5	6.3	48.3	1.4	397	13	63.35	1.93
20TN55A_23_23	13.88	0.40	194.0	5.5	70.4	1.7	324.9	8.5	68.0	1.8	553	18	88.80	3.00
20TN55A_23_24	7.46	1.29	110.3	18.2	42.2	6.2	205.1	30.9	43.0	6.1	362	49	58.59	7.22
20TN55A_23_25	17.64	0.58	227.7	5.5	86.6	2.3	403.0	10.2	85.6	2.0	700	21	116	3
20TN55A_24_1	17.68	0.52	247.0	5.0	90.2	1.0	423.7	6.7	87.1	1.0	717	11	114	2
20TN55A_24_2	15.93	0.70	235.0	8.9	90.7	3.1	446.3	15.3	95.2	3.4	816	24	132	4
20TN55A_24_3	8.54	0.29	119.4	3.9	45.1	0.8	211.0	4.7	44.8	1.2	379	8	65.29	1.43
20TN55A_24_4	15.60	0.48	198.9	4.1	70.3	1.6	314.2	6.9	62.9	1.5	534	13	86.27	2.26
20TN55A_24_7	7.84	0.34	101.2	3.1	37.0	1.2	175.4	4.4	35.9	0.8	307	5	52.94	1.26
20TN55A_24_8	12.46	0.27	159.5	3.7	55.7	1.4	251.2	6.2	49.8	1.4	426	9	71.69	1.59
20TN55A_25_3	14.96	0.73	176.1	7.3	60.6	2.3	264.7	7.8	53.0	1.9	455	13	75.68	1.81
20TN55A_25_6	12.87	0.36	161.0	3.2	55.1	1.1	249.3	5.2	49.5	1.0	419	7	71.95	1.55
20TN55A_25_7	21.11	0.70	236.8	8.1	76.4	1.8	316.1	8.0	59.8	1.7	482	13	78.38	1.93
20TN55A_25_8	11.29	0.46	137.0	4.3	47.0	1.0	201.2	6.5	38.6	0.9	309	8	53.42	1.70
20TN55A_25_16	13.28	0.76	163.5	9.4	54.1	2.8	228.9	11.6	42.5	2.3	335	15	53.99	2.85
20TN55A_25_17	1.38	0.61	16.7	7.2	6.3	2.5	28.1	10.5	5.7	2.0	51	15	9.11	2.58
20TN55A_25_19	12.83	0.40	169.9	3.9	62.7	1.3	293.6	7.1	60.9	1.1	508	11	82.03	1.74
20TN55A_27	22.78	1.93	281.3	22.3	90.7	6.9	393.7	27.1	77.0	5.0	650	40	106	6
20TN55A_28	10.71	0.58	136.7	8.0	48.2	2.7	215.9	13.2	44.7	2.8	377	23	63.56	3.62
20TN55A_30	13.85	0.50	182.1	3.2	64.4	1.3	300.3	6.3	62.2	1.1	517	8	88.05	1.59
20TN55A_39	14.78	0.46	183.0	4.6	63.7	1.7	281.2	6.5	59.2	1.6	497	12	82.51	1.68
20TN55A_40	18.53	1.08	209.0	9.6	68.3	2.7	283.2	9.9	55.2	1.8	431	15	69.91	1.92
20TN55A_42	6.58	0.46	84.2	4.9	33.0	1.7	144.8	5.4	31.1	1.0	259	8	43.83	1.10
20TN55A_43	9.22	0.42	119.5	3.7	43.5	1.3	193.9	3.5	40.7	0.9	325	9	54.12	1.09
20TN55A_44	11.77	0.84	136.5	9.9	46.6	3.3	194.6	13.2	37.0	2.2	286	19	44.97	2.70
20TN55A_46	10.99	0.44	133.7	5.1	48.3	1.7	211.0	6.6	43.0	1.3	340	9	54.19	1.47
20TN55A_47	17.78	0.55	225.3	4.8	86.0	1.7	381.9	7.9	79.4	1.6	641	12	101	2

Sample and Spot Number	Hf (ppm)	±2σ	Ta (ppm)	±2σ	Pb (ppm)	±2σ	Hf (wt. %)	U (ppm)	Th (ppm)	Pb (ppm)
20TN55A_23_21	7764	166	0.92	0.12	25.62	0.57	0.78	12.07	535	490
20TN55A_23_22	7773	108	0.40	0.06	20.36	0.66	0.78	9.75	427	390
20TN55A_23_23	10644	331	1.22	0.11	14.74	0.66	1.06	22.53	239	230
20TN55A_23_24	9832	257	0.17	0.06	13.83	3.72	0.98	17.14	572	512
20TN55A_23_25	13290	321	20.01	6.91	17.06	2.60	1.33	11.54	259	225
20TN55A_24_1	14620	225	2.48	0.35	25.92	0.53	1.46	55.00	393	357
20TN55A_24_2	9952	234	0.20	0.06	11.97	0.59	1.00	27.37	175	156
20TN55A_24_3	5963	150	0.12	0.03	7.18	0.21	0.60	10.19	147	134
20TN55A_24_4	5696	181	4.57	0.29	25.79	0.65	0.57	21.38	592	537
20TN55A_24_7	5551	163	0.11	0.04	5.45	0.25	0.56	5.31	114	104
20TN55A_24_8	6682	216	0.13	0.04	10.74	0.27	0.67	6.42	251	235
20TN55A_25_3	8079	174	1.08	0.12	48.70	5.22	0.81	8.22	1039	1012
20TN55A_25_6	7406	183	1.79	0.12	28.38	0.59	0.74	7.57	690	640
20TN55A_25_7	7778	154	0.61	0.10	53.78	2.36	0.78	6.48	1483	1202
20TN55A_25_8	7293	134	0.28	0.04	27.52	0.56	0.73	6.42	736	664
20TN55A_25_16	6938	223	2.10	0.21	36.64	2.51	0.69	15.99	825	753
20TN55A_25_17	7692	216	0.20	0.04	3.25	1.66	0.77	10.43	575	503
20TN55A_25_19	13216	232	0.28	0.06	9.86	0.26	1.32	22.46	226	209
20TN55A_27	7426	166	1.49	0.21	29.52	2.56	0.74	8.52	703	649
20TN55A_28	7225	166	0.53	0.12	9.31	0.80	0.72	8.07	446	391
20TN55A_30	5866	123	0.18	0.05	10.88	0.35	0.59	14.04	332	302
20TN55A_39	7523	108	0.35	0.06	30.43	0.55	0.75	9.64	1122	1073
20TN55A_40	7211	189	0.56	0.10	55.44	3.14	0.72	9.02	2240	1935
20TN55A_42	5044	159	0.90	0.11	7.84	1.23	0.50	8.03	370	344
20TN55A_43	6424	200	0.20	0.05	11.07	0.64	0.64	8.54	373	356
20TN55A_44	5899	155	0.34	0.06	35.72	2.93	0.59	16.39	1059	1019
20TN55A_46	7461	163	0.31	0.06	21.47	0.63	0.75	19.85	903	845
20TN55A_47	14892	257	0.46	0.06	13.22	0.32	1.49	40.52	348	317

Appendix D: Complete U-Pb Zircon Dataset

Table D.1. U-Pb zircon results determined by LA-ICP-MS for zircon crystals in samples 20TN2, 20TN4D, 20TN13A, 20TN15A, 20TN15B, 20TN16A-2, 20TN17A-2, 20TN20, and 20TN55A from Corundum Dome and Pyrochlore Dome, Pool Creek area, southeast Yukon, Canada.

Sample and Spot Numbers	Note	Isotope Ratios						rho	Dates					
		$^{207}Pb/^{235}U$	±2σ	$^{206}Pb/^{238}U$	±2σ	$^{207}Pb/^{206}Pb$	±2σ		$^{207}Pb/^{235}U$	±2σ	$^{206}Pb/^{238}U$	±2σ	$^{207}Pb/^{206}Pb$	±2σ
20TN2_2	June	0.8234	0.0509	0.1044	0.0026	0.0572	0.0031	0.13	606	28	640	15	458	117
20TN2_4	June	1.0750	0.4084	0.1042	0.0079	0.0693	0.0272	0.40	592	194	638	46	1019	715
20TN2_7	June	1.0602	0.0895	0.1007	0.0024	0.0758	0.0060	0.06	726	43	618	14	1020	161
20TN2_21	June	1.2480	0.3974	0.1083	0.0113	0.0862	0.0256	0.15	759	191	662	65	1083	656
20TN2_25	June	1.0204	0.2458	0.1016	0.0073	0.0752	0.0181	0.16	643	127	623	43	661	604
20TN2_44	July	1.2384	0.2852	0.1076	0.0074	0.0821	0.0189	0.04	735	134	657	43	1108	475
20TN4D_10	June	1.3612	0.1259	0.1083	0.0034	0.0911	0.0075	0.29	860	51	663	20	1375	155
20TN4D_2	June	1.6754	0.2815	0.1059	0.0028	0.1149	0.0196	0.10	958	94	649	16	1644	274
20TN4D_6	June	1.2459	0.1685	0.1013	0.0022	0.0884	0.0110	0.45	798	72	622	13	1234	226
20TN4D_9	June	3.8102	0.2754	0.1009	0.0033	0.2783	0.0187	0.29	1591	56	620	19	3343	99
20TN4D_11	July	8.4530	1.0613	0.1095	0.0070	0.5548	0.0508	0.72	2247	116	669	41	4356	143
20TN4D_12	July	3.4031	0.2775	0.1056	0.0042	0.2324	0.0155	0.62	1485	66	647	25	3026	113
20TN4D_13	July	2.0878	0.2104	0.1060	0.0031	0.1411	0.0116	0.66	1124	67	649	18	2175	146
20TN4D_19	July	1.7455	0.3407	0.1045	0.0023	0.1191	0.0216	0.62	987	116	641	14	1771	293
20TN4D_20	July	4.5593	0.3174	0.1086	0.0060	0.3031	0.0143	0.77	1725	62	664	35	3467	75
20TN4D_27	July	1.2343	0.2668	0.1039	0.0068	0.0867	0.0176	0.03	742	134	636	40	1333	385
20TN4D_28	July	7.2635	1.0230	0.1080	0.0068	0.4772	0.0508	0.78	2083	138	660	40	4102	171
20TN15A_259_1	March	0.8319	0.1144	0.0999	0.0040	0.0800	0.0118	0.08	609	65	614	24	1104	347
20TN15A_281	March	0.6801	0.0801	0.1001	0.0038	0.0590	0.0073	0.05	523	48	615	23	486	272
20TN15A_260_2	March	0.6542	0.0562	0.1007	0.0032	0.0620	0.0056	0.19	510	35	618	19	639	213
20TN15A_284_1	March	0.7630	0.0954	0.1008	0.0024	0.0651	0.0081	0.15	568	55	619	14	630	319
20TN15A_260_3	March	0.6246	0.0354	0.1011	0.0023	0.0619	0.0035	0.36	491	22	621	14	640	129
20TN15A_273_2	March	0.6185	0.0990	0.1015	0.0035	0.0578	0.0098	0.28	481	66	623	20	494	358
20TN15A_264	March	0.6953	0.1129	0.1016	0.0036	0.0656	0.0097	0.03	519	66	623	21	684	346
20TN15A_231_1	March	0.8967	0.1636	0.1017	0.0045	0.0682	0.0129	0.02	636	86	624	27	672	427
20TN15A_250	March	0.7234	0.0659	0.1018	0.0025	0.0695	0.0064	0.17	546	39	625	15	794	207
20TN15A_282	March	0.7770	0.0877	0.1018	0.0025	0.0675	0.0080	0.01	576	50	625	15	727	259

Sample and Spot Numbers	Note	Isotope Ratios						rho	Dates					
		$^{207}Pb/^{235}U$	±2σ	$^{206}Pb/^{238}U$	±2σ	$^{207}Pb/^{206}Pb$	±2σ		$^{207}Pb/^{235}U$	±2σ	$^{206}Pb/^{238}U$	±2σ	$^{207}Pb/^{206}Pb$	±2σ
20TN15A_248	March	0.7845	0.1675	0.1020	0.0066	0.0759	0.0160	0.23	550	94	625	39	699	514
20TN15A_278	March	0.7774	0.0952	0.1019	0.0035	0.0676	0.0081	0.09	578	55	626	20	765	281
20TN15A_276	March	0.6911	0.0500	0.1020	0.0024	0.0622	0.0045	0.10	530	31	626	14	610	183
20TN15A_274_2	March	0.7010	0.0626	0.1022	0.0020	0.0642	0.0058	0.17	532	37	627	11	660	199
20TN15A_253_4	March	0.8008	0.1010	0.1024	0.0026	0.0782	0.0099	0.09	584	55	628	15	1039	233
20TN15A_259_4	March	0.9241	0.1906	0.1025	0.0056	0.0932	0.0204	0.05	644	106	628	33	1027	528
20TN15A_231_4	March	1.0344	0.2166	0.1026	0.0048	0.0806	0.0168	0.14	674	108	629	28	706	555
20TN15A_284_6	March	0.7856	0.0676	0.1027	0.0032	0.0625	0.0060	0.18	583	37	630	18	578	207
20TN15A_265	March	0.6283	0.0676	0.1028	0.0025	0.0602	0.0067	0.07	487	42	631	15	428	278
20TN15A_284_2	March	0.8752	0.1930	0.1029	0.0041	0.0729	0.0147	0.35	620	97	631	24	812	417
20TN15A_252	March	0.6644	0.0888	0.1031	0.0038	0.0634	0.0083	0.08	508	56	632	22	647	310
20TN15A_251	March	1.0201	0.2001	0.1032	0.0030	0.0941	0.0179	0.57	692	104	633	17	1454	329
20TN15A_266	March	0.7312	0.0976	0.1032	0.0025	0.0707	0.0090	0.19	550	56	633	15	853	261
20TN15A_247_1	March	0.7027	0.1324	0.1036	0.0052	0.0657	0.0141	0.27	523	81	635	30	566	471
20TN15A_231_3	March	0.8017	0.1258	0.1036	0.0039	0.0621	0.0102	0.02	574	70	635	23	312	392
20TN15A_274_1	March	0.7219	0.0683	0.1042	0.0027	0.0663	0.0064	0.04	545	40	639	16	686	230
20TN15A_259_3	March	0.6727	0.1035	0.1043	0.0053	0.0667	0.0105	0.15	512	64	639	31	554	493
20TN15A_234	March	0.7556	0.1560	0.1044	0.0047	0.0605	0.0125	0.07	542	88	639	27	552	385
20TN15A_253_3	March	0.7821	0.1008	0.1046	0.0045	0.0751	0.0098	0.04	571	59	641	26	982	262
20TN15A_259_2	March	0.6986	0.1041	0.1048	0.0062	0.0685	0.0116	0.06	517	67	641	37	813	319
20TN15A_233	March	1.0420	0.3187	0.1046	0.0046	0.0756	0.0225	0.44	709	164	641	27	911	688
20TN15A_260_4	March	0.9720	0.2462	0.1048	0.0055	0.0883	0.0206	0.06	673	119	642	32	1242	451
20TN15A_279	March	0.7414	0.0495	0.1050	0.0026	0.0640	0.0041	0.29	560	29	643	15	695	148
20TN15A_231_5	March	1.3199	0.2570	0.1051	0.0046	0.0985	0.0178	0.44	795	109	644	27	1334	343
20TN15A_262	March	0.7675	0.0751	0.1051	0.0029	0.0733	0.0072	0.07	571	44	644	17	959	215
20TN15A_254	March	0.7235	0.0605	0.1052	0.0027	0.0689	0.0059	0.05	547	35	644	16	803	193
20TN15A_261	March	1.3299	0.2191	0.1053	0.0065	0.1285	0.0213	0.22	827	89	645	38	1861	289
20TN15A_284_3	March	0.9767	0.1129	0.1055	0.0021	0.0781	0.0086	0.06	678	54	646	12	1010	217
20TN15A_253_2	March	0.6996	0.1607	0.1056	0.0041	0.0660	0.0153	0.16	524	92	647	24	567	452
20TN15A_283	March	0.7207	0.0412	0.1056	0.0029	0.0595	0.0034	0.28	548	24	647	17	540	129
20TN15A_247_5	March	0.8406	0.0953	0.1056	0.0027	0.0764	0.0069	0.70	611	50	647	16	1038	170
20TN15A_247_6	March	0.6887	0.0455	0.1058	0.0026	0.0622	0.0039	0.04	528	27	648	15	649	143
20TN15A_258	March	0.7349	0.0875	0.1058	0.0024	0.0695	0.0083	0.02	548	52	648	14	789	253
20TN15A_247_3	March	0.7523	0.0623	0.1060	0.0020	0.0685	0.0057	0.08	564	35	649	12	795	169

Sample and Spot Numbers	Note	Isotope Ratios						rho	Dates					
		$^{207}Pb/^{235}U$	±2σ	$^{206}Pb/^{238}U$	±2σ	$^{207}Pb/^{206}Pb$	±2σ		$^{207}Pb/^{235}U$	±2σ	$^{206}Pb/^{238}U$	±2σ	$^{207}Pb/^{206}Pb$	±2σ
20TN15A_232	March	1.3215	0.3629	0.1065	0.0049	0.0984	0.0280	0.05	817	152	652	28	1258	597
20TN15A_247_4	March	0.7554	0.0830	0.1071	0.0029	0.0677	0.0071	0.25	564	48	656	17	747	237
20TN15A_231_2	March	0.9708	0.1882	0.1072	0.0034	0.0715	0.0142	0.09	658	97	656	20	488	544
20TN15A_267_3	March	0.9976	0.1131	0.1073	0.0043	0.0916	0.0105	0.23	693	59	657	25	1354	258
20TN15A_247_2	March	0.6998	0.0709	0.1078	0.0034	0.0626	0.0069	0.02	532	42	660	20	633	215
20TN15A_253_1	March	0.6706	0.1086	0.1079	0.0037	0.0618	0.0104	0.03	501	65	660	22	398	386
20TN15B_133	March	1.5327	0.0912	0.0947	0.0036	0.1312	0.0084	0.32	942	37	583	21	2106	119
20TN15B_158	March	1.2461	0.1209	0.0952	0.0020	0.1034	0.0089	0.48	806	54	586	12	1595	162
20TN15B_156	March	2.0562	0.1599	0.0954	0.0032	0.1719	0.0113	0.62	1120	53	587	19	2532	110
20TN15B_157	March	0.7846	0.0874	0.0955	0.0016	0.0665	0.0079	0.11	579	49	588	10	813	247
20TN15B_132	March	1.3155	0.1352	0.0961	0.0034	0.1115	0.0103	0.74	850	60	591	20	1808	171
20TN15B_140	March	1.3982	0.1424	0.0967	0.0018	0.1191	0.0102	0.38	884	61	595	11	1924	158
20TN16A-2_106	March	0.8505	0.0534	0.0947	0.0017	0.0759	0.0050	0.31	621	29	583	10	1036	136
20TN16A-2_115	March	0.8567	0.0402	0.0955	0.0023	0.0756	0.0032	0.00	626	22	588	13	1060	89
20TN16A-2_101	March	0.9224	0.0598	0.0961	0.0022	0.0806	0.0049	0.01	659	32	591	13	1166	120
20TN16A-2_104	March	0.9260	0.0599	0.0964	0.0023	0.0785	0.0042	0.16	662	30	593	13	1171	122
20TN16A-2_117	March	1.3282	0.2376	0.0977	0.0032	0.1148	0.0194	0.25	827	93	601	19	1696	272
20TN17A-2_92_5	March	0.7026	0.0155	0.0948	0.0009	0.0592	0.0014	0.07	540	9	584	5	567	52
20TN17A-2_97_3	March	0.7605	0.0331	0.0949	0.0028	0.0633	0.0035	0.02	574	19	584	16	702	119
20TN17A-2_90_3	March	0.7498	0.0244	0.0949	0.0012	0.0618	0.0025	0.22	567	14	585	7	650	82
20TN17A-2_98_7	March	0.7714	0.0351	0.0950	0.0023	0.0683	0.0028	0.44	580	20	585	13	866	81
20TN17A-2_92_3	March	0.7444	0.0227	0.0953	0.0010	0.0624	0.0018	0.01	564	13	587	6	679	63
20TN17A-2_90_1	March	0.7768	0.0202	0.0955	0.0009	0.0637	0.0017	0.07	583	12	588	5	722	59
20TN17A-2_90_5	March	0.7755	0.0346	0.0957	0.0017	0.0634	0.0032	0.17	582	19	589	10	704	102
20TN17A-2_92_1	March	0.7286	0.0270	0.0960	0.0016	0.0605	0.0021	0.25	555	16	591	10	610	72
20TN17A-2_99_5	March	0.6769	0.0188	0.0961	0.0015	0.0588	0.0016	0.24	524	11	591	9	548	57
20TN17A-2_89_5	March	0.7404	0.0205	0.0966	0.0013	0.0596	0.0016	0.23	562	12	594	8	578	58
20TN17A-2_92_6	March	0.7160	0.0203	0.0967	0.0015	0.0591	0.0016	0.37	548	12	595	9	564	57
20TN17A-2_96_3	March	0.7277	0.0302	0.0968	0.0023	0.0603	0.0026	0.03	555	18	595	13	604	96
20TN17A-2_96_5	March	0.7468	0.0247	0.0968	0.0012	0.0628	0.0021	0.31	565	14	596	7	688	70
20TN17A-2_90_4	March	0.7416	0.0226	0.0970	0.0009	0.0601	0.0020	0.27	562	13	597	6	591	72
20TN17A-2_98_4	March	0.7088	0.0220	0.0974	0.0011	0.0613	0.0015	0.26	543	13	599	6	641	54
20TN17A-2_97_4	March	0.7542	0.0341	0.0979	0.0018	0.0633	0.0028	0.30	569	20	602	11	699	95
20TN17A-2_89_1	March	0.7572	0.0249	0.0980	0.0011	0.0596	0.0020	0.02	572	15	603	6	575	73

Sample and Spot Numbers	Note	Isotope Ratios						rho	Dates					
		$^{207}Pb/^{235}U$	±2σ	$^{206}Pb/^{238}U$	±2σ	$^{207}Pb/^{206}Pb$	±2σ		$^{207}Pb/^{235}U$	±2σ	$^{206}Pb/^{238}U$	±2σ	$^{207}Pb/^{206}Pb$	±2σ
20TN17A-2_89_4	March	0.7536	0.0228	0.0981	0.0009	0.0595	0.0017	0.02	569	13	603	5	572	64
20TN17A-2_89_2	March	0.7570	0.0193	0.0981	0.0013	0.0594	0.0015	0.30	572	11	603	8	571	56
20TN17A-2_96_4	March	0.7290	0.0308	0.0983	0.0022	0.0590	0.0023	0.39	555	18	604	13	558	83
20TN17A-2_90_2	March	0.8300	0.0285	0.0983	0.0018	0.0664	0.0027	0.22	613	16	605	10	806	89
20TN17A-2_99_3	March	0.7193	0.0264	0.0986	0.0017	0.0614	0.0024	0.07	549	16	606	10	659	71
20TN17A-2_88	March	0.8064	0.0336	0.0990	0.0012	0.0630	0.0028	0.11	599	19	609	7	685	91
20TN17A-2_97_5	March	0.6951	0.0237	0.0991	0.0012	0.0577	0.0026	0.10	535	14	609	7	527	83
20TN17A-2_99_2	March	0.6953	0.0239	0.0997	0.0012	0.0585	0.0018	0.41	535	14	612	7	535	69
20TN17A-2_98_6	March	0.7515	0.0245	0.0997	0.0018	0.0632	0.0020	0.37	568	14	612	10	705	67
20TN17A-2_97_2	March	0.8272	0.0384	0.1000	0.0018	0.0683	0.0033	0.15	611	21	614	11	864	98
20TN17A-2_92_4	March	0.7768	0.0206	0.1001	0.0011	0.0621	0.0016	0.11	583	12	615	7	668	55
20TN17A-2_98_2	March	0.7329	0.0262	0.1002	0.0017	0.0599	0.0018	0.37	557	15	615	10	605	73
20TN17A-2_85	March	0.7931	0.0281	0.1006	0.0010	0.0601	0.0022	0.10	592	16	618	6	587	84
20TN17A-2_92_2	March	0.7199	0.0179	0.1010	0.0012	0.0570	0.0014	0.15	550	11	620	7	481	56
20TN17A-2_86	March	0.7961	0.0248	0.1013	0.0011	0.0602	0.0019	0.07	594	14	622	7	599	68
20TN17A-2_97_1	March	0.7669	0.0243	0.1016	0.0016	0.0624	0.0025	0.24	577	14	624	10	671	86
20TN17A-2_89_3	March	0.7859	0.0281	0.1026	0.0014	0.0598	0.0021	0.25	588	16	629	8	582	75
20TN17A-2_72	March	0.8317	0.0256	0.1032	0.0015	0.0597	0.0019	0.08	614	14	633	9	576	66
20TN17A-2_71	March	0.8585	0.0237	0.1035	0.0012	0.0610	0.0017	0.03	628	13	635	7	626	60
20TN17A-2_76	March	1.0674	0.0535	0.1039	0.0027	0.0772	0.0044	0.22	734	27	637	16	1083	117
20TN17A-2_70	March	0.8950	0.0464	0.1039	0.0023	0.0619	0.0030	0.03	648	24	637	14	655	101
20TN17A-2_75	March	0.8497	0.0189	0.1046	0.0017	0.0605	0.0016	0.10	624	10	641	10	613	57
20TN17A-2_83	March	0.8982	0.0490	0.1050	0.0022	0.0658	0.0041	0.33	649	27	643	13	825	102
20TN20_33	July	1.1757	0.1247	0.1005	0.0029	0.0839	0.0082	0.59	776	51	617	17	1233	194
20TN20_20	June	0.9169	0.0316	0.1008	0.0023	0.0655	0.0020	0.46	660	17	619	14	782	66
20TN20_4	July	0.8648	0.0517	0.1012	0.0044	0.0634	0.0026	0.91	629	27	621	25	695	91
20TN20_11	June	0.7907	0.0446	0.1012	0.0024	0.0568	0.0031	0.24	589	25	621	14	443	124
20TN20_23	June	0.9646	0.1265	0.1013	0.0031	0.0690	0.0088	0.19	667	66	622	18	634	343
20TN20_19	July	0.9296	0.1355	0.1020	0.0048	0.0665	0.0093	0.16	646	76	626	28	661	340
20TN20_25	June	0.8544	0.0413	0.1021	0.0019	0.0608	0.0028	0.32	625	23	627	11	630	90
20TN20_14	June	0.8445	0.0773	0.1025	0.0037	0.0608	0.0052	0.29	619	42	629	22	602	182
20TN20_26	June	0.9168	0.0316	0.1026	0.0018	0.0650	0.0024	0.12	659	17	630	11	756	82
20TN20_21	June	0.9315	0.0511	0.1027	0.0022	0.0659	0.0042	0.31	665	26	630	13	752	134
20TN20_29	July	1.1797	0.0458	0.1029	0.0021	0.0808	0.0038	0.22	789	22	631	13	1214	84

Sample and Spot Numbers	Note	Isotope Ratios						rho	Dates					
		$^{207}Pb/^{235}U$	±2σ	$^{206}Pb/^{238}U$	±2σ	$^{207}Pb/^{206}Pb$	±2σ		$^{207}Pb/^{235}U$	±2σ	$^{206}Pb/^{238}U$	±2σ	$^{207}Pb/^{206}Pb$	±2σ
20TN20_24	July	0.9052	0.0374	0.1029	0.0011	0.0626	0.0025	0.26	653	20	631	6	673	85
20TN20_27	July	0.8927	0.0277	0.1030	0.0013	0.0617	0.0017	0.41	647	15	632	7	654	61
20TN20_26	July	0.9005	0.0265	0.1030	0.0013	0.0623	0.0017	0.34	651	14	632	7	675	59
20TN20_9	July	0.7954	0.0674	0.1032	0.0027	0.0565	0.0051	0.01	588	39	633	16	348	227
20TN20_18	June	0.8907	0.0353	0.1032	0.0016	0.0626	0.0024	0.22	645	19	633	9	674	80
20TN20_30	July	1.3223	0.0602	0.1032	0.0040	0.0917	0.0053	0.03	855	26	633	24	1448	115
20TN20_28	July	0.9037	0.0234	0.1035	0.0014	0.0621	0.0017	0.17	653	12	635	8	669	58
20TN20_21	July	1.2380	0.1047	0.1039	0.0041	0.0859	0.0074	0.31	815	49	637	24	1312	170
20TN20_15	June	0.8491	0.0313	0.1041	0.0013	0.0591	0.0021	0.21	623	17	638	7	555	80
20TN20_24	June	1.0312	0.1875	0.1046	0.0062	0.0741	0.0150	0.06	681	98	640	36	605	488
20TN20_5	June	0.7473	0.0670	0.1045	0.0027	0.0510	0.0041	0.18	560	38	641	16	182	199
20TN20_31	July	1.3946	0.0926	0.1046	0.0024	0.0932	0.0046	0.49	881	38	641	14	1494	103
20TN20_25	July	0.9256	0.0700	0.1046	0.0029	0.0634	0.0049	0.10	660	37	641	17	650	168
20TN20_19	June	1.1633	0.1253	0.1053	0.0020	0.0829	0.0097	0.37	789	63	645	12	1159	201
20TN55A_25_6	March	0.8638	0.1998	0.0961	0.0066	0.0724	0.0181	0.22	575	112	590	39	820	504
20TN55A_23_10	March	0.9933	0.2297	0.0964	0.0070	0.0749	0.0186	0.08	633	116	592	41	521	595
20TN55A_23_8	March	1.3515	0.6302	0.0966	0.0118	0.1140	0.0543	0.06	683	261	593	69	1997	656
20TN55A_23_3	March	0.9878	0.1624	0.0971	0.0045	0.0726	0.0124	0.22	680	87	597	26	752	436
20TN55A_25_19	March	0.8619	0.1502	0.0972	0.0035	0.0650	0.0113	0.11	602	82	598	20	593	353
20TN55A_23_12	March	0.8680	0.2865	0.0985	0.0088	0.0691	0.0239	0.02	542	161	604	52	988	530
20TN55A_25_16	March	0.9534	0.2159	0.0985	0.0056	0.0691	0.0140	0.53	643	113	605	33	332	689
20TN55A_16_2	March	1.7241	1.0696	0.0986	0.0125	0.1174	0.0744	0.59	715	485	605	73	2358	726
20TN55A_24_3	March	0.9415	0.2125	0.0990	0.0061	0.0681	0.0144	0.29	653	124	608	36	838	458
20TN55A_47	March	0.9498	0.1251	0.0990	0.0038	0.0673	0.0091	0.10	661	64	608	22	689	286
20TN55A_44	March	1.0568	0.2709	0.0992	0.0058	0.0726	0.0210	0.06	687	149	609	34	973	457
20TN55A_23_23	March	0.8987	0.1341	0.0992	0.0035	0.0670	0.0098	0.02	625	69	609	21	437	379
20TN55A_23_6	March	1.4358	0.4361	0.0997	0.0124	0.1013	0.0331	0.34	833	216	611	73	1711	469
20TN55A_16_1	March	2.7127	0.9371	0.1006	0.0099	0.2049	0.0760	0.38	1289	328	617	58	2472	774
20TN55A_25_8	March	1.2574	0.2881	0.1008	0.0065	0.1028	0.0255	0.06	770	150	618	38	1639	403
20TN55A_23_18	March	0.9352	0.2954	0.1012	0.0082	0.0715	0.0235	0.09	592	151	620	48	694	631
20TN55A_23_21	March	0.8426	0.1891	0.1011	0.0052	0.0628	0.0145	0.08	592	115	620	31	504	539
20TN55A_23_22	March	0.8734	0.1694	0.1011	0.0058	0.0645	0.0122	0.07	616	106	620	34	689	447
20TN55A_24_4	March	0.8127	0.1250	0.1014	0.0049	0.0599	0.0095	0.05	586	69	622	28	373	376
20TN55A_24_2	March	0.8860	0.1460	0.1014	0.0029	0.0647	0.0105	0.17	622	78	623	17	586	335

Sample and Spot Numbers	Note	Isotope Ratios						rho	Dates					
		$^{207}Pb/^{235}U$	±2σ	$^{206}Pb/^{238}U$	±2σ	$^{207}Pb/^{206}Pb$	±2σ		$^{207}Pb/^{235}U$	±2σ	$^{206}Pb/^{238}U$	±2σ	$^{207}Pb/^{206}Pb$	±2σ
20TN55A_43	March	0.7580	0.2925	0.1015	0.0063	0.0524	0.0219	0.04	508	173	623	37	297	715
20TN55A_14	March	1.2844	0.7737	0.1022	0.0163	0.0906	0.0517	0.06	574	288	623	95	1554	958
20TN55A_30	March	1.1210	0.2406	0.1023	0.0050	0.0797	0.0174	0.12	712	123	628	29	1156	396
20TN55A_23_20	March	0.9253	0.1889	0.1029	0.0055	0.0688	0.0151	0.20	631	95	631	32	256	593
20TN55A_25_17	March	0.7773	0.5575	0.1032	0.0057	0.0528	0.0367	0.21	484	272	633	34	-342	1489
20TN55A_46	March	1.0390	0.1992	0.1033	0.0048	0.0690	0.0131	0.11	697	103	633	28	709	464
20TN55A_23_13	March	0.6639	0.1613	0.1038	0.0080	0.0501	0.0142	0.00	471	100	635	47	-292	622
20TN55A_21_1	March	0.9553	0.4571	0.1037	0.0072	0.0647	0.0313	0.27	622	249	636	42	541	1014
20TN55A_40	March	1.2152	0.2786	0.1039	0.0068	0.0819	0.0184	0.26	720	133	636	40	1027	439
20TN55A_25_7	March	1.3244	0.3315	0.1042	0.0073	0.0988	0.0269	0.09	764	144	637	43	1116	597
20TN55A_27	March	1.0899	0.2259	0.1045	0.0070	0.0753	0.0144	0.01	683	112	639	41	1072	380
20TN55A_24_8	March	0.9965	0.2482	0.1046	0.0091	0.0687	0.0174	0.10	636	127	640	53	716	530
20TN55A_24_1	March	0.8783	0.0734	0.1047	0.0021	0.0617	0.0050	0.27	633	40	642	12	611	171
20TN55A_23_19	March	0.9799	0.1416	0.1048	0.0044	0.0707	0.0109	0.22	665	76	642	26	743	365
20TN55A_23_4	March	1.0301	0.1830	0.1057	0.0057	0.0726	0.0136	0.18	700	100	647	33	809	425
20TN55A_23_24	March	0.8795	0.2529	0.1061	0.0070	0.0542	0.0133	0.01	601	135	649	41	486	569
20TN55A_23_7	March	1.6694	0.4686	0.1042	0.0099	0.1140	0.0336	0.02	828	185	651	64	2085	443
20TN55A_23_25	March	1.7127	0.7970	0.1067	0.0133	0.1101	0.0436	0.46	889	256	652	77	1129	823
20TN55A_39	March	1.1749	0.2341	0.1066	0.0067	0.0786	0.0166	0.04	738	109	652	39	1011	336
20TN55A_23_14	March	1.3936	0.5245	0.1070	0.0104	0.0991	0.0356	0.13	721	241	654	60	1755	506
20TN55A_25_3	March	1.2925	0.4079	0.1069	0.0057	0.0896	0.0288	0.17	742	201	654	33	1015	819
20TN55A_23_5	March	2.1929	0.4046	0.1070	0.0066	0.1411	0.0244	0.14	1105	131	654	38	2052	365
20TN55A_16_7	March	1.1882	1.0711	0.1075	0.0170	0.0612	0.0601	0.52	439	437	656	99	1498	1074
20TN55A_28	March	0.9820	0.1880	0.1075	0.0082	0.0694	0.0169	0.29	710	133	657	48	881	512
20TN55A_24_7	March	1.0906	0.2422	0.1079	0.0080	0.0789	0.0193	0.06	688	117	659	46	787	492
20TN55A_9_9	March	0.8134	0.3052	0.1090	0.0103	0.0563	0.0224	0.21	466	181	664	60	974	520
20TN55A_42	March	1.0349	0.2981	0.1093	0.0073	0.0693	0.0207	0.01	618	153	668	43	693	666
20TN55A_11	March	1.7586	0.7152	0.1097	0.0099	0.1130	0.0452	0.32	964	286	670	58	1358	1067

Table D.2. U-Pb zircon results determined by LA-ICP-MS for standard reference materials BCR2G, NIST610, NIST612, 91500, Plešovice (PL), and Temora2 (Tem).

		Isotope Ratios						rho	Dates					
Sample Spot	Note	$^{207}Pb/^{235}U$	±2σ	$^{206}Pb/^{238}U$	±2σ	$^{207}Pb/^{206}Pb$	±2σ		$^{207}Pb/^{235}U$	±2σ	$^{206}Pb/^{238}U$	±2σ	$^{207}Pb/^{206}Pb$	±2σ
BCR2-G_4	March	198.6450	15.4760	1.6542	0.1575	0.8921	0.0706	0.6128	5382	70	6214	372	4737	151
BCR2-G_20	March	198.8973	18.9581	1.8417	0.1282	0.7952	0.0610	0.6350	5347	99	6689	287	4731	106
BCR2-G_33	March	185.9618	15.5932	1.7178	0.1733	0.8068	0.0619	0.6254	5287	87	6363	391	4714	85
BCR2-G_50	March	198.4532	16.4547	1.6327	0.1376	0.8864	0.0745	0.5956	5355	82	6178	349	4805	72
BCR2-G_67	March	183.4780	14.3465	1.6319	0.1839	0.8641	0.0648	0.7315	5277	78	6140	425	4751	97
BCR2-G_80	March	177.7143	21.4393	1.6150	0.1616	0.7994	0.0585	0.7466	5218	119	6116	392	4678	96
BCR2-G_95	March	165.0730	16.2013	1.6425	0.1677	0.8465	0.0802	0.5832	5159	99	6174	420	4685	108
BCR2-G_110	March	153.4424	17.6490	1.4824	0.1406	0.8627	0.0680	0.6949	5072	118	5796	351	4694	134
BCR2-G_123	March	136.2449	11.8858	1.3764	0.1212	0.8452	0.0623	0.6815	4971	90	5625	389	4720	134
BCR2-G_138	March	144.5918	11.9942	1.5150	0.1739	0.8470	0.0730	0.6121	5034	84	5847	429	4672	107
BCR2-G_153	March	145.7499	14.3017	1.3870	0.1025	0.8761	0.0811	0.4335	5035	96	5568	278	4722	100
BCR2-G_166	March	153.1147	13.7131	1.4723	0.1347	0.8319	0.0646	0.6861	5089	88	5773	342	4733	89
BCR2-G_182	March	191.5832	14.2539	1.7317	0.1543	0.8175	0.0660	0.7051	5344	84	6407	373	4771	59
BCR2-G_197	March	177.3116	16.9686	1.6156	0.1456	0.8115	0.0675	0.5942	5231	98	6135	334	4704	68
BCR2-G_213	March	185.9427	14.9881	1.5740	0.1505	0.8657	0.0590	0.8583	5287	89	6027	354	4778	123
BCR2-G_229	March	190.2889	16.3619	1.7000	0.1647	0.8909	0.0639	0.7380	5307	95	6322	392	4854	65
BCR2-G_242	March	143.3778	13.7086	1.7049	0.1675	0.8585	0.0856	0.5323	5021	86	6325	412	4677	89
BCR2-G_257	March	128.3294	12.3593	1.7708	0.1857	0.8249	0.0884	0.4542	4934	84	6476	420	4709	105
BCR2-G_272	March	131.4278	13.6139	1.5490	0.1648	0.9552	0.0980	0.6137	4957	119	5936	434	4661	112
BCR2-G_289	March	191.7688	19.1002	1.7599	0.1977	0.8682	0.0767	0.5803	5308	102	6440	440	4716	97
BCR2-G	June	181.9925	17.0559	1.7238	0.1764	0.7935	0.0639	0.6914	5253	93	6340	429	4668	96
BCR2-G	June	181.0913	14.4079	1.7320	0.1559	0.7697	0.0594	0.6544	5258	80	6495	417	4658	101
BCR2-G	June	181.7441	18.1048	1.7200	0.1297	0.7509	0.0441	0.7883	5249	96	6389	304	4668	60
BCR2-G	June	186.6785	14.9624	1.6505	0.1261	0.8285	0.0452	0.7937	5284	87	6220	309	4813	64
BCR2-G	June	187.1235	19.5763	1.6717	0.1350	0.8307	0.0848	0.5012	5274	102	6262	339	4635	107
BCR2-G	June	202.4810	16.7681	1.8053	0.1558	0.8157	0.0441	0.7898	5370	80	6568	350	4768	67
BCR2-G	June	181.1024	17.0316	1.5840	0.1098	0.8403	0.0624	0.7620	5273	103	6072	269	4661	99
BCR2-G	June	174.4502	11.7212	1.6632	0.1255	0.7689	0.0486	0.5920	5227	69	6252	311	4735	85
BCR2-G	June	158.5160	14.3782	1.6217	0.1406	0.7177	0.0443	0.7425	5115	93	6136	340	4661	83
BCR2-G	June	177.5580	14.4201	1.6205	0.1469	0.8383	0.0627	0.6409	5261	91	6124	364	4769	58
BCR2-G	June	199.7912	16.5078	1.7181	0.1546	0.8694	0.0695	0.6338	5353	86	6358	364	4782	58

		Isotope Ratios						rho	Dates					
Sample Spot	Note	$^{207}Pb/^{235}U$	±2σ	$^{206}Pb/^{238}U$	±2σ	$^{207}Pb/^{206}Pb$	±2σ		$^{207}Pb/^{235}U$	±2σ	$^{206}Pb/^{238}U$	±2σ	$^{207}Pb/^{206}Pb$	±2σ
BCR2-G	June	208.8588	17.5723	1.7245	0.1492	0.8967	0.0567	0.7800	5400	81	6378	357	4834	72
BCR2-G	June	180.0949	13.2855	1.7769	0.1708	0.7803	0.0516	0.6720	5255	76	6483	389	4727	86
BCR2-G	June	163.6605	11.4905	1.6407	0.1303	0.7420	0.0396	0.7199	5181	78	6193	318	4724	65
BCR2-G	June	176.1811	13.8806	1.6396	0.1305	0.8166	0.0577	0.6311	5230	80	6191	315	4701	91
BCR2-G	June	200.1006	23.4708	1.6801	0.1620	0.8672	0.0599	0.8271	5331	113	6257	385	4722	81
BCR2-G	June	204.2979	19.0334	1.7919	0.1445	0.8347	0.0561	0.6627	5373	87	6548	326	4775	91
BCR2-G	June	201.0756	16.8603	1.6543	0.1207	0.8834	0.0520	0.8156	5381	97	6236	296	4790	85
BCR2-G	June	191.5043	17.9750	1.7681	0.1735	0.8134	0.0661	0.6993	5333	83	6460	393	4712	63
BCR2-G	June	195.0634	14.6862	1.6403	0.1262	0.8562	0.0524	0.7493	5357	66	6284	356	4777	63
BCR	July	192.8962	15.7303	1.7302	0.1242	0.8182	0.0540	0.6525	5320	84	6418	295	4759	79
BCR	July	206.8906	16.7277	1.7756	0.1172	0.8328	0.0537	0.0854	5392	80	6601	307	4773	82
BCR	July	190.5144	13.6960	1.7119	0.1057	0.8252	0.0427	0.7179	5332	76	6390	250	4808	66
BCR	July	203.4289	18.2776	1.7756	0.1332	0.8155	0.0544	0.7659	5367	93	6520	301	4735	80
BCR	July	199.9451	17.7940	1.6850	0.1228	0.8555	0.0380	0.8000	5352	89	6312	285	4873	66
BCR	July	189.5871	14.5315	1.6760	0.1282	0.8297	0.0504	0.6170	5306	77	6286	298	4761	95
BCR	July	185.7624	16.4873	1.7272	0.1625	0.7920	0.0540	0.7854	5274	95	6374	375	4761	55
BCR	July	184.2566	13.8047	1.7240	0.1097	0.7667	0.0426	0.6561	5278	76	6415	260	4733	65
BCR	July	189.0212	17.3862	1.6922	0.1651	0.8279	0.0524	0.8189	5294	88	6282	385	4794	56
BCR	July	197.7102	17.5370	1.6240	0.0999	0.8578	0.0529	0.6689	5341	87	6243	272	4848	43
BCR	July	185.3870	12.5292	1.6666	0.1101	0.8219	0.0509	0.6203	5288	71	6276	266	4782	64
BCR	July	193.5881	12.8514	1.6202	0.0958	0.8809	0.0500	0.5911	5334	65	6174	233	4804	87
BCR	July	209.5924	17.0977	1.7087	0.1355	0.9019	0.0494	0.7903	5403	85	6357	316	4854	63
BCR	July	173.5409	9.3039	1.7014	0.1137	0.7790	0.0541	0.5742	5229	54	6355	279	4701	67
BCR	July	208.9205	12.2680	1.7867	0.1184	0.8497	0.0475	0.6392	5414	62	6636	304	4800	71
BCR	July	202.5659	19.3893	1.8017	0.1604	0.8246	0.0509	0.7519	5359	97	6558	349	4741	95
BCR	July	196.8422	14.3403	1.6568	0.1173	0.8685	0.0442	0.7713	5346	74	6247	278	4877	44
BCR	July	189.6457	11.7663	1.6524	0.1047	0.8495	0.0623	0.4623	5314	64	6242	269	4766	86
BCR	July	189.2395	13.8350	1.5186	0.0864	0.8915	0.0497	0.6737	5307	72	5986	254	4869	54
BCR	July	202.7616	16.0411	1.7113	0.1274	0.8684	0.0518	0.7536	5369	84	6368	302	4805	78
BCR	July	189.3944	17.1005	1.8209	0.1496	0.7659	0.0386	0.8607	5322	95	6699	365	4747	64
BCR	July	194.4879	11.2754	1.7125	0.1045	0.8589	0.0493	0.5816	5358	66	6392	248	4812	70
BCR	July	181.5429	14.0088	1.6322	0.1350	0.8325	0.0497	0.7093	5261	80	6170	321	4836	45
BCR	July	187.2928	14.8440	1.5759	0.1169	0.8913	0.0646	0.5631	5291	82	6041	293	4736	104
BCR	July	197.6235	12.6477	1.6176	0.1111	0.9025	0.0667	0.6120	5370	73	6156	263	4751	102

		Isotope Ratios						rho	Dates					
Sample Spot	Note	$^{207}Pb/^{235}U$	±2σ	$^{206}Pb/^{238}U$	±2σ	$^{207}Pb/^{206}Pb$	±2σ		$^{207}Pb/^{235}U$	±2σ	$^{206}Pb/^{238}U$	±2σ	$^{207}Pb/^{206}Pb$	±2σ
BCR	July	201.5724	17.9862	1.7919	0.1605	0.8218	0.0569	0.6395	5381	84	6528	371	4712	110
BCR	July	193.4981	13.3614	1.6823	0.1123	0.8326	0.0522	0.4849	5330	72	6312	274	4796	73
BCR	July	189.5332	13.8361	1.6041	0.1451	0.8635	0.0511	0.7285	5309	72	6092	338	4755	113
BCR	July	213.4331	17.5573	1.6686	0.1250	0.9295	0.0506	0.7781	5422	82	6268	294	4867	79
BCR	July	196.7453	15.6208	1.6900	0.1355	0.8893	0.0511	0.7703	5361	92	6310	325	4871	48
610_5	March	28.9985	0.4612	0.2291	0.0025	0.9170	0.0114	0.5977	3453	16	1330	13	4979	0
610_32	March	27.1549	0.5431	0.2204	0.0041	0.8986	0.0117	0.7438	3388	19	1284	22	4997	5
610_51	March	28.0514	0.4722	0.2251	0.0036	0.8876	0.0098	0.7454	3420	16	1309	19	4984	0
610_81	March	24.7726	0.4520	0.2127	0.0039	0.8902	0.0114	0.7671	3298	18	1243	21	4986	14
610_102	March	20.0953	0.3601	0.1932	0.0026	0.8808	0.0110	0.6663	3095	17	1139	14	4989	4
610_124	March	19.3580	0.3959	0.1917	0.0037	0.8658	0.0145	0.6118	3059	20	1131	20	4964	25
610_149	March	20.5861	0.3293	0.1985	0.0031	0.8609	0.0128	0.6007	3118	16	1167	16	4970	16
610_167	March	23.0350	0.3915	0.2045	0.0032	0.8785	0.0150	0.4164	3228	16	1199	17	4974	19
610_198	March	25.4082	0.3881	0.2164	0.0031	0.8563	0.0096	0.6937	3323	15	1263	16	4969	13
610_221	March	27.6421	0.5069	0.2251	0.0035	0.8692	0.0124	0.6161	3405	18	1309	18	4961	34
610_243	March	19.9300	0.3721	0.2233	0.0038	0.8777	0.0136	0.5866	3087	18	1299	20	4977	13
610_268	March	18.0884	0.2986	0.2180	0.0040	0.8829	0.0111	0.7461	2994	16	1271	21	4918	0
610_287	March	24.4073	0.4414	0.2220	0.0034	0.8850	0.0115	0.6442	3284	17	1292	18	4978	16
610	June	25.7402	0.5383	0.2201	0.0044	0.8395	0.0099	0.8681	3335	20	1282	23	4953	18
610	June	24.6132	0.3806	0.2185	0.0042	0.8207	0.0116	0.6339	3292	15	1273	22	4933	17
610	June	25.3036	0.5822	0.2121	0.0054	0.8683	0.0103	0.8749	3318	22	1240	29	4976	13
610	June	27.1918	0.6916	0.2218	0.0056	0.8779	0.0116	0.8845	3388	24	1291	29	4975	15
610	June	27.6211	0.4678	0.2234	0.0050	0.9001	0.0114	0.7737	3405	16	1300	26	4979	24
610	June	24.6731	0.4196	0.2188	0.0047	0.8181	0.0118	0.6959	3294	16	1275	25	4923	18
610	June	25.5024	0.3671	0.2079	0.0040	0.8887	0.0084	0.8135	3327	14	1218	21		
610	June	28.2525	0.4764	0.2207	0.0047	0.9265	0.0096	0.8827	3427	16	1285	24		
610	June	23.4953	0.5256	0.2093	0.0043	0.8131	0.0110	0.8341	3246	21	1224	23	4925	16
610	June	25.6642	0.4712	0.2156	0.0050	0.8642	0.0103	0.8306	3333	18	1258	27	4968	13
610	June	29.3420	0.5850	0.2257	0.0058	0.9407	0.0131	0.8131	3463	19	1312	30		
610	June	28.3964	0.5732	0.2201	0.0054	0.9376	0.0117	0.8274	3431	20	1282	28		
610	June	27.8313	0.5896	0.2285	0.0059	0.8838	0.0105	0.8510	3411	21	1326	31	4979	13
610	July	28.4124	0.4667	0.2293	0.0036	0.8986	0.0108	0.7232	3432	16	1331	19		
610	July	28.1012	0.4493	0.2294	0.0040	0.8934	0.0094	0.8593	3422	16	1331	21		
610	July	28.3513	0.5060	0.2270	0.0041	0.9042	0.0090	0.8453	3430	17	1319	22		

		Isotope Ratios						rho	Dates					
Sample Spot	Note	$^{207}Pb/^{235}U$	±2σ	$^{206}Pb/^{238}U$	±2σ	$^{207}Pb/^{206}Pb$	±2σ		$^{207}Pb/^{235}U$	±2σ	$^{206}Pb/^{238}U$	±2σ	$^{207}Pb/^{206}Pb$	±2σ
610	July	28.0644	0.4067	0.2255	0.0032	0.8991	0.0068	0.8098	3421	14	1311	17		
610	July	28.0562	0.5933	0.2229	0.0051	0.9115	0.0104	0.8585	3419	20	1297	26		
610	July	28.0633	0.4478	0.2249	0.0040	0.9013	0.0090	0.8219	3420	16	1308	21		
610	July	28.3495	0.4977	0.2271	0.0044	0.9018	0.0087	0.8579	3430	17	1319	23	4991	0
610	July	28.0070	0.4178	0.2244	0.0038	0.9026	0.0091	0.8013	3418	15	1305	20		
610	July	28.2457	0.4456	0.2263	0.0041	0.9058	0.0094	0.8100	3427	15	1315	22	4985	0
610	July	28.2976	0.4669	0.2263	0.0033	0.9059	0.0105	0.7426	3428	16	1315	17	4956	0
610	July	28.0653	0.4848	0.2256	0.0035	0.9071	0.0103	0.7620	3420	17	1311	19		
610	July	28.3777	0.4499	0.2274	0.0035	0.9105	0.0117	0.6529	3431	15	1321	18	4990	0
610	July	28.3397	0.5673	0.2266	0.0046	0.9116	0.0084	0.8940	3429	20	1316	24		
610	July	28.3736	0.5830	0.2271	0.0039	0.9103	0.0118	0.7782	3430	20	1319	21	4982	0
610	July	28.3261	0.6323	0.2247	0.0043	0.9173	0.0115	0.8347	3428	22	1306	22		
610	July	28.3078	0.6046	0.2242	0.0044	0.9182	0.0114	0.8205	3428	21	1304	23		
610	July	28.4520	0.4735	0.2271	0.0044	0.9097	0.0117	0.7579	3434	16	1319	23		
610	July	27.8478	0.4436	0.2238	0.0041	0.9037	0.0098	0.8152	3417	18	1302	21	4993	0
610	July	28.2917	0.5003	0.2233	0.0042	0.9161	0.0104	0.8094	3428	17	1299	22		
610	July	28.2879	0.5131	0.2258	0.0044	0.9087	0.0108	0.7965	3428	18	1312	23	4996	0
610	July	28.2221	0.4506	0.2264	0.0038	0.9091	0.0096	0.7975	3426	16	1315	20		
610	July	28.5590	0.5362	0.2279	0.0030	0.9156	0.0114	0.7426	3437	18	1323	16	4998	0
610	July	28.2181	0.5937	0.2274	0.0051	0.9140	0.0094	0.8890	3425	20	1320	27	4989	12
610	July	28.1961	0.4786	0.2269	0.0032	0.9140	0.0098	0.7897	3425	17	1318	17		
610	July	28.2323	0.3295	0.2241	0.0040	0.9221	0.0092	0.8155	3427	11	1303	21		
610	July	28.5159	0.4924	0.2231	0.0037	0.9167	0.0113	0.7378	3436	17	1298	19	4974	0
610	July	28.2389	0.3794	0.2200	0.0040	0.9178	0.0093	0.8261	3427	13	1282	21		
610	July	28.4019	0.4947	0.2216	0.0033	0.9155	0.0081	0.8607	3432	17	1290	18		
610	July	28.6757	0.4641	0.2269	0.0038	0.9179	0.0103	0.7796	3441	16	1318	20		
610	July	28.4382	0.5386	0.2285	0.0045	0.9223	0.0110	0.8060	3433	18	1326	24		
612_1	March	32.5339	1.4068	0.2554	0.0085	0.9096	0.0490	0.1089	3560	43	1465	43	4871	71
612_8	March	32.2521	1.0918	0.2518	0.0118	0.9486	0.0375	0.5514	3554	34	1446	60	4956	25
612_17	March	31.0649	0.9580	0.2531	0.0088	0.9075	0.0360	0.1754	3518	30	1453	45	4871	61
612_35	March	30.7897	1.3371	0.2451	0.0118	0.9121	0.0412	0.5297	3506	43	1411	60	4869	108
612_48	March	31.4222	1.2513	0.2494	0.0095	0.8947	0.0357	0.5354	3527	40	1434	49	4887	36
612_64	March	30.0111	1.2653	0.2562	0.0090	0.8646	0.0347	0.4531	3481	42	1469	46	4898	48
612_78	March	28.2528	1.1334	0.2459	0.0102	0.8780	0.0375	0.4412	3423	39	1416	52	4874	40

		Isotope Ratios						rho	Dates					
Sample Spot	Note	$^{207}Pb/^{235}U$	±2σ	$^{206}Pb/^{238}U$	±2σ	$^{207}Pb/^{206}Pb$	±2σ		$^{207}Pb/^{235}U$	±2σ	$^{206}Pb/^{238}U$	±2σ	$^{207}Pb/^{206}Pb$	±2σ
612_93	March	24.7037	0.9546	0.2281	0.0075	0.8801	0.0375	0.2870	3292	38	1324	39	4909	64
612_108	March	22.7568	0.7721	0.2220	0.0075	0.8756	0.0277	0.5971	3213	33	1292	40	4933	31
612_121	March	21.1010	0.9375	0.2121	0.0069	0.8567	0.0405	0.2457	3137	44	1239	37	4836	79
612_136	March	22.3327	0.9004	0.2162	0.0066	0.8828	0.0367	0.2279	3193	39	1261	35	4787	76
612_151	March	23.8007	0.8247	0.2221	0.0067	0.8904	0.0415	0.0103	3256	34	1292	35	4914	36
612_164	March	25.4076	0.9656	0.2299	0.0084	0.8780	0.0339	0.4041	3320	35	1333	44	4908	58
612_180	March	30.3242	1.2666	0.2480	0.0102	0.8725	0.0387	0.4557	3492	42	1427	53	4840	51
612_195	March	28.7332	1.0712	0.2416	0.0081	0.8691	0.0294	0.5594	3440	37	1394	42	4884	39
612_210	March	29.8154	0.9466	0.2430	0.0093	0.8920	0.0303	0.5768	3477	32	1401	48	4908	45
612_227	March	27.8974	1.0520	0.2547	0.0084	0.8486	0.0410	0.1156	3411	38	1461	43	4868	43
612_240	March	22.3557	0.8255	0.2470	0.0076	0.8749	0.0253	0.6596	3195	36	1422	39	4879	43
612_255	March	20.2075	0.6718	0.2465	0.0100	0.8851	0.0356	0.1514	3098	32	1419	52	4895	63
612_270	March	20.5481	0.7525	0.2469	0.0084	0.8788	0.0247	0.6815	3113	37	1422	43	4943	47
612_285	March	26.5508	1.0988	0.2492	0.0074	0.8810	0.0300	0.3962	3362	40	1434	38	4924	29
612_291	March	30.4070	1.1213	0.2563	0.0090	0.8807	0.0443	0.0439	3496	36	1470	46	4859	57
612	June	27.7331	0.8533	0.2408	0.0071	0.8324	0.0308	0.2620	3415	35	1390	37	4876	36
612	June	28.6938	1.0575	0.2577	0.0083	0.8068	0.0290	0.4474	3438	36	1477	42	4846	47
612	June	28.0950	0.9883	0.2511	0.0095	0.8133	0.0306	0.4698	3417	35	1443	49	4861	39
612	June	29.2082	0.9884	0.2472	0.0087	0.8632	0.0350	0.3273	3456	33	1423	45	4879	42
612	June	31.9867	1.1533	0.2519	0.0093	0.9209	0.0297	0.6030	3545	36	1447	48	4892	49
612	June	28.0787	0.8519	0.2361	0.0071	0.8695	0.0284	0.4314	3418	30	1366	37	4914	37
612	June	28.1831	0.8821	0.2444	0.0084	0.8320	0.0214	0.6873	3421	31	1408	43	4896	43
612	June	31.1504	1.0572	0.2527	0.0097	0.8795	0.0309	0.4467	3519	33	1451	50	4913	44
612	June	30.6753	1.0356	0.2446	0.0094	0.9194	0.0322	0.4855	3504	33	1409	48	4919	21
612	June	27.4847	0.8692	0.2454	0.0079	0.8186	0.0281	0.4876	3397	32	1413	41	4876	45
612	June	27.4367	0.9824	0.2422	0.0081	0.8252	0.0345	0.2860	3394	35	1397	42	4843	44
612	June	29.0046	0.7654	0.2386	0.0083	0.8881	0.0294	0.4518	3451	26	1378	43	4909	63
612	June	31.0433	1.1320	0.2434	0.0078	0.9277	0.0306	0.5652	3515	35	1403	41	4941	29
612	June	29.3660	1.1067	0.2550	0.0079	0.8383	0.0281	0.5581	3460	38	1463	40	4868	41
612	June	25.5769	1.0144	0.2381	0.0071	0.7761	0.0251	0.5081	3324	39	1376	37	4819	42
612	June	26.1803	0.8426	0.2378	0.0096	0.8083	0.0314	0.3349	3349	31	1373	50	4823	63
612	June	29.7760	0.8758	0.2509	0.0074	0.8632	0.0217	0.6165	3476	29	1442	38	4952	14
612	June	31.9971	0.9410	0.2508	0.0084	0.9277	0.0296	0.4868	3547	29	1442	43	4911	42
612	June	33.1286	0.9993	0.2416	0.0086	0.9980	0.0313	0.5728	3581	30	1394	45	4976	3

		Isotope Ratios						rho	Dates					
Sample Spot	Note	$^{207}Pb/^{235}U$	±2σ	$^{206}Pb/^{238}U$	±2σ	$^{207}Pb/^{206}Pb$	±2σ		$^{207}Pb/^{235}U$	±2σ	$^{206}Pb/^{238}U$	±2σ	$^{207}Pb/^{206}Pb$	±2σ
612	June	31.7320	1.0116	0.2612	0.0093	0.8924	0.0303	0.4784	3538	31	1494	47	4880	55
612	June	30.8283	1.0055	0.2592	0.0102	0.8776	0.0352	0.4090	3509	32	1484	52	4906	35
612	June	32.4721	1.1453	0.2521	0.0091	0.9314	0.0320	0.5385	3560	34	1448	47	4918	52
612	July	30.3822	0.9853	0.2474	0.0080	0.8941	0.0279	0.5316	3495	32	1424	42	4918	43
612	July	31.7097	0.8755	0.2591	0.0070	0.8903	0.0274	0.3929	3538	27	1484	36	4920	30
612	July	31.3282	0.8952	0.2480	0.0079	0.9192	0.0290	0.4150	3526	29	1427	41	4874	82
612	July	32.1725	0.9587	0.2533	0.0082	0.9231	0.0253	0.6456	3552	29	1454	42	4935	34
612	July	31.1226	1.0090	0.2522	0.0064	0.8956	0.0302	0.3732	3519	33	1449	33	4909	52
612	July	30.5640	1.1004	0.2496	0.0085	0.8886	0.0290	0.4589	3510	40	1435	44	4877	52
612	July	31.9456	0.9716	0.2530	0.0066	0.9145	0.0302	0.3175	3545	30	1453	34	4872	40
612	July	31.4857	0.9583	0.2487	0.0080	0.9194	0.0308	0.4760	3531	30	1431	41	4926	52
612	July	32.3289	0.9116	0.2541	0.0072	0.9251	0.0271	0.4796	3557	28	1459	37	4906	69
612	July	32.2117	1.1142	0.2614	0.0076	0.8985	0.0298	0.4993	3552	34	1496	39	4916	45
612	July	32.0686	1.0103	0.2587	0.0079	0.9064	0.0251	0.5956	3548	31	1482	41	4912	44
612	July	31.0414	1.0895	0.2575	0.0063	0.8819	0.0327	0.2511	3516	34	1477	32	4898	42
612	July	31.2006	1.0816	0.2498	0.0086	0.9149	0.0321	0.5279	3520	34	1436	44	4909	42
612	July	31.8508	0.9100	0.2590	0.0082	0.9016	0.0317	0.2835	3542	28	1483	42	4869	40
612	July	32.6306	0.9559	0.2582	0.0071	0.9238	0.0318	0.2730	3566	30	1480	36	4853	58
612	July	31.7363	0.7187	0.2581	0.0068	0.8979	0.0267	0.3030	3540	22	1479	35	4945	23
612	July	32.4120	1.1036	0.2568	0.0081	0.9192	0.0295	0.4993	3558	34	1472	42	4944	46
612	July	31.8781	0.8789	0.2506	0.0071	0.9233	0.0292	0.3691	3543	27	1441	37	4917	30
612	July	31.7823	0.6924	0.2553	0.0069	0.9044	0.0295	0.1146	3542	22	1465	35	4921	46
612	July	31.4032	0.9346	0.2507	0.0060	0.9099	0.0280	0.3355	3528	29	1442	31	4901	80
612	July	32.8130	1.0383	0.2552	0.0061	0.9389	0.0333	0.2273	3571	31	1465	31	4955	30
612	July	31.6680	1.1684	0.2608	0.0083	0.8910	0.0289	0.5572	3535	36	1493	42	4891	50
612	July	32.0258	1.0511	0.2589	0.0065	0.9139	0.0339	0.2090	3547	32	1483	33	4904	46
612	July	31.7470	0.7757	0.2597	0.0063	0.9035	0.0239	0.4575	3540	24	1488	33	4952	31
612	July	32.8009	0.8203	0.2546	0.0059	0.9380	0.0285	0.1964	3572	25	1461	30	4949	21
612	July	32.3351	0.9257	0.2559	0.0076	0.9142	0.0363	0.0759	3557	28	1468	39	4883	66
612	July	31.8043	0.7716	0.2509	0.0081	0.9147	0.0264	0.5612	3542	24	1442	42	4922	45
612	July	32.3752	0.8461	0.2549	0.0056	0.9174	0.0294	0.3726	3559	26	1463	29	4935	34
612	July	33.0086	1.1547	0.2494	0.0080	0.9610	0.0312	0.5351	3576	35	1434	41	4906	86
612	July	32.4545	0.7707	0.2538	0.0057	0.9429	0.0231	0.5643	3562	24	1458	29	4966	31
91500_3	March	1.6652	0.1230	0.1759	0.0044	0.0680	0.0051	0.1566	988	47	1044	24	816	157

		Isotope Ratios						rho	Dates					
Sample Spot	Note	$^{207}Pb/^{235}U$	±2σ	$^{206}Pb/^{238}U$	±2σ	$^{207}Pb/^{206}Pb$	±2σ		$^{207}Pb/^{235}U$	±2σ	$^{206}Pb/^{238}U$	±2σ	$^{207}Pb/^{206}Pb$	±2σ
91500_18	March	1.8473	0.1536	0.1740	0.0031	0.0779	0.0061	0.3250	1053	53	1034	17	1093	149
91500_36	March	1.8890	0.1112	0.1741	0.0045	0.0780	0.0045	0.3139	1072	39	1034	25	1117	114
91500_49	March	1.8264	0.0920	0.1774	0.0029	0.0726	0.0042	-0.1642	1051	34	1053	16	966	121
91500_66	March	1.7149	0.0844	0.1769	0.0040	0.0719	0.0039	0.0135	1011	32	1050	22	953	113
91500_79	March	1.5931	0.0777	0.1705	0.0046	0.0713	0.0038	0.2336	964	30	1015	25	941	104
91500_94	March	1.4840	0.1071	0.1597	0.0033	0.0757	0.0058	-0.0761	917	44	955	19	1029	165
91500_109	March	1.3266	0.1022	0.1506	0.0033	0.0750	0.0052	0.4863	851	44	904	19	1024	144
91500_122	March	1.3543	0.1189	0.1522	0.0033	0.0767	0.0072	-0.1897	861	52	913	18	1029	204
91500_137	March	1.3102	0.1214	0.1515	0.0031	0.0733	0.0062	0.4238	841	53	909	18	953	181
91500_152	March	1.3217	0.0955	0.1565	0.0041	0.0698	0.0053	0.0199	849	42	937	23	866	165
91500_165	March	1.5284	0.1164	0.1632	0.0038	0.0733	0.0060	-0.0348	935	46	975	21	960	173
91500_181	March	1.7915	0.1032	0.1713	0.0048	0.0741	0.0045	0.1518	1050	31	1019	26	1051	106
91500_196	March	1.7229	0.1319	0.1669	0.0039	0.0754	0.0058	0.0747	1009	48	995	22	1027	152
91500_212	March	1.6780	0.1116	0.1704	0.0050	0.0713	0.0049	0.1749	994	44	1014	28	963	125
91500_228	March	1.5584	0.0909	0.1747	0.0034	0.0693	0.0041	0.1525	950	36	1038	19	875	121
91500_241	March	1.2503	0.1077	0.1762	0.0039	0.0690	0.0057	0.2005	816	49	1046	21	828	185
91500_256	March	1.2286	0.0873	0.1698	0.0040	0.0791	0.0062	-0.1576	809	39	1011	22	1125	149
91500_271	March	1.1498	0.0920	0.1761	0.0039	0.0686	0.0051	0.2315	771	44	1045	21	824	177
91500_286	March	1.5817	0.0873	0.1775	0.0039	0.0733	0.0044	-0.0049	959	34	1053	22	989	125
91500_290	March	1.7636	0.0846	0.1733	0.0039	0.0770	0.0038	0.1828	1029	31	1030	21	1099	98
91500	June	1.6649	0.1103	0.1749	0.0039	0.0692	0.0050	-0.0105	988	43	1038	22	843	154
91500	June	1.6103	0.0927	0.1753	0.0040	0.0672	0.0041	-0.0065	969	36	1041	22	796	135
91500	June	1.8336	0.1139	0.1752	0.0032	0.0754	0.0046	0.2283	1051	41	1040	18	1034	129
91500	June	1.7696	0.1059	0.1716	0.0035	0.0747	0.0042	0.3422	1028	39	1021	19	1021	119
91500	June	1.6227	0.1098	0.1724	0.0034	0.0679	0.0042	0.3512	971	43	1025	19	854	120
91500	June	1.8016	0.1295	0.1768	0.0041	0.0732	0.0051	0.2444	1037	46	1049	22	963	148
91500	June	1.7536	0.1257	0.1740	0.0039	0.0746	0.0047	0.4786	1033	40	1034	21	1012	126
91500	June	1.7789	0.0946	0.1750	0.0043	0.0746	0.0048	-0.2321	1033	35	1039	24	1011	130
91500	June	1.5497	0.1027	0.1740	0.0040	0.0648	0.0043	0.2470	943	40	1034	22	715	137
91500	June	1.7068	0.0855	0.1678	0.0042	0.0739	0.0039	0.0391	1007	31	1000	23	1005	109
91500	June	1.7799	0.0988	0.1681	0.0034	0.0769	0.0043	0.1639	1033	37	1001	19	1114	99
91500	June	1.7341	0.1011	0.1742	0.0036	0.0721	0.0040	0.2789	1015	38	1035	20	985	133
91500	June	1.6720	0.1109	0.1791	0.0039	0.0679	0.0045	0.1356	990	43	1062	21	808	151
91500	June	1.5258	0.0898	0.1647	0.0030	0.0675	0.0040	0.1170	935	37	983	17	808	131

		Isotope Ratios						rho	Dates					
Sample Spot	Note	$^{207}Pb/^{235}U$	±2σ	$^{206}Pb/^{238}U$	±2σ	$^{207}Pb/^{206}Pb$	±2σ		$^{207}Pb/^{235}U$	±2σ	$^{206}Pb/^{238}U$	±2σ	$^{207}Pb/^{206}Pb$	±2σ
91500	June	1.6008	0.1071	0.1708	0.0044	0.0683	0.0048	0.0817	963	42	1016	24	819	149
91500	June	1.7840	0.1184	0.1729	0.0038	0.0748	0.0049	0.2586	1044	39	1028	21	1055	119
91500	June	1.7582	0.1049	0.1819	0.0039	0.0701	0.0044	0.0638	1024	39	1077	21	883	136
91500	June	1.9056	0.1197	0.1752	0.0041	0.0790	0.0049	0.1227	1076	42	1041	22	1124	135
91500	June	1.8219	0.1458	0.1837	0.0050	0.0728	0.0062	0.1360	1042	53	1087	27	927	174
91500	June	1.7184	0.1072	0.1828	0.0038	0.0693	0.0043	0.2490	1009	40	1082	21	864	128
91500	June	1.8292	0.1114	0.1823	0.0038	0.0726	0.0047	-0.0073	1049	41	1079	21	954	137
91500	July	1.8473	0.1116	0.1758	0.0025	0.0759	0.0048	0.0972	1056	39	1044	14	1053	117
91500	July	1.8743	0.0934	0.1764	0.0036	0.0773	0.0041	-0.0214	1067	33	1047	20	1125	96
91500	July	1.9736	0.0830	0.1790	0.0032	0.0800	0.0036	0.0879	1103	28	1061	18	1175	87
91500	July	1.8698	0.0756	0.1758	0.0036	0.0773	0.0034	0.0717	1067	27	1044	20	1104	93
91500	July	1.7716	0.0952	0.1768	0.0041	0.0726	0.0038	0.2586	1030	34	1049	22	971	109
91500	July	1.8613	0.1042	0.1791	0.0027	0.0751	0.0044	0.0596	1062	37	1062	15	1033	114
91500	July	1.8327	0.0916	0.1808	0.0028	0.0733	0.0038	0.0605	1053	33	1071	15	991	104
91500	July	1.8273	0.1200	0.1741	0.0029	0.0759	0.0050	0.1919	1047	44	1035	16	1040	142
91500	July	1.8610	0.0851	0.1780	0.0033	0.0761	0.0037	0.0351	1063	31	1056	18	1069	102
91500	July	1.9134	0.0740	0.1804	0.0035	0.0774	0.0033	0.0341	1083	26	1069	19	1111	86
91500	July	1.7676	0.0818	0.1745	0.0034	0.0741	0.0038	-0.0901	1030	30	1037	19	1014	106
91500	July	1.7716	0.0785	0.1787	0.0029	0.0721	0.0034	0.0218	1032	29	1060	16	961	99
91500	July	1.8164	0.0864	0.1799	0.0032	0.0737	0.0037	0.0981	1047	31	1066	18	1005	100
91500	July	1.8031	0.0970	0.1785	0.0033	0.0736	0.0039	0.2845	1041	36	1059	18	998	108
91500	July	1.8066	0.1249	0.1809	0.0028	0.0728	0.0051	0.0696	1040	44	1072	15	952	141
91500	July	1.7838	0.0996	0.1772	0.0039	0.0732	0.0039	0.3075	1034	36	1052	22	987	108
91500	July	1.8505	0.0943	0.1767	0.0029	0.0759	0.0038	0.2453	1059	33	1049	16	1065	96
91500	July	1.8324	0.1050	0.1780	0.0035	0.0745	0.0043	0.1278	1051	37	1056	19	1016	118
91500	July	1.8573	0.1183	0.1758	0.0030	0.0766	0.0049	0.0342	1059	41	1044	17	1063	131
91500	July	1.8313	0.1029	0.1816	0.0036	0.0735	0.0044	-0.0530	1051	37	1075	19	983	128
91500	July	1.8361	0.0874	0.1799	0.0041	0.0746	0.0039	0.1055	1054	31	1066	22	1028	105
91500	July	1.7849	0.0916	0.1819	0.0032	0.0720	0.0038	0.1149	1035	35	1077	17	980	100
91500	July	1.8522	0.0848	0.1804	0.0044	0.0760	0.0039	0.0389	1060	30	1069	24	1064	103
91500	July	1.8432	0.0977	0.1797	0.0034	0.0755	0.0041	0.0765	1056	35	1065	19	1047	114
91500	July	1.8375	0.0873	0.1801	0.0031	0.0738	0.0033	0.1722	1064	35	1067	17	1038	104
91500	July	1.7263	0.0716	0.1762	0.0038	0.0702	0.0028	0.3032	1015	26	1046	21	916	80
91500	July	1.7628	0.1081	0.1755	0.0030	0.0705	0.0043	-0.2274	1025	39	1042	16	963	121

		Isotope Ratios						rho	Dates					
Sample Spot	Note	$^{207}Pb/^{235}U$	±2σ	$^{206}Pb/^{238}U$	±2σ	$^{207}Pb/^{206}Pb$	±2σ		$^{207}Pb/^{235}U$	±2σ	$^{206}Pb/^{238}U$	±2σ	$^{207}Pb/^{206}Pb$	±2σ
91500	July	1.8154	0.1110	0.1747	0.0033	0.0744	0.0049	-0.1177	1044	40	1038	18	1003	133
91500	July	1.8818	0.0943	0.1797	0.0043	0.0763	0.0042	-0.0037	1070	33	1065	23	1066	114
91500	July	1.8745	0.0926	0.1797	0.0032	0.0770	0.0037	0.2362	1068	33	1065	18	1095	99
PL_2	March	0.3940	0.0164	0.0538	0.0006	0.0522	0.0022	0.0569	337	12	338	4	274	96
PL_7	March	0.3940	0.0256	0.0534	0.0010	0.0535	0.0036	0.0425	336	19	335	6	347	135
PL_19	March	0.3940	0.0170	0.0537	0.0007	0.0538	0.0022	0.2634	337	12	337	4	376	73
PL_31	March	0.3940	0.0153	0.0536	0.0009	0.0538	0.0022	0.0380	337	11	337	5	372	80
PL_45	March	0.3940	0.0224	0.0539	0.0010	0.0516	0.0032	-0.0439	336	17	338	6	268	128
PL_54	March	0.3940	0.0151	0.0535	0.0007	0.0530	0.0021	0.1191	337	11	336	4	310	91
PL_65	March	0.3940	0.0196	0.0537	0.0006	0.0542	0.0028	0.0228	337	14	337	3	349	114
PL_168	March	0.3940	0.0194	0.0538	0.0011	0.0569	0.0027	0.4366	337	14	338	7	464	108
PL_183	March	0.3940	0.0181	0.0536	0.0007	0.0514	0.0026	-0.1077	337	13	337	4	230	119
PL_194	March	0.3940	0.0206	0.0537	0.0009	0.0535	0.0029	0.0341	337	15	337	6	326	126
PL_211	March	0.3940	0.0196	0.0537	0.0008	0.0530	0.0024	0.2899	337	14	337	5	304	104
PL_220	March	0.3940	0.0278	0.0537	0.0009	0.0521	0.0041	-0.3059	336	20	337	6	222	184
PL_292	March	0.3940	0.0142	0.0540	0.0009	0.0525	0.0020	0.0830	337	10	339	5	288	94
PL_293	March	0.3944	0.0210	0.0533	0.0009	0.0508	0.0028	0.2643	337	15	335	6	200	124
PL_294	March	0.3932	0.0232	0.0531	0.0010	0.0509	0.0031	0.1381	336	17	333	6	235	126
PL_295	March	0.3927	0.0199	0.0591	0.0014	0.0519	0.0032	-0.4345	336	15	370	8	242	149
PL_296	March	0.3971	0.0150	0.0509	0.0010	0.0673	0.0028	0.0415	339	11	320	6	831	85
PL_297	March	0.3878	0.0251	0.0532	0.0010	0.0489	0.0034	-0.2183	332	18	334	6	82	171
PL_298	March	0.3986	0.0303	0.0539	0.0010	0.0520	0.0042	-0.1201	339	22	339	6	271	156
PL_299	March	0.3934	0.0206	0.0545	0.0009	0.0506	0.0027	0.1954	336	15	342	6	191	123
PL_300	March	0.3942	0.0303	0.0534	0.0010	0.0505	0.0041	-0.0377	336	22	336	6	147	185
PL	June	0.3956	0.0208	0.0538	0.0010	0.0536	0.0032	-0.0565	337	15	338	6	304	135
PL	June	0.3907	0.0217	0.0535	0.0011	0.0527	0.0027	0.3166	334	16	336	7	279	119
PL	June	0.3960	0.0165	0.0538	0.0008	0.0537	0.0024	0.0940	338	12	338	5	333	102
PL	June	0.3908	0.0178	0.0535	0.0009	0.0526	0.0023	0.2027	334	13	336	5	282	105
PL	June	0.3979	0.0193	0.0538	0.0007	0.0540	0.0026	0.1046	339	14	338	4	338	108
PL	June	0.3934	0.0138	0.0536	0.0006	0.0532	0.0021	0.3502	336	10	337	4	315	86
PL	June	0.3939	0.0197	0.0537	0.0010	0.0531	0.0022	0.5817	336	14	337	6	308	100
PL	June	0.3942	0.0165	0.0537	0.0009	0.0534	0.0024	0.0128	337	12	337	5	318	104
PL	June	0.3941	0.0154	0.0537	0.0007	0.0532	0.0021	0.1189	337	11	337	5	315	93
PL	June	0.3936	0.0213	0.0537	0.0009	0.0531	0.0028	0.2826	336	16	337	6	293	125

		Isotope Ratios						rho	Dates					
Sample Spot	Note	$^{207}Pb/^{235}U$	±2σ	$^{206}Pb/^{238}U$	±2σ	$^{207}Pb/^{206}Pb$	±2σ		$^{207}Pb/^{235}U$	±2σ	$^{206}Pb/^{238}U$	±2σ	$^{207}Pb/^{206}Pb$	±2σ
PL	June	0.3940	0.0208	0.0536	0.0010	0.0534	0.0026	0.4013	336	15	337	6	308	121
PL	June	0.3943	0.0178	0.0537	0.0007	0.0532	0.0024	0.2757	337	13	337	4	310	105
PL	June	0.3940	0.0157	0.0537	0.0008	0.0532	0.0021	0.1924	337	11	337	5	318	86
PL	June	0.3938	0.0198	0.0536	0.0009	0.0533	0.0030	-0.1903	336	15	337	6	292	142
PL	June	0.3939	0.0186	0.0537	0.0009	0.0531	0.0024	0.3138	336	14	337	6	336	91
PL	June	0.3943	0.0204	0.0536	0.0009	0.0534	0.0025	0.3577	337	15	337	6	314	110
PL	June	0.3939	0.0198	0.0537	0.0009	0.0532	0.0027	-0.0178	336	14	337	6	298	120
PL	July	0.3976	0.0203	0.0538	0.0007	0.0537	0.0027	0.1515	339	15	337	4	322	116
PL	July	0.3826	0.0130	0.0532	0.0009	0.0521	0.0016	0.4296	329	10	334	5	275	73
PL	July	0.4029	0.0124	0.0541	0.0008	0.0545	0.0020	0.0765	346	10	340	5	372	80
PL	July	0.3916	0.0149	0.0535	0.0007	0.0530	0.0020	0.2272	335	11	336	4	309	83
PL	July	0.3897	0.0141	0.0535	0.0006	0.0527	0.0019	0.2243	334	10	336	3	295	84
PL	July	0.4111	0.0141	0.0541	0.0008	0.0549	0.0020	0.0529	349	10	340	5	390	82
PL	July	0.3833	0.0172	0.0534	0.0007	0.0519	0.0025	-0.1400	329	12	335	4	250	109
PL	July	0.4049	0.0177	0.0541	0.0008	0.0542	0.0025	0.0432	344	13	340	5	350	102
PL	July	0.3903	0.0170	0.0535	0.0006	0.0530	0.0023	0.0424	334	12	336	3	301	100
PL	July	0.4000	0.0111	0.0539	0.0008	0.0540	0.0014	0.3854	341	8	339	5	360	60
PL	July	0.3887	0.0136	0.0536	0.0007	0.0529	0.0018	0.2521	333	10	336	4	309	77
PL	July	0.3949	0.0190	0.0535	0.0008	0.0538	0.0025	0.2420	337	14	336	5	331	112
PL	July	0.3998	0.0174	0.0541	0.0008	0.0539	0.0023	0.2510	341	13	340	5	339	98
PL	July	0.3661	0.0160	0.0533	0.0007	0.0500	0.0022	0.1586	316	12	335	4	200	91
PL	July	0.4000	0.0174	0.0540	0.0008	0.0540	0.0025	-0.1044	341	13	339	5	338	111
PL	July	0.3916	0.0126	0.0534	0.0008	0.0534	0.0019	-0.0527	335	9	336	5	325	83
PL	July	0.3940	0.0174	0.0534	0.0007	0.0535	0.0023	0.2471	337	13	335	4	324	99
PL	July	0.3943	0.0138	0.0540	0.0005	0.0528	0.0020	-0.1582	337	10	339	3	298	87
PL	July	0.3921	0.0178	0.0532	0.0009	0.0533	0.0022	0.3796	335	13	334	6	316	94
PL	July	0.3938	0.0150	0.0535	0.0007	0.0534	0.0021	0.1246	337	11	336	4	325	90
PL	July	0.3961	0.0135	0.0541	0.0008	0.0534	0.0020	-0.0498	338	10	340	5	326	86
PL	July	0.3863	0.0152	0.0537	0.0007	0.0528	0.0022	0.0100	331	11	337	4	294	97
PL	July	0.4057	0.0157	0.0534	0.0007	0.0558	0.0022	0.1358	345	11	335	4	422	88
PL	July	0.3888	0.0170	0.0538	0.0008	0.0532	0.0023	0.1939	333	13	338	5	310	103
PL	July	0.3916	0.0175	0.0535	0.0005	0.0532	0.0024	0.1327	335	13	336	3	310	105
PL	July	0.3897	0.0161	0.0537	0.0006	0.0522	0.0023	-0.0980	334	12	337	4	266	102
PL	July	0.4059	0.0157	0.0544	0.0009	0.0530	0.0020	0.3336	345	11	342	6	310	86

		Isotope Ratios						rho	Dates					
Sample Spot	Note	$^{207}Pb/^{235}U$	±2σ	$^{206}Pb/^{238}U$	±2σ	$^{207}Pb/^{206}Pb$	±2σ		$^{207}Pb/^{235}U$	±2σ	$^{206}Pb/^{238}U$	±2σ	$^{207}Pb/^{206}Pb$	±2σ
PL	July	0.4018	0.0184	0.0540	0.0008	0.0533	0.0024	0.1064	342	13	339	5	312	108
PL	July	0.3848	0.0170	0.0535	0.0007	0.0520	0.0024	-0.0372	330	13	336	4	255	111
PL	July	0.3958	0.0158	0.0535	0.0007	0.0538	0.0020	-0.0230	338	11	336	4	365	95
TEM_6	March	0.4856	0.0271	0.0690	0.0013	0.0511	0.0025	0.4951	401	18	430	8	221	111
TEM_34	March	0.5191	0.0323	0.0684	0.0012	0.0550	0.0034	0.1396	423	22	426	7	368	148
TEM_52	March	0.5064	0.0381	0.0652	0.0012	0.0558	0.0046	-0.2019	414	26	407	7	368	191
TEM_82	March	0.4365	0.0297	0.0635	0.0011	0.0528	0.0037	0.0572	366	21	397	7	313	142
TEM_103	March	0.3620	0.0265	0.0576	0.0013	0.0535	0.0042	-0.0376	319	24	361	8	322	211
TEM_125	March	0.3456	0.0225	0.0568	0.0010	0.0523	0.0035	0.0731	300	17	356	6	296	138
TEM_150	March	0.3560	0.0240	0.0582	0.0009	0.0506	0.0035	0.0417	308	18	365	6	166	171
TEM_169	March	0.4352	0.0444	0.0594	0.0014	0.0566	0.0058	0.2280	364	32	372	9	349	262
TEM_199	March	0.4404	0.0385	0.0628	0.0015	0.0511	0.0042	0.3522	368	27	393	9	222	182
TEM_222	March	0.5618	0.0298	0.0694	0.0015	0.0572	0.0033	0.0331	451	19	433	9	461	133
TEM_244	March	0.3408	0.0365	0.0640	0.0015	0.0528	0.0058	0.0694	295	28	400	9	179	270
TEM_269	March	0.3629	0.0295	0.0664	0.0015	0.0580	0.0047	0.1983	313	22	415	9	465	172
TEM_288	March	0.4700	0.0402	0.0668	0.0018	0.0558	0.0049	-0.0334	389	28	417	11	349	225
Tem	July	1.2471	0.2019	0.0754	0.0024	0.1189	0.0180	0.3905	787	92	468	14	1762	304
Tem	July	0.5605	0.0623	0.0685	0.0027	0.0593	0.0065	0.3445	445	41	427	16	398	275
Tem	July	0.4815	0.0434	0.0670	0.0014	0.0522	0.0046	0.0828	395	30	418	9	167	230
Tem	July	0.5186	0.0294	0.0675	0.0012	0.0558	0.0032	0.0473	423	19	421	7	397	133
Tem	July	0.4670	0.0428	0.0674	0.0018	0.0504	0.0048	-0.0066	385	30	421	11	60	264
Tem	July	0.5898	0.0519	0.0674	0.0017	0.0655	0.0069	-0.0753	476	37	420	10	664	216
Tem	July	0.4755	0.0617	0.0683	0.0021	0.0508	0.0068	0.0065	400	48	426	13	-27	408
Tem	July	0.6760	0.0758	0.0667	0.0020	0.0741	0.0087	0.0284	516	45	416	12	880	253
Tem	July	0.5161	0.0490	0.0645	0.0016	0.0583	0.0055	0.2153	418	34	403	10	472	230
Tem	July	0.6400	0.0672	0.0692	0.0018	0.0659	0.0066	-0.1594	495	40	431	11	724	228
Tem	July	0.5429	0.0537	0.0682	0.0019	0.0582	0.0056	0.1930	435	34	425	12	419	209
Tem	July	0.5017	0.0584	0.0665	0.0019	0.0553	0.0065	0.0704	406	39	415	11	312	253
Tem	July	0.5644	0.0492	0.0692	0.0018	0.0598	0.0055	-0.1179	450	32	431	11	551	182
Tem	July	0.5087	0.0573	0.0637	0.0015	0.0576	0.0057	0.5130	412	37	398	9	393	212
Tem	July	0.5180	0.0481	0.0659	0.0013	0.0568	0.0053	0.1793	419	33	411	8	354	237
Tem	July	0.5435	0.0550	0.0672	0.0016	0.0585	0.0056	0.2209	435	35	419	10	491	195
Tem	July	0.4769	0.0430	0.0660	0.0014	0.0524	0.0045	0.2575	392	30	412	9	260	179
Tem	July	0.4969	0.0465	0.0664	0.0021	0.0549	0.0051	0.2423	405	32	415	12	273	238

		Isotope Ratios						rho	Dates					
Sample Spot	Note	$^{207}Pb/^{235}U$	±2σ	$^{206}Pb/^{238}U$	±2σ	$^{207}Pb/^{206}Pb$	±2σ		$^{207}Pb/^{235}U$	±2σ	$^{206}Pb/^{238}U$	±2σ	$^{207}Pb/^{206}Pb$	±2σ
Tem	July	0.5129	0.0635	0.0676	0.0017	0.0555	0.0063	0.4264	413	43	422	11	331	260
Tem	July	0.5111	0.0538	0.0681	0.0016	0.0547	0.0054	0.3075	414	36	425	10	237	267
Tem	July	0.5407	0.0491	0.0665	0.0015	0.0593	0.0057	-0.0488	434	33	415	9	446	234
Tem	July	2.1984	0.9873	0.0756	0.0077	0.1677	0.0525	0.9375	930	216	468	45	1921	431
Tem	July	0.5522	0.0353	0.0667	0.0010	0.0592	0.0038	0.0815	444	23	416	6	520	141
Tem	July	0.4921	0.0285	0.0655	0.0010	0.0547	0.0033	-0.0172	405	19	409	6	351	138
Tem	July	0.5178	0.0290	0.0669	0.0009	0.0566	0.0030	0.1015	428	22	418	5	469	140